Cosmological inflation : theoretical aspects and observational constraints

Vincent Vennin

Thèse de Doctorat de l'Université Pierre et Marie Curie

Spécialité: Cosmologie

Ecole Doctorale 127 "Astronomie et Astrophysique d'Île de France"
Institut d'Astrophysique de Paris
$\mathcal{GR}\varepsilon\mathcal{CO}$

Presentée par

Vincent Vennin

Pour obtenir le grade de

Docteur de l'Université Pierre et Marie Curie

Sujet de la thèse:

Inflation Cosmologique: Aspects Théoriques et Contraintes Observationnelles

soutenue le 5 septembre 2014 devant le jury composé de

M.	Jérôme Martin	directeur de thèse
M.	Daniel Baumann	rapporteur
M.	Eiichiro Komatsu	rapporteur
M.	Michael G. F. Joyce	examinateur
M.	Alexei A. Starobinsky	examinateur
M.	Paul J. Steinhardt	examinateur

Acknowledgements

First, I would like to express my deepest gratitude to Jérôme Martin. First as a teacher and then as a Ph.D. director, he introduced me to the beauty of early universe cosmology and he taught me the trade of research with a lot of patience and pedagogy. I learnt a lot from his scientific rigour, his great intellectual honesty and his profund inquisitiveness. With constant support and encouragement, he offered me a very motivating and pleasant environment for doing research.

I want to thank my reporters Daniel Baumann and Eiichiro Komatsu for their patience in light of the size of this manuscript, as well as the members of my thesis jury, Michael Joyce, Aleksei Starobinsky, and Paul Steinhardt. I deeply appreciate their time and effort and I am grateful for their scientific interest in my work.

I am delighted to thank my collaborators, Robert Brandenberger, Laurence Perreault-Levasseur, Patrick Peter, Christophe Ringeval, Roberto Trotta and Jun'ichi Yokoyama with whom I worked closely and from whom I learnt a lot. I thank them for their hospitality and constant advice. Special thanks come to Christophe for having been my "computer hotline" during these three years.

I want to thank the directors of IAP, Laurent Vigroux and Francis Bernardeau, and the director of the $\mathcal{GR}\varepsilon\mathbb{C}\mathcal{O}$ group, Guillaume Faye, for having provided me with ideal conditions for carrying out research, specially in a context of limited funding.

It is a pleasure to thank all those who contributed to make my work environment a very nice one: my office mates Sandrine and Charlotte, and the *Salut Gorêt* championship members Cédric, Jean-Philippe, Jean-Baptiste, Jérôme, Kumiko, Patrick and Stéphane. Above all, my heartfelt gratitude comes to Evaluator-IAP for teaching me interesting english expressions and for his constant encouragement in *getting back to work* (although I never stopped).

Finally, I want to thank my wife Dorothée and my baby daughter Maëlle for their love and support during these years and all the ones to come.

Inflation Cosmologique: Aspects Théoriques et Contraintes Observationelles

Résumé

Dans cette thèse sur articles nous nous intéressons aux contraintes observationnelles sur les modèles d'inflation cosmologique et nous étudions certains aspects fondamentaux liés à la nature quantique de la physique inflationnaire. L'inflation est une période d'expansion accélérée intervenant dans l'Univers primordial à très hautes énergies. En plus d'être une solution possible aux problèmes du modèle standard de la cosmologie dit du "big bang chaud", combinée à la mécanique quantique, l'inflation permet la production causale de fluctuations cosmologiques sur les grandes échelles, qui sont à l'origine des structures cosmiques actuelles. Mettant en jeu des énergies colossales au regard de ce qui peut être réalisé dans un accélérateur de particules, l'inflation est devenue un objet d'intérêt majeur en cosmologie pour tester la physique des hautes énergies au delà de son modèle standard.

Nous commençons par analyser de façon systématique tous les modèles inflationnaires à un champ scalaire et avec terme cinétique standard, à la lumière des mesures du fonds diffus cosmologique les plus récentes. Dans l'approximation du roulement lent, et en intégrant les contraintes venant de la phase de réchauffement, nous dérivons les prédictions associées à environ 75 potentiels. Nous utilisons ensuite les techniques d'inférence Bayésienne pour classer près de 200 modèles inflationnaires et contraindre leurs paramètres. Cela permet d'identifier les modèles favorisés par les observations et de quantifier les niveaux de tensions entre les différents jeux de données. L'intérêt d'une telle approche est renforcé par l'étude de méthodes indépendantes du modèle telle que le "flot de Hubble", qui se révèle biaisé. Nous calculons également le spectre de puissance au deuxième ordre pour les modèles d'inflation-k, afin de permettre leur intégration future dans notre analyse numérique.

Dans une deuxième partie, nous décrivons certains aspects liés à la nature quantique de la physique inflationnaire. Le formalisme de l'inflation stochastique, qui incorpore les corrections quantiques aux dynamiques inflationnaires, est notamment utilisé dans le cadre du modèle à deux champs d'inflation hybride. Nous discutons l'impact de ces corrections sur les prédictions de ce modèle, et à l'aide d'un formalisme récursif, nous nous intéressons à la façon dont elles modifient l'amplitude des perturbations. Finalement, la transition quantique-classique, et le problème de la mesure quantique, sont étudiés dans un contexte cosmologique. Un modèle de réduction dynamique du paquet d'onde est appliqué à la description des perturbations inflationnaires.

Mots Clés: cosmologie, inflation, fonds diffus cosmologique, inflation stochastique, inférence Bayésienne et comparaison de modèles, perturbations quantiques.

Cosmological Inflation: Theoretical Aspects and Observational Constraints

Abstract

This thesis by publication is devoted to the study of the observational constraints on cosmological inflationary models, and to the investigation of fundamental aspects related to the quantum nature of the inflationary physics. Inflation is an early phase of accelerated expansion taking place at very high energy. On top of being a solution for the hot big bang model problems, combined with quantum mechanics, inflation provides a causal mechanism for the production of cosmological fluctuations on large scales, that later give rise to today's cosmic structures. Given that it takes place at energy scales many orders of magnitude larger than what can be achieved in conventional particle physics experiments, inflation has become of great interest to test beyond standard model physics.

We first present a systematic analysis of all single-scalar-field inflationary models with canonical kinetic terms, in light of the most up-to-date Cosmic Microwave Background (CMB) measurements. Reheating consistent slow-roll predictions are derived for ~ 75 potentials, and Bayesian inference and model comparison techniques are developed to arrange a landscape of ~ 200 inflationary models and associated priors. In this way, we discuss what are the best models of inflation in light of the recent observations, and we properly quantify tension between data sets. Related to this massive sampling, we highlight the shortcomings of model independent approaches such as the one of "horizon-flow". We also pave the way for extending our computational pipeline to k-inflation models by calculating the power spectrum at next-to-next-to leading order for this class of models.

In a second part, we describe some aspects related to the quantum nature of the inflationary setup. In particular, we make use of the stochastic inflation formalism, which incorporates the quantum corrections to the inflationary dynamics, in the two-field model of hybrid inflation. We discuss how the quantum diffusion can affect the observable predictions in such models, and we design a recursive strategy that incorporates its effects on the perturbations amplitude. Finally, we investigate the quantum-to-classical transition and the quantum measurement problem in a cosmological context. We apply a dynamical wavefunction collapse model to the description of inflationary perturbations.

Keywords: cosmology, inflation, cosmic microwave background radiation, stochastic inflation, Bayesian inference and model comparison, quantum perturbations.

Introduction

Inflation is a phase of accelerated expansion that took place in the early Universe at very high energy. Originally intended to dispose of some of the hot big bang shortcomings, it was soon realized that inflation may be responsible for a powerful manifestation of our Universe's quantum nature. Indeed, the deviations from homogeneity and isotropy that give rise to today's cosmic structures (galaxies, clusters, filaments, *etc.*) can be traced back to the quantum fluctuations of gravitational and matter fields during inflation. Stretched by the quasi-exponential expansion of space-time to distances of cosmological interest today, these fluctuations serve as the primordial seeds for inhomogeneities that later grow under the influence of gravitational instability. Inflation has become a very active field of research in the past years, since the energy scales involved during this early epoch are many orders of magnitude greater than those accessible in particle physics experiments. Therefore, the early Universe is certainly one of the most promising probes to test beyond standard model physics.

Another consequence of the fact that inflation takes place at energy scales where particle physics remain unknown, is that the physical nature of the fields driving inflation, and their relation with the standard model of particle physics, is still unclear. There have been a crowd of inflationary candidates proposed so far, and an important task is to discriminate between them. On the other hand, there is now a flow of increasingly accurate astrophysical data which provides us with a unique opportunity to constrain the inflationary landscape. These data mostly consist in measurements of the Cosmic Microwave Background (CMB), but they also concern other astrophysical probes such as supernovae, galaxy surveys, and 21 cm observations. It becomes therefore of paramount importance to be able to process such a huge amount of observational data, comprising measurements that are very different in nature, with hundreds of inflationary scenarios, often equally different. It is the first purpose of this thesis to design scientific and technical tools enabling to carry out such a programme, and to determine which inflationary models the data seem to prefer.

At the fundamental level, inflation is also probably one of the only cases in physics where an effect based on General Relativity and Quantum Mechanics leads to predictions that, given our present day technological capabilities, can be tested experimentally. This makes inflation an ideal playground to discuss deep questions related to its quantum aspects. The other purpose of this thesis is to study some of them, ranging from the quantum-to-classical transition of cosmological perturbations, to the quantum corrections to the inflationary dynamics by means of the stochastic inflation formalism.

The present manuscript is a thesis by publication. It presents the works realized at the Institut d'Astrophysique de Paris between September 2011 and September 2014 under the direction of Jérôme Martin. It first contains a brief presentation of the cosmological groundwork for our analysis, which introduces the main aspects of the cosmological standard model and of inflation. Mainly, this part I aims at providing the reader with the conceptual and technical tools that may be helpful to the understanding of the results presented in part II. This second part collects the research articles published during this thesis time (except from section 3.4 which, at the

time of drafting this manuscript, is going through the reviewing process).

More precisely, this document is organized as follows. In chapter 1, we review the cornerstones of the standard model of modern cosmology. In the framework of General Relativity, we describe homogeneous and isotropic universes and derive the associated Einstein equations. By an explicit comparison with the corresponding Newtonian physics, we highlight the deeply relativistic nature of the expansion, especially its possible acceleration. We then give a brief description of the main constituents of the Universe, and of the main lines of its history. Finally, we turn to the presentation of the problems of the hot big band model, namely the horizon, flatness and monopole problems. For each of these problems, we give a detailed calculation of its formulation and show how it can be solved with a phase of accelerated expansion. In particular, we characterize the number of e-folds that is required in each case.

In chapter 2, we review some aspects of cosmological inflation, the physical setups it relies on, the predictions it makes and the fundamental issues it raises. We explain why and under which conditions a single scalar field can support a phase of inflation and we present the "slow-roll" approximation which enables to solve its dynamics perturbatively. It also provides us with a convenient frame of calculation to compare inflationary predictions with observational data, which we make widely use of in chapter 3. We then turn to the description of inflationary perturbations, and show how cosmological fluctuations need to be quantized. For illustrative purpose, we provide a detailed calculation of the power spectrum of scalar perturbations, at first order in slow roll. Finally, we devote a large part of this second chapter to the presentation of the stochastic inflation formalism which is used in chapter 4. We first present a detailed heuristic derivation of the Langevin equation which is at the heart of this formalism, before turning to the question of the time variable that should be used when solving such equations, in order to reproduce results from Quantum Field Theories. Lastly, we address the issue of the calculation of physical observable quantities in stochastic inflation, such as the power spectrum of adiabatic perturbations. We show that the stochastic setup allows to reproduce the standard result, before providing complete solutions which do not rely on an expansion in the noise term. To our knowledge, this is the first time that such a non perturbative calculation of the power spectrum in stochastic inflation is presented. It has not been pre-printed or published yet since it has been derived in the course of drafting this manuscript.

We then turn to part II where the articles published during this thesis are presented and displayed. The first chapter, chapter 3, deals with a systematic analysis of all single-field inflationary models with minimal kinetic terms, in light of the most up-to-date CMB data, especially the ones coming from the Planck experiment and more recently from BICEP2. This somewhat "industrial" project aims at deriving reheating consistent slow-roll predictions for ~ 75 inflationary potentials, and using Bayesian inference and model comparison techniques to arrange a landscape of ~ 200 inflationary models and well studied priors. In this way, one can discuss which are the best models of inflation. This also allows us to assess the compatibility level of the two data sets (Planck and Bicep2) given inflation, or given a specific inflationary model. The relevance of such an approach is further advocated for in an article pointing out the shortcomings of model independent parametrizations of inflation such as the one of "horizon flow", and another one paves the way for including single field k-inflation (*i.e.* non minimal kinetic terms) models in our analysis, by calculating the power spectrum at next-to-next-to leading order for this class of models.

In chapter 4, we turn to the description of some aspects related to the quantum nature of the inflationary setup. In particular, the stochastic inflation formalism incorporates the quantum corrections to the inflationary dynamics by means of stochastic Langevin equations. This gives

rise to non trivial inflationary trajectories, especially when multiple fields are present. This is why we study stochastic effects in hybrid inflation, a two-field model where inflation ends by tachyonic instability, and we discuss how the quantum diffusion can affect the observable predictions in such models. Making use of a recursive formalism for backreacting effects, we also address the issue of evolving cosmological perturbations on top of stochastically shifted backgrounds, in the same type of models. Finally, we investigate the quantum-to-classical transition and the quantum measurement problem in a cosmological context. More precisely, we apply the continuous spontaneous localization modification of the Schrödinger equation to the case of inflationary perturbations. We establish what an efficient collapse of the wavefunction implies for the inflationary predictions, and which constraints can be derived on the collapse models themselves.

Finally, in a last section, we sum up our results and present some concluding remarks and possible prospects for the present work.

Contents

Part I.

Cosmology and Inflation

1. The Cosmological Standard Model

In this chapter, we review the cornerstones of the standard model of modern cosmology. The Hot Big Bang scenario describes a series of events that occurred since an initial singularity 13.7 *billion years ago, and for which we now have accurate observational evidence. Questions left unanswered by this model are discussed, which are solved by the introduction of an era of accelerated expansion in the early Universe. In this section, only a brief and partial overview of the standard cosmological model is given, the various aspects of which are further detailed in a broad range of textbooks [1, 2, 3, 4, 5, 6, 7, 8].*

Considerations about the extent and the structure of the Universe exist in almost every culture and seem to be intrinsic to the development of human awareness. In this sense, Cosmology is a matter of concern which may be considered as old as mankind itself. However, for a very long time, it consisted in a very speculative approach to metaphysical (more than physical) issues in which philosophy or even religion were also at stake. This radically changed only in the first half of the twentieth century with the advent of the theory of general relativity, which provided for the first time a mathematical consistent framework for describing space and time. Cosmological models, in which space is expanding, were derived from this theory and enabled to understand many observations starting with galaxies receding. During these years, Cosmology was mainly about describing and reconstructing *a posteriori* observational effects of this expansion. Then, in the second half of the twentieth century, was formulated the hot big bang model, which includes the description of physical processes occurring in this expanding space-time, and the associated thermal history of the Universe. More recently, Cosmology has entered a precision era with the inflow of high accuracy observational data such as the Cosmic Microwave Background (CMB) measurements, galaxy and supernova surveys, 21 cm astrophysics data, forthcoming cosmic rays and gravitational waves detectors, etc. Together with theoretical developments in high energy and gravitational physics, this enabled to upgrade Cosmology to the status of a genuine Science, *i.e.* a field of research in which falsifiable predictions can be made and tested.

1.1. The Homogeneous and Isotropic Universe

The distribution of galaxies and cosmological structures in space around us appears to be isotropic on large scales [$\sim \mathcal{O}(100)$ Mpc] , which implies that space-time possesses a spherical symmetry around us. This observational fact, combined with the Copernican principle[1] which states that we should not live in a central or specially favoured position in the Universe, leads to the conclusion that the Universe must be homogeneous on large scales. This is the

[1]The Copernican Principle is to be understood as opposed to the anthropocentrist view that human beings should be at the center of the Universe. For example, the Aristotelian model of the solar system in the Middle Ages placed the Earth at the center of the solar system, a unique place since it "appeared" that everything revolves around the Earth. Nicolaus Copernicus demonstrated that this view was incorrect and that the Sun was at the center of the solar system with the Earth in orbit around the Sun.

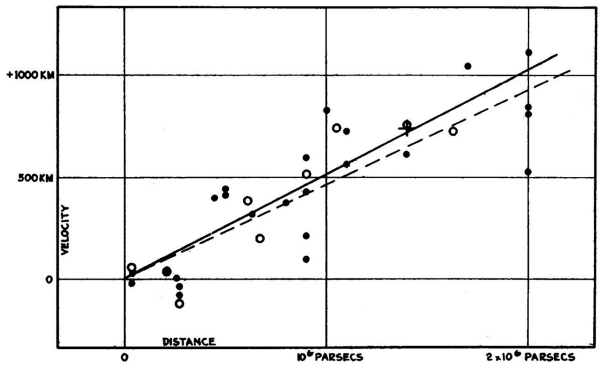

Figure 1.1.: Hubble diagram (*i.e.* velocity against distance) for extra-galactic nebulae, from the 1929 original paper [13] by Edwin Hubble. Such diagrams lead to the hypothesis of an expanding universe with a linear expansion law $v = Hr$. The radial velocities are obtained from redshift measurements and are corrected for solar motion, and distances are estimated from involved stars and mean luminosities of nebulae in a cluster. The black discs and full line represent the solution for solar motion using the nebulae individually; the circles and broken line represent the solution combining the nebulae into groups; the cross represents the mean velocity corresponding to the mean distance of 22 nebulae whose distances could not be estimated individually.

so-called cosmological principle.

1.1.1. The Friedmann-Lemaître-Robertson-Walker Metric

The cosmological principle is a statement about the amount of symmetry present in the observable Universe. As always in physics, this symmetry constrains and simplifies the mathematical description of the system under consideration. In this manner, under the cosmological principle symmetry, the metric of space-time $\mathrm{d}s^2 = g_{\mu\nu}\mathrm{d}x^\mu \mathrm{d}x^\nu$ can be shown to be entirely determined up to a free function of time, the scale factor $a(t)$, and a discrete parameter $\mathcal{K} = -1, 0, 1$ which encodes the spatial curvature (open, flat or closed). With the $(-,+,+,+)$ signature convention, it is of the form [9, 10, 11, 12]

$$\mathrm{d}s^2 = -\mathrm{d}t^2 + a^2(t)\left[\frac{\mathrm{d}r^2}{1-\mathcal{K}r^2} + r^2\left(\mathrm{d}\theta^2 + \sin^2\theta \mathrm{d}\phi^2\right)\right] \tag{1.1}$$

and is called the Friedmann-Lemaître-Robertson-Walker (FLRW) metric. In this parametrization, t is the cosmic time, r is the comoving radial coordinate which is unitless, θ and ϕ are the comoving angular coordinates, and $a(t)$ has units of length.[2]

1.1.1.1. The Hubble Law

From the FLRW metric (1.1), one can see that the physical distance L_{phys} between two points measured on a constant t hypersurface scales as the scale factor a, that is to say

$$L_{\mathrm{phys}} = a(t) L_{\mathrm{com}}\,, \tag{1.2}$$

[2]Hereafter and unless stated otherwise, we work in the unit system where $c = \hbar = k_{\mathrm{B}} = 1$.

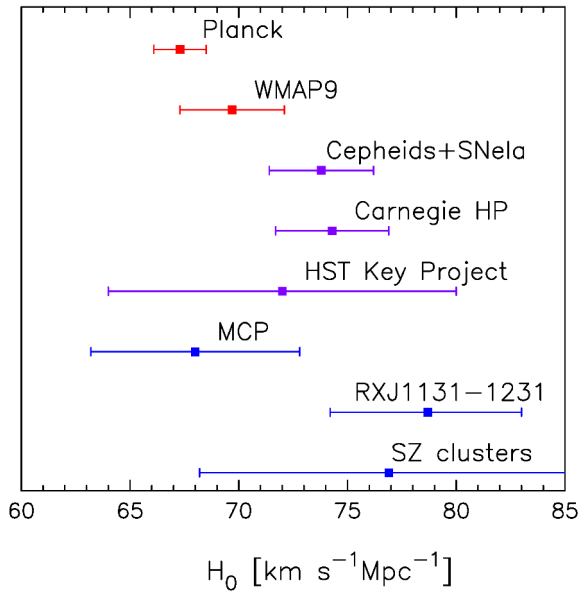

Figure 1.2.: Comparison of H_0 measurements, with estimated of $\pm 1\sigma$ errors, from a number of different astrohphysical techniques, and compared with the spatially-flat ΛCDM model constraints from Planck and WMAP9. Image Credit: Ref. [15].

where $L_{\rm com}$ is the so-called comoving distance, which is constant in time for still objects in the FLRW frame. The scale factor a thus sets the overall expansion (or contraction) level of space hypersurfaces, hence its name. Another consequence of the FLRW metric is a linear relation between distance and velocity. Indeed, from differentiating Eq. (1.2) with respect to cosmic time t, one obtains

$$v = \frac{\mathrm{d}L_{\rm phys}}{\mathrm{d}t} = \frac{\dot{a}}{a} L_{\rm phys} = H L_{\rm phys}\,, \tag{1.3}$$

where we have defined the Hubble parameter $H \equiv \dot{a}/a$. This is the so-called Hubble law. It was first observed in 1929, as presented in Fig. 1.1, where the current value of H, that we denote H_0, was determined to be of the order of 500 km/sec/Mpc. As we will see below, this value contains valuable information about the content of the Universe and this is why it has been the object of much research effort. The first good estimation was realized in 1958 in Ref. [14], where the value 75 km/sec/Mpc was obtained. Finally, the most up to date measurements provided by the Planck mission [15] gave the value 67.80 ± 0.77 km/sec/Mpc for the value of H_0. This value is rather low compared with previous measurements, see Fig. 1.2, and the tension between the CMB-based estimates in the ΛCDM model and the astrophysical measurements of H_0 is still intriguing [15, 16, 17, 18, 19, 20, 21].

The reduced Hubble parameter h is also often used, and is defined as

$$H_0 = 100\, h \text{ km/sec/Mpc}\,. \tag{1.4}$$

The Hubble parameter sets the fundamental physical scale of space-time. It provides a characteristic time scale $H_0^{-1} \simeq 4.551 \times 10^{17}$ sec called the "Hubble time" and a characteristic length scale $H_0^{-1} \simeq 1.364 \times 10^{26}$ m called the "Hubble radius". As we will see later, the Hubble time sets the scale for the age of the Universe, and the Hubble length sets the scale for the size of the observable Universe. These values are displayed in table 1.2 where we collect all the numerical values given and used throughout this section 1.

1.1.1.2. Redshift and Comoving Coordinates

Another interesting property of FLRW space-times is that light gets redshifted as its travels, due to the time dependence of the scale factor. Let us consider an emitting object at rest in the comoving coordinates system, with radial coordinate r_1, while an observer is located at $r_0 = 0$. Light is emitted from this first object at time t_1 with frequency ν_1, and received by the observer at time t_0 with frequency ν_0. Let us determine the relation between ν_0 and ν_1. Since light travels along geodesics with $\mathrm{d}s = 0$, radial light path traveling towards the observer ($\mathrm{d}\theta = \mathrm{d}\phi = 0$ and $\mathrm{d}r/\mathrm{d}t < 0$) follows

$$\frac{\mathrm{d}t}{a\,(t)} = \frac{\mathrm{d}r}{\sqrt{1-\mathcal{K}r^2}}. \tag{1.5}$$

Now consider the emission of two subsequent crests of a light wave. The first one is emitted at (t_1, r_1) and received at $(t_0, 0)$ while the second one is emitted at $(t_1 + \delta t_1, r_1)$ and received at $(t_0 + \delta t_0, 0)$. From Eq. (1.5), one has

$$\int_{r_1}^{0} \frac{\mathrm{d}r}{\sqrt{1-\mathcal{K}r^2}} = \int_{t_1}^{t_0} \frac{\mathrm{d}t}{a(t)} = \int_{t_1+\delta t_1}^{t_0+\delta t_0} \frac{\mathrm{d}t}{a(t)}\,. \tag{1.6}$$

Subtracting the third integral from the second, in the limit $\delta t_0\,,\ \delta t_1 \ll a/\dot{a}$, one obtains

$$\frac{\delta t_0}{a\,(t_0)} = \frac{\delta t_1}{a\,(t_1)}\,. \tag{1.7}$$

Since the time delay δt between two crests is nothing but the inverse frequency, one obtains

$$\frac{\nu_1}{\nu_0} = \frac{a\,(t_0)}{a\,(t_1)} = 1 + z\,, \tag{1.8}$$

where the last equality defines the redshift z. This quantity only depends on the ratio of the scale factor at reception to the scale factor at emission.

In terms of wavelength λ, Eq. (1.8) gives $\lambda_0/\lambda_1 = a(t_0)/a(t_1)$. We see that the wavelength of light just contracts and stretches with the scale factor $\lambda \propto a$. Another way to look at this is to say that a photon traveling through an FRLW space-time loses momentum as the Universe expands,

$$p = h\nu \propto a^{-1}\,(t)\ . \tag{1.9}$$

As shown in appendix 1.A, see Eqs. (1.95) and (1.96), this momentum loss applies to massive particles as well as photons, and any particle moving in an expanding FLRW space-time loses momentum as $p \propto a^{-1}$. This means that a massive particle asymptotically comes to rest relative to the comoving coordinates system. Thus, comoving coordinates represent a preferred reference frame which is such that any free body with a peculiar velocity relative to the comoving frame eventually comes to rest in this frame.

1.1.1.3. Einstein Equations

The Einstein-Hilbert action [22, 23, 24] describes the dynamics of space-time metrics, and reads

$$\mathcal{S}_{\mathrm{grav}} = \frac{1}{2\kappa}\int \mathrm{d}^4x\sqrt{-g}\,(R - 2\Lambda)\ , \tag{1.10}$$

where $\kappa \equiv 8\pi G = 8\pi/m_{\mathrm{Pl}}^2 = 1/M_{\mathrm{Pl}}^2$, where G is the Newton gravitational constant, m_{Pl} is the Planck mass and $M_{\mathrm{Pl}} \simeq 2.4 \times 10^{18}$ GeV is the reduced Planck mass. In the above expression,

Λ is a cosmological constant, g is the determinant of $g_{\mu\nu}$ and R is the Ricci curvature scalar $R \equiv g^{\mu\nu}R_{\mu\nu}$. It is constructed from the Ricci tensor $R_{\mu\nu} = 2\Gamma^{\rho}_{\mu[\nu,\rho]} + 2\Gamma^{\rho}_{\lambda[\rho}\Gamma^{\lambda}_{\nu]\mu}$, where brackets mean anti-symmetrization over the indices and where the Christoffel symbols are given by $\Gamma^{\rho}_{\mu\nu} = \frac{1}{2}g^{\rho\lambda}\left(\partial_\nu g_{\lambda\mu} + \partial_\mu g_{\lambda\nu} - \partial_\lambda g_{\mu\nu}\right)$.

To this action should be added a part $\mathcal{S}_{\rm matter} = \int \mathcal{L}_{\rm matter}\sqrt{-g}\mathrm{d}^4x$ describing matter in the Universe. When varying these two action terms with respect to $g_{\mu\nu}$, one obtains two tensors, namely the Einstein tensor $G_{\mu\nu}$ defined as

$$G_{\mu\nu} + \Lambda g_{\mu\nu} \equiv \frac{2\kappa}{\sqrt{-g}}\frac{\partial \mathcal{S}_{\rm grav}}{\partial g_{\mu\nu}} = R_{\mu\nu} - \frac{1}{2}Rg_{\mu\nu} + \Lambda g_{\mu\nu} \tag{1.11}$$

for the gravity part, and the energy-momentum tensor

$$T_{\mu\nu} \equiv -\frac{2}{\sqrt{-g}}\frac{\partial \mathcal{S}_{\rm matter}}{\partial g_{\mu\nu}} = g_{\mu\nu}\mathcal{L}_{\rm matter} - 2\frac{\delta \mathcal{L}_{\rm matter}}{\delta g^{\mu\nu}} \tag{1.12}$$

for the matter part. This leads to the well-known Einstein equations

$$G_{\mu\nu} + g_{\mu\nu}\Lambda = \kappa T_{\mu\nu}\,. \tag{1.13}$$

Let us now work out the two tensors $G_{\mu\nu}$ and $T_{\mu\nu}$ for an FLRW metric. When the metric (1.1) is plugged into the definition (1.11), one obtains (a detailed calculation is provided in appendix 1.A)

$$G_{00} = 3\left(H^2 + \frac{\mathcal{K}}{a^2}\right), \qquad G_{ij} = -\left(H^2 + 2\frac{\ddot{a}}{a} + \frac{\mathcal{K}}{a^2}\right)g_{ij}\,, \tag{1.14}$$

where the index 0 is for time t, and the indexes i and j are for space coordinates so that g_{ij} is just the spatial part of the full metric $g_{\mu\nu}$.

Given the symmetries of space-time, one can show that the most generic form of the energy-momentum tensor is given by

$$T_{\mu\nu} = \rho u_\mu u_\nu + \frac{p}{a^2}g_{\mu\nu}\,, \tag{1.15}$$

where $g_{\mu\nu} = g_{ij}$ when μ and ν are space indexes and 0 otherwise. In the above expression, ρ and p are two constants depending on time only, and u_μ is the four velocity of a comoving observer for whom space is homogeneous and isotropic. One thus has $u_\mu = \delta_{\mu,0}$, where δ is the Krönecker symbol. Since p is associated to the spatial part of the tensor, it can be interpreted as the pressure of matter, while $\rho = T_{\mu\nu}u^\mu u^\nu$ is the energy density measured by a comoving observer. The above form of $T_{\mu\nu}$ is entirely fixed by the cosmological principle. Finally, let us mention that the time component of the conservation relation $\nabla_\mu T^{\mu\nu} = 0$ leads to

$$\dot{\rho} + 3H\left(\rho + p\right) = 0\,. \tag{1.16}$$

Heuristically, this equation can be understood as a translation of the first law of thermodynamics, $\mathrm{d}U = -p\mathrm{d}V$, with $U = \rho V$ and $V = a^3$.

1.1.2. An Expanding Universe

Let us now detail how this general relativistic framework allows to relate the dynamics of the expansion of space-time to the matter content properties of the Universe.

1.1.2.1. Friedmann and Raychaudhuri Equations

If one plugs the above expressions for $G_{\mu\nu}$, Eqs. (1.14), and for $T_{\mu\nu}$, Eq. (1.15), in the Einstein equation (1.13), one obtains the two following dynamical equations

$$H^2 = \frac{\kappa}{3}\rho - \frac{\mathcal{K}}{a^2} + \frac{\Lambda}{3}\,, \tag{1.17}$$

$$\frac{\ddot{a}}{a} = -\frac{\kappa}{6}(\rho + 3p) + \frac{\Lambda}{3}\,. \tag{1.18}$$

These two equations are known as the Friedmann [25] and the Raychaudhuri [26] equations, respectively. Because of the Bianchi identities, when combined together, one can check that they account for the conservation equation (1.16).

The Friedmann equation relates the change of the scale factor of the Universe to its energy density, spatial curvature and cosmological constant. If the Universe is assumed to be flat ($\mathcal{K} = 0$) and if the cosmological constant vanishes ($\Lambda = 0$), this means that the only presence of energy will cause the Universe to expand ($H > 0$) or to contract ($H < 0$). In the following, we shall mostly consider expanding universes, even if contracting universes are key ingredients of some cosmological models [27, 28, 29, 30, 31, 32, 33, 34].

From the Raychaudhuri equation, one can notice that in absence of a cosmological constant, any form of matter such that $\rho + 3p < 0$ will cause an acceleration of the scale factor $\ddot{a} > 0$ if it dominates the energy budget of the Universe. The energy density is always positive, but in some cases the pressure can be negative and the inequality $\rho + 3p < 0$ may be realized. This simple property is deeply rooted in the inflationary scenario and will be discussed in more details in chapter 2. As we shall now see, it is intimately related to the fundamental principles of general relativity.

1.1.2.2. The Newtonian Expanding Sphere

In order to highlight the relativistic effects in the above setup more clearly, let us derive the Newtonian version [35, 36, 37] of the Friedmann and Raychaudhuri equations. In Fig. 1.3, we sketch the case of an expanding sphere of radius a filled with uniform matter with mass density ρ. Let us consider a particle of mass m sitting on the out-shell of this sphere. The Gauss theorem states that the gravitational attractive force seen by such a particle is given by GmM/a, where $M = 4/3\pi\rho a^3$ is the integrated mass of the sphere. Its acceleration being simply $\ddot{a}$, the second Newton law gives rise to $m\ddot{a} = -MGm/a$, *i.e.*

$$\left.\frac{\ddot{a}}{a}\right|_{\text{Newton}} = -\frac{4}{3}\pi\rho G = -\frac{\kappa}{6}\rho\,. \tag{1.19}$$

This matches the Raychaudhuri equation (1.18) without cosmological constant and without the pressure term. This is why in Newtonian mechanics, one must have $\ddot{a} < 0$ and the expansion of the sphere can only decelerate. The reason why acceleration is allowed in the general relativistic setup is because all forms of energy gravitate, including pressure.[3] As a consequence, the presence of pressure in the Raychaudhuri equation is a crucial signature of the relativistic nature

[3] Acceleration of FRLW space-times is actually one of the only manifestations of pressure's self-gravity [38], otherwise tested only in the context of big bang nucleosynthesis [39] where it is necessary to account for current light element abundances. For example, even in compact objects such as neutron stars, pressure's self-gravity is immeasurable given uncertainties on the equation of state [40, 41].

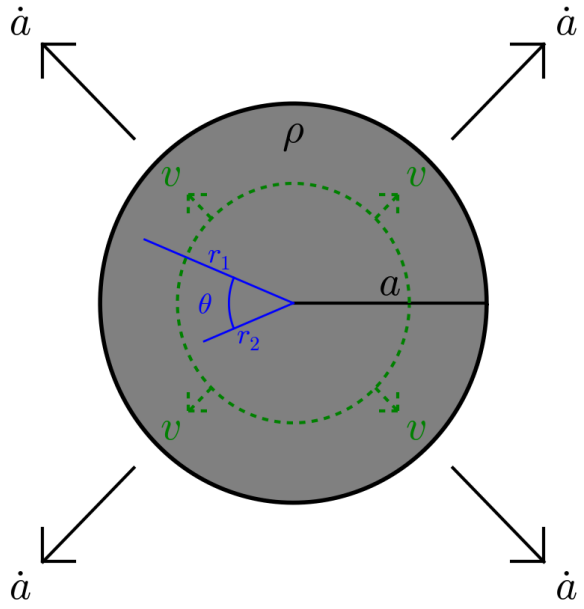

Figure 1.3.: Homogeneous sphere in Newtonian radial expansion.

of the setup. Indeed, in newtonian mechanics, masses source the gravity field, but relativity relates mass to energy. Since energy is not a relativistic invariant but mixes up with momentum when changing frames, momentum, hence pressure, naturally comes into play in a relativistic context.

It is also interesting to calculate the newtonian energy E_{Newton} of the sphere of Fig. 1.3. In order to do this, we first need to derive the velocity profile $v(r)$ of the sphere radial expansion. When diluting, let us assume that the mass density scales as the inverse of the volume to some power $1+w$, $\rho \propto V^{-(1+w)}$ (where for ordinary "newtonian" matter, $w=0$). One can first show[4] that its evolution is given by

$$\dot{\rho} = -(w+1)\left[v'(r) + 2\frac{v(r)}{r}\right]\rho\,. \tag{1.20}$$

In order for the sphere to remain homogeneous (*i.e.* to be such that ρ, hence $\dot{\rho}$, does not depend on r), the term factorizing ρ in the right hand side of the previous relation should not depend on r, *i.e.* one must have $v' + 2v/r =$ constant. This leads to the two-branch solution

$$v(r) = Ar + \frac{B}{r^2} \tag{1.21}$$

for the radial velocity, where A and B are two integration constants that can only depend on time. In this manner the sphere is and remains homogeneous. However, there is no reason why it should be isotropic. Indeed, even if the sphere is taken to be infinite, the direction pointing towards its center is a priori a privileged direction. This is not the case only if the velocity law (1.21) $v(r)$ is valid not only for r being the distance between the center of the sphere and one of its shells, but for r being the distance between any two points within the sphere. As we shall now see, this selects out one of the two branches of the solution (1.21). Let us thus consider

[4] Two shells of radius r_1 and $r_2 = r_1 + \mathrm{d}r$ respectively become, after a $\mathrm{d}t$ long expansion, two shells of radius $r_1' = r_1 + v(r_1)\mathrm{d}t$ and $r_2' = r_1 + \mathrm{d}r + [v(r_1) + v'(r_1)\mathrm{d}r]\,\mathrm{d}t$. The volume contained between these two shells thus evolves from $V = 4\pi r_1^2 \mathrm{d}r$ to $V' = 4\pi {r_1'}^2 (r_2' - r_1') \simeq V\,[1 + 2v(r_1)/r_1 \mathrm{d}t + v'(r_1)\mathrm{d}t]$. From here one gets $\mathrm{d}V/\mathrm{d}t = V\,(v' + 2v/r)$, and with $\rho V^{w+1} =$ constant, Eq. (1.20).

two points of radial distances r_1 and r_2 respectively, and with angular separation θ as in Fig. 1.3. The distance between these two points is simply given by $d_{12} = \sqrt{r_1^2 + r_2^2 - 2r_1 r_2 \cos\theta}$. Since θ is conserved through the radial expansion, its time variation is

$$\dot{d}_{12} = \frac{r_1 v\left(r_1\right) + r_2 v\left(r_2\right) - \left[r_2 v\left(r_1\right) + r_1 v\left(r_2\right)\right]\cos\theta}{d_{12}} \,. \tag{1.22}$$

On the other hand, if the velocity law (1.21) is isotropic, one must have

$$\dot{d}_{12} = v\left(d_{12}\right) \,. \tag{1.23}$$

When the velocity law (1.21) is used in the identification of Eqs. (1.22) and (1.23), it is straightforward to see that $B = 0$. Only the first branch remains, and one has

$$v\left(r\right) = Hr \,, \tag{1.24}$$

where we have renamed $H \equiv A = \dot{a}/a = \dot{r}/r$, which can only depend on time. In a cosmological context, one recovers the Hubble law previously mentioned. In particular, it is in order to stress that it eventually does not depend on the volume scaling power index w.

We are now in a position where we can calculate the energy of the sphere. It is given by the sum of its integrated kinetic energy and its integrated potential energy, that is

$$\begin{aligned} E_{\rm Newton} &= \int_0^a \frac{1}{2}(4\pi r^2 {\rm d}r\rho)(rH)^2 - \int_0^a \frac{G}{r}\left(4\pi r^2 {\rm d}r\rho\right)\left(\frac{4}{3}\pi r^3\rho\right) \\ &= \frac{2}{5}\pi\rho a^5 H^2 - \frac{16\pi^2}{15} G\rho^2 a^5 \\ &= \frac{2}{5}\pi a^5 \rho\left(H^2 - \frac{\kappa}{3}\rho\right) \,. \end{aligned} \tag{1.25}$$

Remembering that ρ scales as $V^{-(w+1)} \propto a^{-3(w+1)}$, one obtains

$$H^2 = \frac{\kappa}{3}\rho + \frac{5E_{\rm Newton}}{2\pi\rho_0 a_0^{3(w+1)}}\frac{1}{a^{2-3w}} \,. \tag{1.26}$$

When the Newtonian energy vanishes, one obtains the Friedmann equation (1.17) in absence of cosmological constant and curvature, the presence of which is therefore a truly relativistic effect. In passing, let us notice that when $E_{\rm Newton} \neq 0$ and for ordinary matter (such that $w = 0$), the second term in the right hand side of Eq. (1.26) plays a role similar to the one of curvature in Eq. (1.17), which scales as a^{-2} and which can be either positive or negative.

A last remark is in order about the conservation equation. In Newtonian mechanics, if one replaces $v(r) = Hr$ in Eq. (1.20), one obtains the conservation equation $\dot{\rho} + 3(w+1)H\rho = 0$, which, in passing, matches Eq. (1.16) if $p = w\rho$. This relation is fairly trivial since it just states that $\rho \propto V^{-(1+w)}$. Thanks to this conservation law, one can check that the two equations (1.19) and (1.26) are actually equivalent when $w = 0$. This is just a consequence of the fact that the conservation of mechanical energy is equivalent to the second Newton law, *i.e.* that Newtonian mechanics derives from a potential. However, in the case of general relativity, the conservation equation (1.16) is not trivial at all and is required to relate the Friedmann and Raychaudhuri equations. One thus really have two independent dynamical equations.

fluid	**equation of state parameter w**	$\rho(a)$	$a(t)$
cold matter	0	$\propto a^{-3}$	$\propto t^{2/3}$
radiation	$1/3$	$\propto a^{-4}$	$\propto t^{1/2}$
spatial curvature	$-1/3$	$\propto a^{-2}$	$\propto t$
cosmological constant	-1	$\propto a^{0}$	$\propto \exp(Ht)$
scalar field	$-1+2\epsilon_1/3$	$\propto a^{-2\epsilon_1}$	t^{1/ϵ_1}

Table 1.1.: Equation of state parameter w for a few fluid examples, with corresponding $\rho(a)$ (1.27) and $a(t)$ (1.30) profiles.

1.1.2.3. Constant Equations of State

It is interesting to notice that the conservation equation (1.16) can be solved in the simple case of a single ideal fluid where the energy density and the pressure are related by a constant equation of state parameter $w \equiv p/\rho$. One obtains

$$\rho = \rho_{\rm in}\left(\frac{a}{a_{\rm in}}\right)^{-3(1+w)} . \tag{1.27}$$

The equation of state parameter of cold matter is simply $w_{\rm mat} = 0$ so that the energy density scales as the inverse volume $\rho_{\rm mat} \propto a^{-3}$, while the equation of state parameter of radiation is $w_{\rm rad} = 1/3$ so that the associated energy density scales as $\rho_{\rm rad} \propto a^{-4}$, which includes both volume dilution effect ($\propto a^{-3}$) and wavelength redshift (1.8) ($\propto a^{-1}$). From the Friedmann equation (1.17), one can also associate an energy density to curvature $\rho_{\mathcal{K}} \equiv -3\mathcal{K}/(\kappa a^2)$ and to the cosmological constant $\rho_\Lambda \equiv \Lambda/\kappa$, so that the Friedmann equation reads

$$H^2 = \frac{\kappa}{3}\left(\rho_{\rm matter} + \rho_{\mathcal{K}} + \rho_\Lambda\right) \equiv \frac{\kappa}{3}\rho_{\rm T} , \tag{1.28}$$

where $\rho_{\rm T}$ denotes the "total" energy density. Here, $\rho_{\rm matter}$ can include ordinary cold matter, radiation, or any other Universe constituent. Since $\rho_{\mathcal{K}} \propto a^{-2}$, this means that curvature can be viewed as a fluid constituent with equation of state parameter $w_{\mathcal{K}} = -1/3$. In the same manner, ρ_Λ is constant and can be viewed as a fluid constituent[5] with equation of state parameter $w_\Lambda = -1$. These values for the equation of state parameters are summarized in table 1.1. The last entry corresponds to a scalar field and will be further explicated in chapter 2.

Interestingly enough, since $p_\Lambda = w_\Lambda \rho_\Lambda = -\rho_\Lambda$, the $\Lambda/3$ term in the right hand side of Eq. (1.18) can also be written $-\kappa/6(\rho_\Lambda + 3p_\Lambda)$. In the same manner, since $p_{\mathcal{K}} = -\rho_{\mathcal{K}}/3$, adding a $-\kappa/6(\rho_{\mathcal{K}} + 3p_{\mathcal{K}}) = 0$ to the right hand side of Eq. (1.18) does not change it, so that similarly to Eq. (1.28), the Raychaudhuri equation can be written as

$$\frac{\ddot{a}}{a} = -\frac{\kappa}{6}\left[\rho_{\rm matter} + \rho_\Lambda + \rho_{\mathcal{K}} + 3\left(p_{\rm matter} + p_\Lambda + p_{\mathcal{K}}\right)\right] = -\frac{\kappa}{6}\left(\rho_{\rm T} + 3p_{\rm T}\right) , \tag{1.29}$$

where $p_{\rm T}$ denotes the "total" pressure. This is why, as far as the two dynamical equations (1.17) and (1.18) are concerned, the curvature can be viewed as an ideal fluid constituent with equation

[5] This should not come as a surprise since the conservation relation $\nabla_\mu T^{\mu\nu} = 0$ is invariant under the redefinition $T_{\mu\nu} \to T_{\mu\nu} + \Lambda g_{\mu\nu}$. This is the reason why a cosmological constant can actually be thought of as being part of the matter side of the Einstein equations.

of state parameter $w_{\mathcal{K}} = -1/3$ and the cosmological constant can be viewed as an ideal fluid constituent with equation of state parameter $w_\Lambda = -1$.

If the scale factor a evolves monotonously with time, the right hand side of the Friedmann equation (1.28) soon gets dominated by a single fluid (the one with the smallest w if space expands, or the one with the largest w if space contracts). In this limit, it can be integrated, leading to

$$a(t) = \begin{cases} a_{\rm in}\left[1 \pm \frac{3}{2}(1+w)\sqrt{\frac{\rho_{\rm in}}{3}}\frac{t-t_{\rm in}}{M_{\rm Pl}}\right]^{\frac{2}{3(1+w)}} & \text{if } w \neq -1 \\ a_{\rm in}\exp\left(\pm\sqrt{\frac{\rho_{\rm in}}{3}}\frac{t-t_{\rm in}}{M_{\rm Pl}}\right) & \text{if } w = -1 \end{cases}, \tag{1.30}$$

where $a_{\rm in}$ and $t_{\rm in}$ are two integration constants. The sign $\pm$ depends on whether space is expanding (plus sign, $H > 0$) or contracting (minus sign, $H < 0$). In what follows, only the case of an expanding space will be considered. The $\rho(a)$ shape (1.27) and the $a(t)$ shape (1.30) are also given in table 1.1 for the fluids mentioned so far.

Finally, it is interesting to notice that the conservation equation (1.16) can also be integrated when the Universe is made of a collection of ideal independent fluids with equations of state $w_i = p_i/\rho_i$. In this case indeed, the conservation equation gives rise to

$$\sum_i \left[\dot{\rho}_i + 3H(1+w_i)\rho_i\right] = 0\,. \tag{1.31}$$

One of the solutions is of course when all the terms of the above sum vanish. Physically, this corresponds to a situation of non interacting independent fluids, where there is no energy transfer from one fluid to another. Obviously, in this case the scaling solution (1.27) applies for all the fluids, and the total energy density is given by

$$\rho_{\rm T} = \sum_i \rho_i^{\rm in}\left(\frac{a}{a_{\rm in}}\right)^{-3(1+w_i)}. \tag{1.32}$$

Unfortunately however, in this case the Friedmann equation $H^2 = \kappa\rho_{\rm T}/3$ cannot be integrated analytically.

1.2. The Present Composition of the Universe

Thanks to Eq. (1.32), we now know how the energy density of each constituent of the Universe evolves with time, at least provided its equation of state parameter is constant. Therefore, up to potential energy transfer between constituents, it is enough to know the energy densities at a single time (most conveniently, now) to derive their value at any other time. This is why we now discuss the present composition of the Universe.

To this end, we first define the critical density $\rho_{\rm crit}$ with respect to the Hubble parameter,

$$\rho_{\rm crit} = \frac{3}{\kappa}H^2\,. \tag{1.33}$$

The total energy density $\rho_{\rm tot}$ is the sum of all contributions but the curvature one, $\rho_{\rm tot} = \rho_{\rm T} - \rho_{\mathcal{K}}$. If one writes $\rho_{\rm tot} = \sum_i \rho_i$, each part ρ_i stands for an ideal fluid i with its own equation of state

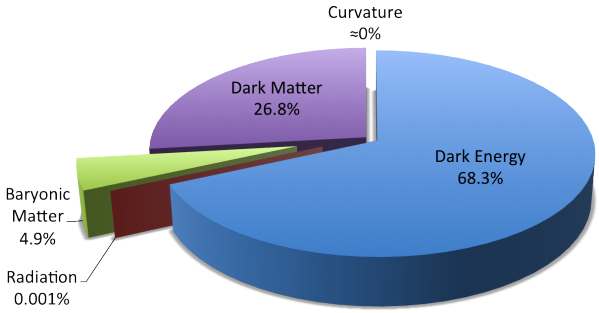

Figure 1.4.: Current Energy Composition of the Universe.

parameter w_i. The dimensionless quantities $\Omega_i = \rho_i/\rho_{\text{crit}}$ then allow to re-write the Friedmann equation (1.28) simply as

$$\Omega_{\text{tot}} = \sum_i \Omega_i = 1 - \Omega_{\mathcal{K}}\,, \tag{1.34}$$

where we stress again that the curvature term (which, contrary to the others, can be either positive or negative) is treated separately. In the present Universe, the components contributing to this relation have the following weights.[6]

Radiation

Most of the photons present in the Universe belong to the Cosmic Microwave Background, see section 1.3.3. They represent a tiny fraction of ρ_{tot}, with [15] $\Omega_{\text{rad}}^{(0)} \approx 9.3 \times 10^{-5}$.

Baryonic Matter

The contribution from ordinary matter (*i.e.* the one we find in atoms, nuclei, *etc.*) to Ω_{tot} is dominated by cold baryons (strongly interacting composite subatomic particles made up of three quarks) which are much heavier than leptons (elementary spin 1/2 particles that do not undergo strong interaction, such as electrons or neutrinos). However, they only amount to [15] $\Omega_{\text{b}}^{(0)} \approx 0.049$.

Nonbaryonic (or "Dark") Matter

In order to consistently explain many observational facts, ranging from galaxy rotation curves and large scale structure formation to the CMB statistics, it is common to postulate the existence of another non-relativistic matter component in the Universe, with $w = 0$ as well, referred to as "dark matter". Its current contribution is [15] $\Omega_{\text{dm}}^{(0)} \approx 0.268$ and therefore, it strongly dominates over ordinary matter. The nature of dark matter is obviously the subject of active study.

[6] All quantities referring to their current (present-day) value are designated by a subscript (or occasionally a superscript) "0" or "(0)".

Curvature

When $\mathcal{K} = 0$, the Universe is globally flat. If $\mathcal{K} = \pm 1$ however ($\mathcal{K} = 1$ corresponds to a closed universe while $\mathcal{K} = -1$ corresponds to an infinite universe), there should be a curvature component in the current Universe energy budget. However, it has not been detected yet, and all the observations made so far are still consistent with $\Omega_{\mathcal{K}}^{(0)} \simeq 0$. The current constraints give [15] $100\Omega_{\mathcal{K}}^{(0)} = -0.10^{+0.62}_{-0.65}$ at 95% confidence level.

Dark Energy

Evidently, after summing over radiation, baryonic and non-baryonic matter, the bulk part of the Universe's energy density is still missing. Together with evidence from a recent acceleration in the expansion of the Universe, this motivates the introduction of a missing fluid named "dark energy", with an equation of state parameter $w \simeq -1$. This is why the cosmological constant Λ (for which $w = -1$ exactly) is one of the candidates for dark energy, even if as for dark matter, the nature of dark energy is the subject of active study (for a nice review, see Ref. [42]). It accounts for the major contribution to $\Omega_{\rm tot}^{(0)}$, *i.e.* [15] $\Omega_{\rm de}^{(0)} \approx 0.683$.

The values mentioned here are given in table 1.2. The relative contributions of these constituents is also displayed in Fig. 1.4. One can see that the Universe is currently dominated by fluids the physical nature of which is still not well understood (dark matter and dark energy). This gives us an idea of the theoretical effort still needed to build a complete and standard description of cosmology.

1.3. The History of the Universe: the Hot Big Bang Model

In the previous section, we have stated the current values of the energy fractions $\Omega_i^{(0)}$ for the Universe main components. Combined with the dynamical considerations of section 1.1.2, this enables us to now infer the main lines of the history of the Universe.

1.3.1. Dominant Constituant

Plugging the previously given values for $\Omega_i^{(0)}$ in Eq. (1.32), $\rho_{\rm tot}/\rho_{\rm cri} = \sum_i \Omega_i^{(0)} (a/a_0)^{-3(1+w_i)}$, allows us to discuss the way $\rho_{\rm tot}$ varies with a. The result is displayed in the left panel of Fig. 1.5. The black dashed line stands for the total sum, while the coloured lines follow each of its components. Because of the different scalings with a, each component of the Universe dominates its content at a different epoch (called "eras" in what follows).

The Universe is currently dominated by dark energy which means that $\rho_{\rm tot} \simeq$ constant. Since cold matter $\rho_{\rm mat} \equiv \rho_{\rm dm} + \rho_{\rm b}$ scales as a^{-3}, its contribution increases when moving backwards in time and becomes larger than the one of dark energy at some point $a_{\rm acc}$ defined by $\rho_{\rm mat}(a_{\rm acc}) = \rho_{\rm de}(a_{\rm acc})$, *i.e.* $a_{\rm acc}/a_0 = \left[\Omega_{\rm mat}^{(0)}/\Omega_{\rm de}^{(0)}\right]^{1/3}$. Here, the subscript "acc" stands for the onset of the dark energy phase.[7] When $a < a_{\rm acc}$, the Universe is dominated by cold matter and one has

[7] One should note that contrary to what the notation may suggest, acceleration of the expansion does not begin

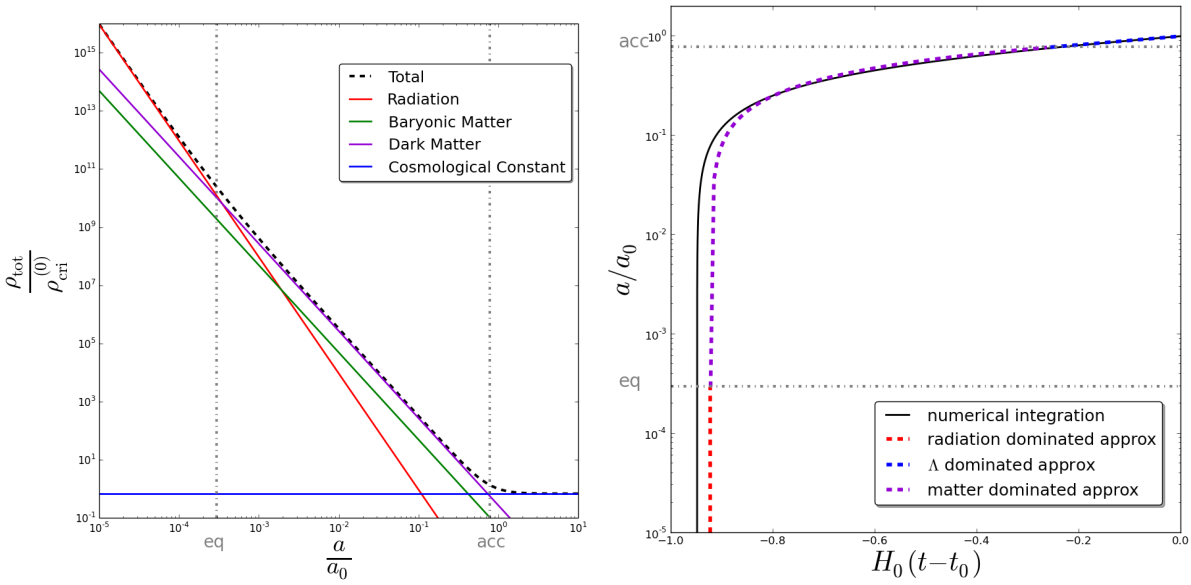

Figure 1.5.: Left panel: energy density (1.32) of the Universe constituents [scaled by the current critical density $\rho_{\rm cri}^{(0)}$] as a function of the scale factor a. The black dashed line stands for the sum of all contributions. The Universe history is made of a radiation era ($a < a_{\rm eq}$), followed by a matter era ($a_{\rm eq} < a < a_{\rm acc}$) and more recently a cosmological constant era ($a > a_{\rm acc}$). Right panel: scale factor a as a function of cosmic time t. The black line corresponds to the numerical integration of Eq. (1.42), and the coloured lines stand for the piecewise approximated solution (1.38). Both panels make use of $\Omega_{\mathcal{K}}^{(0)} = 0$ and the values of $\Omega_i^{(0)}$ recalled in table 1.2, and dark energy is described by means of a cosmological constant ($w_{\rm de} = w_\Lambda = -1$.)

$\rho_{\rm tot} \propto a^{-3}$ and $a \propto t^{2/3}$, see Eq. (1.30).

It can be more convenient to label time t with the redshift z of a photon emitted at time t and reaching its observer now, defined in Eq. (1.8) as

$$1 + z = \frac{a_0}{a}\,. \tag{1.35}$$

With this definition, the transition redshift between matter and dark energy eras is given by

$$z_{\rm acc} = \left[\frac{\Omega_{\rm de}^{(0)}}{\Omega_{\rm mat}^{(0)}}\right]^{1/3} - 1\,. \tag{1.36}$$

With the values of $\Omega_i^{(0)}$ recalled in table 1.2, one obtains $z_{\rm acc} \simeq 0.29$.

Then, since radiation decays faster ($\rho_{\rm rad} \propto 1/a^4$) than matter, its contribution with respect to matter increases when moving backwards in time. Therefore, it dominates the Universe content when $a < a_{\rm eq}$, where $a_{\rm eq}$ is defined by $\rho_{\rm mat}\,(a_{\rm eq}) = \rho_{\rm rad}\,(a_{\rm eq})$, giving rise to

$$z_{\rm eq} = \frac{\Omega_{\rm mat}^{(0)}}{\Omega_{\rm rad}^{(0)}} - 1\,. \tag{1.37}$$

at $a_{\rm acc}$ exactly, since this occurs slightly before when $\rho_{\rm de} = \rho_{\rm mat}/2$.

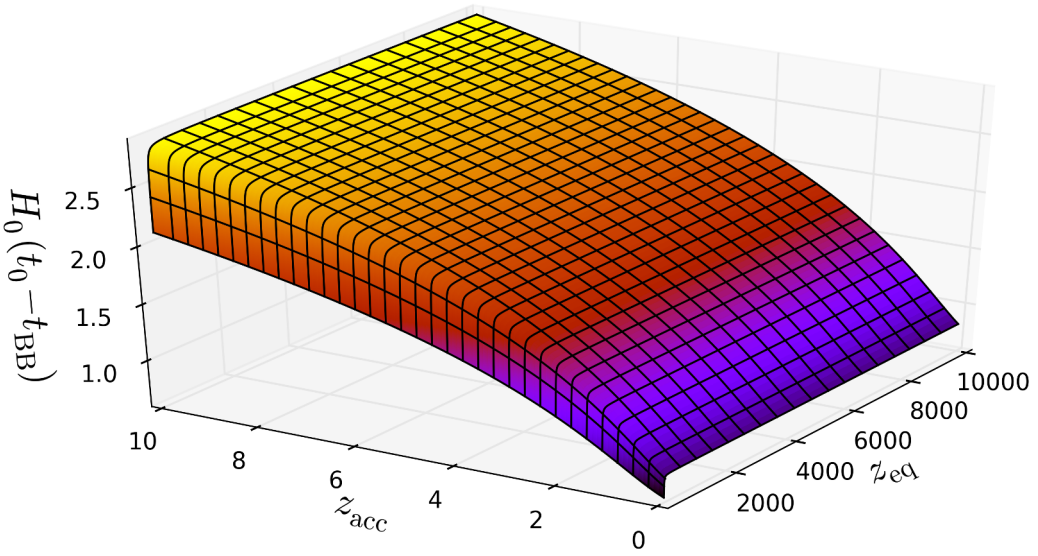

Figure 1.6.: Age of a flat universe as a function of z_{eq} and z_{acc}. The displayed value correspond to a numerical integration of Eq. (1.43).

With the values of $\Omega_i^{(0)}$ recalled in table 1.2, one obtains $z_{eq} \simeq 3402$. Here, the subscript "eq" stands for "equality" between matter and radiation. When $a < a_{eq}$ (or equivalently $z > z_{eq}$), the Universe is dominated by radiation, $\rho_{tot} \propto a^{-4}$ and $a \propto t^{1/2}$.

To conclude, the Universe history is made of three main phases: a radiation era for $z > z_{eq}$ during which $\rho_{tot} \propto 1/a^4$ and $a \propto t^{1/2}$, a matter era for $z_{acc} < z < z_{eq}$ during which $\rho_{tot} \propto 1/a^3$ and $a \propto t^{2/3}$, and a dark energy era for $z < z_{acc}$ during which $\rho_{tot} \simeq$ constant and $a \propto \mathrm{e}^{Ht}$. These three eras can clearly be seen on the left panel of Fig. 1.5. In this discussion, the role played by curvature has not been included. Indeed, since $\rho_{\mathcal{K}}$ decays slower than, say, ρ_{mat}, $\rho_{\mathcal{K}}^{(0)} \ll \rho_{mat}^{(0)}$ implies that this inequality holds at any previous time, and curvature can never have dominated the Universe content. This is why in Fig. 1.5 and in this section 1.3, we consider a flat universe for which $\Omega_{\mathcal{K}}^{(0)} = 0$.

1.3.2. Age of the Universe

When the Universe is dominated by an ideal fluid, the $a(t)$ profile has been derived in Eq. (1.30). Neglecting the transition phases between the three above mentioned eras (during which there are two equally important main constituents), we can therefore derive an approximated piece-wise form for $a(t)$ spanning the whole Universe history. The integration constants ρ_{in} and t_{in} appearing in Eq. (1.30) can be set by requiring continuity of a and $\dot{a}$ at the transition times (so

that H is continuous), and one obtains

$$\frac{a(t)}{a_0} \simeq \begin{cases} \exp\left[H_0\left(t-t_0\right)\right] & \text{if } t > t_{\rm acc} \\ \frac{1}{1+z_{\rm acc}}\left[1+\frac{3}{2}H_0\left(t-t_{\rm acc}\right)\right]^{2/3} & \text{if } t_{\rm eq} < t < t_{\rm acc} \\ \frac{1}{1+z_{\rm eq}}\left[1+2\left(\frac{1+z_{\rm eq}}{1+z_{\rm acc}}\right)^{3/2}H_0\left(t-t_{\rm eq}\right)\right]^{1/2} & \text{if } t_{\rm BB} < t < t_{\rm eq} \end{cases} . \tag{1.38}$$

Here, $t_{\rm acc}$ is the transition time between the matter era and the dark energy era and $t_{\rm eq}$ is the transition time between the radiation era and the matter era. They are such that

$$H_0(t_0 - t_{\rm acc}) = \ln\left(1+z_{\rm acc}\right) , \tag{1.39}$$

$$H_0(t_{\rm acc} - t_{\rm eq}) = \frac{2}{3} - \frac{2}{3}\left(\frac{1+z_{\rm acc}}{1+z_{\rm eq}}\right)^{3/2} . \tag{1.40}$$

The piecewise function $a(t)$ defined by Eq. (1.38) is displayed in the right panel of Fig. 1.5 (coloured lines, each colour corresponds to a different era). It is interesting to notice that when moving backwards in time, a goes to 0 in a finite amount of time. The corresponding singularity is called the Big Bang. Looking at Eq. (1.38), it occurs at the time $t_{\rm BB}$ given by

$$t_0 - t_{\rm BB} \simeq H_0^{-1}\left[\frac{2}{3} + \ln\left(1+z_{\rm acc}\right) - \frac{1}{6}\left(\frac{1+z_{\rm acc}}{1+z_{\rm eq}}\right)^{3/2}\right] . \tag{1.41}$$

One can see that as mentioned in section 1.1.1, the age of the Universe is of the order of the Hubble time H_0^{-1}. More precisely, with the values given in table 1.2, one obtains $t_0 - t_{\rm BB} \simeq 0.92 H_0^{-1} \simeq 1.33 \times 10^{10}$ year.

Obviously, the Friedmann equation (1.28) can also be solved exactly, that is the integral

$$t - t_0 = H_0^{-1}\int_1^{a/a_0} \frac{{\rm d}\left(\tilde{a}/a_0\right)}{\sqrt{\sum_i \Omega_i^{(0)}\left(\frac{\tilde{a}}{a_0}\right)^{-1-3w_i}}} \tag{1.42}$$

can be computed numerically. The result is displayed with the black line in the right panel of Fig. 1.5. The matching with the piecewise approximation is fairly good. With the parameter values recalled in table 1.2, this leads to a slightly different value for the age of the Universe, that is $t_0 - t_{\rm BB} \simeq 0.95 H_0^{-1} \simeq 1.37 \times 10^{10}$ year. Actually, since the approximated expression (1.41) for the age of the Universe is given in terms of $z_{\rm eq}$ and $z_{\rm acc}$, it can be useful to express the integral (1.42) in terms of these two variables only. One obtains for the age of the Universe

$$\begin{aligned} t_0 - t_{\rm BB} \;=\; & H_0^{-1}\sqrt{1+\frac{1}{1+z_{\rm eq}}+\left(1+z_{\rm acc}\right)^3}\times \\ & \int_0^\infty {\rm d}z\left[\left(1+z\right)^5 + \frac{1}{1+z_{\rm eq}}\left(1+z\right)^6 + \left(1+z_{\rm acc}\right)^3\left(1+z\right)^2\right]^{-1/2} . \end{aligned} \tag{1.43}$$

One can numerically check that Eqs. (1.41) and (1.43) give similar results as soon as $z_{\rm eq} > z_{\rm acc}$, and that the age of the Universe increases only mildly with $z_{\rm eq}$, and more notably with $z_{\rm acc}$. The integral (1.43) is displayed in Fig. 1.6 as a function of $z_{\rm eq}$ and $z_{\rm acc}$.

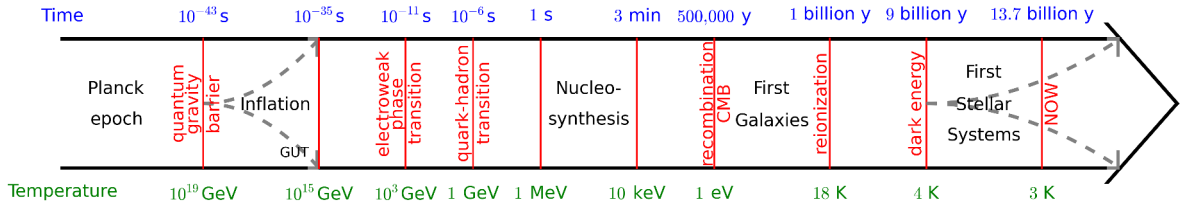

Figure 1.7.: Main events in the Cosmological Standard Scenario.

1.3.3. A Brief Cosmological History

The cosmological redshift (1.8) gives a rule for the behaviour of a black-body spectrum of radiation with temperature T_γ. Indeed, since all photons redshift as exactly the same rate $\lambda \propto a^{-1}$, a system which starts out as a black-body stays as a black-body, with a temperature that decreases with expansion,

$$T_\gamma \propto a^{-1} \,. \tag{1.44}$$

Therefore, when one goes backwards in time during the radiation era, temperature increases as $1/a$. In particular, this means that the initial singularity is also a point of infinite temperature. This leads us to the standard hot Big Bang picture of the Universe: a cosmological singularity at finite time in the past, followed by a hot, radiation dominated expansion, during which the Universe gradually cools down as $T \propto a^{-1}$ and the radiation dilutes, followed by a period of matter dominated expansion during which galaxies, stars and planets form. Finally, the vacuum energy inevitably dominates and the Universe enters a state of exponential expansion.

This simple picture allows us to infer the presence of a few notable events that we now briefly recap, and that are summarized in Fig. 1.7 with orders of magnitude about time, energy and temperature at which these events occur. As one goes backwards in time, one can check that energy or temperature increases.

Inflation takes place at $t \lesssim 10^{-35}$ s and is the object of section 1.4 and chapter 2 (in this section, times are given as elapsed since the initial singularity). This is why we start out our description afterwards, when the Universe is made of a hot plasma containing the fundamental particles of the standard model, at $t \sim 10^{-35}$ s.

At $t \sim 10^{-11}$ s occurs the electroweak phase transition which breaks the $SU(2) \times U(1)$ symmetry of the electroweak field into the $U(1)$ symmetry of the present day electromagnetic field [43, 44, 45, 46, 47, 48, 49]. This transition may be important to understanding the asymmetry between the amount of matter and antimatter in the present Universe through a process of baryogenesis [50, 51, 52, 53, 54]. It occurs at the electroweak scale which is often taken to be at the Higgs *vev*, around 246 GeV.

In the same manner, around $t \sim 10^{-6}$ s, a phase transition (associated with chiral symmetry breaking) occurs that converts a plasma of free quarks and gluons into hadrons [55, 56, 57, 58, 59, 60]. This quark-hadron transition may play an important role in the generation of primordial magnetic fields [61]. It may also give rise to important baryon number inhomogeneities which can affect the distribution of light element abundances from primordial Big Bang nucleosynthesis [62] (see below). It occurs when the temperature drops below the rest energy of nucleons, around 938 MeV.

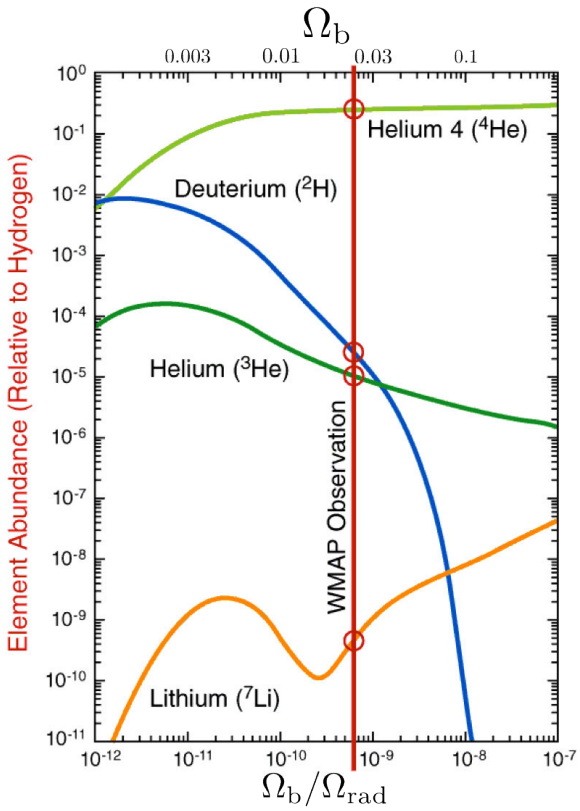

Figure 1.8.: Big Bang Nucleosynthesis. Light elements abundances (relative to hydrogen) as a function of the density of ordinary matter Ω_b and of its density relative to photons Ω_b/Ω_{rad} at time of nucleosynthesis. The WMAP satellite has been able to directly measure this ordinary matter density and found a value [63] of 4.6%(±0.2%), indicated by the vertical red line. This leads to predicted abundances shown by the circles in the graph, which are in good agreement with observed abundances. Image Credit: NASA/WMAP101087.

From there, nuclear fusion begins at $t \sim 0.01$ s and big bang nucleosynthesis proceeds at $t \sim 3$ min. This phase is when light elements (mostly H, D, He, Li and Be) are formed [64, 65, 66, 67]. Reproducing the observed abundances of elements from nuclear physics calculations places tight constraints on the environment it took place in [68, 69, 70, 71, 72, 73, 74, 75]. For example, in Fig. 1.8 are displayed the abundances of early produced light elements as a function of the density of ordinary matter relative to photons, Ω_b/Ω_{rad}. One can see that measures of elements abundances allow to set tight constraints on this ratio, and conversely. Nucleosynthesis begins at temperatures of around 10 MeV (which is the order of magnitude of nuclear binding energies) and ends at temperatures below 100 keV. The corresponding time interval is from a few tenths of a second to up to 10^3 seconds. Heavier elements are only formed later through stellar nucleosynthesis in evolving and exploding stars.

The Universe keeps on cooling down, until it reaches the point where charged electrons and protons become bound to form electrically neutral hydrogen atoms. This phase is often called "recombination" (although nuclei and electrons have never combined before). Since the photon-atom cross section (the Rayleigh cross-section) is much smaller than the photon-electron cross-section (Thomson cross-section), the Universe becomes transparent shortly after when photons decouple from matter (photon decoupling) and travel freely in the Universe. The associated

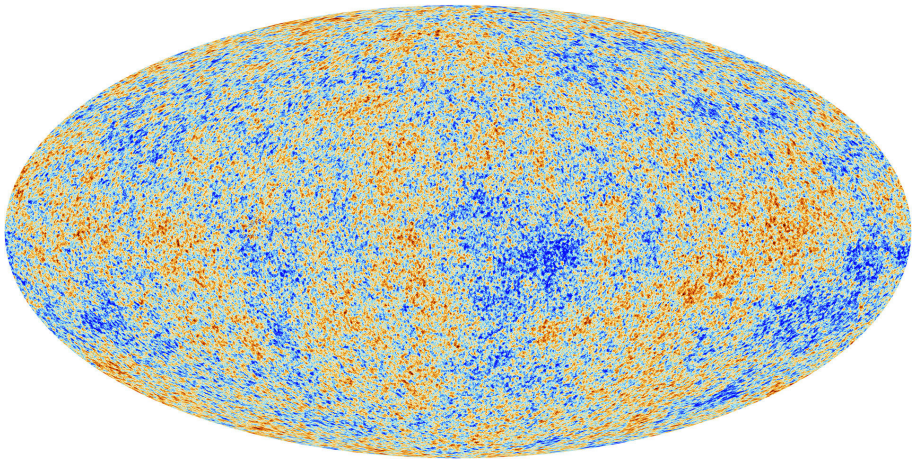

Figure 1.9.: Cosmic Microwave Background temperature fluctuations, as seen by the Planck satellite [76]. Colours encode temperature deviations from the mean temperature (blue points are colder whereas red points are hotter). Image Credit: Planck Collaboration.

relic radiation is called cosmic microwave background (CMB) and is the oldest photograph of the Universe one can get [77]. Its emission occurs at energies around 1 eV, at $t \sim$500,000 y. It reaches us today with the same shape of temperature distribution, *i.e.* a perfect black-body spectrum, with its central temperature redshifted by the amount of expansion $\mathcal{O}(10^3)$ that has occurred since then, to reach the average value $T_{\rm CMB} = 2.725$ K. This temperature is the same for all direction in the sky, up to tiny fluctuations of the order 10^{-5}. This tells us that at recombination time, the Universe is homogeneous and isotropic on all scales up to the present horizon (see section 1.4.1) to at least one part in 100,000. The statistics of the deviations from homogeneity of this radiation is a key prediction of the theory of inflation that we discuss in chapter 2. For illustrative purpose, the spatial map of the CMB temperature fluctuations measured by the Planck satellite is displayed in Fig. 1.9.

Galaxies then start to form, and inside them objects energetic enough to ionize neutral hydrogen. This is the so-called reionization epoch [78, 79, 80, 81]. As these objects form and radiate energy, the Universe indeed goes from being neutral back to being an ionized plasma, between 150 million and one billion years after the Big Bang. Compared with before recombination however, matter is much more diluted because of the expansion of the Universe, and scattering interactions are much less frequent than at this time. This is why the subsequent Universe, full of low density ionized hydrogen, remains transparent, as is the case today.

At $t \sim 9$ billion years, dark energy starts to dominate and the expansion accelerates [84, 85]. First stellar systems form, and large scale structures continue to develop until today. Large scale structures constitute another observational pillar of modern cosmology, since the way they develop is related to the content of the Universe, the physical nature of its dark sector, the underlying theory of gravitation, and the initial cosmological perturbations they start from. For example, in Fig. 1.10 is displayed the result of simulated dark matter distributions for different cosmological models. The left panel is when structures develop in the standard cosmology described so far, the middle panel is when no dark energy is introduced in the model ($\Omega_{\rm de} = 0$), and the right panel is when warm dark matter (*i.e.* such that $w_{\rm de} > 0$) is used instead of cold dark matter. One can see that the features of the structures are different. For example, when no dark energy is present, the Universe expansion does not accelerate at late times, which allows faster structure formation. In this manner, measuring the distribution of matter around us

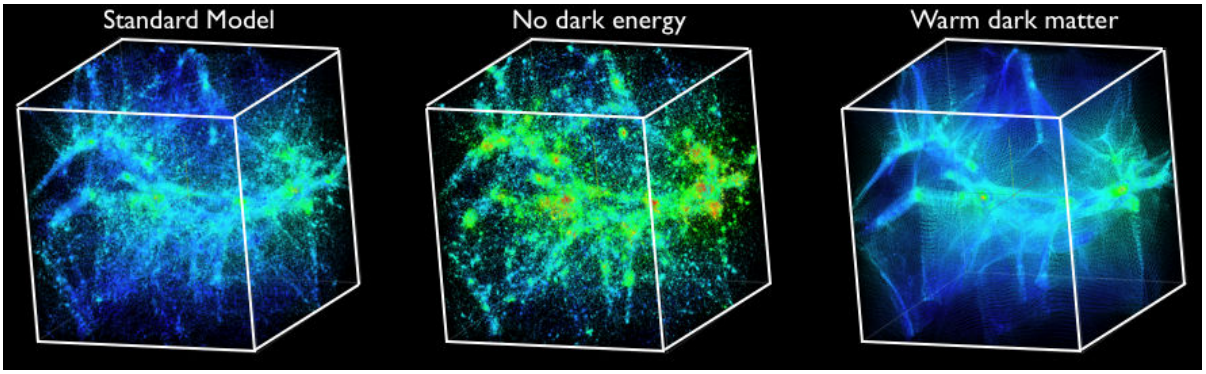

Figure 1.10.: Simulated dark matter distributions for different cosmological models. The colours encode velocities. Left panel: standard cosmological model. Middle panel: without dark energy ($\Omega_{\rm m} = 1$, $\Omega_\Lambda = 0$, $h = 0.7$). Right panel: with warm (instead of cold) dark matter in form of a sterile neutrino. Produced with the MC^2 code [82] run over a small simulation [containing 32^3 particles, with a box size of $(32\,{\rm Mpc}/h)^3$].

Image Credit: Ref. [83].

and understanding, notably by the means of numerical simulations and statistical tools, how it depends on the physical properties of our Universe, is a way to test these properties in the large scales regime.

1.4. The Big Bang Model Problems and Inflation

Now that we have introduced the main aspects of the standard cosmological model, it is worth mentionning that it raises unanswered questions, known as the hot big bang model problems. The horizon problem and the flatness problem deal with the fact that, interpreted within the standard model, observations lead to the conclusion that the Universe must have been extremely flat at early times, and homogeneous even over causally disconnected physical scales. They are not definite impossibility problems, but still serious fine-tuning issues. The monopole problem deals with the density of topological defects arising from symmetry breaking in the early Universe. Described in the standard model, these defects should be well visible at present time, which is in contradiction with experimental investigation for them. In this section, we describe in details these three problems, and we show that even if very different in nature, they can all be solved by the introduction of a phase of accelerated expansion in the early Universe.

1.4.1. The Horizon Problem

One of the properties of the above described cosmology is that it is endowed with a causal horizon, *i.e.* a frontier that separates observable events from non observable ones. Said differently, the set of events causally connected to a reference point in space-time only form a bounded set. Since no physical process can act on scales larger than the horizon, we typically expect the Universe to be strongly inhomogeneous on those scales.

However, as we shall now see, within the cosmological scenario of the standard hot big bang model, the last scattering surface (with respect to us) spans over several causally disconnected

pieces of space-time, that is, the size of the cosmological horizon at time of recombination is smaller than the diameter of the last scattering surface. The last scattering surface should therefore exhibit strong deviations from homogeneity, which is not the case. In this section, we thus calculate the size of the cosmological horizon [86, 87] in a FLRW space-time, and express the angular distance of the horizon at time of recombination, as seen by a current observer on Earth. For the reasons mentioned at the end of section 1.3.1, namely the fact that curvature can never have dominated the Universe content, we consider the case of a flat universe ($\mathcal{K} = 0$). We take the origin of the r coordinate to be the location of Earth, *i.e.* "our" comoving coordinate is $r = 0$.

1.4.1.1. Cosmological Horizon

Let us consider a photon emitted at $t_{\rm em}$ and $r_{\rm em}$ and traveling towards us ($\mathrm{d}\theta = \mathrm{d}\phi = 0$). Its trajectory is given by Eq. (1.5), that is

$$r\left(t\right) = r_{\rm em} - \int_{t_{\rm em}}^{t} \frac{\mathrm{d}\tilde{t}}{a\left(\tilde{t}\right)} \,. \tag{1.45}$$

At time t, the physical distance (or "proper" distance) between the photon and the origin is then given by $d_{\rm P}(t) = a(t)r(t)$. The horizon is defined in the following way. If the photon is received at (or before) time $t_{\rm rec}$, the horizon at time $t_{\rm rec}$ is the proper distance to the furthest point the photon can have been sent from. Clearly, this distance is maximized if the photon was emitted at the earliest possible time, that is $t_{\rm em} = t_{\rm BB}$, and if it is received at the latest allowed time $t_{\rm rec}$, that is $r\left(t_{\rm rec}\right) = 0$. When plugging these two relations in Eq. (1.45), one obtains $r_{\rm em} = \int_{t_{\rm BB}}^{t_{\rm rec}} \mathrm{d}\tilde{t}/a(\tilde{t})$. By definition, the size of the horizon $d_{\rm H}$ at time $t_{\rm rec}$ is then given by

$$d_{\rm H}\left(t_{\rm rec}\right) = a\left(t_{\rm rec}\right) r_{\rm em} = a\left(t_{\rm rec}\right) \int_{t_{\rm BB}}^{t_{\rm rec}} \frac{\mathrm{d}t}{a\left(t\right)} \,. \tag{1.46}$$

If one replaces $t_{\rm rec}$ by the time of recombination $t_{\rm lss}$, one obtains the horizon size at the last scattering surface emission time, $d_{\rm H}\left(t_{\rm lss}\right)$.

1.4.1.2. Angular Distance to $d_{\rm H}\left(t_{\rm lss}\right)$

We now move on to compute the angular distance of the horizon at time of recombination, as seen by a current observer on Earth. This quantity $\Delta\Omega_{d_{\rm H}}\left(t_0\right)$ can be expressed as follows. The last scattering surface is an instantaneous sphere of constant radius and therefore, within the last scattering surface, $\mathrm{d}r = \mathrm{d}t = 0$. The FLRW metric then takes the form $d_{\rm P} = a(t_{\rm lss})r_{\rm lss}\mathrm{d}\Omega$, where $\mathrm{d}\Omega^2 = \mathrm{d}\theta^2 + \sin^2\theta\mathrm{d}\phi^2$. Therefore, the angular extension of the horizon at time of recombination reads

$$\Delta\Omega_{d_{\rm H}}\left(t_0\right) = \frac{d_{\rm H}\left(t_{\rm lss}\right)}{a\left(t_{\rm lss}\right) r_{\rm lss}} \,. \tag{1.47}$$

It only remains to compute $r_{\rm lss}$, which can be done using the same procedure as before. Indeed, applying Eq. (1.45) between $t_{\rm em} = t_{\rm lss}$ and t_0, $r(t_0) = 0$ leads to $r_{\rm lss} = \int_{t_{\rm lss}}^{t_0} \mathrm{d}t/a(t)$. Together with Eq. (1.46) for $t_{\rm rec} = t_{\rm lss}$, one obtains

$$\Delta\Omega_{d_{\rm H}}\left(t_0\right) = \frac{\displaystyle\int_{t_{\rm BB}}^{t_{\rm lss}} \frac{\mathrm{d}t}{a(t)}}{\displaystyle\int_{t_{\rm lss}}^{t_0} \frac{\mathrm{d}t}{a(t)}} \,. \tag{1.48}$$

1.4.1.3. Formulation of the Problem

Let us now evaluate this quantity with the cosmological model of section 1.3, made of a radiation era, a matter era and a dark energy era. Recombination occurs during the matter era ($z_{\rm lss} \simeq 1090$, see Ref. [15]), so that $t_{\rm BB} < t_{\rm eq} < t_{\rm lss} < t_{\rm acc}$. Therefore, thanks to Eq. (1.38), $t_{\rm lss}$ can be expressed in terms of the recombination redshift $z_{\rm lss}$ through $H_0(t_0 - t_{\rm lss}) \simeq 2/3 + \ln(1+z_{\rm acc}) - 2/3\left[(1+z_{\rm acc})/(1+z_{\rm lss})\right]^{3/2}$. Another consequence of this series of events is that the integrals appearing in Eq. (1.48) can be split according to $\int_{t_{\rm BB}}^{t_{\rm lss}} = \int_{t_{\rm BB}}^{t_{\rm eq}} + \int_{t_{\rm eq}}^{t_{\rm lss}}$ and $\int_{t_{\rm lss}}^{t_0} = \int_{t_{\rm lss}}^{t_{\rm acc}} + \int_{t_{\rm acc}}^{t_0}$. Using the piecewise approximation (1.38) for the $a(t)$ profile, each of these integrals can be computed. One obtains

$$a_0 H_0 \int_{t_{\rm BB}}^{t_{\rm eq}} \frac{{\rm d}t}{a} \simeq \frac{(1+z_{\rm acc})^{3/2}}{\sqrt{1+z_{\rm eq}}} \ , \quad a_0 H_0 \int_{t_{\rm eq}}^{t_{\rm lss}} \frac{{\rm d}t}{a} \simeq 2\,(1+z_{\rm acc})^{3/2} \left(\frac{1}{\sqrt{1+z_{\rm lss}}} - \frac{1}{\sqrt{1+z_{\rm eq}}} \right) , \tag{1.49}$$

$$a_0 H_0 \int_{t_{\rm acc}}^{t_0} \frac{{\rm d}t}{a} \simeq z_{\rm acc} \ , \qquad a_0 H_0 \int_{t_{\rm lss}}^{t_{\rm acc}} \frac{{\rm d}t}{a} \simeq 2\,(1+z_{\rm acc})^{3/2} \left(\frac{1}{\sqrt{1+z_{\rm acc}}} - \frac{1}{\sqrt{1+z_{\rm lss}}} \right) .$$

These expressions allow to express $\Delta\Omega_{d_{\rm H}}(t_0)$ in terms of $z_{\rm eq}$, $z_{\rm lss}$ and $z_{\rm acc}$ according to

$$\Delta\Omega_{d_{\rm H}}(t_0) = \frac{\dfrac{2}{\sqrt{1+z_{\rm lss}}} - \dfrac{1}{\sqrt{1+z_{\rm eq}}}}{\dfrac{2+3z_{\rm acc}}{(1+z_{\rm acc})^{3/2}} - \dfrac{2}{\sqrt{1+z_{\rm lss}}}} \, . \tag{1.50}$$

With the parameter values recalled in table 1.2, one obtains $\Delta\Omega_{d_{\rm H}}(t_0) \simeq 0.023$ rad $\simeq 1.31°$. For comparison purpose, let us remind that the angular diameter of the moon seen from the Earth is $\simeq 0.5°$.

Beyond the piecewise approximated form of $a(t)$, like for the age of the Universe in section 1.3.2, an exact calculation can also be carried out using the relation

$$\int_{t_1}^{t_2} \frac{{\rm d}t}{a(t)} = \frac{1}{H_0 a_0} \int_{z_2}^{z_1} \frac{{\rm d}z}{\sqrt{\sum_i \Omega_i^{(0)} (1+z)^{3(1+w_i)}}} \, . \tag{1.51}$$

Such an integral can be computed numerically, and one obtains

$$\Delta\Omega_{d_{\rm H}}(t_0) = \frac{\int_{z_{\rm lss}}^{\infty} {\rm d}z / \sqrt{\sum_i \Omega_i^{(0)} (1+z)^{3(1+w_i)}}}{\int_0^{z_{\rm lss}} {\rm d}z / \sqrt{\sum_i \Omega_i^{(0)} (1+z)^{3(1+w_i)}}} \simeq 0.0054 \text{ rad} \simeq 0.3° \tag{1.52}$$

which is of the same order of magnitude as (but even smaller than) the above approximated result, and which represents $\sim 1/450{,}000$ of the full sky coverage.

As a consequence, one expects the last scattering surface to be made of 450,000 patches whose typical physical properties are *a priori* completely different. This is in contradiction with observations which establish that up to tiny fluctuations of the order $\delta T/T \simeq 10^{-5}$, the CMB radiation is extremely homogeneous and isotropic across the last scattering surface. This paradox is called the horizon problem [88, 89].

A solution to this problem is of course to assume that the initial conditions were identical in all the causally disconnected patches, but it seems very difficult to justify. Another solution is to add a new phase to the standard scenario.

1.4.1.4. Inflation as a Solution to the Horizon Problem

Let us assume that the epoch dominated by radiation can be interrupted during the period $t_{\rm in} < t < t_{\rm end}$, or equivalently $z_{\rm end} < z < z_{\rm in}$. During this interval, we assume that the Universe is dominated by an unknown ideal fluid X with an equation of state parameter w_X. We now wonder whether there are values of $z_{\rm in}$, $z_{\rm end}$ and w_X such that the horizon problem can be solved in this new scenario. Let us thus redo the horizon diameter distance calculation in this new setup.

The piecewise function $a(t)$ now has a new piece, and is given by

$$\frac{a(t)}{a_0} \simeq \begin{cases} \exp\left[H_0\left(t-t_0\right)\right] & \text{if } t > t_{\rm acc} \\ \frac{1}{1+z_{\rm acc}}\left[1+\frac{3}{2}H_0\left(t-t_{\rm acc}\right)\right]^{2/3} & \text{if } t_{\rm eq} < t < t_{\rm acc} \\ \frac{1}{1+z_{\rm eq}}\left[1+2\left(\frac{1+z_{\rm eq}}{1+z_{\rm acc}}\right)^{3/2}H_0\left(t-t_{\rm eq}\right)\right]^{1/2} & \text{if } t_{\rm end} < t < t_{\rm eq} \\ \frac{1}{1+z_{\rm end}}\left[1+\frac{3}{2}\left(1+w_X\right)\left(\frac{1+z_{\rm end}}{1+z_{\rm acc}}\right)^2\sqrt{\frac{1+z_{\rm acc}}{1+z_{\rm eq}}}H_0\left(t-t_{\rm end}\right)\right]^{\frac{2}{3(1+w_X)}} & \text{if } t_{\rm in} < t < t_{\rm end} \\ \frac{1}{1+z_{\rm in}}\left[1+2\left(\frac{1+z_{\rm end}}{1+z_{\rm acc}}\right)^2\sqrt{\frac{1+z_{\rm acc}}{1+z_{\rm eq}}}\left(\frac{1+z_{\rm in}}{1+z_{\rm end}}\right)^{\frac{3}{2}(1+w_X)}H_0\left(t-t_{\rm in}\right)\right]^{1/2} & \text{if } t'_{\rm BB} < t < t_{\rm in} \end{cases} \tag{1.53}$$

where the expressions given for $t_{\rm acc}$ and $t_{\rm eq}$ in Eqs. (1.39) and (1.40) are still valid, and where $t_{\rm end}$, $t_{\rm in}$ and $t'_{\rm BB}$ are such that

$$H_0\left(t_{\rm eq}-t_{\rm end}\right) = \frac{1}{2}\left(\frac{1+z_{\rm acc}}{1+z_{\rm eq}}\right)^{3/2}\left[1-\left(\frac{1+z_{\rm eq}}{1+z_{\rm end}}\right)^2\right], \tag{1.54}$$

$$H_0\left(t_{\rm end}-t_{\rm in}\right) = \frac{2}{3\left(1+w_X\right)}\left(\frac{1+z_{\rm acc}}{1+z_{\rm end}}\right)^2\sqrt{\frac{1+z_{\rm eq}}{1+z_{\rm acc}}}\left[1-\left(\frac{1+z_{\rm end}}{1+z_{\rm in}}\right)^{\frac{3}{2}(1+w_X)}\right], \tag{1.55}$$

$$H_0\left(t_{\rm in}-t'_{\rm BB}\right) = \frac{1}{2}\left(\frac{1+z_{\rm acc}}{1+z_{\rm end}}\right)^2\sqrt{\frac{1+z_{\rm eq}}{1+z_{\rm acc}}}\left(\frac{1+z_{\rm end}}{1+z_{\rm in}}\right)^{\frac{3}{2}(1+w_X)}. \tag{1.56}$$

In this new scenario, the integral decomposition of the numerator in Eq. (1.48) now reads $\int_{t'_{\rm BB}}^{t_{\rm lss}} = \int_{t'_{\rm BB}}^{t_{\rm in}} + \int_{t_{\rm in}}^{t_{\rm end}} + \int_{t_{\rm end}}^{t_{\rm eq}} + \int_{t_{\rm eq}}^{t_{\rm lss}}$, while the integral decomposition of the denominator $\int_{t_{\rm lss}}^{t_0} = \int_{t_{\rm lss}}^{t_{\rm acc}} + \int_{t_{\rm acc}}^{t_0}$ is unchanged. The integrals $\int_{t_{\rm eq}}^{t_{\rm lss}}$, $\int_{t_{\rm lss}}^{t_{\rm acc}}$ and $\int_{t_{\rm acc}}^{t_0}$ have already been calculated in Eq. (1.49) and their expression remains valid. On the other hand, the three new integrals $\int_{t'_{\rm BB}}^{t_{\rm in}}$, $\int_{t_{\rm in}}^{t_{\rm end}}$ and $\int_{t_{\rm end}}^{t_{\rm eq}}$, need to be computed. Using the piecewise approximation (1.53), they are given by

$$\begin{aligned} a_0H_0\int_{t'_{\rm BB}}^{t_{\rm in}}\frac{{\rm d}t}{a} &\simeq \left(1+z_{\rm in}\right)\left(\frac{1+z_{\rm acc}}{1+z_{\rm end}}\right)^2\sqrt{\frac{1+z_{\rm eq}}{1+z_{\rm acc}}}\left(\frac{1+z_{\rm end}}{1+z_{\rm in}}\right)^{\frac{3}{2}(1+w_X)}, \\ a_0H_0\int_{t_{\rm in}}^{t_{\rm end}}\frac{{\rm d}t}{a} &\simeq \frac{2}{1+3w_X}\frac{\left(1+z_{\rm acc}\right)^2}{1+z_{\rm end}}\sqrt{\frac{1+z_{\rm eq}}{1+z_{\rm acc}}}\left[1-\left(\frac{1+z_{\rm end}}{1+z_{\rm in}}\right)^{\frac{1}{2}(1+3w_X)}\right], \\ a_0H_0\int_{t_{\rm end}}^{t_{\rm eq}}\frac{{\rm d}t}{a} &\simeq \frac{\left(1+z_{\rm acc}\right)^{3/2}}{\sqrt{1+z_{\rm eq}}}\frac{z_{\rm end}-z_{\rm eq}}{1+z_{\rm end}}. \end{aligned} \tag{1.57}$$

We can now express the angular extension of the horizon at time of recombination, which reads

$$\Delta\Omega'_{d_{\rm H}}(t_0) = \frac{\frac{2}{\sqrt{1+z_{\rm lss}}} - \frac{1}{\sqrt{1+z_{\rm eq}}} + \frac{\sqrt{1+z_{\rm eq}}}{1+z_{\rm end}}\frac{1-3w_X}{1+3w_X}\left[1-{\rm e}^{-\frac{1}{2}(1+3w_X)N}\right]}{\frac{2+3z_{\rm acc}}{(1+z_{\rm acc})^{3/2}} - \frac{2}{\sqrt{1+z_{\rm lss}}}} \tag{1.58}$$

$$= \Delta\Omega_{d_{\rm H}}(t_0) + \frac{\frac{\sqrt{1+z_{\rm eq}}}{1+z_{\rm end}}\frac{1-3w_X}{1+3w_X}}{\frac{2+3z_{\rm acc}}{(1+z_{\rm acc})^{3/2}} - \frac{2}{\sqrt{1+z_{\rm lss}}}}\left[1-{\rm e}^{-\frac{1}{2}(1+3w_X)N}\right], \tag{1.59}$$

where we have defined the number of e-folds of the new phase $N \equiv \ln(a_{\rm end}/a_{\rm in}) = \ln\frac{1+z_{\rm in}}{1+z_{\rm end}}$ and where in the second line, the standard result (1.52) has been singled out. A first remark is that when $w_X = 1/3$ (*i.e.* the new phase cannot be distinguished from the radiation era in which it intervenes) or when $N = 0$ (*i.e.* the new phase does not exist), one re-obtains Eq. (1.50) as expected. However, when this new phase is switched on, an extra term appears in the angular size of the horizon that can make it much larger, provided

$$w_X < -1/3\,. \tag{1.60}$$

Indeed, if $1+3w_X > 0$, then the argument of the exponential term in Eq. (1.59) is negative and the correction coming from the phase driven by the unknown fluid becomes negligible. If $1+3w_X < 0$ on the other hand, then the correction may be important enough to reach the full sky coverage $\Delta\Omega_{d_{\rm H}}(t_0) > 4\pi$, depending of course on the number of e-folds N.

Let us give some numbers, for the values recalled in table 1.2. If $z_{\rm end} = z_{\rm GUT} \simeq 10^{28}$ (where "GUT" stands for the Grand Unification Theory breaking scale, see section 1.4.3), $\Delta\Omega_{d_{\rm H}}(t_0) > 4\pi$ when $N > 125$ for $w = -2/3$ and when $N > 63$ for $w = -1$. If $z_{\rm end} = 10^{10}$, *i.e.* two orders of magnitude above nucleosynthesis, $\Delta\Omega_{d_{\rm H}}(t_0) > 4\pi$ when $N > 42$ for $w = -2/3$ and when $N > 21$ for $w = -1$. Values of the minimum number of e-folds $N_{\rm min}$ required to have $\Delta\Omega_{d_{\rm H}} > 4\pi$ are displayed in Fig. 1.11 as a function of w_X and for a few values of $z_{\rm end}$.

To sum up this discussion and in order to get a clear formula that is easy to handle, one can simplify Eq. (1.59) in the limit where $z_{\rm lss} \gg 1$ and $z_{\rm acc} \ll 1$. One obtains that the horizon problem is solved provided $w_X < -1/3$ and

$$N \gtrsim -\frac{2}{1+3w_X}\ln\left(\frac{4\pi z_{\rm end}}{\sqrt{z_{\rm eq}}}\right). \tag{1.61}$$

One can check in Fig. 1.11 that this indeed provides a good approximation for the minimum numbers of e-folds .

Finally, from Eq. (1.30), $a \propto t^{\frac{2}{3(1+w)}}$, one can see that the condition $w_X < -1/3$ is equivalent to requiring that the expansion of the Universe is accelerating, that is $\ddot{a} > 0$. This is why the new phase we have introduced in the cosmological standard history is called "inflation" [90, 91].

1.4.1.5. Heuristic Understanding: Conformal Diagrams

Let us try to understand more intuitively what happened. A heuristic way of understanding why a phase of inflation can solve the horizon problem is by means of conformal diagrams. The

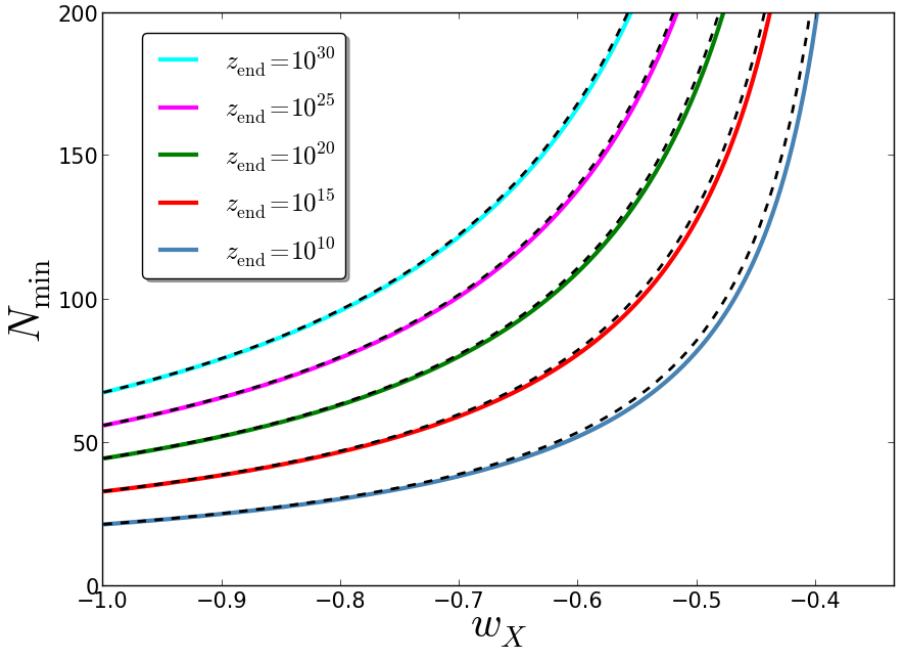

Figure 1.11.: Minimum number of e-folds in order to obtain $\Delta\Omega_{d_{\rm H}}(t_0) > 4\pi$ from Eq. (1.59), as a function of w_X and for a few values of $z_{\rm end}$, with parameter values given in table 1.2 (coloured lines). The black dotted lines correspond to the approximation (1.61).

conformal time η is defined as

$$\mathrm{d}t = a\mathrm{d}\eta\,, \tag{1.62}$$

so that the flat FLRW metric is given by $\mathrm{d}s^2 = a^2(\mathrm{d}\eta^2 - \mathrm{d}r^2)$ (where angular coordinates are omitted). In this time parameterization, null geodesics for the propagation of photons follow the very simple trajectory $\mathrm{d}\eta = \mathrm{d}r$. Therefore, the size of the horizon at time η is straightforwardly given by

$$d_{\rm H}(\eta) = a(\eta)\,(\eta - \eta_{\rm BB})\,. \tag{1.63}$$

When the Universe is dominated by a single ideal fluid with equation of state parameter w, the $a(t)$ profile is given by Eq. (1.30), which, if one sets the origins of time $t_{\rm BB} = 0$, reads

$$a(t) = a_0 \left(\frac{t}{t_0}\right)^{\frac{2}{3(1+w)}}\,. \tag{1.64}$$

From here, integrating Eq. (1.62), one obtains

$$\eta = \frac{3}{a_0 t_0}\frac{1+w}{3w+1}\left(\frac{t}{t_0}\right)^{\frac{3w+1}{3(w+1)}}\,, \tag{1.65}$$

where we have set the origins of conformal times such that its current value is given by $\eta_0 = -3(a_0 t_0)^{-1}(1+w)/(3w+1)$. The calculation of Eq. (1.63) now proceeds along two different cases:

If $w > -1/3$, when $t \to 0$, $\eta \to 0$ in Eq. (1.65), hence $\eta_{\rm BB} = 0$ and the size of the horizon given by Eq. (1.63) is finite, equal to $d_{\rm H} = a\eta$. This is why in this case, a horizon problem can occur. This corresponds the left panel of Fig. 1.12.

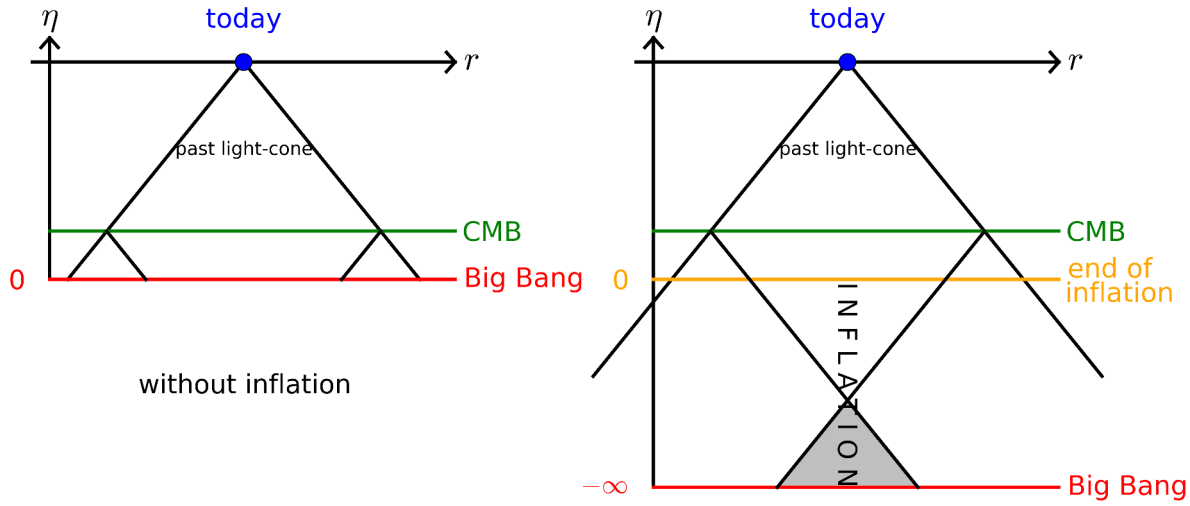

Figure 1.12.: Conformal diagrams. In the (η, r) plane, light propagates along straight lines. The left panel corresponds to the standard Big Bang cosmology. The CMB at last scattering consists of $\sim 10^5$ causally disconnected regions, that is regions the past light cones of which do not intersect because at $\eta = 0$ lies an initial singularity. The right panel corresponds to the inflationary cosmology. Inflation extends conformal time to negative values, so that past light cones of any two points on the CMB surface intersect (grey shaded area).

If $w < -1/3$, when $t \to 0$, $\eta \to -\infty$ in Eq. (1.65), hence $\eta_{\rm BB} = -\infty$ and the size of the horizon given by Eq. (1.63) is infinite. This is the case displayed in the right panel of Fig. 1.12. The singularity $a = 0$ is pushed to the infinite past $\eta \to -\infty$, because $w < -1/3$ allows η to reach negative values. This is why in this case, there is no horizon problem. Actually when $w < -1/3$, the scale factor blows up in the infinite future $t \to \infty$ at $\eta = 0$. This is because in this case, we assume a phase of inflation ($w < -1/3$) which lasts for ever. In practice, inflation ends at some finite time $-1 \ll \eta_{\rm end} < 0$ and the surface $\eta = 0^-$ corresponds to the end of inflation, as displayed in Fig. 1.12.

This is why inflation succeeds in making the size of the horizon expand so much that it is sufficiently large at time of recombination to explain the current homogeneity of the Universe [90].

1.4.2. The Flatness Problem

The flatness problem is also a fine-tuning problem that arises from the observational constraint on $1 - \Omega_{\rm tot} = \Omega_{\mathcal{K}}$. When $\Omega_{\rm tot} = 1$ (or $\mathcal{K} = 0$), the Universe is globally flat, at the border line between a closed finite universe ($\Omega_{\rm tot} > 1$, or $\mathcal{K} = 1$) and an open, infinite universe ($\Omega_{\rm tot} < 1$ or $\mathcal{K} = -1$). Since $\mathcal{K}$ is a constant, the sign of $1 - \Omega_{\rm tot}$ cannot change during the cosmic evolution. Observational constraints put $\Omega_{\rm tot}^{(0)}$ well close to 1, $100\Omega_{\mathcal{K}}^{(0)} = -0.10^{+0.62}_{-0.65}$ at 95% [15]. However, $\Omega_{\rm tot} = 1$ is an unstable equilibrium point. In order for $\Omega_{\rm tot}$ to fall within the given constraints today, it had to be equal to 1 within an extremely high level of fine-tuning in the early Universe. The flatness problem [92, 93] is the puzzle of explaining why the early Universe exhibits such fine-tuning in the value of this parameter.

1.4.2.1. Formulation of the Problem

From the definition (1.33) of $\rho_{\rm cri}$ and of the rescaled variables Ω_i, the deviation from unity of the total rescaled energy density is given by

$$1-\Omega_{\rm tot}=\Omega_{\mathcal{K}}=\frac{1}{1+\dfrac{\sum\Omega_i}{\Omega_{\mathcal{K}}}}\,. \tag{1.66}$$

From table 1.1, let us remember that $\Omega_{\rm rad}\propto a^{-4}$ and $\Omega_{\mathcal{K}}\propto a^{-2}$. This is why, when evaluating this quantity in the early Universe where radiation is the dominant constituent ($\sum\Omega_i\simeq\Omega_{\rm rad}$), one obtains

$$1-\Omega_{\rm tot}\simeq\frac{1}{1+\dfrac{\Omega_{\rm rad}^{(0)}}{1-\Omega_{\rm tot}^{(0)}}\left(\frac{a_0}{a}\right)^2}\simeq\frac{1-\Omega_{\rm tot}^{(0)}}{\Omega_{\rm rad}^{(0)}}\left(\frac{1}{1+z}\right)^2\,. \tag{1.67}$$

If one takes $\left|\Omega_{\mathcal{K}}^{(0)}\right|\simeq10^{-3}$ and $\Omega_{\rm rad}^{(0)}\simeq10^{-4}$ (according to the values given in section 1.2), one obtains $|1-\Omega_{\rm tot}|\simeq10^{-15}$ for $z\simeq10^{10}$ and $|1-\Omega_{\rm tot}|\simeq10^{-55}$ for $z=z_{\rm GUT}\simeq10^{28}$. As a consequence, one can see that the deviation from a flat universe $|1-\Omega_{\rm tot}|$ has to be fine-tuned to a tiny value at early time in order to explain the current flatness of the Universe. This is the so-called flatness problem [92, 93].

1.4.2.2. Inflation as a Solution to the Flatness Problem

As for the horizon problem, a possible explanation consists in adding a new phase which interrupts the radiation epoch between two times $t_{\rm in}$ and $t_{\rm end}$, and where the Universe content is dominated by an ideal fluid X with equation of state w_X. Let us calculate the initial deviation from flatness $|1-\Omega_{\rm tot}|$ required in this new scenario, sketched by Eq. (1.53). Similarly to Eq. (1.67), during this phase, one has

$$1-\Omega_{\rm tot}^{\rm end}=\frac{1}{1+\dfrac{\Omega_X^{\rm in}}{1-\Omega_{\rm tot}^{\rm in}}\left(\dfrac{a_{\rm end}}{a_{\rm in}}\right)^{-1-3w_X}}\,. \tag{1.68}$$

The purpose of this new phase is that starting from a sizable value of $1-\Omega_{\rm tot}^{\rm in}$, it should drive this quantity to a tiny value, $1-\Omega_{\rm tot}^{\rm end}$. Since $a_{\rm end}/a_{\rm in}\gg1$, this is achieved provided $-1-3w_X>0$, that is $w_X<-1/3$, exactly the same condition (1.60) as the one coming from the horizon problem and characterizing an inflationary phase where the expansion is accelerating.

More precisely, let us calculate the minimum number of e-folds $N=\ln(a_{\rm end}/a_{\rm in})$ required to solve the flatness problem. Relating $1-\Omega_{\rm tot}^{\rm end}$ to $1-\Omega_{\rm tot}^{(0)}$ thanks to Eq. (1.67), it is straightforward to write

$$N=\frac{1}{1+3w_X}\ln\left[\frac{\Omega_X^{\rm in}}{1-\Omega_{\rm tot}^{\rm in}}\frac{1-\Omega_{\rm tot}^{(0)}}{\Omega_{\rm rad}^{(0)}}\left(\frac{1}{1+z_{\rm end}}\right)^2\right]\,. \tag{1.69}$$

To avoid initial fine-tuning of the Universe flatness, one takes $\Omega_X^{\rm in}\propto1-\Omega_{\rm tot}^{\rm in}$, so that the flatness problem is solved provided

$$N\gtrsim-\frac{2}{1+3w_X}\ln\left[z_{\rm end}\sqrt{\frac{\Omega_{\rm rad}^{(0)}}{\left|1-\Omega_{\rm tot}^{(0)}\right|}}\right]\,. \tag{1.70}$$

Note that the similarity with Eq. (1.61) is striking. More precisely, from the values for $\Omega_i^{(0)}$ given in table 1.2, the pre-factors in front of $z_{\rm end}$ in the logarithms of Eqs. (1.61) and (1.70) are such that $4\pi/\sqrt{z_{\rm eq}} \sim \sqrt{\Omega_{\rm rad}^{(0)}/(1-\Omega_{\rm tot}^{(0)})}$. Therefore, the values of $N_{\rm min}$ displayed in Fig. 1.11 are such that the flatness problem is also solved.

Let us try to understand more intuitively why it is so. The flatness problem arises because curvature energy density decays slower than the one of matter or radiation. Therefore, if it is small today, it must have been even smaller before. The only way to escape from this fine-tuning issue is to have some phase during which the energy density decays even smaller than curvature. Since $w_{\mathcal{K}} = -1/3$ (see table 1.1), this implies that this phase is driven by a new fluid the equation of state parameter of which is such that $w_X < -1/3$. When this new component dominates the Universe content, curvature decays faster than this new fluid, and is therefore dynamically driven to very small values. If the energy content of this new component X is then transferred to radiation, curvature is automatically subdominant with respect to radiation at the end of this new phase, in a sufficiently large extent provided the duration of inflation N is large enough.

1.4.3. The Monopole Problem

In Grand Unified Theories [94, 95, 96] (GUT), local symmetry under some simple symmetry group is spontaneously broken at an energy $M_{\rm GUT} \simeq 10^{16}$ GeV to the gauge symmetry of the Standard Model under the group $SU(3) \times SU(2) \times U(1)$. In all such cases, the field that breaks the symmetry can be left in twisted configurations that carry non-zero magnetic charge. These topological glitches in the vacuum configuration of gauge fields are magnetic monopoles [97, 98]. Such monopoles are expected to be copiously produced in Grand Unified Theories at high temperature [99, 100], and they should have persisted to the present day, to such an extent that they would become the primary constituent of the Universe [101, 102]. Not only is that not the case, but all searches for them have so far turned out fruitless, placing stringent limits on the density of relic magnetic monopoles in the Universe [103, 104, 105, 106, 107, 108]. These searches show that at present time, monopoles must be typically fewer than $\sim 10^{-30}$ per nucleon.

1.4.3.1. Formulation of the Problem

Let us estimate the current monopole density, in the standard cosmological model sketched in Eq. (1.38). At time $t_{\rm GUT}$ of GUT phase transition, the field that dynamically realizes the symmetry breaking cannot be correlated at length larger than the causal horizon. Therefore, when created, the mean distance $D_{\rm mon}$ between two neighbor monopoles must be smaller than $d_{\rm H}(t_{\rm GUT})$. If monopoles do not find each other to annihilate, this distance is stretched to the current $D_{\rm mon}^{(0)} = a_0/a_{\rm GUT}\, d_{\rm H}(t_{\rm GUT})$. Using Eq. (1.46) to express the horizon distance, one obtains

$$D_{\rm mon}^{(0)} = \int_{t_{\rm BB}}^{t_{\rm GUT}} \frac{{\rm d}t}{a/a_0}\,. \tag{1.71}$$

Making use of Eq. (1.38), this integral can easily be calculated (since the GUT phase transition occurs at energies larger than the one at equivalence, one has $t_{\rm BB} < t_{\rm GUT} < t_{\rm eq}$), and one obtains

$$D_{\rm mon}^{(0)} = \frac{\sqrt{1+z_{\rm eq}}\,(1+z_{\rm acc})^{3/2}}{1+z_{\rm GUT}} H_0^{-1}\,. \tag{1.72}$$

In passing, the value $z_{\rm GUT} \sim 10^{28}$ that has been used so far and that we need here one more time can now be better justified. Indeed, GUT phase transition occurs when $\rho \sim M_{\rm GUT}^4$, hence $H_{\rm GUT} \sim M_{\rm GUT}^2/M_{\rm Pl} \sim 10^{13}$ GeV. During the radiation phase, the time behaviour of $H = \dot{a}/a$ can be calculated from Eq. (1.38), hence $t_{\rm GUT}$ can be expressed in terms of $H_{\rm GUT}$. Using again Eq. (1.38), one then has $a_{\rm GUT}$ in terms of $H_{\rm GUT}$ and in the limit where $z_{\rm GUT} > z_{\rm eq} \gg 1$, this gives rise to

$$z_{\rm GUT} \sim z_{\rm eq}^{1/4}\sqrt{\frac{H_{\rm GUT}}{H_0}} \sim 10^{28}\,. \tag{1.73}$$

This indeed corresponds to the value mentioned before.

Back to the current monopole density calculation, together with the values of $z_{\rm eq}$ and $z_{\rm acc}$ recalled in table 1.2, this allows us to evaluate Eq. (1.72) and one obtains $D_{\rm mon}^{(0)} \simeq 1$ m. Therefore, there should be abount one magnetic monopole per cube meter in our vicinity neighborhood.

In order to better understand this order of magnitude, let us calculate the corresponding rescaled monopole density $\Omega_{\rm mon}^{(0)}$. If the mass of each monopole is of the order $M_{\rm GUT}$, and remembering that the critical energy density is given by Eq. (1.33), this rescaled quantity is given by

$$\Omega_{\rm mon}^{(0)} = \frac{M}{3H_0^2M_{\rm Pl}^2\left[D_{\rm mon}^{(0)}\right]^3} \simeq 10^{15}\,. \tag{1.74}$$

Magnetic monopoles should therefore be the dominant constituent of our current Universe, which is in obvious contradiction with observations. To estimate how far we are from the observational constraints mentioned above (namely less than a monopole per 10^{30} nucleon), one can also calculate the ratio of monopole and nucleon number densities η,

$$\frac{\eta_{\rm mon}^{(0)}}{\eta_{\rm nucl}^{(0)}} = \frac{\Omega_{\rm mon}^{(0)}}{\Omega_{\rm m}^{(0)}}\frac{m_{\rm nucl}}{M_{\rm GUT}} \simeq 5\,, \tag{1.75}$$

where we have assumed that visible cold matter is essentially made of nucleons, and where we have taken the mass of nucleons to be of the order of $m_{\rm nucl} \simeq 938$ MeV. As a consequence, there should be $\mathcal{O}(1)$ magnetic monopole per nucleon, while observations establish that there is less than a monopole per 10^{30} nucleon. This is the so-called monopole problem. Obviously, since magnetic monopoles are supposed to be produced at very high energy where particle physics remains elusive, one can always imagine that the associated symmetry breakings do not occur. However, another elegant solution is again to add a phase of inflation.

1.4.3.2. Inflation as a Solution to the Monopole Problem

If a phase of inflation is added after the GUT phase transition, one may hope to dilute monopoles to such an extent that they would not be visible today. In this case, Eq. (1.71) still applies, but the integral now has to be calculated with Eq. (1.53). Since the GUT phase transition occurs before inflation, one has $t_{\rm BB} < t_{\rm GUT} < t_{\rm in}$ and one obtains

$$D_{\rm mon}^{(0)\,\prime} = \frac{\sqrt{1+z_{\rm eq}}\,(1+z_{\rm acc})^{3/2}}{1+z_{\rm GUT}}H_0^{-1}{\rm e}^{(1-3w_X)\frac{N}{2}}\,, \tag{1.76}$$

where again, N is the amount of e-folds during inflation. Several comments are in order. First, one notices that at first sight, the standard result (1.72) is only modified by the exponential term. When $w_X = 1/3$ or $N = 0$, as before, the standard result (1.72) is recovered. However, the

value of $z_{\rm GUT}$ is actually also modified since the derivation of Eq. (1.73) relies on the standard scenario (1.38). Using this time the modified scheme (1.53) in the calculation of $z_{\rm GUT}$, one obtains

$$z_{\rm GUT} \sim z_{\rm eq}^{1/4}\sqrt{\frac{H_{\rm GUT}}{H_0}}\mathrm{e}^{(1-3w_X)\frac{N}{4}}\,. \tag{1.77}$$

Here also, the standard result is modified by an exponential term, and $z_{\rm GUT}$ actually also depends on the number of e-folds realized during inflation. Plugging back this expression into Eq. (1.76), one finally obtains

$$D^{(0)}_{\rm mon} \simeq z_{\rm eq}^{1/4}\sqrt{\frac{H_0}{H_{\rm GUT}}}H_0^{-1}\mathrm{e}^{(1-3w_X)\frac{N}{4}}\,. \tag{1.78}$$

From here, one can see that the condition on w_X for the new phase to provide a possible solution to the monopole problem is $w_X < 1/3$. This condition is less stringent than the one arisen from the horizon and flatness problems, $w_X < -1/3$. Here, a phase of more rapid expansion than the one driven by radiation is sufficient, and acceleration in itself is a priori not a necessary condition. Obviously, this also depends on the number of inflationary e-folds N.

Let us see which typical numbers of e-folds are required. A first strong requirement would be that there is no magnetic monopole in our entire observable Universe. Since we cannot see beyond the last scattering surface, its size is given by $d_{\rm obs} = a_0 r_{\rm lss} = a_0\int_{t_{\rm lss}}^{t_0}\mathrm{d}t/a$. This integral can be computed making use of Eq. (1.53), and one obtains $d_{\rm obs} \simeq 2/H_0$. This confirms that as mentioned in section 1.1.1 the size of the observable Universe is of the order of the Hubble length. Therefore, requiring that $D^{(0)}_{\rm mon} > d_{\rm obs}$ leads to

$$N > \frac{2}{1-3w_X}\ln\left(\frac{H_{\rm GUT}}{H_0}\sqrt{\frac{2}{z_{\rm eq}}}\right)\,. \tag{1.79}$$

With the values recalled in table 1.2 for $z_{\rm eq}$, $H_{\rm GUT}$ and H_0, one typically obtains $N > 61$ for $w_X = -1$ or $N > 246$ for $w_X = 0$. A less strict requirement is just to meet the observational constraint on $\eta^{(0)}_{\rm mon}/\eta^{(0)}_{\rm nucl}$. This ratio can be calculated as in Eq. (1.75), and one obtains

$$N > \frac{2}{1-3w_X}\ln\left\{\frac{H_{\rm GUT}}{H_0}\sqrt{\frac{1}{z_{\rm eq}}}\left(\frac{m_{\rm nucl}H_0}{3M_{\rm Pl}^2\Omega_{\rm m}}\right)^{2/3}\left[\frac{\eta^{(0)}_{\rm nucl}}{\eta^{(0)}_{\rm mon}}\right]^{2/3}_{\rm min}\right\}\,. \tag{1.80}$$

Using the same values as before together with $\eta^{(0)}_{\rm nucl}/\eta^{(0)}_{\rm mon} > 10^{30}$, this gives $N > 24.5$ for $w_X = -1$ or $N > 98$ for $w_X = 0$.

A last consistency check remains to be done. Indeed, in order for a phase with $w < 1/3$ to solve the monopole problem, its e-folds must be realized after the GUT scale transition and before, say, the equivalence time. One should make sure that there is enough time between these two times for this new phase to proceed, that is

$$\frac{1+z_{\rm in}}{1+z_{\rm end}} < \frac{1+z_{\rm GUT}}{1+z_{\rm eq}}. \tag{1.81}$$

The left hand side of the previous relation is simply given by e^N, while $z_{\rm GUT}$ appearing in the right hand side depends on N through Eq. (1.77). This is why the previous relation translates into a constraint on N itself, which reads

$$N < \frac{2}{3\,(1+w_X)}\ln\left(\frac{H_{\rm GUT}}{H_0}z_{\rm eq}^{-3/4}\right)\,. \tag{1.82}$$

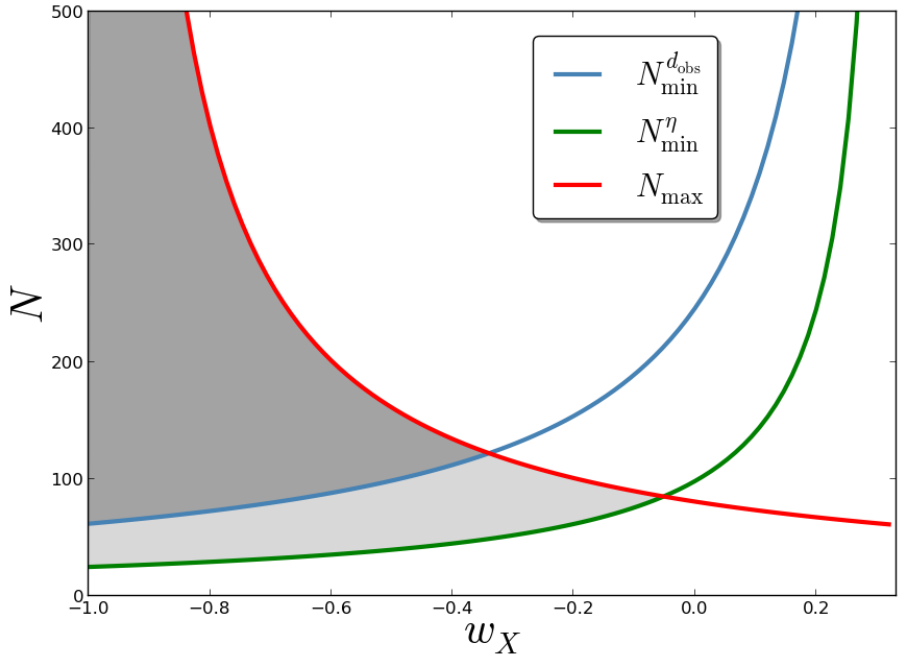

Figure 1.13.: Number of inflationary e-folds required to solve the monopole problem, as a function of w_X. The blue line stands for the minimum number of e-folds in order to dilute the monopoles further than our observable Universe and corresponds to Eq. (1.79). The green line stands for the minimum number of e-folds in order to dilute the monopoles so that the experimental constraint on $\eta_{\rm nucl}/\eta_{\rm mon}$ is satisfied and corresponds to Eq. (1.80). Finally, the red line stands for the maximum number of e-folds between the GUT phase transition and equivalence and corresponds to Eq. (1.82). The shaded areas correspond to when both constraints $N > N_{\rm min}$ and $N < N_{\rm max}$ are satisfied, the darker area being when the stricter constraint on the presence of monopoles in our observable Universe is used. The parameter values used here are the ones of table 1.2.

Obviously, a viable scenario is when Eqs. (1.79) and (1.82) [or Eqs. (1.80) and (1.82)] are satisfied at the same time. Such bounding values of N are displayed in Fig. 1.13. The shaded area stands for values of w_X and N such that both constraints are simultaneously satisfied. Since the maximal value for N given by Eq. (1.82) blows up when $w_X \to -1$, it is always possible to solve the monopole problem, provided w_X is close enough to -1. More precisely, if the criterion (1.80) is adopted, one obtains $w_X < -0.052$, whereas if the criterion (1.79) is adopted, one obtains $w_X < -0.34$. It is remarkable that this last condition is very similar to the one $w_X < -1/3$ that comes from the horizon and flatness problems. Therefore, even for the monopole problem, an accelerating phase seems to be required.

1.A. FLRW Christoffel symbols, Einstein tensor and Geodesics

In this appendix, we give the Christoffel symbols and the Ricci and Einstein tensors of the FLRW metric, and comment on the geodesic equations in comoving coordinate. Starting from the FLRW metric (1.1),

$$\mathrm{d}s^2 = g_{\mu\nu}\mathrm{d}x^\mu \mathrm{d}x^\nu = -\mathrm{d}t^2 + a^2(t)\left[\frac{\mathrm{d}r^2}{1-\mathcal{K}r^2} + r^2\left(\mathrm{d}\theta^2 + \sin^2\theta \mathrm{d}\phi^2\right)\right], \tag{1.83}$$

the Christoffel symbols are formally given by

$$\Gamma^\rho_{\mu\nu} = \frac{1}{2}g^{\rho\lambda}\left(\partial_\nu g_{\lambda\mu} + \partial_\mu g_{\lambda\nu} - \partial_\lambda g_{\mu\nu}\right). \tag{1.84}$$

One can check that they are symmetrical in their lower indices, that is $\Gamma^\rho_{\mu\nu} = \Gamma^\rho_{\nu\mu}$. After a straightforward calculation, up to this symmetry, the only non vanishing Christoffel symbols of the FLRW metric are given by

$$\begin{aligned}
&\Gamma^0_{11} = \frac{a\dot{a}}{1-\mathcal{K}r^2}, && \Gamma^0_{22} = a\dot{a}r^2, \\
&\Gamma^0_{33} = a\dot{a}r^2\sin^2\theta, && \Gamma^1_{11} = \frac{\mathcal{K}r}{1-\mathcal{K}r^2}, \\
&\Gamma^1_{22} = -r\left(1-\mathcal{K}r^2\right), && \Gamma^1_{33} = -r\left(1-\mathcal{K}r^2\right)\sin^2\theta, \\
&\Gamma^2_{33} = -\sin\theta\cos\theta, && \Gamma^1_{01} = \Gamma^2_{02} = \Gamma^3_{03} = \frac{\dot{a}}{a}, \\
&\Gamma^2_{12} = \Gamma^3_{13} = \frac{1}{r}, && \Gamma^3_{23} = \cot\theta,
\end{aligned} \tag{1.85}$$

where index 0 is for time t, 1 is for r, 2 is for θ and 3 is for ϕ. The Ricci tensor is formally expressed as

$$R_{\mu\nu} = 2\Gamma^\rho_{\mu[\nu,\rho]} + 2\Gamma^\rho_{\lambda[\rho}\Gamma^\lambda_{\nu]\mu}, \tag{1.86}$$

where the brackets mean anti-symmetrization under the indices. From the Christoffel symbols (1.85), one can check that its non-zero components are the diagonal ones, given by

$$\begin{aligned}
&R_{00} = -3\frac{\ddot{a}}{a}, && R_{11} = \frac{a\ddot{a} + 2\dot{a}^2 + 2\mathcal{K}}{1-\mathcal{K}r^2}, \\
&R_{22} = r^2\left(a\ddot{a} + 2\dot{a}^2 + 2\mathcal{K}\right), && R_{33} = r^2\left(a\ddot{a} + 2\dot{a}^2 + 2\mathcal{K}\right)\sin^2\theta.
\end{aligned} \tag{1.87}$$

The Ricci curvature scalar is just the contraction of the Ricci tensor with the metric, $R = g^{\mu\nu}R_{\mu\nu}$, and is given by

$$R = 6\left[\left(\frac{\dot{a}}{a}\right)^2 + \frac{\ddot{a}}{a} + \frac{\mathcal{K}}{a^2}\right]. \tag{1.88}$$

Finally, the Einstein tensor $G_{\mu\nu} = R_{\mu\nu} - R/2g_{\mu\nu}$ has non vanishing components

$$\begin{aligned}
&G_{00} = 3\left[\left(\frac{\dot{a}}{a}\right)^2 + \frac{\mathcal{K}}{a^2}\right], && G_{11} = -\left[\left(\frac{\dot{a}}{a}\right)^2 + 2\frac{\ddot{a}}{a} + \frac{\mathcal{K}}{a^2}\right]\frac{a^2}{1-\mathcal{K}r^2}, \\
&G_{22} = -\left[\left(\frac{\dot{a}}{a}\right)^2 + 2\frac{\ddot{a}}{a} + \frac{\mathcal{K}}{a^2}\right]a^2r^2, && G_{33} = -\left[\left(\frac{\dot{a}}{a}\right)^2 + 2\frac{\ddot{a}}{a} + \frac{\mathcal{K}}{a^2}\right]a^2r^2\sin^2\theta.
\end{aligned} \tag{1.89}$$

One can check that this matches the formula (1.14) given in section 1.1.1.3.

Finally, it is interesting to say a few words about the geodesic equation

$$\frac{\mathrm{d}^2 x^\mu}{\mathrm{d}s^2} + \Gamma^\mu_{\nu\rho} \frac{\mathrm{d}x^\nu}{\mathrm{d}s} \frac{\mathrm{d}x^\rho}{\mathrm{d}s} = 0\,. \tag{1.90}$$

Because the FLRW geometry is isotropic with respect to every point, it is always possible to chose a local coordinate system such that a given geodesic initially has a purely radial part, that is $\mathrm{d}\theta/\mathrm{d}s = \mathrm{d}\phi/\mathrm{d}s = 0$ at initial time. Then it is straightforward to see that the geodesic equations for θ and ϕ [$\mu = 2$ or 3 in Eq. (1.90)] imply that it remains so at any later time. In this case, the geodesic equations for t and r are

$$\frac{\mathrm{d}^2 t}{\mathrm{d}s^2} + \frac{a\dot{a}}{1-\mathcal{K}r^2}\left(\frac{\mathrm{d}r}{\mathrm{d}s}\right)^2 = 0\,, \tag{1.91}$$

$$\frac{\mathrm{d}^2 r}{\mathrm{d}s^2} + \frac{\mathcal{K}r}{1-\mathcal{K}r^2}\left(\frac{\mathrm{d}r}{\mathrm{d}s}\right)^2 + 2\frac{\dot{a}}{a}\frac{\mathrm{d}t}{\mathrm{d}s}\frac{\mathrm{d}r}{\mathrm{d}s} = 0\,. \tag{1.92}$$

One can check that a static particle such that $\mathrm{d}t/\mathrm{d}s = 1$ and $\mathrm{d}r/\mathrm{d}t = 0$ is a solution of the above system, which means that still particles in the comoving coordinate system are indeed solutions of the geodesic equations. If one is interested in the more general trajectory $r(t)$ associated with this system, one can work out its solution as

$$\frac{\mathrm{d}t}{\mathrm{d}s} = \left[1 + \left(\frac{b_0}{a}\right)^2\right]^{1/2}\,, \tag{1.93}$$

$$\frac{\mathrm{d}r}{\mathrm{d}s} = \sqrt{1-\mathcal{K}r^2}\frac{b_0}{a^2}\,, \tag{1.94}$$

where b_0 is an integration constant that depends on initial conditions (for example, $b_0 = 0$ for still particles and $b_0 = \infty$ for photons). From here, the physical impulsion p can be obtained,

$$\frac{p}{m} = \sqrt{g_{ij}\frac{\mathrm{d}x^i}{\mathrm{d}s}\frac{\mathrm{d}x^j}{\mathrm{d}s}} = \frac{a}{\sqrt{1-\mathcal{K}r^2}}\frac{\mathrm{d}r}{\mathrm{d}s} = \frac{b_0}{a}\,, \tag{1.95}$$

which confirms the rule $p \propto 1/a$ otherwise derived in section 1.1.1.2. More precisely, the solution for $\mathrm{d}r/\mathrm{d}t$ is given by

$$\frac{\mathrm{d}r}{\mathrm{d}t} = \sqrt{1-\mathcal{K}r^2}\frac{b_0}{a^2}\left[1 + \left(\frac{b_0}{a}\right)^2\right]^{-1/2}\,, \tag{1.96}$$

which means that as time proceeds and a increases (in an expanding universe), $\mathrm{d}r/\mathrm{d}t \propto 1/a^2 \to 0$ for massive particles. Therefore, massive particles asymptotically come to rest relative to the comoving coordinate system, as mentioned in section 1.1.1.2. More precisely, $\mathrm{d}r/\mathrm{d}t \propto 1/a^2$ means that r reaches a finite value in the asymptotic future if a grows strictly faster than $a \propto \sqrt{t}$. This is the case in a matter era, an inflationary era or a dark energy era, but not during a radiation era where $\mathrm{d}r/\mathrm{d}t \to 0$ but $r \to \infty$ if $\mathcal{K} = 0$ or -1 and $r \to 1$ if $\mathcal{K} = 1$.

To be explicit, once the $a(t)$ profile known [see for example Eq. (1.30)], one can calculate

$$r\,(t) = r_{\mathrm{in}} + \begin{cases} \sin\left(\mathcal{I}\right) & \text{if } K = 1 \\ \mathcal{I} & \text{if } K = 0 \\ \sinh\left(\mathcal{I}\right) & \text{if } K = -1 \end{cases}\,, \tag{1.97}$$

where $\mathcal{I}$ is given by

$$\mathcal{I} = b_0 \int_{t_{\rm in}}^{t} \frac{\mathrm{d}\tilde{t}}{a^2 \sqrt{1 + \left(\frac{b_0}{a}\right)^2}} \,. \tag{1.98}$$

Finally, let us mention that for massless particles ($b_0 = \infty$), Eq. (1.98) gives $\mathcal{I} = \int \mathrm{d}t/a$, which is in agreement with Eq. (1.5).

1.B. Numerical Values of Cosmological Parameters

Physical Quantity	**Numerical Value**
M_{Pl}	2.435×10^{18} GeV
H_0	67.3 km/sec/Mpc
H_0^{-1}	4.55×10^{17} sec
H_0^{-1}	1.36×10^{26} m
w_{dm}	0
w_{mat}	0
w_{rad}	$1/3$
$w_{\mathcal{K}}$	$-1/3$
w_{Λ}	-1
$\Omega_{\mathrm{rad}}^{(0)}$	9.3×10^{-5}
$\Omega_{\mathrm{b}}^{(0)}$	0.049
$\Omega_{\mathrm{dm}}^{(0)}$	0.268
$\Omega_{\mathrm{de}}^{(0)}$	0.683
$\lvert\Omega_{\mathcal{K}}\rvert$	$\lesssim 10^{-3}$
z_{acc}	0.29
z_{lss}	1090
z_{eq}	3402
z_{GUT} (without inflation)	10^{28}
M_{GUT}	10^{16} GeV
H_{GUT}	10^{13} GeV

Table 1.2.: Numerical values of cosmological parameters used in section 1.

2. Cosmological Inflation

In this chapter, we review some aspects of cosmological inflation, the physical setups it relies on, the predictions it makes and the fundamental issues it raises. Our purpose is mainly to provide the reader with an understanding of the theoretical and technical tools used in part II where the results obtained during this thesis are presented. This is why in this section, only a brief overview of the physics of inflation is given, the various aspects of which are further detailed in a broad range of textbooks [109, 110, 111, 4, 112, 113, 7, 8].

In chapter 1, we reviewed the cornerstones of the cosmological hot big bang model and the problems it raises. In particular, in section 1.4, we saw that a phase of inflation during which the scale factor accelerates $\ddot{a} > 0$ can solve the hot big bang problems if it occurs prior to (or during) the radiation era [91, 114, 115, 116, 117, 118, 119]. However, we have not discussed which kind of matter component can drive such a phase of inflation. From the the Raychaudhuri equation (1.18), $\ddot{a} > 0$ implies that $\rho + 3p < 0$, hence the pressure must necessarily be negative. One therefore needs to find a physical system able to produce such a negative pressure.

The inflationary phase takes place at very high energy, typically between 10^3 and 10^{15} GeV [120]. At such high energies, field theory is the relevant framework to describe matter, and a natural way to try and realize inflation is therefore to consider that a real scalar field ϕ (dubbed the "inflaton" field) dominates the energy density budget of matter in the early Universe. Moreover, this assumption is compatible with the observed homogeneity, isotropy and flatness of the early Universe. Quite remarkably, it turns out that if the potential $V(\phi)$ of this scalar field is sufficiently flat $\mathrm{d}V/\mathrm{d}\phi \ll V/M_{\mathrm{Pl}}$ so that the field moves slowly, then the corresponding pressure is negative. This is why it is believed that inflation is driven by one (or several) scalar field(s). However, the physical nature of the inflaton and its relation with the standard model of particle physics and its extensions is still unclear. This is not surprising since the inflationary mechanism takes place at energy scales where particle physics remains elusive and has not been tested in accelerators. This is why the shape of its potential is *a priori* not known except that is must be sufficiently flat to support a phase of inflation.

Nonetheless, one of the great achievements of inflation is that, combined with quantum mechanics, it provides a convincing mechanism for the origin of the cosmological fluctuations, the seeds of the CMB anisotropies and of the galaxies. Inflation predicts that their spectrum should be almost scale invariant (*i.e.* equal power on all spatial scales) [121, 122, 123, 124, 125, 126, 127, 128, 129, 130], which is fully consistent with the observations. In passing, this part of the scenario is particularly remarkable since it makes us of General Relativity and Quantum Mechanics [131, 132, 133, 134, 135, 136, 137, 138, 139, 138], two theories that are notoriously difficult to combine. In fact, inflation is probably the only case in physics where an effect based on General Relativity and Quantum Mechanics leads to predictions that, given our present day technological capabilities, can be tested experimentally. Given the confirmation of these predictions by observations and given the fact that, despite many efforts, inflation has not been superseded by its various challengers [140, 29, 141, 27, 142, 143, 144, 145, 146, 147, 148, 149,

150, 31, 34, 151, 152, 153, 154, 32, 155, 156, 157, 158, 159, 160, 161, 162], this scenario has gradually become a crucial part of modern cosmology.

What strongly motivates the investigation of the inflationary period is that there is now a flow of increasingly accurate astrophysical data which gives us a unique opportunity to learn more about inflation. In particular, the recently released Planck satellite data [76, 163, 15], and if confirmed to be of primordial origin, the B-mode detection by the BICEP2 experiment [164], play a crucial role in this process. These missions complement and improve upon observations made by the NASA WMAP satellite [165, 166] and are a major source of information relevant to several cosmological issues including inflation [167, 168]. The CMB small angular scales of Planck are already complemented by ground-based microwave telescopes such as the Atacama Cosmology Telescope [169, 170] or the South Pole Telescope [171, 172] while ultra-sensitive polarization dedicated experiments are on their way [173, 174, 175, 176, 177, 178].

Let us also mention that even if this is what we focus on in this thesis, the flow of new data does not only concern the CMB. The supernovae projects [179, 180, 181, 182] continue to measure the distances to the nearby exploding SN1A stars while the large scale galaxy surveys such as the Sloan Digital Sky Survey (SDSS) [183, 184] are providing an unprecedented picture of the structure of the universe. The "lever arm" in length scales between CMB and galaxy power spectra increases the sensitivity to the small deviations from scale invariance, and thus should be extremely powerful to constrain inflationary models. For this reason, the future Euclid satellite will be another step forward in our understanding of inflation [185]. The possibility of direct detection of the primordial gravitational waves is also currently discussed for high energy inflationary models on large scales [186, 187, 188, 189, 190, 191, 192, 193, 194, 195] and also on small scales [196, 197]. Finally, in a foreseeable future, the yet unexplored length scales are expected to be unveiled by the 21 cm cosmological telescopes. These ones will be sensitive to the redshifted 21 cm line absorbed by hydrogen clouds before the formation of galaxies [198, 199, 200, 201, 202, 203, 204]. With such data, we will have a complete tomography of the universe history from the time of CMB emission at the surface of last scattering to the distribution of galaxies today.

Our ability to see through the inflationary window is crucial since it turns the early universe into a laboratory for ultra-high energy physics, at scales entirely inaccessible to conventional experimentation. In other words, this window offers a unique opportunity to learn about the very early universe and about physics in a regime that cannot be tested otherwise, even in accelerators such as the Large Hadron Collider. In this chapter, we discuss a few aspects that play a key role in this enterprise, and we introduce some of the theoretical and technical tools that are widely used in part II where the results of this thesis are presented. It is organized as follows. In section 2.1, we explain why and under which conditions a single scalar field can support a phase of inflation. In section 2.2, we present a frame of approximation, the "slow-roll approximation", which enables to solve its dynamics perturbatively. It also provides us with a convenient scheme of calculation to compare inflationary predictions with observational data, which we make widely use of in Ref. [205], section 3.2, in Ref. [206], section 3.3 and in Ref. [207], section 3.4. The slow-roll inflationary trajectories are also the subject of Ref. [208], section 3.1, and for this reason it seems important to review the main aspects of this formalism in the present chapter. Then, in section 2.3, we turn to the description of inflationary perturbations. We show how cosmological perturbations need to be quantized, and for illustrative purpose, we provide a detailed calculation of the power spectrum of scalar perturbations. Since such a calculation is modified when extensions to standard quantum mechanics are included in Ref. [138], section 4.3, it is important to first understand how it proceeds in the standard approach. We then specify the obtained result at leading order in the slow-roll approximation. Indeed, in Ref. [209], section 3.5,

this calculation is extended to next-to-leading order in slow roll, and it is generalized in the case where not only the potential but also the kinetic term is a free function. This is why details of the calculation for the leading order in slow roll with canonical kinetic term for the inflaton field may be useful to get acquainted with the employed technique. Finally, in section 2.4, we devote a large part of this introductory chapter to the presentation of the stochastic inflation formalism which is used in Ref. [210], section 4.1 and in Ref. [211], section 4.2. We first present a detailed heuristic derivation of the Langevin equation which is at the heart of this formalism. This allows us to discuss its nature and the assumptions it rests on. Then, we turn to the question of the time variable that should be used when solving such equations, in order to reproduce results from Quantum Field Theories (QFT). Lastly, we address the issue of the calculation of physical observable quantities in stochastic inflation, such as the power spectrum of adiabatic perturbations. We show that the stochastic setup allows us to reproduce the standard result of section 2.3, before providing complete solutions which do not rely on an expansion in the noise term. To our knowledge, this is the first time such a non perturbative calculation of the power spectrum in stochastic inflation is presented, and we plan to further discuss it in a forthcoming article.

2.1. Single-Field Inflation

What makes the inflationary idea quite natural is that the negative pressure condition can simply be met with a single scalar field ϕ, the inflaton field, minimally coupled to gravity. The action of such a system is given by

$$S_\phi = -\int \mathrm{d}^4x\sqrt{-g}\left[\frac{1}{2}g^{\mu\nu}\partial_\mu\phi\partial_\nu\phi + V(\phi)\right]. \tag{2.1}$$

The function $V(\phi)$ is a potential term for the scalar field, that is left unspecified for the moment. Indeed, the physical nature of the inflaton field is still unknown (there are many candidates) and, as a consequence, $V(\phi)$ can have different shapes. From Eq. (1.12), the energy-momentum tensor associated with this action can be derived, and one obtains

$$T^{(\phi)}_{\mu\nu} = \partial_\mu\phi\partial_\nu\phi + g_{\mu\nu}\left[-\frac{1}{2}g^{\rho\sigma}\partial_\rho\phi\partial_\sigma\phi + V(\phi)\right]. \tag{2.2}$$

At the background level, since FRLW space-times are homogeneous and isotropic, ϕ must be homogeneous as well and can only depend on time. Interestingly enough, in such a case, the energy-momentum tensor can be expressed in the form of Eq. (1.15) if one lets

$$\rho = \frac{\dot\phi^2}{2} + V, \tag{2.3}$$

$$p = \frac{\dot\phi^2}{2} - V. \tag{2.4}$$

As a consequence, for an homogeneous scalar field, the condition for the acceleration of the scale factor is fulfilled, $\rho + 3p < 0$, as soon as

$$V > \dot\phi^2. \tag{2.5}$$

This is the condition for inflation to take place. This means that inflation can be obtained provided the inflaton slowly rolls down its potential, so that its potential energy dominates over its kinetic energy. This also shows that the inflaton potential must be sufficiently flat,

a requirement which is not always easy to obtain in realistic situations and which makes the inflationary model building problem a difficult issue [212].

The dynamics of ϕ can be obtained if one plugs the expressions (2.3) and (2.4) into the conservation equation (1.16). Doing so, one gets the Klein-Gordon equation

$$\ddot{\phi} + 3H\dot{\phi} + V' = 0\,, \tag{2.6}$$

where a prime denotes a derivative with respect to ϕ. On the other hand, the Friedmann equation (1.17) gives rise to

$$3M_{\rm Pl}^2 H^2 = V + \frac{\dot{\phi}^2}{2}\,. \tag{2.7}$$

This last quantity is important since it sets the energy scale at which inflation takes place. In section 2.3, we will see that its measurement requires to detect primordial gravity waves. Without such a detection, one can only constrain $\rho^{1/4} \propto \sqrt{M_{\rm Pl}H}$ to be between the Grand Unified Theory (GUT) scale, that is to say $\sim 10^{15}\,$GeV, and $\sim 10^3\,$GeV [120]. However, if the measurement of the B mode polarization of the CMB by the BICEP2 experiment [164] is of primordial origin, the inflationary energy scale should lie close the GUT scale, see the discussion at the end of section 2.3.

The Klein-Gordon equation (2.6) and the Friedmann equation (2.7) form a closed system that can be integrated for any potential $V(\phi)$ and given initial conditions $\phi_{\rm in}$ and $\dot{\phi}_{\rm in}$. A few numerical solutions of this set of equations when $V(\phi) = m^2\phi^2/2$ are displayed in Fig. 2.1 for illustrative purpose. In this figure, the light blue area stands for the region where the condition (2.5) is fulfilled and where inflation takes place. One can see that even if the initial velocity of the inflaton field is too large, it is quickly damped to sufficiently small values so that inflation starts and proceeds. Then, at some point, the system exits the light blue area and inflation naturally stops. Subsequently, the field quickly oscillates at the bottom of the potential, the amplitude of these oscillations being damped due to the expansion, through the term $\propto H\dot{\phi}$ in Eq. (2.6). During this phase, possible coupling between ϕ and other fields can efficiently make the inflaton field parametrically decay into radiation, hence smoothly connecting inflation to the radiation-dominated epoch [213, 214, 215, 216, 217, 218, 219, 196, 220]. This is the so-called reheating period [221, 222, 223, 224, 225].

2.2. The Slow-Roll Approximation

Beyond the numerical solutions of Fig. 2.1, analytical solutions can also be obtained, in the limit where the condition (2.5) is saturated, that is when $V \gg \dot{\phi}^2$. In this limit, one has $p \simeq -\rho$, so that the conservation equation $\dot{\rho} = -3H(\rho + p)$ implies that ρ is almost constant in time. Thanks to the Friedmann equation (1.17), this means that $H = \dot{a}/a$ is almost constant in time too, which implies that space-time is close to the de Sitter universe for which

$$a\,(t) = a_{\rm in} \exp\left[H\,(t - t_{\rm in})\right]\,. \tag{2.8}$$

This is why it is interesting to derive solutions to Eqs. (2.6) and (2.7) in the limit[1] where the Universe is perturbatively close to the one of Eq. (2.8). The "slow-roll approximation" refers to this limit, in which the velocity of the inflaton is small $\dot{\phi} \ll \sqrt{V}$ and the field "slowly rolls" down its potential. At the technical level, the strategy is to define a set of parameters that quantify the deviation from de Sitter space-times, and to perform an expansion in these parameters.

[1] As will be shown in section 2.3.4, such an assumption can be justified *a posteriori*, *e.g.* by the fact that only small deviations from scale invariance are measured, with tight constraints on the level of gravity waves.

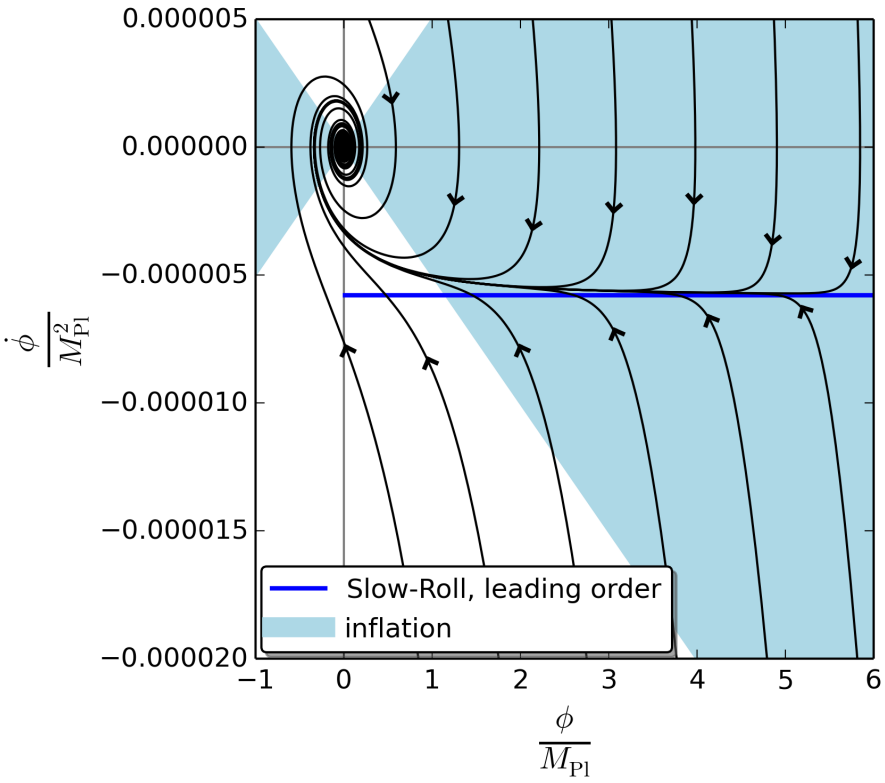

Figure 2.1.: Phase space diagram of the inflaton trajectory for $V = m^2\phi^2/2$, with $m \simeq 7 \times 10^{-6} M_{\rm Pl}$. The black lines correspond to numerical solutions of Eqs. (2.6) and (2.7) with different initial conditions. The arrows indicate in which direction the system evolves. The light blue area stands for the region in phase space where inflation proceeds, that is where the condition (2.5), $V > \dot{\phi}^2$, is fulfilled. Finally, the blue solid line displays the slow-roll trajectory at leading order $\dot{\phi} \simeq -V'/(3H)$, with $H^2 \simeq V/(3M_{\rm Pl}^2)$. One can see that as long as the slow-roll condition $V \gg \dot{\phi}^2$ is met (*i.e.* when one is well inside the light blue area), this trajectory represents an attractor solution.

2.2.1. The Slow-Roll Parameters

Although there are several possible sets of slow-roll parameters, here we choose to introduce the Hubble-flow parameters $\{\epsilon_n\}$ defined by the flow equations [226, 227]. If one lets $\epsilon_0 \equiv H_{\rm in}/H$, this parameter ϵ_0 is constant for a de Sitter space (and equal to 1), so that its time derivatives should be small in the limit we are interested in. This is why, labelling time with the number of e-folds $N \equiv \ln a$, starting from ϵ_0, one iteratively defines

$$\epsilon_{n+1} = \frac{\mathrm{d}\ln|\epsilon_n|}{\mathrm{d}N}\,. \tag{2.9}$$

In this hierarchy, all the ϵ_n are typically of the same order of magnitude. By definition, one has *slow-roll* inflation as long as $|\epsilon_n| \ll 1$, for all $n > 0$. For example, the first slow-roll parameter is given by $\epsilon_1 = -\dot{H}/H^2 = 1 - \ddot{a}/(aH^2)$, which implies that inflation ($\ddot{a} > 0$) takes place provided $\epsilon_1 < 1$.

2.2.2. The Slow-Roll Trajectory

Now, let us see how the system formed by Eqs. (2.6) and (2.7) can be solved perturbatively in the slow-roll limit. Inserting the Klein-Gordon equation in the time derivative of the Friedmann equation, one obtains $\dot{H} = -\dot{\phi}^2/(2M_{\rm Pl}^2)$, hence[2]

$$\epsilon_1 = -\frac{\dot{H}}{H^2} = 3\frac{\dot{\phi}^2/2}{V(\phi)+\dot{\phi}^2/2}\,. \tag{2.10}$$

The condition $\epsilon_1 \ll 1$ thus implies that the kinetic energy of the inflaton is much smaller than its potential energy, which is clearly the limit under study. Under this condition, the Friedmann equation simplifies and gives, at leading order in slow roll, $H^2 \simeq V/(3M_{\rm Pl}^2)$.

One can keep on and play the same game with ϵ_2. Inserting the Klein-Gordon equation (2.6) in the time derivative of the relation $\dot{H} = -\dot{\phi}^2/(2M_{\rm Pl}^2)$ previously obtained, one gets $\ddot{H} = 3H\dot{\phi}^2/M_{\rm Pl}^2 + \dot{\phi}V'/M_{\rm Pl}^2$, and

$$\epsilon_2 = \frac{\ddot{H}}{H\dot{H}} - 2\frac{\dot{H}}{H^2} = 6\left(\frac{\epsilon_1}{3} - \frac{V'}{3H\dot{\phi}} - 1\right)\,. \tag{2.11}$$

The condition $\epsilon_2 \ll 1$ thus implies that, at leading order in slow roll, $\dot{\phi} \simeq -V'/(3H)$, which means that the acceleration term can be neglected in the Klein-Gordon equation (2.6) (such a limit solution is displayed by the solid blue line in Fig. 2.1). This is particularly interesting since it lowers by one the order of the differential equation satisfied by ϕ. As a consequence, it removes the dependency on the initial conditions by singling out a specific trajectory in phase space, and it allows to derive analytical solutions in most cases.

More explicitly, since $\mathrm{d}N = H\mathrm{d}t$, at leading order in slow roll, the Klein-Gordon equation reads $\mathrm{d}N = -3H^2\mathrm{d}\phi/V'$. Plugging in the slow-roll leading order of the Friedmann equation $H^2_{\rm SR,LO} = V/(3M_{\rm Pl}^2)$, one obtains

$$\Delta N^{\rm SR,LO} = -\frac{1}{M_{\rm Pl}^2}\int_{\phi_{\rm in}}^{\phi_{\rm end}}\frac{V}{V'}\mathrm{d}\phi\,, \tag{2.12}$$

where $\Delta N \equiv N_{\rm end} - N_{\rm in}$, $\phi_{\rm in}$ is the value of ϕ at some initial time $N_{\rm in}$, and $\phi_{\rm end}$ is the value of ϕ at some final time $N_{\rm end}$. This represents the leading order (LO) of the slow-roll (SR) trajectory. Inverting this relation yields the value of ϕ as a function of time N.

If one worked at next-to-leading order in slow roll, see section 2.2.3, one would obtain a slightly modified trajectory, so on and so forth, and *the* slow-roll trajectory is by definition the limit towards which this perturbative process converges. It singles out a specific solution to Eqs. (2.6) and (2.7). It is worth mentioning that as can be seen in Fig. 2.1, this slow-roll trajectory is actually a powerful attractor [228] of the inflationary dynamics, that is to say, starting from a large basin of possible initial conditions $\phi_{\rm in}$ and $\dot{\phi}_{\rm in}$, the system quickly converges towards the slow-roll trajectory. This property makes the slow-roll scheme of approximation both convenient and physically well-motivated.

It is also interesting to remark that under the slow-roll approximation, the slow-roll hierarchy can easily be expressed in terms of V and its derivatives. Indeed, making use of Eq. (2.12), one

[2] Notice that with Eq. (2.10), Eqs. (2.3) and (2.4) give rise to $\omega = p/\rho = -1 + 2\epsilon_1/3$, which is consistent with what we displayed in table 1.1.

has

$$\left.\frac{\mathrm{d}}{\mathrm{d}N}\right|^{\mathrm{SR,LO}} = -M_{\mathrm{Pl}}^2 \frac{V'}{V}\frac{\mathrm{d}}{\mathrm{d}\phi}\,. \tag{2.13}$$

Repeatedly applying this identity starting from $\epsilon_0 = H_{\mathrm{in}}/H \simeq H_{\mathrm{in}}\sqrt{3M_{\mathrm{Pl}}^2/V}$, one obtains, at leading order in slow roll,

$$\epsilon_0^{\mathrm{LO}} = H_{\mathrm{in}}\sqrt{\frac{3M_{\mathrm{Pl}}^2}{V}}\,, \tag{2.14}$$

$$\epsilon_1^{\mathrm{LO}} = \frac{M_{\mathrm{Pl}}^2}{2}\left(\frac{V'}{V}\right)^2\,, \tag{2.15}$$

$$\epsilon_2^{\mathrm{LO}} = 2M_{\mathrm{Pl}}^2\left[\left(\frac{V'}{V}\right)^2 - \frac{V''}{V}\right]\,, \tag{2.16}$$

$$\epsilon_3^{\mathrm{LO}} = \frac{2M_{\mathrm{Pl}}^4}{\epsilon_2^{\mathrm{LO}}}\left[\frac{V'''V'}{V^2} - 3\frac{V''V'^2}{V^3} + 2\left(\frac{V'}{V}\right)^4\right]\,, \tag{2.17}$$

and the following slow-roll parameters can be computed in the same manner. One can see that as mentioned above, in order for the first slow-roll parameter to be small and for inflation to take place, the potential needs to be sufficiently flat, and more precisely its logarithm, $(\mathrm{d}/\mathrm{d}\phi)\ln V \ll 1/M_{\mathrm{Pl}}$.

2.2.3. Next-to-Leading Orders in Slow Roll

Most of the time, the leading order of the slow-roll trajectory is sufficiently accurate, but given the precision of observations, it can be useful (and sometimes necessary) to work at higher order in slow roll. Here we explain how the higher contributions can be derived, and as an example, we establish the next-to-leading order (NLO) and the next-to-next-to-leading order (NNLO) versions of the previous expressions. The starting point is to combine equations (2.7) and (2.10) into

$$H^2 = \frac{V}{3M_{\mathrm{Pl}}^2}\left(1 - \frac{\epsilon_1}{3}\right)^{-1}\,, \tag{2.18}$$

which is exact. Together with the Friedmann equation (2.7), this gives rise to $\dot\phi^2 = 2V\epsilon_1/(3-\epsilon_1)$. These two formulas allow us to recast $\mathrm{d}N = H\mathrm{d}\phi/\dot\phi$ as

$$\mathrm{d}N = \pm\frac{1}{M_{\mathrm{Pl}}}\frac{\mathrm{d}\phi}{\sqrt{2\epsilon_1}}\,, \tag{2.19}$$

which is again an exact relation. From here the slow-roll parameters at next-to-leading order can be obtained as follows. Rewriting Eq. (2.18) as $\epsilon_0 = \epsilon_0^{\mathrm{LO}}\sqrt{1-\epsilon_1/3}$, and iteratively applying

$$\left.\frac{\mathrm{d}}{\mathrm{d}N}\right|^{\mathrm{SR,NLO}} = \sqrt{\frac{\epsilon_1^{\mathrm{NLO}}}{\epsilon_1^{\mathrm{LO}}}}\left.\frac{\mathrm{d}}{\mathrm{d}N}\right|^{\mathrm{SR,LO}} \tag{2.20}$$

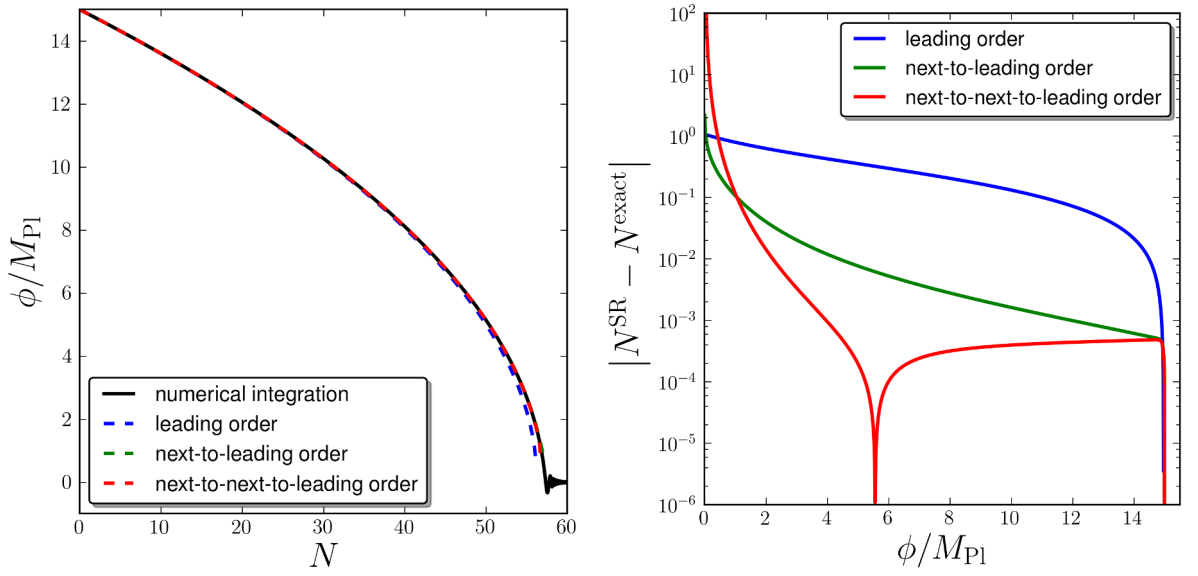

Figure 2.2.: Leading order, next-to-leading order and next-to-next-to leading order of the slow-roll trajectory for $V = m^2\phi^2/2$, with $m \simeq 7 \times 10^{-6} M_{\rm Pl}$. All the trajectories start at $\phi_{\rm in} = 15 M_{\rm Pl}$. In the left panel, the black solid line stands for the numerical solution of Eq. (2.6) where $\mathrm{d}\phi/\mathrm{d}N|_{\rm in}$ is set according to Eq. (2.12). The blue dashed line stand for the leading order slow-roll solution (2.12), the green dashed line stand for the next-to-leading order slow-roll solution (2.30), and the red dashed line stand for the next-to-next-to-leading order slow-roll solution (2.31). One can check that the slow-roll solutions are good approximations to the exact solution. More precisely, in the right panel, the distances from the slow-roll approximations to the exact solution is displayed at each order. Since ϕ decreases during inflation, this plot should be read from the right to the left. Each slow-roll solution is compared with the exact solution of Eq. (2.6) that shares the same initial condition $\mathrm{d}\phi/\mathrm{d}N|_{\rm in}$ at $N = 0$ and $\phi_{\rm in} = 15 M_{\rm Pl}$ (so that the distance to the exact solution exactly vanishes at $\phi = \phi_{\rm in}$ in all three cases). One can check that at each order, the distance to the exact solution is smaller.

which comes from Eq. (2.19), one obtains an expression for the slow-roll parameters at next-to-leading order in terms of the slow-roll parameters at leading order, which reads

$$\epsilon_0^{\rm NLO} = \epsilon_0^{\rm LO}\left(1 - \frac{\epsilon_1^{\rm LO}}{6}\right), \tag{2.21}$$

$$\epsilon_1^{\rm NLO} = \epsilon_1^{\rm LO}\left(1 - \frac{\epsilon_2^{\rm LO}}{3}\right), \tag{2.22}$$

$$\epsilon_2^{\rm NLO} = \epsilon_2^{\rm LO}\left(1 - \frac{\epsilon_2^{\rm LO}}{6} - \frac{\epsilon_3^{\rm LO}}{3}\right), \tag{2.23}$$

$$\epsilon_3^{\rm NLO} = \epsilon_3^{\rm LO}\left(1 - \frac{\epsilon_2^{\rm LO}}{3} - \frac{\epsilon_4^{\rm LO}}{3}\right), \tag{2.24}$$

where the following slow-roll parameters can be computed in the same manner, and where the slow-roll parameters at leading order in the right hand sides are given by Eqs. (2.14)-(2.17). In the same manner, to go to next-to-next-to-leading order, one starts again from

$\epsilon_0 = \epsilon_0^{\rm LO}\sqrt{1-\epsilon_1/3}$, and iteratively applies

$$\left.\frac{\mathrm{d}}{\mathrm{d}N}\right|^{\rm SR,NNLO} = \sqrt{\frac{\epsilon_1^{\rm NNLO}}{\epsilon_1^{\rm LO}}}\left.\frac{\mathrm{d}}{\mathrm{d}N}\right|^{\rm SR,LO} \tag{2.25}$$

which is again a direct consequence of Eq. (2.19). Doing so, one obtains

$$\epsilon_0^{\rm NNLO} = \epsilon_0^{\rm LO}\left[1-\frac{\epsilon_1^{\rm LO}}{6}+\frac{\epsilon_1^{\rm LO}\epsilon_2^{\rm LO}}{18}-\frac{\left(\epsilon_1^{\rm LO}\right)^2}{72}\right], \tag{2.26}$$

$$\epsilon_1^{\rm NNLO} = \epsilon_1^{\rm LO}\left[1-\frac{\epsilon_2^{\rm LO}}{3}+\frac{5}{36}\left(\epsilon_2^{\rm LO}\right)^2-\frac{\epsilon_1^{\rm LO}\epsilon_2^{\rm LO}}{9}+\frac{\epsilon_2^{\rm LO}\epsilon_3^{\rm LO}}{9}\right], \tag{2.27}$$

$$\begin{aligned}\epsilon_2^{\rm NNLO} = \epsilon_2^{\rm LO}\Bigg[1&-\frac{\epsilon_2^{\rm LO}}{6}-\frac{\epsilon_3^{\rm LO}}{3}+\frac{\left(\epsilon_2^{\rm LO}\right)^2}{18}+\frac{\left(\epsilon_3^{\rm LO}\right)^2}{9}\\ &-\frac{\epsilon_1^{\rm LO}\epsilon_2^{\rm LO}}{6}+\frac{5}{18}\epsilon_2^{\rm LO}\epsilon_3^{\rm LO}-\frac{\epsilon_1^{\rm LO}\epsilon_3^{\rm LO}}{9}+\frac{\epsilon_3^{\rm LO}\epsilon_4^{\rm LO}}{9}\Bigg],\end{aligned} \tag{2.28}$$

$$\begin{aligned}\epsilon_3^{\rm NNLO} = \epsilon_3^{\rm LO}\Bigg[1&-\frac{\epsilon_2^{\rm LO}}{3}-\frac{\epsilon_4^{\rm LO}}{3}+\frac{\left(\epsilon_2^{\rm LO}\right)^2}{6}+\frac{\left(\epsilon_4^{\rm LO}\right)^2}{9}-\frac{\epsilon_1^{\rm LO}\epsilon_2^{\rm LO}}{3}+\frac{5}{12}\epsilon_2^{\rm LO}\epsilon_3^{\rm LO}-\frac{\epsilon_1^{\rm LO}\epsilon_4^{\rm LO}}{9}\\ &+\frac{5}{18}\epsilon_3^{\rm LO}\epsilon_4^{\rm LO}+\frac{\epsilon_3^{\rm LO}\epsilon_4^{\rm LO}}{9}+\frac{\epsilon_4^{\rm LO}\epsilon_5^{\rm LO}}{9}-\frac{\epsilon_1^{\rm LO}\left(\epsilon_2^{\rm LO}\right)^2}{\epsilon_3^{\rm LO}}\Bigg],\end{aligned} \tag{2.29}$$

so on and so forth.

Let us move on to the slow-roll trajectory. At next-to-leading order, it proceeds from combining Eq. (2.19) and Eq. (2.22), which gives rise to

$$\Delta N^{\rm SR,NLO} = -\frac{1}{M_{\rm Pl}^2}\int_{\phi_{\rm in}}^{\phi_{\rm end}}\frac{V}{V'}\mathrm{d}\phi+\frac{1}{3}\ln\left(\frac{V'_{\rm end}/V_{\rm end}}{V'_{\rm in}/V_{\rm in}}\right). \tag{2.30}$$

In the same manner, the next-to-next-to-leading order of the slow-roll trajectory can be obtained from combining Eq. (2.19) and Eq. (2.27), and one gets

$$\begin{aligned}\Delta N^{\rm SR,NNLO} = &-\frac{1}{M_{\rm Pl}^2}\int_{\phi_{\rm in}}^{\phi_{\rm end}}\frac{V}{V'}\mathrm{d}\phi+\frac{1}{3}\ln\left(\frac{V'_{\rm end}/V_{\rm end}}{V'_{\rm in}/V_{\rm in}}\right)\\ &+\frac{M_{\rm Pl}^2}{18}\int_{\phi_{\rm in}}^{\phi_{\rm end}}\left[5\left(\frac{V'}{V}\right)^3+2\frac{\left(V''\right)^2}{VV'}-9\frac{V'V''}{V^2}+2\frac{V'''}{V}\right]\mathrm{d}\phi.\end{aligned} \tag{2.31}$$

The slow-roll solutions at leading order (2.12), next-to-leading order (2.30), and next-to-next-to-leading order (2.31) are displayed in Fig. 2.2 for the potential $V(\phi) = m^2\phi^2/2$. In the left panel, they are superimposed to a numerical solution of Eq. (2.6). As already seen in Fig. 2.1, the inflaton rolls down the potential and eventually rapidly oscillates around its minimum, and the slow-roll solutions provide good approximations to the exact trajectory as long as the slow-roll condition is fulfilled. However, it is difficult to distinguish by eye between the different slow-roll orders in this figure. This is why in the right panel, this difference between the slow-roll approximations and the actual trajectory is displayed, in terms of the number of e-folds realized at ϕ, as a function of ϕ (since ϕ decreases during inflation in this model, this plot should be read from the right to the left). Each slow-roll solution is actually compared with the numerical exact solution of Eq. (2.6) that shares the same initial condition $\mathrm{d}\phi/\mathrm{d}N|_{\rm in}$, so that the difference with the exact solution exactly vanishes at $\phi = \phi_{\rm in}$ in all three cases. One can check that at each order, the distance to the exact solution is smaller. Therefore, the slow-roll strategy does provide a perturbative procedure that converges towards a solution (in fact, the attractor solution) of the dynamical system formed by Eqs. (2.6) and (2.7).

2.3. Inflationary Perturbations

What makes inflation appealing is that on top of solving the hot big bang problems, this new phase in the cosmological scenario, combined with quantum mechanics, naturally explains the origin of the CMB anisotropies and of the large-scale structures. In the inflationary paradigm indeed, these deviations from homogeneity and isotropy originate from the unavoidable zero-point quantum fluctuations of the coupled inflaton and gravitational fields. Statistically, the fluctuations are characterized by their two-point correlation function or power spectrum. The observations [229, 230, 120, 231, 232, 15, 163, 164] indicate that it is close to the Harrison-Zel'dovich, scale invariant, power spectrum with equal power on all scales. That this power spectrum represents a good fit to the astrophysical data was in fact realized before the advent of inflation, but no convincing fundamental theory was known to explain this result.

One of the main successes of inflation is that it precisely predicts an almost scale invariant power spectrum, the small deviations from scale invariance being connected to the micro-physics of inflation [122, 123, 124, 125, 126, 127]. The fact that different types of inflationary scenarios lead to a power spectrum which is, at leading order, always close to scale invariance is connected with the fact that the inflationary background is always close to the de Sitter solution (see above) or, equivalently, with the fact that the inflaton potential is always almost flat. The deviations from scale invariance are related to the deviations from a flat potential and, therefore, depend on the detailed shape of the potential. As a consequence, measuring the statistical moments of the cosmological perturbations with accuracy allows us to say something about $V(\phi)$ and there is currently an important effort in this direction, using the high accuracy CMB data that have been released in the past years [233, 234, 235, 236, 237, 205, 206].

Thus in this section, we turn to the description of inflationary perturbations and we see how the results reviewed above can be derived. We show how and why cosmological perturbations need to be quantized, we derive their power spectrum and we verify that it is indeed almost scale invariant. This allows us to highlight some fundamental aspects about the nature of cosmological perturbations and the way they must be dealt with.

2.3.1. Basic Formalism

Clearly, in order to model the cosmological fluctuations, one needs to go beyond homogeneity and isotropy. The most general metric describing small fluctuations on top of a FLRW universe can be written as [129, 8]

$$\mathrm{d}s^2 = a^2(\eta)\left[-(1+2\alpha)\,\mathrm{d}\eta^2 + 2B_i \mathrm{d}x^i \mathrm{d}\eta + (\gamma_{ij}+h_{ij})\,\mathrm{d}x^i \mathrm{d}x^j\right] . \tag{2.32}$$

Notice that here, the metric is written in terms of conformal time η introduced in Eq. (1.62), and that γ_{ij} stands for the spatial part of the unperturbed FLRW metric that can be directly read off from Eq. (1.1). In Eq. (2.32), the three functions α, B_i and h_{ij} are functions of time and space since we consider an inhomogeneous and anisotropic situation.

2.3.1.1. SVT Decomposition

In order to track the dynamics of these cosmological perturbations, it can be useful to decompose them into scalar, vector and tensor components [238] (thereof realizing a "SVT decomposition").

Indeed, any vector field can be decomposed into the divergence of a scalar and a vector with vanishing divergence, that is[3]

$$B_i = \partial_i B + \bar{B}_i\,, \quad \text{with} \quad \partial^i \bar{B}_i = 0\,. \tag{2.33}$$

In the same manner, any tensor field can be decomposed into

$$h_{ij} = -2\psi\gamma_{ij} + 2\partial_i\partial_j E + 2\partial_{(i}\bar{E}_{j)} + 2\bar{E}_{ij}\,, \quad \text{with} \quad \partial_i\bar{E}^{ij} = 0 \quad \text{and} \quad \bar{E}^i_i = 0\,. \tag{2.34}$$

It can be shown that vector modes are rapidly suppressed during inflation [129, 8]. This is why they are often disregarded. Tensor perturbations (*i.e.* gravity waves) and scalar perturbations are instead usually focused on. If one first studies scalar perturbations at linear order, one then has to consider

$$\mathrm{d}s^2\big|_{\mathrm{scal}} = a^2(\eta)\left\{-(1+2\alpha)\,\mathrm{d}\eta^2 + 2\,(\partial_i B)\,\mathrm{d}x^i\mathrm{d}\eta + [(1-2\psi)\,\delta_{ij} + 2\partial_i\partial_j E]\,\mathrm{d}x^i\mathrm{d}x^j\right\}, \tag{2.35}$$

where we take the case of a flat FLRW background for which $\gamma_{ij} = \delta_{ij}$, for the reasons mentioned at the end of section 1.3.1 (namely the fact that the observed spatial curvature is negligible).

2.3.1.2. Gauge Invariant Variables

As is well known, the above approach is redundant because of gauge freedom [129, 239, 240] under space-time diffeomorphisms. A careful study of this question shows that, in the absence of anisotropic stress, the gravitational sector can in fact be described by a single, gauge-invariant, quantity, the Bardeen potential Φ_{B} defined by [239]

$$\Phi_{\mathrm{B}}(\eta,\boldsymbol{x}) = -\alpha + \frac{1}{a}\left[a\left(B - E'\right)\right]', \tag{2.36}$$

where a prime denotes a derivative with respect to the conformal time η. In the same manner, the matter sector can be modelled by the gauge-invariant fluctuation of the scalar field

$$\delta\phi^{(\mathrm{gi})}(\eta,\boldsymbol{x}) = \delta\phi + \phi'\left(B - E'\right)\,. \tag{2.37}$$

The two quantities Φ_{B} and $\delta\phi^{(\mathrm{gi})}$ are related by a perturbed Einstein constraint. This implies that the scalar sector can in fact be described by a single quantity. For this reason, it is useful to introduce the so-called Mukhanov-Sasaki variable [122, 241, 242] which is a combination of the Bardeen potential and of the gauge-invariant field,

$$v(\eta,\boldsymbol{x}) = a\left[\delta\phi^{(\mathrm{gi})} + \phi'\frac{\Phi_{\mathrm{B}}}{\mathcal{H}}\right], \tag{2.38}$$

where $\mathcal{H} \equiv a'/a$. All the other physical scalar quantities can be expressed in terms of $v(\eta,\boldsymbol{x})$ which, therefore, fully characterizes the scalar sector.

2.3.1.3. Equation of Motion for the Perturbations

The next step consists in deriving an equation of motion for $v(\eta,\boldsymbol{x})$. Let us first establish the action for the quantity $v(\eta,\boldsymbol{x})$. Expanding the action of the system [*i.e.* Einstein-Hilbert

[3] For the quantities introduced here, the indexes must be lowered or raised with the unperturbed metric γ_{ij}. For example, $\bar{B}^i = \gamma^{ij}\bar{B}_j$.

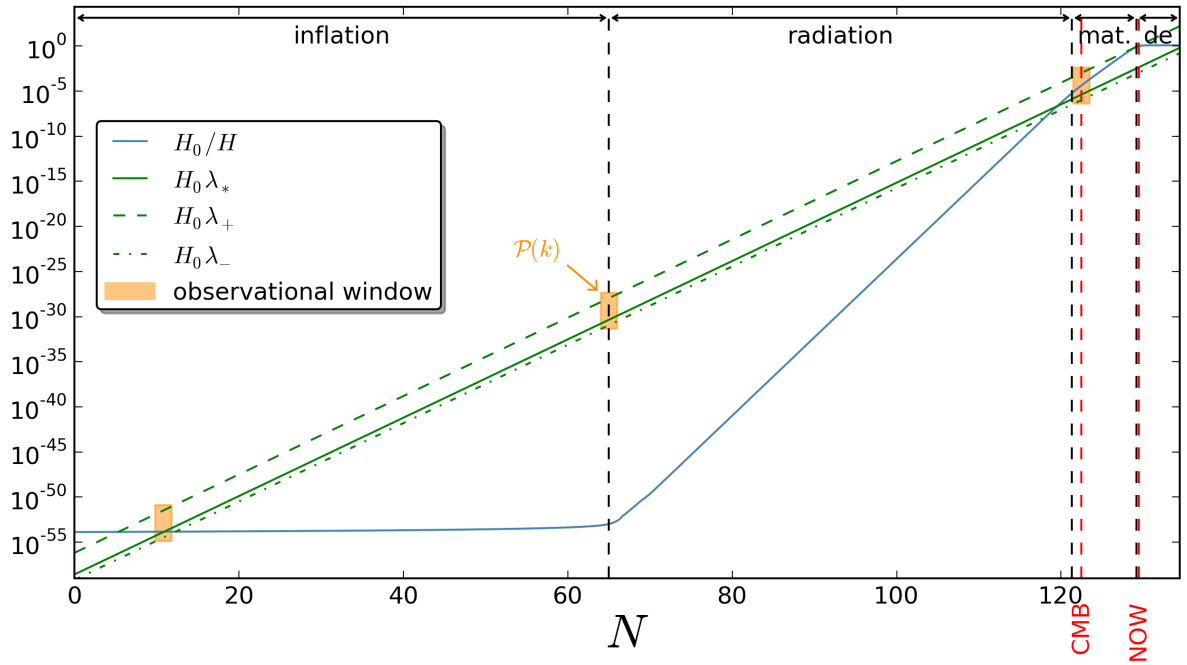

Figure 2.3.: Length scales evolution in the cosmological standard model including a phase of inflation. The blue curve stands for the Hubble radius normalized to its current value, H_0/H. The inflationary phase is implemented with a large field potential $V(\phi) = m^2\phi^2/2$, where m is normalized to the amplitude of the CMB power spectrum $m \simeq 7 \times 10^{-6} M_{\rm Pl}$ (see below), while radiation, cold matter and dark energy components follow the values of table 1.2. As expected, the Hubble radius is roughly constant during inflation and increases afterwards. The green lines stand for the physical length scales probed in the CMB, normalized to the current Hubble radius. They get stretched according to $\lambda = a/k$, as the expansion of the Universe proceeds. The pivot scale λ_* corresponds to $k_* = 0.05$ Mpc^{-1}, and $[\lambda_-, \lambda_+]$ defines the scales directly observed in the CMB, with $k_+ \simeq 0.0002$ Mpc^{-1} and $k_- \simeq 0.2$ Mpc^{-1}. These scales frame the observational window displayed in orange. They cross the Hubble radius during inflation, and at more recent time.

action (1.10) plus the action of the inflaton scalar field (2.1)] up to second order in the perturbations, one obtains [129]

$$ {}^{(2)}\delta S = \frac{1}{2}\int \mathrm{d}^4x \left[\left(v'\right)^2 - \delta^{ij}\partial_i v \partial_j v + \frac{\left(a\sqrt{\epsilon_1}\right)''}{a\sqrt{\epsilon_1}} v^2 \right], \tag{2.39} $$

where ϵ_1 is defined in Eq. (2.10). The next move consists in Fourier transforming the quantity $v(\eta, \boldsymbol{x})$. We follow such a strategy because we work with a linear theory and, as a consequence, all the modes evolve independently. We have

$$ v\left(\eta, \boldsymbol{x}\right) = \frac{1}{\left(2\pi\right)^{3/2}} \int_{\mathbb{R}^3} \mathrm{d}^3\boldsymbol{k}\, v_{\boldsymbol{k}}\left(\eta\right) \mathrm{e}^{i\boldsymbol{k}\cdot\boldsymbol{x}}, \tag{2.40} $$

with $v_{-\boldsymbol{k}} = v_{\boldsymbol{k}}^*$ because $v(\eta, \boldsymbol{x})$ is real. Then, inserting this expansion into Eq. (2.39), one arrives at [129]

$$ {}^{(2)}\delta S = \int \mathrm{d}\eta \int_{\mathbb{R}^+\times\mathbb{R}^2} \mathrm{d}^3\boldsymbol{k} \left\{ v_{\boldsymbol{k}}' v_{\boldsymbol{k}}^{*\prime} + v_{\boldsymbol{k}} v_{\boldsymbol{k}}^* \left[\frac{\left(a\sqrt{\epsilon_1}\right)''}{a\sqrt{\epsilon_1}} - k^2 \right] \right\}, \tag{2.41} $$

where one can see that the integral over $\boldsymbol{k}$ is taken over $\mathbb{R}^+ \times \mathbb{R}^2$, *i.e.* half the Fourier space only, precisely because of the redundancy $v_{-\boldsymbol{k}} = v_{\boldsymbol{k}}^*$. For the same reason, the overall factor 1/2 has been cancelled. This allows us to define $p_{\boldsymbol{k}}$, the variable canonically conjugate to $v_{\boldsymbol{k}}$,

$$p_{\boldsymbol{k}} = \frac{\delta \mathcal{L}}{\delta v_{\boldsymbol{k}}^{*\prime}} = v_{\boldsymbol{k}}^{\prime}\,, \tag{2.42}$$

where $\mathcal{L}$ is the Lagrangian density in Fourier space that can be read off from Eq. (2.41), ${}^{(2)}\delta S = \int \mathrm{d}\eta \mathcal{L}$. This gives rise to the Hamiltonian density $\mathcal{H}$ (not to be confused with the Hubble parameter), defined by the Legendre transform $\mathcal{H} = \int \mathrm{d}^3\boldsymbol{k} v_{\boldsymbol{k}}^{\prime} p_{\boldsymbol{k}} - \mathcal{L}$, which reads

$$\mathcal{H} = \int_{\mathbb{R}^+\times\mathbb{R}^2} \mathrm{d}^3\boldsymbol{k} \left\{ p_{\boldsymbol{k}} p_{\boldsymbol{k}}^* + v_{\boldsymbol{k}} v_{\boldsymbol{k}}^* \left[k^2 - \frac{\left(a\sqrt{\epsilon_1}\right)^{\prime\prime}}{a\sqrt{\epsilon_1}} \right] \right\}. \tag{2.43}$$

This Hamiltonian density represents a collection of parametric oscillators, with one oscillator per mode $\boldsymbol{k}$, the time-dependent frequency of which can be expressed as

$$\omega^2\left(\eta, \boldsymbol{k}\right) = k^2 - \frac{\left(a\sqrt{\epsilon_1}\right)^{\prime\prime}}{a\sqrt{\epsilon_1}}\,. \tag{2.44}$$

We see that the frequency depends on the scale factor and its derivatives (up to the fourth). This means that different inflationary backgrounds (*i.e.* different inflaton potentials) lead to different $\omega(\eta, \boldsymbol{k})$ and, therefore, to different behaviours for $v_{\boldsymbol{k}}(\eta)$. Since Eq. (2.41) gives rise to $\mathcal{L} = \int \mathrm{d}^3\boldsymbol{k} \left(p_{\boldsymbol{k}} p_{\boldsymbol{k}}^* - w^2 v_{\boldsymbol{k}} v_{\boldsymbol{k}}^*\right)$, the equation of motion for the Mukhanov-Sasaki variable can be derived from the variational relation $\partial\mathcal{L}/\partial v_{\boldsymbol{k}}^* = \partial_\eta(\partial\mathcal{L}/\partial p_{\boldsymbol{k}}^*)$. The same result can be obtained making use of Eq. (2.43), $\mathcal{H} = \int \mathrm{d}^3\boldsymbol{k} \left(p_{\boldsymbol{k}} p_{\boldsymbol{k}}^* + w^2 v_{\boldsymbol{k}} v_{\boldsymbol{k}}^*\right)$, and of Hamilton's relation $p_{\boldsymbol{k}}^{\prime} = -\partial\mathcal{H}/\partial v_{\boldsymbol{k}}^*$. In either case, one obtains

$$v_{\boldsymbol{k}}^{\prime\prime} + \omega^2\left(\eta, \boldsymbol{k}\right) v_{\boldsymbol{k}} = 0, \tag{2.45}$$

which confirms that each mode behaves as a parametric oscillator.

Let us comment on the structure of this equation. In the case where ϵ_1 is constant, $\omega^2 = k^2 - a^{\prime\prime}/a$, and since $a \sim \mathrm{e}^{Ht} \propto -1/(\eta H)$, one roughly obtains $\omega^2 \simeq k^2 - 2/\eta^2$. Remember that during inflation, η increases in the range $[-\infty, 0^-]$, see Fig. 1.12. As a consequence, the system undergoes two different regimes. At early time, when $\eta \ll -1/k$, one has $\omega^2 \simeq k^2$ which corresponds to an harmonic oscillator. In this case the Mukhanov-Sasaki variable oscillates with constant amplitude, $v_{\boldsymbol{k}} \propto \cos(k\eta)$, like in Minkowski space-time. On the contrary, at late time when $\eta \gg -1/k$, one has $\omega^2 \simeq -2/\eta^2$ which corresponds to a forced harmonic oscillator, or parametric oscillator. The Mukhanov-Sasaki variable grows as $v_{\boldsymbol{k}} \propto -1/\eta + \eta^2 \simeq -1/\eta$, where the growing mode dominates over the decaying mode in the limit $\eta \to 0^-$. In this regime, curvature of space-time sources the parametric amplification of the cosmological perturbations.

The situation can be better understood looking at Fig. 2.3. In this figure, we have plotted the Hubble radius of a universe made of radiation, cold matter and a cosmological constant according to the values of table 1.2, and which also contains an inflaton field with potential $V(\phi) = m^2\phi^2/2$ (in this discussion, the precise shape of V has no importance). One can check that the Hubble radius is roughly constant during inflation, and increases afterwards during the radiation era and the matter era. On the other hand, the physical length scales λ associated with cosmological perturbations get stretched according to $\lambda = a/k$ (where k is the comoving wavenumber), and always increase as the expansion of the Universe proceeds. As a consequence, at the beginning of inflation, scales of astrophysical interest today are "sub-Hubble", which means that they are smaller than the Hubble radius. Since space-time is locally flat, of the Minkowski type, length

scales far inside the Hubble scale follow harmonic oscillator equations. At some point during inflation, they cross the Hubble radius and become "super-Hubble". From this point on they are impacted by the curvature of space-time, and they undergo parametric amplification. Note that they cross the Hubble radius a second time, at some point between the CMB emission and now, so that they are currently sub-Hubble again.

To go beyond this schematic description, one has of course to work within a specified inflationary model. Once a potential $V(\phi)$ is chosen, the background equations (2.6) and (2.7) can be solved and the corresponding scale factor $a(\eta)$ is inferred. This, in turn, allows us to determine $\omega^2(\eta, \boldsymbol{k})$ and, then, one can solve the equation of motion (2.45) for the Fourier component of the Mukhanov-Sasaki variable $v_{\boldsymbol{k}}$. However, in order to fully specify the solution for $v_{\boldsymbol{k}}$, one also needs to set initial conditions. Classically, there does not seem to exist a natural criterion to choose them. However, as we shall now see, when quantization is performed, if one assumes that the perturbations are sourced by the zero-point fluctuations of the theory, it leads to well-defined initial conditions. We now turn to these questions.

2.3.2. Quantization in the Schrödinger Picture

In this section, we review how the cosmological perturbations must be quantized. Very often in the literature, the quantization is done in the Heisenberg picture. Here, we carry out the quantization in the Schrödinger picture [135, 138] to show that one obtains the same results doing so. In order to properly quantize the system, it is more convenient to work with real variables. Therefore, we introduce the following decompositions

$$v_{\boldsymbol{k}} \equiv \frac{1}{\sqrt{2}}\left(v_{\boldsymbol{k}}^{\mathrm{R}} + i v_{\boldsymbol{k}}^{\mathrm{I}}\right) , \quad p_{\boldsymbol{k}} \equiv \frac{1}{\sqrt{2}}\left(p_{\boldsymbol{k}}^{\mathrm{R}} + i p_{\boldsymbol{k}}^{\mathrm{I}}\right) , \tag{2.46}$$

where $v_{\boldsymbol{k}}^{\mathrm{R}}$, $v_{\boldsymbol{k}}^{\mathrm{I}}$, $p_{\boldsymbol{k}}^{\mathrm{R}}$ and $p_{\boldsymbol{k}}^{\mathrm{I}}$ are real quantities. In the Schrödinger approach, the quantum state of the system is described by a wavefunctional, $\Psi\left[v(\eta, \boldsymbol{x})\right]$. Since we work in Fourier space, and since the theory is free (*i.e.* without mode mixing terms) in the sense that it does not contain terms with power higher than two in the Lagrangian, the wavefunctional can also be factorized into mode components as

$$\Psi\left[v(\eta, \boldsymbol{x})\right] = \prod_{\boldsymbol{k}\in\mathbb{R}^+\times\mathbb{R}^2} \Psi_{\boldsymbol{k}}\left(v_{\boldsymbol{k}}^{\mathrm{R}}, v_{\boldsymbol{k}}^{\mathrm{I}}\right) = \prod_{\boldsymbol{k}\in\mathbb{R}^+\times\mathbb{R}^2} \Psi_{\boldsymbol{k}}^{\mathrm{R}}\left(v_{\boldsymbol{k}}^{\mathrm{R}}\right) \Psi_{\boldsymbol{k}}^{\mathrm{I}}\left(v_{\boldsymbol{k}}^{\mathrm{I}}\right) . \tag{2.47}$$

Quantization is achieved by promoting $v_{\boldsymbol{k}}$ and $p_{\boldsymbol{k}}$ to quantum operators, $\hat{v}_{\boldsymbol{k}}$ and $\hat{p}_{\boldsymbol{k}}$, and by requiring the canonical commutation relations

$$\left[\hat{v}_{\boldsymbol{k}}^{\mathrm{R}}, \hat{p}_{\boldsymbol{q}}^{\mathrm{R}}\right] = i\delta\left(\boldsymbol{k} - \boldsymbol{q}\right) , \quad \left[\hat{v}_{\boldsymbol{k}}^{\mathrm{I}}, \hat{p}_{\boldsymbol{q}}^{\mathrm{I}}\right] = i\delta\left(\boldsymbol{k} - \boldsymbol{q}\right) , \tag{2.48}$$

with $\left[\hat{v}_{\boldsymbol{k}}^{\mathrm{R}}, \hat{p}_{\boldsymbol{q}}^{\mathrm{I}}\right] = \left[\hat{v}_{\boldsymbol{k}}^{\mathrm{I}}, \hat{p}_{\boldsymbol{q}}^{\mathrm{R}}\right] = 0$. These relations admit the following representation

$$\hat{v}_{\boldsymbol{k}}^{\mathrm{R,I}}\Psi = v_{\boldsymbol{k}}^{\mathrm{R,I}}\Psi , \tag{2.49}$$

$$\hat{p}_{\boldsymbol{k}}^{\mathrm{R,I}}\Psi = -i\frac{\partial\Psi}{\partial v_{\boldsymbol{k}}^{\mathrm{R,I}}} . \tag{2.50}$$

The wavefunctional $\Psi\left[v(\eta, \boldsymbol{x})\right]$ obeys the Schrödinger equation which, in this context, is a functional differential equation. However, since each mode evolves independently, this functional

differential equation can be reduced to an infinite number of differential equations for each $\Psi_{\boldsymbol{k}}^{\mathrm{R,I}}$. Concretely, we have

$$i\frac{\Psi_{\boldsymbol{k}}^{\mathrm{R,I}}}{\partial\eta} = \hat{\mathcal{H}}_{\boldsymbol{k}}^{\mathrm{R,I}}\Psi_{\boldsymbol{k}}^{\mathrm{R,I}}, \tag{2.51}$$

where the Hamiltonian densities $\hat{\mathcal{H}}_{\boldsymbol{k}}^{\mathrm{R,I}}$ are related to the direct space Hamiltonian density $\hat{\mathcal{H}}$ by the Fourier expansion $\hat{\mathcal{H}} = \int_{\mathbb{R}^3} \mathrm{d}^3\boldsymbol{k}\left(\hat{\mathcal{H}}_{\boldsymbol{k}}^{\mathrm{R}} + \hat{\mathcal{H}}_{\boldsymbol{k}}^{\mathrm{I}}\right)$. Looking at Eq. (2.43), they can be expressed as

$$\hat{\mathcal{H}}_{\boldsymbol{k}}^{\mathrm{R,I}} = -\frac{1}{2}\frac{\partial^2}{\partial\left(v_{\boldsymbol{k}}^{\mathrm{R,I}}\right)^2} + \frac{1}{2}\omega^2(\eta,\boldsymbol{k})\left(\hat{v}_{\boldsymbol{k}}^{\mathrm{R,I}}\right)^2, \tag{2.52}$$

where we have made use of the representations (2.49) and (2.50), and where the factor $1/2$ accounts for the fact that the $\hat{\mathcal{H}}_{\boldsymbol{k}}$ densities are defined through an integral over $\mathbb{R}^3$ while Eq. (2.43) makes use of an integral over $\mathbb{R}^+\times\mathbb{R}^2$.

We are now in a position where we can solve the Schrödinger equation. Let us consider the following Gaussian state

$$\Psi_{\boldsymbol{k}}^{\mathrm{R,I}}\left(\eta, v_{\boldsymbol{k}}^{\mathrm{R,I}}\right) = N_{\boldsymbol{k}}(\eta)\mathrm{e}^{-\Omega_{\boldsymbol{k}}(\eta)\left(v_{\boldsymbol{k}}^{\mathrm{R,I}}\right)^2}. \tag{2.53}$$

The functions $N_{\boldsymbol{k}}(\eta)$ and $\Omega_{\boldsymbol{k}}(\eta)$ are time dependent and do not carry the superscripts "R" or "I" because as shown below, they are the same for the wavefunctions of the real and imaginary parts. Inserting the state $\Psi_{\boldsymbol{k}}$ given by Eq. (2.53) into the Schrödinger equation (2.51), one can see that such a Gaussian state is a solution of the Schrödinger equation. This is why at linear order in perturbation theory, if the initial state is Gaussian, perturbations remain Gaussian. More precisely, this is the case provided $N_{\boldsymbol{k}}$ and $\Omega_{\boldsymbol{k}}$ obey the following differential equations

$$i\frac{N_{\boldsymbol{k}}'}{N_{\boldsymbol{k}}} = \Omega_{\boldsymbol{k}} \quad \text{and} \quad \Omega_{\boldsymbol{k}}' = -2i\Omega_{\boldsymbol{k}}^2 + \frac{i}{2}\omega^2(\eta,\boldsymbol{k}). \tag{2.54}$$

The solutions can be easily found and read

$$|N_{\boldsymbol{k}}| = \left(\frac{2\Re\mathrm{e}\,\Omega_{\boldsymbol{k}}}{\pi}\right)^{1/4} \quad \text{and} \quad \Omega_{\boldsymbol{k}} = -\frac{i}{2}\frac{f_{\boldsymbol{k}}'}{f_{\boldsymbol{k}}}, \tag{2.55}$$

where $f_{\boldsymbol{k}}$ is a function obeying the equation $f_{\boldsymbol{k}}'' + \omega^2 f_{\boldsymbol{k}} = 0$, that is to say exactly Eq. (2.45). The first equation (2.55) guarantees that the wavefunction is properly normalized, *i.e.* that we have

$$\int_{-\infty}^{\infty}\Psi_{\boldsymbol{k}}^{\mathrm{R,I}}\Psi_{\boldsymbol{k}}^{\mathrm{R,I}*}\mathrm{d}v_{\boldsymbol{k}}^{\mathrm{R,I}} = 1. \tag{2.56}$$

Let us now discuss the initial conditions. A rather natural assumption to make is that the perturbations are initially in their ground state, so that they are only sourced by the zero-point quantum fluctuations. According to the discussion following Fig. 2.3, at the beginning of inflation, all the modes of astrophysical interest today have a physical wavelength which is smaller than the Hubble radius, *i.e.* $k/(aH)\to\infty$. In this regime, one has $\omega^2(\eta,\boldsymbol{k})\to k^2$ and each mode behaves as an harmonic oscillator (as opposed to a parametric oscillator in the generic case) with frequency $\omega = k$. As a consequence, the differential equation for $f_{\boldsymbol{k}}(\eta)$ can easily be solved and the solution reads $f_{\boldsymbol{k}} = A_{\boldsymbol{k}}\mathrm{e}^{ik\eta} + B_{\boldsymbol{k}}\mathrm{e}^{-ik\eta}$, $A_{\boldsymbol{k}}$ and $B_{\boldsymbol{k}}$ being integration constants. Upon using the second equation (2.55), one then has

$$\Omega_{\boldsymbol{k}}\to\frac{k}{2}\frac{A_{\boldsymbol{k}}\mathrm{e}^{ik\eta} - B_{\boldsymbol{k}}\mathrm{e}^{-ik\eta}}{A_{\boldsymbol{k}}\mathrm{e}^{ik\eta} + B_{\boldsymbol{k}}\mathrm{e}^{-ik\eta}} \tag{2.57}$$

in this limit. On the other hand, let us calculate the ground state wavefunction of the harmonic oscillator under consideration. The number of particle operator $\hat{n}_{\boldsymbol{k}} = \hat{a}^{\dagger}_{\boldsymbol{k}}\hat{a}_{\boldsymbol{k}}$ for the harmonic oscillator with $\omega \sim k$ can be expressed in terms of the creation and annihilation operators $a^{\dagger}_{\boldsymbol{k}}$ and $a_{\boldsymbol{k}}$, defined by [243]

$$\hat{a}_{\boldsymbol{k}} = \sqrt{\frac{k}{2}}\left(\hat{v}_{\boldsymbol{k}} + \frac{i}{k}\hat{p}_{\boldsymbol{k}}\right), \tag{2.58}$$

$$\hat{a}^{\dagger}_{\boldsymbol{k}} = \sqrt{\frac{k}{2}}\left(\hat{v}_{\boldsymbol{k}} - \frac{i}{k}\hat{p}_{\boldsymbol{k}}\right), \tag{2.59}$$

so that one has $\hat{n}_{\boldsymbol{k}} = k/2(\hat{v}^2_{\boldsymbol{k}} + \hat{p}^2_{\boldsymbol{k}}/k^2 + i/k[v_{\boldsymbol{k}}, p_{\boldsymbol{k}}]) = k/2(\hat{v}^2_{\boldsymbol{k}} + \hat{p}^2_{\boldsymbol{k}}/k^2 - 1/k)$, where one has made use of the canonical commutation relations (2.48). Here the superscripts "R" and "I" have been removed for simplicity. Making use of the representations (2.49) and (2.50), this allows us to calculate the mean number of particles present in the state (2.53), and one obtains

$$\langle\Psi_{\boldsymbol{k}}|\hat{n}_{\boldsymbol{k}}|\Psi_{\boldsymbol{k}}\rangle = \frac{k}{2}\left[\left\langle\Psi_{\boldsymbol{k}}|\hat{v}^2_{\boldsymbol{k}}|\Psi_{\boldsymbol{k}}\right\rangle\left(1 - 4\frac{\Omega^2_{\boldsymbol{k}}}{k^2}\right) + 2\frac{\Omega_{\boldsymbol{k}}}{k^2} - \frac{1}{k}\right], \tag{2.60}$$

where the quantum mean value of $v^2_{\boldsymbol{k}}$ is just given by the Gaussian integral

$$\begin{aligned}\left\langle\Psi_{\boldsymbol{k}}|\hat{v}^2_{\boldsymbol{k}}|\Psi_{\boldsymbol{k}}\right\rangle &= \int_{-\infty}^{\infty}\mathrm{d}v_{\boldsymbol{k}}\Psi_{\boldsymbol{k}}\left(\eta, v_{\boldsymbol{k}}\right)\Psi^{*}_{\boldsymbol{k}}\left(\eta, v_{\boldsymbol{k}}\right)v^2_{\boldsymbol{k}} \\ &= \sqrt{\frac{2\Re\mathrm{e}\left(\Omega_{\boldsymbol{k}}\right)}{\pi}}\int_{-\infty}^{\infty}\mathrm{d}v_{\boldsymbol{k}}\mathrm{e}^{-2\Re\mathrm{e}\left(\Omega_{\boldsymbol{k}}\right)v^2_{\boldsymbol{k}}}v^2_{\boldsymbol{k}} \\ &= \frac{1}{4\Re\mathrm{e}\left(\Omega_{\boldsymbol{k}}\right)}.\end{aligned} \tag{2.61}$$

Combining the two previous equations together yields an expression for the mean number of particles in the Gaussian state $\Psi_{\boldsymbol{k}}$, only in terms of $\Omega_{\boldsymbol{k}}$. Requiring that this number vanishes, so that $\Psi_{\boldsymbol{k}}$ coincides with the ground state of the Minkowski harmonic oscillator at early time, gives rise to $\Im\mathrm{m}\,\Omega_{\boldsymbol{k}} = 0$ and $\Re\mathrm{e}\,\Omega_{\boldsymbol{k}} = k/2$. Looking back at Eq. (2.57), this means that one must set the initial conditions such that $B_{\boldsymbol{k}} = 0$.

Moreover, it is easy to check that the Wronskian $W \equiv f'_{\boldsymbol{k}}f^{*}_{\boldsymbol{k}} - f'^{*}_{\boldsymbol{k}}f_{\boldsymbol{k}}$ is a conserved quantity, $\mathrm{d}W/\mathrm{d}\eta = 0$, thanks to the equation of motion (2.45) of $f_{\boldsymbol{k}}$. At early time, since $f_{\boldsymbol{k}} = A_{\boldsymbol{k}}\mathrm{e}^{ik\eta} + B_{\boldsymbol{k}}\mathrm{e}^{-ik\eta}$, one has $W = 2ik(|A_{\boldsymbol{k}}|^2 - |B_{\boldsymbol{k}}|^2)$. In the Heisenberg picture, the canonical commutation relations require that $W = i$. Even if in the Schrödinger picture presently used, the specific value of W is irrelevant since it cancels out in all calculable physical quantities, this value is conventionally adopted, which amounts to setting $A_{\boldsymbol{k}} = 1/\sqrt{2k}$ on top of $B_{\boldsymbol{k}} = 0$. However, we insist that a different value of $A_{\boldsymbol{k}}$ can be worked with without modifying the results obtained below, as long as $B_{\boldsymbol{k}} = 0$. The equation for $f_{\boldsymbol{k}}$ (2.45) will thus be solved with the initial condition

$$\lim_{k/(aH)\to+\infty} f_{\boldsymbol{k}} = \frac{1}{\sqrt{2k}}\mathrm{e}^{ik\eta}. \tag{2.62}$$

Such an initial state is often referred to as the Bunch-Davies vacuum [244, 245]. Obviously, if excited states of the harmonic oscillator are chosen as initial conditions instead, one obtains different results [246, 247, 248, 249, 250, 251, 252, 253, 254, 255, 256, 257, 258, 259, 260, 261, 262, 263, 264, 265, 266] and the inflationary predictions are dependent on what one assumes for the initial state of the perturbations.

Once an initial value for $f_{\boldsymbol{k}}$ is chosen, the quantum state for the perturbations is completely specified. Indeed, the wavefunction Ψ is given by Eq. (2.53) and depends on a single parameter

$\Omega_{\boldsymbol{k}}$, for which we know what is the initial state and the equation of motion. We therefore completely know the wavefunction, from which we can further study the quantum state of the perturbations. For example, in section 4.3, we show that on super-Hubble scales, the quantum state is a squeezed one, and we discuss how this squeezing can account for a quantum-to-classical transition of the perturbations. Another relevant quantity to compute is of course the two-point correlation function in the quantum state Ψ, *i.e.* the power spectrum.

2.3.3. The Power Spectrum

Let us now turn to the calculation of the power spectrum. We first introduce the two-point correlation function, defined by $\langle\Psi\left|\hat{v}(\eta,\boldsymbol{x})\hat{v}(\eta,\boldsymbol{x}+\boldsymbol{r})\right|\Psi\rangle$. Making use of the Fourier transform of the Mukhanov-Sasaki variable, Eq. (2.40), and of the mode decomposition of the wavefunction, Eq. (2.47), one has

$$\langle\Psi\left|\hat{v}(\eta,\boldsymbol{x})\hat{v}(\eta,\boldsymbol{x}+\boldsymbol{r})\right|\Psi\rangle = \frac{1}{(2\pi)^3}\int_{\mathbb{R}^3}\mathrm{d}\boldsymbol{p}\,\mathrm{e}^{i\boldsymbol{p}\cdot\boldsymbol{x}}\int_{\mathbb{R}^3}\mathrm{d}\boldsymbol{q}\,\mathrm{e}^{i\boldsymbol{q}\cdot(\boldsymbol{x}+\boldsymbol{r})}\langle\Psi\left|\hat{v}_{\boldsymbol{p}}\hat{v}_{\boldsymbol{q}}\right|\Psi\rangle \tag{2.63}$$

$$= \frac{1}{(2\pi)^3}\int_{\mathbb{R}^3}\mathrm{d}\boldsymbol{p}\,\mathrm{e}^{i\boldsymbol{p}\cdot\boldsymbol{x}}\int_{\mathbb{R}^3}\mathrm{d}\boldsymbol{q}\,\mathrm{e}^{i\boldsymbol{q}\cdot(\boldsymbol{x}+\boldsymbol{r})}\prod_{\boldsymbol{k}\in\mathbb{R}^+\times\mathbb{R}^2}\prod_{\boldsymbol{k}'\in\mathbb{R}^+\times\mathbb{R}^2}\langle\Psi_{\boldsymbol{k}}\left|\hat{v}_{\boldsymbol{p}}\hat{v}_{\boldsymbol{q}}\right|\Psi_{\boldsymbol{k}'}\rangle\,. \tag{2.64}$$

In the above expression, one can see that $\boldsymbol{k}$ and $\boldsymbol{k}'$ take value in $\mathbb{R}^+\times\mathbb{R}^2$ while $\boldsymbol{p}$ and $\boldsymbol{q}$ take value in $\mathbb{R}^3$. In order to have the same integration domain for all variables, it is useful to notice that the $\boldsymbol{p}$-integration (or, in the same manner, the $\boldsymbol{q}$-integration) can be expressed as

$$\int_{\mathbb{R}^3}\mathrm{d}\boldsymbol{p}\,\mathrm{e}^{i\boldsymbol{p}\cdot\boldsymbol{x}}\hat{v}_{\boldsymbol{p}} = \int_{\mathbb{R}^+\times\mathbb{R}^2}\mathrm{d}\boldsymbol{p}\,\mathrm{e}^{i\boldsymbol{p}\cdot\boldsymbol{x}}\hat{v}_{\boldsymbol{p}} + \int_{\mathbb{R}^-\times\mathbb{R}^2}\mathrm{d}\boldsymbol{p}\,\mathrm{e}^{i\boldsymbol{p}\cdot\boldsymbol{x}}\hat{v}_{\boldsymbol{p}} \tag{2.65}$$

$$= \int_{\mathbb{R}^+\times\mathbb{R}^2}\mathrm{d}\boldsymbol{p}\,\mathrm{e}^{i\boldsymbol{p}\cdot\boldsymbol{x}}\hat{v}_{\boldsymbol{p}} + \int_{\mathbb{R}^+\times\mathbb{R}^2}\mathrm{d}\boldsymbol{p}\,\mathrm{e}^{-i\boldsymbol{p}\cdot\boldsymbol{x}}\hat{v}_{-\boldsymbol{p}} \tag{2.66}$$

$$= \int_{\mathbb{R}^+\times\mathbb{R}^2}\mathrm{d}\boldsymbol{p}\,\mathrm{e}^{i\boldsymbol{p}\cdot\boldsymbol{x}}\hat{v}_{\boldsymbol{p}} + \int_{\mathbb{R}^+\times\mathbb{R}^2}\mathrm{d}\boldsymbol{p}\,\mathrm{e}^{-i\boldsymbol{p}\cdot\boldsymbol{x}}\hat{v}^*_{\boldsymbol{p}} \tag{2.67}$$

$$= \int_{\mathbb{R}^+\times\mathbb{R}^2}\mathrm{d}\boldsymbol{p}\left(\mathrm{e}^{i\boldsymbol{p}\cdot\boldsymbol{x}}\hat{v}_{\boldsymbol{p}} + \mathrm{e}^{-i\boldsymbol{p}\cdot\boldsymbol{x}}\hat{v}^*_{\boldsymbol{p}}\right), \tag{2.68}$$

where between the second and the third line we have used the relation $\hat{v}_{-\boldsymbol{p}} = \hat{v}^*_{\boldsymbol{p}}$ mentioned above which comes from the fact that $\hat{v}$ is a real operator in physical space. Plugging the obtained expression in Eq. (2.64), one obtains

$$\langle\Psi\left|\hat{v}(\eta,\boldsymbol{x})\hat{v}(\eta,\boldsymbol{x}+\boldsymbol{r})\right|\Psi\rangle = \frac{1}{(2\pi)^3}\int_{\mathbb{R}^+\times\mathbb{R}^2}\mathrm{d}\boldsymbol{p}\int_{\mathbb{R}^+\times\mathbb{R}^2}\mathrm{d}\boldsymbol{q}\prod_{\boldsymbol{k}\in\mathbb{R}^+\times\mathbb{R}^2}\prod_{\boldsymbol{k}'\in\mathbb{R}^+\times\mathbb{R}^2}\left\langle\Psi_{\boldsymbol{k}}\left|\left[\mathrm{e}^{i\boldsymbol{p}\cdot\boldsymbol{x}}\hat{v}_{\boldsymbol{p}} + \mathrm{e}^{-i\boldsymbol{p}\cdot\boldsymbol{x}}\hat{v}^*_{\boldsymbol{p}}\right]\left[\mathrm{e}^{i\boldsymbol{q}\cdot(\boldsymbol{x}+\boldsymbol{r})}\hat{v}_{\boldsymbol{q}} + \mathrm{e}^{-i\boldsymbol{q}\cdot(\boldsymbol{x}+\boldsymbol{r})}\hat{v}^*_{\boldsymbol{q}}\right]\right|\Psi_{\boldsymbol{k}'}\right\rangle. \tag{2.69}$$

Since the Hilbert spaces associated with each mode are independent at linear order in perturbation theory, and since the $|\Psi_{\boldsymbol{k}}\rangle$ wavefunctions are normalized, $\langle\Psi_{\boldsymbol{k}}|\Psi'_{\boldsymbol{k}}\rangle = \delta(\boldsymbol{k}-\boldsymbol{k}')$, in the above expression the product terms can be written as

$$\left\langle\Psi_{\boldsymbol{k}}\left|\hat{v}^{(*)}_{\boldsymbol{p}}\hat{v}^{(*)}_{\boldsymbol{q}}\right|\Psi_{\boldsymbol{k}'}\right\rangle = \delta\left(\boldsymbol{p}-\boldsymbol{q}\right)\delta\left(\boldsymbol{p}-\boldsymbol{k}\right)\delta\left(\boldsymbol{q}-\boldsymbol{k}'\right)\left\langle\Psi_{\boldsymbol{k}}\left|\hat{v}^{(*)}_{\boldsymbol{p}}\hat{v}^{(*)}_{\boldsymbol{q}}\right|\Psi_{\boldsymbol{k}'}\right\rangle, \tag{2.70}$$

where the superscripts "$(*)$" mean that stars may or may not be present. The delta functions allow to calculate all integrals and products (since they are performed on the same domains) but one, and one obtains

$$\langle\Psi\left|\hat{v}(\eta,\boldsymbol{x})\hat{v}(\eta,\boldsymbol{x}+\boldsymbol{r})\right|\Psi\rangle = \frac{1}{(2\pi)^3}\int_{\mathbb{R}^+\times\mathbb{R}^2}\mathrm{d}\boldsymbol{p} \left\langle\Psi_{\boldsymbol{p}}\left|\left[\mathrm{e}^{i\boldsymbol{p}\cdot\boldsymbol{x}}\hat{v}_{\boldsymbol{p}}+\mathrm{e}^{-i\boldsymbol{p}\cdot\boldsymbol{x}}\hat{v}^*_{\boldsymbol{p}}\right]\left[\mathrm{e}^{i\boldsymbol{p}\cdot(\boldsymbol{x}+\boldsymbol{r})}\hat{v}_{\boldsymbol{p}}+\mathrm{e}^{-i\boldsymbol{p}\cdot(\boldsymbol{x}+\boldsymbol{r})}\hat{v}^*_{\boldsymbol{p}}\right]\right|\Psi_{\boldsymbol{p}}\right\rangle. \tag{2.71}$$

Let us now decompose the product terms into real parts and imaginary parts. Making use of Eq. (2.46), and since $\hat{v}^{\mathrm{R}}_{\boldsymbol{p}}$ and $\hat{v}^{\mathrm{I}}_{\boldsymbol{p}}$ act on independent Hilbert spaces again, $|\Psi_{\boldsymbol{k}}\rangle = |\Psi^{\mathrm{R}}_{\boldsymbol{k}}\rangle|\Psi^{\mathrm{I}}_{\boldsymbol{k}}\rangle$, one has for example

$$\left\langle\Psi_{\boldsymbol{p}}\left|\hat{v}^2_{\boldsymbol{p}}\right|\Psi_{\boldsymbol{p}}\right\rangle = \frac{1}{2}\left\langle\Psi_{\boldsymbol{p}}\left|\left(\hat{v}^{\mathrm{R}}_{\boldsymbol{p}}+i\hat{v}^{\mathrm{I}}_{\boldsymbol{p}}\right)^2\right|\Psi_{\boldsymbol{p}}\right\rangle \tag{2.72}$$

$$= \frac{1}{2}\left\langle\Psi^{\mathrm{R}}_{\boldsymbol{p}}\left|\left(\hat{v}^{\mathrm{R}}_{\boldsymbol{p}}\right)^2\right|\Psi^{\mathrm{R}}_{\boldsymbol{p}}\right\rangle - \frac{1}{2}\left\langle\Psi^{\mathrm{I}}_{\boldsymbol{p}}\left|\left(\hat{v}^{\mathrm{I}}_{\boldsymbol{p}}\right)^2\right|\Psi^{\mathrm{I}}_{\boldsymbol{p}}\right\rangle, \tag{2.73}$$

and in the same manner

$$\left\langle\Psi_{\boldsymbol{p}}\left|\hat{v}_{\boldsymbol{p}}\hat{v}^*_{\boldsymbol{p}}\right|\Psi_{\boldsymbol{p}}\right\rangle = \left\langle\Psi_{\boldsymbol{p}}\left|\hat{v}^*_{\boldsymbol{p}}\hat{v}_{\boldsymbol{p}}\right|\Psi_{\boldsymbol{p}}\right\rangle = \frac{1}{2}\left\langle\Psi^{\mathrm{R}}_{\boldsymbol{p}}\left|\left(\hat{v}^{\mathrm{R}}_{\boldsymbol{p}}\right)^2\right|\Psi^{\mathrm{R}}_{\boldsymbol{p}}\right\rangle + \frac{1}{2}\left\langle\Psi^{\mathrm{I}}_{\boldsymbol{p}}\left|\left(\hat{v}^{\mathrm{I}}_{\boldsymbol{p}}\right)^2\right|\Psi^{\mathrm{I}}_{\boldsymbol{p}}\right\rangle, \tag{2.74}$$

$$\left\langle\Psi_{\boldsymbol{p}}\left|\left(\hat{v}^*_{\boldsymbol{p}}\right)^2\right|\Psi_{\boldsymbol{p}}\right\rangle = \frac{1}{2}\left\langle\Psi^{\mathrm{R}}_{\boldsymbol{p}}\left|\left(\hat{v}^{\mathrm{R}}_{\boldsymbol{p}}\right)^2\right|\Psi^{\mathrm{R}}_{\boldsymbol{p}}\right\rangle - \frac{1}{2}\left\langle\Psi^{\mathrm{I}}_{\boldsymbol{p}}\left|\left(\hat{v}^{\mathrm{I}}_{\boldsymbol{p}}\right)^2\right|\Psi^{\mathrm{I}}_{\boldsymbol{p}}\right\rangle. \tag{2.75}$$

Plugging these relations into Eq. (2.71), one obtains

$$\begin{aligned}\langle\Psi\left|\hat{v}(\eta,\boldsymbol{x})\hat{v}(\eta,\boldsymbol{x}+\boldsymbol{r})\right|\Psi\rangle =& \frac{1}{(2\pi)^3}\int_{\mathbb{R}^+\times\mathbb{R}^2}\mathrm{d}\boldsymbol{p}\left\{\left[\cos\left(\boldsymbol{p}\cdot\boldsymbol{r}\right)+\cos\left(2\boldsymbol{p}\cdot\boldsymbol{x}+\boldsymbol{p}\cdot\boldsymbol{r}\right)\right]\left\langle\Psi^{\mathrm{R}}_{\boldsymbol{p}}\left|\left(\hat{v}^{\mathrm{R}}_{\boldsymbol{p}}\right)^2\right|\Psi^{\mathrm{R}}_{\boldsymbol{p}}\right\rangle\right.\\ &\left.+\left[\cos\left(\boldsymbol{p}\cdot\boldsymbol{r}\right)-\cos\left(2\boldsymbol{p}\cdot\boldsymbol{x}+\boldsymbol{p}\cdot\boldsymbol{r}\right)\right]\left\langle\Psi^{\mathrm{I}}_{\boldsymbol{p}}\left|\left(\hat{v}^{\mathrm{I}}_{\boldsymbol{p}}\right)^2\right|\Psi^{\mathrm{I}}_{\boldsymbol{p}}\right\rangle\right\}.\end{aligned} \tag{2.76}$$

The mean values of $\left(\hat{v}^{\mathrm{R}}_{\boldsymbol{p}}\right)^2$ and $\left(\hat{v}^{\mathrm{I}}_{\boldsymbol{p}}\right)^2$ are the same, and given by Eq. (2.61). This is why the previous expression reduces to

$$\langle\Psi\left|\hat{v}(\eta,\boldsymbol{x})\hat{v}(\eta,\boldsymbol{x}+\boldsymbol{r})\right|\Psi\rangle = \frac{1}{2(2\pi)^3}\int_{\mathbb{R}^+\times\mathbb{R}^2}\mathrm{d}\boldsymbol{p}\,\frac{\cos\left(\boldsymbol{p}\cdot\boldsymbol{r}\right)}{\Re\mathrm{e}\,\left(\Omega_{\boldsymbol{p}}\right)}. \tag{2.77}$$

Now, let us see how the angular part of the $\boldsymbol{p}$-integral can be performed. When p denotes the module of $\boldsymbol{p}$ and r denotes the module of $\boldsymbol{r}$, let θ be the angle between $\boldsymbol{r}$ and $\boldsymbol{p}$. With these notations, one has $\boldsymbol{p}\cdot\boldsymbol{r} = pr\cos\theta$, and from what precedes,[4] $\Omega_{\boldsymbol{p}}$ only depends on p and we use the notation Ω_p. The $\boldsymbol{p}$-integral can be decomposed into radial and angular parts, $\mathrm{d}\boldsymbol{p} = p^2\sin\theta\,\mathrm{d}p\,\mathrm{d}\theta\,\mathrm{d}\varphi$. Because $\boldsymbol{p}$ takes its values in $\mathbb{R}^+\times\mathbb{R}^2$, φ only varies in $[0,\pi]$, and one has

$$\langle\Psi\left|\hat{v}(\eta,\boldsymbol{x})\hat{v}(\eta,\boldsymbol{x}+\boldsymbol{r})\right|\Psi\rangle = \frac{1}{2(2\pi)^3}\int_0^\pi\mathrm{d}\varphi\int_0^\pi\mathrm{d}\theta\sin\theta\int_0^\infty\mathrm{d}p\,p^2\frac{\cos\left(pr\cos\theta\right)}{\Re\mathrm{e}\,\left(\Omega_p\right)} \tag{2.78}$$

$$= \frac{1}{16\pi^2}\int_0^\pi\mathrm{d}\theta\sin\theta\int_0^\infty\mathrm{d}p\,p^2\frac{\cos\left(pr\cos\theta\right)}{\Re\mathrm{e}\,\left(\Omega_p\right)} \tag{2.79}$$

$$= \frac{1}{16\pi^2}\int_0^\infty\mathrm{d}p\,p^2\frac{1}{\Re\mathrm{e}\,\left(\Omega_p\right)}\left[\frac{\sin\left(pr\cos\theta\right)}{-pr}\right]_{\theta=0}^{\theta=\pi} \tag{2.80}$$

$$= \frac{1}{8\pi^2}\int_0^\infty\frac{\mathrm{d}p}{p}\frac{\sin\left(pr\right)}{pr}\frac{p^3}{\Re\mathrm{e}\,\left(\Omega_p\right)}. \tag{2.81}$$

[4] Indeed, $f_{\boldsymbol{p}}$ is initiated in the state (2.62) which only depends on the radial part p of $\boldsymbol{p}$, and follows an equation of motion (2.45) that only depends on p as well. Hence $f_{\boldsymbol{p}} = f_p$, and $\Omega_{\boldsymbol{p}} = \Omega_p$.

We are now in a position where an expression for the power spectrum can be given. The power spectrum $\mathcal{P}_v(\boldsymbol{k})$ is defined as the square of the Fourier amplitude per logarithmic interval at a given scale $\boldsymbol{k}$, *i.e.* it is such that

$$\langle \Psi | \hat{v}(\eta, \boldsymbol{x}) \hat{v}(\eta, \boldsymbol{x}+\boldsymbol{r}) | \Psi \rangle \equiv \int_0^\infty \frac{\mathrm{d}k}{k} \frac{\sin(kr)}{kr} \mathcal{P}_v(\boldsymbol{k}) \,. \tag{2.82}$$

By identifying Eqs. (2.81) and (2.82), it is straightforward to obtain

$$\mathcal{P}_v(\boldsymbol{k}) = \frac{k^3}{8\pi^2} \frac{1}{\Re\mathrm{e}\,(\Omega_k)} \,. \tag{2.83}$$

Finally, let us express $\Re\mathrm{e}\,(\Omega_{\boldsymbol{k}})$ in terms of the function $f_{\boldsymbol{k}}$. From the second Eq. (2.55), one easily shows that

$$\Re\mathrm{e}\,(\Omega_{\boldsymbol{k}}) = -\frac{i}{4} \frac{W}{|f_{\boldsymbol{k}}|^2}. \tag{2.84}$$

One can check that only the ratio $W/|f_{\boldsymbol{k}}|^2$ is involved, so that as announced above, the absolute normalization of $f_{\boldsymbol{k}}$ does not play any role in the Schrödinger picture. Since the initial condition (2.62) is associated with the choice $W = i$, one eventually obtains

$$\mathcal{P}_v(k) = \frac{k^3}{2\pi^2} |f_{\boldsymbol{k}}|^2. \tag{2.85}$$

A last remark is in order. Instead of calculating the power spectrum of the Mukhanov variable $\mathcal{P}_v$, it often proves more convenient to discuss the power spectrum of curvature perturbations $\mathcal{P}_\zeta$. The quantity ζ is related to the Bardeen potential defined in Eq. (2.36) through the following expression [129, 267, 240]

$$\zeta = \frac{2}{3} \frac{\mathcal{H}^{-1}\Phi_{\mathrm{B}}' + \Phi_{\mathrm{B}}}{1+w} + \Phi_{\mathrm{B}}, \tag{2.86}$$

where $w \equiv p/\rho$ is the equation of state parameter. The importance of ζ lies in the fact that it is a conserved quantity on large scales [267, 240]. Therefore, its spectrum, calculated at the end of inflation, can directly be propagated to the recombination time as it is not sensitive to the details of the cosmological evolution, in particular to those of the complicated reheating era [268, 223, 214, 225, 219]. The curvature perturbation can also be expressed in terms of the Mukhanov-Sasaki variable as [267]

$$\zeta = \frac{1}{a\sqrt{2\epsilon_1}} \frac{v}{M_{\mathrm{Pl}}} \,. \tag{2.87}$$

Making use of Eq. (2.85), one then has

$$\mathcal{P}_\zeta(k) = \frac{1}{2a^2 M_{\mathrm{Pl}}^2 \epsilon_1} \mathcal{P}_v(k) = \frac{k^3}{4\pi^2 a^2 \epsilon_1 M_{\mathrm{Pl}}^2} |f_{\boldsymbol{k}}|^2 \,, \tag{2.88}$$

and it only remains to calculate $|f_{\boldsymbol{k}}|^2$.

2.3.4. Power Spectrum at Leading Order in Slow Roll

In the last section, we saw that the calculation of the scalar power spectrum $\mathcal{P}_\zeta(k)$ boils down to solving the differential equation (2.45) for $f_{\boldsymbol{k}}$, with initial condition given by Eq. (2.62). In Eq. (2.45), $\omega^2(\eta, \boldsymbol{k}) = (a\sqrt{\epsilon_1})''/(a\sqrt{\epsilon_1})$ depends on the background function $a(\eta)$, hence on $V(\phi)$ and on the solution of the Klein-Gordon equation (2.6). In practice, it must be solved numerically

once these quantities are specified. However, in the slow-roll approximation, as explained in section 2.2, $a(\eta)$ is close to the de Sitter profile $a(\eta) \propto -1/(H\eta)$, and at the technical level, the slow-roll parameters quantify the deviation of $a(\eta)$ from this de Sitter solution. A priori, $\omega^2(\eta, \boldsymbol{k})$ can therefore be expressed in terms of the slow-roll parameters and Eq. (2.45) can be solved accordingly. This is why in this section, in order to gain some insight on the shape of the power spectrum, we solve Eq. (2.45) at first order in slow roll and we calculate the power spectrum $\mathcal{P}_\zeta(k)$ around some pivot scale k_* at this same order in slow roll.

The first step consists in working out an expression for $a(\eta)$ at first order in slow roll. One can start from the definition of η, given by Eq. (1.62), and write

$$\eta = \int \frac{\mathrm{d}t}{a} = \int \frac{\mathrm{d}a}{a\mathcal{H}}\,, \tag{2.89}$$

where we denote $\mathcal{H} \equiv a'/a = aH$. Writing the last integrand as $1/(a\mathcal{H}) = (\mathrm{d}/\mathrm{d}a)a \times 1/(a\mathcal{H})$, the last integral can be integrated by parts and one obtains

$$\int \frac{\mathrm{d}a}{a\mathcal{H}} = \frac{1}{\mathcal{H}} + \int \frac{\mathrm{d}a}{a\mathcal{H}}(2-\epsilon_1)\,, \tag{2.90}$$

where $\epsilon_1 = 1 - \dot{H}/H^2 = -\mathcal{H}'/\mathcal{H}^2$ has been defined in Eq. (2.10). The above expression gives rise to

$$\int \frac{\mathrm{d}a}{a\mathcal{H}} = -\frac{1}{\mathcal{H}} + \int \frac{\mathrm{d}a}{a\mathcal{H}}\epsilon_1\,. \tag{2.91}$$

Again, the integral in the right hand side can be integrated by parts. Indeed, its integrand can be written as $\epsilon_1/(a\mathcal{H}) = 1/(a\mathcal{H}) \times \epsilon_1 = (\mathrm{d}/\mathrm{d}a)[-1/\mathcal{H} + \int \mathrm{d}a\epsilon_1/(a\mathcal{H})] \times \epsilon_1$, where we have made use of Eq. (2.91) itself to integrate $1/(a\mathcal{H})$. Therefore, one obtains

$$\begin{aligned}
\int \frac{\mathrm{d}a}{a\mathcal{H}}\epsilon_1 &= -\frac{\epsilon_1}{\mathcal{H}} + \epsilon_1 \int \frac{\epsilon_1 \mathrm{d}a}{a\mathcal{H}} + \int \frac{\epsilon_1\epsilon_2 \mathrm{d}a}{a\mathcal{H}} - \int \left[\frac{\mathrm{d}}{\mathrm{d}a}(\epsilon_1) \int \frac{\epsilon_1 \mathrm{d}\bar{a}}{\bar{a}\mathcal{H}}\right] \mathrm{d}a & (2.92)\\
&= -\frac{\epsilon_1}{\mathcal{H}} + \epsilon_1 \int \frac{\epsilon_1 \mathrm{d}a}{a\mathcal{H}} + \int \frac{\epsilon_1\epsilon_2 \mathrm{d}a}{a\mathcal{H}} - \epsilon_1 \int \frac{\epsilon_1 \mathrm{d}a}{a\mathcal{H}} + \int \frac{\epsilon_1^2 \mathrm{d}a}{a\mathcal{H}} & (2.93)\\
&= -\frac{\epsilon_1}{\mathcal{H}} + \int \left[\frac{\epsilon_1}{a\mathcal{H}}(\epsilon_1+\epsilon_2)\right] \mathrm{d}a\,, & (2.94)
\end{aligned}$$

where between the first and the second line the last term has been integrated by parts. Plugging Eq. (2.94) into Eq. (2.91) yields an expression for η, namely

$$\eta = -\frac{1+\epsilon_1}{\mathcal{H}} + \int \frac{\mathrm{d}a}{a\mathcal{H}}\left(\epsilon_1^2 + \epsilon_1\epsilon_2\right)\,. \tag{2.95}$$

Since we want to work at first order in slow roll, the last integral can be dropped and one simply has $\eta \simeq -(1+\epsilon_1)/\mathcal{H}$. However, let us notice that if one wanted to derive higher order in slow-roll terms, the same strategy could be used. The integral in the right hand side of Eq. (2.95) could be integrated by parts making use of Eq. (2.94), noticing that its integrand can be written as $\epsilon_1/(a\mathcal{H}) \times (\epsilon_1 + \epsilon_2)$ and that Eq. (2.94) precisely provides us with a formal integral of the first term $\epsilon_1/(a\mathcal{H})$, so on and so forth. At second order in slow roll for example, one would obtain Eq. (2.5) of Ref. [209], see section 3.5. Here however, we work at first order in slow roll and we have

$$\mathcal{H} \simeq -\frac{1+\epsilon_{1*}}{\eta}\,. \tag{2.96}$$

In the above expression, the first slow-roll parameter has been evaluated at the time η_* where the pivot scale k_* crosses the Hubble radius since as will be shown in Eq. (2.99), deviations of ϵ_1

from this value are slow-roll suppressed quantities. If one integrates the above expression along $\mathrm{d}\eta$, one obtains

$$\ln\left(\frac{a}{a_*}\right) \simeq (1+\epsilon_{1*})\ln\left(\frac{\eta_*}{\eta}\right) \tag{2.97}$$

from which one has after exponentiation, and at first order in slow roll, $a/a_* = \eta_*/\eta[1-\epsilon_{1*}\ln(\eta/\eta_*)]$. Looking at Eq. (2.96), the time η_* can be expressed as $\eta_* = -(1+\epsilon_{1*})/\mathcal{H}_*$, so that one eventually has

$$a \simeq -\frac{1}{H_*\eta}\left[1+\epsilon_{1*}-\epsilon_{1*}\ln\left(\frac{\eta}{\eta_*}\right)\right]. \tag{2.98}$$

We have therefore reached our first goal, namely to find an expression for $a(\eta)$ at first order in slow roll. Notice that when $\epsilon_{1*}=0$, one recovers the de Sitter profile $a(\eta) = -1/(H\eta)$. Now we need to calculate the corresponding behaviour of $\omega^2(\eta,\boldsymbol{k}) = (a\sqrt{\epsilon_1})''/(a\sqrt{\epsilon_1})$ at leading order in slow roll. The first slow-roll parameter ϵ_1 can be expanded at first order in slow roll around the time η_*, and one has

$$\begin{aligned}
\epsilon_1 &\simeq \epsilon_{1*} + \left.\frac{\mathrm{d}\epsilon_1}{\mathrm{d}N}\right|_{\eta_*}(N-N_*) \simeq \epsilon_{1*} + \epsilon_{1*}\epsilon_{2*}\ln\left(\frac{a}{a_*}\right) \\
&\simeq \epsilon_{1*} - \epsilon_{1*}\epsilon_{2*}(1+\epsilon_{1*})\ln\left(\frac{\eta}{\eta_*}\right) \\
&\simeq \epsilon_{1*}\left[1-\epsilon_{2*}\ln\left(\frac{\eta}{\eta_*}\right)\right],
\end{aligned} \tag{2.99}$$

where in the second line we have used Eq. (2.97) to express $\ln(a)$ in terms of η. At this point, with Eqs. (2.98) and (2.99), we are in a position where we can calculate ω^2 at first order in slow roll. After a straightforward calculation, one obtains

$$\frac{\left(a\sqrt{\epsilon_1}\right)''}{a\sqrt{\epsilon_1}} \simeq \frac{2}{\eta^2}\left(1+\frac{3}{2}\epsilon_{1*}+\frac{3}{4}\epsilon_{2*}\right). \tag{2.100}$$

In particular, one notices that the logarithmic terms in η cancel out at first order in slow roll, which makes the previous expression quite simple and easy to handle. Indeed, at this order, Eq. (2.45) reads

$$f_{\boldsymbol{k}}'' + \left[k^2 - \frac{2}{\eta^2}\left(1+\frac{3}{2}\epsilon_{1*}+\frac{3}{4}\epsilon_{2*}\right)\right] f_{\boldsymbol{k}} = 0\,. \tag{2.101}$$

Conveniently enough, such a differential equation can be solved in terms of Hankel functions, and one obtains

$$f_{\boldsymbol{k}} = C_{\boldsymbol{k}}\sqrt{-k\eta}H_\nu^{(1)}(-k\eta) + D_{\boldsymbol{k}}\sqrt{-k\eta}H_\nu^{(2)}(-k\eta)\,, \tag{2.102}$$

with

$$\nu = \frac{3}{2}\sqrt{1+\frac{4}{3}\epsilon_{1*}+\frac{2}{3}\epsilon_{2*}} \tag{2.103}$$

$$\simeq \frac{3}{2}+\epsilon_{1*}+\frac{\epsilon_{2*}}{2}\,. \tag{2.104}$$

In Eq. (2.102), $H_\nu^{(1)}$ and $H_\nu^{(2)}$ are Hankel functions [269] (also called Bessel functions of the third kind), and $C_{\boldsymbol{k}}$ and $D_{\boldsymbol{k}}$ are integration constants.

These constants can be set so that the Bunch-Davies vacuum (2.62) is recovered at early time. In Eq. (2.62) the limit $k/(aH)\to+\infty$ actually corresponds to $k\eta\to-\infty$ since from Eq. (2.96)

one has $k/(aH) = k/\mathcal{H} \simeq -k\eta/(1+\epsilon_{1*})$. Since one has [269] $H_\nu^{(1)}(z) \simeq \sqrt{2/(\pi z)}\exp[i(z - \nu\pi/2 - \pi/4)]$ and $H_\nu^{(2)}(z) \simeq \sqrt{2/(\pi z)}\exp[-i(z-\nu\pi/2-\pi/4)]$ when $z \gg 1$, one obtains

$$f_{\boldsymbol{k}} \underset{k\eta\to-\infty}{\longrightarrow} C_{\boldsymbol{k}}\sqrt{\frac{2}{\pi}}\exp\left[-i\left(k\eta+\frac{\nu\pi}{2}+\frac{\pi}{4}\right)\right] + D_{\boldsymbol{k}}\sqrt{\frac{2}{\pi}}\exp\left[i\left(k\eta+\frac{\nu\pi}{2}+\frac{\pi}{4}\right)\right]. \tag{2.105}$$

This is why in order to match Eq. (2.62), one must set $C_{\boldsymbol{k}} = 0$ and $D_{\boldsymbol{k}} = \sqrt{\pi/k}\exp[-i\pi/2(\nu+1/2)]/2$. One eventually has

$$f_{\boldsymbol{k}} = \frac{1}{2}\sqrt{\frac{\pi}{k}}\sqrt{-k\eta}\mathrm{e}^{-i\frac{\pi}{2}\left(\nu+\frac{1}{2}\right)}H_\nu^{(2)}(-k\eta). \tag{2.106}$$

At the end of inflation, the pivot scale k_* around which we are expanding the power spectrum and which is of astrophysical interest today, is much larger than the Hubble radius, *i.e.* $k_*/(a_{\rm end}H_{\rm end}) \ll 1$. In Fig. 2.3, this corresponds to the observational window located at the end of inflation where $\mathcal{P}(k)$ is calculated. Since we have shown that $k/(aH) \simeq -k\eta$, this means that the power spectrum (2.88), which scales as $|f_{\boldsymbol{k}}|^2$, can be approximated at the end of inflation in the limit $k\eta \to 0^-$. Since one has [269] $H_\nu^{(2)}(z) \simeq -i(2/z)^\nu\Gamma(\nu)/\pi$ when $z \to 0$, one obtains

$$|f_{\boldsymbol{k}}|^2 \underset{k\eta\to0^-}{\longrightarrow} \frac{-k\eta}{4k}\left(\frac{2}{-k\eta}\right)^{2\nu}\frac{\Gamma^2(\nu)}{\pi}. \tag{2.107}$$

In order to be consistent with our first order in slow roll expansion, the slow-roll parameters appearing in ν, see Eq. (2.104), should now be expanded too. One has $\Gamma(\nu) = \Gamma(3/2) + \Gamma'(3/2)(\epsilon_{1*}+\epsilon_{2*}/2)$, where [269] $\Gamma'(3/2) = \Gamma(3/2)(2-2\ln 2-\gamma_{\rm E})$ and $\Gamma(3/2) = \sqrt{\pi}/2$, $\gamma_{\rm E}$ being the Euler-Mascheroni constant. On the other hand, one can write $[-2/(k\eta)]^{2\nu} = \mathrm{e}^{2\nu\ln[-2/(k\eta)]} \simeq [-2/(k\eta)]^3\{1+(2\epsilon_{1*}+\epsilon_{2*})\ln[-2/(k\eta)]\}$. Plugging these expressions in Eq. (2.107), one obtains

$$|f_{\boldsymbol{k}}|^2 \underset{k\eta\to0^-}{\longrightarrow} \frac{1}{2k}\frac{1}{(k\eta)^2}\left\{1+(2\epsilon_{1*}+\epsilon_{2*})\left[2-\ln 2-\gamma_{\rm E}-\ln(-k\eta)\right]\right\}. \tag{2.108}$$

We now have everything one needs to calculate the power spectrum $\mathcal{P}_\zeta$ at first order in slow roll. In Eq. (2.88), let us replace a by Eq. (2.98), ϵ_1 by Eq. (2.99), and $|f_{\boldsymbol{k}}|^2$ by Eq. (2.108). One obtains, at first order in slow roll,

$$\mathcal{P}_\zeta(k) = \frac{H_*^2}{8\pi^2\epsilon_{1*}M_{\rm Pl}^2}\left[2(1-\ln 2-\gamma_{\rm E})\epsilon_{1*} + (2-\ln 2-\gamma_{\rm E})\epsilon_{2*} - (2\epsilon_{1*}+\epsilon_{2*})\ln(-k\eta_*)\right]. \tag{2.109}$$

One can see that quite remarkably, the dependence in η has cancelled out since, as announced, the curvature perturbations are constant on large scales. The time η_* can be expressed in terms of k_* since by definition, it is such that $k_*/(a_*H_*) = 1$. Since Eq. (2.96) gives $k/(aH) = k/\mathcal{H} = -k\eta(1+\epsilon_{1*})$, one simply has $-k\eta_* = (k/k_*)(1+\epsilon_{1*})^{-1}$. Denoting $C \equiv \ln 2 + \gamma_{\rm E} - 2 \simeq -0.7296$ for simplicity, the power spectrum of curvature perturbations calculated at the end of inflation, at first order in slow roll, is finally given by

$$\mathcal{P}_\zeta(k) = \frac{H_*^2}{8\pi^2\epsilon_{1*}M_{\rm Pl}^2}\left[1-2(C+1)\epsilon_{1*} - C\epsilon_{2*} - (2\epsilon_{1*}+\epsilon_{2*})\ln\left(\frac{k}{k_*}\right)\right]. \tag{2.110}$$

This result was derived for the first time in Ref. [128], where the corresponding formula for gravity waves was obtained too. Indeed, the same procedure as the one presented here can be employed to calculate the power spectrum of tensor perturbations $\mathcal{P}_h$. Instead of Eq. (2.45), one has to solve an equation of the form $h'' + (k^2 - a''/a)h = 0$, and one obtains

$$\mathcal{P}_h(k) = \frac{2H_*^2}{\pi^2M_{\rm Pl}^2}\left[1-2(C+1)\epsilon_{1*} - 2\epsilon_{1*}\ln\left(\frac{k}{k_*}\right)\right]. \tag{2.111}$$

Before that, scalar perturbations during inflation were first integrated in Refs. [270, 242] and tensor perturbations in Ref. [121].[5] The same result (2.110) was later re-derived using the Green function method in Ref. [272], using the Wentzel-Kramers-Brillouin (WKB) method in Ref. [273] and using the uniform approximation in Refs. [274, 275]. In fact, the Green function method of Ref. [272] made possible the first determination of the scalar power spectrum at second order in slow roll, since at second order, the mode equation (2.45) describing the evolution of the cosmological perturbations can no longer be solved exactly, hence the need for a new method of approximation.[6] Finally, the first derivation of the tensor power spectrum at second order in slow roll using the Green function method was presented in Ref. [278].

A few comments are in order regarding Eqs. (2.110) and (2.111). First of all, as announced, at leading order in slow roll, these two spectra are scale invariant, that is the power on each scale k does not depend on k. For scalar perturbations, the overall amplitude is measured to be [163, 167] $\mathcal{P}_\zeta(k_*) \simeq 2.203 \times 10^{-9}$. More precisely, the small deviations from scale invariance appear through the logarithm of k, and are controlled by the slow-roll parameters, which quantify the deviation of space-time from de Sitter, see Eq. (2.9), or equivalently the non flatness of the potential, see Eqs. (2.14)-(2.17). As a consequence, measuring the scale dependence of the power spectrum is a way of constraining the inflationary potential $V(\phi)$. For scalar perturbations, the deviation from scale invariance of the power spectrum is often described in terms of the scalar spectral index n_{S}, defined as

$$n_{\mathrm{S}} \equiv 1 + \frac{\mathrm{d}\ln\mathcal{P}_\zeta}{\mathrm{d}\ln k}\,, \tag{2.112}$$

where $n_{\mathrm{S}} = 1$ for exact scale invariance. At first order in slow roll, from Eq. (2.110), it is given by $n_{\mathrm{S}} = 1 - 2\epsilon_{1*} - \epsilon_{2*}$. By definition, the first slow-roll parameter $\epsilon_1 = -\dot{H}/H^2$ is always positive. The second slow-roll parameter is proportional to its time derivative, $\epsilon_2 = (\mathrm{d}\epsilon_1/\mathrm{d}N)/\epsilon_1$. Inflation takes place as long as $\epsilon_1 < 1$, and if it ends with a "graceful exit" when $\epsilon_1 = 1$, it is natural to assume that ϵ_1 increases during inflation, and therefore that ϵ_2 is positive too. As a consequence, a rather natural prediction [122, 279] of slow-roll inflation is that the scalar power spectrum should be almost scale invariant but slightly red, *i.e.* "$n_{\mathrm{S}} < 1$" (as opposed to "blue", for which $n_{\mathrm{S}} > 1$). This is why it is quite remarkable that the most recent observations [163, 167] strongly favour a red scalar spectrum, $n_{\mathrm{S}} = 0.9619 \pm 0.0073$, which excludes exact scale invariance $n_{\mathrm{S}} = 1$ at more than the 5σ confidence level. As for tensors, the deviation from scale invariance is usually described in terms of the tensor spectral index

$$n_{\mathrm{T}} \equiv \frac{\mathrm{d}\ln\mathcal{P}_h}{\mathrm{d}\ln k}\,, \tag{2.113}$$

where $n_{\mathrm{T}} = 0$ for exact scale invariance. At first order in slow roll, from Eq. (2.111), it is given by $n_{\mathrm{T}} = -2\epsilon_{1*}$. Since ϵ_1 is always positive, this means that the tensor spectral index is generically red ($n_{\mathrm{T}} < 0$) in slow-roll inflation. The sign of n_{T} has not been measured so far, but one can see that it would be an additional test for slow-roll inflation. If one ever finds that a blue spectrum $n_{\mathrm{T}} > 0$ is favoured, this would be difficult to explain in the framework presented here, and alternatives such as, for instance, string gas cosmology which predicts a blue spectrum [280], would be a possible solution. Another useful quantity to calculate is the ratio r between the amplitude of both power spectra,

$$r \equiv \frac{\mathcal{P}_h(k_*)}{\mathcal{P}_\zeta(k_*)} \simeq 16\epsilon_{1*}\,, \tag{2.114}$$

[5] In Ref. [271], it was also realized that the power spectrum can be evaluated exactly in the case of power-law inflation, for which $a(\eta) \propto |\eta|^\beta$.

[6] In Refs. [276, 277], it was also shown how to improve the WKB method by adding more adiabatic terms. This improved WKB method has allowed a re-derivation of the scalar and tensor power spectra at second order and confirmed the results of the Green function approach.

where its first order expression in slow roll has been derived thanks to Eqs. (2.110) and (2.111). Since ϵ_1 is a small parameter in slow-roll inflation, this means that tensor perturbations are generically suppressed with respect to scalar perturbations. This is why in practice, it seems difficult to directly measure the gravitational primordial power spectrum. However, tensor perturbations leave an indirect imprint in the polarization pattern of the CMB through its rotational component (dubbed "B mode") that scalar cannot, by definition, produce. Recently the BICEP2 experiment [164] has reported the detection of this B mode signal. If it is of primordial origin, the associated value for r is found to be $r = 0.16^{+0.06}_{-0.05}$. This value carries important physical consequences, notably, it allows to constrain the energy scale $\rho_* = 3M_{\rm Pl}^2 H_*^2$ of inflation. Indeed, combining Eqs. (2.110), (2.111) and (2.114), one obtains

$$\rho_*^{1/4} = 2.0 \times 10^{16} \left(\frac{r}{0.16}\right)^{1/4} \left(\frac{\mathcal{P}}{2.2 \times 10^{-9}}\right)^{1/4} \text{GeV}\,, \tag{2.115}$$

which corresponds to GUT energy scales. If such a detection is confirmed, therefore, inflation is a high energy phenomenon by Particle Physics standard. Such a value of r also implies a large field excursion. Indeed, because of the relation (2.19), one has $\Delta\phi/M_{\rm Pl} \sim \sqrt{2\epsilon_1} M_{\rm Pl} \Delta N = \mathcal{O}(1)\,(r/0.16)^{1/2}$ [281, 282], which indicates that the excursion of the field during inflation is necessarily super-Planckian. This raises model building issues since most inflationary theoretical setups arise as effective field theories relying on sub-Planckian expansions [283].

Finally, a last comment is in order concerning the value of $\mathcal{P}_\zeta \sim 10^{-9}$. Indeed, during the typical inflationary time scale of one e-fold , as just mentioned, the field excursion $\Delta\phi_{\rm cl}$ under the "classical" Klein-Gordon equation (2.6) is given by $\Delta\phi_{\rm cl} \sim \sqrt{2\epsilon_1} M_{\rm Pl}$. On the other hand, as we will see in the next section, quantum fluctuations in the scalar sector modify the inflaton dynamics, which translates into a quantum excursion $\Delta\phi_{\rm qu} = H/(2\pi)$. As a consequence, the ratio between these two field excursions, which roughly quantifies how much the quantum effects modify the inflationary dynamics, is given by $\Delta\phi_{\rm qu}/\Delta\phi_{\rm cl} = H/\sqrt{8\pi^2 M_{\rm Pl}^2 \epsilon_1} = \sqrt{\mathcal{P}_\zeta}$. As a consequence, the small measured value of $\mathcal{P}_\zeta$ indicates that the quantum effects on the inflaton dynamics are small, at least at Hubble exit time of the modes of astrophysical interest today. Hence the classical trajectory (2.6) can safely be used as a first approximation. In the next section, we discuss in more details the implementation of quantum effects on the inflationary dynamics, notably by means of the "stochastic inflation" formalism.

2.4. Stochastic Inflation

As explained in section 2.3, in the standard description of inflation, the homogeneous parts of the fields are usually assumed to behave classically, while the small deviations from homogeneity and isotropy over this classical background are treated quantum mechanically. However, one expects quantum corrections to the classical trajectory to modify the way the background evolves [284, 285, 286, 287, 288, 289]. The stochastic inflation formalism [290, 291, 292, 293, 294, 295, 296, 297, 289, 298] aims at modeling this physics. The idea is to treat the dynamics of the inflaton field coarse-grained over length scales larger than the Hubble radius, by integrating out the sub-Hubble degrees of freedom. It amounts to working out the effective theory for an open quantum system made of the large scale modes of the field operators. When such a theory is derived, it can be shown that the dynamics of the coarse-grained field φ is modified by the presence of a stochastic term, so that its slow-roll equation of motion $\mathrm{d}\varphi/\mathrm{d}N = -V'/(3H^2)$ is modified and becomes a Langevin equation of the form [290]

$$\frac{\mathrm{d}\varphi}{\mathrm{d}N} = -\frac{V'}{3H^2} + \frac{H}{2\pi}\xi\,(N)\,, \tag{2.116}$$

where ξ is a normalized white Gaussian noise, such that $\langle \xi(N) \rangle = 0$ and $\langle \xi(N_1)\xi(N_2) \rangle = \delta(N_1 - N_2)$. What makes this formalism very appealing is that it reproduces results from quantum field theory in curved space-times, even beyond the perturbative level [298, 299, 300, 301]. For example, in Ref. [302], it is shown that stochastic inflation reproduces perturbative calculations of quantum field theories with non-conformal fields, in particular its secular effects which take the form of "infrared logarithms". Not only stochastic inflation accounts for the leading infrared logarithms at each order in perturbation theory, but it can even describe the regimes where inflation proceeds so long that the large logarithms overwhelm small coupling constants. In Refs. [303, 304], this technique was extended to scalar quantum electrodynamics on a de Sitter background. As one can see, stochastic inflation is therefore more than just a qualitative description of some backreaction effects, but it provides us with a very powerful and straightforward frame of calculation for quantum field theoretic effects on inflationary space-times.

This section is organized as follows. First, in section 2.4.1, we detail an heuristic derivation of the Langevin equations of stochastic inflation. This allows us to emphasize a few important aspects of the nature of the formalism and of the assumptions it rests on. Then, in section 2.4.2, we elaborate on the reasons why this equation needs to be written and solved with the number of e-folds as the time variable. Since it happens quite often that a different time variable is used in the literature, it seems important to stress why it is *a priori* wrong to do so. Finally, in section 2.4.3 we address the issue of the calculation of physical observable quantities in stochastic inflation such as the power spectrum of adiabatic perturbations. Making use of the δN formalism, we show that the stochastic setup enables to reproduce the standard result (derived in section 2.3) of linear perturbation theory, in a "classical" limit that we carefully define. Then, we provide complete solutions which do not rely on an expansion in the noise terms and which are therefore valid even when the stochastic effects are large. Generic formulas are provided that can be straightforwardly applied to any single field potential, and as an example, the case of a large field potential $V \propto \phi^p$ is completely worked out. To our knowledge, it is the first time such a non perturbative calculation of the power spectrum in stochastic inflation is presented.

2.4.1. Heuristic Derivation of the Langevin Equations

The basic strategy of stochastic inflation is to introduce a cutoff in Fourier space through a suitable time-dependent window function that filters out the modes whose frequency is higher than the comoving horizon size. The inflaton field is thus split in two differently behaving parts: the short-wavelength part which is treated as a fully quantum operator, and the coarse-grained one which collects the remaining super-horizon modes and which is treated as classical. A Langevin equation of motion for the long-wavelength part can be obtained, where the sub-horizon modes enter as a classical stochastic noise term that perturbs the dynamics of the coarse-grained field. In this section, we give a detailed derivation of such a stochastic equation of motion for the coarse-grained field, based on a heuristic argument dealing with the equation of motion only.

However, it is worth mentioning that a more general approach can be followed that exploits the influence functional method [305, 306] and operates the frequency splitting at the action level, getting rid of the high frequencies via a path-integral over the sub-horizon part of the field. The effective action obtained by this process contains some extra terms that can be interpreted as the coupling of the super-horizon field with a classical random noise source, whose configurations are statistically weighted by an appropriate functional probability distribution, becoming the

origin of the stochastic character of the Langevin equation of motion. In some sense, stochastic inflation is therefore nothing more that a direct application of the well-known non equilibrium quantum field theories for open quantum systems, to inflationary cosmologies.

2.4.1.1. Coarse-Grained Field

The starting point of the stochastic formalism is to divide the inflaton field ϕ into two pieces, $\phi = \varphi + \phi_>$. The coarse-grained field φ contains all wavelengths much larger than the Hubble radius, *i.e.* such that $k < \sigma a H$, where $\sigma \ll 1$ is a fixed parameter that sets the coarse-graining scale. On the other hand, $\phi_>$ collects the small wavelength modes, and can be written as

$$\phi_> (\boldsymbol{x}, N) = \int \frac{\mathrm{d}\boldsymbol{k}}{(2\pi)^{\frac{3}{2}}} W\left(\frac{k}{\sigma a H}\right) \left[\mathrm{e}^{-i\boldsymbol{k}\cdot\boldsymbol{x}} \phi_{\boldsymbol{k}} (N)\, a_{\boldsymbol{k}} + \mathrm{e}^{i\boldsymbol{k}\cdot\boldsymbol{x}} \phi^*_{\boldsymbol{k}} (N)\, a^\dagger_{\boldsymbol{k}}\right] , \tag{2.117}$$

where W is a filter function so that $W \simeq 0$ when its argument is small, $k/(\sigma a H) \ll 1$, and $W \simeq 1$ when its argument is large, $k/(\sigma a H) \gg 1$. The idea is to derive an effective equation of motion for φ, integrating out the degrees of freedom contained in $\phi_>$.

The time dependence in the argument of the window function translates the fact that modes are continuously leaving the small wavelength part of the field $\phi_>$ to source the coarse-grained part φ. Therefore, one expects the dynamics of the coarse-grained field to be kicked by the inflow of modes which cross the Hubble radius during inflation. It is important to stress that the effect one shall obtain is only due to this continuous Hubble crossing of modes, rather than to some fundamental coupling between super-Hubble and sub-Hubble modes.[7]

2.4.1.2. Split Klein-Gordon Equation

We start from the Klein-Gordon equation of the field $\phi(\boldsymbol{x}, t)$ given by Eq. (2.6), but we rewrite it in terms of the number of e-folds $N \equiv \ln a$, that is

$$\frac{\partial^2 \phi (\boldsymbol{x}, N)}{\partial N^2} + (3 - \epsilon_1) \frac{\partial \phi (\boldsymbol{x}, N)}{\partial N} - \frac{\nabla^2}{a^2 H^2} \phi (\boldsymbol{x}, N) + \frac{V' [\phi (\boldsymbol{x}, N)]}{H^2} = 0 . \tag{2.118}$$

The reasons why it is crucial to work with N as the time variable are explained in section 2.4.2. It is important to stress that in the stochastic inflationary setup, the short wavelength perturbations are taken to be test perturbations, in the sense that the background functions H, aH and ϵ_1 appearing in Eq. (2.118) are to be evaluated at the coarse-grained field φ only, through the Friedmann equation (2.7). Written in terms of φ and $\partial\varphi/\partial N$ only, the latter is given by

$$H^2 = \frac{V(\varphi)}{3M_{\mathrm{Pl}}^2 - \frac{1}{2}\left(\frac{\mathrm{d}\varphi}{\mathrm{d}N}\right)^2} . \tag{2.119}$$

Here we have not displayed any gradient term since it is σ-suppressed for φ. In the same manner, the first slow-roll parameter $\epsilon_1 = -(\mathrm{d}H/\mathrm{d}N)/H$ can simply be expressed in terms of $\mathrm{d}\phi/\mathrm{d}N$ as $\epsilon_1 = (\mathrm{d}\phi/\mathrm{d}N)^2/(2M_{\mathrm{Pl}}^2)$, see Eq. (2.15).

Let us now plug the decomposition $\phi = \varphi + \phi_>$ into the Klein-Gordon equation (2.118), and expand the obtained result at first order in $\phi_>$. One obtains

$$\frac{\partial^2 \varphi}{\partial N^2} + (3 - \epsilon_1) \frac{\partial \varphi}{\partial N} + \frac{V'(\varphi)}{H^2} = -\frac{\partial^2 \phi_>}{\partial N^2} - (3 - \epsilon_1) \frac{\partial \phi_>}{\partial N} + \frac{\nabla^2 \phi_>}{(aH)^2} - \frac{V''(\varphi)}{H^2} \phi_> , \tag{2.120}$$

[7] Such couplings would need to be taken into account *e.g.* beyond linear order in perturbation theory.

where the gradient term for φ has been dropped for the same reason as above. Again, H and ϵ_1 have to be understood as functions of φ and $\partial\varphi/\partial N$. The right hand side of this equation can be written with the Fourier expansion (2.117). Before doing so, to simplify notations, we first introduce the hermitian operators $A_{\boldsymbol{k}}$, defined as

$$A_{\boldsymbol{k}}\left(\boldsymbol{x},N\right)=\mathrm{e}^{-i\boldsymbol{k}\cdot\boldsymbol{x}}\phi_{\boldsymbol{k}}\left(N\right)a_{\boldsymbol{k}}+\mathrm{e}^{i\boldsymbol{k}\cdot\boldsymbol{x}}\phi_{\boldsymbol{k}}^{*}\left(N\right)a_{\boldsymbol{k}}^{\dagger}\,, \tag{2.121}$$

so that for example, the Fourier expansion of ϕ is simply given by $(2\pi)^{-3/2}\phi=\int\mathrm{d}\boldsymbol{k}A_{\boldsymbol{k}}$. One obtains

$$\begin{aligned}\frac{\partial^2\varphi}{\partial N^2}+\left(3-\epsilon_1\right)\frac{\partial\varphi}{\partial N}+\frac{V'\left(\varphi\right)}{H^2}=-\int\frac{\mathrm{d}\boldsymbol{k}}{\left(2\pi\right)^{3/2}}\left\{\frac{\partial}{\partial N}W\left(\frac{k}{\sigma aH}\right)\left[2\frac{\partial A_{\boldsymbol{k}}}{\partial N}+\left(3-\epsilon_1\right)A_{\boldsymbol{k}}\right]\right.\\ \left.+\frac{\partial^2}{\partial N^2}W\left(\frac{k}{\sigma aH}\right)A_{\boldsymbol{k}}+W\left(\frac{k}{\sigma aH}\right)\left[\frac{\partial^2A_{\boldsymbol{k}}}{\partial N^2}+\left(3-\epsilon_1\right)\frac{\partial A_{\boldsymbol{k}}}{\partial N}+\left(\frac{V''}{H^2}+\frac{k^2}{a^2H^2}\right)A_{\boldsymbol{k}}\right]\right\}.\end{aligned} \tag{2.122}$$

In this equation, it is clear that the last bracketed term vanishes since from the definition (2.121) of the $A_{\boldsymbol{k}}$ operators, it involves the equation of motion for $\phi_{\boldsymbol{k}}$ and for $\phi_{\boldsymbol{k}}^*$ that one obtains by Fourier expanding Eq. (2.118). This is why, if one lets

$$\xi_1=-\int\frac{\mathrm{d}\boldsymbol{k}}{\left(2\pi\right)^{3/2}}\frac{\partial}{\partial N}\left[W\left(\frac{k}{\sigma aH}\right)\right]A_{\boldsymbol{k}} \tag{2.123}$$

and

$$\xi_2=-\int\frac{\mathrm{d}\boldsymbol{k}}{\left(2\pi\right)^{3/2}}\frac{\partial}{\partial N}\left[W\left(\frac{k}{\sigma aH}\right)\right]\frac{\partial A_{\boldsymbol{k}}}{\partial N}\,, \tag{2.124}$$

the split Klein-Gordon equation can be written as

$$\frac{\partial^2\varphi}{\partial N^2}+\left(3-\epsilon_1\right)\frac{\partial\varphi}{\partial N}+\frac{V'\left(\varphi\right)}{H^2}=\left(3-\epsilon_1\right)\xi_1+\frac{\partial\xi_1}{\partial N}-\xi_2\,. \tag{2.125}$$

2.4.1.3. Stochastic Processes

A crucial ingredient of the stochastic inflationary setup is the statement that the coarse-grained field can be described in terms of a classical stochastic quantity. Indeed, it can be shown that as the cosmological perturbations cross the Hubble radius, they evolve from a coherent vacuum state to a strongly squeezed state [131], the corresponding squeezing being much more important than whatever can be realized in the laboratory [307]. In this limit, the predictions of the quantum formalism are indistinguishable from that of a theory where the fluctuations are just assumed to be realizations of a classical stochastic process [308, 132, 309, 310]. The classical limit is a subtle concept in quantum mechanics but, in this sense, such a system can be characterized as being classical [136]. Moreover, the large-scale cosmological perturbations are not isolated and, as a consequence, the phenomenon of decoherence [311, 312, 313] is relevant for them, which is also considered as playing a role in their quantum-to-classical transition [132, 314, 309, 315, 133, 316, 317, 318, 319].

This is why in the $\sigma\ll1$ limit where φ contains only super-Hubble, largely squeezed modes, the terms ξ_1 and ξ_2 can be treated[8] as classical noise sources acting on a stochastic coarse-grained field φ, through a split Klein-Gordon equation which becomes a Langevin equation for φ. This

[8] This is rigorously showed within the Keldysh formalism, see Refs. [305, 306]

is the stochastic inflationary setup. The mapping between ξ_1 and ξ_2 (which are, strictly speaking, quantum operators) and their classical noise counterparts is made by identifying quantum expectation values with stochastic moments, *i.e.* by requiring that

$$\left\langle \xi_i^p\left(\boldsymbol{x}_1,N_1\right)\xi_j^q\left(\boldsymbol{x}_2,N_2\right)\right\rangle = \left\langle 0\left|T\left[\xi_i^p\left(\boldsymbol{x}_1,N_1\right)\xi_j^q\left(\boldsymbol{x}_2,N_2\right)\right]\right|0\right\rangle , \tag{2.126}$$

where i and j stand for 1 or 2, p and q are natural integers, and where the T-product is the time ordering product. Note that in the left hand side of the above, the angle brackets stand for stochastic average while in the right hand side, they denote the bra and the ket of the vacuum state $|0\rangle$.

2.4.1.4. Noise Moments

Since the field fluctuations $\phi_{\boldsymbol{k}}$ are Gaussian to a good level of approximation, and since ξ_1 and ξ_2 are linearly constructed out of them, they also follow Gaussian statistics and it is enough to calculate their second moments to fully characterize them. First of all, T-products of $A_{\boldsymbol{k}}$'s and $\partial A_{\boldsymbol{k}}/\partial N$'s need to be worked out. Making use of the canonical relations $\langle 0|T[a_{\boldsymbol{k}_1}a^\dagger_{\boldsymbol{k}_2}]|0\rangle = \delta(\boldsymbol{k}_1-\boldsymbol{k}_2)$ and $\langle 0|T[a_{\boldsymbol{k}_1}a_{\boldsymbol{k}_2}]|0\rangle = \langle 0|T[a^\dagger_{\boldsymbol{k}_1}a^\dagger_{\boldsymbol{k}_2}]|0\rangle = \langle 0|T[a^\dagger_{\boldsymbol{k}_1}a_{\boldsymbol{k}_2}]|0\rangle = 0$, from the definition (2.121) one obtains

$$\left\langle A_{\boldsymbol{k}_1}\left(\boldsymbol{x}_1,N_1\right)A_{\boldsymbol{k}_2}\left(\boldsymbol{x}_2,N_2\right)\right\rangle = \phi_{\boldsymbol{k}_1}\left(N_1\right)\phi^*_{\boldsymbol{k}_2}\left(N_2\right)\mathrm{e}^{i\boldsymbol{k}_1\cdot\left(\boldsymbol{x}_2-\boldsymbol{x}_1\right)}\delta\left(\boldsymbol{k}_1-\boldsymbol{k_2}\right), \tag{2.127}$$

$$\left\langle A_{\boldsymbol{k}_1}\left(\boldsymbol{x}_1,N_1\right)\frac{\partial A_{\boldsymbol{k}_2}}{\partial N}\left(\boldsymbol{x}_2,N_2\right)\right\rangle = \phi_{\boldsymbol{k}_1}\left(N_1\right)\frac{\partial\phi^*_{\boldsymbol{k}_2}}{\partial N}\left(N_2\right)\mathrm{e}^{i\boldsymbol{k}_1\cdot\left(\boldsymbol{x}_2-\boldsymbol{x}_1\right)}\delta\left(\boldsymbol{k}_1-\boldsymbol{k_2}\right), \tag{2.128}$$

$$\left\langle \frac{\partial A_{\boldsymbol{k}_1}}{\partial N}\left(\boldsymbol{x}_1,N_1\right)\frac{\partial A_{\boldsymbol{k}_2}}{\partial N}\left(\boldsymbol{x}_2,N_2\right)\right\rangle = \frac{\partial\phi_{\boldsymbol{k}_1}}{\partial N}\left(N_1\right)\frac{\partial\phi^*_{\boldsymbol{k}_2}}{\partial N}\left(N_2\right)\mathrm{e}^{i\boldsymbol{k}_1\cdot\left(\boldsymbol{x}_2-\boldsymbol{x}_1\right)}\delta\left(\boldsymbol{k}_1-\boldsymbol{k_2}\right). \tag{2.129}$$

Let us proceed with the details of the calculation for $\langle\xi_1\xi_1\rangle$, since the expressions for $\langle\xi_1\xi_2\rangle$ and $\langle\xi_2\xi_2\rangle$ will follow accordingly. Making use of Eq. (2.127), one obtains

$$\left\langle \xi_1\left(\boldsymbol{x}_1,N_1\right)\xi_1\left(\boldsymbol{x}_2,N_2\right)\right\rangle = \int\frac{\mathrm{d}\boldsymbol{k}_1\mathrm{d}\boldsymbol{k}_2}{\left(2\pi\right)^3}\frac{\partial}{\partial N}W\left[\frac{k_1}{\sigma a\left(N_1\right)H\left(N_1\right)}\right]\frac{\partial}{\partial N}W\left[\frac{k_2}{\sigma a\left(N_2\right)H\left(N_2\right)}\right]$$
$$\times\phi_{\boldsymbol{k}_1}\left(N_1\right)\phi^*_{\boldsymbol{k}_2}\left(N_2\right)\mathrm{e}^{i\boldsymbol{k}_1\left(\cdot\boldsymbol{x}_2\boldsymbol{x}_1\right)}\delta\left(\boldsymbol{k}_1-\boldsymbol{k}_2\right) \tag{2.130}$$

$$=\int\frac{\mathrm{d}\boldsymbol{k}}{\left(2\pi\right)^3}\frac{\partial}{\partial N}W\left[\frac{k}{\sigma a\left(N_1\right)H\left(N_1\right)}\right]\frac{\partial}{\partial N}W\left[\frac{k}{\sigma a\left(N_2\right)H\left(N_2\right)}\right]\phi_{\boldsymbol{k}}\left(N_1\right)\phi^*_{\boldsymbol{k}}\left(N_2\right)\mathrm{e}^{i\boldsymbol{k}\cdot\left(\boldsymbol{x}_2-\boldsymbol{x}_1\right)}. \tag{2.131}$$

Let θ be the angle between $\boldsymbol{k}$ and $\boldsymbol{x}_2-\boldsymbol{x}_1$, so that $\boldsymbol{k}\cdot\left(\boldsymbol{x}_2-\boldsymbol{x}_1\right)=kr\cos(\theta)$, where $r\equiv|\boldsymbol{x}_2-\boldsymbol{x}_1|$ and $k=|\boldsymbol{k}|$. Decomposing $\mathrm{d}\boldsymbol{k}=k^2\mathrm{d}k\sin(\theta)\mathrm{d}\theta\mathrm{d}\phi$, the ϕ integration can be factorized out and just gives a 2π factor. The θ integral can also be performed, since one has

$$\int_0^\pi\mathrm{d}\theta\sin\left(\theta\right)\mathrm{e}^{ikr\cos(\theta)} = \left[-\frac{\mathrm{e}^{ikr\cos(\theta)}}{ikr}\right]_0^\pi = 2\frac{\sin\left(kr\right)}{kr}. \tag{2.132}$$

It only remains the k-integral, and one has

$$\left\langle \xi_1\left(\boldsymbol{x}_1,N_1\right)\xi_1\left(\boldsymbol{x}_2,N_2\right)\right\rangle = \tag{2.133}$$
$$\int\frac{k^2\mathrm{d}k}{\left(2\pi\right)^2}\frac{\partial}{\partial N}W\left[\frac{k}{\sigma a\left(N_1\right)H\left(N_1\right)}\right]\frac{\partial}{\partial N}W\left[\frac{k}{\sigma a\left(N_2\right)H\left(N_2\right)}\right]\phi_{\boldsymbol{k}}\left(N_1\right)\phi^*_{\boldsymbol{k}}\left(N_2\right)\frac{\sin\left(kr\right)}{kr}.$$

Another quantity we need to compute is $\partial W/\partial N$. One has

$$\frac{\partial}{\partial N}W\left(\frac{k}{\sigma aH}\right) = \frac{\partial}{\partial N}\left(\frac{k}{\sigma aH}\right)W'\left(\frac{k}{\sigma aH}\right) = \frac{k\left(\epsilon_1-1\right)}{\sigma aH}W'\left(\frac{k}{\sigma aH}\right). \tag{2.134}$$

This is why to proceed, one needs to specify the window function.

2.4.1.5. Window Function and Coloured Noises

A very simple choice for the window function consists in taking a Heaviside step function $W(s) = \theta(s-1)$, so that $W \equiv 1$ when $k \geq \sigma aH$ and $W \equiv 0$ when $k < \sigma aH$. In this case, one has

$$\begin{aligned} W'\left(\frac{k}{\sigma aH}\right) &= \theta'\left(\frac{k}{\sigma aH}-1\right) = \delta\left(\frac{k}{\sigma aH}-1\right) \\ &= \sigma aH\delta\left(k-\sigma aH\right) . \end{aligned} \tag{2.135}$$

Combining this relation with Eq. (2.134), one obtains

$$\begin{aligned} &\frac{\partial}{\partial N}W\left[\frac{k}{\sigma a\left(N_1\right)H\left(N_1\right)}\right]\frac{\partial}{\partial N}W\left[\frac{k}{\sigma a\left(N_2\right)H\left(N_2\right)}\right] \\ &= \sigma^2 a\left(N_1\right)H\left(N_1\right)a\left(N_2\right)H\left(N_2\right)\delta\left[k-\sigma a\left(N_1\right)H\left(N_1\right)\right]\delta\left[k-\sigma a\left(N_2\right)H\left(N_2\right)\right] \\ &= \sigma^2 a\left(N_1\right)H\left(N_1\right)a\left(N_2\right)H\left(N_2\right)\delta\left[k-\sigma a\left(N_1\right)H\left(N_1\right)\right]\delta\left[\sigma a\left(N_1\right)H\left(N_1\right)-\sigma a\left(N_2\right)H\left(N_2\right)\right] \\ &= \sigma^2 a\left(N_1\right)H\left(N_1\right)a\left(N_2\right)H\left(N_2\right)\delta\left[k-\sigma a\left(N_1\right)H\left(N_1\right)\right]\frac{\delta\left(N_1-N_2\right)}{\left(1-\epsilon_1\right)\sigma a\left(N_1\right)H\left(N_1\right)} \\ &= \frac{\sigma a\left(N_1\right)H\left(N_1\right)}{1-\epsilon_1}\delta\left[k-\sigma a\left(N_1\right)H\left(N_1\right)\right]\delta\left(N_1-N_2\right) . \end{aligned} \tag{2.136}$$

One can see that due to the presence of the $\delta(N_1 - N_2)$ term, ξ_1 and ξ_2 are white noises, which means that the value they take at time N_1 is uncorrelated with any of their previous (or future) realizations at times N_2, or said differently, that the noises have no memory of their previous history. Thanks to this property, φ describes a Markovian process.

However, one should note that this is directly due to our choice of a step function as the window function. If smooth window functions were considered instead, one would obtain coloured noises, and consequently non-Markovian processes [320, 321, 322]. This have important physical implications, since coloured noises directly affect the shape of the power spectrum [322] and provide an extra source to the production of non Gaussianities [323]. Even though their treatment is more challenging, coloured noises can be argued to be better motivated, since a sharp cutoff in momentum space gives rise to a rather unnatural window function in position space, and since a wide class of smooth window functions give rise to the same asymptotic coloured noise, so that physical quantities remain independent of the exact shape of the window function.

More precisely, it was shown in Ref. [324] that the final correlations of the coarse-grained field are independent of the window function if it satisfies two properties. First, when written in position space, it must be chosen to be spherically symmetric and $\boldsymbol{x}$-dependent only through the combination $|\boldsymbol{x}|/R$, where $R = 1/(\sigma aH)$ is the length scale over which coarse graining is performed. In this way, W is constrained to have the form $W(x, N) \propto R^{-3}w(|x|/R)$, when represented in position space. Second, the function $w(s)$ must decrease at least as s^{-6} for $s \gg 1$. This is not the case for the Heaviside step window function which gives, after Fourier transform,

$$w_{\mathrm{Heav}}\left(s\right) = \frac{\sin\left(s\right)-s\cos\left(s\right)}{2\pi^2 s^3} . \tag{2.137}$$

Such a window function is not everywhere positive and decays too slowly at large distances to satisfy the criterion mentioned above. For simplicity in the following, we will still work with the Heaviside step window function, but one may keep in mind that this choice is not without consequences.

Working with a Heaviside window function, one then obtains

$$\left\langle\xi_1\left(\boldsymbol{x}_1,N_1\right)\xi_1\left(\boldsymbol{x}_2,N_2\right)\right\rangle = \frac{\left(\sigma aH\right)^3}{2\pi^2}\left(1-\epsilon_1\right)\left|\phi_{\boldsymbol{k}}\right|^2_{k=\sigma aH}\frac{\sin\left(\sigma aHr\right)}{\sigma aHr}\delta\left(N_1-N_2\right) . \tag{2.138}$$

Similarly, one gets for $\langle\xi_2\xi_2\rangle$ and $\langle\xi_1\xi_2\rangle$ the following expressions,

$$\langle\xi_2(\boldsymbol{x}_1,N_1)\,\xi_2(\boldsymbol{x}_2,N_2)\rangle = \frac{(\sigma aH)^3}{2\pi^2}(1-\epsilon_1)\left|\frac{\partial\phi_{\boldsymbol{k}}}{\partial N}\right|^2_{k=\sigma aH}\frac{\sin(\sigma aHr)}{\sigma aHr}\delta(N_1-N_2)\,, \tag{2.139}$$

$$\langle\xi_1(\boldsymbol{x}_1,N_1)\,\xi_2(\boldsymbol{x}_2,N_2)\rangle = \frac{(\sigma aH)^3}{2\pi^2}(1-\epsilon_1)\left(\phi_{\boldsymbol{k}}\frac{\partial\phi^*_{\boldsymbol{k}}}{\partial N}\right)_{k=\sigma aH}\frac{\sin(\sigma aHr)}{\sigma aHr}\delta(N_1-N_2)\,, \tag{2.140}$$

and $\langle\xi_2\xi_1\rangle$ is simply given by $\langle\xi_1\xi_2\rangle^*$.

2.4.1.6. Case of a de Sitter Background

In practice, from here, one needs to calculate the amplitude of the Fourier modes $\phi_{\boldsymbol{k}}$ over the background under consideration to work out the correlations of the noises ξ_1 and ξ_2. This must be done by solving the equation of motion for the modes $\phi_{\boldsymbol{k}}$, which is given by the last bracketed term of Eq. (2.122). Here we give the solution in the specific case of a de Sitter background. When writing the equation for the modes in term of the time variable $z\equiv k/(aH)$, one obtains

$$\frac{\mathrm{d}^2\phi_{\boldsymbol{k}}}{\mathrm{d}z^2}-\frac{2}{z}\frac{\mathrm{d}\phi_{\boldsymbol{k}}}{\mathrm{d}z}+\left(1+\frac{V''}{H^2z^2}\right)\phi_{\boldsymbol{k}}\,. \tag{2.141}$$

If V'' is taken to be constant, then the solutions of this equation are given by

$$\phi_{\boldsymbol{k}} = A_{\boldsymbol{k}}z^{3/2}H^{(1)}_\nu(z)+B_{\boldsymbol{k}}z^{3/2}H^{(2)}_\nu(z)\,, \tag{2.142}$$

where $H^{(1)}_\nu$ and $H^{(2)}_\nu$ are the Hankel functions [269] of the first and second class respectively, $A_{\boldsymbol{k}}$ and $B_{\boldsymbol{k}}$ are integration constants, and

$$\nu=\frac{3}{2}\sqrt{1-\frac{4}{9}\frac{V''}{H^2}}\,. \tag{2.143}$$

As explained in section 2.3.2, the integration constants can be set by requiring that the perturbations are initiated in their Bunch-Davies vacuum state $a\phi_{\boldsymbol{k}}=\mathrm{e}^{-ik\eta}/\sqrt{2k}$, see Eq. (2.62), when they are well inside the Hubble radius. Remember that η is the conformal time defined in Eq. (1.62). This amounts to choosing

$$\phi_{\boldsymbol{k}}\underset{z\gg1}{\to}\frac{zH}{\sqrt{2k}k}\mathrm{e}^{-iz}\,. \tag{2.144}$$

Since one has [269] $H^{(1)}_\nu(z)\simeq\sqrt{2/(\pi z)}\exp[i(z-\nu\pi/2-\pi/4)]$ and $H^{(2)}_\nu(z)\simeq\sqrt{2/(\pi z)}\exp[-i(z-\nu\pi/2-\pi/4)]$ when $z\gg1$, this sets the integration constants to be $A_{\boldsymbol{k}}=0$ and $B_{\boldsymbol{k}}=\sqrt{\pi}/2H/k^{3/2}\exp[-i\pi/2(\nu+1/2)]$, so that one has

$$\phi_{\boldsymbol{k}}=\frac{\sqrt{\pi}}{2}H\left(\frac{z}{k}\right)^{3/2}\exp\left[-i\frac{\pi}{2}\left(\nu+\frac{1}{2}\right)\right]H^{(2)}_\nu(z)\,. \tag{2.145}$$

This allows to evaluate $\phi_{\boldsymbol{k}}$ when $k=\sigma aH$, that is when $z=\sigma$. Since one has [269] $H^{(2)}_\nu(\sigma)\simeq i/\pi\Gamma(\nu)(\sigma/2)^{-\nu}$ when $\sigma\ll1$, where Γ is the Euler Gamma function, one can write

$$(\sigma aH)^3\left|\phi_{\boldsymbol{k}}\right|^2_{k=\sigma aH}\simeq\frac{H^2}{4\pi}\Gamma^2(\nu)\,2^{2\nu}\sigma^{3-2\nu}\,. \tag{2.146}$$

In the same manner, making use of the relation [269] $\mathrm{d}H_\nu^{(2)}(z)/\mathrm{d}z = H_{\nu-1}^{(2)}(z) - \nu/zH_\nu^{(2)}(z) \simeq -\nu/zH_\nu^{(2)}(z)$ when $z \ll 1$, and since $\mathrm{d}/\mathrm{d}N = -z\mathrm{d}/\mathrm{d}z$, one has $\mathrm{d}\phi_{\boldsymbol{k}}/\mathrm{d}N \simeq (\nu - 3/2)\phi_{\boldsymbol{k}}$ in this same limit, so that one obtains

$$(\sigma aH)^3 \left|\frac{\mathrm{d}\phi_{\boldsymbol{k}}}{\mathrm{d}N}\right|^2_{k=\sigma aH} \simeq \frac{H^2}{4\pi}\Gamma^2(\nu)\left(\nu-\frac{3}{2}\right)^2 2^{2\nu}\sigma^{3-2\nu}, \tag{2.147}$$

$$(\sigma aH)^3 \left(\phi_{\boldsymbol{k}}\frac{\mathrm{d}\phi^*_{\boldsymbol{k}}}{\mathrm{d}N}\right)_{k=\sigma aH} \simeq \frac{H^2}{4\pi}\Gamma^2(\nu)\left(\nu-\frac{3}{2}\right) 2^{2\nu}\sigma^{3-2\nu}. \tag{2.148}$$

From here, when evaluated at the same point $\boldsymbol{x}$ in space, the cross correlations (2.138)-(2.140) of the noises simply read

$$\langle \xi_1(N_1)\xi_1(N_2)\rangle = \left(\frac{H}{2\pi}\right)^2\left(\frac{\sigma}{2}\right)^{3-2\nu}\frac{4\Gamma^2(\nu)}{\pi}\delta(N_1-N_2), \tag{2.149}$$

$$\langle \xi_2(N_1)\xi_2(N_2)\rangle = \left(\frac{H}{2\pi}\right)^2\left(\nu-\frac{3}{2}\right)^2\left(\frac{\sigma}{2}\right)^{3-2\nu}\frac{4\Gamma^2(\nu)}{\pi}\delta(N_1-N_2), \tag{2.150}$$

$$\langle \xi_1(N_1)\xi_2(N_2)\rangle = \left(\frac{H}{2\pi}\right)^2\left(\nu-\frac{3}{2}\right)\left(\frac{\sigma}{2}\right)^{3-2\nu}\frac{4\Gamma^2(\nu)}{\pi}\delta(N_1-N_2). \tag{2.151}$$

2.4.1.7. Case of a Light Field

We now specify the noises amplitudes when the field is assumed to be light compared to the Hubble factor, that is when $V'' \ll H$. In this case, from Eq. (2.143), one has $\nu \simeq 3/2$. Looking back at Eqs. (2.149)-(2.151), this means that one simply has $\xi_2 = 0$, and that

$$\langle \xi_1(N_1)\xi_1(N_2)\rangle = \left(\frac{H}{2\pi}\right)^2\delta(N_1-N_2). \tag{2.152}$$

This is why it is convenient to express ξ_1 in terms of a normalized white Gaussian noise ξ through $\xi_1 = H/(2\pi)\xi$, so that the Langevin equation for the coarse-grained field is simply given by

$$\frac{\partial^2\varphi}{\partial N^2} + 3\frac{\partial\varphi}{\partial N} + \frac{V'(\varphi)}{H^2} = 3\frac{H}{2\pi}\xi. \tag{2.153}$$

2.4.1.8. Case of a Slow-Rolling Field

Finally, if the field is experiencing slow roll, then as usual the second time derivative can be neglected in the equation of motion and one finally obtains

$$\frac{\partial\varphi}{\partial N} + \frac{V'(\varphi)}{3H^2} = \frac{H}{2\pi}\xi, \tag{2.154}$$

which corresponds to the announced equation (2.116) and which was first derived in Ref. [290].

2.4.2. Why should we use the Number of e-folds as the Time Variable in the Langevin equations?

In section 2.4.1, the Langevin equation has been worked out in terms of the number of e-folds N. A priori, another time variable could have been used, such as cosmic time t for example.

Indeed, in a number of papers (see *e.g.* Refs. [325, 326, 289, 327, 324, 328, 329, 330, 331]), the Langevin equation is written and solved in terms of t instead of N. However, this choice is not without consequences since the transformation from t to N makes use of the stochastic function $H\left[\varphi\left(t\right)\right]$ and as a consequence, leads to a physically different stochastic process with different probability distributions.

2.4.2.1. Steady-State Distributions

The claim we just made can be easily established [289, 332, 333] when deriving *e.g.* the steady-state distribution associated with the stochastic process under study, for different time variables. This distribution can be obtained writing the Fokker-Planck equation for $P(\phi, N)$, which is the probability density for the coarse-grained field to take the value ϕ at time N. If one starts from the Langevin equation (2.116) written in terms of N, in the Itô interpretation [334], one obtains

$$\frac{\partial}{\partial N}P\left(\phi,N\right)=\frac{\partial}{\partial\phi}\left[\frac{V'}{3H^2}P\left(\phi,N\right)\right]+\frac{\partial^2}{\partial\phi^2}\left[\frac{H^2}{8\pi^2}P\left(\phi,N\right)\right]. \tag{2.155}$$

If we denote the steady-state probability distribution by $P_{\rm stat}(\phi)$, the equation for $P_{\rm stat}(\phi)$ is simply given by $\partial P_{\rm stat}(\phi)/\partial N=0$, that is

$$\frac{\partial}{\partial\phi}\left\{\frac{V'}{3H^2}P_{\rm stat}\left(\phi\right)+\frac{\partial}{\partial\phi}\left[\frac{H^2}{8\pi^2}P_{\rm stat}\left(\phi\right)\right]\right\}\equiv\frac{\partial J}{\partial\phi}=0\,, \tag{2.156}$$

where J denotes the probability current. This current thus needs to be independent of ϕ in the steady-state case. In most interesting cases, it is actually 0. For example, if ϕ can take unbounded values, since $\int P_{\rm stat}(\phi){\rm d}\phi=1$, $P_{\rm stat}(\phi)$ needs to decrease at infinity strictly faster than $|\phi|^{-1}$. In this case, $P_{\rm stat}(\phi)$ and $\partial P_{\rm stat}(\phi)/\partial\phi$ vanish at infinity and J is 0 at infinity, hence everywhere. This yields quite a simple equation to solve for $P_{\rm stat}(\phi)$, and one obtains

$$P_{\rm stat}\left(\phi\right)\propto\frac{24\pi^2M_{\rm Pl}^4}{V\left(\phi\right)}\exp\left[\frac{24\pi^2M_{\rm Pl}^4}{V\left(\phi\right)}\right], \tag{2.157}$$

where there is an overall integration constant chosen so that the distribution is normalized, $\int P_{\rm stat}(\phi){\rm d}\phi=1$, and that for simplicity we do not display here. Now, let us redo the same calculation, but starting this time from the Langevin equation written in terms of cosmic time t. Performing a simple change of time variable in Eq. (2.116), the later is given by

$$\frac{{\rm d}\tilde{\phi}}{{\rm d}t}=-\frac{V'}{3H}+\frac{H^{3/2}}{2\pi}\xi\left(t\right), \tag{2.158}$$

where we use the notation $\tilde{\phi}$ to stress the fact that *a priori*, $\tilde{\phi}$ is not the same stochastic process as ϕ. The Fokker-Planck equation corresponding to the above equation reads

$$\frac{\partial}{\partial t}\tilde{P}\left(\tilde{\phi},N\right)=\frac{\partial}{\partial\tilde{\phi}}\left[\frac{V'}{3H}\tilde{P}\left(\tilde{\phi},N\right)\right]+\frac{\partial^2}{\partial\phi^2}\left[\frac{H^3}{8\pi^2}\tilde{P}\left(\tilde{\phi},N\right)\right]. \tag{2.159}$$

In the same manner as before, this equation can be written as $\partial\tilde{P}/\partial t=\partial\tilde{J}/\partial\tilde{\phi}$, and requiring that the current $\tilde{J}$ vanishes gives rise to a differential equation for the steady-state distribution $\tilde{P}_{\rm stat}(\tilde{\phi})$ that can easily be solved, and one obtains

$$\tilde{P}_{\rm stat}\left(\tilde{\phi}\right)\propto\left[\frac{24\pi^2M_{\rm Pl}^4}{V\left(\tilde{\phi}\right)}\right]^{3/2}\exp\left[\frac{24\pi^2M_{\rm Pl}^4}{V\left(\tilde{\phi}\right)}\right]. \tag{2.160}$$

This is, as announced, explicitly different from Eq. (2.157). In this calculation, it can also be made explicit that this difference is intimately related with the fact that the amplitude of the noise depends on the coarse grained field through the function $H(\phi)$. Indeed, if one does the same calculation but assume that H is a constant, then one obtains the same stationary distribution for the two time variables, $P_{\rm stat} = \tilde{P}_{\rm stat} \propto \exp(24\pi^2 M_{\rm Pl}^4/V)$.

In any case, with the example of the steady-state distribution, we have shown that different time variables for the Langevin equation correspond to different stochastic processes. This is why, in the following, we identify the correct time variable one must work with when dealing with stochastic inflation.

2.4.2.2. Perturbations Equation derived from the Background Equation

As suggested in Ref. [335], since the Langevin equation was obtained in section 2.4.1 by performing an expansion in $\phi_>$ in the equation of motion directly, the correct time variable should be the one such that the equations for the perturbations, which must be established at the action level, can correctly be obtained from varying the equation of motion for the background itself, when written in terms of this time variable. In this section, we establish that this condition selects out N as the time variable. This is of course an heuristic argument only, and a more rigorous derivation of this result will be presented in section 2.4.2.3 where it will be shown that N only allows to reproduce results from Quantum Field Theories.

In the case where inflation is driven by a single scalar field ϕ, the action we start from, $S = S_{\rm grav} + S_\phi$ where $S_{\rm grav}$ is given by Eq. (1.10) and S_ϕ is given by Eq. (2.1), reads

$$\mathcal{S} = \int \mathrm{d}^4x\sqrt{-g}\left[\frac{M_{\rm Pl}^2}{2}R - \frac{1}{2}g^{\mu\nu}\partial_\mu\phi\partial_\nu\phi - V(\phi)\right] . \tag{2.161}$$

From this action (and this action only), we first want to derive equations of motion for the scalar perturbations, that can be compared with what will be obtained below from varying the equation of motion itself. To make our point even more convincing, we go up to second order in the perturbations. This is why we expand the background fields $\{\phi, g_{\mu\nu}\}$ at second order in the non-homogeneous scalar perturbations, without fixing any gauge for the moment. With the same notations as in section 2.3.1, when the time variable in the metric is the conformal time η, one has

$$\begin{aligned}
\phi(\eta,\vec{x}) &= \phi^{(0)}(\eta) + \phi^{(1)}(\eta,\vec{x}) + \frac{1}{2}\phi^{(2)}(\eta,\vec{x}) , \\
g_{00} &= a^2\left[-1 - 2\alpha^{(1)} - \alpha^{(2)}\right] , \qquad g_{i0} = -a^2\left[\partial_i B^{(1)} + \frac{1}{2}\partial_i B^{(2)}\right] , \\
g_{ij} &= a^2\left\{\delta_{ij}\left[1 - 2\psi^{(1)} - \psi^{(2)}\right] + 2\partial_i\partial_j\left[E^{(1)} + \frac{1}{2}E^{(2)}\right]\right\} .
\end{aligned} \tag{2.162}$$

Here we have not displayed vector and tensor perturbations, as in Eq. (2.35). As explained in section 2.3.1, the degrees of freedom introduced above are partially redundant and in absence of anisotropic stress, the scalar sector can be described in terms of a single gauge invariant variable. One possible choice is the Mukhanov-Sasaki variable [122, 241, 242] v, which can be defined, order by order, as the scalar field fluctuation $\phi^{(n)}$ on uniform curvature hypersurfaces [336]. To

first and second orders, after a lengthy but straightforward calculation, one obtains [337]

$$v^{(1)} = \phi^{(1)} + \frac{\left(\phi^{(0)}\right)'}{\mathcal{H}}\psi^{(1)}\,, \tag{2.163}$$

$$v^{(2)} = \phi^{(2)} + \frac{\left(\phi^{(0)}\right)'}{\mathcal{H}}\psi^{(2)} + \left(\frac{\psi_1}{\mathcal{H}}\right)^2\left[\left(\phi^{(0)}\right)'' + 2\mathcal{H}\left(\phi^{(0)}\right)' - \frac{\mathcal{H}'}{\mathcal{H}}\left(\phi^{(0)}\right)'\right] + 2\frac{\left(\phi^{(0)}\right)'}{\mathcal{H}^2}\psi_1'\psi_1 + 2\frac{\psi_1}{\mathcal{H}}\left(\phi^{(1)}\right)'\,. \tag{2.164}$$

From varying the expanded action, one can derive an equation of motion for the scalar perturbations, and in particular for a gauge invariant combination of them, say the Mukhanov-Sasaki variable. In this section, we want to compare this action-based equation of motion for the scalar perturbations with an equation of motion for the perturbation in ϕ coming from varying the background Klein-Gordon equation. It is therefore important to work in a gauge where these two quantities, v and the perturbation in ϕ, can be identified. By definition of the Mukhanov-Sasaki variable, this is the case in the Uniform Curvature Gauge, for which one has

$$v^{(n)} = \phi^{(n)} \tag{2.165}$$

to all orders. In this gauge, one notably has $\psi = 0$ to all orders, which indeed gives Eq. (2.165) at first and second order starting from Eqs. (2.163) and (2.164).

The equation of motion for the scalar perturbations $\phi^{(1)}$ and $\phi^{(2)}$ is therefore given by the one for $v^{(1)}$ and $v^{(2)}$ in this gauge. At leading order in the slow-roll approximation, and in the long wavelength limit, they read[9]

$$3H\dot{\phi}^{(1)} + \left(V'' - \frac{V'^2}{3H^2M_{\rm Pl}^2}\right)\phi^{(1)} = 0\,, \tag{2.166}$$

$$3H\dot{\phi}^{(2)} + \left(V'' - \frac{V'^2}{3H^2M_{\rm Pl}^2}\right)\phi^{(2)} = -\frac{1}{2}\left(V''' - \frac{V'V''}{H^2M_{\rm Pl}^2} + \frac{2V'^3}{9H^4M_{\rm Pl}^4}\right)\phi^{(1)2}\,. \tag{2.167}$$

We now need to compare these equations with the ones that arise when varying the equation of motion for the background, and find out for which time variable they match.

If t is used

When cosmic time t is used, the leading order of the slow-roll approximation for the Klein-Gordon equation for the background is given by Eq. (2.12),

$$\frac{\mathrm{d}\phi}{\mathrm{d}t} = -\frac{V'}{3H\left(\phi\right)}\,, \tag{2.168}$$

[9] In spite of the complexity of the field equations at second order, see *e.g.* Ref. [338], in the long wavelength limit, it is sufficient [339] to use the local conservation of energy-momentum to establish Eqs. (2.166) and (2.167). Because this is not the main subject of this section, the corresponding calculations are not reproduced here but they can be found in Refs. [339, 336].

where we take $H^2 \simeq V/(3M_{\rm Pl}^2)$ at leading order in slow roll. When plugging $\phi = \phi^{(0)} + \phi^{(1)} + \phi^{(2)}$ in this equation, one obtains at first and second order in the perturbations

$$3H\dot{\tilde{\phi}}^{(1)} + \left(V'' - \frac{V'^2}{6H^2M_{\rm Pl}^2}\right)\tilde{\phi}^{(1)} = 0\,, \tag{2.169}$$

$$3H\dot{\tilde{\phi}}^{(2)} + \left(V'' - \frac{V'^2}{6H^2M_{\rm Pl}^2}\right)\tilde{\phi}^{(2)} = -\frac{1}{2}\left(V''' - \frac{V'V''}{2H^2M_{\rm Pl}^2} + \frac{V'^3}{12H^4M_{\rm Pl}^4}\right)\tilde{\phi}^{(1)2}\,. \tag{2.170}$$

One should stress that these equations do not apply to $\phi^{(1)}$ and $\phi^{(2)}$ since they are different from Eqs. (2.166) and (2.167), which is why we use the notation $\tilde{\phi}^{(1,2)}$ instead of $\phi^{(1,2)}$. The differences with Eqs. (2.166) and (2.167) are displayed in red. One can see that several factors do not match. This is because in general, the equations for the perturbations must be derived from the action itself and cannot be obtained by simply varying the equation of motion for the background.

If $\mathrm{d}s = H^p a^q \mathrm{d}t$ is used

For this reason, let us look for a time variable s which is such that the equations for the perturbations arise from varying the equation of motion for the background when written in terms of s. Let us assume that s is related to t thanks to a relation of the form

$$\mathrm{d}s = H^p(\phi)\, a^q(\phi)\, \mathrm{d}t\,, \tag{2.171}$$

where p and q are power indexes that we try to determine. For example, when $p = 0$ and $q = 0$, s is the cosmic time t, when $p = 1$ and $q = 0$, s is the number of e-folds N, while when $p = 0$ and $q = -1$, s is the conformal time η. In terms of s, the equation of motion for the background is given by

$$\frac{\mathrm{d}\phi}{\mathrm{d}s} = -\frac{V'}{3H^{p+1}(\phi)}\,, \tag{2.172}$$

where again we take $H^2 \simeq V/(3M_{\rm Pl}^2)$ at leading order in slow roll. When plugging $\phi = \phi^{(0)} + \phi^{(1)} + \phi^{(2)}$, one obtains at first and second order in the perturbations

$$3H\dot{\tilde{\phi}}^{(1)} + \left(V'' - \frac{p+1}{6}\frac{V'^2}{H^2M_{\rm Pl}^2} + 3qH^2\right)\tilde{\phi}^{(1)} = 0\,, \tag{2.173}$$

$$3H\dot{\tilde{\phi}}^{(2)} + \left(V'' - \frac{p+1}{6}\frac{V'^2}{H^2M_{\rm Pl}^2} + 3qH^2\right)\tilde{\phi}^{(2)} = -\frac{1}{2}\left[V''' - \frac{p+1}{2}\frac{V'V''}{H^2M_{\rm Pl}^2} + \frac{(p+1)(p+3)}{36}\frac{V'^3}{H^4M_{\rm Pl}^4} + 3q\frac{H^2V''}{V'} - pq\frac{V'}{M_{\rm Pl}^2} - 18q\frac{H^4}{V'}\right]\tilde{\phi}^{(1)2}\,. \tag{2.174}$$

Again, these equations do not apply to $\phi^{(1)}$ and $\phi^{(2)}$ in general since the correct ones are given by Eqs. (2.166) and (2.167) which is why we use the notation $\tilde{\phi}^{(1,2)}$. The differences between these two sets of equations are displayed in red. In order for the above to match Eqs. (2.166) and (2.167), one must have $q = 0$ and $(p+1)/6 = 1/3$ which gives $p = 1$, $(p+1)/2 = 1$ which also gives $p = 1$, and $(p+1)(p+3)/36 = 2/9$ which gives $p = 1$ or $p = -5$. As a conclusion, with $p = 1$ and $q = 0$ only, the equations for the perturbations (from what is shown here, up to second order in perturbation theory) can be seen as if they were derived from varying the equation of motion for the background. This choice corresponds to the number of e-folds N.

2.4.2.3. Stochastic Inflation and QFT on Curved Space-Times

To go beyond this heuristic argument, one can explicitly show [299, 300] that N is the time variable which allows to consistently connect stochastic inflation with results of QFT on curved space-times. For example, let us consider the leading order of the fluctuations $\delta\phi = \varphi - \phi_{\rm cl}$ in the coarse-grained inflaton field about its classical background value $\phi_{\rm cl}$. By "classical", we mean that $\phi_{\rm cl}$ is the solution of the equation of motion without the noise term. We want to compute the mean square value of $\delta\phi$ and compare what we obtain to results coming from QFT calculations. For example, in Ref. [340], with renormalization obtained by employing the adiabatic subtraction prescription on inflationary backgrounds, it was shown that in quadratic inflation where $V = m^2\phi^2/2$, if $\delta\phi = 0$ at time t_0, one has at leading order see Eq. (48) of Ref. [340]

$$\left\langle (\phi - \phi_{\rm cl})^2 \right\rangle = \frac{H_0^6 - H^6}{8\pi^2 m^2 H^2}\,, \tag{2.175}$$

where H means $H\left(\phi_{\rm cl}\right)$ and H_0 means H evaluated at time t_0. In the same manner, in Ref. [341], it was shown that in power-law inflation where $a(t) \propto t^p$ with $p \gg 1$, the same quantity is given by see Eq. (29) of Ref. [341]

$$\left\langle (\phi - \phi_{\rm cl})^2 \right\rangle = \frac{p}{8\pi^2}\left(H_0^2 - H^2\right)\,. \tag{2.176}$$

Let us see how these results can be derived in the stochastic inflationary framework. We start from the Langevin equation (2.116) that we write

$$\frac{{\rm d}\varphi}{{\rm d}N} = -2M_{\rm Pl}^2\frac{H'}{H} + \frac{H}{2\pi}\xi\left(N\right) \tag{2.177}$$

where we have used $H^2 \simeq V/(3M_{\rm Pl}^2)$ and where a prime denotes a derivative with respect to the inflaton field. Since $\phi_{\rm cl}$ is the solution of the above equation without the noise term, the noise term can be considered as a perturbation captured in $\delta\phi$. After expanding Eq. (2.177) in powers of $\delta\phi$, one gets for the leading order $\delta\phi^{(1)}$

$$\frac{{\rm d}\delta\phi^{(1)}}{{\rm d}N} + 2M_{\rm Pl}^2\left(\frac{H'}{H}\right)'\delta\phi^{(1)} = \frac{H}{2\pi}\xi\,. \tag{2.178}$$

Multiplying this equation by $\delta\phi^{(1)}$ and taking the stochastic average leads to

$$\frac{{\rm d}\left\langle \delta\phi^{(1)2}\right\rangle}{{\rm d}N} + 4M_{\rm Pl}^2\left(\frac{H'}{H}\right)'\left\langle \delta\phi^{(1)2}\right\rangle = \frac{H}{\pi}\left\langle \xi\delta\phi^{(1)}\right\rangle\,. \tag{2.179}$$

In order to obtain a differential equation for $\langle\delta\phi^{(1)2}\rangle$ only, one needs to evaluate the right hand side of the previous equation. This can be done as follows. Letting $\delta\phi^{(1)} = 0$ at time N_0, a formal solution of Eq. (2.178) is given by

$$\delta\phi^{(1)} = \exp\left[-2M_{\rm Pl}^2\int_{N_0}^{N}\left(\frac{H'}{H}\right)'{\rm d}n\right]\int_{N_0}^{N}\left\{\frac{H}{2\pi}\xi\left(n\right)\exp\left[2M_{\rm Pl}^2\int_{N_0}^{n}\left(\frac{H'}{H}\right)'{\rm d}\bar{n}\right]\right\}{\rm d}n\,. \tag{2.180}$$

From this expression, since $\langle\xi\left(N\right)\xi\left(N'\right)\rangle = \delta\left(N - N'\right)$, it is straightforward to see that[10]

$$\left\langle \xi\delta\phi^{(1)}\right\rangle = \frac{H}{4\pi}\,. \tag{2.181}$$

[10]The 1/2 factor comes from the rule $\int_{x_1}^{x_2} f(x)\delta(x - x_2){\rm d}x = f(x_2)/2$ when the Dirac function is centred at a boundary of the integral.

This is why one obtains

$$\frac{\mathrm{d}\left\langle \delta\phi^{(1)\,2}\right\rangle}{\mathrm{d}N}+4M_{\rm Pl}^2\left(\frac{H'}{H}\right)'\left\langle \delta\phi^{(1)\,2}\right\rangle=\frac{H^2}{4\pi^2}\,. \tag{2.182}$$

Since the equation of motion for $\phi_{\rm cl}$ is simply given by $\mathrm{d}N=-H/(2H'M_{\rm Pl}^2)\mathrm{d}\phi_{\rm cl}$, one can change the time variable from N to $\phi_{\rm cl}$ and the formal solution of the above equation can be written as

$$\left\langle \delta\phi^{(1)\,2}\right\rangle=-\frac{1}{8\pi^2M_{\rm Pl}^2}\frac{H'^2}{H^2}\int\frac{H^5}{H'^3}\mathrm{d}\phi_{\rm cl}\,. \tag{2.183}$$

For quadratic inflation where $H=m\phi/(\sqrt{6}M_{\rm Pl})$, this exactly gives rise to Eq. (2.175) while for power-law inflation where[11] $H=H_0\exp\left[-1/\sqrt{2p}(\phi-\phi_0)/M_{\rm Pl}\right]$, one exactly obtains Eq. (2.176). Therefore, stochastic and standard field-theoretical approaches to inflation produce the same results for the amount of field fluctuations. Here we have established this property at leading order in perturbation theory. However, as shown in Refs. [290, 298], the stochastic approach can reproduce QFT results for any finite number of scalar loops and even beyond.

To emphasize the specificity of N as a preferred time variable choice, let us repeat the same procedure using the Langevin equation written in terms of t,

$$\frac{\mathrm{d}\tilde{\phi}}{\mathrm{d}t}=-2M_{\rm Pl}^2H'+\frac{H^{3/2}}{2\pi}\xi\left(t\right)\,. \tag{2.184}$$

Since this corresponds to a different stochastic process as the one written in terms of N, we use again the notation $\tilde{\phi}$ instead of ϕ. At leading order in the noise, one obtains for $\delta\tilde{\phi}^{(1)}$

$$\frac{\mathrm{d}\delta\tilde{\phi}^{(1)}}{\mathrm{d}t}+2M_{\rm Pl}^2H''\delta\tilde{\phi}^{(1)}=\frac{H^{3/2}}{2\pi}\xi\left(t\right)\,. \tag{2.185}$$

Again, multiplying this equation by $\delta\tilde{\phi}^{(1)}$ and taking the stochastic average leads to

$$\frac{\mathrm{d}\left\langle \delta\tilde{\phi}^{(1)\,2}\right\rangle}{\mathrm{d}t}+4M_{\rm Pl}^2H''\left\langle \delta\tilde{\phi}^{(1)\,2}\right\rangle=\frac{H^{3/2}}{\pi}\left\langle \xi\left(t\right)\delta\tilde{\phi}^{(1)}\right\rangle\,. \tag{2.186}$$

In the same manner as before, making use of the formal solution to Eq. (2.185),

$$\delta\tilde{\phi}^{(1)}=\exp\left[-2M_{\rm Pl}^2\int_{t_0}^{t}H''\mathrm{d}u\right]\int_{t_0}^{t}\left\{\frac{H^{3/2}}{2\pi}\xi\left(u\right)\exp\left[2M_{\rm Pl}^2\int_{t_0}^{u}H''\mathrm{d}v\right]\right\}\mathrm{d}u\,, \tag{2.187}$$

one can show that $\left\langle \xi\left(t\right)\delta\tilde{\phi}^{(1)}\right\rangle=H^{3/2}/(4\pi)$, so that one needs to solve

$$\frac{\mathrm{d}\left\langle \delta\tilde{\phi}^{(1)\,2}\right\rangle}{\mathrm{d}t}+4M_{\rm Pl}^2H''\left\langle \delta\tilde{\phi}^{(1)\,2}\right\rangle=\frac{H^3}{4\pi^2}\,. \tag{2.188}$$

Making use of the classical trajectory $\mathrm{d}t=-\mathrm{d}\phi_{\rm cl}/(2M_{\rm Pl}^2H')$, one obtains[12]

$$\left\langle \delta\tilde{\phi}^{(1)\,2}\right\rangle=-\frac{H'^2}{8\pi^2M_{\rm Pl}^2}\int\frac{H^3}{H'^3}\mathrm{d}\phi_{\rm cl} \tag{2.189}$$

[11] In section 3.2, it is shown that the potential associated with power-law inflation, for which $a(t)\propto t^p$, is given by $V(\phi)\propto \mathrm{e}^{-\sqrt{2/p}\phi/M_{\rm Pl}}$. Since $H^2=V(\phi)/(3M_{\rm Pl}^2)$ at leading order in slow roll, one obtains the given $H(\phi)$ profile.

[12] This equation (2.189) also matches Eq. (13) of Ref. [328] where perturbative solutions of stochastic inflation are derived when formulated in terms of the cosmic time.

which is clearly different from Eq. (2.183).[13] For example, for quadratic inflation, it reduces to $\langle \delta\tilde{\phi}^{(1)^2} \rangle = 3(H_0^4 - H^4)/(16\pi^2 m^2)$ which does not coincide with Eq. (2.175) and for power-law inflation, it reduces to $\langle \delta\tilde{\phi}^{(1)^2} \rangle = pH^2/(4\pi^2)\ln(H_0/H)$ which does not coincide with Eq. (2.176).

Finally and in passing, let us derive the corresponding results for the leading order of the mean fluctuation $\langle \delta\phi \rangle$. Since from Eq. (2.178) it is clear that $\langle \delta\phi^{(1)} \rangle = 0$, one has to work out $\langle \delta\phi^{(2)} \rangle$. Expanding $\varphi = \phi_{\rm cl} + \delta\phi^{(1)} + \delta\phi^{(2)}$ in Eq. (2.177), one obtains

$$\frac{\mathrm{d}\delta\phi^{(2)}}{\mathrm{d}N} + 2M_{\rm Pl}^2 \left(\frac{H'}{H}\right)' \delta\phi^{(2)} + M_{\rm Pl}^2 \left(\frac{H'}{H}\right)'' \delta\phi^{(1)^2} = \frac{H'}{2\pi}\delta\phi^{(1)}\xi\left(N\right) . \tag{2.190}$$

When taking the stochastic average of the above equation, $\langle \delta\phi^{(1)^2} \rangle$ is given by Eq. (2.183) and $\langle \delta\phi^{(1)}\xi \rangle$ is given by Eq. (2.181), so that one obtains

$$\frac{\mathrm{d}\left\langle \delta\phi^{(2)} \right\rangle}{\mathrm{d}N} + 2M_{\rm Pl}^2 \left(\frac{H'}{H}\right)' \left\langle \delta\phi^{(2)} \right\rangle = \frac{1}{8\pi^2}\left(\frac{H'}{H}\right)'' \left(\frac{H'}{H}\right)^2 \int \frac{H^5}{H'^3}\mathrm{d}\phi + \frac{HH'}{8\pi^2} . \tag{2.191}$$

Using the classical trajectory $\mathrm{d}\phi_{\rm cl} = -2M_{\rm Pl}^2 H'/H\mathrm{d}N$, this equation can be written in terms of $\phi_{\rm cl}$, and after integration by parts, this gives rise to

$$\left\langle \delta\phi^{(2)} \right\rangle = \frac{1}{2}\frac{(H'/H)'}{H'/H}\left\langle \delta\phi^{(1)^2} \right\rangle + \frac{1}{32M_{\rm Pl}^2\pi^2}\frac{H'}{H}\left(\frac{H_0^4}{H_0'^2} - \frac{H^4}{H'^2}\right) , \tag{2.192}$$

where $\langle \delta\phi^{(1)^2} \rangle$ is given by Eq. (2.181). For example, when applied to quadratic inflation where $V = m^2\phi^2/2$, one obtains

$$\left\langle \delta\phi^{(2)} \right\rangle = \frac{\sqrt{6}}{96\pi^2 m M_{\rm Pl} H}\left[\frac{H^6 - H_0^6}{H^2} - 3\left(H^4 - H_0^4\right)\right] , \tag{2.193}$$

which corresponds to Eq. (49) of Ref. [299]. However, it is again worth noting that one would have obtained a completely different result starting from the Langevin equation written in terms of cosmic time t, namely[14]

$$\left\langle \delta\tilde{\phi}^{(2)} \right\rangle = \frac{1}{2}\frac{H''}{H'}\left\langle \delta\tilde{\phi}^{(1)^2} \right\rangle + \frac{H'}{32\pi^2 M_{\rm Pl}^2}\left(\frac{H_0^3}{H_0 \mathit{l}^2} - \frac{H^3}{H\mathit{l}^2}\right) . \tag{2.194}$$

This obviously differs from Eq. (2.192).

To summarize the discussion, different time variables in the Langevin equation lead to different stochastic processes, and the only time variable which allows the stochastic inflation formalism to reproduce QFT calculations is the number of e-folds N. One should therefore always work with N when dealing with stochastic inflation.

2.4.3. Stochastic Inflation and the Scalar Power Spectrum

In the previous section, we saw that stochastic inflation is able to reproduce QFT results, and we mentioned that this is even true beyond the linear order [298, 302, 299, 300, 301] in

[13] As shown below in section 2.4.3.1, this difference is crucial since it leads *e.g.* to an incorrect result for the power spectrum of scalar perturbations.

[14] This equation (2.194) matches Eq. (15) of Ref. [328] where perturbative solutions of the Langevin equation are derived when formulated in terms of the cosmic time.

perturbations theory. Let us see how this interesting property shall be used. The calculation of the corrections to the power spectrum that arise when perturbations are worked out beyond the linear order [342, 343, 344] is a difficult task, see for example Refs. [345, 346]. Indeed, already at second order, the perturbed Einstein equations $\delta G_{\mu\nu} = \delta T_{\mu\nu}$ are cumbersome. However, as we saw explicitly in sections 2.4.2.2 and 2.4.2.3, stochastic inflation can lead to the same results as the ones coming from a $\delta G_{\mu\nu} = \delta T_{\mu\nu}$ calculation, by means of a Langevin Klein-Gordon equation. This is why in this section, we calculate the power spectrum of scalar adiabatic perturbations, starting from the Langevin equation, and at any order in the noise term.

At linear order, this problem has been treated in Refs. [327, 322, 331] by expanding the coarse-grained field about its classical counterpart at first order, $\varphi = \phi_{\rm cl} + \delta\phi^{(1)}$, where $\phi_{\rm cl}$ is the solution of the Langevin equation (2.116) without the noise term, and by calculating the statistical moments of $\delta\phi^{(1)}$ making use of the same techniques as in section 2.4.2.3. The correlation functions of $\delta\phi^{(1)}$ are related to the power spectrum $\mathcal{P}_\zeta$ of curvature perturbations thanks to the relation [331]

$$\mathcal{P}_\zeta \simeq \frac{1}{H\left(\phi_{\rm cl}\right)} \frac{\mathrm{d}}{\mathrm{d}t} \left\{ \left[\frac{H\left(\phi_{\rm cl}\right)}{\dot{\phi}_{\rm cl}} \right]^2 \left\langle \left[\delta\phi^{(1)} \right]^2 \right\rangle \right\} . \tag{2.195}$$

In this expression, the right hand side needs to be evaluated when the scale associated with the wavenumber k (for which the power spectrum is calculated) exits the Hubble radius. In the references mentioned above, it is important to stress that the Langevin equations are solved in terms of t as the time variable, whereas we have shown in section 2.4.2 that the number of e-folds N must be used instead. This has important consequences. Indeed, if one plugs the expression (2.183) obtained for $\langle {\delta\phi^{(1)}}^2 \rangle$ using the number of e-folds as the time variable into Eq. (2.195), one obtains for the power spectrum $\mathcal{P}_\zeta$ evaluated at the wavenumber k

$$\mathcal{P}_\zeta \simeq \left[\frac{H(\phi_{\rm cl})}{2\pi} \right]^2 \frac{1}{2M_{\rm Pl}^2 \epsilon_1\left(\phi_{\rm cl}\right)} , \tag{2.196}$$

where as above, $\phi_{\rm cl}$ needs to be evaluated when the scale associated with the wavenumber k (for which the power spectrum is calculated) exits the Hubble radius. This expression exactly matches the standard result (2.110) recovered below, see Eq. (2.205). However, if one makes use of the cosmic time t as the time variable and plugs Eq. (2.189) into Eq. (2.195), one obtains instead

$$\mathcal{P}_{\tilde{\zeta}} \simeq \left[\frac{H(\phi_{\rm cl})}{2\pi} \right]^2 \frac{1}{2M_{\rm Pl}^2 \epsilon_1\left(\phi_{\rm cl}\right)} \left\{ 1 + 2 \left[\frac{H'\left(\phi_{\rm cl}\right)}{H\left(\phi_{\rm cl}\right)} \right]^2 \int^{\phi_{\rm cl}} \left[\frac{H\left(\phi_{\rm cl}\right)}{H'\left(\phi_{\rm cl}\right)} \right]^3 \mathrm{d}\phi \right\} \tag{2.197}$$

$$= \mathcal{P}_\zeta \left\{ 1 + 2 \left[\frac{H'\left(\phi_{\rm cl}\right)}{H\left(\phi_{\rm cl}\right)} \right]^2 \int^{\phi_{\rm cl}} \left[\frac{H\left(\phi_{\rm cl}\right)}{H'\left(\phi_{\rm cl}\right)} \right]^3 \mathrm{d}\phi \right\} . \tag{2.198}$$

Here we have adopted the same notation as in section 2.4.2 where a tilde stresses that not the same quantity is actually worked out and ζ is not $\tilde{\zeta}$. This result exactly matches Eq (2.11) of Ref. [331]. However, when in this work it is concluded that, because of the second term in the braces of Eq. (2.198) which is always negative, "the amplitude of the spectrum in the stochastic approach is in general reduced with respect to the amplitude in the standard approach", one can see that such a statement is incorrect since the extra term in Eq. (2.198) is entirely due to a bad choice of time variable. This is why, if such an approach were to be followed and generalized to higher orders, it would again be crucial to work with N as the time variable contrary to what is done in the references mentioned above.

Another strategy is followed in Refs. [347, 348, 349], where methods of statistical physics, such as replica field theory, are employed in a stochastic inflationary context in the case of a free test

field evolving in a de Sitter or power-law background. In particular, dependence on the window function W is studied and it is shown that the effects associated with the choice of the window function vanish at late time so that the power spectrum calculated at the end of inflation is rather independent on W.

Finally, in Refs. [350, 351], the δN formalism is used to relate the curvature perturbations to the number of e-folds perturbations. The Langevin equation is solved numerically over a large number of realizations, and the power spectrum is computed in this manner, numerically, for quadratic potentials and hybrid potentials.

This is this last route that we chose to follow here, since it does not rely on a pertubative expansion in the noise terms and it therefore allows us to describe regimes where the stochastic effects are large. The δN formalism proves very helpful since it relates the scalar power spectrum to stochastic properties of a family of background trajectories, and it is thus well suited to address the issue of stochastic effects on the scalar power spectrum. For the first time, we derive fully analytical and non perturbative results that apply to any single-field potential, and which do not require a numerical solution of the Langevin equation. These results allow us to prove that the usual power spectrum is recovered in the classical limit, for any potential, and to discuss qualitatively and quantitatively the modifications to the standard result that arise due to the stochastic effects. The work presented here has not been pre-printed or published yet since it has been derived in the course of drafting this manuscript.

In this section, we first briefly describe how the δN formalism proceeds. We then turn to the stochastic inflation equations for which we provide generic formal results about ending points probabilities, mean number of e-folds and dispersion in the number of e-folds. For each quantity, we derive analytical non perturbative results that we compute explicitly for the "large field" potential ($V \propto \phi^p$) as an illustrative example. We then derive the generic curvature perturbations power spectrum computed in stochastic inflation, again without using any expansion in the noise term. We make sure that in the classical limit (that we pay attention to carefully define), the standard result (2.110) is recovered. Finally, we completely work out the large field example for which we precisely calculate and discuss the stochastic effects on the scalar power spectrum and its tilt.

2.4.3.1. The δN Formalism

Based on generic considerations, the δN formalism [125, 352, 353, 354, 355, 356] enables to relate statistical properties of cosmological perturbations to the distributions of number of e-folds in some family of homogeneous universes. This leads the way to a very powerful frame of calculation that we now briefly describe. As explained in section 2.3.1, starting from the Friedmann-Lemaître-Robertson-Walker line element $\mathrm{d}s^2 = -\mathrm{d}t^2 + a^2(t)\delta_{ij}\mathrm{d}x^i\mathrm{d}x^j$, deviations from homogeneity and isotropy can be included in a more general metric, which contains some gauge redundancy. A specific gauge choice consists in setting the fixed t-slices of space-time to have uniform energy density, and the fixed x-worldlines to be comoving. When doing so, the perturbed metric becomes [357, 288]

$$\mathrm{d}s^2 = -\mathrm{d}t^2 + a^2(t)\mathrm{e}^{2\zeta(t,\boldsymbol{x})}\gamma_{ij}(t,\boldsymbol{x})\,, \tag{2.199}$$

where ζ is the curvature perturbation. This allows to define a local scale factor $\tilde{a}(t,\boldsymbol{x}) = a(t)\mathrm{e}^{\zeta(t,\boldsymbol{x})}$. Starting from an initial flat slice of space-time at time t_{in}, the amount of expansion $N(t,\boldsymbol{x}) \equiv \ln\left[\tilde{a}(t,\boldsymbol{x})/a(t_{\mathrm{in}})\right]$ to a final slice of uniform energy density is straightforwardly related

to the curvature perturbation

$$\zeta(t,\boldsymbol{x}) = N\left(t,\boldsymbol{x}\right) - N_0(t) \equiv \delta N\,, \tag{2.200}$$

where $N_0(t) \equiv \ln\left[a(t)/a(t_{\rm in})\right]$ is the unperturbed amount of expansion. This result leads to the δN formalism if one further assumes that on super-Hubble scales, the evolution of the Universe at each position is independent and well-approximated by the evolution of an unperturbed universe. This is the so-called "separate universe" assumption [355, 339, 358]. It implies that $N(t,\boldsymbol{x})$ is the amount of expansion in unperturbed universes, so that ζ can be calculated from the knowledge of the evolution of a family of such universes. Written in terms of the inflaton field $\phi(\boldsymbol{x}) = \phi + \delta\phi(\boldsymbol{x})$, made of an unperturbed homogeneous piece ϕ and a perturbation $\delta\phi$ originating from vacuum quantum dispersion, Eq. (2.200) gives rise to

$$\zeta\left(t,\boldsymbol{x}\right) = N\left[\rho\left(t\right),\phi\left(\boldsymbol{x}\right)\right] - N\left[\rho\left(t\right),\phi\right]\,, \tag{2.201}$$

where N is evaluated in unperturbed universes from an initial epoch when the inflaton field has an assigned value ϕ to a final epoch when the energy density has an assigned value ρ. Since the observed curvature perturbations are almost Gaussian, at leading order in perturbation theory, one has

$$\zeta\left(t,\boldsymbol{x}\right) = \delta N \simeq \frac{\partial N}{\partial\phi}\delta\phi\,, \tag{2.202}$$

where $N\left(\phi\right)$ is evaluated with the classical formula

$$N\left(\phi\right) = \frac{1}{M_{\rm Pl}}\int\frac{\mathrm{d}\phi}{\sqrt{2\epsilon_1}}. \tag{2.203}$$

Once ζ is decomposed into Fourier components, $\zeta_{\boldsymbol{k}} = (2\pi)^{-3/2}\int\mathrm{d}^3\boldsymbol{k}\zeta(t,\boldsymbol{k})\exp(i\boldsymbol{k}\cdot\boldsymbol{x})$, the power spectrum $\mathcal{P}_\zeta$, defined with the quantum expected value $\langle\zeta_{\boldsymbol{k}}\zeta_{\boldsymbol{k}'}\rangle \equiv (2\pi)^3 P_\zeta(k)\delta(\boldsymbol{k}+\boldsymbol{k}')$ and $\mathcal{P}_\zeta(k) \equiv \frac{k^3}{2\pi^2}P_\zeta(k)$, can be expressed in terms of the power-spectrum of $\delta\phi$ (defined by similar relations) thanks to Eq. (2.202). For quasi de Sitter inflation, and when the curvature of the inflaton potential is much smaller than H, on super-Hubble scales, the later is given by[15] [244]

$$\mathcal{P}_{\delta\phi}(k) \simeq \left[\frac{H(k)}{2\pi}\right]^2\,, \tag{2.204}$$

where $H(k)$ means H evaluated at the time when the k mode crosses the Hubble radius, *i.e.* when $aH = k$. Together with Eq. (2.203), one therefore obtains

$$\mathcal{P}_\zeta = \left[\frac{H(k)}{2\pi}\right]^2\frac{1}{2M_{\rm Pl}^2\epsilon_1\left(k\right)}\,, \tag{2.205}$$

where again, functions must be evaluated at the time when the corresponding mode k crosses the Hubble radius. This result matches the one coming from the usual calculation [128] presented in section 2.3. Indeed, in the slow-roll approximation, around some pivot scale k_* well chosen in the range of scales probed by the CMB, one has $H \simeq H_*\left[1-\varepsilon_{1*}\ln\left(k/k_*\right)\right]$ and $\epsilon_1 \simeq \epsilon_{1*}\left[1+\varepsilon_{2*}\ln\left(k/k_*\right)\right]$, where we use the second slow-roll parameter $\epsilon_2 \equiv (\mathrm{d}\epsilon_1/\mathrm{d}N)/\varepsilon_1$. This gives rise to

$$\mathcal{P}_\zeta = \frac{H_*^2}{8\pi^2 M_{\rm Pl}^2\epsilon_{1*}}\left[1-(2\epsilon_{1*}+\epsilon_{2*})\ln\left(\frac{k}{k_*}\right)+\cdots\right]\,. \tag{2.206}$$

The standard result (2.110) is retrieved, except that the slow-roll correction to the overall amplitude $1-2(C+1)\epsilon_{1*}-C\epsilon_{2*}$ obtained in Eq. (2.110) is not present here. This is because the

[15] The de Sitter spectrum for $\delta\phi$ (2.204) can be obtained *e.g.* letting $\nu = 3/2$ in Eq. (2.146), since with the above definitions $\mathcal{P}_{\delta\phi}(k) = k^3/2\pi^2|\phi_{\boldsymbol{k}}|^2$.

de Sitter spectrum (2.204) has been used for $\mathcal{P}_{\delta\phi}$ while the slow-roll corrected spectrum should have[16]. However, one can see that this approximation only affects the overall amplitude by a subleading correction, and that the shape of the power spectrum is correctly described. For example, the spectral index, defined in Eq. (2.112), is correctly given by $n_{\rm S} = 1 - 2\epsilon_{1*} - \epsilon_{2*}$ at first order in slow roll.

A fundamental remark is that in the above calculation, the separate universe approximation is assorted with the assumption that once k_* crosses the Hubble radius, the evolution of the inflaton field is governed by its classical equation of motion (2.203). The stochastic dispersion in the number of e-folds thus only comes from the field dispersion at Hubble crossing $\delta\phi_*$. In most cases, this is a good approximation for the following reason. Looking at the Langevin equation (2.116), one can see that during the typical time scale of one e-fold , the classical drift of the inflaton field is of the order $\Delta\phi_{\rm cl} = V'/(3H^2) = \sqrt{2\epsilon_1}M_{\rm Pl}$, while the quantum noise is of the order $\Delta\phi_{\rm qu} = H/(2\pi)$. As in the end of section 2.3.4, this allows us to define a criterion $\eta \equiv \Delta\phi_{\rm qu}/\Delta\phi_{\rm cl}$ that measures the amplitude of the stochastic corrections to the classical trajectory. Looking back at Eqs. (2.205), one can see that this stochastic criterion η can be expressed as

$$\eta = \frac{\Delta\phi_{\rm qu}}{\Delta\phi_{\rm cl}} = \sqrt{\mathcal{P}_\zeta}\,. \tag{2.207}$$

Since $\mathcal{P}_\zeta(k_*) \sim 2\times10^{-9}$, in single field inflation with canonical kinetic term, η is already small when k_* crosses the Hubble radius. If one further assumes that inflation ends "naturally" (*i.e.* by slow-roll violation when ϵ_1 reaches 1) so that ϵ_1 grows during the last stages of inflation, $\mathcal{P}_\zeta \propto H^2/\epsilon_1$ decreases (since H can only decrease) and one is therefore ensured that the stochastic correction to the inflaton trajectory is small after k_* crosses the Hubble radius.

However, it can happen that ϵ_1 decreases after the Hubble crossing time of modes of astrophysical interest today. For example, when the potential has an inflection point [359, 360, 361, 362, 363, 364, 365, 366, 367, 368, 369, 370], see also Refs. [371, 372, 373], ϵ_1 decreases before crossing the inflection point and increases afterwards, so that a transient phase where the stochastic effects can play a non negligible role may happen at some point during the last 60 e-folds . In some other cases, inflation does not end naturally but is triggered *e.g.* by tachyonic instability involving another field, like in hybrid inflation [374, 212, 375, 376, 377, 378]. In such models ϵ_1 monotonously decreases during inflation and the last e-folds may be stochastic dominated. It can also happen, for instance in string theoretical contexts where the inflaton stands for the distance between two branes and evolves in a throat [379, 380, 381, 382], that the inflaton field is allowed to vary only in a bounded interval of values, and that inflation ends by brane annihilation when ϕ reaches a bound of this interval. In these cases again, ϵ_1 may decrease as inflation proceeds, and even if η is small when k_* crosses the Hubble radius, it does not necessarily remain so since it keeps increasing afterwards.[17]

In these cases, it is crucial to study the dispersion δN that arises not only from $\delta\phi_*$ but from the complete stochastic history of the coarse-grained field. In the next sections, we therefore calculate the first statistical moments of the number of e-folds realized between fixed points.

[16] The calculation of $\mathcal{P}_{\delta\phi}$ relies on the de Sitter spectrum (2.204), because the amplitude of the noise term in Eq. (2.116) also relies on it, see sections 2.4.1.6 and 2.4.1.7. This is why in the following, only the leading contributions in slow roll will be derived, and the obtained results should be compared with the reference classical spectrum (2.206). If one wants to go beyond, one needs to add slow-roll corrections to the noise amplitudes.

[17] Another situation of interest is k-inflation for which $\eta \propto \sqrt{\mathcal{P}_\zeta\gamma}$ where $\gamma > 1$ is the Lorentz factor. It can easily happen that $\gamma \gg 1$ in which case $\mathcal{P}_\zeta(k_*) \sim 10^{-9}$ does not necessarily mean that $\eta \ll 1$.

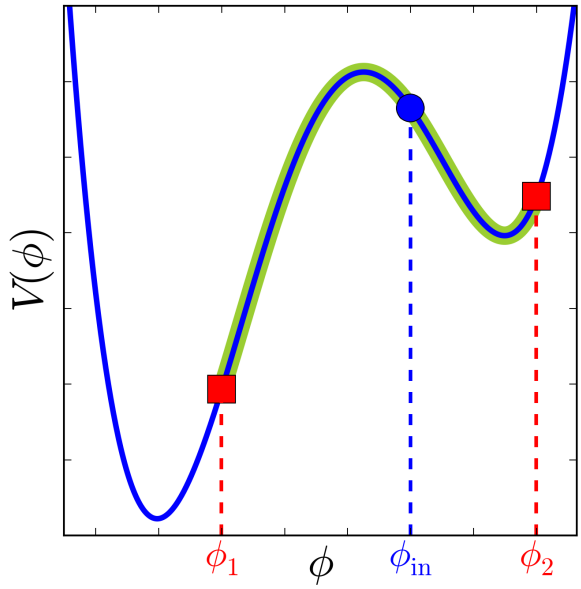

Figure 2.4.: Sketch of the dynamics solved in section 2.4.3. If the inflaton is initially located at $\phi_{\rm in}$, it evolves along some potential $V(\phi)$ thanks to the stochastic Langevin equation (2.208), until it reaches one of the two values ϕ_1 or ϕ_2 where it stops.

2.4.3.2. Stochastic Inflation and Number of e-folds

Let us start from the slow-roll Langevin equation (2.116),

$$\frac{\mathrm{d}\phi}{\mathrm{d}N} = -\frac{V'}{3H^2} + \frac{H}{2\pi}\xi\left(N\right) , \tag{2.208}$$

and work at leading order in slow roll so that $H^2 \simeq V/(3M_{\rm Pl}^2)$. In what follows, we make use of stochastic analysis common tools, introduced *e.g.* in Ref. [383] (see notably p.108 and below). In any case, all the quantities introduced below are self consistently defined. We calculate the mean number of e-folds realized between two points, the dispersion in the number of e-folds realized between two points, and the ending point probability which allows to quantify how much the inflaton can climb up its potential under stochastic effects.

More precisely, let us consider the situation described in Fig. 2.4, where the inflaton is initially located at $\phi_{\rm in}$ and evolves in some potential $V\left(\phi\right)$ under Eq. (2.208). Usually, the inflationary dynamics is stopped when the inflaton reaches some ending value. In the stochastic setup however, since the inflaton can a priori explore any part of the potential thanks to stochastic effects, it makes sense to introduce two possible ending points, located at ϕ_1 and ϕ_2 on each side of $\phi_{\rm in}$. We assume that inflation stops when ϕ reaches ϕ_1 *or* ϕ_2. Let $\mathcal{N}$ be the number of e-folds realized when this happens. Obviously, $\mathcal{N}$ is a stochastic quantity, which means that it is different from one realization to another. In what follows, we compute its first and second moments, as well as the probability that inflation ends at ϕ_1 (or ϕ_2).

A first useful result to establish is the Itô lemma, which is a relation verified by any smooth function f of ϕ. The Taylor expansion of such a function at second order gives $f\left(\phi+\mathrm{d}\phi\right) = f\left(\phi\right) + f'\left(\phi\right)\mathrm{d}\phi + f''\left(\phi\right)/2\,\mathrm{d}\phi^2 + \mathcal{O}\left(\mathrm{d}\phi^3\right)$. Now, if ϕ is a realization of the stochastic process

under study, $\mathrm{d}\phi$ is given by Eq. (2.208) and at first order in $\mathrm{d}N$, one obtains

$$\begin{aligned}\mathrm{d}f\left[\phi\left(N\right)\right] &= f'\left[\phi\left(N\right)\right]\frac{\sqrt{V}\left[\phi\left(N\right)\right]}{2\pi\sqrt{3}M_{\mathrm{Pl}}}\xi\left(N\right)\mathrm{d}N \\ &\quad -f'\left[\phi\left(N\right)\right]\frac{V'\left[\phi\left(N\right)\right]}{V\left[\phi\left(N\right)\right]}M_{\mathrm{Pl}}^2\mathrm{d}N+\frac{1}{24\pi^2M_{\mathrm{Pl}}^2}f''\left[\phi\left(N\right)\right]V\left[\phi\left(N\right)\right]\mathrm{d}N\,. \end{aligned} \tag{2.209}$$

Integrating this relation between $N=0$ where $\phi=\phi_{\mathrm{in}}$ and $N=\mathcal{N}$ where $\phi=\phi_1$ or ϕ_2, one gets the Itô lemma [384]

$$\begin{aligned} f\left(\phi_1 \text{ or } \phi_2\right)-f\left(\phi_{\mathrm{in}}\right) &= \int_0^{\mathcal{N}} f'\left[\phi\left(N\right)\right]\frac{\sqrt{V}\left[\phi\left(N\right)\right]}{2\pi\sqrt{3}M_{\mathrm{Pl}}}\xi\left(N\right)\mathrm{d}N \\ &+\int_0^{\mathcal{N}}\left\{\frac{1}{24\pi^2M_{\mathrm{Pl}}^2}f''\left[\phi\left(N\right)\right]V\left[\phi\left(N\right)\right]-f'\left[\phi\left(N\right)\right]\frac{V'\left[\phi\left(N\right)\right]}{V\left[\phi\left(N\right)\right]}M_{\mathrm{Pl}}^2\right\}\mathrm{d}N\,. \end{aligned} \tag{2.210}$$

2.4.3.3. Ending Point Probability

In this section we calculate the probability p_1 that the inflaton field first reaches the ending point located at ϕ_1 [*i.e.* $\phi\left(\mathcal{N}\right)=\phi_1$], or equivalently the probability $p_2=1-p_1$ that the inflaton field first reaches the ending point located at ϕ_2 [*i.e.* $\phi\left(\mathcal{N}\right)=\phi_2$]. First of all, let $\psi\left(\phi\right)$ be a function that can be expressed as

$$\psi\left(\phi\right)=\frac{h\left(\phi\right)-h\left(\phi_2\right)}{h\left(\phi_1\right)-h\left(\phi_2\right)}\,, \tag{2.211}$$

where $h\left(\phi\right)$ will be specified later. By construction, one has $\psi\left(\phi_1\right)=1$ and $\psi\left(\phi_2\right)=0$. This implies that the mean value of ψ evaluated at $\phi\left(\mathcal{N}\right)$ is given by

$$\left\langle\psi\left[\phi\left(\mathcal{N}\right)\right]\right\rangle=p_1\psi\left(\phi_1\right)+p_2\psi\left(\phi_2\right)=p_1. \tag{2.212}$$

The idea is then to find an appropriate $h\left(\phi\right)$ function which makes easy the evaluation of the left hand side of the previous relation, to deduce p_1. In order to do so, let us apply the Itô lemma (2.210) to $h\left(\phi\right)$. If one requires that the integral of the second line of Eq. (2.210) vanishes, that is

$$h''\left(\phi\right)\frac{V\left(\phi\right)}{24\pi^2M_{\mathrm{Pl}}^4}=h'\left(\phi\right)\frac{V'\left(\phi\right)}{V\left(\phi\right)}\,, \tag{2.213}$$

one obtains

$$h\left[\phi\left(\mathcal{N}\right)\right]-h\left(\phi_{\mathrm{in}}\right)=\int_0^{\mathcal{N}}h'\left[\phi\left(N\right)\right]\frac{\sqrt{V}\left[\phi\left(N\right)\right]}{2\pi\sqrt{3}M_{\mathrm{Pl}}}\xi\left(N\right)\mathrm{d}N\,. \tag{2.214}$$

Using the linear relation (2.211) between h and ψ, this gives rise to the same equation for ψ. Finally, taking the stochastic average of this equation over all the realizations cancels out[18] its right hand side, so that one obtains

$$\left\langle\psi\left[\phi\left(\mathcal{N}\right)\right]\right\rangle=\psi\left(\phi_{\mathrm{in}}\right)\,, \tag{2.215}$$

which is the probability p_1 one is seeking for. Therefore all one needs to do is to solve Eq. (2.213) to obtain $h\left(\phi\right)$, then to plug the obtained expression in Eq. (2.211) to derive $\psi(\phi)$, and finally

[18] The fact that the integral in the right hand side of Eq. (2.214) vanishes when averaged is actually non trivial since both the integrand and the upper bound are stochastic quantities, but it can be shown in a rigorous way (see page 12 of Ref. [383]).

to evaluate this function at $\phi_{\rm in}$ to calculate p_1. A formal solution to Eq. (2.213) can straightforwardly be calculated and one obtains

$$h\left(\phi\right) = A\int_B^{\phi}\exp\left[-\frac{24\pi^2 M_{\rm Pl}^4}{V\left(u\right)}\right]\mathrm{d}u\,, \tag{2.216}$$

where A and B are two integration constants that play no role since they cancel out when calculating ψ thanks to Eq. (2.211). Indeed, this gives rise to

$$p_1 = \frac{\displaystyle\int_{\phi_2}^{\phi_{\rm in}}\exp\left[-\frac{24\pi^2 M_{\rm Pl}^4}{V\left(u\right)}\right]\mathrm{d}u}{\displaystyle\int_{\phi_2}^{\phi_1}\exp\left[-\frac{24\pi^2 M_{\rm Pl}^4}{V\left(u\right)}\right]\mathrm{d}u}\,. \tag{2.217}$$

A few remarks are in order about this equation. Firstly, one can check that since $\phi_{\rm in}$ lies between ϕ_1 and ϕ_2, this probability is ensured to be comprised between 0 and 1. Secondly, the function appearing in the integral, $\exp(-24\pi^2 M_{\rm Pl}^4/V)$, is rather natural for the problem under study, since it has already been encountered (actually, its inverse) when calculating the steady-state distribution in section 2.4.2.1, see Eq. (2.157). Thirdly, a special case that will prove useful in the following (in particular in sections 2.4.3.4 and 2.4.3.5) is when the potential is maximal at $\phi_\infty = \pm\infty$, and when, say, $\phi_1 = \phi_\infty$. In this case one is sure to first reach the ending point located at ϕ_2, that is $p_1 = 0$. Indeed, assuming that the potential is bounded from below, the numerator of Eq. (2.217) must be finite, since a bounded function is integrated over a bounded interval. If the potential is maximal at ϕ_1, and if it is monotonous over an interval of the type $[\phi_0, \phi_1[$, the denominator of Eq. (2.217) is on the contrary larger than the integral of a function bounded from below by a strictly positive number, over an unbounded interval $[\phi_0, \phi_\infty]$. This is why it diverges, and p_1 vanishes.

Example: $V \propto \phi^p$

For illustrative purpose, let us now see what Eq. (2.217) gives in the case where the potential V is monomial in the inflaton field ϕ and is given by

$$V\left(\phi\right) = M^4\left(\frac{\phi}{M_{\rm Pl}}\right)^p\,, \tag{2.218}$$

where p is a positive parameter that sets the shape of the potential (here we take $p > 1$) and M is an overall mass scale normalization. Such models are often referred to as "large field inflation" (LFI), or "chaotic inflation" (for further details about this model, including theoretical justifications, see *e.g.* section 4.2 of Ref. [205], section 3.2). In such cases, if one defines $x \equiv V/(24\pi^2 M_{\rm Pl}^4)$, one obtains

$$p_1 = \frac{\Gamma\left(-\frac{1}{p},\frac{1}{x_2}\right) - \Gamma\left(-\frac{1}{p},\frac{1}{x_{\rm in}}\right)}{\Gamma\left(-\frac{1}{p},\frac{1}{x_2}\right) - \Gamma\left(-\frac{1}{p},\frac{1}{x_1}\right)}\,, \tag{2.219}$$

where $\Gamma\left(s,y\right) \equiv \int_y^\infty t^{s-1}\mathrm{e}^{-t}\mathrm{d}t$ is the upper incomplete gamma function [269]. It is displayed in Fig. 2.5 for a few values of p. One can check that p_1 decreases monotonously between $p_1 = 1$ when $x_{\rm in} = x_1$ and $p_1 = 0$ when $x_{\rm in} = x_2$. Since $\phi_{\rm in}$ is labelled by $x_{\rm in} = V(\phi_{\rm in})/(24\pi^2 M_{\rm Pl}^4)$ in Fig. 2.5, inflation classically proceeds from the right to the left. Therefore, $p_1 < 1$ implies that some realizations of the stochastic process (2.208) climb up the potential and end up at ϕ_2. When $x_1 < x_{\rm in} \ll 1$ however, one has $p_1 =\simeq 1$ [as can be seen in Fig. 2.5, or directly checked in Eq. (2.217)] which means that in this case the inflaton very seldom climbs up the potential. This actually corresponds to the classical limit, on which we elaborate below.

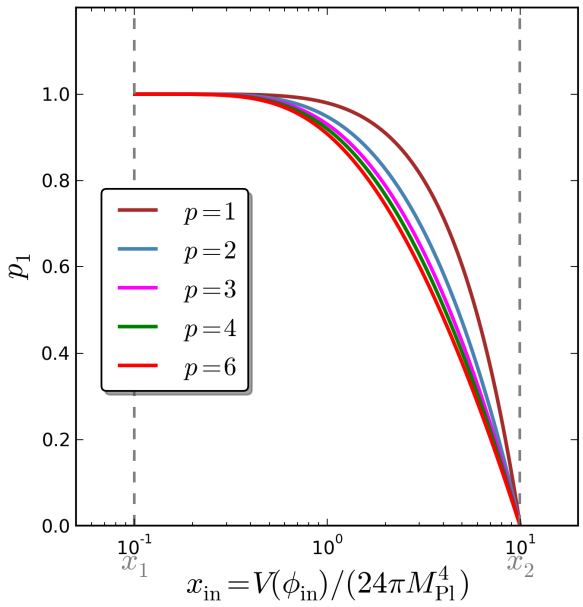

Figure 2.5.: Probability of reaching the ending point located at ϕ_1 first, as a function of $\phi_{\rm in}$ labelled by $x_{\rm in} = V(\phi_{\rm in})/(24\pi^2 M_{\rm Pl}^4)$ (so that inflation classically proceeds from the right to the left), in the large field potentials (LFI). The displayed result corresponds to $p = 1$ (brown), $p = 2$ (blue), $p = 3$ (magenta), $p = 4$ (green) and $p = 6$ (red). It is given by Eq. (2.219). The two ending points are located at $x_1 = 0.1$ and $x_2 = 10$, and are denoted by the dashed grey vertical lines.

2.4.3.4. Mean Number of e-folds

Let us now turn to the calculation of the mean number of e-folds $\langle \mathcal{N} \rangle$. As above, we want to make use of the Itô lemma (2.210). In order to do so, let us choose $f(\phi)$ to be defined as the solution of the differential equation

$$\frac{f''(\phi)}{24\pi^2 M_{\rm Pl}^2} V(\phi) - f'(\phi) \frac{V'(\phi)}{V(\phi)} M_{\rm Pl}^2 = -1 \,, \tag{2.220}$$

with boundary conditions $f(\phi_1) = f(\phi_2) = 0$. Such a solution will be explicitly calculated in due time. For now it is interesting to notice that thanks to this definition, the first term of the left hand side of the Itô equation (2.210), $f(\phi_1$ or $\phi_2)$, vanishes, and that the second integrand of its right hand side is -1. Thus, the Itô equation can be rewritten as

$$\mathcal{N} = f(\phi_{\rm in}) + \int_0^{\mathcal{N}} f'[\phi(N)] \frac{\sqrt{V}[\phi(N)]}{2\pi\sqrt{3} M_{\rm Pl}} \xi(N) \, {\rm d}N \,. \tag{2.221}$$

By averaging over all the realizations, one obtains[19]

$$\langle \mathcal{N} \rangle = f(\phi_{\rm in}) \,. \tag{2.222}$$

Therefore it is enough to solve the deterministic differential equation (2.220) for f with the associated boundary conditions, and to evaluate the obtained solution at $\phi_{\rm in}$, in order to derive

[19] Here also, since both the integrand and the upper bound are stochastic quantities, it is a non trivial fact that the integral in the right hand side of Eq. (2.221) vanishes when averaged. However it can be shown in a rigorous way, see page 12 of Ref. [383].

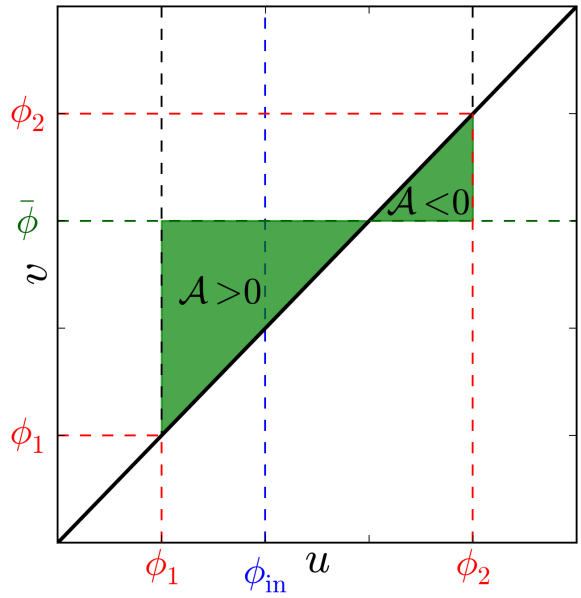

Figure 2.6.: Integration domain of Eq. (2.223) when evaluated at $\phi = \phi_2$, in the case $\phi_1 < \phi_2$ (the opposite case proceeds exactly the same way). The discrete parameter u is integrated between ϕ_1 and ϕ_2, while v varies between $\bar{\phi}$ and u. The resulting integration domain is displayed in green. When $u < \bar{\phi}$, one has $\mathrm{d}u\mathrm{d}v < 0$ and one integrates a positive contribution [remember that a minus sign is stands in front of Eq. (2.223)], and conversely when $u > \bar{\phi}$, one has $\mathrm{d}u\mathrm{d}v > 0$ and one integrates a negative contribution. This is a necessary condition in order for the overall integral to vanish. This is why $\bar{\phi}$ must lie between ϕ_1 and ϕ_2.

the mean value of the realized number of e-folds. Solving Eq. (2.220) gives rise to

$$f\left(\phi\right) = -24\pi^2 M_{\rm Pl}^2 \int_{\phi_1}^{\phi} \mathrm{d}u \int_{\bar{\phi}(\phi_1,\phi_2)}^{u} \frac{\mathrm{d}v}{V\left(v\right)} \exp\left\{24\pi^2 M_{\rm Pl}^4 \left[\frac{1}{V\left(v\right)} - \frac{1}{V\left(u\right)}\right]\right\} , \tag{2.223}$$

where $\bar{\phi}$ is an integration constant that must be chosen in order to have $f(\phi_2) = 0$. More precisely, as can be seen in Fig. 2.6, $\bar{\phi}$ must be such that, when f is evaluated at ϕ_2, the integration domain of Eq. (2.223) possesses a positive part and a negative part, that are able to compensate for each other. This implies that $\bar{\phi}$ lies between ϕ_1 and ϕ_2. Another generic condition comes from splitting the u-integral in Eq. (2.223) into $\int_{\phi_1}^{\phi} \mathrm{d}u = \int_{\phi_1}^{\phi_2} \mathrm{d}u + \int_{\phi_2}^{\phi} \mathrm{d}u$. The first integral vanishes because $f(\phi_2) = 0$, which means that in order for f to be symmetrical in $\phi_1 \leftrightarrow \phi_2$, $\bar{\phi}(\phi_1, \phi_2)$ must abide by this symmetry too, that is

$$\bar{\phi}\left(\phi_1, \phi_2\right) = \bar{\phi}\left(\phi_2, \phi_1\right) . \tag{2.224}$$

Beyond these simple conditions, the actual location of $\bar{\phi}$ needs to be calculated for each potential V explicitly and there is no explicit generic expression for it.

However, in the special case where the potential is maximal at $\phi_\infty = \pm\infty$ (which is the case notably for large field or plateau models), and if one wants to calculate the mean number of e-folds between $\phi_{\rm in}$ and ϕ_1, things can be made clearer regarding the location of $\bar{\phi}$. Indeed, one can set $\phi_2 = \phi_\infty$, since in the case described here the probability to reach ϕ_∞ vanishes, as shown in section 2.4.3.3. Therefore, the quantity we really compute is the mean number of e-folds between $\phi_{\rm in}$ and ϕ_1. In order to make things explicit, let us assume that $V' > 0$ (the

same line of arguments can be followed in the case $V' < 0$). Inflation proceeds at $\phi < \phi_\infty$. In this case, the (absolute value of the) integrand of Eq. (2.226) increases with u and reaches a constant when $u \to \phi_\infty$, while strongly decreasing with v. Looking back at Fig. 2.6, one can convince oneself that, in order for the negative integration domain to cancel out the positive one, $\bar{\phi}$ has therefore to be moved to ϕ_∞,

$$\bar{\phi} = \phi_\infty \,. \tag{2.225}$$

Once the location of $\bar{\phi}$ is determined, from Eqs. (2.222) and (2.223), one obtains

$$\langle \mathcal{N} \rangle = -24\pi^2 M_{\rm Pl}^2 \int_{\phi_1}^{\phi_{\rm in}} {\rm d}u \int_{\bar{\phi}(\phi_1,\phi_2)}^{u} \frac{{\rm d}v}{V\left(v\right)} \exp\left\{ 24\pi^2 M_{\rm Pl}^4 \left[\frac{1}{V\left(v\right)} - \frac{1}{V\left(u\right)} \right] \right\} . \tag{2.226}$$

Here also, one recognizes the same kind of functions as the ones appearing in the steady-state distribution (2.157).

Classical Limit

As a consistency check, let us derive the asymptotic limit of Eq. (2.226) in the classical approximation, and see whether the classical trajectory (2.12) is properly recovered. For simplicity, we consider the situation described above where the potential is maximal at $\phi_\infty = \pm\infty$ and where we thus need to evaluate Eq. (2.226) between $\phi_{\rm in}$ and $\phi_1 = \phi_{\rm end}$, with $\bar{\phi} = \phi_\infty$.

Let us first work out the v-integral, that is to say $\int_{\bar{\phi}}^{u} {\rm d}v/V(v) \exp[24\pi^2 M_{\rm Pl}^4/V(v)]$. Since the integrand varies exponentially with the potential, the strategy is to evaluate it close to its maximum, that is where the potential V is minimum. The potential being maximal at $\phi_\infty = \bar{\phi}$, the integrand is clearly maximal[20] at u. In order for the dominant contributions to the v-integral to come from the close neighbourhood of its ending point u, one needs the argument of the exponential to be large, that is

$$V\left(\phi_{\rm end}\right) \ll 24\pi^2 M_{\rm Pl}^4 \,. \tag{2.227}$$

This assumption is quite natural in the classical limit since $V/M_{\rm Pl}^4$ controls the amplitude of the noise term in Eq. (2.208), but we come back to what it really means below. Taylor expanding $1/V$ at first order around u, $1/V(v) \simeq 1/V(u) - V'(u)/V^2(u)(v-u)$, one obtains, after integrating by parts[21]

$$\int_{\bar{\phi}}^{u} \frac{{\rm d}v}{V(v)} \exp\left[\frac{24\pi^2 M_{\rm Pl}^4}{V(v)} \right] \simeq -\frac{1}{24\pi^2 M_{\rm Pl}^4} \frac{V(u)}{V'(u)} \left[1 - \frac{V(u)}{24\pi^2 M_{\rm Pl}^4} \right] \exp\left[\frac{24\pi^2 M_{\rm Pl}^4}{V(u)} \right] . \tag{2.228}$$

This is similar to a saddle-point approximation [385] (also called Laplace's method). Because of assumption (2.227), the term $1 - V(u)/(24\pi^2 M_{\rm Pl}^4)$ can be approximated to 1. Plugging back this expression in Eq. (2.226), one finally obtains

$$\langle \mathcal{N} \rangle|_{\rm cl} = \int_{\phi_{\rm end}}^{\phi_{\rm in}} \frac{{\rm d}u}{M_{\rm Pl}^2} \frac{V(u)}{V'(u)} \,, \tag{2.229}$$

which exactly matches the classical trajectory (2.12). The classical limit is then properly recovered.

[20] More generally, the calculation presented here only relies on the assumption $V\left(\bar{\phi}\right) > V\left(\phi_{\rm in}\right)$ and on Eq. (2.227).
[21] Since $V(\bar{\phi}) > V(u)$ and since V is monotonous, one can also show that $\exp\left[-24\pi^2 M_{\rm Pl}^4 V'(u)/V^2(u)(\bar{\phi}-u)\right]$ is exponentially vanishing.

A few remarks are in order. First, the classical trajectory appears as a saddle-point limit of the mean stochastic trajectory, analogously to what happens *e.g.* in the context of path integral calculations. The fact that the classical limit corresponds to Eq. (2.227) is also interesting, since it can be shown [386, 387] that $V/M_{\rm Pl}^4$ measures the amplitude of the quantum gravity corrections. Therefore, the "classical" limit needs here to be understood as the limit where corrections from quantum gravity are negligible, and the condition (2.227) is in fact very generic. For this reason, in the following and as we did in section 2.4.3.3, it is convenient to define the ratio

$$x \equiv \frac{V}{24\pi^2 M_{\rm Pl}^4}\,. \tag{2.230}$$

Generic expressions in x will be derived, but the validity range of the present calculation is of course $x < 1$ since we do not incorporate quantum gravity. In the following also, the "classical" limit shall always refer to the $x \ll 1$ limit. Finally and in passing, the fact that x encodes the amplitude of quantum gravity possible effects can be illustrated in the calculation of the steady-state distribution, see section 2.4.2.1. In this section, we made clear that different time variables in the Langevin equation lead to different stochastic processes (and as a consequence, different steady-state distributions) because of the $H(\phi)$ dependence, through which the amplitude of the noise depends on the coarse-grained field. In some sense, because the coarse-grained field is a stochastic quantity, so is H, *i.e.* the metric, and we understand why it has to do with "quantum gravity". In any case, this $H(\phi)$ dependence translates into different steady-state distributions P and $\tilde{P}$ when computed in terms of N or in terms of t respectively. Making use of Eqs. (2.157) and (2.160), the difference between these two distributions can be studied through the ratio

$$\frac{\ln P}{\ln \tilde{P}} = \frac{1 - x\ln x}{1 - \frac{3}{2}x\ln x}\,, \tag{2.231}$$

from which it is clear that the two distributions are identical [and the effects coming from the $H(\phi)$ dependence vanish] in the limit where $x \to 0$.

Example: $V \propto \phi^p$

As an illustrative example, let us now see what Eq. (2.226) gives in the case of the large field potential (2.218). In these models, remember that the classical trajectory proceeds at decreasing values of ϕ. One is interested in the mean number of e-folds realized between $\phi_{\rm in}$ and $\phi_{\rm end}$. Since the large field potential belongs to the category mentioned above where V is maximal at $\phi_\infty = \infty$, one takes $\phi_1 = \phi_{\rm end}$ and $\bar{\phi} = \phi_\infty = \infty$ in Eq. (2.226). One obtains, for $p > 1$,

$$\langle \mathcal{N} \rangle = \frac{1}{p\,(p-1)} \left(\frac{24\pi^2 M_{\rm Pl}^4}{M^4}\right)^{2/p} \int_{x_{\rm end}}^{x_{\rm in}} \mathrm{e}^{-\frac{1}{x}} x^{\frac{2}{p}-2} M\left(1-\frac{1}{p}, 2-\frac{1}{p}, \frac{1}{x}\right) \mathrm{d}x\,, \tag{2.232}$$

where M is the Kummer's confluent hypergeometric function [269] and where we have used the variable $x = V/(24\pi^2 M_{\rm Pl}^4)$, so that the classical limit corresponds to $x \ll 1$. In this limit, one can make use of the asymptotic expansion [269] $M(a, a+1, z) \simeq a\exp(z)/z$ when $z \to \infty$, and one exactly obtains the classical trajectory (2.12) as expected.

An explicit comparison between both trajectories is displayed in Fig. 2.7 for a few values of p. The quantity which is displayed is the derivative of the mean number of e-folds with respect to $\phi_{\rm in}$, to remove the dependence on $\phi_{\rm end}$. It is plotted as a function of $\phi_{\rm in}$, which is labelled by $x_{\rm in}$ to make interpretation easier. Since the energy density must remain sub-Planckian, only the region $x < 1$ makes really sense but we display a larger range of values for x to see how the functions

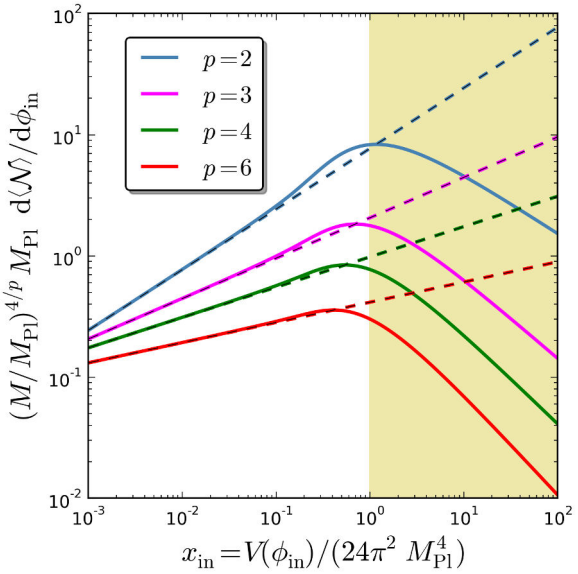

Figure 2.7.: Mean number of e-folds for the models $V \propto \phi^p$ with $p = 2$ (blue), $p = 3$ (magenta), $p = 4$ (green) and $p = 6$ (red). The displayed quantity is the derivative of the mean number of e-folds with respect to the starting point $\phi_{\rm in}$, as a function of $\phi_{\rm in}$ labeled by $x_{\rm in} = V(\phi_{\rm in})/(24\pi^2 M_{\rm Pl}^4)$. The solid lines correspond to Eq. (2.232) while the dashed lines stand for the classical trajectory $\propto V/V'$ given by Eq. (2.12). The later provides a good approximation to the former in the regime $x \ll 1$, as expected. Obviously, the calculation makes sense only when $x < 1$, *i.e.* outside the yellow shaded area, which is displayed for information only.

involved behave in general. On can first check that when $x_{\rm in} \ll 1$, the classical trajectory (2.12) provides a good approximation to the mean number of e-folds given by Eq. (2.232). On the other hand, when $x_{\rm in}$ is large, the deviation between these two quantities starts to be important and the mean stochastic number of e-folds is smaller than the classical one. This is due to the effect of the quantum kicks, which tend to shift the inflaton field faster than what the classical drift does at large field values. More precisely, since the confluent hypergeometric function tends to 1 when its last argument goes to 0, one has ${\rm d}\langle\mathcal{N}\rangle/{\rm d}\phi_{\rm in} \propto x_{\rm in}^{1/p-1}$ when $x_{\rm in} \gg 1$, whereas classically ${\rm d}N/{\rm d}\phi \propto x_{\rm in}^{1/p}$. Finally, there exists an intermediate range of values when $x_{\rm in} \sim 1$ for which the mean number of e-folds is slightly larger than the classical one.

2.4.3.5. Number of e-folds Dispersion

Let us now move on with the calculation of the dispersion in the number of e-folds, that we denote

$$\delta\mathcal{N}^2 = \left\langle \mathcal{N}^2 \right\rangle - \left\langle \mathcal{N} \right\rangle^2 . \tag{2.233}$$

This quantity first requires to compute the mean squared number of e-folds $\left\langle \mathcal{N}^2 \right\rangle$. In order to do so, let us square Eq. (2.221), and take the stochastic average of it. One obtains[22]

$$\left\langle \mathcal{N}^2 \right\rangle = f^2\left(\phi_{\rm in}\right) + \left\langle \int_0^{\mathcal{N}} f'^2\left[\phi\left(N\right)\right] \frac{V\left[\phi\left(N\right)\right]}{12\pi^2 M_{\rm Pl}^2} {\rm d}N \right\rangle . \tag{2.234}$$

[22]This is again a non trivial result since both the integrand and the upper bound of the integral appearing in Eq. (2.221) are stochastic quantities, but it can be shown in a rigorous way (see page 12 of Ref. [383]).

In order to make use of the Itô lemma, let $g(\phi)$ be the function defined by

$$\frac{g''(\phi)V(\phi)}{24\pi^2 M_{\rm Pl}^2} - g'(\phi)\frac{V'(\phi)}{V(\phi)}M_{\rm Pl}^2 = -f'^2(\phi)\frac{V(\phi)}{12\pi^2 M_{\rm Pl}^2}, \tag{2.235}$$

where f is the function introduced in Eq. (2.223). When applied to $g(\phi)$, if one further sets $g(\phi_1) = g(\phi_2) = 0$, the stochastic average of the Itô lemma (2.210) gives rise to

$$\begin{aligned} g(\phi_{\rm in}) &= \left\langle \int_0^{\mathcal{N}} f'^2[\phi(N)]\frac{V[\phi(N)]}{12\pi^2 M_{\rm Pl}^2}{\rm d}N \right\rangle \\ &= \langle \mathcal{N}^2\rangle - f^2(\phi_{\rm in}) \\ &= \langle \mathcal{N}^2\rangle - \langle \mathcal{N}\rangle^2, \end{aligned} \tag{2.236}$$

where the second line is just a consequence of Eq. (2.234) and where the third line is just a consequence of Eq. (2.222). Therefore, what one needs to do is to solve Eq. (2.235) with boundary conditions $g(\phi_1) = g(\phi_2) = 0$, and to evaluate the resulting function at $\phi_{\rm in}$ in order to obtain

$$\delta\mathcal{N}^2 = g(\phi_{\rm in}). \tag{2.237}$$

The differential equation (2.235) can formally be integrated, and one obtains

$$g(\phi_{\rm in}) = 2\int_{\phi_{\rm in}}^{\phi_1}{\rm d}\phi\int_{\hat\phi(\phi_1,\phi_2)}^{\phi}{\rm d}\psi f'^2(\psi)\exp\left[\frac{24\pi^2 M_{\rm Pl}^4}{V(\psi)} - \frac{24\pi^2 M_{\rm Pl}^4}{V(\phi)}\right], \tag{2.238}$$

where $\hat\phi(\phi_1,\phi_2)$ is an integration constant that must be chosen in order to have $g(\phi_2) = 0$. As for $\bar\phi$, it is straightforward to show that $\hat\phi$ must lie between ϕ_1 and ϕ_2 and that it must be symmetric in (ϕ_1,ϕ_2), that is

$$\hat\phi(\phi_1,\phi_2) = \hat\phi(\phi_2,\phi_1). \tag{2.239}$$

In the same manner as for $\bar\phi$, when the potential is maximal at $\phi_\infty = \pm\infty$ and if $\phi_2 = \phi_\infty$, one has $\hat\phi = \phi_\infty$.

Classical Limit

As was done for the mean number of e-folds in section 2.4.3.4, let us derive the classical limit $x \ll 1$ of Eq. (2.238). Obviously, in the classical setup the trajectories are not stochastic and $\delta\mathcal{N}^2 = 0$, and what we mean by "classical limit" here is the non vanishing leading order contribution to $\delta\mathcal{N}^2$ in the limit $x \ll 1$. As in section 2.4.3.4, we consider the situation where the potential is maximal at $\phi_\infty = \pm\infty$ and where we thus need to evaluate Eq. (2.238) between $\phi_{\rm in}$ and $\phi_1 = \phi_{\rm end}$, with $\hat\phi = \phi_\infty$ and $\bar\phi = \phi_\infty$ in the f'^2 term.

Let us first work out the ψ-integral, that is to say $\int_{\hat\phi}^{\phi}{\rm d}\psi f'^2\exp[24\pi^2 M_{\rm Pl}^4/V(\psi)]$, with a saddle-point approximation as before. Since the integrand varies exponentially with the potential, the strategy is again to evaluate it close to its maximum, that is where the potential V is minimum. The potential is maximal at $\phi_\infty = \hat\phi$, so the integrand is clearly maximal at ϕ. Taylor expanding $1/V$ at first order around ϕ, $1/V(\psi) \simeq 1/V(\phi) - V'(\phi)/V^2(\phi)(\psi-\phi)$, one obtains[23]

$$\int_{\hat\phi}^{\phi}{\rm d}\psi f'^2(\psi)\exp\left[\frac{24\pi^2 M_{\rm Pl}^4}{V(\psi)}\right] \simeq -\frac{1}{24\pi^2 M_{\rm Pl}^8}\frac{V^4(\phi)}{V'^3(\phi)}\exp\left[\frac{24\pi^2 M_{\rm Pl}^4}{V(\phi)}\right]. \tag{2.240}$$

[23] In the limit where $V(\phi) \ll 24\pi^2 M_{\rm Pl}^4$, f is close to the classical trajectory (2.229) as shown in section 2.4.3.4, and one can take $f'(\psi) \simeq V(\psi)/V'(\psi)M_{\rm Pl}^{-2}$.

Plugging back this expression in Eq. (2.238), one obtains

$$\delta\mathcal{N}^2\big|_{\rm cl} = \frac{1}{12\pi^2 M_{\rm Pl}^8}\int_{\phi_{\rm end}}^{\phi_{\rm in}} {\rm d}\phi \frac{V^4(\phi)}{V'^3(\phi)} \tag{2.241}$$

which we shall refer to as the classical approximation to $\delta\mathcal{N}^2$.

2.4.3.6. Scalar Power Spectrum

We are now in a position where we can calculate the power spectrum for scalar adiabatic perturbations $\mathcal{P}_\zeta$. The power spectrum of $\delta\mathcal{N}$ is defined by the two-point correlator of $\mathcal{N}$,

$$\mathcal{P}_{\delta\mathcal{N}}(k) = \frac{k^3}{2\pi^2}\int {\rm d}^3x \left\langle \delta\mathcal{N}(0)\,\delta\mathcal{N}(x)\right\rangle {\rm e}^{i\boldsymbol{k}\cdot\boldsymbol{x}}\,. \tag{2.242}$$

Since the quantity $\delta\mathcal{N}^2$ computed between two points $\phi_{\rm in}$ and $\phi_{\rm end}$ is due to an integrated effects of all the modes crossing the Hubble radius between these two points, one has

$$\delta\mathcal{N}^2 = \int_{k_{\rm in}}^{k_{\rm end}} \mathcal{P}_{\delta\mathcal{N}}(k)\frac{{\rm d}k}{k} = \int_{\ln k_{\rm end}-\langle\mathcal{N}\rangle(1-\epsilon_1+\cdots)}^{\ln k_{\rm end}} \mathcal{P}_{\delta\mathcal{N}}{\rm d}N\,, \tag{2.243}$$

where $\langle\mathcal{N}\rangle = \ln(a_{\rm end}/a_{\rm in}) = \ln(k_{\rm end}/k_{\rm in})(1+\epsilon_1+\cdots)$. Here, "$\cdots$" refer to higher order in slow roll terms, but it is enough to keep the zeroth order only since we are just interested in the leading order contributions in slow roll. This is why the above relation leads to

$$\mathcal{P}_\zeta(k) = \mathcal{P}_{\delta\mathcal{N}}(k) = \left.\frac{{\rm d}\delta\mathcal{N}^2}{{\rm d}\langle\mathcal{N}\rangle}\right|_{\langle\mathcal{N}\rangle=\ln(k_{\rm end}/k)}\,. \tag{2.244}$$

Since $\delta\mathcal{N}^2$ is given by $g(\phi)$, see Eq. (2.237), and $\langle\mathcal{N}\rangle$ is given by $f(\phi)$, see Eq. (2.222), noting that ${\rm d}/{\rm d}\langle\mathcal{N}\rangle = ({\rm d}\phi/{\rm d}\langle\mathcal{N}\rangle){\rm d}/{\rm d}\phi = (1/f'){\rm d}/{\rm d}\phi$, this gives rise to

$$\mathcal{P}_\zeta(\phi) = \frac{g'(\phi)}{f'(\phi)} = 2\int_\phi^{\hat\phi}{\rm d}\psi\frac{f'^2(\psi)}{f(\phi)}\exp\left[\frac{24\pi^2M_{\rm Pl}^4}{V(\psi)} - \frac{24\pi^2M_{\rm Pl}^4}{V(\phi)}\right]\,, \tag{2.245}$$

where f is given by Eq. (2.223). Here, by $\mathcal{P}_\zeta(\phi)$, we mean the power spectrum calculated at a scale $\boldsymbol{k}$ such that when it crosses the Hubble radius, the inflaton field value is ϕ. This is the main result of this section since it provides, for the first time, a complete expression of the curvature perturbations power spectrum in stochastic inflation, computed in a non perturbative manner and, therefore, including the full stochastic effects.

Classical Limit

As a consistency check, it is important to make sure that the standard result for the power spectrum (2.205) is properly recovered in the classical limit $x \ll 1$. Since we already derived the classical limit for $\delta\mathcal{N}^2$, given by Eq. (2.241), and the classical limit for $\langle\mathcal{N}\rangle$, given by the classical trajectory (2.229), one can plug these two expressions in Eq. (2.244). Noting again that ${\rm d}/{\rm d}\langle\mathcal{N}\rangle = ({\rm d}\phi/{\rm d}\langle\mathcal{N}\rangle){\rm d}/{\rm d}\phi = (1/f'){\rm d}/{\rm d}\phi$, one obtains

$$P_\zeta\big|_{\rm cl} = \frac{1}{12\pi^2M_{\rm Pl}^6}\frac{V^3(\phi)}{V'^2(\phi)}\,, \tag{2.246}$$

which exactly matches the usual result (2.205), since at leading order in slow roll one has $H^2 \simeq V/(3M_{\rm Pl}^2)$ and $\epsilon_1 = M_{\rm Pl}^2/2(V'/V)^2$. This generalizes the result of Ref. [350], where this

correspondence is shown but only for inflationary models where the Hubble parameter varies linearly with ϕ, that is for inflationary potentials of the specific form given by Eq. (50) in Ref. [208], section 3.1. Here we have extended this result to any potential is single-field slow-roll inflation.

2.4.3.7. Scalar Spectral Index

Finally, it can be interesting to calculate the scalar spectral index, defined in Eq. (2.112) and which characterizes the way $\mathcal{P}_\zeta$ varies with k. Since we established in the last section how $\mathcal{P}_\zeta$ varies with ϕ, see Eq. (2.245), we first need to determine how ϕ varies with k. At leading order in slow roll, one has

$$\frac{\partial}{\partial \ln(k)} \simeq (1+\epsilon_1)\frac{\partial}{\partial N} \tag{2.247}$$

$$\simeq -\frac{1}{\partial \langle \mathcal{N} \rangle / \partial\phi}\frac{\partial}{\partial\phi} \tag{2.248}$$

$$\simeq -\frac{1}{f'(\phi)}\frac{\partial}{\partial\phi}\,. \tag{2.249}$$

When going from Eq. (2.247) to Eq. (2.248), the $1+\epsilon_1$ term has been dropped since it only gives rise to subdominant corrections in slow roll. Making use of Eq. (2.244) for $\mathcal{P}_\zeta$, one obtains

$$n_{\rm S} = 1 - \frac{g''(\phi)}{f'(\phi)\,g'(\phi)} + \frac{f''(\phi)}{f'^2(\phi)}\,, \tag{2.250}$$

where $f(\phi)$ is given by Eq. (2.223) and $g(\phi)$ is given by Eq. (2.238).

Classical Limit

The regular classical result can also be recovered as in section 2.4.3.6. When $f(\phi)$ is given by its classical limit (2.229) and $g(\phi)$ is given by its classical limit (2.241), the above result (2.250) gives rise to

$$n_{\rm S}\big|_{\rm cl} = 1 - M_{\rm Pl}^2\left[3\left(\frac{V'}{V}\right)^2 - 2\frac{V''}{V}\right] = 1 - 2\epsilon_1 - \epsilon_2\,, \tag{2.251}$$

which matches the formula given below Eq. (2.206) since in the slow-roll approximation, the slow-roll parameters ϵ_1 and ϵ_2 can be expressed as

$$\epsilon_1 = \frac{M_{\rm Pl}^2}{2}\left(\frac{V'}{V}\right)^2, \tag{2.252}$$

$$\epsilon_2 = 2M_{\rm Pl}^2\left[\left(\frac{V'}{V}\right)^2 - \frac{V''}{V}\right], \tag{2.253}$$

see Eqs. (2.15) and (2.16).

2.4.3.8. A Complete Example: Large Field Inflation

In sections 2.4.3.3 and 2.4.3.4, we have exemplified the above results in the case of a large field potential. This is why, to gain some intuition on how the stochastic effects modify the power

spectrum, and in order to make clear how the calculation presented here works in practice, we now turn to the complete treatment of large field inflation. We recall that the potential of these models is given by

$$V(\phi) = M^4 \left(\frac{\phi}{M_{\rm Pl}}\right)^p . \tag{2.254}$$

In the figures displayed below, we set the mass scale M^4 to the value that fits the amplitude of the power spectrum P_ζ, when the power spectrum is calculated with the classical formula. The classical trajectory (2.229) can be integrated as $\phi/M_{\rm Pl} = \sqrt{\phi_{\rm end}^2/M_{\rm Pl}^2 - 2p\,(N - N_{\rm end})}$, where $\phi_{\rm end}/M_{\rm Pl} = p/\sqrt{2}$ is the location where $\epsilon_1 \simeq p^2 M_{\rm Pl}^2/(2\phi^2) = 1$. Then, Eq. (2.205) gives rise to

$$\frac{M^4}{M_{\rm Pl}^4} = 12\pi^2 p^2 \left(\frac{p^2}{2} + 2p\Delta N_*\right)^{-1-p/2} \mathcal{P}_{\zeta *} , \tag{2.255}$$

where we take the measured value [163] $\mathcal{P}_{\zeta *} \simeq 2.203 \times 10^{-9}$ and we let $\Delta N_* \simeq 50$. Obviously, when the power spectrum does not match the one given by the classical calculation, this mass normalization needs to be changed accordingly (see section 2.4.3.9) but here we use this value for illustrative purpose.

The aim of this section is to see which corrections to the power spectrum arise due to stochastic effects, and also to check the validity of the formulas derived above with a numerical code that integrates a large number of realizations of the Langevin equation. In passing, it is worth noting that in order to avoid large numerical errors when doing so (due *e.g.* to the small value of $M^4/M_{\rm Pl}^4 \simeq 10^{-11}$), the Langevin equation (2.208) can be written in terms of the rescaled variables

$$y = \left(\frac{M^2}{2\pi\sqrt{3p}M_{\rm Pl}^2}\right)^{2/p} \frac{\phi}{M_{\rm Pl}} \quad \text{and} \quad s = p\left(\frac{M^2}{2\pi\sqrt{3p}M_{\rm Pl}^2}\right)^{4/p} N , \tag{2.256}$$

so that it is given by the simple form

$$\frac{{\rm d}y}{{\rm d}s} = -\frac{1}{y} + y^{p/2}\xi(s) . \tag{2.257}$$

This equation is solved a large number of times (typically $10^6 - 10^7$ realizations are produced) and the mean values of $\mathcal{N}$ and $\mathcal{N}^2$ are computed over the realizations.

Mean number of e-folds

The mean number of e-folds has already been computed and is given by Eq. (2.232). In order to test both the validity of our analytical approach and the reliability of our numerical code, we compare in Fig. 2.8 the integral (2.232) with the ensemble average over a large number of numerical realizations of the Langevin equation (2.257). Since the energy density must remain sub-Planckian, values of x larger than 1 do not really make sense but here, we display them to check the agreement between our code and our calculation in a broader range. Obviously, this agreement is excellent. When the value of $\phi_{\rm in}$ is such that $x_{\rm in} \ll 1$, the classical trajectory (2.229) provides a very good approximation to the mean stochastic trajectory. To go beyond, it proves useful at this point to derive the next-to-leading orders expressions for $\langle\mathcal{N}\rangle$ in the $x \ll 1$ limit, to characterize the deviations from the classical trajectory in this regime. Making use of the expansion [269] $M(1-1/p, 2-1/p, 1/x) \simeq (1-1/p){\rm e}^{1/x}[x + x^2/p + (1+p)/p^2x^3 + \cdots]$ when

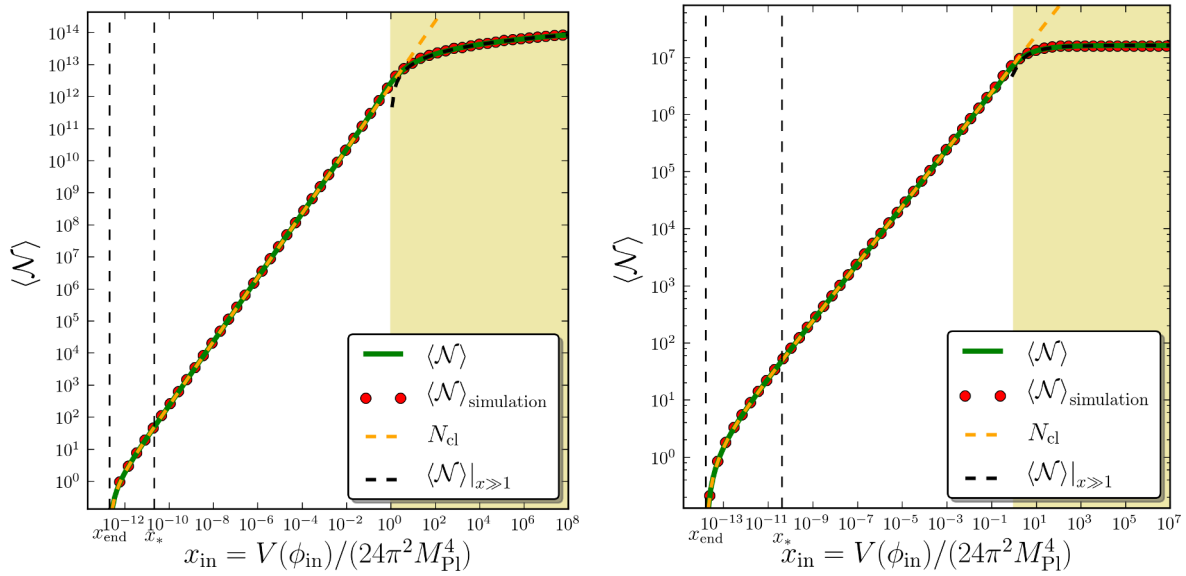

Figure 2.8.: Mean number of e-folds $\langle\mathcal{N}\rangle$ realized in the large field potential (2.254) for $p = 2$ (left panel) and $p = 4$ (right panel), between $x_{\rm in}$ and $x_{\rm end}$, as a function of $x_{\rm in}$, where $x = V/(24\pi^2 M_{\rm Pl}^4)$. The mass scale M^4 is normalized to Eq. (2.255). The location x_* refers to the value of x for which the classical number of e-folds $N_{\rm cl} = 50$ and $x_{\rm end}$ is where $\epsilon_1 = 1$. The green line corresponds to the analytical exact result (2.232), and the red circles are provided by a numerical integration of the Langevin equation (2.257) where a large number of realizations are produced over which the mean value of $\mathcal{N}$ is computed. Obviously, the agreement with the analytical formula is excellent and confirms both approaches. The orange dashed line corresponds to the classical trajectory (2.229), which provides a good approximation to the exact result when $x_{\rm in} \ll 1$. Finally, the black dashed line corresponds to Eq. (2.259) which is the expansion of Eq. (2.232) in the opposite limit $x \gg 1$. Obviously, the calculation makes sense only when $x < 1$, *i.e.* outside the yellow shaded area, which is displayed for information only.

$x \ll 1$, one obtains

$$\langle\mathcal{N}\rangle|_{x_{\rm end}<x_{\rm in}\ll1} \simeq \left(\frac{24\pi^2 M_{\rm Pl}^4}{M^4}\right)^{2/p} \frac{1}{p^2}\left[\frac{p}{2}\left(x_{\rm in}^{2/p} - x_{\rm end}^{2/p}\right) + \frac{1}{p+2}\left(x_{\rm in}^{2/p+1} - x_{\rm end}^{2/p+1}\right) + \frac{1}{2p}\left(x_{\rm in}^{2/p+2} - x_{\rm end}^{2/p+2}\right) + \cdots\right]. \quad (2.258)$$

The term on the first line corresponds to the classical trajectory (2.229), and the following ones are corrections in the regime $x_{\rm in} \ll 1$. Again, the opposite limit $x \gg 1$ corresponds to super-Planckian energy densities where our calculation should not apply. However, it can be interesting to see how Eq. (2.258) breaks when $x \gtrsim 1$. If one expands Eq. (2.232) in the limit

where $x_{\rm in} \gg 1$, one obtains

$$\langle\mathcal{N}\rangle\big|_{x_{\rm end}\ll 1, x_{\rm in}\gg 1} \simeq \begin{cases} \left(\dfrac{24\pi^2 M_{\rm Pl}^4}{M^4}\right)^{2/p} \dfrac{x_{\rm in}^{2/p-1}}{(p-1)(2-p)} & \text{if } 1<p<2 \\ \dfrac{12\pi^2 M_{\rm Pl}^4}{M^4}\ln(x_{\rm in}) & \text{if } p=2 \\ \left(\dfrac{24\pi^2 M_{\rm Pl}^4}{M^4}\right)^{2/p}\left[C(p)-\dfrac{x_{\rm in}^{2/p-1}}{(p-1)(p-2)}\right] & \text{if } p>2 \end{cases} , \tag{2.259}$$

where $C(p)$ is a constant depending on p but which is always of order one. These expressions are also displayed in Fig. 2.8 where one can check that they provide reliable approximations to the exact result when $x_{\rm in} \gg 1$. Interestingly enough, when $p > 2$, the mean number of e-folds that one can realize in the large field potential is always finite even if one starts from $\phi_{\rm in} = \infty$, and is of the order $\mathcal{O}(1)(M/M_{\rm Pl})^{8/p}$. This is not the case when $p \leq 2$ for which the potential is flatter and the mean number of e-folds blows up with $\phi_{\rm in}$.

Number of e-folds dispersion

The calculation of the power spectrum also requires to obtain the dispersion in the number of e-folds . Applying Eq. (2.238) to the potential (2.254), one gets

$$\delta\mathcal{N}^2 = \frac{2}{p^2(p-1)^2}\left(\frac{24\pi^2 M_{\rm Pl}^4}{M^4}\right)^{4/p}\int_{x_{\rm end}}^{x_{\rm in}} {\rm d}s \int_s^\infty {\rm d}t\,(st^3)^{\frac{1}{p}-1}\,{\rm e}^{-\frac{1}{s}-\frac{1}{t}} M^2\left(1-\frac{1}{p}, 2-\frac{1}{p}, \frac{1}{t}\right) . \tag{2.260}$$

This expression is displayed in Fig. 2.9 together with the result of a numerical integration of the Langevin equation for a large number of realizations over which the mean values of $\mathcal{N}$ and $\mathcal{N}^2$ are computed, and $\delta\mathcal{N}^2$ is obtained. Obviously, the agreement is excellent. At this point, it again proves useful to derive the asymptotic limits of Eq. (2.260) in the regimes $x_{\rm in} \ll 1$ and $x_{\rm in} \gg 1$, even if we recall that the later is non-physical. When $x_{\rm end} < x_{\rm in} \ll 1$, if $p > 3/2$, one has

$$\begin{aligned}\delta\mathcal{N}^2\big|_{x_{\rm end}<x_{\rm in}\ll 1} \simeq\ & \frac{2}{p^4}\left(\frac{24\pi^2 M_{\rm Pl}^4}{M^4}\right)^{4/p}\left[\frac{p}{p+4}\left(x_{\rm in}^{4/p+1}-x_{\rm end}^{4/p+1}\right)\right. \\ & \left.+\frac{p+5}{2p+4}\left(x_{\rm in}^{4/p+2}-x_{\rm end}^{4/p+2}\right)+\frac{2p^2+15p+18}{3p^2+4p}\left(x_{\rm in}^{4/p+3}-x_{\rm end}^{4/p+3}\right)\right] .\end{aligned} \tag{2.261}$$

The first line of this expression exactly matches the classical approximation (2.241) to $\delta\mathcal{N}^2$, as expected, while the following terms are corrections in the regime $x \ll 1$. On the other hand, when $x_{\rm end} \ll 1$ but $x_{\rm in} \gg 1$, one has

$$\delta\mathcal{N}^2\big|_{x_{\rm end}\ll 1, x_{\rm in}\gg 1} \simeq \begin{cases} \dfrac{1}{(p-1)^2(2-p)(2p-3)}\left(\dfrac{24\pi^2 M_{\rm Pl}^4}{M^4}\right)^{\frac{4}{p}} x_{\rm in}^{4/p-2} & \text{if } \dfrac{3}{2}<p<2 \\ \left(\dfrac{24\pi^2 M_{\rm Pl}^4}{M^4}\right)^2 \ln(x_{\rm in}) & \text{if } p=2 \\ \left(\dfrac{24\pi^2 M_{\rm Pl}^4}{M^4}\right)^{4/p}\left[\bar{C}(p)-\dfrac{x_{\rm in}^{4/p-2}}{(p-1)^2(p-2)(2p-3)}\right] & \text{if } p>2 \end{cases} , \tag{2.262}$$

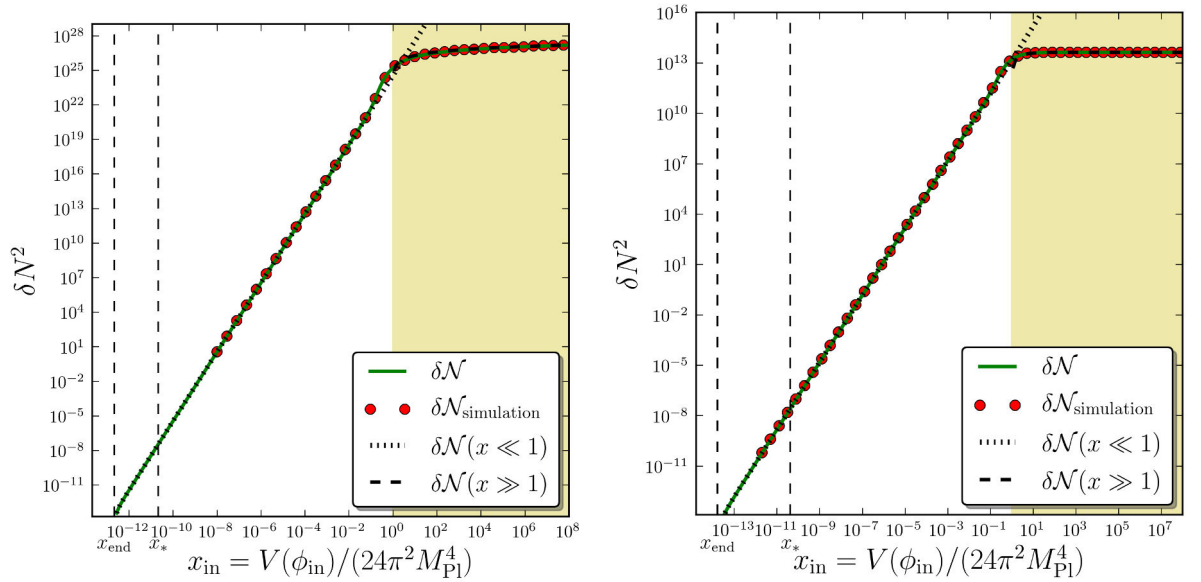

Figure 2.9.: Dispersion of the number of e-folds $\delta\mathcal{N}^2 = \langle\mathcal{N}^2\rangle - \langle\mathcal{N}\rangle^2$ realized in the large field potential (2.254) for $p = 2$ (left panel) and $p = 4$ (right panel), between $x_{\rm in}$ and $x_{\rm end}$, as a function of $x_{\rm in}$, where $x \equiv V/(24\pi^2 M_{\rm Pl}^4)$. The mass scale M^4 is normalized to Eq. (2.255). The location x_* refers to the value of x for which the classical number of e-folds $N_{\rm cl} = 50$ and $x_{\rm end}$ is where $\epsilon_1 = 1$. The green line corresponds to the analytical exact result (2.260), and the red circles are provided by a numerical integration of the Langevin equation (2.257) where a large number of realizations are produced over which the mean values of $\mathcal{N}$ and $\mathcal{N}^2$ are computed. Obviously, the agreement with the analytical formula is excellent and confirms both approaches. The black dotted line corresponds to the classical limit (2.241), which provides a good approximation to the exact result when $x_{\rm in} \ll 1$. Finally, the black dashed line corresponds to Eq. (2.262) which is the expansion of Eq. (2.260) in the opposite limit $x \gg 1$. Again, this limit is non-physical since one must have $x < 1$ in order to keep the energy densities from being super-Planckian, and the yellow shaded area is displayed only to check the agreement between the numerical code and the analytical calculation in a broader range.

where $\bar{C}(p)$ is a constant depending on p but which is always of order one. These expressions are also displayed in Fig. 2.9 where one can check that they provide reliable approximations to the exact result. As for the mean number of e-folds , it is worth noticing that when $p > 2$, $\delta\mathcal{N}^2$ is bounded by $\mathcal{O}(1)(M_{\rm Pl}/M)^{16/p}$, while when $p \leq 2$ it can reach arbitrarily large values in principle.

Power Spectrum

Following section 2.4.3.6, the power spectrum can now be properly computed. Making use of Eq. (2.245), one obtains for the large field potential (2.254)

$$\mathcal{P}_\zeta = \frac{2}{p\,(p-1)}\left(\frac{24\pi^2 M_{\rm Pl}^4}{M^4}\right)^{2/p} \frac{x^{1-1/p}}{M\left(1-\frac{1}{p},2-\frac{1}{p},\frac{1}{x}\right)} \int_x^\infty t^{3/p-3}\mathrm{e}^{-\frac{1}{t}} M^2\left(1-\frac{1}{p},2-\frac{1}{p},\frac{1}{t}\right)\mathrm{d}t\,. \tag{2.263}$$

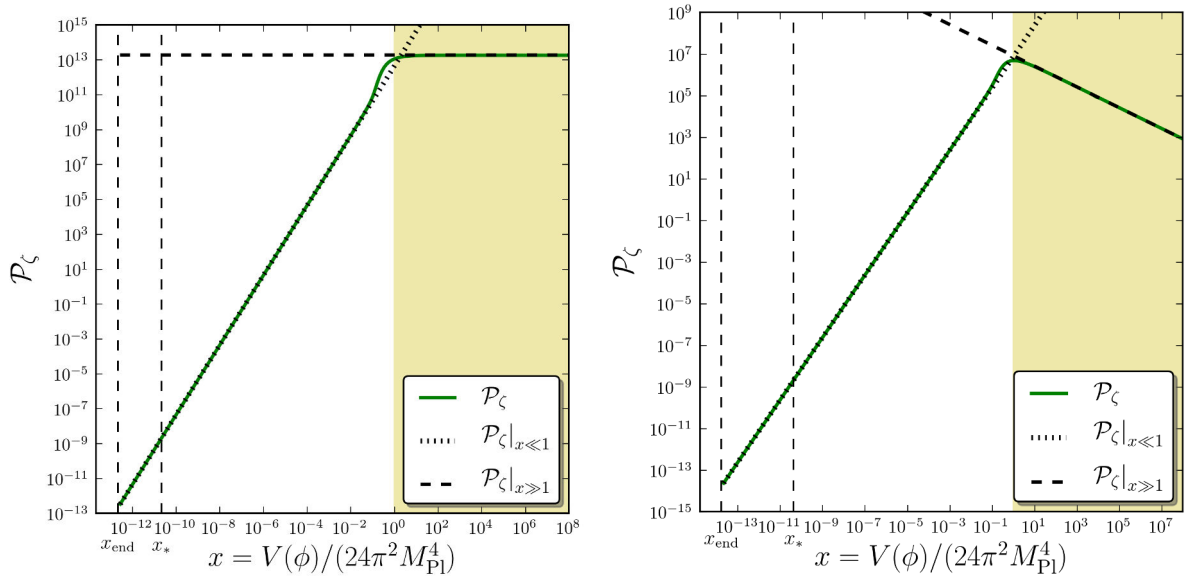

Figure 2.10.: Power Spectrum of curvature perturbations $\mathcal{P}_\zeta$ realized in the large field potential (2.254) for $p = 2$ (left panel) and $p = 4$ (right panel), computed at a scale whose Hubble exit time is labelled by x, where $x = V/(24\pi^2 M_{\rm Pl}^4)$, as a function of x, and where inflation terminates at $x_{\rm end}$. The mass scale M^4 is normalized to Eq. (2.255), so that at x_*, one can check that $\mathcal{P} \simeq 2 \times 10^{-9}$. The location x_* refers to the value of x for which the classical number of e-folds $N_{\rm cl} = 50$ and $x_{\rm end}$ is where $\epsilon_1 = 1$. The green line stands for the analytical exact result (2.263). The black dotted line corresponds to the classical limit (2.246), which provides a good approximation to the exact result when $x \ll 1$. Finally, the black dashed line corresponds to Eq. (2.266) which is the expansion of Eq. (2.263) in the opposite limit $x \gg 1$. As before, the yellow shaded area $x > 1$ may not be physical and it is displayed for illustrative purpose only.

Here, x means the actual value of x at the Hubble exit time of the scale where the power spectrum is calculated. The classical limit of this expression can be obtained either expanding the above formula in $x \ll 1$, or combining Eqs. (2.258) and (2.261). In either case, one obtains

$$\mathcal{P}_\zeta|_{x_{\rm end}<x\ll1} \simeq \frac{2}{p^2}\left(\frac{24\pi^2 M_{\rm Pl}^4}{M^4}\right)^{\frac{2}{p}} x^{1+\frac{2}{p}}\left[1+\left(1+\frac{4}{p}\right)x+\left(2+\frac{13}{p}+\frac{13}{p^2}\right)x^2\right] \quad (2.264)$$

$$\simeq P_\zeta|_{\rm cl}\left[1+\left(1+\frac{4}{p}\right)x+\left(2+\frac{13}{p}+\frac{13}{p^2}\right)x^2\right], \quad (2.265)$$

where $P_\zeta|_{\rm cl}$ is given by Eq. (2.246) and exactly corresponds to the regular "classical" contribution to the power spectrum. To see how this result breaks when $x \gtrsim 1$, it can be interesting to write the opposite limit $x \gg 1$, where the power spectrum can be obtained combining Eqs. (2.259) and (2.262). Interestingly enough, for $\langle\mathcal{N}\rangle$ and $\delta\mathcal{N}^2$, three different cases were to be distinguished according to the value of p. As far as the power spectrum is concerned, they all give rise to the same expression, namely

$$\mathcal{P}_\zeta|_{x_{\rm end}\ll1,x\gg1} \simeq \frac{2}{(p-1)(2p-3)}\left(\frac{24\pi^2 M_{\rm Pl}^4}{M^4}\right)^{2/p} x^{2/p-1}. \quad (2.266)$$

In particular, when $p = 2$, the power spectrum tend to be constant (*i.e.* scale invariant) in the limit $x \gg 1$. This is the limiting case between $p < 2$ where the power spectrum amplitude

increases with ϕ in the $x \gg 1$ limit, and the case $p > 2$ where the power spectrum amplitude decreases with ϕ.

The three formulas (2.263), (2.246) and (2.266) are displayed together in Fig. 2.10 for $p = 2$ and $p = 4$. The mass scale M^4 is normalized to Eq. (2.255), *i.e.* the amplitude of the power spectrum is calibrated to $\mathcal{P}_\zeta \simeq 2 \times 10^{-9}$ when it is computed ~ 50 e-folds before the location defined by $\epsilon_1 = 1$. Of course, if one is interested in a situation where the scales of astrophysical interest today crossed the Hubble radius at a different value of ϕ_* or equivalently x_* (for example, if inflation proceeds at larger fields and ends by tachyonic instability), then the mass scale M^4 needs to be calibrated differently (and the value of $x_{\rm end}$ has to be changed as well). In any case, Fig. 2.10 shows how the amplitude of the power spectrum varies with ϕ for fixed M^4.

A few other comments are in order. First, as expected, when $x \ll 1$, the classical limit provides a good approximation to the exact result. Actually, from Eq. (2.265), the relative difference between the two is given by $\delta\mathcal{P}_\zeta/\,\mathcal{P}_\zeta|_{\rm cl} \simeq (1 + 4/p)x > 0$, which means that the stochastic effects account for a slightly larger amplitude of the power spectrum in this limit.[24] Second, in the regular case where inflation terminates when $\epsilon_1 = 1$ and the power spectrum is computed 50 e-folds before this point, Eq. (2.255) gives rise to $x_* \simeq 10^{-11}$ and the actual stochastic modification to the power spectrum is accordingly small. Therefore, in the large field model, only tiny corrections appear, and we will come back to this point in section 2.4.3.9.

Scalar Spectral Index

Finally, let us calculate the spectral index $n_{\rm S}$ at a given scale whose Hubble exit time is labelled by x. It is given by Eq. (2.250) and can be computed straightforwardly. Its asymptotic limits can also be worked out making use of the previous formulas. In the limit where $x \ll 1$, one obtains

$$n_{\rm S}\big|_{x_{\rm end}<x\ll 1} - 1 \simeq -\left(\frac{M^4}{24\pi^2 M_{\rm Pl}^4}\right)^{2/p} p\,(p+2)\,x^{-\frac{2}{p}}\left[1 + \left(1 - \frac{1}{p} + \frac{2}{p+2}\right)x + \left(3 + \frac{8}{p+2} + \frac{3}{p} - \frac{1}{p^3}\right)x^2 + \mathcal{O}\left(x^3\right)\right] \tag{2.267}$$

$$\simeq \left(n_{\rm S}\big|_{\rm cl} - 1\right)\left[1 + \left(1 - \frac{1}{p} + \frac{2}{p+2}\right)x + \left(3 + \frac{8}{p+2} + \frac{3}{p} - \frac{1}{p^3}\right)x^2 + \mathcal{O}\left(x^3\right)\right], \tag{2.268}$$

where one has used Eq. (2.251) to single out the classical result $n_{\rm S}|_{\rm cl}$. Therefore, one can check that in the classical limit, the regular result is recovered. The scalar index is red ($n_{\rm S} < 1$), and stochastic effects tend to make it even redder by slightly decreasing the actual value of $n_{\rm S}$. Again, even if it corresponds to super-Planckian energy densities, it can be interesting to see how the above result breaks in the regime $x \gtrsim 1$, and one obtains

$$n_{\rm S}\big|_{x_{\rm end}\ll 1, x\gg 1} \simeq 1 - \left(\frac{M^4}{24\pi^2 M_{\rm Pl}^4}\right)^{\frac{2}{p}} (p-1)\,(2-p)\,x^{1-\frac{2}{p}}\,. \tag{2.269}$$

If $p < 2$, the spectral index remains red and keeps increasing with x towards 1 (even if slower than in the classical regime), whereas if $p > 2$, the spectral index becomes blue and starts increasing with x away from 1, *i.e.* away from scale invariance. The case $p = 2$ is singular since, at leading order, the previous expression gives $n_{\rm S} = 1$. This is why one needs to work out

[24] Contrary to what is incorrectly concluded in Ref. [331], as explained in the introductory part of section 2.4.3.

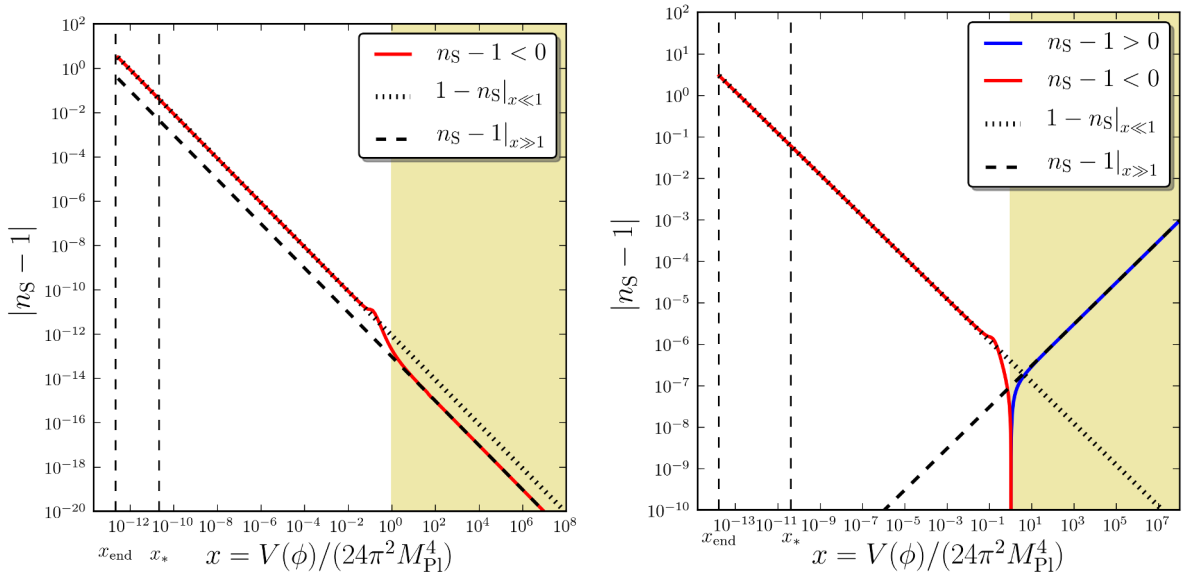

Figure 2.11.: Spectral index $n_{\rm S}$ of the power spectrum of curvature perturbations realized in the large field potential (2.254) for $p=2$ (left panel) and $p=4$ (right panel), computed at a scale whose Hubble exit time is labelled by x, where $x=V/(24\pi^2M_{\rm Pl}^4)$, as a function of x, and where inflation terminates at $x_{\rm end}$. The mass scale M^4 is normalized to Eq. (2.255), the location x_* corresponds to the value of x for which the classical number of e-folds $N_{\rm cl}=50$ and $x_{\rm end}$ is where $\epsilon_1=1$. The coloured lines stand for the analytical exact result (2.250), it is blue when the spectral index is "blue" ($n_{\rm S}>1$), and it is red when the spectral index is "red" ($n_{\rm S}<1$). The black dotted line corresponds to the classical limit (2.251), which provides a good approximation to the exact result when $x\ll1$. Finally, the black dashed line corresponds to Eqs. (2.269) and (2.270) which is the expansion of Eq. (2.250) in the opposite limit $x\gg1$. As before, the yellow shaded area $x>1$ may not be physical and it is displayed for illustrative purpose only.

Eqs. (2.259) and (2.266) at next-to-leading order in $1/x$. After a straightforward calculation, one obtains

$$n_{\rm S}\big|_{x_{\rm end}\ll1,x\gg1}(p=2)\simeq1-\frac{M^4}{24\pi^2M_{\rm Pl}^4}\frac{8}{9x}\,. \tag{2.270}$$

Therefore, in this case, the spectral index also remains red, and increases towards 1 at the same rate than in the classical regime. The exact result (2.250) is compared with these approximations in Fig. 2.11 for $p=2$ (left panel) and $p=4$ (right panel). If $p=2$, one can see that the stochastic effects do not modify much the behaviour of $n_{\rm S}$ even when $x\gtrsim1$ and only add some feature around $x\simeq1$. However, this case is singular and in general, the result radically changes when x approaches 1. When $p>2$, the spectral index can even turn from red to blue.

2.4.3.9. Discussion

At the beginning of section 2.4.3, we explained that, because of the relation $\mathcal{P}_\zeta\propto\eta^2\sim2\times10^{-9}$, the stochastic effects play a negligible role at the time where the scales of astrophysical today cross the Hubble radius. However, we pointed out that it does not mean that η remains small

during all the last ~ 50 e-folds of inflation, and that some substantial effects on the power spectrum may appear in models where it is not the case. The calculation we carried out in this section shows that it is not the case. Indeed, the amplitude of the corrections to the power spectrum is not controlled by η, but by x, which is generically small in order to keep energy densities sub-Planckian. Furthermore, contrary to η, x can only decrease during inflation. For example, in the large field model we studied, one typically has $x_* \sim 10^{-11}$. In general, since at leading order in slow roll, the amplitude of the power spectrum is given by $\mathcal{P}_\zeta \sim H^2/(8\pi^2 M_{\rm Pl}^2\epsilon_1) = x/\epsilon_1$, one has

$$x_* \simeq \epsilon_{1*}\mathcal{P}_{\zeta*} \simeq \frac{r}{16}\mathcal{P}_{\zeta*}\,. \tag{2.271}$$

With $\mathcal{P}_{\zeta*} \sim 2\times 10^{-9}$ and since $r<1$ with certainty, one has $x_* < 10^{-10}$ and the corrections to the power spectrum we have computed are at most tiny $\sim 10^{-10}$ corrections, at least under the assumptions me made (single field and slow roll). However, we have built a scheme in which it is straightforward to calculate these corrections, at any order. Besides, our calculation is well under control even when the stochastic effects dominate the inflationary dynamics (in the sense $\eta \gg 1$), as long as $x<1$.

Let us mention a few prospects. In order to test the ability of stochastic inflation to reproduce results beyond the linear level, it would first be interesting to compare what we obtained with a computation of the power spectrum at second order in the perturbations, using the standard approach. Another interesting idea would be to generalize our scheme to multiple-field scenarios, since it has been shown [388] that the δN formalism performs very well in these situations too. Finally, a straightforward prospect would be to enlarge our procedure to the calculation of non-Gaussianities. Indeed, in the δN formalism and in the large scale limit, the $f_{\rm NL}$ parameters quantifying non-Gaussianities can be related [356, 389, 388] to the third moments of the number of e-folds $\mathcal{N}$ thanks to

$$f_{\rm NL}^{\rm loc} = \frac{\delta\mathcal{N}^3}{(\delta\mathcal{N}^2)^2} = \frac{\left\langle (\mathcal{N}-\langle\mathcal{N}\rangle)^3\right\rangle}{\left\langle (\mathcal{N}-\langle\mathcal{N}\rangle)^2\right\rangle^2}\,. \tag{2.272}$$

In this expression, $\delta\mathcal{N}^2$ has already be calculated and $\delta\mathcal{N}^3$ can be obtained just the same way we calculated $\langle\mathcal{N}\rangle$ and $\langle\mathcal{N}^2\rangle$. In this manner, we could also study non-Gaussianities in the context of stochastic inflation. For single-field models with canonical kinetic terms, the $f_{\rm NL}$ parameters are already known to be small (of the order of the slow-roll parameters), but the same formalism as the one we presented here can be derived *e.g.* for DBI inflation [379, 390, 391, 392, 393, 394, 395, 396, 397, 398, 399] (or general k-inflation). In these models, the kinetic term is not canonical and a larger amount of non-Gaussianities can be produced. The stochastic inflation formalism has been generalized to these models [400, 401, 402, 403] where a modified Langevin equation has been obtained, and the same techniques as the one we developed here can in principle be applied.

Part II.

Results and Publications

3. Inflationary Predictions and Comparison with "Big Data" Observations

Inflation has entered a "big data" era driven by the current flow of high accuracy astrophysical observations, among which are the Cosmic Microwave Background (CMB) measurements. During the time of this thesis notably, the Planck (and if confirmed BICEP2) experiments published unequalled measurements of the CMB maps. It offers an unprecedented opportunity to constrain the inflationary theory. This is however a challenging project given the size of the inflationary landscape which contains hundreds of different scenarios. The objective of this first chapter is to take full advantage of the unprecedented accuracy of the data to determine which models appear to be favoured.

Publications

The inflationary theory contains hundreds of different scenarios. As a consequence, it is a difficult task to single out the ones that are favoured by the observations. In order to take full advantage of the unprecedented accuracy of astrophysical data, which is needed to address this problem, it is necessary to develop new tools and techniques in order to perform a change of scales in the analysis and to adopt a systematic approach.

A first attempt to carry out this programme is to make use of model independent parametrizations of inflation, such as the one of "horizon-flow". In this approach, the analysis is run over quantities describing the way the Hubble parameter H varies with the inflaton field ϕ in single-field inflation. In particular, potential reconstruction and the search for "generic" inflationary predictions have been addressed with this technique. In section 3.1, Ref. [208], we show that in fact, the horizon-flow framework implicitly samples a subclass of phenomenological inflationary

potentials, which strongly bias the analysis. Furthermore, it relies on trajectories in phase space that differ from the slow-roll, that are sometimes even unstable, and that make the horizon-flow setup blind to entire inflationary regimes. Such an approach should therefore be avoided.

On the contrary, slow roll does not suffer from these flaws and this is why in collaboration with Jérôme Martin and Christophe Ringeval, we have used this framework to systematically analyse the inflationary models one by one. For each of them, we derived the corresponding predictions and compared them to the Planck data. The results of this somewhat "industrial" project are presented in section 3.2, Ref. [205]. We focused on the simplest models, the single-field slow-roll models with minimal kinetic term, since there is currently no observational evidence for non-minimal extensions of the inflationary paradigm.

Together with this paper, we developed the publicly available library[1] `ASPIC`, which provides all fortran routines needed to quickly derive reheating consistent observable predictions for all those scenarios. From a systematic scan of the literature, we found that this amounts to including ~ 75 potentials. This number should be compared with three or four representing the previous state of the art. The `ASPIC` library is an evolutive project and is intended to be completed as new models appear.

We then used Bayesian inference and model comparison techniques to rank the `ASPIC` models and find the best ones. Interfacing the `ASPIC` codes with a machine-learned effective likelihood and a nested sampling algorithm, we designed a numerical pipeline that provides the Bayesian evidences and complexities of ~ 200 models of inflation using the Planck 2013 CMB data, from non-committal and well-studied priors. The results of this analysis are presented in section 3.3, Ref. [206]. We showed that one third of the models can now be considered as strongly disfavoured, and that the preferred potentials are of the plateau type, *i.e.* they are such that both the kinetic energy and the kinetic-to-total energy ratio increase during inflation.

When the BICEP2 experiment released its measurements of the CMB polarization, we updated our results including these data in the analysis. This can be found in section 3.4, Ref. [207]. In particular, we investigated the implications for inflation of the detection of B-modes polarization *if* it is of primordial origin. We showed that the sets of inflationary models preferred by Planck alone and BICEP2 alone are almost disjoint, indicating a clear tension between these two data sets. More precisely, we addressed this tension with a Bayesian measure of compatibility between the two data sets, showing that for the Planck-preferred as for the BICEP2-preferred models, they tend to be incompatible. This is why at this point, it seems premature to draw definitive conclusions, and one should better wait for the release of the polarization data from Planck, scheduled by the end of the year, and for a clarification of the dust contribution to the BICEP2 measured signal.

Finally, there are various possible extensions and prospects for this project. One of them is to generalize our analysis and numerical pipeline to models where the speed of sound is varying, but the action for the curvature perturbations remains quadratic. This class of models is called k-inflation. This is why in Ref. [209], presented in section 3.5, we have paved the way for including such models in the analysis, by calculating for the first time the next-to-next-to-leading order scalar and tensor primordial power spectra in k-inflation. We made use of the uniform approximation together with a second order expansion in the Hubble and sound-flow functions.

[1] `http://cp3.irmp.ucl.ac.be/~ringeval/aspic.html`

PHYSICAL REVIEW D **89,** 083526 (2014)

Horizon-flow off-track for inflation

Vincent Vennin*

Institut d'Astrophysique de Paris, UMR 7095-CNRS, Université Pierre et Marie Curie, 98bis boulevard Arago, 75014 Paris, France

(Received 20 January 2014; published 10 April 2014)

Inflation can be parametrized by means of truncated flow equations. In this "horizon-flow" setup, generic results have been obtained, such as typical values for $r/(1-n_S)$. They are sometimes referred to as intrinsic features of inflation itself. In this paper we first show that the phenomenological class of inflationary potentials sampled by horizon flow is directly responsible for such predictions. They are therefore anything but generic. Furthermore, the horizon-flow setup is shown to rely on trajectories in phase space that differ from the slow roll. For a given potential, we demonstrate that this renders horizon flow blind to entire relevant inflationary regimes, for which the horizon-flow trajectory is shown to be unstable. This makes horizon flow a biased parametrization of inflation.

DOI: 10.1103/PhysRevD.89.083526 PACS numbers: 98.80.Cq

I. INTRODUCTION

Inflation is currently the leading paradigm for explaining the physical conditions that prevailed in the very early Universe [1–5]. It describes a phase of accelerated expansion that solves the puzzles of the standard hot big bang model, and it provides a causal mechanism for generating inhomogeneities on cosmological scales [6–11]. These inhomogeneities result from the amplification of the unavoidable vacuum quantum fluctuations of the gravitational and matter fields during the accelerated expansion. In particular, inflation predicts that their spectrum should be almost scale invariant, with small deviations from scale invariance being related to the precise microphysics of inflation. This prediction is consistent with the current high precision astrophysical observations [12–15]. In particular, the recent Planck measurement [15] of the cosmic microwave background temperature map gives together with WMAP polarization data a slightly red tilted scalar spectral index $n_S \simeq 0.96$, ruling out exact scale invariance $n_S = 1$ at over 5σ and enabling us to constrain the inflationary models still allowed by the observations [16,17].

Together with the absence of primordial non-Gaussianities and of isocurvature modes [15], these results indicate that, at this stage, the full set of observations can be accounted for in the minimal setup, where inflation is driven by a single scalar field ϕ, the inflaton field, minimally coupled to gravity, and evolving in some potential $V(\phi)$. The action for such a system is given by (hereafter $M_{\rm Pl}$ denotes the reduced Planck mass)

$$S = \int \left[\frac{M_{\rm Pl}^2}{2}R - \frac{1}{2}\partial_\mu\phi\partial^\mu\phi - V(\phi)\right]\sqrt{-g}\mathrm{d}^4x, \qquad (1)$$

where the background metric is chosen to be of the flat Friedmann-Lemaître-Robertson-Walker type, i.e. the one of a homogeneous and isotropic expanding universe (about which fluctuations are evolved), given by $\mathrm{d}s^2 = -\mathrm{d}t^2 + a^2(t)\mathrm{d}x^2$, where the scale factor $a(t)$ is a free function of time. However, the physical nature of the inflaton and its relation with the standard model of particle physics and its extensions remain elusive, since the inflationary mechanism is supposed to take place at very high energies in a regime where particle physics is not known and has not been tested in accelerators. Therefore the only requirement on V is that it should be sufficiently flat to support inflation, but otherwise the multitude of inflaton candidates (with associated potentials) makes the theory as a whole hardly tractable, unless one restricts to a specific model.

If one does so, within a given inflationary model $V(\phi)$, there exists a frame of approximation, the slow-roll approximation, which provides a set of manageable equations to calculate an attractor solution for the dynamics arising from the action (1), and to consistently derive the statistical properties of cosmological perturbations produced during inflation. This is why, in order to constrain the inflationary scenario at a level matching the accuracy of the current data, a first approach is to scan the full set of models that have been proposed so far, and to test them one by one [16,17] making use of the slow-roll setup.

Another strategy consists in developing model independent approaches and in studying generic parametrizations of inflation. Among these parametrizations is the "horizon-flow" setup [18–22] which relies on truncated flow equations describing the inflationary dynamics. The starting point is to define a set of flow parameters, based on time derivatives of the Hubble scale $H \equiv \dot{a}/a$ during inflation (a dot denoting a derivation with respect to cosmic time t), and to derive a set of equations for their variation in time. A finite subset of these equations is then solved numerically. Since all the observable quantities related to inflation directly depend on H and the way it (slowly) varies with time, this is indeed a generic way to describe a full set of

*vennin@iap.fr

possible inflationary predictions. The goal of this paper is to investigate whether this horizon-flow approach can be used to robustly parametrize inflation.

Both approaches thus use a different function as an input: $V(\phi)$ for the slow-roll setup and $H(\phi)$ for the horizon-flow one. In Sec. II we review how these two strategies address the calculation of inflationary predictions. In particular, we point out that $H(\phi)$ and $V(\phi)$ are explicitly related, and that the horizon-flow parametrization therefore only samples a particular set of inflationary potentials. In Sec. III, we discuss the impact of restraining to such a class of phenomenological potentials, and we show that the typical values for $r/(1-n_S)$ that have been noticed in the literature are in fact in direct correspondence with the inflationary regimes supported by such potentials. However, examples are worked out where those relations break, showing that they are not generic. In Sec. IV, we emphasize that the slow-roll and horizon-flow computational strategies differ by the phase space trajectory they respectively rest on, i.e. the path the system follows in the $(\phi,\dot{\phi})$ plane as inflation proceeds in both setups. We carry out the slow-roll analysis of the potentials associated to the horizon-flow parametrization, computing the inflationary predictions for both trajectories and characterizing the discrepancies. We show that for a given potential, horizon-flow does not sample all possible inflationary regimes, which introduces a bias in the way it parametrizes inflation. In some cases, its trajectory is even shown to be unstable. Finally in Sec. V, we summarize our main results and conclude the discussion.

II. COMPUTING INFLATIONARY PREDICTIONS

In this section we first recall how statistical properties of primordial cosmological fluctuations can be worked out in the framework of canonical single-field cosmological inflation (1). We then review how the slow-roll and horizon-flow setups address the associated calculations.

A. The single-field setup

In order to model the cosmological fluctuations, one needs to go beyond homogeneity and isotropy. When small fluctuations are added [23,24] on top of the Friedman-Lemaître-Robertson-Walker metric introduced above and of the inflaton field, the scalar sector can be fully parametrized in terms of the Mukhanov-Sasaki variable v [6,25]. Expanding and varying the action (1) at leading order in the perturbations, one can show that this gauge invariant quantity follows an equation of motion [26] of the form

$$v_{\boldsymbol{k}}'' + \left[k^2 - \frac{(a\sqrt{\epsilon_1})''}{a\sqrt{\epsilon_1}}\right] v_{\boldsymbol{k}} = 0, \tag{2}$$

where $v_{\boldsymbol{k}}$ is the Fourier mode of v, and where $\epsilon_1 \equiv 1-(a'/a)'/(a'/a)^2$. Here, a prime denotes a derivative with respect to conformal time η, defined by $a\mathrm{d}\eta = \mathrm{d}t$. A similar equation can be obtained for tensor perturbations so that primordial gravity waves can be studied in the same way. Once Eq. (2) is solved, one can evaluate $v_{\boldsymbol{k}}$ at the end of inflation and calculate the power spectrum of curvature perturbations $\zeta = v/(a\sqrt{2\epsilon_1}M_{\mathrm{Pl}})$ at that time, namely

$$\mathcal{P}_\zeta(\boldsymbol{k}) \equiv \frac{k^3}{2\pi^2}|\zeta_{\boldsymbol{k}}|^2 = \frac{k^3}{4\pi^2 a^2 \epsilon_1}|v_{\boldsymbol{k}}|^2. \tag{3}$$

To carry out such a program, two pieces of information are still missing. Firstly, one needs to set initial conditions for v and v' at some reference time. A sensible choice of initial conditions is the Bunch-Davies vacuum where $v_{\boldsymbol{k}} \to \mathrm{e}^{ik\eta}/\sqrt{2k}$ when $k/aH \to \infty$, which corresponds to setting each mode of the scalar perturbations in its Minkowski quantum ground state in the far sub-Hubble past.

Secondly, one needs to specify the background function $a\sqrt{\epsilon_1}$. This is why as mentioned in the introduction, at this point everything depends only on a (or equivalently H) and the way it varies with time. This can be obtained as follows. From varying the action (1) two dynamical equations arise for the background, namely the Friedmann equation, which equals the squared Hubble parameter to the energy density of the inflaton field, and the Klein-Gordon equation, which is the equation of motion of the field ϕ. They are given by

$$H^2 = \frac{V + \dot{\phi}^2/2}{3M_{\mathrm{Pl}}^2}, \tag{4}$$

$$\ddot{\phi} + 3H\dot{\phi} + \frac{\mathrm{d}V}{\mathrm{d}\phi} = 0. \tag{5}$$

Provided some initial conditions ϕ_{in} and $\dot{\phi}_{\mathrm{in}}$, and assuming that the potential $V(\phi)$ is known, this system can be solved and the corresponding time evolution of H (hence of a) can be inferred. Then, Eq. (2) can be solved, and the statistical moments of v can be calculated.

However, such a program is difficult to carry out in practice mainly because of three reasons. First, the system (4–5) and Eq. (2) can generally not be solved analytically. Second, a potential V must be specified even if at these energies there is no unique candidate. Third, in general there is no obvious choice of initial conditions ϕ_{in} and $\dot{\phi}_{\mathrm{in}}$. Both the slow-roll and horizon-flow approaches may simplify some of these issues. We now describe the strategies they rely on.

B. The slow-roll approach

The slow-roll strategy relies on the assumption that the Hubble parameter and its time derivatives slowly vary with time during inflation, i.e. that the deviation from de Sitter

space-time is small.[1] This can be characterized in terms of a hierarchy of "slow-roll parameters."

Although there are several possible sets of slow-roll parameters, in this paper, we choose to work with the Hubble-flow parameters $\{\epsilon_n\}$ defined by the flow equations [27,28]

$$\epsilon_{n+1} = \frac{\mathrm{d}\ln|\epsilon_n|}{\mathrm{d}N}, \tag{6}$$

where the hierarchy is started at $\epsilon_0 \equiv H_{\rm in}/H$, and where $N \equiv \ln a$ is the number of e-folds. With this definition, all the ϵ_n are typically of the same order of magnitude. One has *slow-roll* inflation as long as $|\epsilon_n| \ll 1$, for all $n > 0$, while since $\epsilon_1 = -\dot{H}/H^2 = 1 - \ddot{a}/(aH^2)$, inflation ($\ddot{a} > 0$) takes place provided $\epsilon_1 < 1$. Note that the definition of ϵ_1 is of course consistent with the one introduced below Eq. (2).

Now, when inflation is driven by a single scalar field, let us see how the system (4–5) gets simplified. Inserting the Klein-Gordon equation in the time derivative of the Friedman equation, one obtains $\dot{H} = -\dot{\phi}^2/(2M_{\rm Pl}^2)$, and hence

$$\epsilon_1 = -\frac{\dot{H}}{H^2} = 3\frac{\dot{\phi}^2/2}{V(\phi) + \dot{\phi}^2/2}. \tag{7}$$

The condition $\epsilon_1 \ll 1$ thus implies that the kinetic energy of the inflaton is much smaller than its potential energy, namely $\dot{\phi}^2/2 \ll V(\phi)$. Under this condition, the Friedmann equation simplifies and gives, at leading order in slow roll, $H^2 \simeq V/(3M_{\rm Pl}^2)$.

One can keep on and play the same game with ϵ_2. Inserting the Klein-Gordon equation (5) in the time derivative of the relation $\dot{H} = -\dot{\phi}^2/(2M_{\rm Pl}^2)$ previously obtained, one gets $\ddot{H} = 3H\dot{\phi}^2/M_{\rm Pl}^2 + \dot{\phi}V'/M_{\rm Pl}^2$, and

$$\epsilon_2 = \frac{\ddot{H}}{H\dot{H}} - 2\frac{\dot{H}}{H^2} = 6\left(\frac{\epsilon_1}{3} - \frac{V'}{3H\dot{\phi}} - 1\right). \tag{8}$$

Hereafter and unlike before, a prime denotes a derivative with respect to the field ϕ. The condition $\epsilon_2 \ll 1$ thus implies that, at leading order in slow roll, $\dot{\phi} \simeq -V'/(3H)$, which means that the acceleration term can be neglected in the Klein-Gordon equation. This is particularly interesting since it lowers by 1 the order of the differential equation satisfied by ϕ. As a consequence, it removes dependence on the initial conditions by singling out a specific trajectory, and analytical solutions are available in most cases. In this manner it solves the first and the third difficulties mentioned at the end of Sec. II A.

[1]Such an assumption is justified *a posteriori* e.g. by the fact that only small deviations from scale invariance are measured, with tight constraints on the level of gravity waves.

More explicitly, since $\mathrm{d}N = H\mathrm{d}t$, at leading order in slow roll the Klein-Gordon equation reads $\mathrm{d}N = -3H^2\mathrm{d}\phi/V'$. Plugging in the slow-roll leading order of the Friedman equation $H^2_{\rm SR,LO} = V/(3M_{\rm Pl}^2)$, one obtains

$$\Delta N^{\rm SR,LO} = -\frac{1}{M_{\rm Pl}^2}\int_{\phi_{\rm in}}^{\phi_{\rm end}} \frac{V}{V'}\mathrm{d}\phi, \tag{9}$$

where $\Delta N \equiv N_{\rm end} - N_{\rm in}$, $\phi_{\rm in}$ is the value of ϕ at some initial time $N_{\rm in}$, and $\phi_{\rm end}$ is the value of ϕ at some final time $N_{\rm end}$. This represents the leading order (LO) of the slow-roll (SR) trajectory. Inverting this relation yields the value of ϕ at any time N.

Furthermore, it turns out that the slow-roll trajectory is a powerful attractor [29] of the inflationary dynamics, that is to say, starting from a large basin of possible initial conditions $\phi_{\rm in}$ and $\dot{\phi}_{\rm in}$, the system quickly converges towards the slow-roll trajectory. We will come back to this point in Sec. IV, but we can already notice that it is a strong physical motivation to work within the slow-roll framework.

It is also interesting to remark that under the slow-roll approximation, the slow-roll hierarchy can be easily expressed in terms of V and its derivatives. Indeed, starting from $H^2 \simeq V/(3M_{\rm Pl}^2)$ the derivative relation $\mathrm{d}/\mathrm{d}t = \dot{\phi}\mathrm{d}/\mathrm{d}\phi \simeq -V'/(3H)\mathrm{d}/\mathrm{d}\phi$ gives rise to

$$\left.\frac{\mathrm{d}}{\mathrm{d}N}\right|^{\rm SR,LO} = -M_{\rm Pl}^2\frac{V'}{V}\frac{\mathrm{d}}{\mathrm{d}\phi}. \tag{10}$$

Repeatedly applying this identity, one obtains, at leading order in slow roll,

$$\epsilon_0^{\rm LO} = H_{\rm in}\sqrt{\frac{3M_{\rm Pl}^2}{V}}, \tag{11}$$

$$\epsilon_1^{\rm LO} = \frac{M_{\rm Pl}^2}{2}\left(\frac{V'}{V}\right)^2, \tag{12}$$

$$\epsilon_2^{\rm LO} = 2M_{\rm Pl}^2\left[\left(\frac{V'}{V}\right)^2 - \frac{V''}{V}\right], \tag{13}$$

$$\epsilon_3^{\rm LO} = \frac{2M_{\rm Pl}^4}{\epsilon_2^{\rm LO}}\left[\frac{V'''V'}{V^2} - 3\frac{V''V'^2}{V^3} + 2\left(\frac{V'}{V}\right)^4\right], \tag{14}$$

and the following slow-roll parameters can be computed in the same way.

Since the slow-roll parameters entirely characterize the time evolution of H (and of a), it is now obvious that the solutions to Eq. (2) can be expressed in terms of them, hence the statistical moments of cosmological fluctuations at the end of inflation too. For example, at leading order in slow roll, the scalar power spectrum is given by

$$k^3\mathcal{P}_\zeta = \frac{H_*^2}{8\pi^2 M_{\rm Pl}^2 \epsilon_{1*}}\left[1-(2\epsilon_{1*}+\epsilon_{2*})\ln\frac{k}{k_{\rm P}}+\cdots\right], \quad (15)$$

where a star means that quantities must be evaluated at the Hubble exit time of some pivot scale $k_{\rm P}$ of astrophysical interest today. One can see that the scalar power spectrum is scale invariant, with logarithmic corrections whose amplitude is slow-roll suppressed. They can be described in terms of the spectral index

$$n_{\rm S} \equiv 1+\frac{{\rm d}\ln\mathcal{P}_\zeta}{{\rm d}\ln k} \simeq 1-2\epsilon_{1*}-\epsilon_{2*}, \quad (16)$$

the last expression being given at leading order in slow roll. As already mentioned, the same program can be carried out for tensor modes and the power spectrum of gravity waves $\mathcal{P}_h$ can be obtained in the same manner. The ratio r of its amplitude to the scalar power spectrum amplitude is often used to characterize the primordial level of gravity waves. At leading order in slow roll, one has

$$r \equiv \frac{\mathcal{P}_h}{\mathcal{P}_\zeta} \simeq 16\epsilon_{1*}. \quad (17)$$

The slow-roll program is therefore straightforward. The Hubble crossing time of the pivot scale depends on the subsequent thermal history of the Universe, and is typically located $\Delta N_* \simeq 50$ e-folds before the end of inflation. Given a potential $V(\phi)$, one thus integrates the slow-roll trajectory (9) ΔN_* e-folds prior to the end of inflation (defined as $\epsilon_1 = 1$) and evaluates the potential and its derivatives there. Making use of Eqs. (11)–(14), the slow-roll parameters ϵ_{n*} are obtained, and physical quantities such as $n_{\rm S}$ and r can be computed by means of the formulas (16) and (17).

In the following it will turn useful to make use of next-to-leading order (NLO) expressions in slow roll, i.e. one order further than above. This is why we end this section by deriving such formulas. The starting point is to combine Eqs. (4) and (7) into

$$H^2 = \frac{V}{3M_{\rm Pl}^2}\left(1-\frac{\epsilon_1}{3}\right)^{-1}. \quad (18)$$

Together with the Friedman equation (4), this gives rise to $\dot\phi^2 = 2V\epsilon_1/(3-\epsilon_1)$. These two formulas enable us to recast ${\rm d}N = H{\rm d}\phi/\dot\phi$ as

$${\rm d}N = \pm\frac{1}{M_{\rm Pl}}\frac{{\rm d}\phi}{\sqrt{2\epsilon_1}}. \quad (19)$$

From here the slow-roll parameters at next-to-leading order can be obtained as follows. Rewriting Eq. (18) as $\epsilon_0 = \epsilon_0^{\rm LO}\sqrt{1-\epsilon_1/3}$, and iteratively applying

$$\left.\frac{\rm d}{{\rm d}N}\right|^{\rm SR,NLO} = \sqrt{\frac{\epsilon_1^{\rm NLO}}{\epsilon_1^{\rm LO}}}\left.\frac{\rm d}{{\rm d}N}\right|^{\rm SR,LO} \quad (20)$$

which comes from Eq. (19), one obtains an expression for the slow-roll parameters at next-to-leading order in terms of the slow-roll parameters at leading order, which read

$$\epsilon_0^{\rm NLO} = \epsilon_0^{\rm LO}\left(1-\frac{\epsilon_1^{\rm LO}}{6}\right), \quad (21)$$

$$\epsilon_1^{\rm NLO} = \epsilon_1^{\rm LO}\left(1-\frac{\epsilon_2^{\rm LO}}{3}\right), \quad (22)$$

$$\epsilon_2^{\rm NLO} = \epsilon_2^{\rm LO}\left(1-\frac{\epsilon_2^{\rm LO}}{6}-\frac{\epsilon_3^{\rm LO}}{3}\right), \quad (23)$$

$$\epsilon_3^{\rm NLO} = \epsilon_3^{\rm LO}\left(1-\frac{\epsilon_2^{\rm LO}}{3}-\frac{\epsilon_4^{\rm LO}}{3}\right), \quad (24)$$

where the following slow-roll parameters can be computed in the same manner, and where the slow-roll parameters at leading order in the right-hand sides are given by Eqs. (11)–(14). If one wanted to keep on and go up to next-to-next-to-leading order, one would proceed in exactly the same way, but here it is enough to stop at next-to-leading order.

Let us move on to the slow-roll trajectory. At next-to-leading order, it proceeds from combining Eqs. (19) and (22), which gives rise to

$$\Delta N^{\rm SR,NLO} = -\frac{1}{M_{\rm Pl}^2}\int_{\phi_{\rm in}}^{\phi_{\rm end}}\frac{V}{V'}{\rm d}\phi + \frac{1}{3}\ln\left(\frac{V'_{\rm end}/V_{\rm end}}{V'_{\rm in}/V_{\rm in}}\right). \quad (25)$$

At last, at next-to-leading order in slow roll, the spectral index and the tensor to scalar ratio are given by [30,31]

$$n_{\rm S} = 1-2\epsilon_{1*}-\epsilon_{2*}-2\epsilon_{1*}^2 - (2C+3)\epsilon_{1*}\epsilon_{2*} - C\epsilon_{2*}\epsilon_{3*}, \quad (26)$$

$$r = 16\epsilon_{1*}(1+C\epsilon_{2*}), \quad (27)$$

where $C \equiv \gamma_{\rm E}+\ln 2-2 \simeq -0.7296$, $\gamma_{\rm E}$ being the Euler constant.

C. The horizon-flow approach

Contrary to the slow-roll approach which consists in solving the system (4–5) with some approximation, the horizon-flow strategy [18–22] uses flow equations of the kind (6) as the fundamental input to derive physical observables such as $n_{\rm S}$ or r. In this section we review how this can be achieved.

A first remark is that for single-field inflation, the flow parameters can be cast as functions of ϕ instead of t in full generality. Indeed, since the inflaton field ϕ varies during inflation under the effect of its potential and initial speed, ϕ can be used as a time label itself, which is unambiguous provided ϕ is monotonic in time. Concretely, identifying the expression $\dot{H} = -\dot{\phi}^2/(2M_{\rm Pl}^2)$ found above Eq. (7) with the simple relation $\dot{H} = H'\dot{\phi}$, one obtains

$$\dot{\phi} = -2M_{\rm Pl}^2 H'. \tag{28}$$

This enables us to relate the derivative with respect to the number of e-folds to the derivative with respect to the inflaton field, $\mathrm{d}/\mathrm{d}N = \dot{\phi}H^{-1}\mathrm{d}/\mathrm{d}\phi$, by

$$\frac{\mathrm{d}}{\mathrm{d}N} = -2M_{\rm Pl}^2 \frac{H'}{H}\frac{\mathrm{d}}{\mathrm{d}\phi}. \tag{29}$$

The slow-roll hierarchy $\{\epsilon_n\}$ can thus be expressed only in terms of $H(\phi)$ and its derivatives. Starting from $\epsilon_0 = H_{\rm in}/H$ and repeatedly applying Eq. (29), the flow equation (6) give rise to

$$\epsilon_0 \equiv \frac{H_{\rm in}}{H}, \tag{30}$$

$$\epsilon_1 \equiv \frac{\mathrm{d}\ln|\epsilon_0|}{\mathrm{d}N} = 2M_{\rm Pl}^2\left(\frac{H'}{H}\right)^2, \tag{31}$$

$$\epsilon_2 \equiv \frac{\mathrm{d}\ln|\epsilon_1|}{\mathrm{d}N} = 4M_{\rm Pl}^2\left[\left(\frac{H'}{H}\right)^2 - \frac{H''}{H}\right], \tag{32}$$

$$\epsilon_3 \equiv \frac{\mathrm{d}\ln|\epsilon_2|}{\mathrm{d}N} = 2M_{\rm Pl}^2\left[2\left(\frac{H'}{H}\right)^2 + \frac{H'''}{H'} - 3\frac{H''}{H}\right] \times \left(1 - \frac{HH''}{H'^2}\right)^{-1}, \tag{33}$$

and the following parameters can be iteratively computed in the same manner. Note that contrary to Eqs. (11)–(14), all the above expressions are exact and do not rely on any kind of approximation. It is also clear that the slow-roll parameters depend only on $H(\phi)$ and its derivatives, and that this function therefore contains all the relevant information to derive the physical predictions of inflation.

In the horizon-flow literature [18–22] a different set of flow parameters is often used, which leads the way to a computational program that we now explain. In this set of parameters, ϵ_1 and ϵ_2 are supplemented with [19]

$${}^l\lambda_H = (2M_{\rm Pl}^2)^l \frac{(H')^{l-1}}{H^l}\frac{\mathrm{d}^{l+1}H}{\mathrm{d}\phi^{l+1}}, \quad \text{for } l > 1. \tag{34}$$

From here[2] a set of flow equations similar to Eq. (6) can be derived: $\mathrm{d}\epsilon_1/\mathrm{d}N = \epsilon_1\epsilon_2$, $\mathrm{d}\epsilon_2/\mathrm{d}N = 2({}^2\lambda_H) - 2\epsilon_1^2 - 3\epsilon_1\epsilon_2$, and

$$\frac{\mathrm{d}^l\lambda_H}{\mathrm{d}N} = \left(\frac{l-1}{2}\epsilon_2 - \epsilon_1\right){}^l\lambda_H + {}^{l+1}\lambda_H. \tag{35}$$

One should note that contrary to the hierarchy $\{\epsilon_n\}$, these flow parameters are of increasing order in slow roll. Obviously both hierarchies are explicitly related.

One way to solve the infinite system (35) is to truncate it at some level, by setting all flow parameters beyond a sufficiently high order in the hierarchy to zero, i.e. ${}^l\lambda_H = 0$ for $l > M$, where M is a suitably large integer (in the literature [19–22], $M = 5$ has essentially been investigated). The flow equations then comprise a closed finite set. Once initial conditions on the flow parameters $\epsilon_1, \epsilon_2, {}^2\lambda_H, \ldots, {}^M\lambda_H$ are chosen, the horizon-flow computational program consists in integrating the flow equation (35) forward in time until one of the three following scenarios occurs:

(i) The parameter ϵ_1 reaches 1 and inflation naturally ends. From here the flow equations are integrated ΔN_* e-folds backward in time and the observables are calculated there.
(ii) The system reaches a late-time fixed point, where observables are calculated.
(iii) None of this happens: inflation never ends (after a "long" integration time, typically 1000 e-folds) and no fixed point is reached. In this case the model is just thrown away.

Note that the predictions are computed thanks to the slow-roll approximated formulas (16) and (17) or (26) and (27), expressed in terms of the chosen set of flow parameters.

Then one proceeds with running the same algorithm again, with different values of initial flow parameters and ΔN_*, so on and so forth, until a huge number of predictions are computed among which "typical" features are searched for. The parameters (ΔN_* and initial flow parameters) are usually drawn in predefined ranges of values, the priors. The width of the prior intervals for the initial flow parameters is usually reduced by some factor (typically 5 [22] or 10 [19,21]) for each higher order in the hierarchy.

A crucial remark, made in Ref. [20], is that truncating the hierarchy $\{{}^l\lambda_H\}$ at some order M is actually equivalent to requiring that $\mathrm{d}^{M+2}H/\mathrm{d}\phi^{M+2}$ vanishes, which means that $H(\phi)$ must be a polynomial function of order $M+1$

$$H(\phi) = H_0\left[1 + \sum_{i=1}^{M+1} a_i\left(\frac{\phi}{M_{\rm Pl}}\right)^i\right], \tag{36}$$

[2]These parameters ${}^l\lambda_H$ are related to the parameters ${}^l\beta_H$ defined in Ref. [32] by ${}^l\lambda_H = ({}^l\beta_H)^l$.

the a_i coefficients being directly related to the initial flow parameters of the computational algorithm detailed above. Inflation is thus described in terms of a model depending on $M+1$ free parameters (the a_i, or equivalently, initial values for $\epsilon_1, \epsilon_2, {}^2\lambda_H, \ldots, {}^M\lambda_H$), on which a prior range of variation is set. The dependence on the choice of such priors, and on the parameter set one uses (initial flow parameters ${}^l\lambda_H$, a_i parameters, or other possible choices), is investigated in Ref. [21]. It is shown that while there remains some concentration of points around the above mentioned fixed points under the different parameter sets, there is significant variation in the predictions among them.

Let us insist that in this setup, inflation is parametrized by a free generic function $H(\phi)$, and that it is also the case in the more common approach where one solves Eqs. (4) and (5) with some function $V(\phi)$. Interestingly enough, it turns out [20] that the two functions are straightforwardly related. Indeed, plugging the relation (28) in the Friedman equation (4), one obtains

$$V = 3M_{\rm Pl}^2 H^2 - 2M_{\rm Pl}^4 H'^2. \tag{37}$$

Therefore, horizon flow does not really solve the second difficulty mentioned at the end of Sec. II A (i.e. the necessity to specify a potential) since it implicitly assumes a specific potential, through the choice of H, and a specific initial value $\phi_{\rm in}$ through the choice of the initial flow parameters.

Moreover, the potential $V(\phi)$ derives in principal from the physical origin of the inflaton field, and the free parameters it contains are usually related to physical quantities such as charges, coupling constants, masses, etc. Therefore it may seem more sensible and physically appealing to parametrize inflation in terms of these quantities (and to choose corresponding simple priors on them), instead of using the integration constants of the flow equations, which *a priori* do not carry any particular physical meaning.

In passing, let us note that the horizon-flow computational program has also been used as a potential reconstruction technique [33–39].[3] A selection rule is added to the algorithm detailed previously that specifies an admitted region in observable parameter space (usually defining central values for $n_{\rm S}$ and r with associated error bars). When a trajectory is integrated, its predictions are computed and the trajectory is kept only if these predictions lie in the admitted region. For all the remaining trajectories at the end of the program, the potential is computed using Eq. (37) and all the potentials are superimposed on a single plot to see which typical shape comes out. Obviously, such an approach to potential reconstruction suffers from the same shortcomings discussed in this paper as horizon flow itself.

In the two next sections, we briefly review the two main results of this paper: the origin of the so-called "typical" predictions of horizon-flow inflation, and the bias introduced by horizon-flow trajectories in the parametrization of single-field inflation.

D. "Typical" predictions

In the references mentioned above two typical denser regions turn out to be sampled: either $r_{16}/(1-n_{\rm S}) = 1/2$ or $r_{16} = 0$ (where $r_{16} = r/16$ corresponds to the "r" parameter defined in Refs. [19,21]). Actually, this can be understood with the following heuristic argument. The first order slow-roll relations $r = 16\epsilon_1$ and $n_{\rm S} - 1 = -2\epsilon_1 - \epsilon_2$, combined with the flow equation (6), allow one to express the number of e-fold derivatives of $n_{\rm S}$ and r in terms of $n_{\rm S}$, r and ϵ_3. Working with the two variables $s \equiv -r/8 + (1-n_{\rm S})$ and r instead of $n_{\rm S}$ and r, one obtains

$$\frac{{\rm d}s}{{\rm d}N} = \epsilon_3 s, \tag{38}$$

$$\frac{{\rm d}r}{{\rm d}N} = rs. \tag{39}$$

If the $\{\epsilon_n\}$ hierarchy is truncated at $n=4$ (i.e. ϵ_3 is constant and $\epsilon_{n>3}$ vanish), this system contains two fixed points: either $\epsilon_3 = 0$ and $r=0$, which leads to $r_{16}/(1-n_{\rm S}) = 0$, or $s=0$, which by definition leads to $r_{16}/(1-n_{\rm S}) = 1/2$. This exactly corresponds to the denser regions mentioned above and matches the early results of Refs. [18] (be careful that another normalization is again used in this paper, where $T/S = 10r_{16} = 5r/8$). If this were concluded to be generic predictions of inflation, this would have important consequences for inflation itself, since e.g. the region $r_{16}/(1-n_{\rm S}) = 1/2$ is now strongly disfavored by the most recent observations [15].

In Ref. [19] these fixed points are shown to be generic fixed points of the hierarchy (34) at any order (i.e. for any M) and their stability is studied in Ref. [22]. However in Refs. [19,21] it is also noticed that even if the numerical models generated by the above algorithm cluster not far from the region $r_{16}/(1-n_{\rm S}) = 1/2$, a better fit is given by

$$\frac{r_{16}}{1-n_{\rm S}} \simeq \frac{1}{3}. \tag{40}$$

In this paper we puzzle out this discrepancy for the first time, analytically showing where this number $1/3$ comes from. Indeed, Eq. (37) shows that when using a parametrization of the form (36), only a particular set of inflationary potentials is actually investigated, namely polynomial potentials with some relations among the coefficients. In Sec. III we discuss the impact of restraining

[3] In Ref. [38], note that the horizon-flow setup is extended to noncanonical single-field models with varying speed of sound c_s, the inverse of which is parametrized by a truncated Taylor expansion of the type (36), with associated c_s-flow equations of the type (35).

to such a class of phenomenological models, and we show that the relations $r_{16}/(1-n_S) \sim 1/3$ and $r_{16} \sim 0$ actually correspond to the different inflationary regimes of such potentials.

E. Inflationary trajectories

Even if Eq. (37) explicitly relates H and V, the corresponding horizon-flow and slow-roll analyses are different because they rely on different inflationary trajectories. In this section we first explain why it is so, before we investigate the consequences of this difference.

1. Why horizon-flow and slow-roll trajectories differ

Since the system (4–5) is second order in time derivative, its solutions form a one-dimensional set of inflationary trajectories, i.e. an infinite bundle of paths in phase space $(\phi, \dot{\phi})$ (examples are displayed and commented on in Sec. IV A). As we shall now see, both the slow-roll and horizon-flow setups rely on a single trajectory each, and do not scan this whole set of possible dynamics.

The trajectory on which the slow-roll approach rests has already been explicated in Sec. II B; see Eq. (9) for its leading order expression and Eq. (25) for its next-to-leading order expression. Even if a complete form can only be attained asymptotically by a perturbative calculation, it is nonetheless a well-defined and unique object. One should therefore be aware of the subtlety that "slow roll" both refers to a perturbative computational framework and to a specific inflationary trajectory. The latter is calculable by the former, and is known to be a powerful attractor [29] of the inflationary dynamics. This is why it makes sense to study inflation along its line.

On the other hand, the horizon-flow formalism also implies a particular inflationary trajectory. It does not explicitly make use of it, which is why it has not really been noticed in the literature so far, but such a trajectory is implicitly contained in the computational approach of horizon flow. Indeed, since the H function is defined through Eq. (4) on the full phase space $(\phi, \dot{\phi})$, reducing it to an $H(\phi)$ function only

$$H(\phi, \dot{\phi}) \to H(\phi) \tag{41}$$

necessarily implies some relation $\dot{\phi}(\phi)$, that is, by definition, a trajectory. It is actually given by Eq. (28). More precisely, the trajectory associated to some $H^{\rm HF}(\phi)$ function is basically given by Eq. (29), i.e.

$$\Delta N^{\rm HF} = -\frac{1}{2M_{\rm Pl}^2}\int_{\phi_{\rm in}}^{\phi_{\rm end}} \frac{H^{\rm HF}}{(H^{\rm HF})'}\mathrm{d}\phi, \tag{42}$$

which is exact and does not rely on any approximation, and where "HF" stresses that we are working within the horizon-flow setup.

The problem can therefore be formulated as follows. Starting from an $H^{\rm HF}(\phi)$ function [typically Eq. (36)], horizon flow consists of studying inflation along the trajectory (42). Now, thanks to Eq. (37), a potential V can be associated to $H^{\rm HF}$, so that the slow-roll analysis can be worked out in this potential, and inflation can be studied along the slow-roll trajectory. The question is whether these two trajectories match or not.

In general they do not for the following reason. Thanks to the Friedman equation (4), let us recall that the Hubble parameter H is a function defined along any trajectory supported by a given potential V. All these H functions are different, technically because they correspond to solutions of Eq. (37) (viewed as a differential equation giving H once V is fixed) with different initial conditions $H(\phi_{\rm in})$. Among these functions is the one corresponding to $H^{\rm HF}$ if one chooses $H^{\rm HF}(\phi_{\rm in})$ as an initial condition, but one can also find $H^{\rm SR}$ which corresponds to the slow-roll trajectory if one chooses $H^{\rm SR}(\phi_{\rm in})$ as an initial condition, or any other $\tilde{H}$ function corresponding to any other trajectory and associated initial condition. The sketch displayed in Fig. 1 summarizes the situation. Since there is no reason why $H^{\rm HF}(\phi_{\rm in}) = H^{\rm SR}(\phi_{\rm in})$ *a priori*, the two functions $H^{\rm HF}$ and $H^{\rm SR}$ are different; hence the slow-roll trajectory

$$\Delta N^{\rm SR} = -\frac{1}{2M_{\rm Pl}^2}\int_{\phi_{\rm in}}^{\phi_{\rm end}} \frac{H^{\rm SR}}{(H^{\rm SR})'}\mathrm{d}\phi \tag{43}$$

differs from the horizon-flow one (42) in general.

This being said, since the horizon-flow algorithm imposes that we start from small values of the flow parameters $\epsilon^{\rm HF}$, and since the slow-roll trajectory is in any case an attractor, the departure from slow roll is initially small and should remain so. This is why at first sight, one may claim that predictions should not be too affected since when the slow-roll conditions ($\epsilon \ll 1$) are verified for $H^{\rm SR}$ and $H^{\rm HF}$, the differentials in the predictions of both frames are slow-roll suppressed quantities (and one needs to use next-to-leading order expressions in slow roll to consistently compare them,[4] as in Sec. IV B).

For example, from deriving Eq. (37) with respect to ϕ, one can rewrite Eq. (42) as

[4]A physical quantity $\mathcal{P}$ computed in the horizon-flow parametrization $\mathcal{P}_{\rm HF}$ only differs from the slow-roll one $\mathcal{P}_{\rm SR}$ by slow-roll suppressed quantities; that is, $\mathcal{P}_{\rm HF} = \mathcal{P}_{\rm SR}[1 + \mathcal{O}(\epsilon) + \cdots]$, where ϵ stands for first order terms in slow roll. If $\mathcal{P}_{\rm SR}$ is computed in the slow-roll frame of approximation, $\mathcal{P}_{\rm SR} = \mathcal{P}_{\rm SR}^{\rm LO}[1 + \tilde{\mathcal{O}}(\epsilon) + \cdots]$, one has at leading order $\mathcal{P}_{\rm HF} = \mathcal{P}_{\rm SR}^{\rm LO}[1 + \tilde{\mathcal{O}}(\epsilon) + \mathcal{O}(\epsilon) + \cdots]$. To consistently derive the leading order differential $\mathcal{P}_{\rm HF} - \mathcal{P}_{\rm SR} = \mathcal{P}_{\rm SR}^{\rm LO}\mathcal{O}(\epsilon) + \cdots$, the term $\propto \tilde{\mathcal{O}}(\epsilon)$ must therefore be computed; i.e. the slow-roll quantities must be worked out at next-to-leading order.

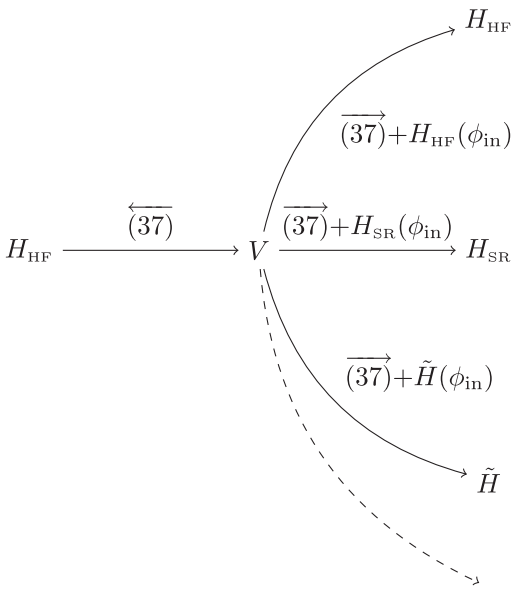

FIG. 1. Relations between H and V functions. Starting from a given $H_{\rm HF}$ function, the associated potential V can be obtained using Eq. (37) from the right-hand side to the left-hand side [hence the direction of the arrow above (37)]. Starting now from this potential V, several H functions can be obtained using Eq. (37) from the left-hand side to the right-hand side (i.e. solving a first order differential equation, that involves one integration constant), depending on the initial condition $H(\phi_{\rm in})$ one chooses. The one corresponding to slow roll, obtained by setting $H(\phi_{\rm in}) = H_{\rm SR}(\phi_{\rm in})$, has *a priori* no reason to mach the initial $H_{\rm HF}$ function corresponding to $H(\phi_{\rm in}) = H_{\rm HF}(\phi_{\rm in})$.

$$\Delta N^{\rm HF} = -\frac{1}{M_{\rm Pl}^2}\int \frac{V}{V'}\frac{1-\epsilon_1^{\rm HF}/3+\epsilon_2^{\rm HF}/6}{1-\epsilon_1^{\rm HF}/3}{\rm d}\phi, \qquad (44)$$

where one has used Eqs. (31) and (32) to introduce $\epsilon_1^{\rm HF}$ and $\epsilon_2^{\rm HF}$. One should notice that the first term of the integrand V/V' actually corresponds to the leading order of the slow-roll trajectory (9). This confirms that when the slow-roll is well verified in the horizon-flow parametrization $\epsilon^{\rm HF} \ll 1$, the two trajectories are similar.

However, beyond this simple argument, the trajectories' difference is the origin of two subtleties which we now describe, and which biases the horizon-flow analysis.

2. H-multivaluated trajectories

Along horizon-flow trajectories, let us first recall that the inflaton field can only vary monotonously. As a consequence, if the complete trajectory is made of several pieces with different signs of $\dot\phi$, only one of them can be described by the horizon-flow parametrization, which therefore may be unable to describe the actual outcome of the process.

Let us illustrate our point on the example of Fig. 2. For the potential displayed in the left panel, the Klein-Gordon equation (5) is integrated from some initial conditions (specified in the caption), and gives the trajectory displayed in the middle panel (colored lines) in the phase plane $(\phi, \dot\phi)$. It is made of several pieces: first the inflaton field climbs up the potential (green); then its velocity vanishes

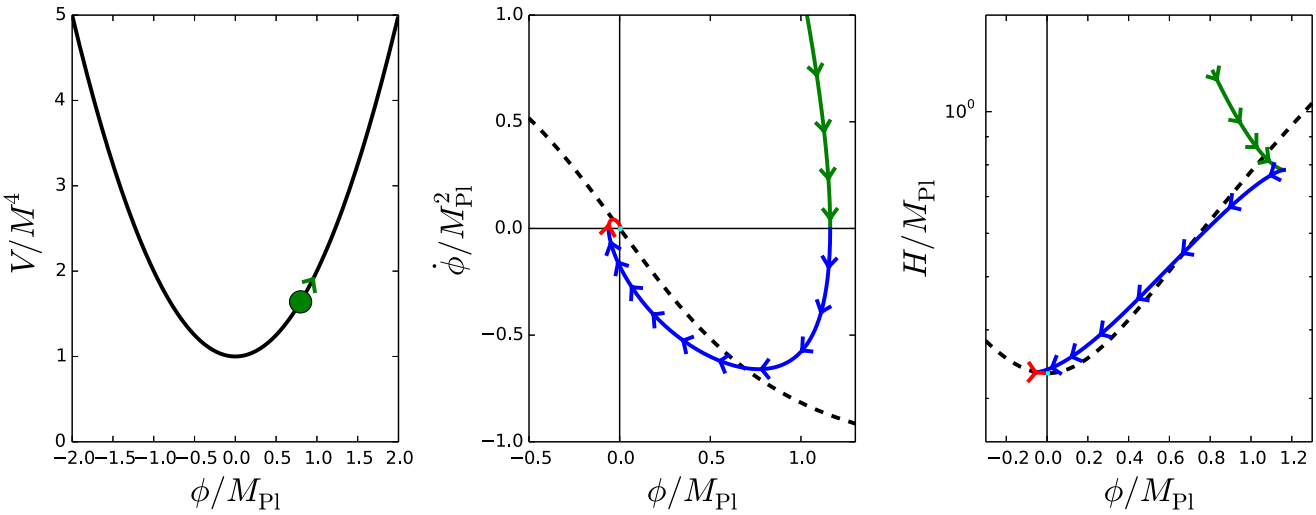

FIG. 2 (color online). Left panel: Potential $V/M^4 = 1 + (\phi/M_{\rm Pl})^2$ as a function of ϕ. The green disk and arrow stand for the initial value and sign of velocity of the inflaton field for the trajectory displayed in the middle and right panels. Middle panel: Numerical integration of equation (5) from $\phi_{\rm in}/M_{\rm Pl} = 0.8$ and $\dot\phi_{\rm in}/M_{\rm Pl}^2 = 2$ (colored line), displayed in the phase plane $(\phi, \dot\phi)$. Each color corresponds to a different piece of it, with alternate signs of $\dot\phi$. The black dashed line stands for the slow-roll leading order trajectory $\dot\phi = -V'/(3H^{\rm SR,LO})$. Right panel: Hubble parameter $H(\phi, \dot\phi)$ evaluated along this trajectory (same color code) with Eq. (4). Note that the logarithmic scale is used for H for display convenience. Again, the black dashed line stands for the slow-roll leading order solution $H^{\rm SR,LO}(\phi) = V(\phi)/(3M_{\rm Pl}^2)$. In the middle and right panels, the arrows indicate in which direction inflation proceeds.

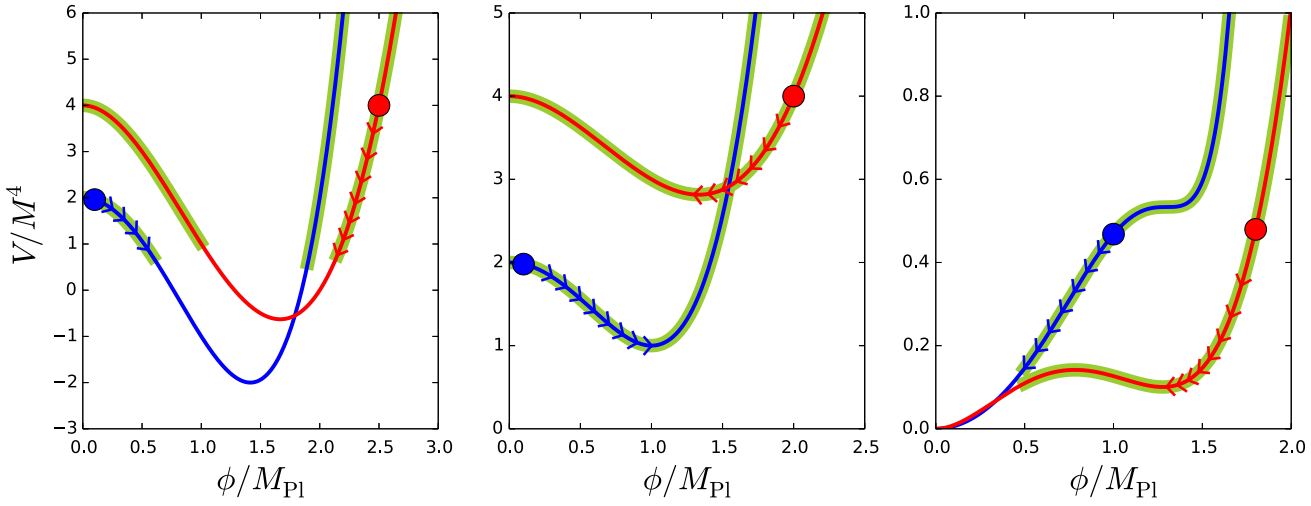

FIG. 3 (color online). Inflationary regimes for a few potential examples (sketch). On each panel, the functional form of V is the same but its coefficients differ (blue and red curves). Regions supporting slow-roll inflation are thickened in green. The horizon-flow trajectory is displayed with the arrows and starts from the location of the disk.

and it goes down the potential, it crosses the minimum and it climbs up on the other side (blue); and then its velocity vanishes again and the same thing happens the other way down (red), so on and so forth. In the right panel, the Hubble parameter $H(\phi, \dot{\phi})$ is evaluated along this trajectory with Eq. (4), and the same color code is adopted. In the middle and right panels, the black dashed line stand for the slow-roll leading order solution, and the arrows indicate in which direction inflation proceeds. One can verify that H always decreases as inflation proceeds.

In this example it is straightforward to understand why the horizon-flow parametrization cannot describe the entire trajectory: in the right panel, one can check that for a single value of ϕ, there are several possible values of H. The Hubble parameter is therefore multivaluated along the full trajectory, and a single $H(\phi)$ function cannot fully stand for it.

Since any physical trajectory within the potential eventually approaches the minimum of the potential $\phi = 0$, in the spirit of the horizon-flow algorithm [especially case (ii); see Sec. II C], this is where the late-time fixed point lies. However, even if the H functions displayed in the right panel of Fig. 2 were completed to be defined for all values of the inflaton field, $\phi = 0$ would be a late-time fixed point for none of them since it is a minimum of H for none of them.[5] Therefore, this kind of situation may not be properly described by the horizon-flow parametrization. These aspects are further developed in Sec. IV A.

3. Inflationary regime bias

In general, a given potential can support inflation in different regimes, but the horizon-flow trajectory is close to the slow-roll one for some of them only. More precisely, letting all the flow parameters vanish beyond some order M sets the functional form of H (hence of V), and drawing the initial values $\epsilon_{\rm in}$ of the remaining flow parameters sets the coefficients of these functions as well as the starting point of the numerical integration. Therefore, each time one draws some $\epsilon_{\rm in}$ coefficients, one draws a specific potential V and an initial value $\phi_{\rm in}$ on it. A few examples are displayed in Fig. 3.

On each panel, the functional form of H from which V is obtained through Eq. (37) is the same but its coefficients are different (blue and red curves). The horizon-flow trajectory is displayed with the arrows and starts from the location $\phi_{\rm in}$ displayed by the disk. On each potential, the green zone denotes where a slow-roll regime of inflation can be supported. One can see that when several slow-roll regimes are possible, $\phi_{\rm in}$ selects out only one of them, such that the other ones are not described. Of course, one can draw other values of $\epsilon_{\rm in}$ so that a similar regime is tracked down (from red to blue case in each panel), but since $\phi_{\rm in}$ and the coefficients of V are entangled by the choice of $\epsilon_{\rm in}$, this will be done on a different potential. In this sense horizon flow is a biased parametrization of inflation, since once the potential is fixed, only a specific regime out of (possibly) many is worked out. This effect is explicitly exemplified and computed in Sec. IV B.

Finally, it is worth mentioning that when the slow-roll conditions are well verified for $H^{\rm SR}$ but not for $H^{\rm HF}$, the horizon-flow and slow-roll trajectories are very different; see Eq. (44). For example, when the second term of Eq. (44) is negative, the horizon-flow dynamics describes a situation where the inflaton field climbs up its potential. In this case the horizon-flow trajectories have nontrivial instability properties that are further investigated in Sec. IV C.

[5]Recall that, since H always decreases during inflation, a late-time fixed point is necessarily a minimum of $H(\phi)$.

F. A warm-up example: $H = 1 + a\phi$

To briefly summarize the computational program of the following sections, and as an illustrative warm-up, let us consider the simple case where the expansion (36) is truncated at first order; that is, $H/H_0 = 1 + ax$, where $x \equiv \phi/M_{\rm Pl}$. The Hubble parameter is positive provided $x > -1/a$ if $a > 0$ and $x < -1/a$ if $a < 0$. For simplicity, we only detail the case $a > 0$ since $a < 0$ is completely symmetrical and can be worked out in exactly the same way. In this section we calculate the ratio $r_{16}/(1 - n_{\rm S})$ predicted by this model, successively making use of the horizon-flow and of the slow-roll setups.

1. Horizon-flow predictions

When $a > 0$, H increases with x; hence from Eq. (28) x decreases as inflation proceeds. It stops when $\epsilon_1 = 2M_{\rm Pl}^2 H'^2/H^2 = 2a^2/(1 + ax)^2 = 1$ [see Eq. (31)], i.e. at the location $x_{\rm end}^{\rm HF}$ given by

$$x_{\rm end}^{\rm HF} = \sqrt{2} - \frac{1}{a}, \tag{45}$$

where as before the superscript HF stresses that for now, the calculation is carried out in the horizon-flow framework. The inflationary trajectory is given by Eq. (42) and the number of e-folds between the Hubble crossing time of the pivot scale and the end of inflation reads

$$\Delta N_*^{\rm HF} = \frac{x_*^{\rm HF}}{2a} + \frac{(x_*^{\rm HF})^2}{4} - \frac{x_{\rm end}^{\rm HF}}{2a} - \frac{(x_{\rm end}^{\rm HF})^2}{4}. \tag{46}$$

This trajectory can be inverted, and making use of Eq. (45), one obtains

$$x_*^{\rm HF} = -\frac{1}{a} + \sqrt{2 + 4\Delta N_*^{\rm HF}}. \tag{47}$$

Then one needs to plug this expression in the slow-roll parameters' ϵ_1 and ϵ_2 expressions, respectively given by Eqs. (31) and (32). Here, since $H'' = 0$, one has $\epsilon_2 = 2\epsilon_1$. Finally, r and $n_{\rm S}$ are evaluated. At leading order in slow roll, they are given by Eqs. (16) and (17), and one obtains

$$\left.\frac{r_{16}}{1 - n_{\rm S}}\right|_{\rm HF}^{\rm LO} = \frac{1}{4}, \tag{48}$$

which neither depends on a nor on ΔN_*. If one goes up to next-to-leading order in slow roll, $n_{\rm S}$ and r are respectively given by Eqs. (26) and (27). Since $H'' = 0$ implies that $\epsilon_3 = 2\epsilon_1$ in Eq. (33), this means that at next-to-leading order in slow roll, one has $r_{16}/(1 - n_{\rm S}) = (1 - 2\epsilon_{1*})/4$, which yields

$$\left.\frac{r_{16}}{1 - n_{\rm S}}\right|_{\rm HF}^{\rm NLO} = \frac{1}{4} - \frac{1}{2 + 4\Delta N_*}, \tag{49}$$

which now mildly depends on ΔN_* but still not on a. For $\Delta N_* \simeq 50$, one obtains $r_{16}/(1 - n_{\rm S}) \simeq 0.245$.

2. Slow-roll predictions

Let us now see what the slow-roll setup predicts for this model. Thanks to Eq. (37), the problem consists in studying slow-roll inflation in the potential

$$V = 3M_{\rm Pl}^2 H_0^2 \left(a^2 x^2 + 2ax + 1 - \frac{2}{3}a^2\right). \tag{50}$$

As before, we restrict ourselves to the case $a > 0$. One can see that the potential is definite positive only if $x > -1/a + \sqrt{2/3}$. Therefore there exists a domain, namely $-1/a < x < -1/a + \sqrt{2/3}$, for which H is well defined but not V. Fortunately $V(x_{\rm end}^{\rm HF}) > 0$ so that this region is never probed, but as explained in Secs. III and IV this is not the case in general. In the same manner, one can check that V and H both increase with x, which means that along the horizon-flow trajectory the inflaton rolls down its potential. However, as mentioned in Sec. II E and further developed in the following, this is also not always necessarily true.

For what matters now, if one uses Eq. (12) to compute $\epsilon_1^{\rm LO}$, the end of inflation is determined to happen at

$$x_{\rm end}^{\rm SR,LO} = \sqrt{\frac{7}{6}} + \frac{1}{\sqrt{2}} - \frac{1}{a}, \tag{51}$$

where again the superscript SR recalls that we are working in the slow-roll framework. The difference with Eq. (45) is not surprising since, here, Eq. (12) is used in a regime where, by definition, the slow-roll approximation is not valid anymore.

At leading order in slow-roll, the slow-roll trajectory (9) gives rise to

$$\Delta N_*^{\rm SR,LO} = \frac{x_*^{\rm SR,LO}}{2a} + \frac{(x_*^{\rm SR,LO})^2}{4} - \frac{x_{\rm end}^{\rm SR,LO}}{2a} - \frac{(x_{\rm end}^{\rm SR,LO})^2}{4} + \frac{1}{3}\ln\left(\frac{1 + ax_{\rm end}^{\rm SR,LO}}{1 + ax_*^{\rm SR,LO}}\right), \tag{52}$$

which resembles the horizon-flow trajectory, but with logarithmic corrections. In practice, Eq. (52) needs to be inverted numerically to get $x_*^{\rm SR}$. However, to allow comparison with the horizon-flow predictions which do not depend on a, let us derive the corresponding slow-roll results in the limit $a \ll 1$. In this case, an approximated formula for the inverted trajectory can be obtained, namely

$$x_*^{\rm SR,LO} \underset{a\ll 1}{\simeq} -\frac{1}{a} + \frac{2\sqrt{2}}{3}\frac{3 + \sqrt{21}}{7 + \sqrt{21}} + \frac{2}{7 + \sqrt{21}} \times \sqrt{23 + 5\sqrt{21} + 4(14 + 3\sqrt{21})\Delta N_*}. \tag{53}$$

The slow-roll parameters at the time of Hubble scale crossing are then obtained by plugging the previous in Eqs. (12) and (13), and n_S and r are computed using Eqs. (16) and (17). One obtains a long but explicit expression. For display convenience and again, to allow an easy comparison with the horizon-flow predictions, it can be simplified in the limit $\Delta N_* \gg 1$, and one gets

$$\left.\frac{r_{16}}{1-n_S}\right|^{\rm LO}_{\rm SR} \underset{\substack{a\ll 1\\ \Delta N_*\gg 1}}{\simeq} \frac{1}{4} - \frac{7-\sqrt{21}}{96\Delta N_*}. \tag{54}$$

Taking $\Delta N_* \simeq 50$, one obtains $r_{16}/(1-n_S) \simeq 0.2496$. Finally, let us see how these expressions are modified when computing them at next-to-leading order in slow roll. First, if one uses $\epsilon_1^{\rm NLO}$ rather than $\epsilon_1^{\rm LO}$ to determine $x_{\rm end}$, then one faces a problem since $\epsilon_1^{\rm NLO}$ reaches a maximum which is less than 1 and then becomes negative as inflation approaches its end. This is because the expansion (22) does not make sense close to the end of inflation where slow roll is violated. In any case the precise value of $x_{\rm end}$ does not play a crucial role. Therefore one can safely continue to work with Eq. (51) as far as the location of the end of inflation is concerned. Then, the slow-roll trajectory (25) gives

$$\begin{aligned}\Delta N_*^{\rm SR,NLO} &= \frac{x_*^{\rm SR,NLO}}{2a} + \frac{(x_*^{\rm SR,NLO})^2}{4} - \frac{x_{\rm end}^{\rm SR,NLO}}{2a}\\ &\quad - \frac{(x_{\rm end}^{\rm SR,NLO})^2}{4} + \frac{2}{3}\ln\left(\frac{1+ax_{\rm end}^{\rm SR,NLO}}{1+ax_*^{\rm SR,NLO}}\right)\\ &\quad + \frac{1}{3}\ln\left[\frac{a^2(x_*^{\rm SR,NLO})^2 + 2ax_*^{\rm SR,NLO} + 1 - 2a^2/3}{a^2(x_{\rm end}^{\rm SR,NLO})^2 + 2ax_{\rm end}^{\rm SR,NLO} + 1 - 2a^2/3}\right].\end{aligned} \tag{55}$$

Again, although this cannot be inverted but numerically, an analytical formula can however be obtained in the limit where $a \to 0$, which reads

$$\begin{aligned}x_*^{\rm SR,NLO} &\underset{a\ll 1}{\simeq} -\frac{1}{a} - \frac{4\sqrt{2}}{3}\frac{9+\sqrt{21}}{13+\sqrt{21}} + \frac{2\sqrt{2}}{3(13+\sqrt{21})}\\ &\quad \times \sqrt{205+44\sqrt{21}+3(43+9\sqrt{21})\Delta N_*}.\end{aligned} \tag{56}$$

The slow-roll parameters at time of pivot scale crossing are then evaluated at this point but this time using the next-to-leading order expressions (21)–(24). Doing so, and again working out the $\Delta N_* \gg 1$ limit for a more convenient comparison of the different results, Eqs. (26) and (27) give rise to[6]

$$\left.\frac{r_{16}}{1-n_S}\right|^{\rm NLO}_{\rm SR} \underset{\substack{a\ll 1\\ \Delta N_*\gg 1}}{\simeq} \frac{1}{4} - \frac{7}{888}\frac{13-\sqrt{21}}{\Delta N_*}. \tag{57}$$

Taking $\Delta N_* \simeq 50$, one obtains $r_{16}/(1-n_S) \simeq 0.2487$.

On can see that the difference between both frames' predictions at next-to-leading order, Eqs. (49) and (57) ($\sim$0.004), is of the same order as the leading order difference Eqs. (48) and (54) ($\sim$0.0037) but does not have the same sign. This confirms that both frames' predictions differ by quantities that need to be consistently computed at next-to-leading order in slow roll.

In this simple toy example, both frames predict similar results and disagree only by subdominant quantities of the order of the percent. However, as will be exemplified in Sec. IV, this is not always the case.

III. WHY HORIZON FLOW PREDICTS $r_{16}/(1-n_S) = 1/3$ OR 0 AND WHY IT SHOULD NOT

The computational program of horizon flow sketched in Sec. II C oversamples two denser regions in the (r_{16}, n_S) plane, namely $r_{16}/(1-n_S) = 1/3$ and $r_{16} = 0$. As explained before, this can be accounted for by a fixed point analysis, which however singles out slightly different predictions, namely $r_{16}/(1-n_S) = 1/2$ and $r_{16} = 0$. In this section we puzzle out this mismatch, going beyond a fixed point analysis and explicitly solving the horizon-flow dynamics when the expansion (36) is truncated at second order (which we argue is sufficient). We then exhibit simple horizon-flow models which completely break these relations. This illustrates how the above mentioned denser regions are intimately related to the specific choice of the parametrization (36), and show that they do not hint at intrinsic properties of single-field inflation itself.

A. Elucidating horizon-flow "predictions"

The inflationary predictions associated with the models (36) cannot be derived analytically in general for an arbitrarily large value of M. However, as we now explain, $M = 1$ already allows us to capture most of the physical effects contained in these models. Indeed, at leading order in slow roll, one has $r_{16} = \epsilon_1$ and $n_S = 1 - 2\epsilon_1 - \epsilon_2$. Looking back at Eqs. (31)–(32), these observables involve up to the second derivative in $H(\phi)$ only. Since H is assumed not to vary too much during inflation, it seems reasonable to first neglect higher derivatives, and thus to study the models defined by

$$H(\phi) = H_0\left[1 + a\frac{\phi}{M_{\rm Pl}} + b\left(\frac{\phi}{M_{\rm Pl}}\right)^2\right]. \tag{58}$$

1. Inflationary regimes

As before, one denotes $x \equiv \phi/M_{\rm Pl}$. The H function (58) is symmetrical with respect to $x_0 = a/(2b)$, and it is

[6]Since expressions are consistently worked out at next-to-leading order in slow roll, the $\propto \epsilon^2$ terms in the right-hand side of Eqs. (26) and (27) are evaluated with the leading order formulas for the slow-roll parameters (11)–(14), while the $\propto \epsilon$ terms are evaluated with the next-to-leading order formulas (21)–(24).

therefore enough to study the inflationary dynamics in the range $x > x_0$ only. If $b > 0$, H increases with x, and if $0 < b < a^2/4$, the Hubble parameter is positive only if $x > x_{H=0}$, where

$$x_{H=0} = \frac{\sqrt{a^2 - 4b} - a}{2b}. \tag{59}$$

On the other hand if $b < 0$, H decreases with x, and is positive only if $x < x_{H=0}$.

The phase space relation (28) implies that H must decrease during inflation. Therefore when $b > 0$, the inflaton ϕ decreases as inflation proceeds, whereas it increases when $b < 0$. Eventually inflation stops when $\epsilon_1 = 1$. In order to determine when this happens, let us calculate the first slow-roll parameters with Eqs. (30)–(33). They are given by

$$\epsilon_1 = 2\left(\frac{a + 2bx}{1 + ax + bx^2}\right)^2, \tag{60}$$

$$\epsilon_2 = 4\frac{a^2 - 2b + 2abx + 2b^2x^2}{(1 + ax + bx^2)^2}, \tag{61}$$

$$\epsilon_3 = 4\left(\frac{a + 2bx}{1 + ax + bx^2}\right)^2 \frac{a^2 - 3b + abx + b^2x^2}{a^2 - 2b + 2abx + 2b^2x^2}, \tag{62}$$

and the following slow-roll parameters can be derived in the same manner. The first slow-roll parameter ϵ_1 equals 1 at

$$x^{\pm}_{\epsilon_1=1} = -\frac{a}{2b} + \sqrt{\frac{a^2}{4b^2} + 2 - \frac{1}{b}} \pm \sqrt{2}, \tag{63}$$

which is defined only when $a^2/4 \geq b - 2b^2$. This leads to five possible regimes that we now describe one by one.

(i) $b < 0$, Fig. 4

In this case inflation proceeds at $x < x_{H=0}$ for increasing values of x (as denoted by the right arrow in Fig. 4), and naturally ends by slow-roll violation since ϵ_1 diverges when x goes to $x_{H=0}$. More precisely, the location at which inflation ends is given by $x_{\rm end} = x^-_{\epsilon_1=1}$. Note that even if the present analysis is detailed for $x > x_0$ only, symmetrical ranges are displayed in the figures, for illustrative purposes.

(ii) $b \geq 0$ and $a^2 > 4b$, Fig. 5

Since $b \geq 0$, inflation proceeds for decreasing values of x, at $x > x_{H=0}$. Again, ϵ_1 diverges when x goes to $x_{H=0}$ and inflation naturally ends by slow-roll violation, but this time at the location $x_{\rm end} = x^+_{\epsilon_1=1}$. The dashed lines attached to the arrows mean that inflation actually proceeds at larger values of the field (where $\epsilon_1 < 1$) than what the position of the arrows indicates.

(iii) $b > 0$ and $a^2/4 = b$, Fig. 6

This case is singular since H vanishes only once at x_0, where the first slow-roll parameter blows up. Inflation naturally ends at $x_{\rm end} = x^+_{\epsilon_1=1}$, which simplifies and reads

$$x_{\rm end} = -\frac{2}{a} + 2\sqrt{2}. \tag{64}$$

(iv) $b > 0$ and $b - 2b^2 \leq a^2/4 < b$, Fig. 7

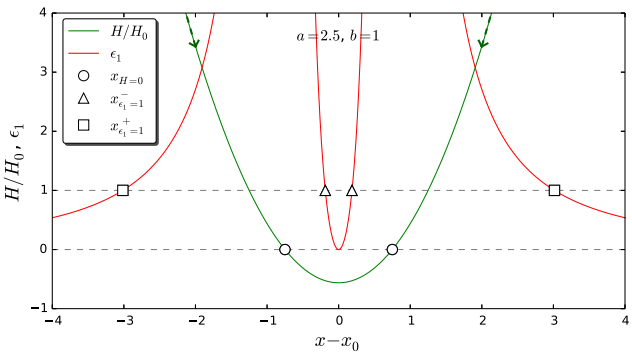

FIG. 5 (color online). Hubble function $H(\phi)$ and first slow-roll parameter ϵ_1 in the case $b \geq 0$ and $a^2 > 4b$ ($a = 2.5$ and $b = 1$).

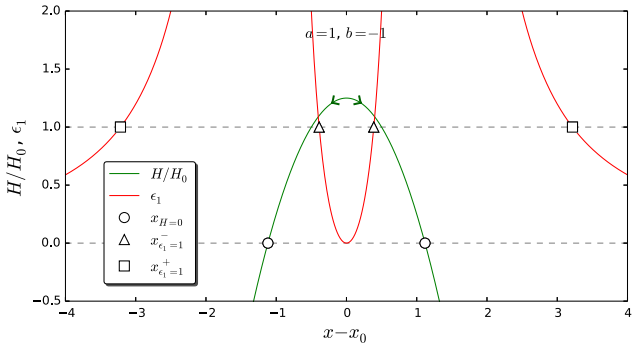

FIG. 4 (color online). Hubble function $H(\phi)$ and first slow-roll parameter ϵ_1 in the case $b < 0$ ($a = 1$ and $b = -1$).

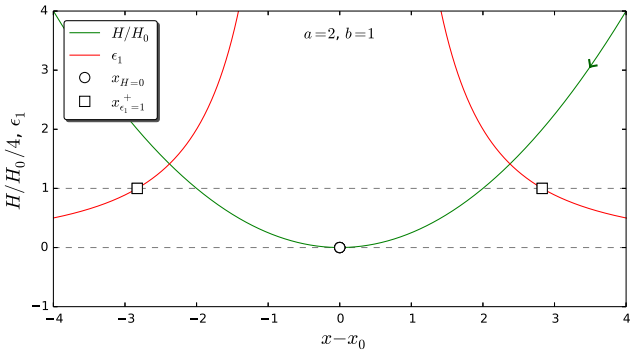

FIG. 6 (color online). Hubble function $H(\phi)$ and first slow-roll parameter ϵ_1 in the case $a^2/4 = b$ ($a = 2$ and $b = 1$).

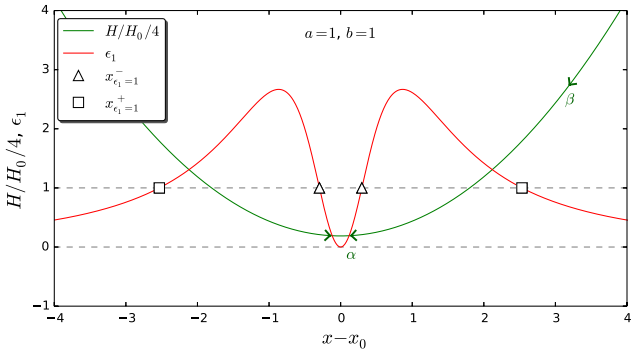

FIG. 7 (color online). Hubble function $H(\phi)$ and first slow-roll parameter ϵ_1 in the case $b>0$ and $b-2b^2<a^2/4<b$ ($a=1$ and $b=1$).

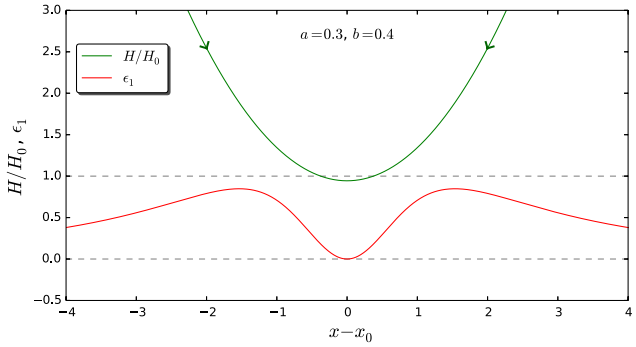

FIG. 8 (color online). Hubble function $H(\phi)$ and first slow-roll parameter ϵ_1 in the case $b>0$ and $a^2/4<b-2b^2$ ($a=0.3$ and $b=0.4$).

In this case H is always positive, and ϵ_1 does not blow up but possesses a maximum that is larger than 1. This leads to two possible regimes: either inflation starts from $x_{\rm in}<x^-_{\epsilon_1=1}$ and never ends [we call this regime (iv-α)], or it starts from $x_{\rm in}>x^+_{\epsilon_1=1}$ and ends at $x_{\rm end}=x^+_{\epsilon_1=1}$ [we call this regime (iv-β)]. In the (iv-α) case, x asymptotically approaches the central value x_0 and stays there forever.

(v) $b>0$ and $a^2/4<b-2b^2$, Fig. 8

This last case occurs only if $0<b<1/2$, and is similar to the previous one except that now the maximum value of ϵ_1 is smaller than 1. Therefore in this situation inflation never ends and x asymptotically approaches the central value x_0 where it stays forever.

2. Inflationary trajectory

We can now move on and compute the inflationary trajectory. Integrating the relation (29) $\mathrm{d}N=-H/H'\mathrm{d}\phi/(2M_{\rm Pl}^2)$ between the time N_* when the modes of astrophysical interest today cross out the Hubble radius and the time $N_*+\Delta N_*=N_{\rm end}$ when inflation stops, one obtains

$$\Delta N_*^{\rm HF}=\frac{x_*^2-x_{\rm end}^2}{8}+\frac{a}{8b}(x_*-x_{\rm end})+\left(1-\frac{a^2}{4b}\right)\frac{1}{4b}\ln\left(\frac{a+2bx_*}{a+2bx_{\rm end}}\right). \quad (65)$$

This trajectory can be inverted to express x_* in terms of a, b and ΔN_* only. The way it proceeds depends on the case under consideration among the five mentioned above.

When $b<0$, case (i), a first remark is that the number of e-folds diverges when $x\to x_0$ and therefore, one is sure to be able to realize a sufficient number of e-folds. Denoting $X\equiv(a+2bx)^2/(4b-a^2)$, one obtains $x_*=-a/(2b)-\sqrt{(4b-a^2)X_*}/(2b)$, where

$$X_*=W_0\left[X_{\rm end}\exp\left(X_{\rm end}+\frac{32b^2}{4b-a^2}\Delta N_*\right)\right] \quad (66)$$

and where W_0 is the 0 branch of the Lambert function.

When $b>0$ and $a^2/4>b$, case (ii), one is also sure to be able to realize a sufficient number of e-folds since ΔN diverges when x goes to infinity. In this case one obtains $x_*=-a/(2b)+\sqrt{(4b-a^2)X_*}/(2b)$ (notice that the sign of the second term in the right-hand side is different from the case $b<0$), with

$$X_*=W_{-1}\left[X_{\rm end}\exp\left(X_{\rm end}+\frac{32b^2}{4b-a^2}\Delta N_*\right)\right], \quad (67)$$

where W_{-1} is the -1 branch of the Lambert function [40].

When $a^2=4b$, case (iii), the logarithm term in Eq. (65) vanishes and the trajectory is simply given by

$$x_*=-\frac{2}{a}+\sqrt{\frac{4}{a^2}+x_{\rm end}^2+\frac{4}{a}x_{\rm end}+8\Delta N_*}. \quad (68)$$

Replacing $x_{\rm end}$ by Eq. (64), this leads to

$$x_*=-\frac{2}{a}+2\sqrt{2}\sqrt{1+\Delta N_*}. \quad (69)$$

Finally when $b>0$ and $a^2/4<b$, cases (iv) and (v), one obtains $x_*=-a/(2b)+\sqrt{(4b-a^2)X_*}/(2b)$ [i.e. with the same sign as for case (ii)], but with

$$X_*=W_0\left[X_{\rm end}\exp\left(X_{\rm end}+\frac{32b^2}{4b-a^2}\Delta N_*\right)\right]. \quad (70)$$

One can check that, as mentioned above, since ΔN diverges when $x\to x_0$, an infinite number of e-folds is realized as x approaches x_0 and inflation never ends in the cases (iii-β) and (iv).

3. Inflationary predictions

The physical predictions can now be derived explicitly in terms of a, b and ΔN_*, especially the ratio $r_{16}/(1-n_S)$ one is interested in. Making use of Eqs. (16) and (17), at first order in slow roll, it is given by

$$\frac{r_{16}}{1-n_S} = \frac{\epsilon_1(x_*,a,b)}{1-2\epsilon_1(x_*,a,b)-\epsilon_2(x_*,a,b)}, \qquad (71)$$

where the slow-roll parameters $\epsilon(x,a,b)$ are given by Eqs. (60)–(62), and the Hubble crossing point $x_*(a,b,\Delta N_*)$ is given by the formulas detailed above in Sec. III A 2. Obviously it would be straightforward to expand Eq. (71) in a (rather long) analytical formula, but one would not learn much doing so. It is instead more instructive to plot the result as a function of a and b, which is what is done in Fig. 9, taking $\Delta N_* = 50$ (where we have made sure that different values of ΔN_* do not modify the result much).

Let us stress that in the case of never-ending inflation, i.e. cases (iv-β) and (v), following the lines of the horizon-flow computational algorithm detailed in Sec. II C, the observational predictions are computed at the late-time attractor x_0, where $\epsilon_1 = 0$ and $\epsilon_2 \neq 0$; hence $r_{16}/(1-n_S) = 0$. This corresponds to the dark blue (iv-β) and black (v) surfaces in Fig. 9, with the "hole" in the blue surface associated with the case (v) where there is no other regime.

It is also worth mentioning that if $a^2 = 4b$, i.e. in case (iii), things are particularly simple since Eqs. (60) and (61) combined with Eq. (69) exactly give $\epsilon_{1*} = \epsilon_{2*} = 1/(1+\Delta N_*)$; hence $r_{16}/(1-n_S) = 1/3$. It is displayed as the blue curved line in Fig. 9, where one can note the

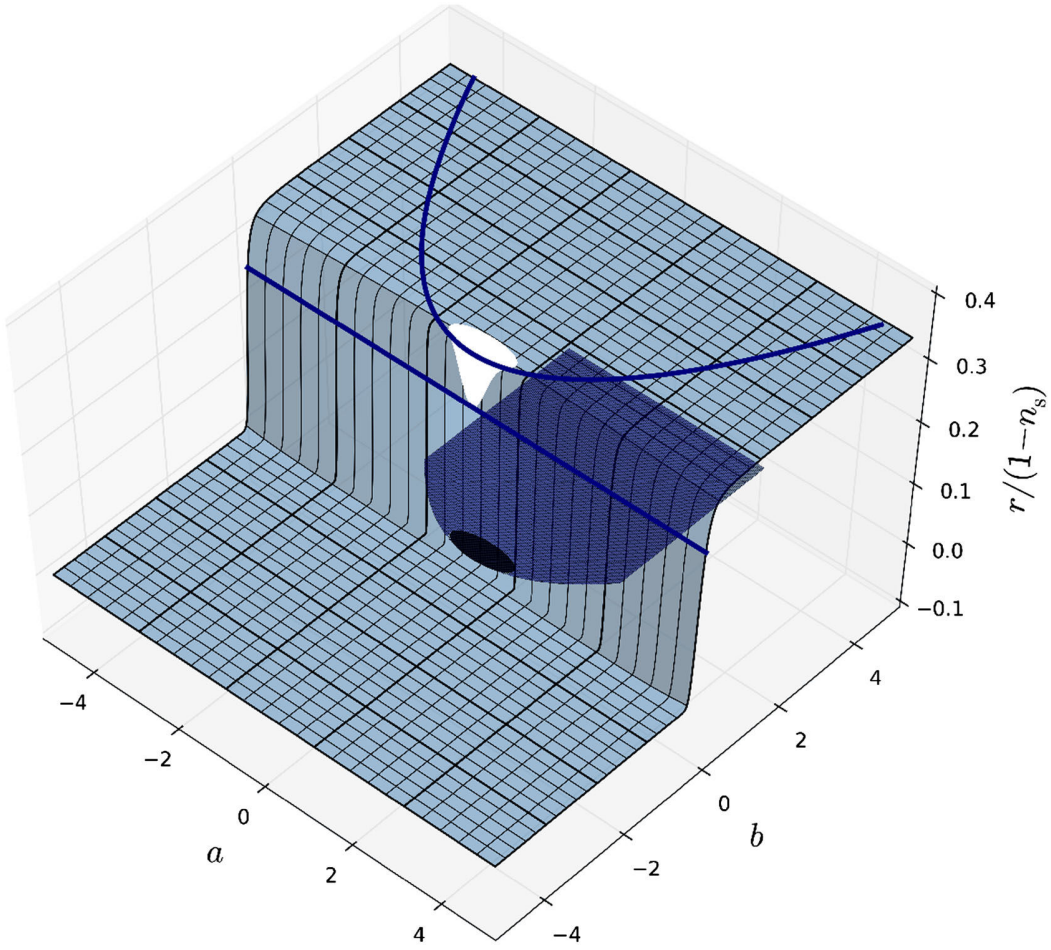

FIG. 9 (color online). Ratio $r_{16}/(1-n_S)$ for the model $H/H_0 = 1 + ax + bx^2$ as a function of a and b, with $\Delta N_* = 50$. The light blue surface stands for the regimes of inflation where it ends naturally, i.e. by slow-roll violation. The "hole" in this surface corresponds to case (v) where there is not such a regime. In this case the predictions are calculated at the late-time attractor x_0 that yields $r_{16} = 0$, which is displayed by the black ellipse behind the light blue surface (and which is the projection of the hole onto the plane $r_{16} = 0$). In the same manner, the dark blue surface corresponds to the case (iv-β) where $r_{16} = 0$ for the same reason. The blue straight line corresponds to $b = 0$ and $r_{16}/(1-n_S) = 1/4$, which matches the calculation of Sec. II F, and the blue curved line corresponds to $a^2 = 4b$, i.e. case (iii), for which $r_{16}/(1-n_S) = 1/3$ exactly.

discontinuity in the predictions when $b \to 0$, this case (iii) being singular. Finally, the blue straight line stands for $b = 0$ and $r_{16}/(1-n_S) = 1/4$, which corresponds indeed to the calculation of Sec. II F.

One can see that when $b \neq 0$, two asymptotic plateaus are quickly reached. When $b < 0$, inflation proceeds close to the maximum of H and in practice, x_* is very close to the local maximum of the potential $x_* \simeq x_0$ where $\epsilon_1 = 0$ and $\epsilon_2 \neq 0$. One then typically has $r_{16} = 0$, as in the cases (iv-β) and (v). When $b > 0$ on the other hand, the asymptotic value of the plateau can be obtained by expanding Eqs. (63), (70), (60) and (61) in the limit $b \gg 1$ and $\Delta N_* \gg 1$, and one obtains $r_{16}/(1-n_S) = 1/3$, as in the case (iii). These results can be schematically summarized as follows:

$$\frac{r_{16}}{1-n_S} \simeq \begin{cases} 0 & \text{in the cases (i), (iv-}\beta\text{), (v)} \\ \frac{1}{3} & \text{in the cases (ii), (iii), (iv-}\alpha\text{)} \end{cases}. \quad (72)$$

It is therefore particularly interesting to notice that the typical results found in the literature can simply be interpreted in this framework: $r_{16} = 0$ corresponds either to inflation proceeding close to a maximum of H or to a never-ending regime of inflation, while $r_{16}/(1-n_S) = 1/3$ is to be associated with a naturally ending inflationary regime where H is not bounded in the far past. This calculation also explains why, as noticed in Refs. [19,21], the denser regions in the observable plane do not lie exactly at the fixed point $r_{16}/(1-n_S) = 1/2$ mentioned in Sec. II C but are better described by $r_{16}/(1-n_S) = 1/3$.

The mismatch between the numerical results of the horizon-flow computational program and the fixed point analysis is therefore elucidated in this example, and a detailed analysis of the inflationary regimes accounts for the two different typical predictions.

B. Breaking horizon-flow "predictions"

However, as we shall now see, these "typical" predictions are a direct consequence of the parametrization (36), and can easily be broken by other choices of the $H(\phi)$ function.

1. $H = 1 + \alpha\phi^p$

Let us first wonder what would happen if, for some reason, the first terms in the expansion (36) vanish. If $a_1 = 0$ and $a_2 \neq 0$ in Eq. (36), the calculation has already been carried out in Sec. III A. Then if $a_1 = a_2 = 0$, the first nonvanishing term of the expansion provides the leading order for r_{16} and n_S, for the same reason as that mentioned at the beginning of Sec. III A. Let us thus investigate a horizon-flow model of the form $H/H_0 = 1 + \alpha x^p$.

The same detailed analysis as before can be carried out, but here we only summarize the results. Again, when inflation proceeds close to a maximum of H, or when inflation never stops and asymptotically reaches a minimum of H, one has $r_{16} \simeq 0$. When $\alpha > 0$, a regime of naturally ending inflation with unbounded values of H in the far past exists for any α if p is odd, but only if α is larger than some value α_c when p is even, given by

$$\alpha_c = 2^{-\frac{p}{2}}(p-1)^{1-p}. \quad (73)$$

Indeed, one can check that if p is even and if $\alpha < \alpha_c$, the first slow-roll parameter ϵ_1 is always smaller than 1. If not, the corresponding location of the end of inflation $x_{\rm end}$ must be determined numerically in general. One can also check that if $p = 2$, the condition $b > 1/2$ of case (v) for the model (58) matches the value of α_c given by Eq. (73). The trajectory can be integrated, and one obtains

$$\Delta N_* = \frac{1}{2\alpha p}\left(\frac{x_*^{2-p} - x_{\rm end}^{2-p}}{2-p} + \alpha\frac{x_*^2 - x_{\rm end}^2}{2}\right). \quad (74)$$

It is singular when $p = 2$, for which the trajectory can directly be read off from Eq. (65) (taking $a = 0$), and it needs to be inverted numerically in general. Doing so, one obtains the value of the field x_* when the modes of astrophysical interest today cross out the Hubble radius. Then, the slow-roll parameters can be evaluated at this point and the corresponding ratio $r_{16}/(1-n_S)$ can be computed. It is displayed in Fig. 10 as a function of α, for integer values of p up to $p = 10$, and taking $\Delta N_* = 50$ (where we have again made sure that different values of ΔN_* do not modify the results much). One can see that when α grows, the ratio $r_{16}/(1-n_S)$ reaches a stationary plateau very quickly, the value of which can be obtained by expanding in $\alpha \gg \alpha_c$ the previous equations. One then finds $x_{\rm end} \simeq p\sqrt{2}$ and $x_* \simeq \sqrt{2p^2 + 4p\Delta N_*}$. From this it follows that $\epsilon_1^* \simeq p/(2\Delta N_* + p)$ and $\epsilon_2^* \simeq 1/(\Delta N_* + p/2)$, and hence

$$\left.\frac{r_{16}}{1-n_S}\right|_{\alpha \gg \alpha_c} \simeq \frac{1}{2(1+\frac{1}{p})}. \quad (75)$$

The values corresponding to Eqs. (73) and (75) are displayed in Fig. 10 (black dotted line), where one can check that the matching with the numerical results is very good. On the other hand, if p is odd, the same plateau exists when $\alpha > \alpha_c$, where inflation proceeds and stops at $x > 0$, but when $\alpha < \alpha_c$, inflation can still end naturally when $\epsilon_1 = 1$ for $x < 0$, and a different behavior arises. In this case the ratio $r_{16}/(1-n_S)$ is negative, and it is displayed by the dashed curves in Fig. 10.

A continuous set of values for the ratio $r_{16}/(1-n_S)$, including negative ones, is therefore described. One sees that it is enough to allow the cancellation of one or several first terms in the expansion (36) to yield different predictions from $r_{16} = 0$ and $r_{16}/(1-n_S) = 1/3$. As a

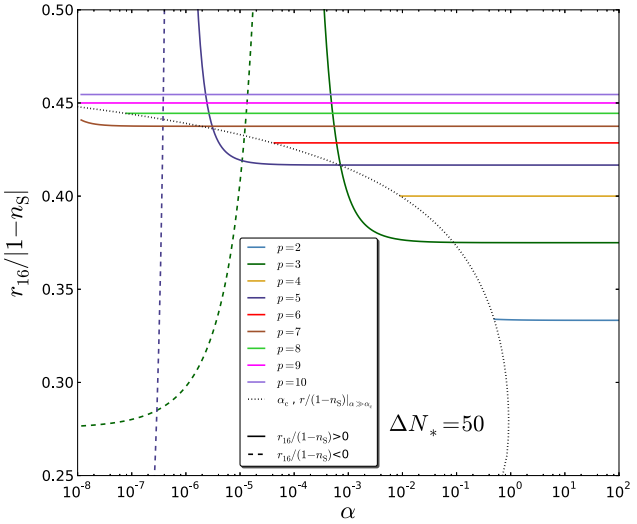

FIG. 10 (color online). Ratio $r_{16}/|1-n_S|$ corresponding to the model $H/H_0 = 1+\alpha x^p$ in the regime of ending inflation, as a function of α, for different values of p and with $\Delta N_* = 50$. Note that the absolute value of the ratio is displayed (continuous lines when it is positive, and dashed lines when it is negative). When p is even, such a regime exists only when α is larger than α_c. The black dotted line stands for the p-parametrized points $(\alpha_c, r_{16}/(1-n_S)|_{\alpha\gg\alpha_c})$, where α_c is given by Eq. (73) and $r_{16}/(1-n_S)|_{\alpha\gg\alpha_c}$ is given by Eq. (75).

consequence, these specific values should not be viewed as generic.

2. $r_{16}/(1-n_S) = f$

One can go even further, adopting a "reverse engineering" approach to design a model that gives $r_{16}/(1-n_S) = f$ for any value of f. Since $r_{16}/(1-n_S) \simeq 1/(2+\epsilon_2/\epsilon_1)$ at first order in slow roll, any value of f can be reached provided $\epsilon_2 = (1/f-2)\epsilon_1$. Plugging Eqs. (31) and (32) in this relation yields a differential equation for H, namely $(H'/H)^2 = 2fH''/H$, which can be solved explicitly:

$$H(x) = \begin{cases} H_0(1+ax)^{\frac{2f}{2f-1}} & \text{if } f \neq \frac{1}{2}, \\ H_0 e^{ax} & \text{if } f = \frac{1}{2}, \end{cases} \tag{76}$$

where a is some integration constant. Such $H(\phi)$ functions therefore provide any value $r_{16}/(1-n_S)$ and do not single out any typical inflationary prediction.

IV. HORIZON-FLOW VERSUS SLOW-ROLL TRAJECTORIES

As explained in Sec. II E, the horizon-flow parametrization selects a specific trajectory in phase space among all the solutions of the Klein-Gordon equation (5) associated with the potential (37) derived from H. In this section we first explicitly characterize such trajectories for a few representative examples of inflationary potentials, and compare them with the slow-roll solution which is known as an efficient attractor [29] of the inflationary dynamics. This allows us to classify horizon-flow trajectories into three categories, and to highlight that in some cases, horizon flow parametrizes inflation along unstable trajectories where the inflaton climbs up its potential. We then go back to the model (58) for which we carry out a complete slow-roll analysis and show that, for a fixed potential, the horizon-flow method is in fact blind to entire inflationary regimes. This introduces a bias in the way it parametrizes inflation. Finally, we numerically investigate, in a reheating consistent manner, the discrepancies in the inflationary predictions obtained from the horizon-flow and the slow-roll trajectories in this model.

A. Horizon-flow trajectories in typical examples

Let us start again from Eq. (37), $V = 3M_{\rm Pl}^2H^2 - 2M_{\rm Pl}^4H'^2$, but let us use it in the opposite way as before: instead of deducing the potential $V(\phi)$ that is associated with a horizon-flow parametrization $H(\phi)$, we now see Eq. (37) as a differential equation giving the $H(\phi)$ functions associated with some potential $V(\phi)$. We shall illustrate our point on several prototypical potential examples.

In the Schwarz- Terrero-Escalante classification [28] of inflationary potentials, three categories arise depending on the time evolution of the kinetic energy density and its ratio with the total energy density during inflation. The first class is constituted by inflationary models where the kinetic energy and its ratio with the total energy density both increase. It is made of concave potentials. Models belonging to the second class are such that the kinetic energy decreases during inflation, but not its ratio with the total energy density. These models have convex potentials, and a vanishing vacuum constant ($V_{\rm min} = 0$). Finally, the third class of inflationary models has a decreasing kinetic energy and a decreasing ratio of the kinetic energy to the total energy density. Its potentials are convex but vacuum dominated ($V_{\rm min} \neq 0$), so that there is no graceful exit to inflation. The third class has been shown [16] to be now ruled out by the most recent observations and we are left with the two first ones. The first class can actually be divided into two subclasses: "hilltop inflation" for which inflation proceeds close to a local maximum of its potential, and "plateau inflation" where it proceeds along an extended flat portion of it, and where the issue of initial conditions is less acute [41].

A prototypical example of hilltop inflation is given by the quadratic "small field" potential

$$V(\phi) = M^4\left[1-\left(\frac{\phi}{\mu}\right)^2\right], \tag{77}$$

where μ is some mass scale and M^4 is an overall energy scale constant, while a common plateau potential is the one of the $f(R) \propto R + R^2$ Starobinsky model [1],

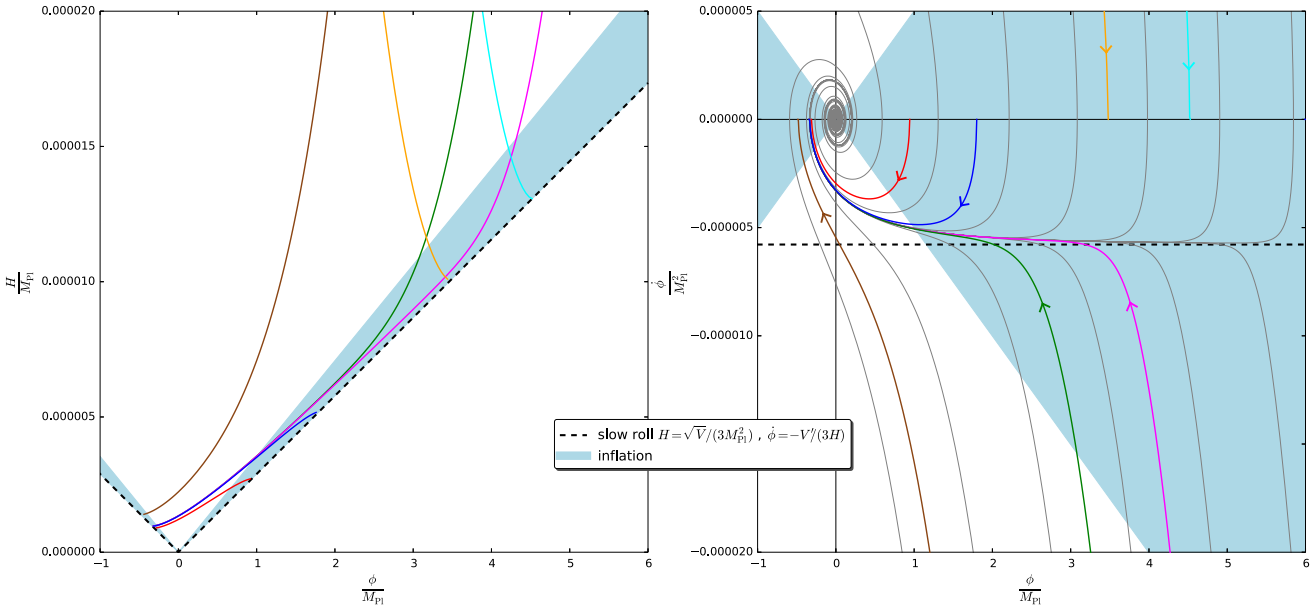

FIG. 11 (color online). Large field inflation [see Eq. (79)]. The colored lines stand for solutions of Eq. (37) for a few different initial conditions, while the black dashed line represents the slow-roll leading order solution $H^2_{\rm SR,LO} \simeq V/3M^2_{\rm Pl}$ (left panel) and $\dot\phi_{\rm SR,LO} \simeq -V'/(3H_{\rm SR,LO})$ (right panel). In the left panel are displayed the $H(\phi)$ functions, and the corresponding trajectories in phase space $(\phi, \dot\phi)$ are shown in the right panel. There, grey lines represent numerical solutions of the Klein-Gordon equation (5) for a few different initial conditions. In both panels, inflation proceeds in the blue surface, defined by $\epsilon_1 < 1$.

$$V(\phi) = M^4\left(1 - e^{-\sqrt{2/3}\phi/M_{\rm Pl}}\right)^2. \tag{78}$$

This potential also appears when inflation is driven by the Higgs field nonminimally coupled to gravity [42,43], which is naturally the case in curved space-time as produced by quantum fluctuations [44]. This is why in the following we refer to it as the "Higgs inflation" model. As a representative of the second class, which is now under observational pressure [16], we take the quadratic potential of "large field" inflation

$$V(\phi) = M^4\left(\frac{\phi}{M_{\rm Pl}}\right)^2. \tag{79}$$

The shape of these three potentials is displayed below:

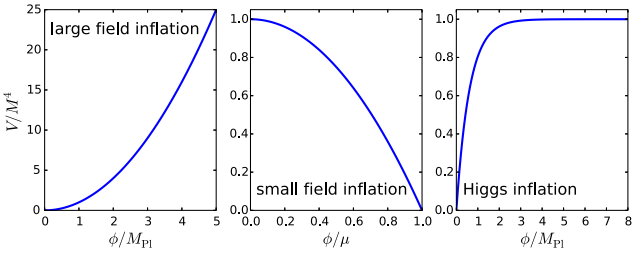

For each of these potentials, we solve Eq. (37) numerically and display a few solutions $H(\phi)$ for different initial conditions (left panels of Figs. 11, 12 and 13). The slow-roll leading order solution $H^2_{\rm SR,LO} \simeq V/(3M^2_{\rm Pl})$ is also shown, and the surface where inflation proceeds [defined by $\epsilon_1 < 1$, or equivalently in the (ϕ, H) plane, $H^2 < V/(2M^2_{\rm Pl})$] is also displayed. Let us notice that in general, the solutions $H(\phi)$ can be very different from the slow-roll expected behavior. More precisely, three kinds of solutions $H(\phi)$ are actually obtained.

1. Hubble functions of the first kind

The first kind is made of Hubble functions which vary with ϕ in the same direction as V (i.e. $H'V' > 0$), and approach the slow-roll solution at late time, i.e. when ϕ decreases for the large field model, and when ϕ increases for the small field and Higgs models. (At very late time, slow roll is violated since inflation ends, and a difference with the slow-roll lowest order solution appears). Such solutions blow up $H^2 \gg H^2_{\rm SR,LO}$ in the opposite direction, where inflation cannot proceed. Examples of this kind are the magenta, green and brown lines in Figs. 11, 12 and 13.

2. Hubble functions of the second kind

Solutions belonging to the second kind share the same properties, except that at early time they are such that $H^2_{\rm SR,LO} < H^2 < (V + \dot\phi^2_{\rm SR,LO}/2)/3M^2_{\rm Pl}$ (where $\dot\phi_{\rm SR,LO} = -V'/3H_{\rm SR,LO}$ is the slow-roll leading order trajectory), and are therefore inflating. However they are not defined in the whole range of possible values for ϕ but only in a subinterval. The blue and red lines in Figs. 11, 12 and 13 are examples of this type.

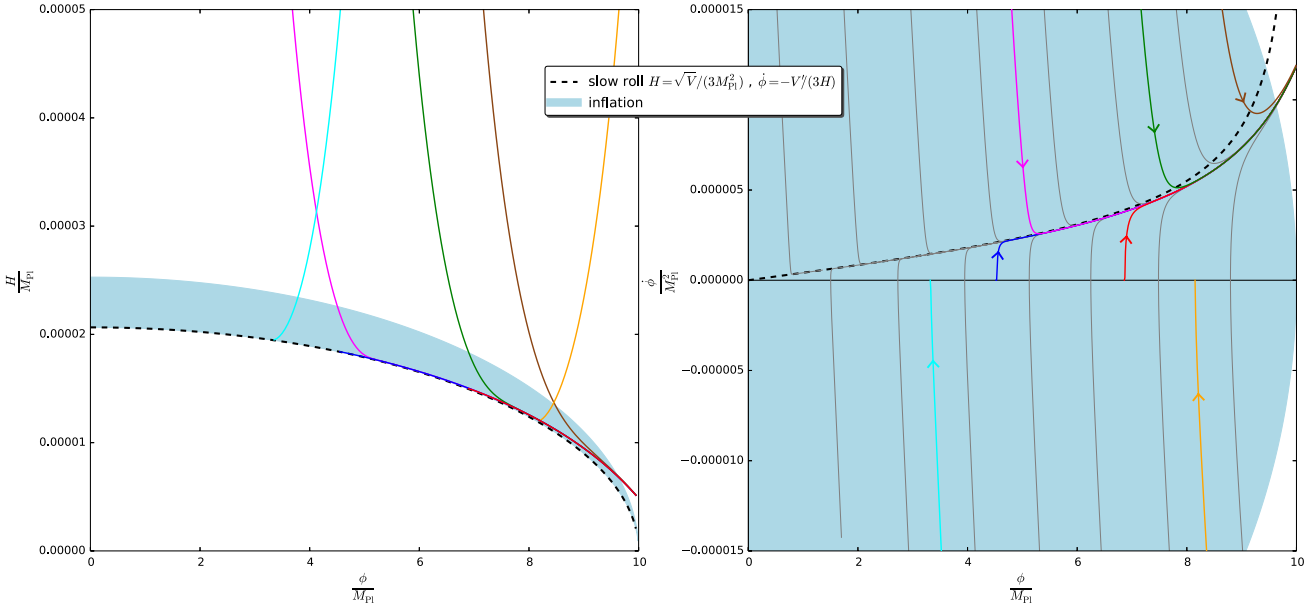

FIG. 12 (color online). Small field inflation [see Eq. (77)] for $\mu = M_{\rm Pl}$. The colored lines stand for solutions of Eq. (37) for a few different initial conditions, while the black dashed line represents the slow-roll leading order solution $H^2_{\rm SR,LO} \simeq V/3M^2_{\rm Pl}$ (left panel) and $\dot\phi_{\rm SR,LO} \simeq -V'/(3H_{\rm SR,LO})$ (right panel). In the left panel are displayed the $H(\phi)$ functions, and the corresponding trajectories in phase space $(\phi, \dot\phi)$ are shown in the right panel. There, grey lines represent numerical solutions of the Klein-Gordon equation (5) for a few different initial conditions. In both panels, inflation proceeds in the blue surface, defined by $\epsilon_1 < 1$.

3. Hubble functions of the third kind

Finally, a third kind is made of solutions which vary with ϕ in the opposite direction from V (i.e. $H'V' < 0$). At late time they approach the lower boundary limit $H^2_{\rm SR,LO}$ where they stop being defined, and they blow up at early time where inflation cannot proceed. Examples of this kind are the yellow and cyan lines in Figs. 11, 12 and 13. It is important to stress that the condition $H^2 > H^2_{\rm SR,LO}$ [so that H' is defined in Eq. (37)] implies that the functions of the second and third kind are not defined in the full range $\phi > 0$.

Let us see how this translates in terms of phase space trajectories. Once the $H(\phi)$ function is numerically integrated, the phase space trajectory is directly given by the relation (28), $\dot\phi = -2M^2_{\rm Pl}H'(\phi)$. The trajectories in phase space $(\phi, \dot\phi)$ corresponding to the $H(\phi)$ functions previously computed are displayed in the right panels of Figs. 11, 12 and 13 for the three models under study, where the same color code is adopted. The slow-roll leading order trajectory $\dot\phi_{\rm SR,LO}$ is displayed too, and the inflationary surface defined by $\epsilon_1 < 1$ [or equivalently $\dot\phi^2 < V(\phi)$ in the $(\phi, \dot\phi)$ plane] is also shown. As before, the obtained trajectories can be very different from the slow-roll one. For illustrative purposes, the Klein-Gordon equation (5) has also been numerically integrated for a few different initial conditions $(\phi_{\rm in}, \dot\phi_{\rm in})$, and the obtained solutions are also displayed. (For the large field model and the Higgs model, the inflaton field oscillates at the bottom of its potential once inflation ends, potentially giving rise to an era of parametric preheating. The oscillations can be noticed in the right panels of Figs. 11 and 13).

The three kinds of Hubble functions listed above can now be easily interpreted. The first kind actually corresponds to an initial overspeed $(\dot\phi^2 > \dot\phi^2_{\rm SR})$ that quickly gets damped to the slow-roll attractor solution (brown, green and magenta lines). On the contrary, functions of the second kind correspond to an initial underspeed $(\dot\phi^2 < \dot\phi^2_{\rm SR})$ that also quickly reaches the slow-roll attractor solution (blue and red lines). Finally, functions of the third kind are such that the initial velocity of the inflaton is of the opposite sign as the slow-roll one $(\dot\phi\dot\phi_{\rm SR} < 0)$. In these cases the inflaton initially climbs up its potential (yellow and cyan lines). It is worth stressing that what actually happens in such situations (and as confirmed by the Klein-Gordon numerical solutions) is that the speed of the inflaton decreases and vanishes at some point. Then, the inflaton rolls down its potential and joins the slow-roll attractor. However, the horizon-flow solutions are not able to reproduce these two-step behaviors. Indeed, this means that a single field value ϕ is attained several times, with different values of $\dot\phi$ (of different signs) each time, and hence different values of H. The full inflationary dynamics cannot therefore be described in terms of a single $H(\phi)$ function, and the complete behavior can only be obtained by connecting together a function of the third kind and a function of the second one. This is one of the reasons why some relevant inflationary regimes can be missed by the horizon-flow parametrization.

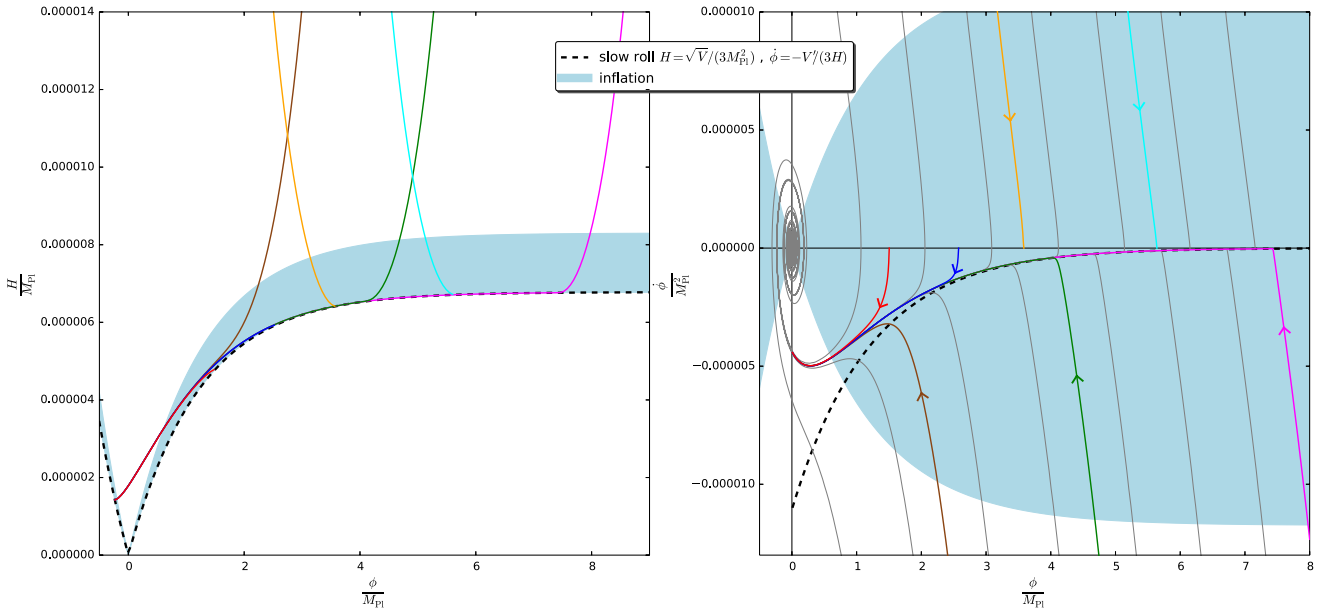

FIG. 13 (color online). Higgs inflation [see Eq. (78)]. The colored lines stand for solutions of Eq. (37) for a few different initial conditions, while the black dashed line represents the slow-roll leading order solution $H^2_{\rm SR,LO} \simeq V/3M^2_{\rm Pl}$ (left panel) and $\dot\phi_{\rm SR,LO} \simeq -V'/(3H_{\rm SR,LO})$ (right panel). In the left panel are displayed the $H(\phi)$ functions, and the corresponding trajectories in phase space $(\phi, \dot\phi)$ are shown in the right panel. There, grey lines represent numerical solutions of the Klein-Gordon equation (5) for a few different initial conditions. In both panels, inflation proceeds in the blue surface, defined by $\epsilon_1 < 1$.

B. Inflationary regimes missed by horizon flow

In order to see how these three kinds of Hubble functions are present in the model (58) of Sec. III A, $H/H_0 = 1 + ax + bx^2$, in this section we turn to the complete slow-roll analysis of this model. In particular, this reveals that, in some cases, the horizon-flow parametrization misses entire inflationary regimes. For an explicit comparison, the predictions provided by both approaches are then also computed in a reheating consistent manner.

The potential associated with the model (58) is given by Eq. (37) and reads

$$V = 3M_{\rm Pl}^2 H_0^2 \left[(1 + ax + bx^2)^2 - \frac{2}{3}(a + 2bx)^2\right], \quad (80)$$

where we define the overall normalization scale $M^4 = 3M_{\rm Pl}^2 H_0^2$. The slow-roll parameters directly follow from Eqs. (11)–(14) at leading order in slow roll, but here we do not write them down since the expressions are complicated and not very instructive.

1. Inflationary regimes

As for H, the potential is symmetrical about $x_0 = -a/(2b)$, and therefore it is only necessary to describe it in the $x > x_0$ region. Following the same logics and notations as in Sec. III A 1, let us detail the different inflationary regimes that can be supported by the potential.

(i) $b < 0$, Fig. 14

In this case the potential has a double-well shape. It vanishes at

$$x^{\pm}_{V=0} = -\frac{a}{2b} + \sqrt{\frac{a^2}{4b^2} + \frac{2}{3} - \frac{1}{b}} \pm \sqrt{\frac{2}{3}}, \quad (81)$$

so that inflation takes place either for $x_0 < x < x^{-}_{V=0}$ (where it proceeds from the left to the right) or for $x > x^{+}_{V=0}$ (where it proceeds from the right to the left). We call these two regimes (i)-a and (i)-b. The potential is minimal at

$$x_{V_{\rm min}} = -\frac{a}{2b} + \sqrt{\frac{a^2}{4b^2} + \frac{4}{3} - \frac{1}{b}}, \quad (82)$$

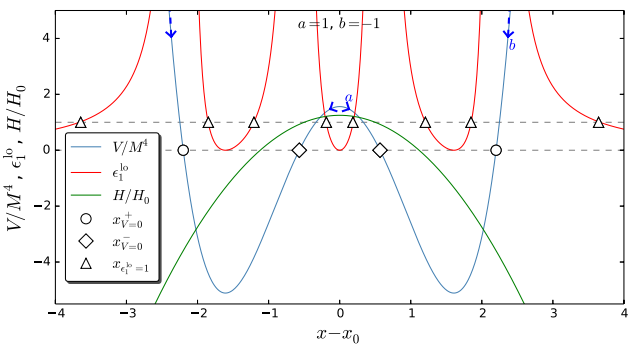

FIG. 14 (color online). Potential $V(\phi)$, first slow-roll parameter $\epsilon_1^{\rm LO}$ and $H(\phi)$ function in the case $b < 0$ ($a = 1$ and $b = -1$).

so that looking back at Eq. (59), one has $x_0 < x^-_{V=0} < x_{H=0} < x_{V_{\min}} < x^+_{V=0}$. Hence there are some values of x (namely $x^-_{V=0} < x < x_{H=0}$) where $H > 0$ whereas $V < 0$. However, one can check that $V(x^-_{\epsilon_1=1}) > 0$ [where $x^-_{\epsilon_1=1}$ is given by Eq. (63) and is the location where inflation ends in the horizon-flow setup] so that this problematic region is never probed by the horizon-flow trajectory. The equation $\epsilon_1^{\rm LO} = 1$ can be solved analytically, but the solutions are rather long expressions in a and b that we do not display because they do not add much to this discussion. What is important is that one of these solutions lies in the range $x_0 < x < x^-_{V=0}$ and another lies in the range $x > x^+_{V=0}$, so that both regimes (i)-a and (i)-b end naturally by slow-roll violation.

Finally, it is worth stressing that compared to the horizon-flow (i) case, which only accounts for the "hilltop" (i)-a regime of inflation (i.e. inflation occurs close to the maximum of its locally concave potential), the slow-roll analysis reveals the presence of another "chaotic" regime (i.e. inflation occurs at large field where the potential is convex, and has a graceful exit), case (i)-b, where the H function (58) is actually negative and therefore helpless to describe such a regime.

(ii) $b \geq 0$ and $a^2 > 4b$, Fig. 15

As far as the potential is concerned, this case is identical to the previous one (i), and two regimes of inflation are supported: a hilltop one, (ii)-a, and a chaotic one, (ii)-b. However, this time the horizon-flow case (ii) only accounts for (ii)-b, since the H function (58) is negative in the (ii)-a regime.

(iii) $b > 0$ and $a^2 = 4b$

As far as the potential is concerned, this case is not singular and can be described as part of case (iv). However the latter gets divided into several subcases for which the potential behaves differently.

(iv.1) $b > 0$ and $b - 2b^2/3 \leq a^2/4 < b$, Fig. 16

In this case the potential still has the same behavior and supports two regimes of inflation as before, (iv.1)-a (hilltop) and (iv.1)-b (chaotic), but now $H(\phi)$ is always positive. This means that contrary to case (ii), the hilltop regime (iv.1)-a can now be described in the horizon-flow setup. However, one should remember that in the corresponding horizon-flow (iv-α) regime, x decreases as inflation proceeds and approaches x_0 where an infinite number of e-folds is realized. Therefore in this case, the inflaton climbs up its potential and settles over its maximum. In this sense case (iv-α) is somewhat pathological, and actually corresponds to a Hubble function of the third kind.

(iv.2) $b > 0$ and $b - 10b^2/9 < a^2/4 < b - 2b^2/3$, Fig. 17

In this case the potential still has a double well shape but it is positive everywhere. As a consequence there are now four regimes of inflation: a hilltop regime (iv.2)-a where inflation proceeds from the left to the right close to the maximum of the potential at x_0, a vacuum dominated regime (iv.2)-b where inflation proceeds from the left to the right close the minimum of the potential at $x < x_{V_{\min}}$ and does not end by slow-roll violation, another vacuum dominated regime (iv.2)-c where inflation proceeds from the right to the left close to the minimum of the potential at

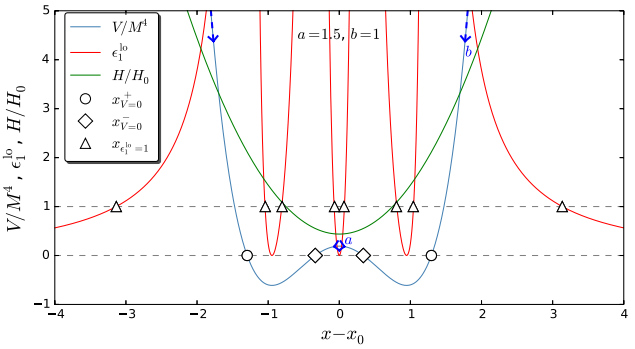

FIG. 16 (color online). Potential $V(\phi)$, first slow-roll parameter $\epsilon_1^{\rm LO}$ and $H(\phi)$ function in the case $b > 0$ and $b - 2b^2/3 \leq a^2/4 < b$ ($a = 1.5$ and $b = 1$).

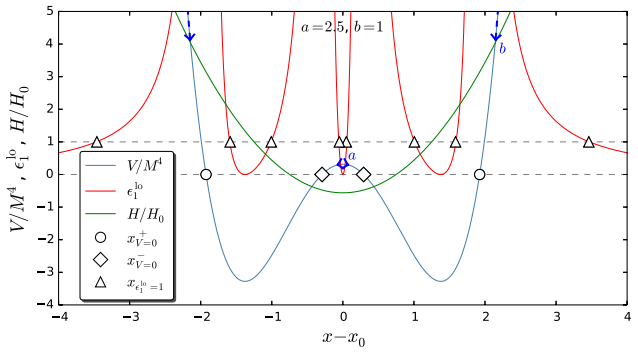

FIG. 15 (color online). Potential $V(\phi)$, first slow-roll parameter $\epsilon_1^{\rm LO}$ and $H(\phi)$ function in the case $b \geq 0$ and $a^2 > 4b$ ($a = 2.5$ and $b = 1$).

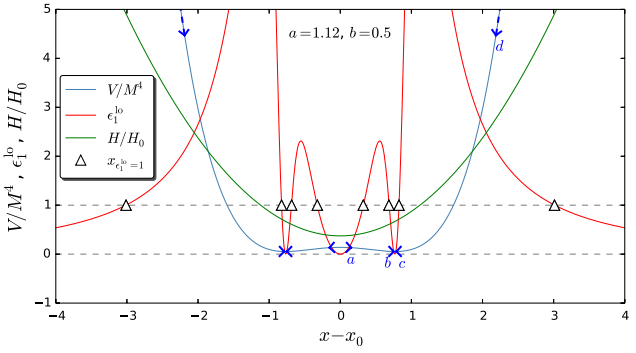

FIG. 17 (color online). Potential $V(\phi)$, first slow-roll parameter $\epsilon_1^{\rm LO}$ and $H(\phi)$ function in the case $b > 0$ and $b - 10b^2/9 < a^2/4 < b - 2b^2/3$ ($a = 1.12$ and $b = 0.5$).

$x > x_{V_{\min}}$, and a chaotic regime (iv.2)-d where inflation proceeds from the right to the left at large fields. One should note that depending on the values of a and b, it can happen that the local maximum of $\epsilon_1^{\rm LO}$ is smaller than 1, in which case (iv.2)-a and (iv.2)-b merge to form a single regime that does not end by slow-roll violation.

Let us compare these regimes to the horizon-flow ones. The regime (iv.2)-a is described by (iv-α) during which the inflaton field value decreases, and therefore climbs up its potential and settles over its maximum. The regimes (iv.2)-b and (iv.2)-c are not described at all, and (iv.2)-d corresponds to (iv-β).

(iv.3) $b > 0$ and $b - 4b^2/3 < a^2/4 < b - 10b^2/9$, Fig. 18

In this case only three regimes exist, namely (iv.3)-a (hilltop, vacuum dominated), (iv.)3-b (vacuum dominated) and (iv.3)-c (chaotic). The first slow-roll parameter ϵ_1 (the one derived from H) happens to be greater than 1 only in the increasing branch of the potential. This means that (iv.3)-a is described by (iv-α) during which the inflaton field value decreases (and again climbs up its potential and settles over its maximum), (iv.3)-b is not described by any horizon-flow regime, and (iv.3)-c is described by (iv-β).

(iv.4) $b > 0$ and $b - 2b^2 < a^2/4 < b - 4b^2/3$, Fig. 19

In this case the potential is convex everywhere. Two regimes of inflation exist, a vacuum dominated regime (iv.4)-a where inflation does not end by slow-roll violation and a chaotic regime (iv.4)-b at large fields. They respectively correspond to (iv-α) and (iv-β).

(v) $b > 0$ and $a^2/4 < b - 2b^2$, Fig. 20

In this case the potential has the same behavior as in the previous case (iv.4). The only difference is that the horizon-flow dynamics only contains a single inflationary regime [remember that in case (v) the first slow-roll parameter ϵ_1, the one derived from H, is always smaller than 1] in which inflation never ends. This corresponds to the regime (v)-a, and regime (v)-b is not described in the horizon-flow setup. However, note that for some values of a and b, the local maximum of $\epsilon_1^{\rm LO}$ is smaller than 1 and the two regimes (v)-a and (v)-b merge in a single regime where inflation does not end by slow-roll violation.

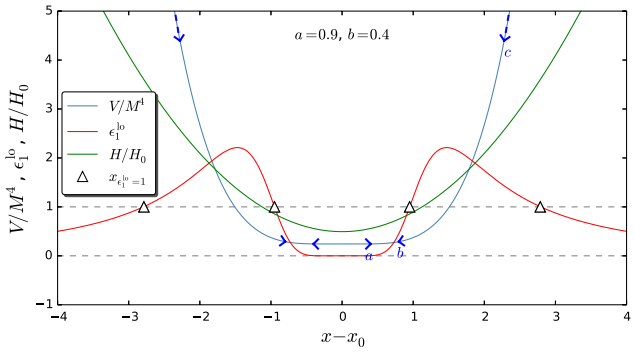

FIG. 18 (color online). Potential $V(\phi)$, first slow-roll parameter $\epsilon_1^{\rm LO}$ and $H(\phi)$ function in the case $4(b - 4b^2/3) < a^2 < 4(b - 10b^2/9)$ ($a = 0.9$ and $b = 0.4$).

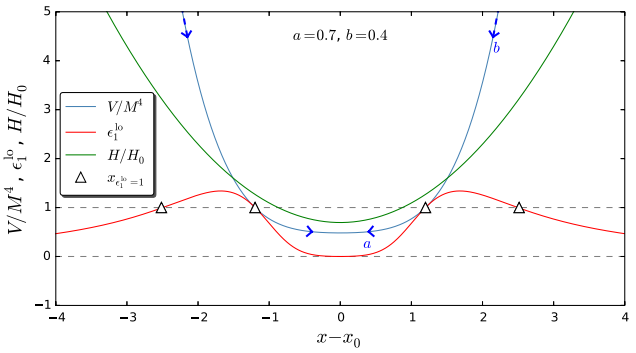

FIG. 19 (color online). Potential $V(\phi)$, first slow-roll parameter $\epsilon_1^{\rm LO}$ and $H(\phi)$ function in the case $b > 0$ and $b - 2b^2 < a^2/4 < b - 4b^2/3$ ($a = 0.7$ and $b = 0.4$).

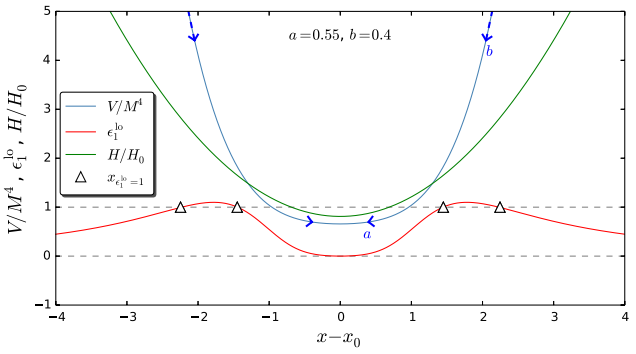

FIG. 20 (color online). Potential $V(\phi)$, first slow-roll parameter $\epsilon_1^{\rm LO}$ and $H(\phi)$ function in the case $b > 0$ and $a^2 < 4(b - 2b^2)$ ($a = 0.55$ and $b = 0.4$).

To sum up the discussion, we saw that there are some regimes which are supported by the inflationary potential but which are not described by the horizon-flow setup, namely (i)-b, (ii)-a, (iv.2)-b, (iv.2)-c, (iv.3)-b and (v)-a; and that some hilltop regimes supported by the potential are described by unnatural trajectories in horizon flow where the inflaton climbs up the potential and settles over its maximum, namely (iv-α) for (iv.1)-a, (iv-α) for (iv.2)-a, and (iv-α) for (iv.3)-a. Such trajectories correspond to Hubble functions of the third kind and are somewhat pathological. They are further studied in Sec. IV C.

2. Inflationary trajectory

For now let us move on to the slow-roll trajectory. As explained in Sec. II E, when slow roll is valid in both the slow-roll and horizon-flow setups, one needs to go up to next-to-leading order in slow roll to consistently compare both frames' predictions. The next-to-leading order slow-roll trajectory (25) can be integrated in our case, and gives rise to

$$\Delta N_*^{\mathrm{SR,NLO}} = \frac{3(a^2-4b)^2}{16b^2(3a^2-12b+16b^2)}\ln\left(\frac{a+2bx_{\mathrm{end}}}{a+2bx_*}\right) - \frac{a}{8b}(x_{\mathrm{end}}-x_*) - \frac{1}{8}(x_{\mathrm{end}}^2-x_*^2) + \frac{1}{3}\frac{3a^2-12b+8b^2}{3a^2-12b+16b^2}\ln\left(\frac{3-4b+3ax_{\mathrm{end}}+3bx_{\mathrm{end}}^2}{3-4b+3ax_*+3bx_*^2}\right) + \frac{1}{3}\ln\left[\frac{2a(3-4b)+2(3a^2+6b-8b^2)x_{\mathrm{end}}+18abx_{\mathrm{end}}^2+12b^2x_{\mathrm{end}}^3}{2a(3-4b)+2(3a^2+6b-8b^2)x_*+18abx_*^2+12b^2x_*^3}\right] - \frac{1}{3}\ln\left[\frac{3-2a^2+2a(3-4b)x_{\mathrm{end}}+(3a^2+6b-8b^2)x_{\mathrm{end}}^2+6abx_{\mathrm{end}}^3+3b^2x_{\mathrm{end}}^4}{3-2a^2+2a(3-4b)x_*+(3a^2+6b-8b^2)x_*^2+6abx_*^3+3b^2x_*^4}\right]. \quad (83)$$

Obviously, this trajectory cannot be inverted analytically and numerical methods must be used in that case.

3. Inflationary predictions

As before, the slow-roll parameters at next-to-leading order, i.e. Eqs. (21)–(24), are evaluated at the location x_* determined by numerically inverting the trajectory (83). The spectral index and tensor to scalar ratio are then given by Eqs. (26) and (27). When inflation does not end by slow-roll violation, like in Sec. III A 3 we calculate the predictions at the location of the late-time attractor which is the minimum of the potential where $\epsilon_1^{\mathrm{NLO}} = 0$ and $\epsilon_2^{\mathrm{NLO}} \neq 0$ hence $r_{16}/(1-n_{\mathrm{S}}) = 0$.

However, before proceeding with evaluating the slow-roll parameters at the Hubble exit, one must say something about the number of e-folds ΔN_*. In Sec. III the rough estimate $\Delta N_* \simeq 50$ was enough since up to the required precision, the results were not sensitive to ΔN_*. Here however, accurate predictions are needed since we want to compare slow-roll and horizon-flow predictions in the regime where slow roll is valid in both frames. The parameter ΔN_* must be set consistently with the thermal subsequent history, in particular the reheating stage. Requiring that the mean energy density during reheating $\bar{\rho}_{\mathrm{reh}}$ be lower than the energy density at the end of inflation, $\bar{\rho}_{\mathrm{reh}} < \rho_{\mathrm{end}}$, and larger than the energy density at, say, the epoch of nucleosynthesis $\bar{\rho}_{\mathrm{reh}} > \rho_{\mathrm{nucl}}$ ($\simeq$ a few MeV) leads [45] to a range of admitted values for ΔN_*. This range depends on the model under consideration and on its parameters,[7] and needs to be computed numerically. Recently the numerical library ASPIC[8] has been made public [16] and implements such a calculation. Making use of this code, the reheating consistent predictions for the model (58) can be worked out, using the horizon-flow formulas of Sec. III A on one hand and the slow-roll ones of this section on the other.

Results are displayed in Fig. 21, in the (n_{S}, r) plane, where the Planck mission observational constraints [15] are superimposed. The cases $b > 0$ and $b < 0$ are treated separately since in the horizon-flow parametrization, they correspond respectively to a chaotic regime ($b > 0$) where H is not bounded in the far past, and to a hilltop regime where inflation proceeds close to a maximum of H ($b < 0$). However, in the slow-roll setup, both regimes can be described in the two cases, and are displayed with different colors to emphasize this crucial point which has important consequences.

For example, one can see that observational constraints favor to a large extent the hilltop regimes with respect to the chaotic ones. Therefore, if, for some reason, one imposes $b > 0$, just looking at the horizon-flow parametrization would lead to the biased conclusion that the model is under pressure, whereas a hilltop slow-roll regime actually exists and solves this tension. In this sense, horizon flow may behave as a biased parametrization of inflation.

In passing, one notices that the limit $b \gg 1$ does not give exactly $r_{16}/(1-n_{\mathrm{S}}) = 1/3$, mainly because of second order terms that here are taken into account. Finally, as expected, the difference between horizon-flow and slow-roll predictions is rather small inside a given regime.

C. Horizon-flow pathological trajectories

In Sec. IV B 1 we made clear that, in the regime (iv-α), where $4(b-4b^2/3) < a^2 < 4b$, horizon flow describes inflation along trajectories where the inflaton climbs up its hilltop potential, realizing an infinite number of e-folds as it approaches the top of the hill.[9] In this case the Hubble function is of the third kind, according to the typology of Sec. IV A. We end this paper by investigating more these somewhat "pathological" trajectories.

A first interesting remark is that they generalize the ultraslow-roll (USR) scenario [46]. This model is obtained when requiring that the potential is exactly flat $V' = 0$ in the Klein-Gordon equation (5), $\ddot{\phi}/(H\dot{\phi}) = -3$, which

[7] The range of admitted values for ΔN_* also depends on the mean equation of state during reheating $\bar{w}_{\mathrm{reh}}$, which in Fig. 21 we have set to $\bar{w}_{\mathrm{reh}} = 0$. Changing its value would not modify the discussion.

[8] http://cp3.irmp.ucl.ac.be/ringeval/aspic.html.

[9] In practice, this does not happen since quantum fluctuations start to dominate the inflationary dynamics, which enters a stochastic regime that pushes it away from the potential maximum and connects it with a regular slow-roll phase.

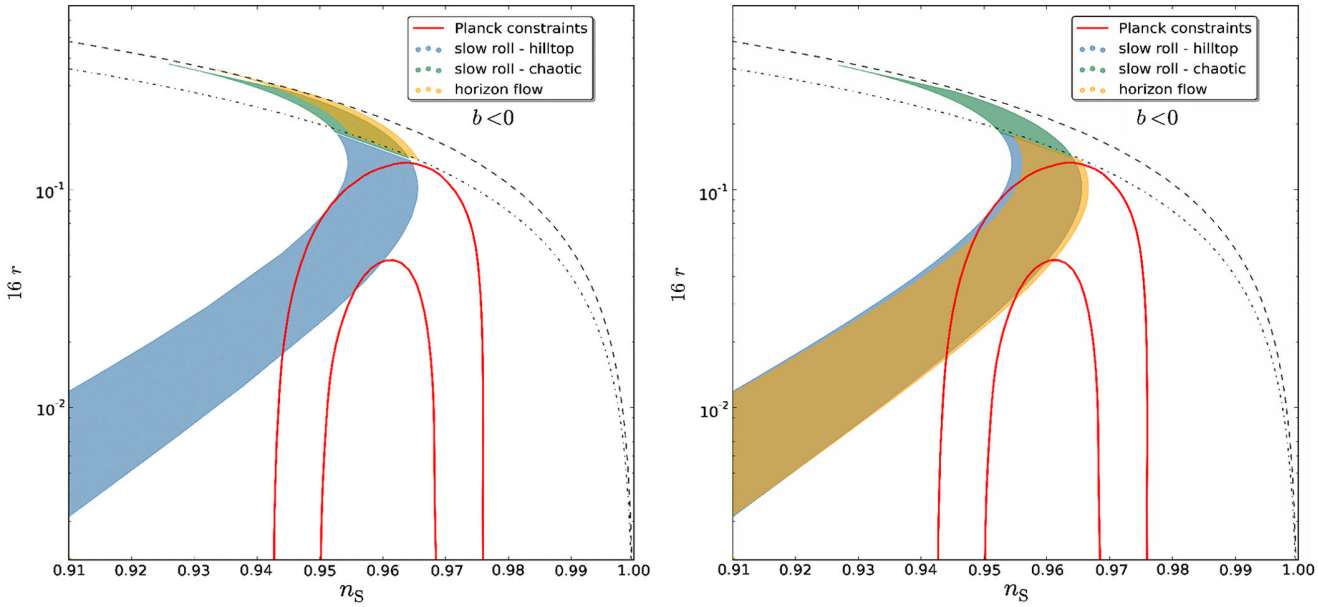

FIG. 21 (color online). Reheating consistent predictions for the model (58) in the case $b > 0$ (left panel), and $b < 0$ (right panel), making use of the horizon-flow setup (yellow area) and the slow-roll one (blue area in the hilltop regime, green area in the chaotic one), and computed at second order in slow roll. The parameters a and b are continuously varied in the ranges $|a|, |b| \in [10^{-3}, 10^{3}]$, and ΔN_* samples values such that $\rho_{\rm nuc} < \bar{\rho}_{\rm reh} < \rho_{\rm end}$ and $\bar{w}_{\rm reh} = 0$. The two red solid contours are the one- and two-sigma Planck confidence intervals (marginalized over second order in slow roll). The black dashed line stands for $r_{16}/(1 - n_{\rm S}) = 1/3$ ($b \gg 1$ limit at first order in slow roll), while the dash-dotted one is for $r_{16}/(1 - n_{\rm S}) = 1/4$ ($b \to 0$ limit at first order in slow roll). One can check that in agreement with Fig. 9, this ratio $r_{16}/(1 - n_{\rm S})$ continuously varies in the range $[0, 1/3]$.

together with Eq. (28) gives a differential equation for $H(\phi)$, namely $M_{\rm Pl}^2 H'' = 3H/2$. One of its solutions is the ultraslow-roll function

$$H_{\rm USR} = H_0 \cosh\left(\sqrt{\frac{3}{2}}\frac{\phi}{M_{\rm Pl}}\right). \tag{84}$$

One can check that Eq. (37) leads to a constant potential $V = 3M_{\rm Pl}^2 H_0^2$. In this model the inflaton field value approaches 0 and freezes out there, even if its potential is exactly flat and regardless of its initial value. The slow-roll approximation is never valid since $\epsilon_{2,\rm USR} = 6$, but the model still produces an exactly scale invariant power spectrum, while it produces sizable non-Gaussianities. However, in Ref. [47], it was shown that such a system is unstable and suffers from many physical problems among which is the difficulty to correctly normalize the amplitude of the scalar perturbations to the observed power spectrum.

The regime (iv-α) provides a generalized version of ultraslow-roll inflation in the following sense. First, in this case, slow roll is also strongly violated, since ϵ_2 approaches the nonvanishing value

$$\epsilon_2 \underset{x\to -a/(2b)}{\longrightarrow} \frac{8b}{1 - a^2/(4b)} > \epsilon_{2,\rm USR} = 6 \tag{85}$$

as the inflaton reaches the top of the hill, where the last condition comes from the fact that, as recalled above, one is working in the case where $4(b - 4b^2/3) < a^2 < 4b$. Therefore, in some sense, the situation is even worse than in the ultraslow-roll scenario. At the top of the hill $x = -a/(2b)$, inflation still proceeds since ϵ_1 vanishes, but ϵ_2 can be arbitrarily large when $a^2 \to 4b$.

The stability of the inflationary trajectory can also be studied. To do this, let us describe possible deviations from Eq. (28) in terms of the modified trajectory

$$\dot{\phi} = -2(1 - \delta) M_{\rm Pl}^2 H'. \tag{86}$$

When $\delta = 0$, one recovers the horizon-flow trajectory (28), but if a small deviation $\delta \neq 0$ is introduced, one is interested in tracking the evolution of its amplitude. First, deriving Eq. (86) with respect to time and introducing the Klein-Gordon equation (5) leads to $\dot{\delta} = [2M_{\rm Pl}^2 H''(2 + \delta) - 3H]\delta$. Now, plugging $\dot{\delta} = \delta'\dot{\phi}$, one obtains, at first order in δ, $\delta' = (3/2H/H' - 2M_{\rm Pl}^2 H''/H')\delta$, which has the generic solution

$$\delta = \delta_0 \frac{H'(\phi_0)}{H'(\phi)} \exp\left[\frac{3}{2}\int_{\phi_0}^{\phi} \frac{H(\varphi)}{H'(\varphi)} {\rm d}\varphi\right], \tag{87}$$

where $\delta_0 = \delta(\phi_0)$ is some integration constant. Now, in the model (58), as x approaches the top of the potential (and the minimum of H) $x_0 = -a/(2b)$, this gives rise to

$$\delta \propto \delta_0 \left(x + \frac{a}{2b} \right)^{\frac{3}{4}\left(\frac{1}{b}-\frac{a^2}{4b^2}\right)-1}. \tag{88}$$

The crucial point is that the exponent appearing in Eq. (88) is negative as soon as $a^2 > 4(b - 4b^2/3)$, i.e. exactly for the case (iv-α) under study, and δ blows up at the top of the potential. The horizon-flow trajectory is therefore highly unstable. As a matter of fact, if $\delta_0 \neq 0$, either ϕ crosses the maximum of its potential and a slow-roll regime possibly occurs on the other half of it ($\delta > 0$), or $\dot{\phi}$ vanishes before reaching the top of the potential and a slow-roll regime of inflation then occurs the other way down ($\delta < 0$). In any case, the instability of the horizon-flow trajectory (28) makes it very unlikely (because the initial condition δ_0 must be fine-tuned to 0 exactly).

On the contrary, one can check on the right panels of Figs. 11, 12 and 13 that the slow-roll solution is a well-behaved attractor, quickly attained from an extended basin of possible initial conditions. More precisely, if initial conditions are such that the kinetic term initially dominates the energy budget of the inflaton field, and that $\dot{\phi}^2 \gg \dot{\phi}^2_{\rm SR}$, the Klein-Gordon equation (5) in this "fast-roll" limit implies that $\dot{\phi} \propto \mathrm{e}^{-3N}$. Remembering that inflation starts when $\dot{\phi}^2 < V$, this means that the speed of the inflaton is damped to the slow-roll one within a few e-folds at most, of the order of $\ln |M_{\rm Pl} V'/V|/3$. This is another reason why the slow-roll setup should be preferred.

V. CONCLUSION

The wide variety of inflationary models makes it tempting to look for model independent approaches for constraining inflationary physics. The horizon-flow strategy has been proposed with exactly this purpose. In this framework generic predictions for the theory of inflation driven by a canonical scalar field have been searched for, and potential reconstruction issues have been investigated.

The present work showed that the horizon-flow method suffers from a number of flaws, rendering it a somewhat misleading parametrization of inflation.

First, it implicitly relies on phenomenological potentials with no physical justification. Furthermore, instead of choosing priors on potential parameters (which usually stand for physical quantities such as charges, masses, coupling constants, etc.), it samples models from priors defined on unphysical quantities corresponding to initial values of flow parameters.

Second, we have shown that the "typical" predictions stemming from this parametrization that have been noticed in the literature are actually originating from this choice of specific potentials. They can be accounted for analytically going beyond the common fixed point analysis of the problem, and we elucidated the mismatch between the results of this fixed point approach and what was actually numerically obtained by the horizon-flow algorithm. Actually, these predictions turn out to be in direct correspondence with the different regimes of inflation supported by the model. This is why they are not generic features of inflation itself, and explicit examples where they are violated have been provided.

Third, horizon flow implicitly relies on a specific trajectory in phase space among all the solutions of the Klein-Gordon equation associated with the potential it selects. This trajectory is different from the slow-roll one, the later yet being known as a well-behaved attractor of inflationary dynamics. At first sight, this only leads to slow-roll suppressed discrepancies in the predictions between both frames, which we have computed. More importantly however, we have found that for a given potential, entire regimes of inflation are missed by the horizon-flow approach, which therefore introduces a bias in the analysis. Interestingly enough, in these missed regimes, the horizon-flow trajectory can be highly unstable (corresponding to an inflaton climbing up its potential and asymptotically approaching its local maximum), and provides a generalized and worsened version of ultraslow-roll inflation.

For these reasons, we conclude that even if convenient, studying inflation along the lines of the horizon-flow program can lead to biased or even inexact results.

ACKNOWLEDGMENTS

I would like to warmly thank J. Martin, P. Peter and C. Ringeval for careful reading of the manuscript and very useful comments.

[1] A. A. Starobinsky, Phys. Lett. **91B**, 99 (1980).
[2] A. H. Guth, Phys. Rev. D **23**, 347 (1981).
[3] A. D. Linde, Phys. Lett. **108B**, 389 (1982).
[4] A. Albrecht and P. J. Steinhardt, Phys. Rev. Lett. **48**, 1220 (1982).
[5] A. D. Linde, Phys. Lett. **129B**, 177 (1983).
[6] V. F. Mukhanov and G. Chibisov, JETP Lett. **33**, 532 (1981).
[7] V. F. Mukhanov and G. Chibisov, Sov. Phys. JETP **56**, 258 (1982).
[8] A. A. Starobinsky, Phys. Lett. **117B**, 175 (1982).
[9] A. H. Guth and S. Y. Pi, Phys. Rev. Lett. **49**, 1110 (1982).
[10] S. Hawking, Phys. Lett. **115B**, 295 (1982), revised version.
[11] J. M. Bardeen, P. J. Steinhardt, and M. S. Turner, Phys. Rev. D **28**, 679 (1983).
[12] Z. Hou, C. Reichardt, K. Story, B. Follin, R. Keisler *et al.*, Astrophys. J. **782**, 74 (2014).
[13] J. L. Sievers, R. A. Hlozek, M. R. Nolta, V. Acquaviva, G. E. Addison *et al.*, J. Cosmol. Astropart. Phys. 10 (2013) 060.

[14] G. Hinshaw *et al.* (WMAP Collaboration), Astrophys. J. Suppl. Ser. **208**, 19 (2013).
[15] P. Ade *et al.* (Planck Collaboration), arXiv:1303.5082.
[16] J. Martin, C. Ringeval, and V. Vennin, arXiv:1303.3787.
[17] J. Martin, C. Ringeval, R. Trotta, and V. Vennin, arXiv:1312.3529.
[18] M. B. Hoffman and M. S. Turner, Phys. Rev. D **64**, 023506 (2001).
[19] W. H. Kinney, Phys. Rev. D **66**, 083508 (2002).
[20] A. R. Liddle, Phys. Rev. D **68**, 103504 (2003).
[21] E. Ramirez and A. R. Liddle, Phys. Rev. D **71**, 123510 (2005).
[22] S. Chongchitnan and G. Efstathiou, Phys. Rev. D **72**, 083520 (2005).
[23] J. M. Bardeen, Phys. Rev. D **22**, 1882 (1980).
[24] P. Peter and J.-P. Uzan, *Primordial Cosmology* (Oxford University Press, UK, 2009).
[25] H. Kodama and M. Sasaki, Prog. Theor. Phys. Suppl. **78**, 1 (1984).
[26] V. F. Mukhanov, H. Feldman, and R. H. Brandenberger, Phys. Rep. **215**, 203 (1992).
[27] D. J. Schwarz, C. A. Terrero-Escalante, and A. A. Garcia, Phys. Lett. B **517**, 243 (2001).
[28] D. J. Schwarz and C. A. Terrero-Escalante, J. Cosmol. Astropart. Phys. 08 (2004) 003.
[29] G. N. Remmen and S. M. Carroll, Phys. Rev. D **88**, 083518 (2013).
[30] J.-O. Gong and E. D. Stewart, Phys. Lett. B **510**, 1 (2001).
[31] J. Martin, C. Ringeval, and V. Vennin, J. Cosmol. Astropart. Phys. 06 (2013) 021.
[32] A. R. Liddle, P. Parsons, and J. D. Barrow, Phys. Rev. D **50**, 7222 (1994).
[33] R. Easther and W. H. Kinney, Phys. Rev. D **67**, 043511 (2003).
[34] H. Peiris *et al.* (WMAP Collaboration), Astrophys. J. Suppl. Ser. **148**, 213 (2003).
[35] W. H. Kinney, E. W. Kolb, A. Melchiorri, and A. Riotto, Phys. Rev. D **69**, 103516 (2004).
[36] C.-Y. Chen, B. Feng, X.-L. Wang, and Z.-Y. Yang, Classical Quantum Gravity **21**, 3223 (2004).
[37] B. A. Powell and W. H. Kinney, J. Cosmol. Astropart. Phys. 08 (2007) 006.
[38] B. A. Powell, K. Tzirakis, and W. H. Kinney, J. Cosmol. Astropart. Phys. 04 (2009) 019.
[39] C. R. Contaldi and J. S. Horner, arXiv:1312.6067.
[40] R. Corless, G. Gonnet, D. Hare, D. Jeffrey, and D. Knuth, Adv. Comput. Math. **5**, 329 (1996).
[41] A. Ijjas, P. J. Steinhardt, and A. Loeb, Phys. Lett. B **723**, 261 (2013).
[42] F. Bezrukov and M. Shaposhnikov, Phys. Lett. B **659**, 703 (2008).
[43] J. Garcia-Bellido, J. Rubio, M. Shaposhnikov, and D. Zenhausern, Phys. Rev. D **84**, 123504 (2011).
[44] N. Birrell and P. Davies, *Quantum Fields in Curved Space* (Cambridge Monographs on Mathematical Physics, Cambridge, 1982).
[45] J. Martin and C. Ringeval, Phys. Rev. D **82**, 023511 (2010).
[46] W. H. Kinney, Phys. Rev. D **72**, 023515 (2005).
[47] J. Martin, H. Motohashi, and T. Suyama, Phys. Rev. D **87**, 023514 (2013).

Encyclopædia Inflationaris

Jérôme Martin,[a] **Christophe Ringeval**[b] **and Vincent Vennin**[a]

[a]Institut d'Astrophysique de Paris, UMR 7095-CNRS, Université Pierre et Marie Curie, 98bis boulevard Arago, 75014 Paris (France)

[b]Centre for Cosmology, Particle Physics and Phenomenology, Institute of Mathematics and Physics, Louvain University, 2 Chemin du Cyclotron, 1348 Louvain-la-Neuve (Belgium)

E-mail: jmartin@iap.fr, christophe.ringeval@uclouvain.be, vennin@iap.fr

Abstract. The current flow of high accuracy astrophysical data, among which are the Cosmic Microwave Background (CMB) measurements by the Planck satellite, offers an unprecedented opportunity to constrain the inflationary theory. This is however a challenging project given the size of the inflationary landscape which contains hundreds of different scenarios. Given that there is currently no observational evidence for primordial non-Gaussianities, isocurvature perturbations or any other non-minimal extension of the inflationary paradigm, a reasonable approach is to consider the simplest models first, namely the slow-roll single field models with minimal kinetic terms. This still leaves us with a very populated landscape, the exploration of which requires new and efficient strategies. It has been customary to tackle this problem by means of approximate model independent methods while a more ambitious alternative is to study the inflationary scenarios one by one. We have developed the new publicly available runtime library `ASPIC`[1] to implement this last approach. The `ASPIC` code provides all routines needed to quickly derive reheating consistent observable predictions within this class of scenarios. `ASPIC` has been designed as an evolutive code which presently supports 74 different models, a number that may be compared with three or four representing the present state of the art. In this paper, for each of the `ASPIC` models, we present and collect new results in a systematic manner, thereby constituting the first *Encyclopædia Inflationaris*. Finally, we discuss how this procedure and `ASPIC` could be used to determine the best model of inflation by means of Bayesian inference.

Keywords: Cosmic Inflation, Slow-Roll, Reheating, Cosmic Microwave Background, Aspic

ArXiv ePrint: 1303.3787

[1] http://cp3.irmp.ucl.ac.be/~ringeval/aspic.html

Contents

1 Introduction

The theory of inflation [1–4] represents a cornerstone of the standard model of modern cosmology (the "hot Big-Bang model" of Lemaître and Friedmann) [5–8]. By definition, it is a phase of accelerated expansion which is supposed to take place in the very early universe, at very high energy (between 200 and 10^{15} GeV). Inflation allows us to understand several puzzles that plagued the pre-inflationary standard model (before 1981) and that could not be understood otherwise. Without inflation, the standard model of cosmology

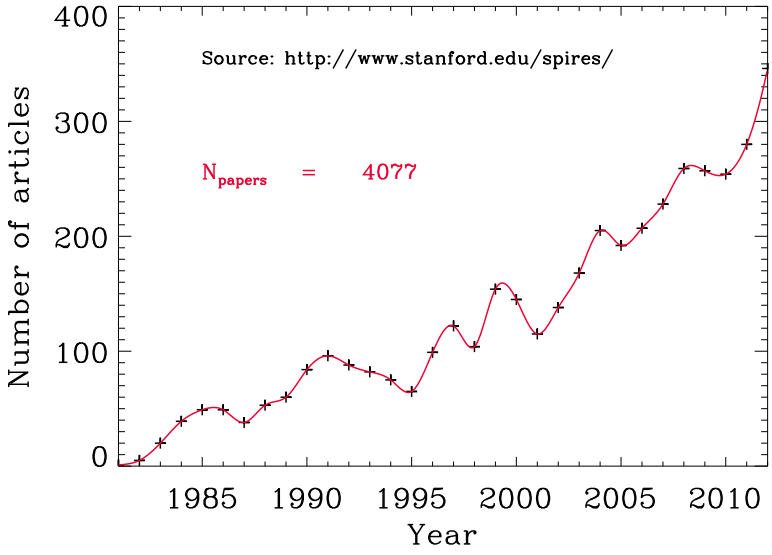

Figure 1. Number of articles containing the word "inflation" and its variations (i.e. "inflating", "inflationary", etc ...) in its title published each year since the advent of inflation. The total number is estimated to be 4077 papers.

would remain incomplete and highly unsatisfactory. The most spectacular achievement of inflation is that, combined with quantum mechanics, it provides a convincing mechanism for the origin of the cosmological fluctuations (the seeds of the galaxies and of the Cosmic Microwave Background - CMB - anisotropies) and predicts that their spectrum should be almost scale invariant (i.e. equal power on all spatial scales) [9–17] which is fully consistent with the observations. Let us notice in passing that this part of the scenario is particularly remarkable since it combines General Relativity and Quantum Mechanics [7, 8, 18–24]. Given all these spectacular successes and given the fact that, despite many efforts, inflation has not been superseded by its various challengers [25–53], this scenario has gradually become a crucial part of modern cosmology. As can be seen in Fig. 1, the number of papers devoted to this topic and published each year is inflating since the advent of inflation.

In order to produce a phase of inflation within General Relativity, the matter content of the universe has to be dominated by a fluid with negative pressure. At very high energy, the correct description of matter is field theory, the prototypical example being a scalar field since it is compatible with the symmetries implied by the cosmological principle. Quite remarkably, if the potential of this scalar field is sufficiently flat (in fact, more precisely, its logarithm) so that the field moves slowly, then the corresponding pressure is negative. This is why it is believed that inflation is driven by one (or several) scalar field(s). For obvious reasons, this scalar field was given the name "inflaton". However, the physical nature of the inflaton and its relation with the standard model of particle physics and its extensions remain elusive. Moreover the shape of its potential is not known except that it must be sufficiently flat. This is not so surprising since, as mentioned above, the inflationary mechanism is supposed to take place at very high energies in a regime where particle physics is not known and has not been tested in accelerators.

Another crucial aspect of the inflationary scenario is how it ends and how it is connected to the subsequent hot Big-Bang phase. It is believed that, after the slow-roll period, the field oscillates at the bottom of its potential, or undergoes tachyonic preheating, but finally decays into radiation. In this way, inflation is smoothly connected to the radiation-dominated epoch [54–63]. Unfortunately, very little is observationally known on this so-called reheating period. Let us stress that adiabatic initial conditions, as favored from the current CMB measurements, naturally stem from such a setup within single field models. Another constraint is that the reheating temperature, $T_{\rm reh}$, must be higher than the nucleosynthesis scale (i.e. a few MeV). If, however, one restricts oneself to specific models, then one can obtain better bounds on $T_{\rm reh}$, as was recently shown for the first time in Ref. [64]. But, so far, these constraints concern a few models only.

We see that, despite the fact that it has become a cornerstone, the inflationary era is not as observationally known as the other parts of the standard model of Cosmology. However, there is now a flow of increasingly accurate astrophysical data which gives us a unique opportunity to learn more about inflation. In particular, the recently released Planck satellite data [65, 66] play a crucial role in this process. The mission complements and improves upon observations made by the NASA WMAP satellite [67, 68] and is a major source of information relevant to several cosmological issues including inflation [69, 70]. But the flow of new data does not only concern the CMB. The Supernovae projects [71–74] continue to measure the distances to the nearby exploding SN1A stars while the large scale galaxy surveys such as the Sloan Digital Sky Survey (SDSS) [75, 76] are providing an unprecedented picture of the structure of the universe. SDSS is planned till 2014 and has recently provided the measure of the so-called Baryonic Acoustic Oscillations (BAO). They are the red-shifted version of the acoustic oscillations observed in the CMB anisotropies which have been transferred to the galaxy power spectrum. The "level arm" in length scales between CMB and galaxy power spectra increases the sensitivity to the small deviations from scale invariance, and thus should be extremely powerful to constrain inflationary models. For this reason, the future Euclide satellite will be another step forward in our understanding of inflation [77]. Let us also mention the possibility of direct detection of the primordial gravitational waves for high energy inflationary models [78–84]. The CMB small angular scales of Planck are already complemented by ground-based microwave telescopes such as the Atacama Cosmology Telescope (ACT) [85, 86] or the South Pole Telescope (SPT) [87, 88] while ultra-sensitive polarization dedicated experiments are on their way [89, 90]. In a foreseeable future, the last bit of yet unexplored length scales are expected to be unveiled by the 21cm cosmological telescopes. These ones will be sensitive to the red-shifted 21cm line absorbed by hydrogen clouds before the formation of galaxies [91–97]. With such data, we will have a complete tomography of the universe history from the time of CMB emission at the surface of last scattering to the distribution of galaxies today.

The main goal of this article is to develop methods that will allow us to constrain the inflationary scenario at a level matching the accuracy of these new data. Since we have now entered the era of massive multi-data analysis, the project aims at a change of scale compared to previous approaches. In particular, one way to deal with this question is to perform systematic and "industrial" studies of this issue. Our ability to see through the inflationary window turns the early universe into a laboratory for ultra-high energy physics, at scales entirely inaccessible to conventional experimentation. In other words, this window offers a unique opportunity to learn about the very early universe and about physics in a regime that cannot be tested otherwise, even in accelerators such as the Large Hadron

Collider (LHC).

1.1 Methodology

Let us now discuss how, in practice, the above described goals can be reached. One issue often raised is that, since there are (literally) a few hundreds different scenarios, it is difficult to falsify inflation. This is, however, not a very convincing argument since different models belong to different classes and usually do differ in their observable predictions. They can thus be observationally distinguished. A natural way to proceed is therefore to test inflationary models step by step, starting with the simplest scenarios. This is consistent with the Occam's razor point of view and the way inference is achieved within Bayesian statistics (see below). With this in mind, we can classify models in three different broad categories: single-field inflation (category I), multiple-field inflation (category II) and models where matter is not described by a scalar field as, for instance, vector inflation [98], chromo-natural inflation [99] and/or gauge-flation [100–102] (category III). Within each category, one could further identify various sub-categories. For example, within category I, the scalar field can possess a minimal kinetic term and a smooth potential (category IA), a minimal kinetic term and a potential with features (category IB), a non-minimal kinetic term with a smooth potential (category IC) or a non-minimal kinetic term and a potential with features (category ID, see for instance Ref. [103]) (a fifth category could be models of warm inflation [104–107]). The same four sub-categories can also be defined within category II [for instance, multiple Dirac Born Infeld (DBI) field inflation [108–110] belongs to category IIC] and so on. As already mentioned, each category leads to different predictions. For instance, all models of category IA predict a negligible level of non-Gaussianities [111–115] while, on the contrary, models of categories IB-ID yield non-negligible non-Gaussianities [116–130]; models belonging to IB and to IC, or II, may not predict exactly the same type of non-Gaussianities [131, 132], etc ... In this context, as already mentioned, a crucial step was the recent release of the Planck data [66, 70, 133, 134]. Together with the polarization data from WMAP, they are compatible with a negligible running $\mathrm{d}n_{\mathrm{S}}/\mathrm{d}\ln k = -0.0134 \pm 0.009$ and a negligible running of the running $\mathrm{d}^2 n_{\mathrm{S}}/\mathrm{d}\ln^2 k = 0.02 \pm 0.016$, with a pivot scale chosen at $k_* = 0.05\,\mathrm{Mpc}^{-1}$. These data are also compatible with adiabaticity at 95% CL such that there is no evidence for isocurvature modes, although the analysis is done with one isocurvature mode at a time only. The Planck data do not find evidence for primordial non-Gaussianity, namely Ref. [70] reports $f_{\mathrm{NL}}^{\mathrm{loc}} = 2.7 \pm 5.8$, $f_{\mathrm{NL}}^{\mathrm{eq}} = -42 \pm 75$ and $f_{\mathrm{NL}}^{\mathrm{ortho}} = -25 \pm 39$. Therefore, at this stage, everything seems to be well described by simplest scenarios of inflation and, as consequence, a reasonable method is to start with the IA-models. Following category IA, if the present observational situation evolves in the future, one should then treat categories IB-ID, then category II and so on. In this way, one can falsify inflation step by step, in a Bayesian motivated fashion.

Bayesian inference for inflation requires some cosmological data that are sensitive to it, such as the ones enumerated above. For the purpose of illustration, let us consider the CMB angular power spectrum. Cosmological measurements give us a set of numbers, C_ℓ^{meas}, that we are able to calculate theoretically within an inflationary model. This means that we know the functions $C_\ell^{\mathrm{th}} \equiv C_\ell^{\mathrm{th}}(\theta_{\mathrm{stand}}, \theta_{\mathrm{inf}})$, where θ_{stand} represents a set of parameters describing post-inflationary physics, i.e. $\theta_{\mathrm{stand}} = (h, \Omega_\Lambda, \Omega_{\mathrm{dm}}, \cdots)$ and θ_{inf} a set of parameters describing inflationary physics. We are interested in constraining the values of those parameters, especially the θ_{inf}'s. Within a given experiment, one is given a likelihood, or an effective chi-squared $\chi^2\left(\theta_{\mathrm{stand}}, \theta_{\mathrm{inf}}\right)$, encoding all the underlying uncertainties. In a frequentist approach, the searched values of θ_{stand} and θ_{inf} would be chosen at the best fit, i.e. those verifying

$\partial\chi^2/\partial\theta = 0$. In a Bayesian approach [135], we are interested in determining the posterior distributions of the parameters, using Bayes's theorem

$$P\left(\theta_{\rm stand}, \theta_{\rm inf}|C_\ell^{\rm meas}\right) = \frac{1}{\mathcal{N}}\mathcal{L}\left(C_\ell^{\rm meas}|\theta_{\rm stand}, \theta_{\rm inf}\right)\pi\left(\theta_{\rm stand}, \theta_{\rm inf}\right), \tag{1.1}$$

where $\mathcal{L}\left(C_\ell^{\rm meas}|\theta_{\rm stand}, \theta_{\rm inf}\right) = e^{-\chi^2(\theta_{\rm stand}, \theta_{\rm inf})/2}$ is the likelihood function, $\pi\left(\theta_{\rm stand}, \theta_{\rm inf}\right)$ the prior distribution, describing our prejudices about the values of the parameters before our information is updated, and $\mathcal{N}$ a normalization factor, also called Bayesian evidence. Because we are interested in the inflationary parameters, one has to integrate over the post-inflationary parameters in order to obtain the marginalized probability distribution $P\left(\theta_{\rm inf}|C_\ell^{\rm meas}\right) = \int P\left(\theta_{\rm stand}, \theta_{\rm inf}|C_\ell^{\rm meas}\right) {\rm d}\theta_{\rm stand}$. CMB physics also tells us that the multipole moment $C_\ell^{\rm th}$ can be written as

$$C_\ell^{\rm th}\left(\theta_{\rm stand}, \theta_{\rm inf}\right) = \int_0^{+\infty} \frac{{\rm d}k}{k} j_\ell(kr_{\ell{\rm ss}}) T(k; \theta_{\rm stand}) \mathcal{P}_\zeta(k; \theta_{\rm inf}), \tag{1.2}$$

where j_ℓ is a spherical Bessel function, $T(k; \theta_{\rm stand})$ is the transfer function which describes the evolution of cosmological perturbations during the standard Friedmann-Lemaître eras and $\mathcal{P}_\zeta$ is the inflationary power spectrum. As a result, the process of constraining inflation from the $C_\ell^{\rm meas}$ reduces to the calculation of $\mathcal{P}_\zeta$. The same lines of reasoning could be generalized to any other cosmological observables sourced during inflation, such as higher order correlation functions.

At this stage, there are, a priori, two possibilities (it is also worth noticing that yet another approach is the reconstruction program [136, 137]). Either one uses a model-independent, necessarily approximate, shape for $\mathcal{P}_\zeta$ or, on the contrary, one scans the inflationary landscape, model by model, and for each of them, calculates $\mathcal{P}_\zeta$ exactly.

The advantage of working with a model-independent technique is obvious. However, it often requires an approximation scheme that may not be available for all models. In practice, an approximate method, the slow-roll approach, is known for the category IA and for the category IC, see the recent papers [138–143]. In this case, the set of inflationary parameters $\theta_{\rm inf}$ becomes the Hubble flow functions: $\theta_{\rm inf} = \{\epsilon_n\}$ where the ϵ_n are defined in Eq. (2.3) and the corresponding expression of $\mathcal{P}_\zeta(k; \epsilon_n)$ is provided in Eqs. (2.18), (2.20), (2.21) and (2.22). Assuming some priors $\pi(\epsilon_n)$ on the Hubble flow functions, this method yields the posterior distributions $P\left(\epsilon_n|C_\ell^{\rm meas}\right)$ for the Hubble flow functions evaluated at the pivot scale. This approach has already been successfully implemented for the WMAP data in Refs. [64, 144–147].

The second approach is more ambitious. It consists in treating exactly all the inflationary models that have been proposed so far and in a systematic manner. For each model, the power spectrum is determined exactly by means of a mode by mode numerical integration, for instance using the `FieldInf` code[1]. Such an approach can also be used with the higher correlation functions with, for instance, the recent release of the `BINGO` code calculating the inflationary bispectrum [148].

In this case, the set of parameters $\theta_{\rm inf}$ differs according to the model considered. For instance, Large Field Inflation (LFI) for which $V(\phi) = M^4\left(\phi/M_{\rm Pl}\right)^p$, has $\theta_{\rm inf} = (M, p)$ while Small Field Inflation (SFI) with $V(\phi) = M^4\left[1 - (\phi/\mu)^p\right]$ has $\theta_{\rm inf} = (M, p, \mu)$. From `FieldInf` one can then compute $\mathcal{P}_\zeta(k; M, p)$ for LFI and $\mathcal{P}_\zeta(k; M, p, \mu)$ for SFI without any

[1] See http://theory.physics.unige.ch/~ringeval/fieldinf.html.

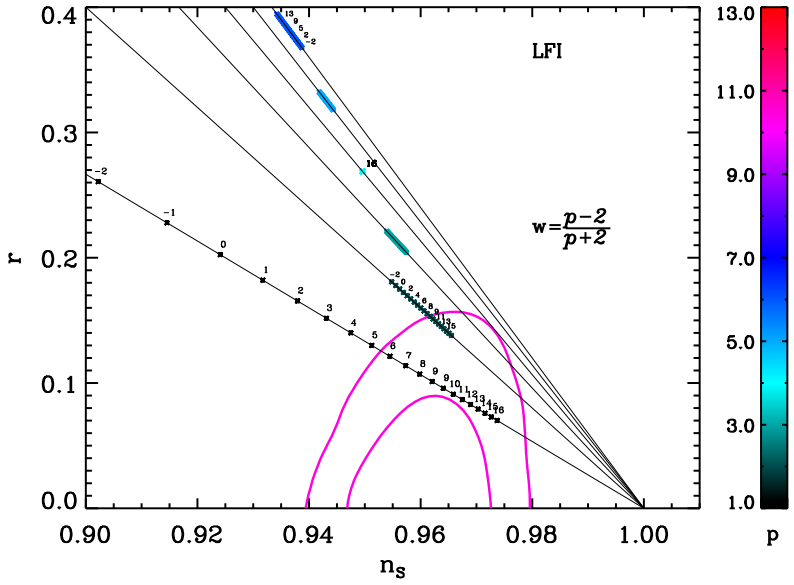

Figure 2. Observational predictions for the LFI models, $V(\phi) \propto \phi^p$, in the plane $(n_{\rm S}, r)$ (i.e. scalar spectral index and gravity wave contribution) compared to the Planck data [66, 69, 70, 133, 134, 153]. Each continuous line and each color represent a different value of p. Along each line, each point (i.e. each small "cross") denotes a different reheating temperature compatible with the constraint $\rho_{\rm end} > \rho_{\rm reh} > \rho_{\rm nuc}$ (the annotations give the logarithm of the reheating temperature in GeV). We see that the details of the reheating stage now matter: along a given line, some reheating temperatures are compatible with the observational constraints while others are not. This means that the CMB observations can now put constraints on $T_{\rm reh}$.

other assumptions than linear perturbation theory and General Relativity. Starting from some priors on the model parameters, e.g. in the case of LFI, $\pi(M, p)$, this method allows us to determine the posterior distributions $P(M|C_\ell^{\rm meas})$ and $P(p|C_\ell^{\rm meas})$, thereby providing parameter inference about the corresponding inflationary model. This approach, which was successfully implemented for the first time in Refs. [145, 149–151], and subsequently used in Ref. [152], has several advantages that we now discuss.

Firstly, the most obvious advantage is that the result is exact. The slow-roll method is an approximation and, for this reason, remains somehow limited. As mentioned before, there are plethora of models, such as single field models with features or multiple field scenarios, for which a numerical integration is mandatory.

A second reason is that a full numerical approach permits a new treatment of reheating. In the standard approach, the influence of the reheating is only marginally taken into account. Any observable predictions depend on the number of e-folds associated with a reheating era. From the fact that the reheating must proceed after the end of inflation and before the electroweak scale, one can put an order of magnitude bound on this number of e-folds [154]. This causes small uncertainties in the inflationary predictions that were not crucial in the past. However, with the accuracy of the present and future data this question now matters. This is illustrated in Fig. 2 which represents the slow-roll predictions of LFI for which $V(\phi) \propto \phi^p$. Each colored segment represents the range of observable predictions for a given value of

p, each point within a segment corresponding to a given number of e-folds for the reheating or, equivalently, to a given reheating temperature $T_{\rm reh}$. We see that, for relatively small values of p, it is necessary to know the number of e-folds the Universe reheated to decide whether the model is compatible with the data or not. Conversely, the data are becoming so accurate that one can start constraining the reheating epoch. Therefore, instead of viewing the reheating parameters as external source of uncertainties, it is more accurate to include them in the numerical approach and consider they are part of the inflationary model. In its simplest description, the reheating epoch can be modeled as a cosmological fluid with a mean equation of state $\overline{w}_{\rm reh} > -1/3$. For a simple quadratic potential, and a parametric reheating, one would have for instance $\overline{w}_{\rm reh} = 0$. In this way, both $\overline{w}_{\rm reh}$ and $T_{\rm reh}$ are added to the inflationary parameters, e.g. we now have $\theta_{\rm inf} = (M, p, T_{\rm reh}, \overline{w}_{\rm reh})$ for LFI, and `FieldInf` computes $\mathcal{P}_\zeta(k; M, p, T_{\rm reh}, \overline{w}_{\rm reh})$. Starting from some priors $\pi(T_{\rm reh}, \overline{w}_{\rm reh})$ one can then obtain the corresponding posterior distributions $P\left(T_{\rm reh}|C_\ell^{\rm meas}\right)$ and $P\left(\overline{w}_{\rm reh}|C_\ell^{\rm meas}\right)$. The feasibility of this method has already been demonstrated in Refs. [64, 145] where constraints on the reheating temperature for LFI and SFI have been derived for the first time (see also Ref. [155]). In view of the expected accuracy of the future data, the preheating/reheating era should become a compulsory element of inflationary model testing. This issue plays an important role in the proposal put forward in this article. In addition, let us also emphasize that a proper treatment of the reheating and preheating stages is mandatory in multiple field inflation because they can affect the evolution of $\mathcal{P}_\zeta$ on large scales. Only a numerical approach can presently deal with this problem.

A third advantage of the numerical approach is to address the question of the priors choice in a particularly well-defined way. A crucial aspect of Bayesian statistics is that the result depends on the choice of the priors. Therefore, these ones must be chosen and discussed carefully. In the slow-roll (approximated) approach described before, the priors are chosen on the slow-roll parameters themselves. For instance, a Jeffreys' prior is typically chosen on ϵ_1 (i.e. uniform prior on $\log \epsilon_1$), as appropriate when the order of magnitude of a parameter is not known. However, from a physical point of view, it is better to choose the priors directly on the parameters of the model, e.g. the parameters entering the potential. For instance, several potentials that we will treat are the results of a one-loop calculation, namely a perturbative calculation with the coupling constant playing the role of the small parameter. It is clear that the prior must encode the fact that this parameter is small. With the numerical approach, this is very conveniently done since we directly compute the power spectrum from the potential itself. As another example, let us consider the case of LFI where $\epsilon_1 \simeq p/\left(4\Delta N_* + p/4\right)$ (ΔN_* is the number of e-folds between Hubble exit and the end of inflation, see below). Owing to the non-trivial relation between the first slow-roll parameter and p, a Jeffreys' prior $\pi(\epsilon_1)$ on ϵ_1 implies a complicated prior $\pi(p)$ on p while a natural choice would be a flat prior. Again, implementing the priors directly on the parameters of the model is a more theoretically justified choice. Conversely, who could dispute that, beside the posterior $P(\epsilon_1|C_\ell^{\rm meas})$, it is theoretically interesting to know the posterior distribution of p, i.e. $P(p|C_\ell^{\rm meas})$. The exact numerical integration is a reliable technique to obtain such distributions.

The numerical approach, however, has also some disadvantages. Firstly, one needs to specify the inflationary scenarios explicitly and, therefore, the constraints obtained are not model-independent. Although this shortcoming can in fact never be avoided (we always need to make some assumptions even in the slow-roll approach) it may be partially overcome by scanning the complete inflationary landscape. Secondly, and more importantly, it is

time consuming since the exact integration of the cosmological perturbations and of the corresponding correlation functions is heavy and can take up to a few minutes for complicated models. Finally, one should expect multiple degeneracies for models having a high number of inflationary parameters since the data have a limited sensitivity to the shape of the primordial observables.

Based on the previous considerations, we conclude that it would be very interesting to have an intermediate method that would allow us to get most of the results that can be derived using the exact numerical approach while being less time consuming and immune to high parameter degeneracies. This is what we suggest in the following. Our strategy is to use the slow-roll approximation in order to skip the numerical calculation of the power spectrum, while being combined with a systematic scan of the whole inflationary landscape and reheating properties. As argued before, the Planck data drive us towards testing inflation with the simplest models first and such a method would therefore need to be implemented for the class of scenarios IA only. More precisely, instead of inferring the posterior distributions of the Hubble flow parameters ϵ_n only, as one would naturally do in the approximate approach discussed before, we take advantage of the fact that the ϵ_n's can be computed in terms of the parameters describing the reheating and $V(\phi)$. In particular, for each model, this permits a quick and efficient extraction of the posterior distributions of those parameters.

In our opinion, this third technique should not be viewed as a competitor of the two others mentioned earlier but rather as complementary and the corresponding results should be compared. Let us also notice that, if, in order to scan all the inflationary scenarios, the full exact numerical approach needs to be carried out at some point, this would by no means render the results derived in the present article useless. Indeed, the slow-roll approach is often a very useful guide of which kind of physics one should expect for a given model (initial conditions, range of the parameters, etc ...). In particular it allows us to understand any eventual parameter degeneracies within the primordial observables. In other words, the slow-roll method is an ideal tool to prepare a full numerical study.

At this point, it is worth making the following remark. The method put forward in this article uses an approximate shape for the power spectrum, namely (k_* is the pivot scale)

$$\mathcal{P}_\zeta(k) \propto a_0\left(\epsilon_n\right) + a_1\left(\epsilon_n\right) \ln\left(\frac{k}{k_*}\right) + \frac{1}{2} a_2\left(\epsilon_n\right) \ln^2\left(\frac{k}{k_*}\right) + \ldots , \tag{1.3}$$

in order to shortcut a numerical integration of $\mathcal{P}_\zeta$ but is otherwise completely self-consistent. In other words, once the slow-roll approximation is accepted, no additional approximation should be made. This may still require some numerical calculations, however, in order to determine the coefficients a_i, or more precisely the explicit expression, at Hubble crossing, of $a_i = a_i\left[\epsilon_n\left(\theta_{\rm inf}\right)\right]$. This is an important issue given the accuracy of the current data as it is illustrated in Fig. 3 (see also Ref. [145]). In this figure, we have represented the slow-roll predictions of a SFI model, $V(\phi) \propto 1 - (\phi/\mu)^4$. Each colored segment represents the *exact* slow-roll predictions of a model given the parameter μ and for different numbers of e-folds during the reheating. These predictions have been computed by solving numerically the slow-roll equations. But, in the same plot, there are also other segments, on the left, and represented in yellow only. They are predictions for different values of μ but based on widespread *approximate* slow-roll formulas used in the literature. We see that, given the accuracy of the data, the approximated formulas are no longer accurate enough: the approximate results would predict that models with $\mu/M_{\rm Pl} > 1$ are strongly disfavored while the correct slow-roll results show that they are still compatible with the data. Another

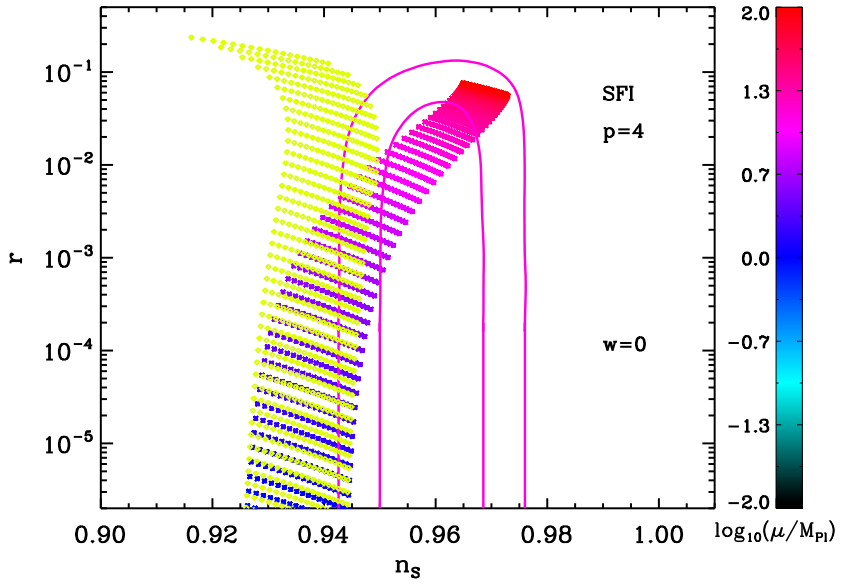

Figure 3. Exact slow-roll predictions for SFI models, $V(\phi) \propto 1 - (\phi/\mu)^4$, compared to the Planck data [66, 69, 70, 133, 134, 153]. Each colored segment represents a different value of μ, the color bar giving the corresponding range of variation. Each segment is made of different points associated with different reheating temperatures. The yellow-only segments on the left represent some extra approximations usually made in the literature on top of slow-roll. We see that both coincide for $\mu/m_{\rm Pl} \ll 1$ but differ in the regime $\mu/m_{\rm Pl} \gg 1$ where the extra approximations become inaccurate. Moreover, these approximations would indicate that this class of models is disfavored while the correct slow-roll predictions show that, on the contrary, they remain compatible with the data.

textbook example is provided by Higgs inflation with radiative corrections (RCHI) and is presented in Fig. 4. This scenario is studied in detail in section 4.1 and depends on one free parameter, $A_{\rm I}$. The colored segments represent the exact predictions for different values of $A_{\rm I}$ (see the color bar on the side of the plot). The red dashed line indicates predictions based on a commonly used approximate equation for the coefficients $a_i = a_i(\epsilon_n)$ at Hubble crossing during inflation. We see that this is no longer sufficient in the range $A_{\rm I} \gtrsim 15$. From these two examples, we conclude that it is safer to use the slow-roll approximation (which is usually extremely good) and nothing else, in particular no extra approximation on top of the slow-roll approximation. The fact that we may still need to use numerical calculations to establish the observational predictions of a model does not make our approach useless. Indeed, the numerics needed to estimate $a_i = a_i[\epsilon_n(\theta_{\rm inf})]$ are, by far, much easier than those needed to exactly compute $\mathcal{P}_\zeta$. Therefore, the gain in computational time mentioned above is huge and allows for a fast and reliable method to constrain the inflationary landscape.

1.2 The ASPIC library

The project described before contains many different aspects that we intend to publish in several companion articles. We now explain the purpose of the present paper and put it in context with the other works that are in preparation. We have coded a public runtime library, named ASPIC for "Accurate Slow-roll Predictions for Inflationary Cosmology", which

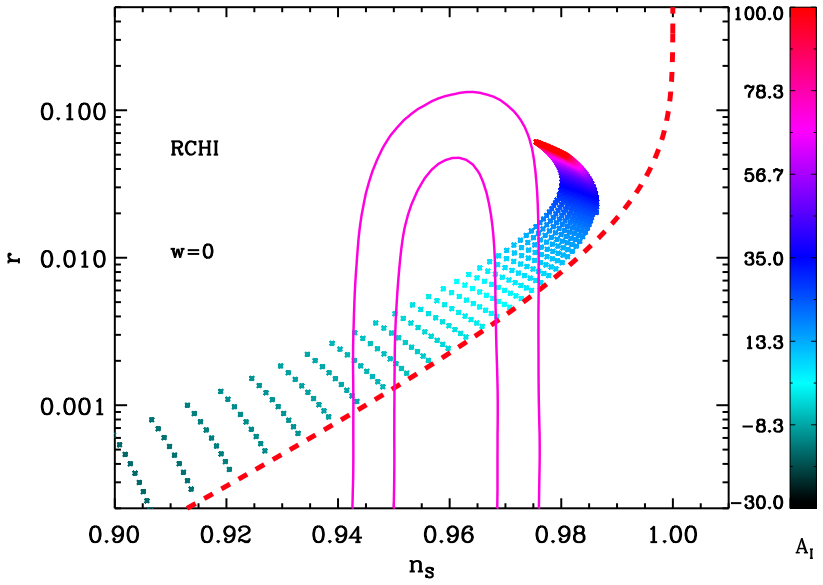

Figure 4. Predictions of the RCHI model in the plane (n_S, r) together with Planck data [66, 69, 70, 133, 134, 153]. These predictions depend on one free parameter, A_I, for details see section 4.1. The colored segments represent the slow-roll predictions (same conventions as in Fig. 3), obtained when the coefficients $a_i = a_i\left[\epsilon_n\left(\theta_{\rm inf}\right)\right]$ are numerically evaluated. On the contrary, the thick red dashed line indicates some approximated predictions. We see that there is a significant difference for $A_I \gtrsim 15$.

is supposed to contain all the inflationary models that can be treated with the method described above. `ASPIC` already has 74 different inflationary scenarios, a number that should be compared to the three or four models that are usually considered. The `ASPIC` library is an open source evolutive project and, although it already contains all the most popular inflationary scenarios, aims at including more models. In this way, it will converge towards a situation where all the category IA models published since the advent of inflation are implemented thereby allowing us to exhaustively scan this part of the inflationary landscape. This article describes the `ASPIC` project and presents its first release and others will follow. The list of the 74 `ASPIC` models, as well as their acronym, is presented in Table 1 at the end of this introduction. If future cosmological data force us to move to more complicated scenarios, the `ASPIC` library will be upgraded accordingly. It can, moreover, already be interfaced with `FieldInf` thereby allowing for a full numerical approach, if needed. This would be especially relevant for all the single field models with modified kinetic terms (category IB) such as DBI models, models with features (category IC) such as the Starobinsky model [156] or multiple field inflationary scenarios (category II) such as double inflation [157–160], double inflation with an interaction term [161], the different versions of hybrid inflation [57, 162, 163] and more [149], assisted inflation [164] or Matrix inflation [165–167, 167]. However, if the data continue to favor simple models, such as those producing negligible non-Gaussianities and isocurvature perturbations, the `ASPIC` library in its present form already contains the most relevant inflationary scenarios. The `ASPIC` library is publicly available at `http://cp3.irmp.ucl.ac.be/~ringeval/aspic.html`.

The `ASPIC` library contains the necessary routines to compare the predictions of any of

the 74 different models to high-accuracy data. The present article presents the general architecture of the ASPIC project and the calculations needed to understand and write these codes. In practice, for each model, we give the calculation of the three first slow-roll parameters, a discussion of how inflation ends, a discussion of the priors, a calculation of the relevant range of variation of the reheating temperature and an exact integration of the slow-roll trajectory. Then, we work out the theoretical predictions and compare them to the Planck data in the planes (ϵ_1, ϵ_2) and $(n_{\rm S}, r)$. Let us stress again that, beside slow-roll, no other approximation is used in the numerical codes of ASPIC.

Most of the ASPIC models have already been partially studied in the literature but let us emphasize that, for each of them, this paper contains new results. In other words, it does not aim at being a review and, therefore, the presentation of already derived results have been kept to the minimal. Firstly, for all the models studied, this is the first time that their observational predictions are worked out when the constraints on the reheating phase are accurately taken into account. As explained in Ref. [64], and briefly reviewed in section 2, it has become too inaccurate to derive the predictions of a model by simply assuming a fixed range for ΔN_*. For instance, this could lead to a reheating energy density larger than the energy density at the end of inflation which is physically irrelevant. Therefore, the predictions have been re-worked in such a consistent fashion (except for the LFI and SFI models which had been studied before [64]). This already constitutes a significant result which goes beyond the current state-of-the-art. Secondly, in the appendix, we present a series of plots which give the predictions of the various ASPIC models in the planes $(n_{\rm S}, r)$ and (ϵ_1, ϵ_2) for different values of the free parameters characterizing each potential. Clearly, this is the first time that the predictions of all these models are compared to the Planck data. The only exception is Ref. [168] which studies a very small subset of the ASPIC scenarios (but also studies non-minimal single field models), Ref. [169] which studies the particular case of power law (PLI) and Ref. [170] which studies the particular case of MSSM inflation (MSSMI). Most often, this is also the first time that these predictions are worked out for such a wide range of parameters and, moreover, this is the first time that these predictions are presented in this fashion. In some sense, our paper can be viewed as the first *Encyclopædia Inflationaris*.

1.3 New results

In order to be completely clear about the fact that this paper is not a review, we now highlight, in a non-exhaustive way, some of the new results obtained in this paper. In this way, we hope it gives a taste of all the new findings described later and the methods advocated earlier.

In the case of Higgs Inflation (HI), for instance, we have found an exact expression of the slow-roll trajectory and discuss the reheating parameter in the case of scalar-tensor theories of gravity. The exact trajectory is also found for radiatively corrected inflation (RCHI) and we show that the exact predictions can differ from the commonly used ones in a certain regime, see also Fig. 4. In the case of Mixed Large Field Inflation (MLFI), the exact expressions of the slow-roll parameters ϵ_2 and ϵ_3 are new. We also calculate exactly $\phi_{\rm end}$, the *vev* at which inflation stops, as well as the exact trajectory $N(\phi)$ and its inverse, $\phi(N)$. Interestingly, since the potential is the sum of a quadratic and a quartic term, one would expect the corresponding predictions to be located between the two lines in the plane $(n_{\rm S}, r)$ representing the quadratic LFI and the quartic LFI models, see for instance Fig. 2. We show that this is not the case. For Natural Inflation (NI), we provide the exact expression of $\phi_{\rm end}$, of the trajectory and its inverse. In addition, it is often claimed that, in the limit $f/M_{\rm Pl} \gg 1$, the model is indistinguishable from a quadratic one (LFI with $p = 2$). We show that it is true

for $n_{\rm S}$ and r but is not accurate for ϵ_3, that is to say for the running $\alpha_{\rm S}$. For the Kähler Moduli Inflation I (KMII) and Kähler Moduli Inflation II (KMIII) models, all our results are basically new. We present, for the first time, the exact expressions of the slow-roll parameters, of the trajectories, their inverses, the possible values of α, a free parameter characterizing the shape of the potentials (not to be confused with the running). We also emphasize the role played by the running in this model: $n_{\rm S}$ and r are perfectly compatible with the data while $\alpha_{\rm S}$ seems to constrain the model more efficiently. However, contrary to what is commonly claimed in the literature, we demonstrate that this does not rule out these models. Within the Logamediate inflation (LMI) scenario, we have derived an analytic expression for the trajectory in terms of hypergeometric functions and exhibited a new inflationary domain LMI2, which is however like almost a pure de Sitter era and currently disfavored. We also have new results for the Coleman Weinberg Inflation (CWI) scenario. We find exact expressions for ϵ_3 and an exact determination of the end of inflation. We discuss, for the first time, the predictions of the model in the full parameter space. In the case of Double Well Inflation (DWI), we present a clear slow-roll analysis. The expressions of ϵ_3, $\phi_{\rm end}$, the slow-roll trajectory, its inverse are all new. Moreover, a detailed comparison with SFI is made and we show that the corresponding predictions actually differ, contrary to what is sometimes written in the literature. In the case of the Minimal Super-Symmetric Model (MSSMI) scenario, we demonstrate several new results. We give the exact expression of the slow-roll parameters ϵ_2 and ϵ_3, the location and the value of the maximum of the first slow-roll parameter ϵ_1, an approximated formula for $\phi_{\rm end}$, the exact slow-roll trajectory and a useful approximated version of it. We also provide a parameter independent treatment of the quantum diffusion regime: usually this is always done using specific values of the parameters whereas we show that the corresponding conclusions are in fact completely general. We also explain why the model is quite strongly disfavored due to the observational constraints on the spectral index. For the Renormalizable Inflection Point Inflation (RIPI) scenario, the slow roll parameters ϵ_2 and ϵ_3, the location and the value of the maximum of ϵ_1, the approximated determination of $\phi_{\rm end}$, the exact slow-roll trajectory and a useful approximated version of it are all new. We also discuss the CMB normalization and calculate the energy scale of inflation very accurately. Last but not the least, we show that the model is strongly disfavored by the data. We have also explored the Generalized MSSM Inflation (GMSSMI) scenario. We provide new formulas for ϵ_2, ϵ_3 and the trajectory. We also give new bounds on the parameters characterizing the potential from the requirement of having a sufficient number of e-folds during inflation. Finally, we show that the model is disfavored by the data. Concerning the Brane Susy Breaking Scenario (BSUSYBI), we have studied the effects coming from the the field value at which inflation ends, in the slow-roll regime. For the ArcTan Inflation (AI) scenario, we work out the slow-roll analysis beyond the approximation of vacuum domination and give an exact expression for ϵ_3 and the slow-roll trajectory. For the class of models leading to a constant spectral index, CNAI, CNBI, CNCI and CNDI, we show how to calculate $\phi_{\rm end}$ and the trajectory exactly. We also demonstrate that the spectral index is in fact constant only in a limited region of the parameter space which turns out to be already disfavored by the data. In the case of Intermediate Inflation (II), we present an analysis which takes into account the two terms of the potential while it is common to keep only the dominant one. We give new expressions for ϵ_3, the slow-roll trajectory and its relation with the exact, non-slow-roll, one. In the case of Twisted Inflation (TWI), we study this model for the first time in a regime where it is not equivalent to DSI. We give new expressions for ϵ_3, the exact trajectory and the CMB normalization. We also discuss how inflation ends and show, contrary to

a naive expectation, that it cannot happen by the end of the slow-rolling phase. For the Pseudo Natural Inflation (PSNI) scenario, we present new formulas for ϵ_2, ϵ_3, $\phi_{\rm end}$ and the trajectory. This is the first time that a slow-roll analysis of Orientifold Inflation (OI) is made. As a consequence, all the corresponding results are new. In particular, we demonstrate that the model is in bad shape because it predicts a too important amount of gravitational waves. The scenario of Spontaneous Symmetry Breaking Inflation (SSBI) is important because it can cover many physically different situations. This model actually contains six different sub-models. The third slow-roll parameter, the trajectory and the CMB normalization are new results obtained for the first time in this paper. In the case of Dynamical Symmetric Inflation (DSI), we present new expressions for ϵ_3, the trajectory and the CMB normalization. Another important result is also a careful analysis of the prior space and the limits derived on the parameters of the model which are such that it is disfavored by observations due to its blue tilt. For the Generalized Mixed Large Field Inflation (GMLFI) model, we present new equations for ϵ_2 and ϵ_3 and the trajectory. Concerning the LPI models, we have exhibited three domains in which inflation could take place, thereafter denoted by LPI1, LPI2 and LPI3. For the Non-Canonical Kähler Inflation model (NCKI), we provide new results for ϵ_2 and ϵ_3, the trajectory and the CMB normalization. We also analyze the predictions for different values of β, a parameter characterizing the potential. We show that the case $\beta < 0$ is ruled out while $\beta > 0$ is disfavored by the observations. We have also studied Loop Inflation (LI). For this model, we give new expressions of ϵ_3, $\phi_{\rm end}$, the trajectory and its inverse in terms of a Lambert function. Also, the slow-roll analysis is carried out in the case where the correcting term is negative which we could not find elsewhere. In the case of Tip Inflation (TI), we also give ϵ_3, $\phi_{\rm end}$ and the trajectory. We also study which amounts of fine-tuning is required by the model and finally show that it is ruled out because its spectrum deviates too strongly from scale invariance. Many other new results are given in this article but, as mentioned above, we do not summarize all of them here due to space limitation. They can be found in the sections devoted to the various models listed in Table 1.

Before concluding this introduction, let us remark that this article and the `ASPIC` library represent important tools to carry out our final goal which consists in assessing how good is a model and in comparing the various inflationary models. This problem can be dealt within Bayesian inference for model comparison. For this purpose, one has to calculate, for each model, the global likelihood which is obtained by integrating the usual likelihood over all of the model parameter values, weighted by their respective prior probability distribution. The resulting quantity is a number associated with each model which gives the "evidence" that the model explains the data [this is the number $\mathcal{N}$ in Eq. (1.1)]. Their respective ratios give the odds that one model explains all data compared to the others. Bayesian methods have the advantage to automatically incorporate the "Occam's razor": complicated inflationary models will be assigned large probability only if the complexity is required by the data. On the practical side, these two steps can be implemented by the use of Markov–Chains–Monte–Carlo (MCMC) methods, which is especially well suited with the exact numerical approach advocated before. These techniques have already been successfully implemented first in Ref. [171], and later on in Ref. [155], and we plan to extent them to all the models of the `ASPIC` library. As a matter of fact, this will allow us to scan the inflationary landscape in a statistically well-defined way and to address the question of "the best model of inflation".

This article is organized as follows. In the next section, section 2, we briefly summarize slow-roll inflation and give the equations needed for the rest of this article. We also discuss the reheating stage and explains how it can be implemented. Then, in section 3, we study

inflationary models which, up to the potential normalization, do not contain any free parameter (concretely, at this stage, Higgs inflation). In sections 4, 5 and 6, we analyze scenarios characterized by one, two and three free parameters, respectively. Finally, in section 7, we present our conclusions and discuss future works. In the appendix A, we give, in the planes $(n_{\rm S}, r)$ and (ϵ_1, ϵ_2), the predictions of all the 74 `ASPIC` models.

Table 1: Models contained in the first release of the `ASPIC` library. For each model, we give the corresponding acronym, the number of free parameters characterizing the potential, the number of sub-models and the shape of the potential. The total number of models is 74.

Name	Parameters	Sub-models	$V(\phi)$
HI	0	1	$M^4\left(1-e^{-\sqrt{2/3}\phi/M_{\rm Pl}}\right)$
RCHI	1	1	$M^4\left(1-2e^{-\sqrt{2/3}\phi/M_{\rm Pl}}+\frac{A_{\rm I}}{16\pi^2}\frac{\phi}{\sqrt{6}M_{\rm Pl}}\right)$
LFI	1	1	$M^4\left(\frac{\phi}{M_{\rm Pl}}\right)^p$
MLFI	1	1	$M^4\frac{\phi^2}{M_{\rm Pl}^2}\left[1+\alpha\frac{\phi^2}{M_{\rm Pl}^2}\right]$
RCMI	1	1	$M^4\left(\frac{\phi}{M_{\rm Pl}}\right)^2\left[1-2\alpha\frac{\phi^2}{M_{\rm Pl}^2}\ln\left(\frac{\phi}{M_{\rm Pl}}\right)\right]$
RCQI	1	1	$M^4\left(\frac{\phi}{M_{\rm Pl}}\right)^4\left[1-\alpha\ln\left(\frac{\phi}{M_{\rm Pl}}\right)\right]$
NI	1	1	$M^4\left[1+\cos\left(\frac{\phi}{f}\right)\right]$
ESI	1	1	$M^4\left(1-e^{-q\phi/M_{\rm Pl}}\right)$
PLI	1	1	$M^4e^{-\alpha\phi/M_{\rm Pl}}$
KMII	1	2	$M^4\left(1-\alpha\frac{\phi}{M_{\rm Pl}}e^{-\phi/M_{\rm Pl}}\right)$
HF1I	1	1	$M^4\left(1+A_1\frac{\phi}{M_{\rm Pl}}\right)^2\left[1-\frac{2}{3}\left(\frac{A_1}{1+A_1\phi/M_{\rm Pl}}\right)^2\right]$
CWI	1	1	$M^4\left[1+\alpha\left(\frac{\phi}{Q}\right)^4\ln\left(\frac{\phi}{Q}\right)\right]$
LI	1	2	$M^4\left[1+\alpha\ln\left(\frac{\phi}{M_{\rm Pl}}\right)\right]$
RpI	1	3	$M^4e^{-2\sqrt{2/3}\phi/M_{\rm Pl}}\left\vert e^{\sqrt{2/3}\phi/M_{\rm Pl}}-1\right\vert^{2p/(2p-1)}$
DWI	1	1	$M^4\left[\left(\frac{\phi}{\phi_0}\right)^2-1\right]^2$
MHI	1	1	$M^4\left[1-\mathrm{sech}\left(\frac{\phi}{\mu}\right)\right]$
RGI	1	1	$M^4\frac{(\phi/M_{\rm Pl})^2}{\alpha+(\phi/M_{\rm Pl})^2}$
MSSMI	1	1	$M^4\left[\left(\frac{\phi}{\phi_0}\right)^2-\frac{2}{3}\left(\frac{\phi}{\phi_0}\right)^6+\frac{1}{5}\left(\frac{\phi}{\phi_0}\right)^{10}\right]$
RIPI	1	1	$M^4\left[\left(\frac{\phi}{\phi_0}\right)^2-\frac{4}{3}\left(\frac{\phi}{\phi_0}\right)^3+\frac{1}{2}\left(\frac{\phi}{\phi_0}\right)^4\right]$

AI	1	1	$M^4\left[1-\frac{2}{\pi}\arctan\left(\frac{\phi}{\mu}\right)\right]$
CNAI	1	1	$M^4\left[3-\left(3+\alpha^2\right)\tanh^2\left(\frac{\alpha}{\sqrt{2}}\frac{\phi}{M_{\rm Pl}}\right)\right]$
CNBI	1	1	$M^4\left[\left(3-\alpha^2\right)\tan^2\left(\frac{\alpha}{\sqrt{2}}\frac{\phi}{M_{\rm Pl}}\right)-3\right]$
OSTI	1	1	$-M^4\left(\frac{\phi}{\phi_0}\right)^2\ln\left[\left(\frac{\phi}{\phi_0}\right)^2\right]$
WRI	1	1	$M^4\ln\left(\frac{\phi}{\phi_0}\right)^2$
SFI	2	1	$M^4\left[1-\left(\frac{\phi}{\mu}\right)^p\right]$
II	2	1	$M^4\left(\frac{\phi-\phi_0}{M_{\rm Pl}}\right)^{-\beta}-M^4\frac{\beta^2}{6}\left(\frac{\phi-\phi_0}{M_{\rm Pl}}\right)^{-\beta-2}$
KMIII	2	1	$M^4\left[1-\alpha\frac{\phi}{M_{\rm Pl}}\exp\left(-\beta\frac{\phi}{M_{\rm Pl}}\right)\right]$
LMI	2	2	$M^4\left(\frac{\phi}{M_{\rm Pl}}\right)^\alpha\exp\left[-\beta(\phi/M_{\rm Pl})^\gamma\right]$
TWI	2	1	$M^4\left[1-A\left(\frac{\phi}{\phi_0}\right)^2e^{-\phi/\phi_0}\right]$
GMSSMI	2	2	$M^4\left[\left(\frac{\phi}{\phi_0}\right)^2-\frac{2}{3}\alpha\left(\frac{\phi}{\phi_0}\right)^6+\frac{\alpha}{5}\left(\frac{\phi}{\phi_0}\right)^{10}\right]$
GRIPI	2	2	$M^4\left[\left(\frac{\phi}{\phi_0}\right)^2-\frac{4}{3}\alpha\left(\frac{\phi}{\phi_0}\right)^3+\frac{\alpha}{2}\left(\frac{\phi}{\phi_0}\right)^4\right]$
BSUSYBI	2	1	$M^4\left(e^{\sqrt{6}\frac{\phi}{M_{\rm Pl}}}+e^{\sqrt{6}\gamma\frac{\phi}{M_{\rm Pl}}}\right)$
TI	2	3	$M^4\left(1+\cos\frac{\phi}{\mu}+\alpha\sin^2\frac{\phi}{\mu}\right)$
BEI	2	1	$M^4\exp_{1-\beta}\left(-\lambda\frac{\phi}{M_{\rm Pl}}\right)$
PSNI	2	1	$M^4\left[1+\alpha\ln\left(\cos\frac{\phi}{f}\right)\right]$
NCKI	2	2	$M^4\left[1+\alpha\ln\left(\frac{\phi}{M_{\rm Pl}}\right)+\beta\left(\frac{\phi}{M_{\rm Pl}}\right)^2\right]$
CSI	2	1	$\frac{M^4}{\left(1-\alpha\frac{\phi}{M_{\rm Pl}}\right)^2}$
OI	2	1	$M^4\left(\frac{\phi}{\phi_0}\right)^4\left[\left(\ln\frac{\phi}{\phi_0}\right)^2-\alpha\right]$
CNCI	2	1	$M^4\left[\left(3+\alpha^2\right)\coth^2\left(\frac{\alpha}{\sqrt{2}}\frac{\phi}{M_{\rm Pl}}\right)-3\right]$
SBI	2	2	$M^4\left\{1+\left[-\alpha+\beta\ln\left(\frac{\phi}{M_{\rm Pl}}\right)\right]\left(\frac{\phi}{M_{\rm Pl}}\right)^4\right\}$
SSBI	2	6	$M^4\left[1+\alpha\left(\frac{\phi}{M_{\rm Pl}}\right)^2+\beta\left(\frac{\phi}{M_{\rm Pl}}\right)^4\right]$
IMI	2	1	$M^4\left(\frac{\phi}{M_{\rm Pl}}\right)^{-p}$
BI	2	2	$M^4\left[1-\left(\frac{\phi}{\mu}\right)^{-p}\right]$

RMI	3	4	$M^4\left[1-\frac{c}{2}\left(-\frac{1}{2}+\ln\frac{\phi}{\phi_0}\right)\frac{\phi^2}{M_{\rm Pl}^2}\right]$
VHI	3	1	$M^4\left[1+\left(\frac{\phi}{\mu}\right)^p\right]$
DSI	3	1	$M^4\left[1+\left(\frac{\phi}{\mu}\right)^{-p}\right]$
GMLFI	3	1	$M^4\left(\frac{\phi}{M_{\rm Pl}}\right)^p\left[1+\alpha\left(\frac{\phi}{M_{\rm Pl}}\right)^q\right]$
LPI	3	3	$M^4\left(\frac{\phi}{\phi_0}\right)^p\left(\ln\frac{\phi}{\phi_0}\right)^q$
CNDI	3	3	$\frac{M^4}{\left\{1+\beta\cos\left[\alpha\left(\frac{\phi-\phi_0}{M_{\rm Pl}}\right)\right]\right\}^2}$

2 Basic Equations

In this section, we very briefly recall the theoretical foundations of inflation and we present the main tools and equations that will be used in the rest of this paper. We start by reviewing the slow-roll phase, where the cosmological fluctuations are generated and, then, we describe how the end of inflation and the transition to the standard hot Big Bang phase can be modeled.

2.1 The slow-roll phase

Let us consider a single-field inflationary model with a minimal kinetic term and a potential $V(\phi)$. The behavior of the system is controlled by the Friedmann-Lemaître and Klein-Gordon equations, namely

$$H^2=\frac{1}{3M_{\rm Pl}^2}\left[\frac{\dot\phi^2}{2}+V(\phi)\right], \tag{2.1}$$

$$\ddot\phi+3H\dot\phi+V_\phi=0, \tag{2.2}$$

where $H\equiv\dot a/a$ denotes the Hubble parameter, $a(t)$ being the Friedmann-Lemaître-Robertson Walker (FLRW) scale factor and $\dot a$ its derivative with respect to cosmic time t. $M_{\rm Pl}=8\pi G$ denotes the reduced Planck mass. A subscript ϕ means a derivative with respect to the inflaton field. In order to describe the evolution of the background, it is convenient to introduce the Hubble flow functions ϵ_n defined by [172, 173]

$$\epsilon_{n+1}\equiv\frac{{\rm d}\ln|\epsilon_n|}{{\rm d}N},\quad n\geq 0, \tag{2.3}$$

where $\epsilon_0\equiv H_{\rm ini}/H$ and $N\equiv\ln(a/a_{\rm ini})$ is the number of e-folds. By definition, inflation is a phase of accelerated expansion, $\ddot a/a>0$, or, equivalently, $\epsilon_1<1$. As a consequence, the end of inflation is defined by the condition $\epsilon_1=1$. On the other hand, the slow-roll conditions (or slow-roll approximation) refer to a situation where all the ϵ_n's satisfy $\epsilon_n\ll 1$. If this is the case, then the parameters ϵ_n can also be expressed in terms of the successive derivatives

of the potential, namely [17]

$$\epsilon_1 \simeq \frac{M_{\rm Pl}^2}{2}\left(\frac{V_\phi}{V}\right)^2, \tag{2.4}$$

$$\epsilon_2 \simeq 2M_{\rm Pl}^2\left[\left(\frac{V_\phi}{V}\right)^2 - \frac{V_{\phi\phi}}{V}\right], \tag{2.5}$$

$$\epsilon_2\epsilon_3 \simeq 2M_{\rm Pl}^4\left[\frac{V_{\phi\phi\phi}V_\phi}{V^2} - 3\frac{V_{\phi\phi}}{V}\left(\frac{V_\phi}{V}\right)^2 + 2\left(\frac{V_\phi}{V}\right)^4\right]. \tag{2.6}$$

Therefore, a measurement of the ϵ_n's also provides information with regards to the shape of the inflationary potential.

In terms of the number of e-folds, one can decouple Eqs. (2.1) and (2.2) to get the field evolution

$$\frac{1}{3-\epsilon_1}\frac{{\rm d}^2\phi}{{\rm d}N^2} + \frac{{\rm d}\phi}{{\rm d}N} = -M_{\rm Pl}^2\frac{{\rm d}\ln V}{{\rm d}\phi}, \tag{2.7}$$

showing that the potential driving the field in FLRW spacetime is $\ln[V(\phi)]$. This equation can be further simplified by using the definition of ϵ_1 and ϵ_2 to get ride of the second order derivatives. From

$$\epsilon_1 = \frac{1}{2M_{\rm Pl}^2}\left(\frac{{\rm d}\phi}{{\rm d}N}\right)^2, \tag{2.8}$$

one gets

$$\left(1+\frac{\epsilon_2}{6-2\epsilon_1}\right)\frac{{\rm d}\phi}{{\rm d}N} = -M_{\rm Pl}^2\frac{{\rm d}\ln V}{{\rm d}\phi}. \tag{2.9}$$

As a result, in the slow-roll approximation, one has

$$\frac{{\rm d}\phi}{{\rm d}N} \simeq -M_{\rm Pl}^2\frac{{\rm d}\ln V}{{\rm d}\phi}. \tag{2.10}$$

This equation can be integrated to give an explicit expression of the classical trajectory. One arrives at

$$N - N_{\rm ini} = -\frac{1}{M_{\rm Pl}^2}\int_{\phi_{\rm ini}}^{\phi}\frac{V(\chi)}{V_\chi(\chi)}\,{\rm d}\chi. \tag{2.11}$$

In this article, for each model, we provide the expressions of the first three Hubble flow parameters, a determination of $\phi_{\rm end}$, the value of the field at which inflation comes to an end (and the corresponding discussion) and an explicit expression of the slow-roll trajectory Eq. (2.11).

Let us now consider the behavior of inflationary cosmological perturbations. The evolution of scalar (density) perturbations can be reduced to the study of a single variable, the so-called Mukhanov–Sasaki variable $v_{\boldsymbol{k}}$. In Fourier space, its equation of motion can be expressed as [6–8, 16]

$$v_{\boldsymbol{k}}'' + \left[k^2 - \frac{\left(a\sqrt{\epsilon_1}\right)''}{a\sqrt{\epsilon_1}}\right]v_{\boldsymbol{k}} = 0. \tag{2.12}$$

Here, a prime denotes a derivative with respect to conformal time and the quantity k is the comoving wave number of the Fourier mode under consideration. This equation is the equation of a parametric oscillator, i.e. an oscillator with a time-dependent frequency. The

time-dependence of the effective frequency is controlled by the dynamics of the background, more precisely by the scale factor and its derivatives (up to fourth order). The quantity $v_{\boldsymbol{k}}$ is related to the curvature perturbation $\zeta_{\boldsymbol{k}}$ through the following expression:

$$\zeta_{\boldsymbol{k}} = \frac{1}{M_{\rm Pl}} \frac{v_{\boldsymbol{k}}}{a\sqrt{2\epsilon_1}}\,. \tag{2.13}$$

The importance of $\zeta_{\boldsymbol{k}}$ lies in the fact that it can be viewed as a "tracer" of the fluctuations on super-Hubble scales, i.e. for all $k\eta \ll 1$, where η denotes the conformal time. Indeed, in the case of single-field inflation, this quantity becomes constant in this limit. Therefore, it can be used to "propagate" the perturbations from inflation to the subsequent cosmological eras. The statistical properties of the fluctuations can be characterized by the n-point correlation functions of $\zeta_{\boldsymbol{k}}$. In particular, the two-point correlation function can be written as an integral over wave numbers (in a logarithmic interval) of the power spectrum $\mathcal{P}_\zeta(k)$, which can be expressed as

$$\mathcal{P}_\zeta(k) \equiv \frac{k^3}{2\pi^2}\left|\zeta_{\boldsymbol{k}}\right|^2 = \frac{k^3}{4\pi^2 M_{\rm Pl}^2}\left|\frac{v_{\boldsymbol{k}}}{a\sqrt{\epsilon_1}}\right|^2\,. \tag{2.14}$$

In order to calculate $\mathcal{P}_\zeta(k)$, one needs to integrate Eq. (2.12), which requires the knowledge of the initial conditions for the mode function $v_{\boldsymbol{k}}$. Since, at the beginning of inflation, all the modes of cosmological interest today were much smaller than the Hubble radius, the initial conditions are chosen to be the Bunch-Davis vacuum which amounts to

$$\lim_{k\eta\to+\infty} v_{\boldsymbol{k}} = \frac{1}{\sqrt{2k}} e^{-ik\eta}\,, \tag{2.15}$$

where $\mathcal{H} = aH$ is the conformal Hubble parameter.

The evolution of tensor perturbations (or primordial gravity waves) can also be reduced to the study of a parametric oscillator. The amplitude of each transverse Fourier mode of the gravity wave, $\mu_{\boldsymbol{k}}(\eta)$, obeys the following equation

$$\mu_{\boldsymbol{k}}'' + \left(k^2 - \frac{a''}{a}\right)\mu_{\boldsymbol{k}} = 0. \tag{2.16}$$

We notice that the time-dependence of the effective frequency differs from that of the scalar case and now involves the derivative of the scale factor up to second order only. It is then straightforward to determine the resulting power spectrum. From a calculation of the two-point correlation function, one obtains

$$\mathcal{P}_h(k) = \frac{2k^3}{\pi^2}\left|\frac{\mu_{\boldsymbol{k}}}{a}\right|^2. \tag{2.17}$$

In order to calculate this quantity, the equation of motion Eq. (2.16) needs to be solved. As it is the case for density perturbations, the initial state is chosen to be the Bunch-Davies vacuum.

The power spectra can be computed exactly by means of a mode by mode integration of Eqs. (2.12) and (2.16), which also requires an exact integration of the background, i.e. of Eqs. (2.1) and (2.2). As discussed in the introduction, this can be done with the help of publicly available codes such as `FieldInf`. We have seen above that the slow-roll approximation can be used to calculate the classical background trajectory. Quite remarkably, the same approximation also permits the derivation of the scalar and tensor power spectra. This

involves a double expansion. The power spectra are expanded around a chosen pivot scale k_* such that

$$\frac{\mathcal{P}(k)}{\mathcal{P}_{_0}} = a_0 + a_1 \ln\left(\frac{k}{k_*}\right) + \frac{a_2}{2}\ln^2\left(\frac{k}{k_*}\right) + \dots\,, \tag{2.18}$$

where

$$\mathcal{P}_{\zeta_0} = \frac{H^2}{8\pi^2\epsilon_1 M_{\rm Pl}^2}\,, \qquad \mathcal{P}_{h_0} = \frac{2H^2}{\pi^2 M_{\rm Pl}^2}\,, \tag{2.19}$$

and, then, the coefficients a_i are determined in terms of the Hubble flow functions. For scalar perturbations, one gets [138, 139, 173–178, 178–180]

$$\begin{aligned} a_0^{(\rm S)} &= 1 - 2\,(C+1)\,\epsilon_1 - C\epsilon_2 + \left(2C^2 + 2C + \frac{\pi^2}{2} - f\right)\epsilon_1^2 \\ &\quad + \left(C^2 - C + \frac{7\pi^2}{12} - g\right)\epsilon_1\epsilon_2 + \left(\frac{1}{2}C^2 + \frac{\pi^2}{8} - 1\right)\epsilon_2^2 \\ &\quad + \left(-\frac{1}{2}C^2 + \frac{\pi^2}{24}\right)\epsilon_2\epsilon_3\,, \end{aligned} \tag{2.20}$$

$$a_1^{(\rm S)} = -2\epsilon_1 - \epsilon_2 + 2(2C+1)\epsilon_1^2 + (2C-1)\epsilon_1\epsilon_2 + C\epsilon_2^2 - C\epsilon_2\epsilon_3\,, \tag{2.21}$$

$$a_2^{(\rm S)} = 4\epsilon_1^2 + 2\epsilon_1\epsilon_2 + \epsilon_2^2 - \epsilon_2\epsilon_3\,, \tag{2.22}$$

where $C \equiv \gamma_{\rm E} + \ln 2 - 2 \approx -0.7296$, $\gamma_{\rm E}$ being the Euler constant, $f = 5$ and $g = 7$. For the gravitational waves, the coefficients a_i read

$$\begin{aligned} a_0^{(\rm T)} &= 1 - 2\,(C+1)\,\epsilon_1 + \left(2C^2 + 2C + \frac{\pi^2}{2} - f\right)\epsilon_1^2 \\ &\quad + \left(-C^2 - 2C + \frac{\pi^2}{12} - 2\right)\epsilon_1\epsilon_2\,, \end{aligned} \tag{2.23}$$

$$a_1^{(\rm T)} = -2\epsilon_1 + 2(2C+1)\epsilon_1^2 - 2(C+1)\epsilon_1\epsilon_2\,, \tag{2.24}$$

$$a_2^{(\rm T)} = 4\epsilon_1^2 - 2\epsilon_1\epsilon_2\,. \tag{2.25}$$

The Hubble flow functions are time-dependent quantities such that in the above expression, it is understood that they should be evaluated at the time at which the pivot scale crosses the Hubble radius during inflation, i.e. at a time η_* such that $k_* = \mathcal{H}(\eta_*)$. Let us notice that setting the pivot at another time affects the previous expression. For instance, setting η_* such that $k_*\eta_* = -1$ would set $f = 3$ and $g = 6$. We will see below that this introduces a dependence in the parameters describing the reheating stage.

The properties of the power spectra can also be characterized by the spectral indices and their "running". They are defined by the coefficients of the Taylor expansions of the power spectra logarithm with respect to $\ln k$, evaluated at the pivot scale k_*. This gives

$$n_{\rm S} - 1 \equiv \left.\frac{{\rm d}\ln\mathcal{P}_\zeta}{{\rm d}\ln k}\right|_{k_*}\,, \qquad n_{\rm T} \equiv \left.\frac{{\rm d}\ln\mathcal{P}_h}{{\rm d}\ln k}\right|_{k_*}\,. \tag{2.26}$$

For the runnings, one similarly has the two following expressions

$$\alpha_{\rm S} \equiv \left.\frac{{\rm d}^2\ln\mathcal{P}_\zeta}{{\rm d}(\ln k)^2}\right|_{k_*}\,, \qquad \alpha_{\rm T} \equiv \left.\frac{{\rm d}^2\ln\mathcal{P}_h}{{\rm d}(\ln k)^2}\right|_{k_*}\,, \tag{2.27}$$

and, in principle, we could also define the running of the running and so on. The slow-roll approximation allows us to calculate the quantities defined above. For instance, we have at first order in the Hubble flow parameters

$$n_{\rm S} = 1 - 2\epsilon_1 - \epsilon_2, \quad n_{\rm T} = -2\epsilon_1. \tag{2.28}$$

Let us also notice that the tensor-to-scalar ratio at leading order can be expressed as

$$r \equiv \frac{\mathcal{P}_h}{\mathcal{P}_\zeta} = 16\epsilon_1. \tag{2.29}$$

In the rest of this article, we give the observational predictions of each inflationary model of the `ASPIC` library in the planes (ϵ_1, ϵ_2) but also $(n_{\rm S}, r)$.

Each inflationary model must also be CMB normalized, that is to say the amplitude of the power spectra, say at $k = k_*$, is completely fixed by the amplitude of the CMB anisotropies measured today. On the largest length scales, this is given to a good approximation by the CMB quadrupole $Q_{\rm rms-PS}/T \equiv \sqrt{5C_2/(4\pi)} \simeq 6 \times 10^{-6}$, where $T \simeq 2.725\,{\rm K}$ is the CMB blackbody temperature. This is achieved if $\mathcal{P}_{\zeta_0} \simeq 60\,Q^2_{\rm rms-PS}/T^2$. Using the slow-roll approximation of the Friedmann-Lemaître equation and writing the potential as $V(\phi) = M^4 v(\phi)$, such that the mass scale M is singled out, one arrives at

$$\left(\frac{M}{M_{\rm Pl}}\right)^4 = 1440\pi^2 \frac{\epsilon_{1*}}{v(\phi_*)} \frac{Q^2_{\rm rms-PS}}{T^2}\,. \tag{2.30}$$

This is a model-depend expression (it depends on v) in which we have rendered explicit the dependence in the pivot time. On a more robust basis, CMB data are strongly constraining the value of $P_* \equiv \mathcal{P}_\zeta(k_*)$ and supplementing the Planck CMB temperature likelihood by the WMAP large-scale polarization data, one gets the one-sigma confidence interval

$$\ln\left(10^{10} P_*\right) = 3.092 \pm 0.026\,, \tag{2.31}$$

at $k_* = 0.05\,{\rm Mpc}^{-1}$. This constraint and the one- and two-sigma contours in the planes (ϵ_1, ϵ_2) and $(n_{\rm S}, r)$ represented in all the figures have been obtained from a slow-roll analysis of the Planck data. Since the analysis is in all point identical to the one of the WMAP seven years data performed in Ref. [64], we do not repeat it here. The interested reader can find all the details in the appendix B of Ref. [64]. Moreover, in order to get a robust inference, we have used the second order expression for the power spectra. Therefore, all the results presented below are marginalized over the second order slow-roll parameters.

Since at leading order in the slow-roll expansion we have $P_* \simeq H_*^2/(8\pi^2\epsilon_{1*}M_{\rm Pl}^2)$, the Friedmann–Lemaître equation allows us to derive the relation

$$\left(\frac{M}{M_{\rm Pl}}\right)^4 = 24\pi^2 \frac{\epsilon_{1*}}{v(\phi_*)} P_*\,, \tag{2.32}$$

which is, as expected, formally identical to Eq. (2.30) with

$$\frac{Q^2_{\rm rms-PS}}{T^2} = 60 P_*. \tag{2.33}$$

It has however the advantage of using P_* which is a well inferred quantity because it is fitted against all the C_ℓ. In the following we will make no-distinction between the so-called COBE

normalization and the CMB normalization, both being identical provided the above equation is used. For each inflationary model, these expressions will completely fix the allowed values for M.

We have shown how to calculate the two point correlation functions in the slow-roll approximation. The next logical step would be to determine the higher correlation functions. However, for the type of models considered here (i.e. category IA models), it is well-known that the corresponding signal is so small that it will stay out of reach for a while [111–115]. Therefore, we now consider the question of how to calculate the values of ϵ_1 and ϵ_2 when the pivot scale exits the Hubble radius and how this result depends on the details of the reheating period.

2.2 The reheating phase

In the last subsection, we have seen that the power spectrum (2.18) can be calculated with the help of the slow-roll approximation and expressed in terms of the Hubble flow parameters evaluated at Hubble radius crossing. Here, we briefly explain how these Hubble flow parameters can be determined. It is easy to calculate ϵ_1, ϵ_2 and ϵ_3 as a function of ϕ from Eqs. (2.4), (2.5) and (2.6). Then, from the trajectory (2.11), one can calculate $N_{\rm end}$, the total number of e-folds during inflation and N_*, the number of e-folds at the point when the pivot scale crosses the Hubble radius. If we denote by $\mathcal{I}$ the following primitive

$$\mathcal{I}(\phi) = \int^{\phi} \frac{V(\psi)}{V_{\psi}(\psi)} \mathrm{d}\psi, \tag{2.34}$$

which is also the slow-roll trajectory of Eq. (2.11), then we have

$$N_{\rm end} = -\frac{1}{M_{\rm Pl}^2}\left[\mathcal{I}(\phi_{\rm end}) - \mathcal{I}(\phi_{\rm ini})\right], \quad N_* = -\frac{1}{M_{\rm Pl}^2}\left[\mathcal{I}(\phi_*) - \mathcal{I}(\phi_{\rm ini})\right], \tag{2.35}$$

where ϕ_* is the vacuum expectation value of the field, again evaluated when the pivot scale crosses the Hubble radius. From these two expressions, it follows that

$$\phi_* = \mathcal{I}^{-1}\left[\mathcal{I}(\phi_{\rm end}) + M_{\rm Pl}^2 \Delta N_*\right], \tag{2.36}$$

where $\Delta N_* \equiv N_{\rm end} - N_*$. Inserting this formula into the expressions of the Hubble flow parameters allows us to find ϵ_{n*} and, therefore, r and $n_{\rm S}$.

However, in order to make the above-described calculation concrete, we need to say something about the quantity ΔN_*. As was explained in details in Ref. [64], this requires to take into account the reheating stage. Let ρ and P be the energy density and pressure of the effective fluid dominating the Universe during reheating. Conservation of energy implies that

$$\rho\left(N\right) = \rho_{\rm end} \exp\left\{-3\int_{N_{\rm end}}^{N}\left[1 + w_{\rm reh}\left(n\right)\right]\mathrm{d}n\right\}, \tag{2.37}$$

where $w_{\rm reh} \equiv P/\rho$ is the "instantaneous" equation of state during reheating. One can also define the mean equation of state parameter, $\overline{w}_{\rm reh}$, by[2]

$$\overline{w}_{\rm reh} \equiv \frac{1}{\Delta N}\int_{N_{\rm end}}^{N_{\rm reh}} w_{\rm reh}(n)\mathrm{d}n, \tag{2.38}$$

[2]In the figures, $\overline{w}_{\rm reh}$ has been denoted by w for simplicity.

where

$$\Delta N \equiv N_{\rm reh} - N_{\rm end}, \tag{2.39}$$

is the total number of e-folds during reheating, $N_{\rm reh}$ being the number of e-folds at which reheating is completed and the radiation dominated era begins. Then, one introduces a new parameter

$$R_{\rm rad} \equiv \frac{a_{\rm end}}{a_{\rm reh}} \left(\frac{\rho_{\rm end}}{\rho_{\rm reh}}\right)^{4}, \tag{2.40}$$

where $\rho_{\rm reh}$ has to be understood as the energy density at the end of the reheating era, i.e. $\rho(N_{\rm reh})$. This definition shows that $R_{\rm rad}$ encodes any deviations the reheating may have compared to a pure radiation era. In fact, $R_{\rm rad}$ completely characterizes the reheating stage and can be expressed in terms of

$$\ln R_{\rm rad} \equiv \frac{\Delta N}{4}\left(-1 + 3\,\overline{w}_{\rm reh}\right), \tag{2.41}$$

which renders explicit that if $\overline{w}_{\rm reh} = 1/3$, i.e. the effective fluid during reheating is equivalent to radiation, then reheating cannot be distinguished from the subsequent radiation dominated era. In this case, one simply has $R_{\rm rad} = 1$. Let us notice that it is also possible to express (or define) $\ln R_{\rm rad}$ as

$$\ln R_{\rm rad} = \frac{1 - 3\,\overline{w}_{\rm reh}}{12(1 + \overline{w}_{\rm reh})} \ln\left(\frac{\rho_{\rm reh}}{\rho_{\rm end}}\right). \tag{2.42}$$

Using entropy conservation till the beginning of the radiation era, the redshift at which inflation ended can be expressed in terms of $R_{\rm rad}$ as

$$1 + z_{\rm end} = \frac{1}{R_{\rm rad}} \left(\frac{\rho_{\rm end}}{\tilde{\rho}_{\gamma}}\right)^{1/4}, \qquad \tilde{\rho}_{\gamma} \equiv \mathcal{Q}_{\rm reh}\rho_{\gamma}. \tag{2.43}$$

The quantity $\rho_{\gamma} = 3H_0^2 M_{\rm Pl}^2 \Omega_{\gamma}$ is the total energy density of radiation today ($\Omega_{\gamma} \simeq 2.471 \times 10^{-5} h^{-2}$) while $\mathcal{Q}_{\rm reh} \equiv g_0^{4/3} g_{\rm reh}/(g_{\rm reh}^{4/3} g_0)$ is the measure of the change of relativistic degrees of freedom between the reheating epoch and today. In this expression q and g respectively denotes the number of entropy and energetic relativistic degrees of freedom. In view of the current CMB data, the precise value for $\mathcal{Q}_{\rm reh}$ is unimportant as this factor has only a minimal effect. At most it can shift the values of $\ln R_{\rm rad}$ by a $\mathcal{O}(1)$ number.

Then, straightforward considerations [64, 181] show that the quantities ΔN_* and $R_{\rm rad}$ are related by

$$\Delta N_* = \ln R_{\rm rad} - N_0 - \frac{1}{4}\ln\left[\frac{9}{\epsilon_{1*}(3 - \epsilon_{1\rm end})}\frac{V_{\rm end}}{V_*}\right] + \frac{1}{4}\ln(8\pi^2 P_*), \tag{2.44}$$

where we have defined[3]

$$N_0 \equiv \ln\left(\frac{k_*/a_0}{\tilde{\rho}_{\gamma}^{1/4}}\right), \tag{2.46}$$

[3]One may also wonder about the influence of the cosmological constant on this result. In fact, one can show that it leads to a negligible correction. Indeed, it simply amounts to redefining N_0 by

$$N_0 \to N_0 + \frac{1}{3}\ln\left[1 - \frac{\Omega_{\Lambda}\Omega_{\gamma}^3}{\Omega_{\rm dm}^4}\left(\frac{g_{\rm eq}}{g_0}\right)^3\left(\frac{q_0}{q_{\rm eq}}\right)^4\right]. \tag{2.45}$$

which is clearly a very tiny modification (the subscript "eq" denotes quantities at the equivalence time between radiation and matter).

which roughly measures the number of e-folds of deceleration of the Friedmann-Lemaître model. From Eq. (2.42), we see that the quantity $\ln R_{\rm rad}$ is not arbitrary since $-1/3 < \overline{w}_{\rm reh} < 1$ and $\rho_{\rm nuc} < \rho_{\rm reh} < \rho_{\rm end}$. As a consequence, the quantity ΔN_* is also constrained to vary in a given range, i.e. $\Delta N_* \in [\Delta N_*^{\rm nuc}, \Delta N_*^{\rm end}]$. Moreover, this range is model-dependent since $\rho_{\rm end}$ or $V_{\rm end}/V_*$ differ for different inflationary scenarios. In fact, for each allowed value of $\ln R_{\rm rad}$, Eq. (2.44) must be viewed as an algebraic equation allowing us to determine the corresponding ϕ_*. Explicitly, using Eq. (2.35), this equation reads

$$-\frac{1}{M_{\rm Pl}^2}\left[\mathcal{I}(\phi_*)-\mathcal{I}(\phi_{\rm end})\right]=\ln R_{\rm rad}-N_0-\frac{1}{4}\ln\left\{\frac{9}{\epsilon_1(\phi_*)[3-\epsilon_1(\phi_{\rm end})]}\frac{V(\phi_{\rm end})}{V(\phi_*)}\right\}+\frac{1}{4}\ln(8\pi^2P_*)\,. \tag{2.47}$$

In general, this equation can not be solved explicitly (except for LFI models, see Ref. [64]) and we have to rely on numerical calculations. Solving for each allowed value of $\ln R_{\rm rad}$, one can determine the range of variation of $\phi_* \in [\phi_*^{\rm nuc}, \phi_*^{\rm end}]$ and, therefore, find the corresponding dispersion in r and $n_{\rm S}$. In this paper, this task is carried out for all the models of the `ASPIC` library. Let us notice that it is compulsory to do so otherwise, assuming blindly say $\Delta N_* \in [40, 60]$, would lead to inconsistent reheating energy densities, either larger than $\rho_{\rm end}$ or smaller than $\rho_{\rm nuc}$. Clearly, this method also allows us to put model-dependent constraints on the reheating temperature. Indeed, for some values of $\rho_{\rm reh}$, the corresponding ϵ_{n*} will turn out to be outside the 1σ or 2σ contours (depending on the criterion one wishes to adopt) thus signaling some tension with the data, see the discussion in the Introduction and Fig. 2.

Before closing this section, let us remind that, for each inflationary model, `ASPIC` gives the expression of the first three Hubble flow parameters, a discussion of the mechanism that ends inflation and the value of $\phi_{\rm end}$, the classical trajectory $\mathcal{I}(\phi)$, the CMB normalization $M/M_{\rm Pl}$ and a determination of the exact range $[\phi_*^{\rm nuc}, \phi_*^{\rm end}]$. Then all these information are compared to CMB data in the planes (ϵ_1, ϵ_2) and $(n_{\rm S}, r)$. This provides a powerful tool to systematically derive the predictions for the `ASPIC` models and, therefore, to scan the inflationary landscape. In the next section, we start the systematic exploration of the category IA models that have been studied in the literature since the advent of inflation.

3 Zero Parameter Models

3.1 Higgs Inflation (HI)

3.1.1 Theoretical Justifications

This model postulates that the inflaton field is the Higgs field h (recently discovered at the Large Hadron Collider, see Refs. [182, 183]) non-minimally coupled to gravity, see Refs. [184–187]. Indeed, one can argue that, in curved spacetime, the simplest model compatible with our knowledge of particle physics is described by a Lagrangian which is the standard model Lagrangian plus an extra term of the form $\xi H^\dagger H R$. This last term is compulsory since, in curved spacetime, it will automatically be generated by quantum corrections [188]. In the Jordan frame, the action of the model can be written as

$$S=\frac{\bar{M}^2}{2}\int {\rm d}^4\boldsymbol{x}\sqrt{-\bar{g}}\left[F\left(h\right)\bar{R}-Z\left(h\right)\bar{g}^{\mu\nu}\partial_\mu h\partial_\nu h-2U\left(h\right)\right]. \tag{3.1}$$

The quantity $\bar{M}$ is a mass scale that, for the moment, is not identified with the Planck scale and the tensor $\bar{g}_{\mu\nu}$ denotes the metric in the Jordan frame (in what follows, all the

quantities with a bar denote quantities evaluated in the Jordan frame; quantities without a bar are quantities evaluated in the Einstein frame). The three functions $F(h)$, $Z(h)$ and $U(h)$ completely characterize the model and are chosen to be

$$F(h) = 1 + \xi h^2, \quad Z(h) = 1, \quad U(h) = \bar{M}^2 \frac{\lambda}{4}\left(h^2 - \frac{v^2}{\bar{M}^2}\right)^2, \tag{3.2}$$

where ξ is a new dimensionless parameter and $U(h)$ is the standard Higgs boson potential with v the Higgs (current) vacuum expectation value and λ the self-interacting coupling constant. Here, the field h is dimensionless (as the functions F and Z) while the potential U is of dimension two. The effective gravitational constant (measured in Cavendish-type experiments) is given by Ref. [189]

$$\frac{1}{M_{\rm Pl}^2} = \frac{1}{\bar{M}^2}\frac{2(1+\xi h^2) + 16\xi^2 h^2}{(1+\xi h^2)[2(1+\xi h^2) + 12\xi^2 h^2]}. \tag{3.3}$$

Since, today, one has $h \simeq v/\bar{M} \ll 1$, it follows that $\bar{M} \simeq M_{\rm Pl}$ with very good accuracy and, from now on, we will always consider that this identification is valid.

The above-described model can also be written in the Einstein frame where the corresponding slow-roll analysis is easier. Denoting the metric tensor in this frame by $g_{\mu\nu}$, the action now takes the form

$$S = 2M_{\rm Pl}^2 \int {\rm d}^4\boldsymbol{x}\sqrt{-g}\left[\frac{R}{4} - \frac{1}{2}g^{\mu\nu}\partial_\mu\chi\partial_\nu\chi - W(\chi)\right], \tag{3.4}$$

where the fields h and χ are related by

$$\frac{{\rm d}\chi}{{\rm d}h} = \frac{\sqrt{1+\xi(1+6\xi)h^2}}{\sqrt{2}(1+\xi h^2)}, \tag{3.5}$$

and the potential is given $V \equiv 2M_{\rm Pl}^2 W = M_{\rm Pl}^2 U/F^2$. Notice also that the canonically normalized field in the Einstein frame can be expressed as $\phi \equiv \sqrt{2}M_{\rm Pl}\chi$. It is also important to recall that, in the Einstein frame, matter is now explicitly coupled to the scalar field ϕ. This has of course important consequences for the description of the reheating period, see Refs. [190–192] and below. The differential equation (3.5) can be integrated exactly and the result reads

$$\chi = \sqrt{\frac{1+6\xi}{2\xi}}\,{\rm arcsinh}\left[h\sqrt{\xi(1+6\xi)}\right] - \sqrt{3}\,{\rm arctanh}\left[\frac{\xi\sqrt{6}h}{\sqrt{1+\xi(1+6\xi)h^2}}\right]. \tag{3.6}$$

The inverse hyperbolic tangent is always well-defined since its argument is always smaller than one. This exact formula between the Einstein and Jordan frame fields was also derived in Ref. [190]. In fact, we are interested in the regime $\xi \gg 1$ and $\xi h \gg 1$. In this case, one can derive an approximated expression for χ. Notice that this limit must be carefully calculated because if one just replaces $1+6\xi$ with ξ in the above expression, one finds that $\chi = 0$! Using the identity ${\rm arcsinh}\,x = \ln\left(x + \sqrt{1+x^2}\right)$, the first term in Eq. (3.6) can be approximated as $\sqrt{3}\ln\left(2\xi\sqrt{6}h\right)$. Then, one can use the identity ${\rm arctanh}\,x = 1/2\ln\left[(1+x)/(1-x)\right]$ and expand the argument of this logarithm in $1/\xi$ and $1/(\xi h)^2$. One finds that the latter reduces to $24\xi^2h^2/(1+\xi h^2)$. Finally, combining the two terms in Eq. (3.6), one arrives at

$$\chi \simeq \frac{\sqrt{3}}{2}\ln\left(1+\xi h^2\right). \tag{3.7}$$

The same expression can also be directly derived from Eq. (3.5) which, in the regime studied here, can be approximated as

$$\frac{\mathrm{d}\chi}{\mathrm{d}h} \simeq \frac{\sqrt{6}\xi h}{\sqrt{2}(1+\xi h^2)}\,. \tag{3.8}$$

The solution to this equation is exactly Eq. (3.7). The last step consists in inserting the expression of h in terms of χ (and, therefore, in terms of ϕ) into the definition of the potential V in the Einstein frame. This leads to the following expression

$$V(\phi) = \frac{M_{\mathrm{Pl}}^4\lambda}{4\xi^2}\left(1 - e^{-\sqrt{2/3}\phi/M_{\mathrm{Pl}}}\right)^2. \tag{3.9}$$

Interestingly enough, the parameters ξ and λ enter the potential only through its overall amplitude. In the following, we define M by $M^4 \equiv M_{\mathrm{Pl}}^4\lambda/(4\xi^2)$. In this sense, Higgs inflation is a "zero parameter model" since the scale M is entirely determined by the amplitude of the CMB anisotropies.

More recently, in Ref. [193], a supergravity realization of this model was presented. We now briefly review how this can be achieved. The model is based on no-scale supergravity and has two fields, a modulus T and the inflaton ϕ. The Kähler and super-potentials are given by $K = -3\ln\left(T + T^\dagger - |\phi|^2/3\right)$ and $W = \hat{\mu}\phi^2 - \lambda\phi^3/3$, respectively. The quantities $\hat{\mu}$ and λ are constants characterizing the model. It follows that the Kähler matrix and its inverse can be written as

$$K_{i\bar{\jmath}} = \frac{3}{\left(T + T^\dagger - |\phi|^2/3\right)^2}\begin{bmatrix}\left(T+T^\dagger\right)/3 & -\phi^\dagger/3\\ -\phi/3 & 1\end{bmatrix}, \tag{3.10}$$

$$K^{k\bar{\jmath}} = \left(T + T^\dagger - \frac{|\phi|^2}{3}\right)\begin{bmatrix}1 & \phi/3\\ \phi^\dagger/3 & (T+T^\dagger)/3\end{bmatrix}. \tag{3.11}$$

Then, assuming that the modulus is stabilized such $\langle T + T^\dagger\rangle = c$ and $\langle T - T^\dagger\rangle = 0$, one obtains the following Lagrangian: $-c|\partial_\mu\phi|^2/\Delta^2 - |\partial W/\partial\phi|^2/\Delta^2$ where $\Delta \equiv c - |\phi|^2/3$. The next step consists in introducing the fields x and y defined by $\phi = \sqrt{3c}\tanh\left[(x+iy)/\sqrt{3}\right]$. Expressed in terms of these two fields, the previous Lagrangian takes the following form

$$\begin{aligned}\mathcal{L}_{\mathrm{eff}} = &-\frac{1}{2\cos^2\left(\sqrt{2/3}y\right)}\left[(\partial_\mu x)^2 + (\partial_\mu y)^2\right]\\ &-\frac{\mu^2}{2}\frac{1}{2\cos^2\left(\sqrt{2/3}y\right)}e^{-\sqrt{2/3}x}\left[\cosh\left(\sqrt{\frac{2}{3}}x\right) - \cos\left(\sqrt{\frac{2}{3}}y\right)\right],\end{aligned} \tag{3.12}$$

where $\mu \equiv \hat{\mu}\sqrt{3/c}$. In order to obtain this formula, we have crucially assumed that

$$\lambda = \frac{\mu}{3}\,. \tag{3.13}$$

The form of the effective Lagrangian has also been studied in Ref. [193] in the case where this relation is no longer valid. The last step consists in remarking that $y = 0$ during inflation. If we expand the above Lagrangian about $y = 0$, then the field x is canonically normalized and the potential becomes precisely the one of Eq. (3.9). Therefore, it constitutes another scenario where this potential arises. Let us also notice that other approaches based on superconformal D-term inflation also lead to the Starobinsky model [194]. Various multifield extensions have also been studied in which the inflationary phase can still be described by the one-field Higgs potential [195–197].

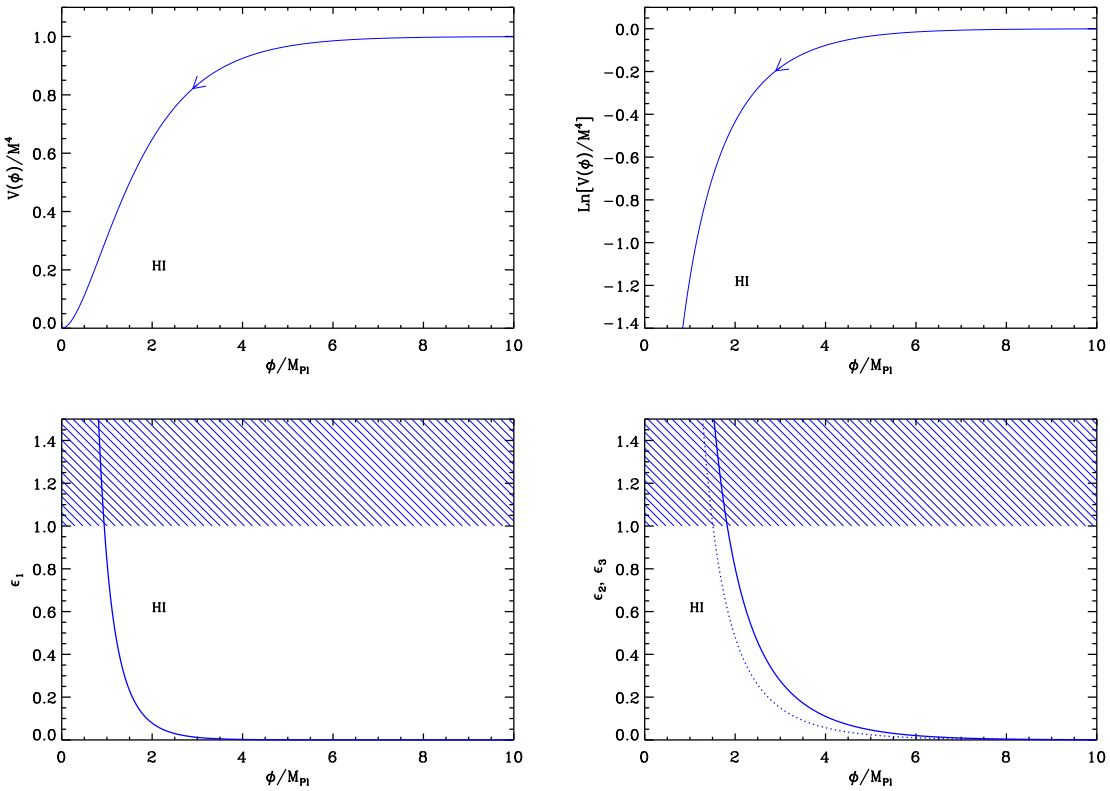

Figure 5. Higgs Inflation (HI). Top left panel: Higgs potential corresponding to Eq. (3.9). Top right panel: logarithm of the Higgs potential. It is clear from these two plots that inflation proceeds from the right to the left. Bottom left panel: slow-roll parameter ϵ_1 as a function of the field ϕ. The shaded area indicates the breakdown of the slow-roll inflation (strictly speaking when the acceleration stops) and we see that, in this model, the end of inflation occurs by violation of the slow-roll conditions. Bottom right panel: slow-roll parameters ϵ_2 (solid line) and ϵ_3 (dotted line) for the same potential.

3.1.2 Slow-Roll Analysis

Having established the shape of the potential, namely

$$V(\phi) = M^4 \left(1 - e^{-\sqrt{2/3}\phi/M_{\rm Pl}}\right)^2 , \tag{3.14}$$

we can now proceed to the slow-roll analysis. For convenience, let us define in the following $x \equiv \phi/M_{\rm Pl}$. Then, the first three slow-roll parameters are given by

$$\begin{aligned} \epsilon_1 &= \frac{4}{3}\left(1 - e^{\sqrt{2/3}x}\right)^{-2}, \qquad \epsilon_2 = \frac{2}{3}\left[\sinh\left(\frac{x}{\sqrt{6}}\right)\right]^{-2}, \\ \epsilon_3 &= \frac{2}{3}\left[\coth\left(\frac{x}{\sqrt{6}}\right) - 1\right]\coth\left(\frac{x}{\sqrt{6}}\right). \end{aligned} \tag{3.15}$$

These quantities are represented in Fig. 5 (left and right bottom panels) together with the potential.

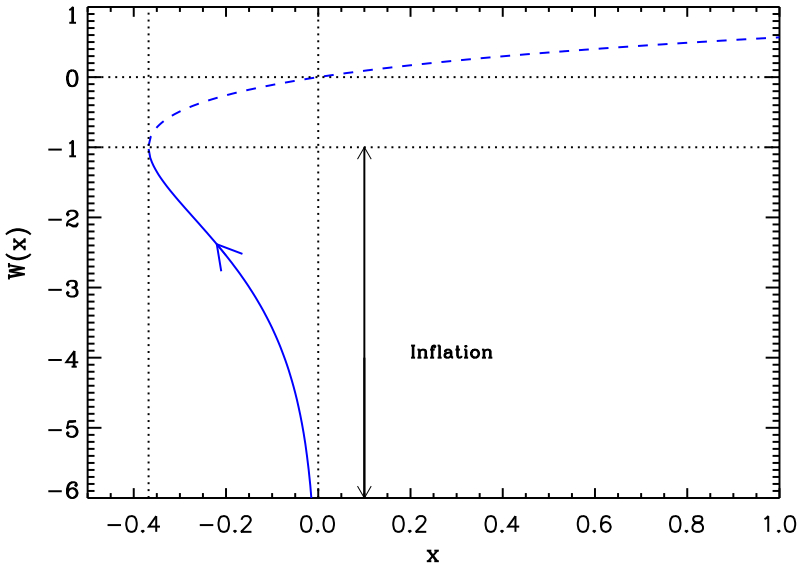

Figure 6. Lambert functions $\mathrm{W}_0(x)$ (dashed line) and $\mathrm{W}_{-1}(x)$ (solid line). During Higgs inflation, inflation proceeds along the "-1" branch in the direction specified by the arrow in the figure.

In this model, as can be noticed on these plots, inflation stops by violation of the slow-roll conditions. The condition $\epsilon_1 = 1$ occurs for $x = x_{\mathrm{end}}$ where x_{end} can be expressed as

$$x_{\mathrm{end}} = \sqrt{\frac{3}{2}} \ln\left(1 + \frac{2}{\sqrt{3}}\right) \simeq 0.94\,. \tag{3.16}$$

In fact, before the end of inflation, the slow-roll approximation breaks down when ϵ_2 becomes greater than 1. This happens for $x = x_{\epsilon_2=1}$ where

$$x_{\epsilon_2=1} = \sqrt{6}\,\mathrm{arcsinh}\left(\sqrt{\frac{2}{3}}\right) \simeq 1.83\,. \tag{3.17}$$

The third slow-roll parameter ϵ_3 also becomes greater than one before the end of inflation (but after the second slow-roll parameter has become unity). The corresponding vacuum expectation value can be written as

$$x_{\epsilon_3=1} = \sqrt{6}\,\mathrm{arctanh}\left(\frac{2}{1+\sqrt{7}}\right) \simeq 1.51\,. \tag{3.18}$$

In the case where the inflaton field is interpreted as the Higgs field, these three vacuum expectation values do not depend on the parameter ξ since this parameter is "hidden" in the mass scale M.

We are now in a position where one can calculate the slow-roll trajectory. Using Eq. (3.14), it can be integrated exactly and yields to

$$N - N_{\mathrm{ini}} = \frac{1}{2}\sqrt{\frac{3}{2}}\,(x - x_{\mathrm{ini}}) - \frac{3}{4}\left(e^{\sqrt{\frac{2}{3}}x} - e^{\sqrt{\frac{2}{3}}x_{\mathrm{ini}}}\right). \tag{3.19}$$

In the regime where $x \gg 1$, the last term is dominant and this is the one usually considered in the literature, see Ref. [184]. The trajectory can be inverted and expressed in term of the "-1-branch" of the Lambert function W_{-1}, leading to

$$x = \sqrt{\frac{3}{2}}\left\{\frac{4}{3}N + \sqrt{\frac{2}{3}}x_{\rm ini} - e^{\sqrt{\frac{2}{3}}x_{\rm ini}} - \mathrm{W}_{-1}\left[-\exp\left(\frac{4}{3}N + \sqrt{\frac{2}{3}}x_{\rm ini} - e^{\sqrt{\frac{2}{3}}x_{\rm ini}}\right)\right]\right\}. \quad (3.20)$$

The fact that inflation proceeds on the -1 branch of the Lambert function W_{-1}, as can be seen in Fig. 6, can be justified by the following considerations. When $N = 0$, the value taken by the Lambert function is $-\exp(\sqrt{2/3}x_{\rm ini})$, which is smaller than -1. On the other hand, if $x = 0$, the value given for N by Eq. (3.19) can be inserted in Eq. (3.20) and one finds that the argument of the Lambert function is -1, i.e. the connection point between the -1 branch and the 0 branch. Therefore inflation takes place between these two points.

Finally, the value of the inflaton field, x_*, calculated $\Delta N_* = N_{\rm end} - N_*$ e-folds before the end of inflation reads

$$\begin{aligned} x_* = \sqrt{\frac{3}{2}}\Bigg(&-\frac{4}{3}\Delta N_* + \ln\left(1+\frac{2}{\sqrt{3}}\right) - \left(1+\frac{2}{\sqrt{3}}\right) \\ &-\mathrm{W}_{-1}\left\{-\exp\left[-\frac{4}{3}\Delta N_* + \ln\left(1+\frac{2}{\sqrt{3}}\right) - \left(1+\frac{2}{\sqrt{3}}\right)\right]\right\}\Bigg). \end{aligned} \quad (3.21)$$

In principle, inserting this formula into the expressions of the slow-roll parameters (3.15) allows us to determine the observational predictions of the model.

At this stage, however, a comment is in order about reheating in the case where the inflaton field is the Higgs field (these remarks do not apply to the supergravity realization of the model). As explained above, all the previous considerations are derived in the Einstein frame. In this frame, matter is not universally coupled to the metric tensor and, therefore, it is compulsory to re-consider the parametrization presented in section 2.2. In the Einstein frame, the matter action is given by $S_{\rm mat}[\psi, A^2(\phi)g_{\mu\nu}]$, where ψ denotes some generic matter field and $g_{\mu\nu} \equiv F(h)\bar{g}_{\mu\nu}$ with $A \equiv F^{-1/2}$, see Ref. [189] (quantities in the Jordan frame are denoted with a bar). In the Jordan frame, the energy density of a (conserved) fluid with a constant equation of state $w = \bar{p}/\bar{\rho}$ scales as $\bar{\rho} \propto \bar{a}^{-3(1+w)}$ while, in the Einstein frame, $\rho \propto A^4\bar{\rho} \propto A^{1-3w}a^{-3(1+w)}$ since the scale factors in the two frames are related by $\bar{a} = Aa$. As explained in Ref. [64] and briefly reviewed in section 2.2, the dependence of the observational predictions on reheating originates from the gradient term $k/\mathcal{H}$ present in the Mukhanov-Sasaki variable equation of motion. In order to evaluate concretely this term, one must relate the comoving wave-number k during inflation with physical scales measured now. Clearly, this depends on the whole history of the Universe and, therefore, explains why the final result depends on the reheating duration. In the Einstein frame, one can show that the gradient term takes the standard form, namely

$$\frac{k}{\mathcal{H}} = \frac{e^{N_{\rm end}-N}}{H}\frac{k}{a_0}\left(\frac{\rho_{\rm end}}{\rho_\gamma}\right)^{1/4}\frac{1}{R_{\rm rad}}, \quad (3.22)$$

with

$$\ln R_{\rm rad} = \frac{1-3w_{\rm reh}}{12(1+w_{\rm reh})}\ln\left(\frac{\rho_{\rm reh}}{\rho_{\rm end}}\right) - \frac{1-3w_{\rm reh}}{3(1+w_{\rm reh})}\ln\left(\frac{A_{\rm reh}}{A_{\rm end}}\right), \quad (3.23)$$

where $w_{\rm reh}$ is the equation of state of the effective dominant fluid during reheating. In the above expressions, it is important to emphasize that all the quantities are defined in the

Einstein frame and that the non-standard scaling of the various energy densities (pressureless matter and radiation) has been systematically taken into account. All the extra terms cancel out except in the definition of the parameter $R_{\rm rad}$ where there is an additional term depending on the function A. Remarkably, this additional term is exactly such that the parameter $R_{\rm rad}$ in the Einstein frame can be re-expressed in terms of the energy densities in the Jordan frame only, namely

$$\ln R_{\rm rad} = \frac{1-3w_{\rm reh}}{12(1+w_{\rm reh})} \ln\left(\frac{\bar{\rho}_{\rm reh}}{\bar{\rho}_{\rm end}}\right). \tag{3.24}$$

Let us stress again that the above equation has an unusual form: it is a quantity in the Einstein frame expressed in terms of quantities defined in the Jordan frame.

It is also important to notice an additional limitation compared to the standard case: in presence of non-minimal coupling to gravity, our parametrization of the reheating stage works only for a constant equation of state $w_{\rm reh}$ while in Ref. [64] it was valid for any $w_{\rm reh}$. We now explain the origin of this limitation. In the Einstein frame, the general expression of the parameter $R_{\rm rad}$ is given by

$$\frac{1}{R_{\rm rad}} = \left(\frac{\rho_{\rm reh}}{\rho_{\rm end}}\right)^{1/4} \frac{a_{\rm reh}}{a_{\rm end}}. \tag{3.25}$$

In order to obtain Eq. (3.23) from that formula, one should express the Einstein frame scale factor in term of the energy density ρ. If the equation of state $w_{\rm reh}$ is a constant, then $a \propto A^{(1-3w_{\rm reh})/(3+3w_{\rm reh})} a^{-1/(3+3w_{\rm reh})}$. This is what has been used above and this led to Eqs. (3.23) and (3.24). But let us now assume that $w_{\rm reh}$ is not a constant (notice that one always has $w = \bar{w}$ since the energy density and the pressure scales with the same power of the function A in the Einstein frame). Then, ρ and a are related by

$$\frac{{\rm d}\rho}{\rho} = (1-3w_{\rm reh})\frac{{\rm d}A}{A} - 3(1+w_{\rm reh})\frac{{\rm d}a}{a}. \tag{3.26}$$

If A is a constant, one can always write [64]

$$\frac{a_{\rm reh}}{a_{\rm end}} = \left(\frac{\rho_{\rm reh}}{\rho_{\rm end}}\right)^{-1/(3+3\overline{w}_{\rm reh})}, \tag{3.27}$$

where $\overline{w}_{\rm reh}$ is the mean equation of state during reheating, namely

$$\overline{w}_{\rm reh} \equiv \frac{1}{N_{\rm reh}-N_{\rm end}} \int_{N_{\rm end}}^{N_{\rm reh}} w_{\rm reh}(n){\rm d}n. \tag{3.28}$$

If A and $w_{\rm reh}$, however, are not constant, it is no longer possible to express the final formula in terms of $\overline{w}_{\rm reh}$. In particular, we do not obtain a term $A^{1-3\overline{w}_{\rm reh}}$ as desired. Therefore, in what follows, we restrict our considerations to the case where the effective fluid dominating the matter content of the Universe has a constant equation of state.

Then, from Eq. (3.22), one can re-express $R_{\rm rad}$ in terms of quantities defined at Hubble radius crossing. One obtains

$$\Delta N_* = \ln R_{\rm rad} - \ln\left(\frac{k/a_0}{\rho_\gamma^{1/4}}\right) + \frac{1}{4}\ln\left(\frac{H_*^2}{M_{\rm Pl}^2\epsilon_{1*}}\right) - \frac{1}{4}\ln\left(\frac{3}{\epsilon_{1*}}\frac{V_{\rm end}}{V_*}\frac{3-\epsilon_{1*}}{3-\epsilon_{1{\rm end}}}\right). \tag{3.29}$$

Of course, this equation resembles a lot Eq. (2.44) but one has to realize that it involves quantities defined in the Einstein frame only. The term $\ln\left[\left(k/a_0\right)/\rho_\gamma^{1/4}\right] = \ln\left[\left(k/\bar{a}_0\right)/\bar{\rho}_\gamma^{1/4}\right]$ and, therefore, its numerical value remains unchanged. The other quantities appearing in this equation are obtained using our standard procedures since they refer to the inflaton sector only. Then, the range of variation of ΔN_* in Eq. (3.29) is determined by putting limits on $\ln R_{\rm rad}$ coming from the fact that reheating must proceed between the end of inflation and the BBN. This means that the physical value of the energy density, that is to say $\bar{\rho}_{\rm reh}$, must be such that $\bar{\rho}_{\rm nuc} \equiv (10{\rm MeV})^4 < \bar{\rho}_{\rm reh} < \bar{\rho}_{\rm end}$. We emphasize that physical limits must of course refer to quantities defined in the Jordan frame. But, precisely, we have shown that $\ln R_{\rm rad}$ in the Einstein frame can be expressed according to the standard formula, provided the energy densities in the argument of the logarithm are Jordan frame energy densities. Therefore, in practice, we have $\Delta N_* \in \left[\Delta N_*^{\rm nuc}, \Delta N_*^{\rm end}\right]$ with

$$\Delta N_*^{\rm end} = -N_0 + \ln\left(\frac{H_*}{M_{\rm Pl}}\right) - \frac{1}{4}\ln\left(\frac{\rho_{\rm end}}{M_{\rm Pl}^4}\right), \tag{3.30}$$

where all the quantities in the above equation are calculated in the Einstein frame and, hence, are directly available since they are, by definition, the outcomes of the `ASPIC` library code. The other limit can be expressed as

$$\Delta N_*^{\rm nuc} = -N_0 + \ln\left(\frac{H_*}{M_{\rm Pl}}\right) - \frac{1}{3(1+w)}\ln\left(\frac{\bar{\rho}_{\rm end}}{M_{\rm Pl}^4}\right) - \frac{1-3w}{12(1+w)}\ln\left(\frac{\bar{\rho}_{\rm nuc}}{M_{\rm Pl}^4}\right). \tag{3.31}$$

The quantity $\bar{\rho}_{\rm nuc}$ is defined in the Jordan frame but its value is explicitly known, see above. On the other hand, we need to evaluate $\bar{\rho}_{\rm end}$ since the code only delivers $\rho_{\rm end}$. By definition, we have

$$\bar{\rho}_{\rm end} = \frac{\rho_{\rm end}}{A_{\rm end}^4} = F_{\rm end}^2\rho_{\rm end} = \left(1+\xi h_{\rm end}^2\right)^2\rho_{\rm end}. \tag{3.32}$$

But $1+\xi h_{\rm end}^2 = e^{2\chi_{\rm end}/\sqrt{3}}$ and $\chi_{\rm end} = \phi_{\rm end}/(\sqrt{2}M_{\rm Pl}) = \sqrt{3}/2\ln\left(1+2/\sqrt{3}\right)$. As a consequence, the relation between the two final energy densities in the two frames can be written as

$$\bar{\rho}_{\rm end} = \left(1+\frac{2}{\sqrt{3}}\right)^2\rho_{\rm end} \simeq 2.15\,\rho_{\rm end}. \tag{3.33}$$

Therefore, the lower bound is only slightly modified (recall that $\bar{\rho}_{\rm end}$ appears in a logarithmic term). Anyway, given the uncertainty in the definition of $\bar{\rho}_{\rm nuc}$, it is irrelevant to include this tiny correction in our determination of ΔN_*. Consequently, we conclude that the range of variation of ΔN_* can be obtained without modifying anything to our usual way to calculate it and one can use the `ASPIC` code without introducing these negligible corrections. Of course, if one considers that the potential studied here comes from supergravity, the above considerations just not apply and one can work with the standard approach.

The reheating consistent observational predictions of Higgs inflation are represented in Fig. 81 where we have displayed their dependence in the reheating temperature defined in the Jordan frame by $g_*^{1/4}\bar{T}_{\rm reh} = \left(30\bar{\rho}_{\rm reh}/\pi^2\right)^{1/4}$. Notice that, a priori, the reheating temperature can be calculated exactly in Higgs inflation since all the couplings between the Higgs and the other fields in the standard model are known. This gives a spectral index which is in good agreement with the data and a small contribution of gravity waves. At this stage, in the Higgs case, we do not have constraints on the parameter ξ since it is hidden in the mass scale

M. Its observational value therefore comes from the amplitude of the CMB anisotropies and reads

$$\frac{M^4}{M_{\rm Pl}^4} = 1920\pi^2 \left(1 - e^{\sqrt{\frac{2}{3}}x_*}\right)^{-4} e^{2\sqrt{\frac{2}{3}}x_*} \frac{Q_{\rm rms-PS}^2}{T^2}\,. \tag{3.34}$$

Upon using the trajectory given by Eq. (3.21), the mass scale M can be written as $M/M_{\rm Pl} \simeq 0.02\,(\Delta N_*)^{-3/2}$, which for the fiducial value $\Delta N_* = 55$, implies that $M \simeq 4\times10^{-5}M_{\rm Pl}$, i.e., roughly speaking, inflation takes place at the GUT scale in this model. Then, using this expression of M, one obtains the following numerical value for the parameter ξ,

$$\xi \simeq 49000\sqrt{\lambda}\,, \tag{3.35}$$

where we have considered $\lambda = m_{\rm H}/v$, with $v \simeq 175{\rm GeV}$ and $m_{\rm H} \simeq 125{\rm GeV}$ (see Refs. [182, 183]). These considerations are in agreement with the conclusions obtained in Refs. [184–186]. If we now consider the supergravity realization of the model, one obtains a constraint on the parameter $\hat{\mu}$, that is to say if one takes $c = 1$ on μ and λ, see Ref. [193].

4 One Parameter Models

4.1 Radiatively Corrected Higgs Inflation (RCHI)

4.1.1 Theoretical Justifications

Let us consider again the model given by Eq. (3.1). The three functions describing this action are modified when quantum corrections are taken into account. As a consequence, the potential which supports inflation is also modified and this leads to a new inflationary scenario that we call Radiatively Corrected Higgs Inflation (RCHI). This scenario has been studied in Refs. [198–203]. At first order, the corrections to the function $Z(h)$ can be neglected while the corrections to $F(h)$ and to $U(h)$ read

$$F(h) = 1 + \xi h^2 + \frac{C}{16\pi^2}h^2 \ln\left(\frac{M_{\rm Pl}^2h^2}{\mu^2}\right), \tag{4.1}$$

$$U(h) = M_{\rm Pl}^2\frac{\lambda}{4}\left(h^2 - \frac{v^2}{M_{\rm Pl}^2}\right)^2 + \frac{\lambda A}{128\pi^2}M_{\rm Pl}^2h^4\ln\left(\frac{M_{\rm Pl}^2h^2}{\mu^2}\right), \tag{4.2}$$

where μ is the renormalization scale and A and C are two new constants given by

$$A = \frac{3}{8\lambda}\left[2g^4 + \left(g^2 + g'^2\right) - 16y_{\rm t}^4\right] + 6\lambda + \mathcal{O}\left(\xi^{-2}\right), \tag{4.3}$$

$$C = 3\xi\lambda + \mathcal{O}\left(\xi^0\right), \tag{4.4}$$

$y_{\rm t}$ being the Yukawa coupling of the top quark and g and g' the coupling constants of the $\mathrm{SU(2)_L}$ and $\mathrm{U(1)_Y}$ groups. The presence of quantum corrections modifies the relation between the Jordan and the Einstein frames and changes the shape of the potential in the Einstein frame. Assuming the smallness of $A/(32\pi^2) \ll 1$ and $C/(8\pi^2\xi) \ll 1$, which is necessary for the consistence of the one-loop calculation (the second condition is in fact equivalent to $C\lambda/(8\pi^2) \ll 1$ because C is proportional to ξ), one obtains the following expression

$$V \simeq \frac{M_{\rm Pl}^4\lambda}{4\xi^2}\frac{\xi^2h^4}{\left(1+\xi h^2\right)^2}\left[1 - \frac{\xi h^2}{1+\xi h^2}\frac{C}{8\pi^2\xi}\ln\left(\frac{M_{\rm Pl}^2h^2}{\mu^2}\right) + \frac{A}{32\pi^2}\ln\left(\frac{M_{\rm Pl}^2h^2}{\mu^2}\right)\right]. \tag{4.5}$$

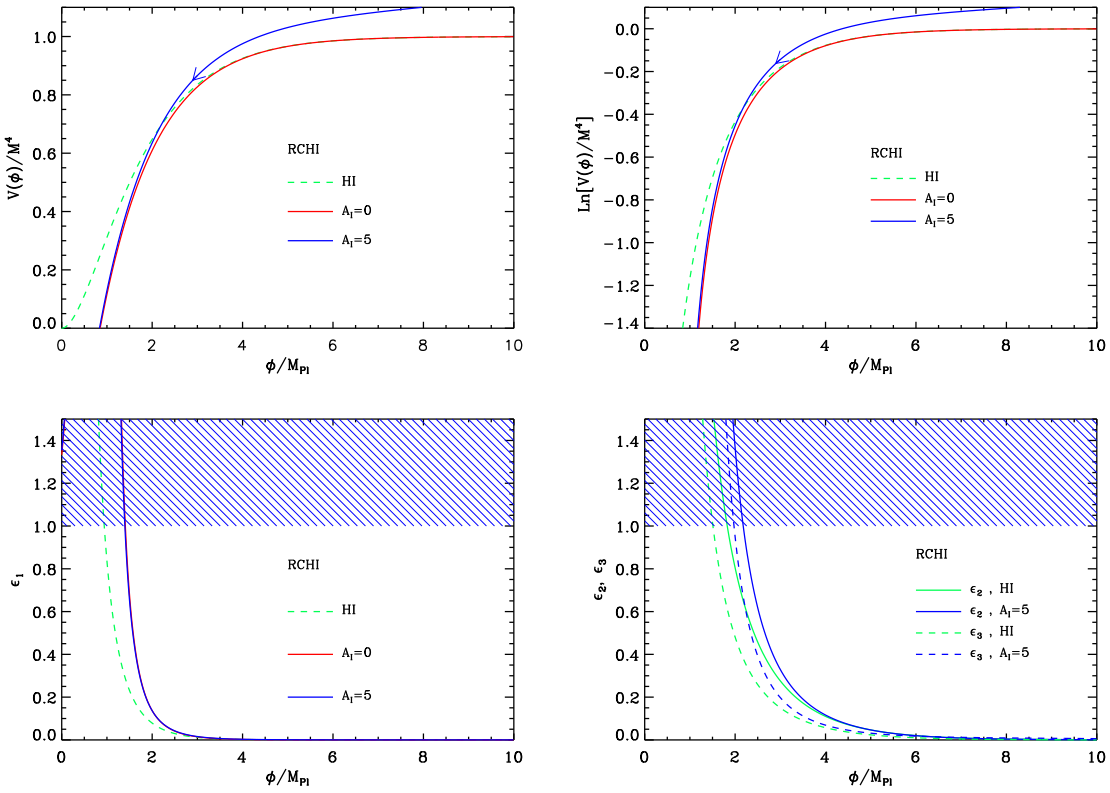

Figure 7. Top left panel: the solid blue line represents the radiatively corrected Higgs potential, see Eq. (4.11), with $A_{\rm I} = 5$. It is compared to the tree level potential given by Eq. (3.9) (dashed green line) and to Eq. (4.11) with $A_{\rm I} = 0$ (solid red line) which is supposed to be a good approximation of the tree level potential. It is obvious that this is indeed the case in the regime of interest, where the *vev* of the Higgs field is not too small. Top right panel: logarithm of potential, the three lines and the color code having the same meaning as in the top left panel. Bottom left panel: slow-roll parameter ϵ_1 as a function of the field ϕ, still with the same convention. As can be seen in this plot, even in presence of radiative corrections, the end of inflation occurs by violation of the slow-roll condition. Bottom right panel: slow-roll parameters ϵ_2 (solid blue line) and ϵ_3 (dashed blue line) for $A_{\rm I} = 5$ compared to their tree level counter parts (solid and dashed green lines, respectively).

Of course, if $A = C = 0$, one checks that this potential reduces to the potential of the previous section. Notice that, at this stage, we have not assumed that $\xi h^2 \gg 1$. If we further postulate that $\xi h^2 \gg 1$ and approximate $\xi^2 h^4/\left(1+\xi h^2\right)^2 \simeq 1 - 2/(\xi h^2)$, then the above formula reduces to

$$V \simeq \frac{M_{\rm Pl}^4 \lambda}{4\xi^2}\left[1 - \frac{2}{\xi h^2} + \frac{A_{\rm I}}{16\pi^2}\ln\left(\frac{M_{\rm Pl} h}{\mu}\right)\right], \tag{4.6}$$

where $A_{\rm I} \equiv A - 12\lambda$ is the inflationary anomalous scaling. This formula coincides with Eq. (6) of Ref. [200] and Eq. (9) of Ref. [202]. Although the above formulas give V in the Einstein frame, it is still expressed in term of h. The expression for the field in the Einstein frame, χ, remains to be established. Assuming the smallness of the loop corrections (but, here, we do

not yet assume that $\xi h^2 \gg 1$), we obtain

$$\frac{\mathrm{d}\chi}{\mathrm{d}h} \simeq \frac{\sqrt{3}h\xi}{(1+\xi h^2)}\left[1+\frac{C}{16\pi^2\xi}+\frac{C}{8\pi^2\xi}\frac{1}{1+\xi h^2}\ln\left(\frac{M_{\rm Pl}h}{\mu}\right)\right]. \tag{4.7}$$

Notice that, in order to obtain this equation, we have neglected a term proportional to $1/(\xi h)^2 \ll 1$. Contrary to the assumption $\xi h^2 \gg 1$, the condition $(\xi h)^2 \gg 1$ was also used in section 3.1. Then, the integration of this differential equation leads to

$$\chi \simeq \frac{\sqrt{3}}{2}\ln\left(1+\xi h^2\right)+\frac{\sqrt{3}C}{16\pi^2\xi}\left[\ln h-\frac{1}{1+\xi h^2}\ln\left(\frac{M_{\rm Pl}h}{\mu}\right)\right]. \tag{4.8}$$

Using only now the limit $\xi h^2 \gg 1$, this expression reduces to

$$\chi \simeq \frac{\sqrt{3}}{2}\ln\left(\xi h^2\right)+\frac{\sqrt{3}C}{16\pi^2\xi}\ln h. \tag{4.9}$$

As expected the relation between the Jordan frame field h and the Einstein frame field χ is modified by the quantum corrections. Inverting the above formula gives

$$\xi^{1/2}h \simeq e^{\chi/\sqrt{3}}-\frac{C}{16\pi^2\xi}e^{\chi/\sqrt{3}}\left(\frac{\chi}{\sqrt{3}}-\frac{1}{2}\ln\xi\right). \tag{4.10}$$

This equation allows us to find the expression of the potential in the Einstein frame. Inserting Eq. (4.10) into Eq. (4.6) and introducing the canonically normalized field $\phi \equiv \sqrt{2}M_{\rm Pl}\chi$, one obtains

$$\begin{aligned} V(\phi) &\simeq \frac{M_{\rm Pl}^4\lambda}{4\xi^2}\left[1-2e^{-2\phi/(\sqrt{6}M_{\rm Pl})}-\frac{C}{4\pi^2\xi}e^{-2\phi/(\sqrt{6}M_{\rm Pl})}\left(\frac{\phi}{\sqrt{6}M_{\rm Pl}}-\frac{1}{2}\ln\xi\right)\right. \\ &\left.+\frac{A_{\rm I}}{16\pi^2}\ln\left(\frac{M_{\rm Pl}}{\mu\sqrt{\xi}}\right)+\frac{A_{\rm I}}{16\pi^2}\frac{\phi}{\sqrt{6}M_{\rm Pl}}\right] \\ &\simeq \frac{M_{\rm Pl}^4\lambda}{4\xi^2}\left[1-2e^{-2\phi/(\sqrt{6}M_{\rm Pl})}+\frac{A_{\rm I}}{16\pi^2}\frac{\phi}{\sqrt{6}M_{\rm Pl}}\right]. \end{aligned} \tag{4.11}$$

We see that we now deal with a "one parameter model", $A_{\rm I}$, since the mass scale $M^4 \equiv M_{\rm Pl}^4\lambda/(4\xi^2)$ is determined by the COBE normalization. In the case $A_{\rm I}=0$, it is also interesting to compare the above potential with the one given by Eq. (3.9). We see that this corresponds to assuming that the exponential $e^{-2\phi/(\sqrt{6}M_{\rm Pl})} \ll 1$ (or, equivalently, $\phi/M_{\rm Pl} \gg 1$) and to expand the corresponding expression at first order in this small parameter. This leads to the following formula: $V \simeq M^4\left[1-2e^{-2\phi/(\sqrt{6}M_{\rm Pl})}\right]$, i.e. exactly Eq. (4.11) for $A_{\rm I}=0$. It is worth remarking that this approximation is not very good towards the end of inflation. Indeed, it is easy to show that (see below), for the potential (4.11) with $A_{\rm I}=0$, $\phi_{\rm end}/M_{\rm Pl} = \sqrt{3/2}\ln\left(2+2/\sqrt{3}\right) \simeq 1.4$ which should be compared with Eq. (3.16) for the potential (3.9) according to which $\phi_{\rm end}/M_{\rm Pl} \simeq 0.94$.

4.1.2 Slow-Roll Analysis

Given the potential (4.11), namely

$$V(\phi) = M^4\left[1-2e^{-2\phi/(\sqrt{6}M_{\rm Pl})}+\frac{A_{\rm I}}{16\pi^2}\frac{\phi}{\sqrt{6}M_{\rm Pl}}\right], \tag{4.12}$$

we can now proceed to the slow-roll analysis. The potential (4.12) is represented and compared with its tree level counterpart in Fig. 7. Defining $x \equiv \phi/M_{\rm Pl}$, the three first slow-roll parameters can be written as

$$\epsilon_1 = \frac{1}{12}\left[\frac{4e^{-\sqrt{2/3}x} + A_{\rm I}/(16\pi^2)}{1 - 2e^{-\sqrt{2/3}x} + A_{\rm I}/(32\pi^2)\sqrt{2/3}x}\right]^2, \tag{4.13}$$

$$\epsilon_2 = \frac{1}{3}\frac{8e^{-\sqrt{2/3}x}\left[1 + A_{\rm I}/(16\pi^2) + A_{\rm I}/(32\pi^2)\sqrt{2/3}x\right] + A_{\rm I}^2/(256\pi^4)}{\left[1 - 2e^{-\sqrt{2/3}x} + A_{\rm I}/(32\pi^2)\sqrt{2/3}x\right]^2}, \tag{4.14}$$

and

$$\begin{aligned}\epsilon_3 = {} & 12\left(4 + \frac{A_{\rm I}}{16\pi^2}e^{\sqrt{2/3}x}\right)\left\{48 + 8\frac{A_{\rm I}}{16\pi^2}\left(9 + \sqrt{6}x\right) + 3\frac{A_{\rm I}^3}{4096\pi^6}e^{2\sqrt{2/3}x}\right. \\ & \left. + 2e^{\sqrt{2/3}x}\left[12 + 18\frac{A_{\rm I}}{16\pi^2}\left(1 + \frac{A_{\rm I}}{16\pi^2}\right) + \sqrt{6}\frac{A_{\rm I}}{16\pi^2}\left(4 + 3\frac{A_{\rm I}}{16\pi^2}\right)x + 2\frac{A_{\rm I}^2}{256\pi^4}x^2\right]\right\} \\ & \times\left[24 + \frac{A_{\rm I}}{16\pi^2}\left(24 + 4\sqrt{6}x + 3\frac{A_{\rm I}}{16\pi^2}e^{\sqrt{2/3}x}\right)\right]^{-1}\left[-12 + e^{\sqrt{2/3}x}\left(6 + \sqrt{6}\frac{A_{\rm I}}{16\pi^2}x\right)\right]^{-2}.\end{aligned} \tag{4.15}$$

These three slow-roll parameters are represented in Fig. 7 (bottom panels). It is interesting to compare these formulas with the expressions derived in Ref. [198] [see Eqs. (22) and (23) of that paper]. An approximate equation for the first slow-roll parameter is obtained by neglecting the second and third terms in the denominator of Eq. (4.13), which, as a matter of fact, consists in writing $V(\phi) \simeq M^4$. Then, it follows that

$$\epsilon_1 \simeq \frac{4}{3}e^{-2\sqrt{2/3}x}\left(1 + \frac{A_{\rm I}}{64\pi^2}e^{\sqrt{2/3}x}\right)^2 \simeq \frac{4}{3}\frac{1}{\xi^2 h^4}\left(1 + \frac{h^2}{h_{\rm I}^2}\right)^2, \tag{4.16}$$

where we have defined $h_{\rm I}^2 \equiv 64\pi^2/(\xi A_{\rm I})$ in agreement with Ref. [198]. The same approximation is made for the second slow-roll parameter (except that Ref. [198] calculates $\hat{\eta} \equiv M_{\rm Pl}^2 V_{\phi\phi}/V$ rather than ϵ_2). The second field derivative of the potential can be written as $V_{\phi\phi} = -4M^4 e^{-\sqrt{2/3}x}/(3M_{\rm Pl}^2)$ and, therefore, if one considers that $V(\phi) \simeq M^4$, then $\hat{\eta} \simeq -4/(3\xi h^2)$. We conclude that our expressions of ϵ_1 and ϵ_2 reproduce Eqs. (22) and (23) of Ref. [198] in the limit where $V(\phi) \simeq M^4$.

Let us now study how inflation ends in this model. From Fig. 7, it is clear that this occurs by violation of the slow-roll conditions. Working out the condition $\epsilon_1 = 1$, it follows that

$$x_{\rm end} = \frac{1}{\sqrt{2}} - \sqrt{\frac{3}{2}}\frac{32\pi^2}{A_{\rm I}} + \sqrt{\frac{3}{2}}{\rm W}_{-1}^{0}\left[\frac{64\pi^2}{A_{\rm I}}\left(1 + \frac{1}{\sqrt{3}}\right)e^{32\pi^2/A_{\rm I} - 1/\sqrt{3}}\right], \tag{4.17}$$

where, if $A_{\rm I} > 0$, ${\rm W}_{-1}^{0} = {\rm W}_0$ while, if $A_{\rm I} < 0$, ${\rm W}_{-1}^{0} = {\rm W}_{-1}$.

We now turn to the slow-roll trajectory. It can be integrated exactly and straightforward manipulations lead to the following expression

$$N - N_{\rm ini} = \sqrt{\frac{3}{2}}\, x - \frac{48\pi^2}{A_{\rm I}} \left[1 + \frac{A_{\rm I}}{32\pi^2}\left(1 + \sqrt{\frac{2}{3}}\, x\right)\right] \ln\left(1 + \frac{A_{\rm I}}{64\pi^2} e^{\sqrt{2/3}\, x}\right) - \frac{3}{2}{\rm Li}_2\left(-\frac{A_{\rm I}}{64\pi^2} e^{\sqrt{2/3}\, x}\right) - \sqrt{\frac{3}{2}} x_{\rm ini} + \frac{48\pi^2}{A_{\rm I}} \left[1 + \frac{A_{\rm I}}{32\pi^2}\left(1 + \sqrt{\frac{2}{3}}\, x_{\rm ini}\right)\right] \times \ln\left(1 + \frac{A_{\rm I}}{64\pi^2} e^{\sqrt{2/3}\, x_{\rm ini}}\right) + \frac{3}{2}{\rm Li}_2\left(-\frac{A_{\rm I}}{64\pi^2} e^{\sqrt{2/3}\, x_{\rm ini}}\right), \tag{4.18}$$

where ${\rm Li}_2$ denotes the dilogarithm function [204, 205]. Let us also notice that if we use the approximation $V(\phi) \simeq M^4$ already discussed before, then one can obtain a much simpler formula, namely

$$N - N_{\rm ini} = -\frac{48\pi^2}{A_{\rm I}} \ln\left(1 + \frac{A_{\rm I}}{64\pi^2} e^{\sqrt{2/3}\, x}\right) + \frac{48\pi^2}{A_{\rm I}} \ln\left(1 + \frac{A_{\rm I}}{64\pi^2} e^{\sqrt{2/3}\, x_{\rm ini}}\right). \tag{4.19}$$

This expression is in agreement with Eq. (24) of Ref. [198]. In this case, the trajectory can even be inverted and the corresponding expression for the field ϕ reads

$$x = \sqrt{\frac{3}{2}} \ln\left[\left(\frac{64\pi^2}{A_{\rm I}} + e^{\sqrt{2/3}\, x_{\rm ini}}\right) e^{A_{\rm I}(N - N_{\rm ini})/(48\pi^2)} - \frac{64\pi^2}{A_{\rm I}}\right]. \tag{4.20}$$

We are now in a position where the predictions of the models can be calculated. They are presented in Fig. 81. We see that very negative values of $A_{\rm I}$ are incompatible with the CMB while large values of $A_{\rm I}$ remain close to the allowed contours. Of course $|A_{\rm I}|$ cannot be too large since we have required $A_{\rm I}/(64\pi^2) \ll 1$. We have chosen the upper bound in Fig. 81 to be $A_{\rm I} = 100$ for which $A_{\rm I}/(64\pi^2) \simeq 0.16$, i.e. still a reasonable number. It is interesting to compare these findings with the existing literature. Using the approximate trajectory (4.19) and neglecting the contribution originating from the end of inflation, one obtains

$$x_* = \sqrt{\frac{3}{2}} \ln\left[\frac{64\pi^2}{A_{\rm I}}\left(e^{x_{\rm BKS}} - 1\right)\right], \tag{4.21}$$

where $x_{\rm BKS} \equiv A_{\rm I}\Delta N_*/(48\pi^2)$ ($x_{\rm BKS}$ is denoted x in Ref. [198]). Then, from Eq. (4.16) and the fact that $\epsilon_2 = 4\epsilon_1 - 2\hat{\eta}$, it follows that

$$\epsilon_1 = \frac{4}{3}\left(\frac{A_{\rm I}}{64\pi^2}\right)^2 \left(\frac{e^{x_{\rm BKS}}}{e^{x_{\rm BKS}} - 1}\right)^2 = \frac{3}{4\Delta N_*^2}\left(\frac{x_{\rm BKS} e^{x_{\rm BKS}}}{e^{x_{\rm BKS}} - 1}\right)^2, \tag{4.22}$$

$$\epsilon_2 = 4\epsilon_1 + \frac{8}{3}\frac{A_{\rm I}}{64\pi^2}\frac{1}{e^{x_{\rm BKS}} - 1} = 4\epsilon_1 + \frac{2}{\Delta N_*}\frac{x_{\rm BKS}}{e^{x_{\rm BKS}} - 1}. \tag{4.23}$$

From these two expressions, one deduces that

$$n_{\rm S} = 1 - \frac{2}{\Delta N_*}\frac{x_{\rm BKS}}{e^{x_{\rm BKS}} - 1}, \quad r = \frac{12}{\Delta N_*^2}\left(\frac{x_{\rm BKS} e^{x_{\rm BKS}}}{e^{x_{\rm BKS}} - 1}\right)^2. \tag{4.24}$$

Notice that, in the formula giving the spectral index, the contribution originating from ϵ_1 has been neglected since it scales $\propto 1/\Delta N_*^2$. These approximate expressions match Eqs. (32)

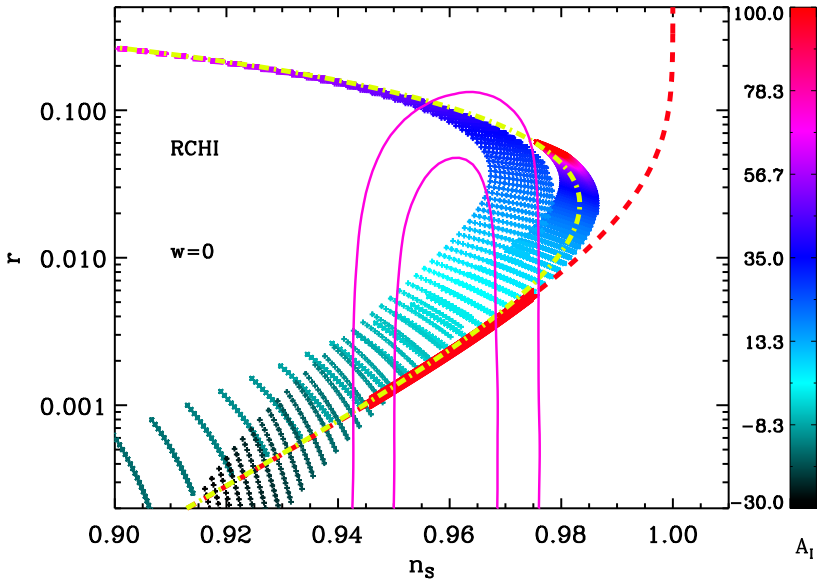

Figure 8. Predictions of the RCHI model in the plane $(n_{\rm S}, r)$. The exact slow-roll predictions (colored segments starting in black/green at the bottom/left part of the plot and ending in red right slightly on the right of the allowed contours) are compared to various approximations represented by the second collection of colored segments, by the red thick dashed line and by the yellow dotted-dashed line, see the text for a detailed explanation. In the regime $10 < A_{\rm I} < 100$, the exact predictions significantly differ from the approximate ones.

and (34) of Ref. [198]. For $\Delta N_* = 60$, they can be represented as a line $r = r(n_{\rm S})$ in the plane $(n_{\rm S}, r)$, the parameter along the curve being $A_{\rm I}$. This line has been plotted in Fig. 8 for $-30 < A_{\rm I} < 100$ (red dashed line). Requiring $0.9457 < n_{\rm S} < 0.9749$ which is the 2σ Planck range [153] (or $0.934 < n_{\rm S} < 0.988$, which is the 2σ range coming from combining the WMAP 9th year data, the Baryon Acoustic Oscillations (BAO) data and the Supernovae measurements), one obtains the solid thick red segment. It follows that $-8 \lesssim A_{\rm I} \lesssim 4$ (or $-12 \lesssim A_{\rm I} \lesssim 14$ with WMAP, again in agreement with Ref. [198]). These predictions are compared to the exact slow-roll predictions of Fig. 81. As before, the slow-roll predictions are represented by a collection of segments, each segment corresponding to different values of $A_{\rm I}$ and each point of a given segment being in one-to-one correspondence with a given reheating temperature. The exact slow-roll predictions are such that, for $A_{\rm I} < 0$, the green segments go to the bottom left side of the figure while for $A_{\rm I} \to 100$, the pink/red segments remain close to the allowed contours (see also Fig. 81). In the limit of "large" positive values of $A_{\rm I}$, the exact slow-roll predictions and the predictions based on Eqs. (4.24) significantly differ. While, in order to remain close to the allowed contours, Eqs. (4.24) tell us that $A_{\rm I} \lesssim 4$, the exact slow-roll predictions show that the model is still viable for any positive values of $A_{\rm I} \lesssim 100$. We conclude that the upper bound $A_{\rm I} \lesssim 4$ (with the WMAP data, $A_{\rm I} \lesssim 14$) is inaccurate and is just an artifact due to the inaccurate nature of the "approximation to the slow-roll approximation".

Let us try to identify the origin of this discrepancy more precisely. In order to investigate this issue, we have also represented in Fig. 8, the predictions obtained when the approximate

trajectory (4.19), the approximate expression of the first slow-roll parameter (4.16) and the relation $\epsilon_2 = 4\epsilon_1 - 2\hat{\eta}$ but, now, without neglecting ϵ_1, are used together with an exact expression for $\phi_{\rm end}$. They are represented by the second collections of segments in Fig. 8. We see that for $A_{\rm I} \gtrsim 0$, they differ from the red thick solid line and bend toward the upper left part of the plot which is also the direction taken by the exact predictions. This suggests that neglecting the term $4\epsilon_1$ in the expression of ϵ_2 causes a non-negligible error. This is confirmed if, instead of using Eq. (4.24) for $n_{\rm S}$, we now take

$$n_{\rm S} = 1 - \frac{3}{2\Delta N_*^2}\left(\frac{x_{\rm BKS}e^{x_{\rm BKS}}}{e^{x_{\rm BKS}}-1}\right)^2 - \frac{2}{\Delta N_*}\frac{x_{\rm BKS}}{e^{x_{\rm BKS}}-1}, \tag{4.25}$$

and plot again the line $r = r(n_{\rm S})$. This gives the yellow dotted-dashed curve which follows the second collection of segments. If, however, we compare the red segments, namely those with $A_{\rm I}$ "large", corresponding the exact predictions to the approximate red ones, we see that including the term $4\epsilon_1$ is not sufficient. For $A_{\rm I} \simeq 60$, the exact predictions are roughly compatible with the data while the segments corresponding to the approximate formulas are not. We conclude that RCHI represents a textbook case for `ASPIC`. It illustrates that, sometimes, "approximating the slow-roll approximation" can lead to too drastic conclusions, especially given the current accuracy of the data. It is an additional motivation to use the slow-roll method without any other scheme of approximations and this is the essence of the `ASPIC` project presented in this article.

A last word is in order concerning the constraints on the parameter $A_{\rm I}$. Particle physics implies that $-48 \lesssim A_{\rm I} \lesssim -20$ and the previously discussed inaccuracies were concerning only a weaker upper limit on $A_{\rm I}$. On the contrary, we see in Fig. 8 that the bound $A_{\rm I} \gtrsim -8$ is accurate whatever the approximation scheme chosen. Therefore, when particle physics and cosmological data are simultaneously taken into account, the conclusions of Ref. [198] are unchanged and RCHI remains disfavored.

Finally, the scale M can be determined from the CMB normalization and this leads to the following expression

$$\frac{M^4}{M_{\rm Pl}^4} = 120\pi^2\frac{Q_{\rm rms-PS}^2}{T^2}\frac{\left[4\,e^{-\sqrt{2/3}x_*} + A_{\rm I}/(16\pi^2)\right]^2}{\left[1 - 2\,e^{-\sqrt{2/3}x_*} + A_{\rm I}/(32\pi^2)\sqrt{2/3}x_*\right]^3}. \tag{4.26}$$

The knowledge of ϕ_* allows us to find the posterior distribution of M, that is to say of λ/ξ^2 or ξ, since the Higgs self coupling, $\lambda = m_{\rm H}/v$, is now known.

4.2 Large Field Inflation (LFI)

4.2.1 Theoretical Justifications

Large fields models, also referred to as chaotic inflation [206], are characterized by the monomial potential [207–211] $V(\phi) \propto M^4\phi^p$. The number p is the only model parameter, in addition to the normalization M of the potential. The index p is usually a positive integer (and it was recently realized in Ref. [212] that this type of scenario can emerge in the context of supergravity) but various models have been proposed in which it can also be a rational number [213–218]. It is interesting to briefly discuss concrete models where this is actually the case. Here, we follow Refs. [217, 218]. These models are supergravity models where one assumes that the Kähler potential is invariant under a generalization of the shift symmetry

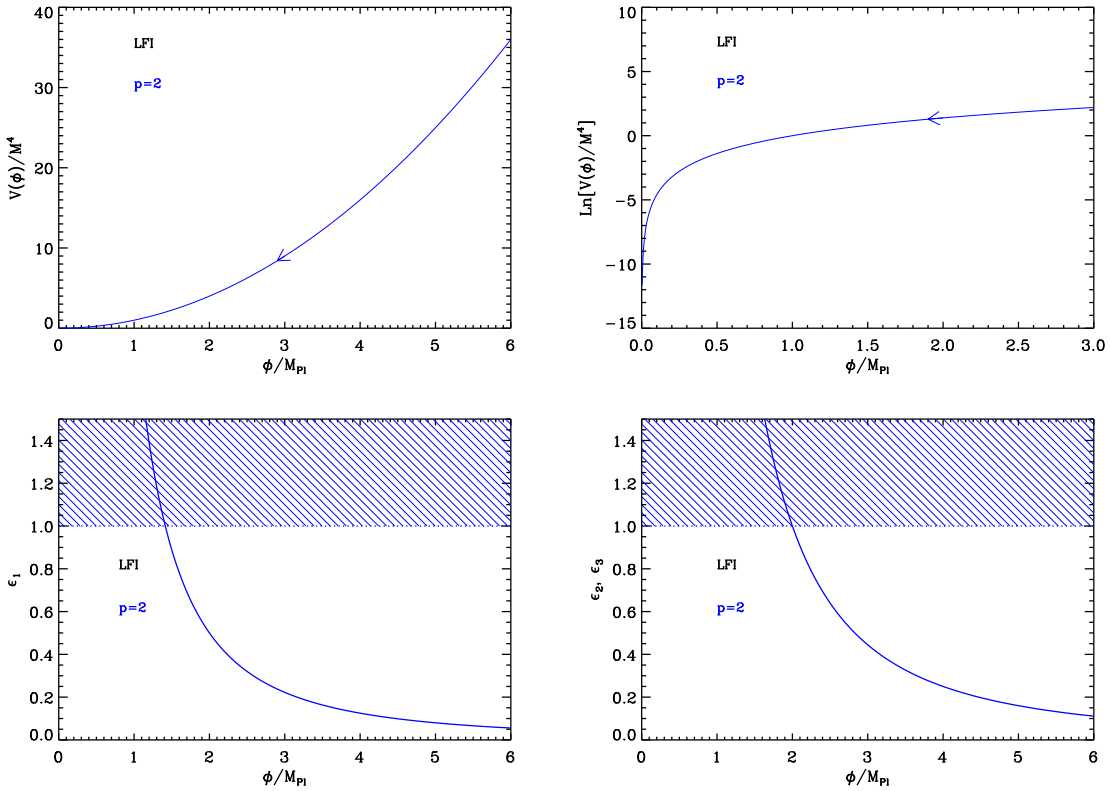

Figure 9. Large Field Inflation (LFI). Top left panel: large field potential for $p = 2$. Top right panel: logarithm of the potential for the same value of p. The required flatness of the potential becomes obvious on this plot. Bottom left panel: slow-roll parameter ϵ_1 for a large field potential with $p = 2$. The shaded area indicates where acceleration stops. Bottom right panel: slow-roll parameters ϵ_2 and ϵ_3 for a large field potential with $p = 2$. Only one curve appears because $\epsilon_2 = \epsilon_3$. On this plot, the shaded region signals the breakdown of the slow-roll approximation, which is not necessarily the end of the accelerated phase.

(usually needed in order to avoid the so called η-problem). In the present case, the transformation is taken to be $\chi^n \to \chi^n + \alpha$ where α is a real number and χ a chiral superfield. This means that the Kähler potential should be a function of $\chi^n - \chi^{\dagger n}$ only. In addition, we allow the presence of a small breaking term in the Kähler potential of the form $b\chi\chi^\dagger$ where $b \ll 1$. We also assume that the superpotential breaks the generalized shift symmetry. Summarizing, we assume that

$$K = b\chi\chi^\dagger + c_1\kappa^{(n-1)/2}\left(\chi^n - \chi^{\dagger n}\right) - \frac{\kappa^{n-1}}{2}\left(\chi^n - \chi^{\dagger n}\right)^2 + XX^\dagger, \tag{4.27}$$

$$W = \lambda X\chi^m, \tag{4.28}$$

where X is another superfield and λ and c_1 (notice that it is pure imaginary) are constant. The model is parametrized by the quantities n and m and $\kappa \equiv 1/M_{\rm Pl}^2$. If, during inflation, X acquires a large mass compared to the Hubble parameter and is stabilized at the origin, $\langle X\rangle = 0$, then it is not difficult to show that this supergravity model can be described by the

following effective Lagrangian

$$\mathcal{L} = -\left[b + n^2\kappa^{n-1}\left(\chi\chi^\dagger\right)^{n-1}\right]\partial_\mu\chi\partial^\mu\chi^\dagger - \exp\left[b\kappa|\chi|^2 + c_1\kappa^{n/2}\left(\chi^n - \chi^{\dagger n}\right) - \frac{\kappa^n}{2}\left(\chi^n - \chi^{\dagger n}\right)^2\right]\lambda^2\left(\chi\chi^\dagger\right)^m. \quad (4.29)$$

Then, one can write the field χ in polar form, $\chi \equiv \alpha e^{i\beta}$ (α is of dimension one and β dimensionless) and the above potential takes the form

$$V = \lambda^2\alpha^{2m}\exp\left[b\kappa\alpha^2 + 2ic_1\kappa^{n/2}\alpha^n\sin(n\beta) + 2\kappa^n\alpha^{2n}\sin^2(n\beta)\right]. \quad (4.30)$$

Writing $\partial V/\partial\beta = 0$, one obtains the condition $2i\kappa^{n/2}\alpha^n\sin(n\beta) = -ic_1$ or $\kappa^{n/2}\left(\chi^n - \chi^{\dagger n}\right) = c_1$. It is thus natural to assume that the inflaton field rolls along that direction. As a consequence, the effective Lagrangian takes the form

$$\mathcal{L} = -\left[b + n^2\kappa^{n-1}\left(\chi\chi^\dagger\right)^{n-1}\right]\partial_\mu\chi\partial^\mu\chi^\dagger - e^{b\kappa|\chi|^2 + c_1^2/2}\lambda^2\left(\chi\chi^\dagger\right)^m. \quad (4.31)$$

Now, in the regime $b\kappa|\chi|^2 \ll 1$, the exponential becomes essentially independent of the field χ and the coefficient b in the kinetic term becomes negligible. It is therefore natural to define a new quantity $\theta \equiv \kappa^{(n-1)/2}\chi^n$ for which one obtains the Lagrangian of a canonically normalized field, namely

$$\mathcal{L} = -\partial_\mu\theta\partial^\mu\theta^\dagger - e^{c_1^2/2}\lambda^2\left(\theta\theta^\dagger\right)^{m/n}. \quad (4.32)$$

Finally, we take the imaginary part of θ to be stabilized to c_1 in order to satisfy the condition discussed above and we define the real field ϕ by $\theta = \phi/\sqrt{2} + c_1/2$. As a consequence, it follows

$$\mathcal{L} \simeq -\frac{1}{2}\partial_\mu\phi\partial^\mu\phi^\dagger - e^{c_1^2/2}\lambda^2\phi^{2m/n}. \quad (4.33)$$

Therefore, we have obtained a LFI model with $p = 2m/n$ (neglecting a term $|c_1|^2$ in V). In Ref. [217], the case $n = 2$ and $m = 1$ was considered and we see that this leads to a linear potential. In Ref. [218], the generalized case considered before was introduced and studied. It is worth mentioning that, when the condition $b\kappa|\chi|^2 \ll 1$ is not satisfied, the potential remains of the LFI form but with a different p, see Ref. [218]. For instance, as shown in Ref. [217], if $n = 2$ and $m = 1$, the potential is in fact quadratic at the origin. This means that the standard relation between p (in the inflationary regime) and the mean equation of state during reheating namely, $\overline{w}_{\rm reh} = (p-2)/(p+2)$ [54], is no longer valid in that case.

4.2.2 Slow-Roll Analysis

Having studied how the LFI model can be implemented in high energy physics, we now turn to the inflationary analysis. In the following, we write $V(\phi)$ as

$$V(\phi) = M^4\left(\frac{\phi}{M_{\rm Pl}}\right)^p. \quad (4.34)$$

This potential is represented in Fig. 9 for $p = 2$. The three Hubble flow functions are straightforwardly obtained from Eqs. (2.4), (2.5) and (2.6). Defining $x \equiv \phi/M_{\rm Pl}$, one gets

$$\epsilon_1 = \frac{p^2}{2x^2}\,, \qquad \epsilon_2 = \frac{2p}{x^2}\,, \qquad \epsilon_3 = \epsilon_2\,. \tag{4.35}$$

These functions are represented in the two bottom panels of Fig. 9. They are monotonic decreasing functions of ϕ. One can immediately deduce that, for a given p, the model in the plane (ϵ_1, ϵ_2) is contained in the line $\epsilon_1 = (p/4)\epsilon_2$.

The slow-roll trajectory is completely explicit and obtained by quadrature from Eq. (2.11)

$$N - N_{\rm end} = -\frac{1}{M_{\rm Pl}^2}\int_{\phi_{\rm end}}^{\phi}\frac{V(\chi)}{V'(\chi)}{\rm d}\chi = -\frac{1}{p}\int_{\phi_{\rm end}/M_{\rm Pl}}^{\phi/M_{\rm Pl}} x{\rm d}x = \frac{1}{2p}\left(x_{\rm end}^2 - x^2\right). \tag{4.36}$$

This expression can be inverted and reads

$$x = \sqrt{x_{\rm end}^2 - 2p\left(N - N_{\rm end}\right)}\,. \tag{4.37}$$

For the large field models, inflation ends naturally when $\epsilon_1 = 1$ (see section 1). Along the $\phi > 0$ branch of the potential, this leads to

$$x_{\rm end} = \frac{p}{\sqrt{2}}\,. \tag{4.38}$$

This expression also allows us to obtain the total number of e-folds. Plugging Eq. (4.38) into Eq. (4.36), one arrives at

$$N_{\rm end} - N_{\rm ini} = \frac{1}{2p}x_{\rm ini}^2 - \frac{p}{4}\,, \tag{4.39}$$

which can be very large if the initial field value is super-Planckian. Notice that this does not imply that the energy density is close to the Planck scale as this one is typically given by the potential and proportional to M^4. In fact, the model remains under control only if the initial energy density is smaller than $M_{\rm Pl}^4$ and this imposes a constraint on both $\phi_{\rm ini}$ and M which reads

$$x_{\rm ini} = \frac{\phi_{\rm ini}}{M_{\rm Pl}} \lesssim \left(\frac{M_{\rm Pl}}{M}\right)^{4/p}. \tag{4.40}$$

Let us notice that, when the inflaton energy density approaches the Planck energy density, quantum effects become important. In this case, the stochastic inflation formalism must be used [219–225].

We now turn to the explicit determination of the slow-roll parameters. We have seen that the model is represented by the trajectory $\epsilon_1 = (p/4)\epsilon_2$ but observable models only lie in a limited portion of this straight line. Indeed, the Hubble flow parameters should be evaluated when the scales of astrophysical interest today left the Hubble radius during inflation. Following the discussion of section 2.2, we assume the pivot mode crossed the Hubble radius for $\phi = \phi_*$ at the e-fold number N_*. From the trajectory, we have

$$x_*^2 = 2p\left(\Delta N_* + \frac{p}{4}\right), \tag{4.41}$$

and the slow-roll parameters read

$$\epsilon_{1*} = \frac{p}{4\left(\Delta N_* + p/4\right)}\,, \qquad \epsilon_{2*} = \frac{1}{\Delta N_* + p/4}\,, \qquad \epsilon_{3*} = \epsilon_{2*}\,. \tag{4.42}$$

Solving Eq. (2.47) for ϕ_* yields the slow-roll predictions represented in Fig. 83. As expected, the whole family lies in the region $\epsilon_2 > 0$ and verifies $\epsilon_1 = p/4\epsilon_2$. From Fig. 83, we see that all the models with $p \gtrsim 3$ lie outside the 2σ contour. The quadratic (or massive) model is under great pressure since it predicts quite a high contribution of gravitational waves, up to $r \simeq 15\%$ level.

Finally, the parameter M can be determined from the amplitude of the CMB anisotropies, and one gets

$$\frac{Q^2_{\rm rms-PS}}{T^2} = \frac{1}{480\pi^2\epsilon_{1*}}\frac{H_*^2}{M_{\rm Pl}^2} = \frac{1}{1440\pi^2\epsilon_{1*}}\frac{V_*}{M_{\rm Pl}^4}\,. \tag{4.43}$$

In the case of large fields model, this implies

$$\left(\frac{M}{M_{\rm Pl}}\right)^4 = \frac{720\pi^2 p^2}{(x_*^2)^{p/2+1}}\frac{Q^2_{\rm rms-PS}}{T^2}\,, \tag{4.44}$$

and given the constraints on p and ΔN_*, this leads to $M/M_{\rm Pl} \simeq 3\times 10^{-3}$. We recover the conclusion that, for large field models, inflation takes place close to the Grand Unified Theory (GUT) scale.

4.3 Mixed Large Field Inflation (MLFI)

This model is a generalization of the LFI model $V(\phi) \propto \phi^p$, see section 4.2, where two monomials $\propto \phi^2$ and $\propto \phi^4$ are added. The MLFI potential reads

$$V(\phi) = M^4\frac{\phi^2}{M_{\rm Pl}^2}\left(1+\alpha\frac{\phi^2}{M_{\rm Pl}^2}\right), \tag{4.45}$$

where α is a positive dimensionless parameter. If $\phi/M_{\rm Pl} \ll 1/\sqrt{\alpha}$, then the potential is of the LFI type with $p=2$, i.e. $V(\phi) \simeq M^4\phi^2/M_{\rm Pl}^2$, whereas if $\phi/M_{\rm Pl} \gg 1/\sqrt{\alpha}$, the potential is of the LFI type with $p=4$, i.e. $V(\phi) \simeq M^4\alpha\phi^4/M_{\rm Pl}^4$. Clearly, the interesting regime is when $\phi/M_{\rm Pl} \simeq 1/\sqrt{\alpha}$, where the two terms are of equal importance. The potential and its logarithm are displayed in Fig. 10. We notice that $V(\phi)$ is an increasing function of the field *vev* and, as a consequence, that inflation proceeds from the right to the left.

This model has been investigated in different contexts. Of course, the shape of the potential appears to be natural and well-motivated since it just represents a free theory (with particles of mass $2M^4/M_{\rm Pl}^2$) corrected by the usual self-interacting quartic term. Therefore, it does not come as a surprise that this potential has been used in many different works. In Ref. [226], this model is studied in the case where a bulk scalar field is driving inflation in large extra dimensions. In Ref. [227], it is considered in a situation where inflation is driven by highly excited quantum states. In Refs. [228, 229], the MLFI potential is utilized in the context of "fresh inflation". The same potential was again considered in Ref. [230] where the role of inflaton is played by the Higgs triplet in a model where the type II seesaw mechanism is used to generate the small masses of left-handed neutrinos. Finally, it is also studied in Ref. [231] where supersymmetric hybrid inflation (in the framework of the Randall-Sundrum type II Braneworld model) is considered. The only constraint on the parameters of the model that is (sometimes) required is that the self-interacting term should be sub-dominant. This leads to the condition $\alpha M^4/M_{\rm Pl}^4 \ll 1$. Given the typical values imposed by CMB normalization, i.e. $M/M_{\rm Pl} \simeq 10^{-3}$ [see Eq. (4.44)], this is not very stringent and α can in fact vary in a quite large range of values.

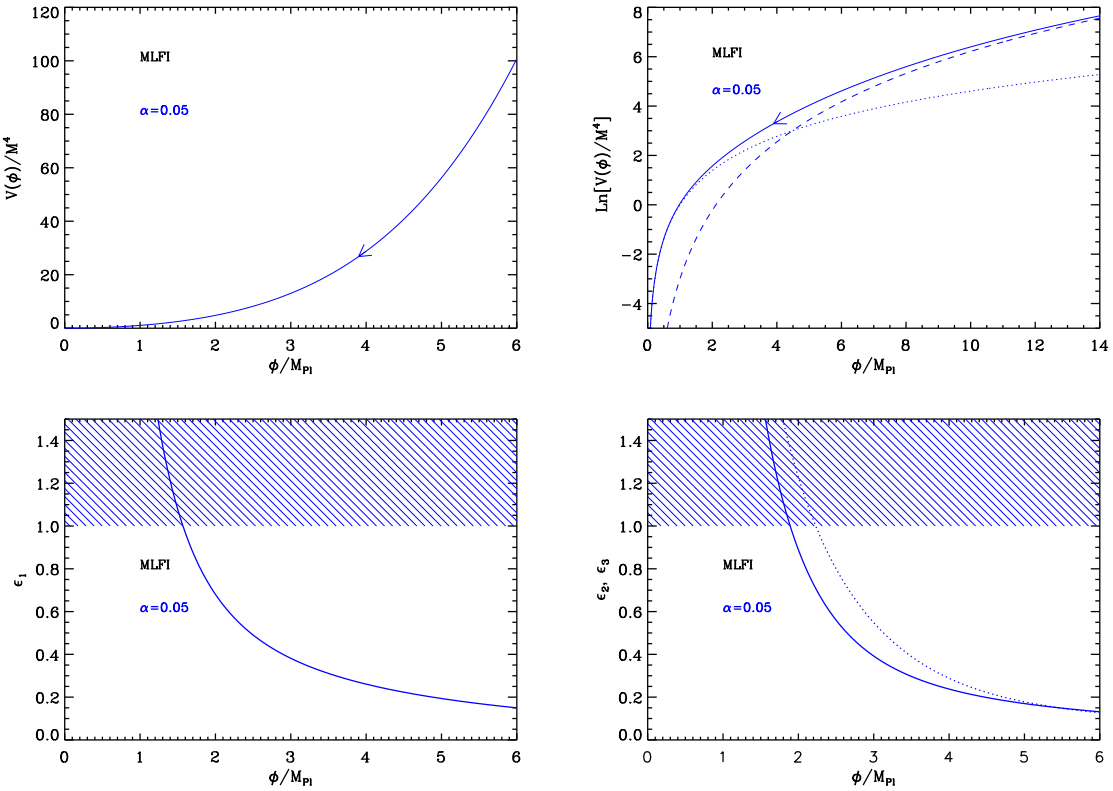

Figure 10. Top left panel: mixed large field (MLFI) potential, see Eq. (4.45), for $\alpha = 0.05$. Top right panel: logarithm of the potential for the same value of α. The dotted line indicates the potential $V(\phi) \simeq M^4\phi^2/M_{\rm Pl}^2$ which is the limit of the MLFI potential in the regime $\phi/M_{\rm Pl} \ll 1/\sqrt{\alpha}$ while the dashed line represents the expression $V(\phi) \simeq M^4\alpha\phi^4/M_{\rm Pl}^4$, the limit of $V(\phi)$ when $\phi/M_{\rm Pl} \gg 1/\sqrt{\alpha}$. For $\alpha = 0.05$ the two lines meet at the following value, $1/\sqrt{\alpha} \simeq 4.5$, as can be directly checked in the figure. The arrow in the top left and right panels indicate in which direction inflation proceeds. Bottom left panel: slow-roll parameter ϵ_1 for a mixed large field potential with $\alpha = 0.05$. Bottom right panel: slow-roll parameters ϵ_2 (solid line) and ϵ_3 (dotted line) still for $\alpha = 0.05$.

Defining $x \equiv \phi/M_{\rm Pl}$, the three first slow-roll parameters can be expressed as

$$\epsilon_1 = \frac{2}{x^2}\left(\frac{1+2\alpha x^2}{1+\alpha x^2}\right)^2, \quad \epsilon_2 = \frac{4}{x^2}\frac{1+\alpha x^2+2\alpha^2x^4}{(1+\alpha x^2)^2}, \tag{4.46}$$

and

$$\epsilon_3 = \frac{M_{\rm Pl}^2}{x^2}\frac{1+2\alpha x^2}{(1+\alpha x^2)^2}\frac{4+12\alpha x^2+8\alpha^3x^6}{1+\alpha x^2+2\alpha^2x^4}. \tag{4.47}$$

They are displayed in Fig. 10. We see that the three slow-roll parameters are decreasing functions of the field *vev*, which means that they are all increasing functions during inflation. As a consequence, inflation can stop by violation of the slow-roll conditions at $x_{\rm end}$ given by $\epsilon_1 = 1$ (see below). We also notice that ϵ_2 and ϵ_3 are larger than one at $x_{\rm end}$. This means that the slow-roll approximation breaks down slightly before the end of inflation and that the last few e-folds of inflation may be not properly described by the slow-roll approximation.

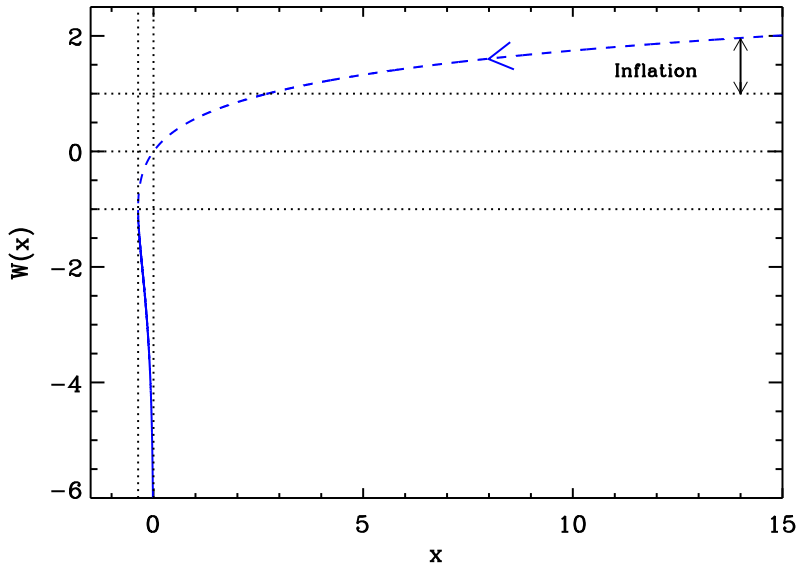

Figure 11. Lambert functions $\mathrm{W}_0(x)$ (dashed line) and $\mathrm{W}_{-1}(x)$ (solid line). During Mixed Large Field inflation, inflation proceeds along the "0" branch above the line $W = 1$ in the direction specified by the arrow.

Let us now study the slow-roll trajectory. It is given by

$$N_{\rm end} - N = -\frac{1}{8}\left[x_{\rm end}^2 + \frac{1}{2\alpha}\ln\left(1+2\alpha x_{\rm end}^2\right) - x^2 - \frac{1}{2\alpha}\ln\left(1+2\alpha x^2\right)\right], \tag{4.48}$$

where $N_{\rm end}$ is the number of e-folds at the end of inflation. One can check that this expression is asymptotically correct. Indeed, when $\alpha \ll 1$, the slow-roll trajectory reduces to

$$x_{\rm end}^2 = x^2 - 4\left(N_{\rm end} - N\right), \tag{4.49}$$

which is the trajectory in the massive case, i.e. LFI with $p = 2$, see Eq. (4.36). On the other hand, in the limit $\alpha \to \infty$, one obtains

$$x_{\rm end}^2 = x^2 - 8\left(N_{\rm end} - N\right), \tag{4.50}$$

which is, as expected, the slow-roll trajectory in the quartic case, i.e. LFI with $p = 4$. In general, the trajectory can be inverted and expressed in terms of the Lambert function. Straightforward manipulations lead to

$$x = \frac{1}{\sqrt{2\alpha}}\sqrt{-1 + \mathrm{W}_0\left[e^{1+2\alpha x_{\rm end}^2}\left(1+2\alpha x_{\rm end}^2\right)e^{-16\alpha\left(N-N_{\rm end}\right)}\right]}. \tag{4.51}$$

The corresponding Lambert function is displayed in Fig. 11, together with the region where inflation proceeds.

We have seen that, in MLFI, inflation stops by violation of the slow-roll condition. Let us therefore determine the corresponding *vev* of the field. The condition $\epsilon_1 = 1$ leads to

$$\alpha x_{\rm end}^3 - 2\sqrt{2}\alpha x_{\rm end}^2 + x_{\rm end} - \sqrt{2} = 0. \tag{4.52}$$

This is a cubic algebraic equation that can be solved exactly. In the limit $\alpha \gg 1$, the solution reads $x_{\rm end} \simeq 2\sqrt{2}$ which is indeed the solution for the quartic case, see Eq. (4.38). On the other hand, if $\alpha \ll 1$, then $x_{\rm end} \simeq \sqrt{2}$ which is also the correct result for the quadratic case. The general solution is

$$x_{\rm end} = \frac{2\sqrt{2}}{3} + \frac{1}{3\alpha}\left\{\frac{1}{4\sqrt{2}}\left[4\alpha^2\left(32\alpha+9\right)+2\alpha\sqrt{4\alpha^2\left(32\alpha+9\right)^2-8\alpha\left(8\alpha-3\right)^3}\right]\right\}^{1/3} + \frac{1}{3}\left(8\alpha-3\right)\left\{\frac{1}{4\sqrt{2}}\left[4\alpha^2\left(32\alpha+9\right)+2\alpha\sqrt{4\alpha^2\left(32\alpha+9\right)^2-8\alpha\left(8\alpha-3\right)^3}\right]\right\}^{-1/3}, \tag{4.53}$$

which is the one used in the `ASPIC` library.

Finally, the parameter M can be determined from the amplitude of the CMB anisotropies, and one gets

$$\left(\frac{M}{M_{\rm Pl}}\right)^4 = \frac{2880\pi^2}{x^4}\frac{\left(1+2\alpha x_*^2\right)^2}{\left(1+\alpha x_*^2\right)^3}\frac{Q_{\rm rms-PS}^2}{T^2}\,. \tag{4.54}$$

Similarly to LFI (see section 4.2), this gives rise to $M/M_{\rm Pl} \simeq 10^{-3}$. The reheating consistent slow-roll predictions for the MLFI models are displayed in Fig. 84. The reheating equation of state parameter $\overline{w}_{\rm reh}$ has been taken to 0 which is consistent with the fact that the potential is quadratic close to its minimum. As expected, when $\alpha \ll 1$ the predictions of the model match those of LFI with $p = 2$ and are aligned along the $\epsilon_1 = \epsilon_2/2$ line. On the other hand, if $\alpha \gg 1$, then the predictions are consistent with those of LFI with $p = 4$ and are aligned along the $\epsilon_1 = \epsilon_2$ line. In the intermediate regime, it is interesting to notice that the MLFI predictions continuously interpolate between these two asymptotic solutions but do not remain inside the domain delimited by those two lines. Indeed, when α is larger than some value, one has $\epsilon_1 > \epsilon_2$. This means that, if one starts from a pure quartic potential (LFI with $p = 4$) and adds a small quadratic term, this extra term has the effect of increasing the "effective value" of p, which is quite counter intuitive. On the other hand, since the quadratic model fits better the data than the quartic one, small values for the parameter α are favored (all the models with $\alpha > 10^{-3}$ lie outside the 2σ contour of the Planck data). High reheating temperatures are also preferred.

4.4 Radiatively Corrected Massive Inflation (RCMI)

This model is based on Ref. [232] and implements radiative corrections due to fermion couplings over the massive ($p = 2$) large field model (see section 4.2). With an appropriate choice of the renormalization scale $\mu = gM_{\rm Pl}$, g denoting the Yukawa coupling, the potential is given by

$$V(\phi) = \frac{1}{2}m^2\phi^2 - \frac{g^4}{16\pi^2}\phi^4\ln\left(\frac{\phi}{M_{\rm Pl}}\right) = M^4\left(\frac{\phi}{M_{\rm Pl}}\right)^2\left[1-2\alpha\frac{\phi^2}{M_{\rm Pl}^2}\ln\left(\frac{\phi}{M_{\rm Pl}}\right)\right], \tag{4.55}$$

where

$$M^4 \equiv \frac{1}{2}m^2M_{\rm Pl}^2, \qquad \alpha \equiv \frac{g^4M_{\rm Pl}^2}{16\pi^2m^2}\,. \tag{4.56}$$

This expression is obtained in the large field regime $\phi \gg m/g$ (this condition coming from the requirement that the fermion loop contribution dominates over the self-interaction loop

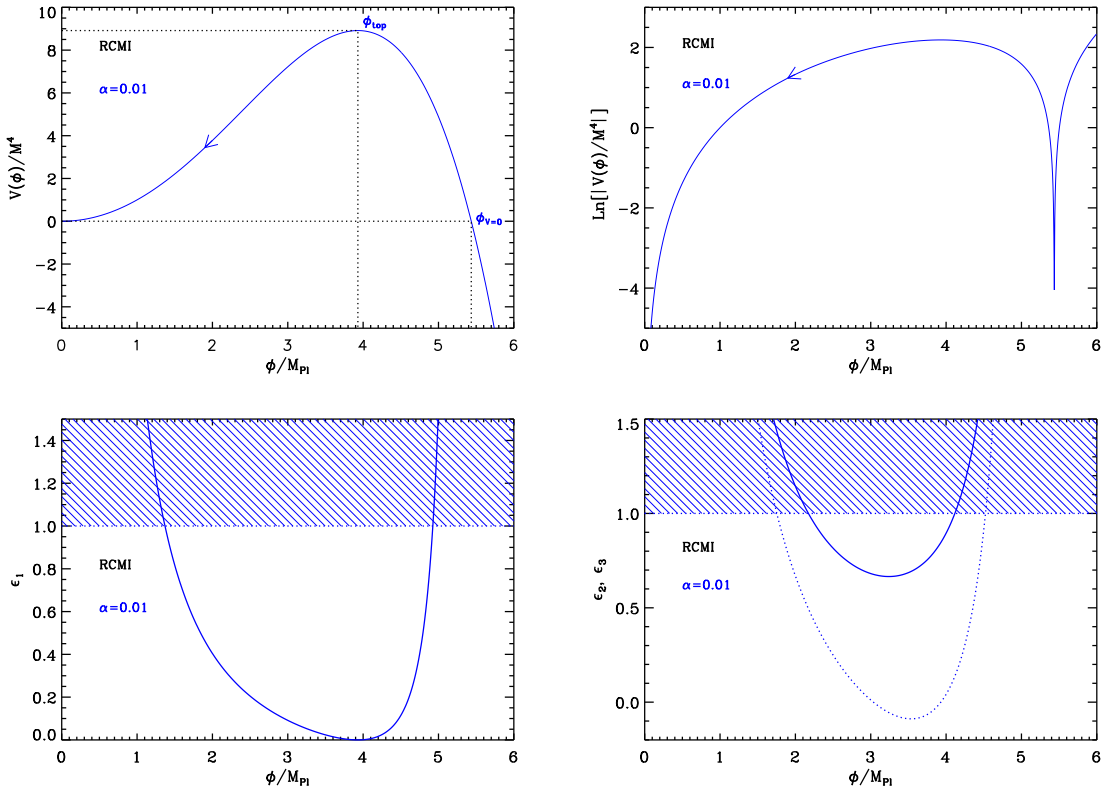

Figure 12. Radiatively Corrected Massive Inflation (RCMI) for $\alpha = 0.01$. Top panels: potential (left) and logarithm of the potential (right). Bottom left panel: slow-roll parameter ϵ_1 with respect to field values. The shaded area indicates where inflation stops. Bottom right panel: slow-roll parameters ϵ_2 (solid line) and ϵ_3 (dotted line).

contribution), i.e. assuming that the inflationary regime takes place under the condition

$$\frac{\phi^4}{M_{\rm Pl}^4} \gg \frac{1}{8\pi^2\alpha}\frac{M^4}{M_{\rm Pl}^4}\,. \tag{4.57}$$

Defining $x \equiv \phi/M_{\rm Pl}$, the Hubble flow functions are given by

$$\epsilon_1 = \frac{2}{x^2}\left(\frac{1-\alpha x^2-4\alpha x^2\ln x}{1-2\alpha x^2\ln x}\right)^2\,, \tag{4.58}$$

$$\epsilon_2 = \frac{4}{x^2}\frac{\left(1+\alpha x^2\right)\left(1+2\alpha x^2\right)-2\alpha x^2\ln x\left(1-\alpha x^2-4\alpha x^2\ln x\right)}{\left(1-2\alpha x^2\ln x\right)^2}\,, \tag{4.59}$$

and

$$\epsilon_3 = \frac{4}{x^2}\frac{1-\alpha x^2-4\alpha x^2\ln x}{\left(1-2\alpha x^2\ln x\right)^2} \times \frac{1-\alpha x^2\left[\alpha x^2\left(4\alpha x^2+9\right)+1\right]-\alpha x^2\ln x\left[4\alpha^2x^4\ln x(4\ln x+1)+\left(\alpha x^2+3\right)\left(6\alpha x^2+2\right)\right]}{\left(1+\alpha x^2\right)\left(1+2\alpha x^2\right)-2\alpha x^2\ln x\left(1-\alpha x^2-4\alpha x^2\ln x\right)}\,. \tag{4.60}$$

If $\alpha = 0$, one recovers the slow-roll parameters of the massive case (namely LFI with $p = 2$, see section 4.2) as expected.

Let us now discuss the field domains in which inflation can take place. It is clear that the above potential is not positive definite for all field values. It becomes negative at the point

$$x_{V=0} = \frac{\phi_{V=0}}{M_{\rm Pl}} = \sqrt{\frac{1}{\alpha \mathrm{W}_0\left(1/\alpha\right)}}\,, \tag{4.61}$$

where W_0 is the 0-branch of the Lambert function. The model is defined only in the regime $\phi < \phi_{V=0}$. On the other hand, the top of the potential, where $V' = 0$ (or equivalently $\epsilon_1 = 0$), is given by

$$x_{\rm top} = \frac{\phi_{\rm top}}{M_{\rm Pl}} = \sqrt{\frac{1}{2\alpha \mathrm{W}_0\left(\dfrac{\sqrt{e}}{2\alpha}\right)}}\,. \tag{4.62}$$

As the model makes sense only if the logarithmic terms do not dominate the potential, the acceptable regime is $\phi < \phi_{\rm top} < \phi_{V=0}$, and a large field region only exists for $\phi_{\rm top}/M_{\rm Pl} \gg 1$. From the above expression, this means that we must be in the regime $\alpha \ll 1$. For $\phi < \phi_{\rm top}$ one can check from Eqs. (4.55) and (4.62) that the loop corrections never exceed α/e.

Let us now turn to the slow-roll trajectory. It is given by

$$N - N_{\rm end} = -\frac{1}{2}\int_{\phi_{\rm end}/M_{\rm Pl}}^{\phi/M_{\rm Pl}} \frac{x - 2\alpha x^3 \ln x}{1 - \alpha x^2 - 4\alpha x^2 \ln x}\mathrm{d}x, \tag{4.63}$$

an integral that cannot be performed analytically and which is numerically evaluated in `ASPIC`. For the purpose of this section, we can nevertheless make an expansion in α to obtain an approximate expression

$$N - N_{\rm end} = -\frac{x^2}{4}\left[1 + \alpha\frac{x^2}{4}\left(1 + 4\ln x\right)\right] + \frac{x_{\rm end}^2}{4}\left[1 + \alpha\frac{x_{\rm end}^2}{4}\left(1 + 4\ln x_{\rm end}\right)\right] + \mathcal{O}\left(\alpha^2\right)\,. \tag{4.64}$$

Inflation stops close to the minimum of the potential when $\epsilon_1 = 1$. This last equation cannot be solved analytically but we can also perform an expansion at first order in α and one gets

$$x_{\rm end} = \frac{\phi_{\rm end}}{M_{\rm Pl}} \simeq \frac{1}{\sqrt{2\alpha \mathrm{W}_0\left[\dfrac{e^{1+1/(4\alpha)}}{2\alpha}\right]}} \simeq \sqrt{2} - 2\sqrt{2}\alpha\,. \tag{4.65}$$

In the limit $\alpha \to 0$, we recover the large field result for $p = 2$, i.e. $x_{\rm end} \to \sqrt{2}$. The maximum total number of e-folds one can realize between $\phi = \phi_{\rm top}$ and $\phi = \phi_{\rm end}$ can be calculated from the previous expressions. It reads

$$\begin{aligned}\Delta N_{\rm max} = N_{\rm end} - N_{\rm top} &= \frac{5}{32\alpha \mathrm{W}_0\left(\dfrac{\sqrt{e}}{2\alpha}\right)} + \frac{1 + 2\alpha - 20\alpha \mathrm{W}_0\left[\dfrac{e^{1+1/(4\alpha)}}{2\alpha}\right]}{128\alpha^2 \mathrm{W}_0^2\left[\dfrac{e^{1+1/(4\alpha)}}{2\alpha}\right]} \\ &\simeq -\frac{5}{32\alpha\ln\left(\alpha\right)}\,.\end{aligned} \tag{4.66}$$

This is a decreasing function of α, so that α has to be small enough if one wants a sufficiently high number of e-folds to take place. Indeed, if one wants at least $\Delta N_{\rm min}$ e-folds to occur, one needs to work with

$$\alpha < \frac{5}{32\Delta N_{\rm min}} \frac{1}{\ln\left(\frac{32\Delta N_{\rm min}}{10}\right)}\,. \tag{4.67}$$

For example, $\Delta N_{\rm min} = 50$ imposes $\alpha < 6 \times 10^{-4}$. The fact that α is bounded from above can be directly checked in Fig. 85. The field ϕ_* value at which the pivot mode crossed the Hubble radius during inflation is obtained from Eq. (2.47) whereas the corresponding e-fold number can be obtained from the trajectory.

Finally, the parameter M can be determined from the amplitude of the CMB anisotropies, and one gets

$$\left(\frac{M}{M_{\rm Pl}}\right)^4 = \frac{2880\pi^2}{x_*^4} \frac{\left(1-2\alpha x_*^2 \ln x_*\right)^3}{\left(1-\alpha x_*^2 - 4\alpha x_*^2 \ln x_*\right)^2} \frac{Q_{\rm rms-PS}^2}{T^2}\,. \tag{4.68}$$

The reheating consistent slow-roll predictions for the RCMI models are represented in Fig. 85. As expected, the LFI quadratic model case is properly recovered for $\alpha \to 0$. From this figure, we see that all models having $\alpha \gtrsim 10^{-3.7}$ lie outside the 2σ contour. Let us emphasize that the value of α cannot be infinitely small due to Eq. (4.57). At zero order, one has $\phi > \phi_{\rm end} \simeq \sqrt{2} M_{\rm Pl}$ such that Eq. (4.57) can be recast into

$$\alpha > \frac{M^4}{8\pi^2 M_{\rm Pl}^4} = \frac{m^2}{16\pi^2 M_{\rm Pl}^2}\,. \tag{4.69}$$

From the COBE normalization, and in the limit of small α, one gets $M/M_{\rm Pl} \gtrsim 10^{-3}$ and the lower bound reads $\alpha > 10^{-15}$.

4.5 Radiatively Corrected Quartic Inflation (RCQI)

This model is similar to RCMI discussed in section 6.1 but implements radiative corrections due to fermion couplings over a quartic ($p = 4$) large field model [232] (see section 4.2). The potential is given by

$$V = \lambda\phi^4 - \frac{g^4}{16\pi^2}\phi^4 \ln\left(\frac{\phi}{M_{\rm Pl}}\right) = M^4 \left(\frac{\phi}{M_{\rm Pl}}\right)^4 \left[1 - \alpha \ln\left(\frac{\phi}{M_{\rm Pl}}\right)\right], \tag{4.70}$$

where

$$M^4 = \lambda M_{\rm Pl}^4, \qquad \alpha \equiv \frac{g^4}{16\pi^2\lambda}\,. \tag{4.71}$$

Defining $x = \phi/M_{\rm Pl}$, the Hubble flow functions in the slow-roll approximation read

$$\epsilon_1 = \frac{8}{x^2}\left(\frac{1-\frac{\alpha}{4}-\alpha\ln x}{1-\alpha\ln x}\right)^2, \qquad \epsilon_2 = \frac{8}{x^2}\frac{1+\frac{\alpha}{4}(\alpha-1)+\alpha\left(\frac{\alpha}{4}-2\right)\ln x+\alpha^2\ln^2 x}{\left(1-\alpha\ln x\right)^2}, \tag{4.72}$$

and

$$\epsilon_3 = \frac{8}{x^2}\frac{\left(1-\frac{\alpha}{2}-\alpha\ln x\right)\left(1-\frac{\alpha}{4}-\alpha\ln x\right)\left[1+\frac{\alpha^2}{2}+\frac{\alpha}{4}-\alpha\left(2+\frac{\alpha}{4}-\alpha\ln x\right)\ln x\right]}{\left(1-\alpha\ln x\right)^2\left[1+\frac{\alpha}{4}(\alpha-1)-\alpha\left(2-\frac{\alpha}{4}-\alpha\ln x\right)\ln x\right]}\,. \tag{4.73}$$

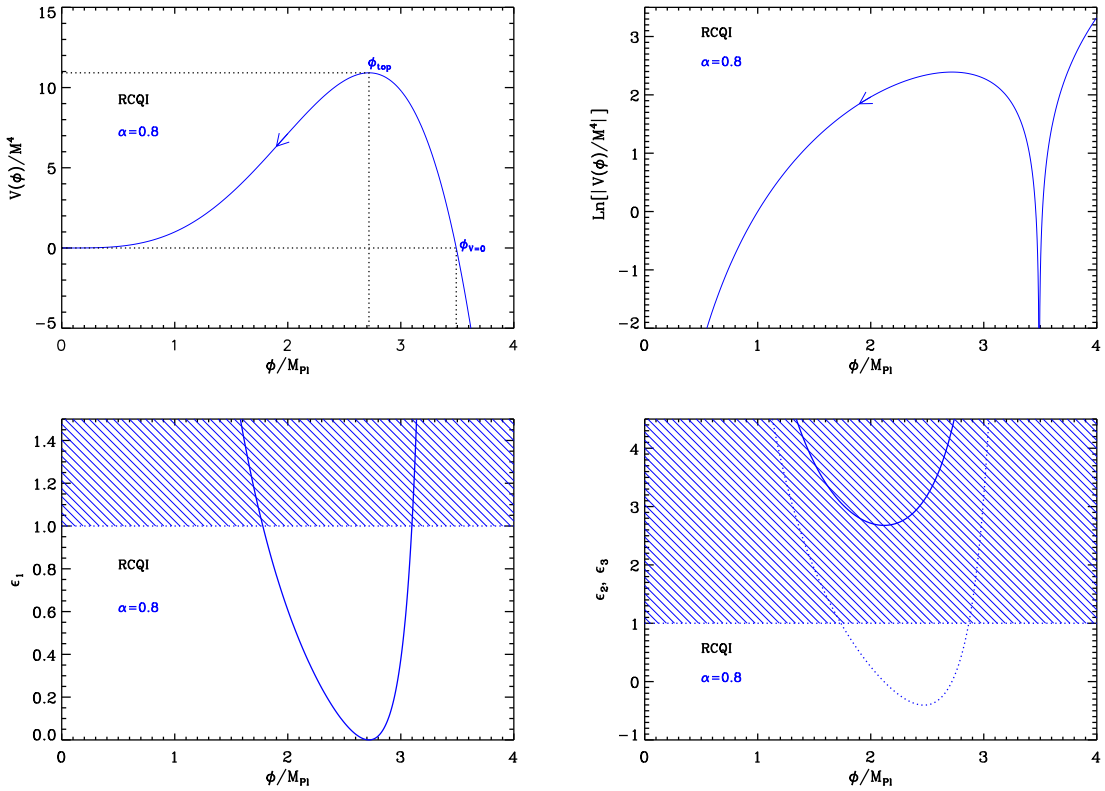

Figure 13. Radiatively Corrected Quartic Inflation (RCQI) for $\alpha = 0.8$. Top panels: the potential and its logarithm as a function of the field values. Bottom left panel: slow-roll parameter ϵ_1. The shaded area indicates where inflation stops. Bottom right panel: slow-roll parameters ϵ_2 (solid line) and ϵ_3 (dotted line). The shaded region for ϵ_2 and ϵ_3 shows where the slow-roll approximation is violated for that value of α.

The shape of the potential and the Hubble flow functions are very similar to the ones of the RCMI model and have been represented in Fig. 13. In particular, the potential is vanishing and maximal at the field values

$$x_{V=0} = \frac{\phi_{V=0}}{M_{\rm Pl}} = e^{1/\alpha}, \quad x_{\rm top} = \frac{\phi_{\rm top}}{M_{\rm Pl}} = e^{1/\alpha - 1/4}, \tag{4.74}$$

respectively. As the model makes sense only if the corrections are small compared to the quartic term, one should consider $\alpha \ll 1$ and not too large super-Planckian field values.

The slow-roll trajectory can integrated analytically from Eqs. (2.11) and (4.70) and one gets

$$\begin{aligned} N - N_{\rm end} = -\frac{1}{16}\Bigg[& 2x^2 - e^{-1/2+2/\alpha}\,{\rm Ei}\left(\frac{1}{2} - \frac{2}{\alpha} + 2\ln x\right) \\ & - 2x_{\rm end}^2 + e^{-1/2+2/\alpha}\,{\rm Ei}\left(\frac{1}{2} - \frac{2}{\alpha} + 2\ln x_{\rm end}\right)\Bigg], \end{aligned} \tag{4.75}$$

where the exponential integral function is defined by

$$\mathrm{Ei}(x) \equiv -\int_{-x}^{+\infty} \frac{e^{-t}}{t}\mathrm{d}t. \tag{4.76}$$

The quartic limit $\alpha \to 0$ is recovered by noticing that

$$\mathrm{Ei}(-2/\alpha) \underset{\alpha\to 0}{\sim} -\frac{\alpha}{2}e^{-2/\alpha}. \tag{4.77}$$

Contrary to the RCMI model, the top of the potential is flat enough to support inflation. Indeed, one sees from Eq. (4.74) that the argument of the exponential integral function vanishes at $x = x_{\mathrm{top}}$. Since for $y \to 0$, one has $\mathrm{Ei}(y) \sim \gamma + \ln y$, whatever the value of x_{end} the total number of e-folds is divergent. This means that it is always possible to realize the required ΔN_* number of e-folds provided inflation starts close enough to the top of the potential.

As for RCMI, inflation stops at $\epsilon_1 = 1$ but this equation can only be solved numerically. For illustrative purpose, one can nevertheless solve it at first order in α to get

$$x_{\mathrm{end}} = \frac{\phi_{\mathrm{end}}}{M_{\mathrm{Pl}}} \simeq 2\sqrt{2} - \frac{\sqrt{2}}{2}\alpha. \tag{4.78}$$

The link between ϕ_* and ΔN_* is given by the slow-roll trajectory with ϕ_* given by Eq. (2.47).

Finally, the parameter M can be determined from the amplitude of the CMB anisotropies, and one gets

$$\lambda = \frac{M^4}{M_{\mathrm{Pl}}^4} = \frac{11520\pi^2}{x_*^6}\frac{\left(1-\frac{\alpha}{4}-\alpha\ln x_*\right)^2}{\left(1-\alpha\ln x_*\right)^3}\frac{Q_{\mathrm{rms-PS}}^2}{T^2}\,. \tag{4.79}$$

The slow-roll predictions for RCQI are represented in Fig. 86 and 87. As expected, the quartic model case is properly recovered in the limit $\alpha \to 0$. From Fig. 86, we see that all the models seem to lie outside the 2σ contour for $\overline{w}_{\mathrm{reh}} = 0$. As the reheating phase takes place at the bottom of a quartic-like potential, we have also represented the prediction for $\overline{w}_{\mathrm{reh}} = 1/3$ in Fig. 87. For a radiation-dominated reheating, ΔN_* is fixed and for each value of α one has only a single point. In that situation, all these models are still disfavored at the two-sigma level.

4.6 Natural Inflation (NI)

4.6.1 Theoretical Justifications

Natural inflation was first proposed as an attempt to solve the so-called "fine-tuning" problem of inflation. In particular, in order to obtain sufficient inflation and the correct normalization for the microwave background anisotropies, the potential $V(\phi)$ of the inflaton must be sufficiently flat. It is usually argued that, on general grounds, such a flatness is not robust under radiative corrections, unless it is protected by some symmetry. This is the reason that has motivated Refs. [233, 234] to put forward Natural Inflation, in which the inflaton potential is flat due to shift symmetries. The model makes use of Nambu-Goldstone bosons [235, 236] which arise whenever a global symmetry is spontaneously broken. The main idea can be very simply illustrated with the following action

$$S = -\int \mathrm{d}\boldsymbol{x}\sqrt{-g}\Bigg[g^{\mu\nu}\partial_\mu\Phi^\dagger\partial_\nu\Phi + i\bar{\Psi}\gamma^\mu\partial_\mu\Psi + \lambda\left(\Phi^\dagger\Phi - \frac{f^2}{2}\right)^2 + g_{\mathrm{f}}\bar{\Psi}_{\mathrm{L}}\Phi\Psi_{\mathrm{R}} + g_{\mathrm{f}}\bar{\Psi}_{\mathrm{R}}\Phi^\dagger\Psi_{\mathrm{L}}\Bigg], \tag{4.80}$$

where Φ is a complex scalar field, Ψ a Dirac spinor and $\Psi_{\rm LR} = (1 \pm \gamma_5)/2\Psi$. The quantity f is the energy scale at which the symmetry is spontaneously broken, λ is a dimensionless coupling constant and $g_{\rm f}$ a dimensionless Yukawa coupling. This action is invariant under the U(1) transformation: $\Phi \to e^{i\alpha}\Phi$, $\Psi_{\rm L} \to e^{i\alpha/2}\Psi_{\rm L}$ and $\Psi_{\rm R} \to e^{-i\alpha/2}\Psi_{\rm R}$, where α is an arbitrary constant. Due to the "Mexican hat" potential for the scalar field, this symmetry is spontaneously broken below the scale f and the scalar field acquires the *vev* $\langle\Phi\rangle = f/\sqrt{2}e^{i\phi/f}$. The field ϕ corresponds to an "angular variable" and is a Goldstone boson. Below the scale of broken symmetry, the effective Lagrangian can be expressed as

$$\mathcal{L} = \frac{1}{2}\partial_\mu\phi\partial^\mu\phi + i\bar{\Psi}\gamma^\mu\partial_\mu\Psi + g_{\rm f}\frac{f}{\sqrt{2}}\left(\bar{\Psi}_{\rm L}\Psi_{\rm R}e^{i\phi/f} + \bar{\Psi}_{\rm R}\Psi_{\rm L}e^{-i\phi/f}\right). \tag{4.81}$$

It is now invariant under $\phi \to \phi + 2\pi f$, $\Psi_{\rm L} \to e^{i\alpha/2}\Psi_{\rm L}$ and $\Psi_{\rm R} \to e^{-i\alpha/2}\Psi_{\rm R}$. Then, we assume that an explicit symmetry breaking takes place, for instance through the appearance of a fermion condensate for which $\langle\bar{\Psi}\Psi\rangle \simeq M_{\rm s}^3$ where $M_{\rm s} < f$ is the scale at which this symmetry breaking occurs. As a consequence, the effective Lagrangian takes the form

$$\mathcal{L} = \frac{1}{2}\partial_\mu\phi\partial^\mu\phi + 2g_{\rm f}M_{\rm s}^3\frac{f}{\sqrt{2}}\cos\left(\frac{\phi}{f}\right). \tag{4.82}$$

We see that the Nambu-Goldstone boson has acquired a cosine potential and the overall scale of the potential is given by $M^4 \simeq g_{\rm f}M_{\rm s}^3 f$. Therefore, if one takes $f \simeq M_{\rm Pl}$, $M_{\rm s}$ slightly below the GUT scale and a Yukawa coupling of order one, one can "naturally" generate a small ratio M/f. A last remark is in order on this model. Suppose that quantum gravity effects generate non-renormalizable higher order terms in the action (4.80) like

$$\Delta V = a_{mn}\frac{|\Phi|^{2m}}{M_{\rm Pl}^{2m+n-4}}\left(\Phi^n + \Phi^{\dagger n}\right), \tag{4.83}$$

where a_{mn} are a priori unknown coefficients. After symmetry breaking, one would therefore obtain a correction of the form

$$\Delta V = a_{mn}M_{\rm Pl}^4\left(\frac{f}{M_{\rm Pl}}\right)^{2m+n}\cos\left(n\frac{\phi}{f}\right). \tag{4.84}$$

If $f \gtrsim M_{\rm Pl}$, as favored by current cosmological data (see below) these terms should dominate unless the coefficients a_{mn} are fine-tuned to very small values. Notice that the overall scale of the potential is now given by $a_{mn}M_{\rm Pl}^4$, which also demands that $a_{mn} \lesssim 10^{-15}$ in order to have the correct CMB normalization. These terms are therefore dangerous for the consistency and the natural character of the model. This model has been studied in more details in Refs. [237–251].

Many other types of candidates have subsequently been explored in order to produce scenarios similar to that of Natural Inflation. For example, in Ref. [252], it was suggested to use a pseudo-Nambu Goldstone boson as the rolling field in double field inflation. Then, NI potentials generated by radiative corrections in models with explicitly broken Abelian [253] and non-Abelian [254, 255] symmetries were considered, showing that NI models with $f \simeq M_{\rm Pl}$ and $f \ll M_{\rm Pl}$ can both be generated. In Refs. [256], the field ϕ is considered to be a Polonyi field [257] and the model predicts that $f = M_{\rm Pl}$. Refs. [258, 259] have examined natural inflation in the context of extra dimensions and Ref. [260] has used pseudo-Nambu Goldstone bosons from little Higgs models to drive hybrid inflation. Also, Refs. [261, 262]

have used the natural inflation idea of pseudo-Nambu Goldstone bosons in the context of braneworld scenarios to drive inflation, Ref. [263] has studied the model in 5-D warped backgrounds. The same potential has also been obtained and studied in Ref. [264] when studying instantons in non-linear sigma models, and in Ref. [265] as providing quintessential inflation. In some of these references the potential is sometimes found with the minus sign in front of the cosine term, which is, up to a shift in the field *vev* $\phi/f \to \phi/f + \pi$, the same potential as already studied before. This last model has also been derived and studied in Refs. [258, 259, 266] in the context of orbifold GUT inflation, where the potential is given by

$$V(\phi) = M^4 \left[F\left(\frac{\phi}{\phi_0}\right) + F\left(2\frac{\phi}{\phi_0}\right) + \frac{F(0)}{2} \right], \tag{4.85}$$

with

$$F(x) = -\sum_{n=1}^{\infty} \frac{\cos(n\pi x)}{n^5}. \tag{4.86}$$

This potential must be studied in its increasing branch, and in the small field limit. At leading order, one recovers the cosine potential.

Finally, an important question is whether a situation where $f > M_{\rm Pl}$ makes sense from the high energy physics and effective field theory point of view. In fact, it was shown in Refs. [267–269] that $f \lessapprox 10^{12}$GeV in order for the corresponding energy density not to exceed the critical energy density. But this constraint applies to the post inflationary Universe and, during inflation, Ref. [270] has argued that it is not relevant. However, it remains the question of whether $f > M_{\rm Pl}$ makes sense or not. To address this issue, an interesting mechanism has been proposed in Ref. [271] (see also Ref. [272]) which shows that two axion fields at sub-Planckian scales can have an effective dynamics similar to the one field Natural Inflation model with $f > M_{\rm Pl}$.

Let us consider a model with two axions, θ and ρ the effective Lagrangian of which is given by

$$\mathcal{L} = \frac{1}{2}\partial_\mu\theta\partial^\mu\theta + \frac{1}{2}\partial_\mu\rho\partial^\mu\rho + M_1^4\left[1 - \cos\left(\frac{\theta}{f} + \frac{\rho}{g_1}\right)\right] + M_2^4\left[1 - \cos\left(\frac{\theta}{f} + \frac{\rho}{g_2}\right)\right], \tag{4.87}$$

where M_1 and M_2, f, g_1 and g_2 are constant, a priori, arbitrary scales. The same model can be re-written in terms of the fields ψ and ξ defined by

$$\psi = \frac{f g_1}{\sqrt{f^2 + g_1^2}}\left(\frac{\theta}{f} + \frac{\rho}{g_1}\right), \qquad \xi = \frac{f g_1}{\sqrt{f^2 + g_1^2}}\left(-\frac{\theta}{g_1} + \frac{\rho}{f}\right). \tag{4.88}$$

It is easy to show that this leads to

$$\begin{aligned}\mathcal{L} = {} & \frac{1}{2}\partial_\mu\psi\partial^\mu\psi + \frac{1}{2}\partial_\mu\xi\partial^\mu\xi + M_1^4\left[1 - \cos\left(\frac{\sqrt{f^2+g_1^2}}{f g_1}\psi\right)\right] \\ & + M_2^4\left[1 - \cos\left(\frac{f^2 + g_1 g_2}{f g_2\sqrt{f^2+g_1^2}}\psi + \frac{g_1 - g_2}{g_2\sqrt{f^2+g_1^2}}\xi\right)\right].\end{aligned} \tag{4.89}$$

Moreover, the mass of the two fields ψ and ξ can be expressed as

$$m_\psi^2 = \left(\frac{1}{f^2} + \frac{1}{g_1^2}\right) M_1^4, \qquad m_\xi^2 = \frac{(g_1 - g_2)^2}{g_2^2\left(f^2 + g_1^2\right)} M_2^4. \tag{4.90}$$

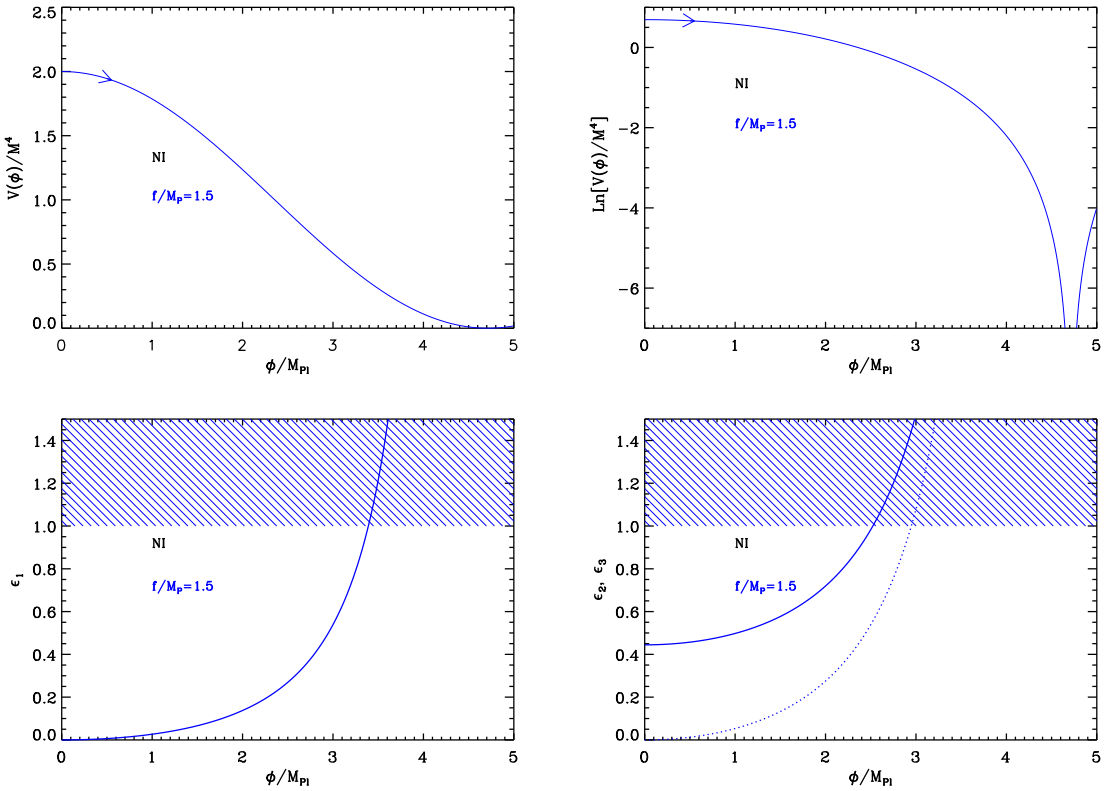

Figure 14. Natural Inflation (NI). Top left panel: potential for $f/M_{\rm Pl} = 1.5$. Top right panel: logarithm of the potential for the same value of f. Bottom left panel: slow-roll parameter ϵ_1 for a potential with $f/M_{\rm Pl} = 1.5$. The shaded area indicates the breakdown of the slow-roll inflation (strictly speaking when the acceleration stops). Bottom right panel: slow-roll parameters ϵ_2 (solid line) and ϵ_3 (dotted line) for a potential with $f/M_{\rm Pl} = 1.5$.

If g_1 is very close to g_2, then the field ξ will be light and, therefore, will have a non-trivial dynamics. In addition, if the field ψ is sufficiently heavy (compared to the Hubble parameter), then its *vev* will be frozen at $\psi = 0$. In this case, we see that the original two fields model effectively reduces to a one field NI model with a scale f_ξ given by

$$f_\xi = \frac{g_2\sqrt{f^2 + g_1^2}}{g_1 - g_2}. \tag{4.91}$$

But, since, g_1 is close to g_2, the scale f_ξ will be large even if the fundamental scales f, g_1 and/or g_2 are sub-Planckian. In this way, one can generate super-Planckian values for the scale f and, at the same time, have a theory which can be consistent from the effective field theory point of view.

4.6.2 Slow-Roll Analysis

Summarizing the above discussion, the model that we consider in this section makes use of a potential that can be written as

$$V(\phi) = M^4\left[1 + \cos\left(\frac{\phi}{f}\right)\right]. \tag{4.92}$$

The scale M is determined by the CMB normalization and the potential depends on one parameter: the a priori unknown scale f. The potential of Eq. (4.92) is displayed with its logarithm in Fig. 14. Since it is a periodic and even function of the field *vev* ϕ, it is enough to study it in the range $\phi \in [0, \pi f]$ where inflation proceeds from the left to the right. If one lets $x \equiv \phi/f$, the slow-roll parameters can be expressed as

$$\epsilon_1 = \frac{M_{\rm Pl}^2}{2f^2}\frac{\sin^2 x}{(1+\cos x)^2}\,, \qquad \epsilon_2 = \frac{2M_{\rm Pl}^2}{f^2}\frac{1}{1+\cos x}\,, \qquad \epsilon_3 = 2\epsilon_1\,. \tag{4.93}$$

They are displayed in Fig. 14, where one can see that they are all increasing functions of the field *vev*, which means that they all increase during inflation. Inflation stops at the position $x_{\rm end}$ given by $\epsilon_1 = 1$ (see below), and one can see that ϵ_2 and ϵ_3 are already greater than one at this point. This means that the slow-roll approximation stops being valid slightly before the end of inflation, and the few last e-folds may not be properly described in this frame of approximations. Another remark to be made is the fact that one generically has

$$\epsilon_2 > \frac{M_{\rm Pl}^2}{f^2}\,. \tag{4.94}$$

This means that in order for the slow-roll approximation to be valid, one must require $f/M_{\rm Pl} \gg 1$ which is not necessarily problematic from a high energy physics point of view (see the above discussion).

The end of inflation occurs when $\epsilon_1 = 1$, i.e. at a position given by

$$x_{\rm end} = \arccos\left(\frac{1-2f^2/M_{\rm Pl}^2}{1+2f^2/M_{\rm Pl}^2}\right). \tag{4.95}$$

From this expression, one can calculate the value of the other slow roll parameters at the end of inflation, namely $\epsilon_2^{\rm end} = 2 + M_{\rm Pl}^2/f^2$ and $\epsilon_3^{\rm end} = 2\epsilon_2^{\rm end}$, which confirms that the last few e-folds may not be described properly in the slow-roll approximation.

Let us now calculate the slow-roll trajectory. It is given by

$$N_{\rm end} - N = \frac{f^2}{M_{\rm Pl}^2}\ln\left(\frac{1-\cos x_{\rm end}}{1-\cos x}\right), \tag{4.96}$$

where $N_{\rm end}$ is the number of e-folds at the end of inflation, and N is the number of e-folds at some point when the scaled field *vev* is x. This trajectory can be inverted and one obtains

$$x = \arccos\left\{1 - (1-\cos x_{\rm end})\exp\left[-\frac{M_{\rm Pl}^2}{f^2}\left(N_{\rm end} - N\right)\right]\right\}. \tag{4.97}$$

Replacing $x_{\rm end}$ by its value [see Eq. (4.95)] gives

$$x = \arccos\left\{1 - \frac{4f^2}{M_{\rm Pl}^2 + 2f^2}\exp\left[-\frac{M_{\rm Pl}^2}{f^2}\left(N_{\rm end} - N\right)\right]\right\}. \tag{4.98}$$

Finally, the amplitude of the CMB anisotropies fixes the parameter M to

$$\left(\frac{M}{M_{\rm Pl}}\right)^4 = 720\pi^2\frac{Q_{\rm rms-PS}^2}{T^2}\frac{M_{\rm Pl}^2}{f^2}\frac{\sin^2 x_*}{(1+\cos x_*)^3}\,. \tag{4.99}$$

If $f/M_{\rm Pl} = \mathcal{O}(1)$, this expression simplifies to

$$\left(\frac{M}{M_{\rm Pl}}\right)^4 \simeq 720\pi^2 \frac{Q^2_{\rm rms-PS}}{T^2} \frac{e^{-2M^2_{\rm Pl}/f^2\Delta N_*}}{1+2f^2/M^2_{\rm Pl}}\,, \tag{4.100}$$

which gives rise to $M/M_{\rm Pl} \simeq 10^{-13}$. On the contrary, if $f/M_{\rm Pl} \gg 1$ one has

$$\left(\frac{M}{M_{\rm Pl}}\right)^4 \simeq 360\pi^2 \frac{Q^2_{\rm rms-PS}}{T^2} \left(\frac{f}{M_{\rm Pl}}\right)^2 \frac{1}{\Delta N_*^2}\,, \tag{4.101}$$

and the potential energy scale goes up. For instance, if $f/M_{\rm Pl} = 10^2$ one has $M/M_{\rm Pl} \simeq 10^{-2}$.

The reheating consistent slow-roll predictions for the natural inflation models are displayed in Fig. 88. The reheating equation of state parameter $\overline{w}_{\rm reh}$ has been taken to 0 since the potential is quadratic close to its minimum. In the limit $f/M_{\rm Pl} \to \infty$, the quadratic model predictions (LFI with $p = 2$, see section 4.2) seem to be recovered. Indeed, from the above formula, one can check that in this limit both $x_{\rm end}$ and x_* approach π and the potential is, at leading order, a parabola. More precisely, one can check from Eq. (4.98) that in the limit $f/M_{\rm Pl} \to \infty$, one has $\cos x_* \simeq -1 + (1+2\Delta N_*)\, M^2_{\rm Pl}/f^2$, from which one deduces that $\epsilon_{1*} \simeq 1/(1+2\Delta N_*)$ and $\epsilon_{2*} \simeq 2/(1+2\Delta N_*) \simeq 2\epsilon_{1*}$. These relations are characteristic of the LFI quadratic models, see Eq. (4.42). However, one has $\epsilon_{3*} = 2\epsilon_{2*}$ which differs from the LFI quadratic relationship $\epsilon_{3*} = \epsilon_{2*}$, and therefore quantities sensitive to ϵ_3, such as the running $\alpha_{\rm S}$, would break the degeneracy between NI and the LFI quadratic model. As expected, large values of $f/M_{\rm Pl}$ seem to be favored by the data (as well as high reheating temperatures), and in practice, $f/M_{\rm Pl} < 4$ appears to be disfavored at the 2σ level by the Planck data.

4.7 Exponential SUSY Inflation (ESI)

4.7.1 Theoretical Justifications

This model has been discussed in Ref. [273] in the context of spin-driven inflation and derived in Ref. [274] in the context of supergravity and superstrings. The potential is given by $V(\phi) \propto \left(1 - e^{-q\phi/M_{\rm Pl}}\right)$. The same potential also appears in Ref. [275] in the context of brane inflation, in Ref. [276] in the context of type IIB string compactification as fiber inflation and more recently in Ref. [277] as unitarized Higgs inflation models. This type of models can be obtained under very general considerations. Suppose that one has a supergravity model with a Kähler potential depending on one field ψ given by $K = -\beta/\kappa \ln\left(1 - \alpha\kappa\psi\psi^\dagger\right)$, where α and β are two free parameters. This model leads to a scalar potential but for a field which is not canonically normalized. The canonically normalized field θ is given by

$$\kappa^{1/2}\theta \simeq \frac{1}{\sqrt{\alpha}}\left(1 - 2e^{-\sqrt{2/\beta}\kappa^{1/2}\psi}\right), \tag{4.102}$$

where we have assumed that inflation takes place at relatively large ψ *vev*'s. Then, suppose that the superpotential leads to a given function $V = f(\theta)$. One can always expand f such that

$$V(\phi) \simeq V_0\left(1 - e^{-\sqrt{2/\beta}\kappa^{1/2}\phi}\right) + \cdots\,, \tag{4.103}$$

where $\kappa^{1/2}\phi \equiv \kappa^{1/2}\theta + \sqrt{\beta/2}\ln\left([2f_\theta/(\sqrt{\alpha}f)\right]$ and V_0 is just the function f evaluated at $1/\sqrt{\alpha}$. We see that one obtains exactly the ESI potential with $q = \sqrt{2/\beta}$. Preferred choices for β are $\beta = 1$ or $\beta = 3$ leading to $q = \sqrt{2}$ or $q = \sqrt{2/3}$. In absence of any more further guidance, it seems reasonable to assume that β, and hence q, is just a number of order one.

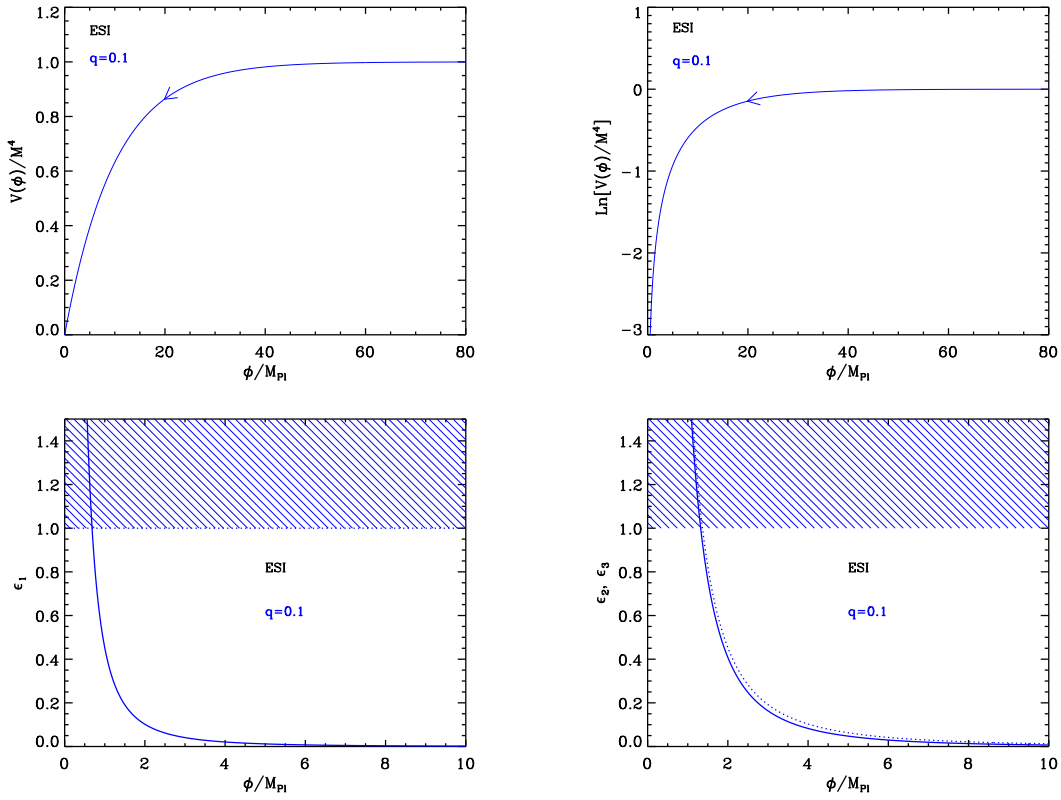

Figure 15. Exponential SUSY Inflation (ESI) for $q = \sqrt{2}$. Top panels: the potential and its logarithm. Bottom left panel: slow-roll parameter ϵ_1. The shaded area indicates where acceleration stops. Bottom right panel: slow-roll parameters ϵ_2 (solid line) and ϵ_3 (dotted line). For those, the shaded region signals the breakdown of the slow-roll approximation but not necessarily the end of the accelerated expansion.

4.7.2 Slow-roll Analysis

Based on the previous considerations, we now study the following potential

$$V(\phi) = M^4 \left(1 - e^{-q\phi/M_{\rm Pl}}\right), \tag{4.104}$$

where q is a positive dimensionless parameter and inflation proceeds at decreasing field values in the region where $\phi/M_{\rm Pl} > 0$. Defining $x \equiv \phi/M_{\rm Pl}$, the Hubble flow functions in the slow-roll approximation read

$$\epsilon_1 = \frac{q^2}{2}\frac{e^{-2qx}}{\left(1-e^{-qx}\right)^2}, \qquad \epsilon_2 = 2q^2\frac{e^{-qx}}{\left(1-e^{-qx}\right)^2}, \qquad \epsilon_3 = q^2\frac{e^{-qx}\left(1+e^{-qx}\right)}{\left(1-e^{-qx}\right)^2}. \tag{4.105}$$

The potential and the Hubble flow functions with respect to the field values are represented in Fig. 15.

The slow-roll trajectory can be integrated analytically from Eq. (2.11) and one finds

$$N - N_{\rm end} = -\frac{e^{qx} - qx}{q^2} + \frac{e^{qx_{\rm end}} - qx_{\rm end}}{q^2}. \tag{4.106}$$

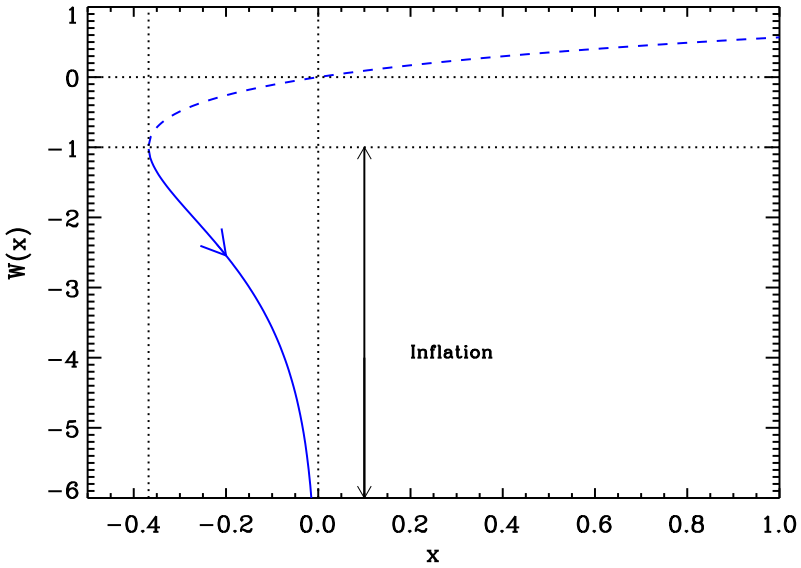

Figure 16. Lambert functions $\mathrm{W}_0(x)$ (dashed line) and $\mathrm{W}_{-1}(x)$ (solid line). During Exponential SUSY inflation, inflation proceeds along the "-1" branch in the direction specified by the arrow on the figure.

This equation can also be inverted in terms of the Lambert function to get the field value in terms of the number of e-folds:

$$x = q(N - N_{\rm end}) - \frac{e^{qx_{\rm end}} - qx_{\rm end}}{q} - \frac{1}{q}\mathrm{W}_{-1}\left\{-\exp\left[q^2(N - N_{\rm end}) - (e^{qx_{\rm end}} - qx_{\rm end})\right]\right\}. \tag{4.107}$$

The fact that one should choose the branch W_{-1} is justified below. The argument of the Lambert function is always negative as the exponential is always positive. Moreover, since $x_{\rm end} > 0$ and $N < N_{\rm end}$, the maximal value of exponential argument is saturated for $x_{\rm end} \to 0$, i.e. for a Lambert function argument equals to $-1/e$. As the result the Lambert function argument varies, at most, in $[-1/e, 0]$. Finally, since $x > 0$, we see directly from Eq. (4.107) that the Lambert function values have to be negative thereby ensuring that inflation proceeds only along the "-1"-branch (see Fig. 16).

With such a potential, inflation ends naturally at $\epsilon_1 = 1$, i.e. at the field value

$$x_{\rm end} = \frac{1}{q}\ln\left(1 + \frac{q}{\sqrt{2}}\right). \tag{4.108}$$

From this equation and the trajectory, we have an explicit relation between the field value ϕ_* at which the pivot mode crossed the Hubble radius during inflation and the corresponding e-fold number ΔN_*.

Finally, the parameter M can be determined from the amplitude of the CMB anisotropies, and one gets

$$\left(\frac{M}{M_{\rm Pl}}\right)^4 = 720q^2\pi^2\frac{e^{-2qx_*}}{(1 - e^{-qx_*})^3}\frac{Q^2_{\rm rms-PS}}{T^2}, \tag{4.109}$$

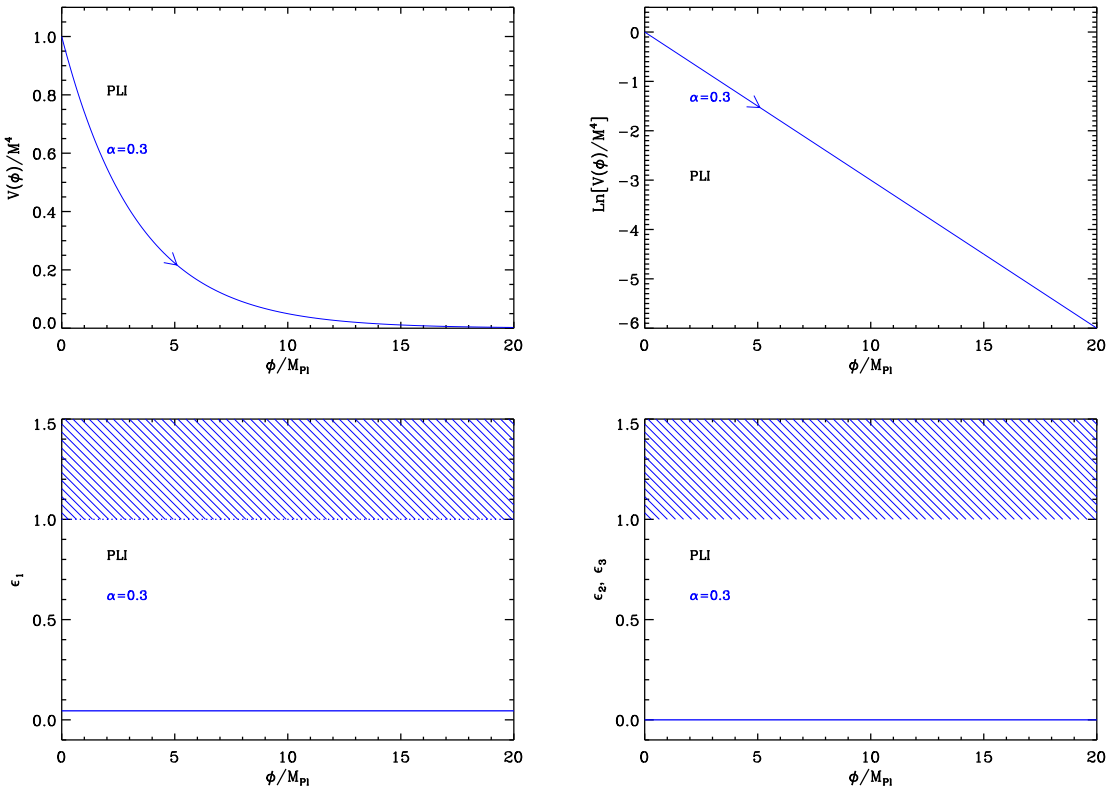

Figure 17. Power Law Inflation (PLI) for $\alpha = 0.3$. Top panels: power law potential (left) and its logarithm (right). Bottom left panel: slow-roll parameter ϵ_1. Bottom right panel: slow-roll parameters $\epsilon_2 = \epsilon_3 = 0$. On these plots, the shaded area indicates the region where slow-roll is violated.

where the value of ϕ_* (or ΔN_*) is obtained from Eq. (2.47). The reheating consistent slow-roll prediction for the exponential Susy models are represented in Figs. 89 and 90. In the limit $q \to 0$, we recover the same prediction as a linear large field model. From Fig. 89, we see that all the models remains compatible with the current data. These figures correspond to $\overline{w}_{\rm reh} = 0$, but one could argue that $\overline{w}_{\rm reh} \gtrsim -1/3$ make more sense if a parametric reheating would feel the linear shape of the potential. This quite extreme situation is represented in Fig. 90. In that case, the low reheating temperatures are clearly disfavored.

4.8 Power Law Inflation (PLI)

These models refer to inflationary potentials of the form

$$V(\phi) = M^4 e^{-\alpha\phi/M_{\rm Pl}}\,, \tag{4.110}$$

where α is a dimensionless parameter. They have been intensively studied since they lead to an exact inflationary dynamics, of the power law form, hence their name. Moreover, the power spectrum can also be determined exactly in this case. The background solution reads $a \propto (t/t_0)^{2/\alpha^2}$ and $\phi = \phi_0 + 2M_{\rm Pl}/\alpha \ln(t/t_0)$ with $t_0^2 = 2M_{\rm Pl}^2/(\alpha^2 M^4)(6/\alpha^2 - 1)e^{\alpha\phi_0/M_{\rm Pl}}$. We see that we have inflation provided $\alpha \in \left[0, \sqrt{2}\right]$.

This scenario was introduced in Ref. [278] where the two point correlation function of the cosmological fluctuations was calculated for the first time (see also Refs. [279, 280]). The

predictions of this model were recently compared to the Planck data in Ref. [169]. Soon after Ref. [278], it was also considered in Refs. [281, 282] but in the context of quintessence, i.e. for models of dark energy in which the energy density of the scalar field redshifts as a power law of the scale factor $\rho \propto a^{-q}$. In that case, one has $\alpha = \sqrt{q/2}$. The same potential also arises in the case where large field inflation is considered (LFI, see section 4.2) but with a non-minimal coupling of the inflaton to the gravity sector, see Refs. [283, 284] (the exponential potential appears after the transformation to the Einstein frame). In Ref. [285], a cosmic no-hair theorem for Bianchi models was proven assuming that the potential of the inflaton is of type (4.110). It was shown that one must have $0 < \alpha < \sqrt{2/3}$ so that the isotropic power law solution is the unique attractor for any initially expanding Bianchi type model (except type IX). In Ref. [286], the potential (4.110) has been studied in the Kantowski-Sachs metric, and it was found that the production of particles by the scalar field acts as viscous forces which enlarges the range of initial conditions leading to successful inflation. In Ref. [287], the nature of the potential $V(\phi)$ relevant to having inflation in presence of a minimally coupled scalar field together with a causal viscous fluid was investigated. It was shown that this leads to an exponential potential. In Refs. [288–290], the exponential potential was used to describe the dynamics of a tachyonic matter field (i.e. with a non-minimal kinetic term). In Ref. [291], the general transformations that leave unchanged the form of the field equations for Bianchi V cosmologies were investigated, and it was found that they admit asymptotic stable points that lead to power law solutions of the type (4.110). In Ref. [292], inflation was studied in the context of M-theory on $S^1/\mathbb{Z}_2$ via the non-perturbative dynamics of M5-branes. The open membrane instanton interactions between the branes give rise to potentials of the type (4.110). Ref. [293] has used the exponential potential (4.110) in the context of Randall-Sandrum type II Braneworld model. Finally, the general dynamics of power law inflation was studied in detail in Refs. [294–303], where various aspects of its phenomenology were highlighted.

The potential and its logarithm are displayed in Fig. 17. They are decreasing functions of the field, hence inflation proceeds from the left to the right. The slow-roll parameters take a simple form given by

$$\epsilon_1 = \frac{\alpha^2}{2}, \quad \epsilon_{i>1} = 0. \tag{4.111}$$

Since the first slow-roll parameter is constant, inflation cannot stop by slow-roll violation and one has to assume that, at some *vev* $\phi_{\rm end}$, a tachyonic instability is triggered. A priori, this means that the model has in fact an additional new free parameter. However, because the slow-roll parameters do not depend on ϕ, as well as all the other properties of the inflationary dynamics (even when the slow-roll approximation is not satisfied, see below), the observational predictions of the model cannot depend on $\phi_{\rm end}$ and this parameter turns out to be irrelevant.

The Hubble flow hierarchy being almost trivial, the exact dynamics of the model can be worked out even if the slow-roll approximation is violated. Indeed, let us first notice that the slow-roll trajectory can be explicitly integrated, and gives

$$\frac{\phi}{M_{\rm Pl}} = \frac{\phi_{\rm end}}{M_{\rm Pl}} + \alpha\,(N_{\rm end} - N)\,. \tag{4.112}$$

Then, one can remark that this trajectory is also a solution of the exact Klein-Gordon

equation of motion, which reads in terms of the number of e-folds N,

$$H^2\frac{\partial^2\phi}{\partial N^2}+\left(3H^2+H\partial\frac{\partial H}{\partial N}\right)\frac{\partial\phi}{\partial N}+\frac{\mathrm{d}V}{\mathrm{d}\phi}=0. \tag{4.113}$$

Indeed, the first term vanishes, and the second term requires

$$H^2=\frac{V+\dot{\phi}^2/2}{3M_{\rm Pl}^2}=\frac{V+\dfrac{H^2}{2}\left(\dfrac{\partial\phi}{\partial N}\right)^2}{3M_{\rm Pl}^2}=\frac{V+\dfrac{H^2}{2}\alpha^2M_{\rm Pl}^2}{3M_{\rm Pl}^2}\,, \tag{4.114}$$

from which one gets

$$H^2=\frac{V}{3M_{\rm Pl}^2}\frac{1}{1-\alpha^2/6}\,. \tag{4.115}$$

From there, one can evaluate all terms in the Klein-Gordon equation, and verify that Eq. (4.112) is indeed a solution of Eq. (4.113). Since it is a second order differential equation, other solutions exist, but it can be shown [281, 282] that the exact solution is an attractor. Let us also notice that combining Eq. (4.115) with Eq. (4.112) gives rise to

$$H=H_{\rm end}\left(\frac{a_{\rm end}}{a}\right)^{\alpha^2/2}, \tag{4.116}$$

which can be integrated and gives

$$a(t)=a_{\rm end}\left(\frac{t}{t_{\rm end}}\right)^{2/\alpha^2}. \tag{4.117}$$

One recovers the solution mentioned at the beginning of this section. Finally, the equation of state $w=P/\rho$ can also be worked out exactly and one gets

$$w=-1+\frac{\alpha^2}{3}\,. \tag{4.118}$$

Again, all the previous expressions are valid even if the slow-roll approximation is not satisfied. One can see that pure de Sitter corresponds to $\alpha=0$. In this case the potential is constant, the equation of state is -1 and the scale factor expands exponentially.

Another nice feature of power-law inflation is that the spectrum of the perturbations can be computed exactly without relying on any approximation. Defining the parameter $\beta\leq-2$ from $\alpha^2/2=(\beta+2)/(\beta+1)$, the primordial scalar power spectrum is given by

$$\mathcal{P}_\zeta=\frac{H_*^2}{\pi\epsilon_1(8\pi M_{\rm Pl}^2)}f(\beta)\left(\frac{k}{k_*}\right)^{2\beta+4}, \tag{4.119}$$

where

$$f(\beta)\equiv\frac{1}{\pi}\left[\frac{(1+\beta)^{1+\beta}}{2^{1+\beta}}\Gamma\left(\frac{1}{2}+\beta\right)\right]^2. \tag{4.120}$$

In particular, $f(\beta=-2)=1$. The power spectrum of gravitational waves can also be obtained remarking that we have $\mu_{\rm S}=\mu_{\rm T}$ for power law inflation. From

$$\mathcal{P}_\zeta=\frac{k^3}{8\pi^2}\left|\frac{\mu_{\rm S}}{a\sqrt{\epsilon_1}}\right|^2, \qquad \mathcal{P}_h=\frac{2k^3}{\pi^2}\left|\frac{\mu_{\rm T}}{a}\right|^2, \tag{4.121}$$

one gets

$$r \equiv \frac{\mathcal{P}_h}{\mathcal{P}_\zeta} = 16\epsilon_1 = \frac{16 n_{\rm T}}{n_{\rm T} - 2}\,, \tag{4.122}$$

since $n_{\rm T} = n_{\rm S} - 1 = 2\beta + 4$.

Finally, the overall amplitude of the CMB anisotropies leads to a determination of the scale M, namely

$$\left(\frac{M}{M_{\rm Pl}}\right)^4 = 720\pi^2\alpha^2 e^{\alpha\phi_*/M_{\rm Pl}} \frac{Q^2_{\rm rms-PS}}{T^2}\,. \tag{4.123}$$

Obviously, this normalization depends on the value of $\phi_{\rm end}$, and it is more relevant to express it in terms of the potential energy, say, at the end of inflation:

$$\frac{V_{\rm end}}{M^4_{\rm Pl}} = 720\pi^2\alpha^2 e^{-\alpha^2\Delta N_*} \frac{Q^2_{\rm rms-PS}}{T^2}\,, \tag{4.124}$$

from which one typically gets $V_{\rm end}^{1/4}/M_{\rm Pl} \simeq 10^{-4}$.

The reheating consistent slow-roll predictions for the power law inflation models are displayed in Fig. 91. Because the slow-roll parameters are constant during inflation, one can check that the predictions of the models do not depend on the energy scale at which the power law reheating ends. One has $n_{\rm S} = 1 - \alpha^2$ and $r = 8\alpha^2$, and from the Planck constraints, all the models are disfavored at more than two-sigma confidence level.

4.9 Kähler Moduli Inflation I (KMII)

These models are stringy models and arise when type IIB string theories via Calabi-Yau flux compactification are used. KMII scenarios have been derived and studied in Refs. [304–310]. More specifically, when internal spaces are weighted projective spaces, one of the Kähler moduli can play the role of an inflaton field and its potential, in the large field limit, reads

$$V(\phi) = M^4\left(1 - \alpha\frac{\phi}{M_{\rm Pl}}e^{-\phi/M_{\rm Pl}}\right), \tag{4.125}$$

α being a positive dimensionless parameter. Actually, since we deal with a modulus, ϕ usually possesses a non-minimal kinetic term. Then, once the inflaton field has been canonically normalized, ϕ has to be replaced with $\propto \phi^{4/3}$. The corresponding corrected potential is studied as "Kähler Moduli Inflation II" (KMIII) in section 5.3. However, sometimes, the potential (4.125) (with ϕ already canonically normalized) is also studied as a toy model (notably in Ref. [310]), the hope being that it can give a simpler description of the physics that naturally appears in the context of moduli inflation. Therefore, in this section, we also consider this scenario.

The potential in Eq. (4.125) depends on one free parameter, α. A priori, there does not exist any bound on its value. However, as explained below, in order for slow-roll inflation to occur, one must restrict the range of possible values for α. Within this range, we will show that the predictions of the model turn out to be almost independent of α (in fact, they logarithmically depend on α). The potential (4.125) and its logarithm are displayed in Fig. 18. It decreases from $\phi = 0$ (where it blows up), reaches a minimum at $\phi = M_{\rm Pl}$, and then increases to the asymptotic value $V = M^4$ when $\phi \to +\infty$. Therefore, two regimes of inflation may a priori exist: either inflation proceeds from the left to the right in the decreasing $\phi < M_{\rm Pl}$ branch of the potential (in this branch the *vev* ϕ increases during inflation) or it

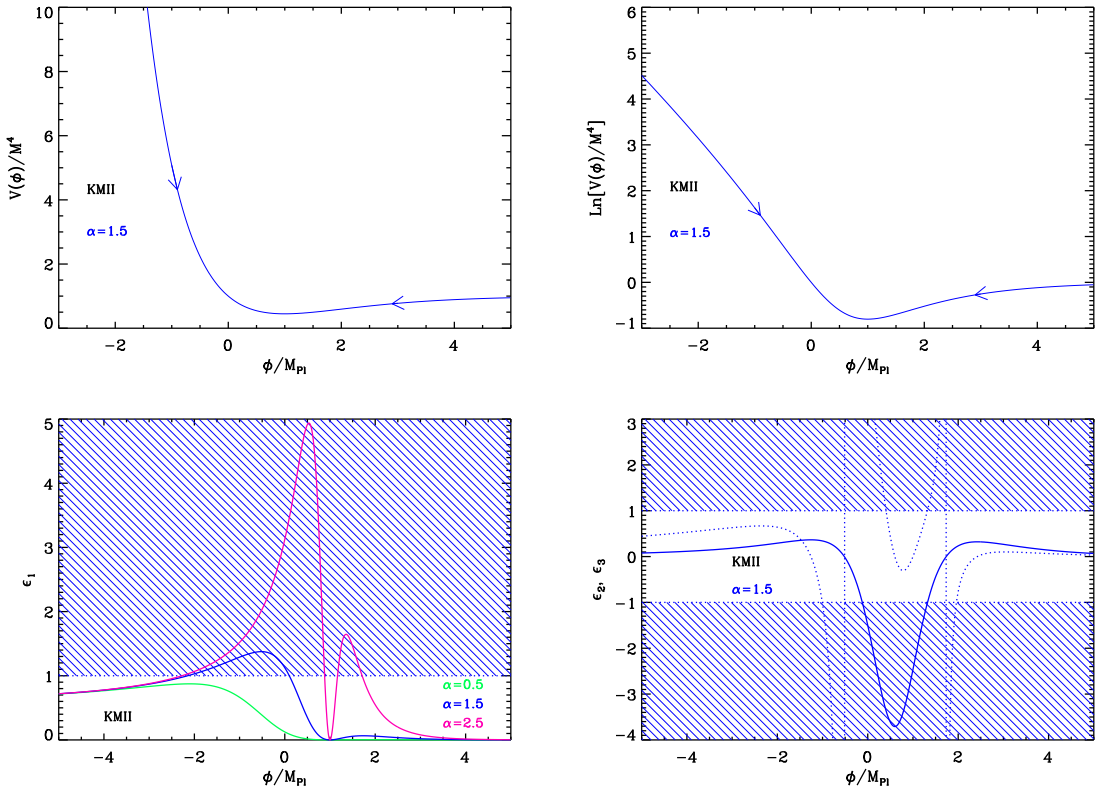

Figure 18. Top left panel: Kähler moduli inflation (KMII) potential for $\alpha = 1.5$. The two arrows indicate the two regions of the potential where inflation can take place. Top right panel: logarithm of the potential for the same value of α. Bottom left panel: slow-roll parameter ϵ_1 for $\alpha = 0.5$ (solid green line), $\alpha = 1.5$ (solid blue line) and $\alpha = 2.5$ (solid pink line). Obviously, the number of solutions of the equation $\epsilon_1 = 1$ depends on the value of α. Bottom right panel: slow-roll parameters ϵ_2 (solid line) and ϵ_3 (dotted line) for $\alpha = 1.5$.

proceeds from the right to the left in the increasing $\phi > M_{\rm Pl}$ branch of the potential (and the *vev* decreases during inflation). However, one should keep in mind that the potential is derived under the large field assumption and, consequently, only the second regime is in fact meaningful. As a toy model, one might nevertheless want to study both regimes but it turns out that, in the first one, inflation could not stop by violation of the slow-roll conditions. This is why we will mainly focus on the second regime in the rest of this section. Let us also notice that the minimum value of the potential is located at $\phi = M_{\rm Pl}$ and is $V_{\rm min} = M^4\,(1 - \alpha/e)$. Therefore, if one requires the potential to be positive definite everywhere, then one must have $0 < \alpha < e \simeq 2.72$. However, this condition may also be ignored if one considers that the potential (4.125) is in any case not valid at $\phi/M_{\rm Pl} \lesssim 1$.

Defining $x \equiv \phi/M_{\rm Pl}$, the three first slow-roll parameters can be expressed as

$$\epsilon_1 = \frac{\alpha^2}{2} e^{-2x} \frac{(1-x)^2}{\left(1-\alpha e^{-x} x\right)^2}\,, \qquad \epsilon_2 = \frac{2\alpha e^{-x}}{\left(1-\alpha e^{-x} x\right)^2}\left(\alpha e^{-x} + x - 2\right), \tag{4.126}$$

and

$$\epsilon_3 = \frac{\alpha e^{-x}(x-1)}{\left(1-\alpha e^{-x}x\right)^2\left(\alpha e^{-x}+x-2\right)}\left[x-3+\alpha e^{-x}\left(x^2-3x+6\right)-2\alpha^2 e^{-2x}\right]. \tag{4.127}$$

Let us now study in more detail how inflation stops in this model. As can be seen in Fig. 18, the number of solutions of $\epsilon_1 = 1$ depends on the value of α. We now define the numbers α_1 and α_2 by

$$\alpha_1 \equiv \frac{\sqrt{2}}{\sqrt{2}-1}e^{\frac{2-\sqrt{2}}{1-\sqrt{2}}} \simeq 0.83, \qquad \alpha_2 \equiv \frac{\sqrt{2}}{\sqrt{2}+1}e^{\frac{2+\sqrt{2}}{1+\sqrt{2}}} \simeq 2.41. \tag{4.128}$$

If $0 < \alpha < \alpha_1$, then there is no solution (this corresponds to the green line in the bottom left panel in Fig. 18). The inflaton field eventually oscillates around the minimum of its potential but remains in a region where inflation continues forever. In this case, in order to stop inflation, one must add an auxiliary field to the model such that a tachyonic instability is triggered at some value $x_{\rm end}$. This of course increases the number of parameters of this model. If $\alpha_1 < \alpha < \alpha_2$ (which corresponds to the blue line in Fig. 18), then two solutions appear:

$$x^-_{\epsilon_1=1}|_{x<1} = x_{\rm end}|_{x<1} = \frac{1}{1-\sqrt{2}} - \mathrm{W}_0\left(\frac{\sqrt{2}}{1-\sqrt{2}}\frac{e^{\frac{1}{1-\sqrt{2}}}}{\alpha}\right) \simeq -2.4 - \mathrm{W}_0\left(-\frac{0.3}{\alpha}\right), \tag{4.129}$$

$$x^+_{\epsilon_1=1}|_{x<1} = \frac{1}{1-\sqrt{2}} - \mathrm{W}_{-1}\left(\frac{\sqrt{2}}{1-\sqrt{2}}\frac{e^{\frac{1}{1-\sqrt{2}}}}{\alpha}\right) \simeq -2.4 - \mathrm{W}_{-1}\left(-\frac{0.3}{\alpha}\right), \tag{4.130}$$

where W_0 and W_{-1} denotes the "0-branch" and the "-1-branch" of the Lambert function respectively. These two solutions are both smaller than one so that they both lie in the decreasing branch of the potential. Correspondingly, two regimes of inflation exist. The first one proceeds from the left to the right and stops at $x_{\rm end}|_{x<1}$. However, using the expression for the slow-roll parameters (4.126), it is easy to see that ϵ_1 is always larger than $1/2$ in this domain. Therefore, the slow-roll approximation breaks down in this case. The second regime takes place in the $\phi/M_{\rm Pl} > 1$ branch of the potential but inflation cannot stop by slow-roll violation. Finally, if $\alpha_2 < \alpha$ (this situation corresponds to the pink line in the bottom left panel in Fig. 18), then four solutions exist: two were already given in Eqs. (4.129), (4.130) and the two new ones read

$$x^-_{\epsilon_1=1}|_{x>1} = \frac{1}{1+\sqrt{2}} - \mathrm{W}_0\left(-\frac{\sqrt{2}}{1+\sqrt{2}}\frac{e^{\frac{1}{1+\sqrt{2}}}}{\alpha}\right) \simeq 0.4 - \mathrm{W}_0\left(\frac{-0.9}{\alpha}\right), \tag{4.131}$$

$$x^+_{\epsilon_1=1}|_{x>1} = x_{\rm end}|_{x>1} = \frac{1}{1+\sqrt{2}} - \mathrm{W}_{-1}\left(-\frac{\sqrt{2}}{1+\sqrt{2}}\frac{e^{\frac{1}{1+\sqrt{2}}}}{\alpha}\right) \simeq 0.4 - \mathrm{W}_{-1}\left(\frac{-0.9}{\alpha}\right). \tag{4.132}$$

The two new solutions are greater than one and therefore lie in the increasing branch of the potential. Thus two regimes exist in this situation. The first one is the same as before, proceeds again from the left to right, stops at $x_{\rm end}|_{x<1}$ and suffers from the fact that ϵ_1 is always larger than $1/2$. The second one proceeds from the right to the left and ends at $x_{\rm end}|_{x>1}$. We conclude that this regime is the regime of interest for the KMII model and that we must therefore require $\alpha > \alpha_2$.

Let us now study the slow-roll trajectory. It can be integrated exactly and its expression can be written as

$$\begin{aligned} N_{\mathrm{end}} - N = x_{\mathrm{end}} - \frac{e}{\alpha}\,\mathrm{Ei}\,(x_{\mathrm{end}} - 1) + \ln\,(x_{\mathrm{end}} - 1) \\ - x + \frac{e}{\alpha}\,\mathrm{Ei}\,(x - 1) - \ln\,(x - 1)\,, \end{aligned} \tag{4.133}$$

where Ei is the exponential integral function [204, 205]. At this point, a few remarks are in order. Firstly, let us notice that N goes to ∞ when x tends to 1. This means that, in the slow-roll approximation, the field can never cross the minimum of its potential. In particular, if $\alpha < \alpha_2$, that is to say if one starts from the $\phi/M_{\mathrm{Pl}} < 1$ branch and rolls down from the left to the right, then one can never reach the physical $\phi/M_{\mathrm{Pl}} > 1$ branch of the potential and inflation can never come to an end. Secondly, when $x \gg 1$, the trajectory can be approximated by

$$N_{\mathrm{end}} - N \simeq \frac{e}{\alpha}\left(\frac{e^x}{x} - \frac{e^{x_{\mathrm{end}}}}{x_{\mathrm{end}}}\right). \tag{4.134}$$

Moreover, in this approximation, it can be inverted exactly and one obtains

$$x \simeq -\mathrm{W}_{-1}\left[-\frac{1}{\alpha\,(N_{\mathrm{end}} - N)\,/e + e^{x_{\mathrm{end}}}/x_{\mathrm{end}}}\right], \tag{4.135}$$

in agreement with what was obtained in Ref. [310]. In the above expression, W_{-1} is the -1 branch of the Lambert function. Let us also notice that, in Ref. [310], the branch of the Lambert function was in fact incorrectly chosen. The fact that the -1 branch of the Lambert function has to be considered comes from the following argument. When $N_{\mathrm{end}} - N \to \infty$, the argument of the Lambert function goes to 0^- and, therefore, since x must tend towards $+\infty$ in this limit, the -1 branch must be chosen. In addition, if $N_{\mathrm{end}} - N \to 0$, then one must have $x \to x_{\mathrm{end}} > 1$ which is also the case if the -1 branch is retained. This is represented in Fig. 19 where the arrow indicates the direction along which inflation proceeds. In the third place, since, when $x \to \infty$, one has $N_{\mathrm{end}} - N \to \infty$, a sufficient number of e-folds can always be realized in this model. Finally, it is inaccurate to assume that $x_{\mathrm{end}} \gg 1$ and, therefore, the above approximated trajectory is not so useful. However, if one only assumes that $x \gg 1$ (which can be checked to be a good approximation, especially at $x = x_*$) but not $x_{\mathrm{end}} \gg 1$, then one can write

$$N_{\mathrm{end}} - N \simeq \frac{e}{\alpha}\frac{e^x}{x} + x_{\mathrm{end}} - \frac{e}{\alpha}\,\mathrm{Ei}\,(x_{\mathrm{end}} - 1)\,, \tag{4.136}$$

which, moreover, can be inverted into

$$x \simeq -\mathrm{W}_{-1}\left[-\frac{1}{\alpha\,(N_{\mathrm{end}} - N)\,e + \mathrm{Ei}\,(x_{\mathrm{end}} - 1) - \alpha x_{\mathrm{end}}/e}\right], \tag{4.137}$$

and which is valid whenever $x \gg 1$. However, one should keep in mind that, now, and contrary to the former approximated trajectory, taking the limit $N \to N_{\mathrm{end}}$ in the above expression is meaningless.

The energy scale M is, as before, given by the CMB normalization and one obtains the following expression

$$\left(\frac{M}{M_{\mathrm{Pl}}}\right)^4 = 720\pi^2\alpha^2\frac{(1 - x_*)^2}{\left(1 - \alpha x_* e^{-x_*}\right)^3}e^{-2x_*}\frac{Q^2_{\mathrm{rms-PS}}}{T^2}\,. \tag{4.138}$$

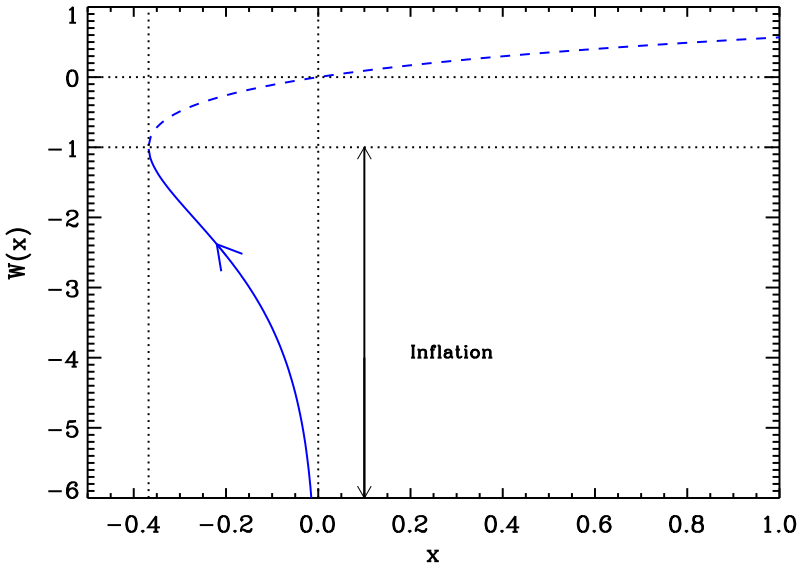

Figure 19. Lambert functions $\mathrm{W}_0(x)$ (dashed line) and $\mathrm{W}_{-1}(x)$ (solid line). During Kähler moduli inflation, inflation proceeds along the "-1" branch in the direction specified by the arrow.

If one uses the $x_* \gg 1$ approximation, then Eq. (4.137) tells us that $x_* \simeq \ln(\alpha\Delta N_*)$ and Eq. (4.138) can be re-written as

$$\left(\frac{M}{M_{\mathrm{Pl}}}\right)^4 = \mathcal{O}(1)\, 720 \frac{\pi^2}{\Delta N_*^2} \frac{Q_{\mathrm{rms-PS}}^2}{T^2}\,. \tag{4.139}$$

It is remarkable that this equation does not depend on α. Using a fiducial value for ΔN_*, one typically gets $M/M_{\mathrm{Pl}} \sim 10^{-3}$.

The predictions of KMII models are displayed in Fig. 92, for $\alpha > \alpha_2$. The reheating equation of state parameter $\overline{w}_{\mathrm{reh}}$ has been taken to 0 since the potential is quadratic close to its minimum [but, it should be reminded that, in principle, the potential Eq. (4.125) cannot be trusted close to its minimum]. One can see that, as announced at the beginning of this section, the predictions depend on α in a very mild way, a conclusion which is in agreement with Refs. [304, 310]. This can be understood as follows. If one assumes that $x_* \gg 1$, then we have already noticed that Eq. (4.137) implies that $x_* \simeq \ln(\alpha\Delta N_*)$. From this result, one obtains that

$$\epsilon_{1*} \simeq \frac{1}{2\Delta N_*^2} \ln^2(\alpha\Delta N_*)\,, \quad \epsilon_{2*} \simeq \frac{2}{\Delta N_*} \ln(\alpha\Delta N_*)\,, \quad \epsilon_{3*} \simeq \frac{1}{\Delta N_*} \ln(\alpha\Delta N_*)\,. \tag{4.140}$$

In these expressions, we notice that the slow-roll parameters (at Hubble crossing) logarithmically depend on α. This explains the weak α dependence observed in Fig. 92. Of course, one can also calculate the corresponding expressions of the spectral index, tensor to scalar ratio and running. One arrives at

$$n_{\mathrm{S}} \simeq 1 - 2\frac{\ln(\alpha\Delta N_*)}{\Delta N_*}\,, \quad r \simeq 8\frac{\ln^2(\alpha\Delta N_*)}{\Delta N_*^2}\,, \quad \alpha_{\mathrm{S}} \simeq -2\frac{\ln^2(\alpha\Delta N_*)}{\Delta N_*^2}\,. \tag{4.141}$$

These expressions are in accordance with the estimates derived in Refs. [304, 310]. However, contrary to what is claimed in Refs. [310], the predicted value of the running is not excluded by the CMB observations since, according to the Planck results [153], one has $\alpha_{\rm s} = -0.013 \pm 0.009$.

4.10 Horizon Flow Inflation at first order (HF1I)

The horizon flow models have been introduced in Ref. [311] and consist into designing field potentials to exactly produce a truncated Taylor expansion of the Hubble parameter with respect to the field. As such they constitute a whole class of phenomenological inflationary models. Here, we are considering a potential designed such that $H(\phi) = H_0(1 + A_1\phi/M_{\rm Pl})$, where A_1 is a free dimensionless parameter. The shape of the potential reads [311]

$$V(\phi) = M^4 \left(1 + A_1 \frac{\phi}{M_{\rm Pl}}\right)^2 \left[1 - \frac{2}{3}\left(\frac{A_1}{1 + A_1 \dfrac{\phi}{M_{\rm Pl}}}\right)^2\right]. \tag{4.142}$$

Denoting $x \equiv \phi/M_{\rm Pl}$, the potential admits a global minimum at $x_{V^{\rm min}} = -1/A_1$, which is negative

$$V_{\rm min} = V\left(\phi_{V^{\rm min}}\right) = -\frac{2}{3} M^4 A_1^2 < 0. \tag{4.143}$$

As a result, there are two disconnected field domains in which the potential remains definite positive, either $x > x^+_{V=0}$ or $x < x^-_{V=0}$ where $x^\pm_{V=0}$ are the two roots of $V(x^\pm_{V=0}) = 0$, i.e.

$$x^+_{V=0} = \sqrt{\frac{2}{3}} - \frac{1}{A_1}, \qquad x^-_{V=0} = -\sqrt{\frac{2}{3}} - \frac{1}{A_1}. \tag{4.144}$$

An interesting consequence of the horizon flow approach is that the Hubble flow functions can be calculated exactly, i.e. without the slow-roll approximation because $H(\phi)$ is exactly known. As discussed in Refs. [17, 312], one could compare them with the other hierarchy of parameters, ϵ_i^V, that are defined by the successive logarithmic derivatives of the potential. In the slow-roll approximation, one precisely uses the potential derivatives to approximate the Hubble flow functions. From $H \propto 1 + A_1 x$, one gets the exact Hubble flow functions

$$\epsilon_1 = 2\left(\frac{A_1}{1 + A_1 x}\right)^2, \qquad \epsilon_2 = \epsilon_3 = 2\epsilon_1, \tag{4.145}$$

whereas the slow-roll functions associated with the potential are

$$\epsilon_1^V = \frac{18 A_1^2 (A_1 x + 1)^2}{\left[3 + 6A_1 x + A^2\left(3x^2 - 2\right)\right]^2}, \qquad \epsilon_2^V = \frac{12 A_1^2\left[3 + 6A_1 x + A_1^2\left(3x^2 + 2\right)\right]}{\left[3 + 6A_1 x + A_1^2\left(3x^2 - 2\right)\right]^2}, \tag{4.146}$$

and

$$\epsilon_3^V = \frac{108 A_1^2 (A_1 x + 1)^2\left[1 + 2A_1 x + A_1^2\left(x^2 + 2\right)\right]}{\left[3 + 6A_1 x + A_1^2\left(3x^2 - 2\right)\right]^2\left[3 + 6A_1 x + A_1^2\left(3x^2 + 2\right)\right]}. \tag{4.147}$$

As shown in Ref. [17], the link between the two hierarchies can be made explicit and one has

$$\epsilon_1^V = \epsilon_1 \left(\frac{1 - \eta/3}{1 - \epsilon_1/3}\right)^2. \tag{4.148}$$

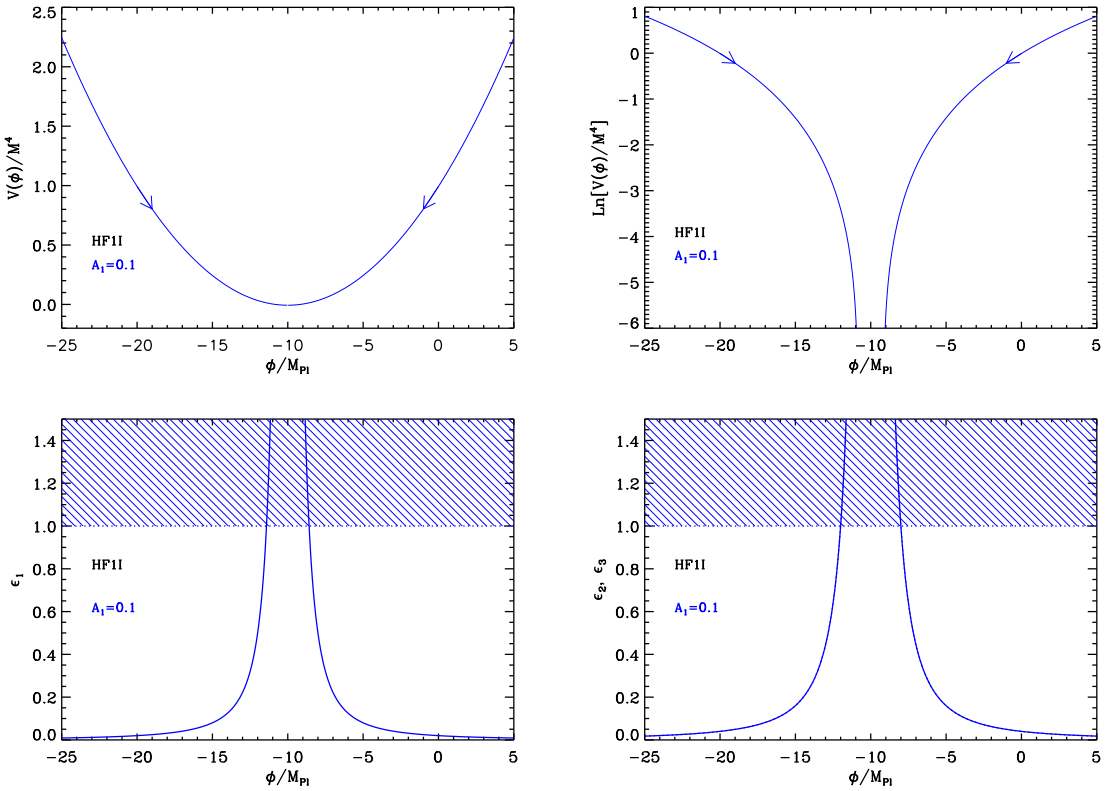

Figure 20. Top left panel: Horizon Flow Inflation at first order potential for $A_1 = 0.1$. Top panels: the potential and its logarithm with respect to the field values. Bottom left panel: the first Hubble flow function ϵ_1 (exact) and the corresponding shaded area where inflation stops. Bottom right panel: Hubble flow functions ϵ_2 (solid line) and ϵ_3 (dotted line) for the same potential. These two functions are equal to $2\epsilon_1$.

The η parameter is defined as

$$\eta \equiv \frac{2}{H}\frac{\mathrm{d}^2 H}{\mathrm{d}x^2}\,, \tag{4.149}$$

and vanishes in our case. As a result, provided $\epsilon_1 \ll 1$, i.e. we are in the slow-roll approximation, both hierarchies give the same results at first order. In order to establish Eq. (4.148), one has to show first that

$$\eta = \epsilon_1 + \frac{1}{\sqrt{2\epsilon_1}}\frac{\mathrm{d}\epsilon_1}{\mathrm{d}x}\,, \tag{4.150}$$

and then that[4]

$$\frac{\mathrm{d}\epsilon_1}{\mathrm{d}x} = (\epsilon_1 - 3)\left(\frac{\mathrm{d}\ln V}{\mathrm{d}x} - \sqrt{2\epsilon_1}\right). \tag{4.151}$$

The potential and the exact Hubble flow functions have been represented in Fig. 20.

Inflation can take place inside the two positive definite domains of the potential, i.e. at negative or positive field values. However, the Hubble parameter has to be positive such that H_0 has to be chosen negative if $1 + A_1 x < 0$ along the field trajectory. Since the potential

[4] A sign in these two equations differs from the ones typeset in Ref. [17], most probably due to a misprint.

is completely symmetric with respect to its minimum $x_{V^{\min}}$, we can study in full generality only the $x > x^{+}_{V=0}$ branch. In particular, as the Hubble flow functions are exact, we can also derive the exact field trajectory

$$N - N_{\rm end} = -\frac{1}{2A_1}\left(x + \frac{1}{2}A_1 x^2 - x_{\rm end} - \frac{1}{2}A_1 x_{\rm end}^2\right). \tag{4.152}$$

Let us notice that, in the slow-roll approximation, one would have derived the trajectory from ϵ_1^V. Doing so, one would have obtained

$$N - N_{\rm end} = -\frac{1}{2A_1}\left(x + \frac{1}{2}A_1 x^2 - x_{\rm end} - \frac{1}{2}A_1 x_{\rm end}^2 - \frac{2}{3}A_1 \ln\left|\frac{1+A_1 x}{1+A_1 x_{\rm end}}\right|\right). \tag{4.153}$$

It is amusing to remark that here, the simplest formula is not given by the slow-roll derived one, but rather by the exact one. From this remark one should keep in mind that, in order to simplify trajectories integration, one can always add factors of order $\mathcal{O}(\epsilon_1)$. The exact trajectory (4.152) can be inverted and one finds

$$x = -\frac{1}{A_1} + \frac{1}{A_1}\sqrt{1 + 2A_1 x_{\rm end} + A_1^2\left[x_{\rm end}^2 - 4(N - N_{\rm end})\right]}. \tag{4.154}$$

Along both the positive and negative branch of the potential, inflation ends naturally at $\epsilon_1 = 1$, that is at

$$x^{\pm}_{\epsilon_1=1} = \frac{-1 \pm \sqrt{2}A_1}{A_1}. \tag{4.155}$$

Along the positive branch we are interested in, we therefore have

$$x_{\rm end} = x^{+}_{\epsilon_1=1} = \frac{-1 + \sqrt{2}A_1}{A_1}. \tag{4.156}$$

Plugging this expression into Eq. (4.154) gives the field value x_* at which the pivot mode crossed the Hubble radius during inflation in terms of the e-fold number $\Delta N_* = N_{\rm end} - N_*$. Let us remember that solving for x_* (or ΔN_*) is made through Eq. (2.47). From Eq. (4.145), one gets

$$\epsilon_{1*} = \frac{1}{1 + 2\Delta N_*} \tag{4.157}$$

which, together with $\epsilon_2 = 2\epsilon_1$, yields

$$n_{\rm S} - 1 = 2n_{\rm T}, \qquad r = 4(1 - n_{\rm S}). \tag{4.158}$$

Notice that this relation is different from the power law case and consistent with Ref. [313]. In that reference, the authors mention that the horizon flow models predicts $r \simeq 4.8(1 - n_{\rm S})$ as a result of Monte-Carlo simulations.

Finally, the potential parameter M can be determined from the CMB normalization

$$\left(\frac{M}{M_{\rm Pl}}\right)^4 = 960\pi^2 \frac{A_1^2}{(1 + A_1 x_*)^4}\frac{Q^2_{\rm rms-PS}}{T^2}. \tag{4.159}$$

It is interesting to notice that the typical energy scale of inflation in these models does not depend on A_1. The previous equation indeed leads to

$$\frac{V(x_*)}{M_{\rm Pl}^4} = \frac{480\pi^2}{1 + 2\Delta N_*}\frac{Q^2_{\rm rms-PS}}{T^2}\left(1 - \frac{1}{3 + 6\Delta N_*}\right) \simeq 10^{-9}. \tag{4.160}$$

The reheating consistent (exact) predictions for the horizon flow inflation I models are represented in Fig. 93. As expected, the relation $\epsilon_2 = 2\epsilon_1$, which is the same as for the LFI quadratic case, is properly recovered. The predictions do not depend much on the potential parameter A_1.

4.11 Colemann-Weinberg Inflation (CWI)

4.11.1 Theoretical Justifications

The potential of this model was first introduced by Coleman and Weinberg in Ref. [314], in the context of spontaneous symmetry breaking generated by radiative corrections. The starting point of this work is to calculate the effective potential for a massless charged meson minimally coupled to the electrodynamic field.

In that reference, the effective action is explicitly constructed from a Legendre transform of the partition function, and expanded into one-particle-irreducible Feynman diagrams with n external lines (and summing up over n). The exact knowledge of the effective potential requires an infinite summation of all these Feynman diagrams, which is in practice intractable. It is thus made use of the one loop expansion method where all diagrams with no closed loops are first summed, then all diagrams with one closed loop are added, and all higher loops diagrams neglected. Starting with a quartic interacting scalar field, and requiring that the renormalized mass vanishes, one obtains a potential of the form

$$V(\phi) \propto 1 + \alpha \left(\frac{\phi}{Q}\right)^4 \ln\left(\frac{\phi}{Q}\right). \tag{4.161}$$

Let us emphasize that another useful frame of approximation is the Gaussian effective potential method. The Gaussian effective potential is a non-perturbative approach to quantum field theory [315–323], originally developed in the context of quantum mechanics, and generalized to field theory afterwards. In quantum mechanics, when studying systems governed by Hamiltonians of the form $H = p^2/2 + V(\phi)$, the idea is to calculate en effective potential V_{GEP} defined as

$$V_{\text{GEP}}(\phi_0) = \min_{\Omega}\left[\langle\psi|\, H\, |\psi\rangle \ , \ \psi(\phi) = \left(\frac{\Omega}{\hbar\pi}\right)^{1/4} e^{-\Omega\left(\phi-\phi_0\right)^2/(2\hbar)}\right], \tag{4.162}$$

i.e. the minimum possible quantum mean energy of a Gaussian wavefunction centered over ϕ_0. Such an object turns out to be a powerful tool to addressing the effects of quantum fluctuations on the physical behavior of a system in a non-perturbative way. It can be easily generalized to quantum field theories, expanding the field operator Φ only over Ω-massive excitations around the classical value ϕ_0 in d dimensions,

$$\Phi(t,\boldsymbol{x}) = \phi_0 + (2\pi)^{(1-d)/2}\int \frac{\mathrm{d}^{d-1}\boldsymbol{k}}{\sqrt{2\sqrt{k^2+\Omega^2}}}\left(a_{\boldsymbol{k}}e^{-i\sqrt{k^2+\Omega^2}t+i\boldsymbol{k}\cdot\boldsymbol{x}} + a^\dagger_{\boldsymbol{k}}e^{i\sqrt{k^2+\Omega^2}t-i\boldsymbol{k}\cdot\boldsymbol{x}}\right), \tag{4.163}$$

where $a^\dagger_{\boldsymbol{k}}$ and $a_{\boldsymbol{k}}$ are the usual creation and annihilation operators, and minimizing the quantum mean value of the Hamiltonian density over Ω. In Ref. [316], the quartic interacting scalar field has been worked out with this method, i.e. starting from $V(\phi) = m^2\phi^2/2 + \lambda\phi^4$. The Gaussian effective potential V_{GEP} obtained in this way can expanded in power of $\hbar$ to show that the first order terms match with the potential of Coleman and Weinberg. This is not surprising as this is equivalent of performing a one loop expansion over the effective

action. However, it should be stressed that the Gaussian effective potential method provides a much more general expression for the potential, that is valid beyond this perturbative limit and that can address regimes where quantum diffusion dominates the dynamics of the scalar field.

The model is defined such that inflation ends by violation of the slow-roll conditions, and is followed by a preheating stage in which the inflaton field oscillates at the bottom of its potential. Therefore this potential minimum must be set to zero, which implies

$$\alpha = 4e\,. \tag{4.164}$$

One is thus left with one mass parameter, Q, which sets the typical *vev* at which inflation takes place. On the other hand, the value taken for Q also depends on the underlying high energy model from which the CW potential emerges.

The CWI potential appears in various other contexts and, in fact, historically, it was the first model of inflation ever proposed [1] (also known as "old inflation"). The idea was that inflation occurs while the field is trapped in a false vacuum state $\langle\phi\rangle = 0$. Then, inflation comes to an end when the field tunnels from this state to the symmetry breaking true minimum. Unfortunately, this models was quickly realized to be ruled out since the above mentioned process is accompanied by bubble formation and these bubbles, while colliding, produce too large inhomogeneities. Then, this problem was solved by a modification of the old inflation scenario called "new inflation" [2, 3]. The main idea is that inflation does not occur while the field is trapped but when the field is rolling down from the origin to its true minimum. Bubbles are also formed but there are so big that our entire universe is contained in one of them. As a consequence, we do not observe bubble collisions and our universe is extremely homogeneous as indicated by the observations. This new inflationary scenario was explicitly implemented in Ref. [2] where the $\mathrm{SU}(5) \to \mathrm{SU}(3) \times \mathrm{SU}(2) \times \mathrm{U}(1)$ phase transition in GUTs is investigated. The model makes use of a CWI potential that can be described by

$$V(\phi) = \frac{5625}{512\pi^2} g^4 \left[\phi^4 \ln\left(\frac{\phi}{\phi_0}\right) - \frac{\phi^4}{4} + \frac{\phi_0^4}{4}\right], \tag{4.165}$$

where $\phi_0 \simeq 10^{14} - 10^{15}\,\mathrm{GeV}$, representing the GUT symmetry breaking scale, and $g^2 \simeq 1/3$ is the SU(5) gauge coupling constant. However, as noticed afterwards in Refs. [324–328], this model has also a fatal flaw. Indeed, one sees in Eq. (4.165) that the overall normalization of the potential reads $M^4 = 5625 g^4 \phi_0^4/(2048\pi^2)$ and that, therefore, the amplitude of the fluctuations is in fact already fixed. Using the value of the SU(5) coupling constant and $Q/M_{\mathrm{Pl}} = e^{1/4}\phi_0/M_{\mathrm{Pl}} \simeq 5 \times 10^{-5} - 5 \times 10^{-4}$, one arrives at $M^4 \simeq \left(10^{-13} - 10^{-17}\right) M_{\mathrm{Pl}}^4$. This turns out to be incompatible with the CMB normalization [see Eq. (4.173) below]. However, the same model was re-considered in Refs. [327, 329] (see also Ref. [330]), but with additional fields and couplings. It was then shown that the scale M acquires a different form and can scale as the inverse of the coupling constants. Since these ones are small, it becomes possible to obtain a higher value for M and to correctly CMB normalize the model. In what follows, we will therefore consider the scale M as a free parameter fixed by the overall amplitude of the cosmological fluctuations.

We also notice that, in Ref. [331], the CWI potential is obtained in the context of Kaluza-Klein inflation, i.e. in higher dimensions and with higher derivative terms and logarithmic dependence on the curvature scalar. Again, the typical value for $Q \simeq 10^{15}\,\mathrm{GeV}$. The CWI potential appears also in Ref. [332], but the value used for Q is rather different, $Q = 0.223 M_{\mathrm{Pl}}$,

and is fine-tuned in order to have two phases of inflation, a "chaotic inflationary" phase followed by a "new inflationary" phase. Finally, in Ref. [333], the Coleman-Weinberg potential is studied in the framework of Einstein-Brans-Dicke gravity, with the same typical value for $Q \simeq 10^{15}\,\mathrm{GeV}$ and the same typical value for $M^4/M_{\mathrm{Pl}}^4 \simeq 10^{-15}$ as in the original paper.

4.11.2 Slow-Roll Analysis

Considering the previous considerations, we take the potential to be

$$V(\phi) = M^4 \left[1 + \alpha \left(\frac{\phi}{Q}\right)^4 \ln\left(\frac{\phi}{Q}\right)\right], \tag{4.166}$$

with a parameter Q/M_{Pl} in the range $\left[10^{-5}, 10^{-3}\right]$ and $\alpha = 4e$. As already mentioned, the mass parameter M will be viewed as free and fixed by the normalization to the amplitude of the CMB anisotropies. The potential is displayed Fig. 21. It starts decreasing with the inflaton *vev* at $\phi = 0$, reaches a minimum at $\phi/Q = e^{-1/4}$ where it vanishes, and then increases and diverges as ϕ goes to ∞. As mentioned above, inflation proceeds along the decreasing branch of the potential, in the direction specified by the arrow in the figure.

Let us now derive the first slow-roll parameters. Defining $x \equiv \phi/Q$, they are given by

$$\epsilon_1 = \frac{M_{\mathrm{Pl}}^2}{Q^2}\frac{\alpha^2}{2}x^6 \left(\frac{1 + 4\ln x}{1 + \alpha x^4 \ln x}\right)^2, \tag{4.167}$$

while

$$\epsilon_2 = 2\frac{M_{\mathrm{Pl}}^2}{Q^2}\alpha x^2 \frac{-7 - 12\ln x + \alpha x^4 + \alpha x^4 \ln x + 4\alpha x^4 \ln^2 x}{\left(1 + \alpha x^4 \ln x\right)^2}, \tag{4.168}$$

and finally

$$\begin{aligned}\epsilon_3 = \frac{M_{\mathrm{Pl}}^2}{Q^2} \big(&-26\alpha x^2 + 21\alpha^2 x^6 - 2\alpha^3 x^{10} - 128\alpha x^2 \ln x \\ &+152\alpha^2 x^6 \ln x - 11\alpha^3 x^{10} \ln x - 96\alpha x^2 \ln^2 x \\ &+368\alpha^2 x^6 \ln^2 x - 14\alpha^3 x^{10} \ln^2 x + 384\alpha^2 x^6 \ln^3 x \\ &-16\alpha^3 x^{10} \ln^3 x - 32\alpha^3 x^{10} \ln^4 x\big) \left(1 + \alpha x^4 \ln x\right)^{-2} \\ &\times \left(7 - \alpha x^4 + 12\ln x - \alpha x^4 \ln x - 4\alpha x^4 \ln^2 x\right)^{-1}.\end{aligned} \tag{4.169}$$

The three of them have the same general behavior. They vanish at $x = 0$, increase with x in the decreasing branch of the potential and diverge at the minimum of the potential. Then they decrease from infinity in the increasing branch of the potential, and reach asymptotically vanishing values when the field *vev* goes to infinity. Inflation stops by slow-roll violation when $\epsilon_1 = 1$. The value of x at which this happens needs to be determined numerically, but in the limit $Q/M_{\mathrm{Pl}} \ll 1$ (remember that $Q/M_{\mathrm{Pl}} \simeq 10^{-4}$) where one expects $x_{\mathrm{end}} \ll 1$, one can derive an analytic approximated formula, namely

$$x_{\mathrm{end}} \simeq e^{-1/4} \exp\left[\mathrm{W}_{-1}\left(-\frac{3\sqrt{2}}{4\alpha}\frac{Q}{M_{\mathrm{Pl}}}e^{3/4}\right)\right], \tag{4.170}$$

where W_{-1} is the -1 branch of the Lambert function. A comparison between this approximated formula and the numerical solution for x_{end} is displayed in Fig. 22. The agreement is excellent.

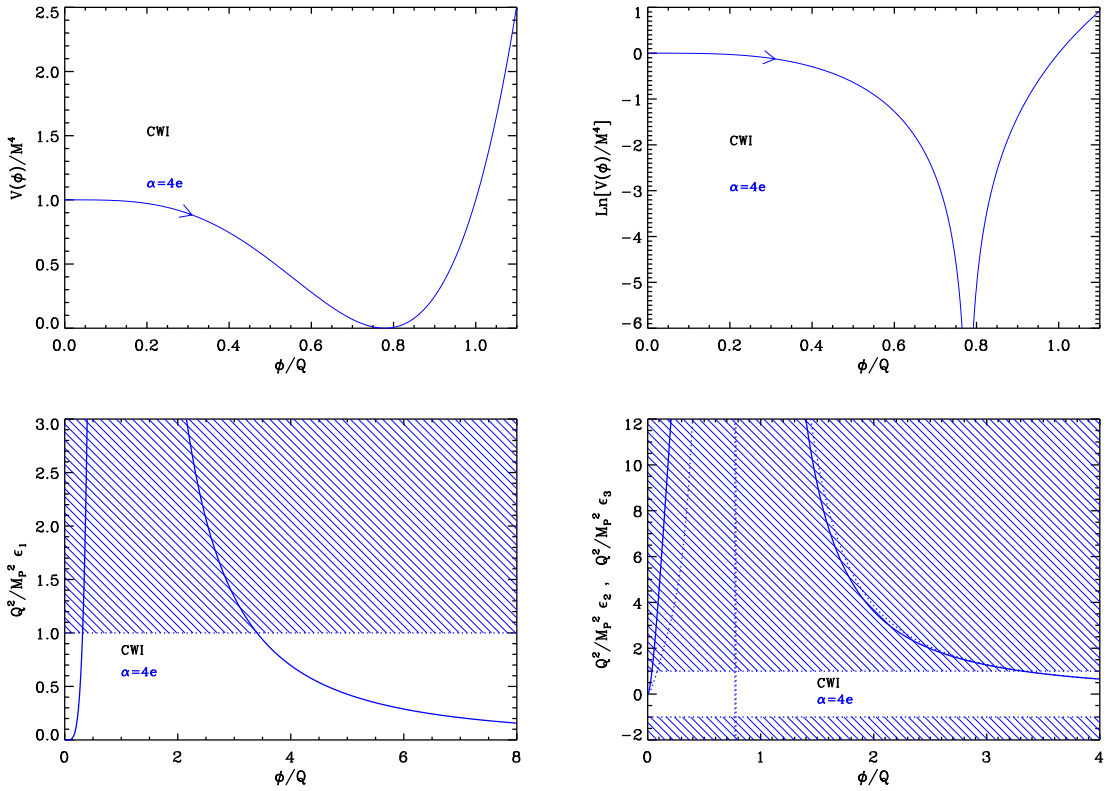

Figure 21. Colemann-Weinberg Inflation (CWI) for $\alpha = 4e$. Top left panel: Colemann-Weinberg Inflation potential as a function of ϕ/Q. Top right panel: logarithm of the potential for the same value of α. Bottom left panel: normalized first slow-roll parameter $Q^2/M_{\rm Pl}^2\,\epsilon_1$. The shaded area indicates the where inflation stops if $Q = M_{\rm Pl}$. Bottom right panel: normalized second and third slow-roll parameters $Q^2/M_{\rm Pl}^2\,\epsilon_2$ (solid line) and $Q^2/M_{\rm Pl}^2\,\epsilon_3$ (dotted line) for the same potential.

Let us now calculate the slow-roll trajectory from Eq. (2.11). It is given by

$$\begin{aligned} N_{\rm end} - N = & \frac{Q^2}{M_{\rm Pl}^2}\frac{\sqrt{e}}{4\alpha}\left[{\rm Ei}\left(-\frac{1}{2}-2\ln x\right)-{\rm Ei}\left(-\frac{1}{2}-2\ln x_{\rm end}\right)\right] \\ & + \frac{Q^2}{M_{\rm Pl}^2}\frac{1}{16\sqrt{e}}\left[{\rm Ei}\left(\frac{1}{2}+2\ln x_{\rm end}\right)-{\rm Ei}\left(\frac{1}{2}+2\ln x\right)\right] \\ & + \frac{1}{8}\frac{Q^2}{M_{\rm Pl}^2}\left(x^2-x_{\rm end}^2\right), \end{aligned} \tag{4.171}$$

where Ei is the exponential integral function, $N_{\rm end}$ is the number of e-folds at the end of inflation and N is the number of e-folds corresponding to the scaled field *vev* x. In the $Q/M_{\rm Pl} \ll 1$ limit where $x \ll 1$, the first term of this expression dominates. Since $\alpha = 4e$, the previous expression can be slightly simplified:

$$\begin{aligned} N_{\rm end} - N = & \frac{Q^2}{M_{\rm Pl}^2}\frac{1}{16\sqrt{e}}\left[{\rm Ei}\left(-\frac{1}{2}-2\ln x\right)-{\rm Ei}\left(-\frac{1}{2}-2\ln x_{\rm end}\right)\right. \\ & \left. + {\rm Ei}\left(\frac{1}{2}+2\ln x_{\rm end}\right)-{\rm Ei}\left(\frac{1}{2}+2\ln x\right)\right] + \frac{1}{8}\frac{Q^2}{M_{\rm Pl}^2}\left(x_{\rm end}^2-x^2\right). \end{aligned} \tag{4.172}$$

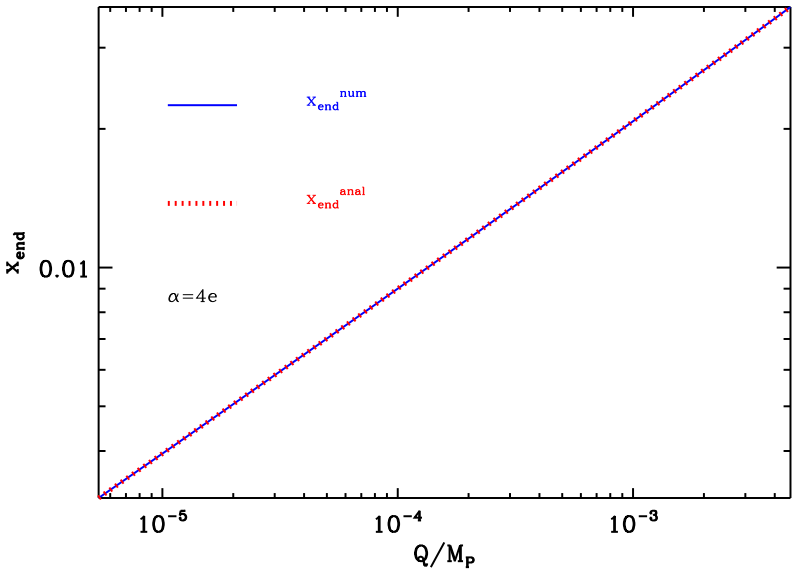

Figure 22. End of inflation in Coleman-Weinberg inflation. The approximated formula of Eq. (4.170) for $x_{\rm end}$ (red dashed line) is compared with the exact numerical solution of $\epsilon_1 = 1$ (blue solid line), for $\alpha = 4e$, in the physically relevant range of values for $Q/M_{\rm Pl}$. The agreement is obviously excellent.

After having solved the above equation for x_*, the field value at which the pivot scale crossed the Hubble radius during inflation, M is fixed by the amplitude of the CMB anisotropies to

$$\left(\frac{M}{M_{\rm Pl}}\right)^4 = 720\pi^2\alpha^2\frac{M_{\rm Pl}^2}{Q^2}x_*^6\left(1+4\ln x_*\right)^2\left(1+\alpha x_*^4\ln x_*\right)^{-3}\frac{Q_{\rm rms-PS}^2}{T^2}\,. \tag{4.173}$$

The reheating consistent slow-roll predictions of the Coleman-Weinberg models are displayed Fig. 94 in the physical range $Q/M_{\rm Pl} \in \left[10^{-5}, 10^{-3}\right]$. The reheating equation of state parameter $\overline{w}_{\rm reh}$ has been taken to 0 since the potential is quadratic close to its minimum $V(x) \simeq 2\alpha M^4 e^{-1/2}\left(x - e^{-1/4}\right)^2$. The typical predicted amount of gravitational waves is extremely small, and a non-negligible deviation from $n_{\rm S} = 1$ is noticed. Also, one could choose to relax the constraint on the parameter Q and study the Coleman-Weinberg potential in general. This was done for instance in Ref. [329] where the Coleman-Weinberg potential predictions are compared with the WMAP observations on general grounds. It is found that the potential normalization should be of the order $M \simeq 10^{16}\,{\rm GeV}$, and that $Q \simeq 10\,M_{\rm Pl}$ in order to match $n_{\rm S} \simeq 0.96$. For this reason the reheating consistent slow-roll predictions are displayed in Fig. 95 in the extended range $Q/M_{\rm Pl} \in [1, 100]$. In the limit $Q/M_{\rm Pl} \gg 1$, the model is well approximated by a quadratic potential around its minimum, and one asymptotically approaches the LFI predictions with $p = 2$ (see section 4.2).

4.12 Loop Inflation (LI)

4.12.1 Theoretical Justifications

The flatness of an inflationary potential is in general altered by radiative corrections. One loop order corrections generically take the form of a logarithmic function, $\ln(\phi/\mu)$, where μ

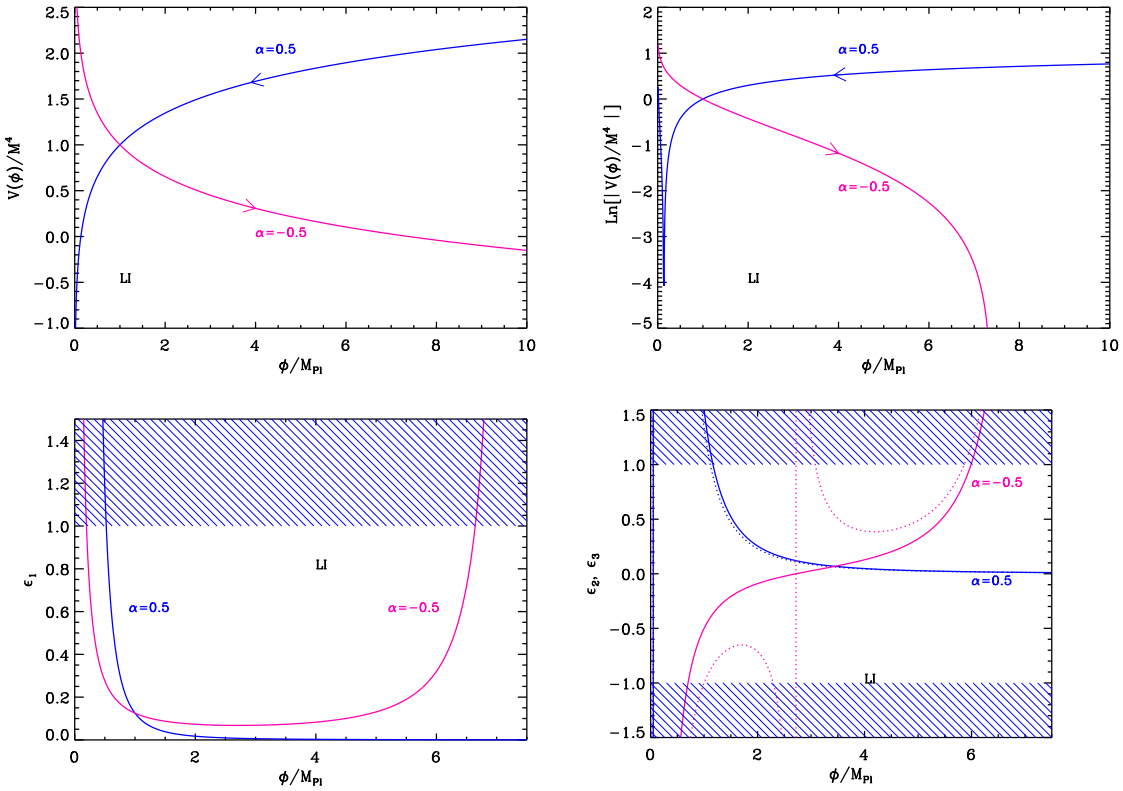

Figure 23. Loop Inflation (LI). Top left panel: Loop Inflation potential for $\alpha = \pm 0.5$, the case $\alpha = 0.5$ being displayed in blue and the case $\alpha = -0.5$ being displayed in pink. Top right panel: logarithm of the potential for the same values of α. Bottom left panel: slow-roll parameter ϵ_1 with the same values of α. The shaded area indicates where inflation stops. Bottom right panel: slow-roll parameters ϵ_2 (solid line) and ϵ_3 (dotted line) for the same values of α.

is a renormalization scale. Starting from a perfectly flat potential, one obtains a potential of the form $V(\phi) = M^4 [1 + \alpha \ln (\phi/M_{\rm Pl})]$ where α is a dimensionless parameter that tunes the strength of the radiative effects. Studying such potentials is therefore a simple way to discuss in which cases the quantum correction "spoil" the flatness of a potential, and how this happens.

In fact, this type of scenarios were invented in the context of F and D-term inflation in Refs. [334–337]. The original motivation was to build an inflationary model in supersymmetry but without the η-problem that appears in the F-term approach. Indeed, if one considers a simple superpotential $W = f/2X\phi^2 - \mu^2 X$ where ϕ and X are two superfields, then it is easy to obtain the supersymmetric potential assuming a minimal Kähler potential: $V = |f\phi^2/2 - \mu^2|^2 + f^2|X|^2|\phi|^2$. There is a flat direction for $\phi = 0$ along the X direction with $V = \mu^4$. Lifting this direction with a one loop correction leads to the LI potential which is suitable for inflation. However, considering non-minimal term in the Kähler potential destroys the flatness of V. The D-term approach was shown to be a viable alternative. The idea is to consider a theory with a U(1) symmetry and three chiral superfields, X, ϕ_+ and ϕ_- with charges 0, +1 and −1 respectively. It then follows that the superpotential has the

form $W = \lambda X \phi_+ \phi_-$. If we compute the corresponding potential in global supersymmetry, one arrives at

$$V = \lambda^2 |X|^2 \left(|\phi_-|^2 + |\phi_+|^2\right) + \lambda^2 |\phi_+ \phi_-|^2 + \frac{g^2}{2}\left(|\phi_+|^2 - |\phi_-|^2 + \xi\right)^2, \tag{4.174}$$

where the part proportional to g (g being the gauge coupling) represents the D-part of V. In this expression ξ is a Fayet-Iliopoulos term. There is a unique supersymmetric vacuum at $X = \phi_+ = 0$ and $|\phi_-| = \sqrt{\xi}$ and a flat direction along the X direction with $\phi_+ = \phi_- = 0$ where the potential $V = g^2\xi^2/2$ can drive inflation. Since supersymmetry is broken along the flat direction, this produces one loop corrections and we obtain

$$V = \frac{g^2}{2}\xi^2 \left[1 + \frac{g^2}{16\pi^2} \ln\left(\frac{\lambda^2 |X|^2}{\mu^2}\right)\right], \tag{4.175}$$

where μ is a renormalization scale. We see that this potential has exactly the form of an LI potential where the scale M is related to the Fayet-Iliopoulos term ξ and where α is in fact the square of the gauge coupling. In particular, this implies that $\alpha > 0$ in this context. One can also reproduce the above calculation in supergravity (with minimal Kähler potentials) and show that the D-part of the theory leads to the same potential which is free of the η problem.

After these initial works on D-term inflation, many other papers addressing different issues were published. Observational constraints on this type of scenarios were discussed in Refs. [338, 339]. Ref. [340] has discussed how to produce D-term inflation and to stabilize the moduli at the same time. Then, in Refs. [341–343], it was shown that the stringy implementation of D-term inflation is problematic. We have seen that the scale M is essentially controlled by the value of the Fayet-Iliopoulos term ξ. Therefore, the CMB normalization allows us to calculate the value of ξ. Anticipating the calculation at the end of this section, if one uses the equation after Eq. (4.187) with $M^4 = g^2\xi^2/2$ and $\alpha = g^2/(8\pi^2)$ [from Eq. (4.175)], then one arrives at

$$\xi \simeq \left[\left(\frac{90}{\Delta N_*}\right)^{1/4} \left(\frac{Q_{\mathrm{rms-PS}}}{T}\right)^{1/2} M_{\mathrm{Pl}}\right]^2 \simeq \left(6.9 \times 10^{15}\mathrm{GeV}\right)^2, \tag{4.176}$$

where we have taken the fiducial value $\Delta N_* \simeq 50$. As noticed in Refs. [341–343], in string theory, one typically obtains $\xi = (\mathrm{Tr}Q) M_{\mathrm{s}}^2/(192\pi^2)$ where M_{s} is the string scale and $\mathrm{Tr}Q \simeq 100$ sums the U(1) charges of all massless states. This leads to $\xi \simeq (\text{few} \times 10^{17}\mathrm{GeV})^2$ and, therefore, does not match the CMB normalization (4.176). Then, Refs. [344, 345] studied more complicated models in the supersymmetric context in order to fix the problem we have just discussed. Other scenarios were also investigated in Refs. [346–349]. D-term inflation in the context of string theory and brane inflation was also discussed in Ref. [231, 350–355]. The same topic was also addressed in Refs. [356, 357] but in the context where the Friedmann equations receives quadratic corrections. Finally, Ref. [358] studied LI potentials in the case of Wess–Zumino models. Let us emphasize again that, in all these models, the constant α is positive and given in terms of the square of a gauge coupling.

The LI potential was also derived in a different framework in Ref. [359]. This article uses the O'Raifeartaigh-Witten model that will be studied in more detail in section 4.23. Therefore, we do not give the details here and only quote results that will be reviewed in that section. In particular, we will see in Eq. (4.338) that the only difference is that the

parameter α is now given in terms of three coupling constants and has a rather involved form which allows for negative α values. For this reason we will not fix the sign of α in the following.

4.12.2 Slow-Roll Analysis

Let us now turn to the slow-roll study of loop inflation. We recall that the potential takes the following form

$$V(\phi) = M^4 \left[1 + \alpha \ln\left(\frac{\phi}{M_{\rm Pl}}\right)\right], \tag{4.177}$$

where α is a dimensionless parameter, that can a priori be either positive or negative (see the above discussion). Let us define the quantity $x \equiv \phi/M_{\rm Pl}$. The potential Eq. (4.177), as well as its logarithm, is displayed in Fig. 23. If $\alpha > 0$, it is an increasing function of the field *vev*, and vanishes at

$$x_{V=0} = e^{-1/\alpha}\,. \tag{4.178}$$

Hence inflation proceeds from the right to the left at $x > x_{V=0}$ in that case. If $\alpha < 0$ however, the potential is a decreasing function of the field, which vanishes at $x_{V=0}$, still given by Eq. (4.178), hence inflation proceeds from the left to the right at $x < x_{V=0}$.

The three first Hubble flow functions in the slow-roll approximation are given by

$$\epsilon_1 = \frac{\alpha^2}{2}\frac{1}{x^2}\left(1+\alpha\ln x\right)^{-2}, \qquad \epsilon_2 = 2\alpha\frac{1}{x^2}\frac{1+\alpha+\alpha\ln x}{\left(1+\alpha\ln x\right)^2}, \tag{4.179}$$

and

$$\begin{aligned}\epsilon_3 =& 2\alpha\frac{1}{x^2}\left(1+\alpha\ln x\right)^{-2}\left(1+\alpha+\alpha\ln x\right)^{-1}\times \\ & \left[1+\frac{3\alpha}{2}+\alpha^2+\left(2\alpha+\frac{3}{2}\alpha^2\right)\ln x+\alpha^2\ln^2 x\right].\end{aligned} \tag{4.180}$$

If $\alpha > 0$, the first slow-roll parameter is a decreasing function of the field *vev*, which diverges at $x_{V=0}$ and vanishes when $x \to \infty$. Therefore inflation stops by slow-roll violation, at the point $x_{\rm end}$ satisfying $\epsilon_1 = 1$ and given by

$$x_{\rm end} = \frac{1}{\sqrt{2}}\left[\mathrm{W}_0\left(\frac{e^{1/\alpha}}{\sqrt{2}}\right)\right]^{-1}, \tag{4.181}$$

where W_0 is the 0-branch of the Lambert function. One can check that since $\mathrm{W}_0(y) < y$ for any y, one always has $x_{\rm end} > x_{V=0}$, as required. When $\alpha \ll 1$, one has $x_{\rm end} \simeq \alpha/\sqrt{2}$. If $\alpha < 0$ on the other hand, the first slow-roll parameter diverges at $x = 0$, decreases with x, reaches a minimum at $x_{\epsilon_2=0} = \exp\left(-1-1/\alpha\right)$, then increases with x and diverges at $x_{V=0}$. The minimum value of ϵ_1 equals $\epsilon_1\left(x_{\epsilon_2=0}\right) = \exp(2+2/\alpha)/2$ which is smaller than unity only if $\alpha > 2/(\ln 2 - 2) \simeq -1.53$. Otherwise $\epsilon_1(x) > 1$ all over the domain and inflation cannot take place. If $\alpha > 2/(\ln 2 - 2)$, the inflationary domain lies between $x^-_{\epsilon_1=1}$ and $x_{\rm end} = x^+_{\epsilon_1=1}$, with

$$x^-_{\epsilon_1=1} = -\frac{1}{\sqrt{2}}\left[\mathrm{W}_{-1}\left(\frac{-e^{1/\alpha}}{\sqrt{2}}\right)\right]^{-1}, \qquad x_{\rm end} = x^+_{\epsilon_1=1} = -\frac{1}{\sqrt{2}}\left[\mathrm{W}_0\left(\frac{-e^{1/\alpha}}{\sqrt{2}}\right)\right]^{-1}, \tag{4.182}$$

and where W_{-1} is the -1-branch of the Lambert function. When $|\alpha| \ll 1$, one has $x_{\rm end} \simeq e^{-1/\alpha} - 1/\sqrt{2} \gg 1$. Let us notice that the end of inflation occurs in the region $\phi \gg M_{\rm Pl}$, where

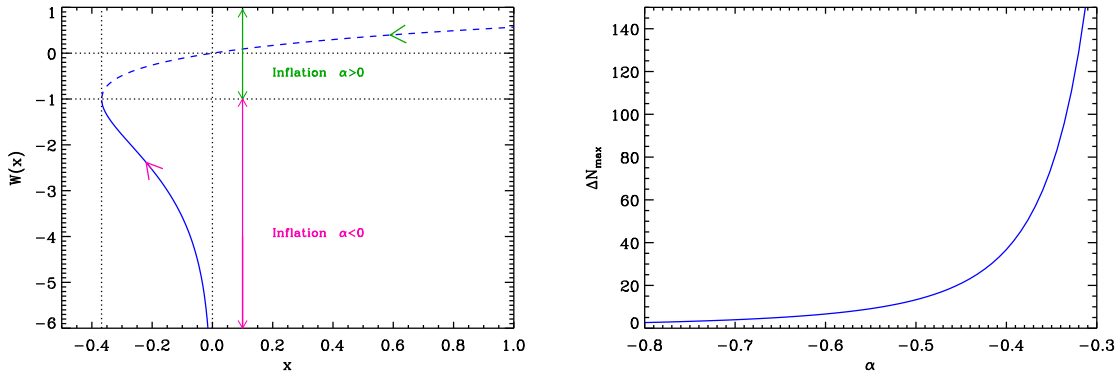

Figure 24. Left panel: Lambert functions $\mathrm{W}_0(x)$ (dashed line) and $\mathrm{W}_{-1}(x)$ (solid line). During loop inflation, inflation proceeds along the "0" branch in the direction specified by the green arrow on the figure if $\alpha > 0$, and along the "-1" branch in the direction specified by the pink arrow on the figure if $\alpha < 0$. Right panel: Maximal number of e-folds $\Delta N_{\rm max}$ one can realize when $\alpha < 0$, between $x^-_{\epsilon_1=1}$ and $x^+_{\epsilon_1=1}$, as a function of α.

Eq. (4.177) may not be well defined. Therefore, depending on the underlying theoretical setting, the end of inflation by slow-roll violation may not be meaningful.

Let us now turn to the slow-roll trajectory. It can be integrated, giving rise to

$$N_{\rm end} - N = \frac{x^2}{2}\left(\ln x + \frac{1}{\alpha} - \frac{1}{2}\right) - \frac{x^2_{\rm end}}{2}\left(\ln x_{\rm end} + \frac{1}{\alpha} - \frac{1}{2}\right). \tag{4.183}$$

When $|\alpha| \ll 1$, it approximately takes the form $2\alpha\,(N_{\rm end} - N) = x^2 - x^2_{\rm end}$. The trajectory Eq. (4.183) can be inverted making use of the Lambert function, and one obtains

$$x^2 = \frac{4\,(N_{\rm end} - N) - x^2_{\rm end}\left[1 - \dfrac{2}{\alpha} - \ln\left(x^2_{\rm end}\right)\right]}{\mathrm{W}_{\substack{0\\-1}}\left\{4\,(N_{\rm end} - N)\,e^{-(1-2/\alpha)} - \left[1 - \dfrac{2}{\alpha} - \ln\left(x^2_{\rm end}\right)\right]\exp\left[-1 + \dfrac{2}{\alpha} + \ln\left(x^2_{\rm end}\right)\right]\right\}}, \tag{4.184}$$

where the 0 branch of the Lambert function must be chosen if $\alpha > 0$, while the -1 branch must be chosen if $\alpha < 0$. The Lambert function is displayed in the left panel of Fig. 24, together with the regions in which inflation proceeds. Let us now comment and check that this expression is valid. Firstly, if $N = N_{\rm end}$, the Lambert function is of the form $\mathrm{W}(-z_{\rm end}e^{-z_{\rm end}}) = -z_{\rm end}$, where $z \equiv (1 - 2/\alpha) - \ln(x^2)$, and this automatically cancels the numerator such that one has indeed $x = x_{\rm end}$. Secondly, if $\alpha > 0$, the condition $x_{\rm end} > x_{V=0}$ implies that $z_{\rm end} < 1$, and the Lambert function at $N_{\rm end}$ is equal to $-z_{\rm end} > -1$. Therefore, at the end of inflation, one should use the zero branch of the Lambert function. Finally, as inflation is under way, the argument of the Lambert function is decreasing which implies that the whole inflationary stage takes place on the zero branch. On the other hand, if $\alpha < 0$ using similar arguments, the whole inflationary stage can be shown to take place on the -1 branch.

In this later case ($\alpha < 0$), it is also interesting to notice that the total number of e-folds is bounded, since inflation can only proceed between $x^-_{\epsilon_1=1}$ and $x^+_{\epsilon_1=1}$. The corresponding

maximal number of e-folds $\Delta N_{\rm max}$ is displayed, as a function of α, in the right panel of Fig. 24. One can see that when $\alpha \lesssim -0.35$, not a sufficient number of e-folds can be realized. For such values of α, one already has $x_{\rm end} > 10$. Since inflation is supposed to take place at sub-Planckian *vevs*, it means that this regime of inflation is a priori forbidden. If one allows slightly super-Planckian field *vevs*, up to $x \simeq 100$ or $x \simeq 1000$, this implies that $\alpha < -0.1$. Therefore even in this case, α must lie in the rather narrow range $-0.3 < \alpha < -0.1$.

Making use of the approximated trajectories and expressions for $x_{\rm end}$, some analytic predictions can be derived in the case $\alpha > 0$. The observable field value x_*, and its associated number of e-folds $\Delta N_* = N_{\rm end} - N_*$ at which the pivot mode crossed the Hubble radius during inflation are obtained from the above equations together with Eq. (2.47). In the limit $\alpha \ll 1$, one obtains the approximate expressions

$$\epsilon_{1*} \simeq \frac{\alpha}{4\Delta N_*}\,, \qquad \epsilon_{2*} \simeq \epsilon_{3*} \simeq \frac{1}{\Delta N_*}\,, \tag{4.185}$$

hence

$$r \simeq \frac{\alpha}{64\Delta N_*}\,, \qquad n_{\rm S} - 1 \simeq -\frac{1}{\Delta N_*}\,, \qquad \alpha_{\rm S} \simeq \frac{1}{\Delta N_*^2}\,. \tag{4.186}$$

Finally, the parameter M can be determined from the amplitude of the CMB anisotropies, and one gets

$$\left(\frac{M}{M_{\rm Pl}}\right)^4 = 720\pi^2 \frac{\alpha^2}{x_*^2} \frac{Q_{\rm rms-PS}^2}{T^2} \left(1 + \alpha \ln x_*\right)^{-3}\,. \tag{4.187}$$

In the small $|\alpha|$ limit, one obtains $M^4/M_{\rm Pl}^4 \simeq 360\pi^2\alpha/\Delta N_* Q_{\rm rms-PS}^2/T^2$ for $\alpha > 0$, and $M^4/M_{\rm Pl}^4 \simeq 720\pi^2\alpha^2 e^{2/\alpha} Q_{\rm rms-PS}^2/T^2$ for negative values of α.

The reheating consistent slow-roll predictions of the loop inflation models are displayed in Fig. 96 for $\alpha > 0$, and in Fig. 97 for $\alpha < 0$. For $\alpha > 0$ and $\alpha \ll 1$, the approximations in Eqs. (4.185) give a good description of what is numerically obtained, namely a deviation from scale invariance which almost does not depend on α, and an amount of gravitational waves which grows linearly with α. For $\alpha < 0$, the predictions blow out of the observational one- and two-sigma contours when α approaches the upper bound derived above, as expected. Correspondingly, the parameter α does not seem to be much constrained when it is positive, whereas close-to-zero values are favored when it is negative.

4.13 $(R + R^{2p})$ Inflation (RpI)

This model is the Einstein frame description of a scalar-tensor theory equivalent to $f(R) = R + \epsilon R^{2p}/\mu^{4p-2}$, where μ is a mass scale, $\epsilon = \pm 1$, and $p > 1/2$ (otherwise the expansion is meaningless). It generalizes the original Starobinsky model [360] obtained for $p = 1$. Such theories are quite generic and appear as limiting cases of more general modified gravity theories [361–365] (see Ref. [366] for a review).

Following Refs. [363, 366], one can introduce the scalar degree of freedom ϕ defined by

$$\frac{\phi}{M_{\rm Pl}} = \sqrt{\frac{3}{2}} \ln\left(|F(R)|\right)\,, \tag{4.188}$$

where $F(R) \equiv \partial f/\partial R$. The quantity $F \equiv \Omega^2$ is also the square of the conformal factor inducing the transformation from the Jordan frame to the Einstein frame. In the Einstein frame, the field ϕ evolves in a potential given by

$$V\left(\phi\right) = \frac{M_{\rm Pl}^2}{2} \frac{|F|}{F} \frac{RF - f}{F^2}\,. \tag{4.189}$$

In the present case, one has

$$F(R) = 1 + 2\epsilon p \left(\frac{R}{\mu^2}\right)^{2p-1} , \tag{4.190}$$

which, for small departures with respect to the Einstein-Hilbert action $R \ll \mu^2$, implies that $F(R) > 0$ as needed. Let us notice that in the opposite situation, accelerated (and super-accelerated) solutions have been shown to exist [366]. Defining the quantity y by

$$y \equiv \sqrt{\frac{2}{3}} \frac{\phi}{M_{\rm Pl}} , \tag{4.191}$$

and inserting Eq. (4.190) into Eq. (4.189) one obtains the Einstein frame potential

$$V = M^4 e^{-2y} \left|e^y - 1\right|^{2p/(2p-1)} . \tag{4.192}$$

The normalization constant M^4 is related to the modified gravity scale μ through the following expression

$$M^4 = \frac{2p-1}{4p} \frac{M_{\rm Pl}^2 \mu^2}{(2p)^{1/(2p-1)}} . \tag{4.193}$$

For $F(R) > 0$, Eq. (4.188) implies that for $\epsilon = 1$, the model is defined in the domain $y > 0$, whereas for $\epsilon = -1$ one should consider the domain $y < 0$ only. Such a potential has also been studied in Ref. [367] for $p = 1$, in Refs. [363, 368] for $p = 4$ and in Ref. [369] for $p = 2$. Let us notice that the case $p = 1$ corresponds to the Higgs inflation potential studied in section 3.1. The case $p = 1/2$ is singular since one recovers $f(R) \propto R$. Taking the limit $p \to \infty$, the potential asymptotes $V \to M^4 e^{-2y} \left|e^y - 1\right|$ and varying p allows us to explore different potential shapes.

Let us first consider the case $y > 0$ ($\epsilon = 1$). If $p > 1$, the potential admits a maximum at

$$y_{\rm max} = \ln\left(\frac{2p-1}{p-1}\right) , \tag{4.194}$$

such that inflation can proceed either for $0 < y < y_{\rm max}$ or $y > y_{\rm max}$. We respectively call these regimes RpI1 and RpI2. If $p < 1$, the potential is an increasing function of y, hence inflation proceeds from the right to the left. We call this regime RpI3. The case $p = 1$ is singular and again, it corresponds to the Higgs inflation potential studied in section 3.1.

The Hubble flow functions in the slow-roll approximation read

$$\epsilon_1 = \frac{4}{3} \frac{\left[1 + (p-1)\, e^y - 2p\right]^2}{(2p-1)^2 \left(e^y - 1\right)^2} , \qquad \epsilon_2 = \frac{8}{3} \frac{p\, e^y}{(2p-1)\left(e^y - 1\right)^2} , \tag{4.195}$$

and

$$\epsilon_3 = -\frac{4}{3} \frac{(e^y + 1)\left[1 + (p-1)\, e^y - 2p\right]}{(2p-1)\left(e^y - 1\right)^2} . \tag{4.196}$$

The potential and the Hubble flow functions for $y > 0$ have been represented in Fig. 25. As one can check on these figures, inflation never stops in the RpI2 regime and one needs to complement the model with a mechanism that can end inflation, as for instance with an extra-field and a tachyonic instability. This adds one additional parameter $y_{\rm end}$ to the model. When

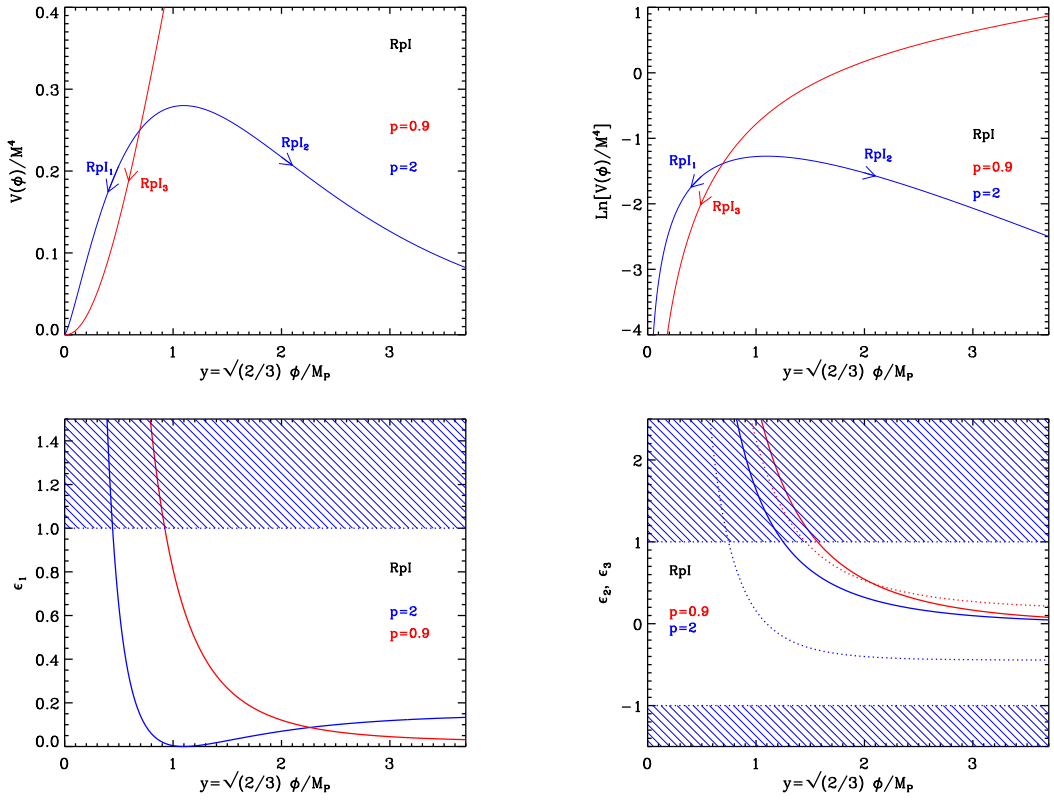

Figure 25. $(R + R^{2p})$ Inflation (RpI) in the Einstein frame for $p = 2$ (RpI1 and RpI2), and $p = 0.9$ (RpI3). Top panels: the potential and its logarithm. Bottom left panel: slow-roll parameter ϵ_1 with the region in which inflation stops (shaded area). In the RpI2 regime, inflation never stops and one has to consider an extra-mechanism to end inflation. Bottom right panel: slow-roll parameters ϵ_2 (solid line) and ϵ_3 (dotted line).

this parameter is large, all the three Hubble flow functions admit asymptotically constant values:

$$\lim_{y\to\infty} \epsilon_1 = \frac{4}{3}\left(\frac{p-1}{2p-1}\right)^2, \qquad \lim_{y\to\infty} \epsilon_2 = 0, \qquad \lim_{y\to\infty} \epsilon_3 = -\frac{4}{3}\frac{p-1}{2p-1}. \tag{4.197}$$

If p is an integer, except for the special case $p = 1$ (see section 3.1), these values are always smaller that unity, but not particularly small. As such, all these models predict large deviation from scale invariance. Indeed, the spectral index at first order is given by

$$n_{\rm S} - 1 \simeq -\frac{8}{3}\left(\frac{p-1}{2p-1}\right)^2, \tag{4.198}$$

which, for $p \geq 2$, remains always smaller than $-8/27 \simeq -0.3$. This is strongly disfavored by current CMB measurements. Therefore, only the models such that p is close enough to 1 are to be considered (i.e. non integer values of p.)

If inflation proceeds in the RpI1 regime, then inflation stops naturally when $\epsilon_1 = 1$, i.e. at the field value

$$y_{\rm end} = \ln\left[(2p-1)\frac{1+2p(\sqrt{3}+1)}{8p^2-4p-1}\right]. \tag{4.199}$$

However, the second Hubble flow function can only take relatively large value. From Eq. (4.195), since $y < y_{\rm max}$, one gets

$$\epsilon_2 > \epsilon_2(y_{\rm max}) = \frac{8}{3}\frac{p-1}{p}. \tag{4.200}$$

For $p \geq 2$, we are in a situation where $\epsilon_2 > 4/3$ and again, the models are ruled out by a simple slow roll analysis. Therefore, as already noticed before, p must take (non integer) close enough to 1 values for the models to be viable.

Finally, in the RpI3 regime, inflation stops naturally when $\epsilon_1 = 1$, with $y_{\rm end}$ still given by Eq. (4.199). This expression is defined only if $p > (1+\sqrt{3})/2 \simeq 0.68$ but the first slow roll parameter continuously decreases with y, and its asymptotic value is again given by Eq. (4.197). Therefore, this regime is viable only when p is close enough to unity.

Let us now turn to the slow-roll trajectory. It is given by

$$N - N_{\rm end} = \frac{3}{4}\left\{\frac{p}{p-1}\ln\left[\frac{(p-1)e^y+1-2p}{(p-1)e^{y_{\rm end}}+1-2p}\right] + y - y_{\rm end}\right\}. \tag{4.201}$$

This expression is not properly defined for $p = 1$ but this case has already been considered in the section on the Higgs inflation model. When $p > 1$, if $y = y_{\rm max}$, the argument of the logarithm vanishes and the total number of e-folds diverges. As a result, provided inflation starts close enough to the top of the potential, it is always possible to find a long enough inflationary period. For $p < 1$, the number of e-folds diverges when $y \to \infty$. The slow-roll trajectory cannot be analytically inverted, but using the same reheating model as in section 3.1, one can solve for the field value y_* at which the pivot mode crossed out the Hubble radius. The corresponding number of e-fold $\Delta N_* = N_{\rm end} - N_*$ being given by Eq. (4.201).

Concerning the case $\epsilon = -1$, i.e. the domain $y < 0$, all of the previous formula still apply but the potential is now a monotonic decreasing function of the field *vev* which is too steep to support inflation. In particular, over the whole negative domain, Eq. (4.195) implies that $\epsilon_1(y<0) > \epsilon_1(y \to -\infty) = 4/3$, independently on whether $p > 1$ or $p < 1$.

Finally, the constant M can be determined from the amplitude of the CMB anisotropies. It follows that

$$\frac{M^4}{M_{\rm Pl}^4} = 1920\pi^2 \frac{\left[1+(p-1)\,e^{y_*}-2p\right]^2 e^{2y_*}}{(2p-1)^2\,(e^{y_*}-1)^{\frac{6p-2}{2p-1}}}\frac{Q_{\rm rms-PS}^2}{T^2}. \tag{4.202}$$

The reheating consistent slow-roll predictions of the RpI models are displayed in Fig. 98 for the RpI1 regime, in Fig. 99 for the RpI2 regime, and in Fig. 100 for the RpI3 regime. In the RpI1 regime, the Higgs inflation model predictions (see Fig. 81) are recovered when $p \to 1$, and one can see that $p < 1.02$ is a necessary condition for the spectral index not to be too red. For RpI2 the limit $p \to 1$ is such that one does not reproduce the Higgs inflation results and for $y_{\rm end} \to \infty$ the predictions lie on the line $\epsilon_{2*} = 0$. Moreover, one can see that when $p > 1.1$, the models predict too much gravity waves to be compatible with the CMB data. Finally for the RpI3 regimes, the Higgs inflation model predictions (see Fig. 81) are recovered when $p \to 1$, and they remain compatible with the data within the two-sigma contours provided $p > 0.99$.

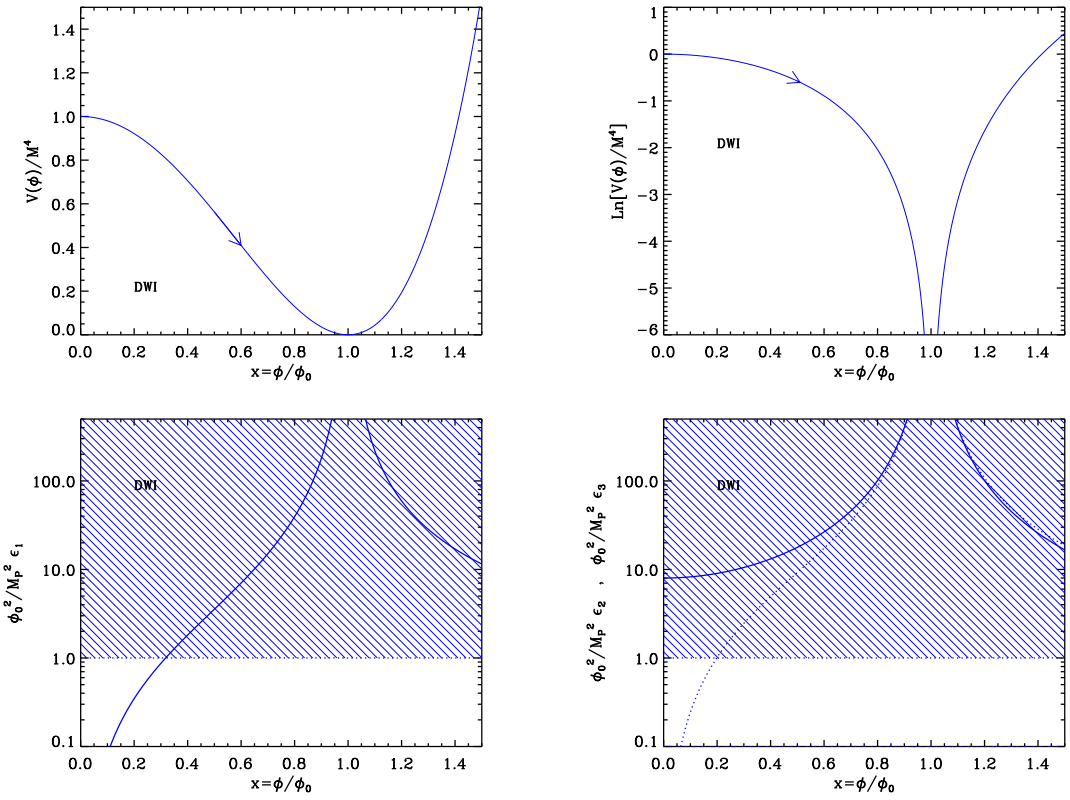

Figure 26. Top left panel: Double Well Inflation (DWI) potential as a function of ϕ/ϕ_0. Only the $\phi > 0$ region is displayed since the potential is symmetric under $\phi \to -\phi$. Top right panel: logarithm of the potential. The arrow indicates in which direction inflation can proceed. Bottom left panel: slow-roll parameter ϵ_1, rescaled by the quantity $M_{\rm Pl}^2/\phi_0^2$, such that the corresponding expression becomes universal, i.e. independent of ϕ_0. Bottom right panel: slow-roll parameters ϵ_2 (solid line) and ϵ_3 (dotted line), rescaled by $M_{\rm Pl}^2/\phi_0^2$ for the same reason as mentioned before.

4.14 Double-Well Inflation (DWI)

In this section, we study the famous "Mexican hat" potential given by

$$V(\phi) = M^4 \left[\left(\frac{\phi}{\phi_0} \right)^2 - 1 \right]^2 . \tag{4.203}$$

Except for the mass M determined by the CMB normalization, it depends on one parameter, the *vev* ϕ_0. Historically, this potential was first introduced by Goldstone in Ref. [370] as a toy model for dynamical symmetry breaking. In cosmology, it is of course utilized to investigate the formation and the microscopic structure of topological defects [371–377]. In the context of inflation, it was first used to construct scenarios of topological inflation [378, 379]. In this case, it is made use of the fact that the discrete $\mathbb{Z}_2$ symmetry, $\phi \to -\phi$, makes the state $\phi = 0$ unstable. Therefore, the Universe will split into two different regions separated by a domain wall. One can then show that inflation takes place within this topological defect. More precisely, the potential is usually written as $V = \lambda/4 \left(\phi^2 - \eta^2\right)^2$ where η represents the position of the minima of the potential. Then, Refs. [378, 379] show that topological inflation

occurs if $\eta > M_{\rm Pl}$. On the other hand, if one writes Eq. (4.203) as $V = M^4/\phi_0^4\left(\phi^2-\phi_0^2\right)^2$, one sees that one can identify η with ϕ_0. And we will precisely show that agreement with the CMB observations requires $\phi_0 > M_{\rm Pl}$. The potential (4.203) was also used in Refs. [380, 381] in the context of open inflation. In a rather different theoretical framework, Eq. (4.203) was studied in Refs. [382, 383] where it was derived in $N = 1$ supergravity coupled to matter. It is also interesting to notice that it was obtained using various stringy constructions as early as the 80's, see Refs. [384, 385]. More recently, this potential was found to be relevant in a large number of different physical situations [329, 386–396]. Let us also mention that this model is sometimes viewed as a realistic version of Small Field Inflation (SFI) with $p = 2$ (see section 5.1), the extra quartic term preventing the potential from becoming negative. However, as will be shown in the following, these two classes of models should actually be described separately since their predictions differ in the relevant range of parameters.

The parameter ϕ_0 sets the typical *vev* at which inflation proceeds and depends on the symmetry breaking scale one considers. In principle, it could vary over a wide range of values, from $\phi_0 \sim 10^{15}$ GeV for GUT symmetry breaking schemes to super-Planckian *vev* in a stringy or supergravity context. As will be shown in the following, it is in fact constrained to be large (super-Planckian) in order for the predictions of the model to be compatible with the CMB data. The DWI potential is displayed in Fig. 26 together with its logarithm. One has represented the region $\phi > 0$ only because the potential is symmetric under $\phi \to -\phi$. We see that it decreases for $\phi < \phi_0$, vanishes at ϕ_0 and then increases for $\phi > \phi_0$. As was already mentioned before, this potential is used to describe dynamical symmetry breaking and, as a consequence, inflation should proceed from the left to the right at $\phi < \phi_0$, in the direction specified by the arrow in Fig. 26.

Let us now calculate the slow-roll parameters. If one defines $x \equiv \phi/\phi_0$ they are given by

$$\epsilon_1 = \left(\frac{M_{\rm Pl}}{\phi_0}\right)^2 \frac{8x^2}{\left(x^2-1\right)^2}, \qquad \epsilon_2 = \left(\frac{M_{\rm Pl}}{\phi_0}\right)^2 \frac{8(1+x^2)}{\left(x^2-1\right)^2}, \qquad \epsilon_3 = \left(\frac{M_{\rm Pl}}{\phi_0}\right)^2 \frac{8(x^4+3x^2)}{\left(x^2-1\right)^2\left(x^2+1\right)}. \tag{4.204}$$

The behavior of these parameters is represented in Fig. 26. The first slow-roll parameter ϵ_1 is an increasing function of ϕ in the range $x \in [0,1]$. It vanishes at $x = 0$ and blows up at $x = 1$. Then, for $x > 1$, it becomes a decreasing function going to zero when x goes to infinity. We see in Fig. 26 that inflation stops by violation of the slow-roll conditions. The slow roll parameters ϵ_2 and ϵ_3 have similar behaviors, except that ϵ_2 does not vanish when $x = 0$ but is equal to $\epsilon_2(x=0) = 8\left(M_{\rm Pl}/\phi_0\right)^2$. Therefore, in order for slow-roll to be valid, this last value should be less than one, which amounts to

$$\frac{\phi_0}{M_{\rm Pl}} > 2\sqrt{2}. \tag{4.205}$$

This constraint on the parameter ϕ_0 shows that the symmetry breaking scale needs to be super-Planckian. If this last condition is verified, then ϵ_2 becomes greater than one during inflation at $\phi_{\epsilon_2=1}$ defined by

$$x_{\epsilon_2=1} = \sqrt{1+4\left(\frac{M_{\rm Pl}}{\phi_0}\right)^2\left[1-\sqrt{1+\left(\frac{\phi_0}{M_{\rm Pl}}\right)^2}\right]}. \tag{4.206}$$

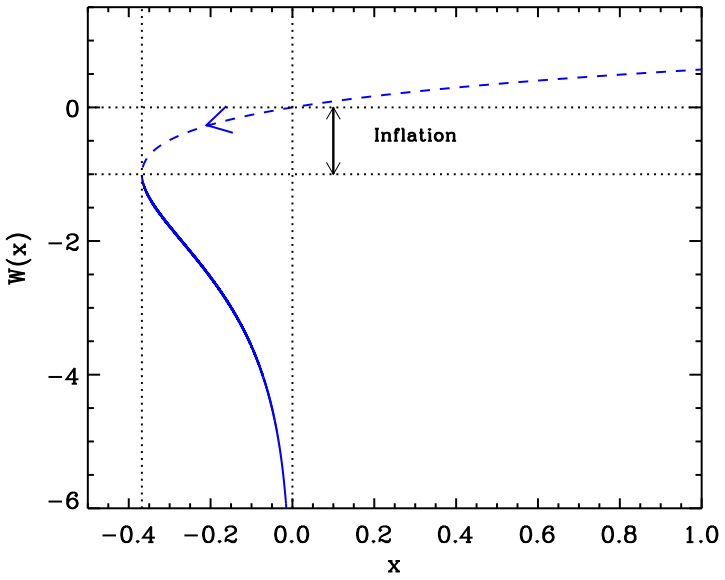

Figure 27. Lambert functions $\mathrm{W}_0(x)$ (dashed line) and $\mathrm{W}_{-1}(x)$ (solid line). In DWI, inflation proceeds along the negative part of the "0" branch in the direction specified by the arrow.

This happens before the end of inflation ($\epsilon_1 = 1$) which occurs at the following value of the field

$$x_{\rm end} = \sqrt{2 + \left(\frac{\phi_0}{M_{\rm Pl}}\right)^2} - \sqrt{2}\,. \tag{4.207}$$

Let us now turn to the slow-roll trajectory. It can be integrated exactly and yields the following formula

$$N_{\rm end} - N = \frac{1}{4}\left(\frac{\phi_0}{M_{\rm Pl}}\right)^2 \left[\ln\left(\frac{x_{\rm end}}{x}\right) - \frac{1}{2}\left(x_{\rm end}^2 - x^2\right)\right], \tag{4.208}$$

where $N_{\rm end}$ is the number of e-folds at the end of inflation. Using the 0-branch of the Lambert function W_0, this trajectory can be inverted. One obtains

$$x = \sqrt{-\mathrm{W}_0\left[-x_{\rm end}^2 e^{-x_{\rm end}^2} e^{8\left(\frac{M_{\rm Pl}}{\phi_0}\right)^2 (N - N_{\rm end})}\right]}\,. \tag{4.209}$$

The fact that the 0-branch of the Lambert function should be chosen comes from the requirement that $x < 1$. The corresponding "trajectory" along the Lambert curve is displayed in Fig. 27, the arrow indicating in which direction inflation proceeds. This trajectory is remarkably similar to the one of SFI with $p = 2$, see section 5.1 and Eq. (5.6), the only difference being that the factor 8 in front of $N - N_{\rm end}$ is just 4 in the case of SFI. Therefore not only these two potentials coincide at small fields, but they also give rise to the same kind of slow-roll trajectory. This is why these two models are sometimes identified, DWI being considered as a realistic realization of SFI. However, as shown below, the observations favors super-Planckian values of ϕ_0 and, in this limit, the two models are not equivalent (of course,

this also has something to do with the debate about whether having super-Planckian *vev* is meaningful or not). In fact, in the regime $\phi_0/M_{\rm Pl} \gg 1$, one can write

$$x_* \simeq 1 - \sqrt{2}\frac{M_{\rm Pl}}{\phi_0}\sqrt{1+2\Delta N_*} + \frac{1}{3}\left(\frac{M_{\rm Pl}}{\phi_0}\right)^2\left(1+2\Delta N_* + \frac{2}{\sqrt{1+2\Delta N_*}}\right) + \ldots . \tag{4.210}$$

From this expression it is clear that, for super-Planckian values of ϕ_0, ϕ_* is close to the minimum of the potential where the quartic term plays an important role and, consequently, where the SFI potential is not a good approximation. A calculation of the Hubble flow parameters at Hubble crossing confirms this conclusion. They are given by

$$\epsilon_{1*} \simeq \frac{1}{1+2\Delta N_*}, \qquad \epsilon_{2*} \simeq \frac{2}{1+2\Delta N_*}, \qquad \epsilon_{3*} \simeq \frac{2}{1+2\Delta N_*}. \tag{4.211}$$

This allows us to establish the corresponding expressions of the tensor to scalar ratio, spectral index and running. One obtains

$$r \simeq \frac{16}{1+2\Delta N_*}, \qquad n_{\rm S} - 1 \simeq -\frac{4}{1+2\Delta N_*}, \qquad \alpha_{\rm S} \simeq -\frac{8}{1+2\Delta N_*}. \tag{4.212}$$

These expressions should be compared with Eqs. (5.17). We see that the first Hubble flow parameter for SFI and DWI differ by a factor close to 4 and that the ϵ_2 roughly differ by a factor of 2. As a consequence, as can be checked in Fig. 101, the DWI predictions are such that $\epsilon_{2*} = 2\epsilon_{1*}$ [or equivalently, $r = 4(1-n_{\rm S})$], whereas, as can be checked in Fig. 112, we have $\epsilon_{2*} = 4\epsilon_{1*}$ for SFI [or equivalently, $r = 8/3(1-n_{\rm S})$]. This explains why the two models can in fact lead to quite different predictions and why DWI cannot be simply viewed as a mere realistic continuation of SFI.

Finally, it is also interesting to constrain the energy scale M. For this purpose, we use the CMB normalization which gives

$$\frac{M^4}{M_{\rm Pl}^4} = 11520\pi^2\left(\frac{M_{\rm Pl}}{\phi_0}\right)^2\frac{x_*^2}{\left(x_*^2-1\right)^4}\frac{Q_{\rm rms-PS}^2}{T^2}. \tag{4.213}$$

Then, using the approximated trajectory $x_* \simeq 1 - \sqrt{2+4\Delta N_*}M_{\rm Pl}/\phi_0$ in the above formula, one obtains the following expression

$$\frac{M^4}{M_{\rm Pl}^4} \simeq 1440\pi^2\left(\frac{\phi_0}{M_{\rm Pl}}\right)^2\frac{1}{\left(1+2\Delta N_*\right)^2}\frac{Q_{\rm rms-PS}^2}{T^2}. \tag{4.214}$$

Then, requiring that $M < M_{\rm Pl}$ leads to the following upper bound on the value of ϕ_0, $\phi_0/M_{\rm Pl} \lesssim 1.5\times 10^5$. Combined with the lower limit (4.205), we see that the possible range of variation of ϕ_0 is quite large.

The reheating consistent slow-roll predictions for the DWI models are displayed in Fig. 101. The reheating equation of state parameter $\overline{w}_{\rm reh}$ has been chosen to be 0 since the potential is quadratic close to its minimum $V(\phi) \simeq 4M^4/\phi_0^2\,(\phi-\phi_0)^2$. As claimed before, one can check that only super-Planckian values of the symmetry breaking scale ϕ_0 are compatible with the data. Actually, this is also true for the SFI models, see section 5.1 and Fig. 112. As already mentioned before, in this regime, the two models differ while, as expected, they are very similar for sub-Planckian values of the field *vev*.

4.15 Mutated Hilltop Inflation (MHI)

This model belongs to the class of hilltop models [397, 398]. In this type of scenarios, inflation is supposed to occur at the top of the potential. In particular, it was shown in Refs. [397, 398] that, by adding the contributions coming from higher order operators, F or D term inflation can be turned into hilltop models. Here, we consider mutated hilltop inflation which was first introduced and discussed in Refs. [399, 400]. The potential is phenomenological only and given by

$$V = M^4 \left[1 - \operatorname{sech}\left(\frac{\phi}{\mu}\right)\right], \tag{4.215}$$

with $\operatorname{sech} x = 1/\cosh x$. As argued in Refs. [399, 400], it can be viewed as small field inflation (hilltop inflation) completed by an infinite number of higher order operators, these operators giving rise to a power series responsible for the appearance of the sech function. From an effective field theory point of view, reasonable values of the parameter μ seem to be such that $\mu < M_{\rm Pl}$ but in other contexts such a restriction may not be necessary. This is why although the model is studied for any value of μ, approximated formula will also be derived in the $\mu \ll M_{\rm Pl}$ approximation.

Defining $x \equiv \phi/\mu$, the three first Hubble flow functions in the slow-roll approximation are given by

$$\epsilon_1 = \frac{M_{\rm Pl}^2}{2\mu^2} \coth^2\left(\frac{x}{2}\right) \operatorname{sech}^2 x, \qquad \epsilon_2 = \frac{M_{\rm Pl}^2}{\mu^2}\left[\operatorname{csch}^2\left(\frac{x}{2}\right) + 2\,\operatorname{sech}^2 x\right], \tag{4.216}$$

$$\epsilon_3 = \frac{M_{\rm Pl}^2}{\mu^2} \frac{\cosh x \coth^2\left(\frac{x}{2}\right) + 2\tanh^2 x}{\cosh x + \sinh^2 x}. \tag{4.217}$$

where $\operatorname{csch} x = 1/\sinh x$. These three quantities are monotonically decreasing functions of the field values and inflation proceeds from large field values towards small field values. Together with the potential, they are represented as a function of x in Fig. 28.

The slow-roll trajectory can be integrated exactly from Eq. (2.11) and reads

$$N - N_{\rm end} = \frac{\mu^2}{M_{\rm Pl}^2}\left\{2\ln\left[\frac{\cosh(x/2)}{\cosh(x_{\rm end}/2)}\right] - \cosh x + \cosh x_{\rm end}\right\}. \tag{4.218}$$

It can also be inverted analytically to give the field values in terms of the number of e-folds using the Lambert function W_{-1}. One obtains

$$x = \operatorname{arccosh}\left(-1 - \mathrm{W}_{-1}\left\{-(1+\cosh x_{\rm end})\exp\left[\frac{M_{\rm Pl}^2}{\mu^2}(N - N_{\rm end}) - 1 - \cosh x_{\rm end}\right]\right\}\right). \tag{4.219}$$

Since $N - N_{\rm end} < 0$ and the function ye^{-y} has a global maximum equals to $1/e$, inflation proceeds along the -1 branch of the Lambert function as represented in Fig. 29. Note that in the $\mu \ll M_{\rm Pl}$ limit, this trajectory simply becomes $N - N_{\rm end} \simeq \mu^2/(2M_{\rm Pl}^2)\,(e^{x_{\rm end}} - e^x)$.

For MHI, inflation naturally stops when $\epsilon_1 = 1$, which has an unique solution given by

$$x_{\rm end} = \operatorname{arcsech}\left[-\frac{1}{3} + \frac{1}{3}\left(1 - 6\frac{\mu^2}{M_{\rm Pl}^2}\right)\left(-1 + 36\frac{\mu^2}{M_{\rm Pl}^2} + 3\sqrt{6}\frac{\mu}{M_{\rm Pl}}\sqrt{4\frac{\mu^4}{M_{\rm Pl}^4} + 22\frac{\mu^2}{M_{\rm Pl}^2} - 1}\right)^{-1/3}\right.$$
$$\left. + \frac{1}{3}\left(-1 + 36\frac{\mu^2}{M_{\rm Pl}^2} + 3\sqrt{6}\frac{\mu}{M_{\rm Pl}}\sqrt{4\frac{\mu^4}{M_{\rm Pl}^4} + 22\frac{\mu^2}{M_{\rm Pl}^2} - 1}\right)^{1/3}\right], \tag{4.220}$$

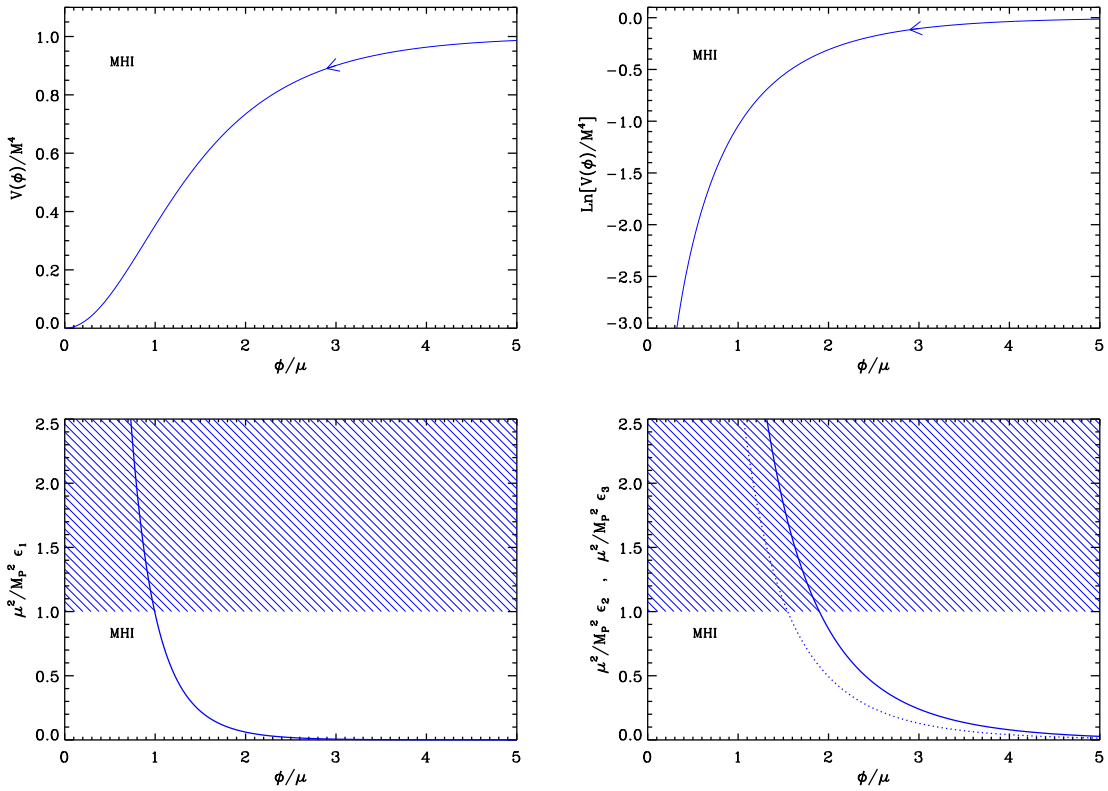

Figure 28. Mutated Hilltop Inflation (MHI). The top panels show the potential and its logarithm as a function of $x = \phi/\mu$. Bottom left panel: Rescaled slow-roll parameter ϵ_1 (divided by $M_{\rm Pl}^2/\mu^2$). The shaded area represents the region in which inflation stops if $\mu = M_{\rm Pl}$. It should be accordingly rescaled for other values of μ. Bottom right panel: slow-roll parameters ϵ_2 (solid line) and ϵ_3 (dotted line), again rescaled by $M_{\rm Pl}^2/\mu^2$ together with the region of slow-roll violation for $\mu = M_{\rm Pl}$.

and with $\operatorname{arcsech} x = \operatorname{arccosh}(1/x)$. One should note that the previous equation is always well defined, regardless of the sign of the square root argument by analytic continuation. Let us notice that from Eq. (4.216) one has

$$\epsilon_2 - \epsilon_1 = \frac{1}{2}\operatorname{csch}^2\left(\frac{x}{2}\right) + \operatorname{sech} x + \frac{5}{2}\operatorname{sech}^2 x > 0. \tag{4.221}$$

Consequently, the slow-roll approximation may become inaccurate before the end of inflation because $\epsilon_2 > 1$ occurs just before $\epsilon_1 = 1$. However, one can check that this happens during a negligible number of e-folds and the observable predictions for MHI remain mostly unaffected. Also, in the limit $\mu \ll M_{\rm Pl}$, Eq. (4.220) gives $x_{\rm end} \simeq \ln\left(\sqrt{2}M_{\rm Pl}/\mu\right)$.

The value $x_* = \phi_*/\mu$ at which the pivot mode crossed the Hubble radius during inflation is obtained by solving Eq. (2.47) for a given reheating energy. In terms of ΔN_*, and in the limit $\mu \ll M_{\rm Pl}$, one has $x_* \simeq \ln\left(2\Delta N_* M_{\rm Pl}^2/\mu^2\right)$. This enables to give estimates for the slow-roll parameters at Hubble crossing, namely

$$\epsilon_{1*} \simeq \frac{1}{2\Delta N_*^2}\left(\frac{\mu}{M_{\rm Pl}}\right)^2, \qquad \epsilon_{2*} \simeq \frac{2}{\Delta N_*}, \qquad \epsilon_{3*} \simeq \frac{1}{\Delta N_*}, \tag{4.222}$$

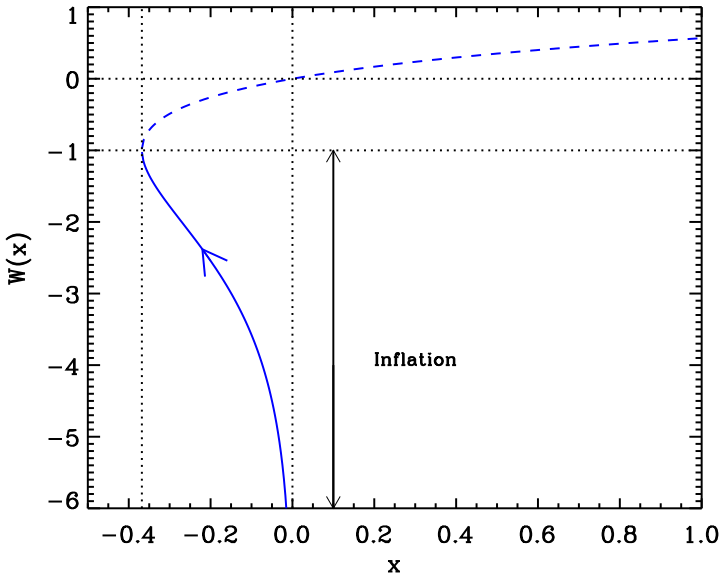

Figure 29. Lambert functions $\mathrm{W}_0(x)$ (dashed line) and $\mathrm{W}_{-1}(x)$ (solid line). During Mutated Hilltop inflation, inflation proceeds along the "−1" branch in the direction specified by the arrow on the figure.

hence, at first order in slow-roll

$$r \simeq \frac{8}{\Delta N_*^2}\left(\frac{\mu}{M_{\rm Pl}}\right)^2, \qquad n_{\rm S} - 1 \simeq -\frac{6}{\Delta N_*}, \qquad \alpha_{\rm S} \simeq -\frac{2}{\Delta N_*^2}. \tag{4.223}$$

One can see that for $\mu/M_{\rm Pl} \ll 1$, the typical predicted amount of gravitational waves is very small, and the deviation from scale invariance almost does not depend on μ.

Finally, the constant M can be determined from the amplitude of the CMB anisotropies

$$\frac{M^4}{M_{\rm Pl}^4} = 90\pi^2 \frac{M_{\rm Pl}^2}{\mu^2}\,\mathrm{csch}^6\left(\frac{x_*}{2}\right)\sinh x_*\tanh x_*\frac{Q_{\rm rms-PS}^2}{T^2}. \tag{4.224}$$

In the $\mu/M_{\rm Pl} \ll 1$ limit, one obtains

$$\frac{M^4}{M_{\rm Pl}^4} \simeq \frac{720\pi^2}{\Delta N_*^2}\frac{\mu^2}{M_{\rm Pl}^2}\frac{Q_{\rm rms-PS}^2}{T^2}. \tag{4.225}$$

Typically, for $\mu/M_{\rm Pl} \simeq 10^{-2}$, one has $M/M_{\rm Pl} \simeq 10^{-4}$.

The reheating consistent slow-roll predictions for MHI have been represented in Fig. 102. As expected, for small values of $\mu/M_{\rm Pl}$, the predicted amount of gravitational waves is extremely small and the deviation from scale invariance almost does not depend on μ.

4.16 Radion Gauge Inflation (RGI)

This model was studied in Ref. [401]. It is an extension of the gauge inflation scenario in which the radius modulus field around which the Wilson loop is wrapped assists inflation as

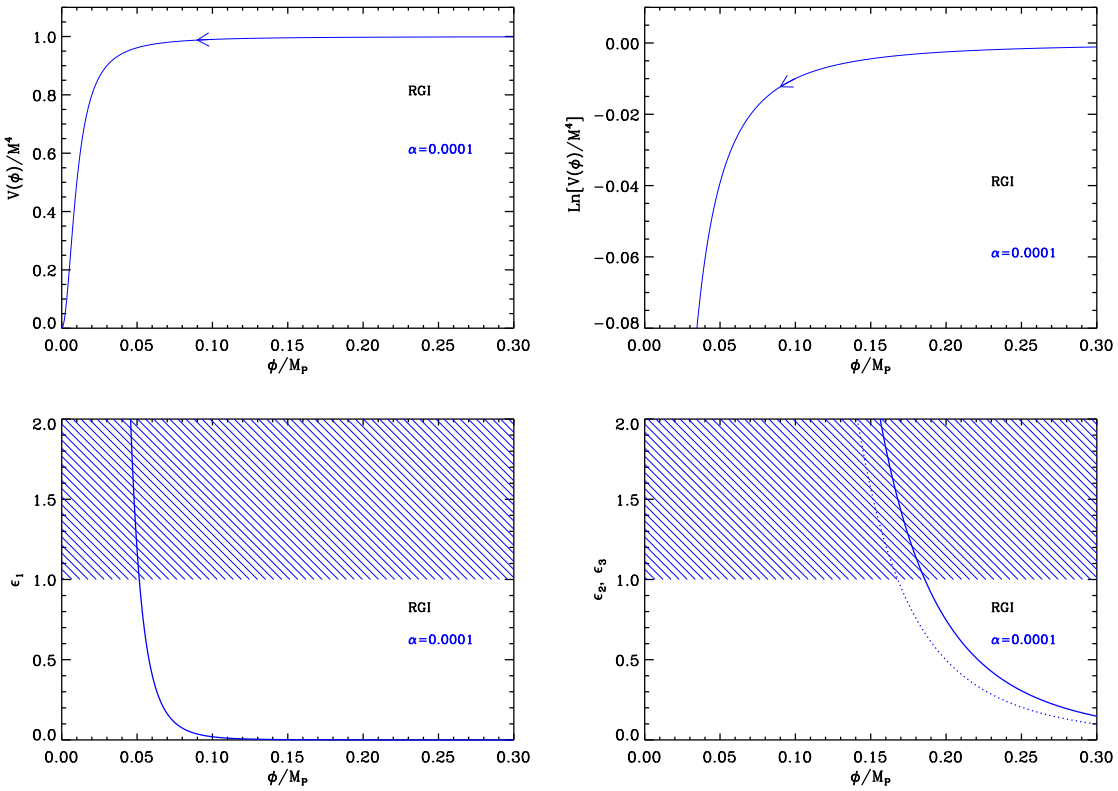

Figure 30. Radion Inflation (RGI) for $\alpha = 10^{-4}$. Top frames: the potential and its logarithm. Bottom left panel: slow-roll parameter ϵ_1 and the shaded area in which inflation stops ($\epsilon_1 > 1$). Bottom right panel: slow-roll parameters ϵ_2 (solid line) and ϵ_3 (dotted line).

it shrinks [233]. Assuming that the radion field value is such that the potential energy is minimal, for each value of the inflaton field ϕ, one can derive an effective potential

$$V(\phi) = M^4 \frac{(\phi/M_{\rm Pl})^2}{\alpha + (\phi/M_{\rm Pl})^2}\,, \tag{4.226}$$

where α is a dimensionless positive parameter. In the context of Ref. [401], the model is natural for $\alpha < 1$ but larger than unity values are not forbidden. The same potential has been obtained in Ref. [402] in the context of S-dual superstring models. In that case, α represents a typical *vev* for the inflaton, in Planck units. Defining $x = \phi/M_{\rm Pl}$, the first three slow-roll parameters read

$$\epsilon_1 = \frac{2\alpha^2}{x^2\left(\alpha + x^2\right)^2}\,, \qquad \epsilon_2 = 4\alpha\frac{\alpha + 3x^2}{x^2\left(\alpha + x^2\right)^2}\,, \qquad \epsilon_3 = 4\alpha\frac{\alpha^2 + 3\alpha x^2 + 6x^4}{x^2\left(\alpha + x^2\right)^2\left(\alpha + 3x^2\right)}\,. \tag{4.227}$$

The potential, its logarithm, and the Hubble flow functions are represented in Fig. 30.

The slow-roll trajectory can be integrated analytically from Eq. (2.11) to obtain

$$N - N_{\rm end} = \frac{x_{\rm end}^2}{4} + \frac{x_{\rm end}^4}{8\alpha} - \frac{x^2}{4} - \frac{x^4}{8\alpha}\,. \tag{4.228}$$

Moreover, it can be inverted explicitly to give the field values in terms of the number of e-folds as

$$x = \sqrt{-\alpha + \sqrt{-8\alpha(N - N_{\rm end}) + (\alpha + x_{\rm end}^2)^2}}\,. \tag{4.229}$$

The end of inflation naturally occurs for $\epsilon_1 = 1$, i.e., from Eq. (4.227), at the field value $x_{\rm end}$ given by

$$x_{\rm end} = \frac{-\sqrt[3]{6}\,\alpha + \left[9\alpha + \sqrt{3\alpha^2(2\alpha+27)}\right]^{2/3}}{162^{1/6}\left[9\alpha + \sqrt{3\alpha^2(2\alpha+27)}\right]^{1/3}}\,. \tag{4.230}$$

As for the MHI models, one should pay attention that

$$\epsilon_2 - \epsilon_1 = 2\alpha\frac{\alpha + 6x^2}{x^2(\alpha + x^2)^2} > 0, \tag{4.231}$$

for any positive values of α. As a result, slow-roll violation, i.e. $\epsilon_2 > 1$, occurs in RGI before inflation ends. However, since the first Hubble flow function is monotonic, this is not very problematic as it happens only during a negligible number of e-folds and only around $N_{\rm end}$. The slow-roll observable predictions therefore remain accurate.

As before, the observable field value x_* is obtained by solving Eq. (2.47) for a given reheating model and allows the determination of the parameter M from the amplitude of the CMB anisotropies. One gets

$$\frac{M^4}{M_{\rm Pl}^4} = \frac{2880\pi^2\alpha^2}{x_*^4\,(\alpha + x_*^2)}\frac{Q_{\rm rms-PS}^2}{T^2}\,. \tag{4.232}$$

The reheating consistent slow-roll predictions for these models are displayed in Fig. 103. Large values of α give back the same predictions as the large field models with $p = 2$ (see section 4.2) having $\epsilon_{2*} = 2\epsilon_{1*}$.

4.17 MSSM Inflation (MSSMI)

4.17.1 Theoretical Justifications

The Minimal Supersymmetric Standard Model (MSSM) is an extension of the Standard Model of particle physics. Its Lagrangian is characterized by the following super potential

$$W_{\rm MSSM} = \lambda_u^{ij} Q_i \cdot H_u U_j^c + \lambda_d^{ij} Q_i \cdot H_d D_j^c + \lambda_e^{ij} L_i \cdot H_d E_j^c + \mu H_u \cdot H_d. \tag{4.233}$$

The quantity Q_i denotes a doublet of left handed quarks super fields where i is a family index. In practice this means that

$$Q_1 = \begin{pmatrix} U \\ D \end{pmatrix}, \quad Q_2 = \begin{pmatrix} C \\ S \end{pmatrix}, \quad Q_3 = \begin{pmatrix} T \\ B \end{pmatrix}, \tag{4.234}$$

where the components of the doublets are super fields. For instance, the scalar part of U is the $\tilde{u}$ squark and its fermionic part is the ordinary u quark. Of course, there is also a color index $a = 1, 2, 3$ and, in fact, one should write the corresponding doublet as Q_{ia}. Moreover, one can also introduce a third $\mathrm{SU(2)_L}$ index $\alpha = 1, 2$ and write $Q_{ia\alpha}$ with, for instance, $Q_{1a1} = U$ and $Q_{1a2} = D$. On the other hand, the quantities U_j^c and D_j^c denotes the right handed super fields where j is the family index (and the color index has been ignored in

order to simplify the notation): for instance, U_2^c means the right handed charm quark super field which is a singlet under $\mathrm{SU(2)_L}$.

In the same fashion, L_i denotes a doublet of left handed lepton superfields

$$L_1 = \begin{pmatrix} N_e \\ E_e \end{pmatrix}, \quad Q_2 = \begin{pmatrix} N_\mu \\ E_\mu \end{pmatrix}, \quad Q_3 = \begin{pmatrix} N_\tau \\ E_\tau \end{pmatrix}, \tag{4.235}$$

where, for instance, N_e denotes the electronic neutrino superfield (the scalar part being the neutralino and the fermionic part the electronic neutrino itself) while E_e denotes the electron superfield. On the other hand, the quantities E_j^c denote the right handed superfields that are singlet under $\mathrm{SU(2)_L}$ (for instance, E_2^c is the right handed muonic superfield). In the superpotential (4.233), there are two terms involving the quarks and only one involving the leptons because, as well-known, there is no right handed neutrinos in the standard model.

The last term in Eq. (4.233) describes the Higgs sector with two Higgs doublet H_u and H_d. The quantity μ is a new dimensionful (of dimension one) parameter of the model. The dot indicates an SU(2) invariant product. Finally, λ_u, λ_d, λ_e are the 3×3 Yukawa matrices.

From the superpotential (4.233), one can determine the scalar potential of the theory by means of the usual supersymmetric machinery. As is well-known, the scalar potential is made of two pieces, the F-term part and the D-term part. Clearly, given the number of fields in the theory, the scalar potential is a complicated object. For inflation, we are especially interested in the flat directions of this potential. A flat direction is a direction such that the F and D-terms vanish, that is to say such that $V_F = 0$, $V_D = 0$ and, therefore, $V \equiv V_F + V_D = 0$. It was shown that the MSSM scalar potential contains nearly 300 gauge invariant flat directions [57, 403, 404]. Finding these directions is a non-trivial task and we now very briefly explain how this can be done. Usually, it consists in putting all the fields to zero except a few ones, these few ones being carefully chosen such that cancellations occur in such a way that the potential exactly vanishes. We now illustrate this method on a particular case. Let us first recall that the general formula giving the D-term potential is

$$V_D = \frac{1}{2} \sum_a g_a^2 D^a D^a, \tag{4.236}$$

where $D^a = \phi^\dagger T^a \phi$, T^a being the generator of the group and ϕ denoting a generic field (of course, the index a should not be confused with the color index discussed above). For the standard model, we have the group $\mathrm{SU(2)_L \times U(1)_Y}$ and, therefore, the explicit expression of the D-term reads

$$V_D = \frac{g^2}{2}\left(D_1^2 + D_2^2 + D_3^2\right) + \frac{g_Y}{2} D_Y^2, \tag{4.237}$$

g and g_Y being the coupling constants of the two groups. For the SU(2) group, the generators T^a are nothing but the Pauli matrices and, therefore, $T^a = \sigma^a/2$. Following Refs. [403, 405], let us consider a situation where all the fields in the MSSM are assumed to have a vanishing *vev* except L_i and E_j^c where we remind that i and j are family indices. If we write $L_i^\uparrow$ and $L_i^\downarrow$ as respectively the upper and lower component of the doublet L_i, then one has (i.e. we put $\phi = L_i$ in the general formula expressing D^a)

$$D_1 = \frac{1}{2}\sum_{i=1}^{3}\left(L_i^{\uparrow *} L_i^\downarrow + L_i^{\downarrow *} L_i^\uparrow\right), \quad D_2 = \frac{i}{2}\sum_{i=1}^{3}\left(L_i^{\uparrow *} L_i^\downarrow - L_i^{\downarrow *} L_i^\uparrow\right), \tag{4.238}$$

$$D_3 = \frac{1}{2}\sum_{i=1}^{3}\left(\left|L_i^\uparrow\right|^2 - \left|L_i^\downarrow\right|^2\right). \tag{4.239}$$

The quantity $E^{\rm c}$ being a SU(2) singlet does not participate to the above expression. On the other hand, the contribution from the U(1) group reads

$$D_Y = \frac{1}{2}\sum_{i=1}^{3}\left(2|e_i|^2 - \left|L_i^{\uparrow}\right|^2 - \left|L_i^{\downarrow}\right|^2\right), \tag{4.240}$$

where e_i denotes the scalar field of the $E_i^{\rm c}$ supersymmetric multiplet. We see that, if we take

$$L_i = \begin{pmatrix}\phi\\0\end{pmatrix}, \quad L_j = \begin{pmatrix}0\\\phi\end{pmatrix}, \quad e_k = \phi, \tag{4.241}$$

then we have $V_D = 0$.

The next step consists in calculating the F-term for the choice (4.241). It is easy to check that $V_F = 0$. Therefore, we have identified a flat direction. It is denoted $L_iL_je_k$ or **LLe** to recall that all family combination are possible. This direction is represented by a "composite operator X_m" formed by the product of the superfields making up the flat direction. In our case $X_3 = L_iL_je_k = \phi^3$ and $m = 3$ since we have three operators participating to the definition of X_3. This direction has been proposed in Ref. [406] as a possible candidate for the inflaton field. Let us also remark that another choice put forward in that reference was **udd**.

We have just seen how to identify flat directions in the MSSM potential. However, this flatness is usually spoiled by the presence of higher order non-renormalizable operators appearing in the MSSM (viewed here as a low energy effective field) and by supersymmetry breaking [57, 403, 404]. Higher order operators are described by the following superpotential

$$W = \frac{\lambda_n}{n}\frac{X_m^k}{M_{\rm Pl}^{mk-3}}, \tag{4.242}$$

where λ_n is a coupling constant, $n \equiv mk$ and $k = 1$ or $k = 2$ depending on whether the flat direction is even or odd under R-parity. Recall that Q, L, $U^{\rm c}$, $D^{\rm c}$ and $E^{\rm c}$ have R-parity -1 and H_u, H_d have R-parity $+1$. It follows that **LLe** (for instance) has odd R-parity and, therefore, that $k = 2$. For the directions **LLe** (this is also true for **uud**), this means that

$$n \equiv mk = 6. \tag{4.243}$$

The above superpotential (4.242) will produce a term $|\partial W/\partial\phi|^2 \propto \phi^{2(km-1)}$ in the scalar potential. Then, we have the contributions originating from supersymmetry breaking. They can be easily calculated if, for instance, we assume that we have an independent hidden sector where supersymmetry is broken and that this breaking is mediated by gravity only. This gives two types of soft terms, one proportional to ϕ^2 and another, the so-called "A-term", proportional to $(\phi\partial W/\partial\phi + {\rm cc})$ that is to say, given Eq. (4.242), proportional to ϕ^{mk}.

More generally, if one starts from a flat direction with a given n, then the superpotential has the form $W = \lambda_n/n\Phi^n M_{\rm Pl}^{3-n}$, where $\Phi = \phi e^{i\theta}$ is the superfield which contains the flat direction. Then, the scalar potential takes the form

$$V(\phi) = \frac{1}{2}m_\phi^2\phi^2 + A\cos(n\theta+\theta_0)\frac{\lambda_n}{n}\frac{\phi^n}{M_{\rm Pl}^{n-3}} + \lambda_n^2\frac{\phi^{2(n-1)}}{M_{\rm Pl}^{2(n-3)}}, \tag{4.244}$$

where the the second term involves the angular part of the superfield via a term $\cos(n\theta+\theta_0)$, which in practice is fixed at -1 to maximize its contribution. As explained below, the fact

that the second term appears with a negative coefficient plays a crucial role in making this scenario a credible inflationary one.

Together with the global minimum at $\phi = 0$, under the condition $A^2 \geq 8(n-1)m_\phi^2$, the potential has a secondary minimum at $\phi_0 \simeq \left(m_\phi M_{\rm Pl}^{n-3}\right)^{1/(n-2)}$. If $A^2 \gg 8(n-1)m_\phi^2$, this secondary minimum becomes the deepest one and thus the true one. The curvature of the potential at this minimum is of the order m_ϕ^2. If inflation occurs there, one gets $H \simeq m_\phi (m_\phi/M_{\rm Pl})^{1/(n-2)}$, which is much smaller than the potential curvature for $m_\phi \ll M_{\rm Pl}$. This implies that the potential is too steep for quantum effects during inflaton to kick ϕ out of the false minimum. Such a situation is similar to the old inflationary scenario. However, this barrier disappears if one saturates the previous inequality and takes

$$A^2 = 8(n-1)m_\phi^2. \tag{4.245}$$

In that case, the potential has a flat inflection point at ϕ_0 and inflation can proceed between this plateau and $\phi = 0$. This is the case we study in this section. This model (and its generalizations) has also been studied in Refs. [407–417]. Its generalizations will be investigated in more details in section 5.6 and section 5.7. Let also us notice that when $n = 3$, the same potential appears in Refs. [418, 419] as "Generalized Chaotic Inflation", and later in Refs. [420–422] as "Punctuated Inflation". In these references, it is shown that slow-roll inflation is briefly interrupted when the inflaton crosses the flat inflection point and this can produce step-like features in the primordial power spectra. These effects are outside the scope of the following slow-roll analysis as we will be dealing with the last slow-roll inflationary stage within this scenario.

4.17.2 Slow-Roll Analysis

We now turn to the slow-roll analysis of MSSM inflation. As discussed before, we assume that the inflaton is the flat direction **LLe** or **uud**. This implies that $n = 6$ in Eq. (4.244). Then, rewriting the potential (4.244) in a more convenient fashion, one arrives at

$$V(\phi) = M^4 \left[\left(\frac{\phi}{\phi_0}\right)^2 - \frac{2}{3}\left(\frac{\phi}{\phi_0}\right)^6 + \frac{1}{5}\left(\frac{\phi}{\phi_0}\right)^{10}\right], \tag{4.246}$$

where we have defined new parameters according to

$$M^8 = \frac{M_{\rm Pl}^3 m_\phi^5}{4\sqrt{10}\lambda_6}, \qquad \phi_0^8 = \frac{M_{\rm Pl}^6 m_\phi^2}{10\lambda_6^2}. \tag{4.247}$$

These definitions ensure that ϕ_0 is the inflection point. Since $m_\phi^2\phi^2$ is a soft SUSY breaking term, we typically expect that $m_\phi \simeq 1\,{\rm TeV}$ and this is the reason why, in what follows, typical values of the field are taken to be

$$\phi_0 \simeq 10^{14}\,{\rm GeV}, \tag{4.248}$$

in agreement with the second of Eqs. (4.247) (the coupling constant λ_6 is taken to be of order one). An interesting feature of this model is that it provides inflation at sub-Planckian *vev* and at low scale $V \simeq (10^9\,{\rm GeV})^4$. As noticed in Ref. [406], higher values than $n = 6$ would produce too small amplitude for the scalar perturbations. This is why the model is commonly studied with $n = 6$ (with $n = 3$, this is RIPI, see section 4.18).

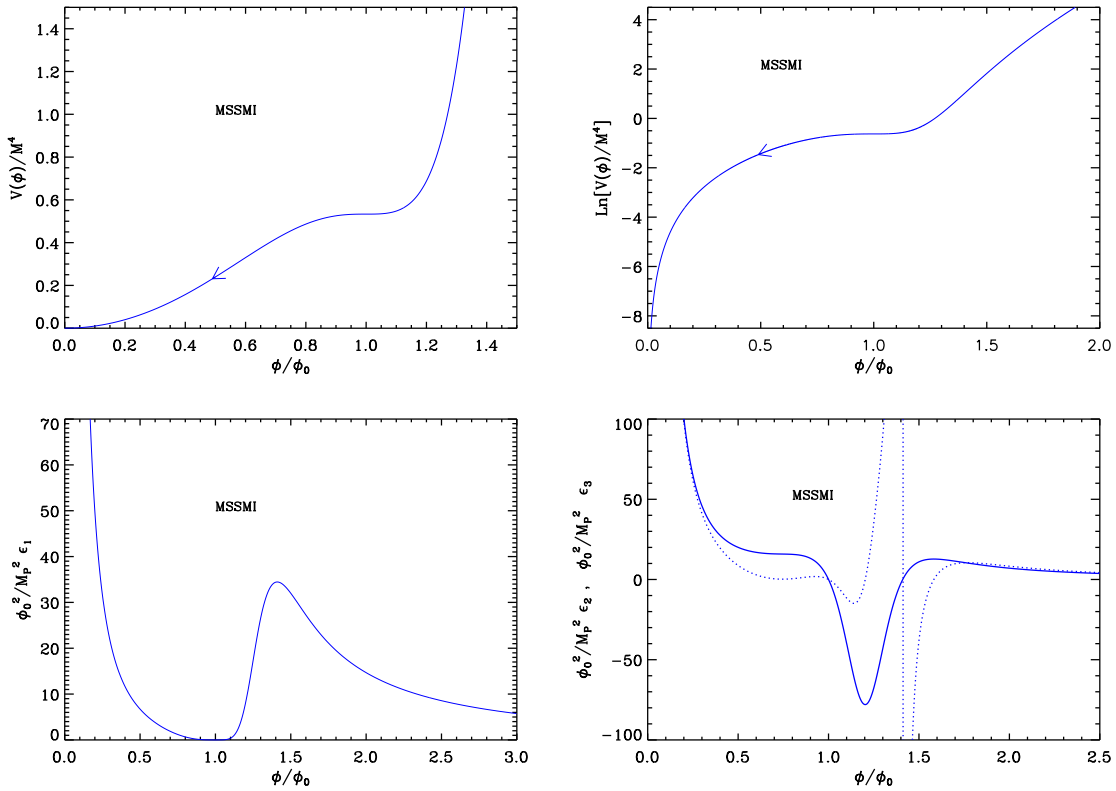

Figure 31. MSSM Inflation (MSSMI). Top left panel: MSSM Inflation potential Eq. (4.246) as a function of ϕ/ϕ_0. Top right panel: logarithm of the potential. Bottom left panel: slow-roll parameter ϵ_1 scaled by $\phi_0^2/M_{\rm Pl}^2$. Bottom right panel: slow-roll parameters ϵ_2 (solid line) and ϵ_3 (dotted line) scaled by $\phi_0^2/M_{\rm Pl}^2$.

The potential in Eq. (4.246) is displayed in Fig. 31, together with its logarithm. It is an increasing function of the field, the derivative of which vanishes at $\phi = 0$ and at its second inflection point $\phi = \phi_0$, the position of the first inflection point being given by $\phi_{V''=0}^- = \phi_0/\sqrt{3}$. Inflation proceeds in the region $\phi \in [0, \phi_0]$, in the direction specified by the arrow in Fig. 31.

Defining the dimensionless quantity x by

$$x \equiv \frac{\phi}{\phi_0}\,, \tag{4.249}$$

the first three Hubble flow functions in the slow-roll approximation are given by

$$\epsilon_1 = 450\frac{M_{\rm Pl}^2}{\phi_0^2}\frac{\left(x^4-1\right)^4}{x^2\left(3x^8-10x^4+15\right)^2}\,, \qquad \epsilon_2 = 60\frac{M_{\rm Pl}^2}{\phi_0^2}\frac{3x^{16}-58x^8+40x^4+15}{x^2\left(3x^8-10x^4+15\right)^2}\,, \tag{4.250}$$

and

$$\epsilon_3 = \frac{M_{\rm Pl}^2}{\phi_0^2}\frac{60}{x^2}\left(-225+1575x^4-3165x^8+395x^{12}+2605x^{16}-1275x^{20}+81x^{24}+9x^{28}\right) \times \left(3x^8-10x^4+15\right)^{-2}\times\left(-15-55x^4+3x^8+3x^{12}\right)^{-1}. \tag{4.251}$$

These two slow-roll parameters diverge when the field *vev* goes to 0, and vanish when the field *vev* goes to infinity. The first slow roll parameter ϵ_1 first decreases, vanishes at the flat inflection point where ϵ_2 vanishes too, then increases to reach a local maximum where ϵ_2 vanishes again, and eventually decreases again, to vanish at infinity where ϵ_2 also goes to zero. Denoting by $x^+_{\epsilon_2=0}$ the position of the second extremum, one has

$$x^+_{\epsilon_2=0} = \left(\frac{1}{3}\right)^{1/4}\left[2^{4/3}\left(i\sqrt{685}-1\right)^{1/3}+14\times 2^{2/3}\left(i\sqrt{685}-1\right)^{-1/3}-1\right]^{1/4} \simeq 1.41022. \tag{4.252}$$

In between the two local extrema of ϵ_1, the second slow-roll parameter ϵ_2 is negative whereas it is positive elsewhere. The value of ϵ_1 at its local maximum is given by

$$\epsilon_1^{\rm max} = \epsilon_1\left(x^+_{\epsilon_2=0}\right) \simeq 34.459\frac{M_{\rm Pl}^2}{\phi_0^2}. \tag{4.253}$$

With the typical above-mentioned value for $\phi_0 \simeq 10^{14}$GeV, one has $M_{\rm Pl}^2/\phi_0^2 \simeq 10^8$ and $\epsilon_1^{\rm max} > 1$. This means that if inflation proceeds for *vev*'s larger than that of the flat inflection point, it can naturally stop by slow-roll violation. However, if this happens, inflation proceeds at $x \gg 1$ and the potential is effectively very close to a large field model one (LFI, see section 4.2) with $p = 10$.

For this reason, we will be focused to the case in which inflation occurs for *vev*'s smaller than that of the flat inflection point. In this case, the value of $x_{\rm end}$ at which inflation stops by slow-roll violation must be determined numerically. In the limit $\phi_0/M_{\rm Pl} \ll 1$ however, one has $x_{\rm end} \simeq 1$ and an approximate analytic formula can be derived

$$x_{\rm end} \simeq 1 - \frac{1}{2^{3/4}\sqrt{15}}\sqrt{\frac{\phi_0}{M_{\rm Pl}}}. \tag{4.254}$$

A comparison between this expression and the numerical solution of $\epsilon_1 = 1$ is displayed in Fig. 32. For physical values $\phi_0 \simeq 10^{-4}M_{\rm Pl}$, the agreement is excellent.

Let us now turn to the slow-roll trajectory. It can be integrated from Eq. (2.11) and leads to

$$N_{\rm end} - N = \left(\frac{\phi_0}{M_{\rm Pl}}\right)^2\left\{\frac{x^2-x_{\rm end}^2}{20}+\frac{1}{15}\left(\frac{x_{\rm end}^2}{x_{\rm end}^4-1}-\frac{x^2}{x^4-1}\right) - \frac{2}{15}\left[\mathrm{arctanh}\left(x_{\rm end}^2\right)-\mathrm{arctanh}\left(x^2\right)\right]\right\},$$

where $N_{\rm end}$ is the number of e-folds at the end of inflation and N is the number of e-folds at some point when the scaled field *vev* is x. A few remarks are in order. Firstly, when $x \simeq 1$, the second term of the previous expression dominates, and one has $N_{\rm end} - N \simeq 1/15\,(\phi_0/M_{\rm Pl})^2[1/(x_{\rm end}^4-1) - 1/(x^4-1)]$, which can be inverted and gives

$$x \simeq 1 - \frac{1}{4}\left[2^{-5/4}\sqrt{15}\sqrt{\frac{M_{\rm Pl}}{\phi_0}}+15\frac{M_{\rm Pl}^2}{\phi_0^2}\left(N_{\rm end}-N\right)\right]^{-1}. \tag{4.255}$$

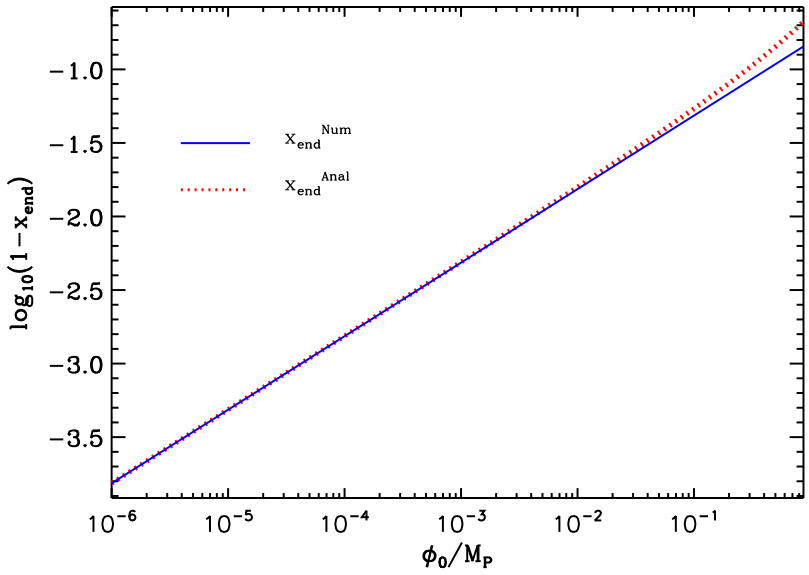

Figure 32. Location of the slow-roll violation induced end of inflation $x_{\rm end} = \phi_{\rm end}/\phi$ for the MSSM inflation models, as a function of $\phi_0/M_{\rm Pl}$. The blue solid curve represents a numerical solution of $\epsilon_1 = 1$, while the red dotted curve corresponds to the approximated analytic solution Eq. (4.254). For physical values $\phi_0 \simeq 10^{-4} M_{\rm Pl}$, the agreement is obviously excellent.

Secondly, one could wonder if a sufficient number of e-folds can be realized in the regime studied here. When $x \to 1$, the corresponding number of e-folds diverges, but in practice, the inflationary dynamics close to the flat inflection point is governed by the quantum diffusion and the classical equation of motion can not be trusted in this domain.

If one introduces the ratio η between the quantum kicks amplitude $H/(2\pi)$ and the classical drift $M_{\rm Pl}^2 V_\phi/V$, when $x \simeq 1$, one has

$$\eta \simeq \frac{1}{90\sqrt{30}\pi} M^2 \phi_0 M_{\rm Pl}^{-3} (x-1)^{-2} \simeq \frac{4\sqrt{10}}{\pi\sqrt{3}} M^2 M_{\rm Pl} \phi_0^{-3} (N_{\rm end} - N)^2 , \tag{4.256}$$

where the last equality comes from the approximate trajectory. In order to estimate the value of η, one needs the value of M which is fixed by the amplitude of the CMB anisotropies. With x_* the observable field value associated with $\Delta N_* = N_{\rm end} - N_*$, one gets

$$\left(\frac{M}{M_{\rm Pl}}\right)^4 = 2880\pi^2 \frac{M_{\rm Pl}^2}{\phi_0^2} \frac{\left(1-x_*^4\right)^4}{x_*^4 \left(1 - \frac{2}{3}x_*^4 + \frac{1}{5}x_*^8\right)^3} \frac{Q_{\rm rms-PS}^2}{T^2} . \tag{4.257}$$

In the $x_* \simeq 1$ approximation, this gives

$$\frac{M^4}{M_{\rm Pl}^4} \simeq \frac{3}{8}\pi^2 \frac{Q_{\rm rms-PS}^2}{T^2} \frac{\phi_0^6}{M_{\rm Pl}^6 (N_{\rm end} - N_*)^4} , \tag{4.258}$$

and thus

$$\eta \simeq \sqrt{20 \frac{Q_{\rm rms-PS}^2}{T^2}} \left(\frac{N_{\rm end} - N}{\Delta N_*}\right)^2 . \tag{4.259}$$

It is quite remarkable that this formula does not depend on ϕ_0 anymore but only on the ratio $(N_{\rm end} - N)/\Delta N_*$. From $Q_{\rm rms-PS}/T \simeq 6 \times 10^{-6}$, one has $N_{\rm end} - N_{\rm min} \simeq 10^4$ in the classical regime [406]. For $\phi_0 \simeq 10^{14}\,{\rm GeV}$, one obtains $M \simeq 10^8 {\rm GeV}$, in agreement with what was announced earlier.

Finally, it can be interesting to write down the approximated slow-roll parameters at Hubble crossing and in the limit $\phi_0/M_{\rm Pl} \ll 1$. One obtains

$$\epsilon_{1*} \simeq \left(\frac{\phi_0}{M_{\rm Pl}}\right)^6 \frac{1}{7200\Delta N_*^4}\,, \qquad \epsilon_{2*} \simeq \frac{4}{\Delta N_*}\,, \qquad \epsilon_{3*} \simeq \frac{1}{\Delta N_*}\,, \tag{4.260}$$

hence

$$r \simeq \left(\frac{\phi_0}{M_{\rm Pl}}\right)^6 \frac{1}{450\Delta N_*^4}\,, \qquad n_{\rm S} \simeq 1 - \frac{4}{\Delta N_*}\,, \qquad \alpha_{\rm S} \simeq -\frac{4}{\Delta N_*^2}\,. \tag{4.261}$$

They are similar with the typical predictions of the RIPI models [see Eq. (4.277)].

The reheating consistent slow-roll predictions of the MSSMI models are displayed in Fig. 104. The reheating equation of state parameter $\overline{w}_{\rm reh}$ has been taken to 0 since the potential is quadratic in the vicinity of its minimum. One can check that, in the limit $\phi_0/M_{\rm Pl} \ll 1$, the first slow-roll parameter is indeed extremely small, while the second slow-roll parameter does not depend much on ϕ_0. Remembering that $\phi_0/M_{\rm Pl} \simeq 10^{-4}$, one can see that these models seem to be disfavored by the data since they predict a too large deviation from scale invariance. In order to better reproduce the constraints on the spectral index, these models should be such that $\phi_0/M_{\rm Pl} \gg 1$, for which they become similar to large field models (LFI, see section 4.2). This can be seen from the previous formulas in the limit $x \gg 1$. Unfortunately, such values for ϕ_0 are not compatible with the MSSM. Finally, comparing Fig. 104 with Fig. 105, one can see that the general features of MSSMI are very similar to the RIPI ones, and that the conclusions drawn here are rather robust against a change in n appearing in Eq. (4.244).

4.18 Renormalizable Inflection Point Inflation (RIPI)

4.18.1 Theoretical Justifications

In section 4.17 inflation is implemented within the Minimal Supersymmetric Standard Model (MSSM) around a flat inflection point. Here, we consider a similar model but with $n = 3$ instead of $n = 6$. Such a scenario can emerge in the following situation, see Refs. [423, 424]. Let us consider the MSSM with three additional superfields N_i representing three right-handed neutrinos. These fields are singlet under the standard model gauge group but this one can be extended to $\mathrm{SU(3)_c} \times \mathrm{SU(2)_L} \times \mathrm{U(1)_Y} \times \mathrm{U(1)_{B-L}}$ and the N_i are assumed to be charged under the extra $\mathrm{U(1)_{B-L}}$. Then, we postulate the following superpotential

$$W = W_{\rm MSSM} + hNH_uL, \tag{4.262}$$

where $h \lesssim 10^{-12}$ in order to explain the neutrino mass, $m_\nu \simeq \mathcal{O}(0.1)$ eV. It follows that NH_uL is a D-flat direction of the potential and we parametrize this direction by ϕ. As a consequence, if one now calculates the corresponding potential, one finds that

$$V = \frac{1}{2}m_\phi^2\phi^2 - \frac{Ah}{6\sqrt{3}}\phi^3 + \frac{h^2}{12}\phi^4, \tag{4.263}$$

where, as usual, we have included the soft supersymmetry breaking terms (since $W \propto \phi^3$, the A-term, proportional to $\phi\partial W/\partial\phi$ is, this time, cubic) and have minimized V along the

angular direction. If A is chosen such that $A = 4m_\phi$, then we have a flat inflection point at $\phi_0 = \sqrt{3}m_\phi/h$. A discussion on the fine-tuning required to get a flat inflection point can be found in section 5.7,

4.18.2 Slow-Roll Analysis

We now turn to the slow-roll analysis of the potential given in Eq. (4.263). For this purpose, it is more convenient to re-write it as

$$V(\phi) = M^4 \left[\left(\frac{\phi}{\phi_0}\right)^2 - \frac{4}{3}\left(\frac{\phi}{\phi_0}\right)^3 + \frac{1}{2}\left(\frac{\phi}{\phi_0}\right)^4 \right], \tag{4.264}$$

where we have defined the quantities M and ϕ_0 by

$$M^4 = \frac{1}{2}m_\phi^2\phi_0^2, \qquad \phi_0 = \sqrt{3}\frac{m_\phi}{h}. \tag{4.265}$$

Relevant values of m_ϕ range from 100 GeV to 10 TeV and $h \simeq 10^{-12}$. This means that [423, 424]

$$\phi_0 \simeq 10^{14}\,\mathrm{GeV}, \tag{4.266}$$

a value that turns out to be similar to the one considered in the MSSMI case (see section 4.17).

Let us now define the quantity x by the following expression

$$x \equiv \frac{\phi}{\phi_0}\,. \tag{4.267}$$

The potential is an increasing function of the field *vev*, hence inflation proceeds from the right to the left. It has two inflection points $x^{\pm}_{V''=0}$, given by

$$x^{-}_{V''=0} = \frac{1}{3} \quad \text{and} \quad x^{+}_{V''=0} = 1, \tag{4.268}$$

the second one being a flat inflection point [i.e. $V'\left(x^{+}_{V''=0}\right) = 0$], close to which inflation takes place. This potential is displayed in Fig. 33, together with its logarithm.

Let us now turn to the slow-roll parameters. The first three Hubble flow functions in the slow-roll approximation are given by

$$\epsilon_1 = 72\frac{M_{\rm Pl}^2}{\phi_0^2}\frac{(x-1)^4}{\left(3x^3-8x^2+6x\right)^2}\,, \qquad \epsilon_2 = 24\frac{M_{\rm Pl}^2}{\phi_0^2}\,(x-1)\,\frac{3x^3-9x^2+10x-6}{\left(3x^3-8x^2+6x\right)^2}\,, \tag{4.269}$$

and

$$\begin{aligned}\epsilon_3 =& 24\frac{M_{\rm Pl}^2}{\phi_0^2}\,(x-1)\left(36-144x+246x^2-236x^3+144x^4-54x^5+9x^6\right)\\ &\times\left(6x-8x^2+3x^3\right)^{-2}\left(10x-9x^2+3x^3-6\right)^{-1}\,.\end{aligned}$$

Both $\epsilon_1(x)$ and $\epsilon_2(x)$ diverge when the field *vev* goes to 0, and vanish when the field *vev* goes to infinity. The first slow-roll parameter ϵ_1 first decreases, vanishes at $x^{+}_{V''=0}$ where ϵ_2 vanishes too, $x^{-}_{\epsilon_2=0} = x^{+}_{V''=0}$, then increases to reach a local maximum at $x^{+}_{\epsilon_2=0}$ where ϵ_2 vanishes again, and eventually decreases again. The value of $x^{+}_{\epsilon_2=0}$ is given by

$$x^{+}_{\epsilon_2=0} = 1 - \frac{1}{3\left(9+\sqrt{82}\right)^{1/3}} + \frac{1}{3}\left(9+\sqrt{82}\right)^{1/3} \simeq 1.75\,. \tag{4.270}$$

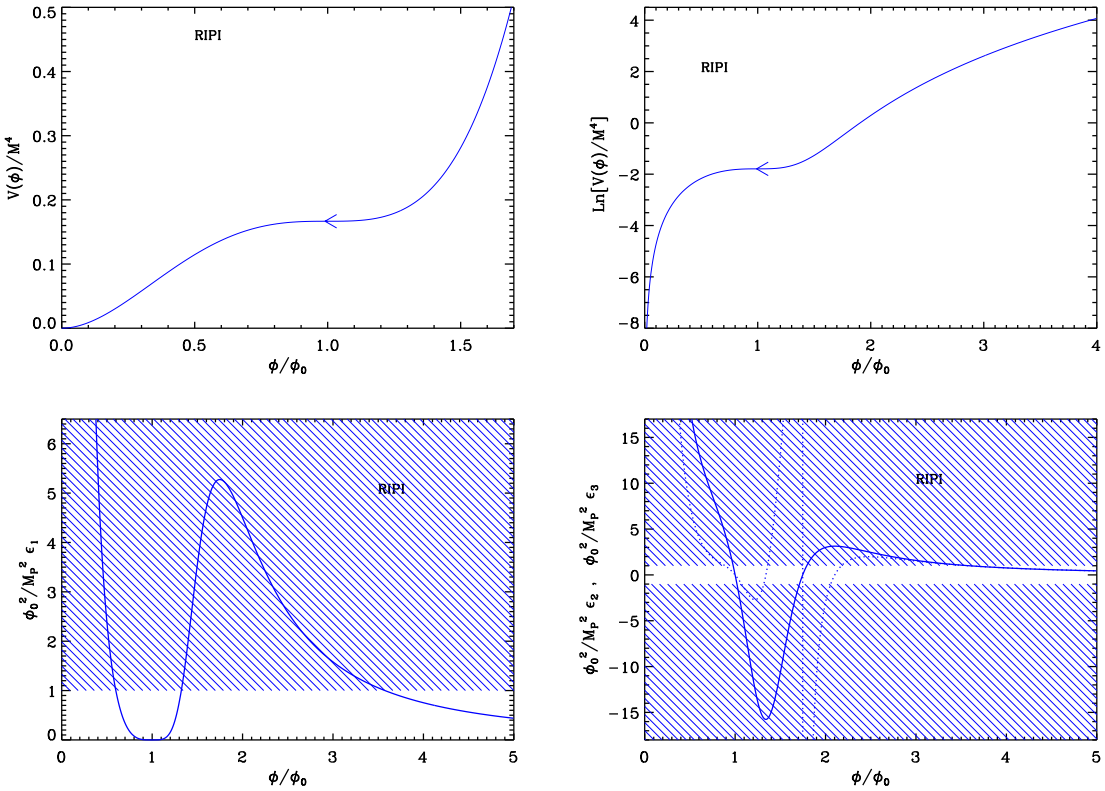

Figure 33. Renormalizable Inflection Point Inflation (RIPI). Top left panel: renormalizable inflection point inflation potential as a function of ϕ/ϕ_0. Top right panel: logarithm of the potential, the required flatness of the potential close to its inflection point becomes obvious on this plot. Bottom left panel: slow-roll parameter ϵ_1 normalized by $M_{\rm Pl}^2/\phi_0^2$. The shaded area indicates the region in which $\epsilon_1 > 1$ and thus where inflation stops (this has to be rescaled for $\phi_0 \neq M_{\rm Pl}$). Bottom right panel: slow-roll parameters ϵ_2 (solid line) and ϵ_3 (dotted line), normalized by $M_{\rm Pl}^2/\phi_0^2$.

In between these two local extrema of ϵ_1, the second slow roll parameter ϵ_2 is negative, and it is positive elsewhere. The value of ϵ_1 at its local maximum, $\epsilon_1^{\rm max}$, is given by

$$\epsilon_1^{\rm max} \simeq 5.2753 \frac{M_{\rm Pl}^2}{\phi_0^2} \,. \tag{4.271}$$

Therefore, if $\phi_0/M_{\rm Pl} \lesssim 2.3$, inflation can stop by slow-roll violation in the region corresponding to *vev*'s larger than that of the second inflection point $x^+_{\epsilon_2=0}$. Remembering that typically $\phi_0 \simeq 10^{14}\,{\rm GeV} \simeq 4 \times 10^{-5} M_{\rm Pl}$, this condition is easily satisfied. In that case, an expression for the *vev* at which inflation ends, $x^+_{\epsilon_1=1}$, can be obtained but is does not add much to the discussion since for reasonable values of ϕ_0, it is extremely far from the flat inflection point (e.g. for $\phi_0/M_{\rm Pl} = 10^{-4}$, one has $x^+_{\epsilon_1=1} \simeq 28285$). Since the potential is introduced in order to study inflation in the vicinity of the flat inflection point, it should be studied in the other regime, as it is the case for MSSM inflation (see section 4.17), i.e. when inflation takes place

between $x=0$ and the second inflection point $x^-_{\epsilon_2=0}$. In that situation, it ends at

$$
\begin{aligned}
x_{\rm end} = x^-_{\epsilon_1=1} = \frac{1}{9}\frac{M_{\rm Pl}}{\phi_0}\Bigg[&6\sqrt{2}+8\frac{\phi_0}{M_{\rm Pl}}+2\left(-36+6\sqrt{2}\frac{\phi_0}{M_{\rm Pl}}-5\frac{\phi_0^2}{M_{\rm Pl}^2}\right)\\
&\times\left(216\frac{\phi_0}{M_{\rm Pl}}-99\sqrt{2}\frac{\phi_0^2}{M_{\rm Pl}^2}+136\frac{\phi_0^3}{M_{\rm Pl}^3}-432\sqrt{2}\right.\\
&\left.+27\sqrt{2}\sqrt{-72\sqrt{2}\frac{\phi_0^3}{M_{\rm Pl}^3}+33\frac{\phi_0^4}{M_{\rm Pl}^4}-16\sqrt{2}\frac{\phi_0^5}{M_{\rm Pl}^5}+12\frac{\phi_0^6}{M_{\rm Pl}^6}}\right)^{-1/3}\\
&-\left(216\frac{\phi_0}{M_{\rm Pl}}-99\sqrt{2}\frac{\phi_0^2}{M_{\rm Pl}^2}+136\frac{\phi_0^3}{M_{\rm Pl}^3}-432\sqrt{2}\right.\\
&\left.+27\sqrt{2}\sqrt{-72\sqrt{2}\frac{\phi_0^3}{M_{\rm Pl}^3}+33\frac{\phi_0^4}{M_{\rm Pl}^4}-16\sqrt{2}\frac{\phi_0^5}{M_{\rm Pl}^5}+12\frac{\phi_0^6}{M_{\rm Pl}^6}}\right)^{1/3}\Bigg]\,.
\end{aligned}
\tag{4.272}
$$

For $\phi_0/M_{\rm Pl}\ll 1$, one can numerically check that this expression is very close to the flat inflection point location $x^-_{\epsilon_2=0}$, namely

$$
x_{\rm end}\simeq 1-\sqrt{6\sqrt{2}\frac{\phi_0}{M_{\rm Pl}}}\,. \tag{4.273}
$$

The whole inflationary stage therefore proceeds in the vicinity of this point.

The slow-roll trajectory is obtained from Eq. (2.11) and reads

$$
\begin{aligned}
N_{\rm end}-N=\frac{\phi_0^2}{M_{\rm Pl}^2}\Bigg[&-\frac{x}{6}+\frac{x^2}{8}+\frac{1}{12\,(1-x)}-\frac{\ln(1-x)}{12}\\
&+\frac{x_{\rm end}}{6}-\frac{x_{\rm end}^2}{8}-\frac{1}{12\,(1-x_{\rm end})}+\frac{\ln(1-x_{\rm end})}{12}\Bigg]\,.
\end{aligned}
\tag{4.274}
$$

Several remarks are in order. Firstly, from this expression, one can see that the number of e-folds diverges when the field approaches the inflection point of the potential. This means that this point is never crossed and that, if inflation proceeds for *vev*'s larger than that of this inflection point, then the field approaches it asymptotically but never actually reaches it. However, an exact numerical integration of the equations of motion reveals that, if the field approaches the inflection point in such a way that the slow-roll conditions are not satisfied, then it can cross it. This is typically the case if its speed is large enough. On the other hand, the field dynamics at the exact location of the inflection point is dominated by quantum diffusion, and a more careful study must be carried out to describe what exactly happens there. Following the considerations of section 4.17, we focus on the inflationary regime only in the region where the *vev* of ϕ is smaller than that of the flat inflection and where deviations from slow-roll and quantum diffusion plays a negligible role. Since for $\phi_0/M_{\rm Pl}\ll 1$ inflation takes place relatively close to the inflection point, the two last terms of Eq. (4.274) dominate over the two first ones. In this limit, the trajectory can be inverted to get

$$
x_*\simeq 1-W_0^{-1}\left\{\exp\left[12\left(\frac{M_{\rm Pl}}{\phi_0}\right)^2\Delta N_*+\frac{1}{1-x_{\rm end}}-\ln(1-x_{\rm end})\right]\right\}\,. \tag{4.275}
$$

Making use of Eq. (4.273), and keeping only the dominant terms in $\phi_0/M_{\rm Pl}$, one obtains

$$x_* \simeq 1 - \frac{1}{12}\left(\frac{\phi_0}{M_{\rm Pl}}\right)^2 \frac{1}{\Delta N_*}\,. \tag{4.276}$$

This expression can be useful to determine typical values for the slow-roll parameters evaluated at Hubble crossing. One obtains

$$\epsilon_{1*} \simeq \frac{1}{288}\frac{1}{\Delta N_*^4}\frac{\phi_0^6}{M_{\rm Pl}^6}\,, \qquad \epsilon_{2*} \simeq \frac{4}{\Delta N_*} \qquad \epsilon_{3*} \simeq \frac{1}{\Delta N_*}\,, \tag{4.277}$$

hence

$$r \simeq \frac{1}{18}\frac{1}{\Delta N_*^4}\frac{\phi_0^6}{M_{\rm Pl}^6}\,, \qquad n_{\rm S} - 1 \simeq -\frac{4}{\Delta N_*}\,, \qquad \alpha_{\rm S} \simeq -\frac{4}{\Delta N_*^2}\,. \tag{4.278}$$

One can see that these models typically predict a tiny amount of gravitational waves, but a substantial deviation from scale invariance $n_{\rm S} - 1 \simeq -4/\Delta N_* \simeq 0.1$. The similarity with Eqs. (4.260) is obvious.

Finally, the parameter M can be determined from the amplitude of the CMB anisotropies and the observable field value $x_* = x(N_*)$ by

$$\left(\frac{M}{M_{\rm Pl}}\right)^4 = 622080\frac{M_{\rm Pl}^2}{\phi_0^2}\pi^2\frac{(x_*-1)^4}{x_*^4\left(3x_*^2-8x_*+3\right)^3}\frac{Q_{\rm rms-PS}^2}{T^2}\,. \tag{4.279}$$

For $\phi_0/M_{\rm Pl} \ll 1$, one can make use of Eq. (4.276) to get the approximate expression

$$\left(\frac{M}{M_{\rm Pl}}\right)^4 \simeq 30\frac{\pi^2}{\Delta N_*^4}\left(\frac{\phi_0}{M_{\rm Pl}}\right)^6\frac{Q_{\rm rms-PS}^2}{T^2}\,. \tag{4.280}$$

Using the typical value $\phi_0 \simeq 10^{14}\,{\rm GeV}$, one gets $M/M_{\rm Pl} \simeq 5\times 10^{-11}$.

The reheating consistent slow-roll predictions of the renormalizable inflection point models are displayed in Fig. 105. The reheating equation of state parameter $\overline{w}_{\rm reh}$ has been taken to 0 since the potential is quadratic close to its minimum. One can check that in the limit $\phi_0/M_{\rm Pl} \ll 1$, the first slow-roll parameter is indeed extremely small, while the second slow-roll parameter does not depend much on ϕ_0. Remembering that $\phi_0/M_{\rm Pl} \simeq 10^{-4}$, one can see that these models are disfavored by the CMB data since they predict a too large deviation from scale invariance. In order to remain inside the two-sigma confidence intervals, these models should be such that $\phi_0/M_{\rm Pl} \gg 1$, for which they are close to the large field models (LFI, see section 4.2). However, such values for ϕ_0 are, a priori, outside the range of validity of the RIPI scenario. Finally, comparing Fig. 104 with Fig. 105, one can see that the general features of RIPI are very close to the MSSMI ones, and that the conclusions drawn before are therefore robust against the precise value of the power index n in Eq. (4.244).

4.19 Arctan Inflation (AI)

This scenario was originally introduced in Ref. [425] as a toy model where the equation of state changes rapidly around $\phi = 0$. The potential reads

$$V(\phi) = M^4\left[1 - \frac{2}{\pi}\arctan\left(\frac{\phi}{\mu}\right)\right], \tag{4.281}$$

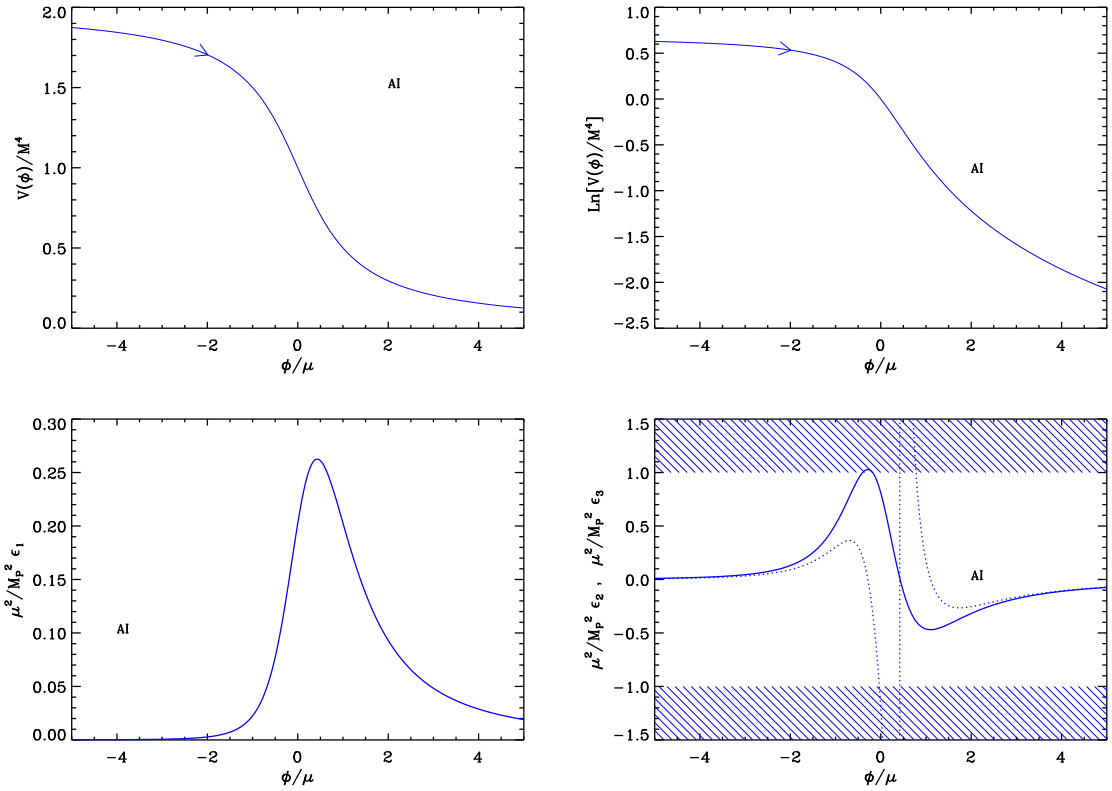

Figure 34. Top left panel: Arctan Inflation (AI) potential as a function of ϕ/μ. Top right panel: logarithm of the potential. Bottom left panel: slow-roll parameter ϵ_1 rescaled by $M_{\rm Pl}^2/\mu^2$ which renders the corresponding expression "universal", i.e. independent of the free parameter μ. Bottom right panel: slow-roll parameters ϵ_2 (solid line) and ϵ_3 (dotted line) rescaled by $M_{\rm Pl}^2/\mu^2$ (for the same reason as mentioned before).

and depends on one free parameter, μ. This model was considered in order to test the reliability of different computational methods and schemes of approximation used in the calculations of the inflationary cosmological perturbations power spectrum, see Ref. [425]. More precisely, in Ref. [180], it was also used to study with which accuracy the first and second slow-roll order power spectra can approximate the actual power spectrum of the fluctuations in the case where the underlying model has both quite large tilt and running. This potential was considered again in Refs. [426, 427] in order to study whether it can lead to the formation of long-lived primordial black holes. In the following slow-roll analysis, μ will be viewed as a free parameter with no restricted range of variation. Let us notice, however, that since it characterizes the typical *vev* at which inflation takes place, it could also be limited to the sub-Planckian regime if one wants inflaton to proceed in a small field regime. As a matter of fact, it will be shown below that this needs to be the case if one wants inflation to end by slow-roll violation.

The potential (4.281), as well as its logarithm, are displayed in Fig. 34. They are decreasing functions of the field and, hence, inflation proceed from the left to the right, in the direction specified by the arrow in Fig. 34.

Let us now compute the three first slow-roll parameters. If one defines $x \equiv \phi/\mu$, their expressions are given by

$$\epsilon_1 = \frac{M_{\rm Pl}^2}{\mu^2}\frac{2}{\left(1+x^2\right)^2\left(\pi - 2\arctan x\right)^2}\,, \qquad \epsilon_2 = 8\frac{M_{\rm Pl}^2}{\mu^2}\frac{1-\pi x + 2x\arctan x}{\left(1+x^2\right)^2\left(\pi - 2\arctan x\right)^2}\,, \tag{4.282}$$

and

$$\epsilon_3 = 2\frac{M_{\rm Pl}^2}{\mu^2}\left[-4 + 6\pi x + \pi^2\left(1-3x^2\right) + 4\left(3\pi x^2 - 3x - \pi\right)\arctan x \right.$$
$$\left. + 4\left(1-3x^2\right)\arctan^2 x\right]\left[\left(1+x^2\right)^2\left(\pi - 2\arctan x\right)^2\left(-1 + \pi x - 2x\arctan x\right)\right]^{-1}. \tag{4.283}$$

They are displayed in Fig. 34. The first slow-roll parameter ϵ_1 increases during inflation, reaches a maximum at $x_{\epsilon_1^{\rm max}}$ and then decreases. Whether inflation can stop by violation of slow-roll or not depends on the value of ϵ_1 at its maximum: $\epsilon_1^{\rm max}$. This value is a solution of the following equation

$$2x_{\epsilon_1^{\rm max}}\arctan\left(x_{\epsilon_1^{\rm max}}\right) + 1 = \pi x_{\epsilon_1^{\rm max}}, \tag{4.284}$$

which can only be solved numerically. One gets $x_{\epsilon_1^{\rm max}} \simeq 0.428978$, from which one deduces that

$$\epsilon_1^{\rm max} \simeq 0.262531\frac{M_{\rm Pl}^2}{\mu^2}\,. \tag{4.285}$$

Therefore, in order for inflation to end by slow-roll violation, one needs to work under the assumption that $\mu/M_{\rm Pl} < 0.512378$. In that case, inflation proceeds along the plateau located at values of x such that $x < x_{\epsilon_1^{\rm max}}$, in the direction specified by the arrow in Fig. 34 (i.e. from the left to the right). Otherwise, if one wants inflation to occur in other parts of the potential and/or for values of μ such that $\mu/M_{\rm Pl} > 0.512378$, another mechanism needs to be consider in order to stop it (typically, we imagine a tachyonic instability in another direction in field space). This means that we also need to introduce an extra parameter $x_{\rm end}$ which gives the location of the *vev* at which the tachyonic instability is triggered. Let us remark that we could also consider a model where the inflaton starts at $x < x_{\epsilon_1^{\rm max}}$, then crosses the region where ϵ_1 has its maximum and then causes the end of inflation by tachyonic instability. This case would give a bump in the power spectrum and, clearly, cannot be properly described in the slow-roll framework. In this article, we restrict ourselves to the first version of the scenario mentioned above. In this situation $x_{\rm end}$ is given by the smallest solution of the equation $\epsilon_1 = 1$ and needs to be computed numerically. Before inflation stops, one can see in Fig. 34 that the second slow-roll parameter ϵ_2 reaches a maximum, the location of which can be numerically computed to be $x_{\epsilon_2^{\rm max}} \simeq -0.28539 < x_{\epsilon_1^{\rm max}}$. At this point, one has $\epsilon_2^{\rm max} \simeq 1.02827 M_{\rm Pl}^2/\mu^2 > \epsilon_1^{\rm max}$. As a consequence, the slow-roll approximation breaks down before the end of inflation. This conclusion is reinforced by the fact that ϵ_3 diverges at $x_{\epsilon_1^{\rm max}}$. This means that the last e-folds of inflation cannot be properly described in the slow-roll framework.

Let us now turn to the slow-roll trajectory. It can be integrated exactly and yields the following expression

$$N_{\rm end} - N = \frac{\mu^2}{M_{\rm Pl}^2}\left[\frac{\pi x_{\rm end}}{2} + \frac{x_{\rm end}^2}{6} + \frac{\pi x_{\rm end}^3}{6} - \left(1 + \frac{x_{\rm end}^2}{3}\right)x_{\rm end}\arctan x_{\rm end} + \frac{1}{3}\ln\left(1+x_{\rm end}^2\right)\right.$$
$$\left. - \frac{\pi x}{2} - \frac{x^2}{6} - \frac{\pi x^3}{6} + \left(1 + \frac{x^2}{3}\right)x\arctan x + \frac{1}{3}\ln\left(1+x^2\right)\right], \tag{4.286}$$

where $N_{\rm end}$ is the number of e-folds at the end of inflation. In the vacuum dominated approximation where the potential is just given by $V(\phi) \simeq M^4$, this trajectory can be approximated by $N_{\rm end} - N = \mu^2/M_{\rm Pl}^2(\pi x_{\rm end} + x_{\rm end}^2/6 + \pi x^3/3 - \pi x - x^2/6 - \pi x^3/3)$, which can be inverted exactly if needed. This formula is valid if $\mu/M_{\rm Pl} \ll 1$, since in that case, $x_{\rm end} \simeq -\sqrt{M_{\rm Pl}/\left(\mu\pi\sqrt{2}\right)} \ll -1$. Under this assumption, one has $x_*^3 \simeq -3M_{\rm Pl}^2/\left(\pi\mu^2\right)\Delta N_*$, from which one can approximate the values of the three first Hubble flow parameters at Hubble radius crossing

$$\epsilon_{1*} = \frac{\left(\mu/M_{\rm Pl}\right)^{2/3}}{2\left(\pi\Delta N_*^2\right)^{2/3}}\,, \qquad \epsilon_{2*} = \frac{4}{3\Delta N_*}\,, \qquad \epsilon_{3*} = \frac{1}{\Delta N_*}\,, \tag{4.287}$$

Then, one can calculate the tensor-to-scalar ratio, the spectral index and the running. One obtains the following expressions

$$r = \frac{8\left(\mu/M_{\rm Pl}\right)^{2/3}}{\left(\pi\Delta N_*^2\right)^{2/3}}\,, \qquad n_{\rm S} - 1 = -\frac{4}{3\Delta N_*} \simeq -0.03\,, \qquad \alpha_{\rm S} = -\frac{4}{3\Delta N_*^2} \simeq -5\times10^{-4}\,. \tag{4.288}$$

These formulas are in agreement with the consistency relation $\alpha_{\rm S} = -3/4\left(n_{\rm S}-1\right)^2$ obtained in Ref. [426].

Finally, it is interesting to estimate the energy scale M from the CMB normalization. This leads to

$$\left(\frac{M}{M_{\rm Pl}}\right)^4 = \frac{2880\pi^3 M_{\rm Pl}^2/\mu^2}{\left(1+x_*^2\right)^2\left(\pi - 2\arctan x_*\right)^3}\frac{Q_{\rm rms-PS}^2}{T^2}\,. \tag{4.289}$$

Under the vacuum dominated approximation ($\mu/M_{\rm Pl} \ll 1$), the above equation can be re-expressed as

$$\left(\frac{M}{M_{\rm Pl}}\right)^4 \simeq \frac{40\times3^{2/3}\pi^{4/3}}{\Delta N_*}\left(\frac{\mu}{M_{\rm Pl}}\right)^{2/3}\frac{Q_{\rm rms-PS}^2}{T^2}\,. \tag{4.290}$$

The requirement $M < M_{\rm Pl}$ is always satisfied form sub-Planckian values of μ. The typical value $M/M_{\rm Pl} \simeq 10^{-3}$ corresponds to $\mu/M_{\rm Pl} \simeq 10^{-2}$.

The slow-roll predictions of the AI models are displayed in Fig. 106, in the range $\mu/M_{\rm Pl} < 0.512378$ (so that inflation can end by slow-roll violation). The reheating equation of state parameter $\overline{w}_{\rm reh}$ has been taken to be 0 but since there is no potential minimum around which the inflaton field can oscillate at the end of inflation, this parameter is a priori unspecified. One can see that this model typically predicts a small amount of gravitational waves, and a deviation from scale invariance which is in accordance with the observations. The predictions in the planes $(n_{\rm S}, r)$ are qualitatively well described by the vacuum dominated analysis (4.288) presented before.

4.20 Constant $n_{\rm S}$ A Inflation (CNAI)

This class of models is designed in order to produce power spectra with constant spectral index. It was studied for the first time in Ref. [428]. The rational behind this approach is that, so far, no evidence for a significant running has been found in the cosmological data. Since, from a Bayesian point of view, one should avoid introducing parameters that are unnecessary in order to reproduce the observations, it makes sense to consider models which lead to exact power-law power spectra. This is of course the case for power-law inflation as discussed in section 4.8 and we will see other examples in sections 4.21, 5.15 and 6.6. In

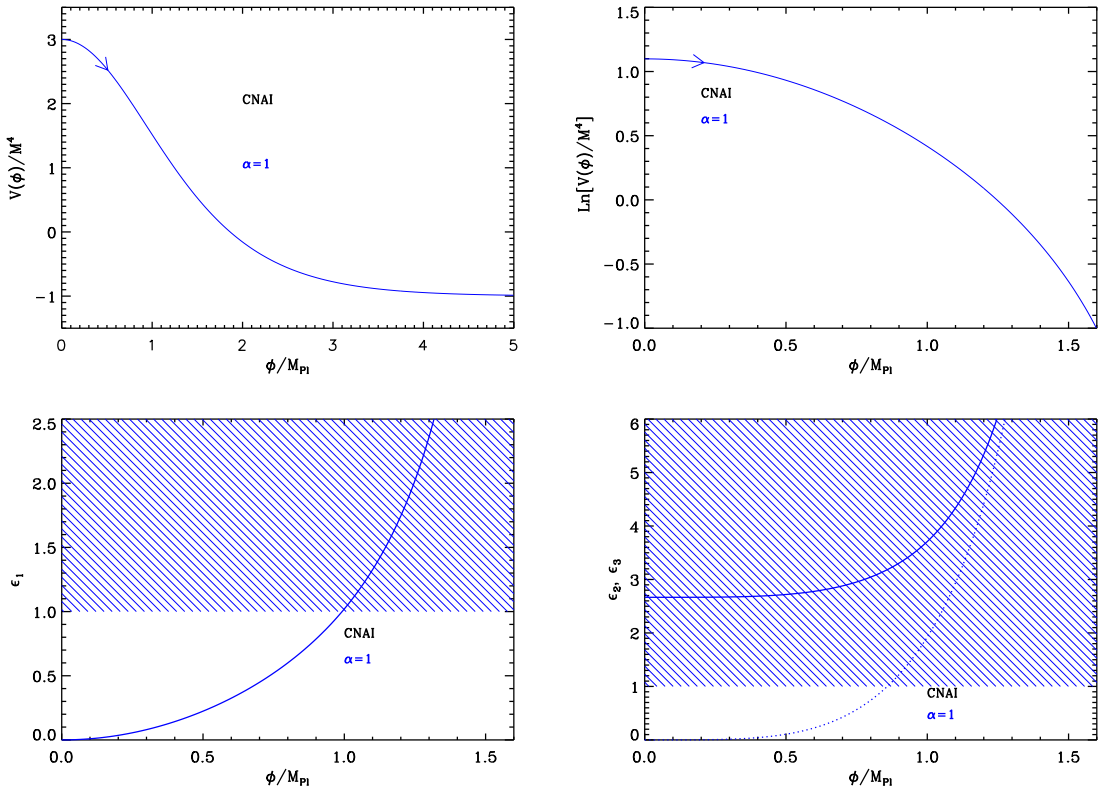

Figure 35. Constant $n_{\rm S}$ A Inflation (CNAI) potential and slow-roll parameters versus the vacuum expectation value of the inflaton field. Top left panel: Constant $n_{\rm S}$ A Inflation potential for $\alpha = 1$. Top right panel: logarithm of the potential for the same value of α. Bottom left panel: slow-roll parameter ϵ_1 (same value of α): inflation stops when $\epsilon_1 = 1$ in this model. Bottom right panel: slow-roll parameters ϵ_2 and ϵ_3 ($\alpha = 1$).

fact, in Ref. [428], a systematic analysis of potentials that yield constant spectral index was carried out. It was found that the following potential belongs to this category of models

$$V(\phi) = M^4 \left[3 - \left(3 + \alpha^2\right) \tanh^2 \left(\frac{\alpha}{\sqrt{2}} \frac{\phi}{M_{\rm Pl}}\right)\right], \tag{4.291}$$

where α is a positive massless parameter (denoted n_0^2 in Ref. [428]) and, in this section, we study this case. This potential is represented in Fig. 35 and, since it is symmetrical under the transformation $\phi \to -\phi$, only the $\phi > 0$ part is displayed. The potential is a decreasing function of the field *vev* and, therefore, inflation proceeds from the left to the right. It is positive provided $\phi < \phi_0$, where

$$\frac{\phi_0}{M_{\rm Pl}} = \frac{\sqrt{2}}{\alpha} \operatorname{arctanh}\left(\sqrt{\frac{3}{3 + \alpha^2}}\right). \tag{4.292}$$

There is no value of α for which the potential is always positive. Defining $x = \phi/M_{\rm Pl}$, the slow-roll parameters are given by

$$\epsilon_1 = \frac{4\alpha^2\left(3+\alpha^2\right)^2\tanh^2\left(\frac{\alpha x}{\sqrt{2}}\right)}{\left[6+\alpha^2-\alpha^2\cosh\left(\sqrt{2}\alpha x\right)\right]^2}\,, \tag{4.293}$$

$$\epsilon_2 = \frac{2\alpha^2\left(3+\alpha^2\right)\left[12+\alpha^2-2\alpha^2\cosh\left(\sqrt{2}\alpha x\right)+\alpha^2\cosh\left(2\sqrt{2}\alpha x\right)\right]}{\left[6+\alpha^2-\alpha^2\cosh\left(\sqrt{2}\alpha x\right)\right]^2\cosh^2\left(\frac{\alpha x}{\sqrt{2}}\right)}\,, \tag{4.294}$$

$$\begin{aligned}\epsilon_3 = {} & 2\alpha^2\left(3+\alpha^2\right)\tanh^2\left(\frac{\alpha}{\sqrt{2}}x\right)\left[6\left(-24+2\alpha^2-\alpha^4\right)+\left(120\alpha^2+7\alpha^4\right)\cosh\left(\sqrt{2}\alpha x\right)\right.\\ & \left.-2\alpha^2\left(\alpha^2-6\right)\cosh\left(2\sqrt{2}\alpha x\right)+\alpha^4\cosh\left(3\sqrt{2}\alpha x\right)\right]\\ & \times\left[6+\alpha^2-\alpha^2\cosh\left(\sqrt{2}\alpha x\right)\right]^{-2}\left[12+\alpha^2-2\alpha^2\cosh\left(\sqrt{2}\alpha x\right)+\alpha^2\cosh\left(2\sqrt{2}\alpha x\right)\right]^{-1}.\end{aligned} \tag{4.295}$$

These slow-roll parameters are displayed in Fig. 35. They all increase as inflation proceeds and diverge when the field approaches ϕ_0. Hence inflation ends by slow-roll violation. Notice that the equation $\epsilon_1 = 1$ can be solved analytically. If we define $y \equiv \sinh^2(\alpha x/\sqrt{2})$, then one has to solve the following cubic equation $\alpha^4 y^3 + (\alpha^4 - 6\alpha^2)y^2 + [9 - 6\alpha^2 - \alpha^2(3+\alpha^2)]y + 9 = 0$. The relevant solution reads

$$y_{\rm end} = \frac{6-\alpha^2}{3\alpha^2} - \frac{1-i\sqrt{3}}{3\times 2^{1/3}}(3+\alpha^2)^2(1+3\alpha^2)P^{-1/3} - \frac{1+i\sqrt{3}}{6\times 2^{1/3}\alpha^4}P^{1/3}, \tag{4.296}$$

where we have defined P by

$$\begin{aligned}P \equiv & -\alpha^6\left(3+\alpha^2\right)^2\left(6-52\alpha^2+9\alpha^4\right)\\ & +\sqrt{-27\alpha^{14}\left(3+\alpha^2\right)^4\left(36-60\alpha^2+96\alpha^4+25\alpha^6+4\alpha^8\right)}\,.\end{aligned} \tag{4.297}$$

The slow-roll parameters ϵ_1 and ϵ_3 both vanish when the field *vev* goes to 0, whereas ϵ_2 has a non-vanishing minimum value, given by $\epsilon_2 \to 2\alpha^2\left(3+\alpha^2\right)/3$ when $x = 0$. Therefore, if α is larger than some maximum value

$$\alpha_{\rm max} = \sqrt{\frac{1}{2}\left(\sqrt{15}-3\right)} \simeq 0.66, \tag{4.298}$$

then ϵ_2 is larger than 1 in the whole inflationary regime and the slow-roll approximation does not hold. It is therefore necessary to work under the assumption $\alpha < \alpha_{\rm max}$ which we assume in the following.

Let now us check that the spectral index $n_{\rm S} - 1 = -2\epsilon_1 - \epsilon_2$ (at first order in slow-roll), can be made constant, as announced previously. Expanding the slow-roll parameters ϵ_1 and ϵ_2 in small values of α, and crucially assuming that αx_* remains small, one obtains $\epsilon_1 = \mathcal{O}\left(\alpha^4\right)$ and $\epsilon_2 = 2\alpha^2 + \mathcal{O}\left(\alpha^4\right)$, so that $n_{\rm S} - 1 = -2\alpha^2 + \mathcal{O}\left(\alpha^4\right)$. Therefore, the corresponding expression is indeed a constant (i.e. does no depend on ϕ_*). Since we have $|n_{\rm S} - 1| \ll 1$, this implies that α should be small which is consistent with the condition $\alpha < \alpha_{\rm max}$ derived above.

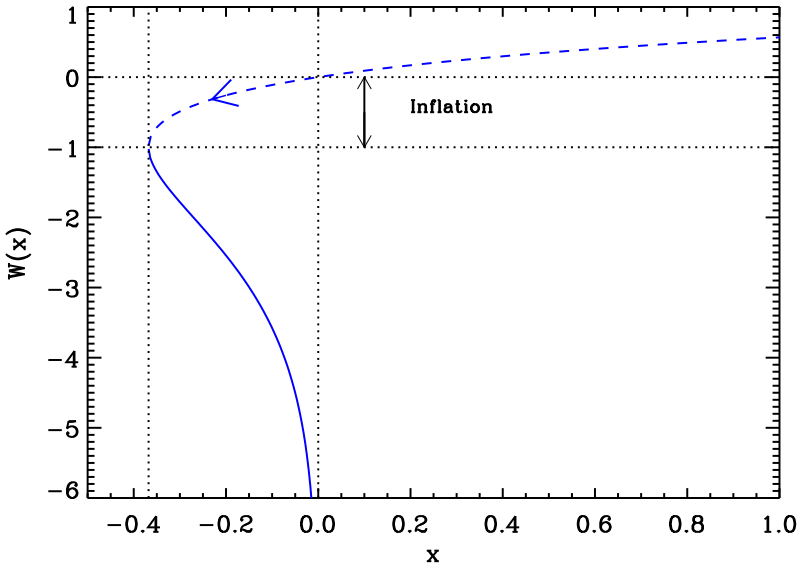

Figure 36. Lambert functions $\mathrm{W}_0(x)$ (dashed line) and $\mathrm{W}_{-1}(x)$ (solid line). During CNAI inflation, inflation proceeds along the "0" branch in the direction specified by the arrow on the figure.

Let us now study the slow-roll trajectory of the system. This one can be integrated exactly leading to the following formula

$$N - N_{\rm end} = \frac{1}{\alpha^2\left(3+\alpha^2\right)}\left\{3\ln\left[\sinh\left(\frac{\alpha}{\sqrt{2}}x\right)\right] - \frac{\alpha^2}{2}\sinh^2\left(\frac{\alpha}{\sqrt{2}}x\right) - 3\ln\left[\sinh\left(\frac{\alpha}{\sqrt{2}}x_{\rm end}\right)\right] + \frac{\alpha^2}{2}\sinh^2\left(\frac{\alpha}{\sqrt{2}}x_{\rm end}\right)\right\}. \tag{4.299}$$

Moreover, this trajectory can be inverted which allows us to explicitly express the *vev* of the inflaton field in terms of the e-folds number. One obtains

$$x = \frac{\sqrt{2}}{\alpha}\,\mathrm{arcsinh}\left[-\frac{3}{\alpha^2}\mathrm{W}_0\left(-\frac{\alpha^2}{3}\exp\left\{\frac{2}{3}\alpha^2\left(3+\alpha^2\right)\left(N-N_{\rm end}\right) + 2\ln\left[\sinh\left(\frac{\alpha}{\sqrt{2}}x_{\rm end}\right)\right] - \frac{\alpha^2}{3}\sinh^2\left(\frac{\alpha}{\sqrt{2}}x_{\rm end}\right)\right\}\right)\right]^{1/2}, \tag{4.300}$$

where W_0 is the 0 branch of the Lambert function as required since $x\left(N\right)$ is an increasing function of N. It is displayed in Fig. 36 where the CNAI trajectory takes place between $\phi/M_{\rm Pl} = 0$ at the origin of the plot, and $x = \phi_0/M_{\rm Pl}$ at the junction between the -1 branch and the 0 branch.

The slow-roll predictions of the CNAI models are displayed in Fig. 107. When α is small (but not too small), the value of $n_{\rm S}$ is indeed constant (and compatible with the considerations presented above) but, unfortunately, too far from scale invariance to be compatible with CMB data. When $\alpha \ll 10^{-1}$, the predictions become roughly compatible with the data but, clearly, $n_{\rm S}$ is no longer constant and no longer given by $-2\alpha^2$. At first sight, this is surprising since we expect the spectral index to tend towards $-2\alpha^2$ when α goes to zero (see above). In

order to understand this point, let us remark that, in the limit where α vanishes, one can expand Eq. (4.296) to find $y_{\rm end} \simeq 3/\alpha^2 - 3/\alpha + \mathcal{O}(\alpha)$ (the term at order α^0 is absent and this plays an important role in what follows). This leads to $x_{\rm end} \simeq (\sqrt{2}/\alpha)\ln\left(2\sqrt{3}/\alpha\right) - 1/\sqrt{2} + \mathcal{O}(\alpha)$. Notice that this last equation is compatible with the behavior of the first Hubble-flow parameter (4.293) in the vicinity of ϕ_0: $\epsilon_1 \simeq M_{\rm Pl}^2/[2(\phi-\phi_0)^2]$. Therefore, the expression of $x_{\rm end}$ found before corresponds in fact to writing $\epsilon_1 = 1$ with this approximated ϵ_1. Then, using the slow-roll trajectory (4.300), one gets

$$\sinh^2\left(\frac{\alpha x_*}{\sqrt{2}}\right) = -\frac{3}{\alpha^2}\mathrm{W}_0\left(-\frac{\alpha^2}{3}e^{-2A/3}\right), \tag{4.301}$$

where A is given by the following expression

$$A \equiv \alpha^2\left(3+\alpha^2\right)\Delta N_* - 3\ln\left[\sinh\left(\frac{\alpha x_{\rm end}}{\sqrt{2}}\right)\right] + \frac{\alpha^2}{2}\sinh^2\left(\frac{\alpha x_{\rm end}}{\sqrt{2}}\right). \tag{4.302}$$

This quantity can be expanded in α using the equation for $y_{\rm end}$ derived above and, at leading order, one obtains

$$-\frac{2}{3}A \simeq -\frac{2}{3}\alpha^2\Delta N_* + \ln\left(\frac{3}{\alpha^2}\right) - 1 - \frac{\alpha^2}{2}. \tag{4.303}$$

For simplicity, the last term in the previous expression can be ignored since $2\Delta N_* \gg 1/2$. It follows that, introducing the formula for $-2A/3$ into Eq. (4.301), one arrives at

$$\sinh^2\left(\frac{\alpha x_*}{\sqrt{2}}\right) = -\frac{3}{\alpha^2}\mathrm{W}_0\left(-\frac{1}{e}e^{-2\alpha^2\Delta N_*}\right). \tag{4.304}$$

If we ignore the exponential in the argument of the Lambert function (since $\alpha \ll 1$) and use the identity $\mathrm{arcsinh}(x) = \ln(x+\sqrt{x^2+1})$, one finally arrives at

$$\alpha x_* \underset{\alpha\to 0}{\sim} \sqrt{2}\ln\left(\frac{2\sqrt{3}}{\alpha}\right). \tag{4.305}$$

We now understand why, in the limit $\alpha \to 0$, the spectral index is no longer constant. The naive expression $n_{\rm S} \simeq -2\alpha^2$ is obtained by expanding the expressions of ϵ_1 and ϵ_2 in α, including the hyperbolic function of argument αx_*. But we have just shown that, when $\alpha \ll 1$, αx_* is not small and, therefore, the Taylor expansion of those terms is no longer justified. This is why, in Fig. 107, we see a deviation from $n_{\rm S}$ constant at very small values of α. In fact, this questions the interest of this model since the condition of constant spectral index is obtained only for values of $n_{\rm S}$ that are already ruled out by the CMB data. On the other hand, when $\alpha \ll 1$, the model seems compatible with the data and, therefore, represents a legitimate inflationary scenario even if the spectral index is not constant in this case.

Finally, it is also interesting to study the energy scale at which inflation takes place in this model. The CMB normalization gives

$$\left(\frac{M}{M_{\rm Pl}}\right)^4 = \frac{11520\pi^2\alpha^2\left(\alpha^2+3\right)^2\sinh^2\left(\frac{\alpha}{\sqrt{2}}x_*\right)}{\left[\alpha^2+6-\alpha^2\cosh\left(\sqrt{2}\alpha x_*\right)\right]^3}\frac{Q_{\rm rms-PS}^2}{T^2}. \tag{4.306}$$

Since we have established the expression of x_* above, it is sufficient to use it in the above formula. We have, however, to be careful about the calculation of the denominator. Indeed,

if we neglect again the exponential in the argument of the Lambert function, Eq. (4.301), then $\sinh^2(\alpha x_*/\sqrt{2}) \simeq 3/\alpha^2$ and the denominator in Eq. (4.306) vanishes. Therefore, one needs to evaluate the Lambert function more precisely and to keep the corrections proportional to ΔN_*. This can be done with the help of Eq. (33) of Ref. [429] which implies that $\sinh^2(\alpha x_*/\sqrt{2}) \simeq 3/\alpha^2 - 6\sqrt{\Delta N_*}/\alpha$. Using this expression, one arrives at

$$\frac{M}{M_{\rm Pl}} \simeq 0.016\, \alpha^{-3/4}\, (\Delta N_*)^{-3/8}\,. \tag{4.307}$$

For an order of magnitude estimate, one can use the fiducial value $\Delta N_* \simeq 55$. This leads to $M/M_{\rm Pl} \simeq 0.0035\, \alpha^{-3/4}$. Requiring $M < M_{\rm Pl}$ puts a lower bound on the parameter α, namely $\alpha \gtrsim 5 \times 10^{-4}$. This roughly corresponds to the range studied in Fig. 107.

4.21 Constant $n_{\rm S}$ B Inflation (CNBI)

This model is another representative of the class of scenarios studied in Ref. [428]. As was already discussed in section 4.20, it is designed such that the corresponding power spectrum has a constant spectral index. The potential is given by

$$V\,(\phi) = M^4 \left[\left(3-\alpha^2\right) \tan^2\left(\frac{\alpha}{\sqrt{2}}\frac{\phi}{M_{\rm Pl}}\right) - 3\right], \tag{4.308}$$

where α is a positive dimensionless parameter [428]. Since the potential is periodic with period $\pi\sqrt{2}/\alpha$ and, moreover, invariant under $\phi \to -\phi$, one can restrict ourselves to the range $0 < \phi/M_{\rm Pl} < \pi/\left(\sqrt{2}\alpha\right)$ without loss of generality. The potential is an increasing function of the field and, as a consequence, inflation proceeds from the right to the left. Finally, $V(\phi)$ is positive provided $\phi > \phi_0$, where

$$\frac{\phi_0}{M_{\rm Pl}} = \frac{\sqrt{2}}{\alpha} \arctan\left(\sqrt{\frac{3}{3-\alpha^2}}\right). \tag{4.309}$$

Obviously, in order for the potential not to be negative everywhere, one needs to impose that $\alpha < \sqrt{3}$ and, as a result, the previous expression is well defined. The potential (and its logarithm) is displayed in Fig. 37, in the relevant range $\phi_0/M_{\rm Pl} < \phi/M_{\rm Pl} < \pi/\left(\sqrt{2}\alpha\right)$.

Then, defining $x = \phi/M_{\rm Pl}$, the slow-roll parameters are given by

$$\epsilon_1 = \frac{4\alpha^2\left(\alpha^2-3\right)^2 \tan^2\left(\dfrac{\alpha}{\sqrt{2}}x\right)}{\left[\alpha^2 + \left(6-\alpha^2\right)\cos\left(\sqrt{2}\alpha x\right)\right]^2}, \tag{4.310}$$

$$\epsilon_2 = \frac{\alpha^2\left(3-\alpha^2\right)\left[6+\alpha^2+2\left(6-\alpha^2\right)\cos\left(\sqrt{2}\alpha x\right)+\left(\alpha^2-6\right)\cos\left(2\sqrt{2}\alpha x\right)\right]}{2\cos^6\left(\dfrac{\alpha}{\sqrt{2}}x\right)\left[3+\left(\alpha^2-3\right)\tan^2\left(\dfrac{\alpha x}{\sqrt{2}}\right)\right]^2}, \tag{4.311}$$

and

$$\begin{aligned}\epsilon_3 = {} & 2\alpha^2\left(\alpha^2-3\right)\tan^2\left(\frac{\alpha}{\sqrt{2}}x\right)\left[6\left(-72+14\alpha^2-\alpha^4\right)+\left(\alpha^2-6\right)\left(7\alpha^2+78\right)\cos\left(\sqrt{2}\alpha x\right)\right.\\ & \left.-2\left(\alpha^4-18\alpha^2+72\right)\cos\left(2\sqrt{2}\alpha x\right)+\left(\alpha^2-6\right)^2\cos\left(3\sqrt{2}\alpha x\right)\right]\\ & \times\left[\alpha^2+\left(6-\alpha^2\right)\cos\left(\sqrt{2}\alpha x\right)\right]^{-2}\left[6+\alpha^2+2\left(6-\alpha^2\right)\cos\left(\sqrt{2}\alpha x\right)\right.\\ & \left.+\left(\alpha^2-6\right)\cos\left(2\sqrt{2}\alpha x\right)\right]^{-1}.\end{aligned} \tag{4.312}$$

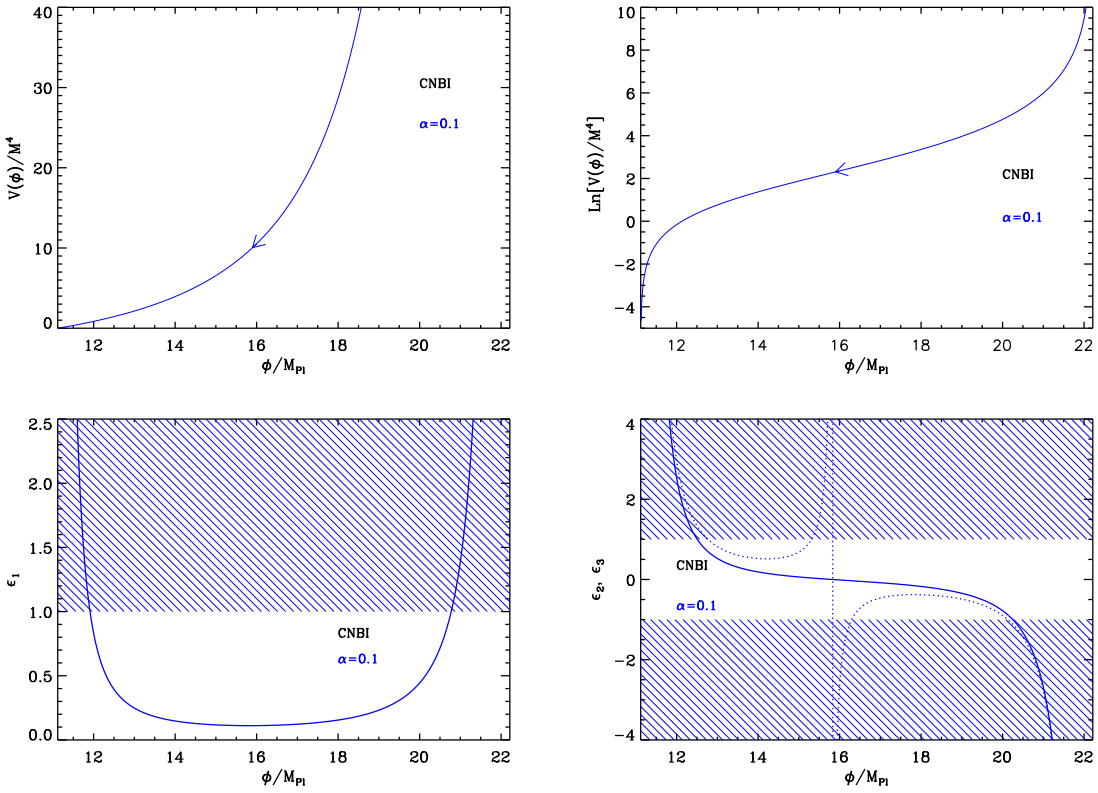

Figure 37. Top left panel: constant $n_{\rm S}$ B Inflation (CNBI) potential for $\alpha = 0.1$, see Eq. (4.308). Top right panel: logarithm of this potential (for the same value of α). Bottom left panel: slow-roll parameter ϵ_1 still for $\alpha = 0.1$. Bottom right panel: slow-roll parameters ϵ_2 and ϵ_3 again for $\alpha = 0.1$.

These slow-roll parameters are displayed in Fig. 37 (bottom panels). The first slow-roll parameter ϵ_1 first decreases as the field *vev* increases and reaches a minimum value at $x_{\epsilon_2=0}$ where ϵ_2 vanishes and then increases. The value of $x_{\epsilon_2=0}$ is given by

$$x_{\epsilon_2=0} = \frac{1}{\alpha\sqrt{2}} \arccos\left[\frac{\alpha^2 - 6 + \sqrt{\alpha^4 - 36\alpha^2 + 180}}{2\left(\alpha^2 - 6\right)}\right] . \tag{4.313}$$

The second slow-roll parameter, ϵ_2, always decreases as inflation proceeds, crossing $\epsilon_2 = 0$ at $x_{\epsilon_2=0}$. The third slow-roll parameter, ϵ_3, is positive for $x < x_{\epsilon_2=0}$. In this domain, it decreases to reach a minimum and then increases and diverges when x approaches $x_{\epsilon_2=0}$. On the contrary, for $x > x_{\epsilon_2=0}$, ϵ_3 becomes negative. It first increases and reaches a local maximum, then decreases and goes to $-\infty$ at $x = \pi/\left(\sqrt{2}\alpha\right)$. The three slow roll parameters diverge when ϕ goes to ϕ_0 and to $M_{\rm Pl}\pi/\left(\sqrt{2}\alpha\right)$.

The minimum value of ϵ_1 at $x_{\epsilon_2=0}$ turns out to be smaller than 1 only if $\alpha < \alpha_{\rm max} \simeq 0.2975$. A (rather long) analytic expression for $\alpha_{\rm max}$ can be derived, but it does not provide much information to the present discussion. Therefore, one must require $\alpha < 0.2975$ in order to realize slow-roll inflation in this model. Then, assuming this is the case, it is clear from Fig. 37 and from the previous considerations that inflation ends by slow-roll violation. If we define $y \equiv \sin^2(\alpha x/\sqrt{2})$, then the condition $\epsilon_1 = 1$ is equivalent to $4(6 - \alpha^2)^2 y^3 - 4(12 -$

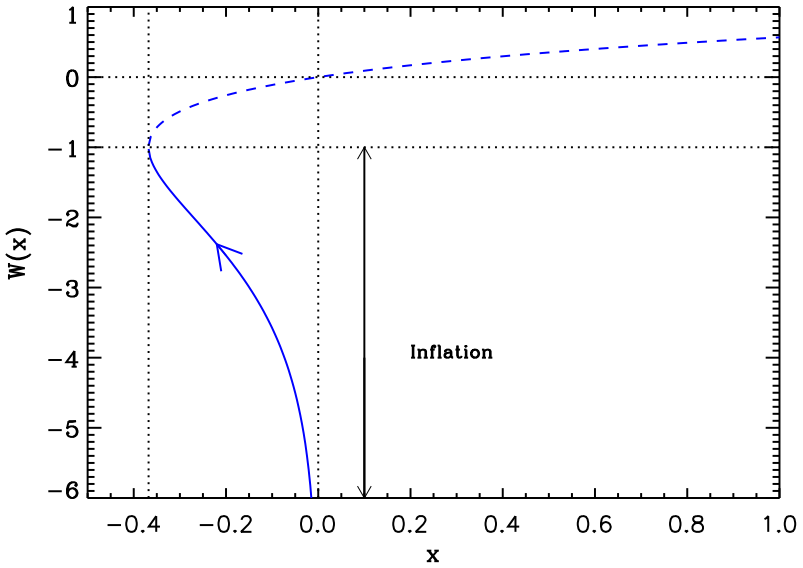

Figure 38. Lambert functions $\mathrm{W}_0(x)$ (dashed line) and $\mathrm{W}_{-1}(x)$ (solid line). During Constant n_S B Inflation, inflation proceeds along the "-1" branch in the direction specified by the arrow.

$\alpha^2)(6-\alpha^2)y^2 + 4(45+3\alpha^2-6\alpha^4+\alpha^6)y - 36 = 0$. The relevant solution is given by

$$y_\mathrm{end} = \frac{12-\alpha^2}{3(6-\alpha^2)} + \frac{4}{3}2^{-2/3}\left(1-i\sqrt{3}\right)\frac{\left(3\alpha^2-1\right)\left(18-9\alpha^2+\alpha^4\right)^2}{\left(6-\alpha^2\right)^2}P^{-1/3} - \left(1+i\sqrt{3}\right)\frac{2^{-1/3}}{24\left(6-\alpha^2\right)^2}P^{1/3}, \tag{4.314}$$

where we have defined the quantity P by

$$P \equiv 64\left(-6+\alpha^2\right)^3\left(-3+\alpha^2\right)^2\left(-6+110\alpha^2-9\alpha^4+3\alpha\sqrt{3} \times \sqrt{-36+408\alpha^2-12\alpha^4-25\alpha^6+4\alpha^8}\right). \tag{4.315}$$

If $\alpha \ll 1$, then $y_\mathrm{end} \simeq 1/2$ and $x_\mathrm{end} \simeq \sqrt{2}/\alpha \arcsin(1/\sqrt{2}) = \pi/(2\sqrt{2}\alpha)$.

As for the CNAI model, the spectral index $n_\mathrm{S} - 1 = -2\epsilon_1 - \epsilon_2$, at first order in slow-roll, can be made constant in some limit. Expanding the slow-roll parameters in α, while assuming αx to be small, gives $\epsilon_1 = x^2\alpha^4/2 + \mathcal{O}(\alpha^6)$ and $\epsilon_2 = 2\alpha^2 + \mathcal{O}(\alpha^4)$, so that $n_\mathrm{S} - 1 = -2\alpha^2 + \mathcal{O}(\alpha^4)$. Therefore, approximate scale-invariance, $|n_\mathrm{S} - 1| \ll 1$, implies α small.

Let us now turn to the slow-roll trajectory. This one can be integrated exactly, leading to the following formula

$$N - N_\mathrm{end} = \frac{1}{\alpha^2\left(3-\alpha^2\right)}\left\{3\ln\left[\sin\left(\frac{\alpha}{\sqrt{2}}x\right)\right] - \frac{6-\alpha^2}{2}\sin^2\left(\frac{\alpha}{\sqrt{2}}x\right) - 3\ln\left[\sin\left(\frac{\alpha}{\sqrt{2}}x_\mathrm{end}\right)\right] + \frac{6-\alpha^2}{2}\sin^2\left(\frac{\alpha}{\sqrt{2}}x_\mathrm{end}\right)\right\}. \tag{4.316}$$

This formula can be inverted and x can be expressed explicitly in terms of the e-folds number. One obtains

$$x = \frac{\sqrt{2}}{\alpha}\arcsin\left[-\frac{3}{6-\alpha^2}\mathrm{W}_{-1}\left(-\frac{6-\alpha^2}{3}\exp\left\{\frac{2}{3}\alpha^2\left(3-\alpha^2\right)\left(N-N_{\mathrm{end}}\right)\right.\right.\right.$$
$$\left.\left.\left.+2\ln\left[\sin\left(\frac{\alpha}{\sqrt{2}}x_{\mathrm{end}}\right)\right]-\frac{6-\alpha^2}{3}\sin^2\left(\frac{\alpha}{\sqrt{2}}x_{\mathrm{end}}\right)\right\}\right)\right]^{1/2}, \tag{4.317}$$

where W_{-1} is the -1 branch of the Lambert function. It is displayed in Fig. 38. When $x = \pi/\left(\sqrt{2}\alpha\right)$, the argument of the Lambert function is $\left(\alpha^2-6\right)\exp\left(\alpha^2/3-2\right)/3$ which is always larger than $-1/e$ for any value of α (this expression decreases with α when $\alpha < \sqrt{3}$), whereas when $x = \phi_0/M_{\mathrm{Pl}}$, the argument of the Lambert function is just given by $-1/e$. For $x > \phi_0/M_{\mathrm{Pl}}$, the value taken by the Lambert function must be less than -1 which indicates that the -1 branch is the relevant one. Therefore, inflation proceeds in the domain displayed in Fig. 38 in which one easily checks that the above trajectory is always well defined.

The slow-roll predictions of the CNBI models are displayed in Fig. 108 for the range $10^{-5} \lesssim \alpha \lesssim 10^{-1.3}$. For very small values of α, the predictions are in agreement with the data with a value of n_{S} centered around the constant value $n_{\mathrm{S}} \simeq 0.97$ and an amount of gravitational waves such that $r \gtrsim 0.07$. But one also notices that the spectral index is not really constant. In fact, it does not come as a surprise that the same phenomenon highlighted in section 4.20 is at work here. Indeed, using the slow-roll trajectory (4.316), one has

$$\sin^2\left(\frac{\alpha x_*}{\sqrt{2}}\right) = -\frac{3}{6-\alpha^2}\mathrm{W}_{-1}\left(-\frac{6-\alpha^2}{3}e^{-2A/3}\right), \tag{4.318}$$

where A is given by the following expression

$$A \equiv \alpha^2\left(3-\alpha^2\right)\Delta N_* - 3\ln\left[\sin\left(\frac{\alpha x_{\mathrm{end}}}{\sqrt{2}}\right)\right] + \frac{6-\alpha^2}{2}\sin^2\left(\frac{\alpha x_{\mathrm{end}}}{\sqrt{2}}\right). \tag{4.319}$$

Using the formula for x_{end} derived above, one obtains, in the limit $\alpha \ll 1$ and at this order of approximation that $x_* \simeq x_{\mathrm{end}}$. Therefore, as in section 4.20, αx_* is not a small quantity and one cannot always Taylor expand the trigonometric functions that appear in the expressions of the slow-roll parameters. This explains why, in the limit $\alpha \ll 1$, the spectral index is in fact not constant (see section 4.20).

Finally, the CMB normalization gives

$$\left(\frac{M}{M_{\mathrm{Pl}}}\right)^4 = \frac{11520\pi^2\alpha^2\left(3-\alpha^2\right)^2\sin^2\left(\frac{\alpha}{\sqrt{2}}x_*\right)}{\left[\left(\alpha^2-6\right)\cos\left(\sqrt{2}\alpha x_*\right)-\alpha^2\right]^3}\frac{Q^2_{\mathrm{rms-PS}}}{T^2}. \tag{4.320}$$

In the limit $\alpha \ll 1$ we are interested in (since we have seen that, if α is not small, then the model is ruled out), the above expression takes the form $M/M_{\mathrm{Pl}} \simeq 0.02\,\alpha^{-1/4}\left(\Delta N_*\right)^{-3/8}$. We obtain almost exactly the same result as for CNAI, see Eq. (4.306), except that the power of α is different. Taking the value $\Delta N_* = 55$, it follows that $M/M_{\mathrm{Pl}} \simeq 0.0044\,\alpha^{-1/4}$ and requiring $M < M_{\mathrm{Pl}}$, one obtains the following lower bound, $\alpha \gtrsim 3.8 \times 10^{-10}$.

4.22 Open String Tachyonic Inflation (OSTI)

4.22.1 Theoretical Justifications

In this section, we consider tachyon inflation. It was shown in Refs. [430–433] that, in bosonic string theory, the four-dimensional action for a tachyon field T on a D3-brane can

be approximated as [432, 433]

$$S_T = T_3 \int \mathrm{d}^4\boldsymbol{x}\sqrt{-g}\left[\alpha' e^{-T/T_0}\partial_\mu\left(\frac{T}{T_0}\right)\partial^\mu\left(\frac{T}{T_0}\right) + \left(1+\frac{T}{T_0}\right)e^{-T/T_0}\right], \tag{4.321}$$

where higher derivative terms have been ignored. In this stringy setting, T_0 is of the order of the string scale $T_0 \simeq M_\mathrm{s} = \ell_\mathrm{s}^{-1} = 1/\sqrt{\alpha'}$, where ℓ_s is the string length. The constant T_3 is the brane tension which can be expressed as $T_3 \propto M_\mathrm{s}^4/g_\mathrm{s}$, g_s being the string coupling. The tachyon is assumed to be minimally coupled to Einstein gravity and the Planck mass in four dimensions can be written as $M_\mathrm{Pl}^2 = M_\mathrm{s}^2 v/g_\mathrm{s}^2$, where $v = (M_\mathrm{s} r)^d/\pi$, r being a radius of compactification and d the number of compactified dimensions. This four dimensional approximation is valid provided $r \gg \ell_\mathrm{s}$ or $v \gg 1$. The action (4.321) can be viewed as a truncated version of the action

$$S_{\bar{T}} = \int \mathrm{d}^4\boldsymbol{x}\sqrt{-g}\,V(\bar{T})\sqrt{1+\alpha'\partial_\mu\left(\frac{\bar{T}}{T_0}\right)\partial^\mu\left(\frac{\bar{T}}{T_0}\right)}. \tag{4.322}$$

Indeed, following Refs. [288, 434, 435], redefining the field $\bar{T}$ by $\bar{T}/T_0 \equiv \sqrt{8(1+T/T_0)}$ with $V\left[\bar{T}(T)\right] \equiv T_3(1+T/T_0)\exp\left(-T/T_0\right)$, it is straightforward to show that the leading terms of Eq. (4.322) give back Eq. (4.321). Conversely, the full action of tachyonic inflation, under the assumptions discussed previously, can thus be described in terms of $\bar{T}$ by Eq. (4.322) with [434]

$$V(\bar{T}) = \frac{T_3 e}{8}\frac{\bar{T}^2}{T_0^2}e^{-\bar{T}^2/(8T_0^2)}. \tag{4.323}$$

Because the action (4.322) is a particular case of k-inflation for which $S = \int \mathrm{d}^4\boldsymbol{x}\sqrt{-g}P(T,X)$ with $X \equiv -g^{\mu\nu}\partial_\mu T\partial_\nu T/2$ and, here, $P(T,X) = \sqrt{1-2X}$, tachyonic inflation could produce observable non-Gaussianities. Therefore, one may wonder how accurate is the truncated action to describe the observable features of the model. On the theoretical point of view, knowing whether the truncated action is a faithful representation of the actual action is a complicated question since even an exact derivation of the complete action is still an open problem. On a more phenomenological point of view, non-Gaussianities are not observed by Planck [70]. More precisely, the parameter f_NL (equilateral configuration) characterizing the amplitude of the bispectrum in Fourier space can be written as [118, 436]

$$f_\mathrm{NL} = \frac{35}{108}\left(\frac{1}{c_\mathrm{S}^2}-1\right) - \frac{5}{81}\left(\frac{1}{c_\mathrm{S}^2}-1-2\Lambda\right), \tag{4.324}$$

where, in our case, $c_\mathrm{S}^2 = 1-2X$ and $1/c_\mathrm{S}^2 - 1 = 2\Lambda$ so that the last term in the above equation cancels out [436]. This leads to $f_\mathrm{NL} = 35X/[54(1-2X)]$. In the range of interest $X \in [0, 1/2]$, the Planck constraint [70], $f_\mathrm{NL} = -42 \pm 75$, yields $X \lesssim 0.495$. As a result, departures from the leading order (4.321) are, a priori, still allowed by the CMB data. We will see at the end of this section that tachyonic inflation has however other problems. For the moment, given that Eq. (4.321) can always be seen as a phenomenological model, we can continue to work with this action in order to see if, at least, this can lead to an inflationary scenario compatible with the CMB data.

4.22.2 Slow-Roll Analysis

The inflationary dynamics can be studied directly from Eq. (4.321) but since it is linear in X, the field can be canonically normalized. Performing the change of variable $e^{-T/T_0} \equiv$

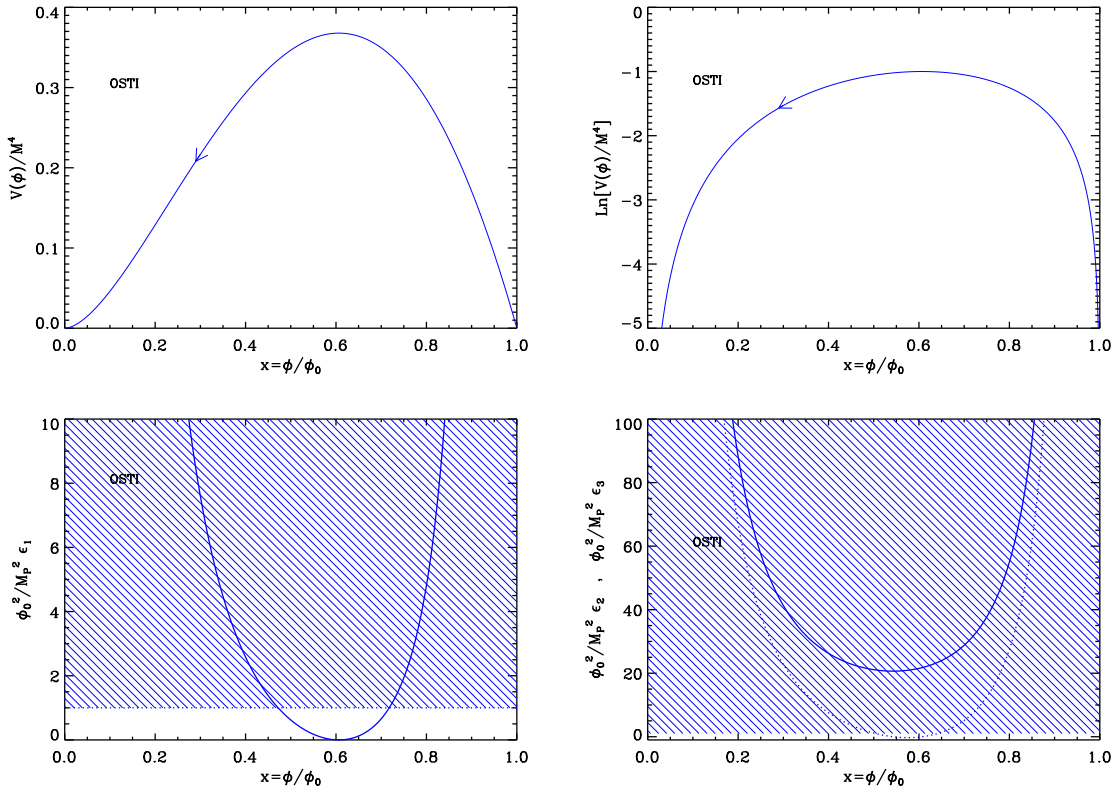

Figure 39. Top left panel: Open String Tachyonic Inflation (OSTI) potential as a function of ϕ/ϕ_0. Top right panel: logarithm of the potential. The arrow indicates in which direction inflation proceeds. Bottom left panel: slow-roll parameter ϵ_1, rescaled by the quantity $M_{\rm Pl}^2/\phi_0^2$, such that the corresponding expression becomes universal, i.e. independent of ϕ_0. Bottom right panel: slow-roll parameters ϵ_2 (solid line) and ϵ_3 (dotted line), rescaled by $M_{\rm Pl}^2/\phi_0^2$ for the same reason as mentioned before.

$(\phi/T_0)^2/8$, the Lagrangian can be re-written with an ordinary kinetic term, as a function of the field ϕ and with a potential given by

$$V(\phi) = -M^4 \left(\frac{\phi}{\phi_0}\right)^2 \ln\left[\left(\frac{\phi}{\phi_0}\right)^2\right], \tag{4.325}$$

where $M^4 \equiv eT_3$ and $\phi_0^2 \equiv 8eT_0^2$. We notice that it corresponds to a particular case of LPI discussed in section 6.5, with $q = 1$ and $p = 2$. Such a potential was also introduced in Ref. [437] as a toy model of tachyon condensation. Let us also comment on the parameter ϕ_0. In the original model $\phi_0 \simeq M_{\rm s}$ and, as such, it is a zero-parameter scenario. Here, given the issues discussed before (see also the end of this section) we consider ϕ_0 as a free parameter. If necessary, one can always recover the situation where ϕ_0 is fixed to the string scale by assuming the corresponding prior $\phi_0 = M_{\rm s}$.

The potential (4.325) in represented in Fig. 39, together with its logarithm (top panels), as a function of $x \equiv \phi/\phi_0$. Since it is invariant under $x \to -x$, and since it is positive definite only if $x^2 < 1$, it is only displayed in the range $0 < x < 1$. The potential vanishes at $x = 0$,

increases with x, reaches a maximum at $x_{V'=0} = e^{-1/2}$, then decreases with x and vanishes at $x_{V=0} = 1$. Inflation is supposed to take place between $x_{V'=0}$, where the effective mass of the inflaton is negative $m_\phi^2 = -4\phi_0^2$, and $x = 0$, where the effective mass is positive and infinite $m_\phi^2 \to +\infty$. Hence it proceeds from the right to the left, at decreasing field values (see Fig. 39).

Let us now calculate the three first slow-roll parameters. They are given by

$$\epsilon_1 = 2\left(\frac{M_{\rm Pl}}{\phi_0}\right)^2 \left[\frac{1+\ln\left(x^2\right)}{x\ln\left(x^2\right)}\right]^2, \tag{4.326}$$

$$\epsilon_2 = 4\left(\frac{M_{\rm Pl}}{\phi_0}\right)^2 \frac{2+\ln\left(x^2\right)+\ln^2\left(x^2\right)}{x^2\ln^2\left(x^2\right)}, \tag{4.327}$$

and

$$\epsilon_3 = 4\left(\frac{M_{\rm Pl}}{\phi_0}\right)^2 \frac{1+\ln\left(x^2\right)}{x^2\ln^2\left(x^2\right)} \frac{4+3\ln\left(x^2\right)+\ln^2\left(x^2\right)+\ln^3\left(x^2\right)}{2+\ln\left(x^2\right)+\ln^2\left(x^2\right)}. \tag{4.328}$$

They are displayed in the bottom panels of Fig. 39. The first slow-roll parameter ϵ_1 diverges when $x \to 0$, decreases with x, vanishes at $x_{V'=0}$ and then increases with x and diverges when $x \to x_{V=0}$. As a consequence, inflation stops by slow-roll violation at a point $x_{\rm end}$ where $\epsilon_1 = 1$ that needs to be determined numerically. The second slow-roll parameter ϵ_2 has the same kind of behavior, except that it has a non-vanishing minimum located at a point $x_{\epsilon_2^{\rm min}}$, which is such that $0 < x_{\epsilon_2^{\rm min}} < x_{V=0}$. An analytic expression for $x_{\epsilon_2^{\rm min}}$ can be derived but it does not add much to the discussion. It yields $\epsilon_2^{\rm min} \simeq 20.65\, M_{\rm Pl}^2/\phi_0^2$. This means that in order for a slow-roll inflationary regime to take place, $\epsilon_2^{\rm min} \ll 1$ requires that the parameter ϕ_0 be sufficiently super-Planckian. Finally, the third slow-roll parameter has the same behavior as the two previous ones, except that it has a negative minimum $\epsilon_3^{\rm min} \simeq -0.2733\, M_{\rm Pl}^2/\phi_0^2$, located between $x_{\epsilon_2^{\rm min}}$ and $x_{V'=0}$ where it vanishes.

Let us now turn to the slow-roll trajectory. It can be integrated, and gives rise to

$$N_{\rm end} - N = \frac{1}{4}\left(\frac{\phi_0}{M_{\rm Pl}}\right)^2 \left[x^2 - \frac{1}{e}\,{\rm Ei}\left(1+\ln x^2\right) - x_{\rm end}^2 + \frac{1}{e}\,{\rm Ei}\left(1+\ln x_{\rm end}^2\right)\right], \tag{4.329}$$

where Ei is the exponential integral function [204, 205] and $N_{\rm end}$ is the number of e-folds at the end of inflation. This trajectory can only be inverted numerically to obtain $\phi(N)$.

Finally, it is interesting to constrain the value of the scale M with the CMB normalization. It follows that

$$\left(\frac{M}{M_{\rm Pl}}\right)^4 = 2880\pi^2 \left(\frac{M_{\rm Pl}}{\phi_0}\right)^2 \frac{\left[1+\ln\left(x_*^2\right)\right]^2}{x_*^4\left|\ln\left(x_*^2\right)\right|^3} \frac{Q_{\rm rms-PS}^2}{T^2}. \tag{4.330}$$

The reheating consistent slow-roll predictions of the open string tachyonic inflation models are displayed in Fig. 109. It is interesting to notice that, as expected, these models are compatible with the CMB data only for super-Planckian values of ϕ_0, $\phi_0/M_{\rm Pl} \gg 1$. In this limit, one has $x_{\rm end} \simeq \sqrt{2}M_{\rm Pl}/\phi_0$, the quadratic terms in the slow roll trajectory Eq. (4.329) dominate over the exponential integral ones, such that one has $x_* \simeq 2M_{\rm Pl}/\phi_0\sqrt{\Delta N_* + \frac{1}{2}}$. It follows that

$$\epsilon_{1*} \simeq \frac{1}{2\Delta N_* + 1}, \qquad \epsilon_{2*} \simeq \epsilon_{3*} \simeq 2\epsilon_{1*}, \tag{4.331}$$

hence

$$r \simeq \frac{16}{2\Delta N_* + 1}\,, \qquad 1 - n_{\rm S} \simeq \frac{4}{2\Delta N_* + 1}\,, \quad \text{and} \quad \alpha_{\rm S} \simeq -\frac{8}{(2\Delta N_* + 1)^2}\,. \tag{4.332}$$

One can check that indeed, in the $\phi_0/M_{\rm Pl} \gg 1$ limit, the prediction points lie in the line $\epsilon_2 = 2\epsilon_1$, or equivalently, $1 - n_{\rm S} = r/4$.

Finally, let us close this section by some additional considerations on the difficulties that tachyonic inflation faces [434]. Using the above equations, it is easy to show that

$$\left(\frac{M}{M_{\rm Pl}}\right)^4 \simeq \frac{2880\pi^2}{16\Delta N_*}\frac{Q^2_{\rm rms-PS}}{T^2}\frac{\phi_0^2}{M_{\rm Pl}^2}\frac{\left[5 - 2\ln(\phi_0/M_{\rm Pl})\right]^2}{\left[4 - 2\ln\left(\phi_0/M_{\rm Pl}\right)\right]^3} \ll 1. \tag{4.333}$$

Given that $T_3 \simeq M^4$, this implies that $g_{\rm s}^3 \ll v^2$. On the other hand, we have seen that the model is compatible with the CMB data only if $\phi_0/M_{\rm Pl} = (g/v)^{1/2} \gg 1$. This last inequality is consistent with $g_{\rm s}^3 \ll v^2$ only if $v \ll 1$. But $v \ll 1$ is in contradiction with the assumption that $r \gg \ell_{\rm s}$, which implies that $v \gg 1$. Therefore, it seems that the constraints obtained from the CMB data invalidates the use of an effective four-dimensional approach to describe tachyonic inflation [434]. On the other hand, this can also justify our approach which just considers this scenario as a phenomenological model.

4.23 Witten-O'Raifeartaigh Inflation (WRI)

4.23.1 Theoretical Justifications

This model arises in different contexts and we now briefly review one of its theoretical motivation. The first situation originates from supersymmetric theories aimed at explaining the gauge hierarchy problem (that is to say why the GUT scale differs so much from the weak scale). In the supersymmetric scenario of Ref. [438], three chiral superfields A, X and Y are considered in a superpotential of the O'Raifeartaigh type [439],

$$W = \lambda X(A^2 - m^2) + gYA, \tag{4.334}$$

where m and g are constant of mass dimension. The corresponding (global) supersymmetric potential can be expressed as

$$V = \lambda^2|A^2 - m^2|^2 + g^2|A|^2 + |2\lambda XA + gY|^2. \tag{4.335}$$

The minimum of this potential is given by $\langle Y\rangle = -2\lambda\langle X\rangle\langle A\rangle/g$ and $\langle A\rangle = 0$ [there is also another minimum at $\langle A\rangle = \sqrt{m^2 - g^2/(2\lambda^2)}$]. Clearly, the potential is minimized regardless of $\langle X\rangle$, that is to say we have a flat direction along X. Along that direction, $V = \lambda^2 m^4$ and supersymmetry is broken since $F_X \equiv \partial W/\partial X \neq 0$. As a consequence, the mass of the real part and imaginary parts of A are split and are given by $4\lambda^2|X|^2 + g^2 \pm 2m^2\lambda^2$. The mass of the fermion field ψ_A is $4\lambda^2|X|^2 + g^2$. The fact that supersymmetry is broken implies that the potential will receive corrections: as is well-known, if supersymmetry is preserved, the corrections originating from bosons and fermions exactly cancel out. Here, this is not the case and the amplitude of the corrections will be determined by the split between the bosonic and fermionic masses that we have just evaluated before. A simple calculation leads to

$$V = \lambda^2 m^4\left[1 + \frac{\lambda^2}{8\pi^2}\ln\left(\frac{|X|^2}{\mu^2}\right)\right], \tag{4.336}$$

where μ is the renormalization scale. Therefore, one obtains an increasing function of the field *vev* and this implies that X cannot become large because it cannot climb its potential. As a consequence, one cannot generate a large hierarchy in this scenario. In fact, as explained in Ref. [438], this is due to the fact that the one loop correction is positive, as appropriate in a theory with scalars and fermions. This can also be understood from the renormalization group perspective where the appearance of the logarithm in the above expression of $V(X)$ can be viewed as the renormalization of the coupling constant such that $\lambda^2 \to \lambda^2\left[1+\lambda^2/(8\pi^2)\ln\left(|X|^2/\mu^2\right)\right]$. The conclusion of Ref. [438] is that if m is the small scale (the weak scale) and $\langle X\rangle$ the large one (the GUT scale), a large hierarchy cannot be achieved in this approach.

However, it is well-known that asymptotic freedom is possible in non-Abelian gauge theories. This means that the renormalization group equations have to produce *negative* one loop corrections. In such a situation, the field could run to infinity, in the non-perturbative regime. For this reason, it is interesting to re-consider the previous model in the framework of a non-Abelian gauge group such as in Grand Unified SU(5) theories. Refs. [440, 441] consider two matter fields A_a^b and Z_a^b in the adjoint representation of SU(5) and one singlet X in a superpotential given by

$$W = \lambda_1 \mathrm{Tr}(ZA^2) + \lambda_2 X\left[\mathrm{Tr}\left(A^2\right) - m^2\right], \tag{4.337}$$

which is the non-Abelian generalization of Eq. (4.334). One can show that supersymmetry is again necessarily broken[5] and that the potential exhibits a flat direction with the value $V = \lambda_1^2\lambda_2^2 m^4/(30\lambda_2^2+\lambda_1^2)$. As it was the case in the first simple example presented above, and since supersymmetry is broken, quantum corrections modify the potential. At the one loop order, one obtains the following expression [440]

$$V(X) = \frac{\lambda_1^2\lambda_2^2 m^4}{30\lambda_2^2+\lambda_1^2}\left(1+\frac{\lambda_2^2}{\lambda_2^2+\lambda_1^2/30}\frac{29\lambda_1^2-50g^2}{80\pi^2}\ln|X|^2\right), \tag{4.338}$$

where g is the SU(5) gauge coupling constant. If $29\lambda_1^2 < 50g^2$, the correction is *negative* contrary to the case studied before. Again, this is precisely because we deal with non-Abelian gauge interaction. The field X will grow and can reach a point where the perturbative approach is no longer valid. However, asymptotic freedom tells us that the potential could develop a minimum in this regime in which X could be stabilized, hence the original motivation for this scenario: the scale m can be taken to be relatively small while $\langle X\rangle$ can now be very large thereby addressing the gauge hierarchy problem.

This class of model was considered in Ref. [442] in order to build a new inflationary scenario. The idea is to start from a potential of the form derived above, namely $V(\phi) = M^4\left(1+\tilde{b}\ln\phi\right)$ with a negative coefficient $\tilde{b}$. Therefore, the field is driven towards a regime where higher corrections must become important. Typically, one expects $\tilde{b}$ to acquire a

[5] For this purpose, it is convenient to write that $A_d^c = (\phi_A)_a^b\,(T_b^a)_d^c$ and $Z_d^c = (\phi_Z)_a^b\,(T_b^a)_d^c$, where T_a^b, $a,b=1,\cdots,5$ is a basis of SU(5) generators. Concretely, one has $(T_b^a)_d^c = \delta_b^c\delta_d^a - \delta_b^a\delta_d^c/5$. As a consequence, the three F-term can be expressed as $F_X = \lambda_2\left[\mathrm{Tr}\left(\phi_A^2\right) - m^2\right]$, $F_Z = \lambda_1\left[\phi_A^2 - \mathrm{Tr}\left(\phi_A^2\right)\mathbb{1}/5\right]$ and $F_A = \lambda_1\left[\phi_Z\phi_A + \phi_A\phi_Z - 2\mathrm{Tr}\left(\phi_Z\phi_A\right)\mathbb{1}/5\right] + 2\lambda_2\phi_X\phi_A$. These expressions are obtained by explicitly writing the superpotential in terms of the components $(\phi_A)_b^a$ and $(\phi_Z)_b^a$ and differentiating W with respect to them. From $F_X = 0$ it follows that $\mathrm{Tr}\left(\phi_A^2\right) = m^2$ and, therefore, $F_Z = 0$ implies that $\phi_A^2 = m^2\mathbb{1}/5$. This last relation is compatible with $\mathrm{Tr}\left(\phi_A^2\right) = m^2$ but not with $\mathrm{Tr}\left(\phi_A\right) = 0$ in five dimensions. The conditions $F_X = 0$ and $F_Z = 0$ are thus incompatible and supersymmetry is spontaneously broken in this model.

logarithmic dependence in ϕ and the potential to develop a minimum at, say $\phi = m_{\rm GUM}$. Therefore, this leads to $V(\phi) = M^4\left[1 + b\ln^2(\phi/m_{\rm GUM})\right]$ where b is a constant. Moreover, if one requires the potential to vanish at the minimum, we are led to $V(\phi) \propto \ln^2(\phi/m_{\rm GUM})$ and this is the potential studied in this section. In Ref. [442], it is argued that $m_{\rm GUM} \simeq M_{\rm Pl}$ and that, initially, $\phi \simeq \mu \simeq (m_{\rm weak}m_{\rm GUM})^{1/2} \simeq 10^{12}$GeV. We will come back to these conditions in what follows.

Another way to obtain the same potential is based on Ref. [443, 444] in which one consider the following action

$$S = -\int \mathrm{d}^4\boldsymbol{x}\sqrt{-g}\left[\hat{g}_{A\bar{B}}\left(z^C, \bar{z}^{\bar{C}}\right) g^{\mu\nu}\partial_\mu z^A \partial_\nu \bar{z}^{\bar{B}} - V\left(z^C, \bar{z}^{\bar{C}}\right)\right]. \tag{4.339}$$

The z^A's are complex scalar fields and $\hat{g}_{A\bar{B}}$ is the Kähler metric. The corresponding equations of motion can be expressed as

$$g^{\mu\nu}\nabla_\mu\nabla_\nu\bar{z}^{\bar{D}} + \Gamma^{\bar{D}}_{\bar{A}\bar{B}} g^{\mu\nu}\partial_\mu\bar{z}^{\bar{A}}\partial_\nu\bar{z}^{\bar{B}} - \hat{g}^{C\bar{D}}\frac{\partial V}{\partial z^C} = 0, \tag{4.340}$$

where $\Gamma^{\bar{D}}_{\bar{A}\bar{B}} \equiv \hat{g}^{C\bar{D}}\partial_{\bar{A}}\hat{g}_{C\bar{B}}$. If we restrict ourselves to cosmological spacetimes, the above equation becomes $\ddot{\bar{z}}^{\bar{D}} + 3H\dot{z}^{\bar{D}} + \Gamma^{\bar{D}}_{\bar{A}\bar{B}}\dot{\bar{z}}^{\bar{A}}\dot{\bar{z}}^{\bar{B}} + \hat{g}^{C\bar{D}}\partial V/\partial z^C = 0$, where H is the Hubble parameter. Then, for simplicity, we assume that there is only one field Z and we denote its real part as u and its imaginary part as v. We also assume that the potential is flat in the v-direction and take $V = V(z + \bar{z})$, $\hat{g}_{Z\bar{Z}} \equiv \hat{g}(Z + \bar{Z})$. It follows that

$$\ddot{u} + 3H\dot{u} + \Gamma(u)\left(\dot{u}^2 - \dot{v}^2\right) + \partial_u V/(2\hat{g}) = 0, \tag{4.341}$$

$$\ddot{v} + 3H\dot{v} + 2\Gamma(u)\dot{u}\dot{v} = 0, \tag{4.342}$$

with $\Gamma = \partial_u\hat{g}/(2\hat{g})$. The second differential equation can be integrated and one obtains $\dot{v} = Qa^{-3}/\hat{g}$, where Q is a constant. The next step consists in defining the field ϕ by $\dot{\phi} \equiv \sqrt{\hat{g}}\dot{u}$. As a consequence, the first differential equation can be re-written as $\ddot{\phi} + 3H\dot{\phi} + \partial_\phi\left[V + Q^2/(\hat{g}a^6)\right] = 0$, that is to say ϕ is now canonically normalized and its evolution is controlled by the effective potential $V(\phi) + Q^2/(\hat{g}a^6)$. One can show that the presence of the additional term proportional to Q^2 is not crucial [443, 444]. Initially, it dominates because a is small but, quickly, since it is proportional to a^{-6}, it goes to zero as the universe expands. As a consequence, one is left with $V(\phi)$ only. A specific version of this scenario has been studied in details in Ref. [443]. In that article, it is assumed that $\hat{g} = e^{-2u}/2$ and $V = 0$. This corresponds to the bosonic action of a model which is superconformal invariant [445]. Then, this invariance is softly broken by adding a term $m^2u^2/2$ and, through the redefinition of the field, one can check that this leads to a potential proportional to $m^2\left(\ln\phi\right)^2$, that is to say of the type studied in this section. Moreover, one can also verifies that, in the regime discussed above where the term $Q^2/(\hat{g}a^6)$ dominates, an exact solution can be found and reads: $a = a_0t^{1/3}$ and $\phi^2(t) = E^2\left(\ln t + C\right)^2 + 4Q^2/(a_0^6E^2)$, where E and C are two integration constants. As a consequence, when the universe expands, $Q^2/(\hat{g}a^6)$ goes to zero and one is left with the logarithmic potential only.

4.23.2 Slow-Roll Analysis

Based on the previous considerations, we study the WRI potential

$$V(\phi) = M^4\ln^2\left(\frac{\phi}{\phi_0}\right), \tag{4.343}$$

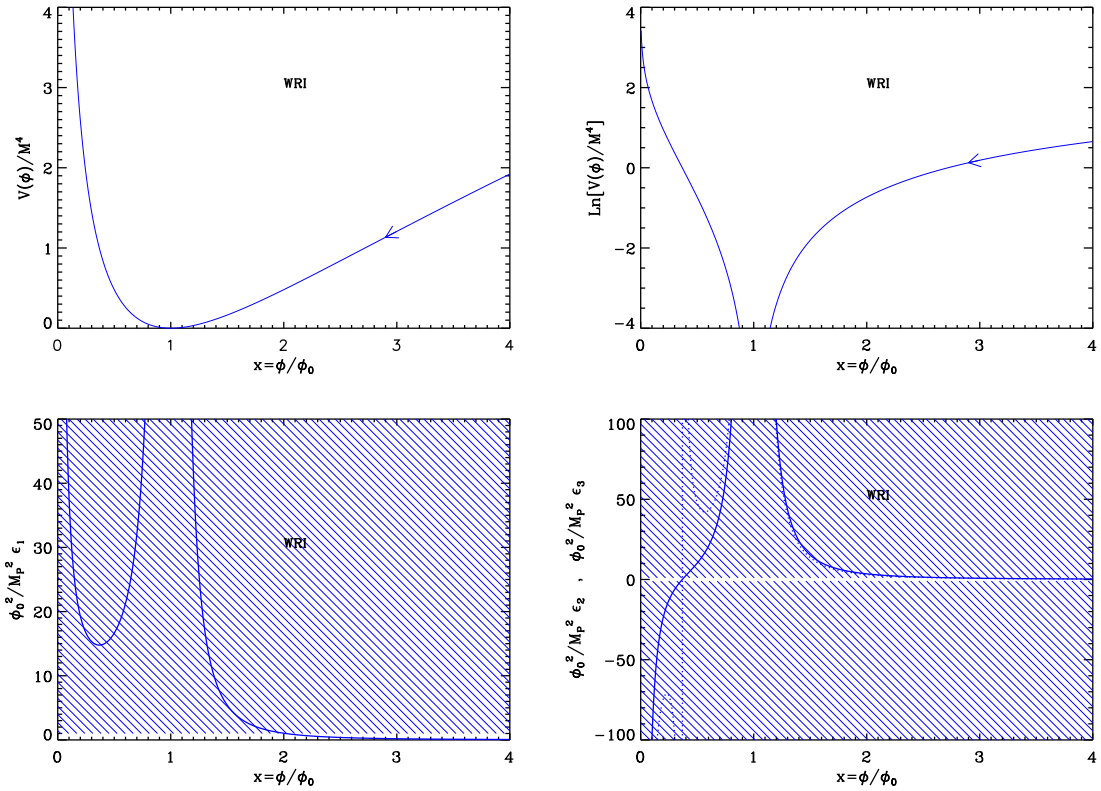

Figure 40. Witten-O'Raifeartaigh Inflation (WRI) potential as a function of ϕ/ϕ_0. Top right panel: logarithm of the potential. The arrow indicates in which direction inflation proceeds. Bottom left panel: slow-roll parameter ϵ_1, rescaled by the quantity $M_{\rm Pl}^2/\phi_0^2$, such that the corresponding expression becomes universal, i.e. independent of ϕ_0. Bottom right panel: slow-roll parameters ϵ_2 (solid line) and ϵ_3 (dotted line), rescaled by $M_{\rm Pl}^2/\phi_0^2$ for the same reason as mentioned before.

where ϕ_0 is viewed as a free parameter but we also keep in mind that a natural prior is $\phi_0 = M_{\rm Pl}$. The potential Eq. (4.343) is displayed in Fig. 40, together with its logarithm (top panels). The arrow indicates that inflation proceeds from the right to the left. Let us now calculate the Hubble flow parameters. If one defines $x \equiv \phi/\phi_0$, they are given by

$$\epsilon_1 = 2\frac{M_{\rm Pl}^2}{\phi_0^2}\frac{1}{x^2\ln^2 x}\,, \tag{4.344}$$

$$\epsilon_2 = 4\frac{M_{\rm Pl}^2}{\phi_0^2}\frac{1+\ln x}{x^2\ln^2 x}\,, \tag{4.345}$$

and

$$\epsilon_3 = 2\frac{M_{\rm Pl}^2}{\phi_0^2}\frac{2+3\ln x+2\ln^2 x}{x^2\ln^2 x\,(1+\ln x)}\,. \tag{4.346}$$

They are displayed in the bottom panels of Fig. 40. One can see that they all vanish when $x \to \infty$, that they increase as inflation proceed, diverging when $x \to 1$. At this stage, a remark is in order about Ref. [442]. As already mentioned above, a natural prior is $\phi_0 = M_{\rm Pl}$. This

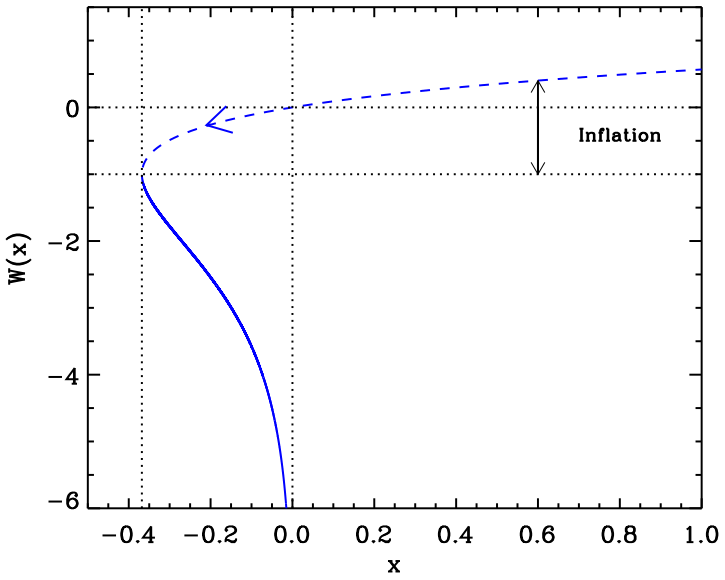

Figure 41. Lambert functions $\mathrm{W}_0(x)$ (dashed line) and $\mathrm{W}_{-1}(x)$ (solid line). During Witten-O'Raifeartaigh inflation, inflation proceeds along the "0" branch in the direction specified by the arrow.

means that if, initially, one has $\phi \simeq \mu$, one is in fact in the decreasing branch of the potential and, as a matter of fact, one cannot have inflation since $\epsilon_1 > 1$ always. Clearly, the only way to have inflation in this branch is to assume that $\phi_0 \gg M_{\rm Pl}$, a case which appears to be difficult to justify in this context. Here, we do not consider this case. In the increasing branch of the potential, inflation stops by slow-roll violation when $\epsilon_1 = 1$, at a *vev* $x_{\rm end}$ given by

$$x_{\rm end} = \exp\left[\mathrm{W}_0\left(\sqrt{2}\frac{M_{\rm Pl}}{\phi_0}\right)\right], \tag{4.347}$$

where W_0 is the 0-branch of the Lambert function, which must be chosen in order to have $x > 1$.

Let us now turn to the slow-roll trajectory. It can be integrated exactly and this leads to the following expression

$$N_{\rm end} - N = \frac{1}{4}\frac{\phi_0^2}{M_{\rm Pl}^2}\left(x^2\ln x - \frac{x^2}{2} - x_{\rm end}^2\ln x_{\rm end} + \frac{x_{\rm end}^2}{2}\right), \tag{4.348}$$

where $N_{\rm end}$ is the number of e-folds at the end of inflation. Interestingly enough, this trajectory can be inverted, and one obtains

$$x = \exp\left\{\frac{1}{2}\mathrm{W}_0\left[\frac{8}{e}\frac{M_{\rm Pl}^2}{\phi_0^2}\left(N_{\rm end} - N\right) + \frac{2}{e}x_{\rm end}^2\ln x_{\rm end} - \frac{x_{\rm end}^2}{e}\right] + \frac{1}{2}\right\}, \tag{4.349}$$

where W_0 is still the 0-branch of the Lambert function. It is displayed in Fig. 41, together with the region where inflation proceeds.

Finally, it is interesting to constrain the value of the scale M with the CMB normalization. It follows that

$$\left(\frac{M}{M_{\rm Pl}}\right)^4 = 2880\pi^2 \left(\frac{M_{\rm Pl}}{\phi_0}\right)^2 \frac{1}{x_*^2 \ln^4 x_*} \frac{Q^2_{\rm rms-PS}}{T^2}\,. \tag{4.350}$$

The reheating consistent slow-roll predictions of the Witten- O'Raifeartaigh inflation models are displayed in Fig. 110. One should remember that in principle, $\phi_0 \simeq M_{\rm Pl}$, even if a wider range of values for ϕ_0 is displayed in order to understand how the predictions depend on this parameter. In particular, when $\phi_0 \gg M_{\rm Pl}$, the predictions lie along the line $\epsilon_2 = 2\epsilon_1$. Indeed, in this limit, Eq. (4.347) shows that $x_{\rm end} \to 1$ while Eq. (4.349) indicates that $x_* \to 1$. As a consequence, one obtains $\epsilon_{2*} \simeq \epsilon_{1*}$ from Eqs. (4.344) and (4.345).

5 Two Parameters Models

5.1 Small Field Inflation (SFI)

This model is proto-typical of inflation occurring at the top of a flat-enough potential. As such it appears in very different contexts. It has been introduced in Ref. [2, 383] and derived in Ref. [3] in the context of radiatively induced symmetry breaking. It appears within superstring models [446], low scale symmetry breaking [254, 447], supersymmetry [338, 448] and supergravity [233, 234, 238, 253, 449–453]. It is also obtained in non-linear sigma models [264] or using moduli as inflatons [454]. It has been discussed in braneworld cosmology in Refs. [455–457] and is more recently referred to as "hilltop inflation" from Ref. [397, 398]. The potential is given by

$$V(\phi) = M^4 \left[1 - \left(\frac{\phi}{\mu}\right)^p\right], \tag{5.1}$$

and has two parameters in addition to the overall normalization M: a typical *vev* μ and the power index p. As this potential can be associated with very different physical frameworks, μ can take any values while $p > 0$ for being at the top of a potential (in the small field limit, namely $\phi \ll \mu$). In particular, we will allow super-Planckian values for μ even though, in the supergravity context, one would require $\mu < M_{\rm Pl}$. Let us stress that Eq. (5.1) is defined only in the domain $\phi < \mu$ as one assumes that the small field potential describes only the field dynamics during inflation. The equation of state during reheating is thus not specified by Eq. (5.1). Defining

$$x \equiv \frac{\phi}{\mu}\,, \tag{5.2}$$

the first three Hubble flow functions read

$$\epsilon_1 = \frac{p^2}{2}\left(\frac{M_{\rm Pl}}{\mu}\right)^2 \frac{x^{2p-2}}{\left(1-x^p\right)^2}\,, \qquad \epsilon_2 = 2p\left(\frac{M_{\rm Pl}}{\mu}\right)^2 x^{p-2}\frac{p-1+x^p}{\left(1-x^p\right)^2}\,, \tag{5.3}$$

and

$$\epsilon_3 = p\left(\frac{M_{\rm Pl}}{\mu}\right)^2 \frac{x^{p-2}\left[2x^{2p}+(p-1)(p+4)x^p+(p-1)(p-2)\right]}{\left(1-x^p\right)^2\left(p-1+x^p\right)}\,. \tag{5.4}$$

They are monotonic functions of the field value but also decreasing functions of the *vev* μ. The potential, its logarithm and the Hubble flow functions are represented in Fig. 42.

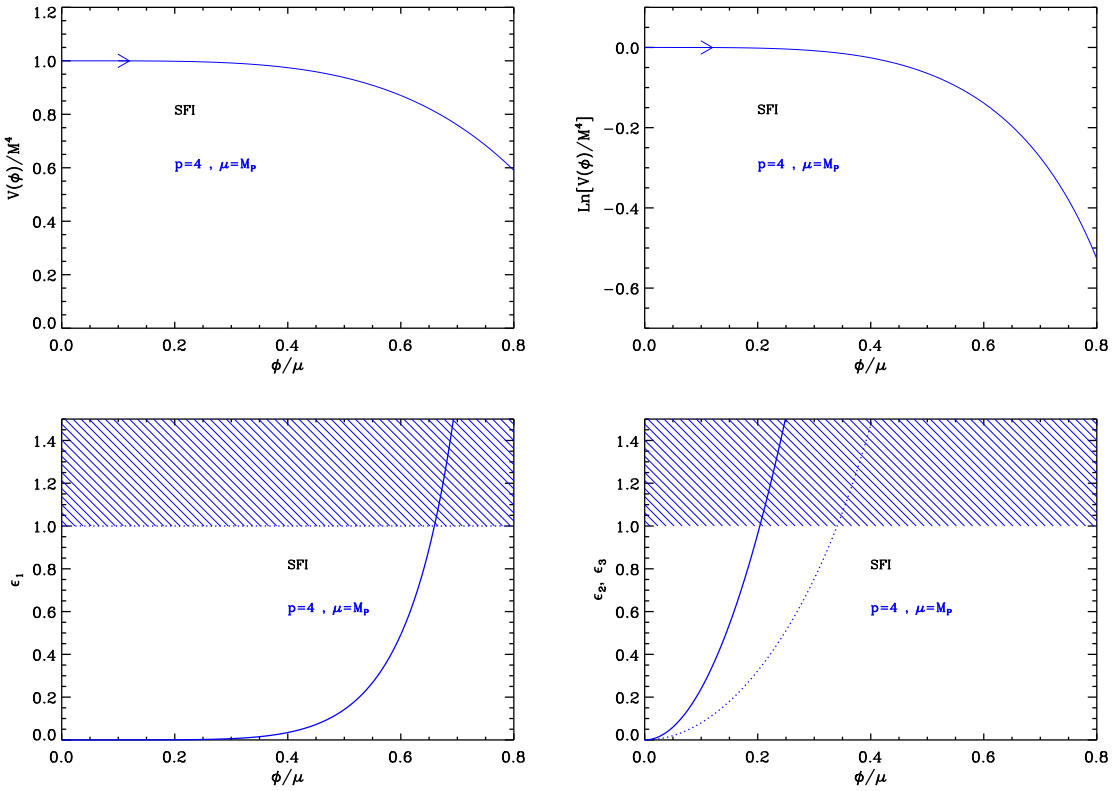

Figure 42. Small Field Inflation (SFI) for $p = 4$ and $\mu = M_{\rm Pl}$. Upper panels: the potential and its logarithm as a function of ϕ/μ. Bottom left panel: slow-roll parameter ϵ_1, the shaded area indicates where inflation stops. Bottom right panel: slow-roll parameters ϵ_2 (solid line) and ϵ_3 (dotted line).

The slow-roll trajectory is obtained by integrating Eq. (2.11) to get

$$N - N_{\rm end} = \frac{1}{2p}\frac{\mu^2}{M_{\rm Pl}^2}\left[-x^2 + x_{\rm end}^2 + \frac{2}{2-p}\left(x^{2-p} - x_{\rm end}^{2-p}\right)\right]. \tag{5.5}$$

This equation seems to be well-defined only for $p \neq 2$. However, the particular case $p = 2$ can be directly obtained from Eqs. (2.11) and (5.1) to get

$$N - N_{\rm end} = \frac{1}{4}\frac{\mu^2}{M_{\rm Pl}^2}\left[-x^2 + x_{\rm end}^2 + 2\ln\left(\frac{x}{x_{\rm end}}\right)\right]. \tag{5.6}$$

This expression can also be viewed as the limit of Eq. (5.5) for $p \to 2$. In general, the trajectory cannot be analytically inverted to give the field value $x(N)$ but one can find some analytic form for almost all integer values of p (e.g. for $p = 1$, $p = 2$, $p = 3$, $p = 4$, $p = 6$) that we do not write down for the sake of clarity.

From the potential Eq. (5.1), inflation can stop naturally at $\epsilon_1(x_{\rm end}) = 1$ with $x_{\rm end} < 1$. This condition gives the algebraic equation

$$x_{\rm end}^p + \frac{p}{\sqrt{2}}\frac{M_{\rm Pl}}{\mu}x_{\rm end}^{p-1} = 1, \tag{5.7}$$

which cannot be solved analytically in full generality. As for the trajectory, there are however explicit solutions for almost all integer values of p, the first two being

$$x_{\rm end}^{(p=1)} = 1 - \frac{M_{\rm Pl}}{\sqrt{2}\mu}, \qquad x_{\rm end}^{(p=2)} = \frac{M_{\rm Pl}}{\sqrt{2}\mu}\left(-1 + \sqrt{1 + 2\frac{\mu^2}{M_{\rm Pl}^2}}\right). \tag{5.8}$$

Together with Eq. (2.47), these equations are enough to allow the determination of the field value x_* at which the observable modes crossed the Hubble radius during inflation. This fixes the value of the parameter M to match the observed amplitude of the CMB anisotropies at

$$\frac{M^4}{M_{\rm Pl}^4} = 720\pi^2 p^2 \frac{M_{\rm Pl}^2}{\mu^2}\frac{x_*^{2p-2}}{\left(1 - x_*^p\right)^3}\frac{Q_{\rm rms-PS}^2}{T^2}. \tag{5.9}$$

The reheating consistent slow-roll predictions for the small field models are represented in Figs. 111 to 113 for $p = 1$, $p = 2$ and $p = 4$. The $p = 1$ case is trivial since one then has $\epsilon_{2*} = 4\epsilon_{1*}$. For $p = 2$ or $p = 4$, one sees that the reheating temperature is limited from below to fit in the observable range. For instance, with $p = 2$, values of μ such that $\mu/M_{\rm Pl} < 10$ are clearly disfavored. Let us notice that the relation $\epsilon_{2*} = 4\epsilon_{1*}$ is recovered in the limit $\mu/M_{\rm Pl} \gg 1$ whereas one clearly observes a systematic shift in $n_{\rm S}$ (or ϵ_2) when $\mu \ll M_{\rm Pl}$. These behaviors can in fact be understood analytically.

Small field models in the supergravity context are commonly studied in the limit $\mu \ll M_{\rm Pl}$. In this situation it is possible to find some approximate solution to both the trajectory and $x_{\rm end}$. Keeping only the dominant term in Eq. (5.7), one gets

$$x_{\rm end}^{(p\neq1)} \simeq \left(\frac{\sqrt{2}}{p}\frac{\mu}{M_{\rm Pl}}\right)^{1/(p-1)}, \tag{5.10}$$

the case $p \leq 1$ being incompatible with the limit $\mu \ll M_{\rm Pl}$ and the consistency requirement that $x_{\rm end} < 1$. The small *vev* limit can also be used to invert Eq. (5.5). Assuming $\mu \ll M_{\rm Pl}$ and $x_{\rm end} \ll 1$, neglecting the quadratic terms for $p > 1$, the approximate trajectory reads

$$N - N_{\rm end} \simeq \frac{\mu^2}{M_{\rm Pl}^2}\frac{x^{2-p} - x_{\rm end}^{2-p}}{p(2-p)}, \tag{5.11}$$

which can be inverted to

$$x \simeq \left[x_{\rm end}^{2-p} - \frac{M_{\rm Pl}^2}{\mu^2}p(2-p)\left(N_{\rm end} - N\right)\right]^{1/(2-p)}. \tag{5.12}$$

Notice that far from the end of inflation, i.e. $N \ll N_{\rm end}$, the first term can be neglected (for $p > 2$) since $x_{\rm end} < 1$ and $M_{\rm Pl}/\mu \gg 1$. Defining $\Delta N_* = N_{\rm end} - N_*$, one can now plug this expression for x_* into the Hubble flow functions of Eqs. (5.3) and (5.4) to get their observable values:

$$\epsilon_{1*} \simeq \frac{p^2}{2}\left(\frac{M_{\rm Pl}}{\mu}\right)^2\left[\Delta N_* p(p-2)\left(\frac{M_{\rm Pl}}{\mu}\right)^2\right]^{-\frac{2(p-1)}{p-2}}, \qquad \epsilon_{2*} \simeq \frac{2}{\Delta N_*}\frac{p-1}{p-2}, \qquad \epsilon_{3*} \simeq \frac{1}{\Delta N_*}. \tag{5.13}$$

It is crucial to keep in mind that the above formulas are valid only in the limit $\mu \ll M_{\rm Pl}$ and $p > 2$. As before, the limiting case $p \to 2$ has to be taken with care and, starting with Eq. (5.6), one obtains

$$\epsilon_{1*}^{(p=2)} = \exp\left(-4\frac{M_{\rm Pl}^2}{\mu^2}\Delta N_*\right), \qquad \epsilon_{2*}^{(p=2)} = 4\frac{M_{\rm Pl}^2}{\mu^2}, \qquad \epsilon_{3*}^{(p=2)} = 6\epsilon_{1*}^{(p=2)}. \tag{5.14}$$

Both Eqs. (5.13) and (5.14) describes the observed behavior in Figs. 111 to 113 when $\mu/M_{\rm Pl} \to 0$ but they do fail in the intermediate region as we have discussed in the introduction (see Fig. 3).

If the theoretical motivations underlying the potential 5.1 do not require the *vev* to be small, one can similarly derive approximate expressions for the observables in the limit $\mu/M_{\rm Pl} \gg 1$ (but still with $x < 1$). Defining $\varepsilon \equiv M_{\rm Pl}/\mu$, one has $x_{\rm end}(\varepsilon)$ and we can search for a Taylor expanded solution of Eq. (5.7) to get

$$x_{\rm end} = 1 - \frac{\varepsilon}{\sqrt{2}} + \frac{p-1}{4}\varepsilon^2 + \mathcal{O}\left(\varepsilon^3\right). \tag{5.15}$$

Similarly one can search for a Taylor expanded solution for the trajectory Eq. (5.5), plugging in the previous expression for $x_{\rm end}$. Doing so yields

$$x_* = 1 - \varepsilon\sqrt{\frac{1}{2} + 2\Delta N_*} + \mathcal{O}\left(\varepsilon^2\right). \tag{5.16}$$

From this, one gets the corresponding Hubble flow functions

$$\epsilon_{1*} \simeq \frac{1}{4\Delta N_* + 1} \qquad \epsilon_{2*} \simeq 4\epsilon_{1*}, \qquad \epsilon_{3*} \simeq \epsilon_1\,. \tag{5.17}$$

This result is quite remarkable since the observable slow-roll parameters become μ and p independent. Performing the same calculation in the singular case $p \to 2$ yields exactly the same result. The spectral index, tensor-to-scalar ratio and running are immediately obtained from Eq. (5.17) with $r = 16\epsilon_{1*}$, $n_{\rm S} - 1 \simeq -3r/8$ and $\alpha \simeq -r$. Again, these expressions match with Figs. 111 to 113 when $\mu/M_{\rm Pl} \to \infty$.

5.2 Intermediate Inflation (II)

This model was introduced in Refs. [458–461] as an implementation of an equation of state of the form

$$\rho + p = \gamma\rho^{\lambda}\,, \tag{5.18}$$

where ρ stands for the energy density and p the pressure. Both $\gamma > 0$ and $\lambda > 1$ are dimensionless constants. As will be made explicit, this equation of state leads to a scale factor which is given by $a(t) \propto \exp\left(At^f\right)$ where $0 < f < 1$. In some sense the expansion is thus faster than power law but slower than de Sitter, hence the name of the model. The pure de Sitter case corresponds to $f = 1$. Inserting the Friedmann-Lemaître equation, $3M_{\rm Pl}^2H^2 = \rho$ as well as the equation of state Eq. (5.18) into the equation of conservation $\dot{\rho}+3H\left(\rho + p\right) = 0$, one obtains a closed equation for ρ which is solved by

$$\rho = \rho_0\left[3\gamma\left(\lambda - 1\right)\ln\left(\frac{a}{a_0}\right)\right]^{1/(1-\lambda)}, \tag{5.19}$$

where ρ_0 and a_0 are positive constants. Making use of the Friedmann-Lemaître equation again, one deduces the behavior for a,

$$\ln\left(\frac{a}{a_0}\right) = 3^{\lambda/(1-2\lambda)}\gamma^{1/(1-2\lambda)}\frac{\left(\lambda-\frac{1}{2}\right)^{(1-\lambda)/(1-2\lambda)}}{\lambda-1}\left(\frac{t}{t_0}\right)^{(1-\lambda)/(1-2\lambda)}, \tag{5.20}$$

i.e. the announced form $a(t) \propto \exp\left(At^f\right)$, with $f = 2(1-\lambda)/(1-2\lambda)$. Since $\lambda > 1$, this means that $0 < f < 1$. Then, one can notice that it is possible to reinterpret the matter source as that of a scalar field with the potential $V(\phi)$ given by

$$\begin{aligned} V(\phi) = {} & 3A^2f^2M_{\rm Pl}^4\left[\frac{\phi-\phi_0}{M_{\rm Pl}\sqrt{8A\left(f^{-1}-1\right)}}\right]^{4(1-1/f)} \\ & - M_{\rm Pl}^4Af\left(1-f\right)\left[\frac{\phi-\phi_0}{M_{\rm Pl}\sqrt{8A\left(f^{-1}-1\right)}}\right]^{2-4/f}. \end{aligned} \tag{5.21}$$

Indeed, starting from this potential, the Klein-Gordon equation with $H = Aft^{f-1}$, has an exact non-trivial solution given by

$$\phi = \phi_0 + M_{\rm Pl}\sqrt{8A\left(f^{-1}-1\right)}\left(\frac{t}{t_0}\right)^{f/2}. \tag{5.22}$$

It is then straightforward to calculate $\rho = \dot{\phi}^2/2 + V$ and $p = \dot{\phi}^2/2 - V$, and to show that they satisfy the equation of state Eq. (5.18). The potential can be recast in the form

$$V(\phi) = M^4\left(\frac{\phi-\phi_0}{M_{\rm Pl}}\right)^{-\beta} - M^4\frac{\beta^2}{6}\left(\frac{\phi-\phi_0}{M_{\rm Pl}}\right)^{-\beta-2}, \tag{5.23}$$

with $\beta = 4(1/f-1)$. The constraint $0 < f < 1$ means that $\beta > 0$. Defining

$$x \equiv \frac{\phi-\phi_0}{M_{\rm Pl}}, \tag{5.24}$$

it is shown below that the model predictions do not depend on ϕ_0. Therefore Intermediate Inflation is a priori a one parameter family of models, but as explained below, one needs an extra parameter $x_{\rm end}$ specifying the field value at which an unspecified mechanism is triggered to end of inflation. It is thus a two parameters model.

This potential appears in the earlier work of Ref. [462] as a solution for a cosmological model containing a string creation term. It is also discussed in the context of tachyon fields in Refs. [463, 464]. Warm intermediate inflation was considered in Refs. [465, 466], intermediate inflation within a Gauss-Bonnet braneworld was studied in Ref. [467], and with Jordan-Brans-Dicke theory in Refs. [468, 469].

The potential (5.23), as well as its logarithm, are displayed in Fig. 43. It is positive definite for $x > x_{V=0} \equiv \beta/\sqrt{6}$. Therefore, one must restrict the inflaton *vev* to lie beyond this value. The potential increases with x, reaches a maximum at $x_{V'=0} \equiv \sqrt{\beta(\beta+2)/6}$, then decreases with x to asymptotically vanish when x goes to infinity. Therefore, a priori, two regimes of inflation exist. Either inflation proceeds at $x < x_{V'=0}$ from the right to the left, either it proceeds at $x > x_{V'=0}$ from the left to the right. However, in Eq. (5.22), one can see that the inflaton *vev* has to increase with time. Therefore only the branch $x > x_{V'=0}$

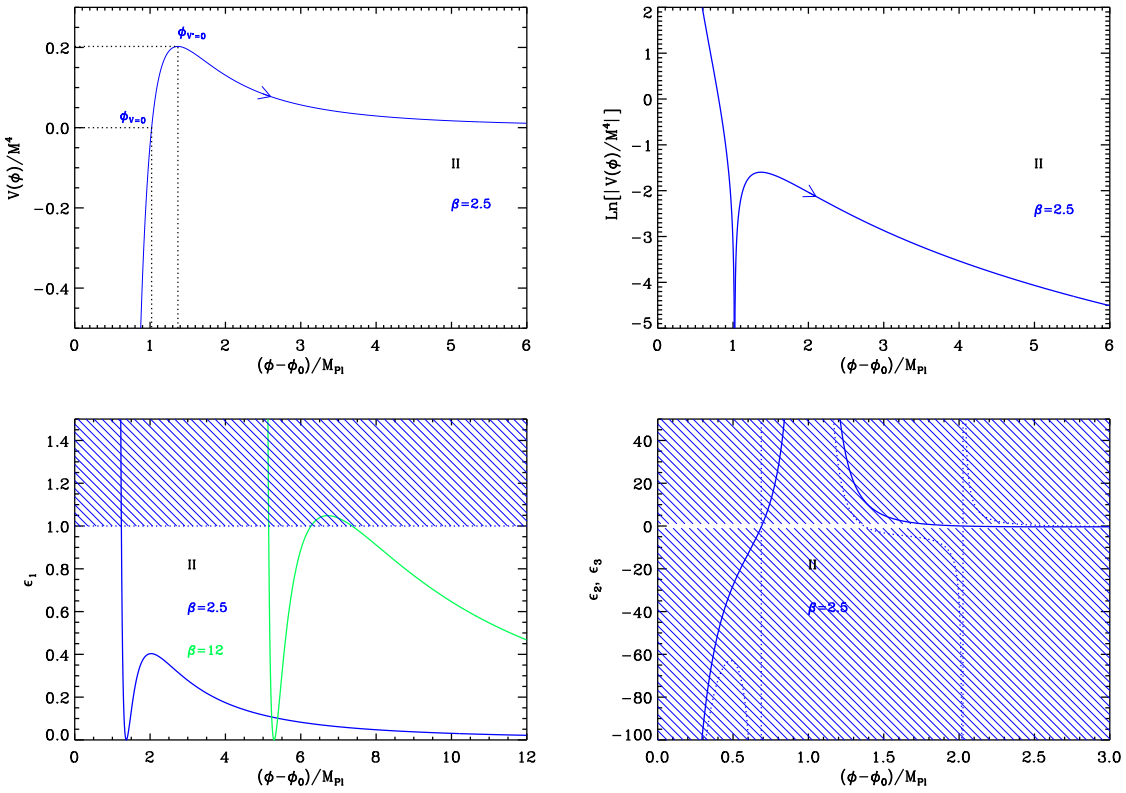

Figure 43. Intermediate Inflation (II). Upper panels: the potential and its logarithm for $\beta = 2.5$. Bottom left panel: slow-roll parameter ϵ_1 for a potential with $\beta = 2.5$ and $\beta = 12$. The position of the maximum of ϵ_1 with respect to one depends on β. The shaded area indicates where inflation stops.. Bottom right panel: slow-roll parameters ϵ_2 (solid line) and ϵ_3 (dotted line) for a potential with $\beta = 2.5$.

can produce an equation of state of the form of Eq. (5.18), which is where the model will be studied in the following.

Let us now turn to the slow-roll parameters. The first three Hubble flow functions in the slow-roll approximation are given by

$$\epsilon_1 = \frac{1}{2}\left[\frac{\beta^2(\beta+2) - 6\beta x^2}{-\beta^2 x + 6x^3}\right]^2, \qquad \epsilon_2 = \frac{-2\beta x^4 + \frac{\beta^2}{3}(2\beta+6)\,x^2 - \frac{\beta^4}{18}(\beta+2)}{\left(x^3 - \frac{\beta^2 x}{6}\right)^2}, \tag{5.25}$$

and

$$\epsilon_3 = \frac{\beta\left[6x^2 - \beta(2+\beta)\right]\left[\frac{\beta^5}{18}(2+\beta) - \beta^3(2+\beta)\,x^2 + 6\beta(4+\beta)\,x^4 - 12x^6\right]}{\left(x^3 - \frac{\beta^2}{6}x\right)^2\left[\beta^3(\beta+2) - 12\beta(\beta+3)\,x^2 + 36x^4\right]}. \tag{5.26}$$

They are displayed in Fig. 43. The first slow-roll parameter diverges where the potential vanishes at $x_{V=0}$, decreases from here and vanishes at the maximum of the potential $x_{V'=0}$.

Then it increases again, reaches a local maximum at $x_{\epsilon_1^{\max}}$, and decreases to asymptotically vanish when x goes to infinity. The location $x_{\epsilon_1^{\max}}$ is given by

$$x_{\epsilon_1^{\max}} = \sqrt{\frac{\beta}{2}\left(1+\frac{\beta}{3}+\sqrt{1+\frac{4\beta}{9}}\right)}\,. \tag{5.27}$$

At this point, the maximum value of ϵ_1 is

$$\epsilon_1^{\max} = \frac{\beta}{9}\frac{\left(1+3\sqrt{1+4\beta/9}\right)^2}{\left(1+\sqrt{1+4\beta/9}\right)^2\left(1+\beta/3+\sqrt{1+4\beta/9}\right)}\,. \tag{5.28}$$

If $\beta < 9/2\left(1+\sqrt{2}\right) \simeq 10.86$, this maximum value is smaller than one. In this case inflation cannot stop by slow-roll violation in the decreasing branch of the potential and an extra parameter $x_{\rm end}$ must be added to the model to specify the location where another mechanism such as e.g. tachyonic instability could trigger the end of inflation. If $\beta > 9/2\left(1+\sqrt{2}\right) \simeq 10.86$, the local maximum value of ϵ_1 is higher than one and in the decreasing branch of the potential, either inflation takes place between $x_{V'=0}$ and the first solution of $\epsilon_1 = 1$, either it takes place between the second solution of $\epsilon_1 = 1$ and $x = \infty$. As will be shown below, only the latter case is consistent with the exact trajectory Eq. (5.22) which allows for an equation of state of the form of Eq. (5.18).

The slow-roll trajectory of the model can be obtained from Eq. (2.11). However, as already mentioned, a non-trivial and exact field evolution is given by Eq. (5.22). Written in terms of the number of e-folds $N - N_0 = \ln(a/a_0) = A(t^f - t_0^f)$, one obtains

$$x = \sqrt{x_{\rm end}^2 + 2\beta\left(N - N_{\rm end}\right)}\,. \tag{5.29}$$

This expression is exact and does not involve any approximations. It can be compared to slow-roll trajectory which reads

$$N_{\rm end} - N = \frac{1}{2\beta}\left(x_{\rm end}^2 - x^2\right) + \frac{1}{6}\ln\left[x_{\rm end}^2 - \frac{\beta\left(\beta+2\right)}{6}\right] - \ln\left[x^2 - \frac{\beta\left(\beta+2\right)}{6}\right], \tag{5.30}$$

where $N_{\rm end}$ is the number of e-folds at the end of inflation and N is the number of e-folds at some point when the scaled field *vev* is x. As mentioned above, the slow-roll trajectory should match the exact one in the decreasing branch of the potential. For $x \to \infty$, one can neglect the logarithmic terms in Eq. (5.30) and one indeed recovers Eq. (5.29). This is expected since in this limit, the slow-roll parameters all go to zero and the slow-roll approximation becomes increasingly accurate. As a result, the domain of validity lies at $x \gg x_{V'=0}$, i.e. between the second solution of $\epsilon_1 = 1$ and $x = \infty$ and inflation cannot stop by slow-roll violation. This justifies the need of the extra-parameter $x_{\rm end}$. This parameter is thus constrained to $x_{\rm end} > x_{V'=0}$ and should be large enough to allow for a sufficient number of e-folding. In order to get $N_{\rm end} - N_{\rm ini}$ e-folds, making use of Eq. (5.29), one gets

$$x_{\rm end} = \sqrt{x_{\rm ini}^2 + 2\beta(N_{\rm end} - N_{\rm ini})}\,. \tag{5.31}$$

If $\beta > 9/2\left(1+\sqrt{2}\right) \simeq 10.86$, $x_{\rm ini}$ is bounded from below by the highest solution of the equation $\epsilon_1 = 1$. This equation admits three solutions which, from the smallest to the

biggest, are given by

$$x^{0}_{\epsilon_1=1} = -\frac{\beta}{3\sqrt{2}} + \frac{\sqrt{2}}{3}\frac{\beta^{4/3}}{\sqrt[3]{9+2\beta+i\sqrt{-81-36\beta+4\beta^2}}} + \frac{\beta^{2/3}}{3\sqrt{2}}\sqrt[3]{9+2\beta+i\sqrt{-81-36\beta+4\beta^2}}\,, \tag{5.32}$$

$$x^{\mp}_{\epsilon_1=1} = \frac{\beta}{3\sqrt{2}} + \frac{1\mp i\sqrt{3}}{3\sqrt{2}}\frac{\beta^{4/3}}{\sqrt[3]{9+2\beta+i\sqrt{-81-36\beta+4\beta^2}}} + \left(1\pm i\sqrt{3}\right)\frac{\beta^{2/3}}{6\sqrt{2}}\sqrt[3]{9+2\beta+i\sqrt{-81-36\beta+4\beta^2}}\,. \tag{5.33}$$

The first solution is located below the maximum of the potential $x^{0}_{\epsilon_1=1} < x_{V'=0}$, while the two others are located beyond it $x^{\mp}_{\epsilon_1=1} > x_{V'=0}$. Using the larger solution as a lower bound for $x_{\rm ini}$, one gets

$$x_{\rm end} > \sqrt{\left(x^{+}_{\epsilon_1=1}\right)^2 + 2\beta(N_{\rm end}-N_{\rm ini})}\,. \tag{5.34}$$

If $\beta < 9/2\left(1+\sqrt{2}\right)$, only one solution to $\epsilon_1 = 1$ exists,

$$x_{\epsilon_1=1} = -\frac{\beta}{3\sqrt{2}} + \frac{\sqrt{2}}{3}\frac{\beta^{4/3}}{\sqrt[3]{9+2\beta+\sqrt{81+36\beta-4\beta^2}}} + \frac{\beta^{2/3}}{3\sqrt{2}}\sqrt[3]{9+2\beta+\sqrt{81+36\beta-4\beta^2}}\,, \tag{5.35}$$

which is located below the maximum of the potential $x^{0}_{\epsilon_1=1} < x_{V'=0}$. In principle $x_{\rm ini}$ is now only bounded from below by $x_{V'=0}$ and one can check from Eq. (5.30) that the total number of e-folds diverges close to $x_{V'=0}$. As a result, provided $x_{\rm ini}$ is fine-tuned to the top of the potential, there is no bound on $x_{\rm end}$. The prior space described by these relations is displayed in Fig. 44.

According to the previous discussion, the observable field value, at which the pivot mode crossed the Hubble radius during inflation, is such that $x_* \gg 1$. In this limit, it is possible to approximate the slow-roll parameters at Hubble crossing with

$$\epsilon_1^* \simeq \frac{\beta^2}{2x_*^2}\,, \qquad \epsilon_2^* \simeq \epsilon_3^* \simeq -\frac{2\beta}{2x_*^2}\,, \tag{5.36}$$

hence

$$r \simeq \frac{8\beta^2}{x_*^2}\,, \qquad n_{\rm S}-1 \simeq \frac{\beta\,(2-\beta)}{x_*^2}\,, \qquad \alpha_{\rm S} = \frac{2\beta^2\,(\beta-2)}{x_*^4}. \tag{5.37}$$

These estimates match with those of Ref. [461]. Finally, the parameter M is obtained from the amplitude of the CMB anisotropies

$$\left(\frac{M}{M_{\rm Pl}}\right)^4 = 720\pi^2\left[\frac{\beta^2\,(\beta+2)}{6}-\beta x_*^2\right]^2\left(x_*^3-\frac{\beta^2 x_*}{6}\right)^{-2}\left(x_*^{-\beta}-\frac{\beta^2}{6}x_*^{-\beta-2}\right)\frac{Q^2_{\rm rms-PS}}{T^2}\,. \tag{5.38}$$

In the $x_* \gg 1$ limit, this gives

$$\frac{M^4}{M_{\rm Pl}^4} \simeq 720\pi^2\beta^2 x_*^{-2-\beta}\frac{Q^2_{\rm rms-PS}}{T^2}\,, \tag{5.39}$$

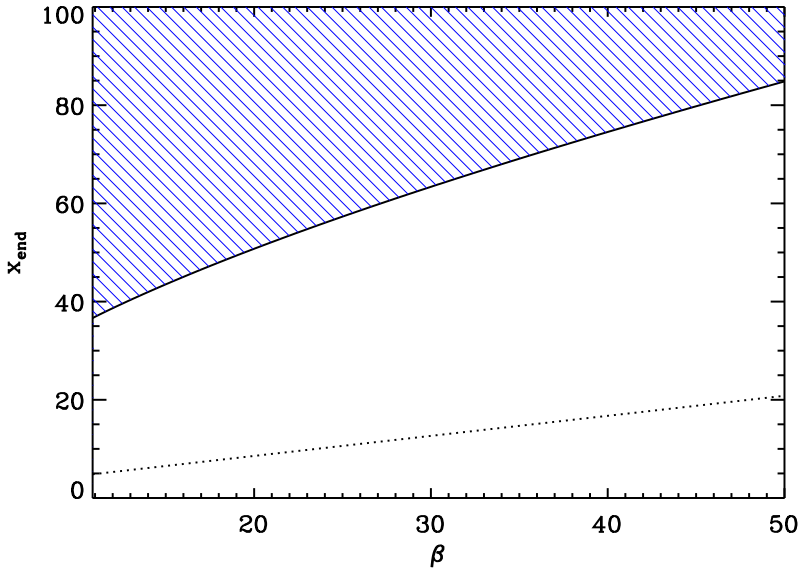

Figure 44. Prior space on $x_{\rm end}$ derived from Eq. (5.34) with $N_{\rm end} - N_{\rm ini} = 60$, as a function of $\beta > 9/2\left(1+\sqrt{2}\right)$ (black solid line). The black dotted line corresponds to $x_{V'=0}$. For $\beta < 9/2\left(1+\sqrt{2}\right)$, provided some fine-tuning on the initial conditions, $x_{\rm end}$ can take any values. The dashed area corresponds to parameters for the model which produce at least the required number of e-folds.

which yields $M/M_{\rm Pl} \lesssim 10^{-2}$.

The reheating consistent slow-roll predictions for the intermediate inflation models are displayed in Fig. 114, for different values of $\beta > 0$, and for $x_{\rm end}$ describing the prior space displayed in Fig. 44. The reheating equation of state parameter $\overline{w}_{\rm reh}$ has been taken to 0 but since there is no potential minimum around which the inflaton field can oscillate at the end of inflation, this parameter is a priori unspecified and can take different values. In any case the reheating temperature is fully degenerate with the parameter $x_{\rm end}$, and therefore these two parameters cannot be constrained independently. However one can see that $x_{\rm end}$ is clearly limited from below as expected. The black solid lines represent the locus of the points such that $\epsilon_1^* = -\beta/4\epsilon_2^*$, or equivalently, $n_{\rm S} - 1 = (1/\beta - 1/2)\, r/4$, these consistency relations arising from Eqs. (5.36). One can check that they provide a good qualitative description of the model predictions. In particular, they explain why, for $\beta < 2$, one has a blue tilt $n_{\rm S} > 1$.

5.3 Kähler Moduli Inflation II (KMIII)

5.3.1 Theoretical Justifications

These models are string motivated scenarios. They arise in the context of type IIB string theory via Calabi-Yau flux compactification. They have been derived and studied in Refs. [304–310], and a two-field generalization of this model has been investigated in Refs. [305–309]. They can be understood in the context of supergravity, viewed as an effective theory. In this framework, one starts with the following superpotential for the moduli T_i

$$W = W_0 + \sum_{i=2}^{n} A_i e^{-a_i T_i}, \tag{5.40}$$

where $a_i = 2\pi/(g_s N)$, N being a positive integer (not to be confused with the e-fold number), g_s the string coupling, and W_0 and A_i are model dependent constants. The Kähler potential can be written as

$$K = -2M_{\rm Pl}^2 \ln\left(\frac{\mathcal{V}}{2\ell_s^6} + \frac{\xi}{2}\right), \tag{5.41}$$

where the constant ξ is given by $\xi = -\zeta(3)\chi(M)/[2(2\pi)^2]$, $\chi(M)$ being the Euler characteristic of the compactification manifold. The quantity $\mathcal{V}$ represents the overall volume of the Calabi-Yau manifold and can be taken to be

$$\mathcal{V} = \frac{\gamma\ell_s^6}{2\sqrt{2}}\left[\left(T_1 + T_1^\dagger\right)^{3/2} - \sum_{i=2}^{n}\lambda_i\left(T_i + T_i^\dagger\right)^{3/2}\right], \tag{5.42}$$

where γ and λ_i are positive constants and depend on the details of the model. From the expression of the Kähler and superpotentials, it is then straightforward to calculate the corresponding F-term potential which is a relatively complex expression that can be found in Ref. [308]. If, however, one consider the limit $\mathcal{V} \gg 1$ (and $T_1 \gg T_i$), then the F-term simplifies a lot and gives rise to the following equation

$$V(\tau_i) \simeq \frac{3\xi W_0^2}{4M_{\rm Pl}^2\mathcal{V}_s^3} + \sum_{i=2}^{n}\left[\frac{4W_0 a_i A_i}{M_{\rm Pl}^2\mathcal{V}_s^2}\tau_i e^{-a_i\tau_i}\cos\left(a_i\theta_i\right) + \frac{8\left(a_i A_i\right)^2}{3M_{\rm Pl}^2\gamma\lambda_i\mathcal{V}_s}\sqrt{\tau_i}e^{-2a_i\tau_i}\right], \tag{5.43}$$

where we have written $T_i = \tau_i + i\theta_i$ and $\mathcal{V}_s \equiv \mathcal{V}/\ell_s^6$. We see that all the constants introduced before, namely a_i, A_i, W_0, ξ, γ and λ_i participate to the expression of the potential. From Eq. (5.43), solving $\partial V/\partial\tau_i = 0$, one can estimate the value of each τ_i at the global minimum of the potential. In the following, we denote this quantity by $\tau_i^{\rm min}$. Then, one can also calculate the value of the potential at this minimum. One finds [where, as usual, we have taken $\cos\left(a_i\theta_i\right) = -1$]

$$V_{\rm min} \simeq \frac{3\xi W_0^2}{4M_{\rm Pl}^2\mathcal{V}_s^3} - \frac{3W_0^2\gamma}{2M_{\rm Pl}^2\mathcal{V}_s^3}\sum_{i=2}^{n}\frac{\lambda_i}{a_i^{3/2}}\left(a_i\tau_i^{\rm min}\right)^{3/2}. \tag{5.44}$$

As a consequence, if for one of the fields, say τ_n, one has $\left(\lambda_n/a_n^{3/2}\right) / \left[\sum_{i=2}^{n-1}(\lambda_i/a_i^{3/2})\right] \ll 1$, then the value of $V_{\rm min}$ is not modified even if one displaces τ_n from $\tau_n^{\rm min}$. In other words, we have an inflationary valley along the τ_n direction and one can use it to produce inflation. In that case, the potential can be re-written as

$$V(\tau_n) \simeq \frac{BW_0^2}{M_{\rm Pl}^2\mathcal{V}_s^3} - \frac{4W_0 a_n A_n}{M_{\rm Pl}^2\mathcal{V}_s^2}\tau_n e^{-a_n\tau_n}, \tag{5.45}$$

where the second exponential in Eq. (5.43) has been neglected, thanks to the condition $a_n\tau_n \gg 1$ and B is a constant that includes the constant term in Eq. (5.43) as well as the contributions of the other fields at their minimum, i.e. $B = 3\xi/4 + \cdots$. It is important to notice that the assumption of large volume translates into a condition on the *vev* of τ_n. The above potential is of the form of the toy model studied as "Kähler Moduli Inflation I (KMII)" in section 4.9. The field is however not canonically normalized since it is a modulus. It is therefore necessary to first canonically normalize it and, then, re-derive the corresponding

potential. Using the form of the Kähler potential given above, denoting by ϕ the canonical field, one arrives at

$$\tau_n = \left(\frac{3\mathcal{V}_{\rm s}}{4\gamma\lambda_n}\right)^{2/3}\left(\frac{\phi}{M_{\rm Pl}}\right)^{4/3}. \tag{5.46}$$

As a consequence, the final form of the inflaton's potential is given by

$$V(\phi) = \frac{BW_0^2}{M_{\rm Pl}^2\mathcal{V}_{\rm s}^3} - \frac{4W_0 a_n A_n}{M_{\rm Pl}^2\mathcal{V}_{\rm s}^2}\left(\frac{3\mathcal{V}_{\rm s}}{4\gamma\lambda_n}\right)^{2/3}\left(\frac{\phi}{M_{\rm Pl}}\right)^{4/3}\exp\left[-a_n\left(\frac{3\mathcal{V}_{\rm s}}{4\gamma\lambda_n}\right)^{2/3}\left(\frac{\phi}{M_{\rm Pl}}\right)^{4/3}\right]. \tag{5.47}$$

Let us now see what are the typical values that the parameters appearing in the above potential can take. As already mentioned, the quantity $\mathcal{V}_{\rm s}$ represents the Calabi-Yau volume and is supposed to be such that $\mathcal{V}_{\rm s} \gg 1$ or $\mathcal{V} \gg \ell_{\rm s}^6$. In Ref. [310] the typical value $\mathcal{V}_{\rm s} \simeq 3\times 10^6$ was chosen. The parameter A_n depends on the complex structure moduli and is typically of order $\mathcal{O}\left(\ell_{\rm s}^3\right)$. This is also the case for W_0. One has $a_n = 2\pi/N$, where N is a positive integer (for $D3$-brane instantons, one has $N = 1$). The dimensionless parameter λ_n is model dependent but is considered to be of order $\mathcal{O}(1)$. The quantity $\xi = \zeta(3)\chi/\left[2(2\pi)^3\right]$, where χ is the Euler number of the internal Calabi-Yau space, is also of order $\mathcal{O}(1)$ as well as the coefficient γ. This means that B is of order $\mathcal{O}(1)$.

5.3.2 Slow-Roll Analysis

We now study the inflationary scenario based on the potential derived above. Re-writing $V(\phi)$ in a more convenient way, we have

$$V(\phi) = M^4\left[1 - \alpha\left(\frac{\phi}{M_{\rm Pl}}\right)^{4/3} e^{-\beta(\phi/M_{\rm Pl})^{4/3}}\right]. \tag{5.48}$$

where we have defined the parameters M, α and β by

$$M^4 = \frac{BW_0^2}{M_{\rm Pl}^2\mathcal{V}_{\rm s}^3}, \quad \alpha = \frac{16\mathcal{V}_{\rm s}a_n}{3}\frac{A_n}{W_0}\left(\frac{3\mathcal{V}_{\rm s}}{4\gamma\lambda_n}\right)^{2/3}, \quad \beta = a_n\left(\frac{3\mathcal{V}_{\rm s}}{4\gamma\lambda_n}\right)^{2/3}. \tag{5.49}$$

Making use of the typical orders of magnitude for the various quantities entering these expression, one sees that

$$\alpha = \mathcal{O}\left(\mathcal{V}_s^{5/3}\right), \qquad \beta = \mathcal{O}\left(\mathcal{V}_s^{2/3}\right), \tag{5.50}$$

with $\mathcal{V}_{\rm s} \gg 1$.

The potential (5.48) and its logarithm are displayed in Fig. 45. $V(\phi)$ decreases from $V/M^4 = 1$ at $\phi = 0$, reaches a minimum at $\phi/M_{\rm Pl} = \beta^{-3/4}$, and then increases to the asymptotic value $V/M^4 = 1$ when $\phi/M_{\rm Pl} \to +\infty$. However, since the potential is derived under the large field assumption, only the increasing branch of the potential is relevant. Inflation proceeds from the right to the left along this branch. The minimum value of the potential at $\phi = M_{\rm Pl}\beta^{-3/4}$ is given by $V_{\rm min} = M^4\left[1 - \alpha/\left(\beta e\right)\right]$. Therefore, if one wants the potential to be definite positive everywhere, one must have $\alpha/\beta < e$. However, from Eq. (5.50), we see that this condition cannot be satisfied since $\alpha/\beta = \mathcal{O}(\mathcal{V}_{\rm s}) \gg 1$. This means that the potential necessarily vanishes at some point. In the increasing branch of the potential, this occurs for a *vev* given by

$$x_{V=0} \equiv \frac{\phi_{V=0}}{M_{\rm Pl}} = \left[-\frac{1}{\beta}\mathrm{W}_{-1}\left(-\frac{\beta}{\alpha}\right)\right]^{3/4}. \tag{5.51}$$

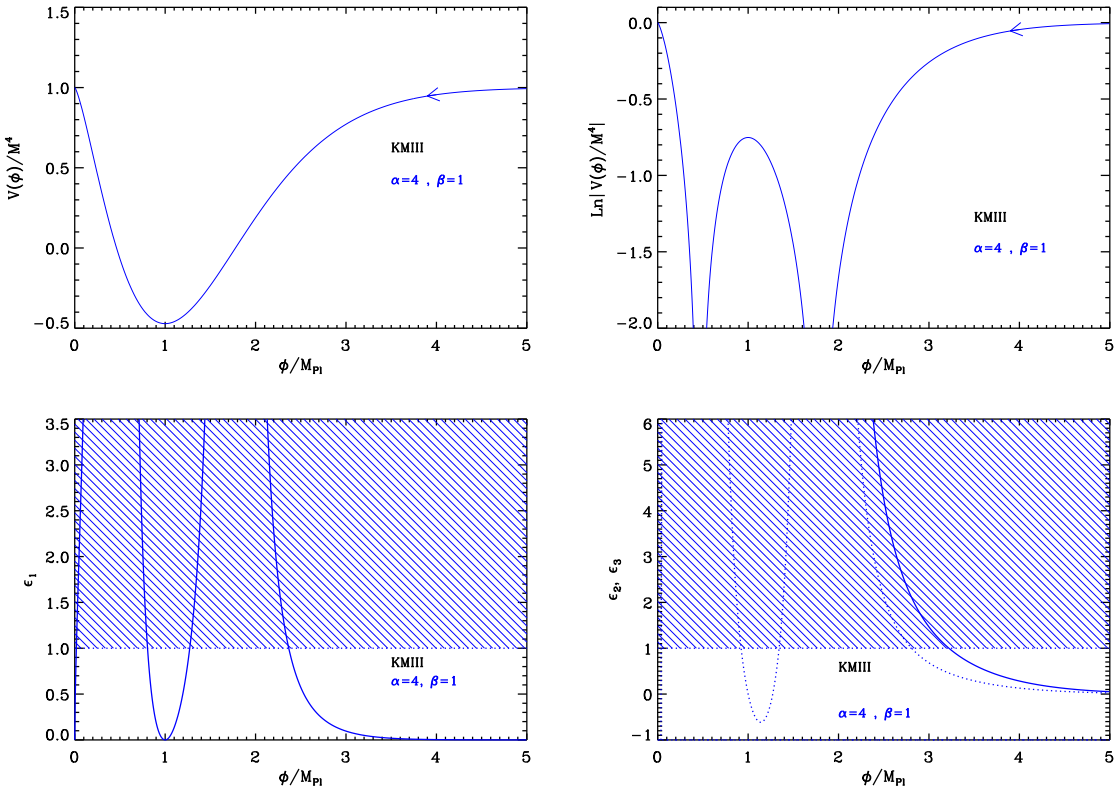

Figure 45. Top left panel: Kähler moduli inflation II (KMIII) potential for $\alpha = 4$ and $\beta = 1$. These parameters are not physical but they are used for display convenience. Top right panel: logarithm of the potential for the same value of α and β. Bottom left panel: slow-roll parameter ϵ_1 for a potential with $\alpha = 4$ and $\beta = 1$. The shaded area indicates the breakdown of the slow-roll inflation (strictly speaking when the acceleration stops). Bottom right panel: slow-roll parameters ϵ_2 (solid line) and ϵ_3 (dotted line) for $\alpha = 4$ and $\beta = 1$.

Anyway, since the potential (5.48) is only valid in the large field region, this criterion does not play an important role in what follows.

Let us now calculate the three first Hubble flow parameters. Defining $x \equiv \phi/M_{\rm Pl}$, they are given by

$$\epsilon_1 = \frac{8\alpha^2}{9} x^{2/3} e^{-2\beta x^{4/3}} \left(\frac{1 - \beta x^{4/3}}{1 - \alpha x^{4/3} e^{-\beta x^{4/3}}} \right)^2 , \tag{5.52}$$

$$\epsilon_2 = \frac{8\alpha}{9} x^{-2/3} e^{-2\beta x^{4/3}} \frac{3\alpha x^{4/3} + \alpha\beta x^{8/3} + e^{\beta x^{4/3}} \left(1 - 9\beta x^{4/3} + 4\beta^2 x^{8/3}\right)}{\left(1 - \alpha x^{4/3} e^{-\beta x^{4/3}}\right)^2}, \tag{5.53}$$

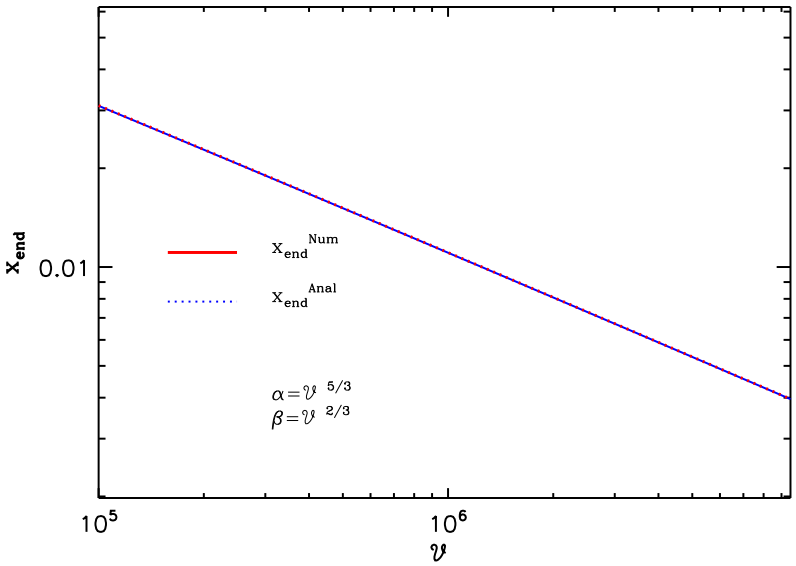

Figure 46. Comparison between the exact numerical value of $x_{\rm end}(\alpha,\beta)$ (blue solid line), and the approximated formula given by Eq. (5.55) (red dotted line) for $\alpha = \mathcal{V}^{5/3}$ and $\beta = \mathcal{V}^{2/3}$. The agreement is excellent but a numerical calculation is used in `ASPIC` anyway.

and

$$\epsilon_3 = \left\{8\alpha\left(1-\beta x^{4/3}\right)\left[\alpha^2 x^{8/3}\left(9+\beta x^{4/3}\right) - 2\alpha e^{\beta x^{4/3}} x^{4/3}\left(-4+19\beta x^{4/3} - 9\beta^2 x^{8/3} + 4\beta^3 x^4\right) - e^{2\beta x^{4/3}}\left(1+11\beta x^{4/3} - 30\beta^2 x^{8/3} + 8\beta^3 x^4\right)\right]\right\}\left\{9x^{2/3}\left(e^{\beta x^{4/3}} - \alpha x^{4/3}\right)^2 \times \left[\alpha x^{4/3}\left(3+\beta x^{4/3}\right) + e^{\beta x^{4/3}}\left(1-9\beta x^{4/3} + 4\beta^2 x^{8/3}\right)\right]\right\}^{-1}. \tag{5.54}$$

Inflation stops when $\epsilon_1(x_{\rm end}) = 1$. As can be seen in Fig. 45, for $\alpha/\beta \gg 1$, the first slow-roll parameter ϵ_1 starts increasing from $\epsilon_1 = 0$ at $x = 0$, diverges at a *vev* that we do not need to compute here, and then decreases to vanish at $x = \beta^{-3/4}$. Then, it increases again, blows up at $x_{V=0}$ and, finally, asymptotically vanishes when $x \to \infty$. Since inflation proceeds at $x > x_{V=0}$ it always stops by violation of the slow-roll conditions. Unfortunately is not possible to find an analytic expression for $x_{\rm end}$ but one can provide the following approximated formula,

$$x_{\rm end} \simeq \left[-\frac{5}{4\beta}{\rm W}_{-1}\left(-\frac{4\times 9^{2/5}}{5\times 8^{2/5}}\alpha^{-4/5}\beta^{1/5}\right)\right]^{3/4}, \tag{5.55}$$

where $\rm W_{-1}$ is the Lambert function. It is compared to the numerical solution for $x_{\rm end}$ implemented in the `ASPIC` code in Fig. 46. The agreement is excellent.

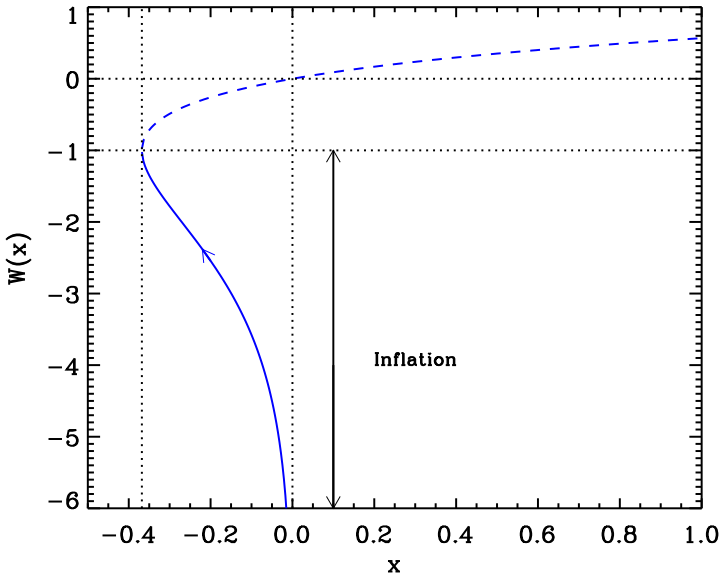

Figure 47. Lambert functions $\mathrm{W}_0(x)$ (dashed line) and $\mathrm{W}_{-1}(x)$ (solid line). During Kähler moduli inflation II, inflation proceeds along the "-1" branch in the direction specified by the arrow.

Let us now turn to the slow-roll trajectory. Unfortunately, KMIII is one of the rare cases for which it cannot be integrated by quadrature. As such, in the `ASPIC` library, the slow-roll trajectory is numerically integrated. However, in the large field limit $x \gg \beta^{-3/4}$, one can obtain an approximate analytic formula given by

$$N_{\mathrm{end}} - N \simeq \frac{9}{16\alpha\beta^2}\left(\frac{e^{\beta x^{4/3}}}{x^2} - \frac{e^{\beta x_{\mathrm{end}}^{4/3}}}{x_{\mathrm{end}}^2}\right), \tag{5.56}$$

from which one deduces that

$$x \simeq \left(-\frac{3}{2\beta}\mathrm{W}_{-1}\left\{-\frac{2}{3}\beta\left[\frac{e^{\beta x_{\mathrm{end}}^{4/3}}}{x_{\mathrm{end}}^2} + \frac{16\alpha\beta^2}{9}\left(N_{\mathrm{end}} - N\right)\right]^{-2/3}\right\}\right)^{3/4}. \tag{5.57}$$

This approximation is in agreement with what was obtained in Ref. [310], up to an incorrect choice of the Lambert function branch. The Lambert function is displayed in Fig. 47 and the part of the curve where inflation proceeds is indicated by the arrow. The fact that the -1 branch of the Lambert function has to be chosen comes from the fact that, when $N_{\mathrm{end}} - N \to \infty$, one must have $x \to \infty$. On the other hand, when $N_{\mathrm{end}} - N \to 0$, $x \to x_{\mathrm{end}} > \beta^{-3/4}$ and this is again consistent with the choice of the -1 branch.

Finally, one can use the CMB normalization to calculate the mass scale M. Without any approximation on top of slow-roll, this leads to the following expression

$$\left(\frac{M}{M_{\mathrm{Pl}}}\right)^4 = 1280\pi^2\alpha^2 x_*^{2/3} e^{-2\beta x_*^{4/3}}\left(1 - \beta x_*^{4/3}\right)^2\left(1 - \alpha x^{4/3} e^{-\beta x_*^{4/3}}\right)^{-2}\frac{Q_{\mathrm{rms-PS}}^2}{T^2}. \tag{5.58}$$

Making use of the approximated trajectory and of the expression for the scale M, one roughly obtains

$$\mathcal{V}_{\rm s} \simeq \frac{\Delta N_*}{\pi\sqrt{720}}\frac{1}{(M_{\rm Pl}\ell_{\rm s})^3}\left[\frac{4Ba_n\left(W_0\ell_{\rm s}^3\right)^2}{3\gamma\lambda_n}\right]\ln^{-5/4}\left(\frac{16\alpha\beta^2}{9}\Delta N_*\right)\frac{T}{Q_{\rm rms-PS}}\,. \tag{5.59}$$

Given that a_n, B, γ, λ_n, $W_0\ell_{\rm s}^3$ are a priori coefficients of order one, we see that the above expression roughly implies that $\mathcal{V}$ is of the order $10^6\ell_{\rm s}$.

The reheating consistent slow-roll predictions for the Kähler moduli inflation II models are displayed in Fig. 115, for $\mathcal{V} \in [10^5, 10^7]$, and taking $\alpha = \mathcal{V}^{5/3}$ and $\beta = \mathcal{V}^{2/3}$. One can check that even if one adds $\mathcal{O}(1)$ factors in these relations, the slow-roll predictions do not depend significantly on them. Also, we notice that ϵ_1 is typically extremely small and that ϵ_2 is almost independent of $\mathcal{V}$. These effects can be analytically understood. Working out Eq. (5.55) and Eqs. (5.52), (5.53), and (5.54) in the large field limit, one obtains

$$\epsilon_{1*} \simeq \frac{1}{324\beta^{3/2}(\Delta N_*)^2}\ln^{5/2}\left(16\sqrt{\frac{9}{8}}\alpha\beta^{1/2}\Delta N_*\right), \qquad \epsilon_{2*} \simeq \frac{2}{\Delta N_*}, \qquad \epsilon_{3*} \simeq \frac{1}{\Delta N_*}, \tag{5.60}$$

from which one deduces that

$$n_{\rm S} \simeq 1 - \frac{2}{\Delta N_*}, \qquad r \simeq \frac{4}{81\beta^{3/2}(\Delta N_*)^2}\ln^{5/2}\left(16\sqrt{\frac{9}{8}}\alpha\beta^{1/2}\Delta N_*\right), \qquad \alpha_{\rm S} \simeq -\frac{2}{\Delta N_*^2}\,. \tag{5.61}$$

Firstly, we see that the slow-roll parameters at Hubble crossing depend on α logarithmically only. This explains the weak dependence in the $\mathcal{O}(1)$ factors mentioned above. Secondly, we also notice that ϵ_{2*} and ϵ_{3*} do not depend on β. In a third place, ϵ_1 is a very small number since it is proportional to the inverse of $\beta^{3/2}$. This also means that, when $\mathcal{V}$ increases, ϵ_1 decreases. All these considerations can be checked in Fig. 115 and the amount of gravitational waves predicted by this model is very small. This is in agreement with the rough estimates given in Refs. [304, 307, 308, 310]. However, contrary to what is claimed in Ref. [310], the predicted value for the running of the spectral index is not excluded by observations since, according to the Planck results [153], $\alpha_{\rm S} = -0.013 \pm 0.009$ while, for the fiducial value $\Delta N_* \simeq 55$, one obtains $\alpha_{\rm S} \simeq -0.0006$.

5.4 Logamediate Inflation (LMI)

Logamediate inflation has been discussed in Refs. [470, 471] and refers to inflationary scenarios in which the scale factor evolves according to

$$a\left(t\right) = a_{_0}\exp\left[A\left(\ln\frac{t}{t_0}\right)^{\lambda}\right], \tag{5.62}$$

where A and λ are two dimensionless parameters and where t_0 has the dimension of a cosmic time. This evolution form for the scale factor is required to occur "at late times", i.e. when $t \gg t_0$. If $\lambda = 1$, one recovers the power law model (see section 4.8), and in that case, t_0 can be absorbed in a rescaling of the scale factor. Otherwise, these three parameters are relevant and one therefore expects LMI to be a two parameters models according to our classification. Following Ref. [470], from Eq. (5.62), one has

$$H \equiv \frac{\dot{a}}{a} = \frac{A\lambda}{t}\left(\ln\frac{t}{t_0}\right)^{\lambda-1}, \tag{5.63}$$

from which one deduces that $A\lambda > 0$ in order to have expansion ($H > 0$). From Eq. (5.62), one can also establish that

$$\frac{\ddot{a}}{a} = \frac{A\lambda}{t^2}\left(\ln\frac{t}{t_0}\right)^{\lambda-1}\left[(\lambda-1)\left(\ln\frac{t}{t_0}\right)^{-1} - 1 + A\lambda\left(\ln\frac{t}{t_0}\right)^{\lambda-1}\right], \tag{5.64}$$

from which one deduces that in order to have inflation at late times (when $t \gg t_0$), one must have $\lambda > 1$, or if $\lambda = 1$, $A > 1$. If this inflationary scenario is implemented within a single minimally coupled scalar field ϕ, one can derive the corresponding potential. From the Friedmann-Lemaître and Klein-Gordon equations one can show that [470]

$$\frac{\dot{\phi}(t)}{M_{\rm Pl}} = \frac{\sqrt{2A\lambda}}{t}\left(\ln\frac{t}{t_0}\right)^{\frac{\lambda-1}{2}}. \tag{5.65}$$

This equation can easily be integrated into

$$\frac{\phi(t)}{M_{\rm Pl}} = \frac{\phi_0}{M_{\rm Pl}} + 2\frac{\sqrt{2A\lambda}}{\lambda+1}\left(\ln\frac{t}{t_0}\right)^{\frac{\lambda+1}{2}}. \tag{5.66}$$

Combining the Friedmann-Lemaître equation $3M_{\rm Pl}^2H^2 = V(\phi) + \dot{\phi}^2/2$ and the relation $2M_{\rm Pl}^2\dot{H} = -\dot{\phi}^2$, one obtains $V(\phi) = 3M_{\rm Pl}^2H^2 + M_{\rm Pl}^2\dot{H}$, namely

$$V(\phi) = \frac{3M_{\rm Pl}^2A^2\lambda^2}{t^2}\left(\ln\frac{t}{t_0}\right)^{2(\lambda-1)} + \frac{M_{\rm Pl}^2A\lambda}{t^2}(\lambda-1)\left(\ln\frac{t}{t_0}\right)^{\lambda-2} - \frac{M_{\rm Pl}^2A\lambda}{t^2}\left(\ln\frac{t}{t_0}\right)^{\lambda-1}. \tag{5.67}$$

Together with Eq. (5.66), this gives a parametric representation of the field potential in terms of t. It can be further simplified since the Logamediate regime occurs in the limit $t \gg t_0$. If $\lambda > 1$, the first term of this expression dominates at late times and one has $V(\phi) = 3M_{\rm Pl}^2A^2\lambda^2\left(\ln t/t_0\right)^{2(\lambda-1)}/t^2$. Defining $x \equiv (\phi-\phi_0)/M_{\rm Pl}$, one makes use of Eq. (5.66) to obtain

$$V(\phi) = M^4x^\alpha\exp\left(-\beta x^\gamma\right), \tag{5.68}$$

where the new parameters are defined by

$$\alpha = 4\frac{\lambda-1}{\lambda+1}, \qquad \beta = 2\left(\frac{\lambda+1}{2\sqrt{2A\lambda}}\right)^{2/(\lambda+1)}, \qquad \gamma = \frac{2}{\lambda+1}, \tag{5.69}$$

and

$$\frac{M^4}{M_{\rm Pl}^4} = \frac{3A^2\lambda^2}{M_{\rm Pl}^2t_0^2}\left(\frac{\lambda+1}{2\sqrt{2A\lambda}}\right)^{4\frac{\lambda-1}{\lambda+1}}. \tag{5.70}$$

The same potential has been studied for $\alpha = 2$, $\beta = 1/8$ and $\gamma = 2$ within tachyon inflation models in Ref. [434]. The case $\lambda = 1$ is particular. At late times, the first term and the last term must be kept in Eq. (5.67), such that $V(\phi) = (3A-1)AM_{\rm Pl}^2/t^2$. In that situation, one has $x = \sqrt{2A}\ln t/t_0$, and the derived potential shares the same expressions for α, β and γ as in Eq. (5.69) but evaluated at $\lambda = 1$. There is a difference however because M^4 now reads $M^4 = (3A-1)AM_{\rm Pl}^2/t_0^2$. We recover explicitly that $\lambda = 1$ corresponds to power law inflation and has already been treated in section 4.8.

In the following, we will work only with the derived parameters β, γ and M^4, noticing that

$$\alpha = 4(1-\gamma). \tag{5.71}$$

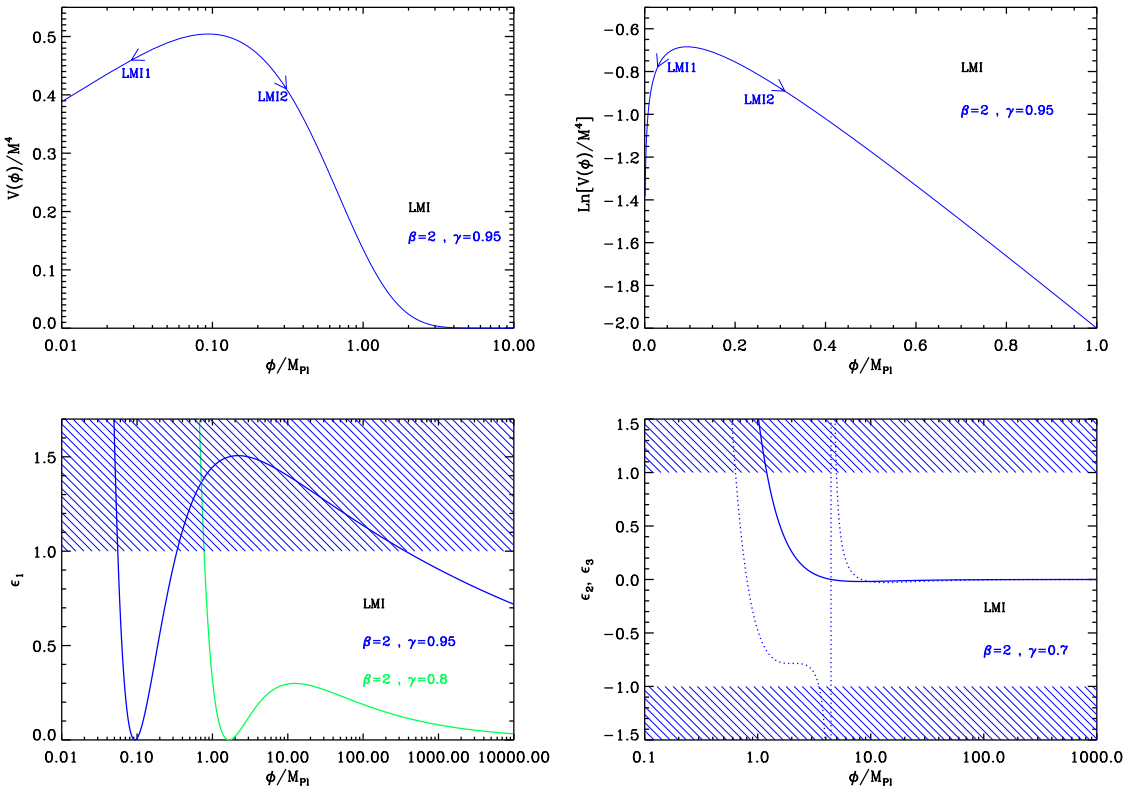

Figure 48. Logamediate Inflation (LMI). Upper panels: the potential and its logarithm for $\beta = 2, \gamma = 0.95$. Bottom left panel: Hubble flow function ϵ_1 for a potential with $\beta = 2, \gamma = 0.95$ (blue curve) and $\beta = 2, \gamma = 0.8$ (green curve). The position of the maximum of ϵ_1 with respect to one depends on γ. The shaded region indicates where inflation stops. Bottom right panel: slow-roll parameters ϵ_2 (solid line) and ϵ_3 (dotted line) for a potential with $\beta = 2, \gamma = 0.7$.

The restrictions $A\lambda > 0$ and $\lambda \geq 1$ translates into the conditions $0 < \gamma \leq 1$ and $\beta > 0$. Following Ref. [471], since there is no fundamental reasons preventing it, we will generalize this model to any possible values of these parameters supporting inflation.

The three first Hubble flow functions in the slow-roll approximation read

$$\epsilon_1 = \frac{(\alpha - \beta\gamma x^\gamma)^2}{2x^2}, \qquad \epsilon_2 = \frac{2}{x^2}\left[\alpha + \beta\left(\gamma - 1\right)\gamma x^\gamma\right], \tag{5.72}$$

$$\epsilon_3 = \frac{\alpha - \beta\gamma x^\gamma}{x^2}\frac{2\alpha - \beta\left(\gamma - 2\right)\left(\gamma - 1\right)\gamma x^\gamma}{\alpha + \beta\left(\gamma - 1\right)\gamma x^\gamma}. \tag{5.73}$$

The potential and the Hubble flow functions in the slow-roll approximation have been represented in Fig. 48.

Inflation can proceed in two regimes: either at decreasing field values, left to the top of the potential (LMI1), or at increasing field values, right to the top of the potential (LMI2). Notice that from Eq. (5.66), ϕ has to increase with time to reproduce the scale factor expansion Eq. (5.62) and this happens only in the regime LMI2 for large values of x. As can be seen in Fig. 48, the slow-roll parameter ϵ_1 diverges when x approaches zero, it vanishes at

the top of the potential for $x = x_{V^{\max}}$ and it is maximal at $x = x_{\epsilon_1^{\max}}$ with

$$x_{V^{\max}} \equiv \left(\frac{\alpha}{\beta\gamma}\right)^{1/\gamma}, \qquad x_{\epsilon_1^{\max}} = \left[\frac{\alpha}{\beta\gamma\,(1-\gamma)}\right]^{1/\gamma}. \tag{5.74}$$

Finally it asymptotes to zero for large values of the field. The value of the local maximum of ϵ_1 reads

$$\epsilon_1^{\max} = \frac{\alpha^2}{2}\left[\frac{\beta\gamma\,(1-\gamma)}{\alpha}\right]^{\frac{2}{\gamma}}\left(\frac{\gamma}{1-\gamma}\right)^2. \tag{5.75}$$

Thus in the regime LMI1, inflation always stops naturally as ϵ_1 becomes larger than unity whereas in the regime LMI2, this may occur only if $\epsilon_1^{\max} > 1$ and if inflation has started from $x_{\rm ini} < x_{\epsilon_1^{\max}}$. Otherwise, if inflation starts with $x_{\rm ini} > x_{\epsilon_1^{\max}}$, or if $\epsilon_1^{\max} < 1$, one needs to add an extra-parameter $x_{\rm end}$ encoding an unspecified mechanism to end inflation. In that situation, the model becomes a three parameters one. If one makes use of $\alpha = 4\,(1-\gamma)$, one obtains $\epsilon_1^{\max} = 8\gamma^2\,(\beta\gamma/4)^{2/\gamma}$. Solving $\epsilon_1^{\max} \geq 1$ for β gives

$$\beta \geq \frac{4}{\gamma\,(8\gamma^2)^{\gamma/2}}\,. \tag{5.76}$$

This condition is therefore required for the model LMI2, if one wants inflation to end naturally. As we will see below, LMI2 inflating in the domain $x_{V^{\max}} < x < x_{\epsilon_1^{\max}}$ is a very fine-tuned situation which is strongly disfavored by the observations. Notice that if one assumes $0 < \gamma \leq 1$, this conditions translates into $\beta > \sqrt{2}$.

Finally, let us notice that for the value of ϵ_2 at the top of the potential to be smaller than some maximal value $\epsilon_{2,\rm top}^{\max}$, one needs to impose the condition

$$\beta < \beta^{\max}\left(\gamma, \epsilon_{2,\rm top}^{\max}\right) = 2^{2-3\gamma/2}\left(\epsilon_{2,\rm top}^{\max}\right)^{\gamma/2}\frac{(1-\gamma)^{1-\gamma/2}}{\gamma^{1+\gamma/2}}\,. \tag{5.77}$$

In the LMI1 model, a slow roll regime of inflation can proceed only if such a condition is verified (with typically $\epsilon_{2,\rm top}^{\max} \simeq 10^{-1}$).

The slow-roll trajectory can be integrated thanks to the hypergeometric function [204, 205] ${}_2F_1$, leading to

$$N - N_{\rm end} = \frac{x_{\rm end}^2}{2\alpha}\,{}_2F_1\left[1, \frac{2}{\gamma}, \frac{2}{\gamma}+1, \left(\frac{x_{\rm end}}{x_{V^{\max}}}\right)^{\gamma}\right] - \frac{x^2}{2\alpha}\,{}_2F_1\left[1, \frac{2}{\gamma}, \frac{2}{\gamma}+1, \left(\frac{x}{x_{V^{\max}}}\right)^{\gamma}\right]. \tag{5.78}$$

One can notice that inserting $\alpha = 4(1-\gamma)$, as a function of $x/x_{V^{\max}}$, this trajectory only involves γ. Plugging $x = x_{V^{\max}}$ into Eq. (5.78) one gets an infinite number of e-folds. This means that the required number of e-folds to solve the problems of the standard Big-Bang scenario can always be realized, both in the decreasing branch of the potential and the increasing one, provided that inflation starts close enough to $x_{V^{\max}}$. However, it can numerically be checked that in the case of LMI2 with $\epsilon_1^{\max} > 1$ and inside the $x_{V^{\max}} < x < x_{\epsilon_1^{\max}}$ region, one has to fine-tune $x_{\rm ini}$ and x_* extremely close to $x_{V^{\max}}$. In that situation $n_{\rm S} = 1$, with vanishing r and vanishing running of the spectral index, can be considered as generic predictions of the model. For this reason, it is more natural to consider LMI2 in the large field regime, namely $x > \max(x_{V^{\max}}, x_{\epsilon_1^{\max}})$, together with the extra-parameter $x_{\rm end}$.

The trajectory in Eq. (5.78) cannot be inverted analytically. However, one can perform some consistency checks in the limit $x/x_{V^{\max}} \gg 1$ in which

$$N - N_{\rm end} \simeq \frac{1}{\beta\gamma\,(2-\gamma)}\left(x^{2-\gamma} - x_{\rm end}^{2-\gamma}\right), \tag{5.79}$$

and

$$x \simeq \left[x_{\rm end}^{2-\gamma} + \beta\gamma\,(2-\gamma)\,(N - N_{\rm end})\right]^{\frac{1}{2-\gamma}}. \tag{5.80}$$

These expressions can be compared to Eq. (5.66)

$$x = 2\frac{\sqrt{2A\lambda}}{\lambda+1}\left(\ln\frac{t}{t_0}\right)^{\frac{\lambda+1}{2}}, \tag{5.81}$$

where t in terms of the number of e-folds N can be obtained from Eq. (5.62). With $N - N_0 = A\,(\ln t/t_0)^{\lambda}$, one gets

$$x = 2\frac{\sqrt{2A\lambda}}{\lambda+1}\left(\frac{N-N_0}{A}\right)^{\frac{\lambda+1}{2\lambda}}. \tag{5.82}$$

The previous calculations are consistent since, making use of Eq. (5.69), Eq. (5.80) and Eq. (5.82) are the same when setting the constants $N_0 = N_{\rm ini}$ and $x_0 = x_{\rm ini} = 0$. This means that in the late times limit $x/x_{V^{\max}} \gg 1$, the slow-roll trajectory coincides with the exact one, as expected.

The amplitude of the CMB anisotropies fixes the value of the parameter M according to

$$\frac{M^4}{M_{\rm Pl}^4} = 720\pi^2\,(\alpha - \beta\gamma x_*^{\gamma})^2\, e^{\beta x_*^{\gamma}} x_*^{-\alpha-2}\frac{Q_{\rm rms-PS}^2}{T^2}, \tag{5.83}$$

where x_* is the observable field value obtained by solving Eq. (2.47) given some assumptions on the reheating. The reheating consistent slow-roll predictions for the models LMI1 and LMI2 (at $x > x_{\epsilon_1^{\max}}$) are displayed in Figs. 116, 117, and 118 for LMI1, and in Figs. 119, 120, and 121 for LMI2. In the case of LMI2, the turning points in the plots precisely correspond to the case where inflation occurs in the fine-tuned domain $x_{V^{\max}} < x_* < x_{\epsilon_1^{\max}}$ and in which the model behaves like a pure de Sitter era.

5.5 Twisted Inflation (TWI)

5.5.1 Theoretical Justifications

This model was introduced in Ref. [472] and is based on higher dimensional supersymmetric gauge theories. The idea is to assume that, in higher dimensions, we have a flat direction ϕ in the potential. Since the theory is supersymmetric, this flat direction will not receive corrections because the bosonic and fermionic contributions exactly cancel out. Then, we compactify the theory down to $3+1$ dimensions but with boundary conditions that break supersymmetry. The typical example given in Ref. [472] is "twisted" circle compactification, hence the name of the model. Since supersymmetry is broken, the "Kaluza-Klein" masses of bosons and fermions will differ. Typically, they can be written as

$$m_{\rm b} = \sqrt{\phi^2 + \frac{n^2}{R^2}}, \qquad m_{\rm f} = \sqrt{\phi^2 + \frac{(n+1/2)^2}{R^2}}, \tag{5.84}$$

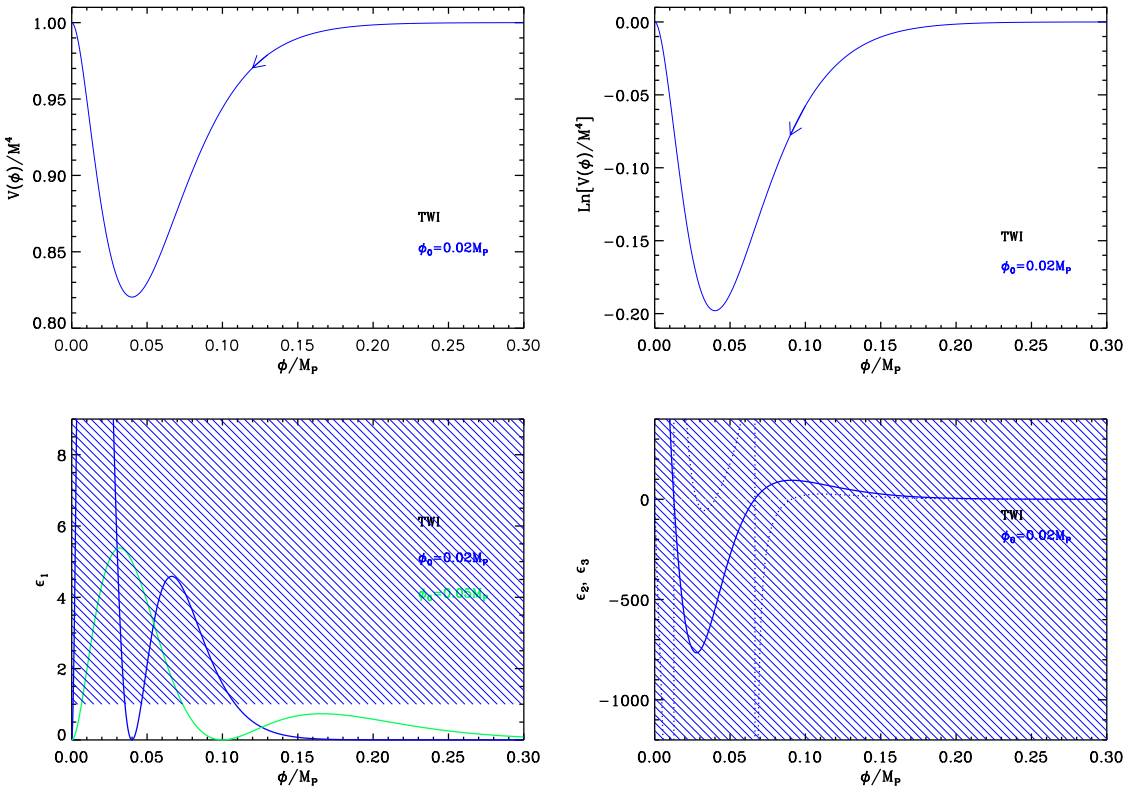

Figure 49. Top left panel: Twisted Potential Inflation (TWI) for $\phi_0 = 0.02 M_{\rm Pl}$. Top right panel: logarithm of the potential for the same value of ϕ_0. Bottom left panel: slow-roll parameter ϵ_1 with $\phi_0 = 0.02 M_{\rm Pl}$ (solid blue line) and $\phi_0 = 0.05 M_{\rm Pl}$ (solid green line). The shaded area indicates the non-inflationary region. Bottom right panel: slow-roll parameters ϵ_2 (solid line) and ϵ_3 (dotted line) with $\phi_0 = 0.02 M_{\rm Pl}$.

where R is the radius of compactification and n an integer. Since $m_{\rm b} \neq m_{\rm f}$, this time, the potential will receive one loop corrections which lift the potential. However, it is clear that, when $\phi R \gg n$, one has approximately $m_{\rm b} \simeq m_{\rm f}$. Therefore, in this regime, we expect the corrections to vanish and the flat direction to remain flat. This is thus particularly well-suited for inflation. In practice, the higher dimensional model considered to implement the above discussed mechanism is a maximally supersymmetric $4+1$ U($\mathcal{N}$) Yang-Mills theory compactified on a circle of radius R. A priori, we have therefore two parameters: $\mathcal{N}$ and the compactification scale R.

5.5.2 Slow-Roll Analysis

As shown in Ref. [472], the above considerations leads to the following expression for the inflaton potential

$$V(\phi) = M^4 \left[1 - A \left(\frac{\phi}{\phi_0} \right)^2 e^{-\phi/\phi_0} \right], \tag{5.85}$$

where A is a constant parameter given by

$$A \equiv \frac{32}{93\zeta\left(5\right)} \simeq 0.33\,, \tag{5.86}$$

and where ϕ_0 is related to the compactification scale R through the following equation

$$\frac{\phi_0}{M_{\rm Pl}} = \frac{1}{2\pi R M_{\rm Pl}}. \tag{5.87}$$

Since the radius R must be larger than the Planck length, i.e. $RM_{\rm Pl} \gg 1$, this implies that $\phi_0/M_{\rm Pl} \ll 1$. On the other hand, the overall normalization can be expressed as

$$M^4 = \frac{8\mathcal{N}}{A\pi^2(2\pi R)^4}\,. \tag{5.88}$$

We see that the scale M depends on the compactification radius R but also on the number $\mathcal{N}$. In addition, one must have $\phi < \sqrt{3/\mathcal{N}}M_{\rm Pl}$ or $\phi \ll M_{\rm Pl}$ which guarantees that the higher order Planck suppressed operators do not alter the potential. The potential (5.85) is the small coupling limit of the model, while the strong coupling limit corresponds to a BI model with $p = 3$, see section 5.19.

The potential Eq. (5.85), as well as its logarithm, is displayed in Fig. 49. Inflation is supposed to take place for *vev*'s larger than the scale ϕ_0, i.e. for $\phi > \phi_0$, in the increasing branch of the potential. This means that it proceeds from the right to the left in the direction indicated by the arrow. The minimum of the potential is located at $\phi/\phi_0 = 2$.

Let us now turn to the calculation of the Hubble flow parameters. If one defines x by $x \equiv \phi/\phi_0$, then they are given by

$$\epsilon_1 = \frac{A^2}{2}\left(\frac{M_{\rm Pl}}{\phi_0}\right)^2 e^{-2x}\left[\frac{x\left(x-2\right)}{1-Ax^2e^{-x}}\right]^2, \qquad \epsilon_2 = 2A\left(\frac{M_{\rm Pl}}{\phi_0}\right)^2 e^{-2x}\frac{2Ax^2+e^x\left(x^2-4x+2\right)}{\left(1-Ax^2e^{-x}\right)^2}, \tag{5.89}$$

and

$$\epsilon_3 = A\left(\frac{M_{\rm Pl}}{\phi_0}\right)^2 x\left(2-x\right)e^{-2x}\frac{4A^2x^3-e^{2x}\left(x^2-6x+6\right)-Axe^x\left(x^3-6x^2+18x-12\right)}{\left(1-Ax^2e^{-x}\right)^2\left[2Ax^2+e^x\left(x^2-4x+2\right)\right]}\,. \tag{5.90}$$

They are displayed in Fig. 49. The first slow-roll parameter ϵ_1 vanishes at the minimum of the potential when $x = 2$, then increases with x and reaches a maximum at $x_{\epsilon_1^{\rm max}}$, and finally decreases to zero when x goes to infinity. The value of ϵ_1 at this local maximum is larger than one if ϕ_0 is smaller than some value that can only be determined numerically. We find

$$\phi_0 < 0.04228 M_{\rm Pl}\,. \tag{5.91}$$

Therefore, a priori, inflation could stop by slow-roll violation. However, by numerically integrating the exact trajectory (i.e. if one does not make use of the slow-roll approximation), one realizes that, in fact, the first Hubble flow function, which is defined by $\epsilon_1^H = -\dot{H}/H^2$, remains smaller than one for all field values, see Fig. 50. This is due to the fact that while the inflaton rolls down its potential and approaches its minimum, the slow-roll parameters continuously increase and the slow-roll approximation is broken before ϵ_1 becomes $\mathcal{O}(1)$. Usually, this leads only to small corrections at the end of inflation. However, in the case

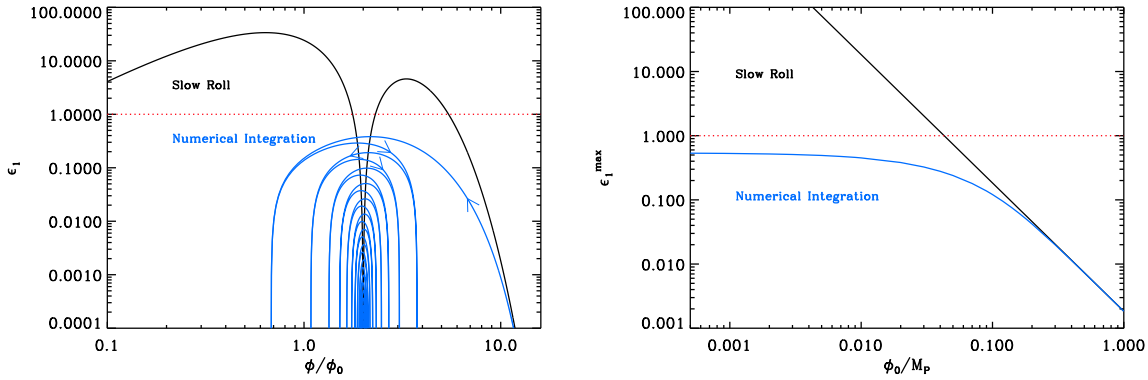

Figure 50. Left panel: slow-roll parameter ϵ_1 as a function of the field *vev* ϕ/ϕ_0, for $\phi_0/M_{\rm Pl} = 0.02 < 0.04228$, see Eq. (5.91). The solid black line corresponds to the approximated slow-roll formula (5.89), i.e. $\epsilon_1^V = M_{\rm Pl}^2/2\,V_\phi^2/V^2$, while the solid blue line represents the exact $\epsilon_1^H = -\dot{H}/H^2$ obtained from a numerical integration starting at $\phi_{\rm ini}/M_{\rm Pl} = 0.33$ and vanishing initial velocity. We see that the exact ϵ_1^H remains in fact always smaller than one and that inflation never stops. The inflaton eventually oscillates around the minimum of its potential located at $\phi = 2\phi_0$ (the arrows indicate the direction of the first oscillations). Right panel: Maximum value taken by ϵ_1^V (solid black line) and ϵ_1^H (solid blue line) for different values of ϕ_0. One can see that ϵ_1^H remains smaller than one for any value of ϕ_0. When ϕ_0 increases, the slow-roll parameters, which scale proportional to $M_{\rm Pl}^2/\phi_0^2$, decrease so that the slow-roll approximation becomes more and more efficient and eventually starts matching the numerical exact predictions.

of twisted inflation, this leads to a radically different picture because the potential does not vanish at its minimum and, therefore, acts as a cosmological constant. In practice, the numerical calculations indicate that the field oscillates around its minimum but always such that $\epsilon_1^H < 1$ and independently on the value of ϕ_0, see Fig. 50. In principle, inflation can never stops in this model since the final stage of the evolution corresponds to an inflaton field sitting for ever at the bottom of the potential and, as already mentioned, it acts as a cosmological constant. However, as explained in Ref. [472], the interactions of the inflaton field with the other degrees of freedom of the standard model starts to play a role in this regime. As a consequence, the energy contained in the inflaton field should quickly be transferred to other fields and a phase of reheating starts. The details of this process are complicated and are discussed in Ref. [472]. In order to model the end of inflation, we therefore introduce the extra parameter $x_{\rm end}$ giving the *vev* at which inflation stops. As a consequence, TWI is in fact a two parameter model, ϕ_0 and $\phi_{\rm end}$.

Let us now turn to the slow-roll trajectory. It can be integrated exactly and leads to the following expression

$$N_{\rm end} - N = \left(\frac{\phi_0}{M_{\rm Pl}}\right)^2 \left\{\frac{1}{2A}\left[{\rm Ei}\left(x_{\rm end}\right) - {\rm Ei}\left(x\right)\right] - \frac{e^2}{2A}\left[{\rm Ei}\left(x_{\rm end}-2\right) - {\rm Ei}\left(x-2\right)\right] + x_{\rm end} - x + 2\ln\left(\frac{x_{\rm end}-2}{x-2}\right)\right\}, \tag{5.92}$$

where $N_{\rm end}$ is the number of e-folds at the end of inflation and Ei is the exponential integral function [204, 205]. This expression is the one used in the `ASPIC` library. However, if one

makes the vacuum dominated approximation, $x \gg 1$, then a simpler formula can be derived for the trajectory, namely

$$N_{\rm end} - N \simeq \frac{1}{A}\left(\frac{\phi_0}{M_{\rm Pl}}\right)^2 \left(\frac{e^x}{x^2} - \frac{e^x_{\rm end}}{x^2_{\rm end}}\right). \tag{5.93}$$

This allows us to obtain an approximated expression for the *vev* of the field at Hubble radius crossing which reads

$$x_* \simeq \ln\left[4A\Delta N_* \left(\frac{M_{\rm Pl}}{\phi_0}\right)^2\right]. \tag{5.94}$$

It is valid provided $\phi_0/M_{\rm Pl} \ll 1$, i.e. precisely in the regime for which the TWI potential was derived. Using this formula, one can estimate the value of the three first Hubble flow parameters at Hubble crossing. One arrives at

$$\begin{aligned} \epsilon_{1*} &\simeq \frac{A^2}{2}\left(\frac{M_{\rm Pl}}{\phi_0}\right)^2 e^{-2x_*} x_*^4 \simeq \frac{1}{32\Delta N_*^2}\left(\frac{\phi_0}{M_{\rm Pl}}\right)^2, \\ \epsilon_{2*} &\simeq \frac{\epsilon_{3*}}{2} \simeq 2A\left(\frac{M_{\rm Pl}}{\phi_0}\right)^2 e^{-x_*} x_*^2 \simeq \frac{1}{2\Delta N_*}. \end{aligned} \tag{5.95}$$

Finally, we can derive an expression for the tensor-to-scalar ratio, the spectral index

$$r \simeq 8A^2\left(\frac{M_{\rm Pl}}{\phi_0}\right)^2 e^{-2x_*} x_*^4 \sim \frac{1}{2\Delta N_*^2}\left(\frac{\phi_0}{M_{\rm Pl}}\right)^2, \qquad n_{\rm S} - 1 \simeq -2A\left(\frac{M_{\rm Pl}}{\phi_0}\right)^2 x_*^2 e^{-x_*} \sim \frac{1}{2\Delta N_*}, \tag{5.96}$$

and the running

$$\alpha_{\rm S} \simeq -2A^2\left(\frac{M_{\rm Pl}}{\phi_0}\right)^4 x_*^4 e^{-2x_*} \simeq -\frac{1}{8\Delta N_*^2}. \tag{5.97}$$

These estimates are in agreement with the ones of Ref. [472], up to a missing factor 4 in Eq. (5.94). However, we have checked that this does not affect the predictions in a significant way.

It is also interesting to discuss the value of the scale M since this is important from the model building point of view. The CMB normalization gives

$$\frac{M^4}{M_{\rm Pl}^4} = 720\pi^2 A^2 \left(\frac{M_{\rm Pl}}{\phi_0}\right)^2 \frac{\left[e^{-x_*} x_* \left(x_* - 2\right)\right]^2}{\left(1 - A x_*^2 e^{-x_*}\right)^3} \frac{Q^2_{\rm rms-PS}}{T^2}. \tag{5.98}$$

In the vacuum dominated approximation, the above expression simplifies and gives $M^4/M_{\rm Pl}^4 \simeq 45\pi^2/\Delta N_*^2 \phi_0^2/M_{\rm Pl}^2 Q^2_{\rm rms-PS}/T^2$. This leads to

$$M_{\rm Pl} R = \sqrt{\frac{2\mathcal{N}}{45A}} \frac{\Delta N_*}{\pi^3} \frac{T}{Q_{\rm rms-PS}} \simeq 1.2 \times 10^5 \sqrt{\mathcal{N}}, \tag{5.99}$$

where we have taken $\Delta N_* \simeq 60$. This also implies that

$$\frac{\phi_0}{M_{\rm Pl}} \simeq \frac{1.35}{\sqrt{\mathcal{N}}} \times 10^{-5}. \tag{5.100}$$

Therefore, we have a rough determination of the compactification radius. The model seems consistent since we obtain that $M_{\rm Pl} R \gg 1$, in agreement with the assumptions made at the beginning of this section.

The predictions for TWI are presented in Fig. 122. The reheating equation of state parameter $\overline{w}_{\rm reh}$ has been taken to be 0 since the potential is quadratic close to its minimum. However, since the details of reheating depend on the details of the interactions between the inflaton field and the others degrees of freedom in the theory, this parameter is a priori unspecified and could very well take different values. In the `ASPIC` code, $\overline{w}_{\rm reh}$ can be freely chosen. Anyway, since the reheating temperature is in fact fully degenerate with the parameter $x_{\rm end}$, these two parameters can not be constrained independently. One can check that the rough description provided by Eqs. (5.96) is correct: the model typically predicts a small amount of gravitational waves which increases with ϕ_0, and a deviation from scale invariance which does not significantly depends on ϕ_0. When $\phi_0/M_{\rm Pl} = \mathcal{O}(1)$, however, one notices a turning point (at fixed values of ϕ_0). This corresponds to the separation between two regimes, one where $x_* < x_{\epsilon_1^{\rm max}}$ and ϵ_1 is an increasing function of x (hence ϵ_{1*} increases with $x_{\rm end}$) and another where $x_* > x_{\epsilon_1^{\rm max}}$ and ϵ_1 is a decreasing function of x (hence ϵ_{1*} decreases with $x_{\rm end}$). If a sufficient number of e-folds can be realized in the $2 < x < x_{\epsilon_1^{\rm max}}$ part of the potential, then ϵ_{2*} can become negative. However, this mostly happens for fine-tuned values of $x_{\rm end} \simeq 2$.

5.6 Generalized MSSM Inflation (GMSSMI)

As for the MSSMI models, see section 4.17, GMSSMI scenarios are based on the Minimal Supersymmetric Model (MSSM) in which a flat direction direction is lifted by soft supersymmetry breaking terms and by superpotential corrections. The potential is of the form

$$V(\phi) = \frac{1}{2}m_\phi^2\phi^2 - A\frac{\lambda_n}{n}\frac{\phi^n}{M_{\rm Pl}^{n-3}} + \lambda_n^2\frac{\phi^{2(n-1)}}{M_{\rm Pl}^{2(n-3)}}\,. \tag{5.101}$$

The MSSMI model corresponds to $n = 6$ and $A^2 = 8(n-1)m_\phi^2$. This last relation is of crucial importance since it implies an exact flat inflection point. Following Refs. [409, 410, 413, 473–476], one may wonder whether the model is robust when this relation is not exactly satisfied. In order to investigate this question, we therefore relax the condition $A^2 = 8(n-1)m_\phi^2$. In this more general case, the potential can be reparametrized in the form

$$V(\phi) = M^4\left[\left(\frac{\phi}{\phi_0}\right)^2 - \frac{2}{3}\alpha\left(\frac{\phi}{\phi_0}\right)^6 + \frac{\alpha}{5}\left(\frac{\phi}{\phi_0}\right)^{10}\right], \tag{5.102}$$

where $\phi_0 \simeq 10^{14}\,{\rm GeV}$, this value being the same as the one found in section 4.17. The positive dimensionless parameter α encodes any deviations from the MSSM case for which it equals unity, $\alpha_{\rm MSSM} = 1$.

The potential is displayed in Fig. 51, where four cases can be distinguished. In the following, we define the quantity x by the expression

$$x \equiv \frac{\phi}{\phi_0}\,. \tag{5.103}$$

If $\alpha < 9/25$, the second derivative of the potential does not vanish and the potential is convex everywhere. This corresponds to the case $\alpha = 0.1$ case in Fig. 51. If $9/25 < \alpha < 1$, the potential has two inflection points $x^{\pm}_{V''=0}$ and is concave in between. It remains an increasing function of the field since its first derivative never vanishes. This is illustrated with the case $\alpha = 0.7$ in Fig. 51. If $\alpha = 1$, this is the MSSM inflation models (see section 4.17) where

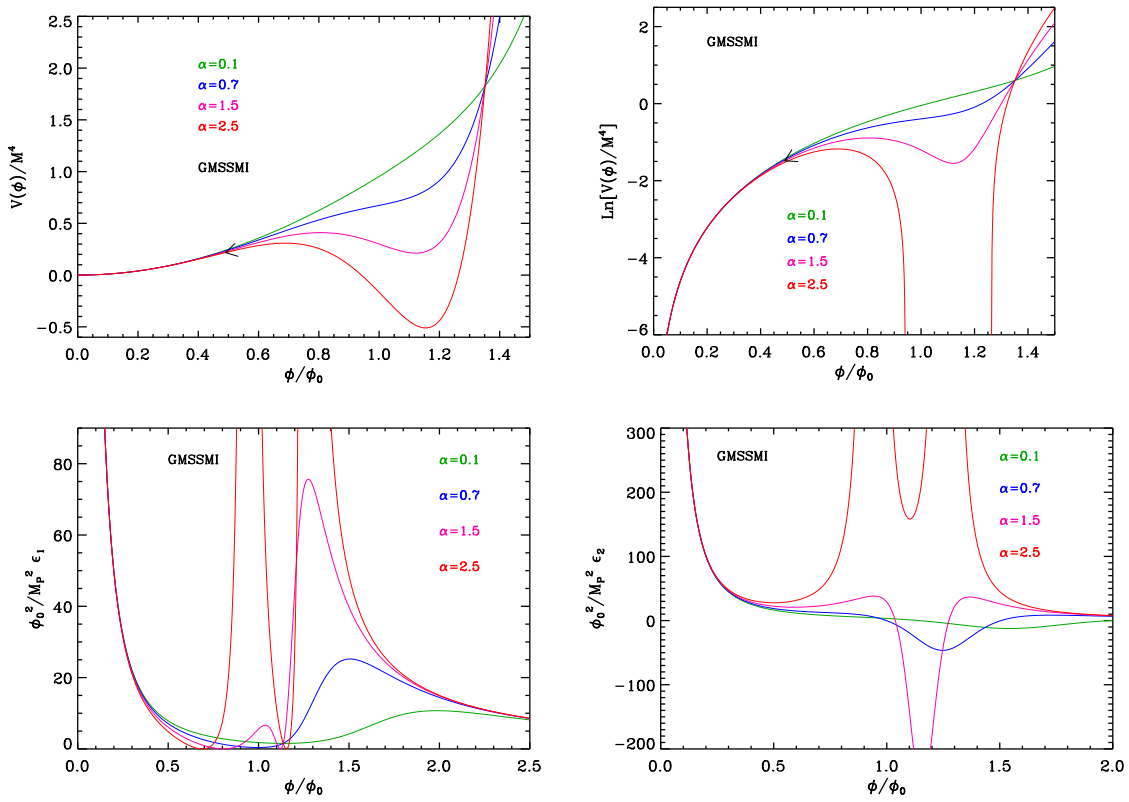

Figure 51. GMSSM Inflation (GMSSMI). Top left panel: GMSSM Inflation potential Eq. (5.102) for $\alpha = 0.1, 0.7, 1.5, 2.5$, as a function of ϕ/ϕ_0. Top right panel: logarithm of the potentials for the same value of α. Bottom left panel: slow-roll parameter ϵ_1 for a potential with the same values of α. Bottom right panel: slow-roll parameter ϵ_2 for a potential with the same values of α. See discussion in the text body.

the potential has a flat inflection point. If $1 < \alpha < 9/5$, the potential decreases in between $x^{\pm}_{V'=0}$ but remains positive everywhere. This is exemplified by the case $\alpha = 1.5$ in Fig. 51. Finally, if $\alpha > 9/5$, the potential becomes negative (hence is not properly defined) between the two points $x^{\pm}_{V=0}$ (see $\alpha = 2.5$ in Fig. 51). The values of the field *vev*'s appearing in this discussion are given by the following formulas:

$$x^{\pm}_{V''=0} = \left[\frac{5}{9}\left(1 \pm \sqrt{1 - \frac{9}{25\alpha}}\right)\right]^{1/4}, \qquad x^{\pm}_{V'=0} = \left(1 \pm \sqrt{1 - \frac{1}{\alpha}}\right)^{1/4}, \tag{5.104}$$

and

$$x^{\pm}_{V=0} = \left[\frac{5}{3}\left(1 \pm \sqrt{1 - \frac{9}{5\alpha}}\right)\right]^{1/4}. \tag{5.105}$$

Let us now calculate the first three Hubble flow functions in the slow-roll approximation.

They are given by

$$\begin{aligned}\epsilon_1 &= 450\left(\frac{M_{\rm Pl}}{\phi_0}\right)^2 \frac{\left(1-2\alpha x^4+\alpha x^8\right)^2}{x^2\left(15-10\alpha x^4+3\alpha x^8\right)^2}\,,\\ \epsilon_2 &= 60\left(\frac{M_{\rm Pl}}{\phi_0}\right)^2 \frac{15+40\alpha x^4+\alpha\left(20\alpha-78\right)x^8+3\alpha^2x^{16}}{x^2\left(15-10\alpha x^4+3\alpha x^8\right)^2}\,,\end{aligned} \tag{5.106}$$

and

$$\begin{aligned}\epsilon_3 = 60\left(\frac{M_{\rm Pl}}{\phi_0}\right)^2 &\left[225-1800\alpha x^4+60\alpha\left(69+10\alpha\right)x^8-40\left(189-100\alpha\right)\alpha^2x^{12}\right.\\ &+10\alpha^2\left(243-504\alpha+402\alpha^2\right)x^{16}+40\alpha^3\left(117-20\alpha\right)x^{20}+12\alpha^3\left(10\alpha-123\right)x^{24}\\ &\left.+72\alpha^4x^{28}+9\alpha^4x^32\right]\times\left[3375x^2+4500\alpha x^6-600\alpha\left(27+10\alpha\right)x^{10}\right.\\ &+100\alpha^2\left(261-20\alpha\right)x^{14}+10\alpha^2\left(200\alpha^2-840\alpha-621\right)x^{18}+60\alpha^3\left(69-20\alpha\right)x^{22}\\ &\left.+48\alpha^3\left(10\alpha-9\right)x^{26}-180\alpha^4x^{30}+27\alpha^4x^{34}\right]^{-1}.\end{aligned} \tag{5.107}$$

The first two slow-roll parameters diverge when $x\to 0$ and vanish asymptotically. In between, their shape depends on α as it is represented in Fig. 51. If $\alpha<1$, ϵ_1 first decreases, reaches a local non-zero minimum where ϵ_2 vanishes, then increases to reach a local maximum where ϵ_2 vanishes again, and eventually decreases again. Let $x^{\pm}_{\epsilon_2=0}$ be the position of these two local extrema. From Ferrari's solutions for depressed quartic equations one gets

$$x^{\pm}_{\epsilon_2=0} = \left[\frac{1}{2\alpha}\sqrt{\frac{5}{3}}\left(\sqrt{\Sigma}\pm 2\sqrt{\frac{39}{5}\alpha-2\alpha^2-\frac{\Sigma}{4}-\frac{12}{\sqrt{15\Sigma}}\alpha^2}\right)\right]^{1/4}, \tag{5.108}$$

where

$$\begin{aligned}\delta &= \frac{736\alpha^2}{25}-\frac{208\alpha^3}{15}+\frac{16\alpha^4}{9}\,,\\ \Delta &= -\frac{430336\alpha^4}{625}+\frac{612352\alpha^5}{1125}-\frac{20992\alpha^6}{225}+\frac{256\alpha^8}{243}\,,\\ \sigma &= -\frac{12896\alpha^3}{125}+\frac{2944\alpha^4}{25}-\frac{416\alpha^5}{15}+\frac{64\alpha^6}{27}+\frac{6}{5}\sqrt{15\Delta}\alpha\,,\\ \Sigma &= \frac{52\alpha}{5}-\frac{8\alpha^2}{3}+\frac{\delta}{\sigma^{1/3}}+\sigma^{1/3},\end{aligned} \tag{5.109}$$

are intermediate quantities introduced solely to reduce the size of Eq. (5.108). If $\alpha>1$, ϵ_1 has two local minimums located at $x^{\pm}_{V'=0}$ where it vanishes. In between it reaches a local maximum or may even diverges for $\alpha>9/5$ (see Fig. 51). The slow-roll parameter ϵ_2 vanishes when ϵ_1 reaches these local maxima, or diverge when ϵ_1 does (for $\alpha>9/5$). As explained in section 4.17, inflation is meant to proceed at $\phi\lesssim\phi_0$. Let us assume that inflation can end for $\epsilon_1>1$ between $x=0$ and the position of the first minimum $x_{\epsilon_1^{\rm min}}$. Following the previous considerations, this latter location is defined as

$$x_{\epsilon_1^{\rm min}} = \begin{cases} x^{-}_{\epsilon_2=0} & \text{if} \quad \alpha<1 \\ x^{-}_{V'=0} & \text{if} \quad \alpha>1 \end{cases}, \tag{5.110}$$

and provides an upper bound to $x_{\rm end}$ the solution of $\epsilon_1(x_{\rm end})=1$. This one can only be determined numerically. The values of $x^{\pm}_{\epsilon_2=0}$ and $x^{\pm}_{V'=0}$ in terms of α are displayed in the

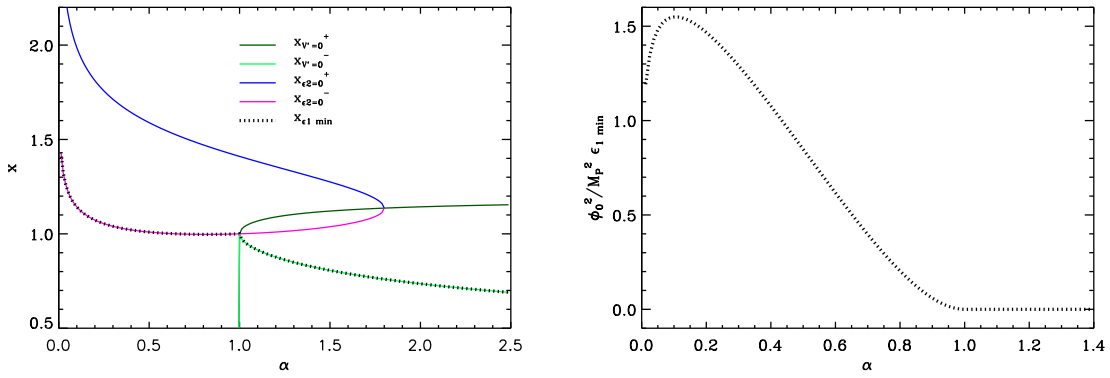

Figure 52. GMSSM Inflation (GMSSMI). Left panel: $x^{\pm}_{\epsilon_2=0}$ defined in Eq. (5.108) and $x^{\pm}_{V'=0}$ defined in Eq. (5.104) together with $x_{\epsilon_1^{\rm min}}$ [see Eq. (5.110)] as a function of α. Right panel: minimal value of the slow-roll parameter ϵ_1 (rescaled by $\phi_0^2/M_{\rm Pl}^2$) as a function of α. When it is greater than unity, inflation cannot occur.

left panel in Fig. 52 together with $x_{\epsilon_1^{\rm min}}$. The right panel of Fig. 52 represents the value of the first slow-roll parameter at this minimum, $\epsilon_1^{\rm min} = \epsilon_1(x_{\epsilon_1^{\rm min}})$. For $\alpha < 1$, one can see that $\epsilon_1^{\rm min} < 1$ only if the parameter $\alpha \lesssim 1$. This defines a minimum value for α, which depends on ϕ_0, such that inflation can take place within this domain. When $\alpha \simeq 1$, one can derive an approximated version of Eq. (5.108), namely, $x^{-}_{\epsilon_2=0} \simeq 1 - (1-\alpha)/32$. Plugging it into the expression for ϵ_1 one obtains

$$\epsilon_1^{\rm min} \simeq \frac{225}{32}(\alpha-1)^2\frac{M_{\rm Pl}^2}{\phi_0^2}\,, \tag{5.111}$$

from which one gets

$$\alpha > 1 - \frac{4\sqrt{2}}{15}\frac{\phi_0}{M_{\rm Pl}}\,. \tag{5.112}$$

For the value suggested in Ref. [406], $\phi_0/M_{\rm Pl} \simeq 10^{-4}$, one obtains $\alpha > 1 - 10^{-5}$, which is in agreement with Ref. [473], and shows that the model needs to be sufficiently fine-tuned (i.e. sufficiently close to regular MSSM inflation) in order to be a viable inflationary model.

On top of that, as shall be seen now, the constraints on α are even tighter if one wants a sufficient number of e-folds to be produced. Let us thus turn to the slow-roll trajectory. It can be integrated, and leads to

$$\begin{aligned} N_{\rm end} - N = \frac{\phi_0^2}{M_{\rm Pl}^2}\Bigg\{ &-\frac{x_{\rm end}^2 - x^2}{20} - \frac{b_+}{10\sqrt{a_+}}\left[\arctan\left(\sqrt{a_+}x_{\rm end}^2\right) - \arctan\left(\sqrt{a_+}x^2\right)\right] \\ &- \frac{b_-}{10\sqrt{a_-}}\left[\arctan\left(\sqrt{a_-}x_{\rm end}^2\right) - \arctan\left(\sqrt{a_-}x^2\right)\right]\Bigg\}\,, \end{aligned} \tag{5.113}$$

where

$$a_\pm = -\alpha \pm \sqrt{\alpha^2-\alpha}\,, \qquad b_\pm = 2\frac{a_\pm + \alpha/3}{a_\pm - a_\mp}\,, \tag{5.114}$$

A few remarks are in order. Firstly, even if the terms appearing in the previous expression are complex, their imaginary contributions cancel out and the resulting expression is truly

a real quantity. Then, one can check that formally, when $\alpha \to 0$, one has $a_\pm \to 0$ and $b_\pm \to 1$, hence $N \simeq -\left(x^2 - x_{\rm ini}^2\right)/4$, which is precisely the LFI slow-roll trajectory for $p = 2$, see section 4.2. This is just a formal check since α is meant to be tuned close to 1 in the GMSSMI scenario. Finally, let us notice that, in the case $\alpha < 1$, and contrary to the MSSM models ($\alpha = 1$), the number of e-folds never diverges at a given point x. Therefore, the total number of e-folds is bounded from above for the field *vev*'s considered here. Working out the limit of Eq. (5.113) when $\alpha \to 1$, one has

$$N_{\rm end} - N_{\rm ini} \leq \left(\frac{\phi_0}{M_{\rm Pl}}\right)^2 \frac{\pi}{30} \frac{1}{\sqrt{1-\alpha}} \,. \tag{5.115}$$

If one require at least $\Delta N = N_{\rm end} - N_{\rm ini}$ e-folds during inflation, then α has to be fine-tuned to

$$\alpha > 1 - \left(\frac{\phi_0}{M_{\rm Pl}}\right)^4 \frac{\pi^2}{900 \Delta N^2} \,. \tag{5.116}$$

Remembering that the small parameter here is $\phi_0/M_{\rm Pl}$, one can see that it is a much tighter constraint than the one of Eq. (5.112). Taking $\phi_0/M_{\rm Pl} \simeq 10^{-4}$ and $\Delta N \simeq 50$, one obtains $\alpha > 1 - 10^{-22}$. This is clearly an extreme fine-tuning which can even make the numerical investigation of the model challenging[6]. As explained below, the same condition $|\alpha - 1| < \phi_0^4/M_{\rm Pl}^4/\Delta N^2$ also applies to the case $\alpha > 1$ in order to maintain an acceptable deviation from scale invariance. This makes GMSSM inflation a severely fine-tuned scenario. Let us also notice that our parameter α is related to the parameter δ of Ref. [474] by $\delta = \sqrt{\alpha^{-2} - 1}$. Ref. [474] finds that, in order for the model to be compatible with the data, $\delta \simeq 10^{-20}$. Therefore, although our method slightly differs from that of Ref. [474], our results are in broad agreement.

Finally, the amplitude of the CMB anisotropies fixes the parameter M to

$$\left(\frac{M}{M_{\rm Pl}}\right)^4 = 2880\pi^2 \frac{M_{\rm Pl}^2}{\phi_0^2} \frac{\left(1 - 2\alpha x_*^4 + \alpha x_*^8\right)^2}{x_*^4 \left(1 - \frac{2}{3}\alpha x_*^4 + \frac{\alpha}{5} x_*^8\right)^3} \frac{Q_{\rm rms-PS}^2}{T^2} \,. \tag{5.117}$$

As explained in section 4.17, this leads to $M/M_{\rm Pl} \simeq 10^8$ GeV for $\phi_0/M_{\rm Pl} \simeq 10^{-4}$.

The reheating consistent slow-roll predictions of the GMSSMI models are displayed in Figs. 123, 124, for $\alpha > 1$ and $\alpha < 1$, respectively. The reheating equation of state parameter $\overline{w}_{\rm reh}$ has been taken to 0 since the potential is quadratic close to its minimum. In both cases, one can see that in the limit $\alpha \to 1$, the standard MSSM predictions are recovered, see Fig. 104. The amount of gravitational waves r seems to be quite independent on α and, therefore, is similar to its regular MSSM counterpart. On the other hand, the spectral index $n_{\rm S}$ strongly depends on α. In the case $\alpha > 1$, larger values of $\alpha - 1$ worsens the spectral index problem, already present in standard MSSMI. These models are therefore strongly disfavored by the data. In the case $\alpha < 1$ however, there is a very narrow range of acceptable values for α. They are well inside the $|\alpha - 1| < \phi_0^4/M_{\rm Pl}^4/\Delta N^2$ condition and the spectral index is inside the two-sigma confidence intervals. But, as can be seen in Fig. 124, the spectral index varies so quickly with α that one has to fine-tune the power of the fine-tuning to remain inside the two-sigma contours. In Refs. [410, 473–476], it is argued that, since the flat saddle point condition is robust against radiative corrections, such a fine-tuning may not be a problem. However, as explained here and in section 4.17, if the flat saddle point condition is exactly satisfied, the model is disfavored by the observations because the spectral index is too red. The only way out is therefore to detune the condition $\alpha = 1$ at an extremely fine-tuned level.

[6] This exceeds the usual 64 bits precision on floating point numbers (FP64).

5.7 Generalized Renormalizable Point Inflation (GRIPI)

As for the MSSMI models (see section 4.17) and for the RIPI models (see section 4.18), the GRIPI models have a potential of the form

$$V(\phi) = \frac{1}{2}m_\phi^2\phi^2 - A\frac{\lambda_n}{n}\frac{\phi^n}{M_{\rm Pl}^{n-3}} + \lambda_n^2\frac{\phi^{2(n-1)}}{M_{\rm Pl}^{2(n-3)}}\,. \tag{5.118}$$

In section 4.18, the particular example $n = 3$ is discussed in the case where the potential has a flat inflection point, i.e. when $A^2 = 16m_\phi^2$. Then, as studied in section 5.6 for MSSMI, comes the question of what happens when we relax this condition. To address this issue, it is convenient to reparametrize the potential as

$$V(\phi) = M^4\left[\left(\frac{\phi}{\phi_0}\right)^2 - \frac{4}{3}\alpha\left(\frac{\phi}{\phi_0}\right)^3 + \frac{\alpha}{2}\left(\frac{\phi}{\phi_0}\right)^4\right], \tag{5.119}$$

where the positive dimensionless parameter α encodes the deviation from the RIPI case (that is to say $\alpha_{\rm RIPI} = 1$). This model was studied in Ref. [477] and in Refs. [478, 479]. In the first reference, the mass m_ϕ is fixed by the soft supersymmetry breaking terms and, in section 4.18, it was shown that this leads to $\phi_0 \simeq 10^{14}\,$GeV. However, in Refs. [478, 479], the scale m_ϕ is no longer controlled by the soft supersymmetry breaking terms but by the right-handed neutrino mass in Type I supersymmetric seesaw and this leads to a different value for ϕ_0, namely $\phi_0 \simeq 10^{17}\,$GeV. Therefore, in what follows, we will use both values.

The potential is displayed in Fig. 53, where four cases can be distinguished. In the following, for convenience, we use the quantity x defined by

$$x \equiv \frac{\phi}{\phi_0}\,. \tag{5.120}$$

If $\alpha < 3/4$, the second derivative of the potential does not vanish and the potential is convex everywhere. This corresponds to the case $\alpha = 0.7$ case in Fig. 53. If $3/4 < \alpha < 1$, the potential has two inflection points $x^\pm_{V''=0}$ and is concave in between. It remains an increasing function of the field since its first derivative never vanishes. This is illustrated by the case $\alpha = 0.85$ in Fig. 53. If $\alpha = 1$, then this is the RIPI model (see section 4.18) where the potential has a flat inflection point. If $1 < \alpha < 9/8$, then the potential decreases between the two values of x, $x^\pm_{V'=0}$, for which the derivative is zero, but remains positive everywhere. Typically, this corresponds to the case $\alpha = 1.094$ in Fig. 53. Finally, if $\alpha > 9/8$, then the potential becomes negative (hence is not properly defined everywhere) between $x^\pm_{V=0}$ (see the case $\alpha = 1.188$ in Fig. 53). The values of the field *vev* in this discussion are given by the following formulas:

$$x^\pm_{V''=0} = \frac{2}{3}\left(1 \pm \sqrt{1 - \frac{3}{4\alpha}}\right), \qquad x^\pm_{V'=0} = 1 \pm \sqrt{\frac{\alpha-1}{\alpha}}\,, \tag{5.121}$$

and

$$x^\pm_{V=0} = \frac{4}{3}\left(1 \pm \sqrt{1 - \frac{9}{8\alpha}}\right). \tag{5.122}$$

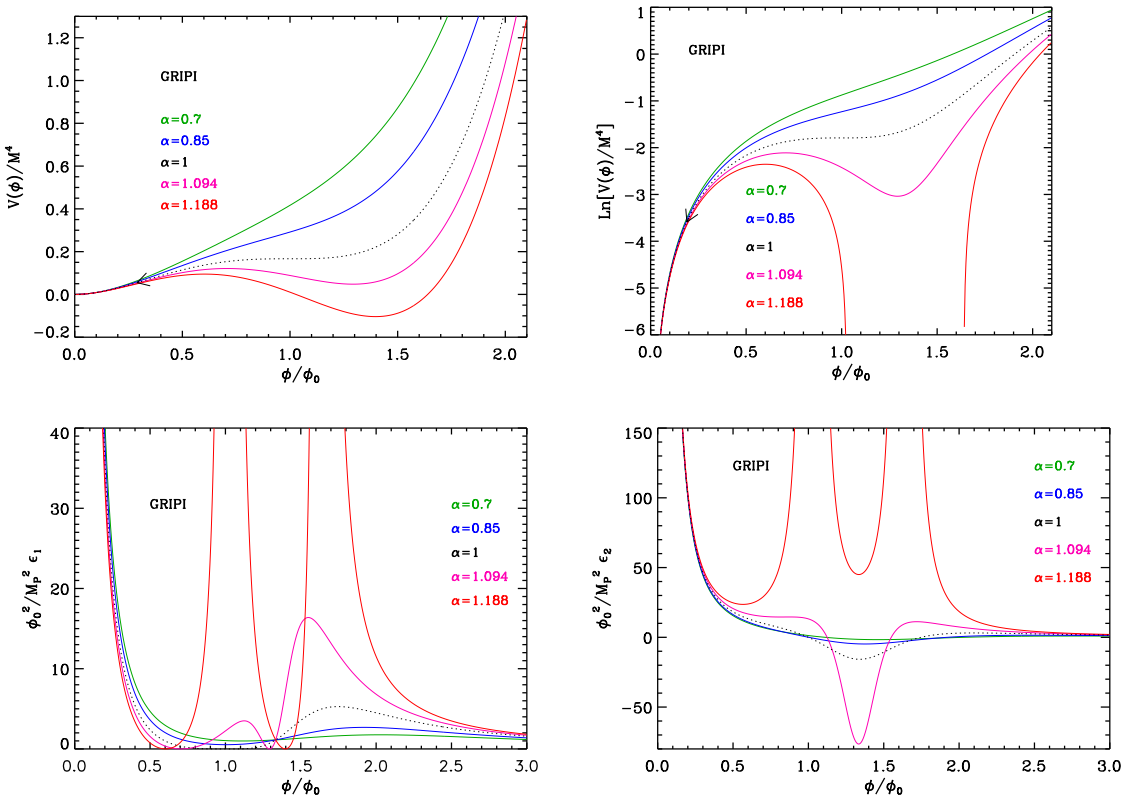

Figure 53. Top left panel: Generalized Renormalizable Point Inflation (GRIPI) potential given by Eq. (5.119) for $\alpha = 0.7, 0.85, 1, 1.094, 1.188$, as a function of ϕ/ϕ_0. Top right panel: logarithm of the potentials for the same values of α. Bottom left panel: slow-roll parameter ϵ_1 rescaled by $M_{\rm Pl}^2/\phi_0^2$, for GRIPI models with the same values of α. Bottom right panel: slow-roll parameter ϵ_2, rescaled by $M_{\rm Pl}^2/\phi_0^2$. A description of these various quantities can be found in the text.

Let us now calculate the first Hubble flow functions in the slow-roll approximation. They are given by

$$\begin{aligned}\epsilon_1 &= 72\left(\frac{M_{\rm Pl}}{\phi_0}\right)^2 \frac{\left(1-2\alpha x+\alpha x^2\right)^2}{x^2\left(6-8\alpha x+3\alpha x^2\right)^2}\,,\\ \epsilon_2 &= 24\left(\frac{M_{\rm Pl}}{\phi_0}\right)^2 \frac{6-16\alpha x+\left(3+16\alpha\right)\alpha x^2-12\alpha^2x^3+3\alpha^2x^4}{x^2\left(6-8\alpha x+3\alpha x^2\right)^2}\,,\end{aligned} \tag{5.123}$$

and

$$\begin{aligned}\epsilon_3 =& 24\left(\frac{M_{\rm Pl}}{\phi_0}\right)^2\left[36-216\alpha x+30\alpha\left(3+16\alpha\right)x^2-8\left(45+64\alpha\right)\alpha^2x^3\right.\\ &+2\left(27+276\alpha+128\alpha^2\right)\alpha^2x^4-2\left(208\alpha+81\right)\alpha^3x^5+9\left(1+28\alpha\right)\alpha^3x^6\\ &\left.-72\alpha^4x^7+9\alpha^4x^8\right]\times\left[x^2\left(6-8\alpha x+3\alpha x^2\right)^2\left(6-16\alpha x+3\alpha x^2+16\alpha^2x^2\right.\right.\\ &\left.\left.-12\alpha^2x^3+3\alpha^2x^4\right)\right]^{-1}.\end{aligned} \tag{5.124}$$

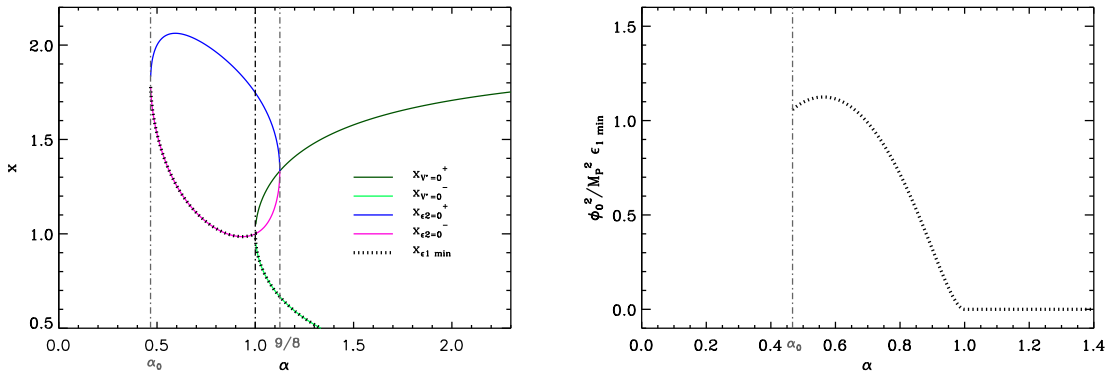

Figure 54. Left panel: $x^{\pm}_{\epsilon_2=0}$ and $x^{\pm}_{V'=0}$ [defined in Eq. (5.121)] together with $x_{\epsilon_1^{\min}}$ [see Eq. (5.126)] as a function of α. Right panel: minimal value of the slow-roll parameter ϵ_1, i.e. $\epsilon_1(x_{\epsilon_1^{\min}})$, rescaled by $\phi_0^2/M_{\mathrm{Pl}}^2$, as a function of α. When it is greater than unity, inflation cannot occur.

The first two slow-roll parameters diverge when $x \to 0$ and asymptotically goes to zero when $x \to \infty$. In between, their behavior depends on α as can be seen in Fig. 53. If $\alpha < \alpha_0$, where

$$\alpha_0 = \frac{3}{16}\left[5 - 3^{2/3}\left(6-2\sqrt{3}\right)^{-1/3} - 2^{-2/3}\left(9-3\sqrt{3}\right)^{1/3}\right] \simeq 0.4671, \tag{5.125}$$

ϵ_1 monotonously decreases with x. If $\alpha_0 < \alpha < 1$, ϵ_1 first decreases, reaches a local non-vanishing minimum at a value of x for which ϵ_2 vanishes, then increases to reach a local maximum where ϵ_2 vanishes again, and eventually decreases for $x \to \infty$, as already mentioned. Let $x^{\pm}_{\epsilon_2=0}$ be the position of these two local extrema. Similarly to Eq. (5.108) for the generalized MSSM inflation models, analytic expressions can be obtained for these two quantities using Ferrari's solutions for depressed quartic equations. They are implemented in `ASPIC` but are not displayed here since this does not add much to the discussion. If $\alpha > 1$, ϵ_1 has two local minima located at $x^{\pm}_{V'=0}$ where it vanishes. In between it reaches a local maximum or may even diverge for $\alpha > 9/8$ (see Fig. 53). The slow-roll parameter ϵ_2 vanishes when ϵ_1 reaches these local maxima, or diverge when ϵ_1 itself diverges (for $\alpha > 9/8$).

As explained in section 4.18, inflation is supposed to proceed at $\phi \lesssim \phi_0$. Let us assume that inflation ends by violation of slow-roll between $x = 0$ and the position of the first minimum $x_{\epsilon_1^{\min}}$. Following the previous considerations, this latter value of x is defined by

$$x_{\epsilon_1^{\min}} = \begin{cases} x^{-}_{\epsilon_2=0} & \text{if} \quad \alpha_0 < \alpha < 1 \\ x^{-}_{V'=0} & \text{if} \quad \alpha > 1 \end{cases}, \tag{5.126}$$

and, moreover, provides an upper bound to determine x_{end} [i.e. the solution of the equation $\epsilon_1(x_{\mathrm{end}}) = 1$]. Let us emphasize that this one can only be determined numerically. The values of $x^{\pm}_{\epsilon_2=0}$ and $x^{\pm}_{V'=0}$ in terms of α are displayed in the left panel of Fig. 54 together with $x_{\epsilon_1^{\min}}$. The right panel of Fig. 54 represents the value of the first slow-roll parameter at this minimum, $\epsilon_1^{\min} = \epsilon_1(x_{\epsilon_1^{\min}})$. For $\alpha < \alpha_0$, one has $\epsilon_1(x=1) > 1.5 M_{\mathrm{Pl}}^2/\phi_0^2$ and, recalling that typically $\phi_0 \simeq 10^{14}\,\mathrm{GeV}$ or $\phi_0 \simeq 10^{17}\,\mathrm{GeV}$, one sees that inflation cannot proceed in this case. For $\alpha_0 < \alpha < 1$, one has $\epsilon_1^{\min} < 1$ only if the parameter $\alpha \lesssim 1$. This defines a minimum

value for α, which depends on ϕ_0, allowing for inflation to take place. When $\alpha \simeq 1$, one can derive an approximated formula for $x^-_{\epsilon_2=0}$, namely, $x^-_{\epsilon_2=0} \simeq 1-(1-\alpha)/2$. Plugging it into the expression for ϵ_1 one obtains

$$\epsilon_1^{\min} \simeq 72(\alpha-1)^2\frac{M_{\rm Pl}^2}{\phi_0^2}\,, \tag{5.127}$$

from which it follows that

$$\alpha > 1-\frac{\sqrt{2}}{12}\frac{\phi_0}{M_{\rm Pl}}\,. \tag{5.128}$$

With $\phi_0/M_{\rm Pl} \simeq 10^{-1}$, one obtains $\alpha > 0.99$, which shows that the model needs to be sufficiently fine-tuned such that it becomes very similar to the regular RIPI scenario. If, on the other hand, $\phi_0/M_{\rm Pl} \simeq 10^{-4}$, the constraint is much tighter. As discussed in Refs. [478, 479], one of the main advantage of the model studied in those references is that a value $\phi_0 \simeq 10^{17}$GeV leads to a less severe fine tuning problem than $\phi_0 \simeq 10^{14}$GeV.

However, the constraints on α are tighter to get a sufficient number of e-folds. Let us therefore now turn to the determination of the slow-roll trajectory. It can be integrated exactly to give

$$\begin{aligned} N_{\rm end}-N = \frac{\phi_0^2}{M_{\rm Pl}^2}\Bigg\{&\frac{5-4\alpha}{12\sqrt{\alpha\,(1-\alpha)}}\arctan\left(\frac{x-1}{\sqrt{1/\alpha-1}}\right)+\frac{x}{2}\left(\frac{x}{4}-\frac{1}{3}\right)\\ &+\left(\frac{1}{8\alpha}-\frac{1}{6}\right)\ln\left[1+\alpha x\,(x-2)\right]-\frac{5-4\alpha}{12\sqrt{\alpha\,(1-\alpha)}}\arctan\left(\frac{x_{\rm end}-1}{\sqrt{1/\alpha-1}}\right)\\ &-\frac{x_{\rm end}}{2}\left(\frac{x_{\rm end}}{4}-\frac{1}{3}\right)-\left(\frac{1}{8\alpha}-\frac{1}{6}\right)\ln\left[1+\alpha x_{\rm end}\,(x_{\rm end}-2)\right]\Bigg\}\,. \end{aligned} \tag{5.129}$$

Exactly the same remarks we have made for the GMSSMI model also applies here (see section 5.6). In particular, for $\alpha < 1$, and contrary to the RIPI models ($\alpha = 1$), the number of e-folds never diverges at a given point x. Therefore, the total number of e-folds is bounded by some maximal finite value. From Eq. (5.129) when $\alpha \to 1$, one has

$$N_{\rm end}-N_{\rm ini} \leq \left(\frac{\phi_0}{M_{\rm Pl}}\right)^2\frac{\pi}{24}\frac{1}{\sqrt{1-\alpha}}\,. \tag{5.130}$$

Therefore, if one require at least $\Delta N = N_{\rm end}-N_{\rm ini}$ e-folds, one has to fine-tune α to

$$\alpha > 1-\left(\frac{\phi_0}{M_{\rm Pl}}\right)^4\frac{\pi^2}{576\Delta N^2}\,. \tag{5.131}$$

Remembering that the small parameter here is $\phi_0/M_{\rm Pl}$, one can see that it is a much tighter constraint than the one of Eq. (5.128). Taking $\phi_0/M_{\rm Pl} \simeq 10^{-1}$ and $\Delta N \simeq 50$, one obtains $\alpha > 1-10^{-10}$. This makes the fine-tuning quite important and, as explained below, the same condition $|\alpha-1| < \phi_0^4/M_{\rm Pl}^4/\Delta N^2$ also applies to the case $\alpha > 1$ to maintain an acceptable deviation from scale invariance, making the whole class of models fine-tuned. However, as already mentioned above, the value $\phi_0 \simeq 10^{17}$GeV makes the fine-tuning issue easier to accept than the value $\phi_0 \simeq 10^{14}$GeV.

Finally, the amplitude of the CMB anisotropies fixes the parameter M to

$$\left(\frac{M}{M_{\rm Pl}}\right)^4 = 622080\pi^2\frac{M_{\rm Pl}^2}{\phi_0^2}\frac{\left(1-2\alpha x_*+\alpha x_*^2\right)^2}{x_*^4\left(6-8\alpha x_*+3\alpha x_*^2\right)^3}\frac{Q_{\rm rms-PS}^2}{T^2}\,. \tag{5.132}$$

As explained in section 4.17, this leads to $M/M_{\rm Pl} \simeq 10^{13}\,{\rm GeV}$ for $\phi_0/M_{\rm Pl} \simeq 10^{-4}$.

The reheating consistent slow-roll predictions of the GRIPI models are displayed in Figs. 125, 126, for $\alpha > 1$ and $\alpha < 1$ respectively, and for values of ϕ_0 such that $\phi_0 \simeq 10^{17}\,{\rm GeV}$: $\phi_0/M_{\rm Pl} = 10^{-2}$, $10^{-1.5}$, 10^{-1}, $10^{-0.5}$, 1. The reheating equation of state parameter $\overline{w}_{\rm reh}$ has been taken to 0 since the potential is quadratic close to its minimum. In both cases, one can see that in the limit $\alpha \to 1$, the standard RIPI predictions are recovered, see Fig. 105. The amount of gravitational waves r seems to be quite independent on α while the spectral index $n_{\rm S}$ strongly depends on it. In the case $\alpha > 1$, the fine-tuning is as important as in the case $\alpha < 1$ as mentioned above. Considering values of α very different from 1 worsens the spectral index problem, already present in standard RIPI. These models are therefore strongly disfavored by the data. In the case $\alpha < 1$ however, there is a very narrow range of acceptable values for α. They are well inside the $|\alpha - 1| < \phi_0^4/M_{\rm Pl}^4/\Delta N^2$ condition and the spectral index is inside the two-sigma confidence intervals. But as can be seen in Fig. 126, the spectral index varies so quickly with α that, even if the fine-tuning is less problematic than in the GMSSMI case (due to the different value of ϕ_0), it is still very important.

5.8 Brane SUSY breaking Inflation (BSUSYBI)

This model has been studied in Ref. [480] in the context of superstrings models[7]. The potential is a sum of two exponential terms

$$V(\phi) = M^4 \left(e^{\sqrt{6}\frac{\phi}{M_{\rm Pl}}} + e^{\sqrt{6}\gamma\frac{\phi}{M_{\rm Pl}}} \right), \tag{5.133}$$

one is a "hard" exponential brought about by a SUSY breaking mechanism and the other is a "slow-roll term" having $0 < \gamma < 1/\sqrt{3}$ and that dominates the eventual inflationary dynamics. It was shown in Ref. [480] that the inflationary dynamics can also generate superimposed oscillations in the primordial power spectrum but we will not focus on this case since, obviously, slow-roll is not satisfied in this situation [481–483]. Let us also notice that if the term in $\sqrt{6}$ in the first exponential function is relaxed to be a free parameter, the potential becomes as in Ref. [484], i.e. a general exponential brane potential. Defining

$$x \equiv \frac{\phi}{M_{\rm Pl}}\,, \tag{5.134}$$

the first three Hubble flow functions in the slow-roll approximation read

$$\epsilon_1 = 3\left(\frac{e^{\sqrt{6}x} + \gamma e^{\sqrt{6}\gamma x}}{e^{\sqrt{6}x} + e^{\sqrt{6}\gamma x}}\right)^2, \qquad \epsilon_2 = -12\,(\gamma-1)^2\,\frac{e^{\sqrt{6}(\gamma+1)x}}{\left(e^{\sqrt{6}x} + e^{\sqrt{6}\gamma x}\right)^2}\,, \tag{5.135}$$

and

$$\epsilon_3 = 6\,(1-\gamma)\,\frac{\left(e^{\sqrt{6}x} - e^{\sqrt{6}\gamma x}\right)\left(e^{\sqrt{6}x} + \gamma e^{\sqrt{6}\gamma x}\right)}{\left(e^{\sqrt{6}x} + e^{\sqrt{6}\gamma x}\right)^2}\,. \tag{5.136}$$

These functions together with the potential are displayed in Fig. 55. The two exponential components are clearly visible on the plot of the logarithm of the potential. The required flatness of the potential is realized only along the γ branch and for negative values of x.

[7] see Eq. (1.1) and Eq. (2.9) in that reference.

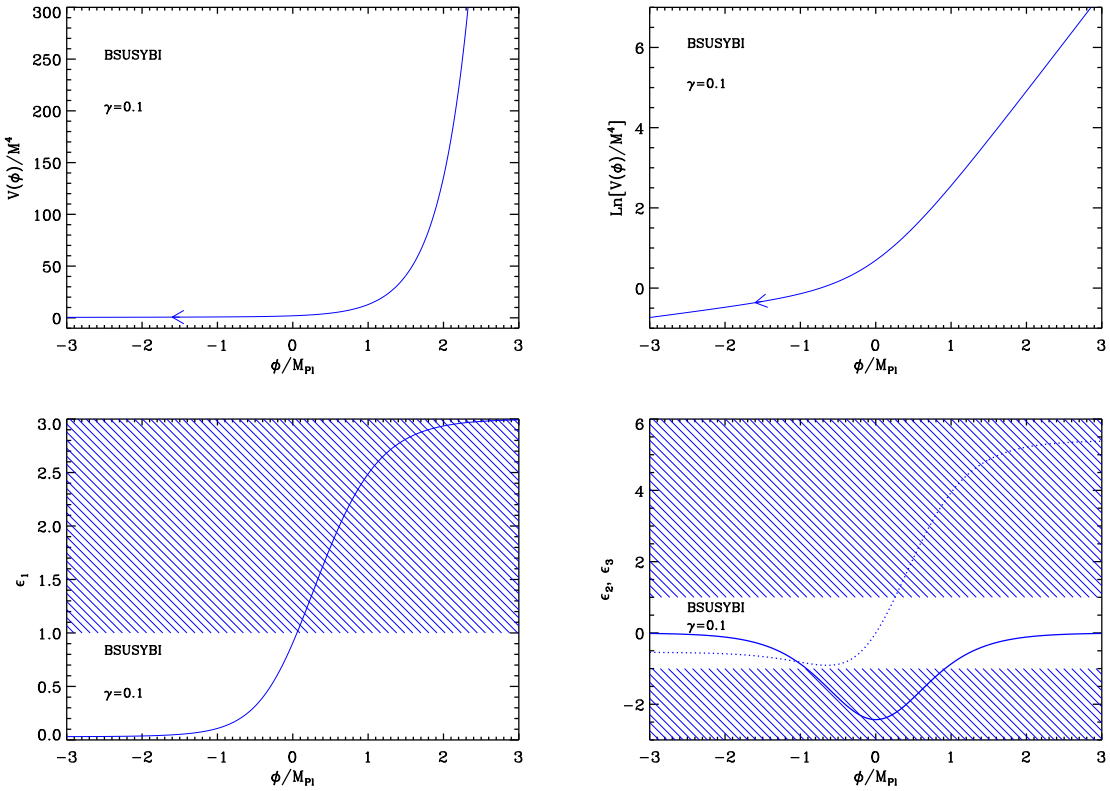

Figure 55. Brane SUSY breaking Inflation (BSUSYBI) for $\gamma = 0.1$. Upper panels: the potential and its logarithm. Bottom left panel: the first slow-roll parameter ϵ_1 as a function of the field value, the shaded area indicates where inflation stops. Bottom right panel: slow-roll parameter ϵ_2 and ϵ_3.

The first Hubble flow function ϵ_1 is an increasing function of x which varies between its asymptotic values:

$$\lim_{x\to-\infty} \epsilon_1 = 3\gamma^2, \qquad \lim_{x\to+\infty} = 3. \tag{5.137}$$

For γ small enough ($\gamma < 1/\sqrt{3}$), there is a regime where it is less than unity. This regime is given by the condition $x < x_{\epsilon_1=1}$ with

$$x_{\epsilon_1=1} = \frac{1}{\sqrt{6}\,(\gamma-1)} \ln\left(\frac{\sqrt{3}-1}{1-\gamma\sqrt{3}}\right). \tag{5.138}$$

As a result, inflation can only proceed in the domain $x < x_{\epsilon_1=1}$ and it never stops. Hence the need for an extra-parameter $x_{\rm end}$ encoding the field value at which some unspecified mechanism (such as a tachyonic instability) is triggered and stops inflation. Let us notice that the slow-roll parameter ϵ_2 is always negative and goes to zero at large $|x|$ with a local minimum in $x = 0$ equals to $\epsilon_2^{\rm min} = -3\,(\gamma-1)^2$. Finally, the slow-roll parameter ϵ_3 vanishes when $x = 0$ and shares the same sign as x. Its asymptotic values are

$$\lim_{x\to-\infty} \epsilon_3 = 6\gamma\,(\gamma-1)\,, \qquad \lim_{x\to+\infty} \epsilon_3 = 6\,(1-\gamma)\,. \tag{5.139}$$

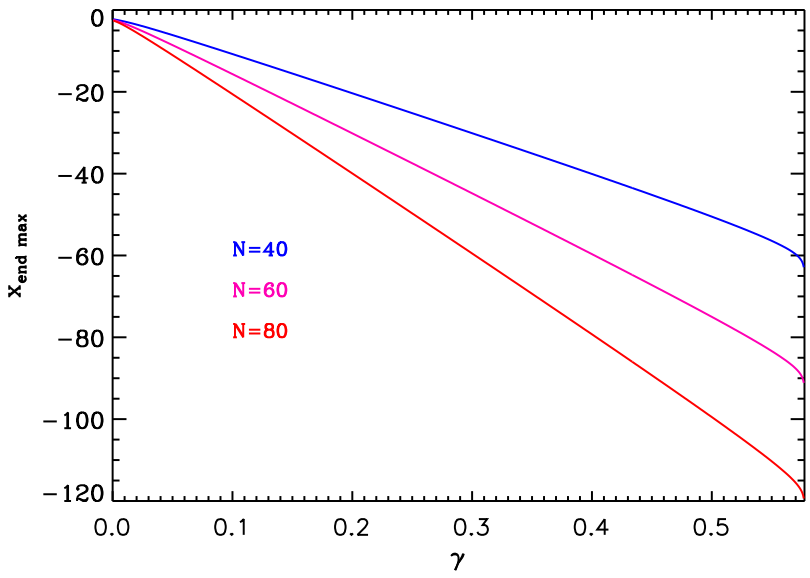

Figure 56. Maximum value of $x_{\rm end}$ in order to realize N e-folds of inflation between $x_{\epsilon_1=1}$ and $x_{\rm end}$ as a function of $0 < \gamma < 1/\sqrt{3}$. This condition defines a prior for the model parameter $x_{\rm end}$, which is the region lying under the curves on the figure.

The slow-roll trajectory can be integrated and gives

$$N - N_{\rm end} = -\frac{1}{\sqrt{6}}\left(x - x_{\rm end}\right) + \frac{1}{6\gamma}\ln\left[\frac{1+\gamma e^{\sqrt{6}(\gamma-1)x}}{1+\gamma e^{\sqrt{6}(\gamma-1)x_{\rm end}}}\right]. \tag{5.140}$$

This equation cannot be analytically inverted but since inflation requires $x < x_{\epsilon_1=1}$, it shows that $x_{\rm end}$ should not be too close to $x_{\epsilon_1=1}$ in order to realize enough e-folds of inflation. This puts some upper bound on $x_{\rm end}$, that can be computed numerically and that is displayed in Fig. 56. This value $x_{\rm end}^{\rm max}$ defines a prior for the model parameter $x_{\rm end}$, which is the region lying under the curves on the figure.

Integrating Eq. (2.47) finally gives the field value x_* at which the pivot mode crossed the Hubble radius during inflation. The parameter M being fixed by the amplitude of the CMB anisotropies

$$\left(\frac{M}{M_{\rm Pl}}\right)^4 = 4320\pi^2\frac{\left(e^{\sqrt{6}x_*}+\gamma e^{\sqrt{6}\gamma x_*}\right)^2}{\left(e^{\sqrt{6}x_*}+e^{\sqrt{6}\gamma x_*}\right)^3}\frac{Q^2_{\rm rms-PS}}{T^2}. \tag{5.141}$$

The reheating consistent slow-roll predictions of the BSUSYBI models have been plotted in Fig. 127. The parameter $x_{\rm end}$ varies between $2x_{\rm end}^{\rm max} < x_{\rm end} < x_{\rm end}^{\rm max}$ with $x_{\rm end}^{\rm max} < 0$, under which the predictions of the model coincide with those of PLI (see section 4.8). Large values for the parameter γ are disfavored and it has to be smaller than $\lesssim 5\times10^{-2}$ to generate a reasonable amount of gravitational waves.

5.9 Tip Inflation (TI)

5.9.1 Theoretical Justifications

This model is a scenario based on string theory in which the motion of branes in extra-dimensions causes the four-dimensional spacetime to inflate, see for instance Refs. [151, 213, 485–490]. Let us assume string theory with flux compactification. In this situation, the six-dimensional Calabi-Yau space has generically the shape of a bulk with warped throat(s) attached to it. The metric in the bulk is usually not known but, along the throat, explicit examples are available. A representative case is the Klebanov-Strassler throat [491] for which one can write the metric as

$$\mathrm{d}s^2 = h^{-1/2}(r)\eta_{\mu\nu}\mathrm{d}x^\mu \mathrm{d}x^\nu + h^{1/2}(r)\left(\mathrm{d}r^2 + r^2 \mathrm{d}s_5^2\right). \tag{5.142}$$

The function $h(r)$ describes the warping along the radial coordinate r of the throat. We see that the throat is in fact a cone with five-dimensional sections given by the metric $\mathrm{d}s_5^2$. For a conifold, these sections are two spheres $S_2 \times S_3$ which shrink to zero at the tip of the cone [492]. Let us recall that a conifold can also be defined by the equation $\sum_{A=1}^4 (Z_A)^2 = 0$, i.e. a six-dimensional (or three complex dimension) surface in $\mathbb{C}^4$. However, if one has a deformed conifold, then, at the tip the S_2 sphere shrinks to zero but the S_3 remains finite [492]. A deformed conifold can similarly be defined by the equation $\sum_{A=1}^4 (Z_A)^2 = \varepsilon^2$ and, at the tip, one has $\sum_{A=1}^4 |Z_A|^2 = \varepsilon^2$. Usually brane inflation takes place when a brane is moving along the radial direction of the throat, see section 5.19. Here, following Ref. [489], we will consider a different situation, namely the case of a brane moving at the tip of the deformed conifold. In addition, we will not only consider radial motion only but also angular motion.

Technically, the above model can be described in the framework of supergravity (viewed, in this context, as a low energy effective field theory). Let us assume that there is a $D3$-brane moving at the tip and that complex structure moduli and the dilaton are stabilized, thanks to the presence of fluxes. Furthermore, following Ref. [489], we suppose that there is only one volume modulus, ρ, plus three fields z_i, $i = 1, \cdots, 3$ describing the $D3$-brane position. It follows that the corresponding Kähler potential is given by

$$K\left(\rho, z_i, z_i^\dagger\right) = -3M_{\mathrm{Pl}}^2 \ln\left[\rho + \rho^\dagger - \gamma k\left(z_i, z_i^\dagger\right)\right], \tag{5.143}$$

where k is a function of the brane coordinates and γ is a constant (of mass dimension -2) related to the brane tension T_3, an approximate expression of which will be given below. In the vicinity of the deformed conifold tip, the function k takes the form

$$k\left(z_i, z_i^\dagger\right) = k_0 + c\varepsilon^{-2/3}\left(\sum_{A=1}^4 |Z_A|^2 - \varepsilon^2\right). \tag{5.144}$$

Here c is a numerical constant $c = 2^{1/6}/3^{1/3} \simeq 0.77$ and k_0 stands for the value of the function k at the tip. The quantity $\varepsilon^{2/3} = r_{\mathrm{tip}}$ can be viewed as the radius of the tip as illustrated in Figs. 1 and 2 of Ref. [489].

The last ingredient of the model is a stack of n $D7$-branes placed far from the tip. Then, the superpotential (Kuperstein embedding [493]) can be written as

$$W = W_0 + A(z_1)e^{-a\rho} = W_0 + A_0\left(1 - \frac{z_1}{\mu}\right)^{1/n} e^{-a\rho}. \tag{5.145}$$

In this expression, $\mu^{2/3}$ represents the distance between the stack of $D7$-branes and the tip (see Fig. 2 of Ref. [489] for an illustration). We always assume that this distance is much larger than the size of the tip, i.e. $\epsilon/\mu \ll 1$. The quantities W_0, A_0 and a are constants. It is interesting to remark that the above superpotential only depends on z_1 and therefore breaks the symmetry of the tip.

We are now in a position where the potential and the kinetic term can be calculated for the fields z_i and ρ. The F-term potential reads

$$V(\sigma, x_1) = \frac{2ae^{-a\sigma}}{M_{\rm Pl}^2 U^2}\left(\frac{aU}{6}|A|^2 e^{-a\sigma} + |A|^2 e^{-a\sigma} - |W_0 A|\right) + \frac{e^{-2a\sigma}}{3M_{\rm Pl}^2\gamma U^2}\frac{|A|^2}{n^2\mu^2}\frac{\varepsilon^{2/3}}{c}\left(1 - \frac{x_1^2}{\varepsilon^2}\right)\left(1 - \frac{x_1}{\mu}\right)^{-2} + \frac{D}{U^b}, \tag{5.146}$$

where we have taken, from the definition $z_i = x_i + iy_i$, $z_1 = x_1$ at the tip. Because of our choice of the superpotential, V no longer depends on x_2, x_3. In the above expression, we have defined $\rho = \sigma + i\tau$ and τ is chosen such that V is minimal. The quantity U is defined by $U = \rho + \rho^\dagger - k = 2\sigma - k_0$ at the tip. Finally, the last term D/U^b, with D and b constant, is an uplifting term which is added in order to avoid having an anti-de Sitter minimum. In practice, uplifting potentials generically have $b = 3$ [494].

The calculation of the kinetic term is difficult since the Kähler matrix mixes all the fields z_i. For this reason, it is easier to use another parametrization such where $z_1 = \varepsilon\cos\varphi$, $z_2 = \varepsilon\sin\varphi\cos\theta$, $z_3 = \varepsilon\sin\varphi\sin\theta\cos\psi$ and $z_4 = \varepsilon\sin\varphi\sin\theta\sin\psi$, as appropriate since the tip of the deformed conifold is S_3. In this case, the Kähler matrix becomes diagonal and expanding everything in the small parameter $\epsilon/\mu \ll 1$, one obtains

$$V(\sigma, \varphi) = \Lambda(\sigma) + B(\sigma)\cos\varphi + C(\sigma)\sin^2\varphi + \cdots, \tag{5.147}$$

where

$$\Lambda(\sigma) = \frac{2a|A_0|e^{-a\sigma}}{M_{\rm Pl}^2 U^2}\left(\frac{aU}{6}|A_0|e^{-a\sigma} + |A_0|e^{-a\sigma} - |W_0|\right) + \frac{D}{U^b}, \tag{5.148}$$

$$B(\sigma) = \frac{2a|A_0|e^{-a\sigma}}{M_{\rm Pl}^2 U^2 n}\frac{\varepsilon}{\mu}\left(-\frac{aU|A_0|}{3}e^{-a\sigma} - 2|A_0|e^{-a\sigma} + |W_0|\right), \tag{5.149}$$

$$C(\sigma) = \frac{|A_0|^2 e^{-2a\sigma}}{3M_{\rm Pl}^2 U^2\gamma\mu^2 n^2}\frac{\varepsilon^{2/3}}{c}. \tag{5.150}$$

Let us now discuss this result. If one ignores, for the moment, all terms depending on the brane position, it remains only the term $\Lambda(\sigma)$ which is nothing but the Kachru-Kallosh-Linde-Trivedi (KKLT) potential for the volume modulus [494]. We see that in absence of the uplifting term D/U^b, its minimum given by $\partial\Lambda/\partial\sigma = 0$ would be located at $\sigma = \sigma_0$, solution of the implicit equation

$$W_0 = -A_0\left[1 + \frac{a}{3}(2\sigma_0 - k_0)\right]e^{-a\sigma_0}. \tag{5.151}$$

The corresponding value of the potential would actually be negative (anti-de Sitter) and given by

$$\Lambda(\sigma_0) = -\frac{a^2|A_0|^2}{3M_{\rm Pl}^2 U}e^{-2a\sigma_0} < 0. \tag{5.152}$$

Hence the required uplifting term from which one can find a new minimum at which V is positive. This is precisely how KKLT managed to find a de Sitter minimum instead of an anti de Sitter one for the first time in string theory [494].

If the position of the minimum were not changed by adding the uplifting term, one would obtain a vanishing value of V for

$$D_0 = \frac{a^2|A_0|^2 U^{b-1}(\sigma_0)}{3M_{\rm Pl}^2} e^{-2a\sigma_0}. \tag{5.153}$$

This suggests to introduce a new parameter β, defined by

$$\beta \equiv D \frac{3M_{\rm Pl}^2}{a^2|A_0|^2 U^{b-1}(\sigma_0)} e^{2a\sigma_0}, \tag{5.154}$$

such that one can trade D for β in all the uplifting terms. Therefore, $\beta = 1$ represents a situation in which the potential is uplifted while the position of its minimum is unchanged. In general, as expected in presence of the brane, the KKLT minimum σ_0 of $\Lambda(\sigma)$ will be shifted. The correction due to the uplifting terms can be evaluated perturbatively and one obtains the following expression

$$\sigma_{\rm min} = \sigma_0 + \frac{b\beta}{2a^2\sigma_0} + \cdots, \tag{5.155}$$

valid provided $b\beta/(2a^2\sigma_0) \ll 1$. For $\beta = 0$, one recovers that $\sigma_{\rm min} = \sigma_0$ as expected without uplifting terms (and with a negative minimum for V). There are other corrections to the position of the minimum due to the presence of the brane but one can show that they do not play an important role (they are calculated in Ref. [489]). The final argument consists in considering that the modulus is stabilized at this minimum. Then, one obtains a single field model $V(\varphi) = V(\sigma_{\rm min}, \varphi)$ where the coefficients in Eq. (5.147) are now given by

$$\Lambda\left(\sigma_{\rm min}\right) \equiv \Lambda \simeq \frac{a^2|A_0|^2 e^{-2a\sigma_0}}{6M_{\rm Pl}^2\sigma_0}\left[(\beta - 1) + \cdots\right], \tag{5.156}$$

$$B\left(\sigma_{\rm min}\right) \equiv B \simeq \frac{a|A_0|^2\varepsilon e^{-2a\sigma_0}}{6M_{\rm Pl}^2 n\mu\sigma_0^2}\left[(b\beta - 3) + \frac{b\beta}{4a\sigma_0}\left(14 - 3b\beta\right) + \cdots\right], \tag{5.157}$$

$$C\left(\sigma_{\rm min}\right) \equiv C \simeq \frac{|A_0|^2\varepsilon^{2/3} e^{-2a\sigma_0}}{12M_{\rm Pl}^2 n^2\mu^2\sigma_0^2\gamma c} + \cdots. \tag{5.158}$$

The above relations express the parameters of the potential in terms of the stringy parameters. We see that, if $\beta > 1$, we have that the KKLT potential is positive at the minimum that could account for a cosmological constant today for $\beta - 1 = \mathcal{O}\left(\sigma_0^{-2}\right)$ [489].

Finally, the kinetic term for φ remains to be calculated. Using the explicit form of the Kähler metric, one obtains

$$K_{I\bar{J}}\partial_\mu z^I \partial^\mu z^{\bar{J}} \simeq \frac{3M_{\rm Pl}^2}{U}\gamma c\varepsilon^{4/3}\partial_\mu\varphi\partial^\mu\varphi + \cdots, \tag{5.159}$$

where, at the minimum, one has

$$\gamma \simeq \frac{\sigma_0 T_3}{3M_{\rm Pl}^2}, \tag{5.160}$$

T_3 being the brane tension. Therefore, in the large volume limit, the canonical field ϕ is $\phi = \sqrt{T_3 c}\varepsilon^{2/3}\varphi$. As a consequence, the final form of the potential reads

$$V(\phi) = \Lambda + B\cos\left(\frac{\phi}{\sqrt{T_3 c}\varepsilon^{2/3}}\right) + C\sin^2\left(\frac{\phi}{\sqrt{T_3 c}\varepsilon^{2/3}}\right). \tag{5.161}$$

To end this section, it is interesting to discuss the orders of magnitude of the parameters appearing in the above potential. For this purpose, it is useful to recall that σ_0, being a volume modulus, is related to the size (or volume) of the extra-dimensions, $V_6 \simeq \sigma_0^{3/2}\alpha'^3$. The brane tension can be written as $T_3 = (2\pi)^{-3} g_{\rm s}^{-1}\alpha'^{-2}$ while the Planck mass takes the form $M_{\rm Pl}^2 = 2(2\pi)^{-7} V_6 g_{\rm s}^{-2}\alpha'^{-4}$ ($g_{\rm s}$ is the string coupling). As already mentioned, the distance $\mu^{2/3}$ can be viewed as the distance between the stack of $D7$-branes and the tip. It is therefore of the order of the size of the throat which allows us to write that $\mu \simeq (27\pi g_{\rm s}\mathcal{N}\alpha'^2/4)^{3/8}$ where the positive integer $\mathcal{N}$ is the total background Ramond-Ramond charge.

In order to have a successful slow-roll scenario, we must assume that the potential vanishes at its minimum. This amounts to take $\Lambda = B$ which can always be achieved by choosing $\beta = \beta_{\rm sr}$ such that (with $b = 3$, see before)

$$\beta_{\rm sr} = 1 + \frac{45\varepsilon}{4n\mu a^2\sigma_0^2} + \cdots, \tag{5.162}$$

where we have performed a large volume expansion. Then, at the top of the potential, one has $\partial^2 V/\partial\phi^2 \simeq 2C - \Lambda$ and if one wants a flat potential $2C - \Lambda = 2C - B$ must be a very small quantity, i.e. $C/B \simeq 1/2$. Using the equations established above, one can write

$$\frac{C}{B} = \Upsilon\frac{\sigma_0^{3/2}}{g_{\rm s}(g_{\rm s}\pi\mathcal{N})^{3/8}}\left(\frac{r_{\rm tip}}{\ell_{\rm s}}\right)^{-1/2}, \tag{5.163}$$

where the numerical factor $\Upsilon = (12/15)\times(4/27)^{3/8}/[(2\pi)^4 nc] \simeq 5\times 10^{-5}$ and $r_{\rm tip} \equiv \varepsilon^{2/3}$. The string length is given by $\ell_{\rm s} = \sqrt{\alpha'}$. Let us also recall that we have taken $b = 3$. We see in the above expressions, especially Eq. (5.157), that this case is special because $\beta_{\rm sr} \simeq 1$ and we have an additional suppression. It is also interesting to discuss the mass scale which appears in the arguments of the trigonometric functions. Straightforward calculations lead to

$$\frac{\sqrt{T_3 c}\varepsilon^{2/3}}{M_{\rm Pl}} = (2\pi)^2\sqrt{\frac{c}{2}}g_{\rm s}^{1/2}\sigma_0^{-3/4}\left(\frac{r_{\rm tip}}{\ell_{\rm s}}\right). \tag{5.164}$$

For fixed $g_{\rm s}$ and $\mathcal{N}$, the two inflationary parameters C/B and $\sqrt{T_3 c}\varepsilon^{2/3}/M_{\rm Pl}$ are in fact controlled by the radius of the tip and the volume of the extra-dimensions.

Finally, if one requires $C/B = 1/2$, as appropriate in a slow-roll analysis, then the above equations imply that

$$\frac{\sqrt{T_3 c}\varepsilon^{2/3}}{M_{\rm Pl}} \simeq 2\times 10^8\sigma_0^{9/4}. \tag{5.165}$$

This equation is relevant for the question of the priors that should be put on the model parameters.

5.9.2 Slow-roll Analysis

We now turn to the slow-roll analysis of the model. For the canonically normalized inflaton field, we have just seen that the potential is given by

$$V = M^4\left(1 + \cos\frac{\phi}{\mu} + \alpha\sin^2\frac{\phi}{\mu}\right), \tag{5.166}$$

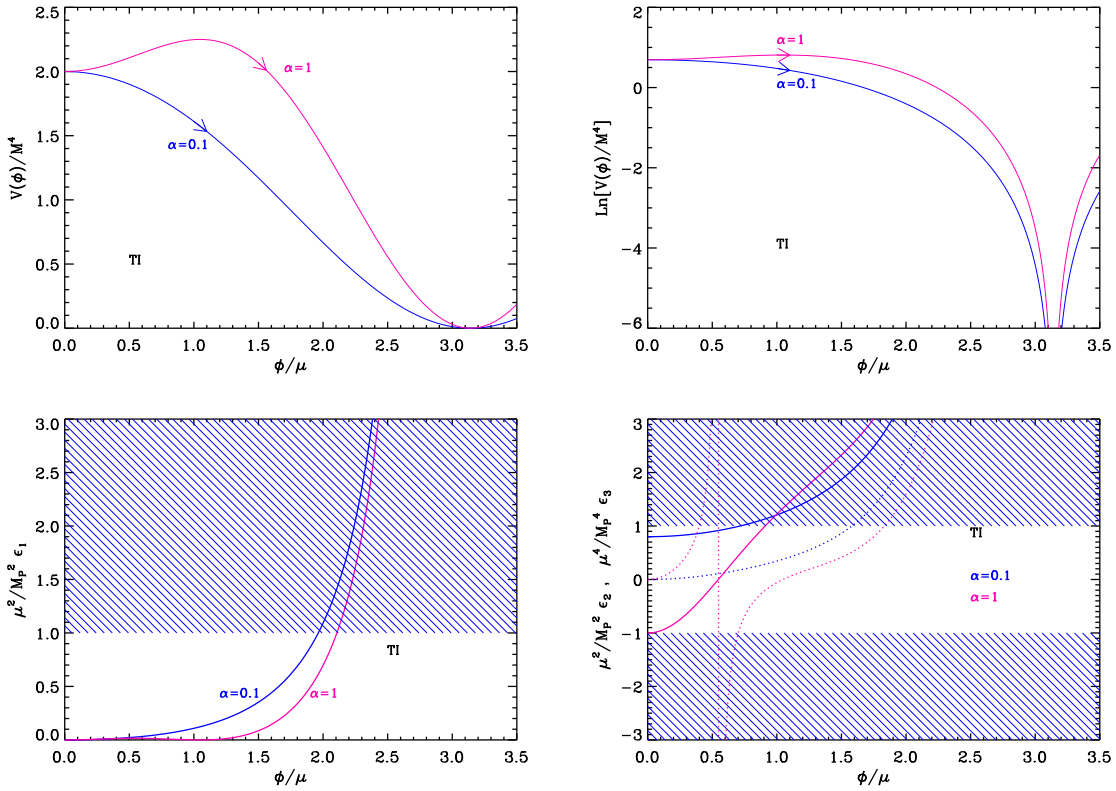

Figure 57. Tip Inflation (TI). Upper panels: Tip Inflation potential and its logarithm for $\alpha = 0.1$ (blue line) and $\alpha = 1$ (pink line), as a function of ϕ/μ. Bottom left panel: slow-roll parameter ϵ_1 normalized by $M_{\rm Pl}^2/\mu^2$. The shaded area indicates the breakdown of the slow-roll inflation if $\mu = M_{\rm Pl}$ (strictly speaking when the acceleration stops). Bottom right panel: slow-roll parameter ϵ_2 (solid line) and ϵ_3 (dotted line), again rescaled by $M_{\rm Pl}^2/\mu^2$.

where inflation proceeds in the region $0 < \phi/\mu < \pi$. Here, we have written $\Lambda = M^4$, $C/B = \alpha$ and $\mu = \sqrt{T_3 c}\varepsilon^{2/3}$ (not to be confused with the scale μ introduced above and related to the distance between the stack of branes and the tip). When $\alpha \ll 1$, the potential reduces to the natural inflation (NI) one. Yet, it was shown in section 4.6 that only super-Planckian decay constants $\mu/M_{\rm Pl} > \mathcal{O}(1)$ could make the natural inflation models compatible with observations (see e.g. Fig. 88). As noticed in Ref. [489], this means that tip inflation models with $\alpha \ll 1$ are not viable. On the other hand, as was discussed in detail in the previous sub-section, if α is fine-tuned to $\alpha \simeq 1/2$, then the potential of Eq. (5.166) becomes very flat at the top and a phenomenologically successful slow-roll inflationary stage could occur. This is why, in the following, these models are studied with $\alpha \simeq 1/2$.

Defining

$$x \equiv \frac{\phi}{\mu}\,, \tag{5.167}$$

the potential of Eq. (5.166) and its logarithm with respect to x are displayed in Fig. 57. Its general shape depends on the value of α. If $\alpha < 1/2$, it is a decreasing function of the field *vev*, hence inflation proceeds from the left to the right, and it has a vanishing minimum at $x = \pi$. Its first derivative vanishes at the top of the potential for $x = 0$ while its second

derivative $V''(x=0) \propto 2\alpha - 1$. It vanishes there when $\alpha = 1/2$ and the potential becomes flat enough to support inflation. If $\alpha > 1/2$, the potential maximum is not located at $x = 0$ anymore but at $x = \arccos\left[1/(2\alpha)\right]$. Let us thus define

$$x_{V'=0} = \begin{cases} 0 & \text{if} \quad \alpha < 1/2, \\ \arccos\left(\dfrac{1}{2\alpha}\right) & \text{if} \quad \alpha > 1/2. \end{cases} \tag{5.168}$$

If $\alpha > 1/2$, the potential decreases with the field *vev* in the range $x_{V'=0} < x < \pi$, where inflation proceeds from the left to the right. Again, the first derivative of the potential vanishes at the top of the potential while its second derivative $V''(x = x_{V'=0}) \propto 1/(2\alpha) - 2\alpha$ again vanishes when $\alpha = 1/2$. This is why α must be close enough to $1/2$ in order for a viable slow-roll inflationary regime to take place.

Let us calculate the Hubble flow functions within the slow-roll approximation. They read

$$\epsilon_1 = \frac{M_{\rm Pl}^2}{\mu^2} \frac{(1 - 2\alpha\cos x)^2 \sin^2 x}{2\left(1 + \cos x + \alpha \sin^2 x\right)^2}, \tag{5.169}$$

$$\epsilon_2 = \frac{M_{\rm Pl}^2}{\mu^2} \frac{2\cos^2\frac{x}{2}}{\left(1 + \cos x + \alpha \sin^2 x\right)^2} \left[2 + \alpha\left(3 + 4\alpha\right) - 2\alpha\left(3 + 2\alpha\right)\cos x - \alpha\cos\left(2x\right)\right], \tag{5.170}$$

and

$$\epsilon_3 = \frac{M_{\rm Pl}^2}{\mu^2} \left\{ -2 - \frac{2 + 4\alpha}{\left(1 + \alpha - \alpha\cos x\right)^2} + \frac{5 + 3\alpha}{1 + \alpha - \alpha\cos x} + \frac{1}{\cos^2\left(\frac{x}{2}\right)} + \frac{4\left(1 + \alpha + 3\alpha^2\right) - 2\alpha\left(7 + 4\alpha\right)\cos x}{\alpha\left[\cos\left(2x\right) + \left(6 + 4\alpha\right)\cos x - 3 - 4\alpha\right] - 2} \right\}. \tag{5.171}$$

They are displayed in Fig. 57 and are increasing functions of the field *vev* in the inflationary domain $x_{V'=0} < x < \pi$. Notice that they diverge when $x \to \pi$. The first and third slow-roll parameters ϵ_1 and ϵ_3 vanish at the potential maximum. However, the second slow-roll parameter ϵ_2 takes a non-vanishing positive value given by

$$\epsilon_2\left(x = x_{V'=0}\right) = \begin{cases} \dfrac{M_{\rm Pl}^2}{\mu^2}\left(1 - 2\alpha\right) & \text{if} \quad \alpha < 1/2, \\ 4\dfrac{M_{\rm Pl}^2}{\mu^2}\dfrac{2\alpha - 1}{2\alpha + 1} & \text{if} \quad \alpha > 1/2. \end{cases} \tag{5.172}$$

Requiring $|\epsilon_2| < 1$ implies again to adjust α close to $1/2$ such that $|\alpha - 1/2| \ll \mu^2/M_{\rm Pl}^2 \ll 1$.

Inflation stops when $\epsilon_1 = 1$ at the position $x_{\rm end}$ given by

$$x_{\rm end} = \arccos\left[\Sigma + \frac{\left(1 + i\sqrt{3}\right)\sigma}{3 \times 2^{2/3}\left(\delta + \sqrt{\Delta}\right)^{1/3}} - \frac{\left(1 - i\sqrt{3}\right)\sigma'}{6 \times 2^{1/3}}\left(\delta + \sqrt{\Delta}\right)^{1/3}\right]. \tag{5.173}$$

In this formula, we have defined

$$\Delta = -864\alpha^6\left(2\alpha + 1\right)^3 \frac{\mu^2}{M_{\rm Pl}^2}\left(\frac{\mu^2}{M_{\rm Pl}^2} + 2\right)^2 \times \left\{\left(2\alpha - 1\right)^3 + 2\left(2\alpha + 1\right)\left[\left(\alpha - 10\right)\alpha - 2\right]\frac{\mu^2}{M_{\rm Pl}^2} - 4\left(2\alpha + 1\right)^2\frac{\mu^4}{M_{\rm Pl}^4}\right\}, \tag{5.174}$$

and

$$\delta = 8\alpha^3 \left[2\left(2\alpha-1\right)^3 - 3\left(1+2\alpha\right)\left(5+2\alpha\right)\left(1+4\alpha\right)\frac{\mu^2}{M_{\rm Pl}^2} \right. \\ \left. - 15\left(1+\alpha\right)\left(1+2\alpha\right)^2\frac{\mu^4}{M_{\rm Pl}^4} - 2\left(1+2\alpha\right)^3\frac{\mu^6}{M_{\rm Pl}^6}\right], \tag{5.175}$$

together with

$$\sigma = 3 + 4\alpha\left(1-\alpha\right) - 2\frac{\mu^2}{M_{\rm Pl}^2}\left(1+2\alpha\right)^2 - \frac{8}{2+\dfrac{\mu^2}{M_{\rm Pl}^2}}, \qquad \sigma' = \frac{1}{2\alpha^2\left(2+\dfrac{\mu^2}{M_{\rm Pl}^2}\right)}. \tag{5.176}$$

Let us now turn to the slow-roll trajectory. It can be integrated explicitly, leading to

$$N_{\rm end} - N = \frac{\mu^2}{M_{\rm Pl}^2}\frac{1}{2\alpha-1}\ln\left(\frac{1-\cos x}{1-\cos x_{\rm end}}\right) - \frac{\mu^2}{2M_{\rm Pl}^2}\frac{2\alpha+1}{2\alpha-1}\ln\left(\frac{1-2\alpha\cos x}{1-2\alpha\cos x_{\rm end}}\right). \tag{5.177}$$

For $\alpha = 1/2$, this expression is singular, and one has

$$N_{\rm end} - N = \frac{\mu^2}{M_{\rm Pl}^2}\left[\frac{1}{1-\cos x} - \frac{1}{1-\cos x_{\rm end}} - \frac{1}{2}\ln\left(\frac{1-\cos x}{1-\cos x_{\rm end}}\right)\right]. \tag{5.178}$$

Finally, the parameter M can be determined from the amplitude of the CMB anisotropies and the observable field value x_* [see Eq. (2.47)], and one gets

$$\left(\frac{M}{M_{\rm Pl}}\right)^4 = 720\pi^2\frac{M_{\rm Pl}^2}{\mu^2}\frac{\left(1-2\alpha\cos x_*\right)^2\sin^2 x_*}{\left(1+\cos x_* + \alpha\sin^2 x_*\right)^3}\frac{Q_{\rm rms-PS}^2}{T^2}. \tag{5.179}$$

The reheating consistent slow-roll predictions of the TI models are displayed in Fig. 128 for $\alpha < 1/2$ and in Fig. 129 for $\alpha > 1/2$, with $\mu/M_{\rm Pl} = 10^{-6}$, 10^{-4} and 10^{-2}. In both cases, one can see that α needs to be sufficiently adjusted to 1/2, namely $|2\alpha - 1| \ll \mu^2/M_{\rm Pl}^2$, otherwise the deviation from scale invariance is too important. The typical amount of gravitational waves is very small. To see how $\mu/M_{\rm Pl}$ is constrained, the slow-roll predictions are displayed for $\alpha = 1/2$ in Fig. 130, and with μ varying. One can see that even if one allows values of μ larger than the typical ones ($\mu/M_{\rm Pl} \simeq 10^{-4}$) these models are disfavored by the observations since they deviate too much from scale invariance.

5.10 β exponential inflation (BEI)

This model was introduced and studied in Ref. [495] as a phenomenological generalization of the PLI exponential potential (see section 4.8). The potential is given by

$$V(\phi) = M^4\exp_{1-\beta}\left(-\lambda\frac{\phi}{M_{\rm Pl}}\right), \tag{5.180}$$

where the generalized exponential function $\exp_{1-\beta}$ is defined by

$$\exp_{1-\beta}(f) = \begin{cases} \left(1+\beta f\right)^{1/\beta} & \text{for } \ 1+\beta f > 0\,, \\ 0 & \text{otherwise}\,. \end{cases} \tag{5.181}$$

As discussed in Ref. [495], for $f > 0$ and $g > 0$, this function satisfies the following identities:

$$\exp_{1-\beta}\left[\ln_{1-\beta}(f)\right] = f, \qquad \ln_{1-\beta}(f) + \ln_{1-\beta}(g) = \ln_{1-\beta}(fg) - \beta\left[\ln_{1-\beta}(f)\ln_{1-\beta}(g)\right], \tag{5.182}$$

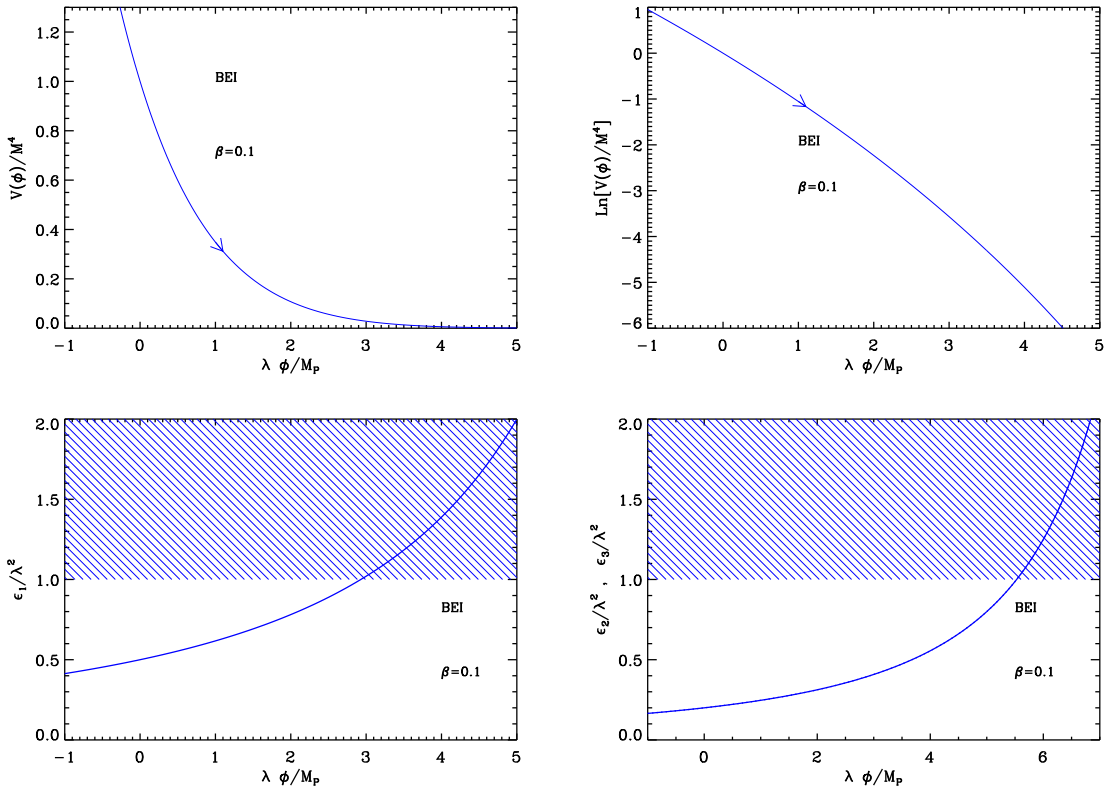

Figure 58. β exponential inflation (BEI) for $\beta = 0.1$. Upper panels: the potential and its logarithm. Bottom left panel: slow-roll parameter ϵ_1 with respect to the field values. The shaded area indicates where inflation stops if $\lambda = 1$. Bottom right panel: slow-roll parameters $\epsilon_2 = \epsilon_3$.

where $\ln_{1-\beta}(f) = \left(f^{\beta} - 1\right)/\beta$ is the generalized logarithmic function. In the limit $\beta \to 0$, all the above expressions reproduce the usual exponential and logarithm properties. Therefore, the limit $\beta \to 0$ reproduces the PLI potential (see section 4.8). However, as discussed below, this is not the case for the observable predictions which remain different. Defining the quantity x by

$$x \equiv \frac{\phi}{M_{\rm Pl}}\,, \tag{5.183}$$

the range of field *vev* for which inflation occurs depends on the sign of β. For $\beta > 0$, the field values are such that $x < 1/(\beta\lambda)$, whereas if $\beta < 0$, the potential is defined for $x > 1/(\beta\lambda)$. In both cases, inflation proceeds from the left to the right. The first three Hubble flow functions in the slow-roll approximation are given by

$$\epsilon_1 = \frac{\lambda^2}{2\left(1-\beta\lambda x\right)^2}\,, \qquad \epsilon_2 = \frac{2\beta\lambda^2}{\left(1-\beta\lambda x\right)^2} = 4\beta\epsilon_1, \qquad \epsilon_3 = \epsilon_2. \tag{5.184}$$

Together with the potential, they are represented in Fig. 58.

One immediately sees that ϵ_1 is an increasing function of x only for the case where $\beta > 0$. Therefore inflation can naturally stop at $x_{\rm end}$ such that $\epsilon_1(x_{\rm end}) = 1$. In the opposite situation, namely $\beta < 0$, inflation has to be ended by some additional mechanism and $x_{\rm end}$

would become an extra-parameter. Since this model is purely phenomenological, in the following, we restrict ourselves to the case $\beta > 0$ for which

$$x_{\rm end} = \frac{1}{\beta}\left(\frac{1}{\lambda} - \frac{1}{\sqrt{2}}\right). \tag{5.185}$$

The next step consists in determining the slow-roll trajectory. It can be integrated explicitly and the result reads

$$N - N_{\rm end} = \frac{1}{\lambda}\left(x - x_{\rm end}\right) - \frac{\beta}{2}\left(x^2 - x_{\rm end}^2\right). \tag{5.186}$$

It can also be inverted and one obtains the following expression for x as a function of the e-folds number

$$x = \frac{1}{\lambda\beta} - \sqrt{\left(x_{\rm end} - \frac{1}{\lambda\beta}\right)^2 - \frac{2}{\beta}(N - N_{\rm end})}. \tag{5.187}$$

Using these expressions, the observable field value x_* can be related to the number of e-folds $\Delta N_* = N_{\rm end} - N_*$ at which the pivot scale crossed out the Hubble radius during inflation. Making use of Eq. (5.185), one gets

$$x_* = \frac{1}{\lambda\beta} - \sqrt{\frac{1}{2\beta^2} + \frac{2}{\beta}\Delta N_*}. \tag{5.188}$$

Inserting this expression into the slow-roll parameters formulas yields

$$\epsilon_{1*} = \frac{1}{1 + 4\beta\Delta N_*}, \qquad \epsilon_{2*} = \epsilon_{3*} = 4\beta\epsilon_{1*}. \tag{5.189}$$

Therefore, the slow-roll predictions of these models do not depend on the parameter λ. Moreover, the limit $\beta \to 0$ does not give the same observable predictions as for the PLI models due to the singular behavior of $x_{\rm end}$. These models can therefore be viewed as a completely different class.

Finally, the amplitude of the CMB anisotropies fixes the parameter M with

$$\left(\frac{M}{M_{\rm Pl}}\right)^4 = 720\pi^2\lambda^2\left(1 - \beta\lambda x_*\right)^{-2-\frac{1}{\beta}}\frac{Q_{\rm rms-PS}^2}{T^2}. \tag{5.190}$$

Notice that, from Eq. (5.188), the above expression can be written in terms of ΔN_* and that it does not depend on λ anymore. The reheating consistent slow-roll predictions for the BEI models are displayed in Fig. 131. The parameter β must be such that $\beta \gtrsim 0.6$ in order for the predictions of the model to remain inside the two-sigma confidence intervals, while the parameter λ remains totally unconstrained.

5.11 Pseudo Natural Inflation (PSNI)

5.11.1 Theoretical Justifications

Pseudo Natural Inflation (PSNI) was introduced and studied in Ref. [259]. This model has common points with NI, see section 4.6. Indeed, in PSNI, the inflaton field is also a pseudo-Nambu Goldstone boson which appears after symmetry breaking. The corresponding potential is nearly flat which is well-suited for inflation. The main ideas behind this

construction are reviewed in section 4.6. The main difference with respect to natural inflation, for which the broken symmetry is a shift symmetry, is that in pseudo natural inflation the broken symmetry is now a $U(1)$ one. A concrete implementation of this idea has been proposed in Ref. [259] and starts with the following supersymmetric hybrid superpotential

$$W\left(S,X,\varphi,\psi_1,\psi_2\right)=\lambda_0 S\left(\psi_1^2+\psi_2^2-f^2\right)+\frac{\lambda_1}{2}\psi_1\varphi^2+\lambda_2 X\left(\varphi^2-v^2\right), \tag{5.191}$$

with $\lambda_1^2 f^2>2\lambda_2^2 v^2$, where S, X, ψ_1, ψ_2 and φ are scalar fields and λ_0, λ_1 and λ_2 are coupling constants. We see that the $U(1)$ symmetry is explicitly broken by the term proportional to λ_1. The corresponding potential can be written as

$$V=\lambda_0^2\left|\psi_1^2+\psi_2^2-f^2\right|^2+\left|2\lambda_0 S\psi_1+\frac{\lambda_1}{2}\varphi^2\right|^2+4\lambda_0^2\left|S\psi_2\right|^2+|\varphi|^2\left|\lambda_1\psi_1+2\lambda_2 X\right|^2+\lambda_2^2\left|\varphi^2-v^2\right|^2. \tag{5.192}$$

The flat directions of this superpotential can be reparametrized as

$$\psi_1+i\psi_2\equiv(f+\sigma)\,e^{i\phi/f}\,,\quad \psi_1-i\psi_2\equiv(f-\sigma)\,e^{-i\phi/f}, \tag{5.193}$$

where ϕ is the Nambu-Goldstone boson associated to the broken $U(1)$ symmetry and σ is a modulus. One can assume that σ is stabilized and sits at $\sigma=0$, the minimum of a potential originating from supersymmetry breaking. The field ϕ plays the role of the inflaton. Using the above expressions and the condition $\sigma=0$, one obtains that $\psi_1=f\cos(\phi/f)$ and $\psi_2=f\sin(\phi/f)$. In that case, a flat direction for ϕ is obtained for $\varphi=0$ and $S=0$ since then we have

$$V=\lambda_2^2 v^4. \tag{5.194}$$

Notice that SUSY is broken because $F_X\equiv\langle\partial W/\partial X\rangle=\lambda_2 v^2\neq 0$. As a consequence, the corresponding vacuum energy density is indeed given by $V_0\simeq|F_X|^2=\lambda_2^2 v^4$.

This tree level potential is corrected by two kind of contributions. First, supergravity induces a soft SUSY breaking mass of order H for every scalar, but since ϕ is a pseudo Nambu-Goldstone boson, it only receives a potential due to the explicit breaking term proportional to λ_1. The corresponding contribution is loop suppressed, $m_\phi^2\simeq 3\lambda_1^2 H^2/(16\pi^2)$, as soon as $\lambda_1\lesssim 1$ which will be assumed. Second, the potential receives a direct Yukawa mediated contribution through a φ loop and Ref. [259] has shown that it takes the form

$$V(\phi)\simeq V_0\left(1+\frac{\lambda_2^2}{4\pi^2}\ln\frac{\lambda_1\psi_1}{\mu}\right)=V_0\left[1+\frac{\lambda_2^2}{4\pi^2}\ln\frac{\cos(\phi/f)}{\mu/f}\right]. \tag{5.195}$$

where μ is some renormalization scale. The above formula gives rise to a new type of potential that we study in the next sub-section.

5.11.2 Slow-Roll Analysis

We now turn to the slow-roll analysis of the PSNI model. Using more friendly notations, the potential (5.195) can be re-expressed as

$$V=M^4\left[1+\alpha\ln\left(\cos\frac{\phi}{f}\right)\right], \tag{5.196}$$

with the following definitions

$$M^4=\lambda_2^2 v^4\left[1+\frac{\lambda_2^2}{4\pi^2}\ln\left(\frac{\lambda_1 f}{\mu}\right)\right],\qquad \alpha=\frac{\lambda_2^2/\left(4\pi^2\right)}{1+\lambda_2^2/\left(4\pi^2\right)\ln\left(\frac{\lambda_1 f}{\mu}\right)}. \tag{5.197}$$

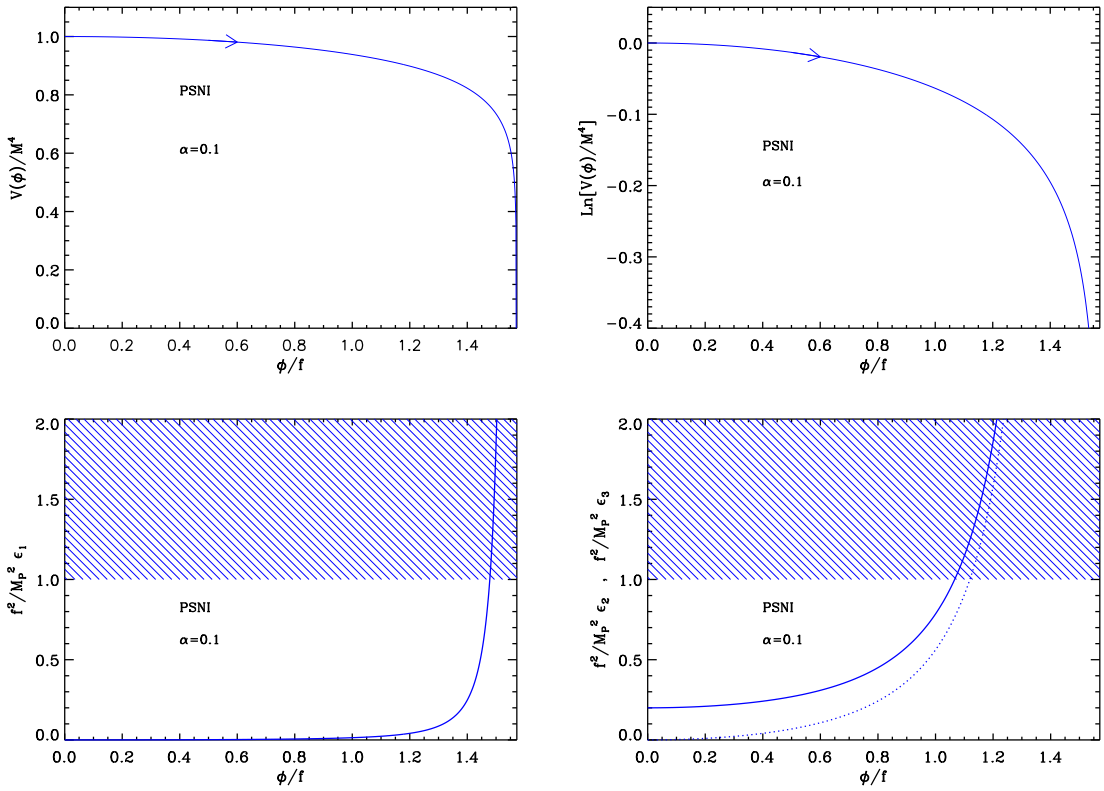

Figure 59. Top left panel: Pseudo Natural Inflation (PSNI) potential, for $\alpha = 0.1$, as a function of ϕ/f. Top right panel: logarithm of the potential for the same value of α. Bottom left panel: slow-roll parameter ϵ_1, rescaled by the quantity $M_{\rm Pl}^2/f^2$ such that it acquires a universal form, for the same value of α. Bottom right panel: slow-roll parameter ϵ_2 (solid line) and ϵ_3 (dotted line), rescaled by the quantity $M_{\rm Pl}^2/f^2$, still for the same value of α.

Therefore, one typically has $\alpha \ll 1$, and the scale f should a priori be such that $f \lesssim M_{\rm Pl}$ in order to avoid the usual problems of natural inflation.

The potential (5.196) as well as its logarithm are displayed in Fig. 59. Since ϕ is assumed to be such that $\phi \simeq 0$ initially, the potential must be studied in the range $\phi/f \in [0, \pi/2]$. It is positive definite in the range $\phi/f \in \left[0, \arccos\left(e^{-1/\alpha}\right)\right]$. We see that it is a decreasing function of the inflaton *vev*, which means that inflation proceeds from the left to the right in the direction specified by the arrow in Fig. 59.

Let us now turn to the slow-roll parameters. If one defines $x \equiv \phi/f$, then the three first Hubble flow parameters are given by

$$\epsilon_1 = \frac{M_{\rm Pl}^2}{2f^2}\frac{\alpha^2\tan^2 x}{(1+\alpha\ln\cos x)^2}, \qquad \epsilon_2 = 2\alpha\frac{M_{\rm Pl}^2}{f^2}\frac{1+\alpha+\alpha\ln\cos x-\alpha\cos^2 x}{\cos^2 x\,(1+\alpha\ln\cos x)^2}, \tag{5.198}$$

$$\epsilon_3 = \alpha\frac{M_{\rm Pl}^2}{f^2}(\tan x)^2\frac{2+3\alpha+\alpha^2-\alpha^2\cos(2x)+(4+3\alpha)\,\alpha\ln\cos x+2\alpha^2\ln^2\cos x}{(1+\alpha\ln\cos x)^2\left(1+\alpha\ln\cos x+\alpha\sin^2 x\right)}. \tag{5.199}$$

They are displayed in Fig. 59. We see on this plot that the slow-roll parameters ϵ_1 and ϵ_3 vanish when x goes to 0 and diverge when x goes to $\pi/2$. On the other hand, the slow-roll

parameter ϵ_2 has a non-zero limit when x goes to 0, namely

$$\lim_{x\to 0}\epsilon_2 = 2\frac{M_{\rm Pl}^2}{f^2}\alpha. \tag{5.200}$$

This quantity should be small in order for slow-roll to be valid. This means that, at a fixed scale f, the parameter α needs to be smaller than $f^2/M_{\rm Pl}^2$. From the monotonous behavior of ϵ_1, one also notices that inflation naturally stops at $\epsilon_1 = 1$. Unfortunately, this equation cannot be solved exactly and the solution needs to be determined numerically. However, since we are in a regime where $f/M_{\rm Pl} \ll 1$ and $\alpha M_{\rm Pl}^2/f^2 \ll 1$, $x_{\rm end}$ must be close to $\pi/2$. One can derive a better approximation by solving the equation $\epsilon_1 = 1$ using an expansion in the small quantities of the problem. One arrives at

$$x_{\rm end} \simeq \frac{\pi}{2} - \frac{\alpha}{\sqrt{2}}\frac{M_{\rm Pl}}{f}\,, \tag{5.201}$$

that is to say the first correction to $\pi/2$ is linear in $\alpha M_{\rm Pl}/f$ and, as expected, negative. As usual, the `ASPIC` code makes use of the complete slow-roll solution.

Let us now turn to the slow-roll trajectory. It can be integrated exactly in terms of the dilogarithm function Li_2 (also referred to as Spence's function, or Joncquière function). This function was already used in this paper, for instance in section 4.1. The explicit expression of the trajectory reads

$$\begin{aligned} N_{\rm end} - N = {} & \frac{f^2}{\alpha M_{\rm Pl}^2}\left[(1+\alpha\ln\cos x_{\rm end})\ln\sin x_{\rm end} + \frac{\alpha}{4}\mathrm{Li}_2\left(\cos^2 x_{\rm end}\right)\right] \\ & -\frac{f^2}{\alpha M_{\rm Pl}^2}\left[(1+\alpha\ln\cos x)\ln\sin x + \frac{\alpha}{4}\mathrm{Li}_2\left(\cos^2 x\right)\right], \end{aligned} \tag{5.202}$$

where $N_{\rm end}$ is the number of e-folds at the end of inflation. Unfortunately, this trajectory cannot be inverted analytically. However, if one uses the two conditions $f/M_{\rm Pl} \ll 1$ and $\alpha M_{\rm Pl}^2/f^2 \ll 1$, one can simplify a lot its expression. In particular, at Hubble crossing, one can write

$$\Delta N_* \simeq \frac{f^2}{2\alpha M_{\rm Pl}^2}\left[\left(x_* - \frac{\pi}{2}\right)^2 - \left(x_{\rm end} - \frac{\pi}{2}\right)^2\right], \tag{5.203}$$

from which one can obtain an explicit formula for x_*

$$x_* \simeq \frac{\pi}{2} - \sqrt{2\alpha\Delta N_*}\frac{M_{\rm Pl}}{f}\,. \tag{5.204}$$

Then, this also allows us to derive useful approximated equations for the first three Hubble flow parameters, namely

$$\epsilon_{1*} \simeq \frac{\alpha}{4\Delta N_*}\,, \qquad \epsilon_{2*} \simeq \epsilon_{3*} \simeq \frac{1}{\Delta N_*}\,. \tag{5.205}$$

The expressions of the tensor-to-scalar ratio, spectral index and running are

$$r \simeq \frac{4\alpha}{\Delta N_*}\,, \qquad n_{\rm S} - 1 \simeq \alpha_{\rm S} \simeq -\frac{1}{\Delta N_*}\,, \tag{5.206}$$

These formulas are in agreement with the estimates given in Ref. [259]. Interestingly enough, we see that these predictions are independent of the scale f and that the spectral index (and the running) is even independent of α.

The last step consists in using the CMB normalization in order to extract the mass scale M. Straightforward manipulations lead to

$$\left(\frac{M}{M_{\rm Pl}}\right)^4 = 720\pi^2\alpha^2\frac{M_{\rm Pl}^2}{f^2}\frac{\tan^2 x_*}{\left(1+\alpha\ln\cos x_*\right)^3}\frac{Q_{\rm rms-PS}^2}{T^2}\,. \tag{5.207}$$

Under the two conditions $f/M_{\rm Pl} \ll 1$ and $\alpha M_{\rm Pl}^2/f^2 \ll 1$ and using the same method as before, this leads to

$$\left(\frac{M}{M_{\rm Pl}}\right)^4 \simeq \frac{360\pi^2\alpha}{\Delta N_*}\frac{Q_{\rm rms-PS}^2}{T^2}\,. \tag{5.208}$$

Requiring $M < M_{\rm Pl}$ is easily achieved since, for the fiducial value $\Delta N_* \simeq 55$, this is equivalent to $\alpha \lesssim 2580$ whereas we have $\alpha \ll 1$. Taking the more realistic value $\alpha \simeq 10^{-6}$ and $\Delta N_* \simeq 55$, one typically obtains that $M/M_{\rm Pl} \simeq 10^{-3}$.

The predictions of the PSNI models are displayed in Fig. 132 for $f/M_{\rm Pl} = 10^{-3}, 10^{-1}, 10$ respectively (although this last value is considered just for the purpose of illustration since super-Planckian values of f are not very physical). The reheating equation of state parameter $\overline{w}_{\rm reh}$ has been taken to 0 but since there is no potential minimum around which the inflaton field can oscillate at the end of inflation, this parameter is a priori unspecified and can take different values (in the `ASPIC` code, this parameter can be freely chosen). One can see that the rough description provided by Eqs. (5.205) is correct: when $\alpha M_{\rm Pl}^2/f^2 \ll 1$, the deviation from scale invariance does not depend on the model parameters and is of the order of $n_{\rm S} \simeq 1 - 1/\Delta N_* \simeq 0.975$, while $r \simeq 4\alpha/\Delta N_*$ is typically very small.

5.12 Non Canonical Kähler Inflation (NCKI)

5.12.1 Theoretical Justifications

This model was introduced and studied in Ref. [397] as a way to model hilltop inflation. The idea is to consider F or D term inflation in which we have a flat direction lifted by one loop corrections. This gives rise to loop inflation as discussed in section 4.12. The LI potential has been obtained, however, under the assumption of a minimal Kähler potential. Now, corrections originating from higher order operators, always present in the Kähler potential, should typically produce a mass term and, therefore, the scalar potential gets modified and takes the form

$$V\left(\phi\right) \simeq V_0 + \alpha\ln\left(\frac{\phi}{Q}\right) + b\phi^2, \tag{5.209}$$

where Q is a renormalization scale. This is the model we study in this section. Let us notice that the coefficient b can be positive or negative. The case $b > 0$ has been investigated in Refs. [496, 497] as "hybrid inflation with quasi-canonical supergravity" and the case $b < 0$ was studied in Ref. [397]. For $b > 0$, the potential (5.209) can be viewed as a valley hybrid potential [VHI, see section 6.2 and Eq. (6.29)] plus logarithmic radiative corrections. Therefore, a consistency check of our calculations will be that, when $\alpha \to 0$, all the formulas derived below must reproduce those derived in section 6.2. Finally, let us mention that the potential (5.209) has also been studied in Ref. [498] for $b < 0$ under the name "SUSY breaking potential" and in Ref. [499] in the context of supersymmetric hybrid inflation.

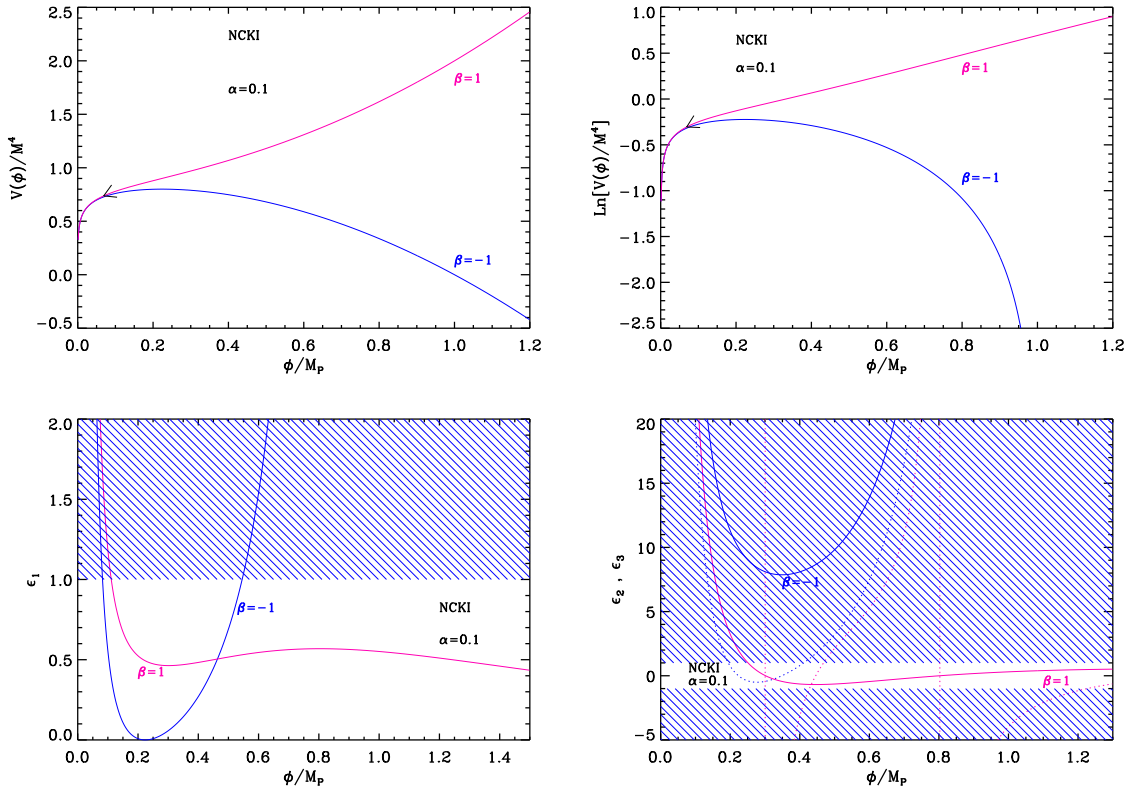

Figure 60. Top left panel: Non Canonical Kähler Inflation (NCKI) potential for $\alpha = 0.1$ and $\beta = \pm 1$. The solid blue line represents the case $\beta = -1$ while the solid pink line represents the case $\beta = 1$. Top right panel: logarithm of the potential for the same values of α and β. Bottom left panel: slow-roll parameter ϵ_1, for a potential with the same values of α and β and the same color code. The shaded area indicates the region where inflation is not possible. Bottom right panel: slow-roll parameters ϵ_2 (solid blue and pink lines) and ϵ_3 (dotted blue and pink lines), for a potential with the values of α and β already considered in the other panels.

5.12.2 Slow-Roll Analysis

In this sub-section, we now turn to the slow-roll analysis of the NCKI scenario. For this purpose, it is convenient to re-write the potential (5.209) under the following form

$$V = M^4 \left[1 + \alpha \ln \left(\frac{\phi}{M_{\rm Pl}} \right) + \beta \left(\frac{\phi}{M_{\rm Pl}} \right)^2 \right], \tag{5.210}$$

where α is a small positive dimensionless parameter and β a dimensionless parameter of order $\mathcal{O}(1)$ which can be either positive or negative. Notice that the coefficient α has be redefined and that β is directly related to b.

The potential (5.210), as well as its logarithm, are displayed in Fig. 60. We now describe its shape. For this purpose, let us first define the quantity $x \equiv \phi/M_{\rm Pl}$. If $\beta > 0$, the potential is definite positive provided $x > x^-_{V=0}$, where

$$x^-_{V=0} = \left[\frac{\alpha}{2\beta} \mathrm{W}_0 \left(\frac{2\beta}{\alpha} e^{-2/\alpha} \right) \right]^{1/2}, \tag{5.211}$$

and where W_0 is the "0"-branch of the Lambert function. In this case, the potential is an increasing function of the field *vev* and, therefore, inflation proceeds from the right to the left in the direction indicated by the arrow in Fig. 60. Let us also notice that, in this case, the potential has an inflection point located at $x_{V''=0} = \sqrt{\alpha/(2\beta)}$. If $\beta < 0$, we must have $2\beta/\alpha \exp(1-2/\alpha) > -1$ in order to avoid the situation where the potential is everywhere negative. This implies that either $\beta > -1$ or $\beta < -1$ and, in this last case, $\alpha < -2/\mathrm{W}_{-1}[1/(e\beta)]$ or $\alpha > -2/\mathrm{W}_0[1/(e\beta)]$. If one of these conditions is satisfied (which is generically the case when $\alpha \ll 1$), the potential is positive provided $x^-_{V=0} < x < x^+_{V=0}$, where $x^-_{V=0}$ is defined in Eq. (5.211) and where

$$x^+_{V=0} = \left[\frac{\alpha}{2\beta}\mathrm{W}_{-1}\left(\frac{2\beta}{\alpha}e^{-2/\alpha}\right)\right]^{1/2}, \tag{5.212}$$

W_{-1} being the -1 branch of the Lambert function. In this case, the potential is a concave function of the field *vev*, with a maximum located at $x_{V'=0} = \sqrt{-\alpha/(2\beta)}$. Typically, inflation proceeds from the right to the left at small values of the field *vev* compared to the Planck mass.

The Hubble flow functions in the slow-roll approximation are given by

$$\epsilon_1 = \frac{\left(\alpha+2\beta x^2\right)^2}{2x^2\left(1+\alpha\ln x+\beta x^2\right)^2}, \tag{5.213}$$

$$\epsilon_2 = 2\frac{\alpha(\alpha+1)+(5\alpha-2)\beta x^2+2\beta^2x^4+\alpha\left(\alpha-2\beta x^2\right)\ln x}{x^2\left(1+\alpha\ln x+\beta x^2\right)^2}, \tag{5.214}$$

and

$$\begin{aligned}\epsilon_3 = \frac{1}{x^2}\Bigg[&\frac{2\left(\alpha+2\beta x^2\right)^2}{\left(1+\alpha\ln x+\beta x^2\right)^2}+\frac{\alpha-2\beta x^2}{1+\alpha\ln x+\beta x^2}\\ &+\frac{\alpha^2+8\alpha\beta x^2-4\beta^2x^4}{\alpha(\alpha+1)+(5\alpha-2)\beta x^2+2\beta^2x^4+\alpha\left(\alpha-2\beta x^2\right)\ln x}\Bigg].\end{aligned} \tag{5.215}$$

The are displayed in the bottom panels in Fig. 60. If $\beta > 0$, the first slow-roll parameter ϵ_1 diverges when $x \to x^-_{V=0}$. For $x > x^-_{V=0}$, it first decreases, then reaches a minimum, then increases and reaches a local maximum. Finally, from this maximum, it decreases again and vanishes at infinity. Therefore, inflation stops at a *vev* x_{end} solution of $\epsilon_1(x_{\mathrm{end}}) = 1$, which cannot be solved analytically. It can be noticed that the value of ϵ_1 as its local maximum increases when α decreases. In the limit $\alpha \ll 1$, one has

$$\epsilon_1^{\mathrm{max}} \simeq \frac{\beta}{2}, \tag{5.216}$$

which is reached at $x_{\epsilon_1^{\mathrm{max}}} \simeq 1/\sqrt{\beta}$ (still in the limit of very small β). This sets an upper bound on β in order for this local maximum to satisfy $\epsilon_1 \ll 1$. If not, inflation would proceed in the part of the potential beyond its inflection point, corresponding to "large values" of the field *vev* and the model would formally be equivalent to a quadratic model (LFI_2, see section 4.2).

If $\beta < 0$, the first slow-roll parameter diverges when $x \to x^-_{V=0}$. For $x > x^-_{V=0}$, ϵ_1 decreases, vanishes at the potential local maximum $x_{V'=0}$, and then increases to blow up when $x \to x^+_{V=0}$. At the same time, the second slow-roll parameter ϵ_2 decreases in the inflationary

range $x_{V=0}^{-} < x < x_{V'=0}$. Let us also notice that, since $\epsilon_2(x_{V'=0}) \propto 2\alpha - \alpha^2 + \alpha^2 \ln\left[-\alpha/(2\beta)\right]$, one has $\epsilon_2 > 0$, thanks to the condition $2\beta/\alpha \exp\left(1 - 2/\alpha\right) > -1$. Therefore the minimum value of ϵ_2 in the increasing branch of the potential is reached at the potential maximum and is given by

$$\epsilon_2^{\min} = \frac{-16\beta}{2 - \alpha\left[1 + \ln\left(-2\frac{\beta}{\alpha}\right)\right]}. \tag{5.217}$$

For $\alpha < -2\beta/e$ (which is generically the case since $\alpha \ll 1$), this number is such that $\epsilon_2^{\min} > -8\beta$, which puts a lower bound on β in order for ϵ_2 to remain small and slow-roll to be satisfied. As it was the case for $\beta > 0$, inflation also ends when $\epsilon_1 = 1$. Notice that the exact calculations are implemented in the `ASPIC` routines.

Let us now turn to the slow-roll trajectory. It can be analytically integrated using the dilogarithm function Li_2 and the corresponding expression reads

$$\begin{aligned} N_{\rm end} - N = &\left(1 - \frac{\alpha}{2} + \alpha \ln x\right)\frac{\ln\left(\alpha + 2\beta x^2\right)}{4\beta} + \frac{x^2}{4} - \frac{\alpha}{4\beta}\ln\alpha \ln x + \frac{\alpha}{8\beta}\mathrm{Li}_2\left(-2\frac{\beta}{\alpha}x^2\right) \\ &- \left(1 - \frac{\alpha}{2} + \alpha \ln x_{\rm end}\right)\frac{\ln\left(\alpha + 2\beta x_{\rm end}^2\right)}{4\beta} - \frac{x_{\rm end}^2}{4} + \frac{\alpha}{4\beta}\ln\alpha \ln x_{\rm end} - \frac{\alpha}{8\beta}\mathrm{Li}_2\left(-2\frac{\beta}{\alpha}x_{\rm end}^2\right), \end{aligned} \tag{5.218}$$

where $N_{\rm end}$ is the number of e-folds at the end of inflation. An approximate and simpler expression can be derived in the limit $\alpha \ll 1$. In that limit, one obtains $N_{\rm end} - N = x^2/4 + \ln(x)/(2\beta) - x_{\rm end}^2/4 - \ln(x_{\rm end})/(2\beta)$, which is precisely the slow-roll trajectory for the VHI models with $\mu = M_{\rm Pl}/\sqrt{\beta}$ and $p = 2$, see Eq. (6.35). For $\alpha \neq 0$, the exact trajectory cannot be inverted analytically.

Finally, the parameter M can be determined from the CMB normalization. One obtains the following expression

$$\left(\frac{M}{M_{\rm Pl}}\right)^4 = 720\pi^2 \frac{\left(\alpha + 2\beta x_*^2\right)^2}{x_*^2\left(1 + \alpha \ln x_* + \beta x_*^2\right)^3}\frac{Q_{\rm rms-PS}^2}{T^2}. \tag{5.219}$$

The slow-roll predictions of the NCKI models are displayed in Fig. 133 and Fig. 134 for $\beta > 0$ and $\beta < 0$, respectively. The reheating equation of state parameter $\overline{w}_{\rm reh}$ has been taken to be 0 but, since there is no potential minimum around which the inflaton field can oscillate at the end of inflation, this parameter is in fact unspecified. Some remarks are in order at this point. Firstly, when $\beta > 0$, we notice that ϵ_2 at Hubble crossing is either positive or negative while, when $\beta < 0$, it is always positive. This is in agreement with what we have discussed before. Secondly, when $\beta > 0$ and $\alpha \ll 1$, one can check that the predictions of the models are similar to the VHI ones with $p = 2$ (compare with Fig. 174). Again, this is consistent with the previous considerations. Thirdly, when $|\beta| \gtrsim \mathcal{O}(1)$, the predictions of the models do not depend much on β . Finally, as expected, when $\beta \to 0$, one recovers the predictions of the LI models, see section 4.12 and Fig. 96. Now, in the regime $|\beta| = \mathcal{O}(1)$ and $\alpha \ll 1$, Fig. 133 and Fig. 134 indicate that the case $\beta > 0$ is disfavored by the observations. The situation is even worst for $\beta < 0$, the deviation from scale invariance being clearly too important to satisfy the observational constraints.

5.13 Constant Spectrum Inflation (CSI)

This potential belongs to the class of models discussed in Ref. [500] and is constructed in order to produce a power spectrum $P(k) \propto k^0$ for the primordial density fluctuations, i.e. a

power spectrum with constant spectral index such that $n_{\rm S} = 1$ (exact scale invariance). It reads

$$V(\phi) = \frac{M^4}{\left(1 - \alpha\dfrac{\phi}{M_{\rm Pl}}\right)^2}. \tag{5.220}$$

There is a symmetry for $\phi/M_{\rm Pl} \to 2/\alpha - \phi/M_{\rm Pl}$ and inflation can proceed indifferently in the branch $\phi/M_{\rm Pl} < 1/\alpha$ or in the branch $\phi/M_{\rm Pl} > 1/\alpha$, leading to the same physical predictions. For this reason, in the following, we will be interested in the branch $\phi/M_{\rm Pl} < 1/\alpha$. Defining the quantity x by

$$x \equiv \frac{\phi}{M_{\rm Pl}}, \tag{5.221}$$

the first three Hubble flow functions in the slow-roll approximation are given by

$$\epsilon_1 = \frac{2\alpha^2}{(\alpha x - 1)^2}, \qquad \epsilon_2 = \epsilon_3 = -2\epsilon_1. \tag{5.222}$$

The previous relation $\epsilon_2 = -2\epsilon_1$ means that, at first order in slow-roll, the spectral index is indeed equals to unity, $n_{\rm S} - 1 = 0$. Recall that the potential of this model is precisely constructed in order for this relation to be true. Let us notice, however, that, at second order in slow-roll, $\epsilon_2 = \epsilon_3 = -2\epsilon_1$ yields $n_{\rm S} - 1 = 4\epsilon_1^2 > 0$. One should note that another way to realize $n_{\rm S} - 1 = 0$ at first order in slow-roll is to take the large field inflation potential LFI (see section 4.2) with a negative power index $p = -2$. In that case one also has $\epsilon_2 = \epsilon_3 = -2\epsilon_1$ and, at second order, $n_{\rm S} - 1 = 4\epsilon_1^2$ is also verified. However, since the explicit expressions of ϵ_1 for CSI and LFI ($p = -2$) are different, the actual value of the spectral index at second order is also different. The potential and the Hubble flow functions have been represented in Fig. 61.

As can be checked in this figure, ϵ_1 is a monotonous function of x in both branches of the potential. It diverges at $x = 1/\alpha$ and vanishes for $x \to \pm\infty$. Inflation can therefore take place in the region $x < x^-_{\epsilon_1=1}$ for the branch $x < 1/\alpha$ (or $x > x^+_{\epsilon_1=1}$ for the branch $x > 1/\alpha$), where $x^\pm_{\epsilon_1=1}$ are the field values at which $\epsilon_1 = 1$:

$$x^\pm_{\epsilon_1=1} = \frac{1 \pm \sqrt{2}\alpha}{\alpha}. \tag{5.223}$$

Since the field evolution proceeds from the right to the left from $x^\pm_{\epsilon_1=1}$, inflation does not stop by slow-roll violation and an extra mechanism parametrized by $x_{\rm end}$ should be considered in order to end it. For this reason, CSI is in fact a two parameters model. Let us also notice that the slow-roll parameters $\epsilon_2 = \epsilon_3$ are negative monotonous functions of x in both branches of the potential and cross the line $\epsilon_2 = \epsilon_3 = -1$ at

$$x^\pm_{\epsilon_2=-1} = x^\pm_{\epsilon_3=-1} = \frac{1 \pm 2\alpha}{\alpha}. \tag{5.224}$$

As a result, there is a small domain $x^-_{\epsilon_2=-1} < x < x^-_{\epsilon_1=1}$ where we have inflation but where the slow-roll approximation is violated (this is also true for the other branch). This is not problematic since the system is driven away from this regime towards a situation in which all the Hubble flow functions become small (see Fig. 61).

The slow-roll trajectory can be integrated explicitly and reads

$$N - N_{\rm end} = \frac{x^2}{4} - \frac{x}{2\alpha} + \frac{x_{\rm end}^2}{4} - \frac{x_{\rm end}}{2\alpha}. \tag{5.225}$$

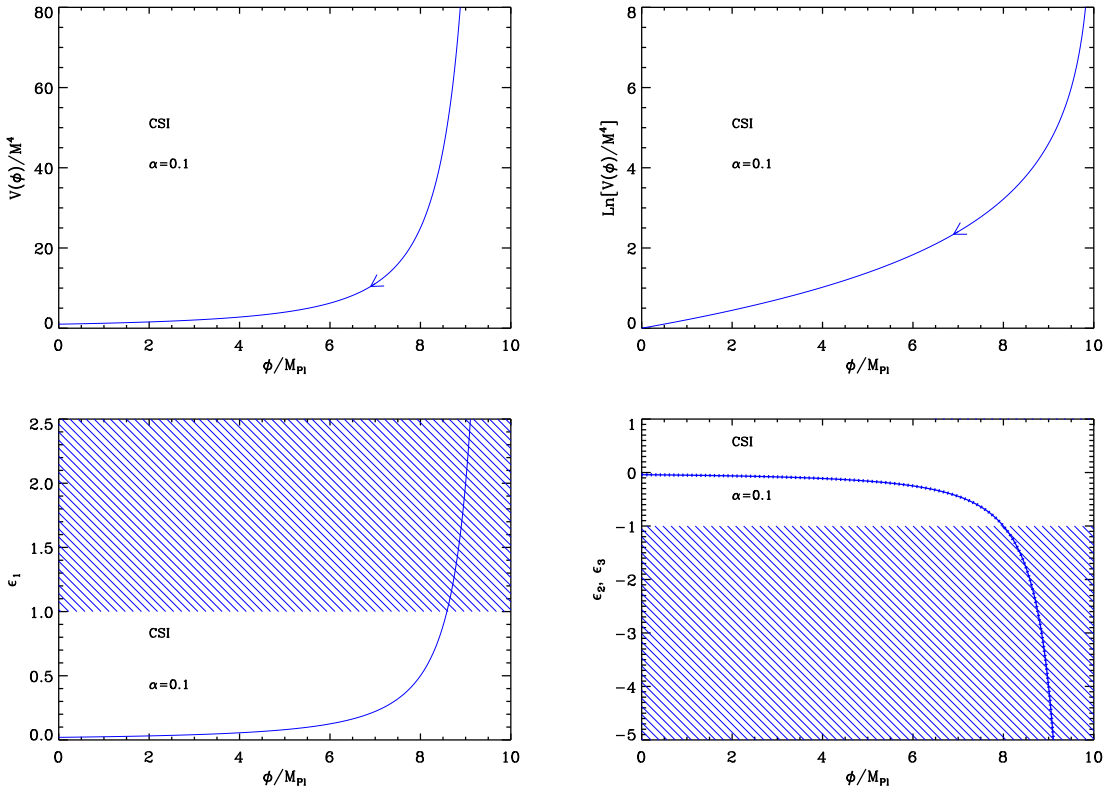

Figure 61. Constant Spectrum Inflation (CSI) for $\alpha = 0.1$. Upper panels: the potential and its logarithm along the branch $x < 1/\alpha$. Bottom left panel: slow-roll parameter ϵ_1 together with the region in which it is larger than unity and in which inflation cannot occur (shaded). Bottom right panel: slow-roll parameter $\epsilon_2 = \epsilon_3$ along the same branch $x < 1/\alpha$.

It can also be inverted analytically and it follows that

$$x = \frac{1 \pm \sqrt{1 - 2\alpha x_{\rm end} + \alpha^2 x_{\rm end}^2 + 4\alpha^2 \left(N - N_{\rm end}\right)}}{\alpha}\,. \tag{5.226}$$

The sign $\mp$ depends on whether one works in the $x < 1/\alpha$ branch or in the $x > 1/\alpha$ branch, respectively. A consequence of this formula is the fact that, if one requires $N_{\rm end} - N_{\rm ini}$ e-folds during inflation, then $x_{\rm end}$ should be smaller than some value $x_{\rm end}^{\rm max}$ given by

$$x_{\rm end}^{\rm max} = \frac{1}{\alpha} - \sqrt{2 + 4\left(N_{\rm end} - N_{\rm ini}\right)}\,, \tag{5.227}$$

in the $x < 1/\alpha$ branch. Equivalently, taking the minus sign in this expression would lead to $x_{\rm end}^{\rm min}$ for the branch $x > 1/\alpha$.

Finally, the observable field value x_* is obtained by solving Eq. (2.47) while the amplitude of the CMB anisotropies fixes the parameter M to

$$\left(\frac{M}{M_{\rm Pl}}\right)^4 = 2880\pi^2\alpha^2\frac{Q_{\rm rms-PS}^2}{T^2}\,. \tag{5.228}$$

Interestingly enough, it only depends on α, and not on x_* (i.e. it has no explicit dependence on the reheating). The reheating consistent slow-roll predictions for the CSI models are represented in Figs. 135 and 136 for $\alpha = 10^{-3}$ and $\alpha = 1$, respectively.

5.14 Orientifold Inflation (OI)

5.14.1 Theoretical Justifications

The model is based on the following considerations. Let us start with a $N = 1$ supersymmetric Yang-Mills gauge theory the Lagrangian of which can be written as

$$\mathcal{L} = -\frac{1}{4}F^a_{\mu\nu}F^{a\mu\nu} + \frac{i}{2}\bar{\lambda}^a \not{D}_{ab}\lambda^b, \tag{5.229}$$

with $a = 1, \cdots, N_c^2$, N_c being the number characterizing the group $SU(N_c)$. $F^a_{\mu\nu}$ is the field strength, λ^a a spinor field and $\not{D}$ a covariant derivative. A is a composite scalar field, i.e. a bound state denoted by $\varphi \simeq \lambda\bar{\lambda}$, can actually appear in the theory if a strongly interacting regime takes place. The effective Lagrangian aimed at describing its dynamics has been derived in Ref. [501] and reads

$$\mathcal{L}_{YV} = -\frac{N_c^2}{\alpha_{OI}}\left(\varphi\varphi^\dagger\right)^{-2/3}\partial_\mu\varphi\partial^\mu\varphi^\dagger - \frac{4\alpha_{OI}N_c^2}{9}\left(\varphi\varphi^\dagger\right)^{2/3}\ln\left(\frac{\varphi}{\Lambda^3}\right)\ln\left(\frac{\varphi^\dagger}{\Lambda^3}\right), \tag{5.230}$$

where α_{OI} is a constant and Λ a mass scale. This class of theories are discussed in more detail in section 6.5. However, in Ref. [502], it was argued that in "orientifold theories", the above Lagrangian can be slightly deformed and now takes the form

$$\mathcal{L}_{OI} = -\frac{N_c^2}{\alpha_{OI}}\left(\varphi\varphi^\dagger\right)^{-2/3}\partial_\mu\varphi\partial^\mu\varphi^\dagger - \frac{4\alpha_{OI}N_c^2}{9}\left(\varphi\varphi^\dagger\right)^{2/3}\left[\ln\left(\frac{\varphi}{\Lambda^3}\right)\ln\left(\frac{\varphi^\dagger}{\Lambda^3}\right) - \beta\right], \tag{5.231}$$

where $\beta = \mathcal{O}(1/N_c)$. Ref. [502] raised the possibility that φ (or, rather, its canonically conjugated version) could be the inflaton. In fact, in order to study this question, one must also specify the gravitational coupling. In Ref. [502], the scalar field φ is non-minimally coupled to gravity such that, in the Jordan frame,

$$S = \int \mathrm{d}^4\boldsymbol{x}\sqrt{-g}\left[-\frac{M^2 + N_c^2\xi\left(\varphi\varphi^\dagger\right)^{1/3}}{2}R + \mathcal{L}_{OI}\right], \tag{5.232}$$

where M is a mass scale. There is a new parameter in the problem, ξ, which describes the strength of the non-minimal coupling to gravity (as it was the case for Higgs inflation, see section 3.1). Then, in the Einstein frame, one can write the above model as Ref. [502]

$$S = \int \mathrm{d}^4\boldsymbol{x}\sqrt{-g}\Bigg\{-\frac{1}{2}M_{Pl}^2R - \frac{N_c^2}{\alpha_{OI}}\Omega^{-2}\left[1 + \frac{\alpha_{OI}N_c^2\xi^2}{3M_{Pl}^2}\Omega^{-2}\left(\varphi\varphi^\dagger\right)^{1/3}\right]\left(\varphi\varphi^\dagger\right)^{-2/3}\partial_\mu\varphi\partial^\mu\varphi^\dagger$$
$$-\Omega^{-4}V_{OI}\Bigg\}. \tag{5.233}$$

In this expression, V_{OI} refers to the second term in Eq. (5.231) and

$$\Omega^2 \equiv \frac{M^2 + N_c^2\xi\left(\varphi\varphi^\dagger\right)^{1/3}}{M_{Pl}^2}. \tag{5.234}$$

In the following, we consider two situations: the case where $\xi \neq 0$ such that $\Omega^2 \simeq N_c^2 \xi \varphi^{2/3}/M_{\rm Pl}^2$, i.e. the second term in the definition of Ω^2 dominates (the large field limit) and the case $\xi = 0$. In the first case, taking $\varphi = \varphi^\dagger$ and canonically normalizing the field one finds

$$V(\varphi) = \frac{4\alpha_{\rm OI} M_{\rm Pl}^4}{9 N_c^2 \xi^2} \left[\left(\ln \frac{\varphi}{\Lambda^3} \right)^2 - \beta \right]. \tag{5.235}$$

The canonically normalized field is $\phi/M_{\rm Pl} \propto \ln \varphi$. Since β is a small number, it can be neglected and this model is in fact a LFI model with $V(\phi) \propto \phi^2$ which was already studied in section 4.2. For the second case, it is sufficient to restart from Eq. (5.231). Then, the canonically normalized field reads

$$\frac{\varphi}{\Lambda^3} = \left(\frac{\phi}{\phi_0} \right)^3, \tag{5.236}$$

with

$$\phi_0 = 3 N_c \left(\frac{2}{\alpha_{\rm OI}} \right)^{1/3} \Lambda. \tag{5.237}$$

It follows that the potential can be written as

$$V = \alpha_{\rm OI} N_c^2 \Lambda^4 \left(\frac{\phi}{\phi_0} \right)^4 \left[\ln^2 \left(\frac{\phi}{\phi_0} \right) - \frac{\beta}{9} \right]. \tag{5.238}$$

This model is studied in detail in the next subsection. The case $\beta = 0$ will also be investigated in section 6.5.

5.14.2 Slow-Roll Analysis

We now turn to the slow-roll study of the potential derived previously in Eq. (5.238). This one can be re-written as

$$V(\phi) = M^4 \left(\frac{\phi}{\phi_0} \right)^4 \left[\left(\ln \frac{\phi}{\phi_0} \right)^2 - \alpha \right], \tag{5.239}$$

where we have defined

$$M^4 = \alpha_{\rm OI} N_c^2 \Lambda^4, \qquad \alpha \equiv \frac{\beta}{9}. \tag{5.240}$$

One should be careful that $\alpha_{\rm OI}$ appearing in the first of the two above equations stems from the Lagrangian used in the previous subsection while the observable constant α only refers to the quantity $\beta/9 = \mathcal{O}(1/N_c) \ll 1$. The scale ϕ_0 is defined in Eq. (5.237) and will be chosen such that $\phi_0 \simeq 10^{16}$ GeV. The potential as well as its logarithm are displayed in Fig. 62.

Defining the quantity x by the following expression

$$x \equiv \frac{\phi}{\phi_0}, \tag{5.241}$$

the potential remains positive provided $x < x_{V=0}^-$ or $x > x_{V=0}^+$, where

$$x_{V=0}^\pm = e^{\pm\sqrt{\alpha}}. \tag{5.242}$$

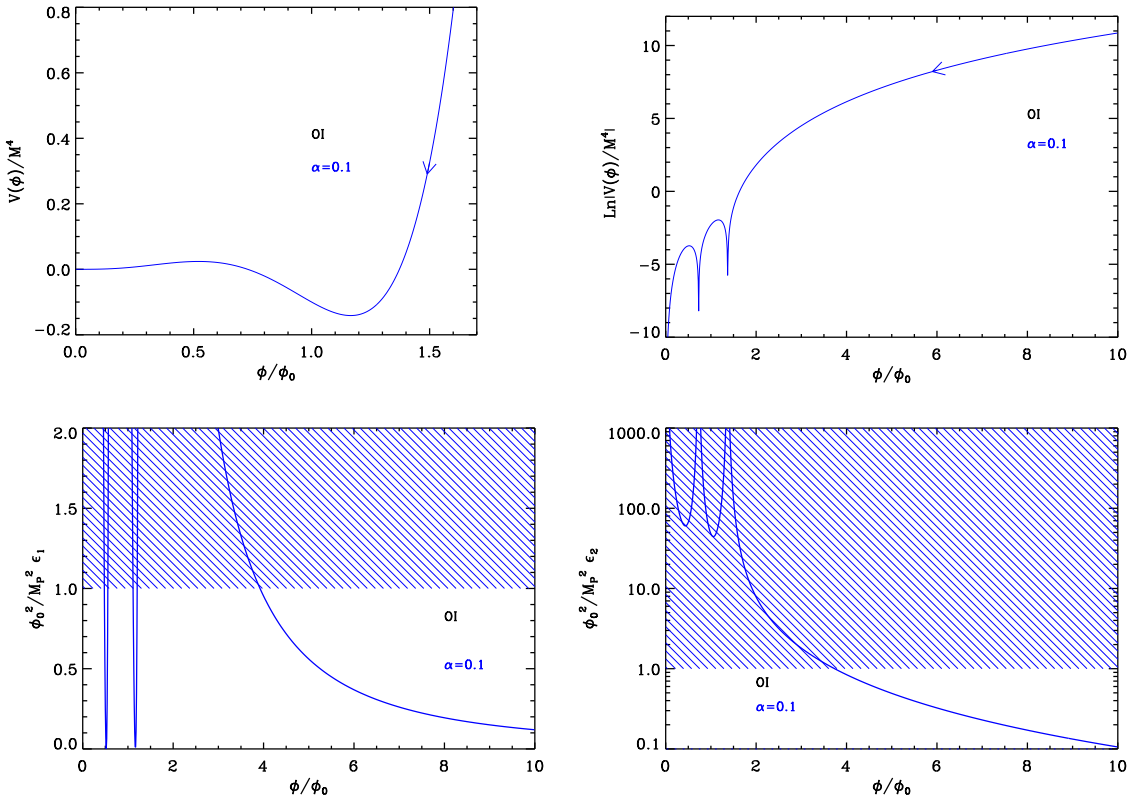

Figure 62. Orientifold Inflation (OI) for $\alpha = 0.1$. Upper panels: the potential and its logarithm. Bottom left panel: slow-roll parameter ϵ_1, rescaled by the factor $\phi_0^2/M_{\rm Pl}^2$. The shaded area indicates where inflation cannot occur (for $\phi_0 = M_{\rm Pl}$). Bottom right panel: rescaled slow-roll parameter ϵ_2.

It vanishes at $x = 0$, then increases to reach a local maximum at $x^-_{V'=0}$, decreases again to become negative at $x^-_{V=0}$, reaches a local minimum at $x^+_{V'=0}$, then increases again to become positive at $x^+_{V=0}$ and diverges asymptotically. The values of $x^-_{V'=0}$ and $x^+_{V'=0}$ are given by

$$x^\pm_{V'=0} = e^{-\frac{1}{4}\pm\sqrt{\frac{1}{16}+\alpha}}. \tag{5.243}$$

A priori three regimes of inflation may exist: $x < x^-_{V'=0}$ and inflation proceeds from the right to the left, $x^-_{V'=0} < x < x^-_{V=0}$ and inflation proceeds from the left to the right, $x^+_{V=0} < x$ and inflation proceeds from the right to the left in the direction specified by the arrow in Fig. 62. As explained below, only the third possibility allows us to have a slow-roll inflationary regime.

Let us now calculate the quantities ϵ_n. The first three Hubble flow functions in the slow-roll approximation are given by

$$\epsilon_1 = 2\frac{M_{\rm Pl}^2}{\phi_0^2}\left(\frac{2\ln^2 x + \ln x - 2\alpha}{x\ln^2 x - \alpha x}\right)^2, \tag{5.244}$$

$$\epsilon_2 = 4\frac{M_{\rm Pl}^2}{\phi_0^2}\frac{2\ln^4 x + \ln^3 x + (1-4\alpha)\ln^2 x - \alpha\ln x + \alpha + 2\alpha^2}{\left(x\ln^2 x - \alpha x\right)^2}, \tag{5.245}$$

and

$$\epsilon_3 = 2\frac{M_{\rm Pl}^2}{\phi_0^2}\left[8\alpha^4+6\alpha^3-\alpha^2\left(8\alpha+15\right)\ln x+2\alpha\left(3-16\alpha^2-2\alpha\right)\ln^2 x\right.$$
$$+8\alpha\left(3\alpha+1\right)\ln^3 x+2\left(24\alpha^2-5\alpha+1\right)\ln^4 x+\left(7-24\alpha\right)\ln^5 x+8\left(1-4\alpha\right)\ln^6 x \qquad (5.246)$$
$$\left.+8\ln^7 x+8\ln^8 x\right]\left(x\ln^2 x-\alpha x\right)^{-2}$$
$$\times\left[2\alpha^2+\alpha-\alpha\ln x+\left(1-4\alpha\right)\ln^2 x+\ln^3 x+2\ln^4 x\right]^{-1}.$$

They have been represented in Fig. 62. One can see that the slow-roll regime can only take place in the $x > x_{V=0}^{+}$ region, where ϵ_1 continuously increase as inflation proceeds from the right to the left, and diverges at $x_{V=0}^{+}$. In the other domains, ϵ_2 remains too large to support slow-roll inflation. Within the $x > x_{V=0}^{+}$ domain, inflation naturally ends by slow-roll violation, but the field value $x_{\rm end}$ at which this occurs has to be determined numerically. However, since $\phi_0 \simeq 10^{16}\,{\rm GeV}$, one can derive an approximated formula for $x_{\rm end}$ in the $\phi_0 \ll M_{\rm Pl}$ limit, namely

$$x_{\rm end} \simeq 2\sqrt{2}\frac{M_{\rm Pl}}{\phi_0}. \qquad (5.247)$$

The next step is to derive the slow-roll trajectory. It can be obtained from Eq. (2.11) and reads

$$N_{\rm end}-N = -\frac{\phi_0^2}{M_{\rm Pl}^2}\left\{\frac{x_{\rm end}^2-x^2}{8}+\frac{\ln^2\left(x_{V'=0}^{+}\right)-\alpha}{2\sqrt{1+16\alpha}}\left(x_{V'=0}^{+}\right)^2\left[{\rm Ei}\left(2\ln\frac{x_{\rm end}}{x_{V'=0}^{+}}\right)\right.\right.$$
$$\left.-{\rm Ei}\left(2\ln\frac{x}{x_{V'=0}^{+}}\right)\right]-\frac{\ln^2\left(x_{V'=0}^{-}\right)-\alpha}{2\sqrt{1+16\alpha}}\left(x_{V'=0}^{-}\right)^2\left[{\rm Ei}\left(2\ln\frac{x_{\rm end}}{x_{V'=0}^{-}}\right)-{\rm Ei}\left(2\ln\frac{x}{x_{V'=0}^{-}}\right)\right]\left.\right\}, \qquad (5.248)$$

where Ei is the exponential integral function, and where $x_{V'=0}^{\pm}$ have been defined in Eq. (5.243). In the $\phi_0 \ll M_{\rm Pl}$ limit, this trajectory reduces to $\Delta N_* \simeq \phi_0^2/(8M_{\rm Pl}^2)(x_*^2-x_{\rm end}^2)$, where we have introduced the observable field value x_* at which the pivot scale crossed the Hubble radius during inflation. It can be inverted to give x_* in terms of $\Delta N_* = N_{\rm end}-N_*$ and one gets

$$x_* \simeq 2\sqrt{2}\frac{M_{\rm Pl}}{\phi_0}\sqrt{\Delta N_*+1}. \qquad (5.249)$$

Plugging this into Eqs. (5.244), (5.245) and (5.246) gives the approximated expressions

$$\epsilon_{1*} \simeq \epsilon_{2*} \simeq \epsilon_{3*} \simeq \frac{1}{\Delta N_*+1}, \qquad (5.250)$$

hence

$$r \simeq \frac{16}{\Delta N_*+1}, \qquad n_{\rm S}-1 \simeq -\frac{3}{\Delta N_*+1}, \qquad \alpha_{\rm S} \simeq -\frac{3}{\left(\Delta N_*+1\right)^2}. \qquad (5.251)$$

From x_*, the parameter M is fixed by the amplitude of the CMB anisotropies and one obtains

$$\left(\frac{M}{M_{\rm Pl}}\right)^4 = \frac{2880\pi^2\left(2\ln^2 x_*+\ln x_*-2\alpha\right)^2}{x_*^6\left(\ln^2 x_*-\alpha\right)^3}\frac{M_{\rm Pl}^2}{\phi_0^2}\frac{Q_{\rm rms-PS}^2}{T^2}. \qquad (5.252)$$

In the $\phi_0 \ll M_{\rm Pl}$ limit, the previous expression reduces to the following formula

$$\left(\frac{M}{M_{\rm Pl}}\right)^4 \simeq \frac{45\pi^2}{2\left(\Delta N_* + 1\right)^3}\left(\frac{\phi_0}{M_{\rm Pl}}\right)^4 \frac{1}{\ln^2\left(2\sqrt{2}\dfrac{M_{\rm Pl}}{\phi_0}\sqrt{\Delta N_* + 1}\right)}\frac{Q^2_{\rm rms-PS}}{T^2}\,. \tag{5.253}$$

With $\phi_0 \simeq 10^{16}\,{\rm GeV}$, this typically gives $M/M_{\rm Pl} \simeq 5\times 10^{-4}$.

The reheating consistent slow-roll predictions for the orientifold inflation models are displayed in Fig. 137, for $\phi_0/M_{\rm Pl} = 10^{-4}$,$10^{-2}$, and 1. Let us recall that natural values are around $\phi_0 \simeq 10^{16}\,{\rm GeV}$ and $\alpha \in \left[10^{-3}, 1\right]$. The reheating equation of state parameter has been fixed to $\overline{w}_{\rm reh} = 0$ since the potential is quadratic in the vicinity of its minimum. According to the rough picture provided by Eq. (5.250), the predictions of these models almost do not depend on its parameters ϕ_0 and α, which is why all the points in Fig. 137 are superimposed. In particular, one can see that these models generically predict an important amount of gravitational waves which is disfavored by the observations.

5.15 Constant $n_{\rm S}$ C Inflation (CNCI)

This model has been obtained in Ref. [428] and is the third example of a class of scenarios already studied in sections 4.20 and 4.21. As explained in those sections, the corresponding potential is designed in order to produce a power spectrum with constant spectral index. The potential studied in this section reads

$$V\left(\phi\right) = M^4\left[\left(3+\alpha^2\right)\coth^2\left(\frac{\alpha}{\sqrt{2}}\frac{\phi}{M_{\rm Pl}}\right) - 3\right], \tag{5.254}$$

where α is a positive dimensionless parameter (denoted n_0 in Ref. [428]). The potential being symmetrical in $\phi \to -\phi$, only the $\phi > 0$ part is displayed in Fig. 63. It is a decreasing function of the field *vev*, and its asymptotic value when $\phi/M_{\rm Pl}$ goes to infinity is given by $\alpha^2 M^4$, hence the potential is always positive.

Defining $x = \phi/M_{\rm Pl}$, the three first slow-roll parameters are given by

$$\epsilon_1 = \frac{4\alpha^2\left(3+\alpha^2\right)^2\coth^2\left(\dfrac{\alpha x}{\sqrt{2}}\right)}{\left[6+\alpha^2+\alpha^2\cosh\left(\sqrt{2}\alpha x\right)\right]^2}\,, \tag{5.255}$$

$$\epsilon_2 = -\frac{2\alpha^2\left(3+\alpha^2\right)\left[12+\alpha^2+2\alpha^2\cosh\left(\sqrt{2}\alpha x\right)+\alpha^2\cosh\left(2\sqrt{2}\alpha x\right)\right]}{\left[6+\alpha^2+\alpha^2\cosh\left(\sqrt{2}\alpha x\right)\right]^2\sinh^2\left(\dfrac{\alpha x}{\sqrt{2}}\right)}\,, \tag{5.256}$$

and

$$\begin{aligned}\epsilon_3 = &-2\alpha^2\left(3+\alpha^2\right)\left[6\left(24-2\alpha^2+\alpha^4\right)+\left(120\alpha^2+7\alpha^4\right)\cosh\left(\sqrt{2}\alpha x\right)\right.\\ &\left.+\,2\alpha^2\left(\alpha^2-6\right)\cosh\left(2\sqrt{2}\alpha x\right)+\alpha^4\cosh\left(3\sqrt{2}\alpha x\right)\right]\coth^2\left(\frac{\alpha}{\sqrt{2}}x\right)\\ &\times\left[6+\alpha^2+\alpha^2\cosh\left(\sqrt{2}\alpha x\right)\right]^{-2}\left[12+\alpha^2+2\alpha^2\cosh\left(\sqrt{2}\alpha x\right)+\alpha^2\cosh\left(2\sqrt{2}\alpha x\right)\right]^{-1}.\end{aligned} \tag{5.257}$$

These slow-roll parameters are displayed in Fig. 63 (bottom panels). We see that the first slow-roll parameters monotonously decreases during inflation. It blows up as the field *vev*

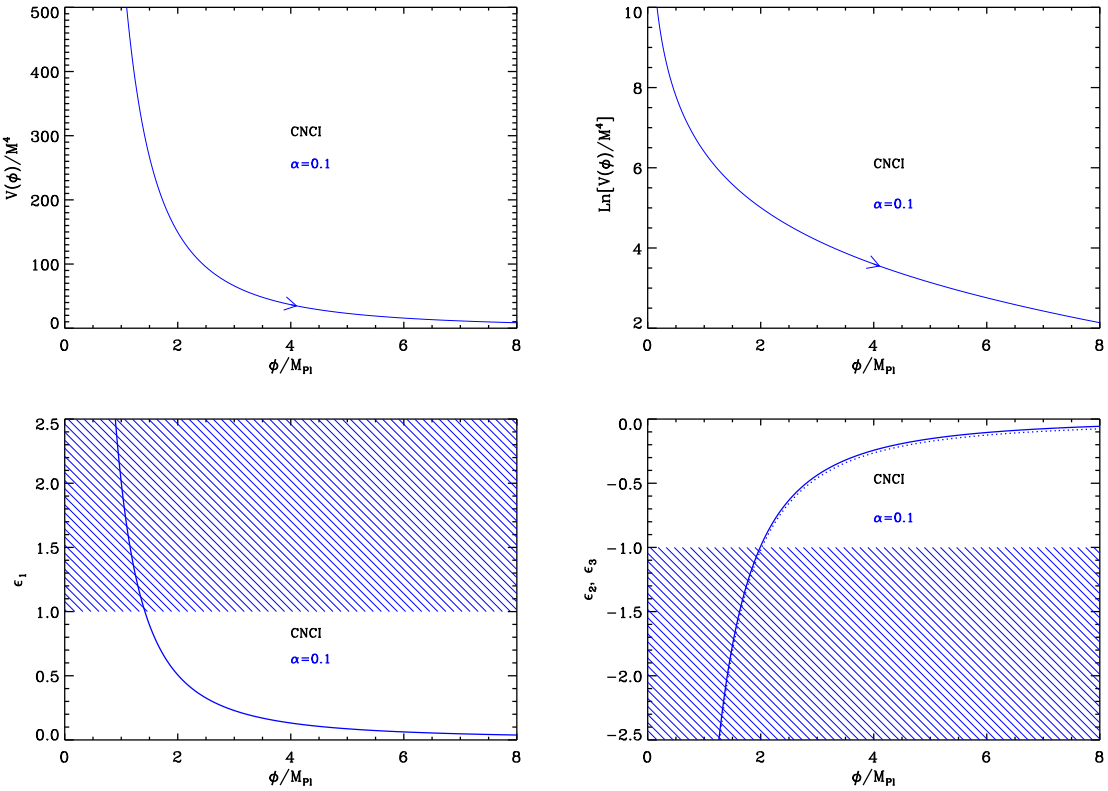

Figure 63. Top left panel: Constant $n_{\rm S}$ C inflaton potential for $\alpha = 0.1$. Inflation proceeds from the left to the right as indicated by the arrow. Top right panel: logarithm of the potential for the same value of α. Bottom left panel: the first slow-roll parameter ϵ_1 for $\alpha = 0.1$. Bottom right panel: slow-roll parameters ϵ_2 and ϵ_3, still for $\alpha = 0.1$.

approaches zero and tends to zero when the field *vev* goes to infinity. On the contrary, the second and third slow-roll parameters monotonously increase from $-\infty$ to zero as inflation proceeds.

Given the above described behavior of ϵ_1, it is clear that inflation cannot stop by slow-roll violation. Therefore, it should be stopped by instability which means that an extra parameter $x_{\rm end}$ should be added to the model.

As for CNAI and CNBI, the spectral index $n_{\rm S} - 1 = -2\epsilon_1 - \epsilon_2$ at first order in slow-roll, can be made constant in some limit. Expanding the slow-roll parameters ϵ_1 and ϵ_2 in α, assuming that $x\alpha$ remains small, one obtains $\epsilon_1 = 2/x^2 + 2\alpha^2/3 + \mathcal{O}\left(\alpha^4\right)$ and $\epsilon_2 = -4/x^2 + 2\alpha^2/3 + \mathcal{O}\left(\alpha^4\right)$, so that $n_{\rm S} - 1 = -2\alpha^2 + \mathcal{O}\left(\alpha^4\right)$. As for the similar calculations performed in sections 4.20 and 4.21, one should remark that, if $x_{\rm end}$ is such that $\alpha x_* \gtrsim 1$, the previous expansion can be inaccurate and some deviations from constant $n_{\rm S}$ may appear.

Let us now consider the slow-roll trajectory. It can be integrated analytically and is

given by the following formula

$$N - N_{\rm end} = \frac{1}{\alpha^2\left(3+\alpha^2\right)}\left\{3\ln\left[\cosh\left(\frac{\alpha}{\sqrt{2}}x\right)\right] + \frac{\alpha^2}{2}\cosh^2\left(\frac{\alpha}{\sqrt{2}}x\right) - 3\ln\left[\cosh\left(\frac{\alpha}{\sqrt{2}}x_{\rm end}\right)\right] - \frac{\alpha^2}{2}\cosh^2\left(\frac{\alpha}{\sqrt{2}}x_{\rm end}\right)\right\}. \tag{5.258}$$

Moreover, this expression can be explicitly inverted. As a consequence, the function $x(N)$ can be written as

$$x = \frac{\sqrt{2}}{\alpha}\,\mathrm{arccosh}\left[\frac{3}{\alpha^2}\mathrm{W}_0\left(\frac{\alpha^2}{3}\exp\left\{\frac{2}{3}\alpha^2\left(3+\alpha^2\right)\left(N-N_{\rm end}\right) + 2\ln\left[\cosh\left(\frac{\alpha}{\sqrt{2}}x_{\rm end}\right)\right] + \frac{\alpha^2}{3}\cosh^2\left(\frac{\alpha}{\sqrt{2}}x_{\rm end}\right)\right\}\right)\right]^{1/2}, \tag{5.259}$$

where W_0 is the Lambert function. The fact that we deal with the 0-branch is obvious since the argument of this function is positive definite.

The predictions of the CNCI models are displayed in Fig. 138, for $\alpha = 10^{-3}$, 0.1 and 0.2. The thin black solid lines are the lines such that $n_{\rm S} - 1 = -2\alpha^2$. We see that, for very small values of α, the predictions are indeed such that the spectral index is constant. For α not too small, however, we also notice deviations from this law and the larger α the stronger these deviations. This is reminiscent with the phenomenon observed in sections 4.20 and 4.21 but now $x_{\rm end}$ is a free parameter and, for a given value of α, the deviations from $n_{\rm S} - 1 = -2\alpha^2$ become larger when $x_{\rm end}$ increase (i.e. when the line becomes redder in Fig. 138). In this case, the Taylor expansion of the trigonometric functions which appear in the expressions of the slow-roll parameters is no longer valid because a larger $x_{\rm end}$ implies a larger x_*. This has for consequence that CNCI inflation is only marginally consistent with the data. Indeed, it is precisely in the region where $n_{\rm S} - 1 = -2\alpha^2$ would be compatible with the observations that the deviations play an important role and push the predictions away from the allowed contours. In fact, these properties can be better illustrated by deriving explicitly x_*. Using Eq. (5.258), one gets

$$\cosh^2\left(\frac{\alpha x_*}{\sqrt{2}}\right) = \frac{3}{\alpha^2}\mathrm{W}_0\left(\frac{\alpha^2}{3}e^{2A/3}\right), \tag{5.260}$$

where we have defined the quantity A by

$$A \equiv -\alpha^2\left(3+\alpha^2\right)\Delta N_* + 3\ln\left[\cosh\left(\frac{\alpha x_{\rm end}}{\sqrt{2}}\right)\right] + \frac{\alpha^2}{2}\cosh^2\left(\frac{\alpha x_{\rm end}}{\sqrt{2}}\right). \tag{5.261}$$

In the regime where both $\alpha \ll 1$ and $\alpha x_{\rm end} \ll 1$, the previous expression reduces to $x_*^2 \simeq x_{\rm end}^2 - 4\Delta N_*$. This last formula is identical to the slow-roll trajectory for LFI provided $p = -2$, see Eq. (4.36). At the beginning of this section, we have show that, at leading order $\epsilon_1 \simeq 2/x^2$ and $\epsilon_2 \simeq -4/x^2$ and, comparing with Eqs. (4.35), we notice that these are also the slow-roll parameters for LFI with $p = -2$. In fact, expanding Eq. (5.254), one sees that $V(\phi) \propto \phi^{-2}$ which confirms the previous considerations. In the regime where $\alpha \ll 1$ and $\alpha x_{\rm end} \ll 1$, the model is very close to LFI with $p = -2$. On the contrary, if $\alpha x_{\rm end}$ is not small, then the above relation does not hold anymore and one does not recover a constant spectral index.

Finally, we conclude this section by discussing how the mass scale M can be chosen. The CMB normalization gives

$$\left(\frac{M}{M_{\rm Pl}}\right)^4 = \frac{11520\pi^2\alpha^2\left(3+\alpha^2\right)^2\cosh^2\left(\frac{\alpha}{\sqrt{2}}x_*\right)}{\left[6+\alpha^2+\alpha^2\cosh\left(\sqrt{2}\alpha x_*\right)\right]^3}\frac{Q^2_{\rm rms-PS}}{T^2}\,. \tag{5.262}$$

From Eq. (5.260), one deduces that $\cosh^2(\alpha x_*/\sqrt{2}) \simeq 1 - 2\alpha^2\Delta N_* + \alpha^2 x^2_{\rm end}/2 \simeq 1$. Inserting this formula into Eq. (5.262), and taking the leading order in α, one obtains $M/M_{\rm Pl} \simeq 0.02\sqrt{\alpha}$. This implies that $M < M_{\rm Pl}$ if $\alpha \lesssim 2420$, which is largely the case for the predictions displayed in Fig. 138.

5.16 Supergravity Brane Inflation (SBI)

5.16.1 Theoretical Justifications

This model can emerge in different contexts. Following Ref. [232], let us consider a model with a scalar field and a massive fermion interacting through a Yukawa type term (with a coupling constant g). The corresponding Lagrangian can be written as

$$-\mathcal{L} = \frac{1}{2}\partial_\mu\phi\partial^\mu\phi + \frac{i}{2}\bar{\psi}\gamma^\mu\partial_\mu\psi + \frac{1}{2}m^2\phi^2 + \frac{\lambda}{4!}\phi^4 + m_{\rm f}\bar{\psi}\psi + \frac{1}{2}g\phi\bar{\psi}\psi, \tag{5.263}$$

where we have assumed the most general renormalizable scalar potential. At one loop level, the potential takes the form

$$\begin{aligned} V(\phi) = V_0 + \frac{1}{2}m^2\phi^2 + \frac{\lambda}{4!}\phi^4 + \frac{1}{64\pi^2}\left(m^2+\frac{\lambda}{2}\phi^2\right)^2\ln\left(\frac{m^2+\lambda\phi^2/2}{\mu^2}\right) \\ - \frac{2}{64\pi^2}\left(g\phi+m_{\rm f}\right)^4\ln\left[\frac{\left(g\phi+m_{\rm f}\right)^2}{\mu^2}\right], \end{aligned} \tag{5.264}$$

where μ is a renormalization scale. Then, assuming that, for some reason, the bosonic and fermionic massive terms are negligible, the potential can be expressed as

$$V(\phi) \simeq V_0 + \left[\frac{\lambda}{4!} + \frac{\lambda^2}{256\pi^2}\ln\left(\frac{\lambda}{2}\right) - \frac{g^4}{16\pi^2}\ln g\right]\phi^4 + \frac{1}{64\pi^2}\left(\frac{\lambda^2}{2} - \frac{g^4}{4}\right)\phi^4\ln\left(\frac{\phi}{\mu}\right). \tag{5.265}$$

This is the type of potential that we study in this section. Notice that a change in the renormalization scale μ is in fact equivalent to a change in the coefficient of the terms $\propto \phi^4$ and $\propto \phi\ln(\phi/\mu)$. This potential was also studied in Ref. [503] but the coefficient of the ϕ^4 term was chosen such that, at its minimum, the potential exactly vanishes. This particular case will also be treated in what follows. Finally, it is interesting to remark that this model was also proposed in Refs. [504, 505] in the context of brane cosmology within a supergravity bulk spacetime.

5.16.2 Slow-Roll Analysis

Let us now turn to the slow-roll analysis of the potential given by Eq. (5.265). It is more convenient to write it under the following form

$$V\left(\phi\right) = M^4\left\{1 + \left[-\alpha + \beta\ln\left(\frac{\phi}{M_{\rm Pl}}\right)\right]\left(\frac{\phi}{M_{\rm Pl}}\right)^4\right\}, \tag{5.266}$$

where α and β are dimensionless quantities that must be considered as small quantities since they are typically proportional to coupling constants, see Eq. (5.265). It is worth noticing that setting $\alpha = 0$ in the above expression allows us to recover the Coleman-Weinberg CWI models already studied in section 4.11. Defining the quantity x by the following expression

$$x \equiv \frac{\phi}{M_{\rm Pl}}\,, \tag{5.267}$$

one sees that the potential decreases from $x = 0$ to reach a minimum located at $x = x_{V'=0}$, then increases and diverges when x goes to infinity. The value of $x_{V'=0}$ is given by

$$x_{V'=0} = \exp\left(\frac{\alpha}{\beta} - \frac{1}{4}\right). \tag{5.268}$$

Since the logarithm terms in Eq. (5.266) are one loop corrections, they should not dominate the leading order terms. As a result, inflation can take place only in the domain $x < x_{V'=0}$ if one wants the model to be such that additional corrections to $V(\phi)$ are negligible. The value of the potential at the minimum reads

$$V_{\rm min} = V(x_{V'=0}) = M^4\left(1 - \frac{\beta}{4}e^{4\alpha/\beta-1}\right), \tag{5.269}$$

which is negative or vanishing if the following condition is satisfied

$$\alpha \geq \alpha_{\rm min}\left(\beta\right) = \frac{\beta}{4}\left[1 - \ln\left(\frac{\beta}{4}\right)\right]. \tag{5.270}$$

Inflation proceeds from the left to the right in the range $0 < x < x_{V=0} < x_{V'=0}$ where $x_{V=0}$ is the value at which the potential vanishes. It is given by

$$x_{V=0} = \left[\frac{-4/\beta}{\mathrm{W}_{-1}\left(-4/\beta e^{-4\alpha/\beta}\right)}\right]^{1/4}, \tag{5.271}$$

where W_{-1} is the -1 branch of the Lambert function. In this situation, inflation stops by slow-roll violation at $x = x_{V=0}$. As noticed above, the case $\alpha = \alpha_{\rm min}(\beta)$ is also interesting. It corresponds to tuning the parameters α and β such that the minimum of the potential exactly vanishes. When this condition is satisfied the previous formula reduces to $x_{V=0} = x_{V'=0} = (\beta/4)^{-1/4}$. Then, the first slow roll parameter ϵ_1 diverges at this point (see below) and, as a consequence, inflation also ends by slow roll violation.

The first three Hubble flow functions in the slow-roll approximation are given by

$$\epsilon_1 = \frac{x^6\left(-4\alpha + \beta + 4\beta\ln x\right)^2}{2\left(1 - \alpha x^4 + \beta x^4\ln x\right)^2}\,, \tag{5.272}$$

$$\epsilon_2 = 2\frac{\left(12\alpha - 7\beta - 12\beta\ln x\right)x^2 + \left(4\alpha^2 - \alpha\beta + \beta^2 + \beta^2\ln x - 8\alpha\beta\ln x + 4\beta^2\ln^2 x\right)x^6}{\left[1 + x^4\left(-\alpha + \beta\ln x\right)\right]^2}\,, \tag{5.273}$$

$$\begin{aligned}\epsilon_3 = {} & \frac{8}{x^2} + 2\frac{\left(-4 + \beta x^4\right)^2}{x^2\left(1 - \alpha x^4 + \beta x^4\ln x\right)^2} + \frac{1}{x^2}\frac{-52 + 9\beta x^4}{1 - \alpha x^4 + \beta x^4\ln x} \\ & + \frac{144\alpha - 84\beta + \left(28\alpha - 11\beta\right)\beta x^4 - 4\beta\left(36 + 7\beta x^4\right)\ln x}{\left(12\alpha - 7\beta - 12\beta\ln x\right)x^2 + \left(4\alpha^2 - \alpha\beta + \beta^2 - 8\alpha\beta\ln x + \beta^2\ln x + 4\beta^2\ln^2 x\right)x^6}\,.\end{aligned} \tag{5.274}$$

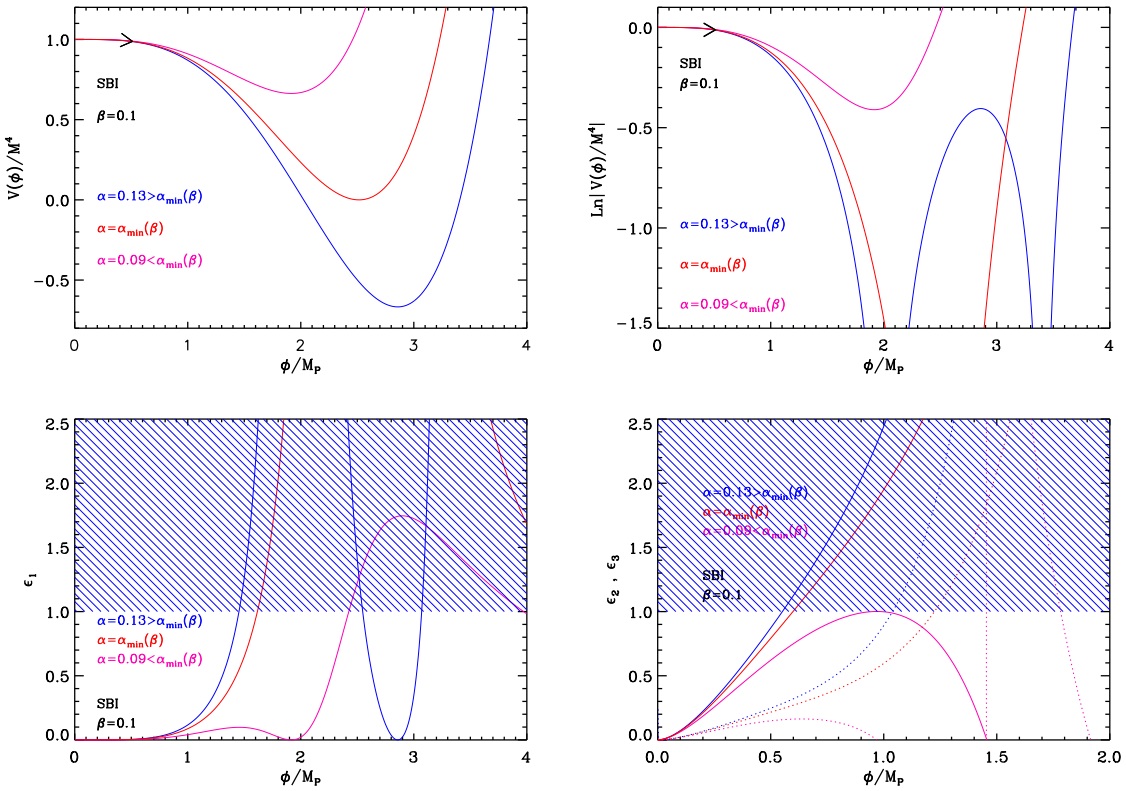

Figure 64. Supergravity Brane Inflation (SBI) for $\beta = 0.7$ and $\alpha = 0.13 > \alpha_{\rm min}(\beta)$, $\alpha = \alpha_{\rm min}(\beta)$, and $\alpha = 0.09 < \alpha_{\rm min}(\beta)$ (where $\alpha_{\rm min}$ is defined in Eq. (5.270)). Upper panels: the potential and its logarithm. Inflation proceeds in the place and direction labeled by the arrow. Bottom left panel: slow-roll parameter ϵ_1. The shaded area indicates where inflation stops. Bottom right panel: slow-roll parameters ϵ_2 (solid line) and ϵ_3 (dotted line), only displayed in the branch of the potential where inflation proceeds.

Together with the potential, they are represented in Fig. 64 for the physical branch $0 < x < x_{V=0}$.

As already mentioned, inflation stops by violation of the slow-roll conditions. This happens when $x = x_{\rm end}$ where $x_{\rm end}$ is the solution of $\epsilon_1(x_{\rm end}) = 1$. We see in Eq. (5.272) that there is no simple analytic solution for $x_{\rm end}$ and this equation must in fact be solved numerically. We have, however, already stressed that, when $\alpha \leq \alpha_{\rm min}(\beta)$, ϵ_1 diverges for $x \to x_{V=0}$, and therefore one already knows that $x_{\rm end} < x_{V=0}$.

Let us now consider the slow-roll trajectory. It can be integrated analytically and one obtains the following expression

$$N - N_{\rm end} = \frac{e^{2\frac{\alpha}{\beta}-\frac{1}{2}}}{16}\left[{\rm Ei}\left(\frac{1}{2} - 2\frac{\alpha}{\beta} + 2\ln x\right) - {\rm Ei}\left(\frac{1}{2} - 2\frac{\alpha}{\beta} + 2\ln x_{\rm end}\right)\right] - \frac{e^{\frac{1}{2}-2\frac{\alpha}{\beta}}}{4\beta}\left[{\rm Ei}\left(-\frac{1}{2} + 2\frac{\alpha}{\beta} - 2\ln x\right) - {\rm Ei}\left(-\frac{1}{2} + 2\frac{\alpha}{\beta} - 2\ln x_{\rm end}\right)\right] - \frac{x^2 - x_{\rm end}^2}{8}\,. \tag{5.275}$$

The field value x_* at which the pivot scale crossed the Hubble radius during inflation is obtained by solving Eq. (2.47). Clearly, it must also been done numerically and those calculations are implemented in the corresponding `ASPIC` routines.

Finally, the parameter M is fixed by the amplitude of the CMB anisotropies and one obtains

$$\left(\frac{M}{M_{\rm Pl}}\right)^4 = \frac{720\pi^2\,(4\alpha-\beta-4\beta\ln x_*)^2}{(-1+\alpha x_*^4-\beta x_*^4\ln x_*)^3}\,\frac{Q^2_{\rm rms-PS}}{T^2}\,. \tag{5.276}$$

The reheating consistent slow-roll predictions for the SBI models are displayed in Figs. 139 and 140, for $\beta = 5\times10^{-5}$ and $\beta = 10^{-3}$, respectively, and with $\alpha \leq \alpha_{\rm min}(\beta)$. These plots show that the larger values of β, the more negligible the amount of gravitational waves. The predictions for the special case $\alpha = \alpha_{\rm min}(\beta)$ are also displayed in Fig. 141, where it is clear that smaller values of β are preferred.

5.17 Spontaneous Symmetry Breaking Inflation (SSBI)

5.17.1 Theoretical Justifications

The potential that we study in this section is given by the following expression

$$V(\phi) = V_0 + a\phi^2 + b\phi^4, \tag{5.277}$$

where a and b are constant coefficients the sign of which is not a priori determined. Before turning to the slow-roll analysis, it is interesting to study in which context such a potential can arise.

First of all, it is clear that this potential is very general since it is just made of the three first terms of a general Taylor expansion. Therefore, it can just be considered as a phenomenological description of a generic inflaton potential. This view was for instance adopted in Ref. [328], where this potential was used as a toy model to implement "new inflation". In the same fashion, it was also considered in Ref. [506] (with the assumptions $a<0$ and $b>0$) in the framework of models with spontaneous symmetry breaking where ϕ represents one of the components of a Higgs field. In Ref. [507], it was also studied in the context of "mixmaster inflation".

However, there are also models where this specific shape explicitly arises and, here, when necessary, we also briefly review them.

The first example is given by Refs. [508, 509]. In these articles, inflation was investigated in the context of gauge mediated SUSY breaking scenarios. One of the basic idea of this approach is that the inflaton field should not be an extra field added to the theory on purpose but rather a field which is already present in known high energy theories. In the MSSM, see also section 4.17, we know that the Higgs sector superpotential contains the term $\mu H_{\rm u}\cdot H_{\rm d}$ where μ should be of the order of the electroweak scale, that is to say far from the Planck scale. This is the so-called μ-problem. One possible solution is to consider that this term dynamically arises due to the presence of another superfield (usually a singlet), S, in the theory. Refs. [508, 509] take advantage of this fact and build a model where S can also play the role of the inflaton. Since the model is also formulated in the framework of gauge-mediated supersymmetry breaking scenarios, there is an additional superfield X such that its scalar component (also denoted X) and auxiliary component F_X acquire non-vanishing *vev*. Let us now consider the following super-potential

$$W = -\beta\frac{XS^4}{M_{\rm Pl}^2} + \frac{S^5}{M_{\rm Pl}^2} + \lambda\frac{S^2}{M_{\rm Pl}}H_{\rm u}\cdot H_{\rm d} + \bar{W}, \tag{5.278}$$

where the function $\bar{W}$ describes all the other extra terms in W and, crucially, is assumed to be independent of S. The quantities λ and β are constant coefficients. As argued in Refs. [508, 509], this form of W can be enforced by discrete symmetries. In particular, we notice the absence of a term $SH_{\rm u}\cdot H_{\rm d}$. Another important ingredient of the model is the assumption that the *vev* F_X comes from the extra-terms in the above superpotential, i.e. $F_X \simeq \partial\bar{W}/\partial X$. Then, the scalar potential reads

$$V = \left(F_X - \beta\frac{S^4}{M_{\rm Pl}^2}\right)^2 + \left(5\frac{S^4}{M_{\rm Pl}^2} - 4\beta\frac{X}{M_{\rm Pl}^2}S^3\right)^2 . \tag{5.279}$$

Taking into account supergravity corrections, which are typically of the form $(\partial W/\partial X)/M_{\rm Pl}^2$, i.e. $m^2 = aF_X^2/M_{\rm Pl}^2$, where a is a coefficient of order one we are led to

$$V \simeq F_X^2 - a\frac{F_X^2}{M_{\rm Pl}^2}S^2 - 2\beta F_X\frac{S^4}{M_{\rm Pl}^2} + 16\beta^2\frac{X^2}{M_{\rm Pl}^4}S^6 - 40\beta\frac{X}{M_{\rm Pl}^4}S^7 + (25+\beta^2)\frac{S^8}{M_{\rm Pl}^4}. \tag{5.280}$$

In addition, making the reasonable assumption that the field X is stabilized at a *vev* such that $X/M_{\rm Pl} \ll 1$, one can neglect higher order terms in this expression. Then, we see that S can play the role of the inflaton with a potential of the form given by Eq. (5.277), namely

$$V \simeq F_X^2\left(1 - a\frac{S^2}{M_{\rm Pl}^2} - \frac{2\beta M_{\rm Pl}^2}{F_X}\frac{S^4}{M_{\rm Pl}^4}\right). \tag{5.281}$$

At the minimum of the potential, $S^4 \simeq M_{\rm Pl}^2 F_X$ and this implies a μ term for the MSSM of the form $\mu \simeq \lambda\sqrt{F_X}$. As explained before, this model dynamically produces the μ term while obtaining a candidate for the inflaton field. Finally, let us remark that the CMB normalization will determine the scale F_X and that the spectrum of the superparticles depends on the ratio F_X/X. Therefore, given a value of F_X, one can always choose X in order to obtain reasonable values for the superparticle masses.

The SSBI potential was also used, as a toy model, in Refs. [510, 511] to study a model of "Spinodal Inflation". After the 90's, it was considered again several times: in the context of the Randall-Sundrum model in Ref. [512] (but within the framework of Brans-Dicke theories), in the context of the little Higgs model in Ref. [259] and in the context of induced gravity inflation in Ref. [513]. In this last reference, a potential of the form (5.277) was considered but in the Jordan frame. Since the potential is different in the Einstein frame, in fact, this model does not belong to the class of scenarios studied here. Finally, it was also considered in the context of electroweak inflation in Ref. [514].

In Ref. [515], an inflationary scenario was studied in which the superpartner of the right-handed neutrino plays the role of the inflaton field. Let us denote by N the singlet neutrino superfield, ϕ the super waterfall field (that can be put to zero during inflation) and S another singlet superfield (which can also be put to zero during inflation). Then, on very general grounds, the Kähler potential can be written as

$$\begin{aligned} K = {} & |S|^2 + |\phi|^2 + |N|^2 + \kappa_S\frac{|S|^4}{4M_{\rm Pl}^2} + \kappa_N\frac{|N|^4}{4M_{\rm Pl}^2} + \kappa_\phi\frac{|\phi|^4}{4M_{\rm Pl}^2} + \kappa_{S\phi}\frac{|S|^2|\phi|^2}{M_{\rm Pl}^2} + \kappa_{SN}\frac{|S|^2|N|^2}{M_{\rm Pl}^2} \\ & + \kappa_{N\phi}\frac{|N|^2|\phi|^2}{M_{\rm Pl}^2} + \cdots , \end{aligned} \tag{5.282}$$

where the dimensionless coefficients κ are a priori of order one. The superpotential can be expressed as

$$W = \kappa S\left(\frac{\phi^4}{M'^2} - M^2\right) + \frac{\lambda}{M_*}N^2\phi^2 + \cdots , \tag{5.283}$$

where M, M' and M_* are three mass scales and κ and λ are coupling constants. Since the three fields introduced before are singlets the potential does not contain D-term contributions. As a consequence, for $S \simeq 0$ and $\phi \simeq 0$, we are left with the F-term potential only and this one can be written as

$$V(N) \simeq \kappa^2 M^4 \left[1 + (1 - \kappa_{SN}) \frac{N^2}{M_{\rm Pl}^2} + \left(\frac{1}{2} + \frac{\kappa_N}{4} - \kappa_{SN} + \kappa_{SN}^2\right) \frac{N^4}{M_{\rm Pl}^4} + \cdots\right]. \tag{5.284}$$

We see that it has the form of Eq. (5.277). Ref. [515] also discusses how to stop inflation by tachyonic instability. Since the field ϕ is viewed as the waterfall field, one has to calculate his mass to see when the instability is triggered. This can be done by evaluating the quadratic correction in ϕ to the potential calculated before. This leads to

$$m_\phi^2 = \left(1 + \kappa_{N\phi} \frac{N^2}{M_{\rm Pl}^2} - \kappa_{S\phi}\right) \frac{\kappa^2 M^4}{M_{\rm Pl}^2} + 4 \frac{\lambda^2}{M_*^2} N^4. \tag{5.285}$$

Neglecting the term $N^2/M_{\rm Pl}^2 \ll 1$ in this expression, the effective mass vanishes for

$$N_{\rm cri} \simeq \frac{\kappa M^2 M_*}{2\lambda M_{\rm Pl}} \sqrt{-(1 - \kappa_{S\phi})}\,. \tag{5.286}$$

We see that this requires $1 - \kappa_{S\phi} < 0$. On the other hand, this model also provides an expression for the coefficients a and b in terms of the fundamental coefficients of the Kähler potential. Except from the above mentioned condition, there is no other constraint on the coefficients κ and, as a consequence, the sign of a and b is, a priori, not fixed in this scenario.

Another context in which Eq. (5.277) arises is "racetrack inflation" [516, 517]. Racetrack inflation is a string inspired inflationary scenario where the inflaton is a volume modulus. Therefore, this model belongs to the same class as KMIII, see section 5.3. The Kähler and super potentials are given by standard formulas, namely

$$K = -\frac{3}{\kappa} \ln\left(T + T^\dagger\right), \qquad W = W_0 + A e^{-aT} + B e^{-bT}. \tag{5.287}$$

Writing $T = X + iY$, it follows that the scalar F-term potential reduces to

$$\begin{aligned} V(X,Y) = \frac{\kappa}{6X^2} \Big\{ & aA^2 (3 + aX) e^{-2aX} + bB^2 (3 + bX) e^{-2bX} + 3aAW_0 e^{-aX} \cos(aY) \\ & + 3bBW_0 e^{-bX} \cos(bY) + AB \left[2abX + 3(a + b)\right] e^{-(a+b)X} \cos\left[(a - b) Y\right] \Big\} + \frac{E}{X^\alpha}, \end{aligned} \tag{5.288}$$

where an uplifting term $\propto X^{-\alpha}$ has been added. Let us mention that X and Y are not canonically normalized and their kinetic term reads $3[(\partial_\mu X)^2 + (\partial_\mu Y)^2]/(4\kappa X^2)$. The above potential has a very rich structure and for $W_0 = 0$ and $a = b$, we have a flat direction in Y. Moreover, for $Y = 0$, one can find a minimum in the X direction. If we then combine the two above remarks, then it is clear that there exists a choice of parameters such that one has a saddle point around $Y = 0$ (a specific example was exhibited in Ref. [516]). This point seems suitable for inflation. Around such a point, it is argued in Ref. [517] that one can write

$$V(Y) = V_0 \left(1 + \frac{\eta_0}{2} y^2 + \frac{C}{4} y^4 + \cdots\right), \tag{5.289}$$

where y is now the canonically normalized field when X is stabilized. This is again a potential of the type given by Eq. (5.277). In order to phenomenologically reproduce racetrack inflation, one should have η_0 small and negative and C large and positive.

The potential of Eq. (5.277) was also used, as a toy model, in the context of minimal left-right symmetric models with spontaneous D-parity breaking in Ref. [518] and in the context of hilltop supernatural inflation in Refs. [519–521]. A justification based on high energy physics was offered and the idea is to assume that the full potential has a SUSY flat direction. The approach is therefore similar to what was already investigated in section 4.17. In that situation, one can write $V(\phi)$ as

$$V = V_0 + \frac{1}{2}m^2\phi^2 - A\frac{\lambda_p\phi^p}{pM_{\rm Pl}^{p-3}} + \lambda_p^2\frac{\phi^{2p-2}}{M_{\rm Pl}^{2p-6}}, \tag{5.290}$$

where the term V_0 is added by hand. If one chooses $p = 4$ and neglects the last term (for instance if $\phi \ll M_{\rm Pl}$), then one arrives at

$$V(\phi) \simeq V_0 + \frac{1}{2}m^2\phi^2 - \frac{\lambda_4 A}{4M_{\rm Pl}}\phi^4, \tag{5.291}$$

which is of the form of Eq. (5.277). In this framework, m and A are SUSY soft terms and, therefore, should be taken of $\mathcal{O}(\mathrm{TeV})$. The term $V_0 = M_{\rm s}^4$ where $M_{\rm s}$ is the SUSY breaking scale, $M_{\rm s} \simeq 10^{11}\,\mathrm{GeV}$.

Finally, let us mention that SSBI was also considered in the context of a supersymmetric B-L extension of the standard model in Refs. [522, 523] and in the context of Kähler-driven "tribrid inflation" in Ref. [524]. In this last case, one obtains a situation very similar to the one discussed above for sneutrino inflation. In particular, the coefficients a and b can be expressed in terms of the coefficients appearing in the Kähler potential. To end this part, let us notice that the potential (5.277) also arises in the context of Higgs inflation, as shown in Refs. [525–527].

As already mentioned above, these works differ on the signs of α and β. Summarizing, Refs. [507, 515] require $\alpha > 0$, $\beta > 0$ while Refs. [259, 328, 506, 510, 511, 513, 514, 517, 518] assume $\alpha < 0$, $\beta > 0$. On the other hand, Refs. [519–521] consider that $\alpha > 0$ and $\beta < 0$ and Refs. [508, 509, 525–527] have $\alpha < 0$, $\beta < 0$. We see that the four possible combinations have all been studied. Also, in Refs. [522, 523], one has $\alpha, \beta \lesssim \mathcal{O}(1)$ and inflation only takes place in the increasing branches of the potential (see below). Finally, in Refs. [512, 524], β is taken to be positive and the sign of α is left unspecified.

5.17.2 Slow-Roll Analysis

Let us now turn to the slow-roll analysis of SSBI. For this purpose, it is more convenient to rewrite the potential (5.277) as

$$V(\phi) = M^4\left[1 + \alpha\left(\frac{\phi}{M_{\rm Pl}}\right)^2 + \beta\left(\frac{\phi}{M_{\rm Pl}}\right)^4\right], \tag{5.292}$$

where α and β are two dimensionless parameters. Based on the previous brief review of the literature, we conclude that it is necessary to study the model in full generality and, therefore, in what follows, we investigate all possible situations. As mentioned above, four cases should be distinguished: $\alpha > 0$, $\beta > 0$; $\alpha < 0$, $\beta < 0$; $\alpha > 0$, $\beta < 0$ and $\alpha < 0$, $\beta > 0$, with two

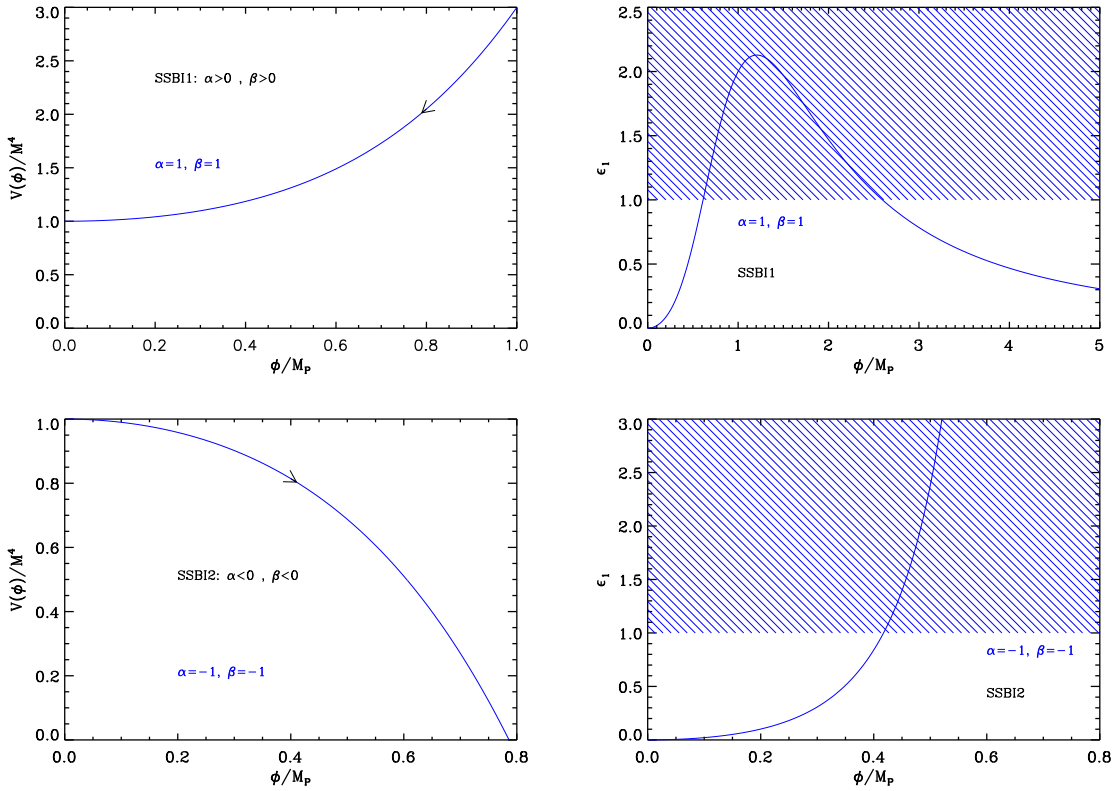

Figure 65. Spontaneous Symmetry Breaking Inflation (SSBI) potential and the corresponding Hubble flow parameter ϵ_1 for the two cases $\alpha > 0$, $\beta > 0$ (SSBI1), and $\alpha < 0$, $\beta < 0$ (SSBI2). The values of the parameters are chosen to be $\alpha, \beta = \pm 1$. The four other possibilities, namely SSBI3, SSBI4, SSBI5, SSBI6 are displayed in Fig. 66.

possible domains of inflation in the two latter cases. Therefore we have six regimes of inflation that we label SSBI1, SSBI2, SSBI3, SSBI4, SSBI5 and SSBI6. The different potentials and inflationary regimes are displayed and defined in Fig. 65 and Fig. 66. Since the potential is symmetric under $\phi/M_{\rm Pl} \to -\phi/M_{\rm Pl}$, it is only displayed and studied for $\phi > 0$.

Let us now calculate the slow-roll parameters. If one defines x by $x \equiv \phi/M_{\rm Pl}$, then the three first Hubble parameters are given by the following expressions

$$\epsilon_1 = \frac{2\left(\alpha x + 2\beta x^3\right)^2}{\left(1+\alpha x^2+\beta x^4\right)^2}, \qquad \epsilon_2 = \frac{4\left[-\alpha + \left(\alpha^2 - 6\beta\right)x^2 + \alpha\beta x^4 + 2\beta^2 x^6\right]}{\left(1+\alpha x^2+\beta x^4\right)^2}, \tag{5.293}$$

and

$$\epsilon_3 = \frac{4x^2\left(\alpha+2\beta x^2\right)\left[-3\alpha^2+6\beta+\alpha\left(\alpha^2-12\beta\right)x^2+3\left(\alpha^2-8\beta\right)\beta x^4+2\beta^3 x^8\right]}{\left(1+\alpha x^2+\beta x^4\right)^2\left[-\alpha+\left(\alpha^2-6\beta\right)x^2+\alpha\beta x^4+2\beta^2 x^6\right]}. \tag{5.294}$$

The first slow-roll parameter ϵ_1 is displayed in the right panels of Figs. 65 and 66 while the second and third slow-roll parameters ϵ_2 and ϵ_3 are displayed in Fig. 67. Let us describe the behavior of these slow-roll parameters, for the six models under consideration. For SSBI1, ϵ_1 vanishes at $x = 0$, reaches a maximum at $x^{\rm SSBI1}_{\epsilon_2=0}$ (where ϵ_2 vanishes and ϵ_3 diverges) and

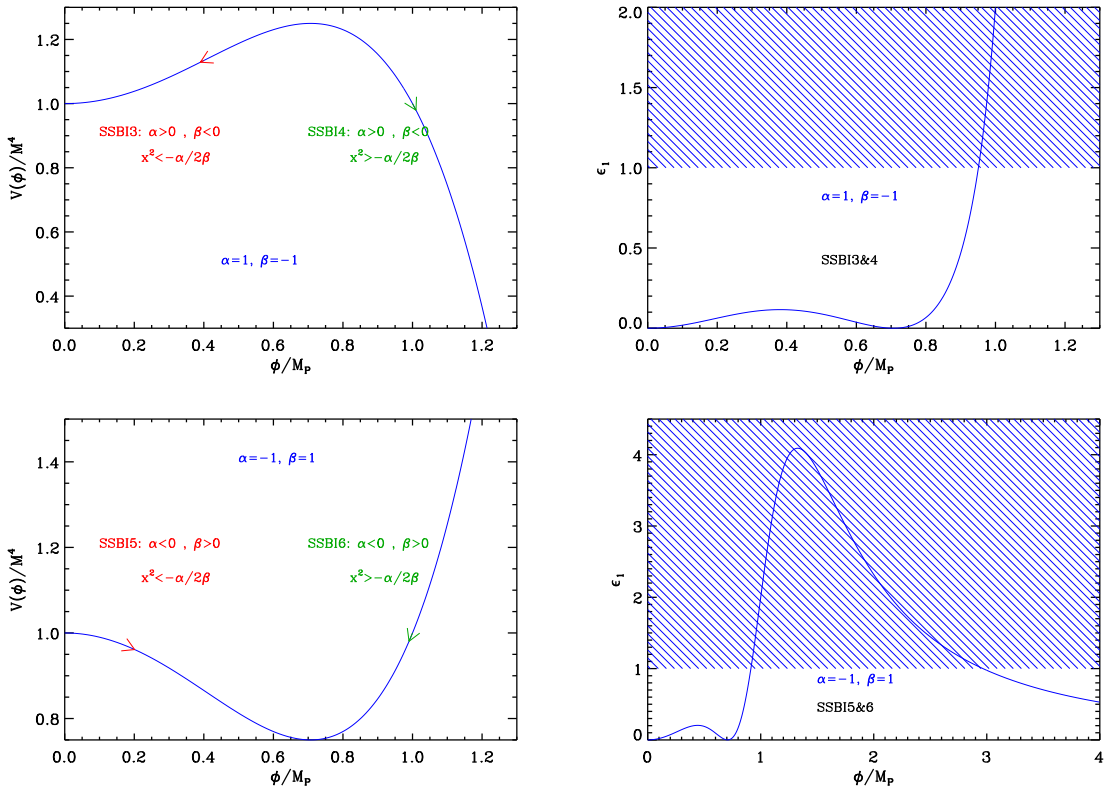

Figure 66. Spontaneous Symmetry Breaking Inflation (SSBI) potential and the corresponding Hubble flow parameter ϵ_1 for the two cases $\alpha > 0$, $\beta < 0$ (corresponding to SSBI3 to SSBI4) and $\alpha < 0$, $\beta > 0$ (corresponding to SSBI5 and to SSBI6). In each of these cases, the direction in which inflation proceeds is indicated by the arrow.

then decreases to asymptotically vanish when x goes to infinity. The value of $x_{\epsilon_2=0}^{\rm SSBI1}$ is given by

$$x_{\epsilon_2=0}^{\rm SSBI1\&3\&6} = \left\{ -\frac{\alpha}{6\beta} + \frac{1}{6\beta}\left[8\alpha^3 + \sqrt{64\alpha^6 + (5\alpha^2 - 36\beta)^3}\right]^{1/3} + \frac{36\beta - 5\alpha^2}{6\beta}\left[8\alpha^3 + \sqrt{64\alpha^6 + (5\alpha^2 - 36\beta)^3}\right]^{-1/3} \right\}^{1/2} . \tag{5.295}$$

Whether the maximum of ϵ_1 at this point is larger or smaller than 1 depends on α and β. In the following, we restrict ourselves to the physical regime where $\alpha, \beta \lesssim \mathcal{O}(1)$. For each value of β, there is a minimum value of α, denoted $\alpha_{\rm min}$, above which the maximum is larger than 1. The line $\alpha_{\rm min}(\beta)$ is displayed in Fig. 68 and the shaded area in this plot represents the region in the parameter space where inflation stops by slow-roll violation. When $\beta \ll 1$, $\alpha_{\rm min}(\beta)$ approaches 2 as can be noticed in the figure. In addition, for $\beta \gtrsim 0.25$, the maximum value for ϵ_1 becomes larger than 1 for any value of α.

For SSBI2, the three first slow-roll parameters are monotonic increasing functions of

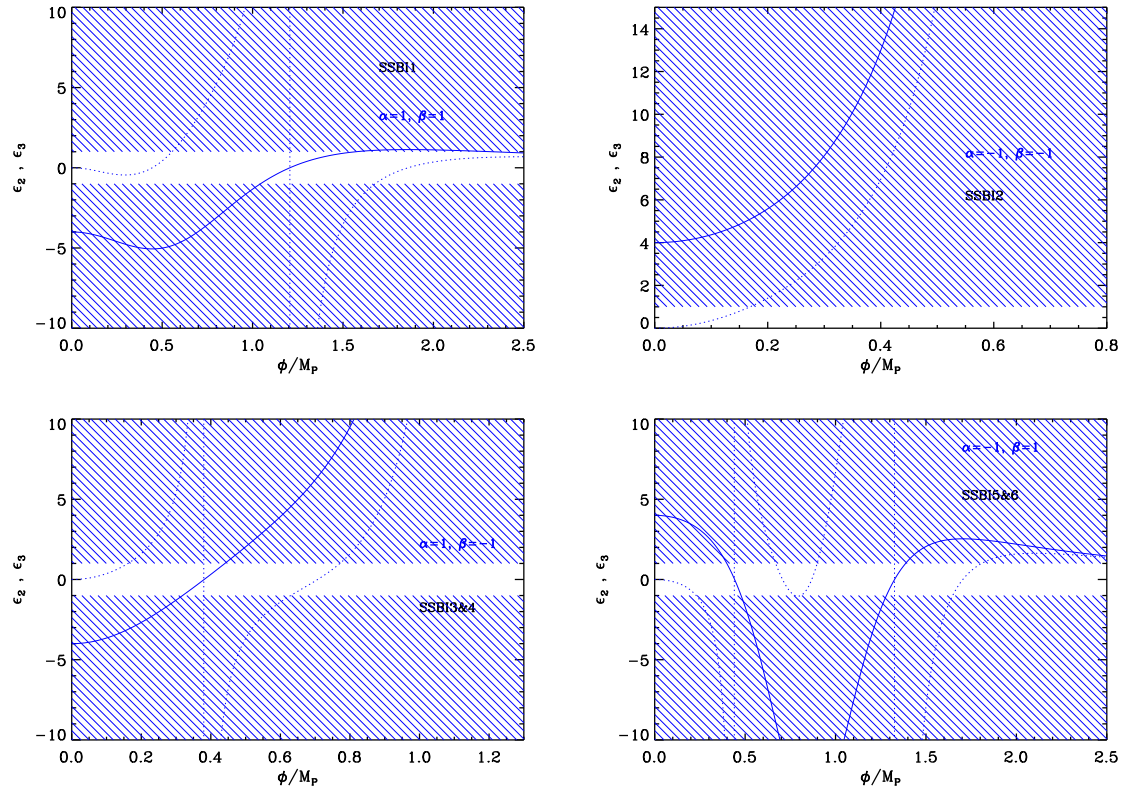

Figure 67. Second slow-roll parameter ϵ_2 (solid line) and third slow-roll parameter ϵ_3 (dotted line), for the six SSBI models studied in this section. The free parameters of the models are chosen to be $\alpha, \beta = \pm 1$.

the field *vev* and diverge when the potential vanishes at

$$x_{V=0}^{\mathrm{SSBI2\&4\&5}} = \sqrt{-\frac{\alpha + \sqrt{\alpha^2 - 4\beta}}{2\beta}}\,. \tag{5.296}$$

Hence inflation ends by slow-roll violation at x_{end}. Unfortunately, the corresponding *vev* cannot be found exactly and one has to rely on numerical calculations. Let us also notice that, while the first and third slow-roll parameters ϵ_1 and ϵ_3 vanish at $x = 0$, ϵ_2 is equal to $\epsilon_2^{\mathrm{min}} = -4\alpha$ at this point. Therefore, in order for the slow-roll approximation to be valid, one needs to work with $|\alpha| \ll 1$.

For SSBI3, the first slow-roll parameter ϵ_1 vanishes at $x = 0$ and at $x = \sqrt{-\alpha/(2\beta)}$. In between, it reaches a maximum located at

$$x_{\epsilon_2=0}^{\mathrm{SSBI3}} = x_{\epsilon_2=0}^{\mathrm{SSBI1}}\,, \tag{5.297}$$

a point where ϵ_2 vanishes and ϵ_3 diverges. Whether the maximum of ϵ_1 at this point is larger or smaller than 1 depends again on α and β. For each value of β, there is a minimum value for α above which inflation stops by slow-roll violation, similarly to the SSBI1 case. This corresponds to the green dotted line in Fig. 68 (top right panel). One way to estimate

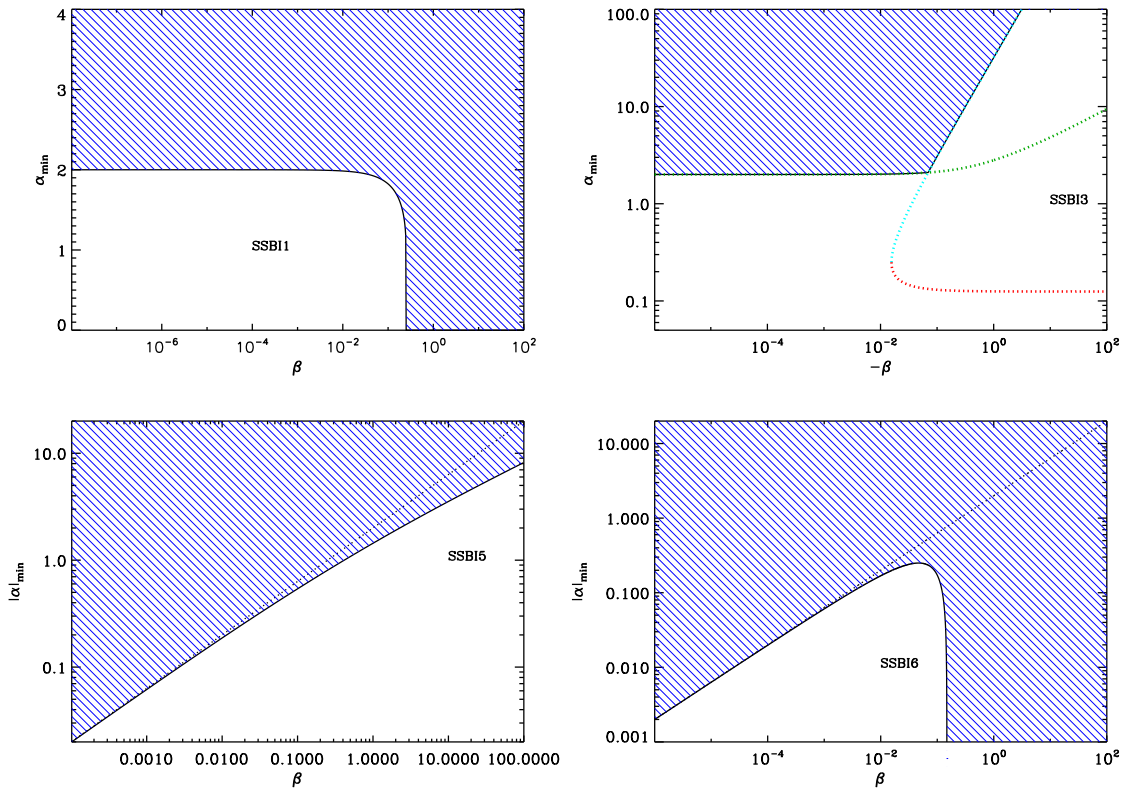

Figure 68. The black solid line gives the minimum value of $|\alpha|$, denoted here by $\alpha_{\rm min}$, as a function of β in order for inflation to stop by slow-roll violation for SSBI1 (top left panel), SSBI5 (bottom left panel) and SSBI6 (bottom right panel). For SSBI3 (top right panel), the green dotted line denotes the minimum value of α for inflation to stop by slow-roll violation, and the cyan and red dotted line restrict the values of α for which $\epsilon_2^{\rm top} > 1$ (defined only for $\beta < -1/64$). In the bottom panels, the dotted lines correspond to $\alpha^2 = 4\beta$, see the discussion in the text. In all the panels, the region above the black solid curve (shaded region) represents the allowed region (i.e. the one where a slow roll regime of inflation stops because ϵ_1 reaches one). For SSBI1, when $\beta \gtrapprox 0.25$, this is always the case. For SSBI1 and SSBI3, $\alpha_{\rm min}$ approaches the asymptotic value $\alpha_{\rm min} = 2$ when $|\beta| \ll 1$. For SSBI5 and SSBI6, inflation stops by slow-roll violation when $\alpha < -|\alpha_{\rm min}|$.

whether a slow roll regime of inflation can occur in the decreasing branch of ϵ_1 is to look at the value of ϵ_2 at the top of the potential. It is given by

$$\epsilon_2^{\rm top} = \frac{-32\alpha\beta}{\alpha^2 - 4\beta}\,. \tag{5.298}$$

This number is smaller than one when $\beta < -1/64$, or when α lies outside the range with limits given by $-16\beta \pm \sqrt{\beta(1+64\beta)}$, displayed in Fig. 68 with the red and cyan dotted lines. Therefore, requiring that $\epsilon_2^{\rm top} < 1$ and that inflation stops by slow roll violation leads to the allowed space $\alpha > \alpha_{\rm min}$, represented by the shaded region in Fig. 68.

For SSBI4, the three first slow-roll parameters are monotonic increasing functions of the field *vev* and diverge when the potential vanishes at $x_{V=0}^{\rm SSBI2\&4}$. The first and third slow-roll parameters ϵ_1 and ϵ_3 vanish when $x = \sqrt{-\alpha/(2\beta)}$ while ϵ_2 has a non-zero value $\epsilon_2^{\rm min} =$

$8\alpha\beta/(\beta^2-\alpha^2/4)$ at this point. From the above discussion, it is clear that, in this version of the scenario, inflation also stops by violation of the slow-roll condition. As for SSBI2, however, the corresponding *vev* can not be determined exactly and a numerical calculation is needed.

For SSBI5, the behavior of the slow-roll parameters depend on α^2/β. If $\alpha^2/\beta \geq 4$, the minimum of the potential at $x = \sqrt{-\alpha/(2\beta)}$ is negative. The potential vanishes at $x_{V=0}^{\mathrm{SSBI2\&4\&5}}$ and the three first slow-roll parameters continuously increase between $x = 0$ where they vanish (except ϵ_2 for which $\epsilon_2^{\mathrm{min}} = -4\alpha$) and $x_{V=0}^{\mathrm{SSBI2\&4\&5}}$ where they diverge. Inflation ends by slow-roll violation at some point x_{end} that needs to be determined numerically. On the other hand, if $\alpha^2/\beta \leq 4$, ϵ_1 vanishes at $x = 0$, reaches a maximum at $x_{\epsilon_2=0}^{\mathrm{SSBI5}}$ (where ϵ_2 vanishes and ϵ_3 diverges), then decreases and finally vanishes at $x = \sqrt{-\alpha/(2\beta)}$. The value of $x_{\epsilon_2=0}^{\mathrm{SSBI5}}$ is given by

$$x_{\epsilon_2=0}^{\mathrm{SSBI5}} = \left\{ -\frac{\alpha}{6\beta} - \frac{1+i\sqrt{3}}{12\beta}\left[8\alpha^3 + \sqrt{64\alpha^6 + (5\alpha^2-36\beta)^3}\right]^{1/3} + \frac{5\alpha^2-36\beta}{12\beta}\left(1-i\sqrt{3}\right)\left[8\alpha^3 + \sqrt{64\alpha^6 + (5\alpha^2-36\beta)^3}\right]^{-1/3} \right\}^{1/2}. \tag{5.299}$$

Whether the maximum of ϵ_1 at this point is larger or smaller than 1 depends on α and β and is again similar to what has already been discussed before. The region in the parameter space where inflation ends by slow-roll violation is displayed in Fig. 68 and corresponds to the points such that $\alpha < -|\alpha_{\mathrm{min}}|$. In this plot, the dotted line represents the curve $\alpha^2 = 4\beta$, above which one is sure that inflation ends by slow-roll violation since the minimum of the potential is negative in this case. For values of $\beta \ll 1$, one can see that $|\alpha_{\mathrm{min}}| \simeq 2\sqrt{\beta}$ and the allowed region becomes negligible.

Finally the case SSBI6 remains to be treated. The behavior of the slow roll parameters depend on α^2/β in the same way as before. If $\alpha^2/\beta \geq 4$, the minimum of the potential at $x = \sqrt{-\alpha/(2\beta)}$ is negative. The potential vanishes at $x_{V=0}^{\mathrm{SSBI6}}$ and the slow-roll parameters continuously decrease from this value (where they blow up) and go to zero at infinity. The value of $x_{V=0}^{\mathrm{SSBI6}}$ can be expressed as

$$x_{V=0}^{\mathrm{SSBI6}} = \sqrt{\frac{-\alpha+\sqrt{\alpha^2-4\beta}}{2\beta}}. \tag{5.300}$$

On the other hand, if $\alpha^2/\beta \leq 4$, ϵ_1 vanishes at $x = \sqrt{-\alpha/(2\beta)}$, reaches a maximum at $x_{\epsilon_2=0}^{\mathrm{SSBI6}}$ and then decreases. At infinity, it goes to zero. The value of $x_{\epsilon_2=0}^{\mathrm{SSBI6}}$ is given by

$$x_{\epsilon_2=0}^{\mathrm{SSBI6}} = x_{\epsilon_2=0}^{\mathrm{SSBI3}} = x_{\epsilon_2=0}^{\mathrm{SSBI1}}. \tag{5.301}$$

Whether the maximum of ϵ_1 at this point is larger or smaller than 1 depends on α and β. The corresponding region in the parameter space is displayed in Fig. 68 and corresponds to the inequality $\alpha < -|\alpha_{\mathrm{min}}|$. The dotted line represents the law $\alpha^2 = 4\beta$. Above this line, one is sure that inflation can stop by slow-roll violation since, in this case, the potential becomes negative at some point. It is also interesting to notice that, when $\beta \gtrsim 1.48$, the maximum value of ϵ_1 is larger than 1 for any value of α. On the other hand, if $\beta \ll 1$, the allowed region shrinks to zero.

Let us now turn to the slow-roll trajectory. This one can be integrated analytically to get

$$N_{\rm end} - N = -\frac{1}{2\alpha}\ln\left(\frac{x_{\rm end}}{x}\right) - \frac{x_{\rm end}^2 - x^2}{8} - \frac{\alpha^2 - 4\beta}{16\alpha\beta}\ln\left(\frac{1+\frac{2\beta}{\alpha}x_{\rm end}^2}{1+\frac{2\beta}{\alpha}x^2}\right), \tag{5.302}$$

where $N_{\rm end}$ is the number of e-folds at the end of inflation. It is important to notice that the argument of the logarithm is always positive. This trajectory cannot be inverted analytically. But, numerically, it is easy to use this expression in order to determine x_*, the value of x at Hubble radius crossing.

Finally, it is interesting to constrain the value of the scale M with the CMB normalization. It follows that

$$\left(\frac{M}{M_{\rm Pl}}\right)^4 = \frac{2880\left(\alpha x_* + 2\beta x_*^3\right)^2\pi^2}{\left(1+\alpha x_*^2+\beta x_*^4\right)^3}\frac{Q_{\rm rms-PS}^2}{T^2}. \tag{5.303}$$

We are now in a position where we can discuss the predictions of the six versions of this model. The reheating consistent slow-roll predictions for the SSBI1 models are displayed in Figs. 142, 143 and 144 for $\beta = 10^{-3}$, $\beta = 10^{-1}$ and $\beta = 10$, respectively. SSBI1 seems to be disfavored by the observations. The predictions of SSBI2 models are displayed in Fig. 145 for different values of β and α. We notice that they depend on the parameter α quite strongly. The spectral index is clearly red and, for values of β of order one, the contribution of gravity waves becomes very small. For SSBI3, the predictions are presented in Figs. 146, 147 and 148 for $\beta = -10^{-3}$, $\beta = -5\times10^{-3}$ and $\beta = -10^{-2}$, respectively. As we increase β, the points start spreading in the plane $(n_{\rm S}, r)$. For this class of models, the spectrum is red and the level of gravity waves quite important. The predictions for the SSBI4 models are displayed in Figs. 149, 150, and 151 for $\beta = -10^{-5}$, $\beta = -10^{-4}$, $\beta = -10^{-3}$, respectively. One can notice that the typical predicted values for ϵ_1 decrease with the absolute value of β. As before the spread of the points increases with β. The tilt is still red and the contribution of gravity waves is small for small values of α. The predictions for the SSBI5 models are displayed in Figs. 152, 153 and 154 for $\beta = 10^{-6}$, $\beta = 10^{-5}$ and $\beta = 10^{-4}$, respectively. Once again, for $\mathcal{O}(1)$ values of β, one can see that the model predict a small amount of gravitational waves but has a deviation from scale invariance strongly disfavored by the observational constraints. Finally, the reheating consistent slow-roll predictions for the SSBI6 models are displayed in Figs. 155, 156 and 157 for $\beta = 10^{-6}$, $\beta = 10^{-1}$ and $\beta = 1$, respectively. When $\beta \ll 1$ the predictions of the model do not depend on β. Moreover, for values of β of order one, the predictions become almost independent of the two parameters of the model.

5.18 Inverse Monomial Inflation (IMI)

These models are characterized by the inverse monomial potential given by

$$V(\phi) = M^4\left(\frac{\phi}{M_{\rm Pl}}\right)^{-p}, \tag{5.304}$$

where p is a positive number. This scenario has been studied in many different situations: in Refs. [281, 528, 529] it was considered in the context of quintessential inflation, in Refs. [530–533] in the context of tachyon inflation, in Refs. [459, 461] in the context of intermediate

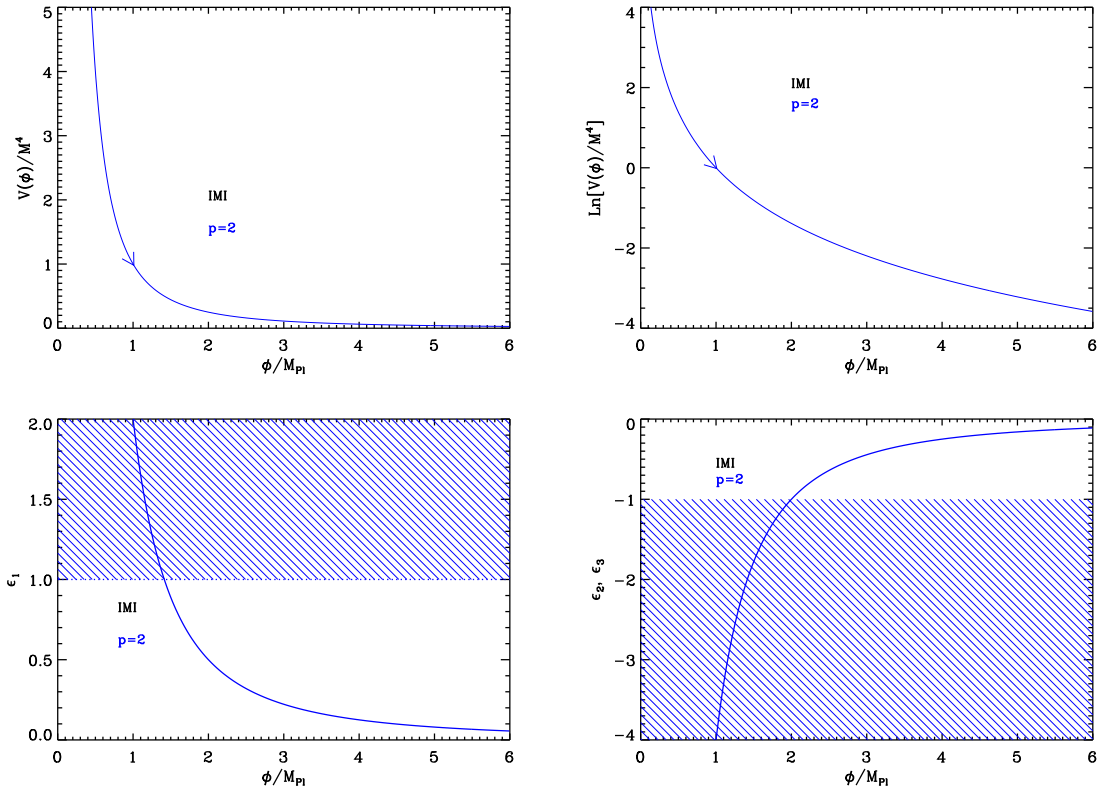

Figure 69. Top left panel: Inverse Monomial Inflation (IMI) potential for $p = 2$. Top right panel: logarithm of the potential for the same value of p. Bottom left panel: slow-roll parameter ϵ_1 for $p = 2$. Bottom right panel: slow-roll parameters ϵ_2 and ϵ_3 for $p = 2$. Only one line appears because $\epsilon_2 = \epsilon_3$. On these plots, the shaded region represents the region where the slow-roll approximation breaks down.

inflation and in Ref. [293] in the context of Randall-Sundrum braneworld models. In all these articles, the potential was just postulated. An attempt to derive this potential from high energy considerations was made in Refs. [534, 535] in the context of supersymmetric QCD. Let us, however, notice that this was done in order to build a model of quintessence and not of inflation. The model uses the group $\mathrm{SU}(N_\mathrm{c})$ and has N_f flavors. The quarks Q^i, $i = 1, \cdots, N_\mathrm{f}$ are placed in the fundamental representation of $\mathrm{SU}(N_\mathrm{c})$ and the anti-quarks $Q_i^\dagger$ in the conjugate representation [534]. At scales below the gauge breaking scale Λ, the relevant degrees of freedom are the pions $\pi_j^i = Q^i Q_j^\dagger$ and one can show that the corresponding superpotential is given by [536, 537]

$$W = (N_\mathrm{c} - N_\mathrm{f}) \frac{\Lambda^{3(N_\mathrm{c}-N_\mathrm{f})/(N_\mathrm{c}-N_\mathrm{f})}}{(\det \pi)^{1/(N_\mathrm{c}-N_\mathrm{f})}} \,. \tag{5.305}$$

The potential (5.304) then follows from the F-term associated to the above superpotential.

The potential is represented in Fig. 69 for $p = 2$. It is a decreasing function of the field *vev* and, hence, inflation proceeds from the left to the right, in the direction specified by the arrow in the figure.

The three Hubble flow functions are straightforwardly obtained from Eqs. (2.4), (2.5) and (2.6). Defining $x \equiv \phi/M_{\rm Pl}$, one gets

$$\epsilon_1 = \frac{p^2}{2x^2}\,, \qquad \epsilon_2 = -\frac{2p}{x^2}\,, \qquad \epsilon_3 = \epsilon_2. \tag{5.306}$$

These functions are represented in the two bottom panels in Fig. 69. The first slow-roll parameter is a monotonic decreasing function of ϕ while ϵ_2 and ϵ_3 are negative increasing functions. From these expressions, one can also immediately deduce that, for a given p, the model in the plane (ϵ_1, ϵ_2) is represented by the line $\epsilon_1 = -(p/4)\epsilon_2$. Since inflation proceeds from the left to the right, it cannot stop by slow-roll violation. As a consequence, an extra-mechanism, such as e.g. tachyonic instability, must be implemented to end inflation. Let us denote $x_{\rm end}$ the position at which such a process occurs. The model has therefore two free parameters: p and $x_{\rm end}$.

The slow-roll trajectory can be obtained by quadrature from Eq. (2.11), and one obtains

$$N - N_{\rm end} = \frac{1}{2p}\left(x^2 - x_{\rm end}^2\right). \tag{5.307}$$

This expression can be inverted and reads

$$x = \sqrt{x_{\rm end}^2 + 2p\left(N - N_{\rm end}\right)}\,. \tag{5.308}$$

Let us now derive some prior condition on $x_{\rm end}$. One can notice that when $x < x_{\epsilon_1=1} = p/\sqrt{2}$, one has $\epsilon_1 > 1$ and inflation cannot take place. This means that inflation can only proceed between $x_{\epsilon_1=1}$ and $x_{\rm end}$, where the maximum number of e-folds is, using Eq. (5.307), $\Delta N_{\rm max}\left(x_{\rm end}\right) = \left(x_{\rm end}^2 - x_{\epsilon_1=1}^2\right)/(2p)$. Put it differently, if one wants to realize at least ΔN e-folds, then one has to work with $x_{\rm end} > x_{\rm end}^{\rm min}$ where

$$x_{\rm end}^{\rm min}\left(\Delta N\right) = \sqrt{p^2/2 + 2p\Delta N}\,. \tag{5.309}$$

This defines a prior condition on $x_{\rm end}$.

Finally, the parameter M can be determined from the amplitude of the CMB anisotropies, and it follows that

$$\left(\frac{M}{M_{\rm Pl}}\right)^4 = 720\pi^2 p^2 x_*^{p-2}\frac{Q_{\rm rms-PS}^2}{T^2}\,. \tag{5.310}$$

The reheating consistent slow-roll predictions for the IMI models are displayed in Fig. 158. For a given value of p, they lie along the line $(1-2/p)\,r = 8\,(1-n_{\rm S})$, i.e. $\epsilon_1 = -(p/4)\epsilon_2$. As expected, large values of $x_{\rm end}$, or small values of the reheating temperature (these two parameters being degenerate), are preferred.

5.19 Brane Inflation (BI)

5.19.1 Theoretical Justifications

This section is devoted to brane inflation, a class of models widely discussed in the literature [151, 337, 353, 387, 538–541, 541–551]. The idea is that inflation is caused by branes moving in the extra dimensions as it was already the case in TI, see section 5.9. For this reason, the setup is very similar to the one considered in that section. One starts from type IIB superstring theory where six dimensions are compactified. The effective, low energy,

description of the model contains various fields among which are the dilaton, the axion and the (tensorial) gravitational field. One also has anti-symmetric fields with their corresponding field strength. The compact dimensions form a Calabi-Yau space and, generically, this Calabi-Yau space is made of a bulk plus throats attached to it. Along a given throat, a solution for the ten-dimensional metric is given by the conifold already discussed in section 5.9 whose metric is given in Eq. (5.142). In this equation, the metric $\mathrm{d}s_5^2$ lives on the five-dimensional section Σ_5 and r is the "radial" coordinate. In the following, we will denote by r_{UV} the radial coordinate at which the cone is glued to the bulk and r_0 the coordinate at the tip of the cone. The volume of the cone section is denoted by $\mathrm{Vol}(\Sigma_5)$ and will be measured in terms of the volume of the five-dimensional sphere, namely

$$v \equiv \frac{\mathrm{Vol}(\Sigma_5)}{\mathrm{Vol}(S_5)}\,. \tag{5.311}$$

The geometry of the section Σ_5 depends on the background fluxes, denoted by $\mathcal{M}$ and $\mathcal{K}$, that are quantities related to the values of the anti-symmetric fields. If these fluxes vanish then the five-dimensional sections are simply given by $S_2 \times S_3$. In that case, the conifold can be written as $\sum_{i=1}^{4} w_i^2 = 0$ where w_i are four complex coordinates, see also section 5.9. Moreover, an exact expression for the warp function $h(r)$ can be found and reads

$$h(r) = C_2 + \frac{C_1}{r^4}\,, \tag{5.312}$$

C_1 and C_2 being constants. On the other hand, if the fluxes are turned on, then the background geometry responses accordingly and, as a consequence, the geometry of the cone is modified. It is now given by a "deformed conifold", $\sum_{i=1}^{4} w_i^2 = z$, where z is a number which depends on $\mathcal{M}$ and $\mathcal{K}$. The warp function acquires a more complicated form and, obviously, becomes z-dependent, i.e. $h(r,z)$. The explicit form of this warp function is not needed here but it is interesting to notice that, far from the tip, one has $h(r,z) \simeq h(r)$. In other words, the modification of the extra-dimensional geometry due to the fluxes is significant only in the vicinity of the tip. Notice that, provided the depth of the throat is comparable to its width, the radial coordinate r_{UV} can be expressed in terms of the quantity $\mathcal{N} \equiv \mathcal{M}\mathcal{K}$. One obtains [552]

$$r_{\mathrm{UV}}^4 = 4\pi g_{\mathrm{s}} \alpha'^2 \frac{\mathcal{N}}{v}, \tag{5.313}$$

where g_{s} is the string coupling and $\alpha' \equiv \ell_{\mathrm{s}}^2$, ℓ_{s} being the string length.

Finally, an anti-$D3$ brane is placed at the tip of the conifold, i.e. at the bottom of the throat. This brane is heavy and is supposed to slightly disturb the geometry of the throat in a way that has been calculated for instance in Refs. [151, 550, 553]. Then, in this geometry, one studies the motion of a light $D3$ brane with tension

$$T_3 = \frac{1}{(2\pi)^3 g_{\mathrm{s}} \alpha'^2}\,. \tag{5.314}$$

This brane is attracted by the anti-$D3$ brane and as a consequence moves radially along the throat. In principle it possesses a DBI kinetic term but one can show that, in the regime considered here, it always reduces to an ordinary, minimal, kinetic term, see Ref. [151]. If r represents the distance between the two branes, then the effective Lagrangian of the system can be expressed as

$$\mathcal{L} = -\frac{1}{2}\left(\frac{\partial\phi}{\partial t}\right)^2 - \frac{2T_3 r_0^4}{r_{\mathrm{UV}}^4}\left(1 - \frac{r_0^4 T_3^2}{\mathcal{N}}\frac{1}{\phi^4}\right), \tag{5.315}$$

where $\phi \equiv \sqrt{T_3} r$. The shape of the potential is now completely fixed and the behavior $\propto \phi^{-4}$ is of course due to the particular scaling $\propto r^{-4}$ of the warp function given by Eq. (5.312).

In order to be valid, the effective model described above must satisfy some conditions that we now discuss in more detail. Defining $\phi_0 \equiv \sqrt{T_3} r_0$ and $\phi_{\rm UV} \equiv \sqrt{T_3} r_{\rm UV}$, it is clear that the presence of the brane in the throat implies that $\phi_0 < \phi < \phi_{\rm UV}$. In addition, as discussed for instance in Ref. [151], from the trivial fact that the volume of the throat, $V_6^{\rm throat} = 2\pi^4 g_{\rm s} \mathcal{N} \alpha'^2 r_{\rm UV}^2$, cannot be bigger than the volume of the total Calabi-Yau manifold $V_6^{\rm tot}$, one can derive the bound

$$\phi_{\rm UV} < \frac{m_{\rm Pl}}{\sqrt{2\pi\mathcal{N}}}\,, \tag{5.316}$$

where the Planck mass can be expressed as $m_{\rm Pl}^2 = 8\pi V_6^{\rm tot}/\kappa_{10}$ and $\kappa_{10} = (2\pi)^7 g_{\rm s}^2 \alpha'^4/2$. Another constraint comes from the fact that the effective model is valid only if the proper distance between the two branes is larger than the Planck length. One can show, see Ref. [151], that this means $r > r_{\rm stg}$ where

$$r_{\rm stg} \equiv r_0 e^{\sqrt{\alpha'}/r_{\rm UV}}. \tag{5.317}$$

In particular, as will be seen in the following, the value of $r_{\rm stg}$ plays an important role regarding the mechanism ending inflation. In the next section, we carry out the slow-roll analysis of this model.

Let us also mention that the same potential arises in the context of tachyon inflation [554, 555], in the context of SQCD inflation [556] and in the context of the strong coupling limit of twisted models of SQCD inflation, (see TWI, section 5.5 and Ref. [472]). It is also worth noticing that the same kind of inverse power law potential is sometimes used in quintessence models [281, 528, 529].

5.19.2 Slow-Roll Analysis

We now turn to the slow-roll analysis of BI. For this purpose, it is more convenient to re-write the potential appearing in Eq. (5.315) in the following way

$$V(\phi) = M^4 \left[1 - \left(\frac{\phi}{\mu}\right)^{-p}\right], \tag{5.318}$$

where μ and p are free parameters. Compared to Eq. (5.315), we have generalized by hand the expression of $V(\phi)$ by considering an arbitrary p. In such a way, this potential can be viewed as a generalization of the small field models to negative values of p (see section 5.1). In the following, we will also consider the non-approximated KKLT potential

$$V(\phi) = \frac{M^4}{1 + \left(\frac{\phi}{\mu}\right)^{-p}}\,, \tag{5.319}$$

from which (5.318) is the $\mu \ll M_{\rm Pl}$ limit.

In the context of the brane inflationary scenario, the value $p = 4$ is special in the sense that, as explained above, it corresponds to the motion of a test $D3$ brane in a warped throat and is, therefore, a case of physical interest. Let us notice that the parameters of the potential are related to their stringy counterparts by

$$M^4 = \frac{2T_3 r_0^4}{r_{\rm UV}^4} = \frac{4\pi^2 v}{\mathcal{N}} \phi_0^4, \qquad \mu^4 = \frac{T_3^2 r_0^4}{\mathcal{N}} = \frac{M^4}{4\pi^2 v}\,. \tag{5.320}$$

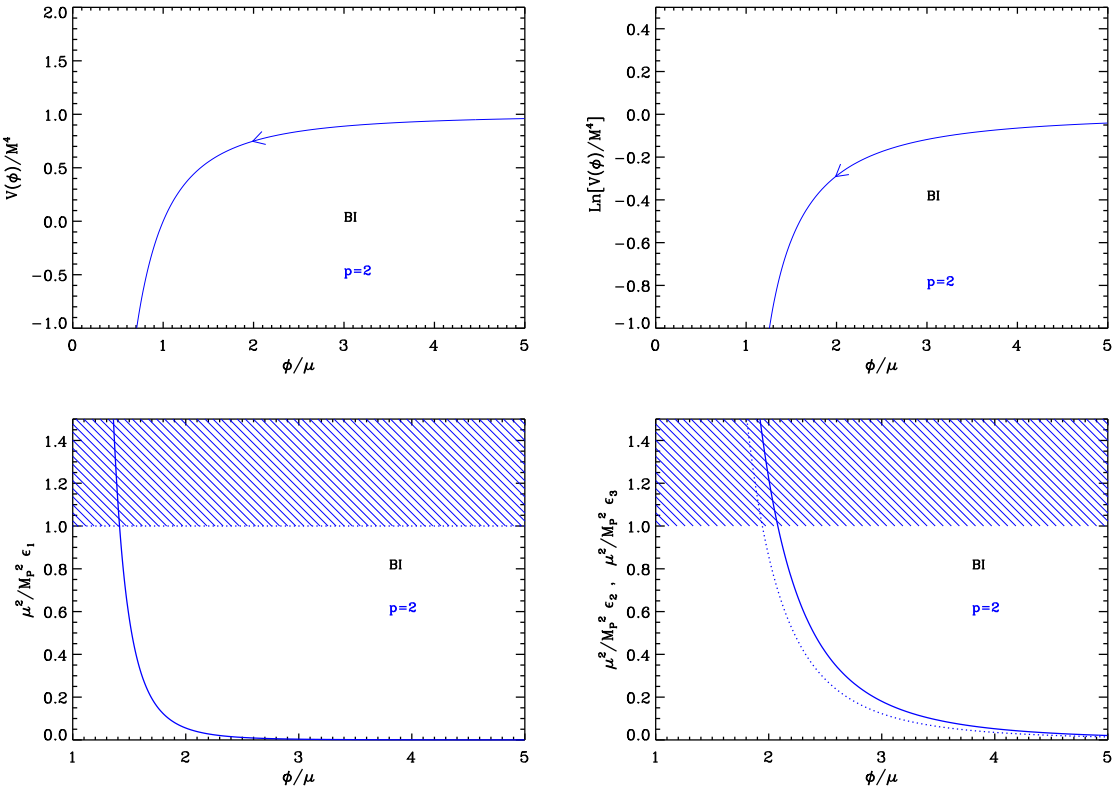

Figure 70. Brane Inflation (BI) for $p = 2$. Upper panels: the potential and its logarithm as a function of ϕ/μ. Bottom left panel: slow-roll parameter ϵ_1 rescaled by $M_{\rm Pl}^2/\mu^2$. The shaded area indicates the region in which inflation cannot occur for $\mu = M_{\rm Pl}$. Bottom right panel: slow-roll parameters ϵ_2 (solid line) and ϵ_3 (dotted line), rescaled by $M_{\rm Pl}^2/\mu^2$.

Moreover, brane inflation proceeds under the condition $\mu/M_{\rm Pl} \ll 1$. Indeed, using the formulas established in the previous subsection, it is easy to show that

$$\frac{\mu^4}{M_{\rm Pl}^4} = \frac{1}{\mathcal{N}}\left(\frac{\phi_0}{M_{\rm Pl}}\right)^4 < \frac{1}{\mathcal{N}}\left(\frac{\phi_{\rm UV}}{M_{\rm Pl}}\right)^4 < \frac{16}{\mathcal{N}^3} \ll 1, \tag{5.321}$$

where we have used the condition $\phi_0 < \phi_{\rm UV}$ and Eq. (5.316). Finally, let us stress that the brane motion in the throat ends by a tachyonic instabilities at $\phi = \phi_{\rm stg}$. As we discuss below, the observable predictions of the model crucially depends on whether the universe is still inflating at $\phi \gtrsim \phi_{\rm stg}$, or not. Therefore, in the context of string theory, we necessarily have $\mu/M_{\rm Pl} \ll 1$, $p = 4$ and an additional model parameter $\phi_{\rm stg}$.

In the following, we will first consider arbitrary values for μ and p viewing Eq. (5.318) as a phenomenological potential in which $\phi_{\rm stg}$ has no meaning, and then, the discussion will be focused on the stringy scenario. BI is another proto-typical case exemplifying how two models having exactly the same potential can lead to different observable predictions. Here this will be due to the mechanism ending inflation.

The potential (5.318), as well as its logarithm, are displayed in Fig. 70. It is an increasing function of the field, hence inflation proceeds from the right to the left. It vanishes for $\phi/\mu = 1$

and, hence, it should be studied in the $\phi/\mu > 1$ region only. Let us calculate the slow-roll parameters. Defining the quantity x by the following expression

$$x \equiv \frac{\phi}{\mu}\,, \tag{5.322}$$

one can express the first three Hubble flow functions in the slow-roll approximation as

$$\epsilon_1 = \left(\frac{M_{\rm Pl}}{\mu}\right)^2 \frac{p^2}{2x^2\left(1-x^p\right)^2}\,, \qquad \epsilon_2 = 2p\left(\frac{M_{\rm Pl}}{\mu}\right)^2 \frac{(1+p)\,x^p - 1}{x^2\left(1-x^p\right)^2}\,, \tag{5.323}$$

and

$$\epsilon_3 = p\left(\frac{M_{\rm Pl}}{\mu}\right)^2 \frac{2 + (p-4)\,(p+1)\,x^p + (1+p)\,(2+p)\,x^{2p}}{x^2\left(1-x^p\right)^2\left[(1+p)\,x^p - 1\right]}\,. \tag{5.324}$$

These functions are displayed in Fig. 70. They become very small at large fields $x \gg 1$, and diverge when the potential vanishes at $x \to 1$. Therefore inflation can naturally end with slow-roll violation at a field value $x_{\rm end}$, solution of $\epsilon_1(x_{\rm end}) = 1$, i.e., verifying

$$x_{\rm end}^{p+1} - x_{\rm end} = \frac{p}{\sqrt{2}}\frac{M_{\rm Pl}}{\mu}\,. \tag{5.325}$$

Unless p takes integer values, this equation has to be solved numerically (see also section 5.1).

However, in the limits $\mu/M_{\rm Pl} \ll 1$ and $\mu/M_{\rm Pl} \gg 1$ we can find an approximate expression for $x_{\rm end}$. Solving perturbatively the equation $\epsilon_1 = 1$, one obtains

$$x_{\rm end} \underset{\mu\ll M_{\rm Pl}}{\simeq} \left(\frac{pM_{\rm Pl}}{\sqrt{2}\mu}\right)^{\frac{1}{p+1}} + \frac{1}{p+1}\left(\frac{pM_{\rm Pl}}{\sqrt{2}\mu}\right)^{\frac{1-p}{1+p}}\,, \qquad x_{\rm end} \underset{\mu\gg M_{\rm Pl}}{\simeq} 1 + \frac{1}{\sqrt{2}}\frac{M_{\rm Pl}}{\mu} - \frac{p+1}{4}\frac{M_{\rm Pl}^2}{\mu^2}\,. \tag{5.326}$$

It is also interesting to find the solution of $\epsilon_2 = 1$. As before, this cannot be done exactly but, perturbatively, one obtains

$$x_{\epsilon_2=1} \underset{\mu\ll M_{\rm Pl}}{\simeq} \left[2p(1+p)\left(\frac{M_{\rm Pl}}{\mu}\right)^2\right]^{\frac{1}{p+2}}\,, \qquad x_{\epsilon_2=1} \underset{\mu\gg M_{\rm Pl}}{\simeq} 1 + \sqrt{2}\frac{M_{\rm Pl}}{\mu}\,. \tag{5.327}$$

From the above expressions, we deduce that slow-roll violation always occurs before the end of inflation, that is to say ϵ_2 becomes unity before ϵ_1. This has not effect on the observable predictions since only a few e-folds of inflation are spent in this regime (see Fig. 70).

The slow-roll trajectory can be integrated explicitly from Eq. (2.11) and one obtains

$$N_{\rm end} - N = \frac{\mu^2}{2pM_{\rm Pl}^2}\left(x_{\rm end}^2 - \frac{2}{p+2}x_{\rm end}^{p+2} - x^2 + \frac{2}{p+2}x^{p+2}\right), \tag{5.328}$$

an expression which cannot be inverted in general. However, in the $\mu \ll M_{\rm Pl}$ and $\mu \gg M_{\rm Pl}$ limits, one has $x \gg 1$ and $x \simeq 1$ respectively and the previous equation can be approximately inverted leading to the following expressions

$$x_* \underset{\mu\ll M_{\rm Pl}}{\simeq} \left[p(p+2)\frac{M_{\rm Pl}^2}{\mu^2}\Delta N_* + x_{\rm end}^{p+2}\right]^{\frac{1}{p+2}}\,, \qquad x_* \underset{\mu\gg M_{\rm Pl}}{\simeq} 1 + \frac{M_{\rm Pl}}{\mu}\sqrt{\frac{1}{2} + 2\Delta N_*}\,, \tag{5.329}$$

where use has been made of Eq. (5.326). Also, making use of the full KKLT potential (5.319), the slow roll trajectory reads

$$N_{\rm end} - N = \frac{\mu^2}{2pM_{\rm Pl}^2}\left(-x_{\rm end}^2 - \frac{2}{p+2}x_{\rm end}^{p+2} + x^2 + \frac{2}{p+2}x^{p+2}\right), \tag{5.330}$$

which coincides with (5.328) in the limit $\mu \ll M_{\rm Pl}$.

The mass scale M is given by the CMB normalization and verifies

$$\left(\frac{M}{M_{\rm Pl}}\right)^4 = 720\pi^2 p^2 \left(\frac{M_{\rm Pl}}{\mu}\right)^2 \frac{x_*^{p-2}}{\left(x_*^p - 1\right)^3}\frac{Q_{\rm rms-PS}^2}{T^2}. \tag{5.331}$$

which can be further simplified in the appropriate limits using Eqs. (5.326) and (5.329).

The reheating consistent slow-roll predictions for the phenomenological models are displayed in Figs. 159, 160, 161 for $p = 2$, $p = 3$ and $p = 4$, respectively, and with $\mu/M_{\rm Pl} \in \left[10^{-3}, 10^3\right]$. The reheating equation of state parameter $\overline{w}_{\rm reh} = 0$ but since the shape of the potential is unknown at $x < 1$, this parameter is a priori unspecified and could take different values. For small values of μ, we see that $n_{\rm S} \simeq 0.96$ and $r \ll 1$. In the opposite case, $\mu \gg M_{\rm Pl}$, the model predictions lie around $\epsilon_2 \simeq 4\epsilon_1$ with $n_{\rm S} \simeq 0.97$ and $r \simeq 0.08$. These behaviors can be recovered by plugging the approximated expressions given in Eqs. (5.326) and (5.329) into the Hubble flow functions. For $\mu \ll M_{\rm Pl}$, one obtains

$$\epsilon_{1*} \simeq \frac{p^2}{2}\left[p\left(p+2\right)\Delta N_*\right]^{-\frac{2p+2}{p+2}}\left(\frac{\mu}{M_{\rm Pl}}\right)^{\frac{2p}{p+2}}, \qquad \epsilon_{2*} \simeq \frac{2}{\Delta N_*}\frac{p+1}{p+2}, \qquad \epsilon_{3*} \simeq \frac{1}{\Delta N_*}, \tag{5.332}$$

and the spectral index is of the order $n_{\rm S} \simeq 1 - 2/\Delta N_*(p+1)/(p+2) \sim 0.96$ with $r \ll 1$. Similarly, for $\mu \gg M_{\rm Pl}$ limit, the Hubble flow parameters at Hubble crossing behave as

$$\epsilon_{1*} \simeq \frac{1}{4\Delta N_*}, \qquad \epsilon_{2*} \simeq \frac{1}{\Delta N_*}, \qquad \epsilon_{3*} \simeq \frac{1}{\Delta N_*}. \tag{5.333}$$

Therefore, the predicted level of gravity waves is now of the order $r \simeq 4/\Delta N_* \simeq 0.08$ and the spectral index is $n_{\rm S} \simeq 1 - 3/(2\Delta N_*) \simeq 0.97$, which is again in agreement with the numerical results.

Finally, the predictions for the KKLTI models, i.e. using the full potential (5.319), are displayed in Figs. 163, 164, 165 for the same parameters. One can see that they deviate from the ones of brane inflation only when $\mu \gg M_{\rm Pl}$.

5.19.3 Slow-Roll Analysis of the Stringy Scenario

In the case where the model is interpreted as a stringy scenario, with $p = 4$, we have seen before that the low energy description is valid provided $r > r_{\rm stg}$, or $x > x_{\rm stg}$ with

$$x_{\rm stg} \equiv \frac{\sqrt{T_3}\, r_{\rm stg}}{\mu} = \mathcal{N}^{1/4}\exp\left[\left(4\pi g_{\rm s}\frac{\mathcal{N}}{v}\right)^{-1/4}\right]. \tag{5.334}$$

If slow-roll violation occurs before the system reaches $x_{\rm stg}$, then the effective string description is always valid and the observable predictions will be exactly the same as those derived in the previous paragraph (for $p = 4$ and $\mu \ll M_{\rm Pl}$). However, if, on the contrary, slow-roll violation occurs after the field crosses the value $x_{\rm stg}$, then inflation stops by instability at

$x_{\rm stg}$ instead of the naively expected $x_{\rm end}$. Indeed, in this case, a tachyon appears and triggers the process of branes annihilation. Therefore, the mechanism ending inflation in this model depends on whether slow-roll violation occurs in a regime where the distance between the branes is larger or smaller than the string length. And this question depends on the value of the parameters characterizing BI. One can determine the two regimes by evaluating the ratio

$$\frac{x_{\epsilon_2=1}}{x_{\rm stg}} = 40^{1/6}\left(\frac{M}{M_{\rm Pl}}\right)^{-1/3}\mathcal{N}^{-1/4}(4\pi^2 v)^{1/12}\exp\left[-\left(4\pi g_{\rm s}\frac{\mathcal{N}}{v}\right)^{-1/4}\right], \tag{5.335}$$

in which we have used Eqs. (5.320), (5.327) and (5.334) (with $p = 4$ and $\mu \ll M_{\rm Pl}$). If this ratio is larger than one, inflation stops by slow-roll violation and if it is smaller than one by instability. The complicated part of the analysis lies in the fact that the above equation depends on the mass scale M. In order to have an explicit expression of M in terms of the parameters of the model, one must first CMB normalize the model which, in turn, requires the knowledge of the mechanism ending inflation. However, we are interested in calculating the frontier where $x_{\epsilon_2=1} = x_{\rm stg}$ and, therefore, the two possible mechanisms for stopping inflation coincide in that case. Replacing $x_{\rm end}$ by $x_{\rm stg} = x_{\epsilon_2=1}$ in Eq. (5.329) yields

$$x_*^{\rm f} \simeq \left[24\frac{M_{\rm Pl}^2}{\mu^2}\left(\Delta N_* + \frac{5}{3}\right)\right]^{1/6}, \tag{5.336}$$

from which one can obtain an explicit formula for the first slow-roll coefficient (5.323) at Hubble radius crossing

$$\epsilon_{1*}^{\rm f} \simeq 8\left[24\left(\Delta N_* + \frac{5}{3}\right)\right]^{-5/3}\left(\frac{\mu}{M_{\rm Pl}}\right)^{4/3}. \tag{5.337}$$

Comparing this expression to Eq. (5.332), we see that there is a very small shift by 5/3 in ΔN_*. It accounts for the difference of e-folds between the time at which slow-roll violations occur, i.e. for $x = x_{\epsilon_2=1}$, and the end of inflation at $x_{\rm end}$. As argued before, we see that these effects are too small to be observable and completely degenerated with the reheating duration. Plugging this expression into the CMB normalization, and using the relation $M^4 = 4\pi^2 v\mu^4$, one arrives at the following expression for M

$$\frac{M}{M_{\rm Pl}} = C(4\pi^2 v)^{-1/8}\left(\Delta N_* + \frac{5}{3}\right)^{-5/8}, \tag{5.338}$$

where we have defined

$$C \equiv 3^{-5/8}(8\pi^2 Q_*)^{3/8}, \qquad Q_* \equiv 45\frac{Q_{\rm rms-PS}^2}{T^2} = 2700P_*. \tag{5.339}$$

We can now insert this expression of M in Eq. (5.335) to get the equation defining the frontier in the string parameter space, namely

$$\left.\frac{x_{\epsilon_2=1}}{x_{\rm stg}}\right|_{\rm f} = 1 = \left(\frac{40}{C^2}\right)^{1/6}\left(\Delta N_* + \frac{5}{3}\right)^{5/24}(4\pi^2 v)^{1/8}\mathcal{N}^{-1/4}\exp\left[-\left(4\pi g_{\rm s}\frac{\mathcal{N}}{v}\right)^{-1/4}\right]. \tag{5.340}$$

Following Ref. [151], if one defines the two following rescaled stringy parameters

$$y \equiv 4\pi g_{\rm s}\frac{\mathcal{N}}{v}, \qquad \bar{v} \equiv \frac{v}{(4\pi g_{\rm s})^2}, \tag{5.341}$$

then the frontier (5.340) is defined by the following "universal" form

$$y^{1/4}e^{y^{-1/4}}\bar{v}^{1/8} - \left(\frac{40}{C^2}\right)^{1/6}\left(\Delta N_* + \frac{5}{3}\right)^{5/24}\left(4\pi^2\right)^{1/8} = 0, \tag{5.342}$$

which is independent of the string coupling $g_{\rm s}$. As represented in Fig. 71, in the plane $(y,\bar{v})$, this relation is a curve that separates the region where inflation stops by slow-roll violation (below the curve) and the region where inflation stops by instability due to brane annihilation (above the curve).

The requirement of having the throat contained within the Calabi-Yau manifold can equally be written in terms of the universal variables. From Eqs. (5.316) and (5.341), one gets

$$y^{3/2}\bar{v} < 8\pi^2 M_{\rm Pl}^2\ell_{\rm s}^2, \tag{5.343}$$

which therefore depends on the string length $\ell_{\rm s} = \sqrt{\alpha'}$ but not on the string coupling $g_{\rm s}$.

Finally, the last theoretical prior comes from requiring that the brane motion remains located inside the throat, i.e. $x < x_{\rm UV}$ with

$$x_{\rm UV} \equiv \frac{\sqrt{T_3}r_{\rm UV}}{\mu} = \frac{M_{\rm Pl}}{M}\left(\frac{\mathcal{N}}{4\pi^3\alpha'^2 g_{\rm s}}\right)^{1/4}. \tag{5.344}$$

Since during inflation x decreases, this condition gives an upper limit on the admissible initial field values. However, the initial field values depends on the *total* number of e-folds of inflation, say $\Delta N_{\rm tot}$, and on the field value at which inflation ends, i.e. either $x_{\rm stg}$ or $x_{\epsilon_2=1}$ depending on if brane annihilation occurs before slow-roll violations.

Let us first assume that brane annihilation occurs well after the end of inflation, i.e. we are in lower part of the string parameter space $(y,\bar{v})$ separated by Eq. (5.342). For the relevant limit, $\mu \ll M_{\rm Pl}$, the initial field value is given by

$$x_{\rm ini}^{\epsilon_2} \simeq \left[24\frac{M_{\rm Pl}^2}{\mu^2}\left(\Delta N_{\rm tot} + \frac{5}{3}\right)\right]^{1/6}. \tag{5.345}$$

This expression involves μ and therefore M through Eq. (5.320). Again, one has to determine M using the CMB normalization and we are assuming that inflation ends at $x_{\epsilon_2=1}$, i.e. exactly Eq. (5.338). Plugging everything together and making use of the universal variables, one gets

$$y\bar{v} \underset{x_{\rm stg}<x_{\epsilon_2=1}}{>} C^{8/3}\pi^2 M_{\rm Pl}^2\ell_{\rm s}^4\left[24\left(\Delta N_{\rm tot} + \frac{5}{3}\right)\right]^{2/3}\left(\Delta N_* + \frac{5}{3}\right)^{-5/3}. \tag{5.346}$$

If inflation ends by brane annihilation at $x = x_{\rm stg}$, i.e. the string parameters $(y,\bar{v})$ lie above the curve given by Eq. (5.338), then $x_{\rm ini}$ and x_* are accordingly modified. For $\mu \ll M_{\rm Pl}$, their new expressions are however still given by Eq. (5.329), up to the replacement $x_{\rm end} \to x_{\rm stg}$, i.e.

$$x_{\rm ini}^{\rm stg} \simeq \left(24\frac{M_{\rm Pl}^2}{\mu^2}\Delta N_{\rm tot} + x_{\rm stg}^6\right)^{1/6}, \qquad x_*^{\rm stg} \simeq \left(24\frac{M_{\rm Pl}^2}{\mu^2}\Delta N_* + x_{\rm stg}^6\right)^{1/6}. \tag{5.347}$$

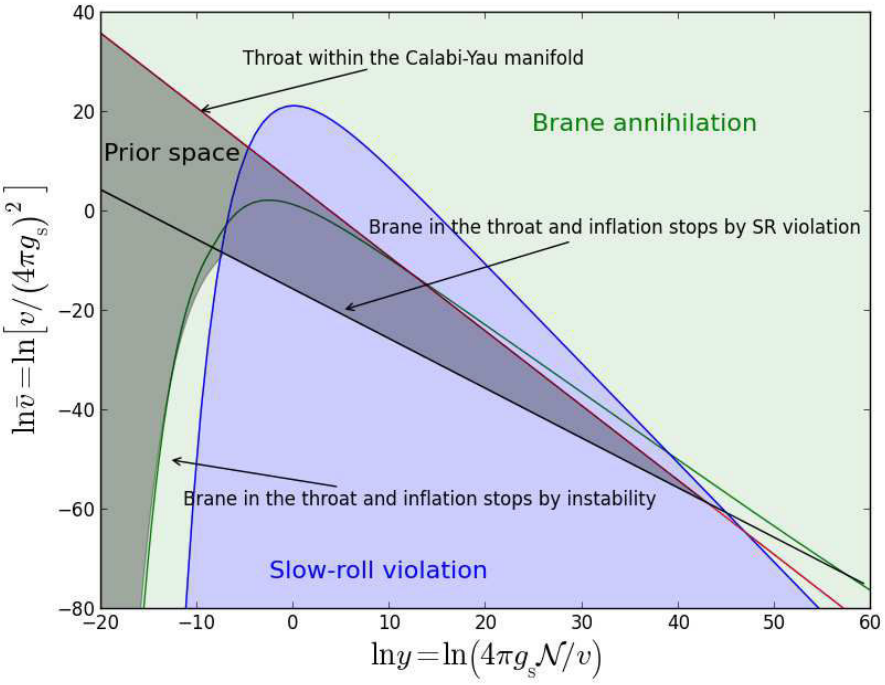

Figure 71. Theoretical prior space for the stringy scenario of brane inflation [151] in the plane of the "universal" coordinates $(y, \bar{v})$. The solid blue line is the frontier above which inflation ends by tachyonic pre-heating triggered by brane annihilation (light green region). Only in the region enclosed by this curve (light blue region), inflation ends by slow-roll violation. The upper thick red line is the volume bound of Eq. (5.343). The lower black straight line is the "UV" limit given by (5.346) and is relevant only if inflation stops by slow-roll violation. The solid green curve is given by (5.350) and also represents the "UV" limit but, this time, in the regime where inflation stops when the two branes collide. As a consequence, the admissible region is the one shaded in light black. We see that, even in this allowed region, inflation can either end by tachyonic instability or slow-roll violation depending on the string parameter values. In principle, the blue, black and green lines should cross at a single point. Due to the approximations used here, we see that this is true only approximately. In order to give a more faithful description of the allowed region, the light black area has been slightly deformed around the crossing point (see Ref. [151] for an exact determination of these frontiers).

As before, $x_{\rm ini}^{\rm stg}$ and $x_*^{\rm stg}$ depend on μ and therefore on M, which is determined by the CMB normalization. However, since inflation now ends by tachyonic instability this one has to be re-determined by plugging $x_*^{\rm stg}$ into Eq. (5.331). Doing so gives an implicit expression for M

$$\frac{M}{M_{\rm Pl}} \simeq C(4\pi^2 v)^{-1/8}\left(\Delta N_* + \frac{\mu^2}{M_{\rm Pl}^2}\frac{x_{\rm stg}^6}{24}\right)^{-5/8} = C(4\pi^2 v)^{-1/8}\left[\Delta N_* + \frac{5}{3}\left(\frac{x_{\rm stg}}{x_{\epsilon_2=1}}\right)^6\right]^{-5/8}, \tag{5.348}$$

where use has been made of Eq. (5.327), for $\mu \ll M_{\rm Pl}$. This equation cannot be analytically solved for M because μ, and $x_{\epsilon_2=1}$, depends on M. However, if brane annihilation occurs well before slow-roll violation, one has $x_{\rm stg} \gg x_{\epsilon_2=1}$ such that the term in ΔN_* can be neglected. In that situation, from $\mu^4 = M^4/(4\pi^2 v)$, one gets the approximate expression

$$\frac{M}{M_{\rm Pl}} \underset{x_{\rm stg}\gg x_{\epsilon_2=1}}{\simeq} 24^{5/18} C^{4/9} (4\pi^2 v)^{1/12} x_{\rm stg}^{-5/3}. \tag{5.349}$$

Requiring $x_{\rm ini}^{\rm stg} < x_{\rm UV}$ finally yields

$$y^{19/6}\bar{v}^{7/3}\exp\left(\frac{20}{3}y^{-1/4}\right) \underset{x_{\rm stg}\gg x_{\epsilon_2=1}}{>} \left(8\pi^2\ell_{\rm s}^2\right)^3 Q_* \left[y^{2/3}\bar{v}^{1/3}\exp\left(\frac{8}{3}y^{-1/4}\right) + \frac{6\Delta N_{\rm tot}}{Q_*^{1/3}}\right], \tag{5.350}$$

which completes the bounds coming from $x_{\rm UV}$.

Brane inflation within the string scenario has therefore a rather involved set of priors. In addition to have $p = 4$ and $\mu \ll M_{\rm Pl}$, the model parameters should simultaneously verify Eq. (5.343) and either Eq. (5.346), or Eq. (5.350), according to the sign of the left hand side of Eq. (5.342). All these equations involve the amplitude of the CMB anisotropies, which is well measured, the total number of e-folds $\Delta N_{\rm tot}$, which is an unknown quantity, and the number of e-folds ΔN_* before the end of inflation at which the pivot mode crossed the Hubble radius. As discussed in section 2.2, ΔN_* can only be obtained by solving Eq. (2.44), i.e. after having specified the reheating parameter. As the result, the reheating slow-roll predictions for the string scenario can only be sorted out numerically, paying attention that for a given reheating history, all of the previous theoretical constraints are satisfied. As an illustration, we have plotted in Fig. 71 the bounds for the typical values $\Delta N_* = 50$ and $\Delta N_{\rm tot} = 60$ with $\alpha' M_{\rm Pl}^2 \simeq 1/4$ [151, 557].

The reheating consistent slow-roll predictions for the string models are displayed in Figs. 162 for a set of realistic fundamental parameters. Also, making use of the full potential (5.319), the predictions of the corresponding KKLT inflation models are displayed in Figs. 166. One can check that they match perfectly.

6 Three parameters Models

6.1 Running-mass Inflation (RMI)

6.1.1 Theoretical Justifications

This model has been derived and studied in Refs. [338, 558–566]. Following Ref. [561], let us briefly discuss its physical origin. At tree level, a potential can always be expanded as $V(\phi) \simeq M^4 + m^2\phi^2/2 + \lambda\phi^4/4 + \cdots$. Since the potential must be flat to support inflation, quantum corrections may play an important role. Typically, they modify the potential with a term of the form $\left(c_1 + c_2\phi^2 + c_4\phi^4\right)\ln\left(\phi/\mu\right)$, where μ is the renormalization scale. In a non-supersymmetric framework, the quartic term dominates and one is led to models similar to RCMI, RCQI or CWI, see section 4.4, 4.5 and 4.11. On the other hand, in a supersymmetric context, at least if supersymmetry is spontaneously broken, the quadratic and the quartic terms cancel and one is left with a model similar to LI, see sections 4.12. If, however, supersymmetry is explicitly broken by the presence of soft terms, then the most important term will be the quadratic one.

Concretely, the above reasoning leads to a specific shape for the inflaton potential. We start from a flat direction in supersymmetry. Then, we assume that supersymmetry is explicitly broken and, as a consequence, that the potential receives corrections $\propto m^2\phi^2$, where m is a soft mass. Higher order terms are supposed to be negligible since we assume $\phi/M_{\rm Pl} \ll 1$. We thus have

$$V = V_0 + \frac{1}{2}m^2\phi^2 + \cdots, \tag{6.1}$$

The one loop corrections to this tree potential will typically induces a logarithmic dependence of the soft mass through the renormalization group equation

$$\frac{\mathrm{d}m^2}{\mathrm{d}\ln\phi} = \beta_{\mathrm{mat}}, \tag{6.2}$$

where β_{mat} is proportional to the inflaton couplings with the other fields present in the theory. Therefore, by Taylor expanding the solution of the previous equation aroused $\phi = \bar{\phi}$, we can write

$$m^2 = m^2(\bar{\phi}) + \beta_{\mathrm{mat}} \ln\left(\frac{\phi}{\bar{\phi}}\right) + \cdots . \tag{6.3}$$

As a consequence, the potential (6.1) can be re-expressed as

$$V(\phi) = V_0 + \frac{1}{2}m^2(\bar{\phi})\phi^2 + \frac{1}{2}\beta_{\mathrm{mat}}\phi^2 \ln\left(\frac{\phi}{\bar{\phi}}\right). \tag{6.4}$$

As noticed in Refs. [561, 564, 566], the beta function can typically be expressed as

$$\beta_{\mathrm{mat}} = \frac{-2C}{\pi}\alpha\tilde{m}^2 + \frac{D}{16\pi^2}|\lambda|^2 m^2_{\mathrm{loop}}, \tag{6.5}$$

if we assume that the inflaton interacts with gauge bosons and fermions. The quantity α is the coupling constant between ϕ and the gauge boson, λ is a Yukawa coefficient, $\tilde{m}$ is the gaugino mass, m the fermionic mass and C and D are dimensionless numbers of order one.

In the next section, we explore the cosmological consequences of this type of potential. In particular, we will see that it can lead to four different kind of inflationary scenarios.

6.1.2 Slow-Roll Analysis

We now perform the slow-roll analysis of the potential previously derived. In order to carry out this task, it is more convenient to re-write the potential as follows

$$V(\phi) = M^4\left[1 - \frac{c}{2}\left(-\frac{1}{2} + \ln\frac{\phi}{\phi_0}\right)\frac{\phi^2}{M_{\mathrm{Pl}}^2}\right], \tag{6.6}$$

where we have defined the two parameters c and ϕ_0 by

$$c = -\frac{M_{\mathrm{Pl}}^2\beta_{\mathrm{mat}}}{2V_0}, \quad m^2(\bar{\phi}) = -\beta_{\mathrm{mat}}\left[\frac{1}{2} + \ln\left(\frac{\phi_0}{\bar{\phi}}\right)\right]. \tag{6.7}$$

In this expression, M, c and ϕ_0 are free parameters. The dimensionless parameter c can be positive or negative. With the form of the beta function given in Eq. (6.5), the coefficient c is given by $\alpha m^2 M_{\mathrm{Pl}}^2/V_0$. If one assumes that the soft masses are of order $m \simeq H \simeq V_0^{1/2}/M_{\mathrm{Pl}}^2$, then $c \simeq \alpha \simeq 10^{-2}$ to 10^{-1} or may be smaller depending on the assumption on the couplings. This also mean that, in order for the expansion (6.3) to be valid, one has $|\ln(\phi/\phi_0)| \ll 1$. Also, the model is commonly worked out in the vacuum dominated regime (otherwise it is equivalent to a large field model, LFI, see section 4.2), which means that $c\phi_0^2/M_{\mathrm{Pl}}^2 \ll 1$. The location $\phi = \phi_0$ is an extremum of $V(\phi)$, a maximum if $c > 0$ and a minimum if $c < 0$. The potential and its logarithm are represented in Fig. 72.

Running mass inflation can be realized in four different ways [561], denoted as RMI1, RMI2, RMI3 and RMI4 in what follows. RMI1 corresponds to the case where $c > 0$ and

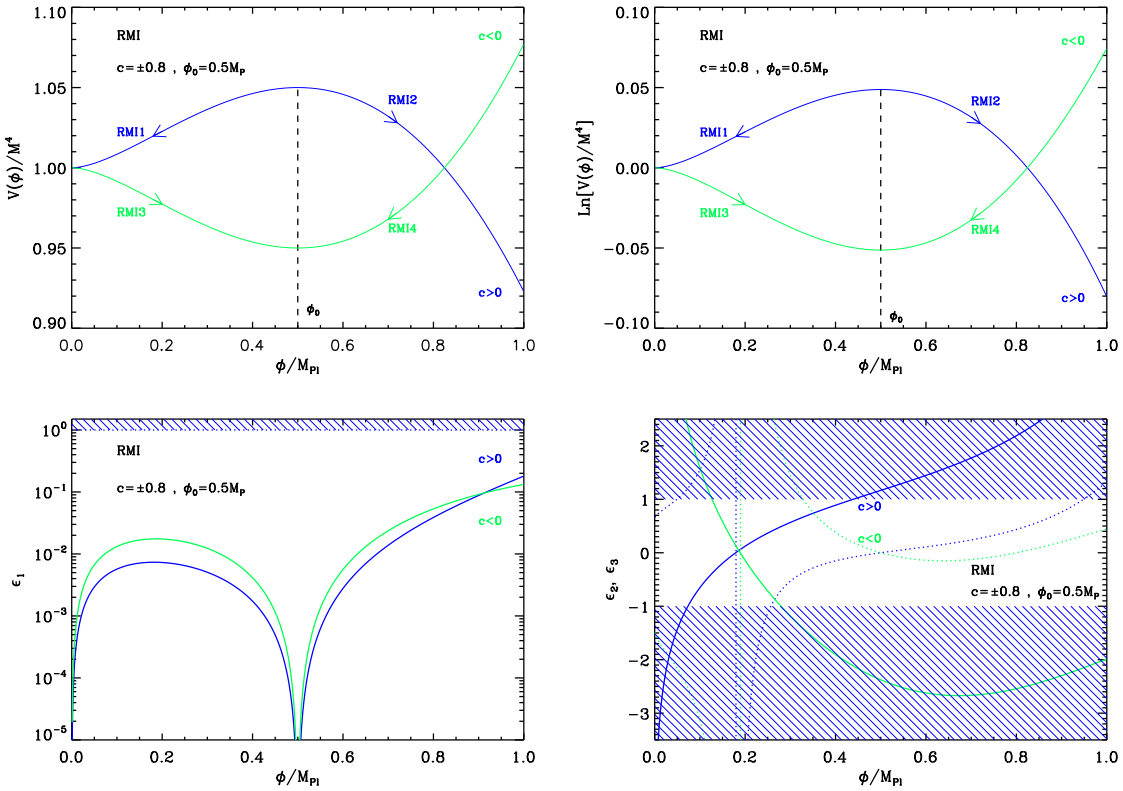

Figure 72. Top left panel: running mass potential for $c = 0.8$ (blue line) or $c = -0.8$ (green line) and $\phi_0 = 0.5 M_{\rm Pl}$. Top right panel: logarithm of the potentials for the same values of c and ϕ_0. Bottom left panel: slow-roll parameter ϵ_1 for a potential with $c = \pm 0.8$ and $\phi_0 = 0.5 M_{\rm Pl}$. Bottom right panel: slow-roll parameters ϵ_2 (solid line) and ϵ_3 (dotted line) for $c = \pm 0.8$ and $\phi_0 = 0.5 M_{\rm Pl}$. The value $c = \pm 0.8$ may not be physical and was chosen only in order to produce a clear plot.

$\phi < \phi_0$, see Fig. 72 (top panels). In this case, ϕ decreases during inflation which proceeds from the right to the left. RMI2 also corresponds to $c > 0$ but with $\phi > \phi_0$ and ϕ increases during inflation which now proceeds from the left to the right. RMI3 refers to the situation where $c < 0$ and $\phi < \phi_0$ all the time. In this case, ϕ increases during inflation which proceeds from the left to the right. Finally, RMI4 has $c < 0$ and $\phi > \phi_0$ decreases as inflation proceeds from the right to the left.

Using the potential (6.6), one can calculate the three slow-roll parameters ϵ_1, ϵ_2 and ϵ_3. Defining $x \equiv \phi/\phi_0$, one obtains the following expressions

$$\epsilon_1 = \frac{c^2}{2}\left[\frac{\dfrac{\phi_0}{M_{\rm Pl}} x \ln x}{1 - \dfrac{c}{2}\dfrac{\phi_0^2}{M_{\rm Pl}^2}\left(-\dfrac{1}{2} + \ln x\right) x^2}\right]^2 , \tag{6.8}$$

$$\epsilon_2 = 2c\,\frac{1+\dfrac{c}{4}\dfrac{\phi_0^2}{M_{\rm Pl}^2}x^2+\left(1-\dfrac{c}{4}\dfrac{\phi_0^2}{M_{\rm Pl}^2}x^2\right)\ln x+\dfrac{c}{2}\dfrac{\phi_0^2}{M_{\rm Pl}^2}x^2\ln^2 x}{\left[1-\dfrac{c}{2}\dfrac{\phi_0^2}{M_{\rm Pl}^2}\left(-\dfrac{1}{2}+\ln x\right)x^2\right]^2}\,, \tag{6.9}$$

and

$$\begin{aligned}\epsilon_3 = {} & \frac{c\ln x}{\left[1-\dfrac{c}{2}\dfrac{\phi_0^2}{M_{\rm Pl}^2}\left(-\dfrac{1}{2}+\ln x\right)x^2\right]^2}\left[1+\frac{c}{4}\frac{\phi_0^2}{M_{\rm Pl}^2}x^2+\left(1-\frac{c}{4}\frac{\phi_0^2}{M_{\rm Pl}^2}x^2\right)\ln x+\frac{c}{2}\frac{\phi_0^2}{M_{\rm Pl}^2}x^2\ln^2 x\right]^{-1}\\ & \times\left[1+\frac{c}{2}\frac{\phi_0^2}{M_{\rm Pl}^2}x^2+\frac{c^2}{16}\frac{\phi_0^4}{M_{\rm Pl}^4}x^4+c\left(2\frac{\phi_0^2}{M_{\rm Pl}^2}x^2+\frac{c}{2}\frac{\phi_0^4}{M_{\rm Pl}^4}x^4\right)\ln x\right.\\ & \left.+\,c\left(3\frac{\phi_0^2}{M_{\rm Pl}^2}x^2-\frac{c}{2}\frac{\phi_0^4}{M_{\rm Pl}^4}x^4\right)\ln^2 x+\frac{c^2}{2}\frac{\phi_0^4}{M_{\rm Pl}^4}x^4\ln^3 x\right].\end{aligned} \tag{6.10}$$

The slow-roll parameters are represented in the bottom panels in Fig. 72.

Let us now examine how inflation ends in this model. The slow-roll parameter ϵ_1 has a maximum in the $x<1$ region and a maximum in the $x>1$ region, see Fig. 72. If these maxima were larger than one, inflation could in principle stop by violation of the slow-roll conditions. In the vacuum dominated approximation, however, we see from Eq. (6.8), that $\epsilon_1 \simeq (c^2/2)(\phi_0^2/M_{\rm Pl}^2)x^2\ln^2 x$. This means that the *vev* $x_{\rm end}$ satisfies $x_{\rm end}\ln x_{\rm end} = \pm(\sqrt{2}/c)(M_{\rm Pl}/\phi_0)$. But we have established previously that the vacuum dominated condition precisely implies that $cM_{\rm Pl}/\phi_0 \gg 1$ and one would have $\ln x_{\rm end} \gg 1$. But for the model to be valid, we have already mentioned that the condition $|\ln x| \ll 1$ should be enforced. We conclude that the value of $x_{\rm end}$ obtained above lies outside the regime of validity of the potential. The end of inflation either occurs by violation of slow-roll but in a regime where additional unknown corrections arise and modify the shape of $V(\phi)$, or by tachyonic instability. In this last case, inflation stops in a regime where our calculations are valid. This also means that we must consider an additional parameter in the model, namely $x_{\rm end}$. In this article, this is the assumption made which implies that RMI is indeed a three parameters model.

We now turn to the calculation of the observable predictions. The first step is to obtain the slow-roll trajectory. One obtains

$$\begin{aligned}N-N_{\rm end} = {} & \frac{1}{c}\left(\ln|\ln x|-\ln|\ln x_{\rm end}|\right)-\frac{1}{4}\frac{\phi_0^2}{M_{\rm Pl}^2}(x^2-x_{\rm end}^2)\\ & +\frac{1}{4}\left(\frac{\phi_0}{M_{\rm Pl}^2}\right)^2\left[{\rm Ei}\left(2\ln x\right)-{\rm Ei}\left(2\ln x_{\rm end}\right)\right],\end{aligned} \tag{6.11}$$

where the exponential integral function Ei is defined by ${\rm Ei}(x) \equiv -\int_{-x}^{+\infty}{\rm d}te^{-t}/t$ [204, 205]. This expression cannot be inverted analytically. However, in the limit $(c\phi_0/M_{\rm Pl})x \ll 1$ (the vacuum dominated regime), the above expression can be approximated by

$$N-N_{\rm end} \simeq \frac{1}{c}\left(\ln|\ln x|-\ln|\ln x_{\rm end}|\right), \tag{6.12}$$

from which it follows that

$$x(N) = \exp\left[e^{c(N-N_{\rm end})}\ln x_{\rm end}\right]. \tag{6.13}$$

The slow-roll predictions of the four models, RMI1, RMI2, RMI3 and RMI4 are presented in Figs. 167, 168, 169 and 170 for $|c| = 10^{-2}$, $\phi_0/M_{\rm Pl} < 1/\sqrt{|c|}$, and $1/e < x_{\rm end} < e$, respectively. In order to interpret them, it is interesting to use some approximations. From the trajectory (6.13), it is straightforward to calculate x_*. Recalling that inflation is supposed to stop at $x_{\rm end}$, one obtains $x_* = \exp\left(e^{-c\Delta N_*}\ln x_{\rm end}\right)$. Then, using Eqs. (6.8), (6.9) and (6.10) in the vacuum dominated limit, we find that

$$\epsilon_{1*} \simeq \frac{c^2}{2}\left(\frac{\phi_0}{M_{\rm Pl}}\right)^2 \exp\left(2\mathrm{e}^{-c\Delta N_*}\ln x_{\rm end}\right) e^{-2c\Delta N_*}\ln^2 x_{\rm end}, \tag{6.14}$$

$$\epsilon_{2*} \simeq 2c\left(1 + e^{-c\Delta N_*}\ln x_{\rm end}\right). \tag{6.15}$$

In fact, in order to compare with the existing literature, it turns out to be convenient to define the following quantity

$$s \equiv c\ln x_* = -c\, e^{-c\Delta N_*}\ln x_{\rm end}. \tag{6.16}$$

For RMI1 and RMI4, $s > 0$ while for RMI2 and RMI3 one has $s < 0$. In terms of s Eqs. (6.14) and (6.15) can be re-written as

$$\epsilon_{1*} \simeq \frac{s^2}{2}\left(\frac{\phi_0}{M_{\rm Pl}}\right)^2 e^{-2s/c}, \qquad \epsilon_{2*} \simeq 2c\left(1 - \frac{s}{c}\right). \tag{6.17}$$

These equations imply that the locus of the model predictions in the plane (ϵ_1, ϵ_2) are given by $\epsilon_2 \simeq 2(c-s) + 4\epsilon_1 M_{\rm Pl}^2/\phi_0^2$. If we neglect ϵ_{1*} (with respect to ϵ_{2*}) one recovers the formula derived in Refs. [561, 564, 566], namely $n_{\rm S} - 1 \simeq 2(s-c)$. The same route for the third slow-roll parameter gives $\epsilon_2\epsilon_3 \simeq -2cs$ and neglecting again ϵ_1 gives the scalar running $\alpha_{\rm S} \simeq 2sc$. The above analytic estimates agree well with the complete slow-roll predictions represented in Figs. 167, 168, 169 and 170.

From the CMB normalization, we obtain the following expression for the mass scale

$$\frac{M^4}{M_{\rm Pl}^4} = 720\pi^2 c^2 \frac{Q_{\rm rms-PS}^2}{T^2}\frac{\phi_0^2}{M_{\rm Pl}^2}\frac{x_*^2\ln^2(x_*)}{\left\{1 - \frac{c}{2}\frac{\phi_0^2}{M_{\rm Pl}^2}\left[-\frac{1}{2} + \ln(x_*)\right]x_*^2\right\}^3}. \tag{6.18}$$

In the vacuum dominated regime, this expression can be approximated by

$$\frac{M^4}{M_{\rm Pl}^4} \simeq 720\pi^2 s^2 \frac{Q_{\rm rms-PS}^2}{T^2}\frac{\phi_0^2}{M_{\rm Pl}^2}e^{s/c}. \tag{6.19}$$

One can then easily deduce the mass scale M for a given value of c, ϕ_0 and $x_{\rm end}$, the three parameters of the model.

6.2 Valley Hybrid Inflation (VHI)

6.2.1 Theoretical Justifications

Hybrid inflation is a two-fields model with the potential given by the following expression [162, 240, 338, 567–570]

$$V(\phi,\psi) = \frac{1}{2}m^2\phi^2 + \frac{\lambda'}{4}\left(\psi^2 - \Delta^2\right)^2 + \frac{\lambda}{2}\phi^2\psi^2, \tag{6.20}$$

where ϕ is the inflaton, ψ the waterfall field, λ and λ' are two coupling constants and Δ a constant of dimension one. A priori, given the above potential, inflation can occur in different regimes. However, the standard lore is that inflation can proceed along the valley given by $\psi = 0$ and, in this case, the potential reduces to an effective single field potential that can be written as

$$V(\phi) = M^4 \left[1 + \left(\frac{\phi}{\mu}\right)^p\right], \tag{6.21}$$

with $p = 2$ and where one has used the following parameter redefinition

$$M = \frac{\lambda'^{1/4}\Delta}{\sqrt{2}}, \qquad \mu = \sqrt{\frac{\lambda'}{2}}\frac{\Delta^2}{m}. \tag{6.22}$$

Inflation along the valley has been shown to be a dynamical attractor of the two-field dynamics in Refs. [571, 572]. However, as recently shown in Ref. [573], the hybrid potential can also support an inflationary phase along a mixed valley-waterfall trajectory, which is genuinely a two-fields dynamics. As we use a single field description here, those effects cannot be described by the potential of Eq. (6.21). For this reason, we will refer to the single field approximation as the "valley hybrid regime". Let us stress that, if the waterfall inflationary regime occurs, then it will erase any observable effects coming the valley hybrid regime. As a result, Eq. (6.21) is a good description of hybrid inflation only if the model parameters are such that the waterfall regime remains sub-dominant. According to Ref. [573, 574], this is the case provided

$$\sqrt{\lambda'}\frac{\Delta^3}{m} \ll M_{\rm Pl}^2, \tag{6.23}$$

a condition that will be assumed in the following. The effective potential (6.21) was also obtained in Ref. [575] in the context of supergravity brane inflation, and in Ref. [521] in the context of hilltop supernatural inflation. It depends on three parameters, namely M, μ and p. In fact, as mentioned before, $p = 2$ for the two-field model given in Eq. (6.20) but we will consider the most general situation with $p > 0$ unspecified. Let us stress again that all multifield effects such as the generation of isocurvature modes or cosmic strings cannot be accounted within the single field dynamics [149, 576–578].

It is also worth mentioning that the potential (6.21) with $p = 2$ can also be obtained in the supergravity context [579–582]. The main idea is to consider a supergravity model which is not R-symmetry invariant and described by the following Kähler and super-potentials:

$$K = XX^\dagger + \frac{b}{6M^2}\left(XX^\dagger\right)^2 - \frac{c}{9M^2}XX^\dagger\left[X^2 + \left(X^\dagger\right)^2\right], \tag{6.24}$$

$$W = fX, \tag{6.25}$$

Here X is a superfield, $M < M_{\rm Pl}$ a mass scale and b, c two dimensionless constants, a priori of order one. The quantity f is a constant of dimension two that can be viewed as the supersymmetry breaking scale. From these expressions, the scalar potential reads

$$V = f^2\left[1 - \frac{2b}{3M^2}XX^\dagger + \frac{c}{3M^2}\left(X^2 + X^{\dagger 2}\right) + \mathcal{O}\left(\frac{1}{M^4}\right)\right], \tag{6.26}$$

or, re-writing $X = \alpha + i\beta$, it reads

$$V \simeq f^2\left[1 + \frac{2}{3M^2}(b-c)\alpha^2 - \frac{2}{3M^2}(b+c)\beta^2\right]. \tag{6.27}$$

For a field evolution along the α direction, we recover a potential of the VHI type with $p = 2$ ($b - c$ must be positive). In this setup, $\alpha/M \ll 1$ is required in order for the field α to be approximately canonically normalized, the Kähler potential being not minimal. It is also interesting to comment on the η-problem in this model since this is a generic issue in supergravity. If one calculates the slow-roll parameter $\eta \equiv M_{\rm Pl}^2 V_{\alpha\alpha}/V$, one finds that

$$\eta = \frac{4M_{\rm Pl}^2}{3M^2}(b-c). \tag{6.28}$$

Therefore, one must take $M \lesssim M_{\rm Pl}$ and fine-tune the difference $b - c$ to a small number.

6.2.2 Slow-Roll analysis

We now turn to the slow-roll analysis of the VHI scenario. Recall that we consider the following potential

$$V(\phi) = M^4\left[1 + \left(\frac{\phi}{\mu}\right)^p\right], \tag{6.29}$$

where the parameter M and μ have been expressed in terms of the parameters of the two-field model in Eq. (6.22). The first three Hubble flow functions in the slow-roll approximation can be derived from Eq. (6.29) in a straightforward fashion. Defining the quantity x by the following expression

$$x \equiv \frac{\phi}{\mu}, \tag{6.30}$$

they read

$$\epsilon_1 = \frac{p^2}{2}\left(\frac{M_{\rm Pl}}{\mu}\right)^2 \frac{x^{2p-2}}{\left(1+x^p\right)^2}, \qquad \epsilon_2 = 2p\left(\frac{M_{\rm Pl}}{\mu}\right)^2 x^{p-2}\frac{x^p - p + 1}{\left(1+x^p\right)^2}, \tag{6.31}$$

and

$$\epsilon_3 = p\left(\frac{M_{\rm Pl}}{\mu}\right)^2 x^{p-2}\frac{2x^{2p} - (p-1)(p+4)x^p + (p-1)(p-2)}{\left(1+x^p\right)^2\left(x^p - p + 1\right)}. \tag{6.32}$$

A specific feature of hybrid inflation in comparison to large and small field models is that ϵ_2 and ϵ_3 can be negative (see Fig. 73). In particular

$$\epsilon_2 \underset{x\to 0}{\simeq} -2p(p-1)\left(\frac{M_{\rm Pl}}{\mu}\right)^2 x^{p-2}, \tag{6.33}$$

and ϵ_3 blows up in the limit $x^p \to p - 1$. Together with the potential, the three Hubble flow functions have been represented in Fig. 73.

The slow-roll trajectory is obtained by integrating Eq. (2.11) with the valley hybrid potential and reads

$$N - N_{\rm end} = \frac{1}{2p}\frac{\mu^2}{M_{\rm Pl}^2}\left[-x^2 + x_{\rm end}^2 + \frac{2}{2-p}\left(x_{\rm end}^{2-p} - x^{2-p}\right)\right], \tag{6.34}$$

which is, up to a sign, the same as for the SFI models [see Eq. (5.5)]. The case $p = 2$ requires special attention, but as for SFI, is recovered as the limit $p \to 2$ in the previous equation. One obtains

$$N - N_{\rm end} = \frac{1}{4}\frac{\mu^2}{M_{\rm Pl}^2}\left[-x^2 + x_{\rm end}^2 - 2\ln\left(\frac{x}{x_{\rm end}}\right)\right], \tag{6.35}$$

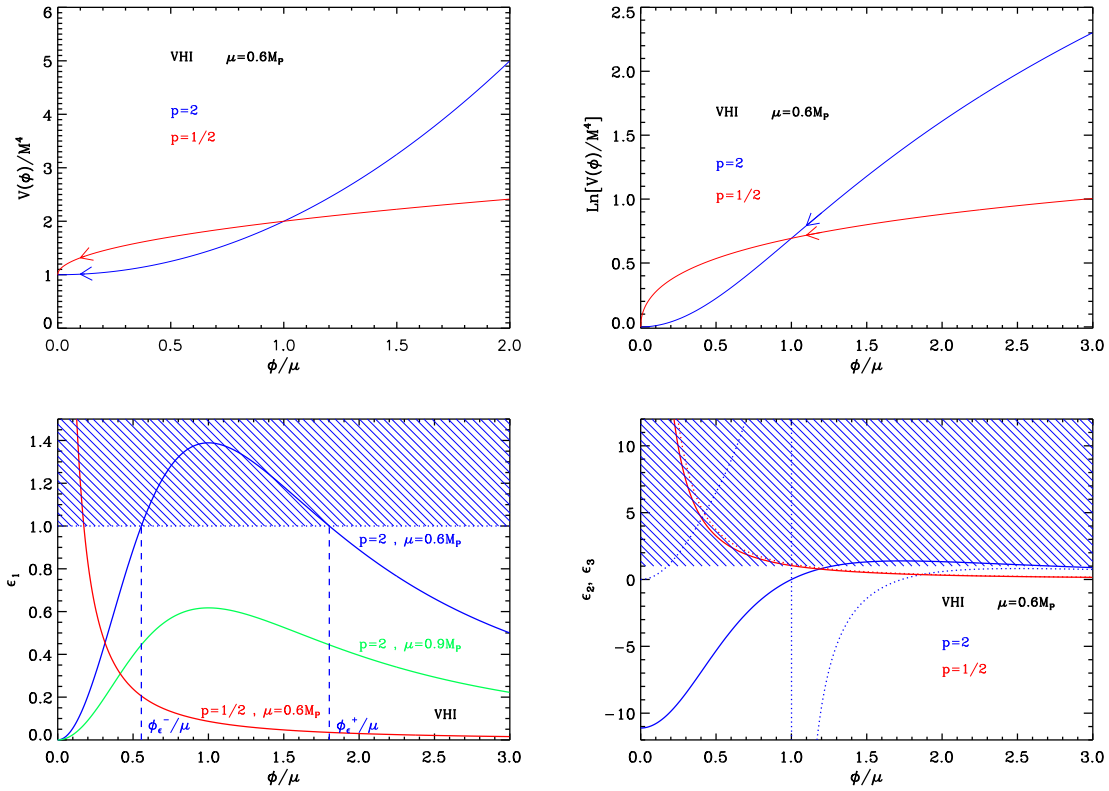

Figure 73. Valley Hybrid inflation (VHI) for $p = 1/2$ (red line) and $p = 2$ (blue line). Upper panels: the potential and its logarithm for $\mu = 0.6M_{\rm Pl}$. Bottom left panel: slow-roll parameter ϵ_1 for $p = 1/2$, $\mu = 0.6M_{\rm Pl}$ (red line), $p = 2$, $\mu = 0.6M_{\rm Pl}$ (blue line) and $p = 2$, $\mu = 0.9M_{\rm Pl}$ (green line). For small values of μ and $p > 1$, the inflationary regions are separated into a large field one and the vacuum dominated one. The latter may not exist due to slow-roll violations if the field first rolls down the potential in the large field domain (see the text for a detailed discussion). The shaded area indicates the regions in which acceleration cannot occur. Bottom right panel: slow-roll parameters ϵ_2 (solid line) and $\epsilon 3$ (dotted line) for $\mu = 0.6M_{\rm Pl}$.

which is again very similar to SFI, up to a sign. The trajectory (6.34) cannot be inverted analytically in the general case. It is however possible to perform this inversion for many integer values of p, but those expressions will be omitted for the sake of clarity. We simply give an approximate solution valid only in the limit $x \ll 1$ and $p > 2$

$$x \simeq \left[x_{\rm end}^{2-p} + p(p-2)\frac{M_{\rm Pl}^2}{\mu^2}(N - N_{\rm end}) \right]^{1/(2-p)} . \tag{6.36}$$

If the waterfall inflation does not take place, i.e. under the condition (6.23), valley hybrid inflation ends by a tachyonic instability in the small field regime $x < 1$, also referred to as "the vacuum dominated regime". From the two-fields potential (6.20), one sees that the transverse direction becomes tachyonic at the inflaton value

$$\phi_{\rm end} = \sqrt{\frac{\lambda'}{\lambda}}\Delta. \tag{6.37}$$

In the single field approach, $x_{\rm end}$ is therefore an extra-parameter and VHI is a three parameters model according to our classification. However, as can be seen in Fig. 73, one should pay attention to the various domains in which inflation can take place. They are given by the behavior of $\epsilon_1(x)$.

If $p > 1$, the slow-roll parameter ϵ_1 vanishes when the field goes to zero and at infinity while it reaches a maximum for

$$x_{\epsilon_1^{\rm max}} = (p-1)^{1/p} \, , \tag{6.38}$$

equals to

$$\epsilon_1^{\rm max} = \frac{1}{2}\left(\frac{M_{\rm Pl}}{\mu}\right)^2 (p-1)^{\frac{2p-2}{p}} \, . \tag{6.39}$$

Defining

$$\mu_\epsilon \equiv \frac{M_{\rm Pl}}{\sqrt{2}}(p-1)^{1-1/p} \, , \tag{6.40}$$

for all $\mu > \mu_\epsilon$, one has $\epsilon_1(x) < 1$ and inflation can proceed all over the domain $x > 0$. On the contrary, if $\mu < \mu_\epsilon$, then inflation can, a priori, proceed in two disconnected domains. Either $0 < x < x^-_{\epsilon_1=1}$ or $x > x^+_{\epsilon_1=1}$ where $x^\pm_{\epsilon_1=1}$ are the two roots of $\epsilon_1 = 1$, i.e. the solutions of

$$x^{2p} + 2x^p - \frac{p^2}{2}\left(\frac{M_{\rm Pl}}{\mu}\right)^2 x^{2p-2} + 1 = 0. \tag{6.41}$$

This equation cannot be solved explicitly in the general case but, as for the trajectory, there are explicit analytic expressions for many integer values of p. For instance, for $p = 2$, one gets

$$x^{\pm(p=2)}_{\epsilon_1=1} = \frac{1}{\sqrt{2}}\frac{M_{\rm Pl}}{\mu}\left(1 \pm \sqrt{1 - 2\frac{\mu^2}{M_{\rm Pl}^2}}\right). \tag{6.42}$$

The positive sign corresponds to the largest root while the minus one to the smallest (see Fig. 73). In the limit $\mu \ll M_{\rm Pl}$, one has $x^+_{\epsilon_1=1} \simeq pM_{\rm Pl}/(\sqrt{2}\,\mu)$ which is also the expression of $x_{\rm end}$ for the large field model LFI (see section 4.2). This does not come as a surprise since in that situation Eq. (6.29) is indeed dominated by the monomial term. In fact, the two above-mentioned domains precisely corresponds to a large field one for $x > x^+_{\epsilon_1=1}$ and a vacuum dominated one for $x < x^-_{\epsilon_1=1}$. It is a common mistake to assume that the large field domain remains unobservable due to the existence of the vacuum dominated one. In fact, as shown in Ref. [571], the large field regime becomes observable provided $\mu \ll \mu_\epsilon$. In that situation, after having crossed $x^+_{\epsilon_1=1}$, the field fast-rolls in the region $\epsilon_1(x) > 1$. Then, it enters the domain $x < x^-_{\epsilon_1=1}$ with a strong initial velocity and, as a consequence, crosses the whole vacuum dominated region, still in fast-roll, to reach $x_{\rm end}$. All observable predictions in such a situation are therefore similar to that obtained in the LFI models. Let us notice that, if there exists a mechanism that can gently put the field without a strong initial velocity inside the $x < x^-_{\epsilon_1=1}$ domain, then inflation can still occur in the vacuum dominated region, even though $\mu < \mu_\epsilon$. But if the field is coming from the region $x > x^+_{\epsilon_1=1}$, then this regime does not exist anymore.

For $p = 1$, $\epsilon_1(x)$ is a decreasing function of the field and takes a finite value $M_{\rm Pl}^2/(2\mu^2)$ for $x \to 0$. The behavior is similar to the case $p > 1$ and if $\mu > M_{\rm Pl}/\sqrt{2}$ inflation can take place all over $x > x_{\rm end}$. However, if $\mu < M_{\rm Pl}/\sqrt{2}$ then the vacuum dominated region does not exist anymore and $x_{\epsilon_1=1} = x^+_{\epsilon_1=1} = M_{\rm Pl}/(\sqrt{2}\mu) - 1$ One should also notice that if $p = 1$ the relation $\epsilon_2 = 4\epsilon_1$ applies.

Finally, for $p < 1$, $\epsilon_1(x)$ is a decreasing function of the field but it blows up when $x \to 0$. In that situation, inflation stops at $x = \max(x^-_{\epsilon_1=1}, x_{\rm end})$ but the field will still fast-roll till the tachyonic instability develops at $x_{\rm end}$. As a result, even if for some cases $x^-_{\epsilon_1=1} > x_{\rm end}$, the observable predictions remain mostly the same.

According to the previous discussion, for $p > 1$, the VHI effective potential is therefore adequate to describe the vacuum dominated regime only, i.e. for $x_{\rm end} < x < x^-_{\epsilon_1=1}$ where $x_{\rm end}$ is the instability point given by Eq. (6.37). In that situation, solving Eq. (2.47) together with the trajectory (6.34) gives the observable field value x_* at which the pivot mode crossed the Hubble radius during inflation. The potential parameter M is fixed from the amplitude of the CMB anisotropies

$$\frac{M^4}{M_{\rm Pl}^4} = 720\pi^2 p^2 \frac{M_{\rm Pl}^2}{\mu^2} \frac{x_*^{2p-2}}{(1+x_*^p)^3} \frac{Q^2_{\rm rms-PS}}{T^2}\,. \tag{6.43}$$

The reheating consistent slow-roll predictions are displayed in Figs. 171, 172, 173, 174 and 175 for $p = 0.5$, $p = 1$, $p = 1.5$, $p = 2$ and $p = 3$, respectively. For $p > 1$ and $x_{\epsilon_1}^{\rm max} > 1$, $x_{\rm end}$ is varied between 0 and an upper bound such that $x_{\rm in} < x^-_{\epsilon_1=1}$. One the other hand, if $x_{\epsilon_1}^{\rm max} < 1$, then one simply takes $x_{\rm end} < 10$. For $p \leq 1$, $x_{\rm end}$ is varied on a wider range, with no particular constraints. For $p = 1$, the predictions lie on the line $\epsilon_2 = 4\epsilon_1$ as expected whereas for $p > 1$ one recovers a blue spectral index when $x_{\epsilon_1}^{\rm max} > 1$, while a red spectral index can be obtained when $x_{\epsilon_1}^{\rm max} < 1$ and $x_* > x_{\epsilon_1}^{\rm max}$, with $x_* < 1$ (that is to say, the large field regime).

6.3 Dynamical Supersymmetric Inflation (DSI)

6.3.1 Theoretical Justifications

This model has been studied in Refs. [583, 584]. As for the IMI scenario, see section 5.18, the model is based on Ref. [537] which has shown that inverse power law potentials naturally arise in supersymmetric theories. The fact that we have an inverse power law behavior, rather than the usual positive power law behavior, can be traced back to the presence of non-perturbative effects, such as for instance gaugino condensation, see section 5.18. Based on the previous considerations, one can write that

$$V = V_0 + \frac{\Lambda_3^{p+4}}{\phi^p} + \frac{\phi^{q+4}}{M_{\rm Pl}^q}, \tag{6.44}$$

where the last term encodes a correction to $V(\phi)$ due to a non-renormalizable operator. It is Planck suppressed since $M_{\rm Pl}$ is the only explicit scale present in the theory. This term implies that there is a minimum located at

$$\phi_{V^{\rm min}} = \left(\frac{p}{q+4}\Lambda_3^{p+4} M_{\rm Pl}^q\right)^{\frac{1}{p+q+4}}\,. \tag{6.45}$$

This means that the extra term can be neglected in the region $\phi \ll \phi_{V^{\rm min}}$ and, in the following, we assume that this is the case. The difference with the IMI scenario is the presence of the constant term V_0 which will be assumed to be dominant.

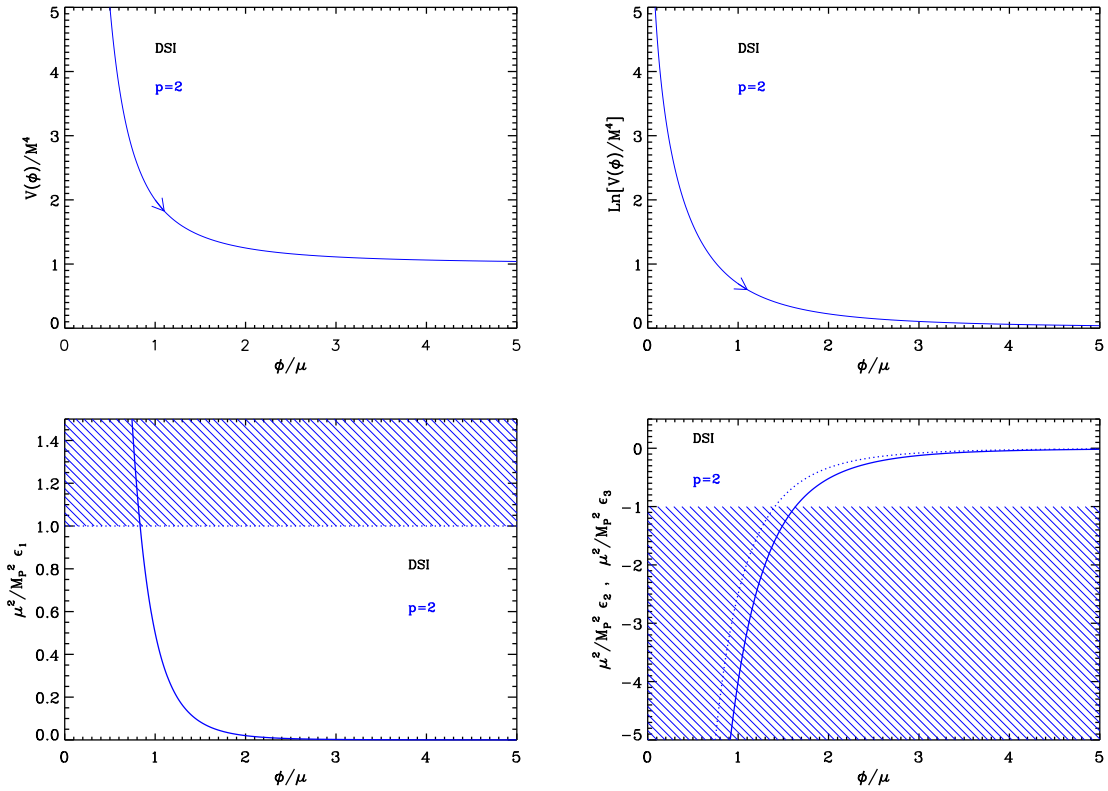

Figure 74. Dynamical Supersymmetric Inflation (DSI) for $p = 2$. Upper panels: the potential and its logarithm as a function of ϕ/μ. Bottom left panel: slow-roll parameter ϵ_1 rescaled by $M_{\rm Pl}^2/\mu^2$. The shaded area indicates the region in which inflation cannot occur for $\mu = M_{\rm Pl}$. Bottom right panel: slow-roll parameters ϵ_2 (solid line) and ϵ_3 (dotted line), rescaled by $M_{\rm Pl}^2/\mu^2$.

6.3.2 Slow-Roll Analysis

In this sub-section, we now turn to the slow-roll analysis of the DSI scenario. For this purpose, we rewrite the potential as

$$V(\phi) = M^4 \left[1 + \left(\frac{\phi}{\mu}\right)^{-p}\right], \tag{6.46}$$

where p is a free index parameter and where we defined

$$V_0 = M^4, \qquad \mu^p = \frac{\Lambda_3^{p+4}}{M^4}. \tag{6.47}$$

As already mentioned, in order for inflation to take place in the vacuum dominated regime, we must assume that $\phi \gg \mu$. In Refs. [583, 584], it was argued that natural values for Λ_3 and M are 10^6GeV and 10^{10}GeV, respectively. This means that a scale of order $\mu \simeq 10^{6+14/p}$ GeV is a reasonable prior for μ.

The potential (6.46), as well as its logarithm, is displayed in Fig. 74. It is a decreasing function of the field, hence inflation proceeds from the left to the right. Defining the quantity

$$x \equiv \frac{\phi}{\mu}, \tag{6.48}$$

the first three Hubble flow functions in the slow-roll approximation read

$$\epsilon_1 = \frac{p^2}{2}\left(\frac{M_{\rm Pl}}{\mu}\right)^2 \frac{x^{-2p-2}}{\left(1+x^{-p}\right)^2}\,, \qquad \epsilon_2 = -2p\left(\frac{M_{\rm Pl}}{\mu}\right)^2 x^{-p-2}\frac{x^{-p}+p+1}{\left(1+x^{-p}\right)^2}\,, \tag{6.49}$$

and

$$\epsilon_3 = -p\left(\frac{M_{\rm Pl}}{\mu}\right)^2 x^{-p-2}\frac{\left[2x^{-2p}+(p+1)(p-4)x^{-p}+(p+1)(p+2)\right]}{\left(1+x^{-p}\right)^2\left(x^{-p}+p+1\right)}\,. \tag{6.50}$$

Let us already notice that, from these expressions, one has

$$-2\epsilon_1-\epsilon_2 = \left(\frac{M_{\rm Pl}}{\mu}\right)^2 \frac{px^{-p-2}}{\left(1+x^{-p}\right)^2}\left[px^{-p}+2p(p+1)x^{-p-2}\right] > 0, \tag{6.51}$$

which implies a blue spectral index for the scalar power spectrum since, at first order, $n_{\rm S}-1 = -2\epsilon_{1*}-\epsilon_{2*}$. The three slow-roll parameters become very small at large fields $x \gg 1$. There is a value $x_{\epsilon_1=1}$ such that $\epsilon_1 = 1$. For x such that $x < x_{\epsilon_1=1}$, $\epsilon_1 > 1$ and inflation cannot take place. This value has to be determined numerically, but since the natural values for μ are such that $\mu/M_{\rm Pl} \ll 1$, an approximate expression can be derived

$$x_{\epsilon_1=1} \simeq \left(\frac{p}{\sqrt{2}}\frac{M_{\rm Pl}}{\mu}\right)^{1/(p+1)}\,. \tag{6.52}$$

Because the potential is decreasing with x, inflation can only take place in the domain $x > x_{\epsilon_1=1} \gg 1$ if $\mu \ll M_{\rm Pl}$. It cannot stop by slow-roll violation and another mechanism such as, e.g. a tachyonic instability, has to be introduced. We will denote by $x_{\rm end}$ the field value at which this occurs. It represents an extra parameter of the model. Obviously, it must be such that $x_{\epsilon_1=1} < x_{\rm end} \ll x_{V^{\rm min}}$.

Let us now turn to the slow-roll trajectory. It can be integrated explicitly from Eq. (2.11) and one obtains

$$N_{\rm end}-N = \frac{\mu^2}{2pM_{\rm Pl}^2}\left(x_{\rm end}^2+\frac{2}{p+2}x_{\rm end}^{p+2}-x^2-\frac{2}{p+2}x^{p+2}\right). \tag{6.53}$$

In the $\mu/M_{\rm Pl} \ll 1$ limit, one has $x > x_{\epsilon_1=1} \gg 1$, and the previous trajectory can be approximated by

$$N_{\rm end}-N \simeq \frac{\mu^2}{p(p+2)M_{\rm Pl}^2}\left(x_{\rm end}^{p+2}-x^{p+2}\right). \tag{6.54}$$

This expression can be analytically inverted to get the observable field value x_* in terms of $\Delta N_* = N_{\rm end}-N_*$ as

$$x_* \simeq \left[x_{\rm end}^{p+2}-\frac{M_{\rm Pl}^2}{\mu^2}p(p+2)\Delta N_*\right]^{\frac{1}{p+2}}\,. \tag{6.55}$$

One can notice that the total amount of e-folds is bounded because $x_{\rm end} \ll x_{V^{\rm min}}$ and cannot take infinitely large values. In order to get a number of e-folds, $\Delta N > \Delta N_{\rm min}$, $x_{\rm end}$ should be sufficiently large with $x_{\rm end} > x_{\rm end}^{\rm min}$. More precisely, setting $x_{\rm ini} = x_{\epsilon_1=1}$, one has

$$x_{\rm end}^{\rm min} \simeq \left[p(p+2)\frac{M_{\rm Pl}^2}{\mu^2}\Delta N_{\rm min}+\left(\frac{p}{\sqrt{2}}\frac{M_{\rm Pl}}{\mu}\right)^{\frac{p+2}{p+1}}\right]^{\frac{1}{p+2}} \simeq \left[p(p+2)\frac{M_{\rm Pl}^2}{\mu^2}\Delta N_{\rm min}\right]^{\frac{1}{p+2}}\,. \tag{6.56}$$

In practice one wants $\Delta N_{\rm min} > 50$ to solve the problems of the standard Big-Bang scenario. Whether this value is compatible, or not, with the condition $x_{\rm end} \ll x_{V^{\rm min}}$ depends on the value of M^4 appearing in Eq. (6.45), which is itself determined by the amplitude of the CMB anisotropies. This one reads

$$\left(\frac{M}{M_{\rm Pl}}\right)^4 = 720\pi^2 p^2 \left(\frac{M_{\rm Pl}}{\mu}\right)^2 x_*^{-2p-2}\left(1+x_*^{-p}\right)^{-3}\frac{Q^2_{\rm rms-PS}}{T^2}\,. \tag{6.57}$$

In the limit $\mu/M_{\rm Pl} \ll 1$, one has $x_* \gg 1$ and this expression can be approximated by

$$\frac{M^4}{M_{\rm Pl}^4} \simeq 720\pi^2 p^2 \frac{M_{\rm Pl}^2}{\mu^2} x_*^{-2p-2}\frac{Q^2_{\rm rms-PS}}{T^2}\,. \tag{6.58}$$

Therefore, from Eq. (6.45), one has

$$x_{V^{\rm min}} \simeq \left[720\pi^2\frac{p^3}{q+4}\left(\frac{M_{\rm Pl}}{\mu}\right)^{6+q} x_*^{-2p-2}\frac{Q^2_{\rm rms-PS}}{T^2}\right]^{\frac{1}{p+q+4}}\,, \tag{6.59}$$

with x_* depending on $x_{\rm end}$ through Eq. (6.55). One can see that the previous expression decreases with x_* and the condition $x_{\rm end} \ll x_{V^{\rm min}}$ imposes an upper bound on $x_{\rm end} < x_{\rm end}^{\rm max}$ with

$$x_{\rm end}^{\rm max} \simeq \left[720\pi^2\frac{p^3}{q+4}\frac{Q^2_{\rm rms-PS}}{T^2}\left(\frac{M_{\rm Pl}}{\mu}\right)^{q+6}\right]^{1/(3p+q+6)}\,. \tag{6.60}$$

The prior condition on $x_{\rm end}$ is therefore of the type $x_{\rm end}^{\rm min} < x_{\rm end} \ll x_{\rm end}^{\rm max}$, with $x_{\rm end}^{\rm min}$ defined by Eq. (6.56) and $x_{\rm end}^{\rm max}$ defined by Eq. (6.60). For any $q > 0$, these two equations show that there exists an upper bound $\mu < \mu_{\rm max}$ under which the condition $x_{\rm end}^{\rm min} \ll x_{\rm end}^{\rm max}$ is satisfied. It reads

$$\frac{\mu_{\rm max}}{M_{\rm Pl}} \simeq \frac{\left(720\pi^2\frac{p^3}{q+4}\frac{Q^2_{\rm rms-PS}}{T^2}\right)^{(p+2)/(pq)}}{[p(p+2)\Delta N_{\rm min}]^{(3p+q+6)/(pq)}}\,, \tag{6.61}$$

and has been represented in Fig. 75. One can see that a typical value $\mu/M_{\rm Pl} \simeq 10^{10}$ GeV (see Ref. [583]) is not allowed for realistic values of p and q. As such, the prior space for p, μ, and $x_{\rm end}$ is constrained and should be handled carefully.

The reheating consistent slow-roll predictions of the dynamical supersymmetric models are displayed in Figs. 176, 177 and 178 for $p = 2$, $p = 3$ and $p = 4$, respectively, and with $10^{-10} M_{\rm Pl} < \mu < \mu_{\rm max}$ (where $\mu_{\rm max}$ has been calculated taking $q = 8$ and $\Delta N_{\rm min} = 60$ to cover a large prior space). The reheating equation of state parameter $\overline{w}_{\rm reh}$ has been taken to 0 but since there is no potential minimum around which the inflaton field can oscillate at the end of inflation, this parameter is a priori unspecified and can take different values. In any case the reheating temperature is strongly degenerated with the parameter $x_{\rm end}^{\rm min} < x_{\rm end} < x_{\rm end}^{\rm max}$ preventing their inference. One can check that the spectral index is blue, as announced earlier, making these models disfavored by the observations. The typical amount of gravitational waves is very small, in agreement with the results of Ref. [583].

6.4 Generalized Mixed Inflation (GMLFI)

This model is a generalization of MLFI (see section 4.3) and is, by definition, the sum of two monomial functions with arbitrary power indices. The corresponding potential can be

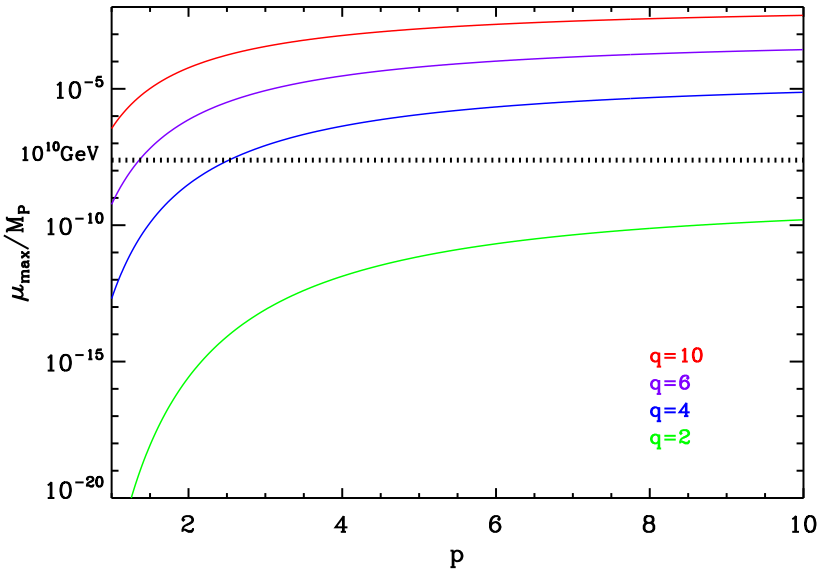

Figure 75. Dynamical Supersymmetric Inflation. Maximal value of $\mu/M_{\rm Pl}$ with respect to p, and for different values of q, such that the condition $x_{\rm end}^{\rm min} < x_{\rm end}^{\rm max}$ is satisfied. We have fixed $\Delta N_{\rm max} = 50$. The black dotted line show a typical value for $\mu/M_{\rm Pl} \simeq 10^{10}$ GeV [583].

written as

$$V = M^4 \left(\frac{\phi}{M_{\rm Pl}}\right)^p \left[1 + \alpha \left(\frac{\phi}{M_{\rm Pl}}\right)^q\right], \tag{6.62}$$

where α, p and q are three dimensionless positive parameters. It can be seen as a generalization of the large field inflation potential (LFI, see section 4.2), which is recovered when $\alpha \to 0$ or $\alpha \to \infty$. The parameter α therefore controls the relative weight of the two terms. Since the potential is an increasing function of the inflaton *vev*, inflation proceeds from the right to the left and occurs in the large field regime $\phi/M_{\rm Pl} \gg 1$. Defining the quantity x by

$$x \equiv \frac{\phi}{M_{\rm Pl}}, \tag{6.63}$$

the first three Hubble flow functions in the slow-roll approximation can be expressed as

$$\epsilon_1 = \frac{1}{2x^2}\left[\frac{p + \alpha\,(p+q)\,x^q}{1+\alpha x^q}\right]^2, \tag{6.64}$$

$$\epsilon_2 = \frac{2}{x^2}\frac{p + \alpha^2\,(p+q)\,x^{2q} + \alpha\left(2p + q - q^2\right)x^q}{\left(1+\alpha x^q\right)^2}, \tag{6.65}$$

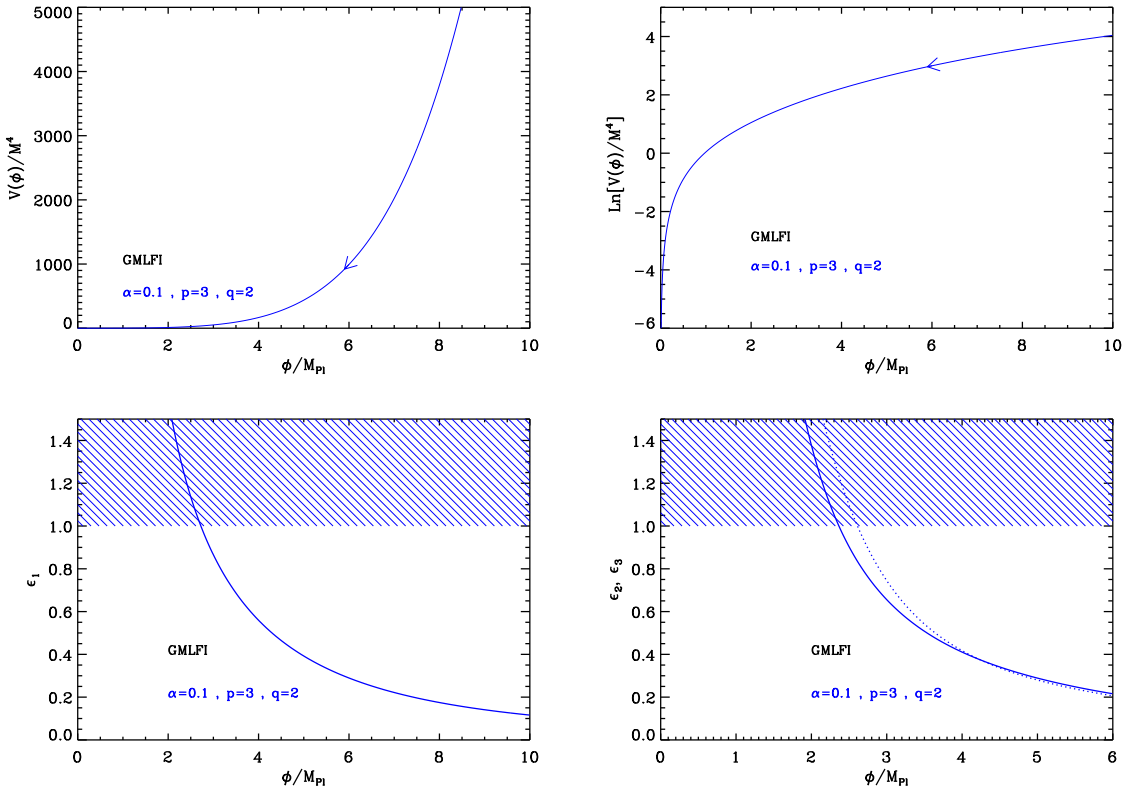

Figure 76. Generalized Mixed Inflation (GMLFI) for $p = 3, q = 2$ and $\alpha = 0.1$. Upper panels: the potential and its logarithm with respect the field value. Bottom left panel: slow-roll parameter ϵ_1, the shaded region is where inflation stops. Bottom right panel: slow-roll parameters ϵ_2 (solid line) and ϵ_3 (dotted line).

and

$$\epsilon_3 = \frac{1}{x^2\left(1+\alpha x^q\right)^2}\left[pq^2+\alpha^2q^2\left(p+q\right)x^{2q}+\alpha q^2\left(2p+q-q^2\right)x^q\right]^{-1}$$
$$\times\left\{2q^2\left[p^2+\alpha^4(p+q)^2\right]x^{4q}+\alpha^2q^2\left[12p^2+6pq\left(2-q\right)+\left(q-2\right)\left(q-1\right)q^2\right]x^{2q}\right. \tag{6.66}$$
$$\left.+\alpha^3q^3\left(p+q\right)\left[8\frac{p}{q}+\left(1-q\right)\left(4+q\right)\right]x^{3q}+\alpha pq^2\left[8p+q\left(4+q^2-3q\right)\right]x^q\right\}.$$

They are decreasing functions of the field, vanishing when $x \to \infty$ and diverging when $x \to 0$. Together with the potential and its logarithm, the Hubble flow functions are represented in Fig. 76.

In Fig. 76, one sees that inflation ends by slow-roll violation at $x = x_{\rm end}$, the solution of the equation $\epsilon_1(x_{\rm end}) = 1$. From Eq. (6.64), one obtains

$$\sqrt{2}\alpha x_{\rm end}^{q+1}+\sqrt{2}x_{\rm end} = \pm\left[p+\alpha\left(p+q\right)x_{\rm end}^q\right]. \tag{6.67}$$

One can check that, for $\alpha = 0$, one recovers the LFI-p result $x_{\rm end} = p/\sqrt{2}$ (see section 4.2) and that, for $\alpha \to \infty$, one gets $x_{\rm end} = (p+q)/\sqrt{2}$, which correspond again to the LFI-$p+q$

solution. The above equation cannot be solved analytically for arbitrary values of p, q. This is possible only in some particular cases, namely $q = 0$, $q = 1$ or $q = 2$. For $q = 0$, this is LFI whereas $q = 2$ corresponds to MLFI, both solutions being given in section 4.2 and section 4.3, respectively. For $q = 1$, one obtains

$$x_{\rm end} = \frac{\sqrt{2}}{4}(p+1) - \frac{1}{2\alpha} + \frac{\sqrt{4 + 4\sqrt{2}\alpha\,(p-1) + 2\alpha^2\,(p+1)^2}}{4\alpha}\,, \tag{6.68}$$

but, in general, $x_{\rm end}$ has to be determined numerically.

The slow-roll trajectory can be integrated explicitly using Eq. (2.11) and this leads to

$$\begin{aligned} N_{\rm end} - N = {} & \frac{1}{2\,(p+q)} x^2 \left\{ 1 + \frac{q}{p} {}_2F_1\left[1, \frac{2}{q}, 1+\frac{2}{q}, -\alpha q \left(\frac{1}{p}+\frac{1}{q}\right) x^q\right]\right\} \\ & - \frac{1}{2\,(p+q)} x_{\rm end}^2 \left\{ 1 + \frac{q}{p} {}_2F_1\left[1, \frac{2}{q}, 1+\frac{2}{q}, -\alpha q \left(\frac{1}{p}+\frac{1}{q}\right) x_{\rm end}^q\right]\right\}. \end{aligned} \tag{6.69}$$

Here, ${}_2F_1$ stands for the Gauss hypergeometric function [204, 205]. Since it is equal to unity when its last argument vanishes, one can check that, in the limit $\alpha \to 0$, one recovers the slow-roll trajectory for the LFI-p models while the limit $\alpha \to \infty$ leads to the trajectory of the LFI-$(p+q)$ models. Finally, since ${}_2F_1\,(1,1,2,x) = -\ln(1-x)/x$, one can also check that the MLFI case corresponds to $p = q = 2$. The previous expression can only be inverted for $q = 0$ (LFI) and $q = 2$ (MLFI), and they have been already discussed in section 4.2 and section 4.3, respectively. The case $q = 1$ can also be simplified using ${}_2F_1\,(1,2,3,x) = -2/x - 2\ln(1-x)/x^2$. In general, one has to inverse this slow-roll trajectory numerically.

The parameter M can be determined from the amplitude of the CMB anisotropies and the Hubble crossing *vev* x_*. One obtains

$$\frac{M^4}{M_{\rm Pl}^4} = 720\pi^2 \frac{\left[p + \alpha\,(p+q)\,x_*^q\right]^2}{x_*^{p+2}\,(1+\alpha x_*^q)^3} \frac{Q_{\rm rms-PS}^2}{T^2}\,. \tag{6.70}$$

The reheating consistent slow-roll predictions for the generalized mixed large field models are displayed in Figs 179, 180, and 181 for ($p = 2$ and $q = 1$), ($p = 2$ and $q = 3$) and ($p = 3$ and $q = 2$), respectively. As for MLFI, the predictions lie between the LFI-p and LFI-$(p+q)$ models, but can actually exit this region for large enough values of α. This means that, if one starts from a pure $V \propto \phi^{p+q}$ potential and adds a small $\propto \phi^p$ term, then this extra term has the effect of increasing the "effective value" of the power index of the potential. Moreover, since for large field inflation models, the p-model fits the data better than the $(p+q)$-one, it follows that small values for the parameter α are favored, together with high reheating temperatures.

6.5 Logarithmic Potential Inflation (LPI)

6.5.1 Theoretical Justifications

This class of model assumes that inflation is driven by a composite state in a strongly interacting theory, see Refs. [502, 585, 586]. Let us consider the following model, see section 5.14 for more details

$$\mathcal{L}_{\rm GI} = -\varphi^{-3/2}\partial_\mu\varphi\partial^\mu\varphi - \frac{\varphi}{2}\ln\left(\frac{\varphi}{\Lambda^4}\right), \tag{6.71}$$

where Λ is a mass scale. Moreover, let us consider the situation where the model has a general non-minimal coupling to gravity of the form

$$S = \int \mathrm{d}^4\boldsymbol{x}\sqrt{-g}\left[-\frac{1}{2}\left(M^2 + \xi\varphi^{1/2}\right)R + \mathcal{L}_{\mathrm{GI}}\right]. \tag{6.72}$$

The coupling to gravity is characterized by the parameter ξ. Then, the action in the Einstein frame reads [502, 585, 586]

$$S = \int \mathrm{d}^4\boldsymbol{x}\sqrt{-g}\left[-\frac{1}{2}M_{\mathrm{Pl}}^2 R - \Omega^{-2}\left(1 + \frac{3\xi^2\varphi^{1/2}}{4M_{\mathrm{Pl}}^2}\Omega^{-2}\right)\varphi^{-3/2}\partial_\mu\varphi\partial^\mu\varphi - \Omega^{-4}V_{\mathrm{GI}}\right], \tag{6.73}$$

where V_{GI} refers to the potential in Eq. (6.71) and $\Omega^2 = \left(M^2 + \xi\varphi^{1/2}\right)/M_{\mathrm{Pl}}^2$. If $\xi \neq 0$ and if we are in the large field limit, then $\Omega^2 \simeq \xi\varphi^{1/2}/M_{\mathrm{Pl}}^2$ and the canonically normalized field ϕ is such that $\phi \propto \ln\varphi$. In that case the potential reduces to $\Omega^{-4}V_{\mathrm{GI}} \propto \ln\varphi \propto \phi$. Therefore, we have obtained a LFI model with $p = 1$, see section 4.2. On the other hand, if one assumes that $\xi = 0$, then $\varphi = \phi^4/(4\sqrt{2})^4$ and

$$V = 2\Lambda^4\left(\frac{\phi}{\phi_0}\right)^4 \ln\left(\frac{\phi}{\phi_0}\right), \tag{6.74}$$

with $\phi_0 \equiv 4\sqrt{2}\Lambda$. This resembles the potential found in section 5.14 which, for $\beta = 0$ (see the precise definition in that section), was such that $V \propto \phi^4\ln^2(\phi/\phi_0)$. These considerations motivate the next section devoted to the slow-roll analysis of this class of scenarios.

6.5.2 Slow-Roll Analysis

Based on the previous discussion, we now turn to the slow-roll analysis of the models described by the following potential

$$V(\phi) = M^4\left(\frac{\phi}{\phi_0}\right)^p\left(\ln\frac{\phi}{\phi_0}\right)^q. \tag{6.75}$$

We have just seen that, for $p = 4$ and $q = 2$, the model discussed in Ref. [502] is recovered, see section 5.14, while for $p = 4$ and $q = 1$, this model matches with the so-called Glueball Inflation of Ref. [585]. This class of models has also been studied on general grounds in Ref. [587]. In the following, we keep p and q unspecified. Defining the quantity x by the following relation

$$x \equiv \frac{\phi}{\phi_0}, \tag{6.76}$$

the potential has a local maximum at $x = x_{V^{\max}}$ and a local minimum (at which the potential vanishes) at $x = x_{V=0}$ with

$$x_{V^{\max}} = e^{-q/p}, \qquad x_{V=0} = 1. \tag{6.77}$$

For $x > x_{V=0}$, $V(x)$ increases and finally diverge when x goes to infinity. The potential is always definite positive in the $x > 1$ branch, whereas it is definite positive in the $x < 1$ branch only if q is an even integer. The first three Hubble flow functions in the slow-roll approximation are given by

$$\epsilon_1 = \frac{M_{\mathrm{Pl}}^2}{\phi_0^2}\frac{(q + p\ln x)^2}{2x^2\ln^2 x}, \qquad \epsilon_2 = 2\frac{M_{\mathrm{Pl}}^2}{\phi_0^2}\frac{q + q\ln x + p\ln^2 x}{x^2\ln^2 x}, \tag{6.78}$$

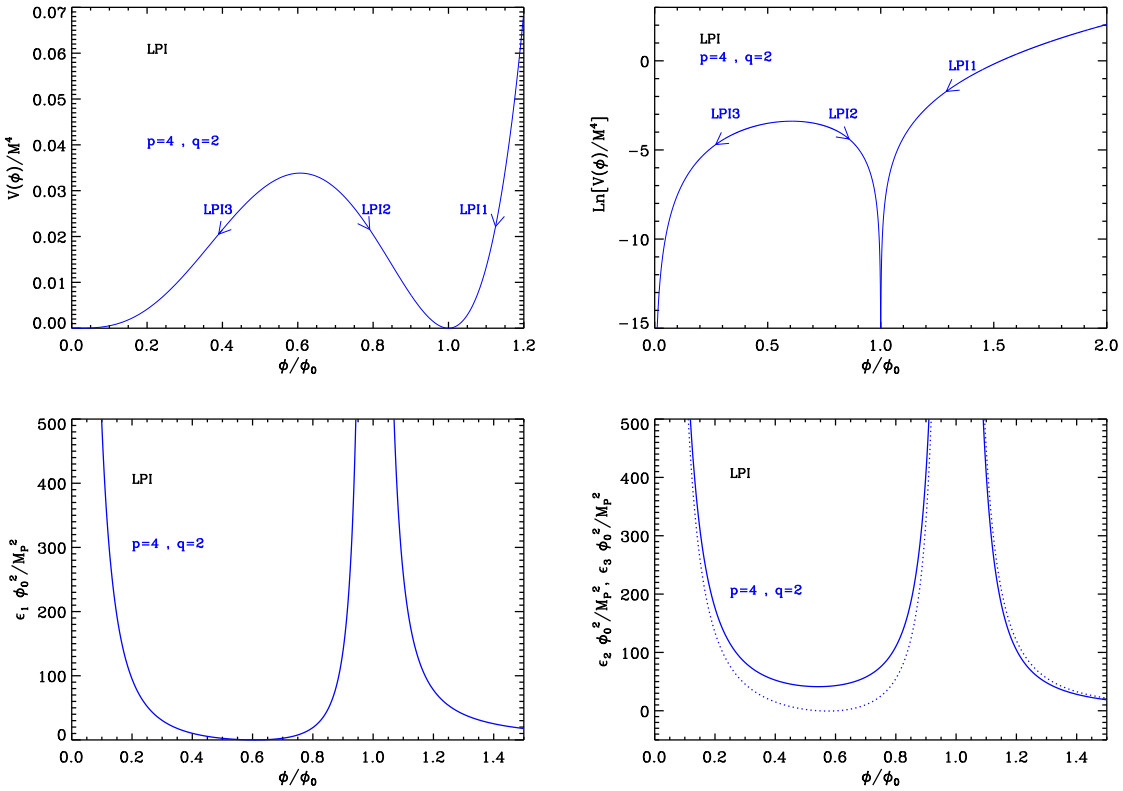

Figure 77. Logarithmic Potential Inflation (LPI) for $p = 4, q = 2$. Upper panels: the potential and its logarithm. Bottom left panel: slow-roll parameter ϵ_1. Bottom right panel: slow-roll parameters ϵ_2 (solid line) and ϵ_3 (dotted line).

and

$$\epsilon_3 = \frac{M_{\rm Pl}^2}{\phi_0^2}\,(q + p\ln x)\,\frac{2q + 3q\ln x + 2q\ln^2 x + 2p\ln^3 x}{x^2\ln^2 x\,(q + q\ln x + p\ln^2 x)}\,. \tag{6.79}$$

Together with the potential, they are displayed in Fig. 77.

As can be checked on this figure, and assuming q is even, the behavior of $\epsilon_1(x)$ exhibits three domains in which inflation can occur and can naturally end. Either $x > 1$ and inflation proceeds from the right to the left (LPI1), or $x_{V^{\max}} < x < 1$ and inflation proceeds from the left to the right (LPI2), or $0 < x < x_{V^{\max}}$ and inflation proceeds from the right to the left (LPI3), see the three arrows in Fig. 77. For these three cases, the slow-roll trajectory can be integrated analytically and one has

$$N - N_{\rm end} = \left(\frac{\phi_0}{M_{\rm Pl}}\right)^2 \left\{-\frac{x^2 - x_{\rm end}^2}{2p} + \frac{q}{p^2}e^{-2q/p}\left[{\rm Ei}\left(\frac{2q}{p} + 2\ln\,x\right) - {\rm Ei}\left(\frac{2q}{p} + 2\ln\,x_{\rm end}\right)\right]\right\}. \tag{6.80}$$

Let us remark that for $x \to +\infty$ (LPI1), one recovers the large field inflation (LFI) trajectory of section 4.2 with p becoming the same parameter of LFI.

In the three above described regimes, inflation ends at the field value $x_{\rm end}$ solution of

$\epsilon_1(x_{\rm end}) = 1$, i.e. verifying

$$p \ln(x_{\rm end}) + q \mp \sqrt{2}\frac{\phi_0}{M_{\rm Pl}} x_{\rm end} \ln x_{\rm end} = 0. \tag{6.81}$$

This is a transcendental equation that cannot be solved analytically for any values of p and q. It can nevertheless be solved numerically in each of the three above-mentioned situations. Together with Eq. (2.47), Eq. (6.80) uniquely determines the observable field value x_* at which the pivot scale crossed out the Hubble radius during inflation. Therefore, according to our classification, LPI is a three parameters model with p, q and ϕ_0.

Finally, the parameter M is fixed by the amplitude of the CMB anisotropies to

$$\frac{M^4}{M_{\rm Pl}^4} = 720\pi^2 \left(\frac{M_{\rm Pl}}{\phi_0}\right)^2 \frac{(q + p \ln x_*)^2}{x_*^{2+p} \ln^{2+q} x_*} \frac{Q_{\rm rms-PS}^2}{T^2}\,. \tag{6.82}$$

The reheating consistent slow-roll predictions for the LPI1 models with $p = 4$ are represented in Figs 182, 183, and 184 for $q = 2$, $q = 1$ and $q = 3$, respectively. The predictions for LPI2 are displayed in Figs 185, 186, and 187 for ($p = 1$, $q = 2$), ($p = 2$, $q = 2$) and ($p = 3$, $q = 4$), respectively. For the LPI3 scenario, the predictions have been plotted in Figs 188, 189, and 190 for ($p = 1$, $q = 2$), ($p = 2$, $q = 2$) and ($p = 3$, $q = 4$), respectively. One can see that the current CMB data generically require LPI inflation to take place with super-Planckian values for ϕ_0 while some combinations of p and q are already disfavored at more than two-sigma.

6.6 Constant $n_{\rm S}$ D Inflation (CNDI)

This model has been studied in Ref. [500]. Its potential is designed to produce a power law power spectrum $\propto k^n$ (where n is a constant). In this sense, the approach followed here is similar to the one investigated in sections 4.20, 4.21 and 5.15. The potential studied in this section is given by

$$V(\phi) = \frac{M^4}{\left\{1 + \beta \cos\left[\alpha\left(\dfrac{\phi - \phi_0}{M_{\rm Pl}}\right)\right]\right\}^2}\,, \tag{6.83}$$

where α and β are two dimensionless parameters. Since the potential is an even function of $x \equiv (\phi - \phi_0)/M_{\rm Pl}$ and is 2π-periodic, it can be studied without loss of generality in the range $x \in [0, \pi/\alpha]$ only (with $\alpha > 0$, $\beta > 0$). The potential and its logarithm are displayed in Fig. 78 (top panels) for two different representative values of β. If $\beta < 1$ (blue curve), it is an increasing function of the field, hence inflation proceeds from the right to the left. On the contrary, if $\beta \geq 1$ (pink curve), it diverges at $x_{V\to\infty} = \arccos(-1/\beta)/\alpha$. Then, for $x < x_{V\to\infty}$ it is an increasing function of x and inflation proceeds from the right to the left, whereas for $x > x_{V\to\infty}$ it is an decreasing function of x and inflation proceeds from the left to the right.

The three first slow-roll parameters are given by the following expressions

$$\epsilon_1 = \frac{2\alpha^2\beta^2 \sin^2(\alpha x)}{[1 + \beta\cos(\alpha x)]^2}\,, \qquad \epsilon_2 = \frac{-4\alpha^2\beta\,[\beta + \cos(\alpha x)]}{[1 + \beta\cos(\alpha x)]^2}\,, \tag{6.84}$$

and

$$\epsilon_3 = \frac{-2\alpha^2\beta\,[2\beta^2 - 1 + \beta\cos(\alpha x)]\sin^2(\alpha x)}{[\beta + \cos(\alpha x)]\,[1 + \beta\cos(\alpha x)]^2}\,. \tag{6.85}$$

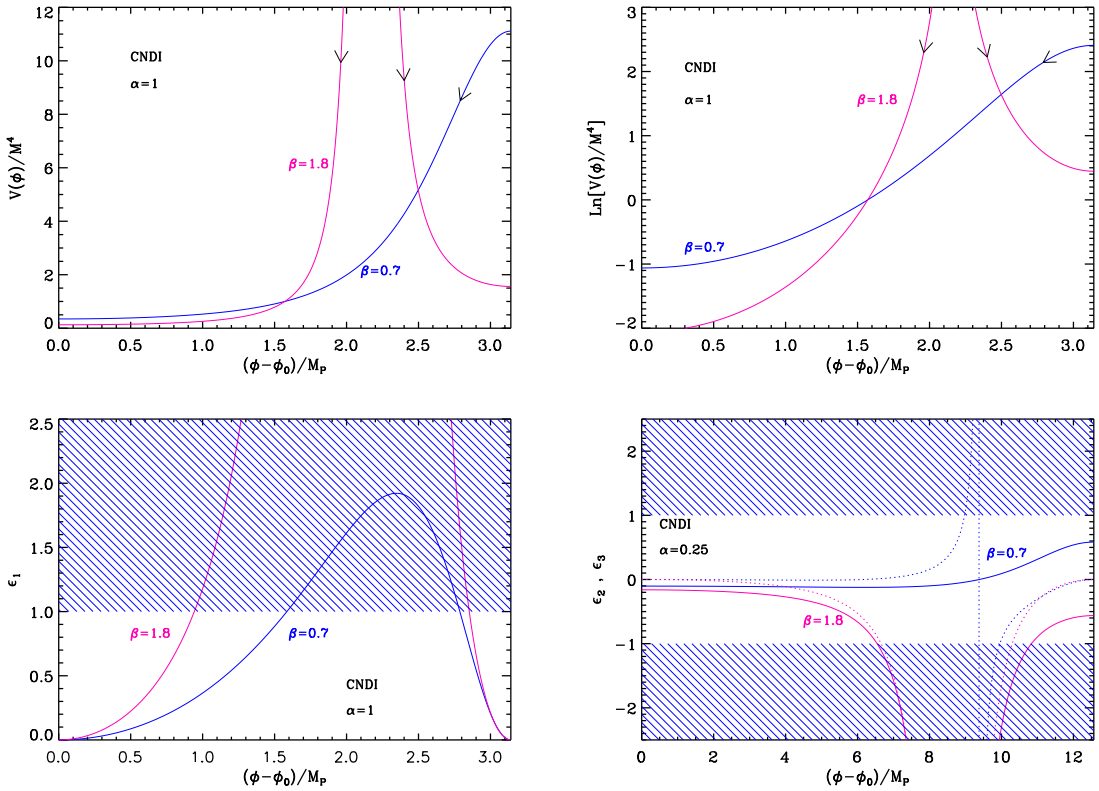

Figure 78. Top left panel: constant $n_{\rm S}$ D inflaton potential for $\alpha = 1$ and two values of β, namely $\beta = 0.7$ (solid blue line) and $\beta = 1.3$ (solid pink line). Top right panel: logarithm of the potential for the same values of α and β and with the same color code. Bottom left panel: first slow-roll parameter ϵ_1 for a potential with $\alpha = 1$ and $\beta = 0.7$ (solid blue line), $\beta = 1.8$ (solid pink line). The shaded area indicates the breakdown of slow-roll inflation (strictly speaking where acceleration cannot occur). Bottom right panel: second and third slow-roll parameters ϵ_2 and ϵ_3 for $\alpha = 0.25$ and the same values of β as in the other plots.

They are displayed in Fig. 78 (bottom panels). Let us now study in more detail the behavior of ϵ_1 and ϵ_2. It depends on whether β is larger or smaller than 1. If $\beta < 1$, the first slow-roll parameter ϵ_1 vanishes at $x = 0$ and $x = \pi/\alpha$, and reaches a maximum in between at $x_{\epsilon_2=0}$. This maximum is larger than one provided $\alpha > \alpha_{\rm min}\,(\beta)$, where

$$\alpha_{\rm min}\,(\beta) = \sqrt{\frac{1-\beta^2}{2\beta^2}}\,. \tag{6.86}$$

In that case, inflation can stop by slow-roll violation, at the position $x_{\rm end}$ given by

$$x_{\rm end} = x^+_{\epsilon_1=1} = \frac{1}{\alpha}\arccos\left[\frac{\alpha\sqrt{2\beta^2\left(1+2\alpha^2\right)-2}-1}{\beta+2\alpha^2\beta}\right], \tag{6.87}$$

and proceeds in the range $[x_{\rm end}, \pi/\alpha]$ (from the right to the left). On the other hand, the second slow-roll parameter ϵ_2 is a monotonous increasing function of x, which vanishes at $x_{\epsilon_2=0} = \arccos\left(-\beta\right)/\alpha$. If $\beta \geq 1$, as can be seen in Fig. 78, the first slow-roll parameter ϵ_1

diverges at $x_{V\to\infty} = \arccos(-1/\beta)/\alpha$, so that inflation cannot stop by slow-roll violation in that case. This means that inflation must end by another mechanism and, therefore, that the model depends on an additional parameter. The second slow-roll parameter ϵ_2 is always negative and also diverges at $x_{V\to\infty}$. Let us notice that, for $\beta < 1$ and $\alpha > \alpha_{\rm min}(\beta)$, and for $\beta > 1$ (for any α), we will need below the other solution of $\epsilon_1 = 1$, namely

$$x^{-}_{\epsilon_1=1} = \frac{1}{\alpha}\arccos\left[-\frac{\alpha\sqrt{2\beta^2\left(1+2\alpha^2\right)-2}+1}{\beta+2\alpha^2\beta}\right]. \tag{6.88}$$

We are now in a position where the slow-roll trajectory can be determined. It turns out that this one can be integrated analytically and reads

$$N-N_{\rm end} = \frac{1}{2\alpha^2}\left\{-\ln\left[\sin\left(\alpha x\right)\right] - \frac{1}{\beta}\ln\left[\tan\left(\alpha\frac{x}{2}\right)\right] + \ln\left[\sin\left(\alpha x_{\rm end}\right)\right] + \frac{1}{\beta}\ln\left[\tan\left(\alpha\frac{x_{\rm end}}{2}\right)\right]\right\}. \tag{6.89}$$

Because of the logarithmic functions, a sufficient number of e-folds can be realized only if the initial conditions are fine-tuned and $x_{\rm ini}$ is chosen to be extremely close to π/α.

Indeed, inserting Eq. (6.87) into Eq. (6.89), the total number of e-folds during inflation becomes a function of $x_{\rm ini}$ and of the two parameters α and β. For given values of those parameters, one can check that $(N_{\rm end} - N_{\rm ini})(x_{\rm ini})$ remains always small compared to unity, unless $x_{\rm ini} \to \pi/\alpha$ where it blows up. Let us write $x_{\rm ini}$ as $\pi/\alpha + \delta x_{\rm ini}$ with $\delta x_{\rm ini} \ll 1$ and defining $A \equiv \ln\left[\sin\left(\alpha x_{\rm end}\right)\right] + \ln\left[\tan\left(\alpha x_{\rm end}/2\right)\right]/\beta$, one arrives at

$$\delta x_{\rm ini} \simeq \left[\alpha\left(\frac{\alpha}{2}\right)^{-1/\beta} e^{-A}\right]^{\beta/(1-\beta)} e^{-2\alpha^2\beta(N_{\rm end}-N_{\rm ini})/(1-\beta)}. \tag{6.90}$$

The coefficient between the squared brackets only depends on α and β which are, a priori, coefficients of order one. On the other hand, the argument of the exponential is $2(N_{\rm end} - N_{\rm ini}) > 120$, times a negative term of order one. This means that $\delta x_{\rm ini}$ must be exponentially small to obtain a significant number of e-folds and one can question the physical relevance of such a fine-tuning. The typical predictions of the model (taking $x_* \simeq \pi/\alpha$) actually are $\epsilon_1 \simeq 0$, $\epsilon_2 \simeq 4\alpha^2\beta/(1-\beta)$, and $\epsilon_3 \simeq 0$. It follows that the condition $\alpha > \alpha_{\rm min}(\beta)$ implies $\epsilon_2 > 2(1+\beta)/\beta > 4$, which is is completely ruled out by the observations. Therefore, we conclude that the case $\beta < 1$ is not of cosmological interest.

The only remaining possibility is $\beta > 1$. Inflation cannot end by slow-roll violation and $x_{\rm end}$ is an additional parameter, making the model a three parameters one. In the range $\alpha x_{\rm end} \ll 1$, one has $\epsilon_1 \ll 1$ and $\epsilon_2 \simeq -4\alpha^2\beta/(1+\beta)$ such that the spectral index is given by $n_{\rm S} \simeq 1 + 4\alpha^2\beta/(\beta+1)$. Therefore, it is indeed a constant.

The CMB normalization gives the mass scale M as

$$\left(\frac{M}{M_{\rm Pl}}\right)^4 = 2880\alpha^2\beta^2\pi^2\sin^2\left(\alpha x_*\right)\frac{Q^2_{\rm rms-PS}}{T^2}, \tag{6.91}$$

which has to be numerically evaluated when if αx_* is not small. The predictions of CNDI inflation are displayed in Figs. 191 and 192. We see that, in the regime $\alpha x_{\rm end} \ll 1$, the spectral index is constant, as expected. However, this occurs in a regime where the predictions are not consistent with the observations (the spectrum is too blue). On the other hand, when $\alpha x_{\rm end}$ is no longer small, we observe strong deviations from $n_{\rm S} \simeq 1 + 4\alpha^2\beta/(\beta+1)$ but, for intermediate values of $\alpha \simeq 0.3$, this renders the predictions compatible with the data. Obviously, these considerations bear some resemblance with the findings of sections 4.20, 4.21 and 5.15.

7 Conclusions

Let us very briefly recap our main findings and present some directions for future works.

In this article, we have discussed the question of how the inflationary theory can be constrained given that we now have at our disposal high accuracy cosmological data. We have argued that this can be done by means of the slow-roll approximation which has the advantage of being relatively model independent. Although this approximation cannot be used if one has to deal with more complicated models, it produces interesting but limited information on inflation. Concretely, it leads to the Hubble flow posterior distributions $P\left(\epsilon_n|C_\ell^{\mathrm{meas}}\right)$. This is interesting since it gives a general constraint on the derivatives of the inflaton potential. But, at the same time, this does not answer some legitimate fundamental questions one might have about the plethora of inflationary scenarios studied so far. For instance, it does not tell us rigorously which constraints exist on the parameters of a given model. Indeed, suppose that we are interested in LFI, $V(\phi) \propto \phi^p$. It is obvious that we would like to know for which values of p this class of models is compatible with the data and for which values it is not.

In order to complement the slow-roll approximation and to address the above mentioned issues, we have argued that it is interesting to scan the inflationary landscape model by model and have provided the public code `ASPIC` to do so. Such a strategy has to be done for all the inflationary scenarios since it would be arbitrary to consider only a restricted class while ignoring the others. In fact, this question deserves to be discussed in more detail. One could indeed imagine that it is not necessary to consider all the models one by one and that considering a representative for each class is sufficient. Indeed, to simplify the discussion, it is common to distinguish three broad types of scenarios: large field models (LFI), small field models (SFI) and Hybrid models (VHI). Such a classification is not very precise and biased because it pushes to the front line these three models. It could be reasonably argued that a better classification is the one of Schwarz and Terrero-Escalante introduced in Ref. [588]. For a scalar field, the ratio of the kinetic energy to the total energy density is given by $\epsilon_1/3 = \dot{\phi}^2/(2\rho)$. Because ϵ_2 is, by definition, the logarithmic derivative of ϵ_1 with respect to the e-fold number, the kinetic contribution to the total energy density increases if $\epsilon_2 > 0$ and decreases if $\epsilon_2 < 0$. On the other hand, we also have

$$\frac{\mathrm{d}(\dot{\phi}^2/2)}{\mathrm{d}t} = H\frac{\dot{\phi}^2}{2}\left(\epsilon_2 - 2\epsilon_1\right), \tag{7.1}$$

and, therefore, the absolute value of the kinetic energy increases if $\epsilon_2 > 2\epsilon_1$ whereas it decreases if $\epsilon_2 < 2\epsilon_1$. This allows us to identify three different regions: $\epsilon_2 > 0$ and $2\epsilon_1 < \epsilon_2$ (region 1), $\epsilon_2 < 2\epsilon_1$ (region 2), $\epsilon_2 < 0 < 2\epsilon_1$ (region 3).

These three regions are identified in Fig. 79 together with Planck and WMAP9 bounds[8]. If we use the first order slow-roll expressions, the condition $\epsilon_2 > 0$ is equivalent to $r < 8(1-n_{\mathrm{S}})$ while $\epsilon_2 > 2\epsilon_1$ amounts to $r < 4(1-n_{\mathrm{S}})$. These two lines are also represented in Fig. 79 (solid black lines). We have also superimposed the predictions of LFI, SFI and VHI (upper panel). We see that the three regions defined above roughly correspond to the cases large field, small field and hybrid. However, the correspondence is not perfect and we notice, for instance, that the predictions of VHI can penetrate region 2.

[8]The slight shift visible on the one- and two-sigma contours between the two plots come from the different priors used, either flat on ϵ_1 or flat on $\log\epsilon_1$ (Jeffreys' prior).

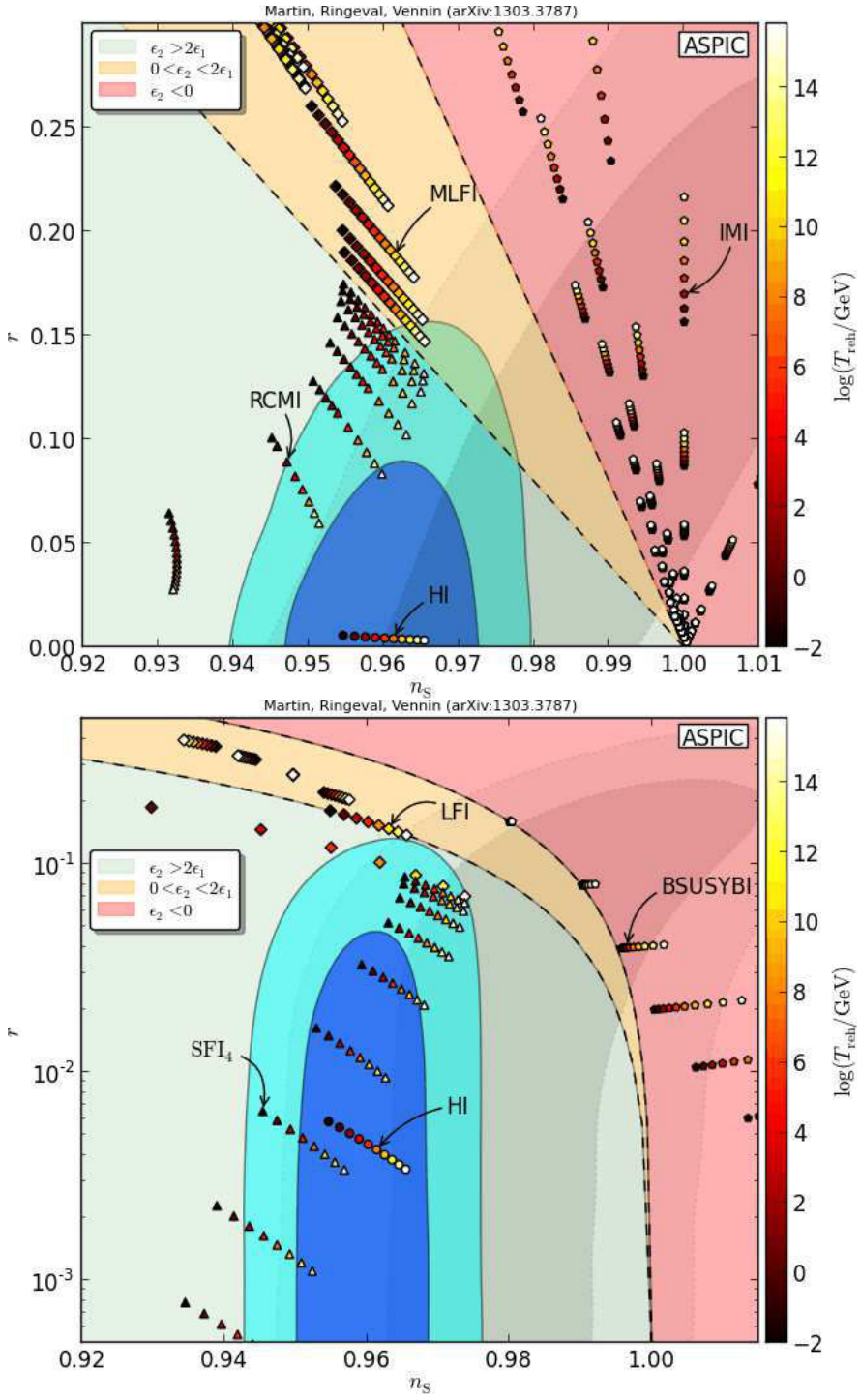

Figure 79. Upper panel: various `ASPIC` scenarios in the (n_S, r) plane using the Schwarz-Terrero-Escalante classification [588] and compared to the Planck data [66, 69, 70, 133, 134, 153] (blue contours) and the WMAP9 data [67, 68] (light gray shading). Bottom panel: same plot in logarithmic scale for another sample of models.

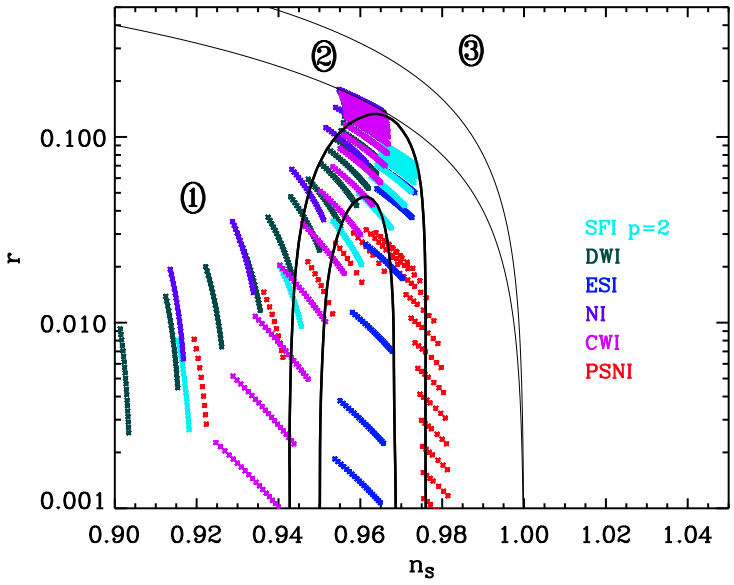

Figure 80. Observable predictions in the (n_S, r) plane for various models belonging to region 1 of the Schwarz-Terrero-Escalante classification (see Fig. 79). Despite the fact that they are in the same broad class, the accuracy of the CMB data allows us to discriminate among them thereby justifying a detailed navigation within the inflationary landscape.

Having identified three broad classes of scenarios, the question is whether testing only a representative model for each class could be sufficient. In Fig. 80, we have considered the predictions of six different models that all belong to region 1. This plot clearly shows that inside this region, these six models span different domains that are separated enough to be distinguishable within current and future data. Given the quality of the current data, working only with broad classes of models seems to be no longer justified. Therefore, if one really wants to scan the inflationary landscape, the approach advocated in this paper is well-suited.

With `ASPIC`, we have provided a new tool to treat any model of inflation and this has led us to derive observational predictions for 74 models. `ASPIC` is an evolutive project and therefore the next steps will be to complete and upgrade it with new models. Finally, the ultimate goal is to identify which `ASPIC` model is performing the best for explaining cosmological data. In order to carry out this task, an appropriate method is to use Bayesian evidence and model comparison. Then, we should be able to identify, in a statistically well-defined manner, what might be called "the best model of inflation".

A Reheating consistent slow-roll predictions

A.1 Higgs Inflation (HI)

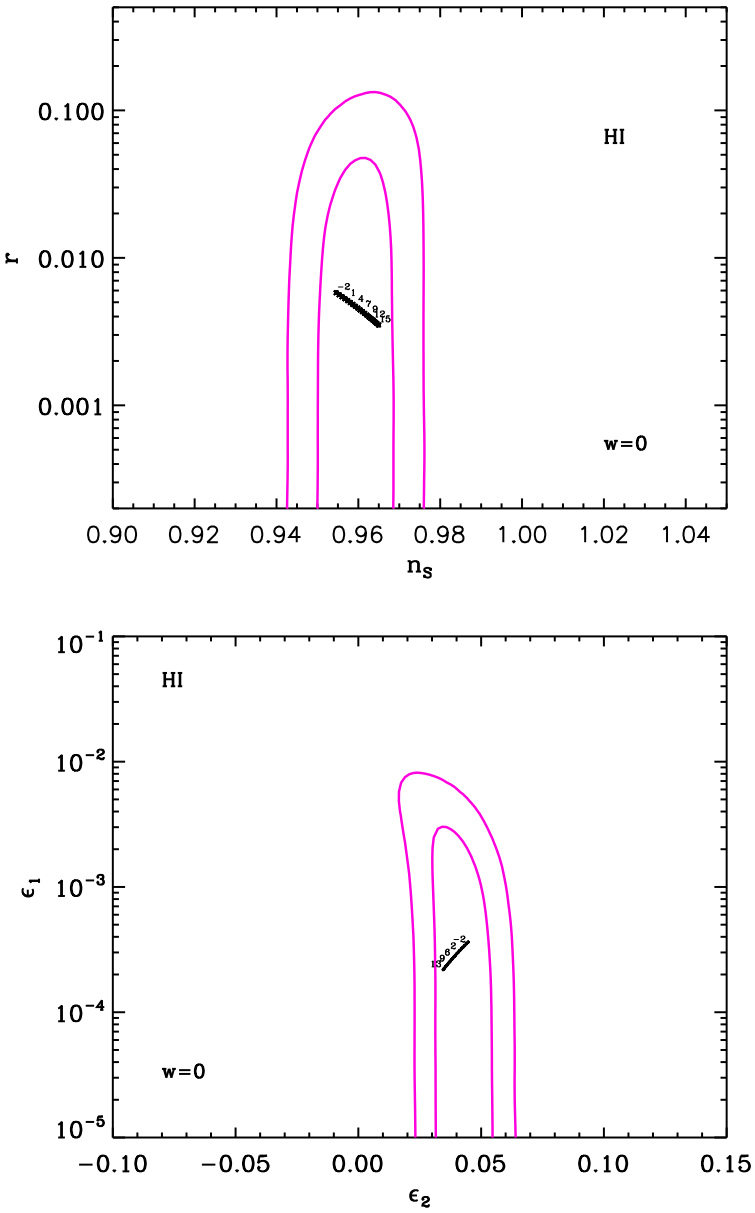

Figure 81. Reheating consistent slow-roll predictions for the Higgs model in the plane $(n_{\rm S}, r)$ (top panel) and the plane (ϵ_1, ϵ_2) (bottom panel). The two pink solid contours are the one and two-sigma Planck confidence intervals (marginalized over second order slow-roll). The annotations trace the energy scale at which the large field reheating ends and correspond to $\log(g_*^{1/4} T_{\rm reh}/{\rm GeV})$.

A.2 Radiatively Corrected Higgs Inflation (RCHI)

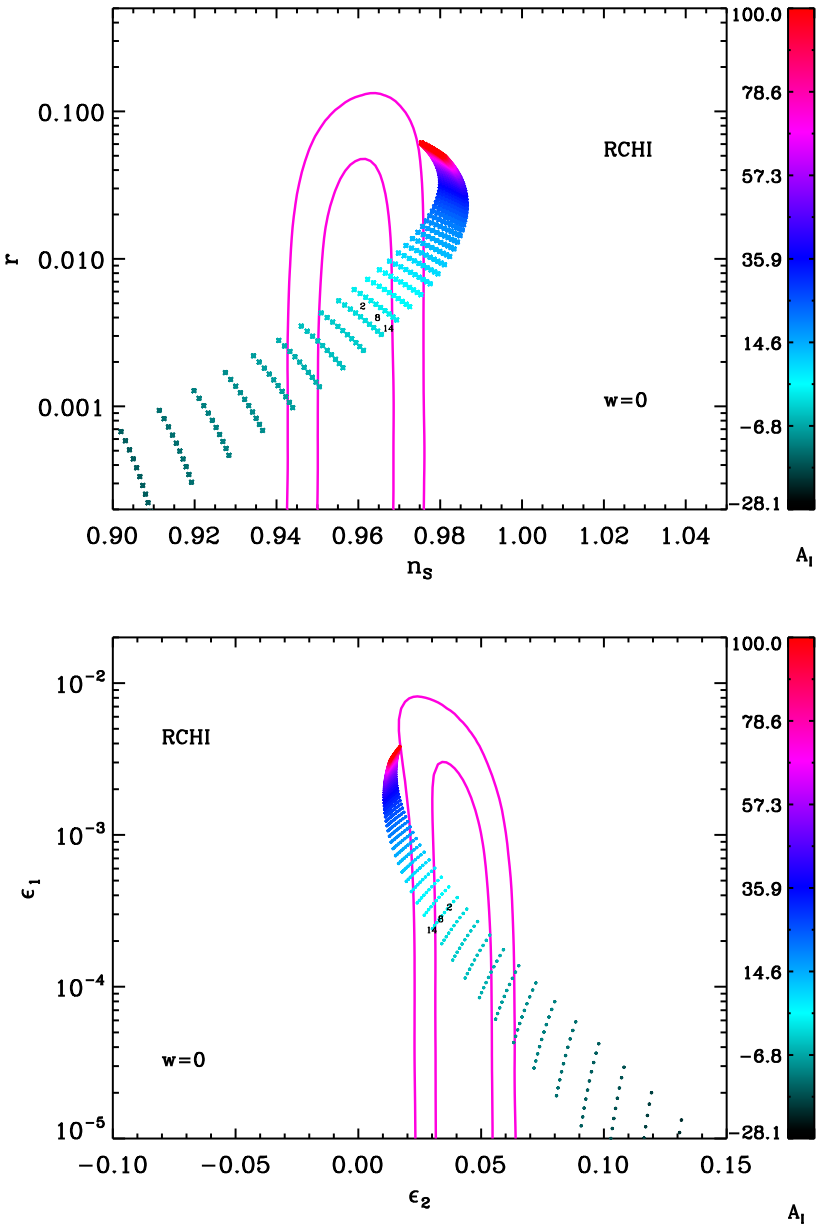

Figure 82. Reheating consistent slow-roll predictions for the radiatively corrected Higgs model in the plane $(n_{\rm s}, r)$ (top panel) and the plane (ϵ_1, ϵ_2) (bottom panel). The two pink solid contours are the one and two-sigma Planck confidence intervals (marginalized over second order slow-roll). The annotations trace the energy scale at which the large field reheating ends and correspond to $\log(g_*^{1/4} T_{\rm reh}/{\rm GeV})$.

A.3 Large Field Inflation (LFI)

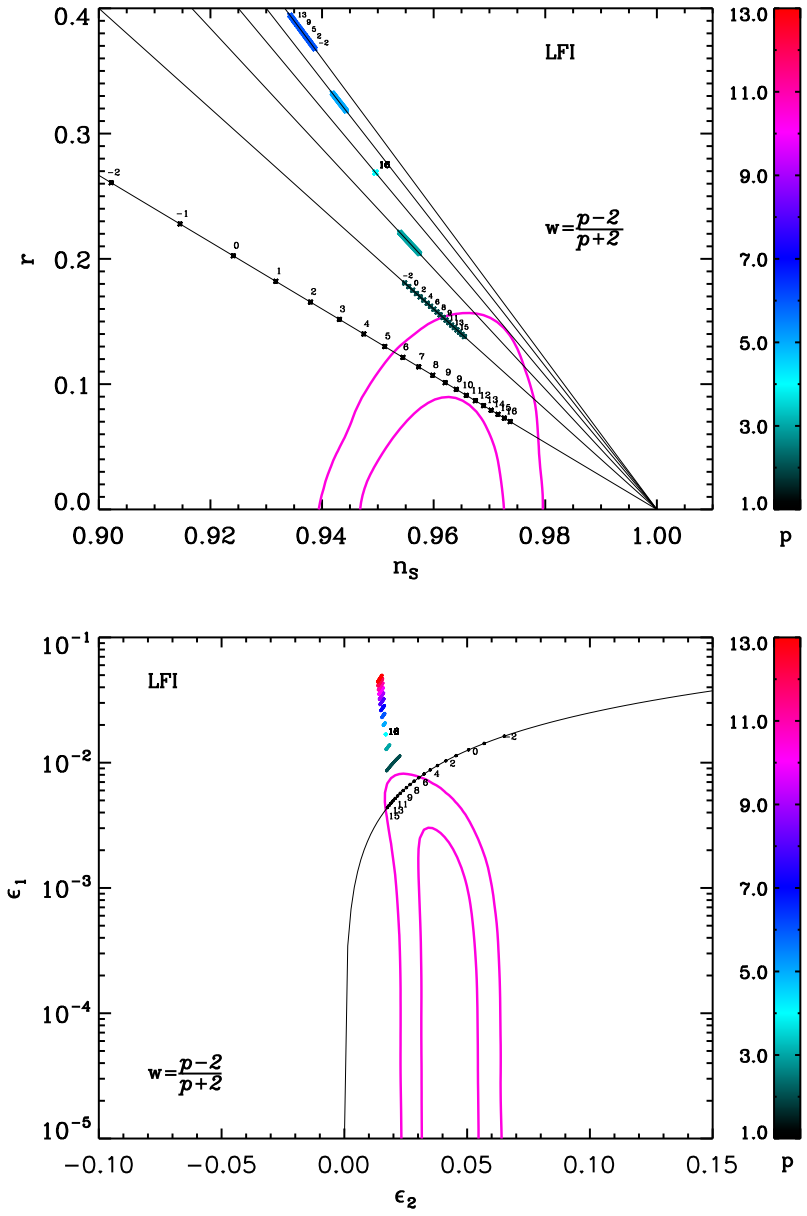

Figure 83. Reheating consistent slow-roll predictions for the large field models in the plane $(n_{\rm S}, r)$ (top panel) and the plane (ϵ_1, ϵ_2) (bottom panel). The two pink solid contours are the one and two-sigma Planck confidence intervals (marginalized over second order slow-roll). The black solid lines represent the locus of different LFI-p models [for which $(1+2/p)\,r = 8\,(1-n_{\rm S})$, i.e. $\epsilon_1 = (p/4)\epsilon_2$]. The annotations trace the energy scale at which the large field reheating ends and correspond to $\log(g_*^{1/4} T_{\rm reh}/{\rm GeV})$. Large reheating temperatures are preferred and models with $p > 2$ are disfavored at two sigma confidence level.

A.4 Mixed Large Field Inflation (MLFI)

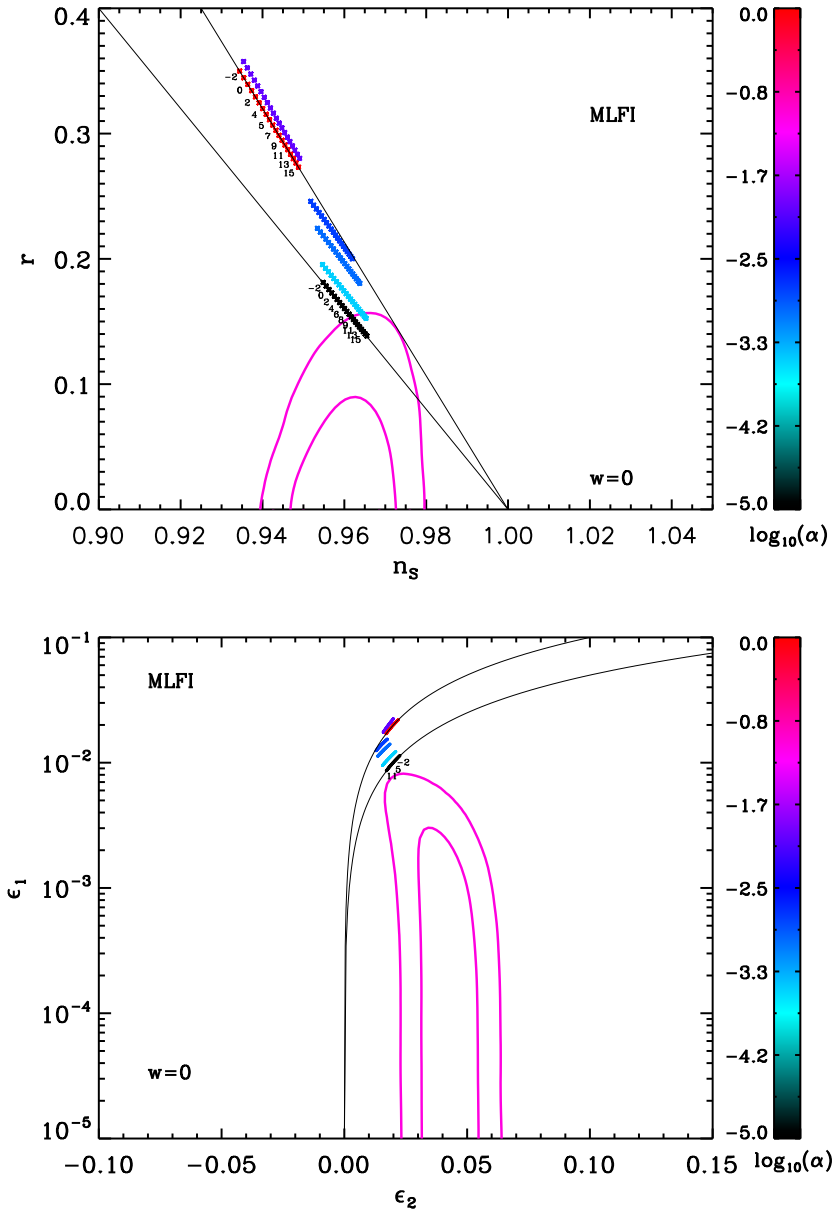

Figure 84. Reheating consistent slow-roll predictions for the mixed large field models in the plane $(n_{\rm S}, r)$ (top panel) and the plane (ϵ_1, ϵ_2) (bottom panel). The two pink solid contours are the one and two-sigma Planck confidence intervals (marginalized over second order slow-roll). The reheating equation of state parameter $\overline{w}_{\rm reh}$ has been taken to 0 since the potential is quadratic close to its minimum. The black solid lines represent the locus of the quadratic model (namely LFI with $p = 2$) and of the quartic model (namely LFI with $p = 4$) [for which $(1 + 2/p)\, r = 8\,(1 - n_{\rm S})$, i.e. $\epsilon_1 = (p/4)\epsilon_2$]. The annotations trace the energy scale at which the mixed large field reheating ends and correspond to $\log(g_*^{1/4} T_{\rm reh}/{\rm GeV})$. Clearly, these values are limited from below to stay inside the two-sigma contours and models with $\alpha > 10^{-3}$ are excluded at two-sigma confidence level.

A.5 Radiatively Corrected Massive Inflation (RCMI)

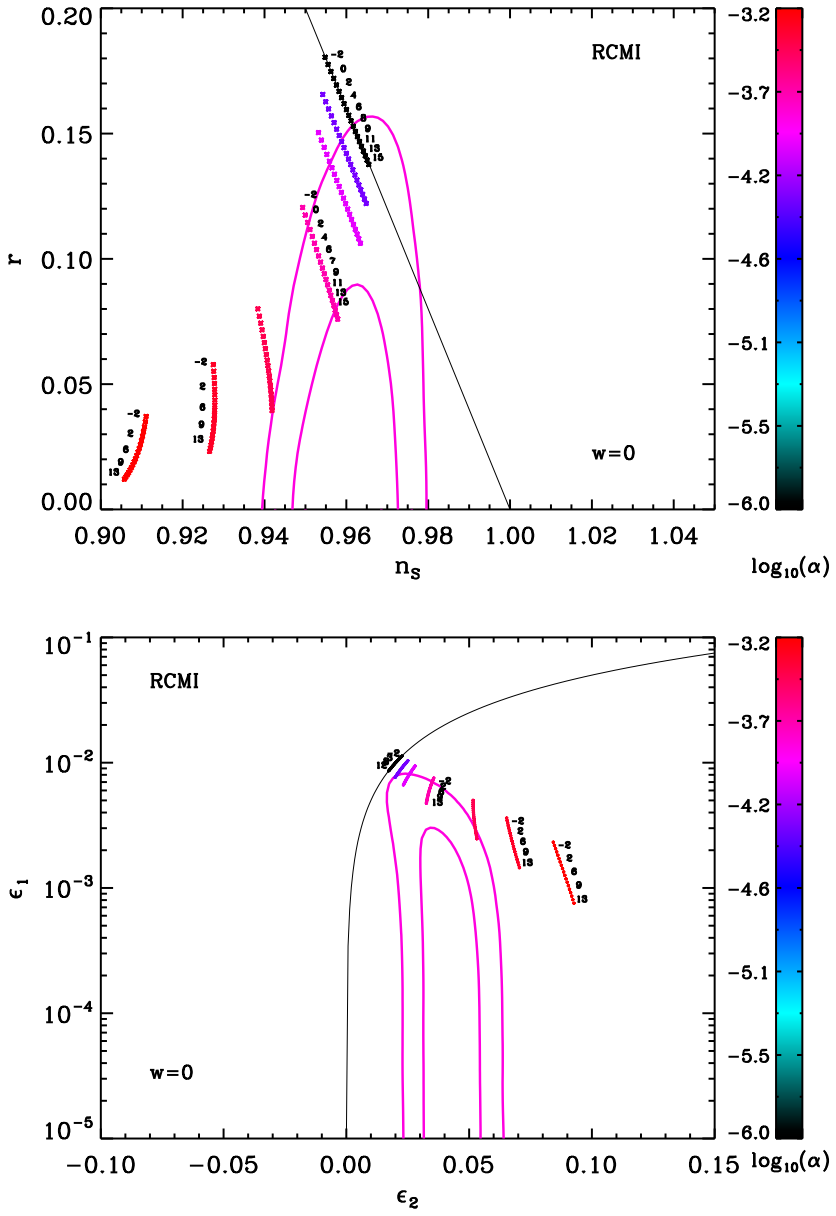

Figure 85. Reheating consistent slow-roll predictions for the radiatively corrected massive models in the plane $(n_{\rm S}, r)$. The two pink solid contours are the one and two-sigma Planck confidence intervals (marginalized over second order slow-roll). The black solid line represent the locus of the quadratic model [i.e. LFI with $p = 2$, for which $r = 4\,(1 - n_{\rm S})$, i.e. $\epsilon_1 = \epsilon_2/2$]. The annotations trace the energy scale at which the radiatively corrected massive reheating ends and correspond to $\log(g_*^{1/4} T_{\rm reh}/{\rm GeV})$. Clearly, these values are limited from below to stay inside the two-sigma contours and models with $\alpha > 10^{-3.5}$ are disfavored at two sigma confidence level.

A.6 Radiatively Corrected Quartic Inflation (RCQI)

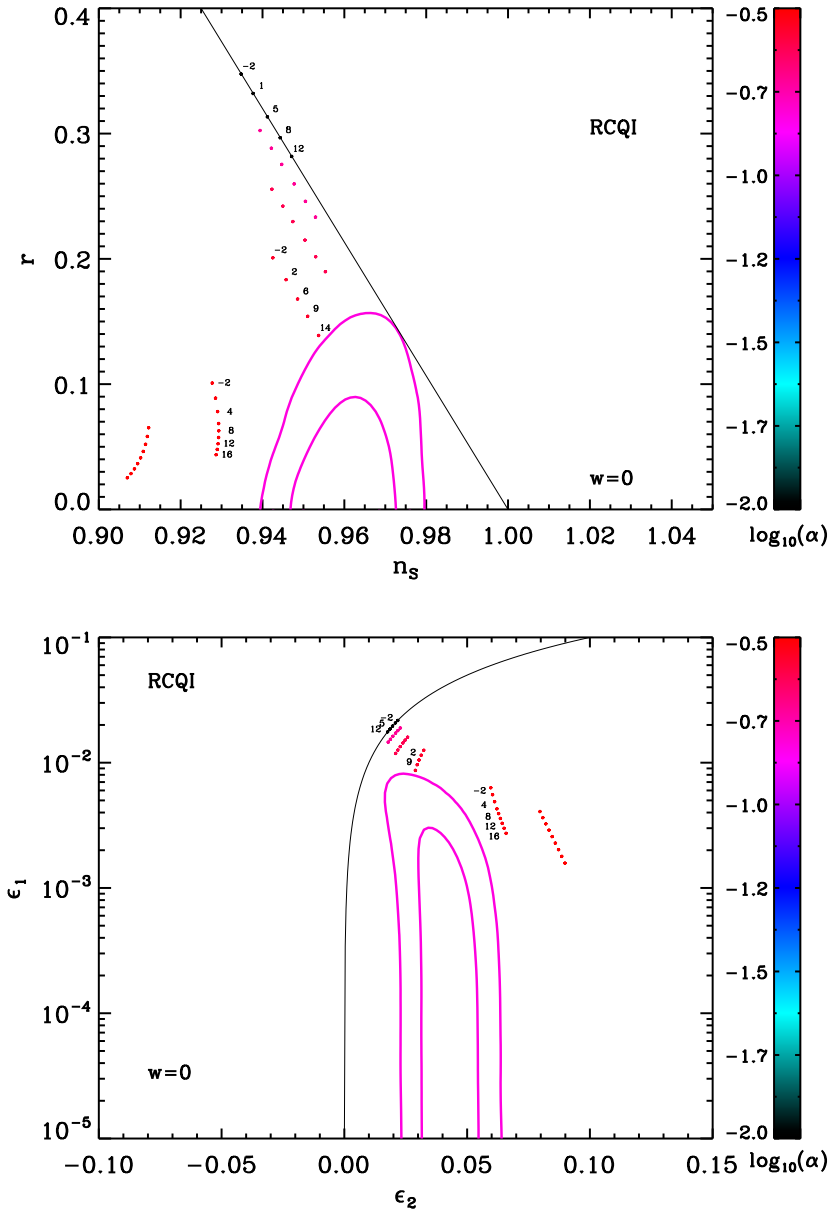

Figure 86. Reheating consistent slow-roll predictions for the radiatively corrected quartic models in the plane $(n_{\rm S}, r)$ (top panel) and the plane (ϵ_1, ϵ_2) (bottom panel), with $\overline{w}_{\rm reh} = 0$. The two pink solid contours are the one and two-sigma Planck confidence intervals (marginalized over second order slow-roll). The black solid line represent the locus of the quartic model [i.e. LFI with $p = 4$, for which $r = (16/3)\,(1 - n_{\rm S})$, i.e. $\epsilon_1 = \epsilon_2$]. The annotations trace the energy scale at which the radiatively corrected quartic reheating ends and correspond to $\log(g_*^{1/4} T_{\rm reh}/{\rm GeV})$. Clearly, these values are limited from below, and regardless of them, these models seem to be disfavored at two sigma confidence level.

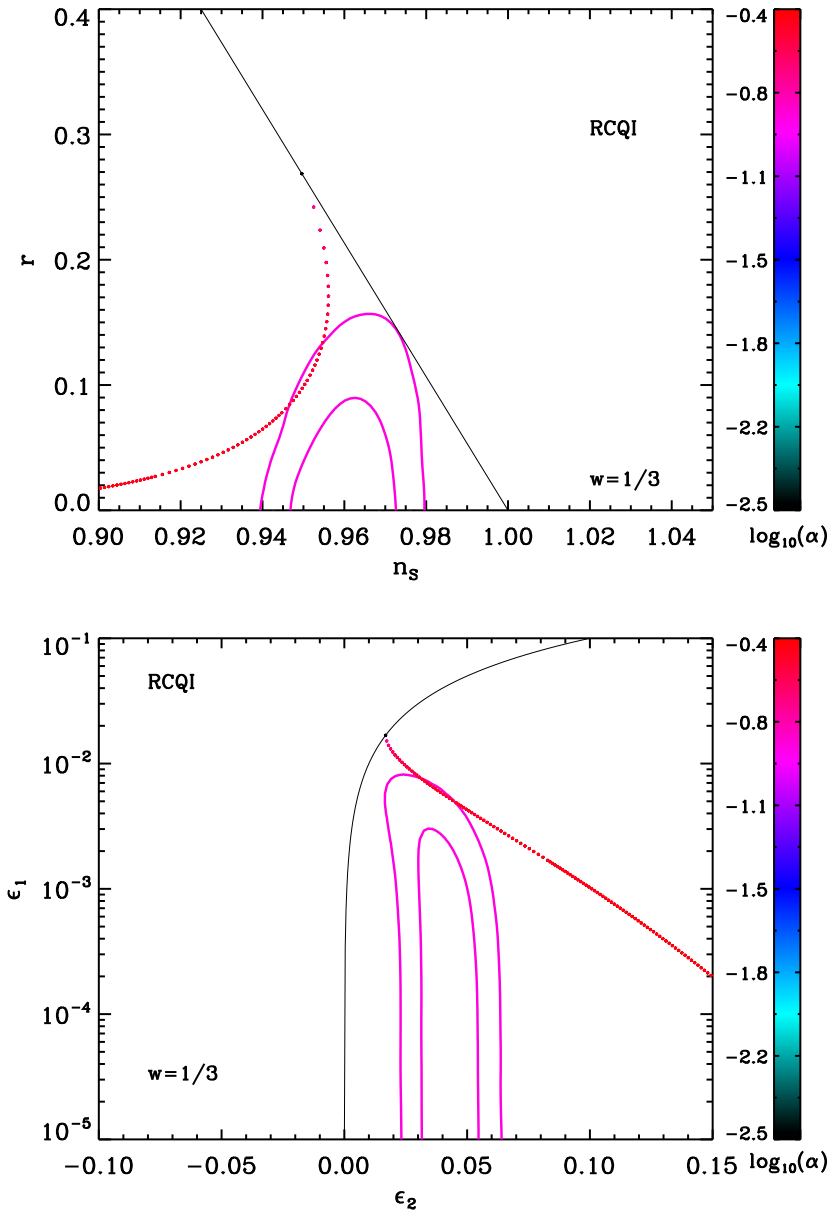

Figure 87. Reheating consistent slow-roll predictions for the radiatively corrected quartic models in the plane $(n_{\rm S}, r)$ (top panel) and the plane (ϵ_1, ϵ_2) (bottom panel), with $\overline{w}_{\rm reh} = \frac{1}{3}$. This value of $\overline{w}_{\rm reh}$ may be more physically justified if the reheating phase takes place at the bottom of the potential, which is quartic in a good approximation, and for which one has $\overline{w}_{\rm reh} = 1/3$. The two pink solid contours are the one and two-sigma Planck confidence intervals (marginalized over second order slow-roll). The black solid line represent the locus of the quartic model [i.e. LFI with $p = 4$, for which $r = (16/3)\,(1 - n_{\rm S})$, i.e. $\epsilon_1 = \epsilon_2$]. Clearly, these models are disfavored at two sigma confidence level.

A.7 Natural Inflation (NI)

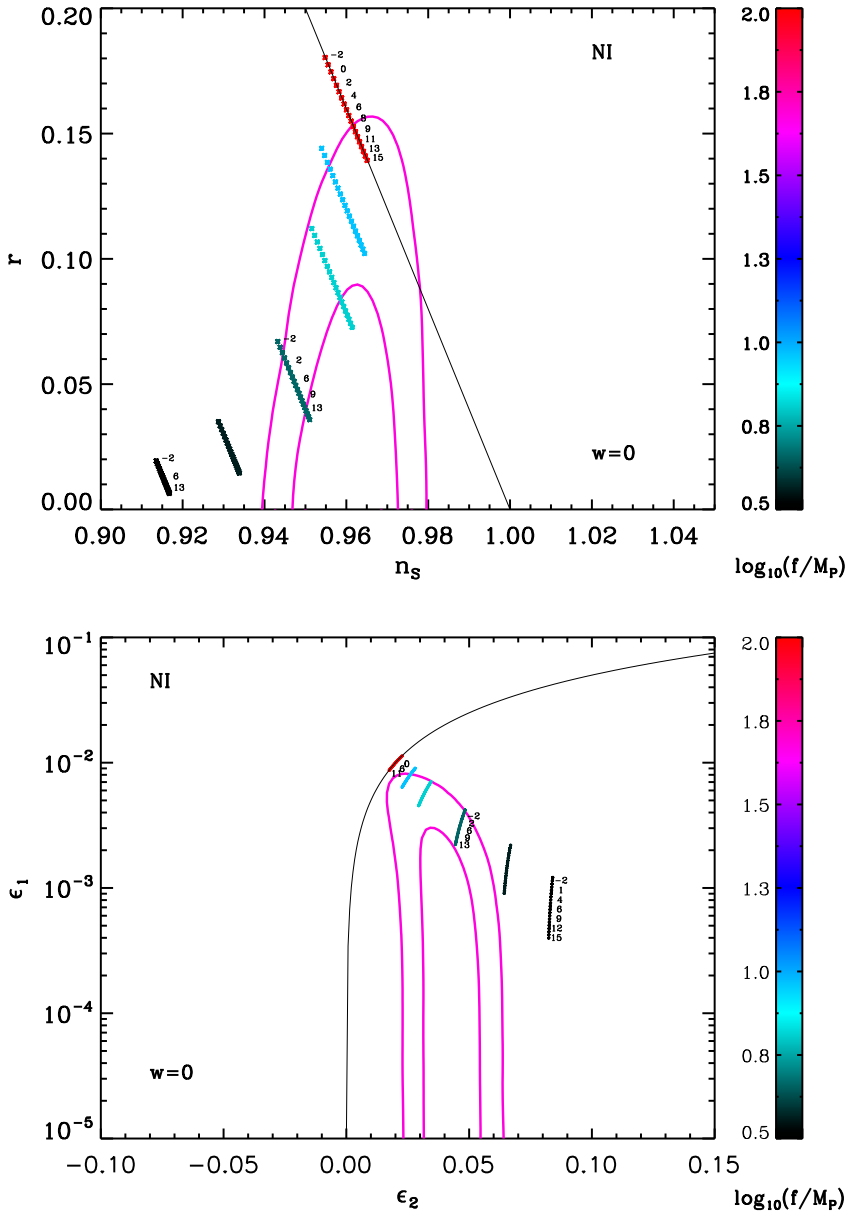

Figure 88. Reheating consistent slow-roll predictions for the natural inflation models in the plane $(n_{\rm S}, r)$ (top panel) and the plane (ϵ_1, ϵ_2) (bottom panel). The two pink solid contours are the one and two-sigma Planck confidence intervals (marginalized over second order slow-roll). The reheating equation of state parameter $\overline{w}_{\rm reh}$ has been taken to 0 since the potential is quadratic close to its minimum. The black solid line represent the locus of the quadratic model points [i.e. LFI with $p = 2$, for which $r = 4\,(1 - n_{\rm S})$, i.e. $\epsilon_1 = \epsilon_2/2$]. The annotations trace the energy scale at which the natural reheating ends and correspond to $\log(g_*^{1/4} T_{\rm reh}/{\rm GeV})$. Clearly, high values of $f/M_{\rm Pl}$ seem to be favored by the data, as well as high reheating temperatures.

A.8 Exponential SUSY Inflation (ESI)

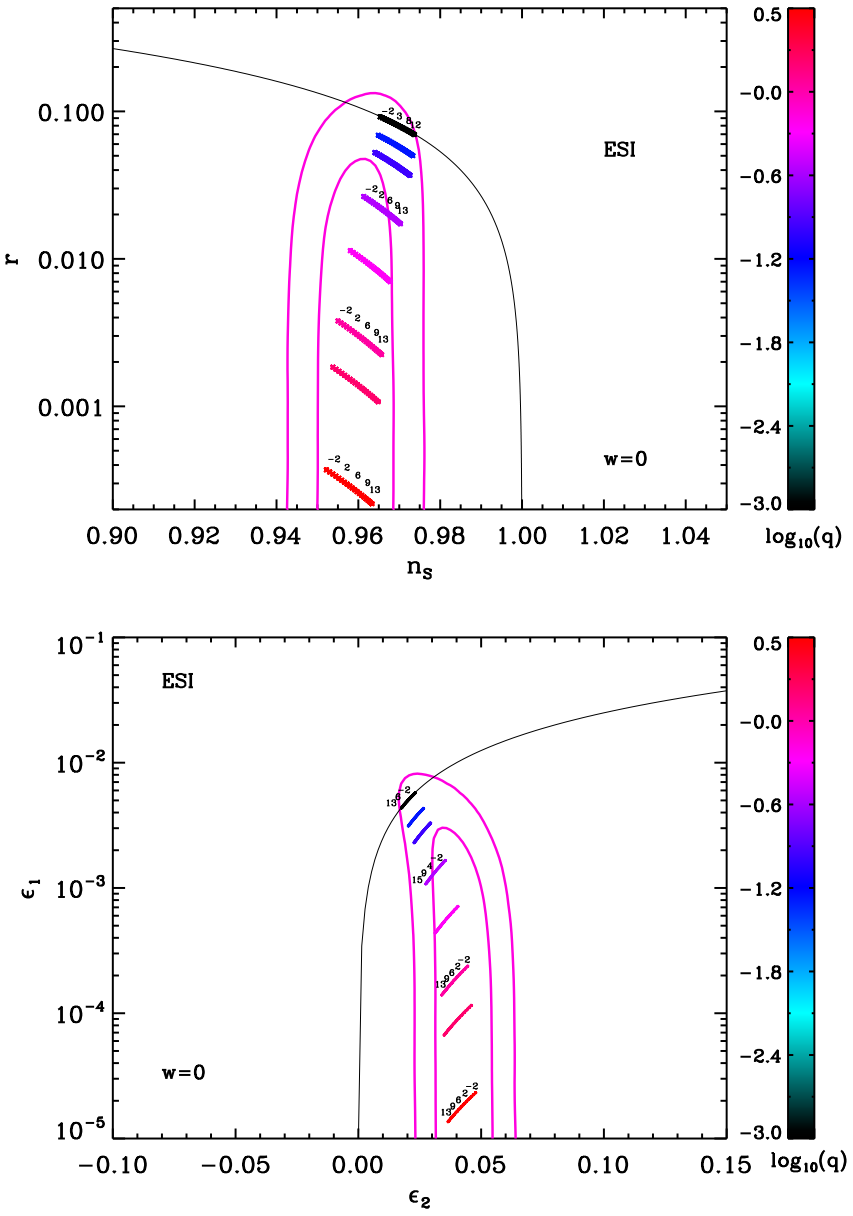

Figure 89. Reheating consistent slow-roll predictions for the exponential Susy models in the plane $(n_{\rm s}, r)$ (top panel) and the plane (ϵ_1, ϵ_2) (bottom panel), with $\overline{w}_{\rm reh} = 0$. The two pink solid contours are the one and two-sigma Planck confidence intervals (marginalized over second order slow-roll). The black solid line represent the locus obtained from the linear large field model [with $p = 1$, for which $r = (8/3)\,(1 - n_{\rm s})$, i.e. $\epsilon_1 = \epsilon_2/4$]. The annotations trace the energy scale at which the exponential Susy reheating ends and correspond to $\log(g_*^{1/4} T_{\rm reh}/{\rm GeV})$. Clearly, all these models seem to be consistent with observations.

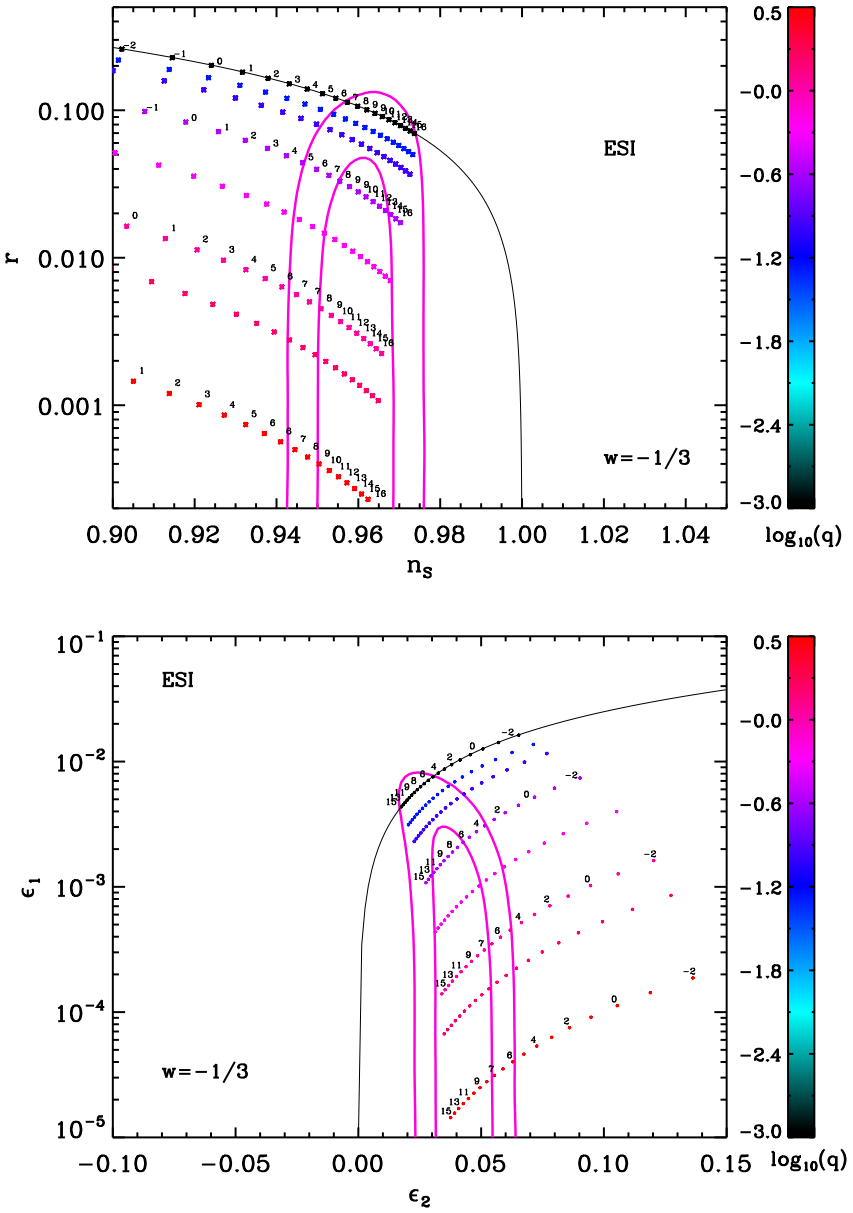

Figure 90. Reheating consistent slow-roll predictions for the exponential Susy models in the plane $(n_{\rm S}, r)$ (top panel) and the plane (ϵ_1, ϵ_2) (bottom panel), with $\overline{w}_{\rm reh} = -1/3$. This value of $\overline{w}_{\rm reh}$ may be more physically justified (although rather extreme) if a parametric reheating feels the bottom of the potential, which is linear in a good approximation. The two pink solid contours are the one and two-sigma Planck confidence intervals (marginalized over second order slow-roll). The black solid line represent the locus of the linear large field model [with $p = 1$, for which $r = (8/3)\,(1 - n_{\rm S})$, i.e. $\epsilon_1 = \epsilon_2/4$]. The annotations trace the energy scale at which the exponential Susy reheating ends and correspond to $\log(g_*^{1/4} T_{\rm reh}/{\rm GeV})$. Clearly in that case, these values are limited from below.

A.9 Power Law Inflation (PLI)

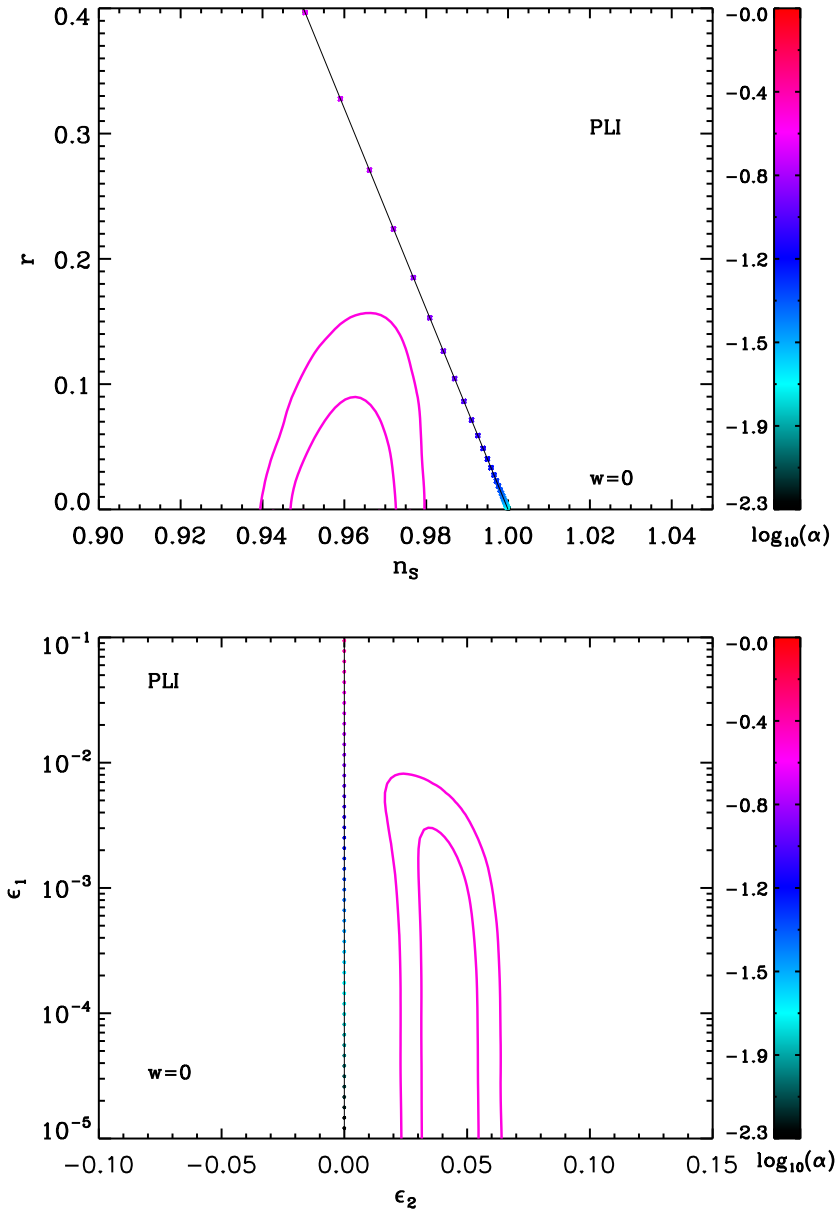

Figure 91. Reheating consistent slow-roll predictions for the power law models in the plane $(n_{\rm S}, r)$ (top panel) and the plane (ϵ_1, ϵ_2) (bottom panel). The two pink solid contours are the one and two-sigma Planck confidence intervals (marginalized over second order slow-roll). The black solid line represents the locus of the points such that $r = -8\,(n_{\rm S} - 1)$, i.e. $\epsilon_2 = 0$. The annotations of the energy scale at which reheating ends are not displayed since the predictions of these models do not depend on this parameter. Clearly, these models are excluded at more than two sigma confidence level.

A.10 Kähler Moduli Inflation I (KMII)

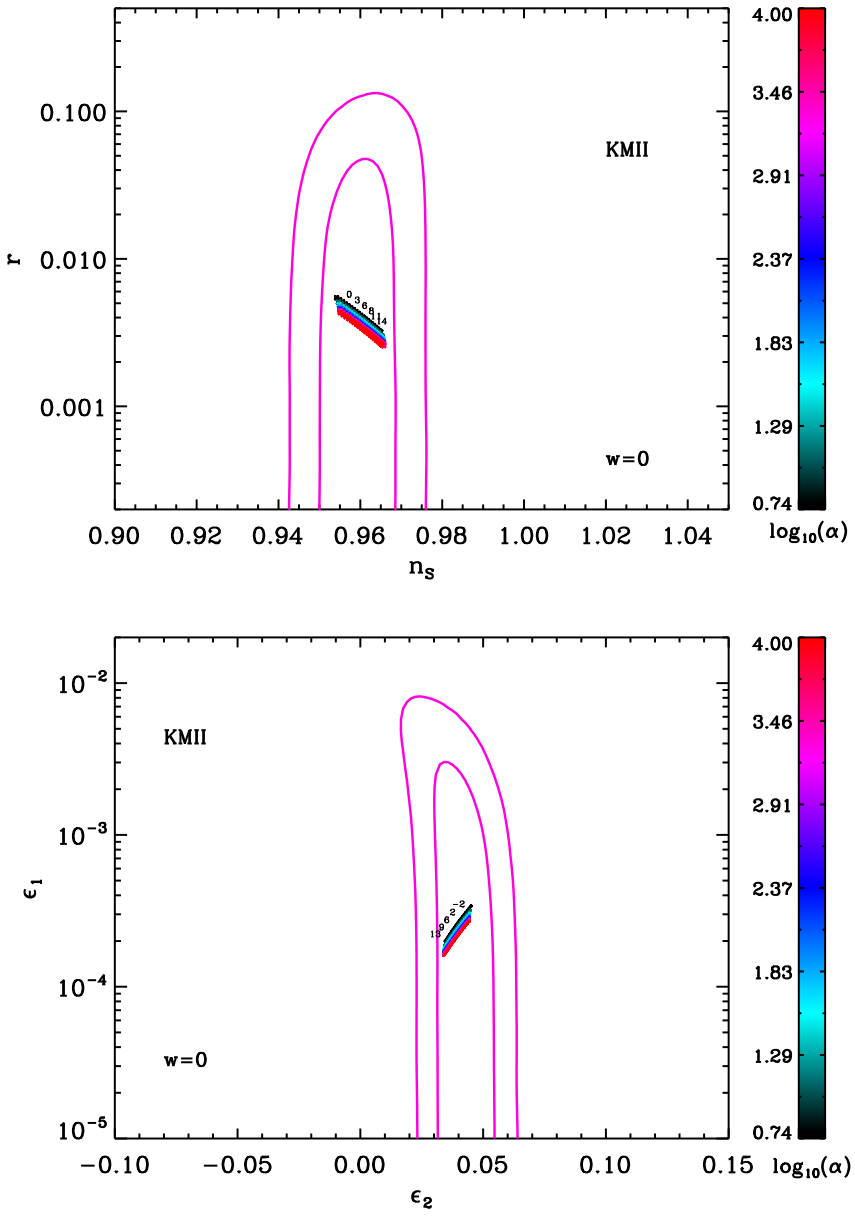

Figure 92. Reheating consistent slow-roll predictions for the Kähler Moduli I models in the plane $(n_{\rm S}, r)$ (top panel) and the plane (ϵ_1, ϵ_2) (bottom panel). The two pink solid contours are the one and two-sigma Planck confidence intervals (marginalized over second order slow-roll). The reheating equation of state parameter $\overline{w}_{\rm reh} = 0$ since the potential is quadratic close to its minimum. The annotations trace the energy scale at which reheating ends and correspond to $\log(g_*^{1/4} T_{\rm reh}/{\rm GeV})$.

A.11 Horizon Flow Inflation at first order (HF1I)

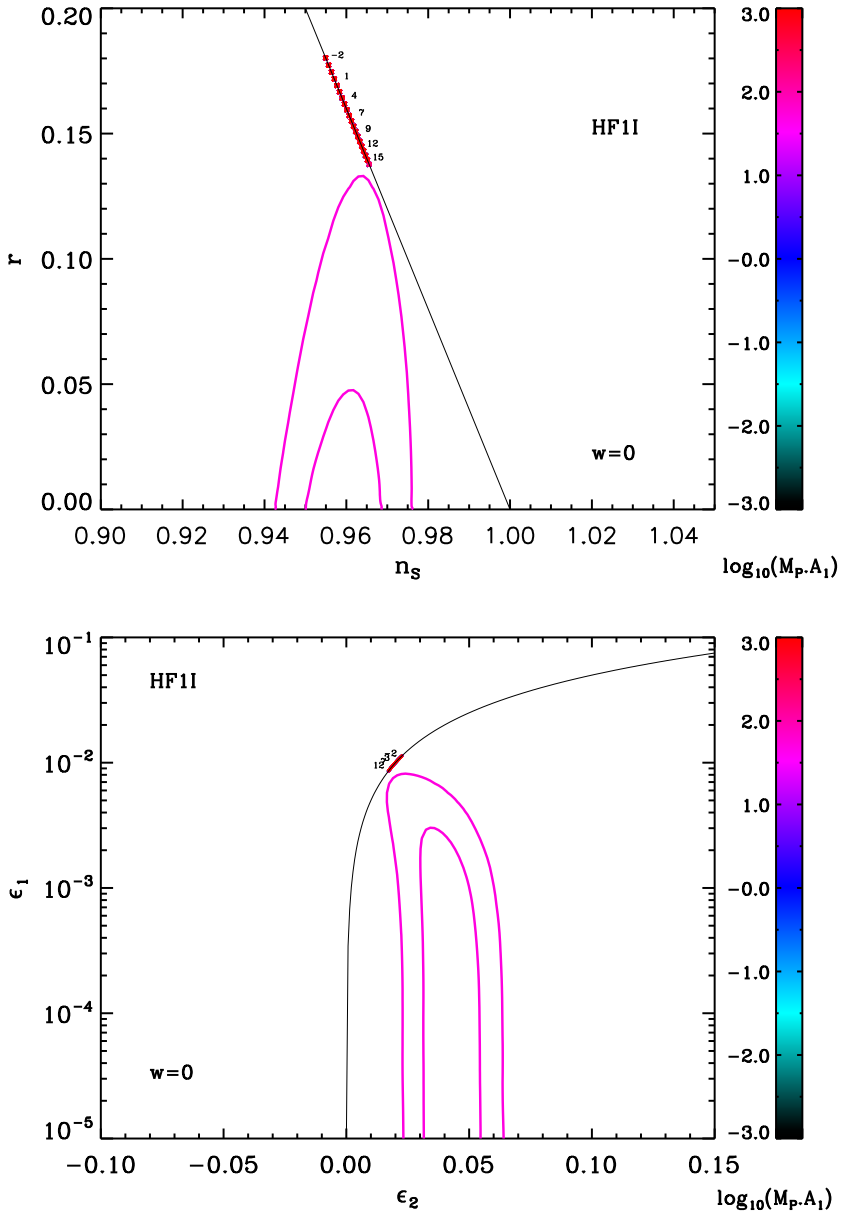

Figure 93. Reheating consistent (exact) predictions for the horizon flow inflation at first order models in the plane $(n_{\rm s}, r)$ (top panel) and the plane (ϵ_1, ϵ_2) (bottom panel). The two pink solid contours trace the two-sigma Planck confidence intervals (marginalized over second order slow-roll). The black solid line represent the locus of the quadratic large field model [with $p = 2$, for which $r = 4\,(1 - n_{\rm s})$, i.e. $\epsilon_1 = \epsilon_2/2$]. The annotations trace the energy scale at which reheating ends and correspond to $\log(g_*^{1/4} T_{\rm reh}/{\rm GeV})$. Clearly, a high energy scale reheating is preferred for these models to remain inside the two-sigma contours. Notice that, up to the amplitude of the CMB anisotropies, the predictions do not depend much on A_1 as they are all superimposed.

A.12 Colemann-Weinberg Inflation (CWI)

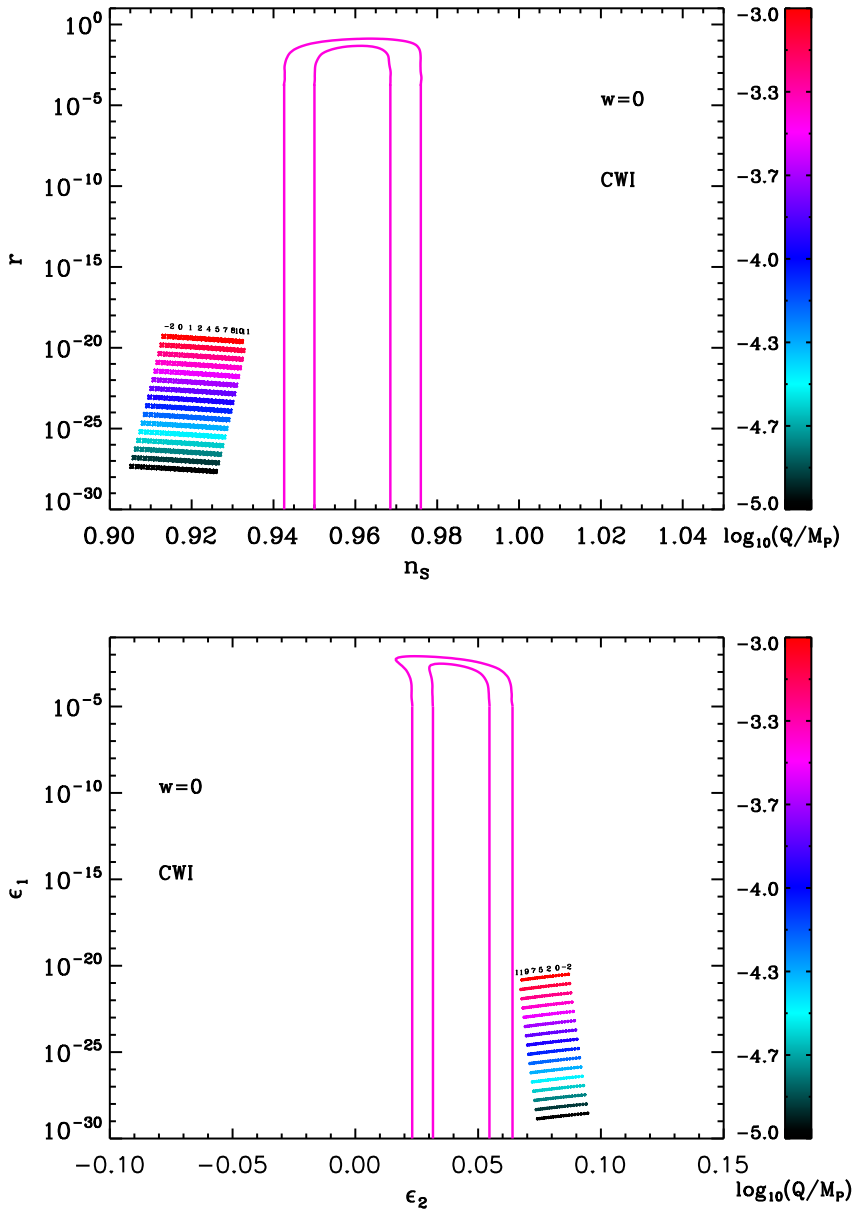

Figure 94. Reheating consistent slow-roll predictions for the Colemann-Weinberg models in the plane $(n_{\rm S}, r)$ (top panel) and the plane (ϵ_1, ϵ_2) (bottom panel), in the physical domain $Q/M_{\rm Pl} \in [10^{-5}, 10^{-3}]$. The two pink solid contours are the one and two-sigma Planck confidence intervals (marginalized over second order slow-roll). The annotations trace the energy scale at which reheating ends and correspond to $\log(g_*^{1/4} T_{\rm reh}/{\rm GeV})$. The typical amount of gravitational waves is extremely small.

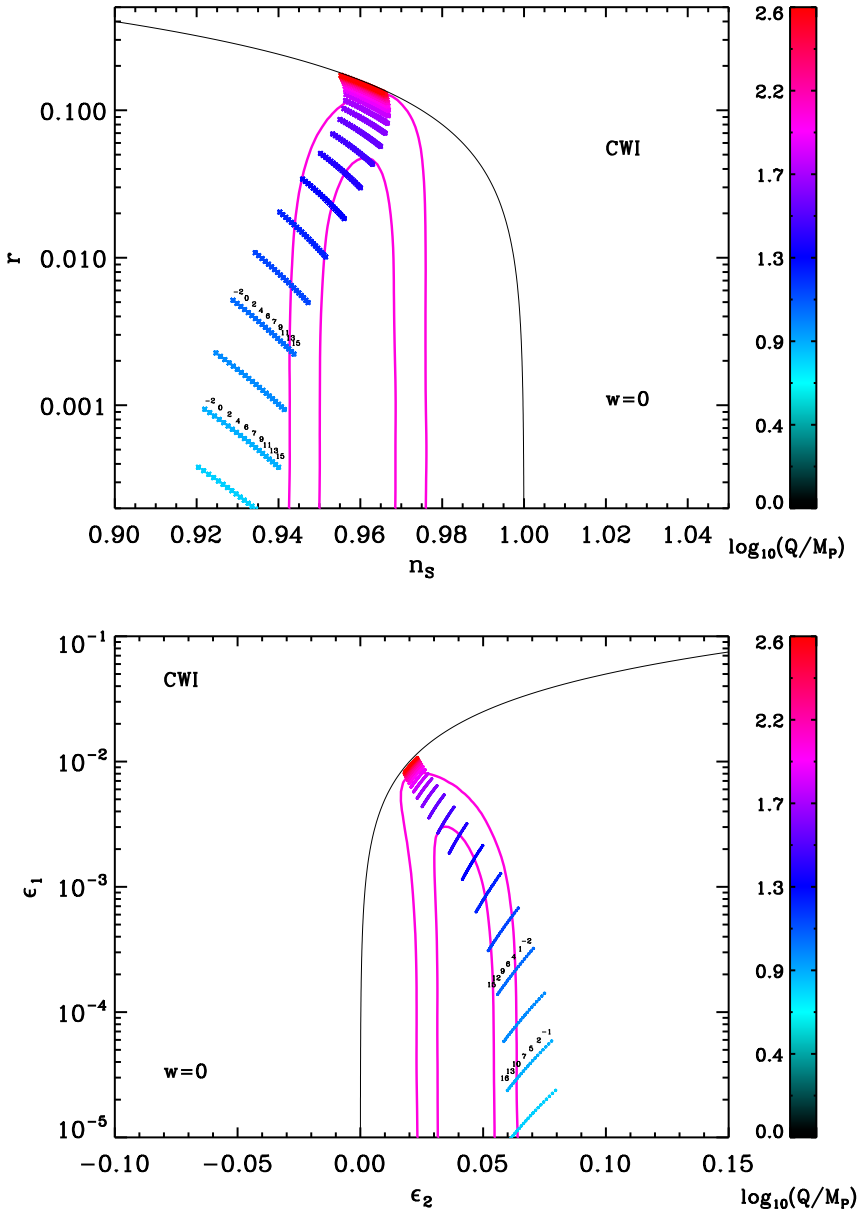

Figure 95. Reheating consistent slow-roll predictions for the Colemann-Weinberg models in the plane $(n_{\rm S}, r)$ (top panel) and the plane (ϵ_1, ϵ_2) (bottom panel), in the domain $Q/M_{\rm Pl} \in [1, 100]$. The two pink solid contours are the one and two-sigma Planck confidence intervals (marginalized over second order slow-roll). The annotations trace the energy scale at which reheating ends and correspond to $\log(g_*^{1/4} T_{\rm reh}/{\rm GeV})$. When $Q/M_{\rm Pl} \gg 1$, the model is similar to a quadratic potential close to its minimum, and the predictions match the LFI $\epsilon_1 = \epsilon_2/2$ relation (see section 4.2) represented by the black lines.

A.13 Loop Inflation (LI)

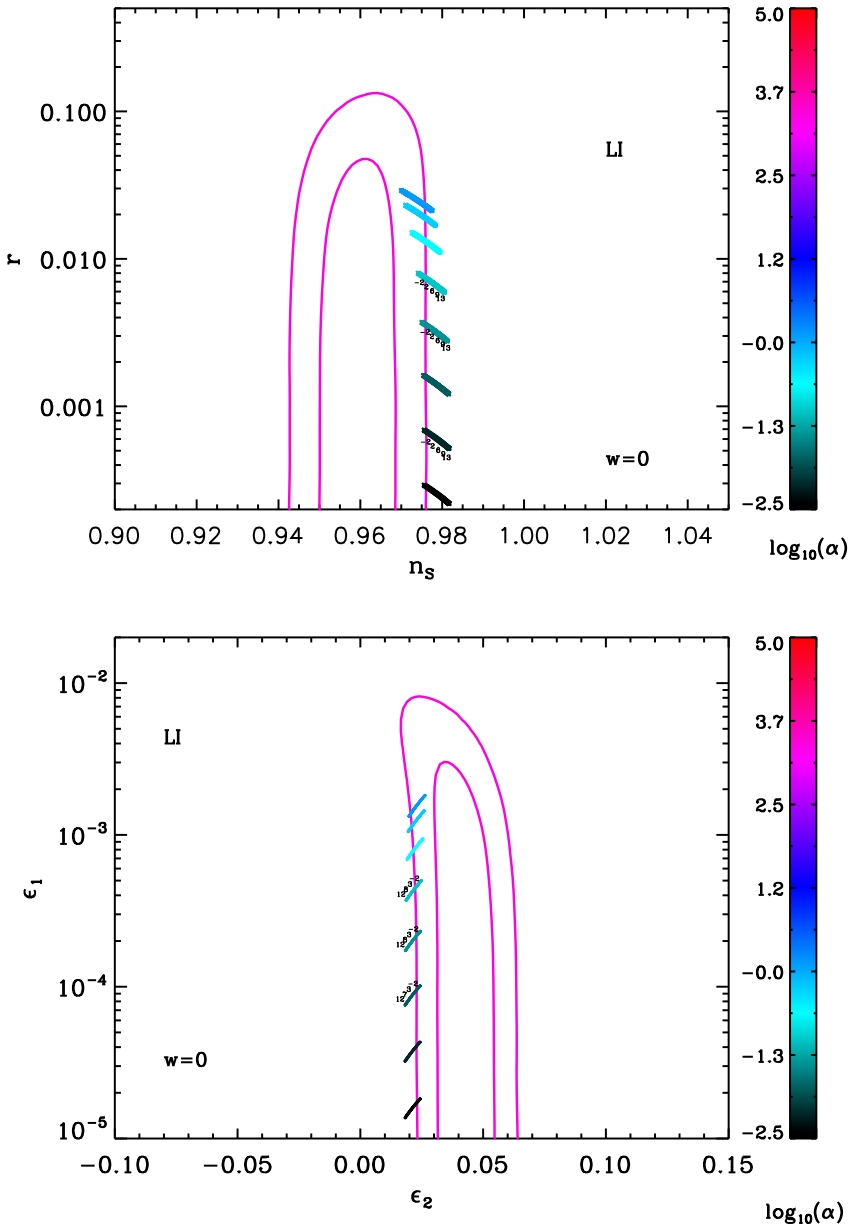

Figure 96. Reheating consistent slow-roll predictions for the loop inflation models for $\alpha > 0$, in the plane $(n_{\rm S}, r)$ (top panel), and the plane (ϵ_1, ϵ_2) (bottom panel). The two pink solid contours are the one and two-sigma Planck confidence intervals (marginalized over second order slow-roll). The annotations trace the energy scale at which reheating ends and correspond to $\log(g_*^{1/4} T_{\rm reh}/{\rm GeV})$.

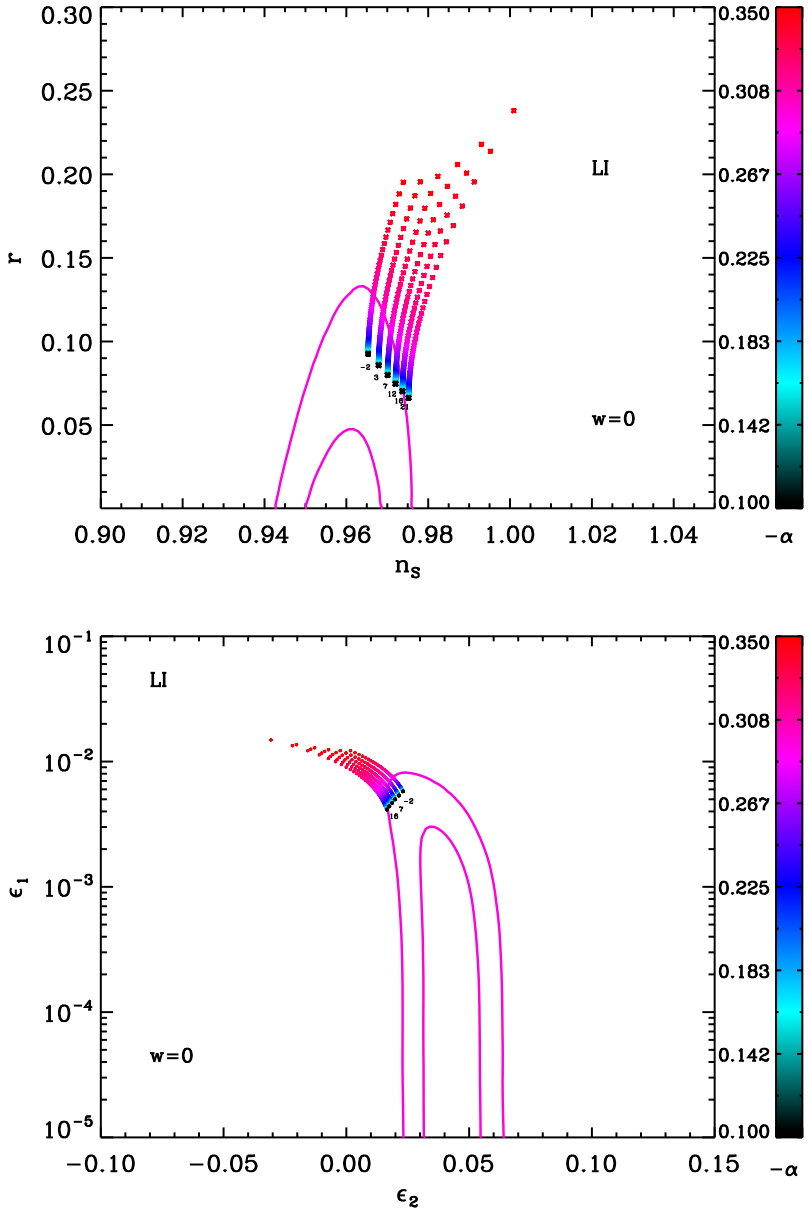

Figure 97. Reheating consistent slow-roll predictions for the loop inflation models for $\alpha < 0$, in the plane $(n_{\rm S}, r)$ (top panel), and the plane (ϵ_1, ϵ_2) (bottom panel). The two pink solid contours are the one and two-sigma Planck confidence intervals (marginalized over second order slow-roll). The annotations trace the energy scale at which reheating ends and correspond to $\log(g_*^{1/4} T_{\rm reh}/{\rm GeV})$.

A.14 $R + R^{2p}$ Inflation (RpI)

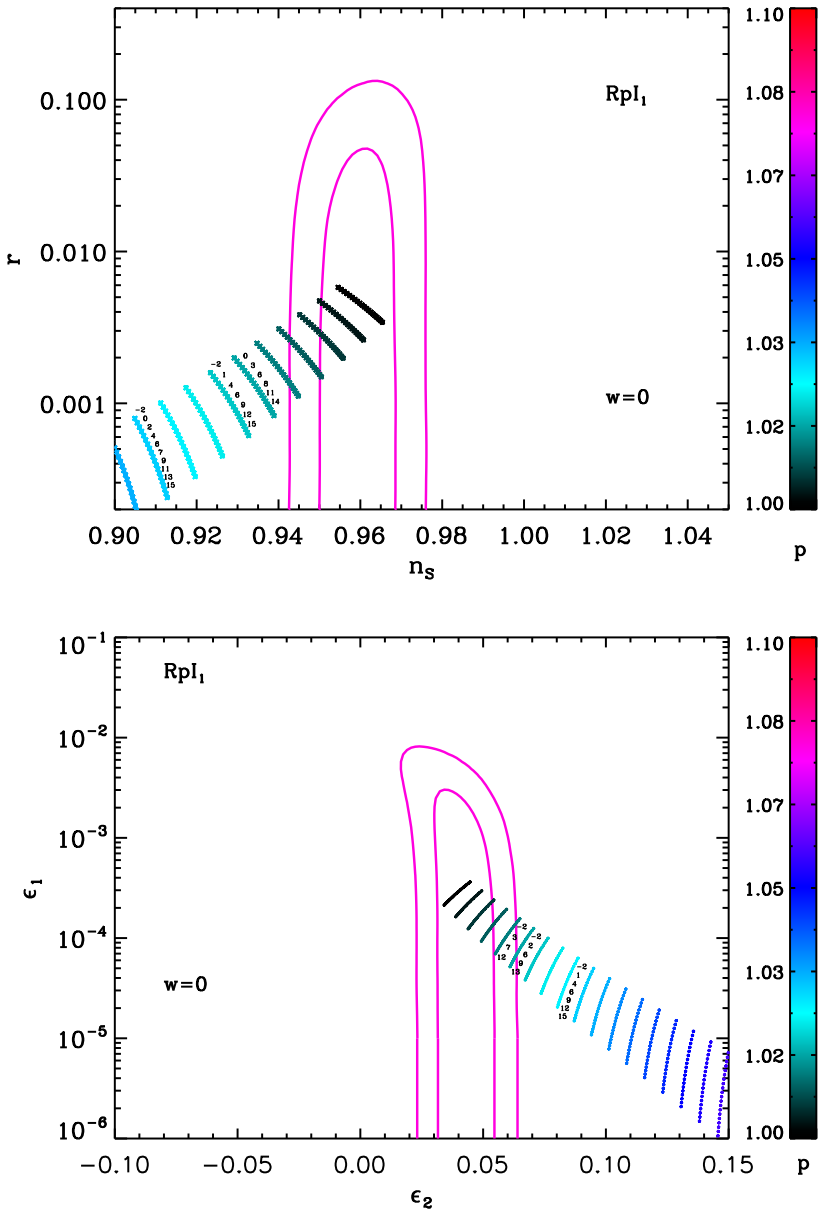

Figure 98. Reheating consistent slow-roll predictions for the $R + R^{2p}$ inflation models in the RpI1 regime, in the plane (n_s, r) (top panel), and the plane (ϵ_1, ϵ_2) (bottom panel). The two pink solid contours are the one and two-sigma Planck confidence intervals (marginalized over second order slow-roll). The annotations trace the energy scale at which reheating ends and correspond to $\log(g_*^{1/4} T_{\rm reh}/{\rm GeV})$.

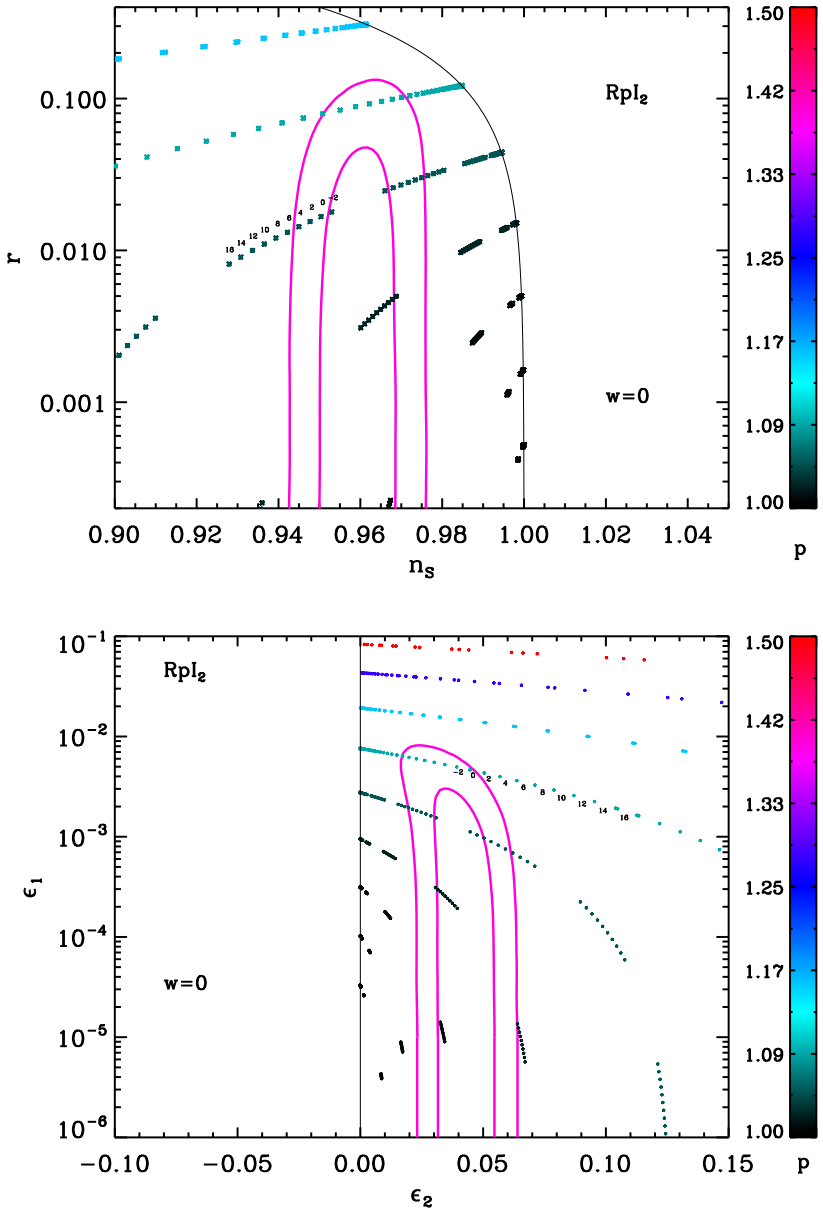

Figure 99. Reheating consistent slow-roll predictions for the $R + R^{2p}$ inflation models in the RpI2 regime, in the plane $(n_{\rm s}, r)$ (top panel), and the plane (ϵ_1, ϵ_2) (bottom panel). The two pink solid contours are the one and two-sigma Planck confidence intervals (marginalized over second order slow-roll). The color of the data points encodes the value of p, while different data blocks correspond to different values of $y_{\rm end}$. Inside a given bock, the annotations trace the energy scale at which reheating ends and correspond to $\log(g_*^{1/4} T_{\rm reh}/{\rm GeV})$. When $y_{\rm end} >> 1$, one has $\epsilon_2 \to 0$ which is denoted by the black line.

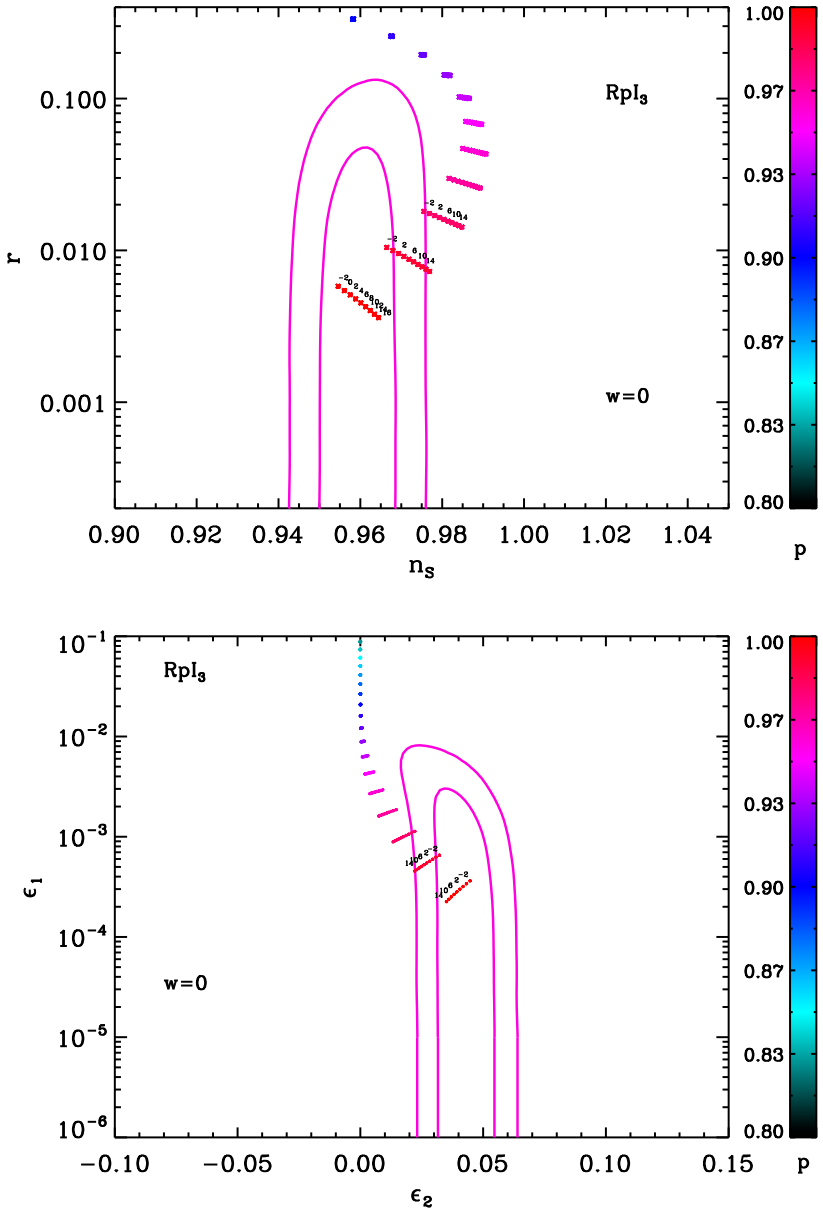

Figure 100. Reheating consistent slow-roll predictions for the $R + R^{2p}$ inflation models in the RpI3 regime, in the plane $(n_{\rm s}, r)$ (top panel), and the plane (ϵ_1, ϵ_2) (bottom panel). The two pink solid contours are the one and two-sigma Planck confidence intervals (marginalized over second order slow-roll). The annotations trace the energy scale at which reheating ends and correspond to $\log(g_*^{1/4} T_{\rm reh}/{\rm GeV})$.

A.15 Double Well Inflation (DWI)

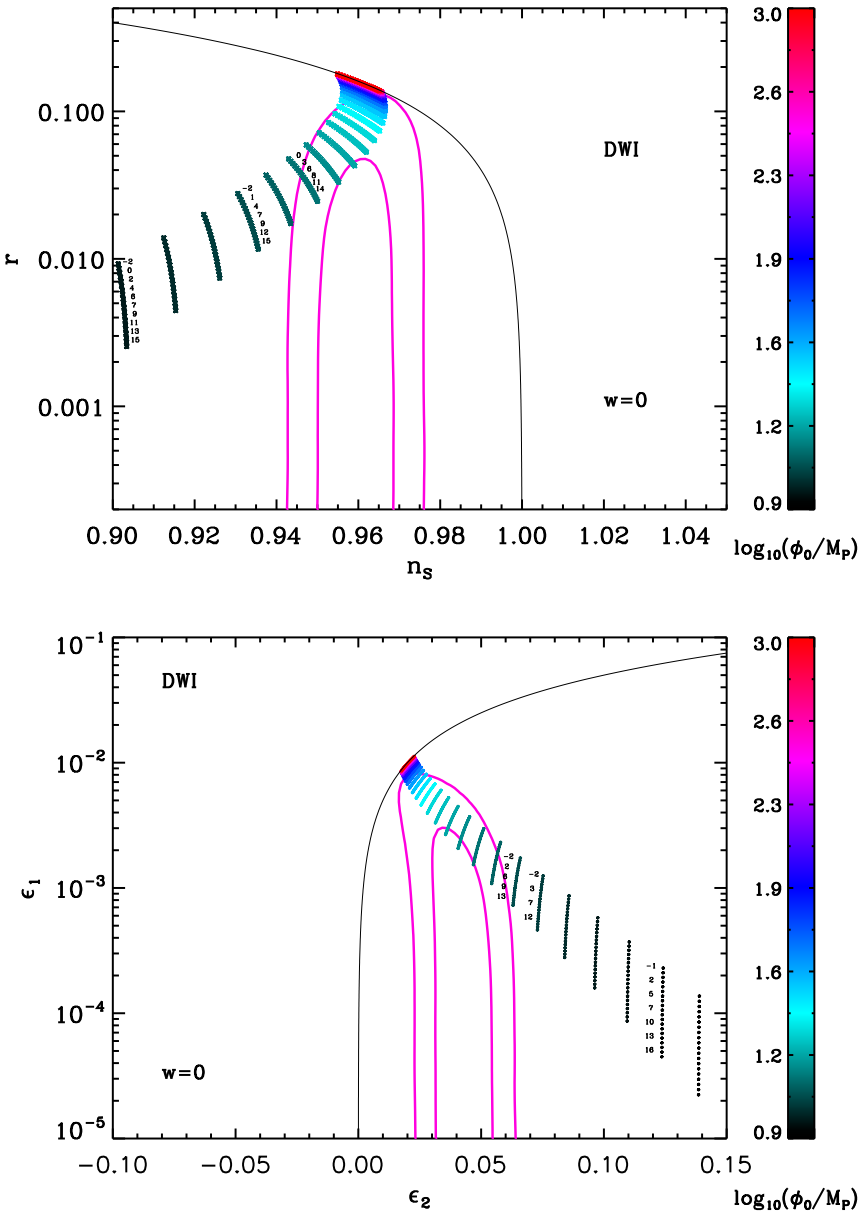

Figure 101. Reheating consistent slow-roll predictions for the double well models in the plane $(n_{\rm S}, r)$ (top panel) and the plane (ϵ_1, ϵ_2) (bottom panel). The two pink solid contours are the one and two-sigma Planck confidence intervals (marginalized over second order slow-roll). The annotations trace the energy scale at which reheating ends and correspond to $\log(g_*^{1/4} T_{\rm reh}/{\rm GeV})$. The shape of the zone covered by the models predictions is similar to the one for Small Field Inflation (SFI, see Fig. 112), except in the domain $\phi_0 \gg M_{\rm Pl}$, which is the one favored by the observations. The black solid line represents the locus of the points such that $r = 4\,(1 - n_{\rm S})$, i.e. $\epsilon_2 = 2\epsilon_1$, on which this model lies for $\phi_0/M_{\rm Pl} \gg 1$.

A.16 Mutated Hilltop Inflation (MHI)

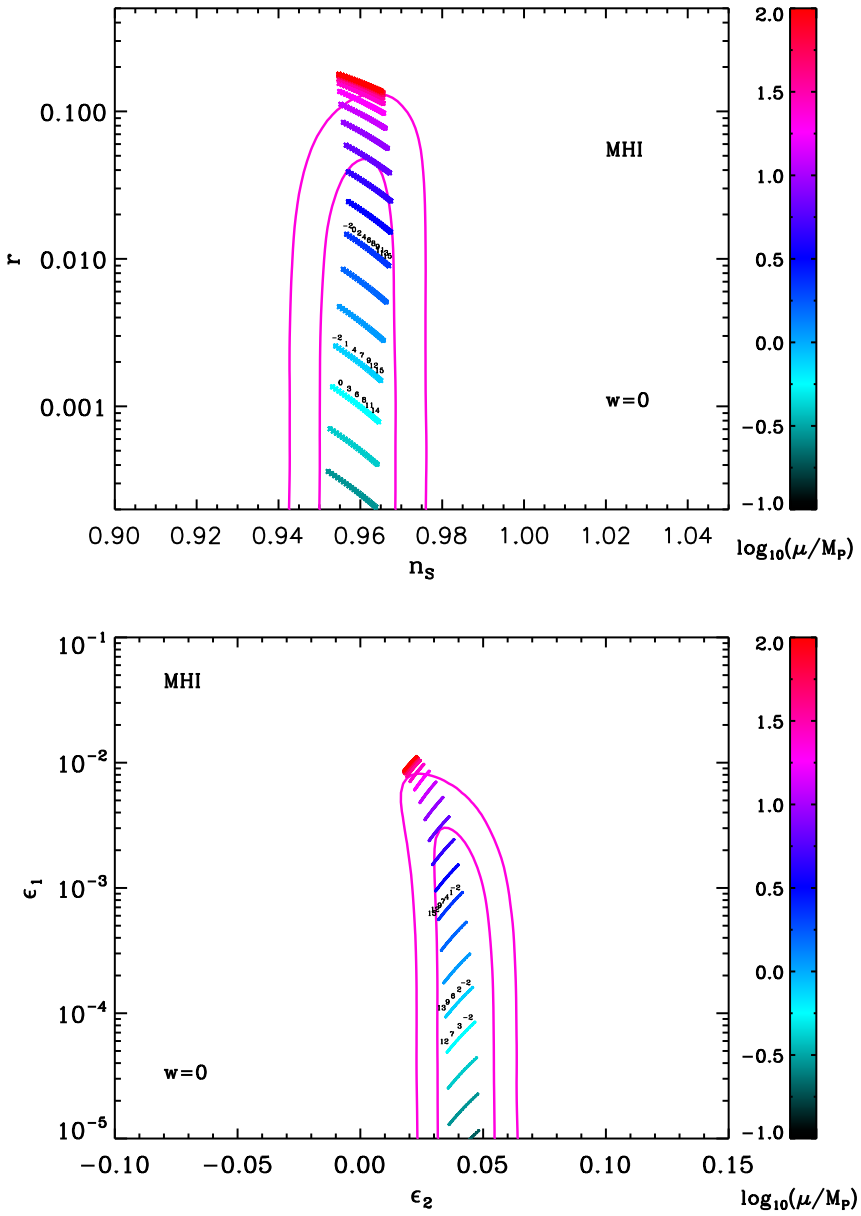

Figure 102. Reheating consistent slow-roll predictions for the mutated hilltop models in the plane $(n_{\rm S}, r)$ (top panel) and the plane (ϵ_1, ϵ_2) (bottom panel). The two pink solid contours are the one and two-sigma Planck confidence intervals (marginalized over second order slow-roll). The annotations trace the energy scale at which reheating ends and correspond to $\log(g_*^{1/4} T_{\rm reh}/{\rm GeV})$. For small values of $\mu/M_{\rm Pl}$, this model predicts a very small amount of gravitational waves

A.17 Radion Gauge Inflation (RGI)

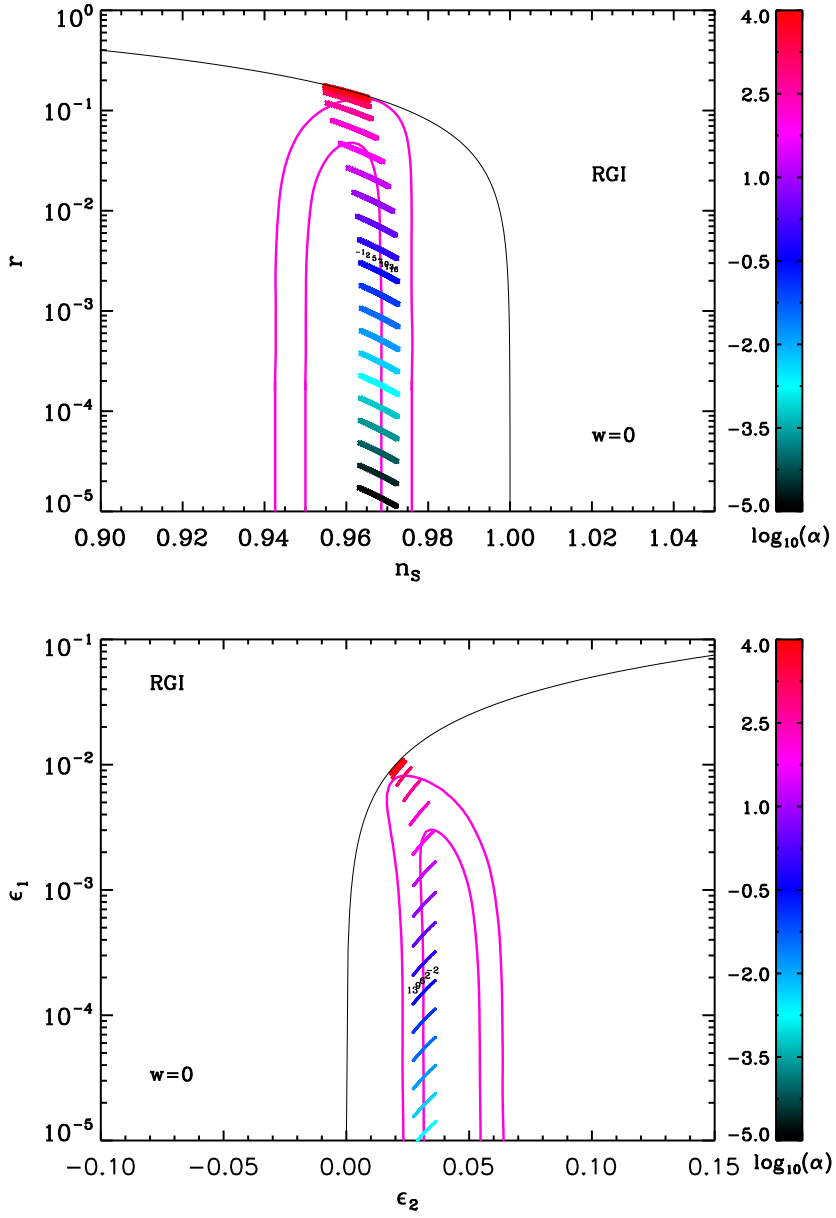

Figure 103. Reheating consistent slow-roll predictions for the radion gauge models in the plane $(n_{\rm S}, r)$ (top panel) and the plane (ϵ_1, ϵ_2) (bottom panel). The two pink solid contours are the one and two-sigma Planck confidence intervals (marginalized over second order slow-roll). The annotations trace the energy scale at which reheating ends and correspond to $\log(g_*^{1/4} T_{\rm reh}/{\rm GeV})$. At large values of α, the predictions are the same as the large field model with $p = 2$ (see Fig. 83) for which $\epsilon_2 = 2\epsilon_1$ (black solid line).

A.18 MSSM Inflation (MSSMI)

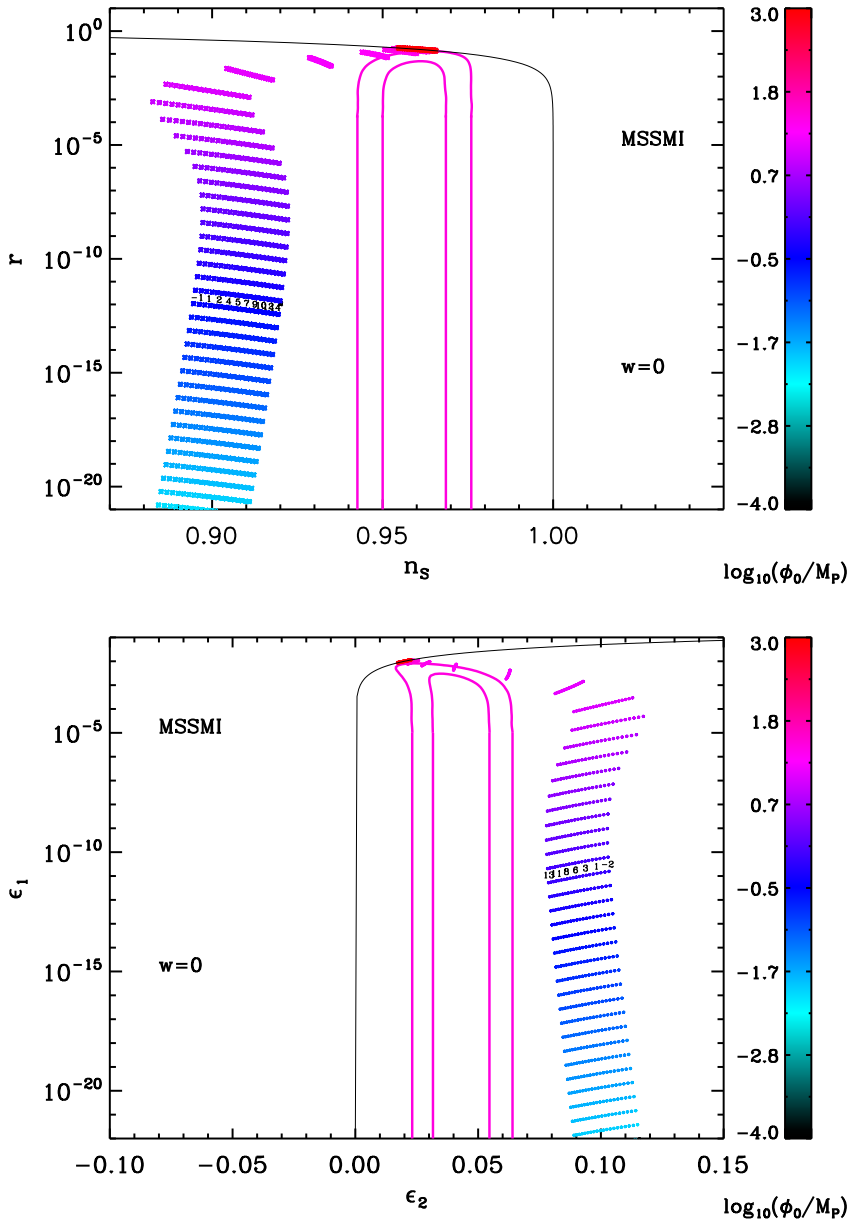

Figure 104. Reheating consistent slow-roll predictions for the MSSMI models in the plane $(n_{\rm S}, r)$ (top panel) and the plane (ϵ_1, ϵ_2) (bottom panel). The two pink solid contours are the one and two-sigma Planck confidence intervals (marginalized over second order slow-roll). The annotations trace the energy scale at which reheating ends and correspond to $\log(g_*^{1/4} T_{\rm reh}/{\rm GeV})$. The black solid line represent the locus of the points such that $r = 4\,(1 - n_{\rm S})$, i.e. $\epsilon_2 = 2\epsilon_1$, on which this model lies for for $\phi_0/M_{\rm Pl} \gg 1$. However, the physical relevant value is closer to $\phi_0/M_{\rm Pl} \simeq 10^{-4}$.

A.19 Renormalizable Inflection Point Inflation (RIPI)

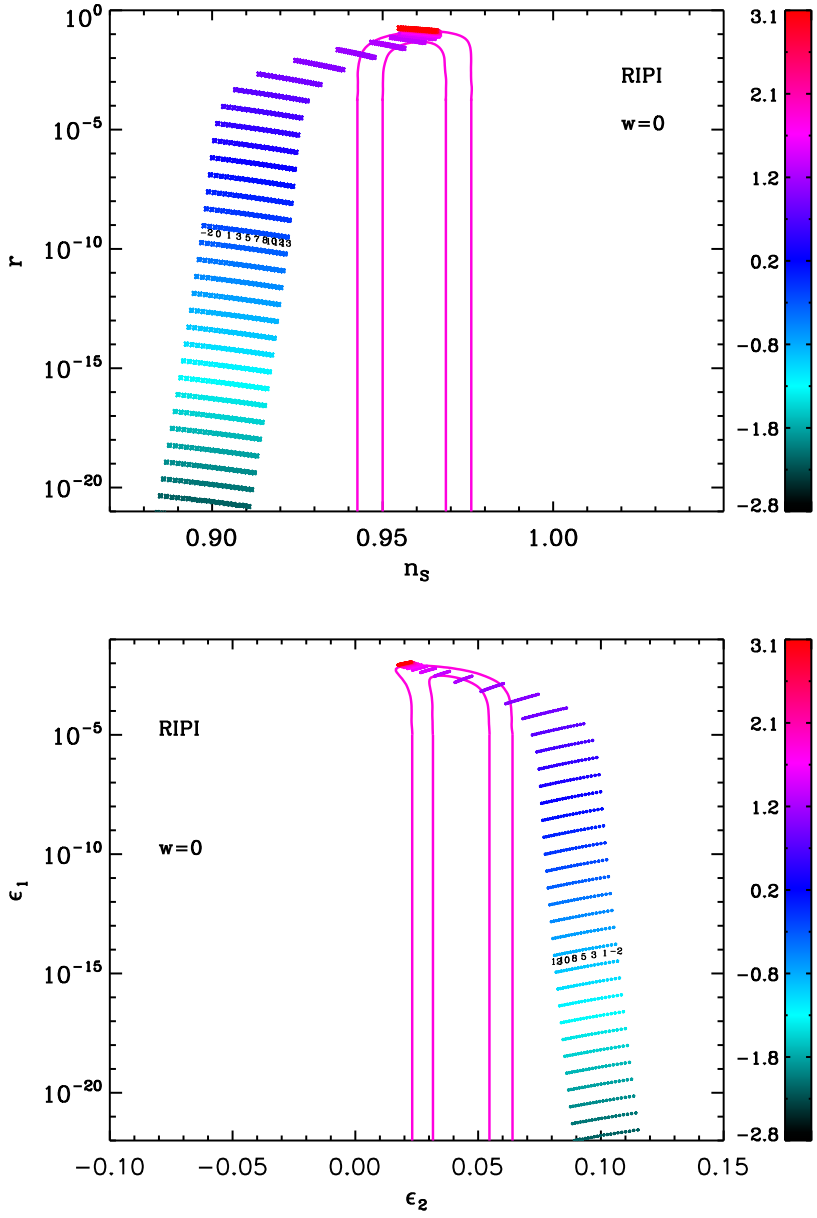

Figure 105. Reheating consistent slow-roll predictions for the renormalizable inflection point models in the plane $(n_{\rm S}, r)$ (top panel) and the plane (ϵ_1, ϵ_2) (bottom panel). The two pink solid contours are the one and two-sigma Planck confidence intervals (marginalized over second order slow-roll). The annotations trace the energy scale at which reheating ends and correspond to $\log(g_*^{1/4} T_{\rm reh}/{\rm GeV})$.

A.20 Arctan Inflation (AI)

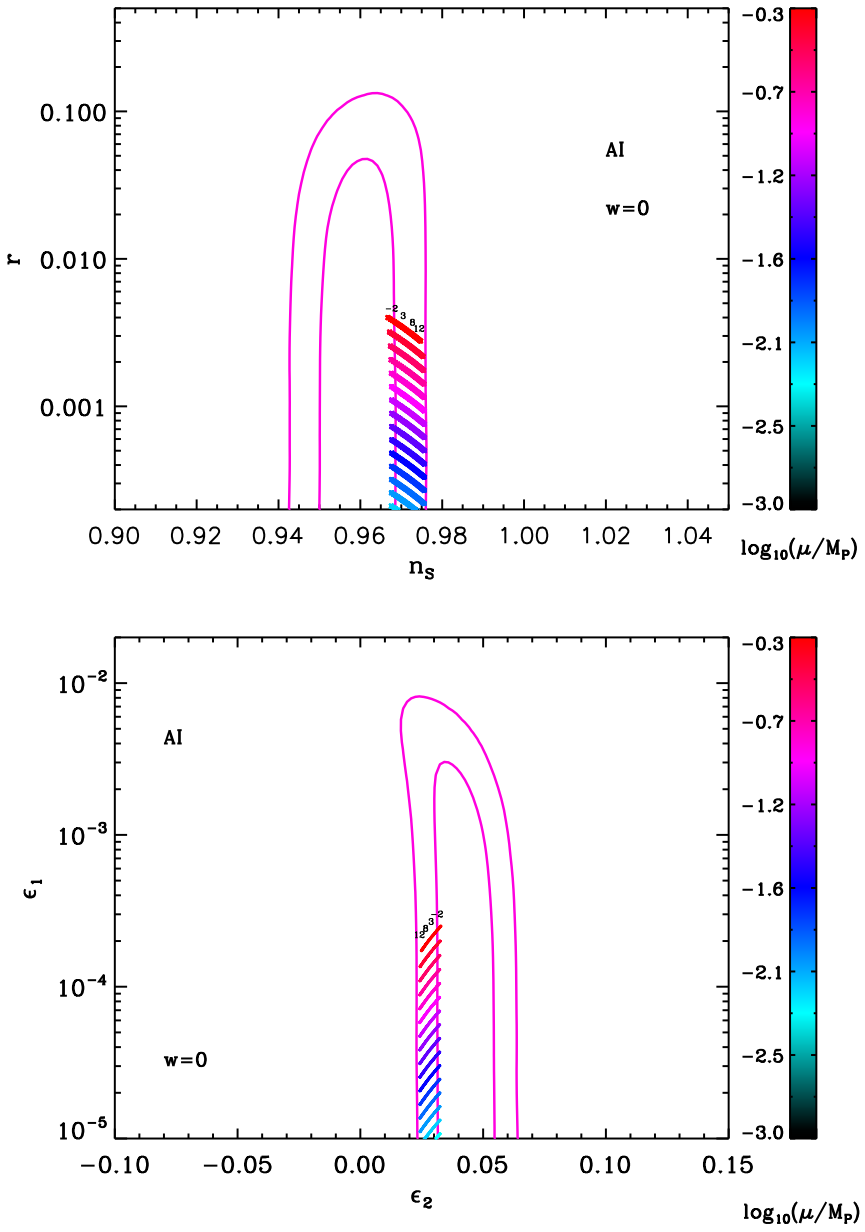

Figure 106. Reheating consistent slow-roll predictions for the ArcTan models in the plane $(n_{\rm S}, r)$ (top panel) and the plane (ϵ_1, ϵ_2) (bottom panel), when the reheating equation of state is $\overline{w}_{\rm reh} = 0$. The two pink solid contours are the one and two-sigma Planck confidence intervals (marginalized over second order slow-roll). The annotations trace the energy scale at which reheating ends and correspond to $\log(g_*^{1/4} T_{\rm reh}/{\rm GeV})$.

A.21 Constant $n_{\rm S}$ A Inflation (CNAI)

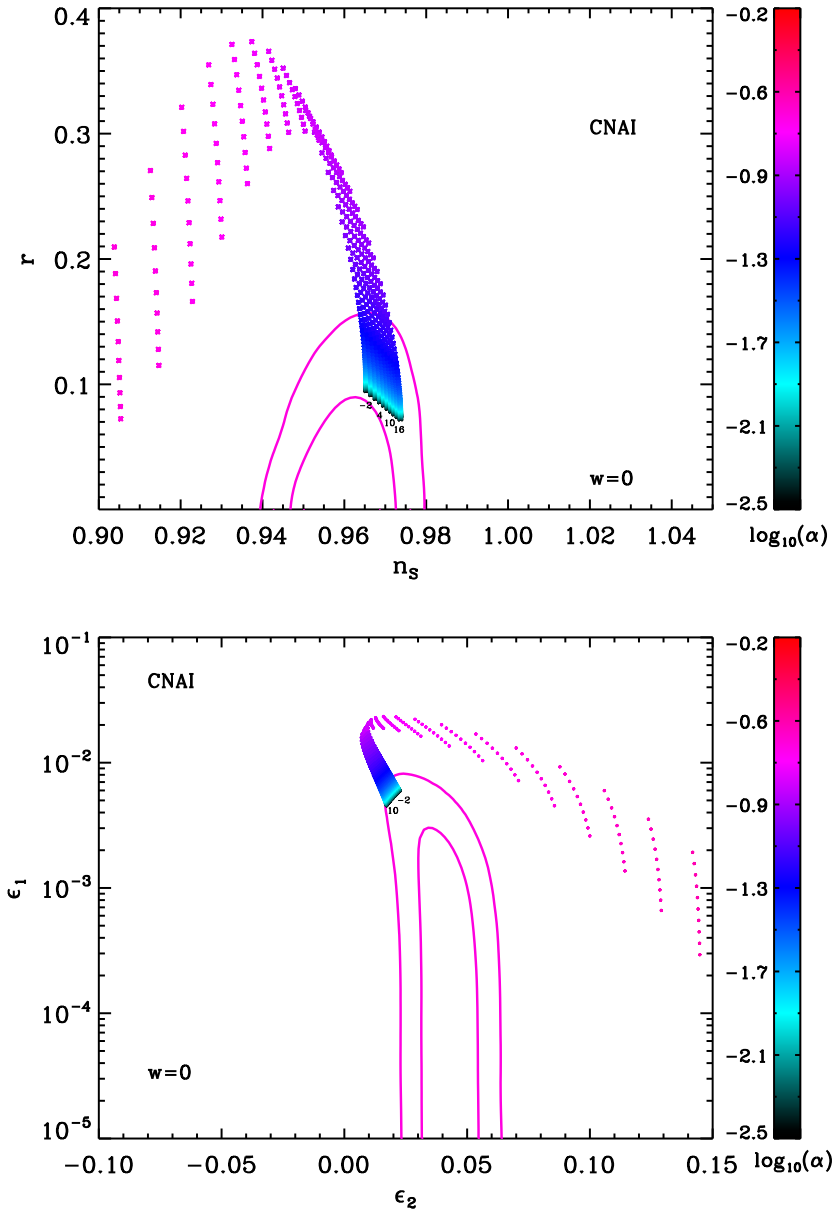

Figure 107. Reheating consistent slow-roll predictions for the constant $n_{\rm S}$ A models in the plane $(n_{\rm S}, r)$ (top panel) and the plane (ϵ_1, ϵ_2) (bottom panel). The two pink solid contours are the one and two-sigma Planck confidence intervals (marginalized over second order slow-roll). The annotations trace the energy scale at which reheating ends and correspond to $\log(g_*^{1/4} T_{\rm reh}/{\rm GeV})$.

A.22 Constant $n_{\rm S}$ B Inflation (CNBI)

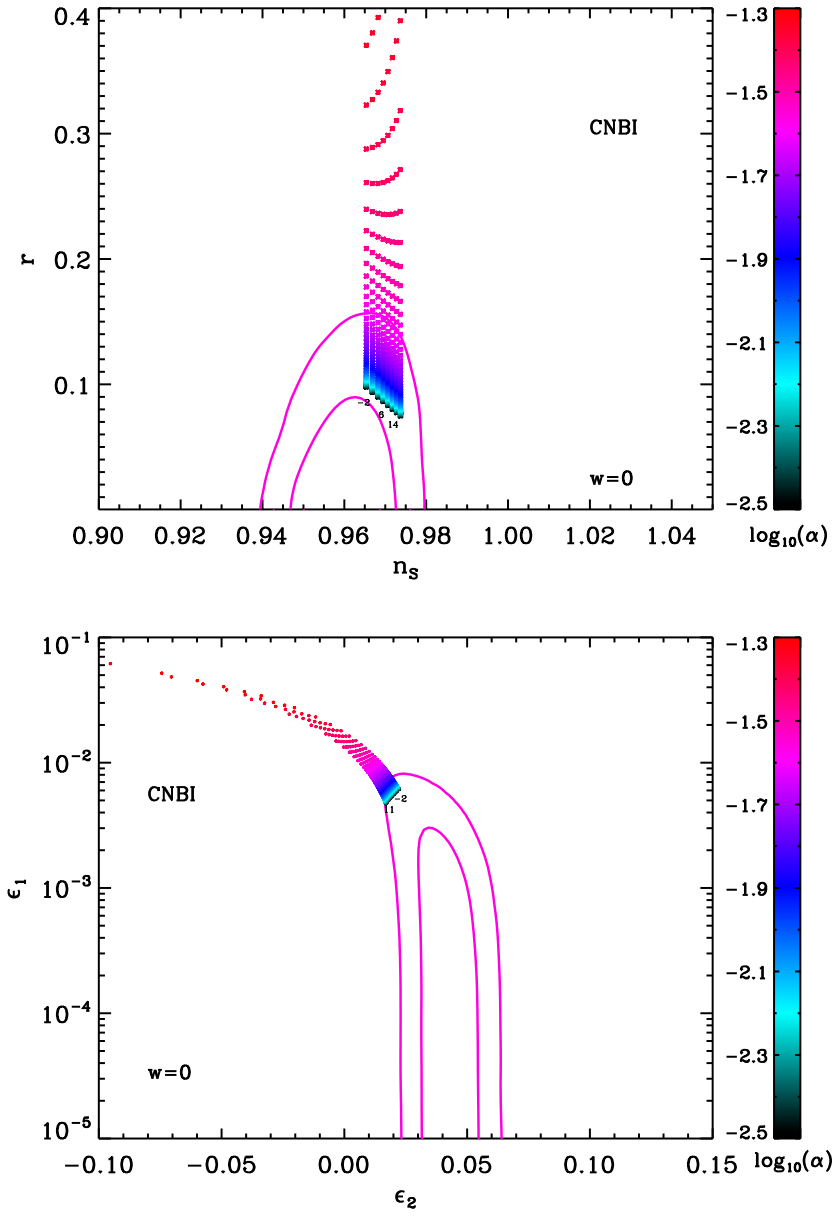

Figure 108. Reheating consistent slow-roll predictions for the constant $n_{\rm S}$ B models in the plane $(n_{\rm S}, r)$ (top panel) and the plane (ϵ_1, ϵ_2) (bottom panel). The two pink solid contours are the one and two-sigma Planck confidence intervals (marginalized over second order slow-roll). The annotations trace the energy scale at which reheating ends and correspond to $\log(g_*^{1/4} T_{\rm reh}/{\rm GeV})$.

A.23 Open String Tachyonic Inflation (OSTI)

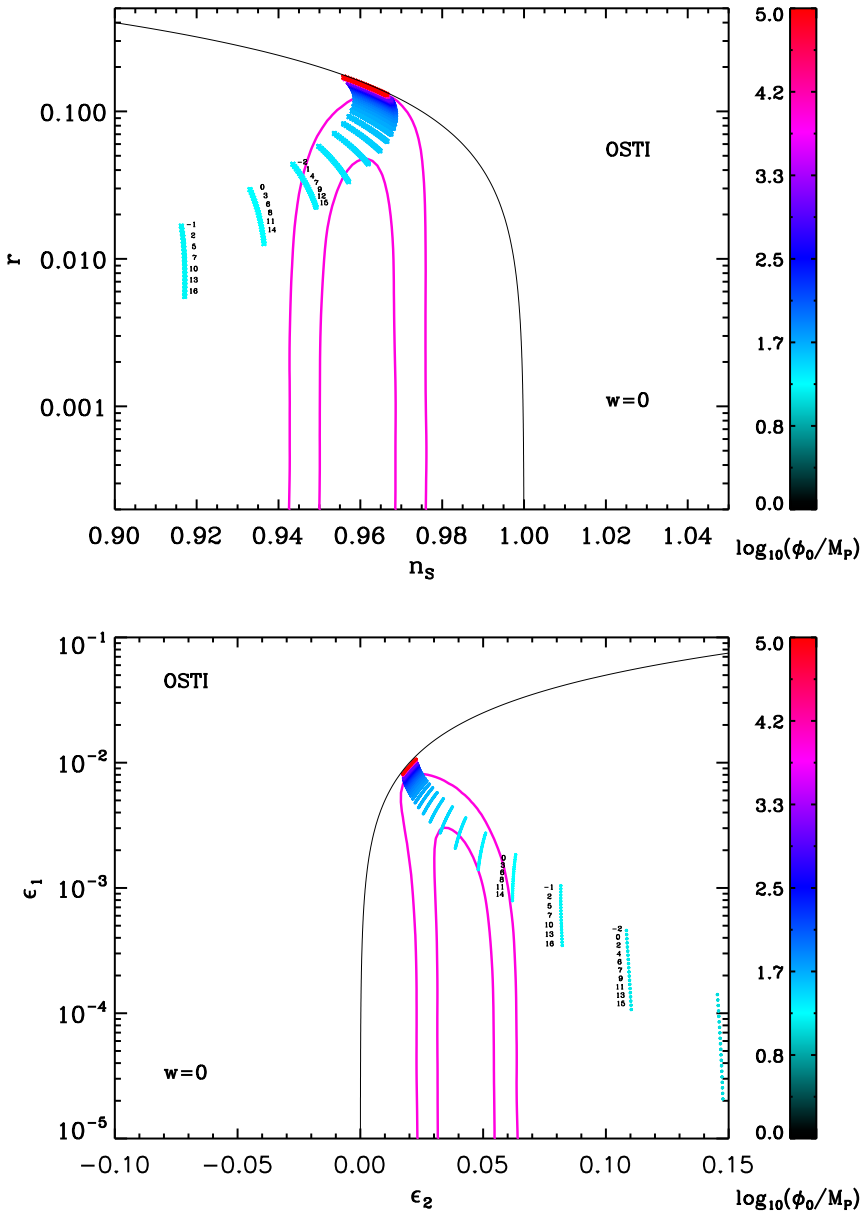

Figure 109. Reheating consistent slow-roll predictions for the open string tachyonic models in the plane $(n_{\rm S}, r)$ (top panel) and the plane (ϵ_1, ϵ_2) (bottom panel). The two pink solid contours are the one and two-sigma Planck confidence intervals (marginalized over second order slow-roll). The annotations trace the energy scale at which reheating ends and correspond to $\log(g_*^{1/4} T_{\rm reh}/{\rm GeV})$. The black solid line represents the locus of the points such that $r = 4\,(1 - n_{\rm S})$, i.e. $\epsilon_2 = 2\epsilon_1$, on which this model lies for $\phi_0/M_{\rm Pl} \gg 1$.

A.24 Witten-O'Raifeartaigh Inflation (WRI)

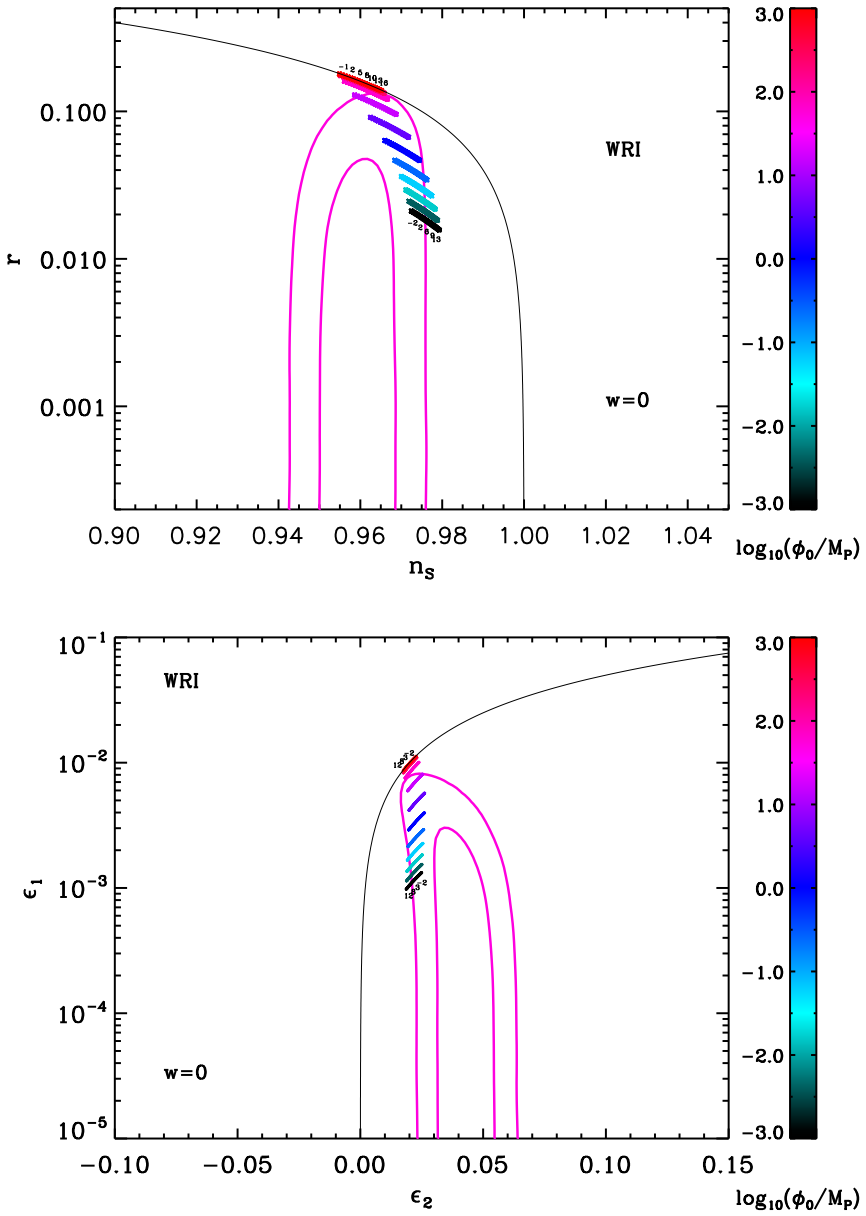

Figure 110. Reheating consistent slow-roll predictions for the Witten-O'Raifeartaigh models in the plane $(n_{\rm S}, r)$ (top panel) and the plane (ϵ_1, ϵ_2) (bottom panel). The two pink solid contours are the one and two-sigma Planck confidence intervals (marginalized over second order slow-roll). The annotations trace the energy scale at which reheating ends and correspond to $\log(g_*^{1/4} T_{\rm reh}/{\rm GeV})$. The black solid line represents the locus of the points such that $r = 4\,(1 - n_{\rm S})$, i.e. $\epsilon_2 = 2\epsilon_1$, on which this model lies for $\phi_0/M_{\rm Pl} \gg 1$.

A.25 Small Field Inflation (SFI)

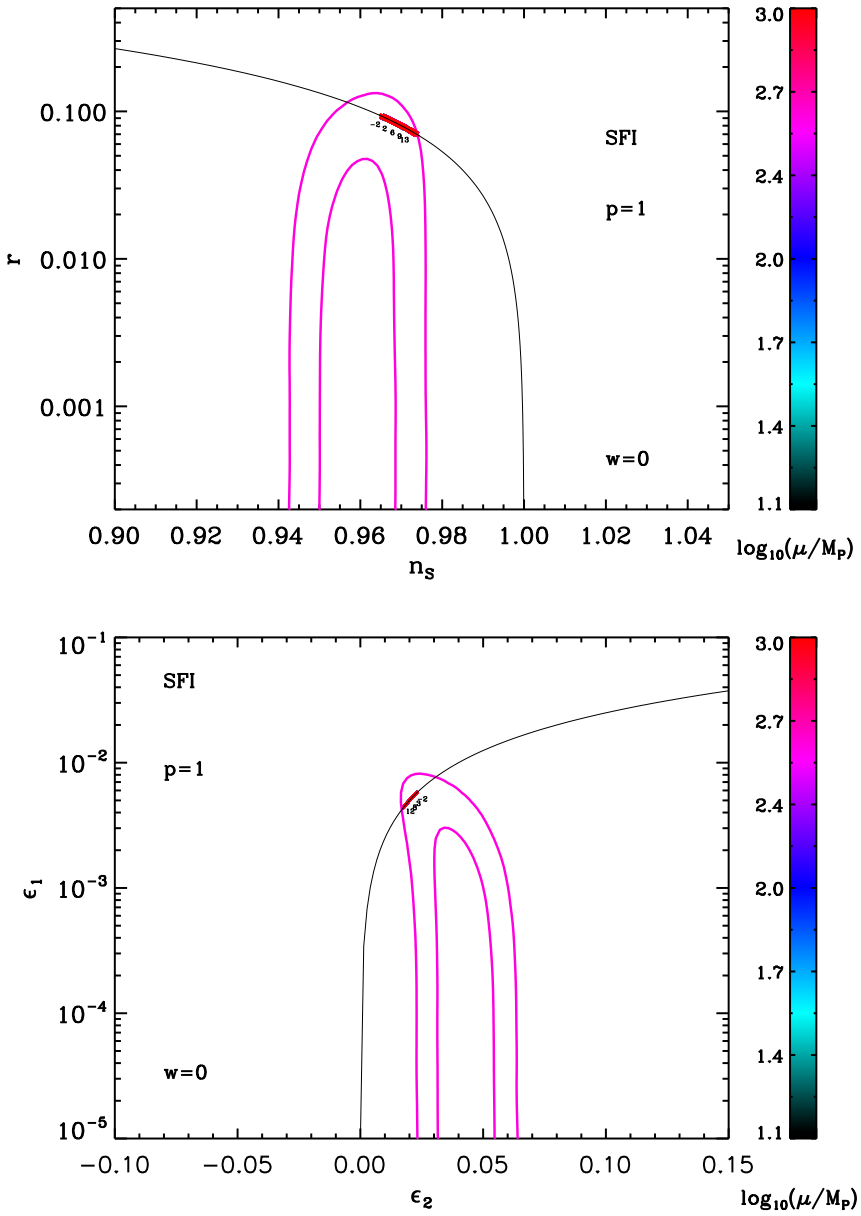

Figure 111. Reheating consistent slow-roll predictions for the small field models with $p = 1$ in the plane $(n_{\rm S}, r)$ (top panel) and the plane (ϵ_1, ϵ_2) (bottom panel). The two pink solid contours are the one and two-sigma Planck confidence intervals (marginalized over second order slow-roll). The annotations trace the energy scale at which reheating ends and correspond to $\log(g_*^{1/4} T_{\rm reh}/{\rm GeV})$. The black solid line represent the locus of the points such that $r = (8/3)\,(1 - n_{\rm S})$, i.e. $\epsilon_2 = 4\epsilon_1$, on which this model must lie.

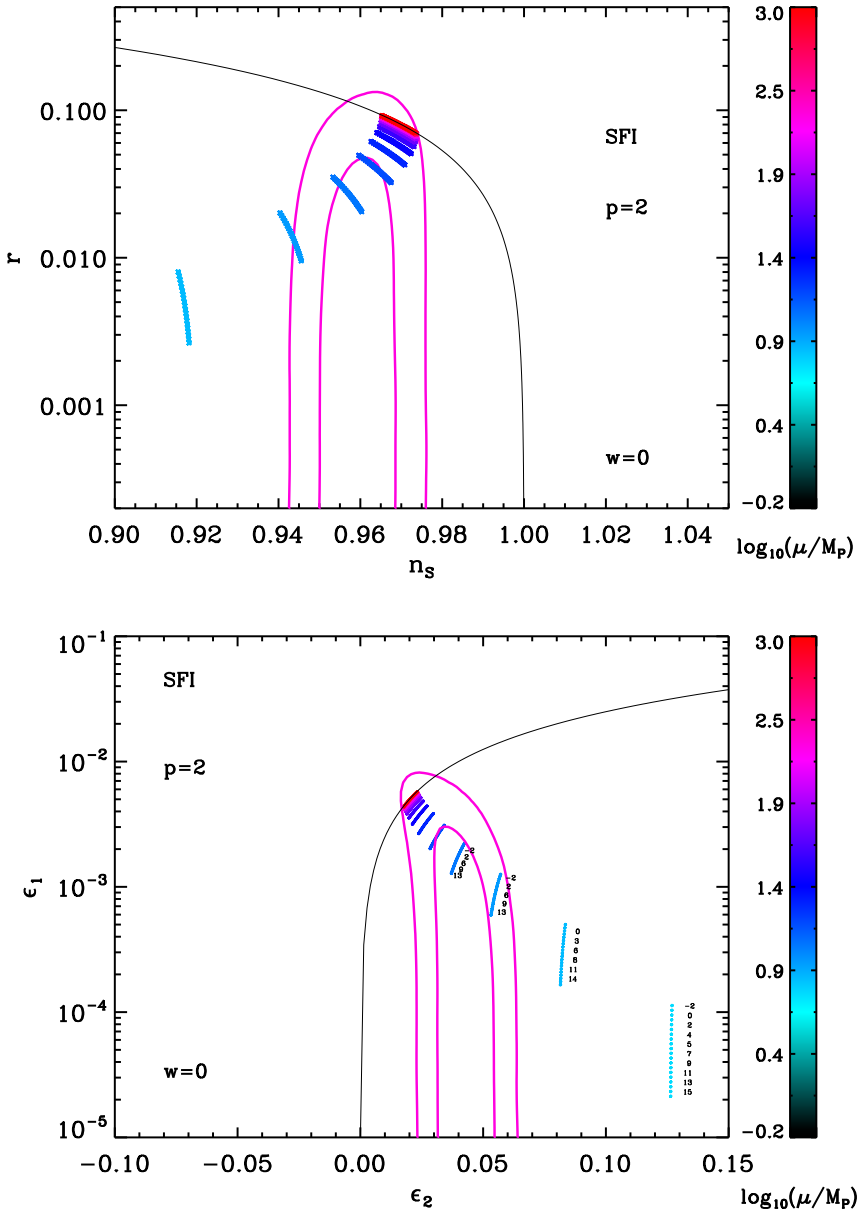

Figure 112. Reheating consistent slow-roll predictions for the small field models with $p = 2$ in the plane $(n_{\rm S}, r)$ (top panel) and the plane (ϵ_1, ϵ_2) (bottom panel). The two pink solid contours are the one and two-sigma Planck confidence intervals (marginalized over second order slow-roll). The annotations trace the energy scale at which reheating ends and correspond to $\log(g_*^{1/4} T_{\rm reh}/{\rm GeV})$. Clearly, if $\mu/M_{\rm Pl}$ is not too high these values are limited from below to stay inside the two-sigma contours, and $\mu/M_{\rm Pl} < 10$ seems to be disfavored by the data. The black solid line represent the locus of the points such that $r = (8/3)\,(1 - n_{\rm S})$, i.e. $\epsilon_2 = 4\epsilon_1$, on which this model lies for $\mu/M_{\rm Pl} \gg 1$.

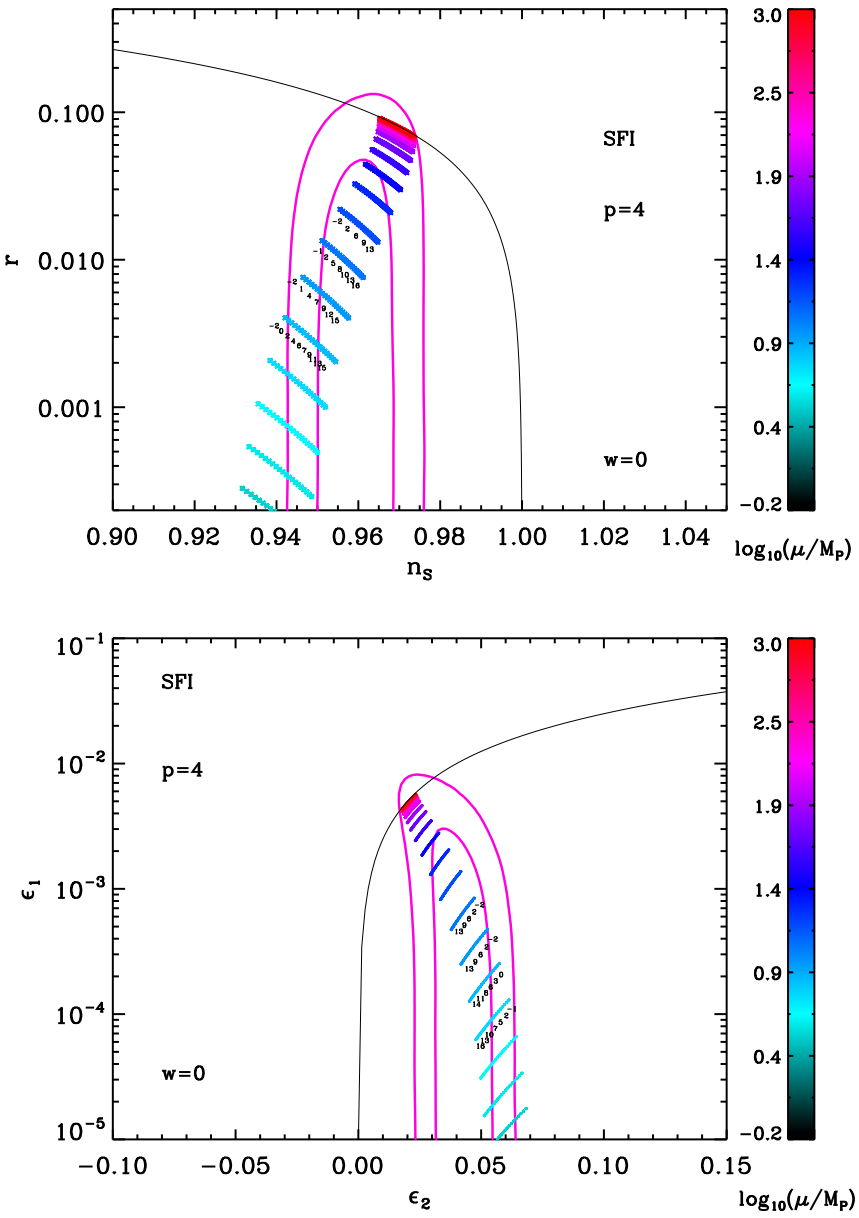

Figure 113. Reheating consistent slow-roll predictions for the small field models with $p = 4$ in the plane $(n_{\rm S}, r)$ (top panel) and the plane (ϵ_1, ϵ_2) (bottom panel). The two pink solid contours are the one and two-sigma Planck confidence intervals (marginalized over second order slow-roll). The annotations trace the energy scale at which reheating ends and correspond to $\log(g_*^{1/4} T_{\rm reh}/{\rm GeV})$. Clearly, if $\mu/M_{\rm Pl}$ is not too high these values are limited from below to stay inside the two-sigma contours. The black solid line represent the locus of the points such that $r = (8/3)\,(1 - n_{\rm S})$, i.e. $\epsilon_2 = 4\epsilon_1$, on which this model lies for $\mu/M_{\rm Pl} \gg 1$.

A.26 Intermediate Inflation (II)

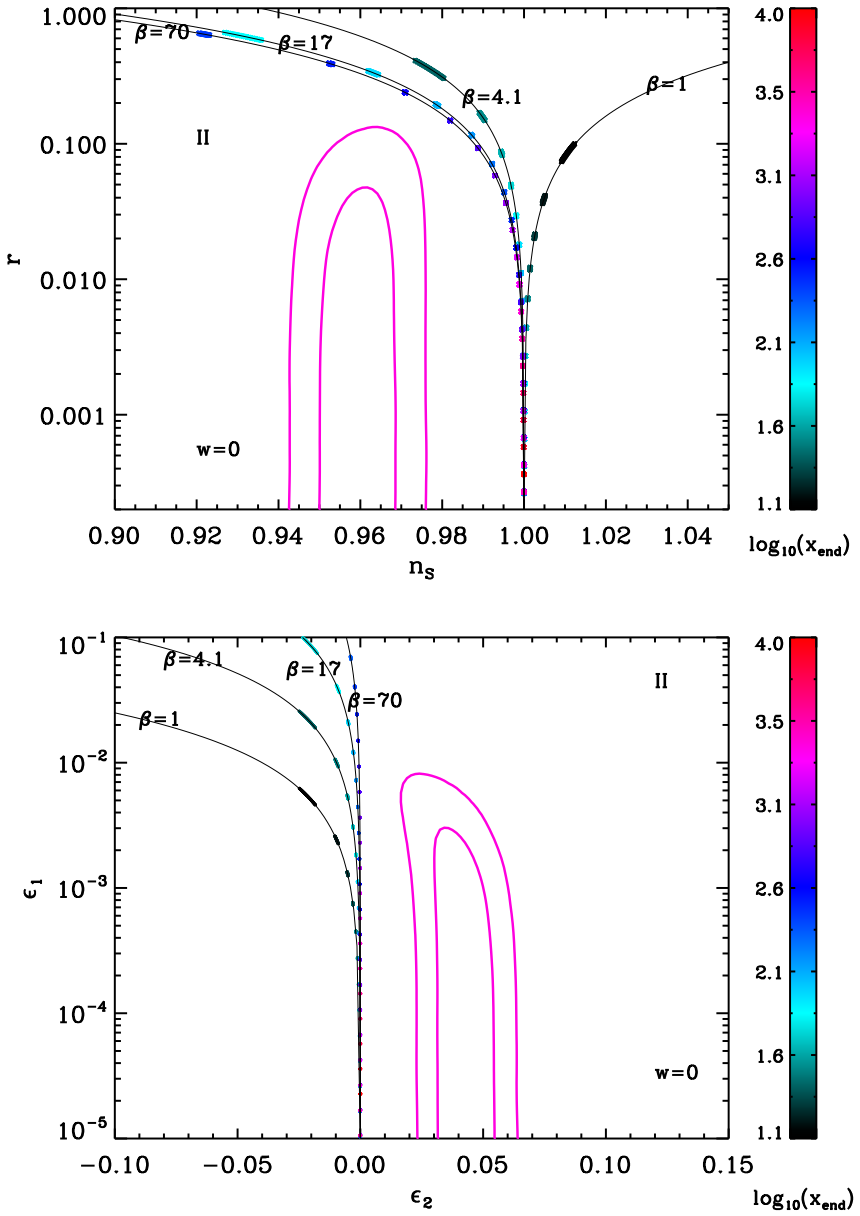

Figure 114. Reheating consistent slow-roll predictions for the intermediate inflation models in the plane $(n_{\rm S}, r)$ (top panel) and the plane (ϵ_1, ϵ_2) (bottom panel). The two pink solid contours are the one and two-sigma Planck confidence intervals (marginalized over second order slow-roll). Four different values of β are displayed (namely $\beta = 1, 4.1, 17, 70$), and for each of them the black solid lines correspond to the points such that $\epsilon_1 = -(\beta/4)\epsilon_2$, on which the predictions should lie for $x_{\rm end} \gg 1$, which is very well verified. The annotations of the energy scale at which reheating ends are not displayed since this parameter is degenerated with $x_{\rm end}$.

A.27 Kähler Moduli Inflation II (KMIII)

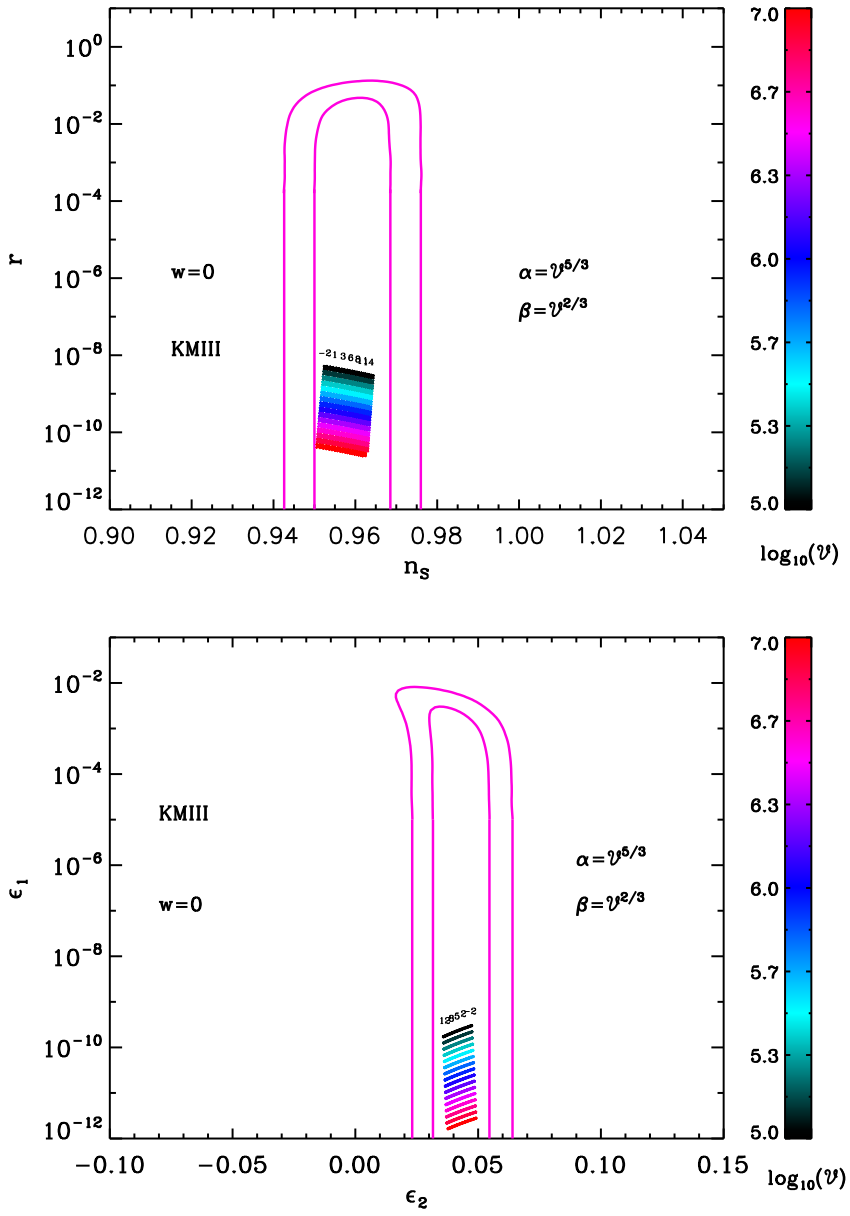

Figure 115. Reheating consistent slow-roll predictions for the Kähler moduli III models in the plane $(n_{\rm S}, r)$ (top panel) and the plane (ϵ_1, ϵ_2) (bottom panel), for $10^5 < \mathcal{V} < 10^7$, $\alpha = \mathcal{V}^{5/3}$ and $\beta = \mathcal{V}^{2/3}$. The two pink solid contours are the one and two-sigma Planck confidence intervals (marginalized over second order slow-roll). The annotations trace the energy scale at which reheating ends and correspond to $\log(g_*^{1/4} T_{\rm reh}/{\rm GeV})$.

A.28 Logamediate Inflation (LMI)

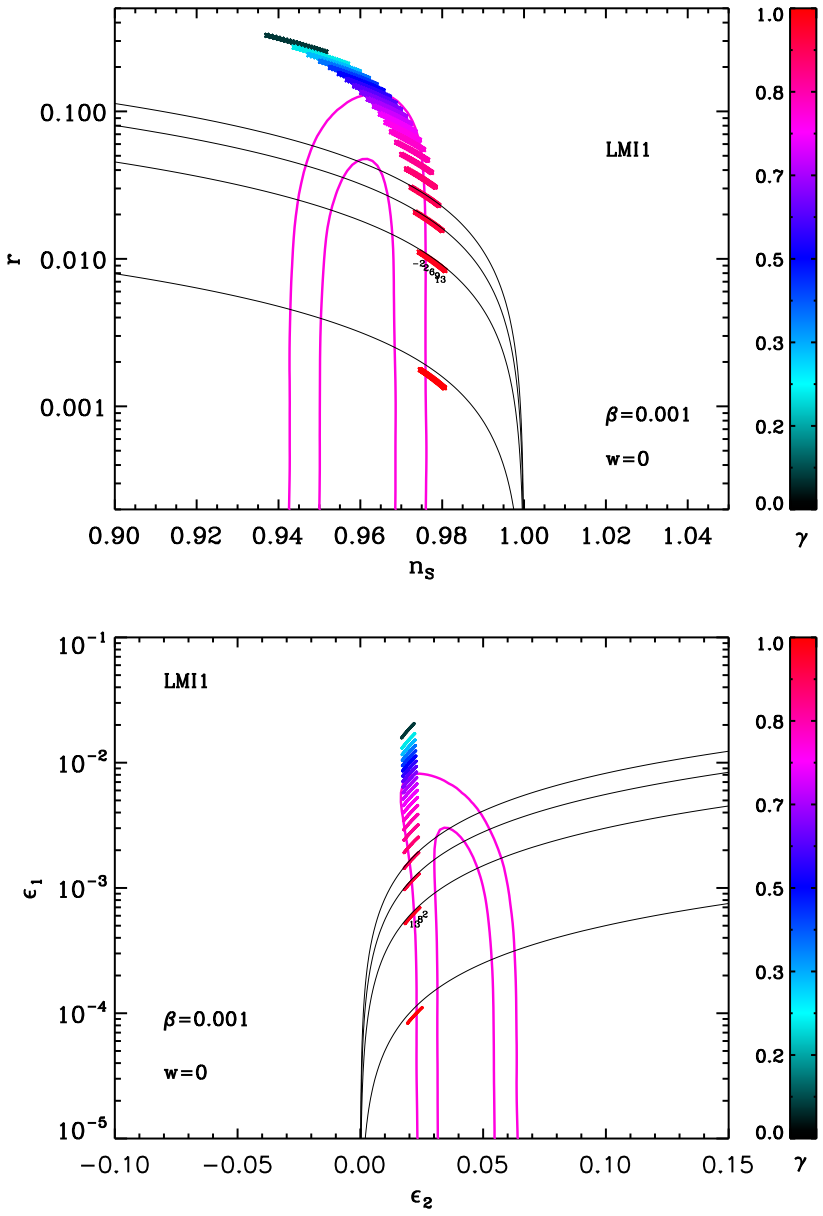

Figure 116. Reheating consistent slow-roll predictions for the Logamediate Inflation 1 models with $\beta = 10^{-3}$, in the plane $(n_{\rm S}, r)$ (top panel) and the plane (ϵ_1, ϵ_2) (bottom panel). Inflation proceeds at decreasing field values $x < x_{V^{\rm max}}$. The two pink solid contours are the one and two-sigma Planck confidence intervals (marginalized over second order slow-roll). The annotations trace the energy scale at which reheating ends and correspond to $\log(g_*^{1/4} T_{\rm reh}/{\rm GeV})$. For $\beta \ll 1$, the exponential term in the potential Eq. (5.68) is almost constant so that the model is close to large field inflation (LFI, see section 4.2). In that limit, one has $\epsilon_1 = \alpha\epsilon_2/4 = (1-\gamma)\,\epsilon_2$, which corresponds to the black solid lines.

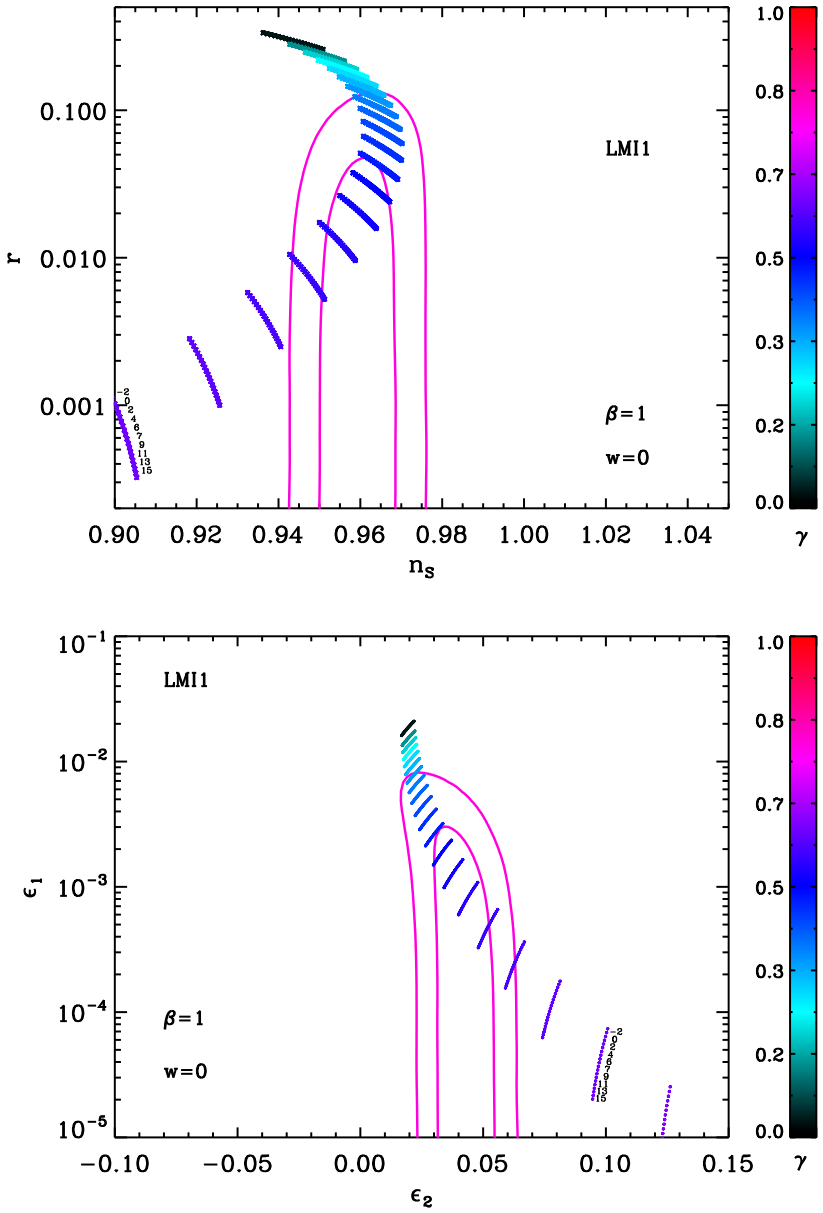

Figure 117. Reheating consistent slow-roll predictions for the Logamediate Inflation 1 models with $\beta = 1$ in the plane $(n_{\rm S}, r)$ (top panel) and the plane (ϵ_1, ϵ_2) (bottom panel). Inflation proceeds as in Fig. 116, at decreasing field values and with $x < x_{V^{\rm max}}$. The two pink solid contours are the one and two-sigma Planck confidence intervals (marginalized over second order slow-roll). The annotations trace the energy scale at which reheating ends and correspond to $\log(g_*^{1/4} T_{\rm reh}/{\rm GeV})$.

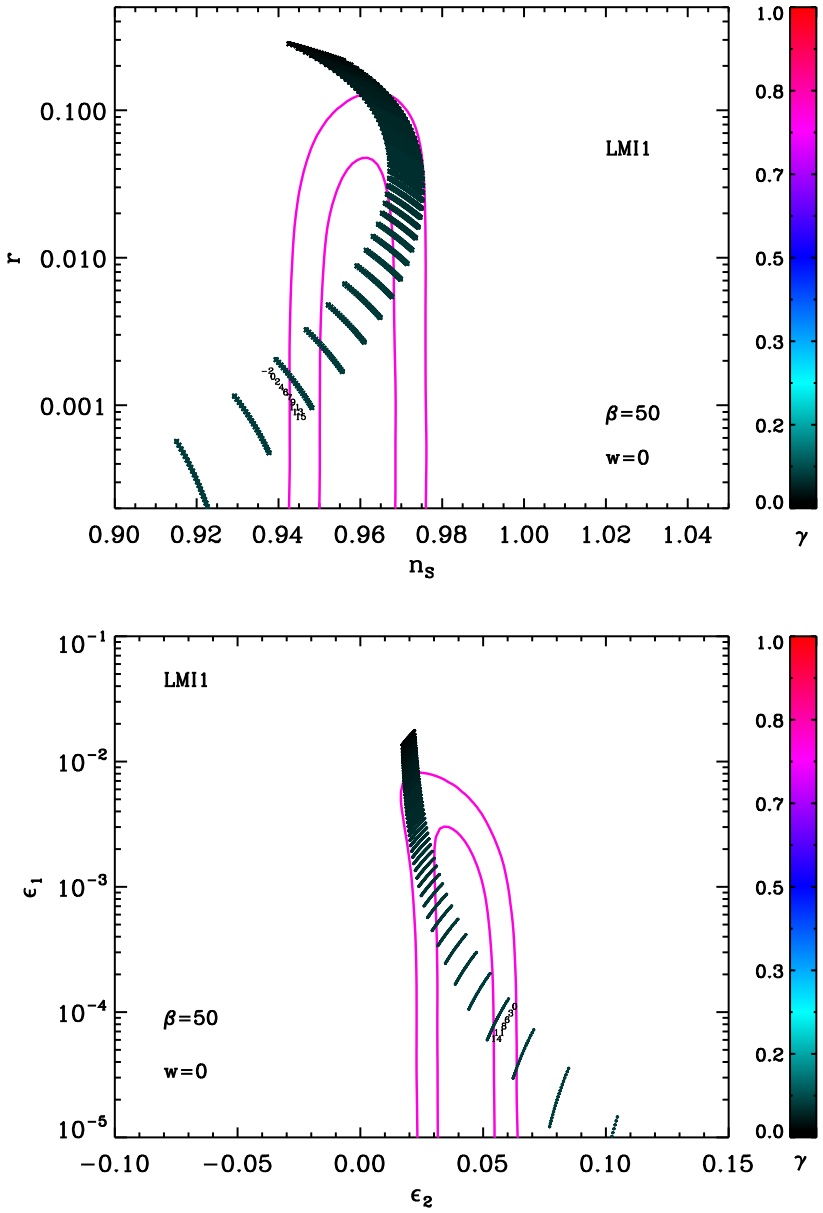

Figure 118. Reheating consistent slow-roll predictions for the Logamediate Inflation 1 models ($x < x_{V^{\max}}$) with $\beta = 50$, in the plane $(n_{\rm S}, r)$ (top panel) and the plane (ϵ_1, ϵ_2) (bottom panel). The two pink solid contours are the one and two-sigma Planck confidence intervals (marginalized over second order slow-roll). The annotations trace the energy scale at which reheating ends and correspond to $\log(g_*^{1/4} T_{\rm reh}/{\rm GeV})$. For such high values of β, only small values of γ are in agreement with observations.

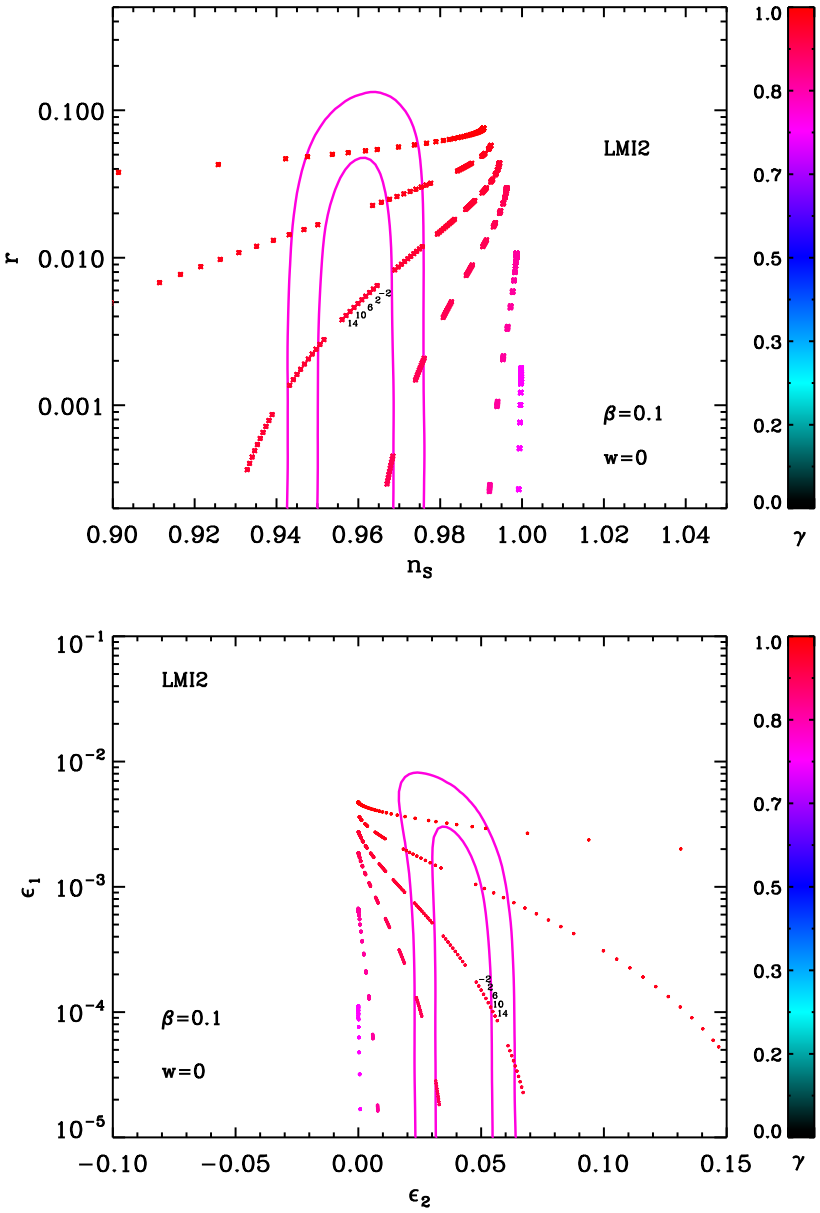

Figure 119. Reheating consistent slow-roll predictions for the Logamediate Inflation 2 models with $\beta = 0.1$, in the plane $(n_{\rm S}, r)$ (top panel) and the plane (ϵ_1, ϵ_2) (bottom panel). Inflation proceeds at increasing field values and with $x > x_{V^{\rm max}}$. The color of the data points encodes the value of γ, while different data blocks correspond to different values of $x_{\rm end}$. Inside a given bock, the annotations trace the energy scale at which reheating ends and correspond to $\log(g_*^{1/4} T_{\rm reh}/{\rm GeV})$. The two pink solid contours are the one and two-sigma Planck confidence intervals (marginalized over second order slow-roll).

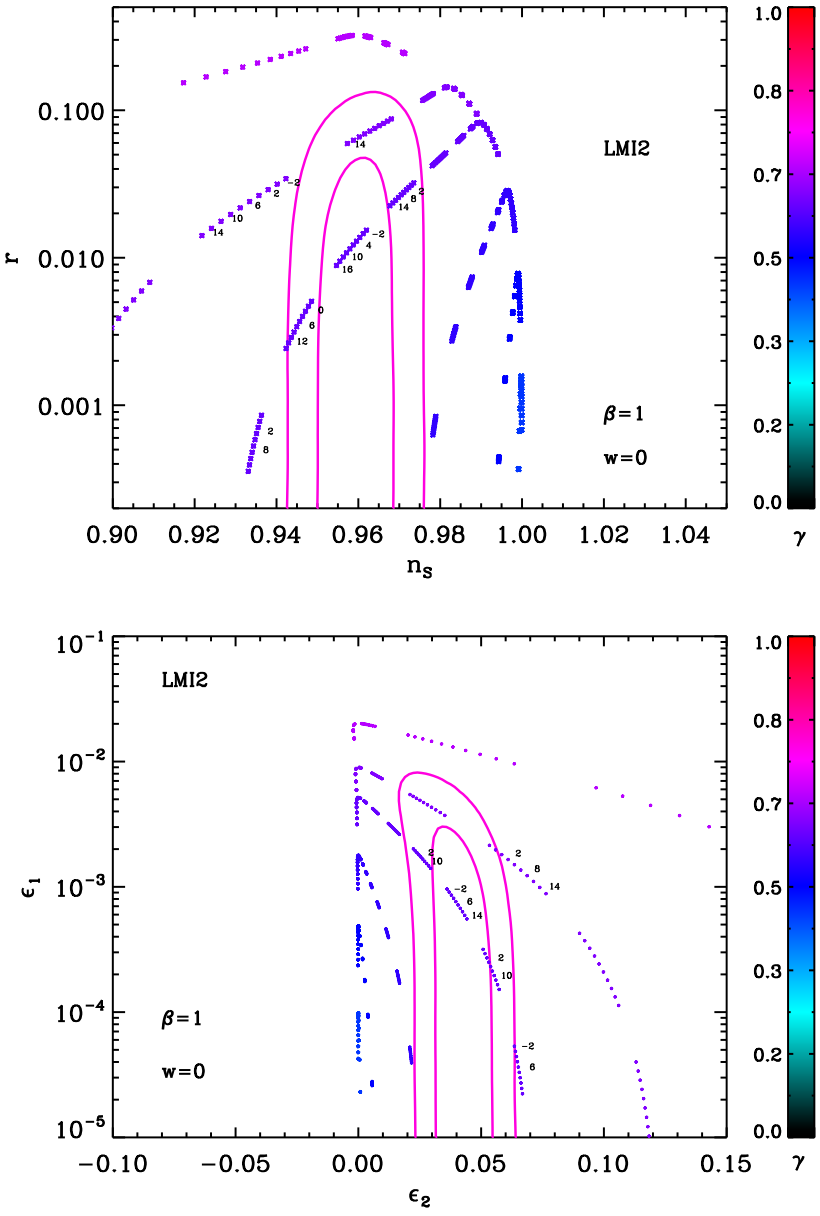

Figure 120. Reheating consistent slow-roll predictions for the Logamediate Inflation 2 models ($x > x_{V^{\max}}$) with $\beta = 1$, in the plane $(n_{\rm S}, r)$ (top panel) and the plane (ϵ_1, ϵ_2) (bottom panel). The color of the data points encodes the value of γ, while different data blocks correspond to different values of $x_{\rm end}$. Inside a given bock, the annotations trace the energy scale at which reheating ends and correspond to $\log(g_*^{1/4} T_{\rm reh}/{\rm GeV})$. The two pink solid contours are the one and two-sigma Planck confidence intervals (marginalized over second order slow-roll). For fixed γ, the turning point in the predictions line occurs when $x_{\rm end}$ lies in the fine-tuned region of LMI2, i.e. $x_{V^{\max}} < x < x_{\epsilon_1^{\max}}$. One sees that the predictions become infinitely close to pure de-Sitter.

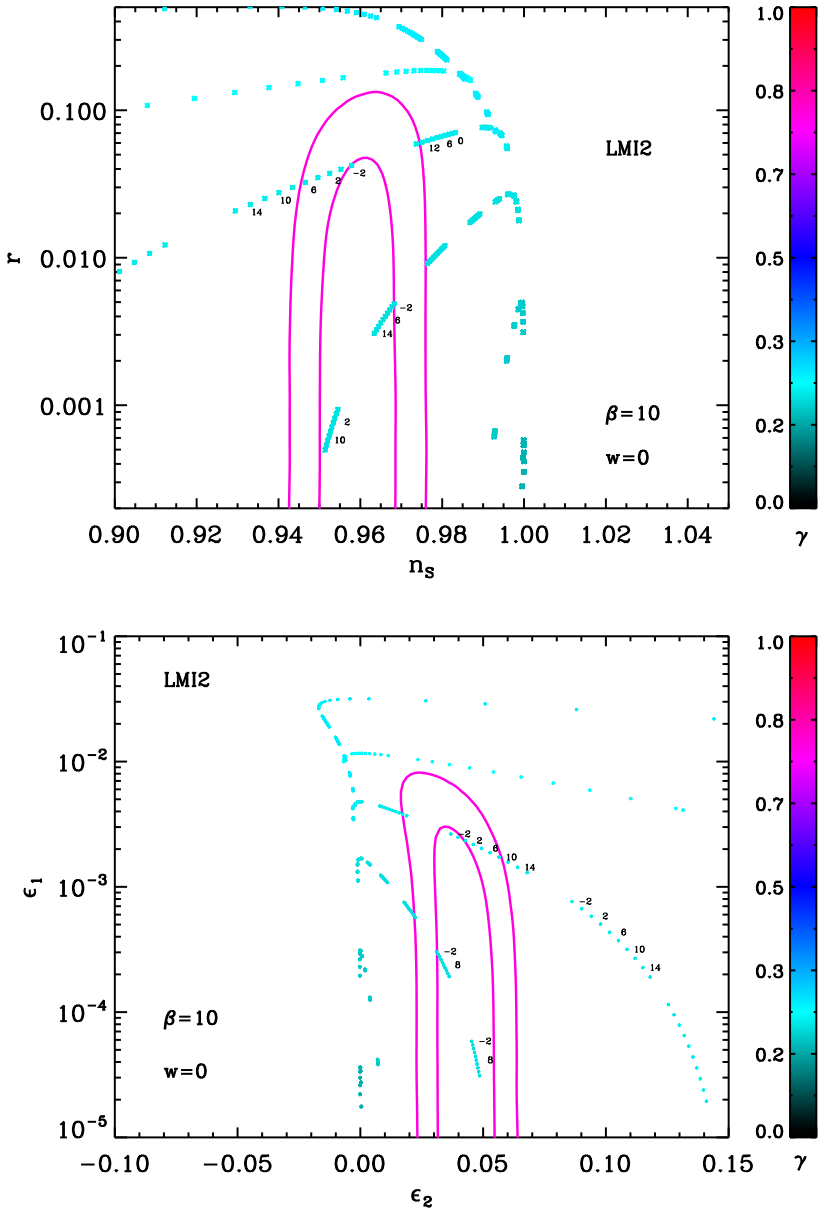

Figure 121. Reheating consistent slow-roll predictions for the Logamediate Inflation 2 models ($x > x_{V^{\max}}$) with $\beta = 10$, in the plane $(n_{\rm S}, r)$ (top panel) and the plane (ϵ_1, ϵ_2) (bottom panel). The color of the data points encodes the value of γ, while different data blocks correspond to different values of $x_{\rm end}$. Inside a given bock, the annotations trace the energy scale at which reheating ends and correspond to $\log(g_*^{1/4} T_{\rm reh}/{\rm GeV})$. The two pink solid contours are the one and two-sigma Planck confidence intervals (marginalized over second order slow-roll). For fixed γ, the turning point in the predictions line occurs when $x_{V^{\max}} < x < x_{\epsilon_1^{\max}}$.

A.29 Twisted Inflation (TWI)

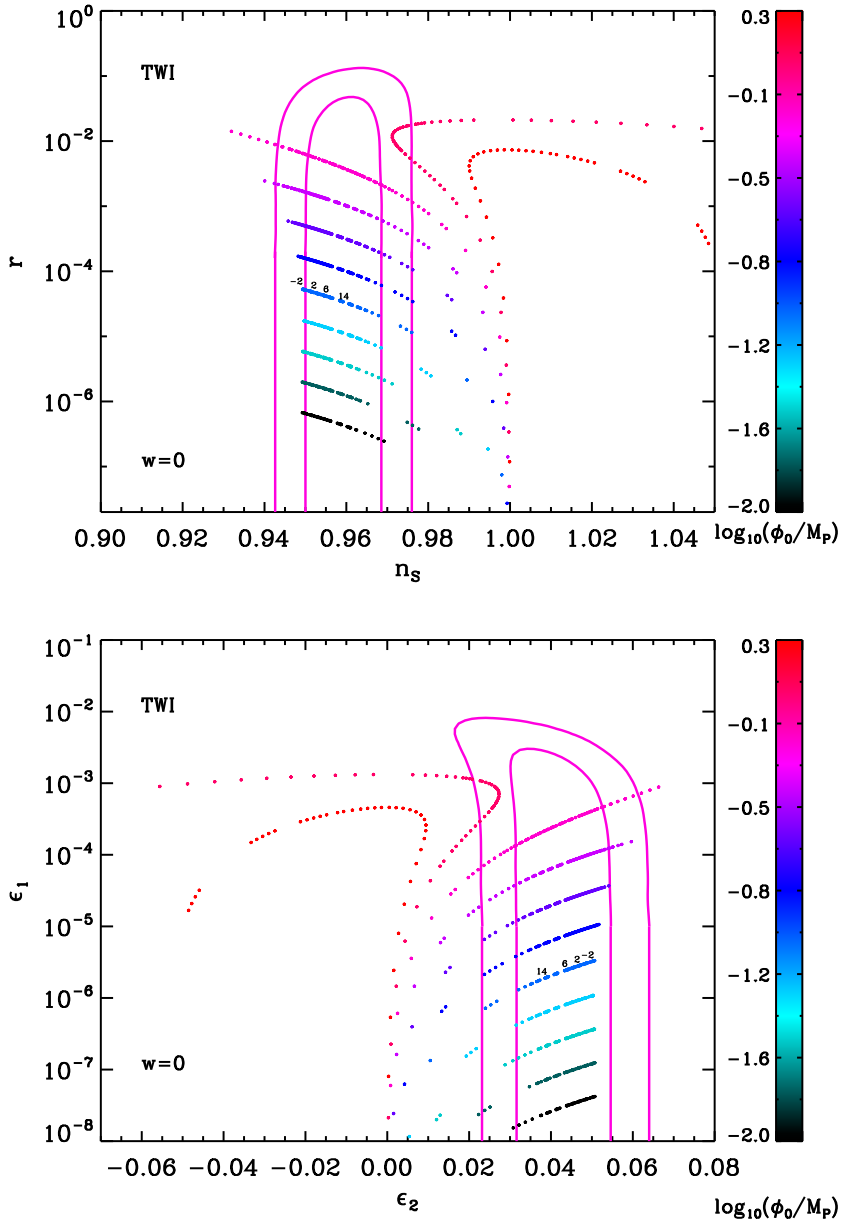

Figure 122. Reheating consistent slow-roll predictions for the twisted models in the plane $(n_{\rm S}, r)$ (top panel) and the plane (ϵ_1, ϵ_2) (bottom panel). The two pink solid contours are the one and two-sigma Planck confidence intervals (marginalized over second order slow-roll). The color of the data points encodes the value of ϕ_0, while different data blocks correspond to different values of $x_{\rm end}$. Inside a given bock, the annotations trace the energy scale at which reheating ends and correspond to $\log(g_*^{1/4} T_{\rm reh}/{\rm GeV})$.

A.30 GMSSM Inflation (GMSSMI)

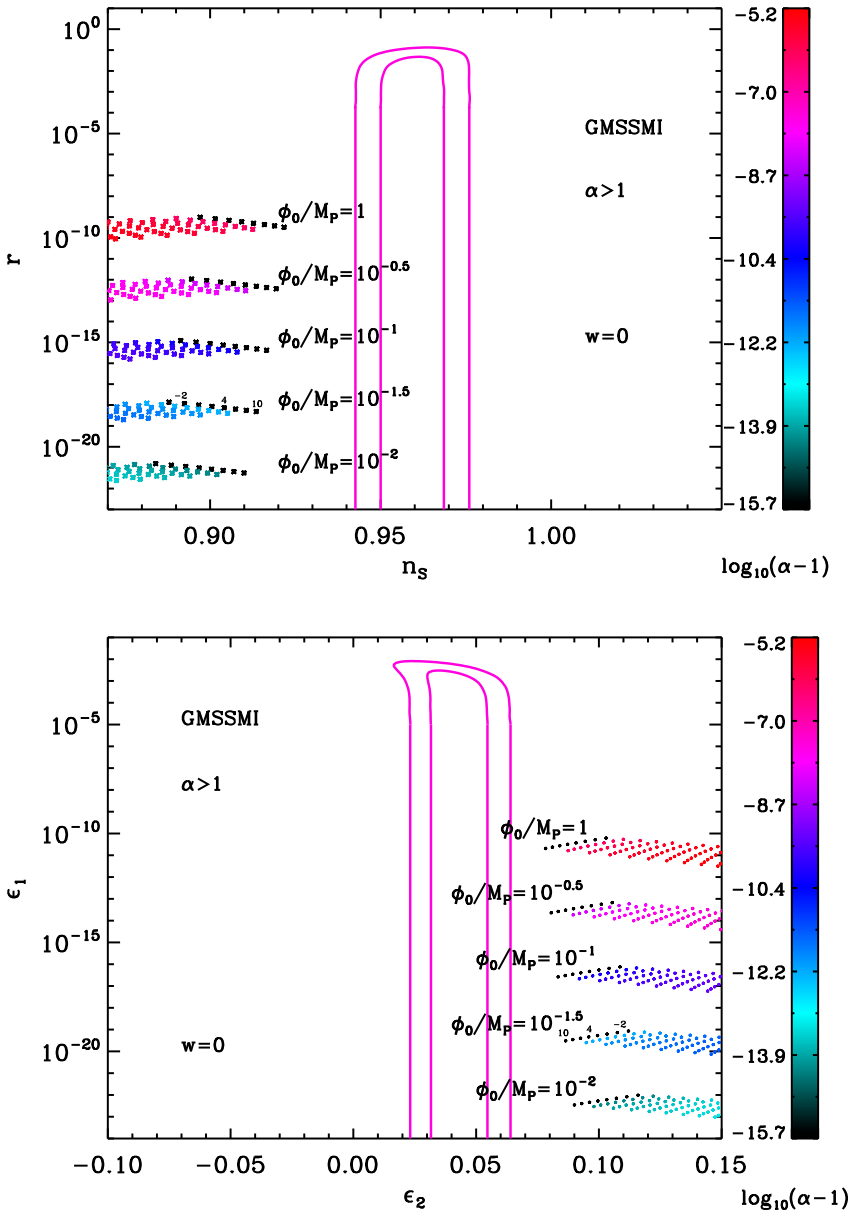

Figure 123. Reheating consistent slow-roll predictions for the GMSSMI models in the plane $(n_{\rm S}, r)$ (top panel) and the plane (ϵ_1, ϵ_2) (bottom panel), for $1 < \alpha < 1 + \phi_0^4/M_{\rm Pl}^4\pi^2/900/(N_{\rm end} - N_{\rm ini})^2$. The two pink solid contours are the one and two-sigma Planck confidence intervals (marginalized over second order slow-roll). The annotations trace the energy scale at which reheating ends and correspond to $\log(g_*^{1/4}T_{\rm reh}/{\rm GeV})$. When $\alpha \to 1$, one recovers the standard MSSM predictions, see Fig. 104.

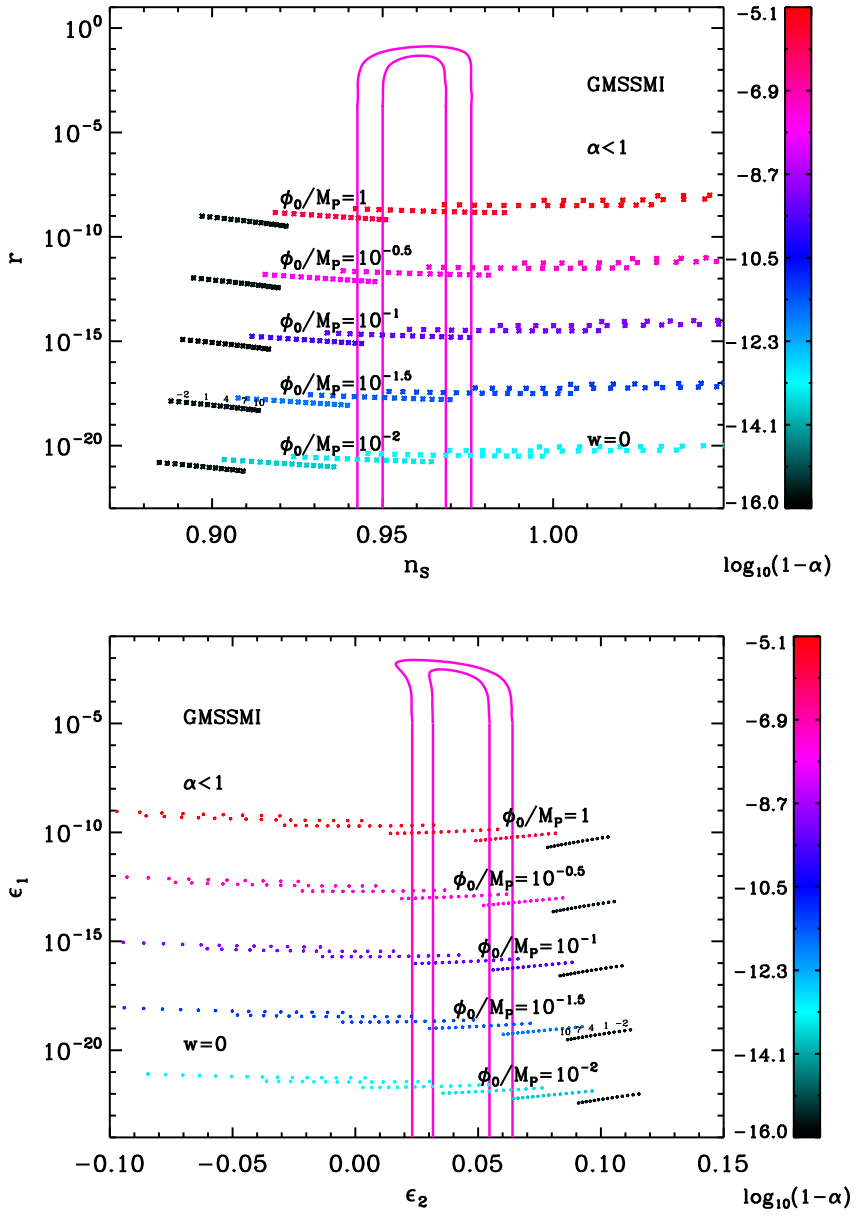

Figure 124. Reheating consistent slow-roll predictions for the GMSSMI models in the plane $(n_{\rm S}, r)$ (top panel) and the plane (ϵ_1, ϵ_2) (bottom panel), for $1 - \phi_0^4/M_{\rm Pl}^4\pi^2/900/(N_{\rm end} - N_{\rm ini})^2 < \alpha < 1$. The two pink solid contours are the one and two-sigma Planck confidence intervals (marginalized over second order slow-roll). The annotations trace the energy scale at which reheating ends and correspond to $\ln(g_*^{1/4}T_{\rm reh}/{\rm GeV})$. When $\alpha \to 1$, one recovers the standard MSSM predictions, see Fig. 104.

A.31 Generalized Renormalizable Inflection Point Inflation (GRIPI)

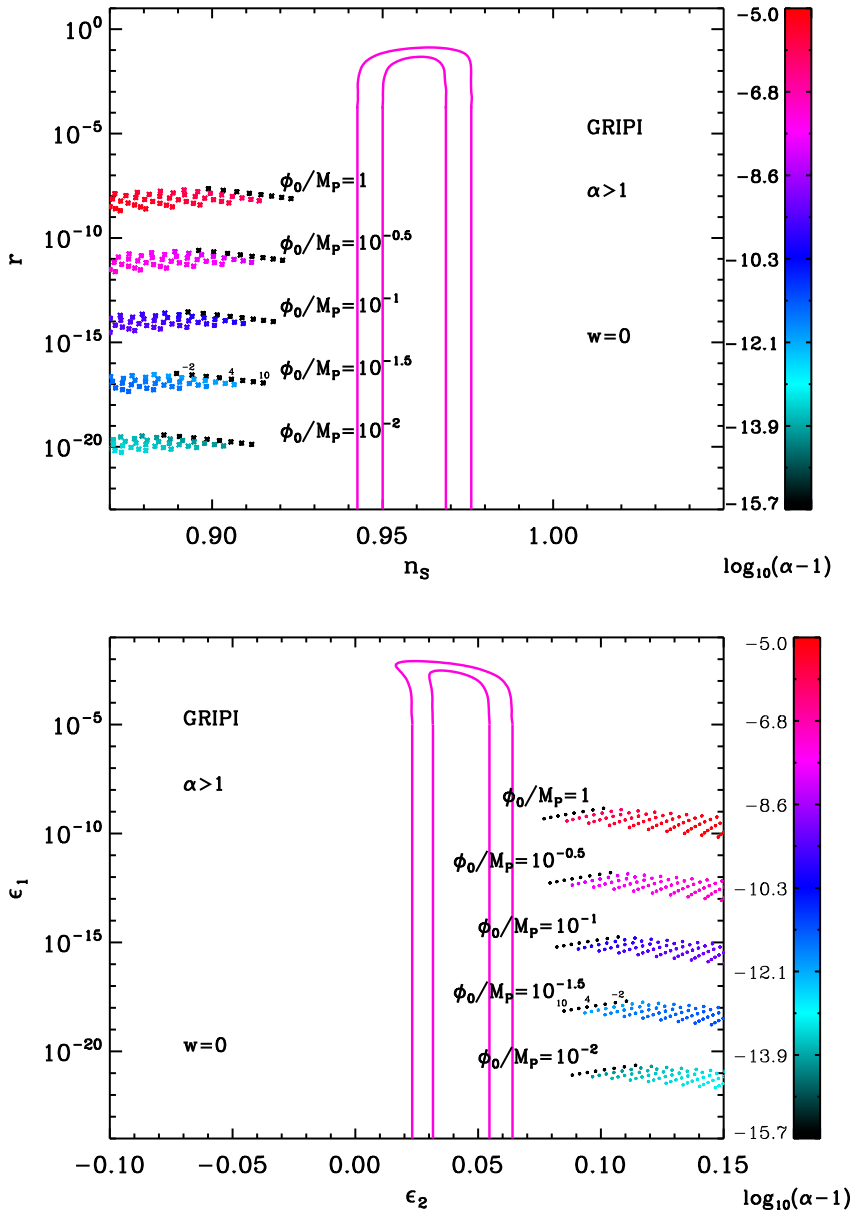

Figure 125. Reheating consistent slow-roll predictions for the generalized renormalizable inflection point models in the plane $(n_{\rm S}, r)$ (top panel) and the plane (ϵ_1, ϵ_2) (bottom panel), for $1 < \alpha < 1 + \phi_0^4/M_{\rm Pl}^4\pi^2/576/(N_{\rm end} - N_{\rm ini} = 60)^2$. The two pink solid contours are the one and two-sigma Planck confidence intervals (marginalized over second order slow-roll). The annotations trace the energy scale at which reheating ends and correspond to $\log(g_*^{1/4}T_{\rm reh}/{\rm GeV})$. When $\alpha \to 1$, one recovers the standard RIPI predictions, see Fig. 105.

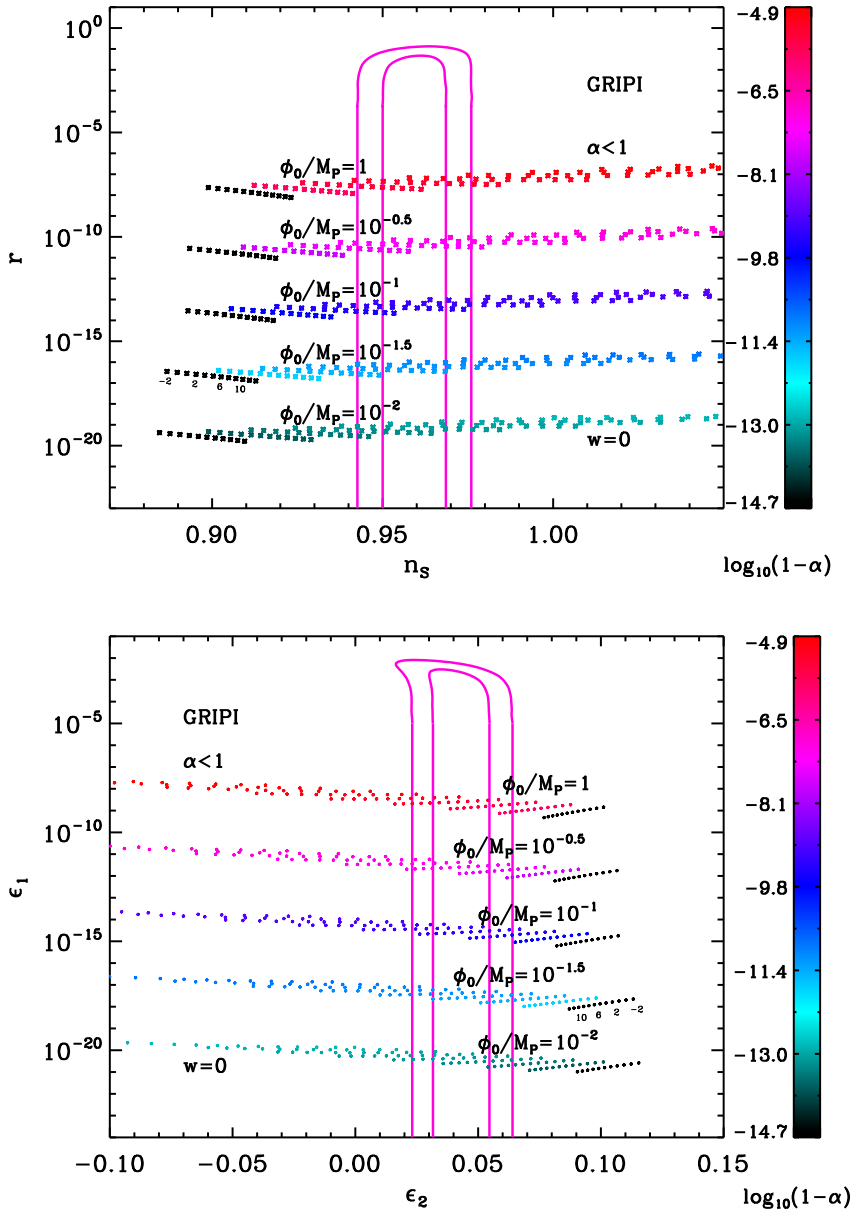

Figure 126. Reheating consistent slow-roll predictions for the generalized renormalizable inflection point models in the plane $(n_{\rm S}, r)$ (top panel) and the plane (ϵ_1, ϵ_2) (bottom panel), for $1 - \phi_0^4/M_{\rm Pl}^4\pi^2/576/(N_{\rm end} - N_{\rm ini} = 60)^2 < \alpha < 1$. The two pink solid contours are the one and two-sigma Planck confidence intervals (marginalized over second order slow-roll). The annotations trace the energy scale at which reheating ends and correspond to $\ln(g_*^{1/4} T_{\rm reh}/{\rm GeV})$. When $\alpha \to 1$, one recovers the standard RIPI predictions, see Fig. 105.

A.32 Brane SUSY breaking Inflation (BSUSYBI)

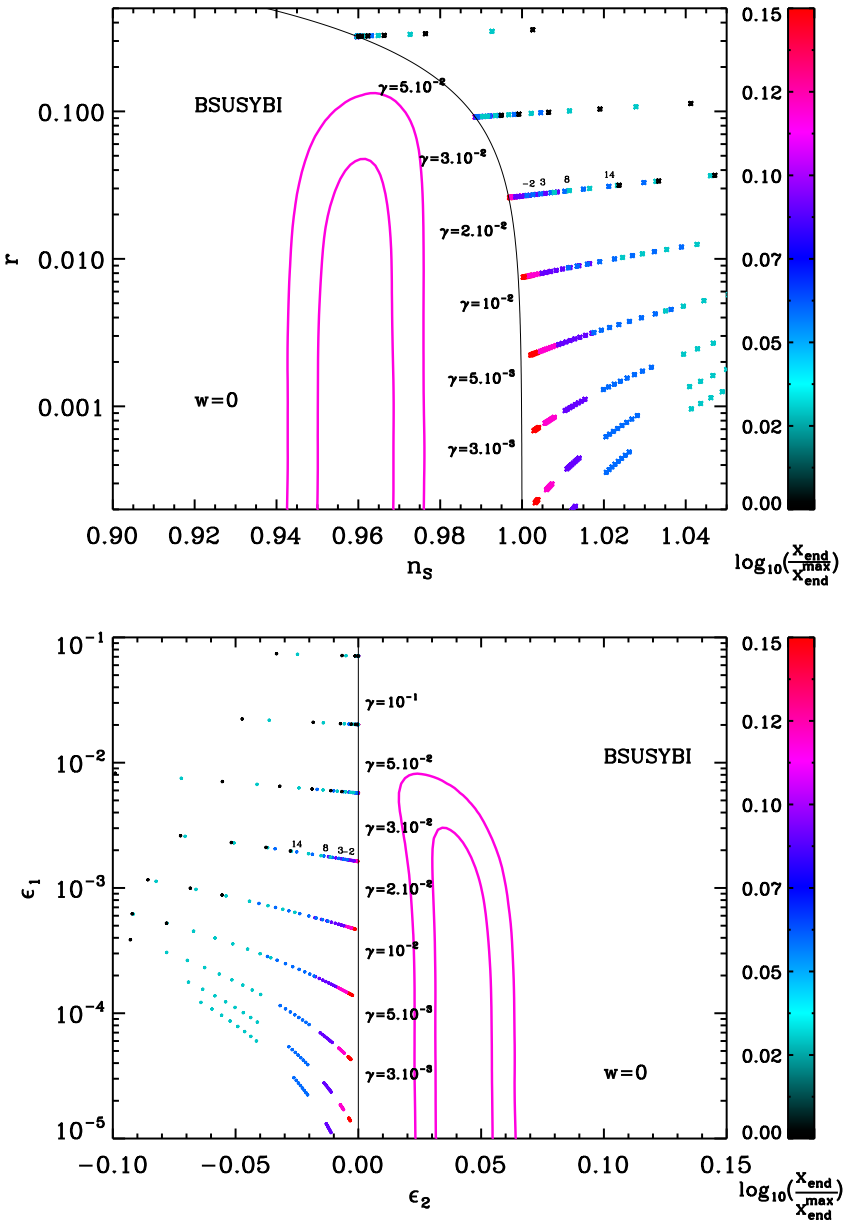

Figure 127. Reheating consistent slow-roll predictions for the BSUSYBI models in the plane $(n_{\rm S}, r)$ (top panel) and the plane (ϵ_1, ϵ_2) (bottom panel). The two pink solid contours are the one and two-sigma Planck confidence intervals (marginalized over second order slow-roll). The parameter $x_{\rm end}$ varies between $2x_{\rm end}^{\rm max} < x_{\rm end} < x_{\rm end}^{\rm max}$ ($x_{\rm end}^{\rm max} < 0$), under which the predictions of the model coincide with the line $\epsilon_2 = 0$ (black solid), i.e. PLI (see section 4.8). The annotations trace the energy scale at which reheating ends and correspond to $\log(g_*^{1/4} T_{\rm reh}/{\rm GeV})$. The parameter γ should be $\lesssim 5 \times 10^{-2}$ to predict a reasonable amount of gravitational waves.

A.33 Tip Inflation (TI)

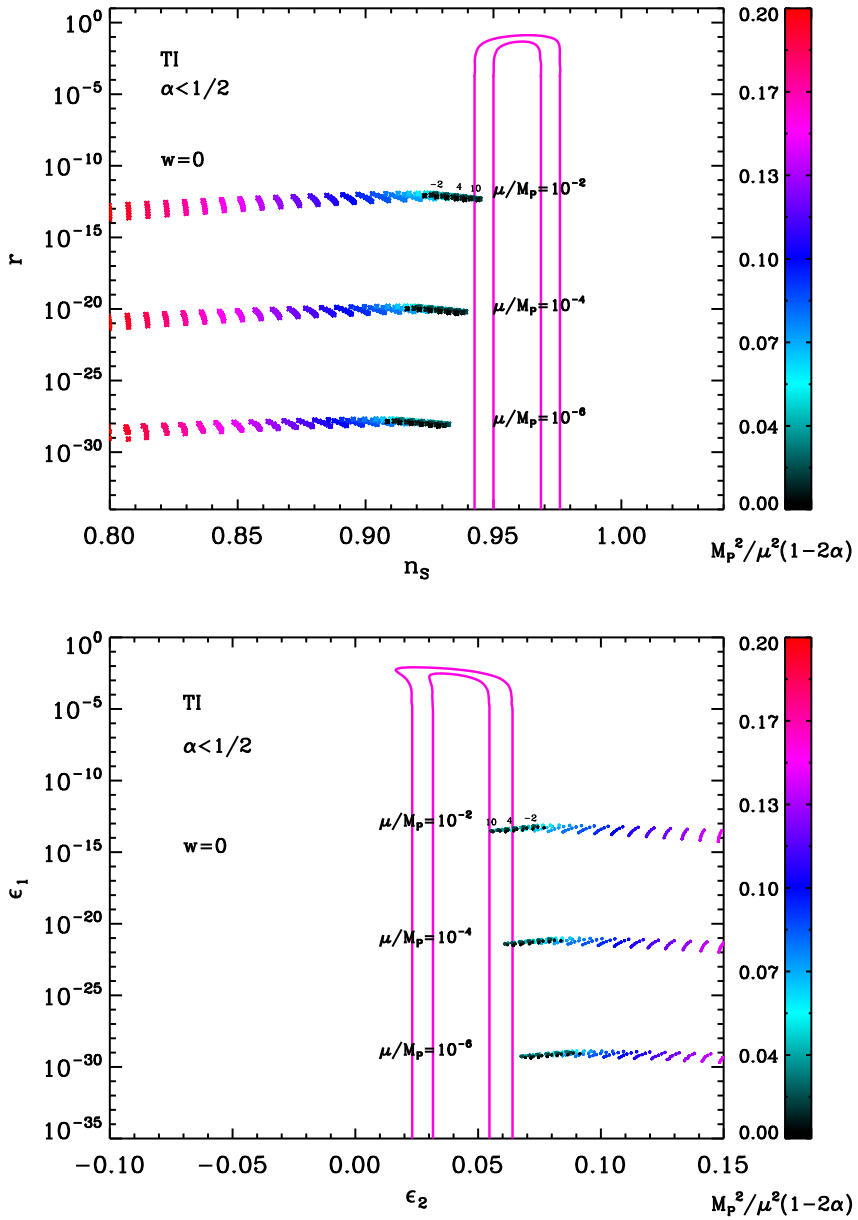

Figure 128. Reheating consistent slow-roll predictions for the tip inflation models with $\alpha < 1/2$, and for $\mu/M_{\rm Pl} = 10^{-6}, 10^{-4}, 10^{-2}$ in the plane $(n_{\rm S}, r)$ (top panel) and the plane (ϵ_1, ϵ_2) (bottom panel). The two pink solid contours are the one and two-sigma Planck confidence intervals (marginalized over second order slow-roll). The annotations trace the energy scale at which reheating ends and correspond to $\log(g_*^{1/4} T_{\rm reh}/{\rm GeV})$.

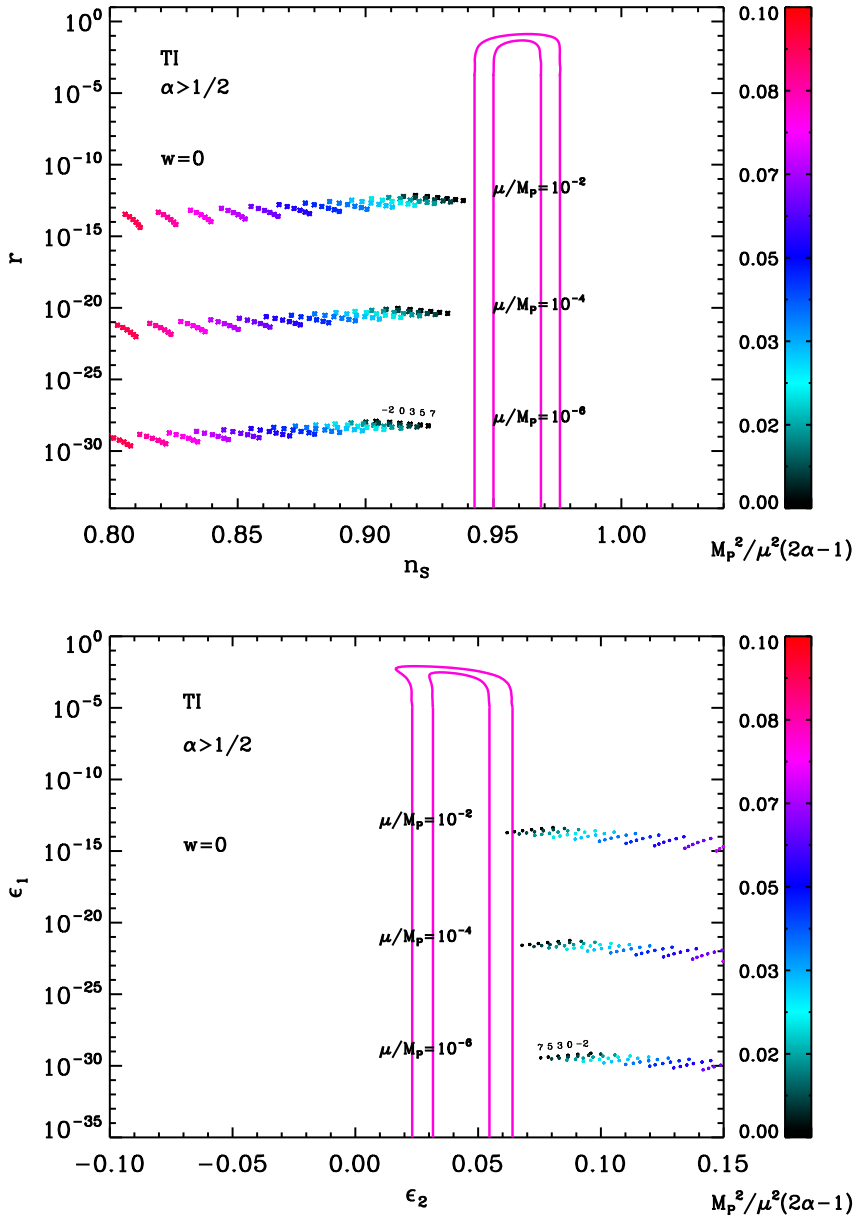

Figure 129. Reheating consistent slow-roll predictions for the tip inflation models with $\alpha > 1/2$, and for $\mu/M_{\rm Pl} = 10^{-6}, 10^{-4}, 10^{-2}$ in the plane $(n_{\rm S}, r)$ (top panel) and the plane (ϵ_1, ϵ_2) (bottom panel). The two pink solid contours are the one and two-sigma Planck confidence intervals (marginalized over second order slow-roll). The annotations trace the energy scale at which reheating ends and correspond to $\log(g_*^{1/4} T_{\rm reh}/{\rm GeV})$.

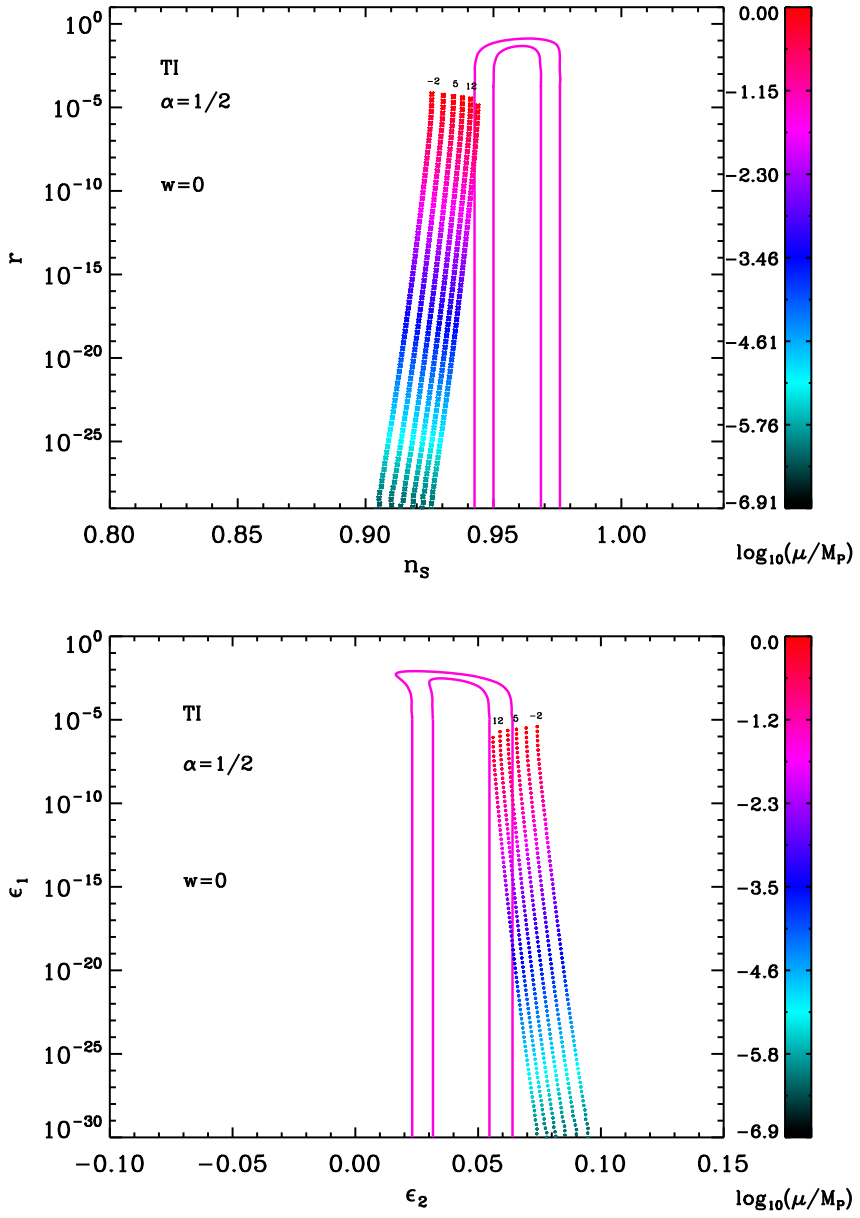

Figure 130. Reheating consistent slow-roll predictions for the tip inflation models with $\alpha = 1/2$ in the plane $(n_{\rm S}, r)$ (top panel) and the plane (ϵ_1, ϵ_2) (bottom panel). The two pink solid contours are the one and two-sigma Planck confidence intervals (marginalized over second order slow-roll). The annotations trace the energy scale at which reheating ends and correspond to $\log(g_*^{1/4} T_{\rm reh}/{\rm GeV})$.

A.34 β Exponential Inflation (BEI)

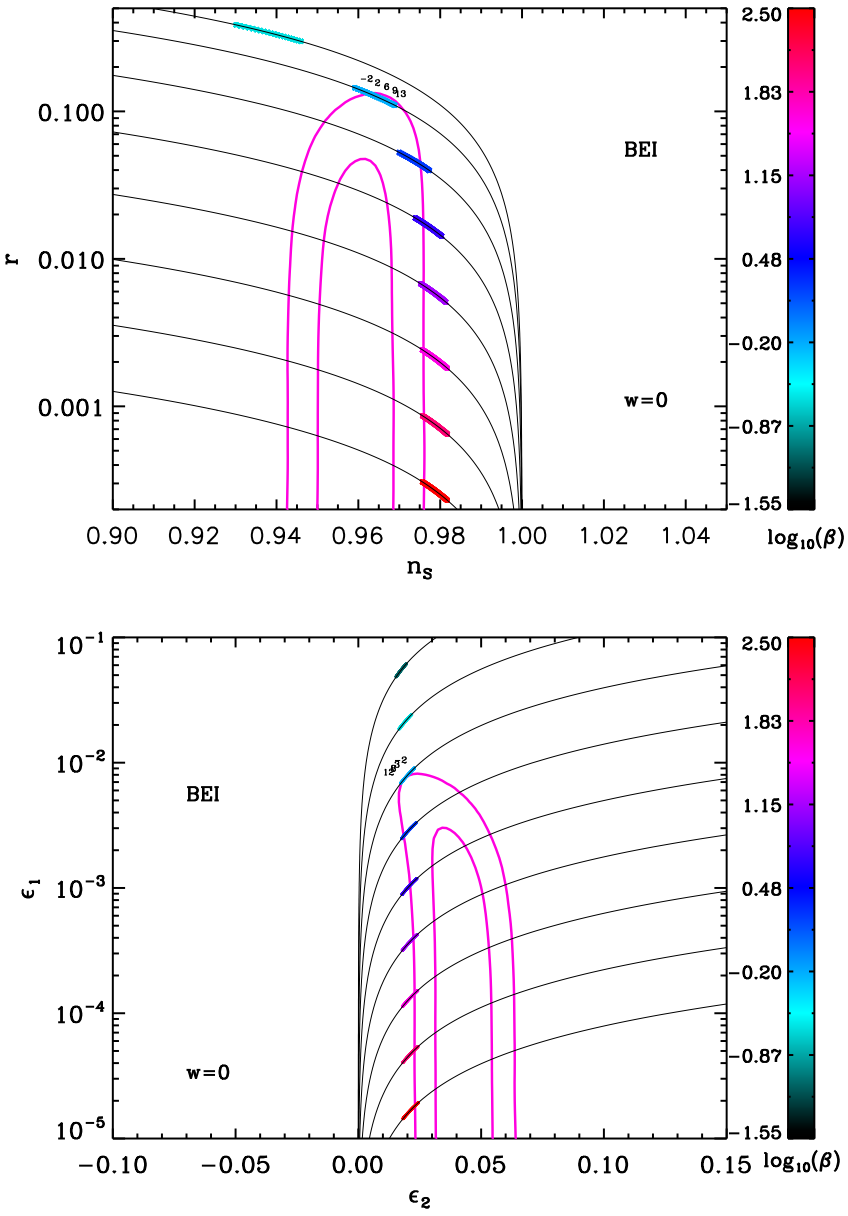

Figure 131. Reheating consistent slow-roll predictions for the β exponential inflation models in the plane $(n_{\rm s}, r)$ (top panel) and the plane (ϵ_1, ϵ_2) (bottom panel). The parameter λ varies in the range $10^{-6} < \lambda < 10^{3}$ but the predictions almost do not depend on it (and cannot be distinguished in the figure). The two pink solid contours are the one and two-sigma Planck confidence intervals (marginalized over second order slow-roll). The black solid lines represent the locus of the points such that $\epsilon_2 = 4\beta\epsilon_1$. The annotations trace the energy scale at which reheating ends and correspond to $\log(g_*^{1/4} T_{\rm reh}/{\rm GeV})$.

A.35 Pseudo Natural Inflation (PSNI)

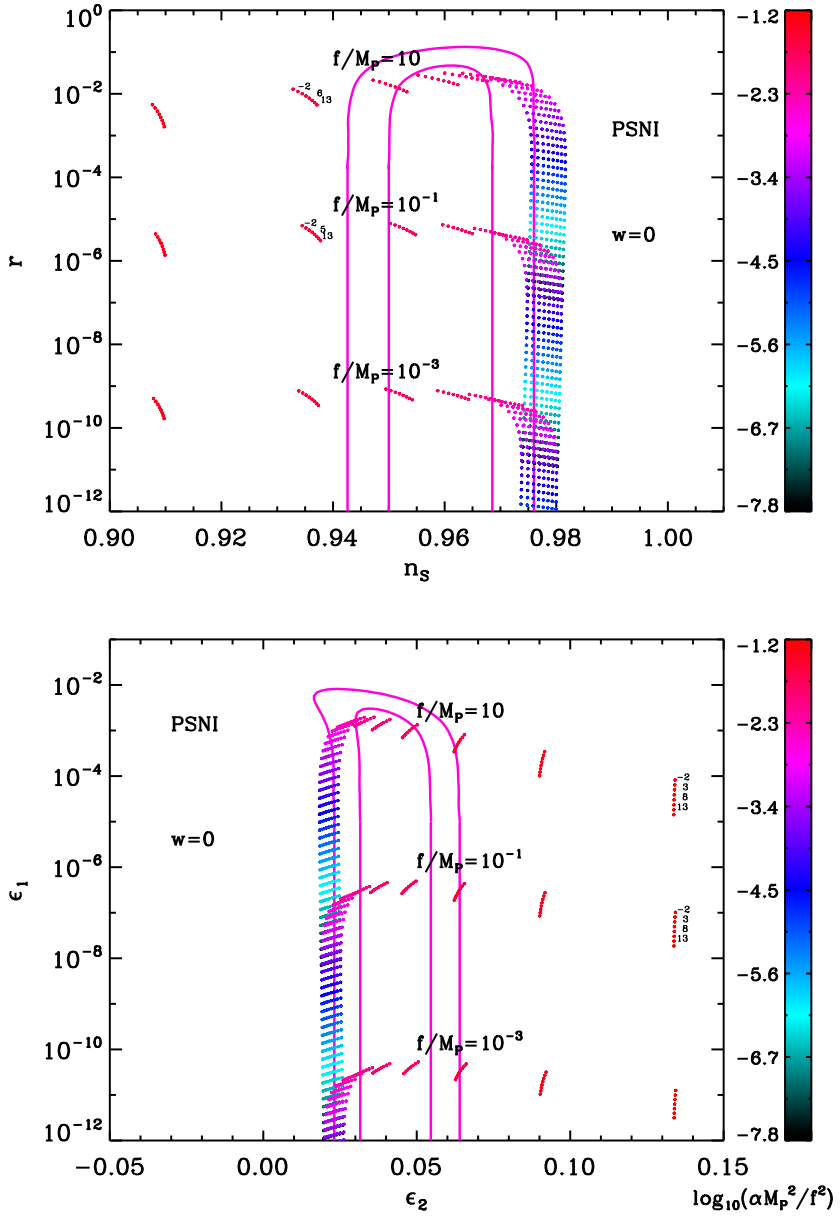

Figure 132. Reheating consistent slow-roll predictions for the pseudo natural inflation models with $\mu/M_{\rm Pl} = 10, 10^{-1}, 10^{-3}$, in the plane $(n_{\rm S}, r)$ (top panel) and the plane (ϵ_1, ϵ_2) (bottom panel). The two pink solid contours are the one and two-sigma Planck confidence intervals (marginalized over second order slow-roll). The annotations trace the energy scale at which reheating ends and correspond to $\log(g_*^{1/4} T_{\rm reh}/{\rm GeV})$.

A.36 Non Canonical Kähler Inflation (NCKI)

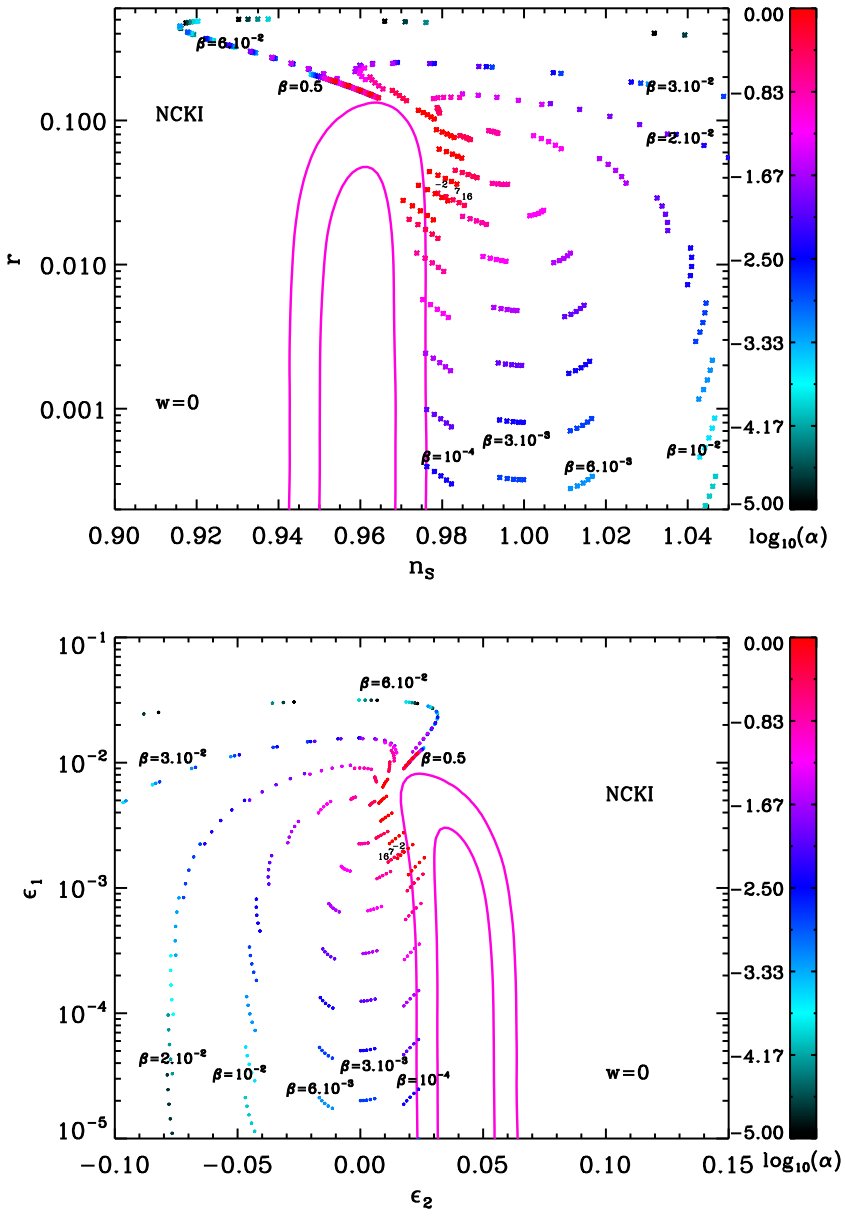

Figure 133. Reheating consistent slow-roll predictions for the non canonical Kähler inflation models with $\beta > 0$ in the plane $(n_{\rm s}, r)$ (top panel) and the plane (ϵ_1, ϵ_2) (bottom panel). The two pink solid contours are the one and two-sigma Planck confidence intervals (marginalized over second order slow-roll). The annotations trace the energy scale at which reheating ends and correspond to $\log(g_*^{1/4} T_{\rm reh}/{\rm GeV})$. When $\beta \gtrsim 1$, the predictions are almost identical to those displayed here.

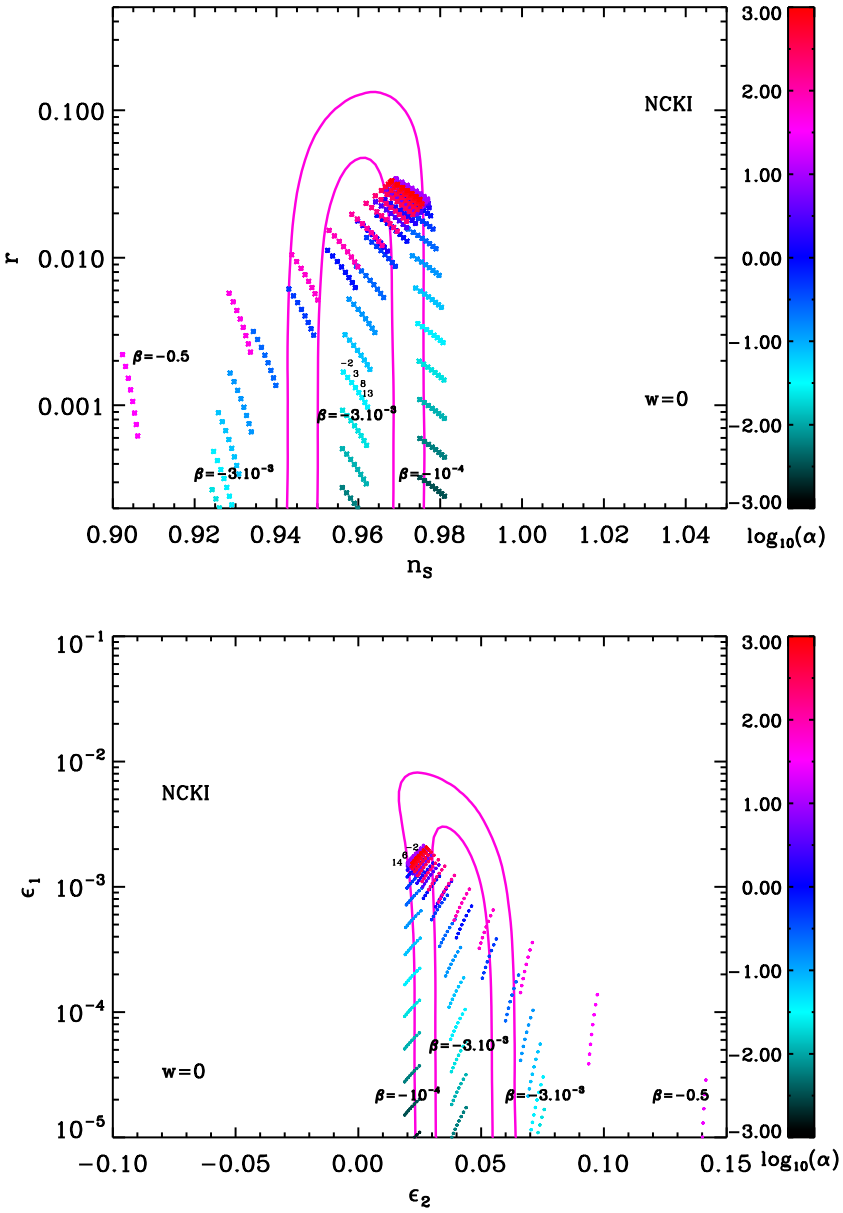

Figure 134. Reheating consistent slow-roll predictions for the non canonical Kähler inflation models with $\beta < 0$, in the plane $(n_{\rm S}, r)$ (top panel) and the plane (ϵ_1, ϵ_2) (bottom panel). The two pink solid contours are the one and two-sigma Planck confidence intervals (marginalized over second order slow-roll). The annotations trace the energy scale at which reheating ends and correspond to $\log(g_*^{1/4} T_{\rm reh}/{\rm GeV})$. When $\beta \lesssim -1$, the predictions remain almost unchanged.

A.37 Constant Spectrum Inflation (CSI)

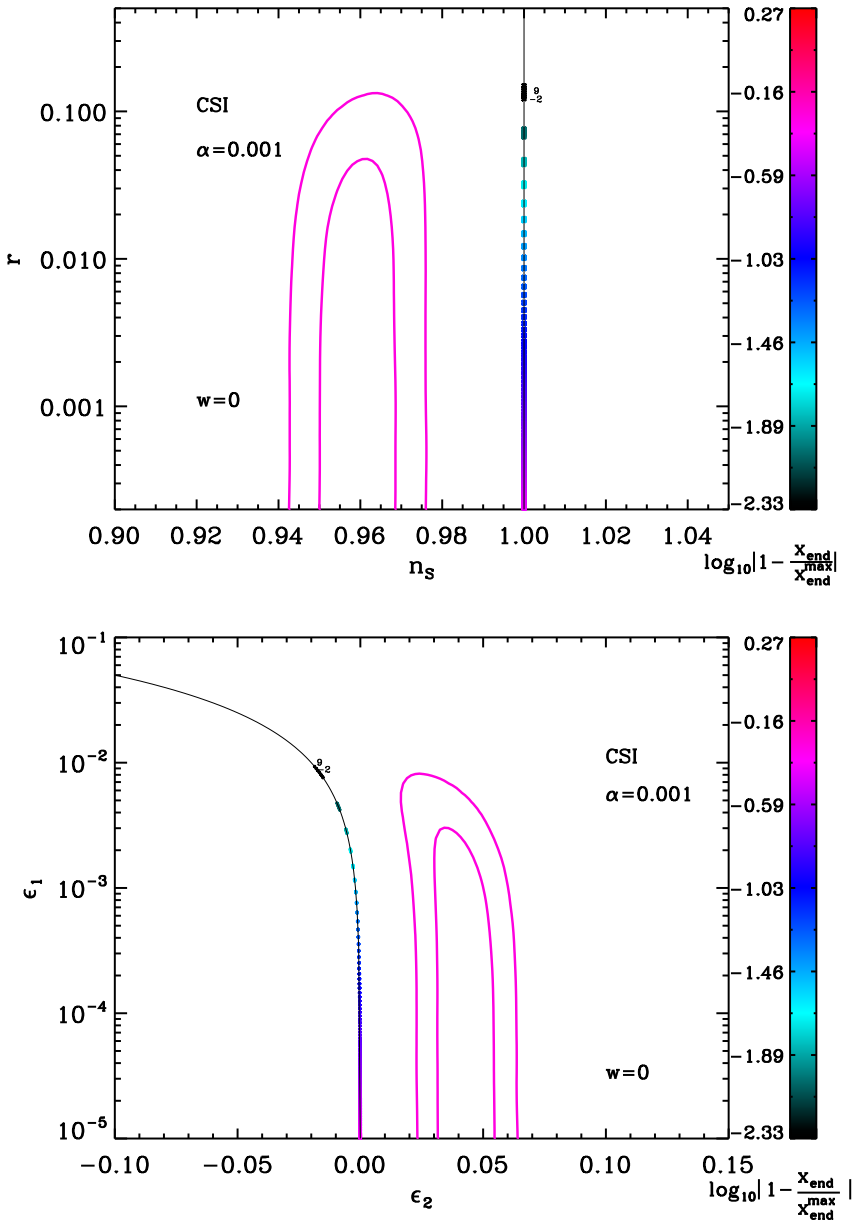

Figure 135. Reheating consistent slow-roll predictions for the Constant Spectrum models in the plane $(n_{\rm S}, r)$ (top panel) and the plane (ϵ_1, ϵ_2) (bottom panel), for $\alpha = 10^{-3}$. The two pink solid contours are the one and two-sigma Planck confidence intervals (marginalized over second order slow-roll). The black solid lines correspond to $n_{\rm S} = 1$, and the annotations trace the energy scale at which reheating ends and correspond to $\log(g_*^{1/4} T_{\rm reh}/{\rm GeV})$.

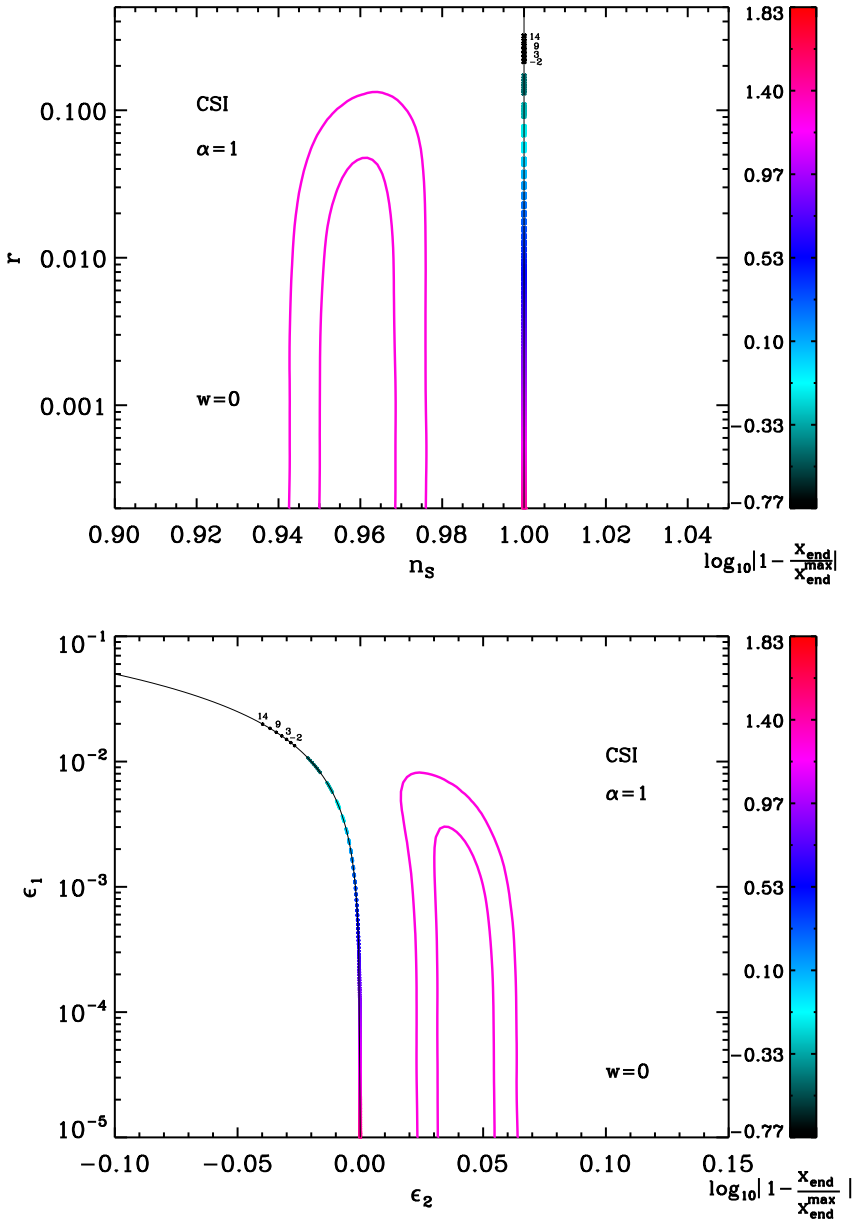

Figure 136. Reheating consistent slow-roll predictions for the Constant Spectrum models in the plane $(n_{\rm S}, r)$ (top panel) and the plane (ϵ_1, ϵ_2) (bottom panel), for $\alpha = 1$. The two pink solid contours are the one and two-sigma Planck confidence intervals (marginalized over second order slow-roll). The black solid lines correspond to $n_{\rm S} = 1$, and the annotations trace the energy scale at which reheating ends and correspond to $\log(g_*^{1/4} T_{\rm reh}/{\rm GeV})$.

A.38 Orientifold Inflation (OI)

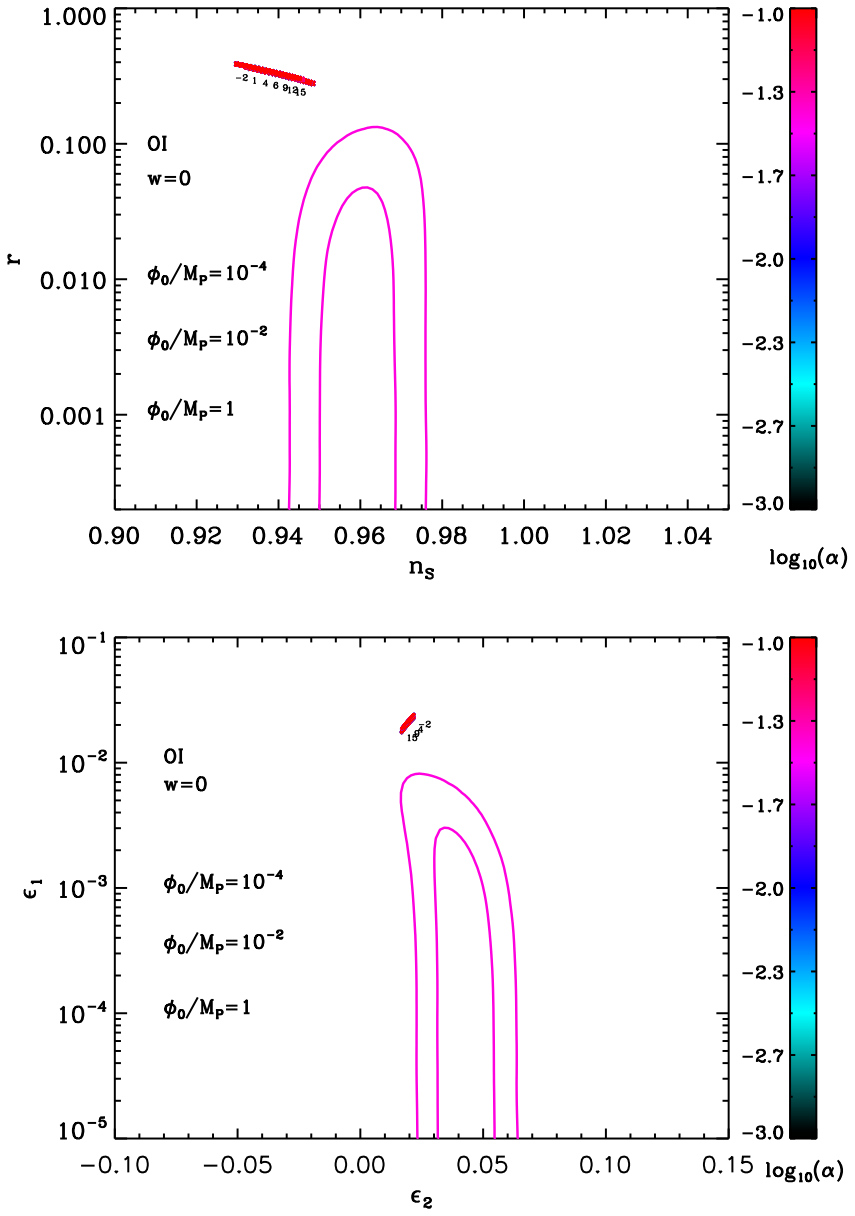

Figure 137. Reheating consistent slow-roll predictions for the orientifold inflation models for $\phi_0/M_{\rm Pl} = 10^{-4}$, 10^{-2}, 1 and $\alpha \in \left[10^{-3}, 10^{-1}\right]$, in the plane $(n_{\rm S}, r)$ (top panel) and the plane (ϵ_1, ϵ_2) (bottom panel). The two pink solid contours are the one and two-sigma Planck confidence intervals (marginalized over second order slow-roll). The annotations trace the energy scale at which reheating ends and correspond to $\log(g_*^{1/4} T_{\rm reh}/{\rm GeV})$. Since the predictions of these models almost do not depend on its parameters, they are all superimposed and one cannot distinguish the different values of ϕ_0 are α.

A.39 Constant $n_{\rm S}$ C Inflation (CNCI)

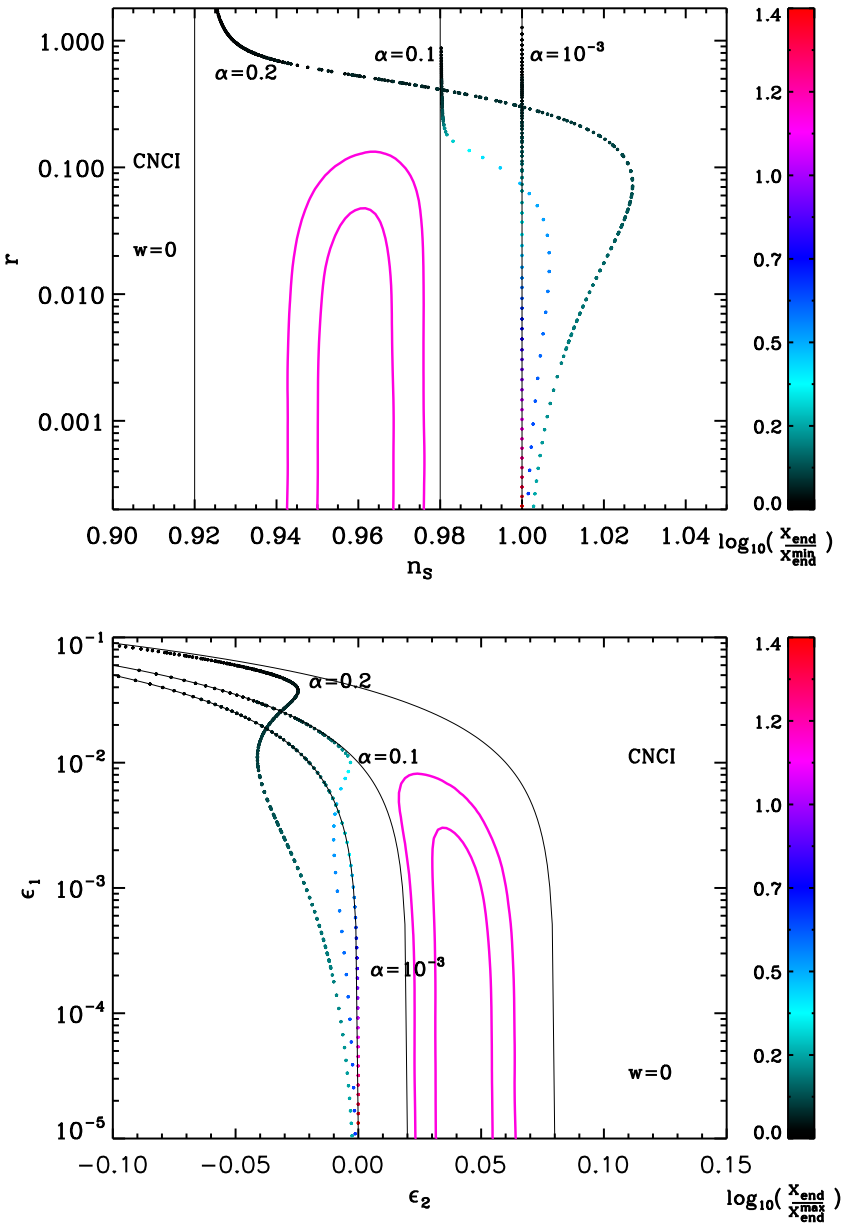

Figure 138. Reheating consistent slow-roll predictions for the constant $n_{\rm S}$ C inflation models for $\alpha = 10^{-3}, 0.1, 0.2$ in the plane $(n_{\rm S}, r)$ (top panel) and the plane (ϵ_1, ϵ_2) (bottom panel). The black solid lines are the $n_{\rm S} - 1 = -2\alpha^2$ contours, for the displayed values of α. The two pink solid contours are the one and two-sigma Planck confidence intervals (marginalized over second order slow-roll). The energy scale at which reheating ends is degenerated with the parameter $x_{\rm end}$, which is why it is not labeled.

A.40 Supergravity Brane Inflation (SBI)

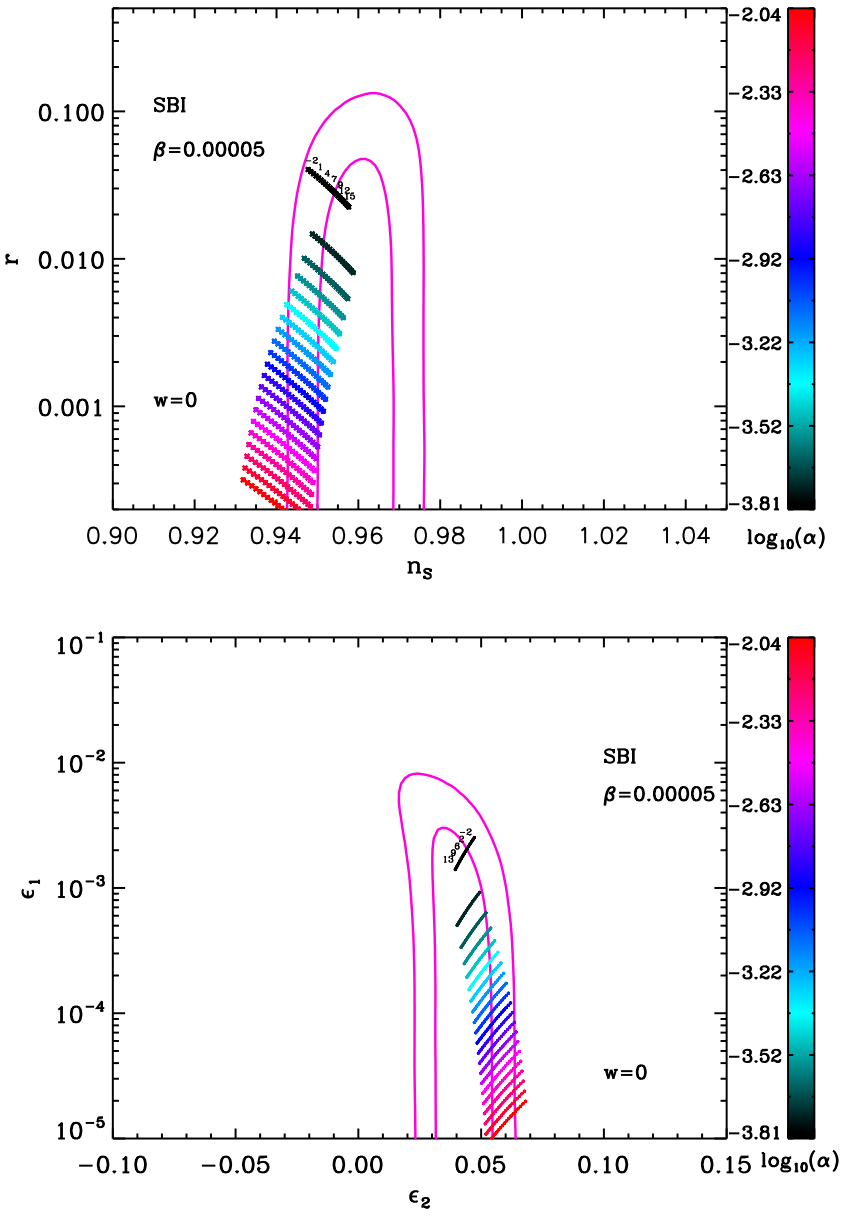

Figure 139. Reheating consistent slow-roll predictions for the supergravity brane inflation models for $\beta = 5 \times 10^{-5}$ in the plane $(n_{\rm S}, r)$ (top panel) and the plane (ϵ_1, ϵ_2) (bottom panel). The two pink solid contours are the one and two-sigma Planck confidence intervals (marginalized over second order slow-roll). The annotations trace the energy scale at which reheating ends and correspond to $\log(g_*^{1/4} T_{\rm reh}/{\rm GeV})$.

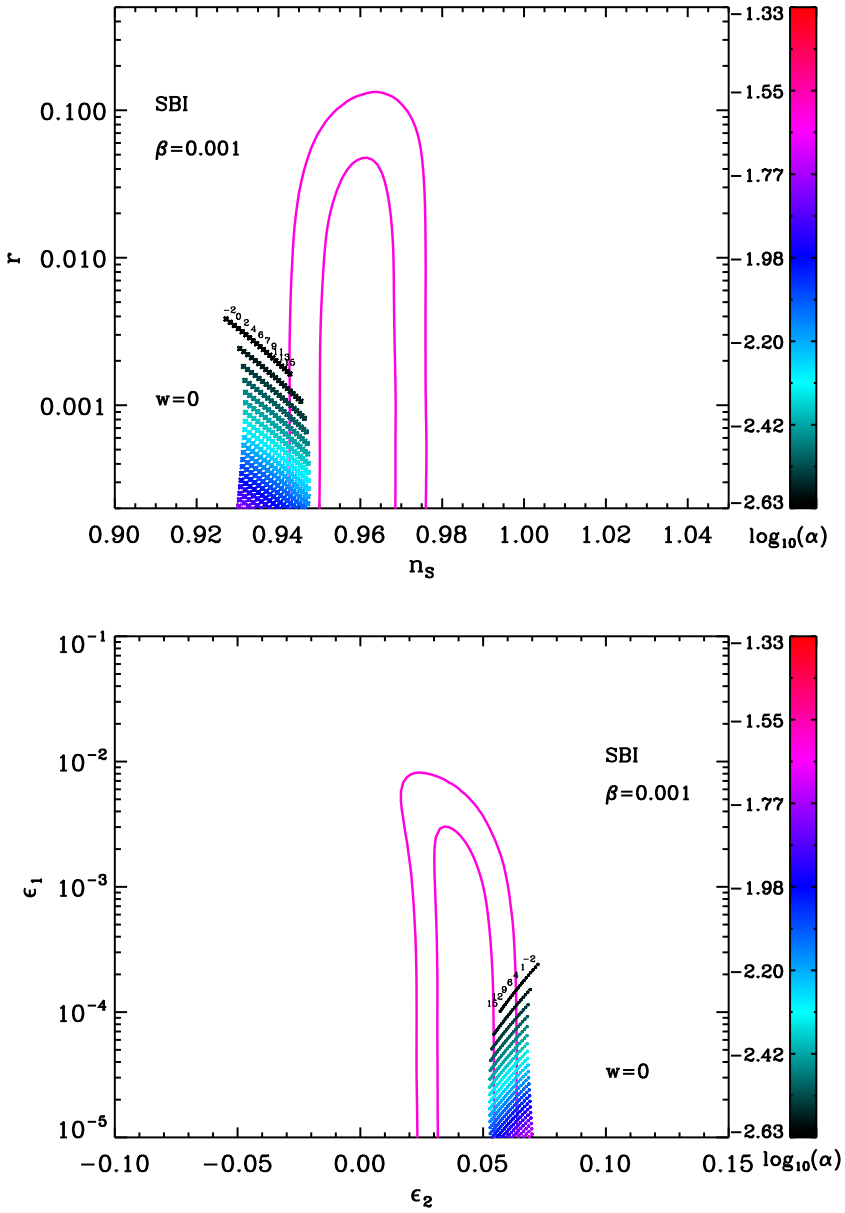

Figure 140. Reheating consistent slow-roll predictions for the supergravity brane inflation models for $\beta = 10^{-3}$ in the plane $(n_{\rm s}, r)$ (top panel) and the plane (ϵ_1, ϵ_2) (bottom panel). The two pink solid contours are the one and two-sigma Planck confidence intervals (marginalized over second order slow-roll). The annotations trace the energy scale at which reheating ends and correspond to $\log(g_*^{1/4} T_{\rm reh}/{\rm GeV})$.

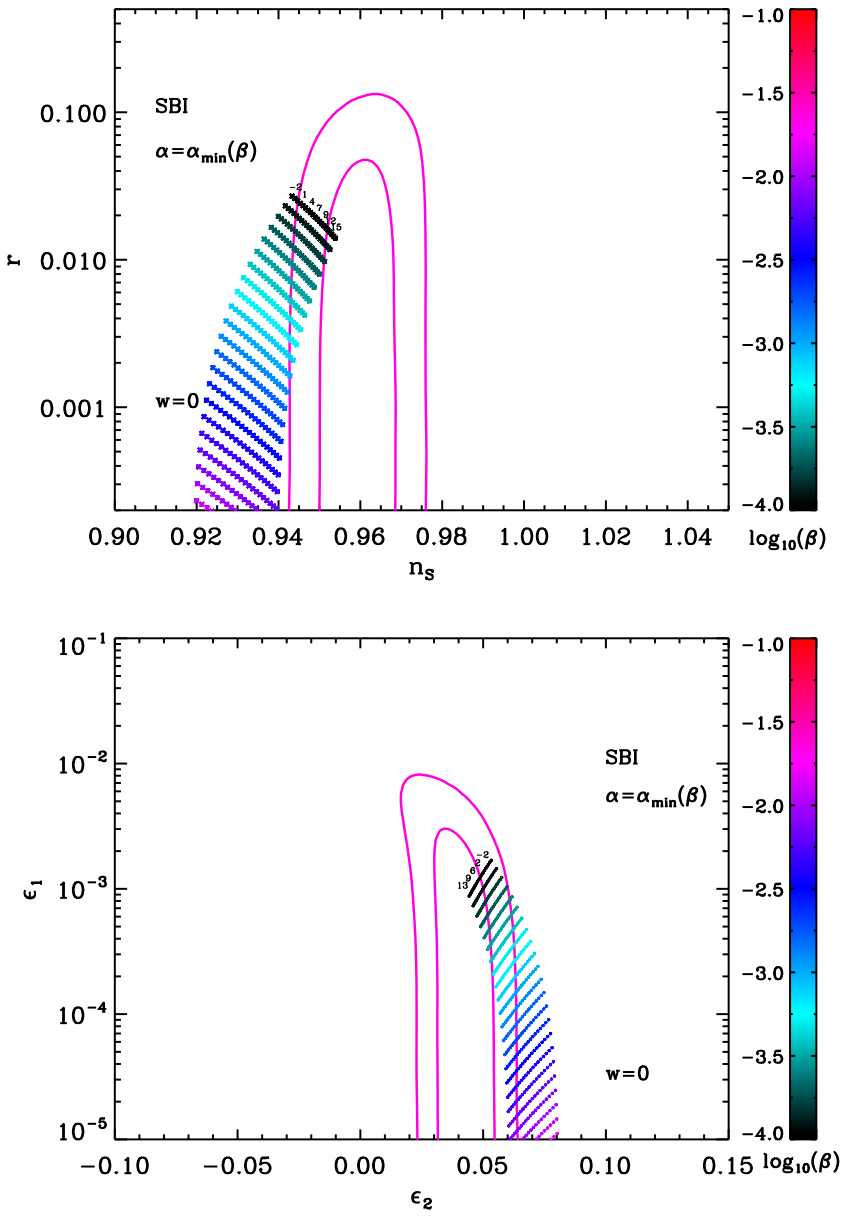

Figure 141. Reheating consistent slow-roll predictions for the supergravity brane inflation models for $\alpha = \alpha_{\rm min}(\beta)$ in the plane $(n_{\rm S}, r)$ (top panel) and the plane (ϵ_1, ϵ_2) (bottom panel). The two pink solid contours are the one and two-sigma Planck confidence intervals (marginalized over second order slow-roll). The annotations trace the energy scale at which reheating ends and correspond to $\log(g_*^{1/4} T_{\rm reh}/{\rm GeV})$.

A.41 Spontaneous Symmetry Breaking Inflation 1 (SSBII)

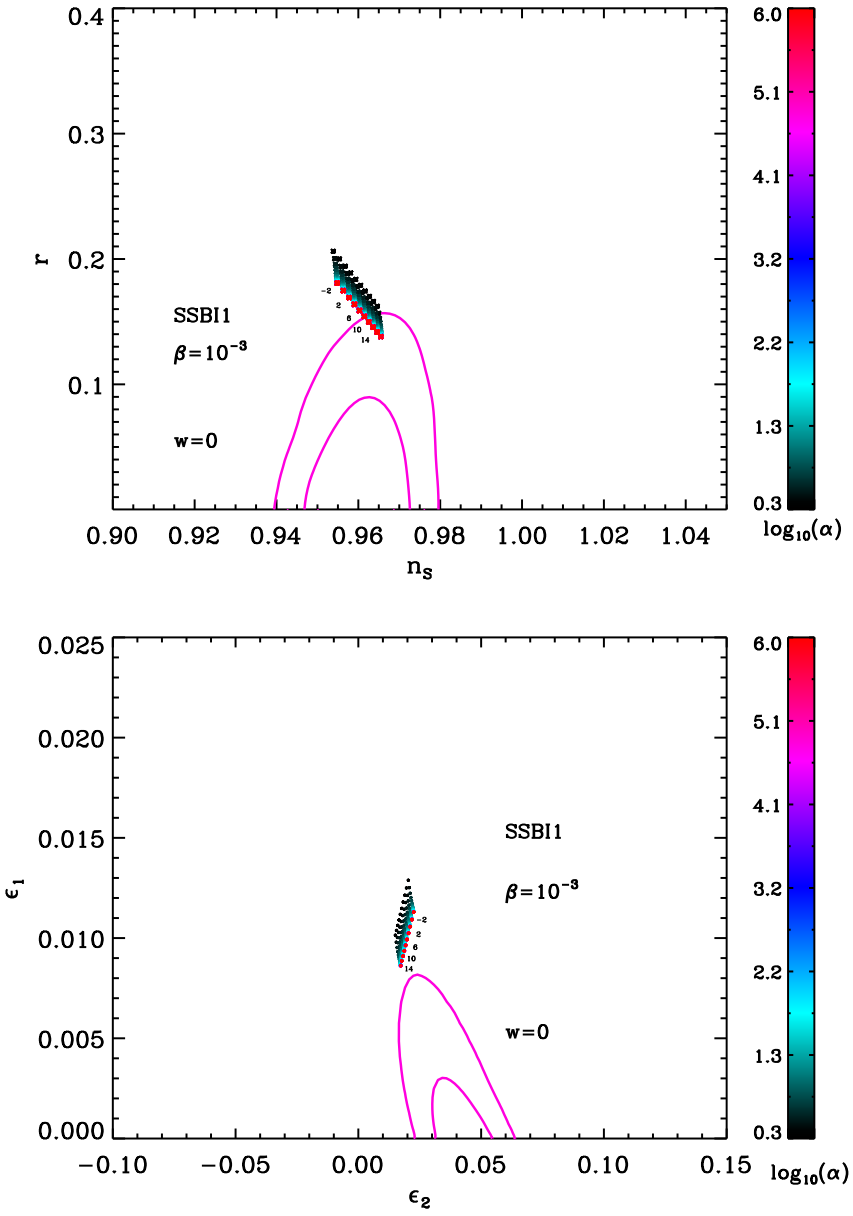

Figure 142. Reheating consistent slow-roll predictions for the spontaneous symmetry breaking 1 inflation ($\alpha > 0, \beta > 0$) models with $\beta = 10^{-3}$, in the plane $(n_{\rm S}, r)$ (top panel) and the plane (ϵ_1, ϵ_2) (bottom panel). The two pink solid contours are the one and two-sigma Planck confidence intervals (marginalized over second order slow-roll). The annotations trace the energy scale at which reheating ends and correspond to $\log(g_*^{1/4} T_{\rm reh}/{\rm GeV})$. The parameter α is varied between $\alpha_{\rm min}(\beta) < \alpha < 10^6 \alpha_{\rm min}(\beta)$.

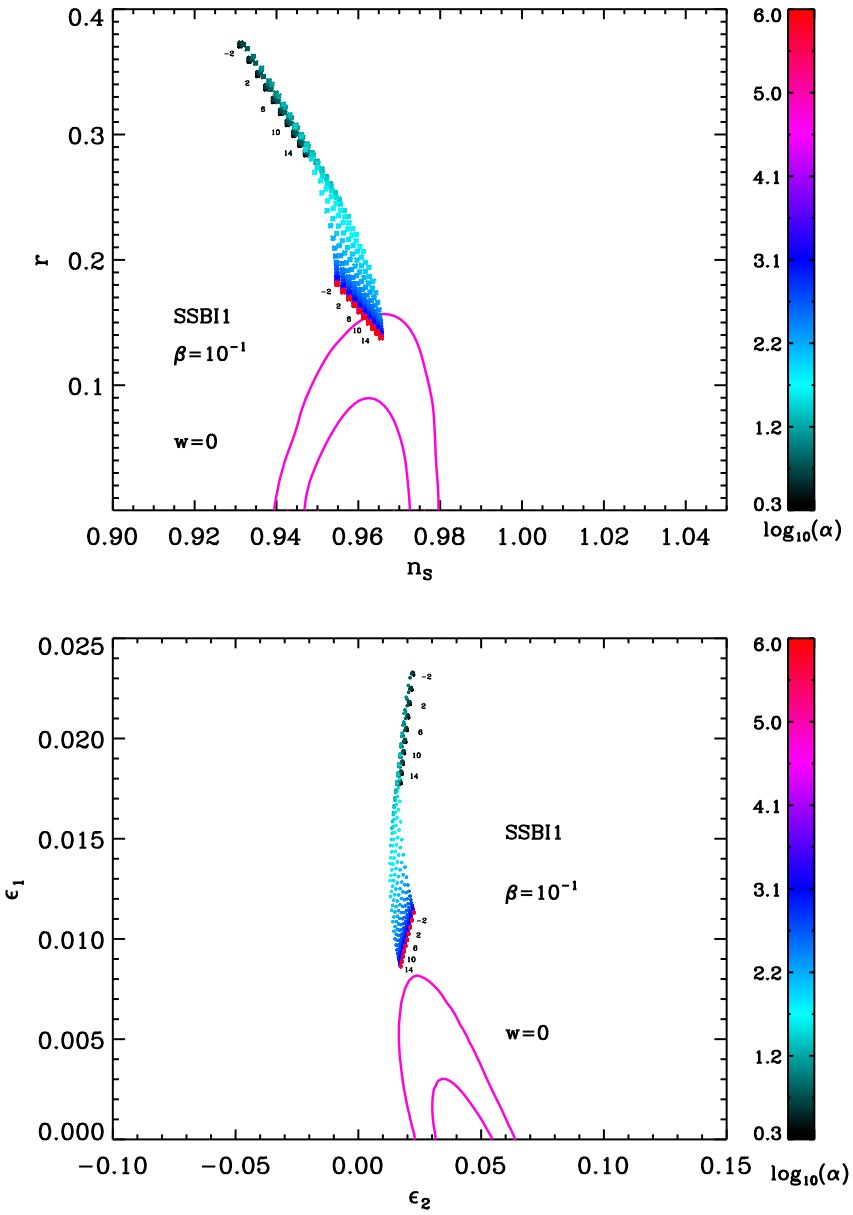

Figure 143. Reheating consistent slow-roll predictions for the spontaneous symmetry breaking 1 inflation ($\alpha > 0, \beta > 0$) models with $\beta = 10^{-1}$, in the plane $(n_{\rm S}, r)$ (top panel) and the plane (ϵ_1, ϵ_2) (bottom panel). The two pink solid contours are the one and two-sigma Planck confidence intervals (marginalized over second order slow-roll). The annotations trace the energy scale at which reheating ends and correspond to $\log(g_*^{1/4} T_{\rm reh}/{\rm GeV})$. The parameter α is varied between $\alpha_{\rm min}(\beta) < \alpha < 10^6 \alpha_{\rm min}(\beta)$.

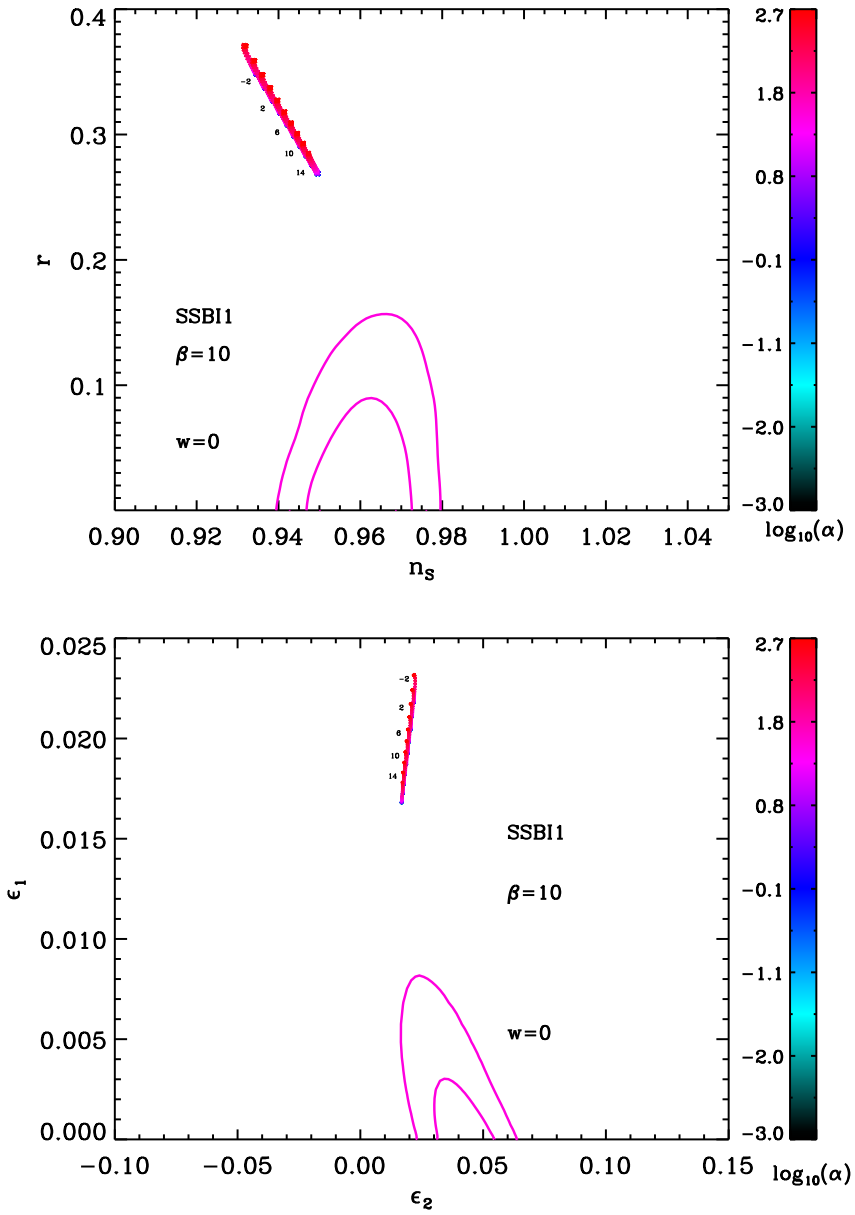

Figure 144. Reheating consistent slow-roll predictions for the spontaneous symmetry breaking 1 inflation ($\alpha > 0, \beta > 0$) models with $\beta = 10$, in the plane $(n_{\rm S}, r)$ (top panel) and the plane (ϵ_1, ϵ_2) (bottom panel). The two pink solid contours are the one and two-sigma Planck confidence intervals (marginalized over second order slow-roll). The annotations trace the energy scale at which reheating ends and correspond to $\log(g_*^{1/4} T_{\rm reh}/{\rm GeV})$. The parameter α is varied between $\alpha_{\rm min}(\beta) < \alpha < 10^6 \alpha_{\rm min}(\beta)$.

A.42 Spontaneous Symmetry Breaking Inflation 2 (SSBI2)

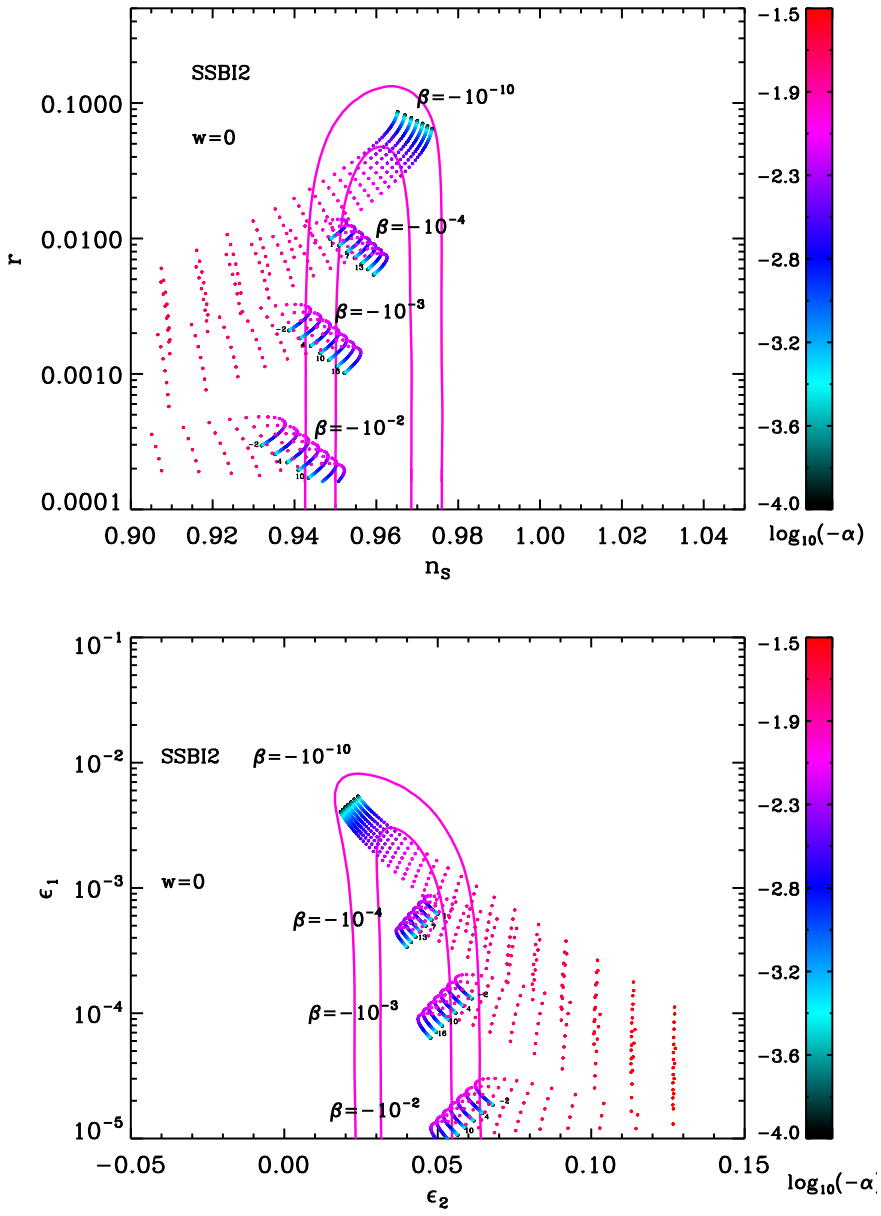

Figure 145. Reheating consistent slow-roll predictions for the spontaneous symmetry breaking 2 inflation ($\alpha < 0, \beta < 0$) models, in the plane $(n_{\rm s}, r)$ (top panel) and the plane (ϵ_1, ϵ_2) (bottom panel). The two pink solid contours are the one and two-sigma Planck confidence intervals (marginalized over second order slow-roll). The annotations trace the energy scale at which reheating ends and correspond to $\log(g_*^{1/4} T_{\rm reh}/{\rm GeV})$.

A.43 Spontaneous Symmetry Breaking Inflation 3 (SSBI3)

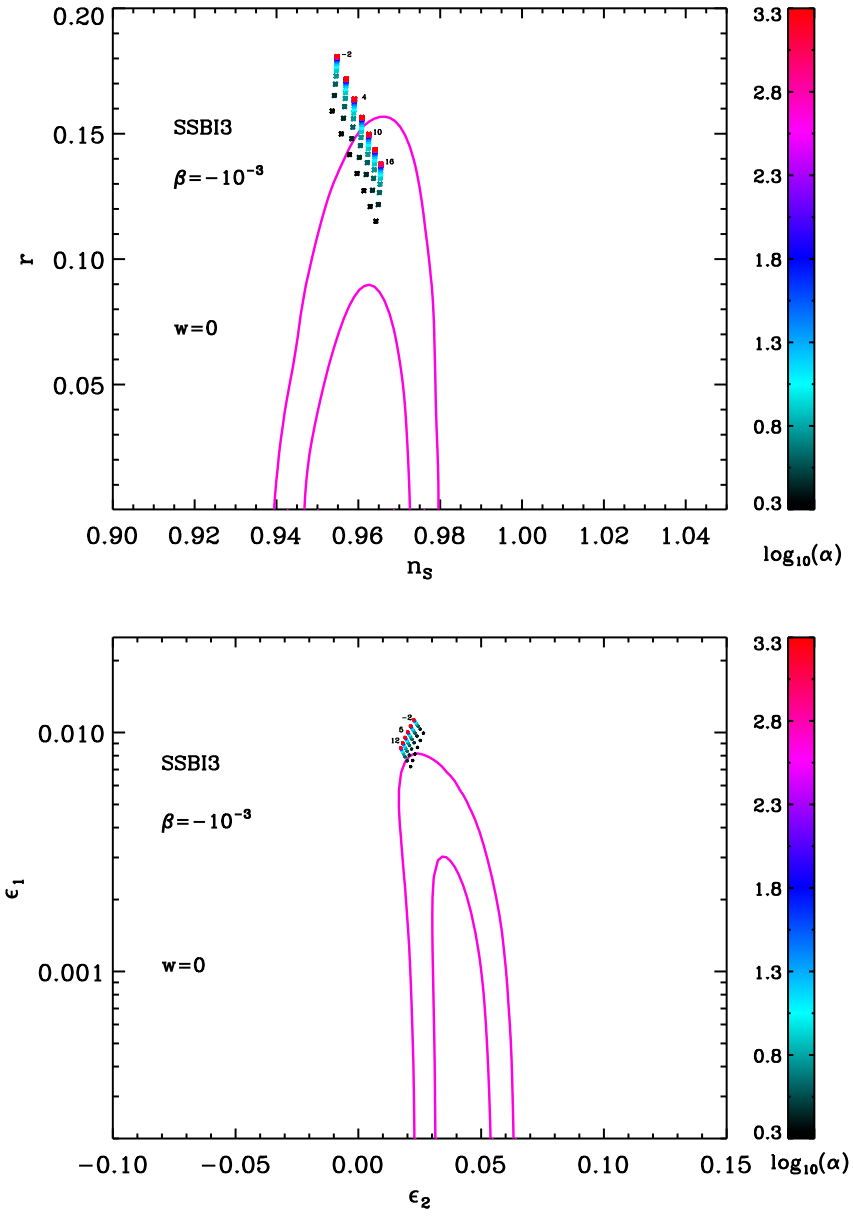

Figure 146. Reheating consistent slow-roll predictions for the spontaneous symmetry breaking 3 inflation $[\alpha > 0, \beta < 0, x^2 < -\alpha/(2\beta)]$ models for $\beta = -10^{-3}$, in the plane $(n_{\rm S}, r)$ (top panel) and the plane (ϵ_1, ϵ_2) (bottom panel). The two pink solid contours are the one and two-sigma Planck confidence intervals (marginalized over second order slow-roll). The annotations trace the energy scale at which reheating ends and correspond to $\log(g_*^{1/4} T_{\rm reh}/{\rm GeV})$. The parameter α is varied between $\alpha_{\rm min}(\beta) \simeq 2 < \alpha < 10^3 \alpha_{\rm min}(\beta)$.

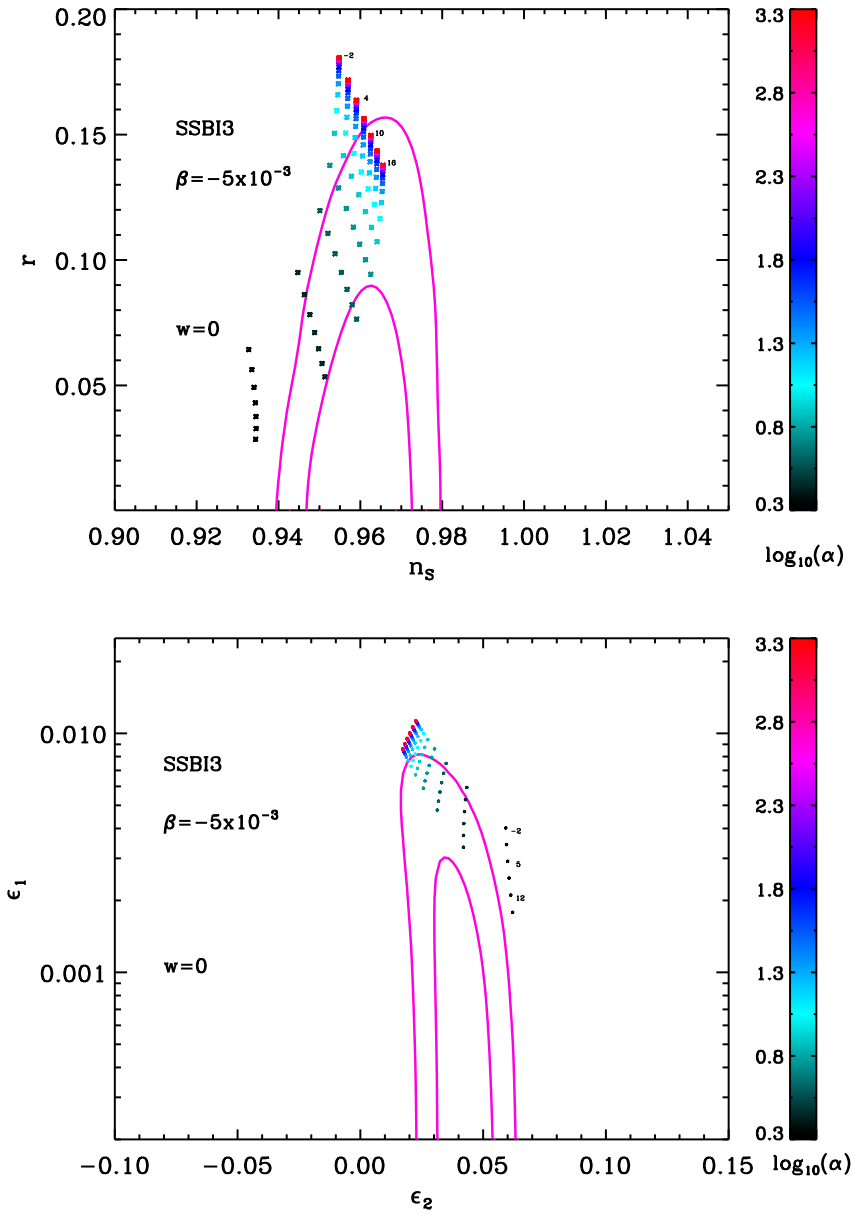

Figure 147. Reheating consistent slow-roll predictions for the spontaneous symmetry breaking 3 inflation $[\alpha > 0, \beta < 0, x^2 < -\alpha/(2\beta)]$ models for $\beta = -5 \times 10^{-3}$, in the plane $(n_{\rm S}, r)$ (top panel) and the plane (ϵ_1, ϵ_2) (bottom panel). The two pink solid contours are the one and two-sigma Planck confidence intervals (marginalized over second order slow-roll). The annotations trace the energy scale at which reheating ends and correspond to $\log(g_*^{1/4} T_{\rm reh}/{\rm GeV})$. The parameter α is varied between $\alpha_{\rm min}(\beta) \simeq 2 < \alpha < 10^3 \alpha_{\rm min}(\beta)$.

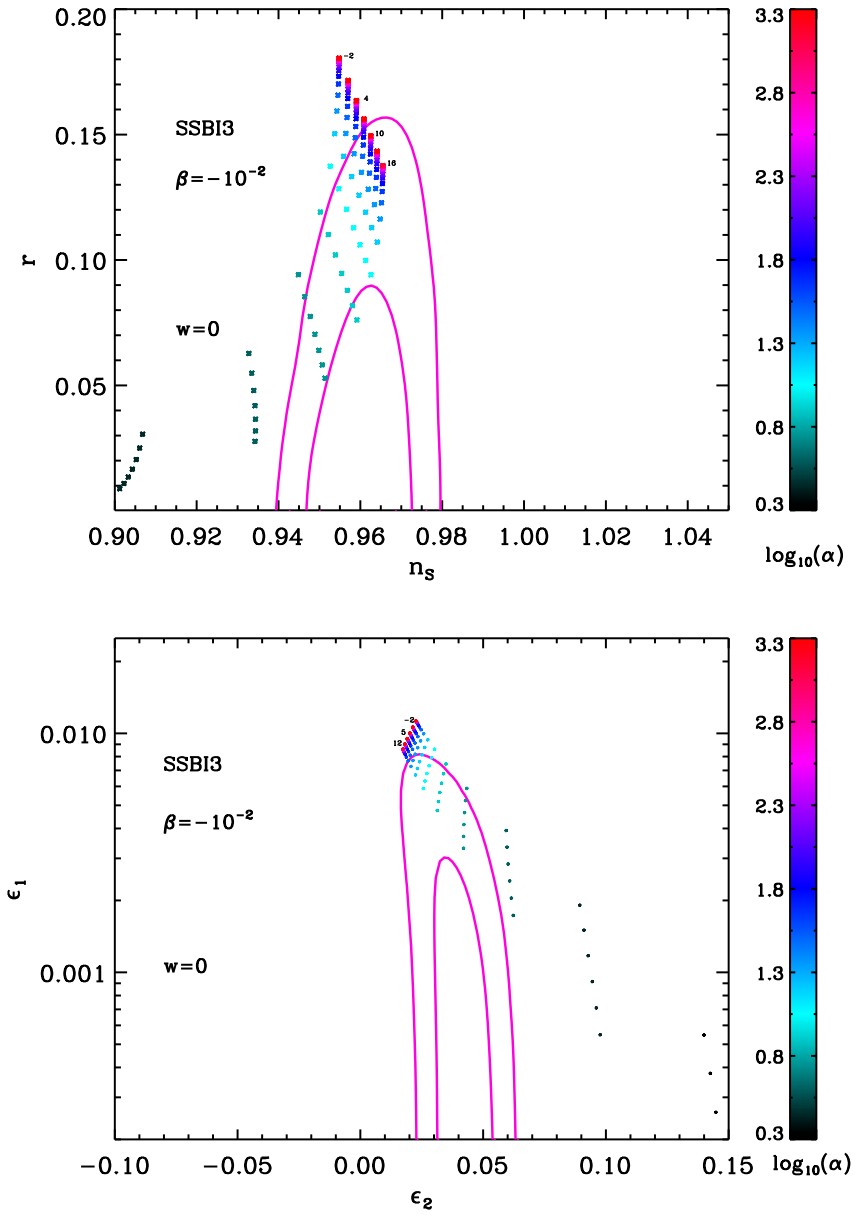

Figure 148. Reheating consistent slow-roll predictions for the spontaneous symmetry breaking 3 inflation $[\alpha > 0, \beta < 0, x^2 < -\alpha/(2\beta)]$ models for $\beta = -10^{-2}$, in the plane $(n_{\rm S}, r)$ (top panel) and the plane (ϵ_1, ϵ_2) (bottom panel). The two pink solid contours are the one and two-sigma Planck confidence intervals (marginalized over second order slow-roll). The annotations trace the energy scale at which reheating ends and correspond to $\log(g_*^{1/4} T_{\rm reh}/{\rm GeV})$. The parameter α is varied between $\alpha_{\rm min}(\beta) \simeq 2 < \alpha < 10^3 \alpha_{\rm min}(\beta)$.

A.44 Spontaneous Symmetry Breaking Inflation 4 (SSBI4)

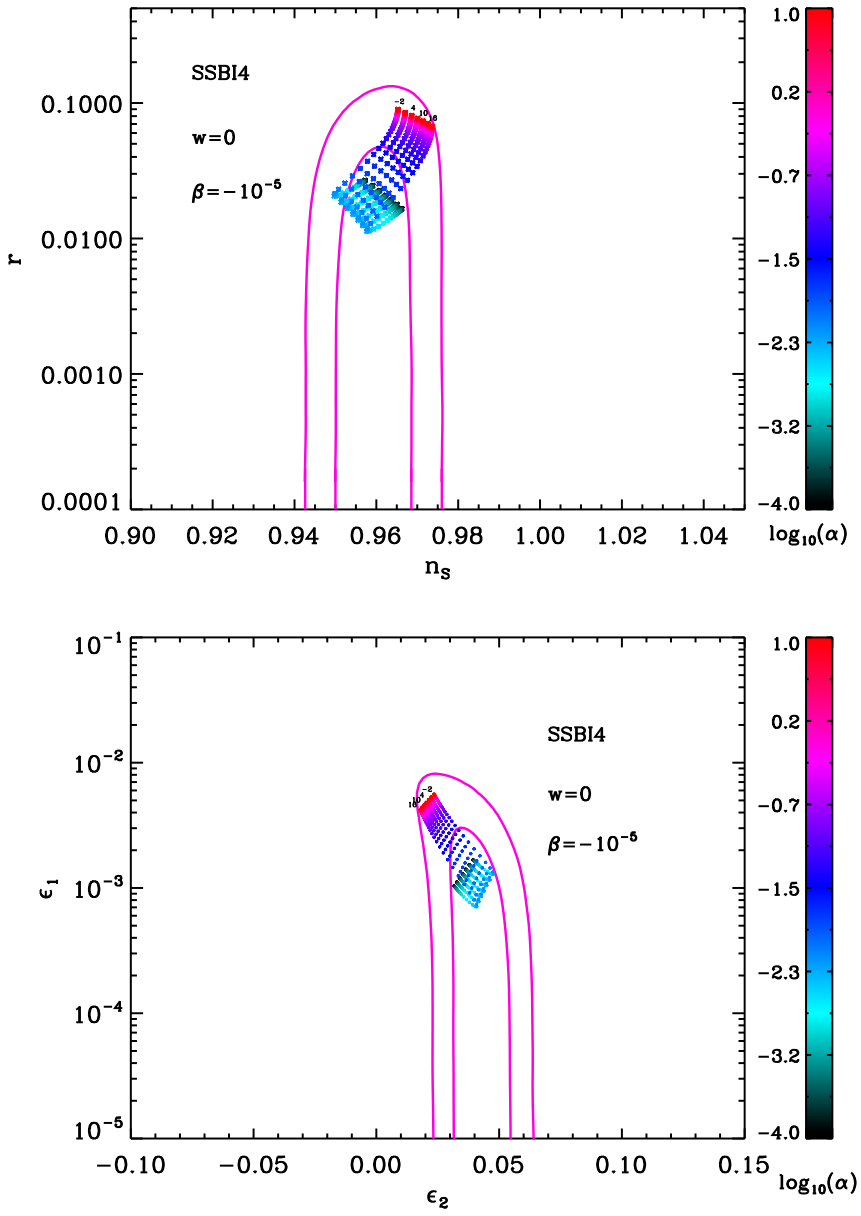

Figure 149. Reheating consistent slow-roll predictions for the spontaneous symmetry breaking 4 inflation $[\alpha > 0, \beta < 0, x^2 > -\alpha/(2\beta)]$ models for $\beta = -10^{-5}$, in the plane $(n_{\rm S}, r)$ (top panel) and the plane (ϵ_1, ϵ_2) (bottom panel). The two pink solid contours are the one and two-sigma Planck confidence intervals (marginalized over second order slow-roll). The annotations trace the energy scale at which reheating ends and correspond to $\log(g_*^{1/4} T_{\rm reh}/{\rm GeV})$.

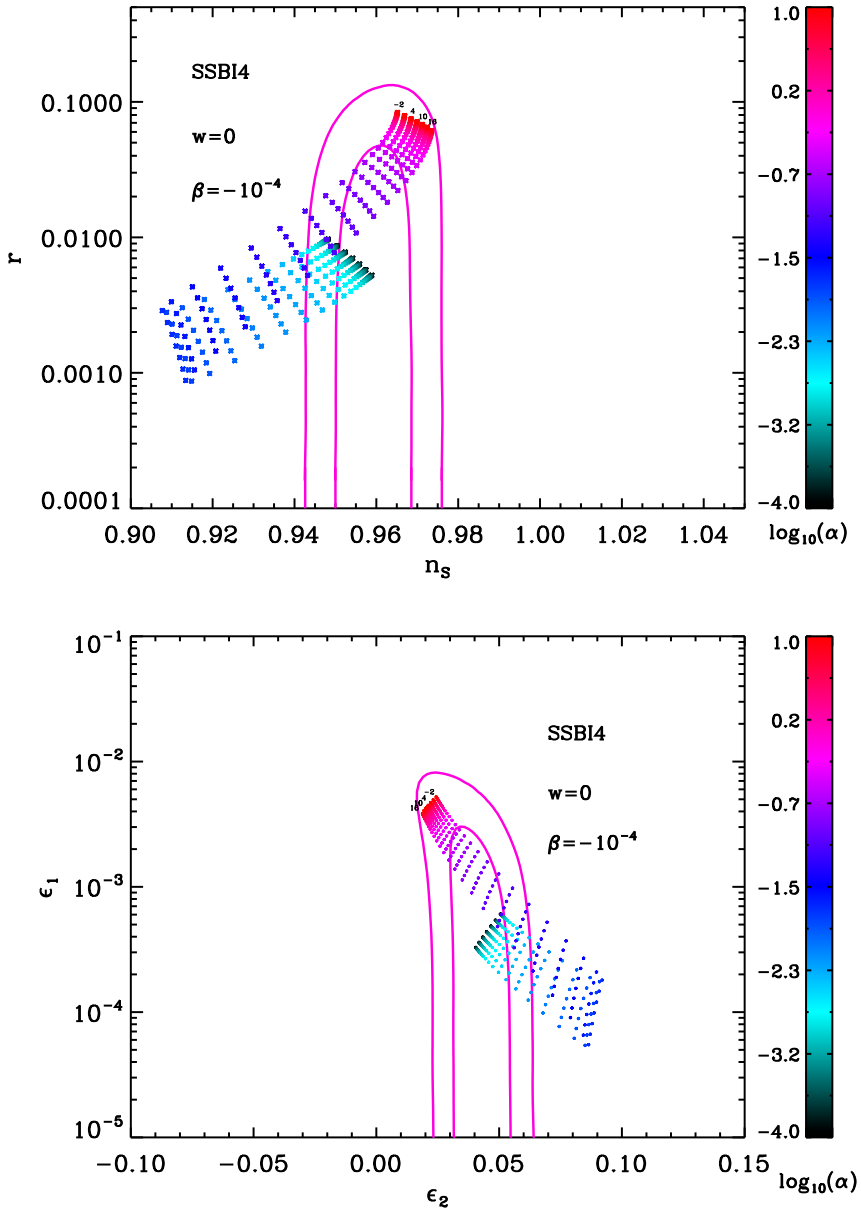

Figure 150. Reheating consistent slow-roll predictions for the spontaneous symmetry breaking 4 inflation $[\alpha > 0, \beta < 0, x^2 > -\alpha/(2\beta)]$ models for $\beta = -10^{-4}$, in the plane $(n_{\rm S}, r)$ (top panel) and the plane (ϵ_1, ϵ_2) (bottom panel). The two pink solid contours are the one and two-sigma Planck confidence intervals (marginalized over second order slow-roll). The annotations trace the energy scale at which reheating ends and correspond to $\log(g_*^{1/4} T_{\rm reh}/{\rm GeV})$.

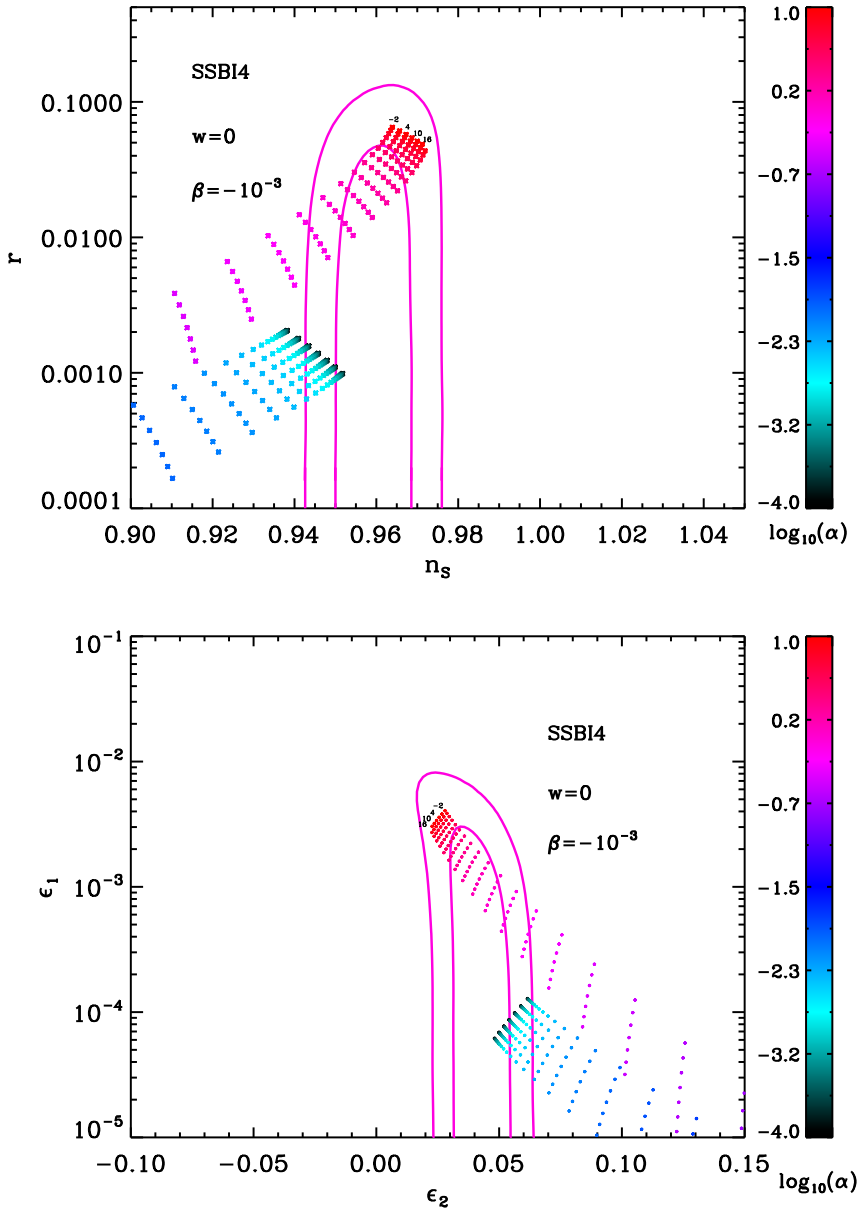

Figure 151. Reheating consistent slow-roll predictions for the spontaneous symmetry breaking 4 inflation $[\alpha > 0, \beta < 0, x^2 > -\alpha/(2\beta)]$ models for $\beta = -10^{-3}$, in the plane $(n_{\rm S}, r)$ (top panel) and the plane (ϵ_1, ϵ_2) (bottom panel). The two pink solid contours are the one and two-sigma Planck confidence intervals (marginalized over second order slow-roll). The annotations trace the energy scale at which reheating ends and correspond to $\log(g_*^{1/4} T_{\rm reh}/{\rm GeV})$.

A.45 Spontaneous Symmetry Breaking Inflation 5 (SSBI5)

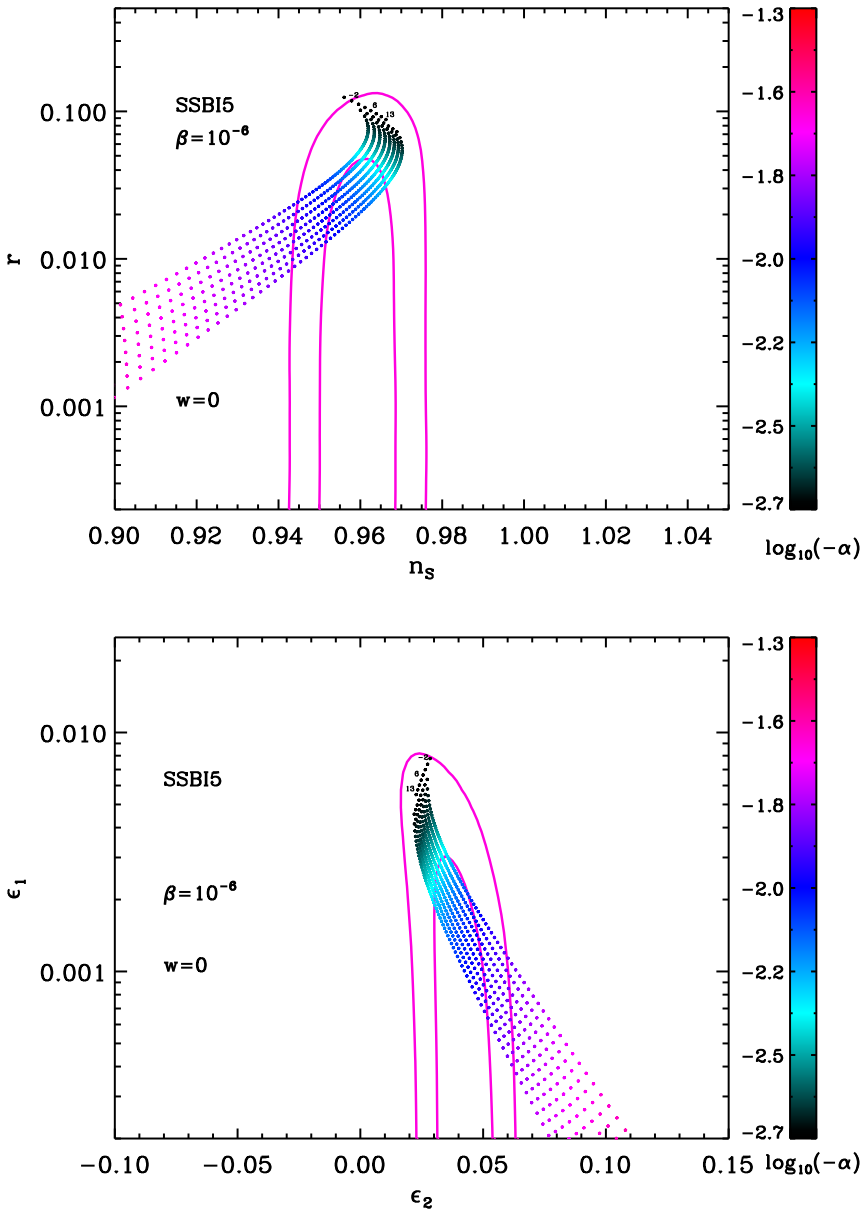

Figure 152. Reheating consistent slow-roll predictions for the spontaneous symmetry breaking 5 inflation $[\alpha < 0, \beta > 0, x^2 < -\alpha/(2\beta)]$ models for $\beta = 10^{-6}$, in the plane $(n_{\rm S}, r)$ (top panel) and the plane (ϵ_1, ϵ_2) (bottom panel). The two pink solid contours are the one and two-sigma Planck confidence intervals (marginalized over second order slow-roll). The annotations trace the energy scale at which reheating ends and correspond to $\log(g_*^{1/4} T_{\rm reh}/{\rm GeV})$. The parameter α is varied between $|\alpha_{\rm min}(\beta)| < |\alpha| < 10|\alpha_{\rm min}(\beta)|$.

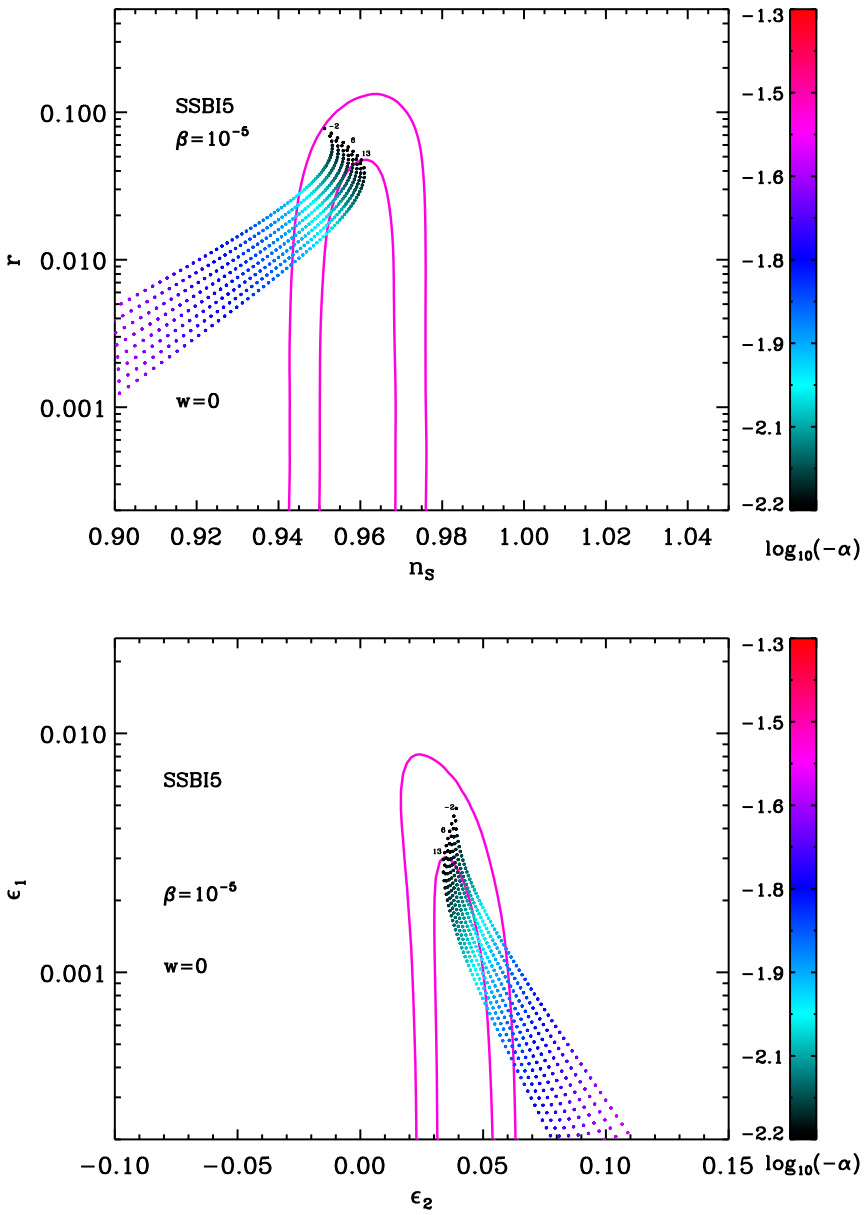

Figure 153. Reheating consistent slow-roll predictions for the spontaneous symmetry breaking 5 inflation $[\alpha < 0, \beta > 0, x^2 < -\alpha/(2\beta)]$ models for $\beta = 10^{-5}$, in the plane $(n_{\rm S}, r)$ (top panel) and the plane (ϵ_1, ϵ_2) (bottom panel). The two pink solid contours are the one and two-sigma Planck confidence intervals (marginalized over second order slow-roll). The annotations trace the energy scale at which reheating ends and correspond to $\log(g_*^{1/4} T_{\rm reh}/{\rm GeV})$.The parameter α is varied between $|\alpha_{\rm min}(\beta)| < |\alpha| < 10|\alpha_{\rm min}(\beta)|$.

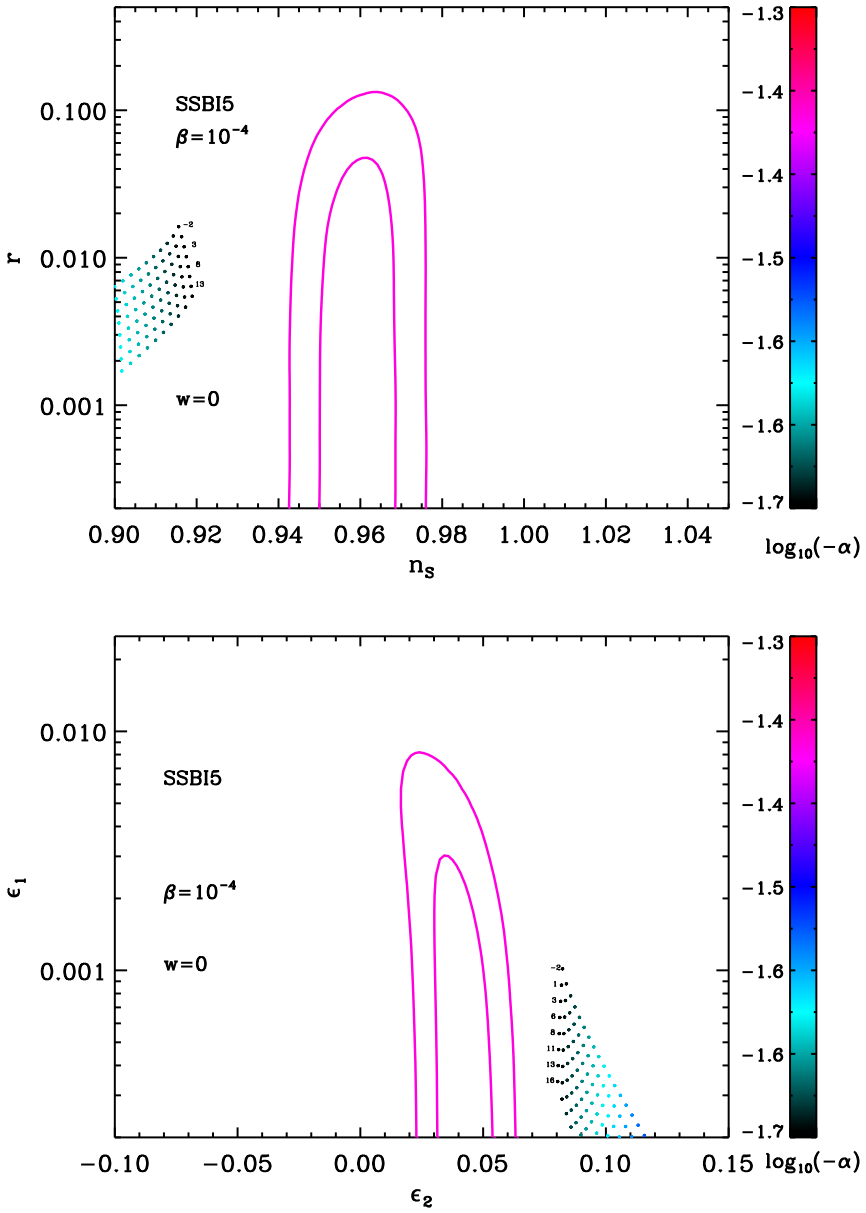

Figure 154. Reheating consistent slow-roll predictions for the spontaneous symmetry breaking 5 inflation $[\alpha < 0, \beta > 0, x^2 < -\alpha/(2\beta)]$ models for $\beta = 10^{-4}$, in the plane $(n_{\rm S}, r)$ (top panel) and the plane (ϵ_1, ϵ_2) (bottom panel). The two pink solid contours are the one and two-sigma Planck confidence intervals (marginalized over second order slow-roll). The annotations trace the energy scale at which reheating ends and correspond to $\log(g_*^{1/4} T_{\rm reh}/{\rm GeV})$.The parameter α is varied between $|\alpha_{\rm min}(\beta)| < |\alpha| < 10|\alpha_{\rm min}\,(\beta)\,|$.

A.46 Spontaneous Symmetry Breaking Inflation 6 (SSBI6)

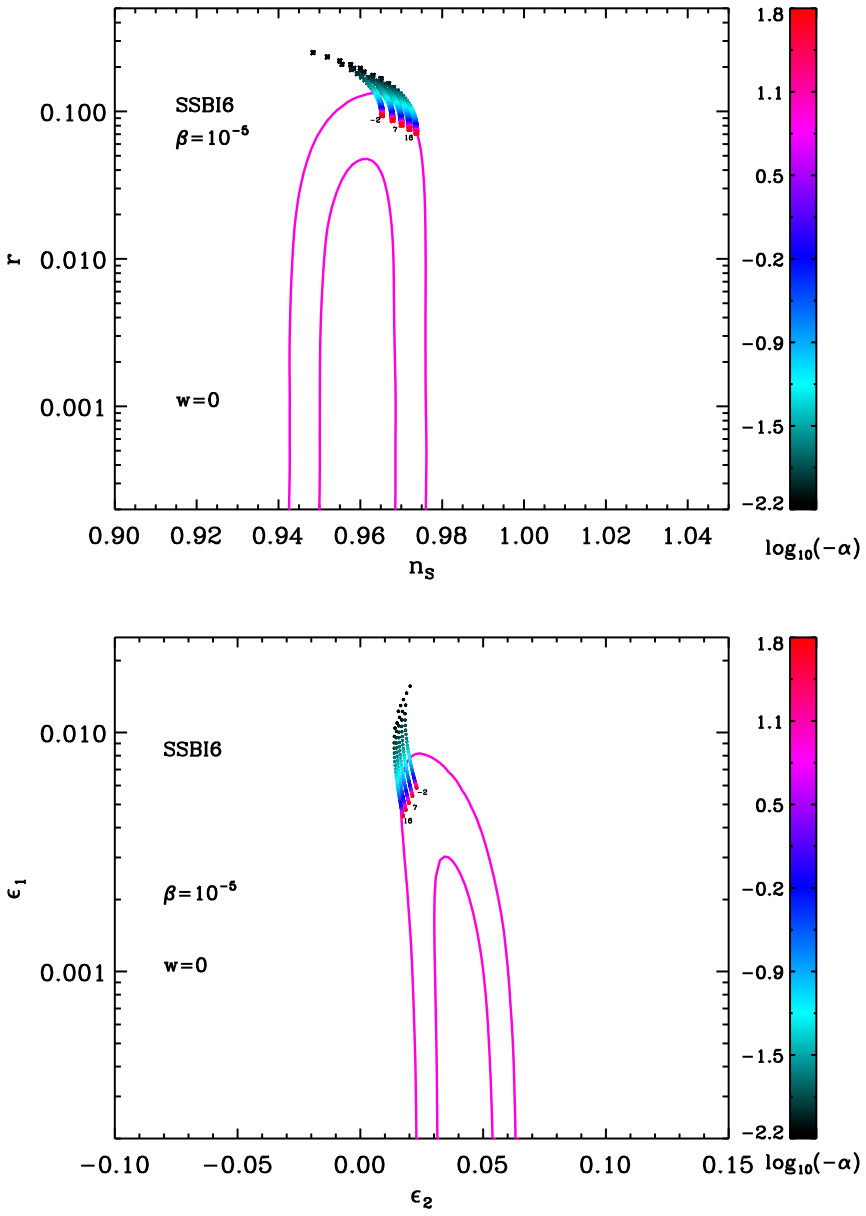

Figure 155. Reheating consistent slow-roll predictions for the spontaneous symmetry breaking 6 inflation $[\alpha < 0, \beta > 0, x^2 > -\alpha/(2\beta)]$ models for $\beta = 10^{-5}$, in the plane $(n_{\rm S}, r)$ (top panel) and the plane (ϵ_1, ϵ_2) (bottom panel). The two pink solid contours are the one and two-sigma Planck confidence intervals (marginalized over second order slow-roll). The annotations trace the energy scale at which reheating ends and correspond to $\log(g_*^{1/4} T_{\rm reh}/{\rm GeV})$. The parameter α is varied between $|\alpha_{\rm min}(\beta)| < |\alpha| < 10^4 |\alpha_{\rm min}(\beta)|$.

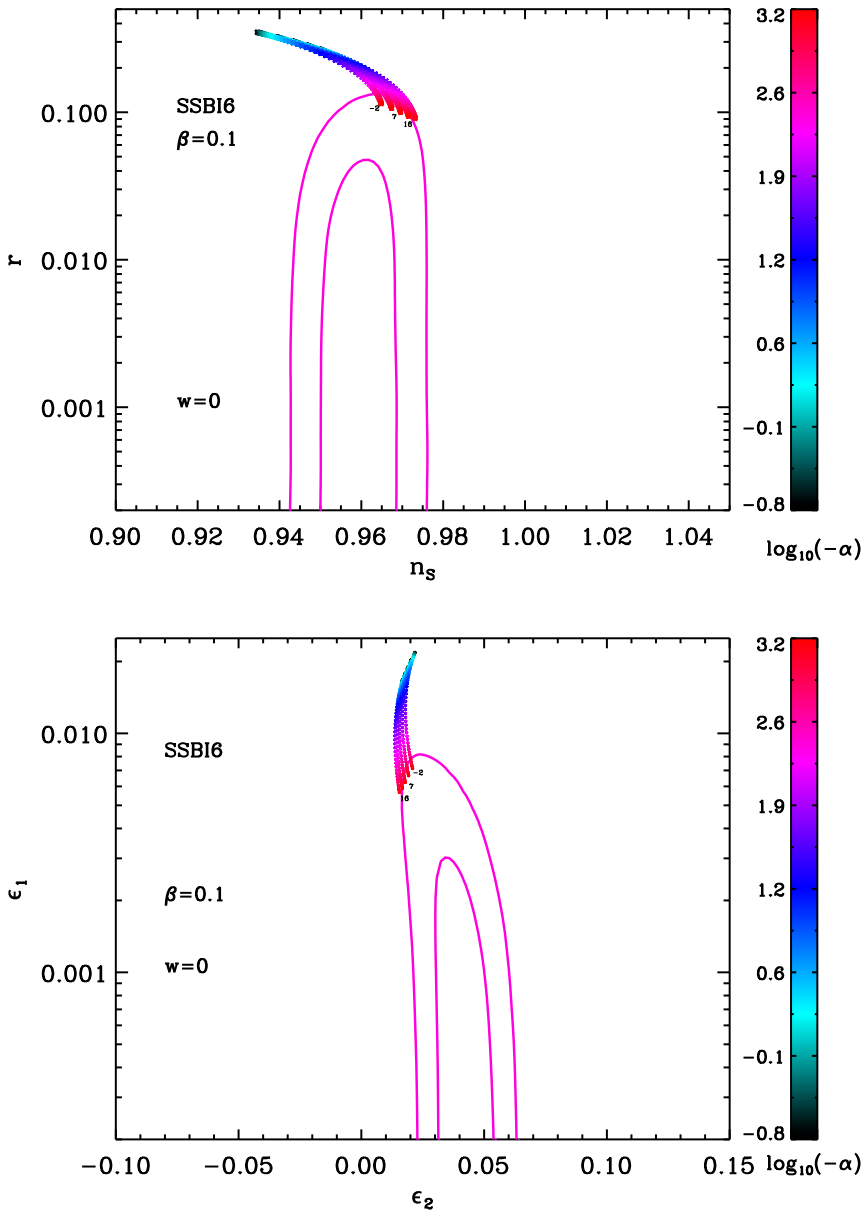

Figure 156. Reheating consistent slow-roll predictions for the spontaneous symmetry breaking 6 inflation $[\alpha < 0, \beta > 0, x^2 > -\alpha/(2\beta)]$ models for $\beta = 10^{-1}$, in the plane $(n_{\rm S}, r)$ (top panel) and the plane (ϵ_1, ϵ_2) (bottom panel). The two pink solid contours are the one and two-sigma Planck confidence intervals (marginalized over second order slow-roll). The annotations trace the energy scale at which reheating ends and correspond to $\log(g_*^{1/4} T_{\rm reh}/{\rm GeV})$. The parameter α is varied between $|\alpha_{\rm min}(\beta)| < |\alpha| < 10^4 |\alpha_{\rm min}(\beta)|$.

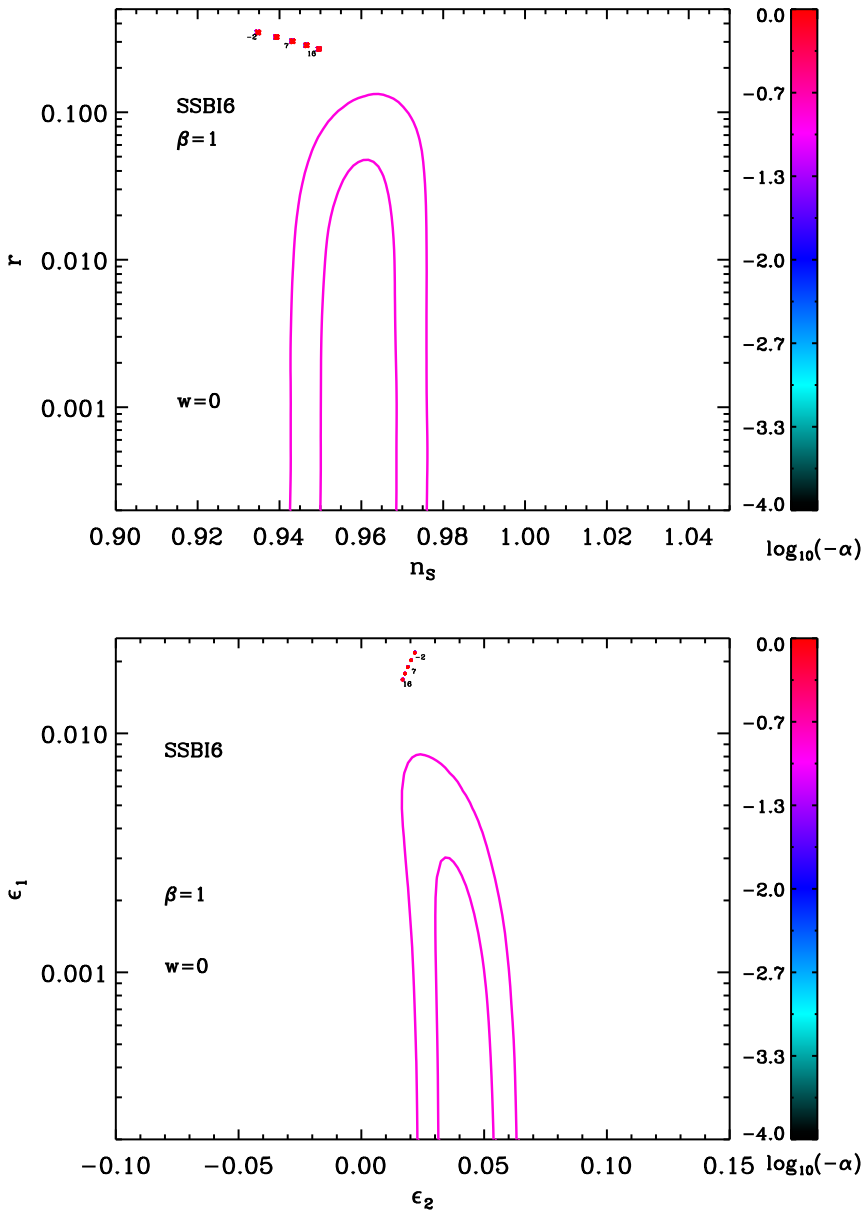

Figure 157. Reheating consistent slow-roll predictions for the spontaneous symmetry breaking 6 inflation $[\alpha < 0, \beta > 0, x^2 > -\alpha/(2\beta)]$ models for $\beta = 1$, in the plane $(n_{\rm S}, r)$ (top panel) and the plane (ϵ_1, ϵ_2) (bottom panel). The two pink solid contours are the one and two-sigma Planck confidence intervals (marginalized over second order slow-roll). The annotations trace the energy scale at which reheating ends and correspond to $\log(g_*^{1/4} T_{\rm reh}/{\rm GeV})$. The parameter α is varied between $|\alpha_{\rm min}(\beta)| < |\alpha| < 10^4 |\alpha_{\rm min}(\beta)|$.

A.47 Inverse Monomial Inflation (IMI)

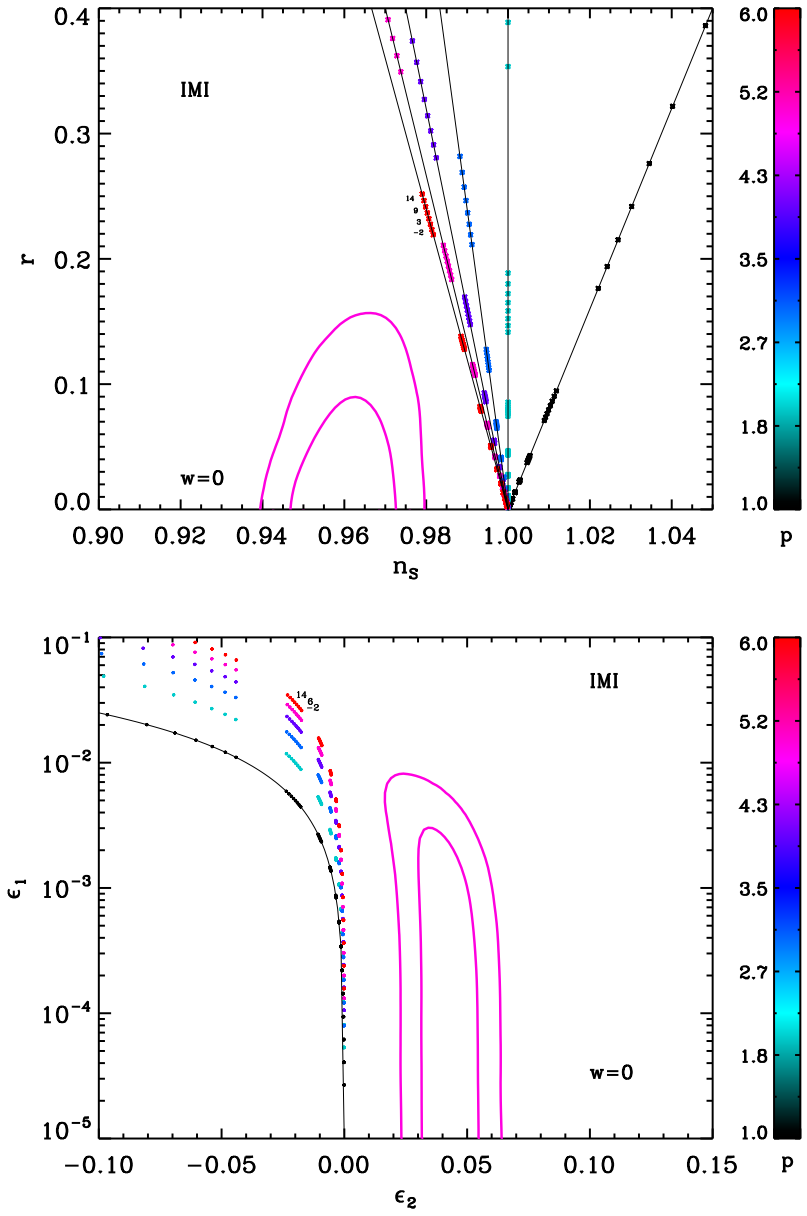

Figure 158. Reheating consistent slow-roll predictions for the IMI models in the plane $(n_{\rm S}, r)$ (top panel) and the plane (ϵ_1, ϵ_2) (bottom panel). The two pink solid contours are the one and two-sigma Planck confidence intervals (marginalized over second order slow-roll). The parameter $x_{\rm end}$ varies above $x_{\rm end}^{\rm min}$ ($\Delta N = 65\, e-$folds). It is not labeled since it is fully degenerate with the reheating temperature. The annotations trace the energy scale at which reheating ends and correspond to $\log(g_*^{1/4} T_{\rm reh}/{\rm GeV})$. The black solid lines represent the locus of different IMI-p models [for which $(1-2/p)\, r = 8\,(1-n_{\rm S})$, i.e. $\epsilon_1 = -(p/4)\epsilon_2$].

A.48 Brane Inflation (BI)

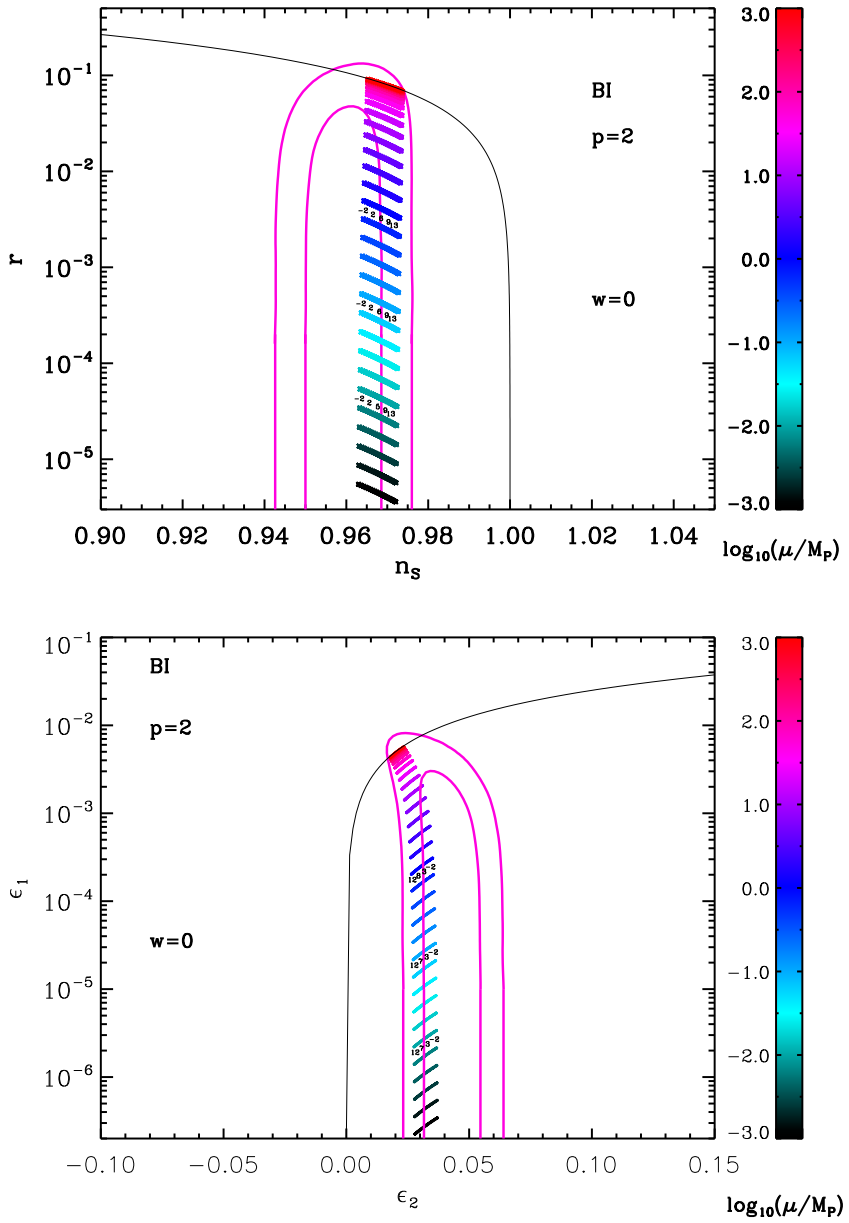

Figure 159. Reheating consistent slow-roll predictions for the brane inflation models with $p = 2$ in the plane $(n_{\rm S}, r)$ (top panel) and the plane (ϵ_1, ϵ_2) (bottom panel). The two pink solid contours are the one and two-sigma Planck confidence intervals (marginalized over second order slow-roll). The annotations trace the energy scale at which reheating ends and correspond to $\log(g_*^{1/4} T_{\rm reh}/{\rm GeV})$. The black solid line represent the locus of the points such that $r = (8/3)\,(1 - n_{\rm S})$, i.e. $\epsilon_2 = 4\epsilon_1$, on which this model must lie for $\mu \gg M_{\rm Pl}$.

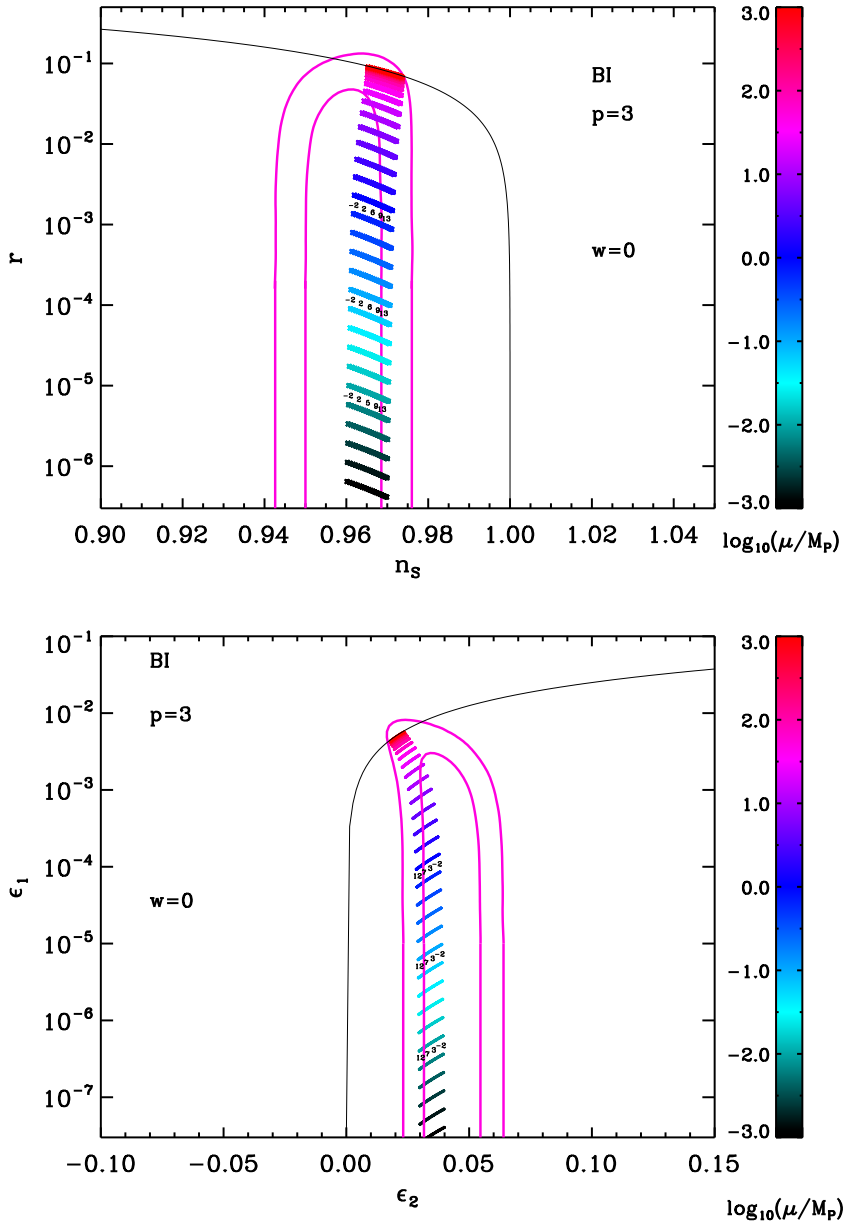

Figure 160. Reheating consistent slow-roll predictions for the brane inflation models with $p = 3$ in the plane $(n_{\rm S}, r)$ (top panel) and the plane (ϵ_1, ϵ_2) (bottom panel). The two pink solid contours are the one and two-sigma Planck confidence intervals (marginalized over second order slow-roll). The annotations trace the energy scale at which reheating ends and correspond to $\log(g_*^{1/4} T_{\rm reh}/{\rm GeV})$. The black solid line represent the locus of the points such that $r = (8/3)\,(1 - n_{\rm S})$, i.e. $\epsilon_2 = 4\epsilon_1$, on which this model must lie for $\mu \gg M_{\rm Pl}$.

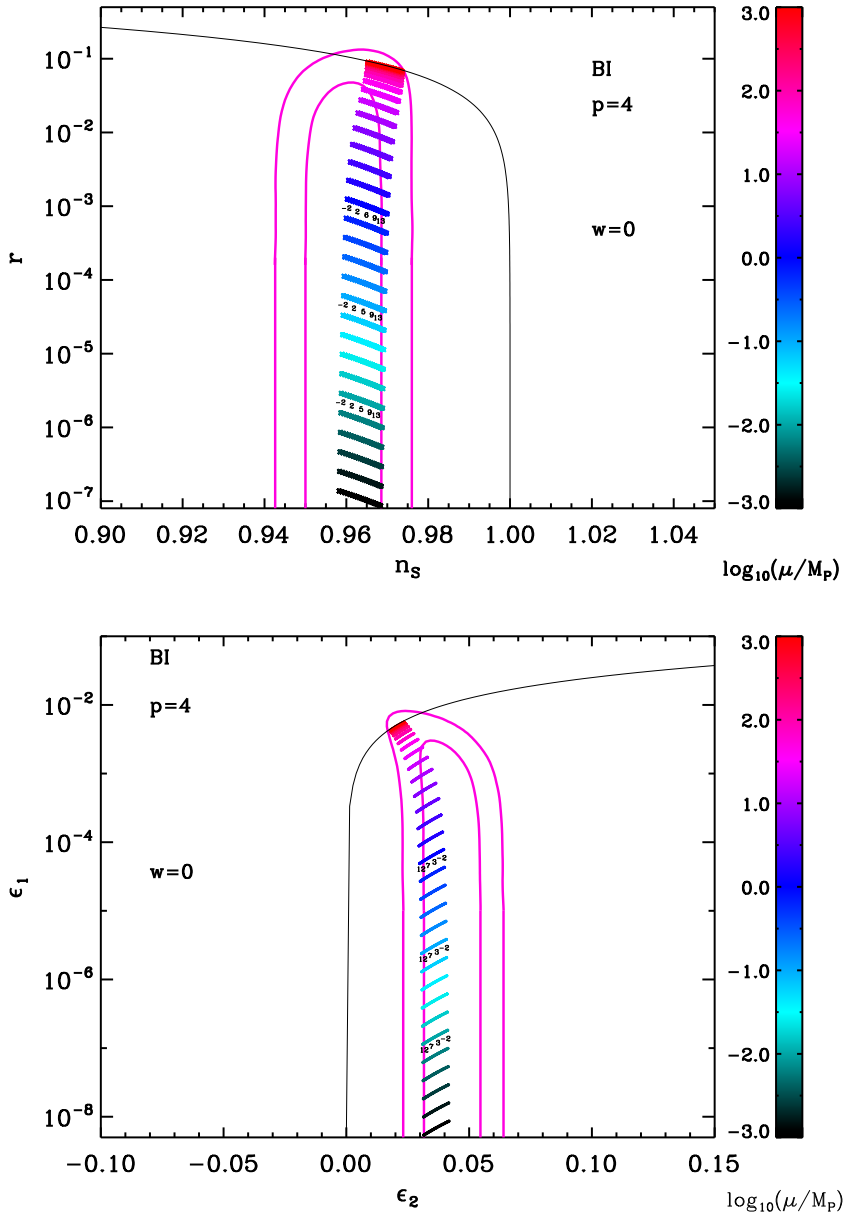

Figure 161. Reheating consistent slow-roll predictions for the brane inflation models with $p = 4$ in the plane $(n_{\rm S}, r)$ (top panel) and the plane (ϵ_1, ϵ_2) (bottom panel). The two pink solid contours are the one and two-sigma Planck confidence intervals (marginalized over second order slow-roll). The annotations trace the energy scale at which reheating ends and correspond to $\log(g_*^{1/4} T_{\rm reh}/{\rm GeV})$. The black solid line represent the locus of the points such that $r = (8/3)\,(1 - n_{\rm S})$, i.e. $\epsilon_2 = 4\epsilon_1$, on which this model must lie for $\mu \gg M_{\rm Pl}$.

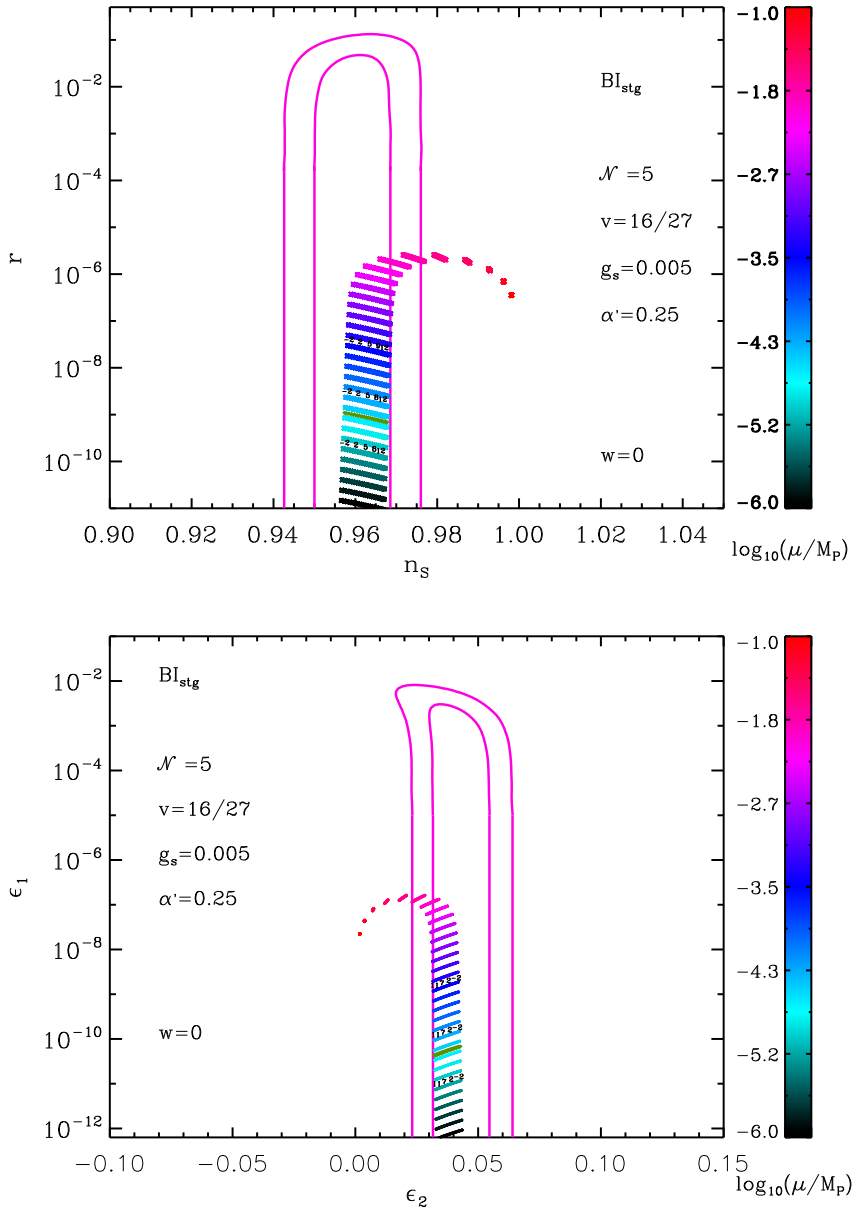

Figure 162. Reheating consistent slow-roll predictions for the brane inflation models in the string framework ($p = 4$, $\mu \ll M_{\rm Pl}$, for the fundamental parameters displayed in the figures), in the plane $(n_{\rm S}, r)$ (top panel) and the plane (ϵ_1, ϵ_2) (bottom panel). The two pink solid contours are the one and two-sigma Planck confidence intervals (marginalized over second order slow-roll). The annotations trace the energy scale at which reheating ends and correspond to $\log(g_*^{1/4} T_{\rm reh}/{\rm GeV})$. The green points delimitate the prediction points such that inflation end by slow roll violation (for $\mu/M_{\rm Pl} > 0.02$, above the green points) from the ones where inflation end by tachyonic instability (below the green points).

A.49 KKLT Inflation (KKLTI)

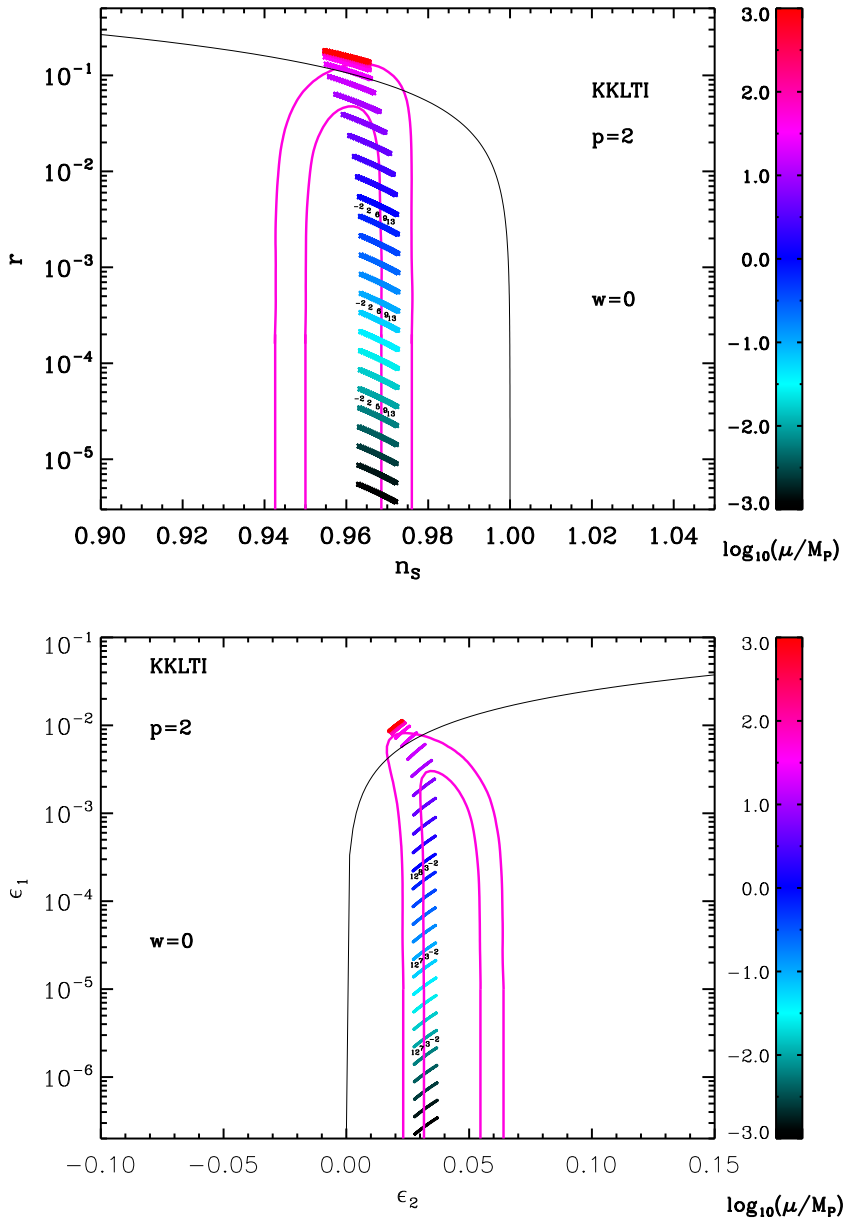

Figure 163. Reheating consistent slow-roll predictions for the KKLT inflation models with $p = 2$ in the plane $(n_{\rm S}, r)$ (top panel) and the plane (ϵ_1, ϵ_2) (bottom panel). The two pink solid contours are the one and two-sigma Planck confidence intervals (marginalized over second order slow-roll). The annotations trace the energy scale at which reheating ends and correspond to $\log(g_*^{1/4} T_{\rm reh}/{\rm GeV})$. The black solid line represent the locus of the points such that $r = (8/3)\,(1 - n_{\rm S})$, i.e. $\epsilon_2 = 4\epsilon_1$, on which BI lies for $\mu \gg M_{\rm Pl}$ and deviates from KKLTI.

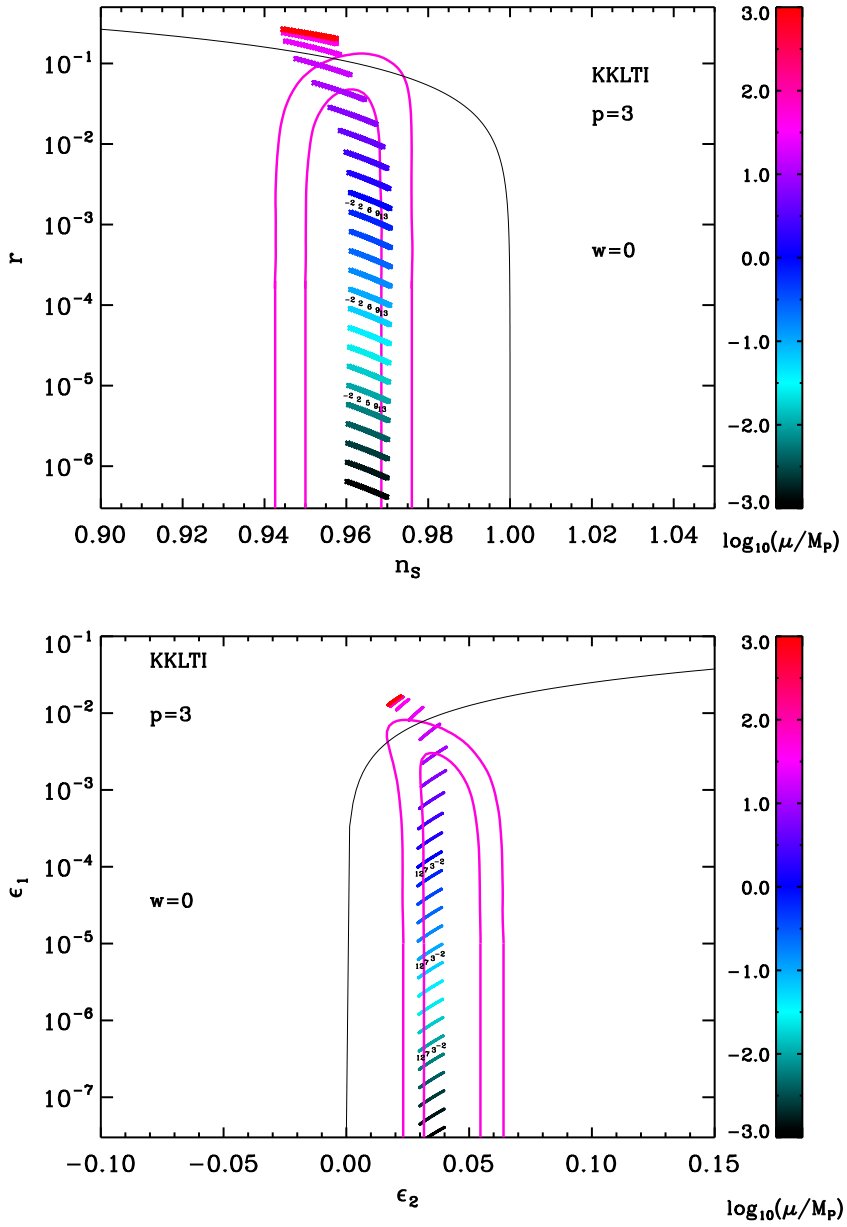

Figure 164. Reheating consistent slow-roll predictions for the KKLT inflation models with $p = 3$ in the plane $(n_{\rm S}, r)$ (top panel) and the plane (ϵ_1, ϵ_2) (bottom panel). The two pink solid contours are the one and two-sigma Planck confidence intervals (marginalized over second order slow-roll). The annotations trace the energy scale at which reheating ends and correspond to $\log(g_*^{1/4} T_{\rm reh}/{\rm GeV})$. The black solid line represent the locus of the points such that $r = (8/3)\,(1 - n_{\rm S})$, i.e. $\epsilon_2 = 4\epsilon_1$, on which BI lies for $\mu \gg M_{\rm Pl}$ and deviates from KKLTI.

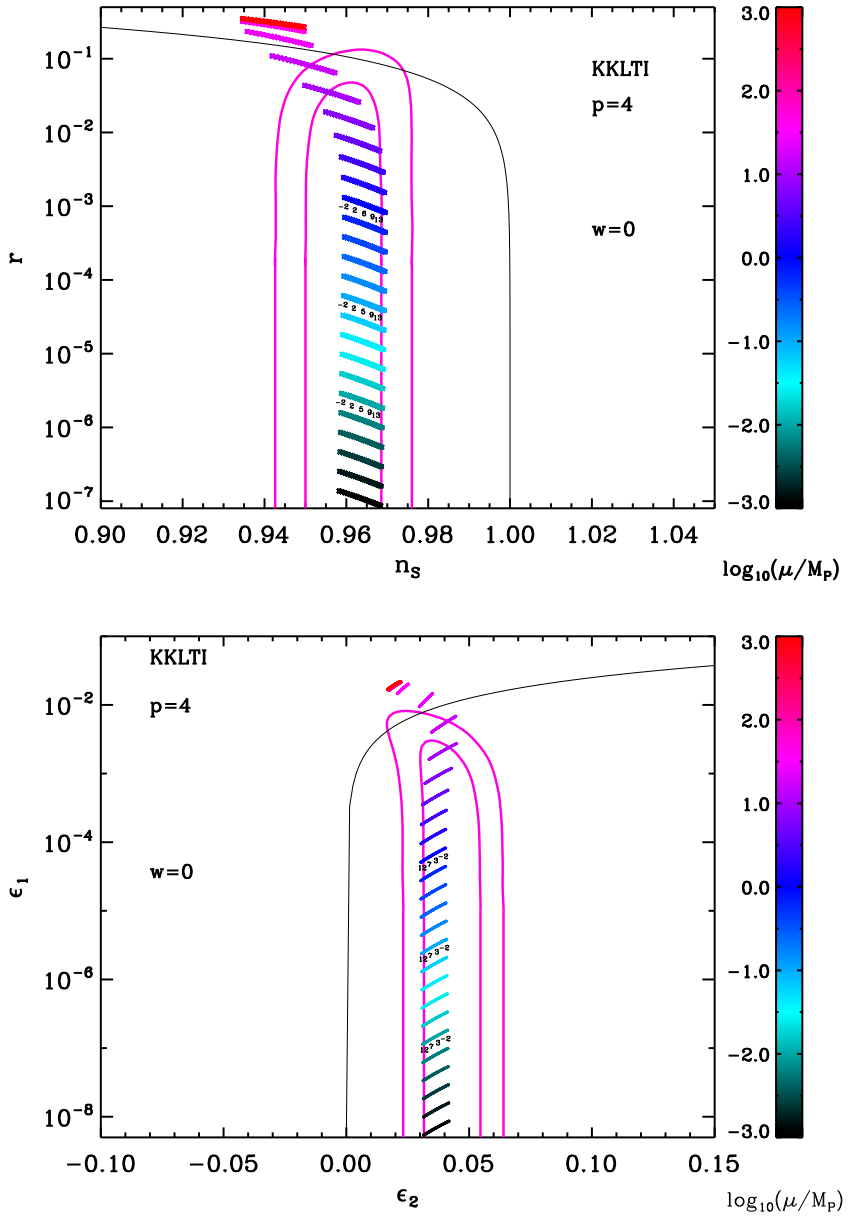

Figure 165. Reheating consistent slow-roll predictions for the KKLT inflation models with $p = 4$ in the plane $(n_{\rm S}, r)$ (top panel) and the plane (ϵ_1, ϵ_2) (bottom panel). The two pink solid contours are the one and two-sigma Planck confidence intervals (marginalized over second order slow-roll). The annotations trace the energy scale at which reheating ends and correspond to $\log(g_*^{1/4} T_{\rm reh}/{\rm GeV})$. The black solid line represent the locus of the points such that $r = (8/3)\,(1 - n_{\rm S})$, i.e. $\epsilon_2 = 4\epsilon_1$, on which BI lies for $\mu \gg M_{\rm Pl}$ and deviates from KKLTI.

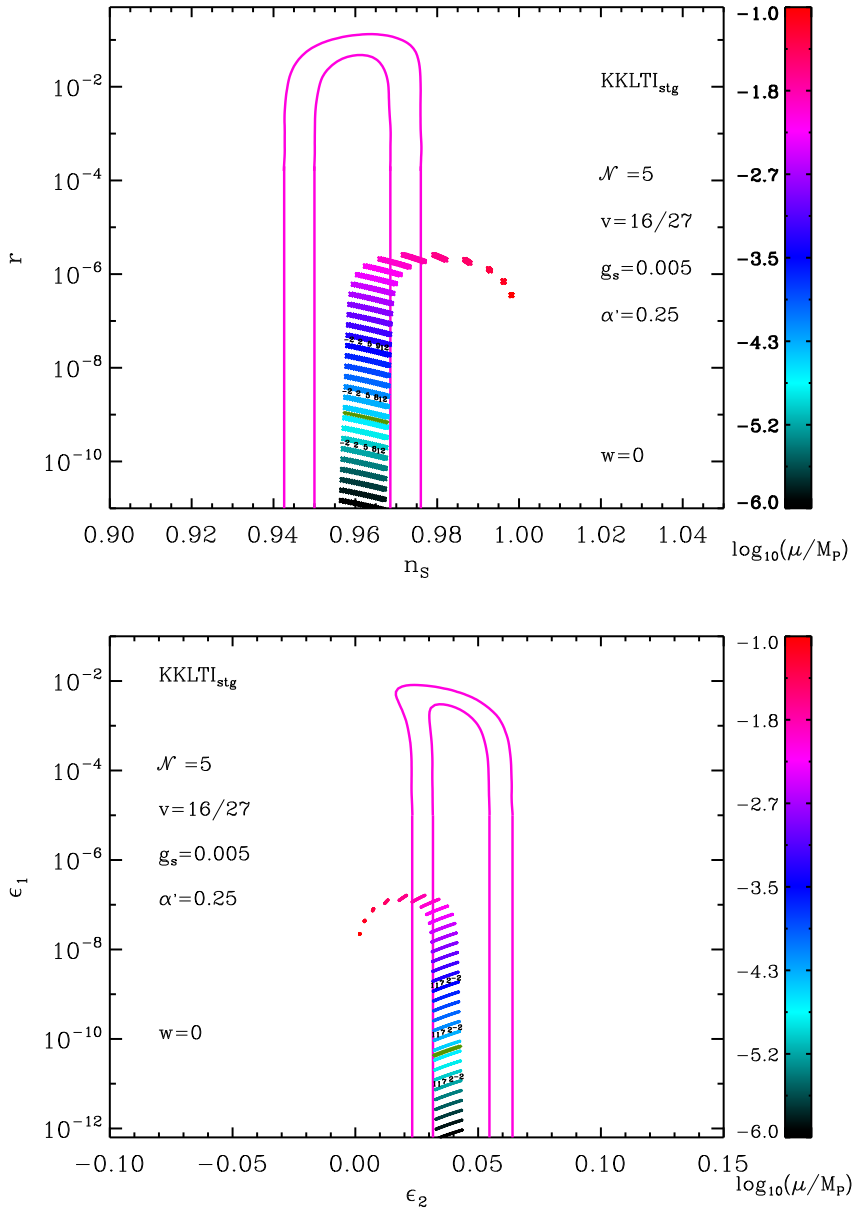

Figure 166. Reheating consistent slow-roll predictions for the KKLT inflation models in the string framework ($p = 4$, $\mu \ll M_{\rm Pl}$, for the fundamental parameters displayed in the figures), in the plane $(n_{\rm S}, r)$ (top panel) and the plane (ϵ_1, ϵ_2) (bottom panel). The two pink solid contours are the one and two-sigma Planck confidence intervals (marginalized over second order slow-roll). The annotations trace the energy scale at which reheating ends and correspond to $\log(g_*^{1/4} T_{\rm reh}/{\rm GeV})$. The green points delimit the prediction points such that inflation end by slow roll violation (for $\mu/M_{\rm Pl} > 0.02$, above the green points) from the ones where inflation end by tachyonic instability (below the green points).

A.50 Running Mass Inflation 1 (RMI1)

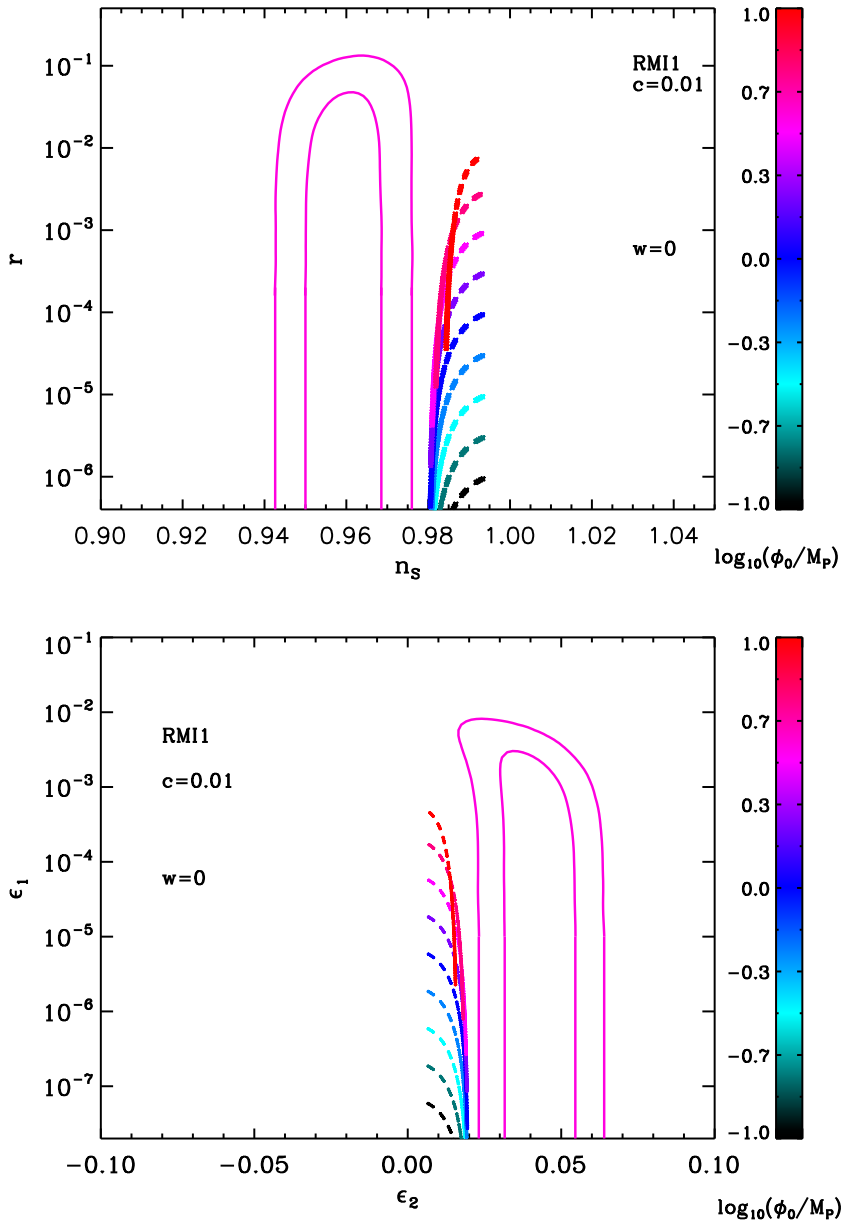

Figure 167. Reheating consistent slow-roll predictions for the running mass inflation 1 models ($c > 0$, $x < 1$) with $c = 0.01$, $\phi_0/M_{\rm Pl} < 1/\sqrt{c}$, $1/e < x_{\rm end} < 1$, in the plane $(n_{\rm S}, r)$ (top panel) and the plane (ϵ_1, ϵ_2) (bottom panel). The two pink solid contours are the one and two-sigma Planck confidence intervals (marginalized over second order slow-roll). The energy scale at which reheating ends and the field *vev* when inflation stops $x_{\rm end} = \phi_{\rm end}/\phi_0$ are degenerated, which is the reason why they are not displayed.

A.51 Running Mass Inflation 2 (RMI2)

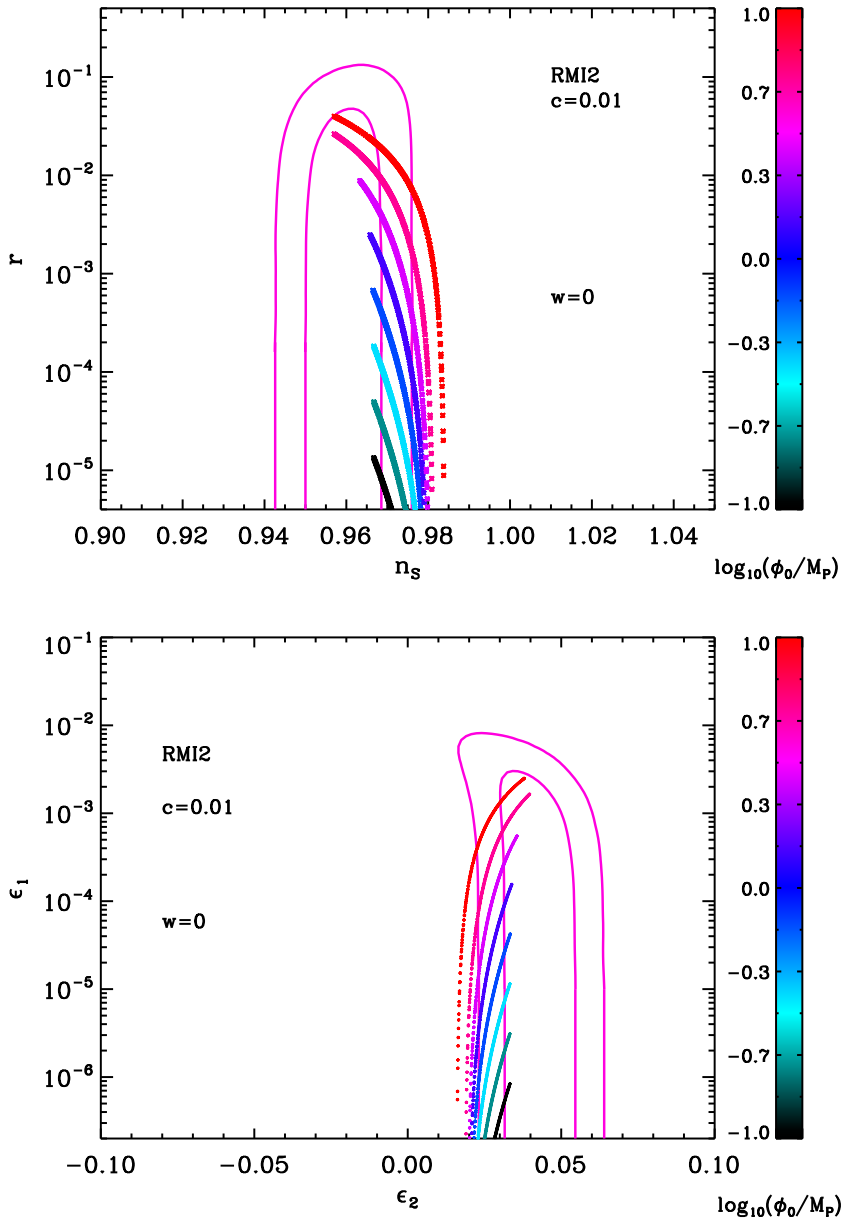

Figure 168. Reheating consistent slow-roll predictions for the running mass inflation 2 models ($c > 0$, $x > 1$) with $c = 0.01$, $\phi_0/M_{\rm Pl} < 1/\sqrt{c}$, $1 < x_{\rm end} < e$, in the plane $(n_{\rm S}, r)$ (top panel) and the plane (ϵ_1, ϵ_2) (bottom panel). The two pink solid contours are the one and two-sigma Planck confidence intervals (marginalized over second order slow-roll). The energy scale at which reheating ends and the field *vev* when inflation stops $x_{\rm end}$ are degenerated and not represented.

A.52 Running Mass Inflation 3 (RMI3)

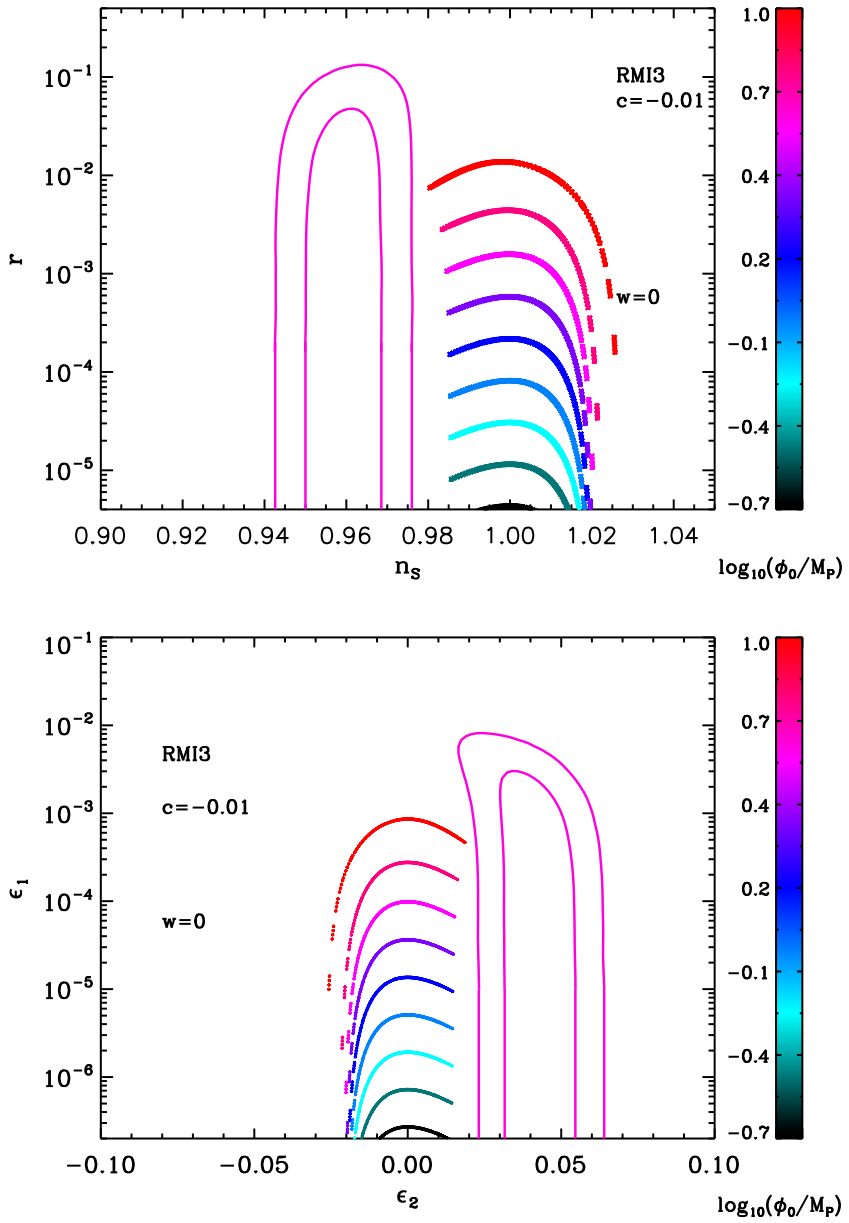

Figure 169. Reheating consistent slow-roll predictions for the running mass inflation 3 models ($c < 0$, $x < 1$) with $c = -0.01$, $\phi_0/M_{\rm Pl} < 1/\sqrt{-c}$, $1/e < x_{\rm end} < 1$, in the plane $(n_{\rm S}, r)$ (top panel) and the plane (ϵ_1, ϵ_2) (bottom panel). The two pink solid contours are the one and two-sigma Planck confidence intervals (marginalized over second order slow-roll). The energy scale at which reheating ends and the field *vev* when inflation stops $x_{\rm end}$ are degenerated and have not been represented.

A.53 Running Mass Inflation 4 (RMI4)

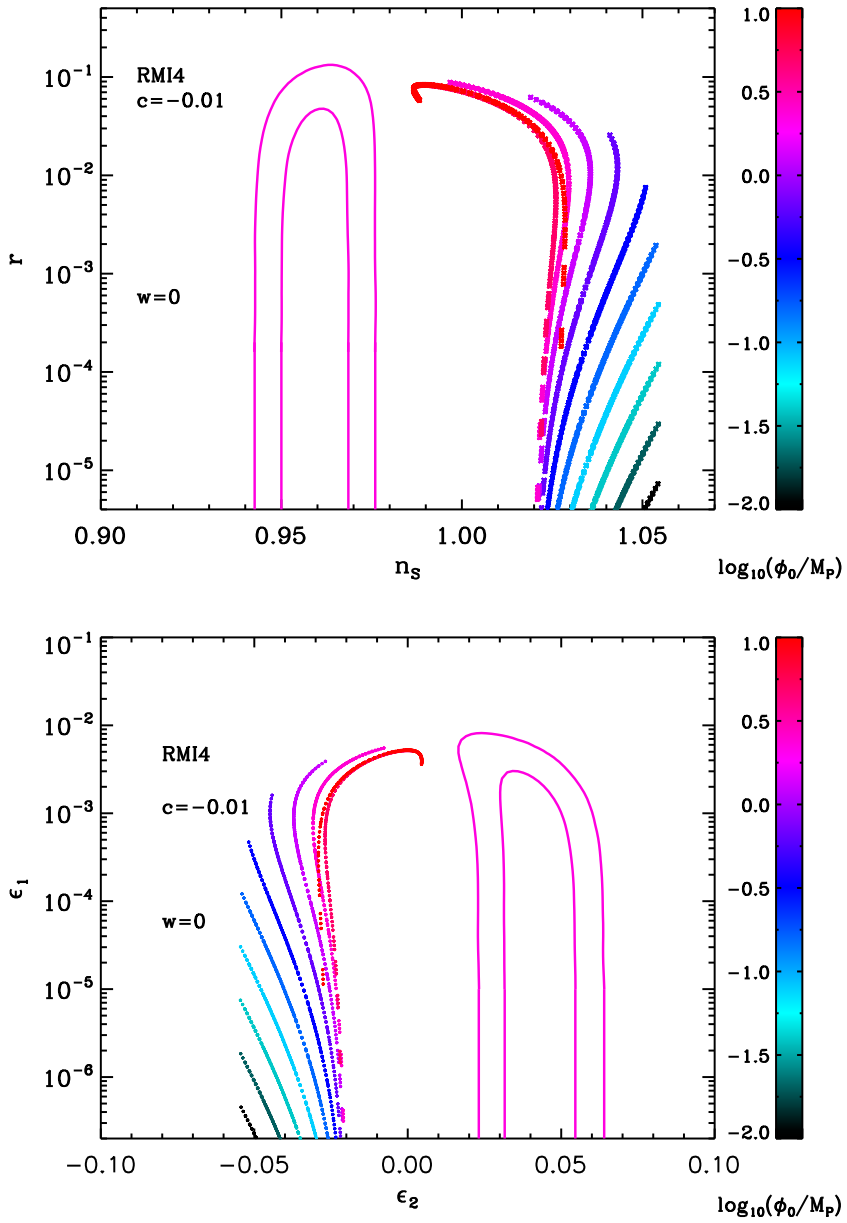

Figure 170. Reheating consistent slow-roll predictions for the running mass inflation 4 models ($c < 0$, $x > 1$) with $c = -0.01$, $\phi_0/M_{\rm Pl} < 1/\sqrt{-c}$, $1 < x_{\rm end} < e$, in the plane $(n_{\rm s}, r)$ (top panel) and the plane (ϵ_1, ϵ_2) (bottom panel). The two pink solid contours are the one and two-sigma Planck confidence intervals (marginalized over second order slow-roll). The energy scale at which reheating ends and the field *vev* $x_{\rm end}$ are degenerated and not displayed.

A.54 Valley Hybrid Inflation (VHI)

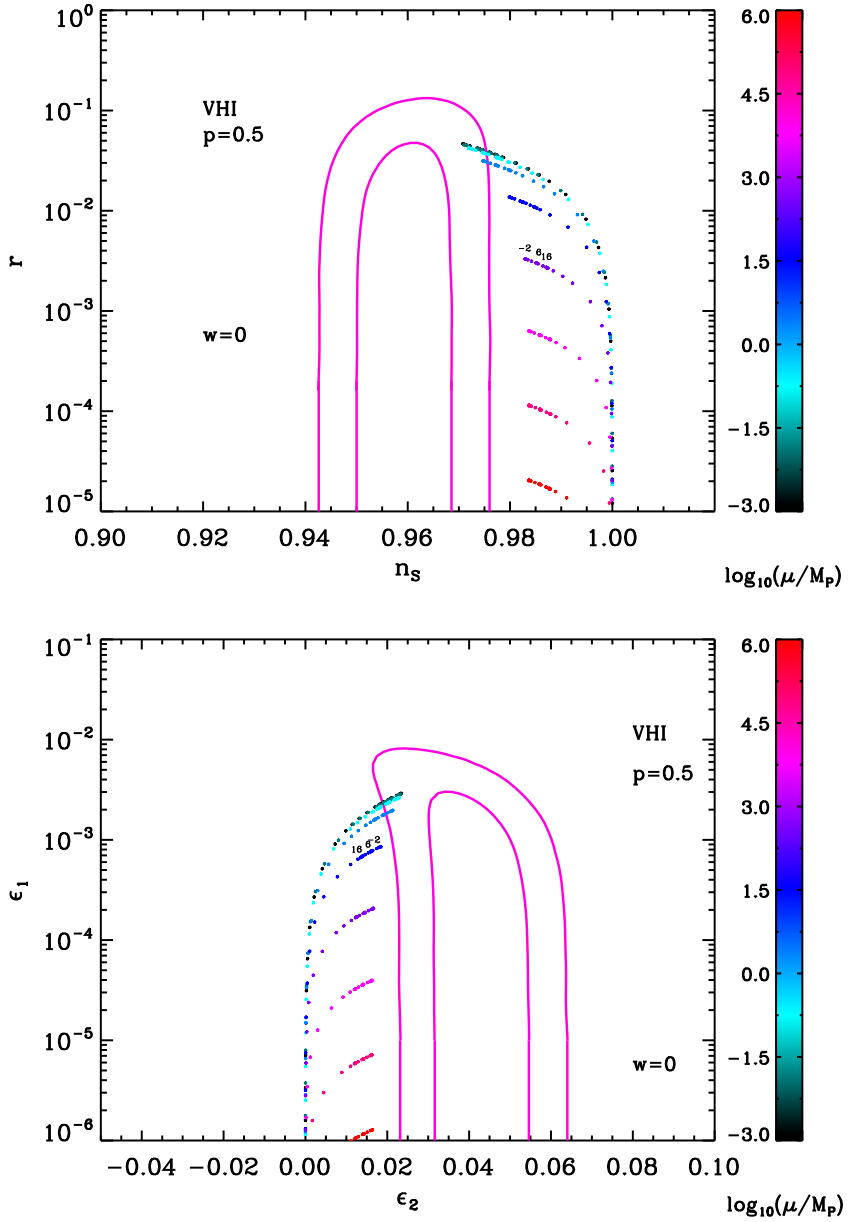

Figure 171. Reheating consistent slow-roll predictions for the valley hybrid inflation models with $p = 0.5$, in the plane $(n_{\rm S}, r)$ (top panel) and the plane (ϵ_1, ϵ_2) (bottom panel). The two pink solid contours are the one and two-sigma Planck confidence intervals (marginalized over second order slow-roll). The color of the data points encodes the value of μ, while different data blocks correspond to different values of $x_{\rm end}$. Inside a given bock, the annotations trace the energy scale at which reheating ends and correspond to $\log(g_*^{1/4} T_{\rm reh}/{\rm GeV})$.

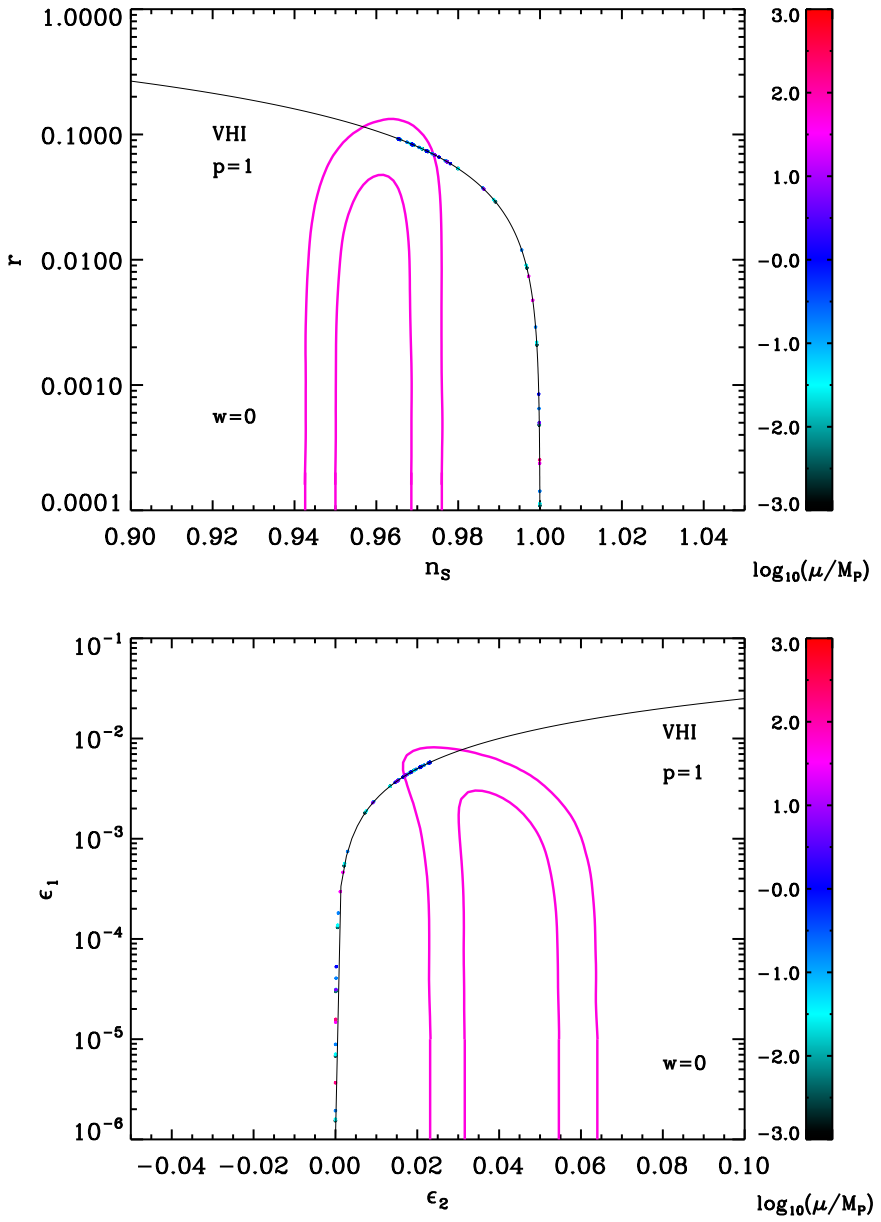

Figure 172. Reheating consistent slow-roll predictions for the valley hybrid inflation models with $p = 1$, in the plane $(n_{\rm S}, r)$ (top panel) and the plane (ϵ_1, ϵ_2) (bottom panel). The two pink solid contours are the one and two-sigma Planck confidence intervals (marginalized over second order slow-roll). The color of the data points encodes the value of μ, while different data blocks correspond to different values of $x_{\rm end}$. Inside a given bock, the annotations trace the energy scale at which reheating ends and correspond to $\log(g_*^{1/4} T_{\rm reh}/{\rm GeV})$. The black solid line represent the locus of the points such that $\epsilon_2 = 4\epsilon_1$.

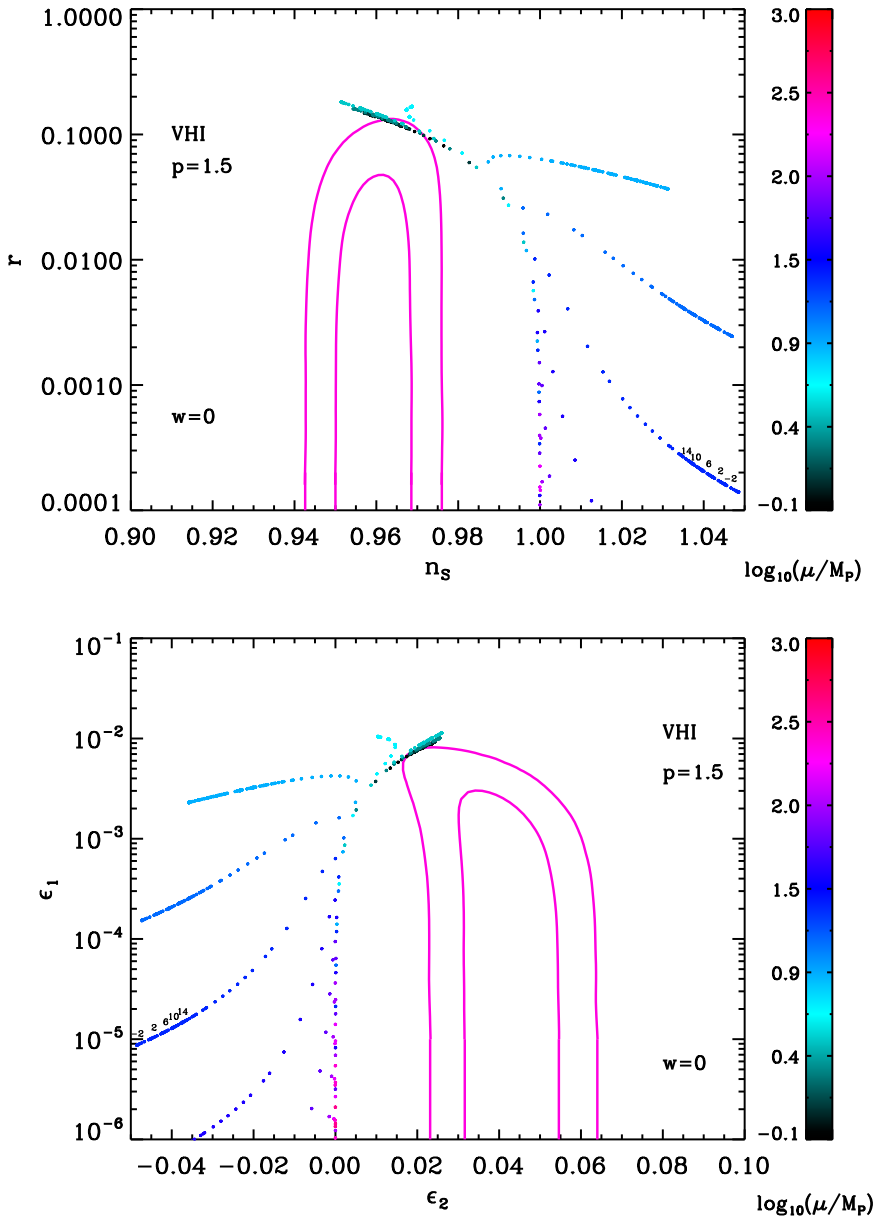

Figure 173. Reheating consistent slow-roll predictions for the valley hybrid inflation models with $p = 1.5$, in the plane $(n_{\rm S}, r)$ (top panel) and the plane (ϵ_1, ϵ_2) (bottom panel). The two pink solid contours are the one and two-sigma Planck confidence intervals (marginalized over second order slow-roll). The color of the data points encodes the value of μ, while different data blocks correspond to different values of $x_{\rm end}$. Inside a given bock, the annotations trace the energy scale at which reheating ends and correspond to $\log(g_*^{1/4} T_{\rm reh}/{\rm GeV})$.

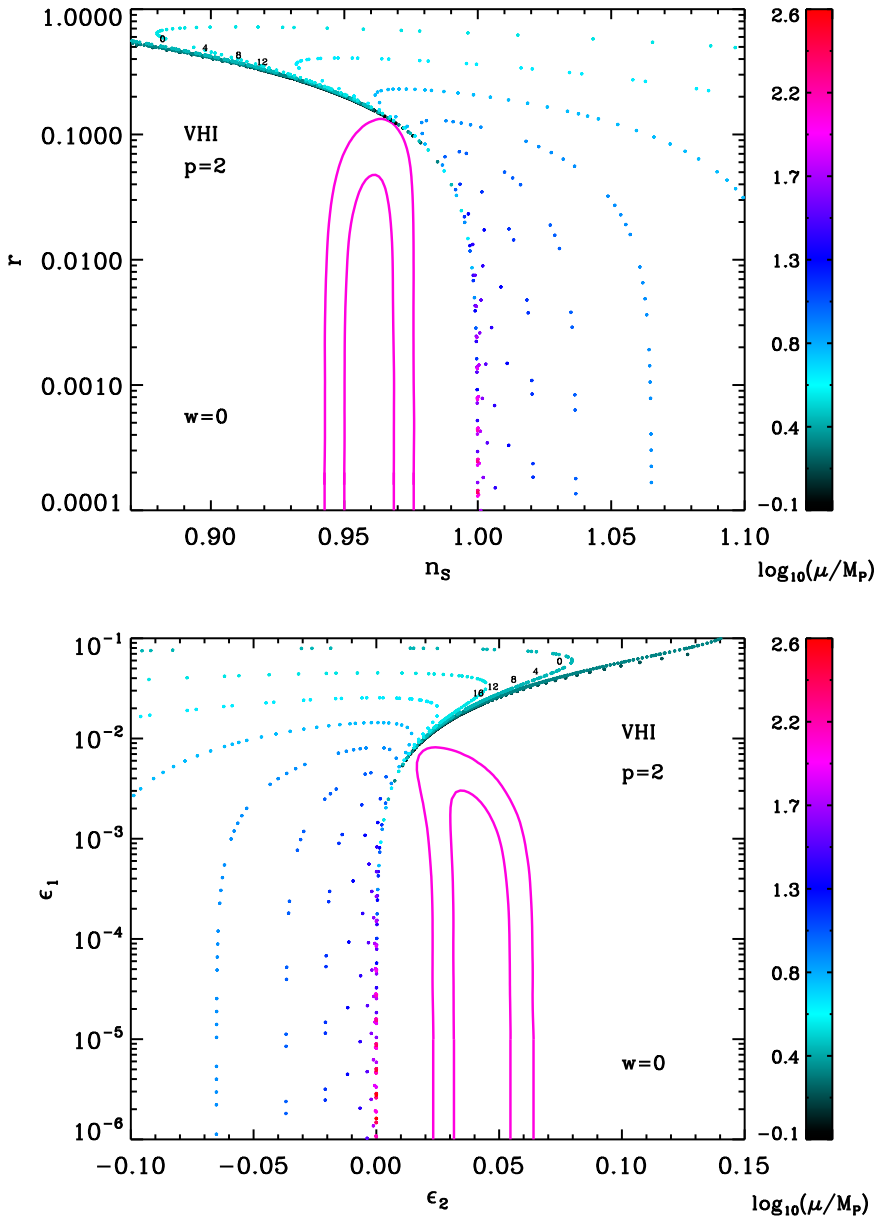

Figure 174. Reheating consistent slow-roll predictions for the valley hybrid inflation models with $p = 2$, in the plane $(n_{\rm S}, r)$ (top panel) and the plane (ϵ_1, ϵ_2) (bottom panel). The two pink solid contours are the one and two-sigma Planck confidence intervals (marginalized over second order slow-roll). The color of the data points encodes the value of μ, while different data blocks correspond to different values of $x_{\rm end}$. Inside a given bock, the annotations trace the energy scale at which reheating ends and correspond to $\log(g_*^{1/4} T_{\rm reh}/{\rm GeV})$.

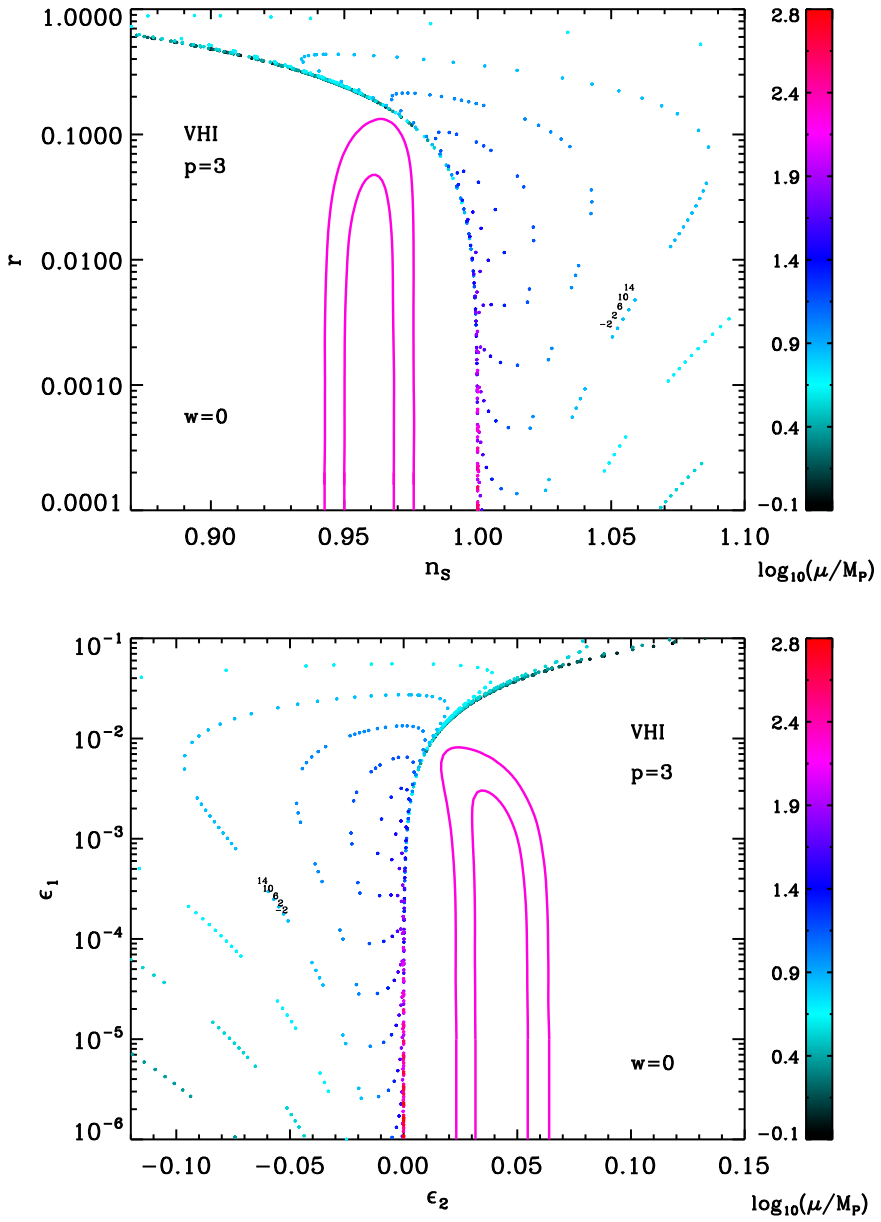

Figure 175. Reheating consistent slow-roll predictions for the valley hybrid inflation models with $p = 3$, in the plane $(n_{\rm S}, r)$ (top panel) and the plane (ϵ_1, ϵ_2) (bottom panel). The two pink solid contours are the one and two-sigma Planck confidence intervals (marginalized over second order slow-roll). The color of the data points encodes the value of μ, while different data blocks correspond to different values of $x_{\rm end}$. Inside a given bock, the annotations trace the energy scale at which reheating ends and correspond to $\log(g_*^{1/4} T_{\rm reh}/{\rm GeV})$.

A.55 Dynamical Supersymmetric Inflation (DSI)

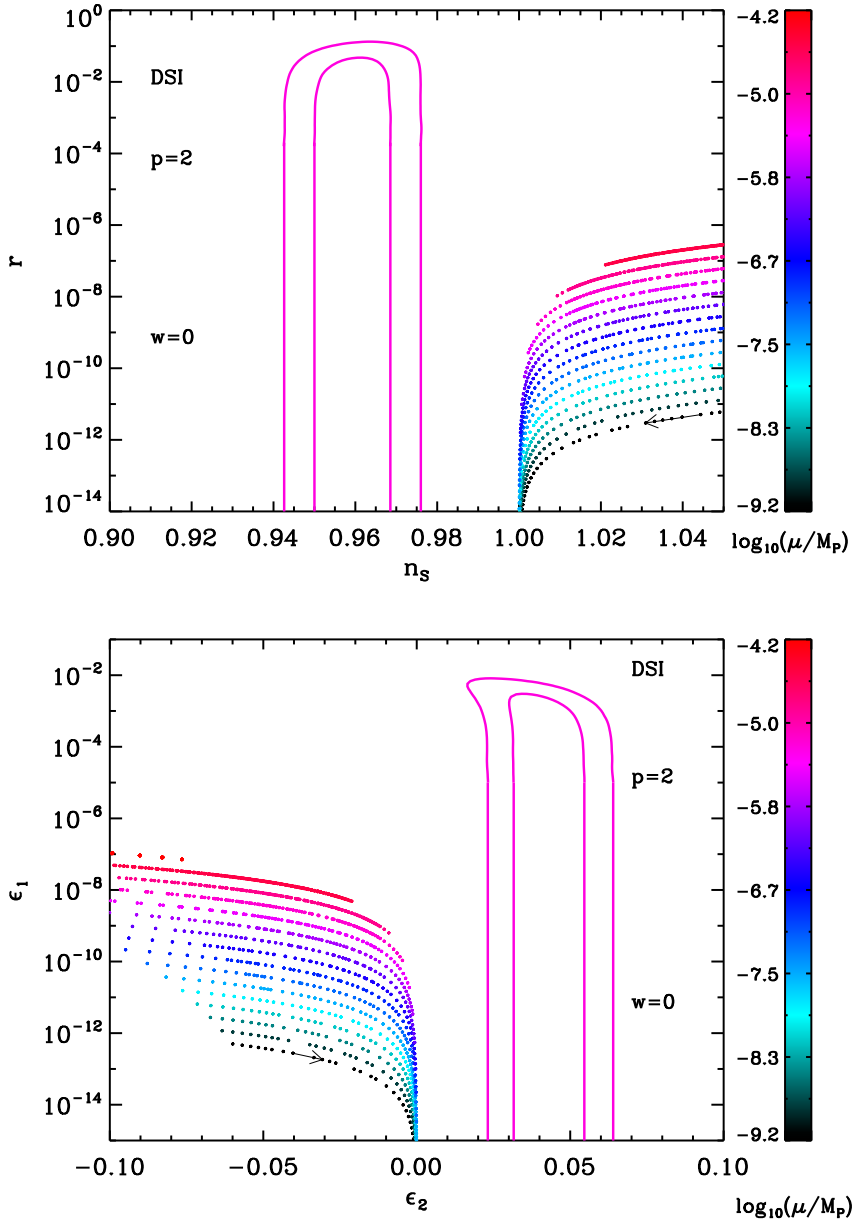

Figure 176. Reheating consistent slow-roll predictions for the dynamical supersymmetric inflation models with $p = 2$, $10^{-10} < \mu/M_{\rm Pl} < \mu_{\rm max}/M_{\rm Pl}$, and $x_{\rm end}^{\rm min} < x_{\rm end} < x_{\rm end}^{\rm max}$ in the plane $(n_{\rm S}, r)$ (top panel) and the plane (ϵ_1, ϵ_2) (bottom panel). The two pink solid contours are the one and two-sigma Planck confidence intervals (marginalized over second order slow-roll). The parameter $x_{\rm end}$ increases along the direction specified by the arrows, and is degenerate with the energy scale at which reheating ends.

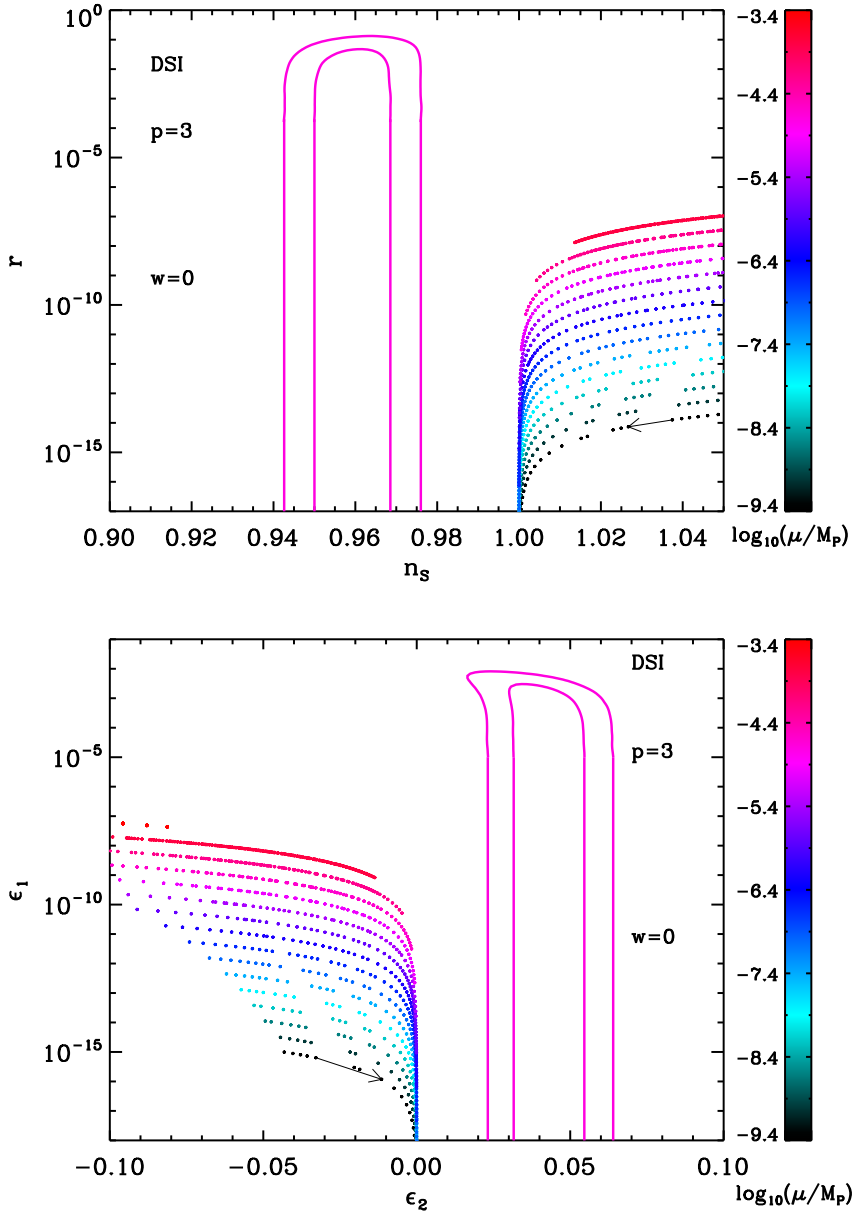

Figure 177. Reheating consistent slow-roll predictions for the dynamical supersymmetric inflation models with $p = 3$, $10^{-10} < \mu/M_{\rm Pl} < \mu_{\rm max}/M_{\rm Pl}$, and $x_{\rm end}^{\rm min} < x_{\rm end} < x_{\rm end}^{\rm max}$, in the plane $(n_{\rm S}, r)$ (top panel) and the plane (ϵ_1, ϵ_2) (bottom panel). The two pink solid contours are the one and two-sigma Planck confidence intervals (marginalized over second order slow-roll). The parameter $x_{\rm end}$ increases along the direction specified by the arrows, and is degenerated with the energy scale at which reheating ends.

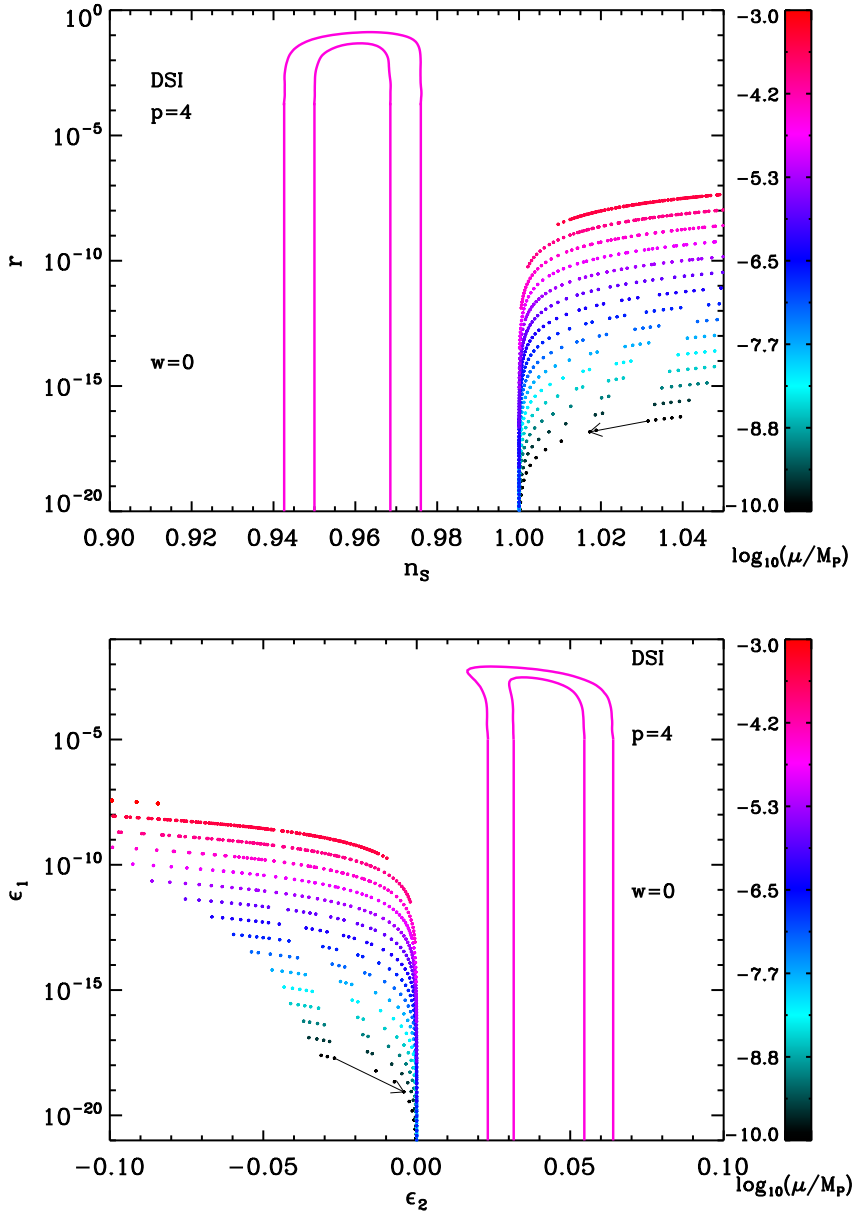

Figure 178. Reheating consistent slow-roll predictions for the dynamical supersymmetric inflation models with $p = 4$, $10^{-10} < \mu/M_{\rm Pl} < \mu_{\rm max}/M_{\rm Pl}$, and the prior $x_{\rm end}^{\rm min} < x_{\rm end} < x_{\rm end}^{\rm max}$ in the plane $(n_{\rm S}, r)$ (top panel) and the plane (ϵ_1, ϵ_2) (bottom panel). The two pink solid contours are the one and two-sigma Planck confidence intervals (marginalized over second order slow-roll). The parameter $x_{\rm end}$ increases along the direction specified by the arrows and is degenerated with the energy scale at which reheating ends.

A.56 Generalized Mixed Inflation (GMLFI)

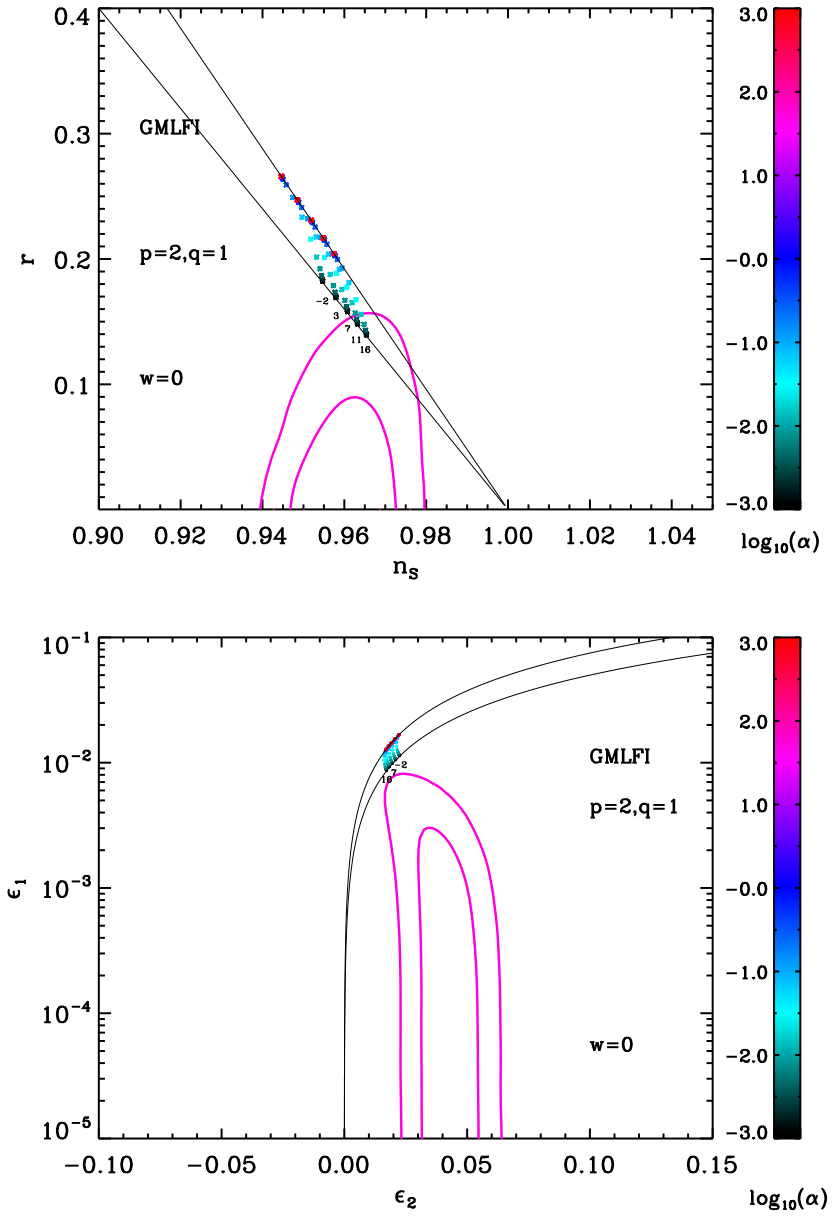

Figure 179. Reheating consistent slow-roll predictions for the generalized mixed inflation models with $p = 2$ and $q = 1$, in the plane $(n_{\rm S}, r)$ (top panel) and the plane (ϵ_1, ϵ_2) (bottom panel). The two pink solid contours are the one and two-sigma Planck confidence intervals (marginalized over second order slow-roll). The annotations trace the energy scale at which reheating ends and correspond to $\log(g_*^{1/4} T_{\rm reh}/{\rm GeV})$. The black solid lines represent the locus of the LFI-p and LFI-$(p+q)$ models (for which $\epsilon_2 = (4/p)\epsilon_1$ and $\epsilon_2 = 4\epsilon_1/(p+q)$ respectively).

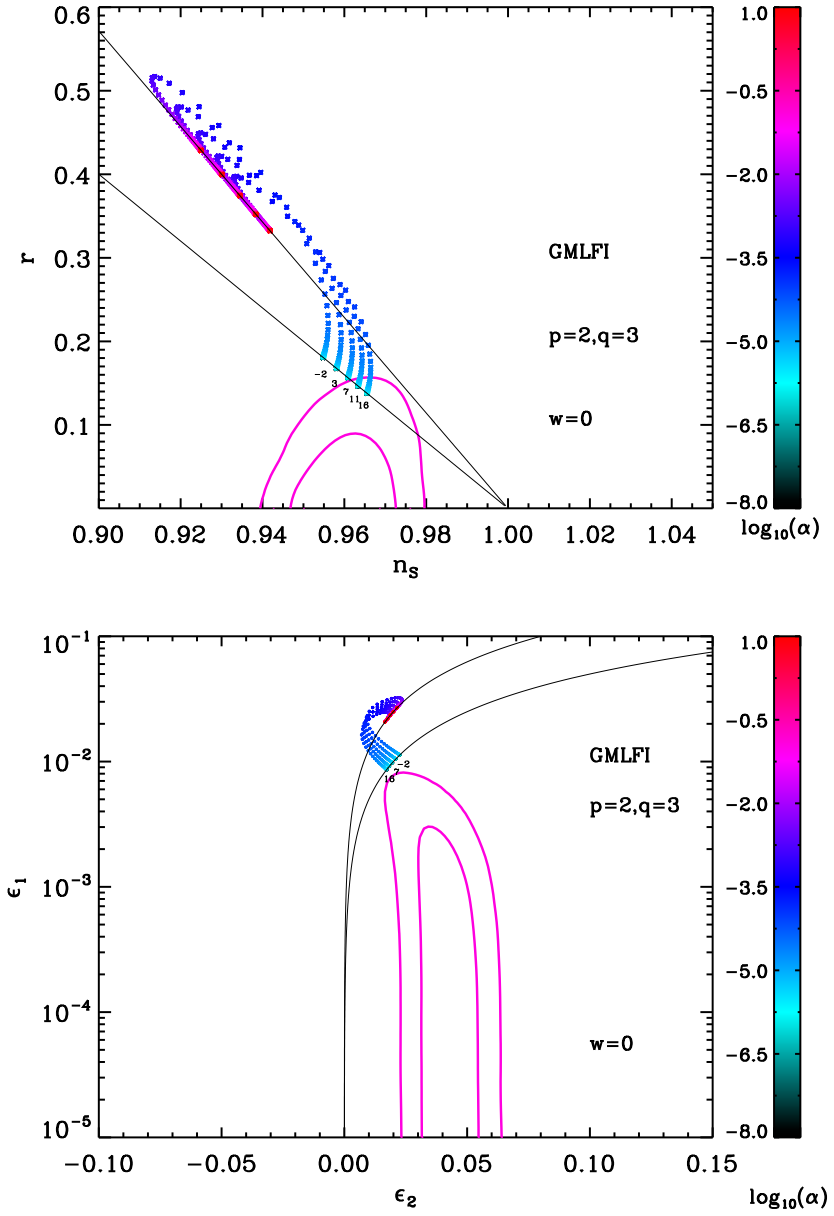

Figure 180. Reheating consistent slow-roll predictions for the generalized mixed inflation models with $p = 2$ and $q = 3$, in the plane $(n_{\rm S}, r)$ (top panel) and the plane (ϵ_1, ϵ_2) (bottom panel). The two pink solid contours are the one and two-sigma Planck confidence intervals (marginalized over second order slow-roll). The annotations trace the energy scale at which reheating ends and correspond to $\log(g_*^{1/4} T_{\rm reh}/{\rm GeV})$. The black solid lines represent the locus of the LFI-p and LFI-$(p+q)$ models (for which $\epsilon_2 = (4/p)\epsilon_1$ and $\epsilon_2 = 4\epsilon_1/(p+q)$ respectively).

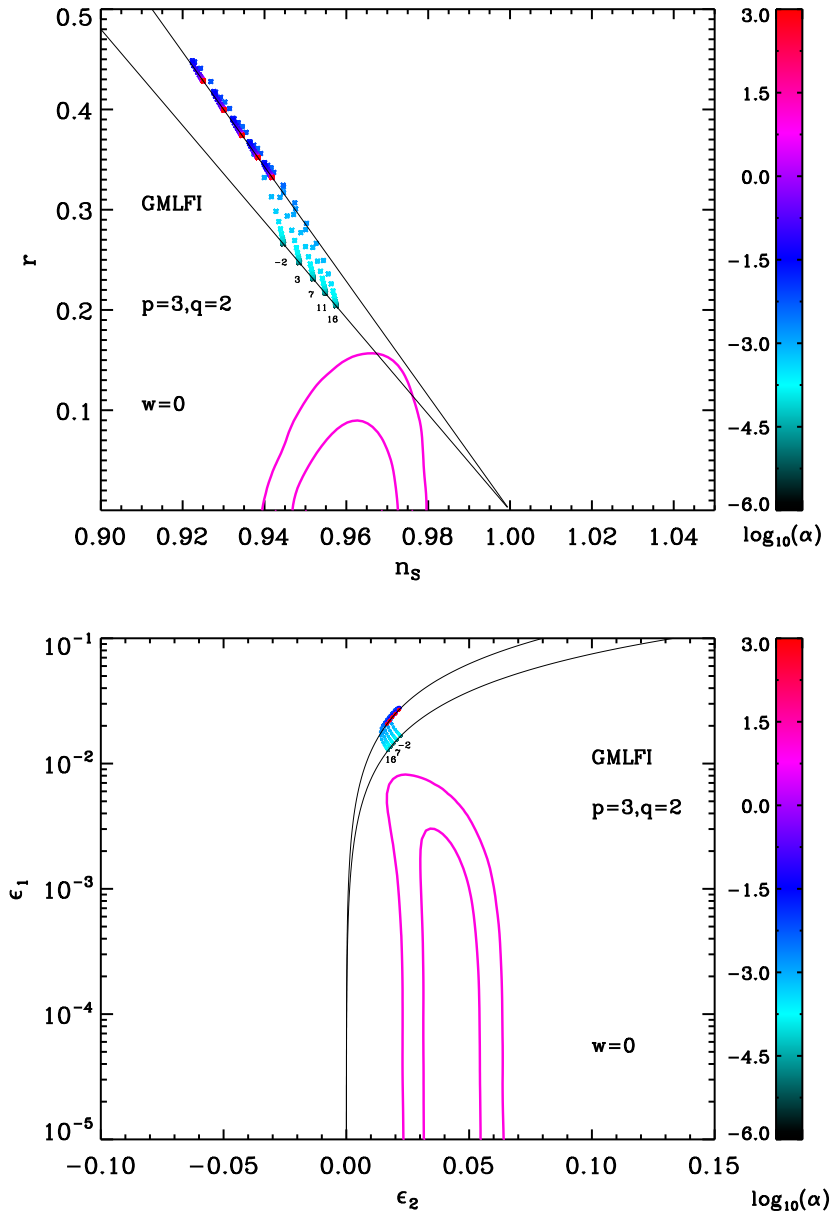

Figure 181. Reheating consistent slow-roll predictions for the generalized mixed inflation models with $p = 3$ and $q = 2$, in the plane $(n_{\rm S}, r)$ (top panel) and the plane (ϵ_1, ϵ_2) (bottom panel). The two pink solid contours are the one and two-sigma Planck confidence intervals (marginalized over second order slow-roll). The annotations trace the energy scale at which reheating ends and correspond to $\log(g_*^{1/4} T_{\rm reh}/{\rm GeV})$. The black solid lines represent the locus of the LFI-p and LFI-$(p+q)$ models (for which $\epsilon_2 = (4/p)\epsilon_1$ and $\epsilon_2 = 4\epsilon_1/(p+q)$ respectively).

A.57 Logarithmic Potential Inflation 1 (LPI1)

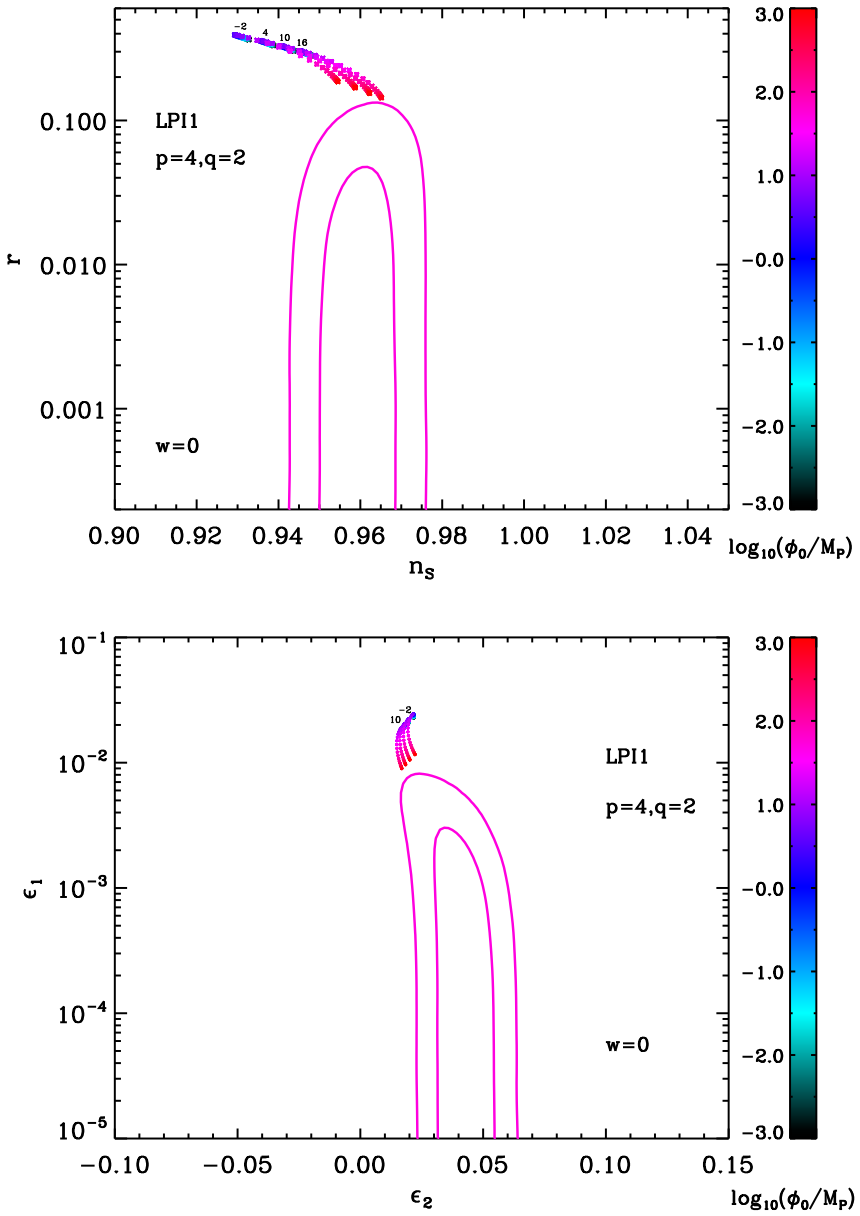

Figure 182. Reheating consistent slow-roll predictions for the logarithmic potential inflation 1 models for $p = 4$ and $q = 2$ in the plane $(n_{\rm S}, r)$ (top panel) and the plane (ϵ_1, ϵ_2) (bottom panel). The two pink solid contours are the one and two-sigma Planck confidence intervals (marginalized over second order slow-roll). The annotations trace the energy scale at which reheating ends and correspond to $\log(g_*^{1/4} T_{\rm reh}/{\rm GeV})$.

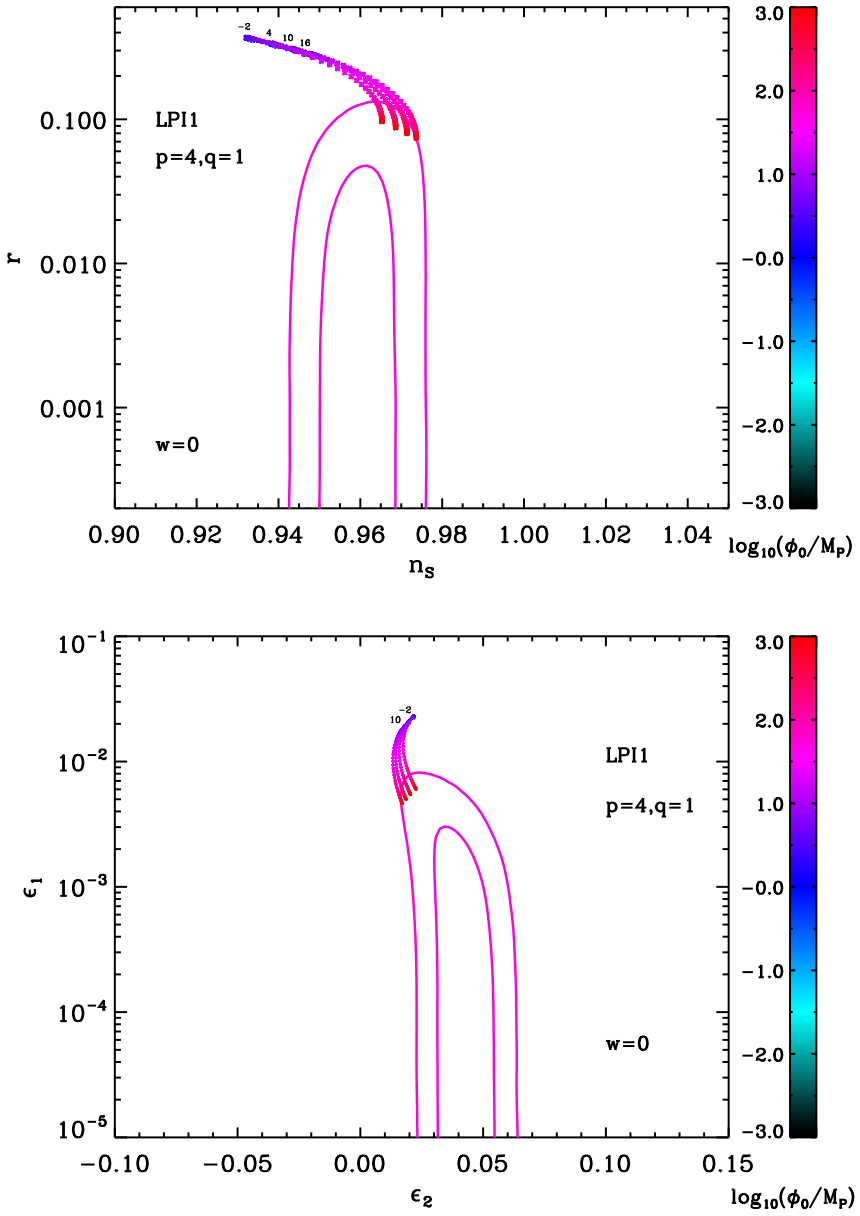

Figure 183. Reheating consistent slow-roll predictions for the logarithmic potential inflation 1 models for $p = 4$ and $q = 1$ in the plane $(n_{\rm S}, r)$ (top panel) and the plane (ϵ_1, ϵ_2) (bottom panel). The two pink solid contours are the one and two-sigma Planck confidence intervals (marginalized over second order slow-roll). The annotations trace the energy scale at which reheating ends and correspond to $\log(g_*^{1/4} T_{\rm reh}/{\rm GeV})$.

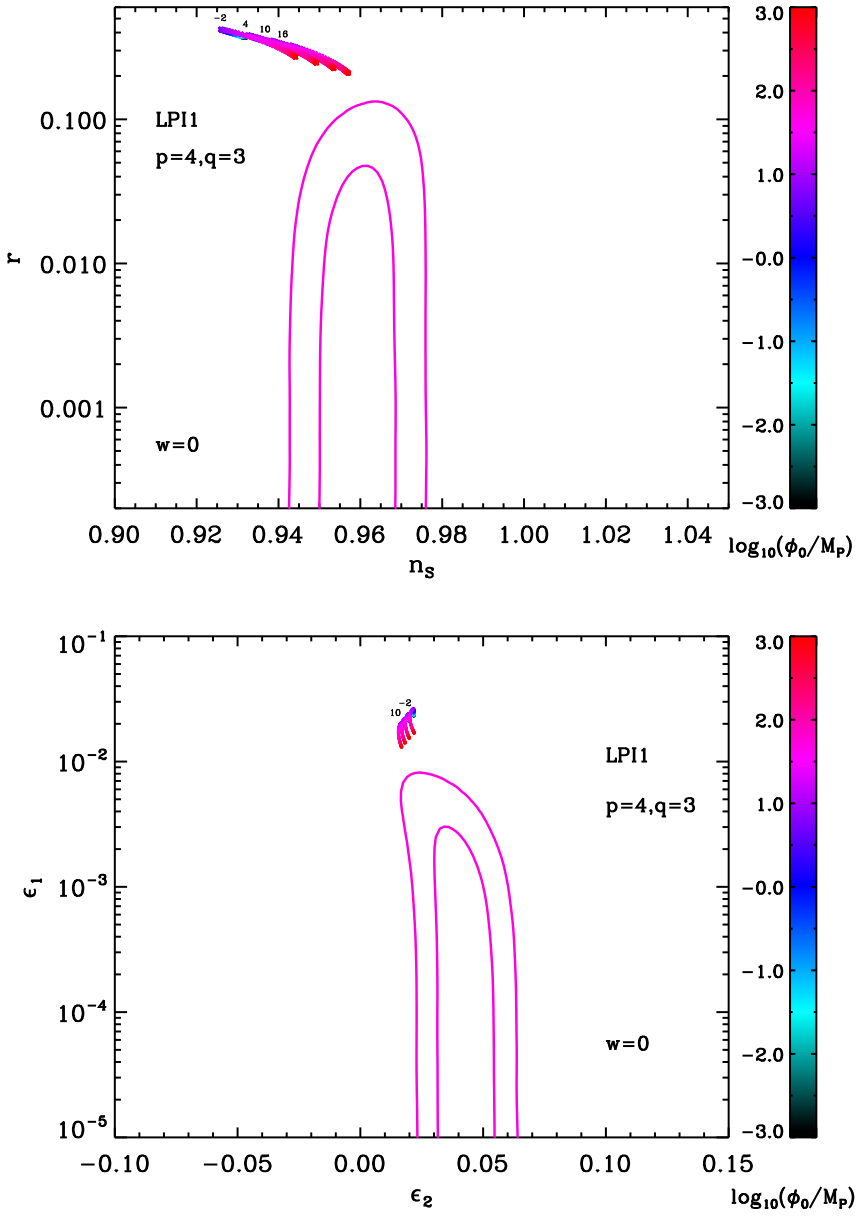

Figure 184. Reheating consistent slow-roll predictions for the logarithmic potential inflation 1 models for $p = 4$ and $q = 3$ in the plane $(n_{\rm S}, r)$ (top panel) and the plane (ϵ_1, ϵ_2) (bottom panel). The two pink solid contours are the one and two-sigma Planck confidence intervals (marginalized over second order slow-roll). The annotations trace the energy scale at which reheating ends and correspond to $\log(g_*^{1/4} T_{\rm reh}/{\rm GeV})$.

A.58 Logarithmic Potential Inflation 2 (LPI2)

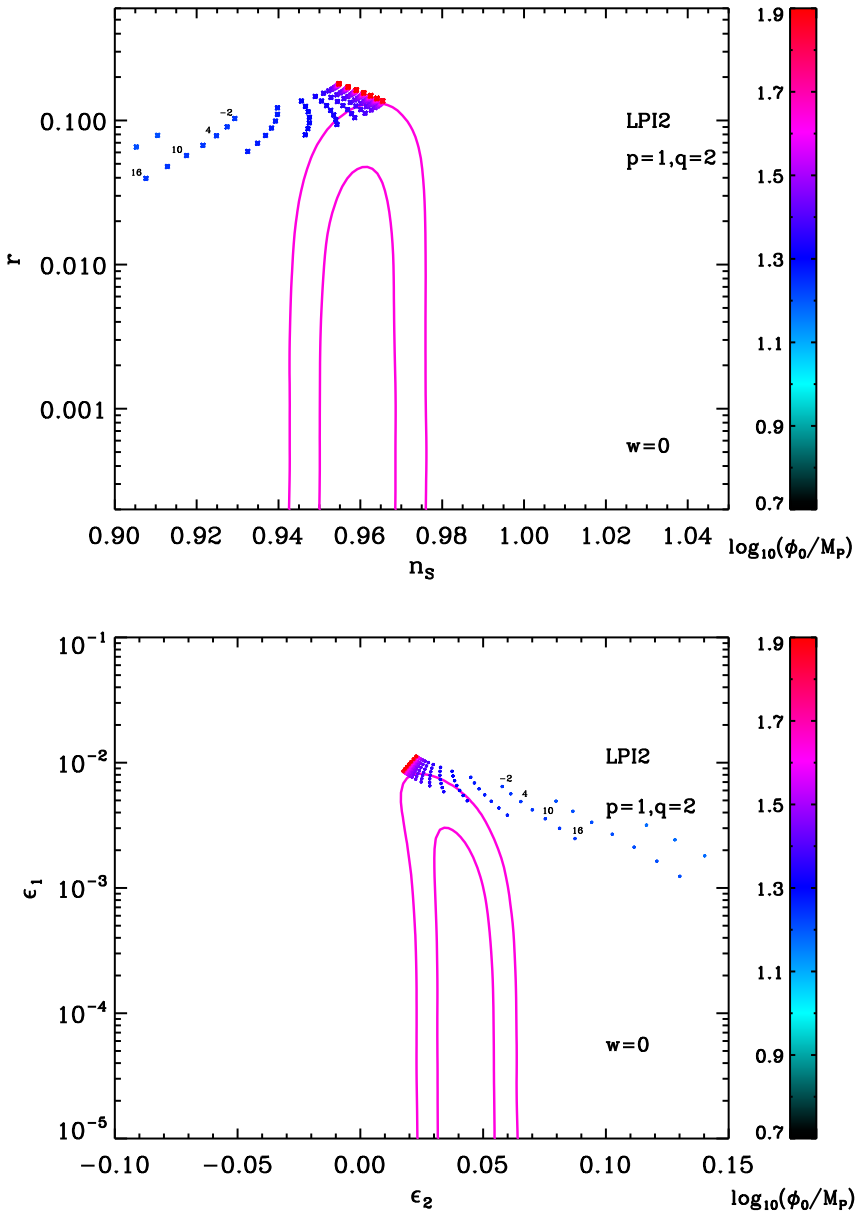

Figure 185. Reheating consistent slow-roll predictions for the logarithmic potential inflation 2 models for $p = 4$ and $q = 2$ in the plane $(n_{\rm S}, r)$ (top panel) and the plane (ϵ_1, ϵ_2) (bottom panel). The two pink solid contours are the one and two-sigma Planck confidence intervals (marginalized over second order slow-roll). The annotations trace the energy scale at which reheating ends and correspond to $\log(g_*^{1/4} T_{\rm reh}/{\rm GeV})$.

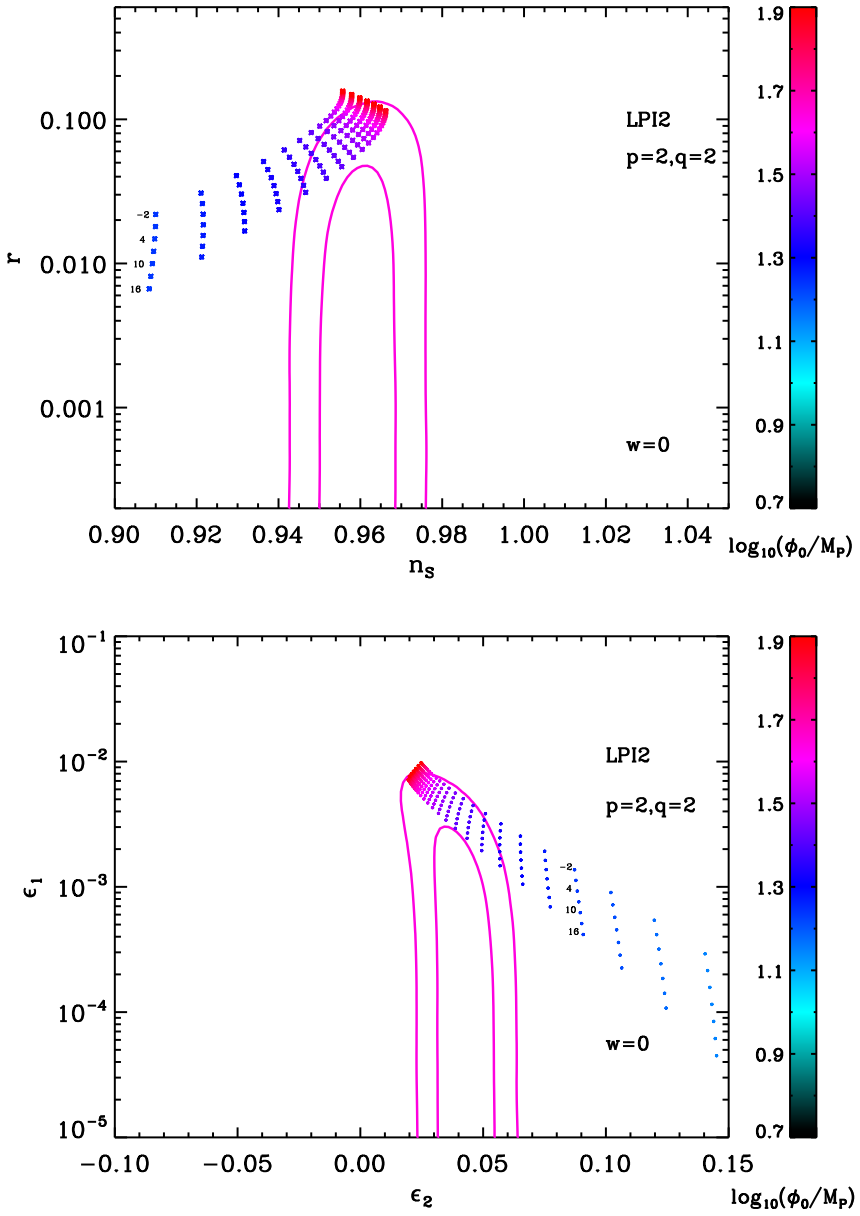

Figure 186. Reheating consistent slow-roll predictions for the logarithmic potential inflation 2 models for $p = 4$ and $q = 1$ in the plane $(n_{\rm S}, r)$ (top panel) and the plane (ϵ_1, ϵ_2) (bottom panel). The two pink solid contours are the one and two-sigma Planck confidence intervals (marginalized over second order slow-roll). The annotations trace the energy scale at which reheating ends and correspond to $\log(g_*^{1/4} T_{\rm reh}/{\rm GeV})$.

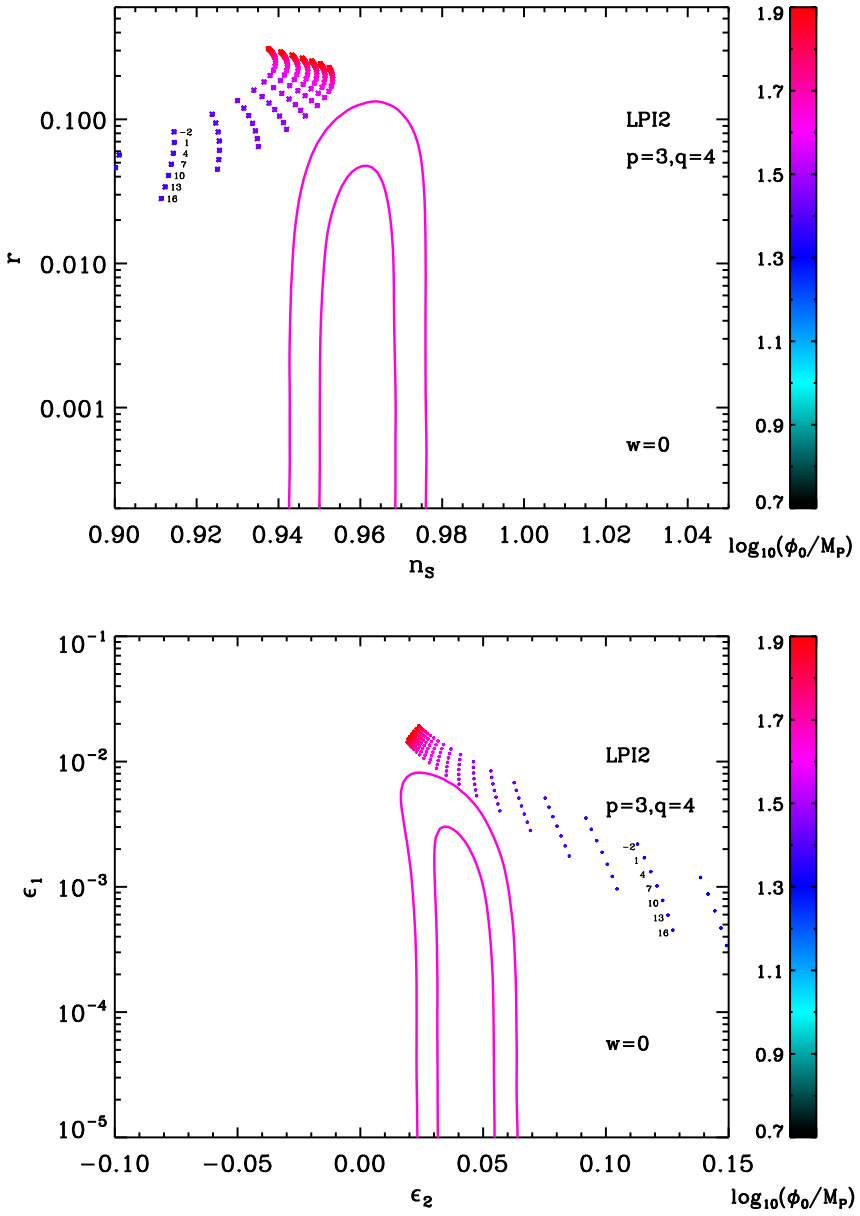

Figure 187. Reheating consistent slow-roll predictions for the logarithmic potential inflation 2 models for $p = 4$ and $q = 3$ in the plane $(n_{\rm S}, r)$ (top panel) and the plane (ϵ_1, ϵ_2) (bottom panel). The two pink solid contours are the one and two-sigma Planck confidence intervals (marginalized over second order slow-roll). The annotations trace the energy scale at which reheating ends and correspond to $\log(g_*^{1/4} T_{\rm reh}/{\rm GeV})$.

A.59 Logarithmic Potential Inflation 3 (LPI3)

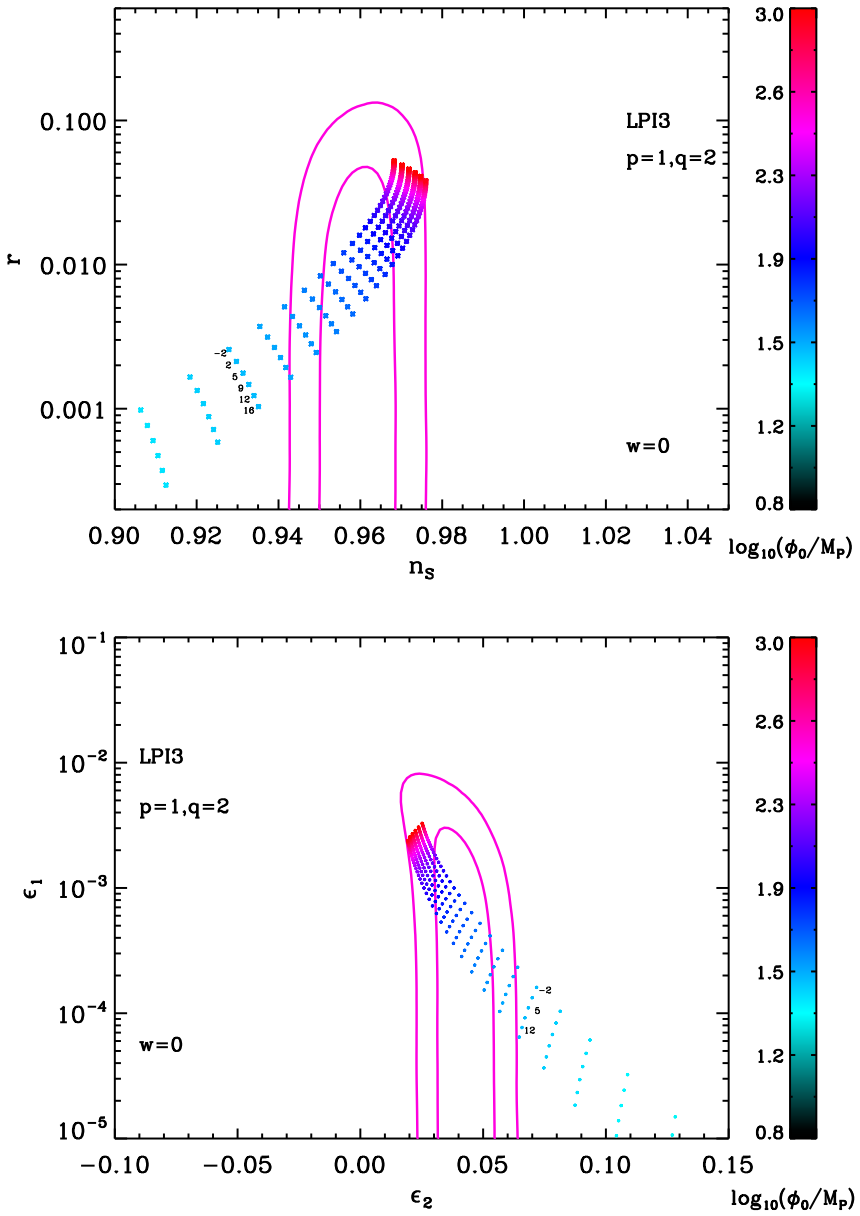

Figure 188. Reheating consistent slow-roll predictions for the logarithmic potential inflation 3 models for $p = 4$ and $q = 2$ in the plane $(n_{\rm S}, r)$ (top panel) and the plane (ϵ_1, ϵ_2) (bottom panel). The two pink solid contours are the one and two-sigma Planck confidence intervals (marginalized over second order slow-roll). The annotations trace the energy scale at which reheating ends and correspond to $\log(g_*^{1/4} T_{\rm reh}/{\rm GeV})$.

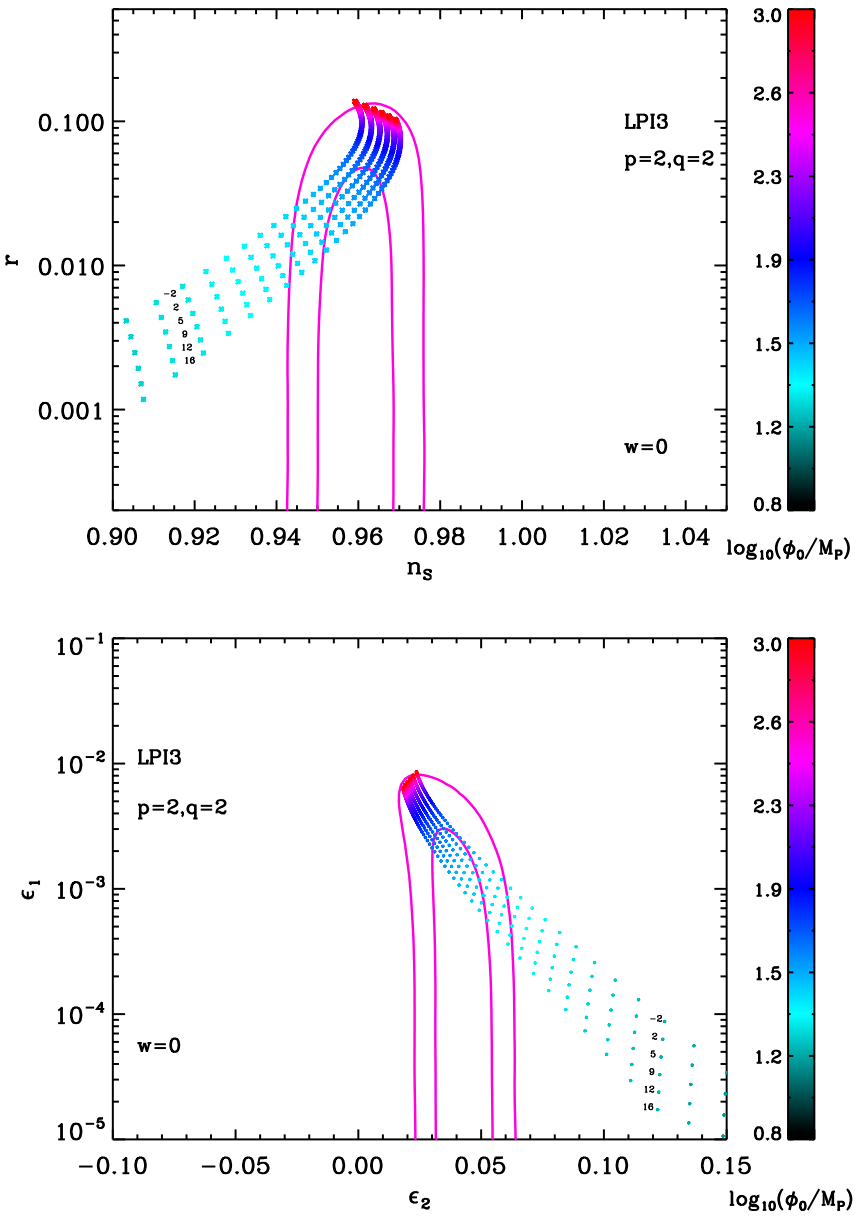

Figure 189. Reheating consistent slow-roll predictions for the logarithmic potential inflation 3 models for $p = 4$ and $q = 1$ in the plane $(n_{\rm S}, r)$ (top panel) and the plane (ϵ_1, ϵ_2) (bottom panel). The two pink solid contours are the one and two-sigma Planck confidence intervals (marginalized over second order slow-roll). The annotations trace the energy scale at which reheating ends and correspond to $\log(g_*^{1/4} T_{\rm reh}/{\rm GeV})$.

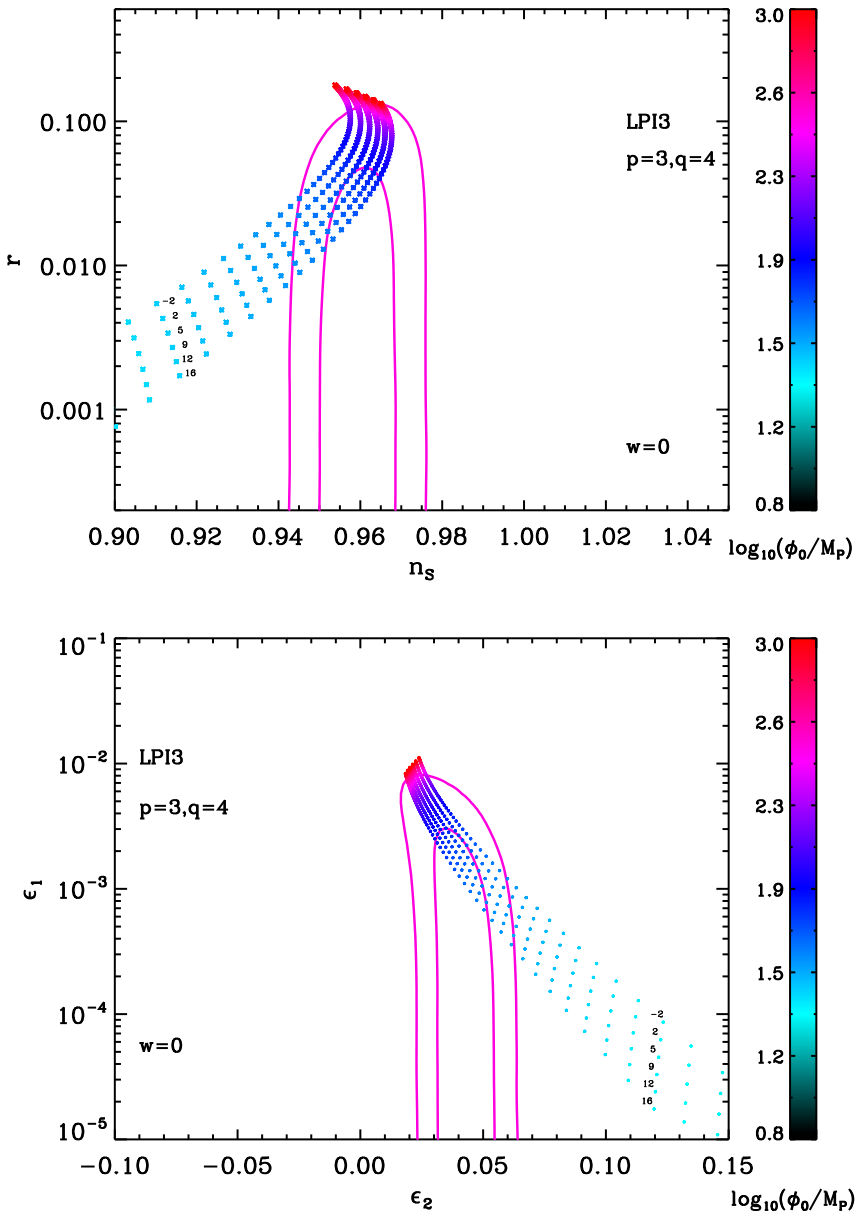

Figure 190. Reheating consistent slow-roll predictions for the logarithmic potential inflation 3 models for $p = 4$ and $q = 3$ in the plane $(n_{\rm S}, r)$ (top panel) and the plane (ϵ_1, ϵ_2) (bottom panel). The two pink solid contours are the one and two-sigma Planck confidence intervals (marginalized over second order slow-roll). The annotations trace the energy scale at which reheating ends and correspond to $\log(g_*^{1/4} T_{\rm reh}/{\rm GeV})$.

A.60 Constant $n_{\rm S}$ D Inflation (CNDI)

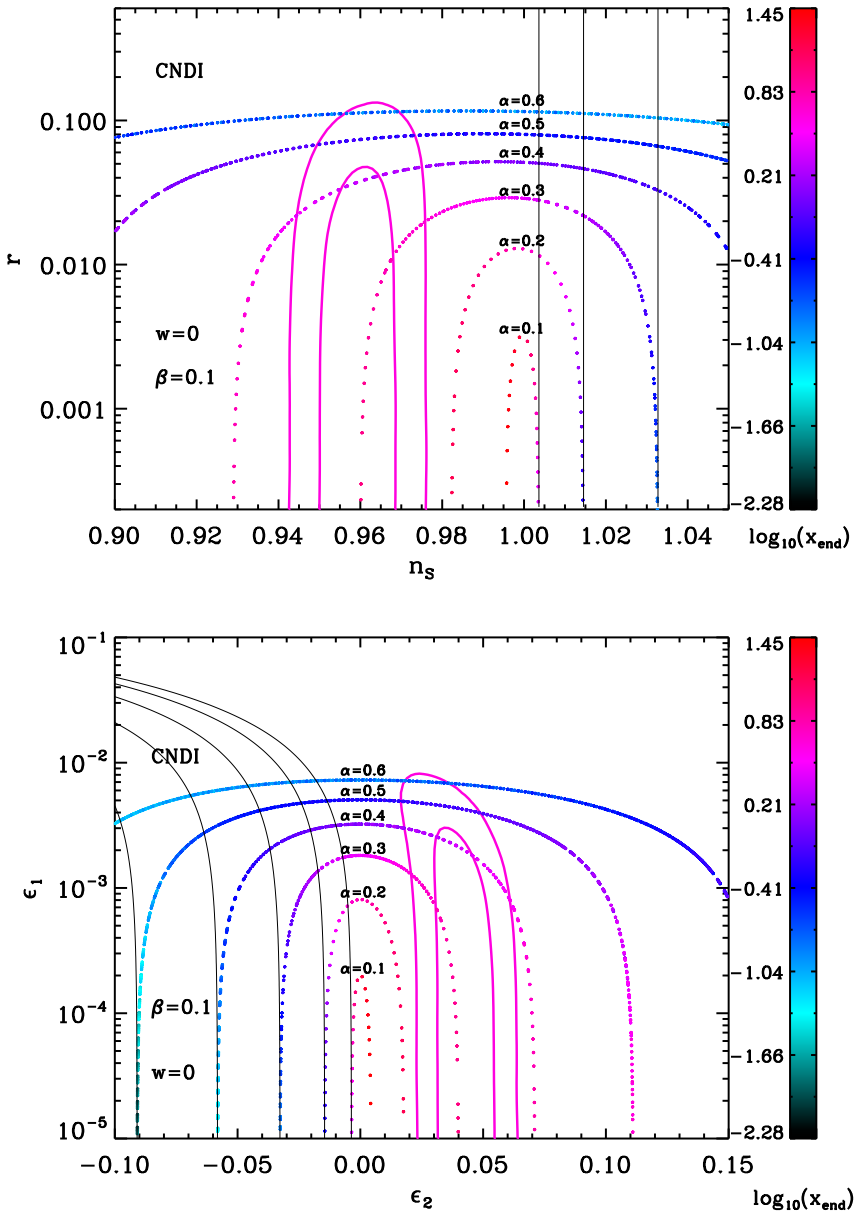

Figure 191. Reheating consistent slow-roll predictions for the constant $n_{\rm S}$ D inflation models for $\beta = 0.1$ in the plane $(n_{\rm S}, r)$ (top panel) and the plane (ϵ_1, ϵ_2) (bottom panel). The two pink solid contours are the one and two-sigma Planck confidence intervals (marginalized over second order slow-roll). The energy scale at which reheating ends is not annotated since it is degenerated with the parameter $x_{\rm end}$. The black solid lines stand for the points such that $n_{\rm S} = 1 + 4\alpha^2\beta/(\beta + 1)$.

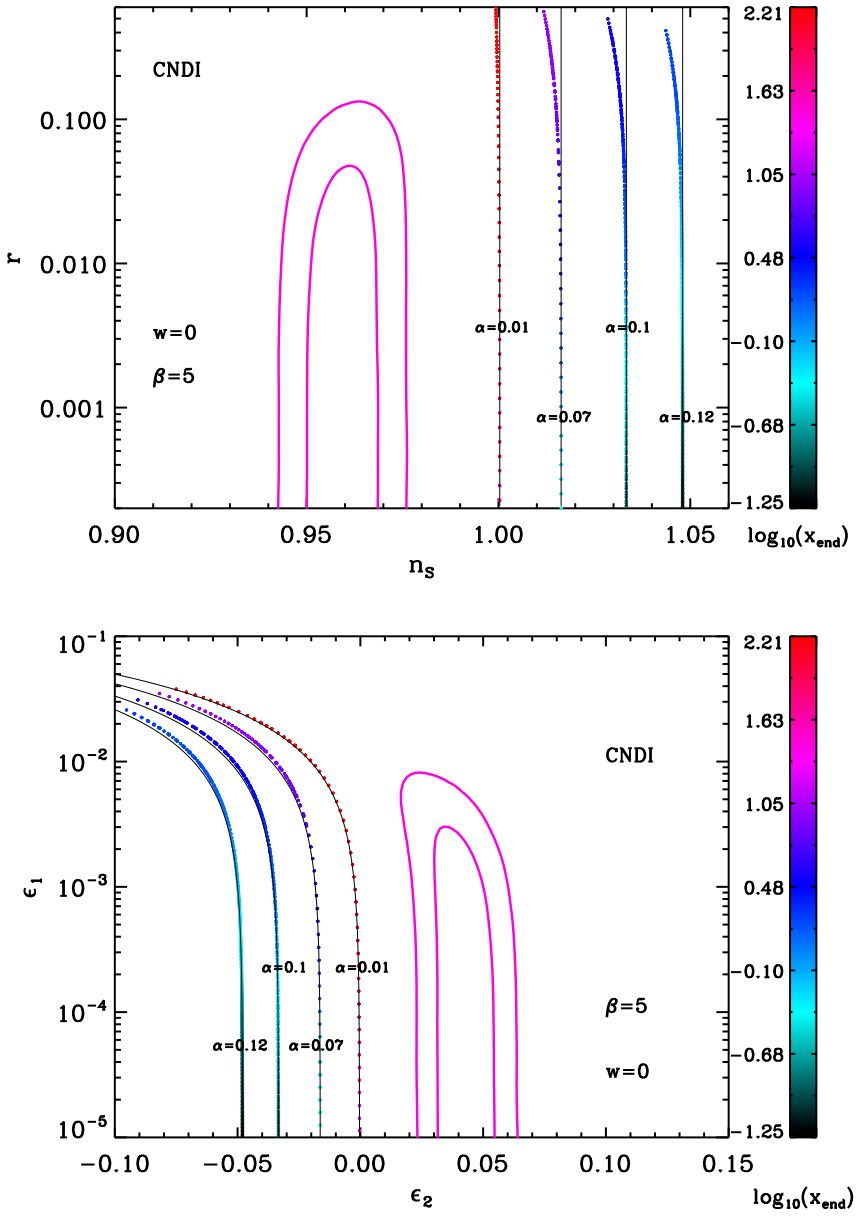

Figure 192. Reheating consistent slow-roll predictions for the constant $n_{\rm S}$ D inflation models for $\beta = 5$ in the plane $(n_{\rm S}, r)$ (top panel) and the plane (ϵ_1, ϵ_2) (bottom panel). The two pink solid contours are the one and two-sigma Planck confidence intervals (marginalized over second order slow-roll). The energy scale at which reheating ends is not annotated since it is degenerated with the parameter $x_{\rm end}$. The black solid lines stand for the points such that $n_{\rm S} = 1 + 4\alpha^2\beta/(\beta + 1)$.

Acknowledgments

This work is partially supported by the ESA Belgian Federal PRODEX Grant No. 4000103071 and the Wallonia-Brussels Federation grant ARC No. 11/15-040. We would like to thank `EvaluatorIAP` for his everyday encouragements.

References

[1] A. H. Guth, *The Inflationary Universe: A Possible Solution to the Horizon and Flatness Problems*, *Phys. Rev.* **D23** (1981) 347–356.

[2] A. D. Linde, *A New Inflationary Universe Scenario: A Possible Solution of the Horizon, Flatness, Homogeneity, Isotropy and Primordial Monopole Problems*, *Phys.Lett.* **B108** (1982) 389–393.

[3] A. Albrecht and P. J. Steinhardt, *Cosmology for Grand Unified Theories with Radiatively Induced Symmetry Breaking*, *Phys.Rev.Lett.* **48** (1982) 1220–1223.

[4] A. D. Linde, *Chaotic Inflation*, *Phys. Lett.* **B129** (1983) 177–181.

[5] A. D. Linde, *Inflationary Cosmology*, *Lect. Notes Phys.* **738** (2008) 1–54, [arXiv:0705.0164].

[6] J. Martin, *Inflation and precision cosmology*, *Braz. J. Phys.* **34** (2004) 1307–1321, [astro-ph/0312492].

[7] J. Martin, *Inflationary cosmological perturbations of quantum- mechanical origin*, *Lect. Notes Phys.* **669** (2005) 199–244, [hep-th/0406011].

[8] J. Martin, *Inflationary perturbations: The cosmological Schwinger effect*, *Lect. Notes Phys.* **738** (2008) 193–241, [arXiv:0704.3540].

[9] A. A. Starobinsky, *Relict Gravitation Radiation Spectrum and Initial State of the Universe. (In Russian)*, *JETP Lett.* **30** (1979) 682–685.

[10] V. F. Mukhanov and G. Chibisov, *Quantum Fluctuation and Nonsingular Universe. (In Russian)*, *JETP Lett.* **33** (1981) 532–535.

[11] S. Hawking, *The Development of Irregularities in a Single Bubble Inflationary Universe*, *Phys. Lett.* **B115** (1982) 295. Revised version.

[12] A. A. Starobinsky, *Dynamics of Phase Transition in the New Inflationary Universe Scenario and Generation of Perturbations*, *Phys. Lett.* **B117** (1982) 175–178.

[13] A. H. Guth and S. Y. Pi, *Fluctuations in the New Inflationary Universe*, *Phys. Rev. Lett.* **49** (1982) 1110–1113.

[14] J. M. Bardeen, P. J. Steinhardt, and M. S. Turner, *Spontaneous Creation of Almost Scale - Free Density Perturbations in an Inflationary Universe*, *Phys. Rev.* **D28** (1983) 679.

[15] E. D. Stewart and D. H. Lyth, *A More accurate analytic calculation of the spectrum of cosmological perturbations produced during inflation*, *Phys. Lett.* **B302** (1993) 171–175, [gr-qc/9302019].

[16] V. F. Mukhanov, H. A. Feldman, and R. H. Brandenberger, *Theory of cosmological perturbations. Part 1. Classical perturbations. Part 2. Quantum theory of perturbations. Part 3. Extensions*, *Phys. Rept.* **215** (1992) 203–333.

[17] A. R. Liddle, P. Parsons, and J. D. Barrow, *Formalizing the slow roll approximation in inflation*, *Phys. Rev.* **D50** (1994) 7222–7232, [astro-ph/9408015].

[18] L. Grishchuk and Y. Sidorov, *Squeezed quantum states of relic gravitons and primordial density fluctuations*, *Phys.Rev.* **D42** (1990) 3413–3421.

[19] D. Polarski and A. A. Starobinsky, *Semiclassicality and decoherence of cosmological perturbations*, *Class.Quant.Grav.* **13** (1996) 377–392, [gr-qc/9504030].

[20] C. Kiefer, D. Polarski, and A. A. Starobinsky, *Quantum to classical transition for fluctuations in the early universe*, *Int.J.Mod.Phys.* **D7** (1998) 455–462, [gr-qc/9802003].

[21] C. Kiefer and D. Polarski, *Why do cosmological perturbations look classical to us?*, *Adv.Sci.Lett.* **2** (2009) 164–173, [arXiv:0810.0087].

[22] D. Sudarsky, *Shortcomings in the Understanding of Why Cosmological Perturbations Look Classical*, *Int.J.Mod.Phys.* **D20** (2011) 509–552, [arXiv:0906.0315].

[23] J. Martin, V. Vennin, and P. Peter, *Cosmological Inflation and the Quantum Measurement Problem*, *Phys.Rev.* **D86** (2012) 103524, [arXiv:1207.2086].

[24] J. Martin, *The Quantum State of Inflationary Perturbations*, *J.Phys.Conf.Ser.* **405** (2012) 012004, [arXiv:1209.3092].

[25] S. Alexander, R. H. Brandenberger, and D. Easson, *Brane gases in the early universe*, *Phys.Rev.* **D62** (2000) 103509, [hep-th/0005212].

[26] P. J. Steinhardt and N. Turok, *Cosmic evolution in a cyclic universe*, *Phys.Rev.* **D65** (2002) 126003, [hep-th/0111098].

[27] J. Khoury, B. A. Ovrut, N. Seiberg, P. J. Steinhardt, and N. Turok, *From big crunch to big bang*, *Phys.Rev.* **D65** (2002) 086007, [hep-th/0108187].

[28] J. Khoury, B. A. Ovrut, P. J. Steinhardt, and N. Turok, *The Ekpyrotic universe: Colliding branes and the origin of the hot big bang*, *Phys.Rev.* **D64** (2001) 123522, [hep-th/0103239].

[29] J. Martin, P. Peter, N. Pinto Neto, and D. J. Schwarz, *Passing through the bounce in the ekpyrotic models*, *Phys.Rev.* **D65** (2002) 123513, [hep-th/0112128].

[30] P. Steinhardt and N. Turok, *A cyclic model of the universe*, *Science* **296** (2002) 1436–1439.

[31] F. Finelli and R. Brandenberger, *On the generation of a scale invariant spectrum of adiabatic fluctuations in cosmological models with a contracting phase*, *Phys.Rev.* **D65** (2002) 103522, [hep-th/0112249].

[32] R. Brandenberger, D. A. Easson, and D. Kimberly, *Loitering phase in brane gas cosmology*, *Nucl.Phys.* **B623** (2002) 421–436, [hep-th/0109165].

[33] R. Kallosh, L. Kofman, and A. D. Linde, *Pyrotechnic universe*, *Phys.Rev.* **D64** (2001) 123523, [hep-th/0104073].

[34] J. Martin, P. Peter, N. Pinto-Neto, and D. J. Schwarz, *Comment on'Density perturbations in the ekpyrotic scenario'*, *Phys.Rev.* **D67** (2003) 028301, [hep-th/0204222].

[35] P. Peter and N. Pinto-Neto, *Primordial perturbations in a non singular bouncing universe model*, *Phys.Rev.* **D66** (2002) 063509, [hep-th/0203013].

[36] S. Tsujikawa, R. Brandenberger, and F. Finelli, *On the construction of nonsingular pre - big bang and ekpyrotic cosmologies and the resulting density perturbations*, *Phys.Rev.* **D66** (2002) 083513, [hep-th/0207228].

[37] L. Kofman, A. D. Linde, and V. F. Mukhanov, *Inflationary theory and alternative cosmology*, *JHEP* **0210** (2002) 057, [hep-th/0206088].

[38] J. Khoury, P. J. Steinhardt, and N. Turok, *Designing cyclic universe models*, *Phys.Rev.Lett.* **92** (2004) 031302, [hep-th/0307132].

[39] J. Martin and P. Peter, *On the causality argument in bouncing cosmologies*, *Phys.Rev.Lett.* **92** (2004) 061301, [astro-ph/0312488].

[40] J. Martin and P. Peter, *Parametric amplification of metric fluctuations through a bouncing phase*, *Phys.Rev.* **D68** (2003) 103517, [hep-th/0307077].

[41] J. Martin and P. Peter, *On the properties of the transition matrix in bouncing cosmologies*, *Phys.Rev.* **D69** (2004) 107301, [hep-th/0403173].

[42] A. Nayeri, R. H. Brandenberger, and C. Vafa, *Producing a scale-invariant spectrum of perturbations in a Hagedorn phase of string cosmology*, *Phys.Rev.Lett.* **97** (2006) 021302, [hep-th/0511140].

[43] P. Peter, E. J. Pinho, and N. Pinto-Neto, *A Non inflationary model with scale invariant cosmological perturbations*, *Phys.Rev.* **D75** (2007) 023516, [hep-th/0610205].

[44] F. Finelli, P. Peter, and N. Pinto-Neto, *Spectra of primordial fluctuations in two-perfect-fluid regular bounces*, *Phys.Rev.* **D77** (2008) 103508, [arXiv:0709.3074].

[45] L. R. Abramo and P. Peter, *K-Bounce*, *JCAP* **0709** (2007) 001, [arXiv:0705.2893].

[46] F. T. Falciano, M. Lilley, and P. Peter, *A Classical bounce: Constraints and consequences*, *Phys.Rev.* **D77** (2008) 083513, [arXiv:0802.1196].

[47] A. Linde, V. Mukhanov, and A. Vikman, *On adiabatic perturbations in the ekpyrotic scenario*, *JCAP* **1002** (2010) 006, [arXiv:0912.0944].

[48] L. R. Abramo, I. Yasuda, and P. Peter, *Non singular bounce in modified gravity*, *Phys.Rev.* **D81** (2010) 023511, [arXiv:0910.3422].

[49] R. Brandenberger, *Matter Bounce in Horava-Lifshitz Cosmology*, *Phys.Rev.* **D80** (2009) 043516, [arXiv:0904.2835].

[50] R. H. Brandenberger, *String Gas Cosmology: Progress and Problems*, *Class.Quant.Grav.* **28** (2011) 204005, [arXiv:1105.3247].

[51] R. H. Brandenberger, *The Matter Bounce Alternative to Inflationary Cosmology*, arXiv:1206.4196.

[52] Y.-F. Cai, D. A. Easson, and R. Brandenberger, *Towards a Nonsingular Bouncing Cosmology*, *JCAP* **1208** (2012) 020, [arXiv:1206.2382].

[53] Y.-F. Cai, R. Brandenberger, and P. Peter, *Anisotropy in a Nonsingular Bounce*, arXiv:1301.4703.

[54] M. S. Turner, *Coherent Scalar Field Oscillations in an Expanding Universe*, *Phys. Rev.* **D28** (1983) 1243.

[55] L. Kofman, A. D. Linde, and A. A. Starobinsky, *Towards the theory of reheating after inflation*, *Phys. Rev.* **D56** (1997) 3258–3295, [hep-ph/9704452].

[56] B. A. Bassett, S. Tsujikawa, and D. Wands, *Inflation dynamics and reheating*, *Rev. Mod. Phys.* **78** (2006) 537–589, [astro-ph/0507632].

[57] A. Mazumdar and J. Rocher, *Particle physics models of inflation and curvaton scenarios*, *Phys. Rept.* **497** (2011) 85–215, [arXiv:1001.0993].

[58] F. Finelli and R. H. Brandenberger, *Parametric amplification of gravitational fluctuations during reheating*, *Phys.Rev.Lett.* **82** (1999) 1362–1365, [hep-ph/9809490].

[59] B. A. Bassett, D. I. Kaiser, and R. Maartens, *General relativistic preheating after inflation*, *Phys.Lett.* **B455** (1999) 84–89, [hep-ph/9808404].

[60] F. Finelli and R. H. Brandenberger, *Parametric amplification of metric fluctuations during reheating in two field models*, *Phys. Rev.* **D62** (2000) 083502, [hep-ph/0003172].

[61] K. Jedamzik, M. Lemoine, and J. Martin, *Collapse of Small-Scale Density Perturbations during Preheating in Single Field Inflation*, *JCAP* **1009** (2010) 034, [arXiv:1002.3039].

[62] K. Jedamzik, M. Lemoine, and J. Martin, *Generation of gravitational waves during early structure formation between cosmic inflation and reheating*, *JCAP* **1004** (2010) 021, [arXiv:1002.3278].

[63] R. Easther, R. Flauger, and J. B. Gilmore, *Delayed Reheating and the Breakdown of Coherent Oscillations*, *JCAP* **1104** (2011) 027, [arXiv:1003.3011].

[64] J. Martin and C. Ringeval, *First CMB Constraints on the Inflationary Reheating Temperature*, *Phys. Rev.* **D82** (2010) 023511, [arXiv:1004.5525].

[65] J.-M. Lamarre, J.-L. Puget, P. A. R. Ade, F. Bouchet, G. Guyot, A. E. Lange, F. Pajot, A. Arondel, K. Benabed, J.-L. Beney, A. Benoît, J.-P. Bernard, R. Bhatia, Y. Blanc, J. J. Bock, E. Bréelle, T. W. Bradshaw, P. Camus, A. Catalano, J. Charra, M. Charra, S. E. Church, F. Couchot, A. Coulais, B. P. Crill, M. R. Crook, K. Dassas, P. de Bernardis, J. Delabrouille, P. de Marcillac, J.-M. Delouis, F.-X. Désert, C. Dumesnil, X. Dupac, G. Efstathiou, P. Eng, C. Evesque, J.-J. Fourmond, K. Ganga, M. Giard, R. Gispert, L. Guglielmi, J. Haissinski, S. Henrot-Versillé, E. Hivon, W. A. Holmes, W. C. Jones, T. C. Koch, H. Lagardère, P. Lami, J. Landé, B. Leriche, C. Leroy, Y. Longval, J. F. Macías-Pérez, T. Maciaszek, B. Maffei, B. Mansoux, C. Marty, S. Masi, C. Mercier, M.-A. Miville-Deschênes, A. Moneti, L. Montier, J. A. Murphy, J. Narbonne, M. Nexon, C. G. Paine, J. Pahn, O. Perdereau, F. Piacentini, M. Piat, S. Plaszczynski, E. Pointecouteau, R. Pons, N. Ponthieu, S. Prunet, D. Rambaud, G. Recouvreur, C. Renault, I. Ristorcelli, C. Rosset, D. Santos, G. Savini, G. Serra, P. Stassi, R. V. Sudiwala, J.-F. Sygnet, J. A. Tauber, J.-P. Torre, M. Tristram, L. Vibert, A. Woodcraft, V. Yurchenko, and D. Yvon, *Planck pre-launch status: The HFI instrument, from specification to actual performance*, *Astron. & Astrophys.* **520** (Sept., 2010) A9.

[66] **Planck Collaboration** Collaboration, P. Ade et al., *Planck 2013 results. I. Overview of products and scientific results*, arXiv:1303.5062.

[67] C. Bennett, D. Larson, J. Weiland, N. Jarosik, G. Hinshaw, et al., *Nine-Year Wilkinson Microwave Anisotropy Probe (WMAP) Observations: Final Maps and Results*, arXiv:1212.5225.

[68] G. Hinshaw, D. Larson, E. Komatsu, D. Spergel, C. Bennett, et al., *Nine-Year Wilkinson Microwave Anisotropy Probe (WMAP) Observations: Cosmological Parameter Results*, arXiv:1212.5226.

[69] **Planck Collaboration** Collaboration, P. Ade et al., *Planck 2013 results. XXII. Constraints on inflation*, arXiv:1303.5082.

[70] **Planck Collaboration** Collaboration, P. Ade et al., *Planck 2013 Results. XXIV. Constraints on primordial non-Gaussianity*, arXiv:1303.5084.

[71] **Supernova Search Team** Collaboration, J. L. Tonry et al., *Cosmological results from high-z supernovae*, *Astrophys.J.* **594** (2003) 1–24, [astro-ph/0305008].

[72] **Supernova Search Team** Collaboration, A. G. Riess et al., *Type Ia supernova discoveries at z¿1 from the Hubble Space Telescope: Evidence for past deceleration and constraints on dark energy evolution*, *Astrophys.J.* **607** (2004) 665–687, [astro-ph/0402512].

[73] A. G. Riess, L.-G. Strolger, S. Casertano, H. C. Ferguson, B. Mobasher, et al., *New Hubble Space Telescope Discoveries of Type Ia Supernovae at z¿1: Narrowing Constraints on the Early Behavior of Dark Energy*, *Astrophys.J.* **659** (2007) 98–121, [astro-ph/0611572].

[74] A. G. Riess, L. Macri, S. Casertano, H. Lampeitl, H. C. Ferguson, et al., *A 3Telescope and Wide Field Camera 3*, *Astrophys.J.* **730** (2011) 119, [arXiv:1103.2976].

[75] **SDSS Collaboration** Collaboration, J. K. Adelman-McCarthy et al., *The Sixth Data Release of the Sloan Digital Sky Survey*, *Astrophys.J.Suppl.* **175** (2008) 297–313, [arXiv:0707.3413].

[76] **SDSS Collaboration** Collaboration, K. N. Abazajian et al., *The Seventh Data Release of the Sloan Digital Sky Survey*, *Astrophys.J.Suppl.* **182** (2009) 543–558, [arXiv:0812.0649].

[77] **Euclid collaboration** Collaboration, J. Amiaux et al., *Euclid Mission: building of a Reference Survey*, arXiv:1209.2228.

[78] M. S. Turner, M. J. White, and J. E. Lidsey, *Tensor perturbations in inflationary models as a probe of cosmology*, *Phys.Rev.* **D48** (1993) 4613–4622, [astro-ph/9306029].

[79] M. Maggiore, *Gravitational wave experiments and early universe cosmology*, *Phys.Rept.* **331** (2000) 283–367, [gr-qc/9909001].

[80] H. Kudoh, A. Taruya, T. Hiramatsu, and Y. Himemoto, *Detecting a gravitational-wave background with next-generation space interferometers*, *Phys.Rev.* **D73** (2006) 064006, [gr-qc/0511145].

[81] S. Kuroyanagi, C. Gordon, J. Silk, and N. Sugiyama, *Forecast Constraints on Inflation from Combined CMB and Gravitational Wave Direct Detection Experiments*, *Phys.Rev.* **D81** (2010) 083524, [arXiv:0912.3683].

[82] S. Kawamura, M. Ando, N. Seto, S. Sato, T. Nakamura, et al., *The Japanese space gravitational wave antenna: DECIGO*, *Class.Quant.Grav.* **28** (2011) 094011.

[83] P. Amaro-Seoane, S. Aoudia, S. Babak, P. Binetruy, E. Berti, et al., *eLISA: Astrophysics and cosmology in the millihertz regime*, arXiv:1201.3621.

[84] S. Kuroyanagi, C. Ringeval, and T. Takahashi, *Early Universe Tomography with CMB and Gravitational Waves*, *Phys. Rev. D* **87** (2013) 083502, [arXiv:1301.1778].

[85] J. Dunkley, E. Calabrese, J. Sievers, G. Addison, N. Battaglia, et al., *The Atacama Cosmology Telescope: likelihood for small-scale CMB data*, arXiv:1301.0776.

[86] J. L. Sievers, R. A. Hlozek, M. R. Nolta, V. Acquaviva, G. E. Addison, et al., *The Atacama Cosmology Telescope: Cosmological parameters from three seasons of data*, arXiv:1301.0824.

[87] Z. Hou, C. Reichardt, K. Story, B. Follin, R. Keisler, et al., *Constraints on Cosmology from the Cosmic Microwave Background Power Spectrum of the 2500-square degree SPT-SZ Survey*, arXiv:1212.6267.

[88] K. Story, C. Reichardt, Z. Hou, R. Keisler, K. Aird, et al., *A Measurement of the Cosmic Microwave Background Damping Tail from the 2500-square-degree SPT-SZ survey*, arXiv:1210.7231.

[89] **CMBPol Study Team** Collaboration, D. Baumann et al., *CMBPol Mission Concept Study: Probing Inflation with CMB Polarization*, *AIP Conf.Proc.* **1141** (2009) 10–120, [arXiv:0811.3919].

[90] B. Crill, P. Ade, E. Battistelli, S. Benton, R. Bihary, et al., *SPIDER: A Balloon-borne Large-scale CMB Polarimeter*, arXiv:0807.1548.

[91] M. Zaldarriaga, S. R. Furlanetto, and L. Hernquist, *21 Centimeter fluctuations from cosmic gas at high redshifts*, *Astrophys.J.* **608** (2004) 622–635, [astro-ph/0311514].

[92] A. Lewis and A. Challinor, *The 21cm angular-power spectrum from the dark ages*, *Phys. Rev.* **D76** (2007) 083005, [astro-ph/0702600].

[93] M. Tegmark and M. Zaldarriaga, *The Fast Fourier Transform Telescope*, *Phys. Rev.* **D79** (2009) 083530, [arXiv:0805.4414].

[94] V. Barger, Y. Gao, Y. Mao, and D. Marfatia, *Inflationary Potential from 21 cm Tomography and Planck*, *Phys. Lett.* **B673** (2009) 173–178, [arXiv:0810.3337].

[95] Y. Mao, M. Tegmark, M. McQuinn, M. Zaldarriaga, and O. Zahn, *How accurately can 21 cm tomography constrain cosmology?*, *Phys. Rev.* **D78** (2008) 023529, [arXiv:0802.1710].

[96] P. Adshead, R. Easther, J. Pritchard, and A. Loeb, *Inflation and the Scale Dependent Spectral Index: Prospects and Strategies*, *JCAP* **1102** (2011) 021, [arXiv:1007.3748].

[97] S. Clesse, L. Lopez-Honorez, C. Ringeval, H. Tashiro, and M. H. Tytgat, *Background reionization history from omniscopes*, *Phys.Rev.* **D86** (2012) 123506, [arXiv:1208.4277].

[98] A. Golovnev, V. Mukhanov, and V. Vanchurin, *Vector Inflation*, *JCAP* **0806** (2008) 009, [arXiv:0802.2068].

[99] P. Adshead and M. Wyman, *Chromo-Natural Inflation: Natural inflation on a steep potential with classical non-Abelian gauge fields*, *Phys.Rev.Lett.* **108** (2012) 261302, [arXiv:1202.2366].

[100] A. Maleknejad and M. Sheikh-Jabbari, *Gauge-flation: Inflation From Non-Abelian Gauge Fields*, arXiv:1102.1513.

[101] A. Maleknejad and M. Sheikh-Jabbari, *Non-Abelian Gauge Field Inflation*, *Phys.Rev.* **D84** (2011) 043515, [arXiv:1102.1932].

[102] A. Maleknejad, M. Sheikh-Jabbari, and J. Soda, *Gauge Fields and Inflation*, arXiv:1212.2921.

[103] S. Avila, J. Martin, and D. Steer, *Superimposed Oscillations in Brane Inflation*, arXiv:1304.3262.

[104] A. Berera, *Warm inflation*, *Phys.Rev.Lett.* **75** (1995) 3218–3221, [astro-ph/9509049].

[105] J. Yokoyama and A. D. Linde, *Is warm inflation possible?*, *Phys.Rev.* **D60** (1999) 083509, [hep-ph/9809409].

[106] M. Bastero-Gil, A. Berera, and R. O. Ramos, *Dissipation coefficients from scalar and fermion quantum field interactions*, *JCAP* **1109** (2011) 033, [arXiv:1008.1929].

[107] S. Bartrum, A. Berera, and J. G. Rosa, *Warming up for Planck*, arXiv:1303.3508.

[108] M. Alishahiha, E. Silverstein, and D. Tong, *DBI in the sky*, *Phys.Rev.* **D70** (2004) 123505, [hep-th/0404084].

[109] D. Langlois, S. Renaux-Petel, D. A. Steer, and T. Tanaka, *Primordial perturbations and non-Gaussianities in DBI and general multi-field inflation*, *Phys.Rev.* **D78** (2008) 063523, [arXiv:0806.0336].

[110] D. Langlois, S. Renaux-Petel, and D. A. Steer, *Multi-field DBI inflation: Introducing bulk forms and revisiting the gravitational wave constraints*, *JCAP* **0904** (2009) 021, [arXiv:0902.2941].

[111] A. Gangui, F. Lucchin, S. Matarrese, and S. Mollerach, *The Three point correlation function of the cosmic microwave background in inflationary models*, *Astrophys.J.* **430** (1994) 447–457, [astro-ph/9312033].

[112] A. Gangui, *NonGaussian effects in the cosmic microwave background from inflation*, *Phys.Rev.* **D50** (1994) 3684–3691, [astro-ph/9406014].

[113] A. Gangui and J. Martin, *Cosmic microwave background bispectrum and slow roll inflation*, *Mon.Not.Roy.Astron.Soc.* (1999) [astro-ph/9908009].

[114] L.-M. Wang and M. Kamionkowski, *The Cosmic microwave background bispectrum and inflation*, *Phys.Rev.* **D61** (2000) 063504, [astro-ph/9907431].

[115] J. M. Maldacena, *Non-Gaussian features of primordial fluctuations in single field inflationary models*, *JHEP* **0305** (2003) 013, [astro-ph/0210603].

[116] D. Seery and J. E. Lidsey, *Primordial non-Gaussianities in single field inflation*, *JCAP* **0506** (2005) 003, [astro-ph/0503692].

[117] X. Chen, *Running non-Gaussianities in DBI inflation*, *Phys.Rev.* **D72** (2005) 123518, [astro-ph/0507053].

[118] X. Chen, M.-x. Huang, S. Kachru, and G. Shiu, *Observational signatures and non-Gaussianities of general single field inflation*, *JCAP* **0701** (2007) 002, [hep-th/0605045].

[119] X. Chen, *Primordial Non-Gaussianities from Inflation Models*, *Adv.Astron.* **2010** (2010) 638979, [arXiv:1002.1416].

[120] X. Chen, R. Easther, and E. A. Lim, *Large Non-Gaussianities in Single Field Inflation*, *JCAP* **0706** (2007) 023, [astro-ph/0611645].

[121] X. Chen, R. Easther, and E. A. Lim, *Generation and Characterization of Large Non-Gaussianities in Single Field Inflation*, *JCAP* **0804** (2008) 010, [arXiv:0801.3295].

[122] S. Hannestad, T. Haugbolle, P. R. Jarnhus, and M. S. Sloth, *Non-Gaussianity from Axion Monodromy Inflation*, *JCAP* **1006** (2010) 001, [arXiv:0912.3527].

[123] R. Flauger and E. Pajer, *Resonant Non-Gaussianity*, *JCAP* **1101** (2011) 017, [arXiv:1002.0833].

[124] P. Adshead, C. Dvorkin, W. Hu, and E. A. Lim, *Non-Gaussianity from Step Features in the Inflationary Potential*, *Phys.Rev.* **D85** (2012) 023531, [arXiv:1110.3050]. Typos fixed, supersedes journal version.

[125] J. Martin and L. Sriramkumar, *The scalar bi-spectrum in the Starobinsky model: The equilateral case*, *JCAP* **1201** (2012) 008, [arXiv:1109.5838].

[126] X. Chen, *Folded Resonant Non-Gaussianity in General Single Field Inflation*, *JCAP* **1012** (2010) 003, [arXiv:1008.2485].

[127] A. Gangui, J. Martin, and M. Sakellariadou, *Single field inflation and non-Gaussianity*, *Phys.Rev.* **D66** (2002) 083502, [astro-ph/0205202].

[128] R. Holman and A. J. Tolley, *Enhanced Non-Gaussianity from Excited Initial States*, *JCAP* **0805** (2008) 001, [arXiv:0710.1302].

[129] W. Xue and B. Chen, *alpha-vacuum and inflationary bispectrum*, *Phys.Rev.* **D79** (2009) 043518, [arXiv:0806.4109].

[130] P. D. Meerburg, J. P. van der Schaar, and P. S. Corasaniti, *Signatures of Initial State Modifications on Bispectrum Statistics*, *JCAP* **0905** (2009) 018, [arXiv:0901.4044].

[131] J.-L. Lehners and S. Renaux-Petel, *Multifield Cosmological Perturbations at Third Order and the Ekpyrotic Trispectrum*, *Phys.Rev.* **D80** (2009) 063503, [arXiv:0906.0530].

[132] S. Renaux-Petel, S. Mizuno, and K. Koyama, *Primordial fluctuations and non-Gaussianities from multifield DBI Galileon inflation*, *JCAP* **1111** (2011) 042, [arXiv:1108.0305].

[133] **Planck collaboration** Collaboration, P. Ade et al., *Planck 2013 results. XV. CMB power spectra and likelihood*, arXiv:1303.5075.

[134] **Planck Collaboration** Collaboration, P. Ade et al., *Planck 2013 results. XXV. Searches for cosmic strings and other topological defects*, arXiv:1303.5085.

[135] R. Trotta, *Bayes in the sky: Bayesian inference and model selection in cosmology*, *Contemp.Phys.* **49** (2008) 71–104, [arXiv:0803.4089].

[136] J. E. Lidsey, A. R. Liddle, E. W. Kolb, E. J. Copeland, T. Barreiro, et al., *Reconstructing the inflation potential : An overview*, *Rev.Mod.Phys.* **69** (1997) 373–410, [astro-ph/9508078].

[137] H. de Oliveira and C. A. Terrero-Escalante, *Troubles for observing the inflaton potential*, *JCAP* **0601** (2006) 024, [astro-ph/0511660].

[138] J. Martin, C. Ringeval, and V. Vennin, *K-inflationary Power Spectra at Second Order*, arXiv:1303.2120.

[139] J. B. Jimenez, M. Musso, and C. Ringeval, *Exact Mapping between Tensor and Most General Scalar Power Spectra*, arXiv:1303.2788.

[140] D. Boyanovsky, H. J. de Vega, and N. G. Sanchez, *Clarifying Inflation Models: Slow-roll as an expansion in 1/N efolds*, *Phys.Rev.* **D73** (2006) 023008, [astro-ph/0507595].

[141] C. Destri, H. J. de Vega, and N. Sanchez, *MCMC analysis of WMAP3 and SDSS data points to broken symmetry inflaton potentials and provides a lower bound on the tensor to scalar ratio*, *Phys.Rev.* **D77** (2008) 043509, [astro-ph/0703417].

[142] C. Burigana, C. Destri, H. de Vega, A. Gruppuso, N. Mandolesi, et al., *Forecast for the Planck precision on the tensor to scalar ratio and other cosmological parameters*, *Astrophys.J.* **724** (2010) 588–607, [arXiv:1003.6108].

[143] D. Boyanovsky, C. Destri, H. De Vega, and N. Sanchez, *The Effective Theory of Inflation in the Standard Model of the Universe and the CMB+LSS data analysis*, *Int.J.Mod.Phys.* **A24** (2009) 3669–3864, [arXiv:0901.0549].

[144] S. M. Leach and A. R. Liddle, *Constraining slow - roll inflation with WMAP and 2dF*, *Phys.Rev.* **D68** (2003) 123508, [astro-ph/0306305].

[145] J. Martin and C. Ringeval, *Inflation after WMAP3: Confronting the slow-roll and exact power spectra to CMB data*, *JCAP* **0608** (2006) 009, [astro-ph/0605367].

[146] L. Lorenz, J. Martin, and C. Ringeval, *Constraints on Kinetically Modified Inflation from WMAP5*, *Phys. Rev.* **D78** (2008) 063543, [arXiv:0807.2414].

[147] F. Finelli, J. Hamann, S. M. Leach, and J. Lesgourgues, *Single-field inflation constraints from CMB and SDSS data*, *JCAP* **1004** (2010) 011, [arXiv:0912.0522].

[148] D. K. Hazra, L. Sriramkumar, and J. Martin, *BINGO: A code for the efficient computation of the scalar bi-spectrum*, arXiv:1201.0926.

[149] C. Ringeval, P. Brax, C. van de Bruck, and A.-C. Davis, *Boundary Inflation and the WMAP Data*, *Phys. Rev.* **D73** (2006) 064035, [astro-ph/0509727].

[150] C. Ringeval, *The exact numerical treatment of inflationary models*, *Lect.Notes Phys.* **738** (2008) 243–273, [astro-ph/0703486].

[151] L. Lorenz, J. Martin, and C. Ringeval, *Brane inflation and the WMAP data: a Bayesian analysis*, *JCAP* **0804** (2008) 001, [arXiv:0709.3758].

[152] M. J. Mortonson, H. V. Peiris, and R. Easther, *Bayesian Analysis of Inflation: Parameter Estimation for Single Field Models*, *Phys.Rev.* **D83** (2011) 043505, [arXiv:1007.4205].

[153] **Planck Collaboration** Collaboration, P. Ade et al., *Planck 2013 results. XVI. Cosmological parameters*, arXiv:1303.5076.

[154] A. R. Liddle and S. M. Leach, *How long before the end of inflation were observable perturbations produced?*, *Phys. Rev.* **D68** (2003) 103503, [astro-ph/0305263].

[155] R. Easther and H. V. Peiris, *Bayesian Analysis of Inflation II: Model Selection and Constraints on Reheating*, *Phys.Rev.* **D85** (2012) 103533, [arXiv:1112.0326].

[156] A. A. Starobinsky, *Spectrum of adiabatic perturbations in the universe when there are singularities in the inflation potential*, *JETP Lett.* **55** (1992) 489–494.

[157] J. Silk and M. S. Turner, *Double Inflation*, *Phys.Rev.* **D35** (1987) 419.

[158] P. Peter, D. Polarski, and A. A. Starobinsky, *Confrontation of double inflationary models with observations*, *Phys.Rev.* **D50** (1994) 4827–4834, [astro-ph/9403037].

[159] D. Polarski and A. A. Starobinsky, *Structure of primordial gravitational waves spectrum in a double inflationary model*, *Phys.Lett.* **B356** (1995) 196–204, [astro-ph/9505125].

[160] D. Parkinson, S. Tsujikawa, B. A. Bassett, and L. Amendola, *Testing for double inflation with WMAP*, *Phys.Rev.* **D71** (2005) 063524, [astro-ph/0409071].

[161] S. Tsujikawa, D. Parkinson, and B. A. Bassett, *Correlation - consistency cartography of the double inflation landscape*, *Phys.Rev.* **D67** (2003) 083516, [astro-ph/0210322].

[162] A. D. Linde, *Hybrid inflation*, *Phys.Rev.* **D49** (1994) 748–754, [astro-ph/9307002].

[163] D. H. Lyth and E. D. Stewart, *More varieties of hybrid inflation*, *Phys.Rev.* **D54** (1996) 7186–7190, [hep-ph/9606412].

[164] A. R. Liddle, A. Mazumdar, and F. E. Schunck, *Assisted inflation*, *Phys.Rev.* **D58** (1998) 061301, [astro-ph/9804177].

[165] A. Ashoorioon, H. Firouzjahi, and M. Sheikh-Jabbari, *M-flation: Inflation From Matrix Valued Scalar Fields*, *JCAP* **0906** (2009) 018, [arXiv:0903.1481].

[166] A. Ashoorioon, H. Firouzjahi, and M. M. Sheikh-Jabbari, *Matrix Inflation and the Landscape of its Potential*, *JCAP* **1005** (2010) 002, [arXiv:0911.4284].

[167] A. Ashoorioon and M. Sheikh-Jabbari, *Gauged M-flation, its UV sensitivity and Spectator Species*, *JCAP* **1106** (2011) 014, [arXiv:1101.0048].

[168] S. Tsujikawa, J. Ohashi, S. Kuroyanagi, and A. De Felice, *Planck constraints on single-field inflation*, arXiv:1305.3044.

[169] S. Unnikrishnan and V. Sahni, *Resurrecting power law inflation in the light of Planck results*, arXiv:1305.5260.

[170] S. Choudhury, A. Mazumdar, and S. Pal, *Low and High scale MSSM inflation, gravitational waves and constraints from Planck*, arXiv:1305.6398.

[171] J. Martin, C. Ringeval, and R. Trotta, *Hunting Down the Best Model of Inflation with Bayesian Evidence*, *Phys. Rev.* **D83** (2011) 063524, [arXiv:1009.4157].

[172] M. B. Hoffman and M. S. Turner, *Kinematic constraints to the key inflationary observables*, *Phys.Rev.* **D64** (2001) 023506, [astro-ph/0006321].

[173] D. J. Schwarz, C. A. Terrero-Escalante, and A. A. Garcia, *Higher order corrections to primordial spectra from cosmological inflation*, *Phys. Lett.* **B517** (2001) 243–249, [astro-ph/0106020].

[174] J. Martin and D. J. Schwarz, *WKB approximation for inflationary cosmological perturbations*, *Phys.Rev.* **D67** (2003) 083512, [astro-ph/0210090].

[175] R. Casadio, F. Finelli, M. Luzzi, and G. Venturi, *Improved WKB analysis of cosmological perturbations*, *Phys.Rev.* **D71** (2005) 043517, [gr-qc/0410092].

[176] R. Casadio, F. Finelli, M. Luzzi, and G. Venturi, *Higher order slow-roll predictions for inflation*, *Phys.Lett.* **B625** (2005) 1–6, [gr-qc/0506043].

[177] R. Casadio, F. Finelli, M. Luzzi, and G. Venturi, *Improved WKB analysis of slow-roll inflation*, *Phys.Rev.* **D72** (2005) 103516, [gr-qc/0510103].

[178] J.-O. Gong and E. D. Stewart, *The Density perturbation power spectrum to second order corrections in the slow roll expansion*, *Phys.Lett.* **B510** (2001) 1–9, [astro-ph/0101225].

[179] J. Choe, J.-O. Gong, and E. D. Stewart, *Second order general slow-roll power spectrum*, *JCAP* **0407** (2004) 012, [hep-ph/0405155].

[180] S. M. Leach, A. R. Liddle, J. Martin, and D. J. Schwarz, *Cosmological parameter estimation and the inflationary cosmology*, *Phys.Rev.* **D66** (2002) 023515, [astro-ph/0202094].

[181] C. Ringeval, T. Suyama, and J. Yokoyama, *Magneto-reheating constraints from curvature perturbations*, arXiv:1302.6013.

[182] **ATLAS Collaboration** Collaboration, G. Aad et al., *Observation of a new particle in the search for the Standard Model Higgs boson with the ATLAS detector at the LHC*, *Phys.Lett.* **B716** (2012) 1–29, [arXiv:1207.7214].

[183] **CMS Collaboration** Collaboration, S. Chatrchyan et al., *Observation of a new boson at a mass of 125 GeV with the CMS experiment at the LHC*, *Phys.Lett.* **B716** (2012) 30–61, [arXiv:1207.7235].

[184] F. Bezrukov and M. Shaposhnikov, *The Standard Model Higgs boson as the inflaton*, *Phys.Lett.* **B659** (2008) 703–706, [arXiv:0710.3755].

[185] F. L. Bezrukov, A. Magnin, and M. Shaposhnikov, *Standard Model Higgs boson mass from inflation*, *Phys.Lett.* **B675** (2009) 88–92, [arXiv:0812.4950].

[186] F. Bezrukov and M. Shaposhnikov, *Standard Model Higgs boson mass from inflation: Two loop analysis*, *JHEP* **0907** (2009) 089, [arXiv:0904.1537].

[187] J. Garcia-Bellido, J. Rubio, M. Shaposhnikov, and D. Zenhausern, *Higgs-Dilaton Cosmology: From the Early to the Late Universe*, *Phys.Rev.* **D84** (2011) 123504, [arXiv:1107.2163].

[188] N. D. Birrell and P. C. W. Davies, *Quantum Fields In Curved Space*. Cambridge Univ. Pr., 1982.

[189] G. Esposito-Farese and D. Polarski, *Scalar tensor gravity in an accelerating universe*, *Phys.Rev.* **D63** (2001) 063504, [gr-qc/0009034].

[190] J. Garcia-Bellido, D. G. Figueroa, and J. Rubio, *Preheating in the Standard Model with the Higgs-Inflaton coupled to gravity*, *Phys.Rev.* **D79** (2009) 063531, [arXiv:0812.4624].

[191] O. Bertolami, P. Frazao, and J. Paramos, *Reheating via a generalized non-minimal coupling of curvature to matter*, *Phys.Rev.* **D83** (2011) 044010, [arXiv:1010.2698].

[192] H. Motohashi and A. Nishizawa, *Reheating after f(R) inflation*, *Phys.Rev.* **D86** (2012) 083514, [arXiv:1204.1472].

[193] J. Ellis, D. V. Nanopoulos, and K. A. Olive, *A No-Scale Supergravity Realization of the Starobinsky Model*, arXiv:1305.1247.

[194] W. Buchmuller, V. Domcke, and K. Kamada, *The Starobinsky Model from Superconformal D-Term Inflation*, arXiv:1306.3471.

[195] R. N. Lerner and J. McDonald, *Gauge singlet scalar as inflaton and thermal relic dark matter*, *Phys.Rev.* **D80** (2009) 123507, [arXiv:0909.0520].

[196] J. Elias-Miro, J. R. Espinosa, G. F. Giudice, H. M. Lee, and A. Strumia, *Stabilization of the Electroweak Vacuum by a Scalar Threshold Effect*, *JHEP* **1206** (2012) 031, [arXiv:1203.0237].

[197] C. Arina, J.-O. Gong, and N. Sahu, *Unifying darko-lepto-genesis with scalar triplet inflation*, *Nucl.Phys.* **B865** (2012) 430–460, [arXiv:1206.0009].

[198] A. Barvinsky, A. Y. Kamenshchik, and A. Starobinsky, *Inflation scenario via the Standard Model Higgs boson and LHC*, *JCAP* **0811** (2008) 021, [arXiv:0809.2104].

[199] A. De Simone, M. P. Hertzberg, and F. Wilczek, *Running Inflation in the Standard Model*, *Phys.Lett.* **B678** (2009) 1–8, [arXiv:0812.4946].

[200] A. Barvinsky, A. Y. Kamenshchik, C. Kiefer, A. Starobinsky, and C. Steinwachs, *Higgs boson, renormalization group, and naturalness in cosmology*, *Eur.Phys.J.* **C72** (2012) 2219, [arXiv:0910.1041].

[201] F. Bezrukov, A. Magnin, M. Shaposhnikov, and S. Sibiryakov, *Higgs inflation: consistency and generalisations*, *JHEP* **1101** (2011) 016, [arXiv:1008.5157].

[202] C. F. Steinwachs and A. Y. Kamenshchik, *Non-minimal Higgs Inflation and Frame Dependence in Cosmology*, arXiv:1301.5543.

[203] F. Bezrukov, G. K. Karananas, J. Rubio, and M. Shaposhnikov, *Higgs-Dilaton Cosmology: an effective field theory approach*, *Phys.Rev.* **D87** (2013) 096001, [arXiv:1212.4148].

[204] M. Abramowitz and I. A. Stegun, *Handbook of mathematical functions with formulas, graphs, and mathematical tables*. National Bureau of Standards, Washington, US, ninth ed., 1970.

[205] I. S. Gradshteyn and I. M. Ryzhik, *Table of Integrals, Series, and Products*. Academic Press, New York and London, 1965.

[206] A. Vilenkin, *Eternal inflation and chaotic terminology*, gr-qc/0409055.

[207] A. D. Linde, *Chaotic Inflating Universe*, *JETP Lett.* **38** (1983) 176–179.

[208] M. Madsen and P. Coles, *CHAOTIC INFLATION*, *Nucl.Phys.* **B298** (1988) 701–725.

[209] G. Lazarides and Q. Shafi, *A Predictive inflationary scenario without the gauge singlet*, *Phys.Lett.* **B308** (1993) 17–22, [hep-ph/9304247].

[210] L. Kofman, A. D. Linde, and A. A. Starobinsky, *Reheating after inflation*, *Phys.Rev.Lett.* **73** (1994) 3195–3198, [hep-th/9405187].

[211] G. Lazarides and Q. Shafi, *Topological defects and inflation*, *Phys.Lett.* **B372** (1996) 20–24, [hep-ph/9510275].

[212] M. Kawasaki, M. Yamaguchi, and T. Yanagida, *Natural chaotic inflation in supergravity*, *Phys.Rev.Lett.* **85** (2000) 3572–3575, [hep-ph/0004243].

[213] D. Baumann, A. Dymarsky, I. R. Klebanov, and L. McAllister, *Towards an Explicit Model of D-brane Inflation*, *JCAP* **0801** (2008) 024, [arXiv:0706.0360].

[214] E. Silverstein and A. Westphal, *Monodromy in the CMB: Gravity Waves and String Inflation*, *Phys.Rev.* **D78** (2008) 106003, [arXiv:0803.3085].

[215] R. H. Brandenberger, A. Knauf, and L. C. Lorenz, *Reheating in a Brane Monodromy Inflation Model*, *JHEP* **0810** (2008) 110, [arXiv:0808.3936].

[216] K. Nakayama and F. Takahashi, *Higgs Chaotic Inflation in Standard Model and NMSSM*, *JCAP* **1102** (2011) 010, [arXiv:1008.4457].

[217] F. Takahashi, *Linear Inflation from Running Kinetic Term in Supergravity*, *Phys.Lett.* **B693** (2010) 140–143, [arXiv:1006.2801].

[218] K. Nakayama and F. Takahashi, *Running Kinetic Inflation*, *JCAP* **1011** (2010) 009, [arXiv:1008.2956].

[219] A. Vilenkin, *Quantum Fluctuations in the New Inflationary Universe*, *Nucl. Phys.* **B226** (1983) 527.

[220] A. Vilenkin, *The Birth of Inflationary Universes*, *Phys. Rev.* **D27** (1983) 2848.

[221] A. Goncharov, A. D. Linde, and V. F. Mukhanov, *The Global Structure of the Inflationary Universe*, *Int. J. Mod. Phys.* **A2** (1987) 561–591.

[222] A. D. Linde, D. A. Linde, and A. Mezhlumian, *From the Big Bang theory to the theory of a stationary universe*, *Phys. Rev.* **D49** (1994) 1783–1826, [gr-qc/9306035].

[223] A. A. Starobinsky, *Stochastic De Sitter (Inflationay) Stage in the Early Universe*, .

[224] J. Martin and M. Musso, *Solving stochastic inflation for arbitrary potentials*, *Phys. Rev.* **D73** (2006) 043516, [hep-th/0511214].

[225] J. Martin and M. Musso, *On the reliability of the Langevin perturbative solution in stochastic inflation*, *Phys. Rev.* **D73** (2006) 043517, [hep-th/0511292].

[226] R. Mohapatra, A. Perez-Lorenzana, and C. A. de Sousa Pires, *Inflation in models with large extra dimensions driven by a bulk scalar field*, *Phys.Rev.* **D62** (2000) 105030, [hep-ph/0003089].

[227] F. Cao, *Generalized chaotic inflation*, astro-ph/0205207.

[228] M. Bellini, *Fresh inflation with nonminimally coupled inflaton field*, *Gen.Rel.Grav.* **34** (2002) 1953–1961, [hep-ph/0205171].

[229] M. Bellini, *Fresh inflation with increasing cosmological parameter*, *Phys.Rev.* **D67** (2003) 027303, [gr-qc/0211044].

[230] C.-S. Chen and C.-M. Lin, *Type II Seesaw Higgs Triplet as the inflaton for Chaotic Inflation and Leptogenesis*, *Phys.Lett.* **B695** (2011) 9–12, [arXiv:1009.5727].

[231] A. Bouaouda, R. Zarrouki, H. Chakir, and M. Bennai, *F-term braneworld inflation in light of five-year WMAP observations*, *Int.J.Mod.Phys.* **A25** (2010) 3445–3451, [arXiv:1010.4884].

[232] V. N. Senoguz and Q. Shafi, *Chaotic inflation, radiative corrections and precision cosmology*, *Phys. Lett.* **B668** (2008) 6–10, [arXiv:0806.2798].

[233] K. Freese, J. A. Frieman, and A. V. Olinto, *Natural inflation with pseudo - Nambu-Goldstone bosons*, *Phys.Rev.Lett.* **65** (1990) 3233–3236.

[234] F. C. Adams, J. R. Bond, K. Freese, J. A. Frieman, and A. V. Olinto, *Natural inflation: Particle physics models, power law spectra for large scale structure, and constraints from COBE*, *Phys.Rev.* **D47** (1993) 426–455, [hep-ph/9207245].

[235] R. Peccei and H. R. Quinn, *Constraints Imposed by CP Conservation in the Presence of Instantons*, *Phys.Rev.* **D16** (1977) 1791–1797.

[236] R. Peccei and H. R. Quinn, *CP Conservation in the Presence of Instantons*, *Phys.Rev.Lett.* **38** (1977) 1440–1443.

[237] D. Lyth, *Axions and inflation: Sitting in the vacuum*, *Phys.Rev.* **D45** (1992) 3394–3404.

[238] L. Knox and A. Olinto, *Initial conditions for natural inflation*, *Phys.Rev.* **D48** (1993) 946–949.

[239] J. Garcia-Bellido, A. D. Linde, and D. Wands, *Density perturbations and black hole formation in hybrid inflation*, *Phys. Rev.* **D54** (1996) 6040–6058, [astro-ph/9605094].

[240] D. H. Lyth and A. Riotto, *Particle physics models of inflation and the cosmological density perturbation*, *Phys. Rept.* **314** (1999) 1–146, [hep-ph/9807278].

[241] S. Tsujikawa and T. Torii, *Spinodal effect in the natural inflation model*, *Phys.Rev.* **D62** (2000) 043505, [hep-ph/9912499].

[242] X. Wang, B. Feng, M. Li, X.-L. Chen, and X. Zhang, *Natural inflation, Planck scale physics and oscillating primordial spectrum*, *Int.J.Mod.Phys.* **D14** (2005) 1347, [astro-ph/0209242].

[243] K. Freese and W. H. Kinney, *On: Natural inflation*, *Phys.Rev.* **D70** (2004) 083512, [hep-ph/0404012].

[244] C. Savage, K. Freese, and W. H. Kinney, *Natural Inflation: Status after WMAP 3-year data*, *Phys.Rev.* **D74** (2006) 123511, [hep-ph/0609144].

[245] G. Panotopoulos, *Cosmic strings and natural inflation*, *JHEP* **0706** (2007) 080, [arXiv:0706.2747].

[246] T. W. Grimm, *Axion inflation in type II string theory*, *Phys.Rev.* **D77** (2008) 126007, [arXiv:0710.3883].

[247] K. Freese, C. Savage, and W. H. Kinney, *Natural Inflation: The Status after WMAP 3-year data*, *Int.J.Mod.Phys.* **D16** (2008) 2573–2585, [arXiv:0802.0227].

[248] S. Mohanty and A. Nautiyal, *Natural inflation at the GUT scale*, *Phys.Rev.* **D78** (2008) 123515, [arXiv:0807.0317].

[249] A. Ashoorioon, K. Freese, and J. T. Liu, *Slow nucleation rates in Chain Inflation with QCD Axions or Monodromy*, *Phys.Rev.* **D79** (2009) 067302, [arXiv:0810.0228].

[250] M. E. Olsson, *Inflation assisted by heterotic axions*, *JCAP* **0704** (2007) 019, [hep-th/0702109].

[251] D. Maity, *Kinetic Gravity Braiding and axion inflation*, arXiv:1209.6554.

[252] K. Freese, *A Coupling of pseudoNambu-Goldstone bosons to other scalars and role in double field inflation*, *Phys.Rev.* **D50** (1994) 7731–7734, [astro-ph/9405045].

[253] W. H. Kinney and K. Mahanthappa, *Natural inflation from Fermion loops*, *Phys.Rev.* **D52** (1995) 5529–5537, [hep-ph/9503331].

[254] W. H. Kinney and K. T. Mahanthappa, *Inflation at Low Scales: General Analysis and a Detailed Model*, *Phys. Rev.* **D53** (1996) 5455–5467, [hep-ph/9512241].

[255] G. G. Ross and G. German, *Hybrid natural inflation from non Abelian discrete symmetry*, *Phys.Lett.* **B684** (2010) 199–204, [arXiv:0902.4676].

[256] G. German, A. Mazumdar, and A. Perez-Lorenzana, *Angular inflation from supergravity*, *Mod.Phys.Lett.* **A17** (2002) 1627–1634, [hep-ph/0111371].

[257] D. Bailin and A. Love, *Supersymmetric Gauge Field Theory and String Theory*. IOP (Graduate student series in physics), 1994.

[258] N. Arkani-Hamed, H.-C. Cheng, P. Creminelli, and L. Randall, *Extra natural inflation*, *Phys.Rev.Lett.* **90** (2003) 221302, [hep-th/0301218].

[259] N. Arkani-Hamed, H.-C. Cheng, P. Creminelli, and L. Randall, *Pseudonatural inflation*, *JCAP* **0307** (2003) 003, [hep-th/0302034].

[260] D. E. Kaplan and N. J. Weiner, *Little inflatons and gauge inflation*, *JCAP* **0402** (2004) 005, [hep-ph/0302014].

[261] H. Firouzjahi and S. H. Tye, *Closer towards inflation in string theory*, *Phys.Lett.* **B584** (2004) 147–154, [hep-th/0312020].

[262] J. P. Hsu and R. Kallosh, *Volume stabilization and the origin of the inflaton shift symmetry in string theory*, *JHEP* **0404** (2004) 042, [hep-th/0402047].

[263] R. Gonzalez Felipe and N. Santos, *Natural inflation in 5-D warped backgrounds*, *Phys.Rev.* **D78** (2008) 023519, [arXiv:0711.0022].

[264] B. A. Ovrut and S. Thomas, *Instanton induced periodic potentials in nonlinear sigma models*, *Phys.Lett.* **B267** (1991) 227–232.

[265] J. E. Kim, *Axion and almost massless quark as ingredients of quintessence*, *JHEP* **9905** (1999) 022, [hep-ph/9811509].

[266] S. C. Park, *Orbifold GUT inflation*, *JCAP* **0711** (2007) 001, [arXiv:0704.3920].

[267] J. Preskill, M. B. Wise, and F. Wilczek, *Cosmology of the Invisible Axion*, *Phys.Lett.* **B120** (1983) 127–132.

[268] L. Abbott and P. Sikivie, *A Cosmological Bound on the Invisible Axion*, *Phys.Lett.* **B120** (1983) 133–136.

[269] M. Dine and W. Fischler, *The Not So Harmless Axion*, *Phys.Lett.* **B120** (1983) 137–141.

[270] A. D. Linde, *Inflation and Axion Cosmology*, *Phys.Lett.* **B201** (1988) 437.

[271] J. E. Kim, H. P. Nilles, and M. Peloso, *Completing natural inflation*, *JCAP* **0501** (2005) 005, [hep-ph/0409138].

[272] S. Dimopoulos, S. Kachru, J. McGreevy, and J. G. Wacker, *N-flation*, *JCAP* **0808** (2008) 003, [hep-th/0507205].

[273] Y. N. Obukhov, *Spin driven inflation*, *Phys.Lett.* **A182** (1993) 214–216, [gr-qc/0008015].

[274] E. D. Stewart, *Inflation, supergravity and superstrings*, *Phys.Rev.* **D51** (1995) 6847–6853, [hep-ph/9405389].

[275] G. Dvali and S. H. Tye, *Brane inflation*, *Phys.Lett.* **B450** (1999) 72–82, [hep-ph/9812483].

[276] M. Cicoli, C. Burgess, and F. Quevedo, *Fibre Inflation: Observable Gravity Waves from IIB String Compactifications*, *JCAP* **0903** (2009) 013, [arXiv:0808.0691].

[277] G. F. Giudice and H. M. Lee, *Unitarizing Higgs Inflation*, *Phys.Lett.* **B694** (2011) 294–300, [arXiv:1010.1417].

[278] L. Abbott and M. B. Wise, *Constraints on Generalized Inflationary Cosmologies*, *Nucl.Phys.* **B244** (1984) 541–548.

[279] V. Sahni, *SCALAR FIELD FLUCTUATIONS AND INFRARED DIVERGENT STATES IN COSMOLOGICAL MODELS WITH POWER LAW EXPANSION*, *Class.Quant.Grav.* **5** (1988) L113.

[280] V. Sahni, *THE ENERGY DENSITY OF RELIC GRAVITY WAVES FROM INFLATION*, *Phys.Rev.* **D42** (1990) 453–463.

[281] B. Ratra and P. Peebles, *Cosmological Consequences of a Rolling Homogeneous Scalar Field*, *Phys.Rev.* **D37** (1988) 3406.

[282] P. G. Ferreira and M. Joyce, *Cosmology with a primordial scaling field*, *Phys.Rev.* **D58** (1998) 023503, [astro-ph/9711102].

[283] D. La and P. J. Steinhardt, *Extended Inflationary Cosmology*, *Phys.Rev.Lett.* **62** (1989) 376.

[284] E. W. Kolb, *First order inflation*, *Phys.Scripta* **T36** (1991) 199–217.

[285] Y. Kitada and K.-i. Maeda, *Cosmic no hair theorem in power law inflation*, *Phys.Rev.* **D45** (1992) 1416–1419.

[286] L. E. Mendes and A. B. Henriques, *Inflation in a simple Kantowski-Sachs model*, *Phys.Lett.* **B254** (1991) 44–48.

[287] N. Banerjee and S. Sen, *Power law inflation and scalar field cosmology with a causal viscous fluid*, *Phys.Rev.* **D57** (1998) 4614–4619.

[288] M. Fairbairn and M. H. Tytgat, *Inflation from a tachyon fluid?*, *Phys.Lett.* **B546** (2002) 1–7, [hep-th/0204070].

[289] M. Sami, P. Chingangbam, and T. Qureshi, *Aspects of tachyonic inflation with exponential potential*, *Phys.Rev.* **D66** (2002) 043530, [hep-th/0205179].

[290] V. H. Cardenas, *Tachyonic quintessential inflation*, *Phys.Rev.* **D73** (2006) 103512, [gr-qc/0603013].

[291] J. M. Aguirregabiria, L. P. Chimento, A. S. Jakubi, and R. Lazkoz, *Symmetries leading to inflation*, *Phys.Rev.* **D67** (2003) 083518, [gr-qc/0303010].

[292] K. Becker, M. Becker, and A. Krause, *M-theory inflation from multi M5-brane dynamics*, *Nucl.Phys.* **B715** (2005) 349–371, [hep-th/0501130].

[293] M. Bennai, H. Chakir, and Z. Sakhi, *On Inflation Potentials in Randall-Sundrum Braneworld Model*, *Eur.J.Phys.* **9** (2006) 84–93, [arXiv:0806.1137].

[294] F. Lucchin and S. Matarrese, *Power Law Inflation*, *Phys.Rev.* **D32** (1985) 1316.

[295] J. Yokoyama and K.-i. Maeda, *On the Dynamics of the Power Law Inflation Due to an Exponential Potential*, *Phys.Lett.* **B207** (1988) 31.

[296] A. R. Liddle, *POWER LAW INFLATION WITH EXPONENTIAL POTENTIALS*, *Phys.Lett.* **B220** (1989) 502.

[297] B. Ratra, *INFLATION IN AN EXPONENTIAL POTENTIAL SCALAR FIELD MODEL*, *Phys.Rev.* **D45** (1992) 1913–1952.

[298] B. Ratra, *QUANTUM MECHANICS OF EXPONENTIAL POTENTIAL INFLATION*, *Phys.Rev.* **D40** (1989) 3939.

[299] H.-J. Schmidt, *New exact solutions for power law inflation Friedmann models*, *Astron.Nachr.* **311** (1990) 165, [gr-qc/0109004].

[300] R. Maartens, D. Taylor, and N. Roussos, *Exact inflationary cosmologies with exit*, *Phys.Rev.* **D52** (1995) 3358–3364.

[301] E. J. Copeland, A. R. Liddle, and D. Wands, *Exponential potentials and cosmological scaling solutions*, *Phys.Rev.* **D57** (1998) 4686–4690, [gr-qc/9711068].

[302] S. Hirai and T. Takami, *Length of inflation and WMAP data in the case of power-law inflation*, astro-ph/0506479.

[303] J. M. Heinzle and A. D. Rendall, *Power-law inflation in spacetimes without symmetry*, *Commun.Math.Phys.* **269** (2007) 1–15, [gr-qc/0506134].

[304] J. P. Conlon and F. Quevedo, *Kahler moduli inflation*, *JHEP* **0601** (2006) 146, [hep-th/0509012].

[305] J. R. Bond, L. Kofman, S. Prokushkin, and P. M. Vaudrevange, *Roulette inflation with Kahler moduli and their axions*, *Phys.Rev.* **D75** (2007) 123511, [hep-th/0612197].

[306] H.-X. Yang and H.-L. Ma, *Two-field Kahler moduli inflation on large volume moduli stabilization*, *JCAP* **0808** (2008) 024, [arXiv:0804.3653].

[307] S. Krippendorf and F. Quevedo, *Metastable SUSY Breaking, de Sitter Moduli Stabilisation and Kahler Moduli Inflation*, *JHEP* **0911** (2009) 039, [arXiv:0901.0683].

[308] J. J. Blanco-Pillado, D. Buck, E. J. Copeland, M. Gomez-Reino, and N. J. Nunes, *Kahler Moduli Inflation Revisited*, *JHEP* **1001** (2010) 081, [arXiv:0906.3711].

[309] M. Kawasaki and K. Miyamoto, *Kahler moduli double inflation*, *JCAP* **1102** (2011) 004, [arXiv:1010.3095].

[310] S. Lee and S. Nam, *Káhler moduli inflation and WMAP7*, *Int. J. Mod. Phys.* **A26** (2011) 1073–1096, [arXiv:1006.2876].

[311] A. R. Liddle, *On the inflationary flow equations*, *Phys. Rev.* **D68** (2003) 103504, [astro-ph/0307286].

[312] E. J. Copeland, I. J. Grivell, E. W. Kolb, and A. R. Liddle, *On the reliability of inflaton potential reconstruction*, *Phys. Rev.* **D58** (1998) 043002, [astro-ph/9802209].

[313] E. Ramirez and A. R. Liddle, *Stochastic approaches to inflation model building*, *Phys. Rev.* **D71** (2005) 123510, [astro-ph/0502361].

[314] S. R. Coleman and E. J. Weinberg, *Radiative Corrections as the Origin of Spontaneous Symmetry Breaking*, *Phys.Rev.* **D7** (1973) 1888–1910.

[315] P. M. Stevenson, *The Gaussian Effective Potential. 1. Quantum Mechanics*, *Phys.Rev.* **D30** (1984) 1712.

[316] P. M. Stevenson, *The Gaussian Effective Potential. 2. Lambda phi**4 Field Theory*, *Phys.Rev.* **D32** (1985) 1389–1408.

[317] P. M. Stevenson and I. Roditi, *THE GAUSSIAN EFFECTIVE POTENTIAL. III. PHI**6 THEORY AND BOUND STATES*, *Phys.Rev.* **D33** (1986) 2305–2315.

[318] P. M. Stevenson, *DIMENSIONAL CONTINUATION AND THE TWO lambda phi**4 in four-dimensions THEORIES*, *Z.Phys.* **C35** (1987) 467.

[319] P. M. Stevenson and R. Tarrach, *The Return of Lambda phi**4*, *Phys.Lett.* **B176** (1986) 436.

[320] P. M. Stevenson, B. Alles, and R. Tarrach, *O(n) Symmetric Lambda phi**4 Theory: The Gaussian Effective Potential Approach*, *Phys.Rev.* **D35** (1987) 2407.

[321] P. M. Stevenson, G. Hajj, and J. Reed, *FERMIONS AND THE GAUSSIAN EFFECTIVE POTENTIAL*, *Phys.Rev.* **D34** (1986) 3117.

[322] G. Hajj and P. M. Stevenson, *FINITE TEMPERATURE EFFECTS ON THE GAUSSIAN EFFECTIVE POTENTIAL*, *Phys.Rev.* **D37** (1988) 413.

[323] R. Ibanez-Meier, I. Stancu, and P. M. Stevenson, *Gaussian effective potential for the U(1) Higgs model*, *Z.Phys.* **C70** (1996) 307–320, [hep-ph/9207276].

[324] L. Abbott, *GRAVITATIONAL EFFECTS ON THE SU(5) BREAKING PHASE TRANSITION FOR A COLEMAN-WEINBERG POTENTIAL*, *Nucl.Phys.* **B185** (1981) 233.

[325] J. R. Ellis, D. V. Nanopoulos, K. A. Olive, and K. Tamvakis, *PRIMORDIAL SUPERSYMMETRIC INFLATION*, *Nucl.Phys.* **B221** (1983) 524.

[326] A. Albrecht, L. G. Jensen, and P. J. Steinhardt, *INFLATION IN SU(5) GUT MODELS COUPLED TO GRAVITY*, *Nucl.Phys.* **B239** (1984) 290.

[327] Q. Shafi and A. Vilenkin, *Inflation with SU(5)*, *Phys.Rev.Lett.* **52** (1984) 691–694.

[328] A. Albrecht and R. H. Brandenberger, *ON THE REALIZATION OF NEW INFLATION*, *Phys.Rev.* **D31** (1985) 1225.

[329] M. U. Rehman, Q. Shafi, and J. R. Wickman, *GUT Inflation and Proton Decay after WMAP5*, *Phys.Rev.* **D78** (2008) 123516, [arXiv:0810.3625].

[330] R. Langbein, K. Langfeld, H. Reinhardt, and L. von Smekal, *Natural slow roll inflation*, *Mod.Phys.Lett.* **A11** (1996) 631–646, [hep-ph/9310335].

[331] P. Gonzalez-Diaz, *PRIMORDIAL KALUZA-KLEIN INFLATION*, *Phys.Lett.* **B176** (1986) 29–32.

[332] J. Yokoyama, *Chaotic new inflation and primordial spectrum of adiabatic fluctuations*, *Phys.Rev.* **D59** (1999) 107303.

[333] Y.-g. Gong, *Constraints on inflation in Einstein-Brans-Dicke frame*, *Phys.Rev.* **D59** (1999) 083507, [gr-qc/9808057].

[334] P. Binetruy and G. Dvali, *D term inflation*, *Phys.Lett.* **B388** (1996) 241–246, [hep-ph/9606342].

[335] E. Halyo, *Hybrid inflation from supergravity D terms*, *Phys.Lett.* **B387** (1996) 43–47, [hep-ph/9606423].

[336] G. Dvali, *Natural inflation in SUSY and gauge mediated curvature of the flat directions*, *Phys.Lett.* **B387** (1996) 471–477, [hep-ph/9605445].

[337] G. Dvali, Q. Shafi, and S. Solganik, *D-brane inflation*, hep-th/0105203.

[338] L. Covi, *Models of inflation, supersymmetry breaking and observational constraints*, hep-ph/0012245.

[339] A. Safsafi, A. Bouaouda, R. Zarrouki, H. Chakir, and M. Bennai, *Supersymmetric braneworld inflation in light of WMAP7 observations*, *Int.J.Theor.Phys.* **51** (2012) 1774–1782.

[340] T. Matsuda, *Successful D term inflation with moduli*, *Phys.Lett.* **B423** (1998) 35–39, [hep-ph/9705448].

[341] J. Espinosa, A. Riotto, and G. G. Ross, *D - term inflation in superstring theories*, *Nucl.Phys.* **B531** (1998) 461–477, [hep-ph/9804214].

[342] C. F. Kolda and D. H. Lyth, *D term inflation and M theory*, hep-ph/9812234.

[343] E. Halyo, *D term inflation in type I string theory*, *Phys.Lett.* **B454** (1999) 223–227, [hep-ph/9901302].

[344] D. Suematsu, *D term inflation and neutrino mass*, *JHEP* **0210** (2002) 014, [hep-ph/0207041].

[345] A.-C. Davis and M. Majumdar, *Inflation in supersymmetric cosmic string theories*, *Phys.Lett.* **B460** (1999) 257–262, [hep-ph/9904392].

[346] J. Urrestilla, A. Achucarro, and A. Davis, *D term inflation without cosmic strings*, *Phys.Rev.Lett.* **92** (2004) 251302, [hep-th/0402032].

[347] C.-M. Lin and J. McDonald, *Supergravity modification of D-term hybrid inflation: Solving the cosmic string and spectral index problems via a right-handed sneutrino*, *Phys.Rev.* **D74** (2006) 063510, [hep-ph/0604245].

[348] C.-M. Lin and J. McDonald, *Supergravity and two-field inflation effects in right-handed sneutrino modified D-term inflation*, *Phys.Rev.* **D77** (2008) 063529, [arXiv:0710.4273].

[349] M. Kawasaki and F. Takahashi, *Inflation model with lower multipoles of the CMB suppressed*, *Phys.Lett.* **B570** (2003) 151–153, [hep-ph/0305319].

[350] M. Gomez-Reino and I. Zavala, *Recombination of intersecting D-branes and cosmological inflation*, *JHEP* **0209** (2002) 020, [hep-th/0207278].

[351] E. Halyo, *P-term inflation on D-branes*, hep-th/0405269.

[352] A. Hebecker, S. C. Kraus, D. Lust, S. Steinfurt, and T. Weigand, *Fluxbrane Inflation*, *Nucl.Phys.* **B854** (2012) 509–551, [arXiv:1104.5016].

[353] N. T. Jones, H. Stoica, and S. H. Tye, *Brane interaction as the origin of inflation*, *JHEP* **0207** (2002) 051, [hep-th/0203163].

[354] E. Halyo, *Inflation on fractional branes: D-brane inflation as D term inflation*, *JHEP* **0407** (2004) 080, [hep-th/0312042].

[355] K. Dasgupta, J. P. Hsu, R. Kallosh, A. D. Linde, and M. Zagermann, *D3/D7 brane inflation and semilocal strings*, *JHEP* **0408** (2004) 030, [hep-th/0405247].

[356] J. McDonald, *F term hybrid inflation, the eta problem and extra dimensions*, *JHEP* **0212** (2002) 029, [hep-ph/0201016].

[357] G. Panotopoulos, *D-term inflation in D-brane cosmology*, *Phys.Lett.* **B623** (2005) 185–191, [hep-ph/0503071].

[358] E. Halyo, *Inflation in Wess–Zumino Models*, arXiv:1001.4812.

[359] C. Vayonakis, *NATURAL VALUES OF COUPLING CONSTANTS AND COSMOLOGICAL INFLATION IN A SUPERSYMMETRIC MODEL*, *Phys.Lett.* **B123** (1983) 396.

[360] A. A. Starobinsky, *A new type of isotropic cosmological models without singularity*, *Phys. Lett.* **B91** (1980) 99–102.

[361] K. Stelle, *Classical Gravity with Higher Derivatives*, *Gen.Rel.Grav.* **9** (1978) 353–371.

[362] P. Teyssandier and P. Tourrenc, *The Cauchy problem for the R+R**2 theories of gravity without torsion*, *J.Math.Phys.* **24** (1983) 2793.

[363] K.-i. Maeda, *Towards the Einstein-Hilbert Action via Conformal Transformation*, *Phys. Rev.* **D39** (1989) 3159.

[364] D. Wands, *Extended gravity theories and the Einstein-Hilbert action*, *Class.Quant.Grav.* **11** (1994) 269–280, [gr-qc/9307034].

[365] A. De Felice, S. Tsujikawa, J. Elliston, and R. Tavakol, *Chaotic inflation in modified gravitational theories*, *JCAP* **1108** (2011) 021, [arXiv:1105.4685].

[366] A. De Felice and S. Tsujikawa, *f(R) theories*, *Living Rev.Rel.* **13** (2010) 3, [arXiv:1002.4928].

[367] L. Kofman, A. D. Linde, and A. A. Starobinsky, *Inflationary Universe Generated by the Combined Action of a Scalar Field and Gravitational Vacuum Polarization*, *Phys.Lett.* **B157** (1985) 361–367.

[368] S. Kaneda, S. V. Ketov, and N. Watanabe, *Slow-roll inflation in (R+R*4) gravity*, *Class.Quant.Grav.* **27** (2010) 145016, [arXiv:1002.3659].

[369] S. V. Ketov and A. A. Starobinsky, *Embedding (R+R$\hat{2}$)-Inflation into Supergravity*, *Phys.Rev.* **D83** (2011) 063512, [arXiv:1011.0240].

[370] J. Goldstone, *Field Theories with Superconductor Solutions*, *Nuovo Cim.* **19** (1961) 154–164.

[371] E. Witten, *Superconducting Strings*, *Nucl.Phys.* **B249** (1985) 557–592.

[372] P. Peter, *Spontaneous current generation in cosmic strings*, *Phys.Rev.* **D49** (1994) 5052–5062, [hep-ph/9312280].

[373] B. Carter and P. Peter, *Supersonic string models for Witten vortices*, *Phys.Rev.* **D52** (1995) 1744–1748, [hep-ph/9411425].

[374] P. Peter, *Surface current carrying domain walls*, *J.Phys.* **A29** (1996) 5125–5136, [hep-ph/9503408].

[375] P. Peter and C. Ringeval, *Fermionic current carrying cosmic strings: Zero temperature limit and equation of state*, hep-ph/0011308.

[376] C. Ringeval, *Equation of state of cosmic strings with fermionic current carriers*, *Phys.Rev.* **D63** (2001) 063508, [hep-ph/0007015].

[377] C. Ringeval, *Fermionic massive modes along cosmic strings*, *Phys.Rev.* **D64** (2001) 123505, [hep-ph/0106179].

[378] A. D. Linde and D. A. Linde, *Topological defects as seeds for eternal inflation*, *Phys.Rev.* **D50** (1994) 2456–2468, [hep-th/9402115].

[379] A. Vilenkin, *Topological inflation*, *Phys.Rev.Lett.* **72** (1994) 3137–3140, [hep-th/9402085].

[380] A. M. Green and A. R. Liddle, *Open inflationary universes in the induced gravity theory*, *Phys.Rev.* **D55** (1997) 609–615, [astro-ph/9607166].

[381] J. Garcia-Bellido and A. R. Liddle, *Complete power spectrum for an induced gravity open inflation model*, *Phys.Rev.* **D55** (1997) 4603–4613, [astro-ph/9610183].

[382] A. D. Linde, *SUPERGRAVITY AND INFLATIONARY UNIVERSE. (IN RUSSIAN)*, *Pisma Zh.Eksp.Teor.Fiz.* **37** (1983) 606–608.

[383] A. D. Linde, *PRIMORDIAL INFLATION WITHOUT PRIMORDIAL MONOPOLES*, *Phys.Lett.* **B132** (1983) 317–320.

[384] J. Casas and C. Munoz, *INFLATION FROM SUPERSTRINGS*, *Phys.Lett.* **B216** (1989) 37.

[385] J. Casas, J. Moreno, C. Munoz, and M. Quiros, *COSMOLOGICAL IMPLICATIONS OF AN ANOMALOUS U(1): INFLATION, COSMIC STRINGS AND CONSTRAINTS ON SUPERSTRING PARAMETERS*, *Nucl.Phys.* **B328** (1989) 272.

[386] J. Cervantes-Cota and H. Dehnen, *Induced gravity inflation in the standard model of particle physics*, *Nucl.Phys.* **B442** (1995) 391–412, [astro-ph/9505069].

[387] S. H. Alexander, *Inflation from D - anti-D-brane annihilation*, *Phys.Rev.* **D65** (2002) 023507, [hep-th/0105032].

[388] R. Easther, J. Khoury, and K. Schalm, *Tuning locked inflation: Supergravity versus phenomenology*, *JCAP* **0406** (2004) 006, [hep-th/0402218].

[389] J.-O. Gong, *Modular thermal inflation without slow-roll approximation*, *Phys.Lett.* **B637** (2006) 149–155, [hep-ph/0602106].

[390] R. Kallosh and A. D. Linde, *Testing String Theory with CMB*, *JCAP* **0704** (2007) 017, [arXiv:0704.0647].

[391] G. Lazarides and A. Vamvasakis, *Standard-smooth hybrid inflation*, *Phys.Rev.* **D76** (2007) 123514, [arXiv:0709.3362].

[392] M. U. Rehman and Q. Shafi, *Higgs Inflation, Quantum Smearing and the Tensor to Scalar Ratio*, *Phys.Rev.* **D81** (2010) 123525, [arXiv:1003.5915].

[393] F. Bauer and D. A. Demir, *Higgs-Palatini Inflation and Unitarity*, *Phys.Lett.* **B698** (2011) 425–429, [arXiv:1012.2900].

[394] A. O. Barvinsky, *Standard Model Higgs Inflation: CMB, Higgs Mass and Quantum Cosmology*, *Prog.Theor.Phys.Suppl.* **190** (2011) 1–19, [arXiv:1012.4523].

[395] G. Barenboim, *Inflation might be caused by the right: Handed neutrino*, *JHEP* **0903** (2009) 102, [arXiv:0811.2998].

[396] R. Kallosh and A. Linde, *New models of chaotic inflation in supergravity*, *JCAP* **1011** (2010) 011, [arXiv:1008.3375].

[397] L. Boubekeur and D. Lyth, *Hilltop inflation*, *JCAP* **0507** (2005) 010, [hep-ph/0502047]. Latex, 20 pages, 5 figures. Minor changes, references added.

[398] K. Tzirakis and W. H. Kinney, *Inflation over the hill*, *Phys.Rev.* **D75** (2007) 123510, [astro-ph/0701432].

[399] B. K. Pal, S. Pal, and B. Basu, *Mutated Hilltop Inflation : A Natural Choice for Early Universe*, *JCAP* **1001** (2010) 029, [arXiv:0908.2302].

[400] B. K. Pal, S. Pal, and B. Basu, *A semi-analytical approach to perturbations in mutated hilltop inflation*, *Int.J.Mod.Phys.* **D21** (2012) 1250017, [arXiv:1010.5924].

[401] M. Fairbairn, L. Lopez Honorez, and M. Tytgat, *Radion assisted gauge inflation*, *Phys.Rev.* **D67** (2003) 101302, [hep-ph/0302160].

[402] A. de la Macorra and S. Lola, *Inflation in S dual superstring models*, *Phys.Lett.* **B373** (1996) 299–305, [hep-ph/9511470].

[403] T. Gherghetta, C. F. Kolda, and S. P. Martin, *Flat directions in the scalar potential of the supersymmetric standard model*, *Nucl.Phys.* **B468** (1996) 37–58, [hep-ph/9510370].

[404] K. Enqvist and A. Mazumdar, *Cosmological consequences of MSSM flat directions*, *Phys.Rept.* **380** (2003) 99–234, [hep-ph/0209244].

[405] M. Dine, L. Randall, and S. D. Thomas, *Baryogenesis from flat directions of the supersymmetric standard model*, *Nucl.Phys.* **B458** (1996) 291–326, [hep-ph/9507453].

[406] R. Allahverdi, K. Enqvist, J. Garcia-Bellido, and A. Mazumdar, *Gauge invariant MSSM inflaton*, *Phys.Rev.Lett.* **97** (2006) 191304, [hep-ph/0605035].

[407] J. Garcia-Bellido, *Flat direction MSSM (A-term) inflation*, *AIP Conf.Proc.* **878** (2006) 277–283, [hep-ph/0610152].

[408] R. Allahverdi, *MSSM flat direction inflation*, *eConf* **C0605151** (2006) 0020, [hep-ph/0610180].

[409] D. H. Lyth, *MSSM inflation*, *JCAP* **0704** (2007) 006, [hep-ph/0605283].

[410] R. Allahverdi and A. Mazumdar, *Spectral tilt in A-term inflation*, hep-ph/0610069.

[411] R. Allahverdi, B. Dutta, and A. Mazumdar, *Probing the parameter space for an MSSM inflation and the neutralino dark matter*, *Phys.Rev.* **D75** (2007) 075018, [hep-ph/0702112].

[412] K. Enqvist, L. Mether, and S. Nurmi, *Supergravity origin of the MSSM inflation*, *JCAP* **0711** (2007) 014, [arXiv:0706.2355].

[413] R. Allahverdi, B. Dutta, and A. Mazumdar, *Attraction towards an inflection point inflation*, *Phys.Rev.* **D78** (2008) 063507, [arXiv:0806.4557].

[414] K. Kamada and J. Yokoyama, *On the realization of the MSSM inflation*, *Prog.Theor.Phys.* **122** (2010) 969–986, [arXiv:0906.3402].

[415] R. Allahverdi, B. Dutta, and Y. Santoso, *MSSM inflation, dark matter, and the LHC*, *Phys.Rev.* **D82** (2010) 035012, [arXiv:1004.2741].

[416] K. Enqvist, A. Mazumdar, and P. Stephens, *Inflection point inflation within supersymmetry*, *JCAP* **1006** (2010) 020, [arXiv:1004.3724].

[417] K. Kohri and C.-M. Lin, *Hilltop Supernatural Inflation and Gravitino Problem*, *JCAP* **1011** (2010) 010, [arXiv:1008.3200].

[418] A. D. Linde and A. Mezhlumian, *Inflation with Omega not = 1*, *Phys.Rev.* **D52** (1995) 6789–6804, [astro-ph/9506017].

[419] A. D. Linde, *A Toy model for open inflation*, *Phys.Rev.* **D59** (1999) 023503, [hep-ph/9807493].

[420] R. K. Jain, P. Chingangbam, J.-O. Gong, L. Sriramkumar, and T. Souradeep, *Punctuated inflation and the low CMB multipoles*, *JCAP* **0901** (2009) 009, [arXiv:0809.3915].

[421] R. K. Jain, P. Chingangbam, L. Sriramkumar, and T. Souradeep, *The tensor-to-scalar ratio in punctuated inflation*, *Phys.Rev.* **D82** (2010) 023509, [arXiv:0904.2518].

[422] D. A. Lowe and S. Roy, *Punctuated eternal inflation via AdS/CFT*, *Phys.Rev.* **D82** (2010) 063508, [arXiv:1004.1402].

[423] R. Allahverdi, B. Dutta, and A. Mazumdar, *Unifying inflation and dark matter with neutrino masses*, *Phys.Rev.Lett.* **99** (2007) 261301, [arXiv:0708.3983].

[424] R. Allahverdi, A. Kusenko, and A. Mazumdar, *A-term inflation and the smallness of neutrino masses*, *JCAP* **0707** (2007) 018, [hep-ph/0608138].

[425] L.-M. Wang, V. F. Mukhanov, and P. J. Steinhardt, *On the problem of predicting inflationary perturbations*, *Phys.Lett.* **B414** (1997) 18–27, [astro-ph/9709032].

[426] M. Drees and E. Erfani, *Running Spectral Index and Formation of Primordial Black Hole in Single Field Inflation Models*, *JCAP* **1201** (2012) 035, [arXiv:1110.6052].

[427] M. Drees and E. Erfani, *Dark Matter Primordial Black Holes and Inflation Models*, arXiv:1205.4012.

[428] A. Vallinotto, E. J. Copeland, E. W. Kolb, A. R. Liddle, and D. A. Steer, *Inflationary potentials yielding constant scalar perturbation spectral indices*, *Phys.Rev.* **D69** (2004) 103519, [astro-ph/0311005].

[429] D. Veberic, *Lambert w function for applications in physics*, *CoRR* **abs/1209.0735** (2012).

[430] E. Witten, *On background independent open string field theory*, *Phys.Rev.* **D46** (1992) 5467–5473, [hep-th/9208027].

[431] E. Witten, *Some computations in background independent off-shell string theory*, *Phys.Rev.* **D47** (1993) 3405–3410, [hep-th/9210065].

[432] A. A. Gerasimov and S. L. Shatashvili, *On exact tachyon potential in open string field theory*, *JHEP* **0010** (2000) 034, [hep-th/0009103].

[433] D. Kutasov, M. Marino, and G. W. Moore, *Some exact results on tachyon condensation in string field theory*, *JHEP* **0010** (2000) 045, [hep-th/0009148].

[434] L. Kofman and A. D. Linde, *Problems with tachyon inflation*, *JHEP* **0207** (2002) 004, [hep-th/0205121].

[435] D. Choudhury, D. Ghoshal, D. P. Jatkar, and S. Panda, *On the cosmological relevance of the tachyon*, *Phys.Lett.* **B544** (2002) 231–238, [hep-th/0204204].

[436] J. E. Lidsey and D. Seery, *Primordial Non-Gaussianity and Gravitational Waves: Observational Tests of Brane Inflation in String Theory*, *Phys.Rev.* **D75** (2007) 043505, [astro-ph/0610398].

[437] J. A. Minahan and B. Zwiebach, *Field theory models for tachyon and gauge field string dynamics*, *JHEP* **0009** (2000) 029, [hep-th/0008231].

[438] E. Witten, *Mass Hierarchies in Supersymmetric Theories*, *Phys.Lett.* **B105** (1981) 267.

[439] L. O'Raifeartaigh, *Spontaneous Symmetry Breaking for Chiral Scalar Superfields*, *Nucl.Phys.* **B96** (1975) 331.

[440] E. Witten, *Dynamical Breaking of Supersymmetry*, *Nucl.Phys.* **B188** (1981) 513.

[441] S. Dimopoulos and S. Raby, *Geometric Hierarchy*, *Nucl.Phys.* **B219** (1983) 479.

[442] A. Albrecht, S. Dimopoulos, W. Fischler, E. W. Kolb, S. Raby, et al., *NEW INFLATION IN SUPERSYMMETRIC THEORIES*, *Nucl.Phys.* **B229** (1983) 528.

[443] E. Papantonopoulos, T. Uematsu, and T. Yanagida, *NATURAL CHAOTIC INFLATION*, *Phys.Lett.* **B183** (1987) 282.

[444] M. Pollock, *ON THE POSSIBILITY OF CHAOTIC INFLATION FROM A SOFTLY BROKEN SUPERCONFORMAL INVARIANCE*, *Phys.Lett.* **B194** (1987) 518–522.

[445] K.-i. Kobayashi and T. Uematsu, *NONLINEAR REALIZATION OF SUPERCONFORMAL SYMMETRY*, *Nucl.Phys.* **B263** (1986) 309.

[446] P. Binetruy and M. Gaillard, *Candidates for the Inflaton Field in Superstring Models*, *Phys.Rev.* **D34** (1986) 3069–3083.

[447] W. H. Kinney and K. Mahanthappa, *Inflation from symmetry breaking below the Planck scale*, *Phys.Lett.* **B383** (1996) 24–27, [hep-ph/9511460].

[448] M. Kawasaki and M. Yamaguchi, *A Supersymmetric topological inflation model*, *Phys.Rev.* **D65** (2002) 103518, [hep-ph/0112093].

[449] K. Kumekawa, T. Moroi, and T. Yanagida, *Flat potential for inflaton with a discrete R invariance in supergravity*, *Prog.Theor.Phys.* **92** (1994) 437–448, [hep-ph/9405337].

[450] J. A. Adams, G. G. Ross, and S. Sarkar, *Natural supergravity inflation*, *Phys.Lett.* **B391** (1997) 271–280, [hep-ph/9608336].

[451] K.-I. Izawa and T. Yanagida, *Natural new inflation in broken supergravity*, *Phys.Lett.* **B393** (1997) 331–336, [hep-ph/9608359].

[452] K. Izawa, M. Kawasaki, and T. Yanagida, *R invariant topological inflation*, *Prog.Theor.Phys.* **101** (1999) 1129–1133, [hep-ph/9810537].

[453] W. Buchmuller, K. Hamaguchi, M. Ratz, and T. Yanagida, *Gravitino and goldstino at colliders*, hep-ph/0403203.

[454] T. Banks, M. Berkooz, S. Shenker, G. W. Moore, and P. Steinhardt, *Modular cosmology*, *Phys.Rev.* **D52** (1995) 3548–3562, [hep-th/9503114].

[455] Y. Himemoto and M. Sasaki, *Brane world inflation without inflaton on the brane*, *Phys.Rev.* **D63** (2001) 044015, [gr-qc/0010035].

[456] N. Sago, Y. Himemoto, and M. Sasaki, *Quantum fluctuations in brane world inflation without inflaton on the brane*, *Phys.Rev.* **D65** (2002) 024014, [gr-qc/0104033].

[457] X. Chen, *Inflation from warped space*, *JHEP* **0508** (2005) 045, [hep-th/0501184].

[458] J. D. Barrow, *Graduated Inflationary Universes*, *Phys. Lett.* **B235** (1990) 40–43.

[459] J. D. Barrow and P. Saich, *The Behavior of intermediate inflationary universes*, *Phys. Lett.* **B249** (1990) 406–410.

[460] J. D. Barrow and A. R. Liddle, *Perturbation spectra from intermediate inflation*, *Phys. Rev.* **D47** (1993) 5219–5223, [astro-ph/9303011].

[461] J. D. Barrow, A. R. Liddle, and C. Pahud, *Intermediate inflation in light of the three-year WMAP observations*, *Phys. Rev.* **D74** (2006) 127305, [astro-ph/0610807].

[462] J. D. Barrow, *String-Driven Inflationary and Deflationary Cosmological Models*, *Nucl.Phys.* **B310** (1988) 743–763.

[463] S. del Campo, R. Herrera, and A. Toloza, *Tachyon Field in Intermediate Inflation*, *Phys.Rev.* **D79** (2009) 083507, [arXiv:0904.1032].

[464] H. Farajollahi and A. Ravanpak, *Tachyon Field in Intermediate Inflation on the Brane*, *Phys.Rev.* **D84** (2011) 084017, [arXiv:1106.2211].

[465] S. del Campo and R. Herrera, *Warm-Intermediate inflationary universe model*, *JCAP* **0904** (2009) 005, [arXiv:0903.4214].

[466] S. del Campo, R. Herrera, and J. Saavedra, *Tachyon warm inflationary universe model in the weak dissipative regime*, *Eur.Phys.J.* **C59** (2009) 913–916, [arXiv:0812.1081].

[467] R. Herrera and N. Videla, *Intermediate inflation in Gauss-Bonnet braneworld*, *Eur.Phys.J.* **C67** (2010) 499–505, [arXiv:1003.5645].

[468] A. Cid and S. del Campo, *Constraints from CMB in the intermediate Brans-Dicke inflation*, *JCAP* **1101** (2011) 013, [arXiv:1101.4588].

[469] A. Cid and S. del Campo, *Intermediate Inflation in the Jordan-Brans-Dicke Theory*, *AIP Conf.Proc.* **1471** (2012) 114–117, [arXiv:1210.5273].

[470] J. D. Barrow and N. J. Nunes, *Dynamics of Logamediate Inflation*, *Phys. Rev.* **D76** (2007) 043501, [arXiv:0705.4426].

[471] P. Parsons and J. D. Barrow, *Generalized scalar field potentials and inflation*, *Phys.Rev.* **D51** (1995) 6757–6763, [astro-ph/9501086].

[472] J. L. Davis, T. S. Levi, M. Van Raamsdonk, and K. R. L. Whyte, *Twisted Inflation*, *JCAP* **1009** (2010) 032, [arXiv:1004.5385].

[473] D. H. Lyth and A. Riotto, *Generating the Curvature Perturbation at the End of Inflation in String Theory*, *Phys.Rev.Lett.* **97** (2006) 121301, [astro-ph/0607326].

[474] J. Bueno Sanchez, K. Dimopoulos, and D. H. Lyth, *A-term inflation and the MSSM*, *JCAP* **0701** (2007) 015, [hep-ph/0608299].

[475] R. Allahverdi, K. Enqvist, J. Garcia-Bellido, A. Jokinen, and A. Mazumdar, *MSSM flat direction inflation: Slow roll, stability, fine tunning and reheating*, *JCAP* **0706** (2007) 019, [hep-ph/0610134].

[476] A. Chatterjee and A. Mazumdar, *Tuned MSSM Higgses as an inflaton*, *JCAP* **1109** (2011) 009, [arXiv:1103.5758].

[477] S. Hotchkiss, A. Mazumdar, and S. Nadathur, *Inflection point inflation: WMAP constraints and a solution to the fine-tuning problem*, *JCAP* **1106** (2011) 002, [arXiv:1101.6046].

[478] C. S. Aulakh and I. Garg, *Supersymmetric Seesaw Inflation*, *Phys.Rev.* **D86** (2012) 065001, [arXiv:1201.0519].

[479] C. S. Aulakh, *Susy Seesaw Inflation and NMSO(10)GUT*, arXiv:1210.2042.

[480] E. Dudas, N. Kitazawa, S. Patil, and A. Sagnotti, *CMB Imprints of a Pre-Inflationary Climbing Phase*, arXiv:1202.6630.

[481] J. Martin and C. Ringeval, *Superimposed oscillations in the WMAP data?*, *Phys.Rev.* **D69** (2004) 083515, [astro-ph/0310382].

[482] J. Martin and C. Ringeval, *Addendum to 'Superimposed oscillations in the WMAP data?'*, *Phys.Rev.* **D69** (2004) 127303, [astro-ph/0402609].

[483] J. Martin and C. Ringeval, *Exploring the superimposed oscillations parameter space*, *JCAP* **0501** (2005) 007, [hep-ph/0405249].

[484] J. Trudeau and J. M. Cline, *Warped Radion Inflation*, *JHEP* **1202** (2012) 081, [arXiv:1111.4257].

[485] C. P. Burgess, J. M. Cline, K. Dasgupta, and H. Firouzjahi, *Uplifting and Inflation with D3 Branes*, *JHEP* **0703** (2007) 027, [hep-th/0610320].

[486] A. Krause and E. Pajer, *Chasing brane inflation in string-theory*, *JCAP* **0807** (2008) 023, [arXiv:0705.4682].

[487] D. Baumann, A. Dymarsky, I. R. Klebanov, L. McAllister, and P. J. Steinhardt, *A Delicate universe*, *Phys.Rev.Lett.* **99** (2007) 141601, [arXiv:0705.3837].

[488] O. DeWolfe, L. McAllister, G. Shiu, and B. Underwood, *D3-brane Vacua in Stabilized Compactifications*, *JHEP* **0709** (2007) 121, [hep-th/0703088].

[489] E. Pajer, *Inflation at the Tip*, *JCAP* **0804** (2008) 031, [arXiv:0802.2916].

[490] F. Chen and H. Firouzjahi, *Dynamics of D3-D7 Brane Inflation in Throats*, *JHEP* **0811** (2008) 017, [arXiv:0807.2817].

[491] I. R. Klebanov and M. J. Strassler, *Supergravity and a confining gauge theory: Duality cascades and chi SB resolution of naked singularities*, *JHEP* **0008** (2000) 052, [hep-th/0007191].

[492] P. Candelas and X. C. de la Ossa, *Comments on Conifolds*, *Nucl.Phys.* **B342** (1990) 246–268.

[493] S. Kuperstein, *Meson spectroscopy from holomorphic probes on the warped deformed conifold*, *JHEP* **0503** (2005) 014, [hep-th/0411097].

[494] S. Kachru, R. Kallosh, A. D. Linde, and S. P. Trivedi, *De Sitter vacua in string theory*, *Phys.Rev.* **D68** (2003) 046005, [hep-th/0301240].

[495] J. S. Alcaniz and F. Carvalho, *Beta-exponential inflation*, *Europhys.Lett.* **79** (2007) 39001, [astro-ph/0612279].

[496] C. Panagiotakopoulos, *Hybrid inflation with quasicanonical supergravity*, *Phys.Lett.* **B402** (1997) 257–262, [hep-ph/9703443].

[497] C. Panagiotakopoulos, *Blue perturbation spectra from hybrid inflation with canonical supergravity*, *Phys.Rev.* **D55** (1997) 7335–7339, [hep-ph/9702433].

[498] L. M. Hall and H. V. Peiris, *Cosmological Constraints on Dissipative Models of Inflation*, *JCAP* **0801** (2008) 027, [arXiv:0709.2912].

[499] B. Kyae, *Spectral Index and Non-Gaussianity in Supersymmetric Hybrid Inflation*, *Eur.Phys.J.* **C72** (2012) 1857, [arXiv:0910.4092].

[500] H. Hodges and G. Blumenthal, *Arbitrariness of inflationary fluctuation spectra*, *Phys.Rev.* **D42** (1990) 3329–3333.

[501] G. Veneziano and S. Yankielowicz, *An Effective Lagrangian for the Pure N=1 Supersymmetric Yang-Mills Theory*, *Phys.Lett.* **B113** (1982) 231.

[502] P. Channuie, J. Joergensen, and F. Sannino, *Composite Inflation from Super Yang-Mills, Orientifold and One-Flavor QCD*, arXiv:1209.6362.

[503] Q. Shafi and V. N. Senoguz, *Coleman-Weinberg potential in good agreement with wmap*, *Phys.Rev.* **D73** (2006) 127301, [astro-ph/0603830].

[504] S. Choudhury and S. Pal, *Brane inflation in background supergravity*, *Phys.Rev.* **D85** (2012) 043529, [arXiv:1102.4206].

[505] S. Choudhury and S. Pal, *Brane inflation: A field theory approach in background supergravity*, arXiv:1209.5883.

[506] I. Moss, *PRIMORDIAL INFLATION WITH SPONTANEOUS SYMMETRY BREAKING*, *Phys.Lett.* **B154** (1985) 120.

[507] B. Hu and D. O'Connor, *MIXMASTER INFLATION*, *Phys.Rev.* **D34** (1986) 2535.

[508] M. Dine and A. Riotto, *An Inflaton candidate in gauge mediated supersymmetry breaking*, *Phys.Rev.Lett.* **79** (1997) 2632–2635, [hep-ph/9705386].

[509] A. Riotto, *Inflation and the nature of supersymmetry breaking*, *Nucl.Phys.* **B515** (1998) 413–435, [hep-ph/9707330].

[510] D. Cormier and R. Holman, *Spinodal inflation*, *Phys.Rev.* **D60** (1999) 041301, [hep-ph/9812476].

[511] D. Cormier and R. Holman, *Spinodal decomposition and inflation: Dynamics and metric perturbations*, *Phys.Rev.* **D62** (2000) 023520, [hep-ph/9912483].

[512] S. Bhattacharya, D. Choudhury, D. P. Jatkar, and A. A. Sen, *Brane dynamics in the Randall-Sundrum model, inflation and graceful exit*, *Class.Quant.Grav.* **19** (2002) 5025–5038, [hep-th/0103248].

[513] W.-F. Wang, *Exact solution in the cosmological chaotic inflation model with induced gravity*, *Phys.Lett.* **A328** (2004) 255–260.

[514] T. Fukuyama, T. Kikuchi, and W. Naylor, *Electroweak inflation and reheating in the NMSSM*, hep-ph/0511105.

[515] S. Antusch, *Sneutrino hybrid inflation*, *AIP Conf.Proc.* **878** (2006) 284–290, [hep-ph/0608261].

[516] J. Blanco-Pillado, C. Burgess, J. M. Cline, C. Escoda, M. Gomez-Reino, et al., *Racetrack inflation*, *JHEP* **0411** (2004) 063, [hep-th/0406230].

[517] P. Brax, S. C. Davis, and M. Postma, *The Robustness of n(s) ¡ 0.95 in racetrack inflation*, *JCAP* **0802** (2008) 020, [arXiv:0712.0535].

[518] J.-O. Gong and N. Sahu, *Inflation in minimal left-right symmetric model with spontaneous D-parity breaking*, *Phys.Rev.* **D77** (2008) 023517, [arXiv:0705.0068].

[519] L.-Y. Lee, K. Cheung, and C.-M. Lin, *Comments on SUSY inflation models on the brane*, *Mod.Phys.Lett.* **A25** (2010) 2105–2110, [arXiv:0912.5423].

[520] C.-M. Lin and K. Cheung, *Reducing the Spectral Index in Supernatural Inflation*, *Phys.Rev.* **D79** (2009) 083509, [arXiv:0901.3280].

[521] C.-M. Lin, *Hilltop Supernatural Inflation*, *Prog.Theor.Phys.Suppl.* **190** (2011) 20–25, [arXiv:1012.2647].

[522] S. Khalil and A. Sil, *Right-handed Sneutrino Inflation in SUSY B-L with Inverse Seesaw*, *Phys.Rev.* **D84** (2011) 103511, [arXiv:1108.1973].

[523] S. Khalil and A. Sil, *Sneutrino inflation in supersymmetric B-L with inverse seesaw*, *AIP Conf.Proc.* **1467** (2012) 294–297.

[524] S. Antusch and D. Nolde, *Káhler-driven Tribrid Inflation*, arXiv:1207.6111.

[525] I. Masina and A. Notari, *Standard Model False Vacuum Inflation: Correlating the Tensor-to-Scalar Ratio to the Top Quark and Higgs Boson masses*, *Phys.Rev.Lett.* **108** (2012) 191302, [arXiv:1112.5430].

[526] I. Masina and A. Notari, *The Higgs mass range from Standard Model false vacuum Inflation in scalar-tensor gravity*, *Phys.Rev.* **D85** (2012) 123506, [arXiv:1112.2659].

[527] I. Masina and A. Notari, *Inflation from the Higgs field false vacuum with hybrid potential*, *JCAP* **1211** (2012) 031, [arXiv:1204.4155].

[528] P. Peebles and B. Ratra, *Cosmology with a Time Variable Cosmological Constant*, *Astrophys.J.* **325** (1988) L17.

[529] G. Huey and J. E. Lidsey, *Inflation, brane worlds and quintessence*, *Phys.Lett.* **B514** (2001) 217–225, [astro-ph/0104006].

[530] A. Feinstein, *Power law inflation from the rolling tachyon*, *Phys.Rev.* **D66** (2002) 063511, [hep-th/0204140].

[531] M. Sami, *Implementing power law inflation with rolling tachyon on the brane*, *Mod.Phys.Lett.* **A18** (2003) 691, [hep-th/0205146].

[532] B. Wang, E. Abdalla, and R.-K. Su, *Dynamics and holographic discreteness of tachyonic inflation*, *Mod.Phys.Lett.* **A18** (2003) 31–40, [hep-th/0208023].

[533] L. R. W. Abramo and F. Finelli, *Cosmological dynamics of the tachyon with an inverse power-law potential*, *Phys.Lett.* **B575** (2003) 165–171, [astro-ph/0307208].

[534] P. Binetruy, *Models of dynamical supersymmetry breaking and quintessence*, *Phys.Rev.* **D60** (1999) 063502, [hep-ph/9810553].

[535] P. Brax and J. Martin, *The Robustness of quintessence*, *Phys.Rev.* **D61** (2000) 103502, [astro-ph/9912046].

[536] T. Taylor, G. Veneziano, and S. Yankielowicz, *Supersymmetric QCD and Its Massless Limit: An Effective Lagrangian Analysis*, *Nucl.Phys.* **B218** (1983) 493.

[537] I. Affleck, M. Dine, and N. Seiberg, *Dynamical Supersymmetry Breaking in Four-Dimensions and Its Phenomenological Implications*, *Nucl.Phys.* **B256** (1985) 557.

[538] C. Burgess, M. Majumdar, D. Nolte, F. Quevedo, G. Rajesh, et al., *The Inflationary brane anti-brane universe*, *JHEP* **0107** (2001) 047, [hep-th/0105204].

[539] G. Shiu and S. H. Tye, *Some aspects of brane inflation*, *Phys.Lett.* **B516** (2001) 421–430, [hep-th/0106274].

[540] J. Garcia-Bellido, *Inflation from branes at angles*, astro-ph/0306195.

[541] L. Pogosian, S. H. Tye, I. Wasserman, and M. Wyman, *Observational constraints on cosmic string production during brane inflation*, *Phys.Rev.* **D68** (2003) 023506, [hep-th/0304188].

[542] T. Matsuda, *F term, D term and hybrid brane inflation*, *JCAP* **0311** (2003) 003, [hep-ph/0302078].

[543] T. Matsuda, *Brane Q ball, branonium and brane Q ball inflation*, *JCAP* **0410** (2004) 014, [hep-ph/0402223].

[544] H.-X. Yang, *D3/D7 inflation in a Type-0B string background*, hep-th/0504096.

[545] Q.-G. Huang, M. Li, and J.-H. She, *Brane Inflation After WMAP Three Year Results*, *JCAP* **0611** (2006) 010, [hep-th/0604186].

[546] R. Bean, S. E. Shandera, S. Henry Tye, and J. Xu, *Comparing brane inflation to WMAP*, *JCAP* **0705** (2007) 004, [hep-th/0702107].

[547] R. A. Battye, B. Garbrecht, A. Moss, and H. Stoica, *Constraints on Brane Inflation and Cosmic Strings*, *JCAP* **0801** (2008) 020, [arXiv:0710.1541].

[548] S.-H. Henry Tye, *Brane inflation: String theory viewed from the cosmos*, *Lect.Notes Phys.* **737** (2008) 949–974, [hep-th/0610221].

[549] R. H. Brandenberger, A. R. Frey, and L. C. Lorenz, *Entropy fluctuations in brane inflation models*, *Int.J.Mod.Phys.* **A24** (2009) 4327–4354, [arXiv:0712.2178].

[550] L. Lorenz, *Constraints on brane inflation from WMAP3*, arXiv:0801.4891.

[551] Y.-Z. Ma and X. Zhang, *Brane inflation revisited after WMAP five year results*, *JCAP* **0903** (2009) 006, [arXiv:0812.3421].

[552] D. Baumann and L. McAllister, *A Microscopic Limit on Gravitational Waves from D-brane Inflation*, *Phys.Rev.* **D75** (2007) 123508, [hep-th/0610285].

[553] L. C. Lorenz, *Primordial Fluctuations in String Cosmology*, arXiv:1002.2087.

[554] K. L. Panigrahi and H. Singh, *Assisted Inflation from Geometric Tachyon*, *JHEP* **0711** (2007) 017, [arXiv:0708.1679].

[555] P. S. Kwon, G. Y. Jun, K. L. Panigrahi, and M. Sami, *Inflation driven by single geometric tachyon with D-brane orbiting around NS5-branes*, *Phys.Lett.* **B712** (2012) 10–15, [arXiv:1106.4118].

[556] P. Brax, C. A. Savoy, and A. Sil, *SQCD Inflation & SUSY Breaking*, *JHEP* **0904** (2009) 092, [arXiv:0902.0972].

[557] S. Kachru, R. Kallosh, A. D. Linde, J. M. Maldacena, L. P. McAllister, et al., *Towards inflation in string theory*, *JCAP* **0310** (2003) 013, [hep-th/0308055].

[558] E. D. Stewart, *Flattening the inflaton's potential with quantum corrections*, *Phys.Lett.* **B391** (1997) 34–38, [hep-ph/9606241].

[559] E. D. Stewart, *Flattening the inflaton's potential with quantum corrections. 2.*, *Phys.Rev.* **D56** (1997) 2019–2023, [hep-ph/9703232].

[560] L. Covi, D. H. Lyth, and L. Roszkowski, *Observational constraints on an inflation model with a running mass*, *Phys.Rev.* **D60** (1999) 023509, [hep-ph/9809310].

[561] L. Covi and D. H. Lyth, *Running-mass models of inflation, and their observational constraints*, *Phys. Rev.* **D59** (1999) 063515, [hep-ph/9809562].

[562] S. M. Leach, I. J. Grivell, and A. R. Liddle, *Black hole constraints on the running mass inflation model*, *Phys.Rev.* **D62** (2000) 043516, [astro-ph/0004296].

[563] D. H. Lyth, *Observational constraints on models of inflation from the density perturbation and gravitino production*, hep-ph/0012065.

[564] L. Covi, D. H. Lyth, and A. Melchiorri, *New constraints on the running-mass inflation model*, *Phys. Rev.* **D67** (2003) 043507, [hep-ph/0210395].

[565] K. Kadota and E. D. Stewart, *Inflation on moduli space and cosmic perturbations*, *JHEP* **0312** (2003) 008, [hep-ph/0311240].

[566] L. Covi, D. H. Lyth, A. Melchiorri, and C. J. Odman, *The running-mass inflation model and WMAP*, *Phys. Rev.* **D70** (2004) 123521, [astro-ph/0408129].

[567] A. D. Linde, *Axions in inflationary cosmology*, *Phys. Lett.* **B259** (1991) 38–47.

[568] E. J. Copeland, A. R. Liddle, D. H. Lyth, E. D. Stewart, and D. Wands, *False vacuum inflation with Einstein gravity*, *Phys. Rev.* **D49** (1994) 6410–6433, [astro-ph/9401011].

[569] C. Panagiotakopoulos, *Hybrid inflation and supergravity*, hep-ph/0011261.

[570] G. Lazarides, *Supersymmetric hybrid inflation*, hep-ph/0011130.

[571] S. Clesse and J. Rocher, *Avoiding the blue spectrum and the fine-tuning of initial conditions in hybrid inflation*, *Phys. Rev.* **D79** (2009) 103507, [arXiv:0809.4355].

[572] S. Clesse, C. Ringeval, and J. Rocher, *Fractal initial conditions and natural parameter values in hybrid inflation*, *Phys. Rev.* **D80** (2009) 123534, [arXiv:0909.0402].

[573] S. Clesse, *Hybrid inflation along waterfall trajectories*, *Phys. Rev.* **D83** (2011) 063518, [arXiv:1006.4522].

[574] H. Kodama, K. Kohri, and K. Nakayama, *On the waterfall behavior in hybrid inflation*, *Prog.Theor.Phys.* **126** (2011) 331–350, [arXiv:1102.5612].

[575] M. Bento, O. Bertolami, and A. Sen, *Supergravity inflation on the brane*, *Phys.Rev.* **D67** (2003) 023504, [gr-qc/0204046].

[576] J. Rocher and M. Sakellariadou, *Constraints on Supersymmetric Grand Unified Theories from Cosmology*, *JCAP* **0503** (2005) 004, [hep-ph/0406120].

[577] M. Bastero-Gil, S. F. King, and Q. Shafi, *Supersymmetric hybrid inflation with non-minimal Kaehler potential*, *Phys. Lett.* **B651** (2007) 345–351, [hep-ph/0604198].

[578] J. Martin and V. Vennin, *Stochastic Effects in Hybrid Inflation*, *Phys.Rev.* **D85** (2012) 043525, [arXiv:1110.2070].

[579] Z. Komargodski and N. Seiberg, *From Linear SUSY to Constrained Superfields*, *JHEP* **0909** (2009) 066, [arXiv:0907.2441].

[580] L. Alvarez-Gaume, C. Gomez, and R. Jimenez, *A Minimal Inflation Scenario*, *JCAP* **1103** (2011) 027, [arXiv:1101.4948].

[581] L. Alvarez-Gaume, C. Gomez, and R. Jimenez, *Minimal Inflation*, *Phys.Lett.* **B690** (2010) 68–72, [arXiv:1001.0010].

[582] L. Alvarez-Gaume, C. Gomez, and R. Jimenez, *Phenomenology of the minimal inflation scenario: inflationary trajectories and particle production*, *JCAP* **1203** (2012) 017, [arXiv:1110.3984].

[583] W. H. Kinney and A. Riotto, *Dynamical supersymmetric inflation*, *Astropart. Phys.* **10** (1999) 387–395, [hep-ph/9704388].

[584] W. H. Kinney and A. Riotto, *A Signature of inflation from dynamical supersymmetry breaking*, *Phys.Lett.* **B435** (1998) 272–276, [hep-ph/9802443].

[585] F. Bezrukov, P. Channuie, J. J. Joergensen, and F. Sannino, *Composite Inflation Setup and Glueball Inflation*, *Phys.Rev.* **D86** (2012) 063513, [arXiv:1112.4054].

[586] P. Channuie and K. Karwan, *Observational Constraints on Composite Inflationary Models*, arXiv:1307.2880.

[587] J. D. Barrow and P. Parsons, *Inflationary models with logarithmic potentials*, *Phys.Rev.* **D52** (1995) 5576–5587, [astro-ph/9506049].

[588] D. J. Schwarz and C. A. Terrero-Escalante, *Primordial fluctuations and cosmological inflation after WMAP 1.0*, *JCAP* **0408** (2004) 003, [hep-ph/0403129].

Journal of Cosmology and Astroparticle Physics
An IOP and SISSA journal

The best inflationary models after Planck

Jérôme Martin,[a] **Christophe Ringeval,**[b] **Roberto Trotta**[c] **and Vincent Vennin**[a]

[a]Institut d'Astrophysique de Paris, UMR 7095-CNRS, Université Pierre et Marie Curie, 98bis boulevard Arago, 75014 Paris, France
[b]Centre for Cosmology, Particle Physics and Phenomenology, Institute of Mathematics and Physics, Louvain University, 2 Chemin du Cyclotron, 1348 Louvain-la-Neuve, Belgium
[c]Imperial College London, Astrophysics & Imperial Centre for Inference and Cosmology, Blackett Laboratory, Prince Consort Road, London SW7 2AZ, United Kingdom

E-mail: jmartin@iap.fr, christophe.ringeval@uclouvain.be, r.trotta@imperial.ac.uk, vennin@iap.fr

Received December 20, 2013
Revised February 8, 2014
Accepted February 18, 2014
Published March 19, 2014

Abstract. We compute the Bayesian evidence and complexity of 193 slow-roll single-field models of inflation using the Planck 2013 Cosmic Microwave Background data, with the aim of establishing which models are favoured from a Bayesian perspective. Our calculations employ a new numerical pipeline interfacing an inflationary effective likelihood with the slow-roll library `ASPIC` and the nested sampling algorithm `MultiNest`. The models considered represent a complete and systematic scan of the entire landscape of inflationary scenarios proposed so far. Our analysis singles out the most probable models (from an Occam's razor point of view) that are compatible with Planck data, while ruling out with very strong evidence 34% of the models considered. We identify 26% of the models that are favoured by the Bayesian evidence, corresponding to 15 different potential shapes. If the Bayesian complexity is included in the analysis, only 9% of the models are preferred, corresponding to only 9 different potential shapes. These shapes are all of the plateau type.

Keywords: inflation, CMBR experiments, physics of the early universe, cosmological parameters from CMBR

ArXiv ePrint: 1312.3529

doi:10.1088/1475-7516/2014/03/039

JCAP03(2014)039

Contents

JCAP03(2014)039

1 Introduction

The recent release of the Planck satellite data has had important and profound consequences for our understanding of primordial cosmology. These data clearly support the idea that inflation is the correct description of the physical conditions that prevailed in the early universe since they are in agreement with several important and generic predictions made by the inflationary theory. For instance, a basic property of inflation is that spatial curvature should vanish. And one indeed finds that $100\Omega_K = -0.05^{+0.65}_{-0.66}$ by combining Planck with Wilkinson Microwave Anisotropy Probe (WMAP) large-scale polarisation (denoted WP in ref. [1]) and Baryon Acoustic Oscillations (BAO) measurements. Another important consequence of the Planck data is the detection of a spectral tilt, $n_{\rm S} = 0.9603 \pm 0.0073$ thus ruling out scale invariance at more than 5σ, a level of significance predicted in ref. [2], and convincingly confirming a crucial inflationary prediction. Moreover, the Planck data seem to point to the simplest (but non-trivial) version of inflation. Indeed, neither a significant running nor a significant running of the running have been detected since it is found that $\mathrm{d}n_{\rm S}/\mathrm{d}\ln k = -0.0134 \pm 0.009$ (Planck+WP) and $\mathrm{d}^2 n_{\rm S}/\mathrm{d}\ln^2 k = 0.02 \pm 0.016$ (Planck+WP), with a pivot scale chosen at $k_* = 0.05\mathrm{Mpc}^{-1}$. The data are also compatible with adiabaticity at 95% CL. If one defines $\alpha_{ab}^{(\ell_{\rm min},\ell_{\rm max})} \equiv (\Delta T)^2_{ab}\,(\ell_{\rm min},\ell_{\rm max})/\,(\Delta T)^2_{\rm tot}\,(\ell_{\rm min},\ell_{\rm max})$, with $a, b = \mathcal{R}, \mathcal{I}$, where $\mathcal{I}$ stands for Cold Dark Isocurvature (CDI), Neutrino Density Isocurvature (NDI) or Neutrino Velocity Isocurvature (NVI) and $(\Delta T)^2_X\,(\ell_{\rm min},\ell_{\rm max}) = \sum_{\ell=\ell_{\rm min}}^{\ell=\ell_{\rm max}} (2\ell+1)\,C^{TT}_{\ell,X}$, then one obtains $\alpha_{\mathcal{R}\mathcal{R}}^{(2,2500)} \in [0, 98, 1.07]$ and $\alpha_{\mathcal{R}\mathcal{I}}^{(2,2500)} \in [-0.093, 0.014]$ for $\mathcal{I} = $ CDI, $\alpha_{\mathcal{R}\mathcal{R}}^{(2,2500)} \in [0, 99, 1.09]$ and $\alpha_{\mathcal{R}\mathcal{I}}^{(2,2500)} \in [-0.18, 0.0]$ for $\mathcal{I} = $ NDI, $\alpha_{\mathcal{R}\mathcal{R}}^{(2,2500)} \in [0, 96, 1.05]$ and $\alpha_{\mathcal{R}\mathcal{I}}^{(2,2500)} \in [-0.09, 0.026]$

JCAP03(2014)039

for $\mathcal{I} = \mathrm{NVI}$. This implies that isocurvature modes are compatible with zero although the analysis is done with one isocurvature mode at a time only. A quite large non-adiabatic contribution remains possible but, as discussed in ref. [3], this is in fact driven by the data in the range $\ell \leq 40$. The Planck data also imply that primordial non-Gaussianity is compatible with zero, namely $f_{\mathrm{NL}}^{\mathrm{loc}} = 2.7 \pm 5.8$, $f_{\mathrm{NL}}^{\mathrm{eq}} = -42 \pm 75$ and $f_{\mathrm{NL}}^{\mathrm{ortho}} = -25 \pm 39$ [4]. Some anomalies or "glitches" have also been reported but the corresponding statistical significance is unclear and, in any case, not yet sufficient to claim a detection.

Therefore, the overall picture that emerges is that the inflationary mechanism is non-trivial but, at the same time, "non-exotic". In particular, the complicated scenarios that were considered, at some point, as attractive are now disfavoured (but not necessarily ruled out). Therefore, in accordance with an Occam's razor principle, that the simplest viable explanation for the observations at hand ought to be preferred, it is appropriate to consider — at least for the moment — the simplest scenarios, namely single field slow-roll inflation with a standard kinetic term. This type of scenarios is characterised by one free function, the potential $V(\phi)$. Therefore, identifying the "best model of inflation" boils down to determining the potential $V(\phi)$ which fits the data the best with the smallest number of free parameters and the least fine-tuning.

In order to achieve this task, it is first necessary to identify all the scenarios belonging to the above-mentioned class. This is not so easy since, even if restricted to a small part of the inflationary landscape, the "single-field region" remains densely populated. This was accomplished recently in the "*Encyclopædia Inflationaris*" of ref. [5]. Once all the single-field models have been identified, one needs to quantify statistically whether a model is "better" than another. This question can be addressed in the framework of Bayesian model comparison, which requires the computation of the Bayesian evidence, or global likelihood, i.e. the integral of the likelihood over the prior space for each model. The ratio of such evidences then gives the Bayes factor, representing the degree by which the Planck data have modified our a priori relative belief in each pair of models. From the Bayes factors, one can then evaluate the posterior probability for each model, and thus identify the "best" (in a Bayesian sense) model of inflation. The calculation of the Bayesian evidence of each of the *Encyclopædia Inflationaris* scenarios constitutes the main subject of the present paper.

This article is organised as follows. In the next section, section 2, we briefly present the theory of Bayesian inference and how it can be used to perform model comparison. In sub-section 2.1, we recall the definition of the Bayesian evidence and, in sub-section 2.2, we discuss how this quantity depends on the prior choices. In sub-section 2.3, we also introduce the Bayesian complexity and explains its meaning. In section 3, we discuss how the Bayesian evidences and complexities can be calculated efficiently and rapidly from the `ASPIC`[1] library. In sub-section 3.1, we present the idea behind the method introduced in ref. [6] (and used in the present article) and, in sub-section 3.2, we detail how the effective likelihood, which is the crucial tool of the method of ref. [6], can be determined from the Planck 2013 data. In sub-section 3.3, we describe the numerical methods used in order to calculate the evidences from the effective likelihood. We also specify the priors chosen on the non-primordial parameters. In sub-section 3.4, we briefly discuss the accuracy of our calculations and its limitations. Then, in section 4, we present our results, namely the numerical values of the evidence and complexity for all the models considered and we discuss the physical implications of our calculations. In section 5, we summarise our findings and present our conclusions. Finally,

[1] `http://cp3.irmp.ucl.ac.be/~ringeval/aspic.html`.

JCAP03(2014)039

in appendix A, we review in detail how the priors, for each model, have been chosen. Special attention has been paid to their physical origin and we discuss how the Bayesian evidence would be modified if the priors were changed.

2 Bayesian inference and model comparison

In this section, we briefly review Bayesian inference theory and Bayesian model comparison, which we adopt to compare the performance of the *Encyclopædia Inflationaris* scenarios.

2.1 Bayes factor and posterior model probability

Let $\mathcal{M}_i$ be a collection of $N^{\rm mod}$ models ($i = 1, \cdots, N^{\rm mod}$) describing a given physical situation. In this paper, we will denote by "model" a choice of inflationary potential, together with the specification of a prior distribution for its parameters. A given shape of the potential can support different prior choices, and we call the selection of a potential shape (without specification of a prior for its parameters) a "scenario". Thus within a given inflationary scenario there can be multiple models. The following considerations are however fully general. A model $\mathcal{M}_i$ is specified by a set of N_i parameters θ_{ij} (with $j = 1, \cdots, N_i$) and by the prior probability distribution of each of its parameters, namely $\pi(\theta_{ij}|\mathcal{M}_i)$. In the context of inference on the model's parameter (where the model is assumed to be correct), the prior can be set from the posterior of a previous observation. However, if one is interested in assessing a model's performance via Bayesian model comparison, it is preferable to understand the priors in terms of the a priori available parameter space under the theory represented by model $\mathcal{M}_i$ (see e.g. refs. [7–15] for further details).

Bayesian inference uses Bayes' theorem to update our degree of belief in hypotheses when some new data D becomes available (here, we think of D as the Cosmic Microwave Background - CMB - Planck data but the formalism is generic). Assuming that model $\mathcal{M}_i$ is true, from Bayes' theorem, the posterior probability of its parameters θ_{ij}'s can be expressed as

$$p\left(\theta_{ij}|D, \mathcal{M}_i\right) = \frac{1}{\mathcal{E}(D|\mathcal{M}_i)} \mathcal{L}\left(\theta_{ij}\right) \pi\left(\theta_{ij}|\mathcal{M}_i\right), \tag{2.1}$$

where $\mathcal{L}(\theta_{ij}) = p\left(D|\theta_{ij}, \mathcal{M}_i\right)$ is the likelihood function for the parameters of model $\mathcal{M}_i$. The quantity $\mathcal{E}(D|\mathcal{M}_i)$ is just a normalisation factor, called the Bayesian evidence or model likelihood, and it is given by

$$\mathcal{E}\left(D|\mathcal{M}_i\right) = \int \mathrm{d}\theta_{ij} \mathcal{L}(\theta_{ij}) \pi\left(\theta_{ij}|\mathcal{M}_i\right). \tag{2.2}$$

If we are only interested in constraining the parameters θ_{ij} of the model, then the Bayesian evidence can be neglected. However, in the following we shall focus on the question of assessing the posterior model's probability, for which the Bayesian evidence plays a central role.

Using again Bayes' theorem, one obtains the posterior probability of the model $\mathcal{M}_i$, which is given by

$$p(\mathcal{M}_i|D) = \frac{\mathcal{E}(D|\mathcal{M}_i)\pi(\mathcal{M}_i)}{p(D)}, \tag{2.3}$$

where $\pi(\mathcal{M}_i)$ is the prior belief in model $\mathcal{M}_i$. The quantity $p(D)$ is a normalisation factor (which only depends on the data but not on the model under consideration), given by

$$p(D) = \sum_i \mathcal{E}(D|\mathcal{M}_i)\pi(\mathcal{M}_i). \tag{2.4}$$

JCAP03(2014)039

$\lvert \ln B^i_{\rm REF} \rvert$	Odds	Strength of evidence
< 1.0	$\lesssim 3:1$	Inconclusive
1.0	$\sim 3:1$	Weak evidence
2.5	$\sim 12:1$	Moderate evidence
5.0	$\sim 150:1$	Strong evidence

Table 1. Jeffreys' scale for evaluating the strength of evidence when comparing two models, $\mathcal{M}_i$ versus a reference model $\mathcal{M}_{\rm REF}$, here slightly modified following the prescriptions given in refs. [15, 16].

When comparing two models against each other, this factor cancels. If one defines a "reference model", $\mathcal{M}_{\rm REF}$, against which all other models are compared, the posterior odds between a model $\mathcal{M}_i$ and the reference model are given by

$$\frac{p(\mathcal{M}_i|D)}{p(\mathcal{M}_{\rm REF}|D)} = B^i_{\rm REF}\frac{\pi(\mathcal{M}_i)}{\pi(\mathcal{M}_{\rm REF})}\,. \tag{2.5}$$

Here, we have introduced the Bayes factor $B^i_{\rm REF}$ which can be expressed as the ratio of the evidences, namely

$$B^i_{\rm REF} \equiv \frac{\mathcal{E}(D|\mathcal{M}_i)}{\mathcal{E}(D|\mathcal{M}_{\rm REF})}\,. \tag{2.6}$$

Under the principle of indifference, we can assume non-committal model priors, i.e. we give all models the same a priori probability, $\pi(\mathcal{M}_i) = 1/N^{\rm mod}$, in which case the Bayes factor becomes identical with the posterior odds. With this assumption, a Bayes factor larger (smaller) than one means a preference for the model $\mathcal{M}_i$ over the reference model (a preference for the reference model over $\mathcal{M}_i$). The "Jeffreys' scale", see table 1, gives an empirical prescription for translating the values of $B^i_{\rm REF}$ into strengths of belief.

With non-committal model priors, the posterior probability for model $\mathcal{M}_i$ is then given by

$$p(\mathcal{M}_i|D) = \frac{B^i_{\rm REF}}{\sum_j B^j_{\rm REF}}\,. \tag{2.7}$$

This implicitly further assumes that the list of $N^{\rm mod}$ is reasonably complete — i.e. that there isn't a yet undiscovered better models that have not been considered a priori (see ref. [17] for a Bayesian method leading to the discovery of such unknown models).

The fundamental idea underpinning Bayesian model comparison is that "economic" models that fit well the data while exhibiting strong predictivity are rewarded, while models with a large number of free parameters that turn out not to be required by the data are penalised for the wasted parameter space. Therefore, in a Bayesian sense, the "best" model is the one that achieves the best compromise between quality of fit and simplicity (see ref. [15, 18] for further details and ref. [19, 20] for a discussion of issues in Bayesian-frequentist calibrations). One of the attractive features of Bayesian model comparison is that it automatically embodies a quantitative version of Occam's razor, that is to say, the principle of simplicity (see ref. [21] for a critical discussion and comparison with frequentist methods). The price to pay is that the Occam's razor effect depends in an irreducible way on the choice of prior (and particularly on its range) hence the latter must be set according to physical considerations stemming from the model. We now turn to the crucial question of prior sensitivity.

JCAP03(2014)039

2.2 Prior sensitivity considerations

As mentioned above, since the priors $\pi(\theta_{ij}|\mathcal{M}_i)$ play a crucial role, a detailed description on how they have been chosen is provided for each model in appendix A. We also discuss how the evidence is affected by alternative prior choices within various theoretical scenarios. For this reason, the number of evidences presented in this paper is much larger than the number *Encyclopædia Inflationaris* scenarios. Indeed, a given field potential can support several prior choices motivated by different theories, each of them leading to different evidences. We thus consider them as different models.

For each field potential, physical considerations have been used to determine the shape of the prior. If a parameter is small but its order of magnitude is unknown, as it is typically the case for a coupling constant used in a perturbative expansion, then a Jeffreys' prior (uniform in the logarithm of the parameter) is the most uninformative. If, on the contrary, we deal with a parameter whose order of magnitude is known, then this is a scale parameter and a uniform prior on the parameter itself is appropriate. As priors must be proper (i.e., normalised), the support of the prior $[\theta_{\rm min}, \theta_{\rm max}]$ must also be chosen according to the natural values allowed by the underlying physical scenario. Indeed, the strength of the Occam's razor effect depends on this range, as generically the Bayesian evidence scales as (for uniform priors)

$$\mathcal{E}(D|\mathcal{M}_i) \propto \frac{1}{\theta_{\rm max} - \theta_{\rm min}}\,, \tag{2.8}$$

for cases where the support of the likelihood is much smaller than the support of the prior. However, since the Jeffreys' scale is logarithmic in the Bayes factor, the dependence on the prior range is relatively mild. Still, there are many cases in which $\theta_{\rm min}$ and $\theta_{\rm max}$ remain unspecified by the model. When this happens, attention has been paid on how the evidence is affected when this range is modified.

From the above argument it follows that one can estimate the variation in the evidence that one would get from a change of the range of the prior simply by rescaling it proportionally to the ratio of the prior volumes in the parameter space. This holds approximately true as long as the support of the likelihood is well within that of the prior. This is more detailed in appendix A where, if necessary, we discuss for each model how this calculation can be done in practice.

Another often-encountered situation is when the likelihood is flat along the θ_{ik} direction, i.e. the data are insensitive to one of the parameters of the model under consideration. In this case, the posterior for that parameter is identical to the prior and the Bayes factor reduces to unity — the Bayesian evidence is insensitive to the number of *unconstrained* parameters in a model. For such flat directions in parameter space, the prior boundary does not matter (as long as the likelihood stays flat), and the evidence is unchanged by a rescaling of the boundaries of the prior. A second quantity is thus required to measure the number of effective parameters that the data can constrain in a given model. This can be implemented in various way, as for instance by using Kullback-Leiber divergence between the prior and the posterior, leading to the notion of model complexity that we now discuss [15, 22, 23].

2.3 Bayesian complexity

The number of parameters in a model is a poor description of its "complexity", as parameters that are not constrained by the data should not be counted. A better evaluation of complexity (in a Bayesian sense) has been introduced by [24], who advocates using the relative entropy

JCAP03(2014)039

between the prior and the posterior distribution (i.e., the Kullback-Leibler divergence) as a better suited measure of the number of free parameters in a model that the data can actually constrain.

As shown in ref. [23], such an effective number of parameters, or Bayesian complexity, $\mathcal{C}$, can be written as

$$\mathcal{C}_i = \langle -2 \log \mathcal{L}(\theta_{ij}) \rangle + 2 \log \mathcal{L}\left(\theta_{ij}^{\rm ML}\right), \tag{2.9}$$

where $\langle \cdot \rangle$ denotes averaging over the posterior $p(\theta_{ij}|D, \mathcal{M}_i)$ and $\theta_{ij}^{\rm ML}$ is the maximum-likelihood estimate of the model's parameters which can be approximately obtained from the posterior samples used to map out the posterior distribution[2]. The Bayesian complexity is thus not an absolute measure of the number of constrained parameters — rather it assesses the constraining power of the data with respect to the measure provided by the prior.

The use of model complexity together with the Bayesian evidence allows us to distinguish between cases where $\mathcal{E}(D|\mathcal{M}_i) \simeq \mathcal{E}(D|\mathcal{M}_j)$ (i.e., two models exhibiting approximately the same Bayesian evidence) but $\mathcal{C}_i \simeq \mathcal{C}_j$, in which case the data is insufficient to distinguish between the two models (as their effective complexities are the same); or the case where $\mathcal{C}_i > \mathcal{C}_j$, which means that the data are sufficient to measure extra parameters of model i but that those parameters are not required by the evidence, in which case we ought to prefer model j, as the one with the smallest (measured) complexity.

3 Fast Bayesian evidence calculation

The computation of the Bayesian evidence can be a numerically demanding task, as it requires the evaluation of the multi-dimensional integral of eq. (2.2). This is particularly computationally intensive for Markov Chains Monte-Carlo (MCMC)-based methods. In recent years, a powerful tool has emerged in the shape of nested sampling, and its implementation in the `MultiNest` code [26, 27]. Even with such a highly efficient algorithm, the Bayesian evidence requires hundreds of thousands of likelihood evaluations for each model. A typical analysis based on the Planck likelihood coupled with an exact inflationary code to integrate the perturbations requires roughly 3×10^5 CPU hours (or 3.4 CPU years) of computing time on modern `x86_64` processors. Performing this for each model considered here would become prohibitively time consuming, even with high-performance computing.

In this section, we briefly describe the method introduced in ref. [6] which allows us to calculate the Bayesian evidences in a fraction of the time that would be required using conventional tools. We also mention the limitation of the method, especially the fact that the very low evidences may be poorly approximated.

3.1 Effective likelihood via slow-roll reparameterisation

Let us denote by $a_{\ell m}^{\rm obs}$ the CMB temperature map recently observed by the Planck satellite. From this map, one can estimate the measured multipole moments $C_\ell^{\rm obs} = \langle a_{\ell m}^{\rm obs} a_{\ell m}^{\rm obs\star} \rangle$. From the ΛCDM model (or any other post-inflationary history) and the scenario of inflation, one can compute the theoretical prediction for those multipole moments, $C_\ell^{\rm th}(\theta_{\rm s}, \theta_{\rm reh}, \theta_{\rm inf})$ as a function of the parameters in the model. Here, $\theta_{\rm s}$ represents a set of parameters describing post-inflationary physics, see eq. (3.12) for a precise definition, $\theta_{\rm reh}$ are the parameters of reheating and $\theta_{\rm inf}$ describe the shape of the potential $V(\phi)$. The reheating epoch can be

[2] See however ref. [25] for the caveats that apply when one wants to derive maximum likelihood estimates from Bayesian posterior maps.

JCAP03(2014)039

described either with $\theta_{\rm reh} = (\rho_{\rm reh}, \overline{w}_{\rm reh})$, namely the energy density of the universe at the end of reheating and the mean equation of state parameter during reheating; or with the completely generic rescaled reheating parameter $\theta_{\rm reh} = \ln(R)$, defined by

$$R \equiv R_{\rm rad} \frac{\rho_{\rm end}^{1/4}}{M_{\rm Pl}}, \qquad R_{\rm rad} \equiv \frac{a_{\rm end}}{a_{\rm reh}} \left(\frac{\rho_{\rm end}}{\rho_{\rm reh}}\right)^{1/4}. \tag{3.1}$$

Here the indices "end" and "reh" denote the end of inflation and end of the reheating era (i.e. the beginning of the radiation dominated era, see ref. [5] for further details), ρ and a being the energy density of the universe and the FLRW scale factor, respectively. Here, we have chosen to sample over the same optimised set discussed in refs. [6, 28–30], see also refs. [31, 32]. All possible reheating histories are sampled using the rescaled reheating parameter and with a prior uniform in its logarithm,

$$\pi(\theta_{\rm reh}) = \pi[\ln(R)] = U(-46, 15). \tag{3.2}$$

The boundaries of the prior support encompass all reheating histories satisfying the constraints that the mean equation of state during reheating verifies $-1/3 < \overline{w}_{\rm reh} < 1$, and $\rho_{\rm nuc} < \rho_{\rm reh} < \rho_{\rm end}$. The last inequality enforces that reheating takes place after inflation and before Big-Bang Nucleosynthesis (BBN). Practically, we have chosen $\rho_{\rm nuc}^{1/4} \equiv 10\,{\rm MeV}$. More details can be found in refs. [28–30, 33–37].

The expression for $C_\ell^{\rm th}$ can be written as

$$C_\ell^{\rm th}\left(\theta_{\rm s}, \theta_{\rm reh}, \theta_{\rm inf}\right) = \int_0^{+\infty} \frac{{\rm d}k}{k} j_\ell(k r_{\ell {\rm ss}}) T(k; \theta_{\rm s}) \mathcal{P}_\zeta(k; \theta_{\rm reh}, \theta_{\rm inf}), \tag{3.3}$$

j_ℓ being a spherical Bessel function, $r_{\ell {\rm ss}}$ the comoving radial distance to the last scattering surface, $T(k; \theta_{\rm s})$ the transfer function which describes the evolution of cosmological perturbations during the standard Friedmann-Lemaître eras and $\mathcal{P}_\zeta$ the inflationary power spectrum.

The posterior distribution for the parameters of interest is given by

$$p\left(\theta_{\rm s}, \theta_{\rm reh}, \theta_{\rm inf} | a_{\ell m}^{\rm obs}\right) = \frac{1}{\mathcal{E}} \mathcal{L}\left(\theta_{\rm s}, \theta_{\rm reh}, \theta_{\rm inf}\right) \pi\left(\theta_{\rm s}, \theta_{\rm reh}, \theta_{\rm inf}\right), \tag{3.4}$$

where $\mathcal{L}\left(\theta_{\rm s}, \theta_{\rm reh}, \theta_{\rm inf}\right) = p\left(a_{\ell m}^{\rm obs} | \theta_{\rm s}, \theta_{\rm reh}, \theta_{\rm inf}\right) \propto e^{-\chi^2(\theta_{\rm s}, \theta_{\rm reh}, \theta_{\rm inf})/2}$ is the likelihood function (and the normalisation constant in front is irrelevant), χ^2 being the effective chi-squared. The prior distribution $\pi\left(\theta_{\rm s}, \theta_{\rm reh}, \theta_{\rm inf}\right)$ describes our a priori state of knowledge about the values of the parameters before our information is updated. Notice that, for clarity, we have dropped the dependence on the model $\mathcal{M}$ under scrutiny. In eq. (3.4), $\mathcal{E}$ is the Bayesian evidence discussed in the previous section and reads

$$\mathcal{E} = \int {\rm d}\theta_{\rm s} {\rm d}\theta_{\rm reh} {\rm d}\theta_{\rm inf} \mathcal{L}\left(\theta_{\rm s}, \theta_{\rm reh}, \theta_{\rm inf}\right) \pi\left(\theta_{\rm s}, \theta_{\rm reh}, \theta_{\rm inf}\right). \tag{3.5}$$

It is the quantity we need to calculate for the 193 models considered here.

The effective chi-squared, and, therefore, the likelihood function, is a function of $C_\ell^{\rm th}$ and of the data, namely

$$\chi^2\left(\theta_{\rm s}, \theta_{\rm reh}, \theta_{\rm inf}\right) = \chi^2\left[C_\ell^{\rm th}\left(\theta_{\rm s}, \theta_{\rm reh}, \theta_{\rm inf}\right), a_{\ell m}^{\rm obs}, \Sigma\right], \tag{3.6}$$

JCAP03(2014)039

where Σ is the noise covariance matrix of the measurement. The above expression is only illustrative — in practice one has to deal with more complex issues, including foregrounds, instrumental systematics and the measurements of polarisation in addition to temperature [38]. Assuming that the post-inflationary physics is the same for all inflationary scenarios, different models have different evidences because they have a different power spectrum $\mathcal{P}_\zeta(k;\theta_{\rm reh},\theta_{\rm inf})$. In order to calculate the evidence of a given inflationary model, one must therefore evaluate $\mathcal{P}_\zeta(k;\theta_{\rm reh},\theta_{\rm inf})$ for the sampled values of $\theta_{\rm reh}$ and $\theta_{\rm inf}$, then perform the integral (3.5). In general, $\mathcal{P}_\zeta(k;\theta_{\rm reh},\theta_{\rm inf})$ is only known numerically and this procedure is computationally intensive.

It is, however, possible to speed up dramatically this calculation if one uses the fact that the inflationary models under consideration here are all slow-roll models. In that case, there exists a general parametrisation of the power spectrum which is given by (k_* is the pivot scale)

$$\begin{aligned}\mathcal{P}_\zeta(k) &= \mathcal{P}_0\left[a_0\left(\epsilon_n\right)+a_1\left(\epsilon_n\right)\ln\left(\frac{k}{k_*}\right)+\frac{1}{2}a_2\left(\epsilon_n\right)\ln^2\left(\frac{k}{k_*}\right)+\ldots\right]\\ &= P_*\left[1+\frac{a_1(\epsilon_n)}{a_0(\epsilon_n)}\ln\left(\frac{k}{k_*}\right)+\frac{a_2(\epsilon_n)}{a_0(\epsilon_n)}\ln^2\left(\frac{k}{k_*}\right)+\ldots\right],\end{aligned} \tag{3.7}$$

where ϵ_n are the Hubble-flow parameters evaluated at Hubble exit and $\mathcal{P}_0$ represents the overall normalisation [39, 40]. We have rendered explicit the well-measured quantity $P_* = a_0(\epsilon_n)\mathcal{P}_0 = \mathcal{P}_\zeta(k_*)$ which fixes the amplitude of the CMB anisotropies. The explicit form of the a_i's as functions of ϵ_n is known [41].

Furthermore, one can express the Hubble flow parameters as a function of the more fundamental inflationary parameters for every scenario. The explicit functionals $\epsilon_n(\theta_{\rm reh},\theta_{\rm inf})$ are all provided in the `ASPIC` library and in the *Encyclopædia Inflationaris*.

The central idea, introduced in [6], is that the likelihood function entering the evidence is invariant under a reparameterisation of the primordial power spectrum parameters. We can thus rewrite the multipole moments (and hence the likelihood function which depends on them) as $C_\ell^{\rm th}(\theta_{\rm s},\theta_{\rm reh},\theta_{\rm inf}) = C_\ell^{\rm th}\left[\theta_{\rm s}, P_*(\theta_{\rm reh},\theta_{\rm inf}), \epsilon_n(\theta_{\rm reh},\theta_{\rm inf})\right]$. The evidence of eq. (3.5) becomes

$$\mathcal{E} = \int \mathrm{d}\theta_{\rm s}\mathrm{d}\theta_{\rm reh}\mathrm{d}\theta_{\rm inf}\mathcal{L}\left[\theta_{\rm s}, P_*(\theta_{\rm reh},\theta_{\rm inf}), \epsilon_n(\theta_{\rm reh},\theta_{\rm inf})\right]\pi(\theta_{\rm s})\pi(\theta_{\rm reh},\theta_{\rm inf}) \tag{3.8}$$

$$= \int \mathrm{d}\theta_{\rm reh}\mathrm{d}\theta_{\rm inf}\mathcal{L}_{\rm eff}\left[P_*(\theta_{\rm reh},\theta_{\rm inf}), \epsilon_n(\theta_{\rm reh},\theta_{\rm inf})\right]\pi(\theta_{\rm reh})\pi(\theta_{\rm inf}), \tag{3.9}$$

where we have defined the effective likelihood, marginalised over the post-inflationary parameters, $\theta_{\rm s}$, as

$$\mathcal{L}_{\rm eff}\left[P_*(\theta_{\rm reh},\theta_{\rm inf}), \epsilon_n(\theta_{\rm reh},\theta_{\rm inf})\right] \equiv \int \mathrm{d}\theta_{\rm s} e^{-\frac{1}{2}\chi^2\left[C_\ell^{\rm th}(\theta_{\rm s},P_*,\epsilon_n),a_{\ell m}^{\rm obs},\Sigma\right]}\pi\left(\theta_{\rm s}\right). \tag{3.10}$$

In eq. (3.9) we have made the reasonable assumption that the prior on the post-inflationary, reheating and primordial parameters are separable,[3] i.e.

$$\pi(\theta_{\rm s},\theta_{\rm reh},\theta_{\rm inf}) = \pi(\theta_{\rm s})\pi(\theta_{\rm reh})\pi(\theta_{\rm inf}). \tag{3.11}$$

[3] More precisely, it is sufficient to require that $\pi(\theta_{\rm s},\theta_{\rm reh},\theta_{\rm inf}) = \pi(\theta_{\rm s})\pi(\theta_{\rm reh},\theta_{\rm inf})$. However, it is sensible to assume that the reheating and inflationary parameters are separable, too, thus leading to eq. (3.11).

JCAP03(2014)039

The effective likelihood, eq. (3.10), can be computed as a function of the slow-roll parameters, P_*, ϵ_n, using machine-learning algorithms to interpolate the functional form of $\mathcal{L}_{\rm eff}(P_*, \epsilon_n)$. Seen as a function of the slow-roll parameters, $\mathcal{L}_{\rm eff}$ needs only to be computed once for all inflationary models considered here. To then use it for a specific inflationary model, it is sufficient to map its potential parameters $\theta_{\rm inf}$ and reheating parameters $\theta_{\rm reh}$ onto the corresponding functionals, $P_*(\theta_{\rm inf}, \theta_{\rm reh})$, $\epsilon_n(\theta_{\rm inf}, \theta_{\rm reh})$.

The computational advantages of our method are twofold. First, the evaluation of the effective likelihood is very fast, since it is obtained as the output of a neural network interpolator (typically, one evaluation requires less than a μs of CPU-time on standard `x86_64` processor). Second, by integrating out once and for all the post-inflationary parameters from the likelihood, we are left with a much reduced parameter space over which the Bayesian evidence integral has to be computed. The dimensionality of $\theta_{\rm inf}$ is at most three, while the reheating is described by just one parameter, so that the Bayesian evidence integral is at most four-dimensional. Thanks to this vastly increased efficiency, we were able to compute a large number of Bayesian evidences with a much reduced numerical effort. More details about the method can be found in ref. [6].

3.2 Effective likelihood from Planck 2013

In order to determine $\mathcal{L}_{\rm eff}$, we have used the Planck 2013 data [42] together with the second order slow-roll expansion of the primordial power spectra for both the scalar and tensor perturbations. The full Planck likelihood is provided by the Planck collaboration [38]. Concerning the post-inflationary universe, it is assumed to be a flat ΛCDM model such that the parameters $\theta_{\rm s}$ are:

$$\begin{aligned}\theta_{\rm s} = \big(&\Omega_{\rm b}h^2, \Omega_{\rm dm}h^2, \tau, 100\theta_{\rm MC}, A_{100}^{\rm PS}, A_{143}^{\rm PS}, A_{217}^{\rm PS}, r_{143\times217}^{\rm PS}, A_{143}^{\rm CIB}, A_{217}^{\rm CIB}, r_{143\times217}^{\rm CIB}, \gamma^{\rm CIB},\\ &A_{\rm tSZ}, A_{\rm kSZ}, \xi^{\rm tSZ\times CIB}, c_{100}, c_{217}, \beta_1^1\big)\,.\end{aligned} \tag{3.12}$$

The usual ΛCDM parameters are the density of baryons $\Omega_{\rm b}$, of cold dark matter $\Omega_{\rm dm}$, the reduced Hubble parameter today h, the Thompson optical depth τ to last scattering and an angle, $\theta_{\rm MC}$, related to the angular size of the sound horizon on the last scattering surface [43]. The remaining parameters describe astrophysical signals on top of the CMB and any relevant instrumental distortions, as they have been modelled by the Planck collaboration [1]. They are the power contribution at $\ell = 3000$ of unresolved point sources at 100 GHz, at 143 GHz, at 217 GHz and their cross correlation ($A_{100}^{\rm PS}$, $A_{143}^{\rm PS}$, $A_{217}^{\rm PS}$, $r_{143\times217}^{\rm PS}$). The next are their equivalent for the Cosmic Infrared Background (CIB), namely $A_{143}^{\rm CIB}$, $A_{217}^{\rm CIB}$, $r_{143\times217}^{\rm CIB}$, and $\gamma^{\rm CIB}$ stands for the spectral index of the CIB angular power spectrum. The Sunyaev-Zel'dovich (SZ) signals, either thermal or kinetic, and their correlations with the CIB are encoded in the parameters $A_{\rm tSZ}$, $A_{\rm kSZ}$, $\xi^{\rm tSZ\times CIB}$. Finally, calibration and beam uncertainties are taken into account in the last three parameters. More details on how these signals are accounted for can be found in ref. [38].

Using the Planck likelihood and its associated public code `CLIK`, we have performed a MCMC exploration of the parameter space $(\theta_{\rm s}, P_*, \epsilon_1, \epsilon_2, \epsilon_3)$. In order to do so, we have used the public code `COSMOMC` [43] complemented by a modified version of the `CAMB` code [44] in order to implement as initial conditions the slow-roll primordial power spectra discussed above. All ϵ_n in these equations are evaluated at the conformal time η_* defined by $k_*\eta_* = -1$, $k_* = 0.05\,{\rm Mpc}^{-1}$ being the pivot scale.

The prior choices for the parameters $\theta_{\rm s}$ have been chosen as in ref. [1]. For the primordial parameter space, we have chosen a Jeffreys' prior for P_* such that $\ln(10^{10}P_*) \in [2.7, 4.2]$, i.e. centred around its well-measured value. The order of magnitude of the tensor-to-scalar

JCAP03(2014)039

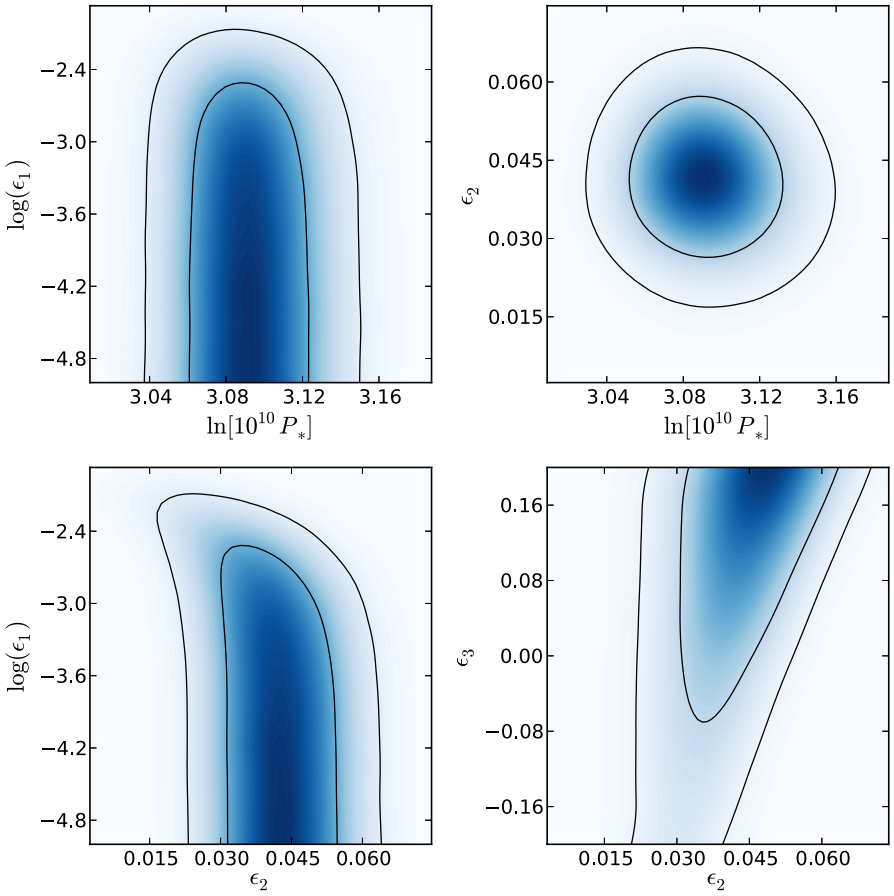

Figure 1. Two-dimensional marginalised posterior distributions of the slow-roll parameters (P_*, ϵ_1, ϵ_2, ϵ_3) using the Planck 2013 data.

ratio being unknown, we have chosen a wide Jeffreys' prior on ϵ_1 as $\log(\epsilon_1) \in [-5, -0.7]$, the upper bound being such that $\epsilon_1 < 0.2$ to be within the slow-roll approximation. Finally, for ϵ_2 and ϵ_3 we have chosen uniform priors in $[-0.2, 0.2]$. The MCMC exploration has been stopped once the total number of samples reached two millions, which corresponds to the R-statistics convergence of `COSMOMC` (the Gelman-Rubin criterion) to be less than 10^{-3} (see ref. [43]). The thus obtained two-dimensional marginalised posterior probability distributions for the slow-roll parameters are shown in figure 1. More details on the analysis can be found in ref. [6]. In particular, all the posteriors are compatible with those obtained by the Planck Collaboration in refs. [1, 3].

These MCMC samples have then be used to determine the effective likelihood for inflation $\mathcal{L}_{\rm eff}$ according to eq. (3.10), i.e. by marginalisation over all the $\theta_{\rm s}$. However, as shown in figure 1, ϵ_3 is not well constrained. Therefore, following ref. [6], it is more convenient to fit a three-dimensional likelihood $\mathcal{L}_{\rm eff}(P_*, \epsilon_1, \epsilon_2)$ by additionally marginalising over ϵ_3. Notice that doing so renders our analysis robust with respect to any uncertainties that are associated with the unconstrained second order terms. The fit itself have been implemented by a multivariate interpolation using a modified quadratic Shepard's method [45, 46]. Discussions on the method's accuracy can be found in ref. [6] and we emphasise that the effective likelihood is only well approximated within the bounds $\ln(\mathcal{L}_{\rm eff}^{\rm min}/\mathcal{L}_{\rm eff}^{\rm max}) = -10$. Lower values

JCAP03(2014)039

of the likelihood have been extrapolated by assuming Gaussian tails. As a result, for a given model, the contribution to the Bayesian evidence from regions in parameter space where the likelihood is smaller than this value are not reliable. In practice, this is unlikely to be problematic because the contribution of regions with exceedingly small likelihood values to the evidence integral is minimal. Furthermore, models that never achieve a large value of the likelihood are in any case clearly ruled out, even though the value for their Bayesian evidence is only approximate.

Let us also stress that, for our purpose, $\mathcal{L}_{\rm eff}(P_*, \epsilon_1, \epsilon_2)$ is now numerically known for any input values of P_*, ϵ_1 and ϵ_2 within the prior bounds mentioned earlier. As can be seen in the posterior of ϵ_1 (see figure 1), $\mathcal{L}_{\rm eff}$ has a flat direction for very small values of ϵ_1. As a result, and only for ϵ_1, $\mathcal{L}_{\rm eff}$ has been extrapolated by a constant along its flat direction for $\log(\epsilon_1) < -5$, without loss of accuracy.

3.3 Computing the evidences

From the effective likelihood, and within a given model of inflation, we have used the nested sampling algorithm `MultiNest` [26, 27] to perform the multidimensional integral of eq. (3.9). For each slow-roll scenario of the *Encyclopædia Inflationaris*, the analytic form of the functionals $\epsilon_n(\theta_{\rm reh}, \theta_{\rm inf})$ have been derived in ref. [5] and they have been numerically evaluated using the public code `ASPIC`. The evidences reported below have been obtained by requiring a `MultiNest` target accuracy of 10^{-4} on the evidence and a number of live points equals to 30000. Typically, this amounts to a few hundred thousand samples for each model and around one hour of CPU time. We have not reported any numerical error on the evidences because, with such a target accuracy, they remain completely negligible with respect to the prior sensitivity effects.

Moreover, for all of the models, we have traded the parameter M, namely the mass scale giving the normalisation of the potential $V(\phi)$, by the amplitude P_* of the scalar primordial power spectrum at the pivot wavenumber. Both of these parameters are indeed in one-to-one correspondence once the functionals $\epsilon_n(\theta_{\rm reh}, \theta_{\rm inf})$ are given, but using P_* instead of M has the advantage of minimising superfluous degeneracies in the parameter space, as does the choice of using the rescaled parameter R instead of $R_{\rm rad}$. From the Friedmann-Lemaître equation, one indeed has [6]

$$M^4 = 24\pi^2 \frac{\epsilon_1}{v_*} P_*, \tag{3.13}$$

at first order in slow-roll. Here $v_* \equiv V(\phi_*)/M^4$, and $\phi_* = \phi(\eta_*)$.

These prior choices have important consequences for the evidence calculation. They imply that, for all models tested, the prior space on both the reheating, and the potential normalisation are the same. As a result, the Occam's razor factors for those parameters cancel out when computing the Bayes' factor between two models (this can be seen at once by employing the Savage-Dickey density ratio, see [14, 15]). In other words, we assume that all models have the same ability to reheat the universe after inflation and to produce the observed amplitude of the CMB anisotropies. As definite reheating predictions are almost absent in all the models we have explored, and those same models do not predict definite values of M, this is a fair assumption.

However, if one imagines a situation in which M is an actual output of the model under scrutiny, its evidence should be reviewed. One may envisage two cases. Either the predicted values for M (and ϵ_1) yield a prior on P_* whose support is outside the range we have used, i.e. $\ln(10^{10}P_*) \in [2.7, 4.2]$ (see figure. 1), which is compatible with the data — in which case such a model would be ruled out; or it overlaps with it and the evidence should be

JCAP03(2014)039

recomputed by sampling the parameter space directly over M. In the situation for which the model's predictions for M would actually match very well the observed amplitude of the CMB anisotropies, one should expect the Bayesian evidence of that precise model to be boosted in accordance with the Occam's razor principle. The same remarks hold concerning the reheating parameter [47]. Let us stress, however, that we have not encountered such a situation in all the models tested here.

3.4 Fine-tuning issues

For some of the models presented here, the slow-roll regime of inflation takes place only for a very limited range of values for some of their parameters. Such "fine-tuning" of parameters which have, a priori, no reason to take exactly such specific values, is disfavoured by the Occam's razor penalty in-built into the Bayesian evidence. From a technical point of view, the likelihood can reliably be worked out only in regimes where the slow-roll is (at least roughly) valid. Otherwise, the inflationary dynamics is very difficult to track and not described by our modelisation. On the other hand, when the slow-roll is completely violated, one knows that the associated predictions are ruled out by observations, and that the likelihood in this region of parameter space, being essentially 0, does not contribute to the the total evidence. Therefore such situations result into an Occam's razor effect which suppresses the evidence computed over "compatible" parameters (the ones for which slow-roll inflation exist) by a factor equal to the ratio of the volume of compatible parameters over the whole prior volume. For the models in which this occurs, we have added some discussions in the appendix.

4 Results and discussion

For all the models listed in the appendix A, i.e. $N^{\mathrm{mod}} = 193$, we have computed the Bayes factors B^i_{HI} with respect to the Starobinsky model [48–50] or Higgs Inflation (HI), which is our reference model. We have also evaluated each model's Bayesian complexity $\mathcal{C}_i$.

Our main results are displayed in figure 2, which represents all the Bayes factors. Each model is represented by a horizontal bar indicating the value of $\ln B^i_{\mathrm{HI}}$. A bar extending to the left corresponds to $\ln B^i_{\mathrm{HI}} < 0$ and the model under consideration is disfavoured with respect to the the reference model. If, on the contrary, the bar extends to the right, then $\ln B^i_{\mathrm{HI}} > 0$ and the model is preferred to Higgs inflation. Obviously, the Bayes factor of the reference model is one and, therefore, its logarithm vanishes: this is why there is no bar for HI. In front of (or inside) each bar, we have reported the exact numerical value of $\ln B^i_{\mathrm{HI}}$. We have also included the Jeffreys' scale of table 1, as dashed vertical lines, as an indication of the viability of a given model compared to HI.

Bars are colour-coded according to the Schwarz-Terrero-Escalante (STE) classification associated with the slow-roll parameters of the model under consideration [40]. Following the notation used in ref. [5], region 1 are models predicting $\epsilon_2 > 2\epsilon_1 > 0$, i.e. the kinetic energy increases during inflation as well as the ratio of the kinetic energy to the total energy. Region 2 stands for potentials associated with $0 < \epsilon_2 < 2\epsilon_1$ for which the kinetic energy decreases while the ratio of the kinetic energy to the total energy still increases. Finally, region 3 is such that both quantities decrease during inflation. As shown in ref. [5], the Planck 2013 results disfavour models living in regions 2 and 3 and the Bayes factors also reflect this. Let us stress that the parameter space of some models may span more than one region, i.e. for some values of its parameters the predictions of a model can fall in region 1 (say) while, for some other regime, they can be in region 2. It is referenced in the captions of figure 2 where the colour code takes this fact into account.

JCAP03(2014)039

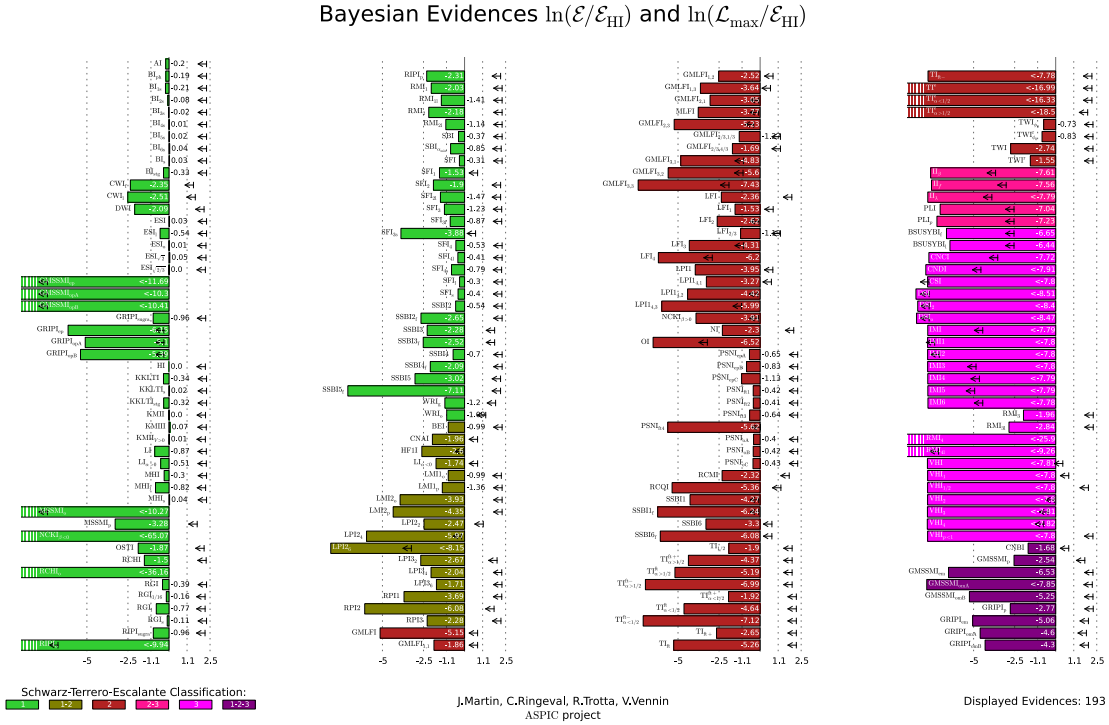

Figure 2. Bayes factors (bars) and absolute upper bound to the Bayes factors (arrows) for the *Encyclopædia Inflationaris* inflationary scenarios, with Higgs inflation as the reference model (see the text for a more accurate description).

JCAP03(2014)039

Finally, for each model, we have also calculated the maximum value of the evidence, that is to say the value that is obtained when all the prior mass for the model under consideration is concentrated in a delta-function centred at the maximum likelihood location. Clearly, in that case, one has $\mathcal{E}_{\rm max} = \mathcal{L}_{\rm max}$. It represents an absolute upper bound on the evidence: any choice of priors necessarily leads to a value of the evidence smaller than $\mathcal{E}_{\rm max}$. This upper bound is represented by black left-pointing arrows in figure 2. Let us also remark that this quantity would be relevant in a frequentist analysis where the p-value obtained from the maximum likelihood ratio would be used to compare the performances of different models.

Let us now analyse our results in more detail. Firstly, the answer to the central question of this paper, namely "what is the best model of inflation given the Planck 2013 data?" is KMIII inflation [51–53], whose Bayes factor with respect to Higgs inflation is $\ln B_{\rm HI}^{\rm KMIII} = 0.07 > 0$. However, the preference is extremely mild, so much so that it is within the margin of uncertainty of our analysis, and for all practical purposes KMIII inflation has to be regarded as being on the same footing with Higgs inflation, from the point of view of the Planck data.

We can use the Jeffreys' scale as an indication for which of the models remain viable, and which are disfavoured at various levels of evidence with respect to the best models. We find 52 models in the "inconclusive" region (with respect to the best model), 41 in the "weakly disfavoured" region, 34 in the "moderately disfavoured" region and 66 in the "strongly disfavoured". Therefore, our analysis concludes that surviving models (i.e. those in the "inconclusive" region) represent 26% of the total. On the contrary, the number of models that are conclusively ruled out (i.e. those in the "strong" region) represent 34% of the total numbers of models. The models in the "inconclusive region", which are to be considered the best models of inflation after the Plank data, are (in alphabetical order):[4] AI, $\rm BI_{ph}$, $\rm BI_{s}$, $\rm BI_{1s}$, $\rm BI_{2s}$, $\rm BI_{3s}$, $\rm BI_{4s}$, $\rm BI_{5s}$, $\rm BI_{6s}$, $\rm BI_{stg}$, ESI, $\rm ESI_{l}$, $\rm ESI_{\sqrt{2/3}}$, $\rm ESI_{\sqrt{2}}$, $\rm ESI_{o}$, HI, KKLTI, $\rm KKLTI_{s}$, $\rm KKLTI_{stg}$, KMIII, KMII, $\rm KMII_{V>0}$, LI, $\rm LI_{\alpha>0}$, MHI, $\rm MHI_{l}$, $\rm MHI_{s}$, $\rm PSNI_{ft1}$, $\rm PSNI_{ft2}$, $\rm PSNI_{ft3}$, $\rm PSNI_{oA}$, $\rm PSNI_{oB}$, $\rm PSNI_{oC}$, $\rm PSNI_{epA}$, $\rm PSNI_{epB}$, RGI, $\rm RGI_{s}$, $\rm RGI_{l}$, $\rm RGI_{1/16}$, SBI, $\rm SBI_{\alpha_{min}}$, SFI, $\rm SFI_{3l}$, $\rm SFI_{4}$, $\rm SFI_{4l}$, $\rm SFI_{4s}$, $\rm SFI_{l}$, $\rm SFI_{s}$, SSBI2, SSBI4, $\rm TWI_{\phi_0}$ and $\rm TWI^{r}_{\phi_0}$. As explained above, there are more models than potential shapes because a given potential can support different priors, which are considered as separate model choices. As a consequence, the above 52 models in the "inconclusive region" encompass only 15 different potentials or scenarios.

Further insight can be garnered by considering the Bayesian complexity for each *Encyclopædia Inflationaris* model. We are particularly interested in evaluating the number of unconstrained parameters for the best models identified via the Bayesian evidence, i.e. the ones that are in the "inconclusive region". Since the Bayesian complexity measures the number of effective parameters supported by the data, one can define a measure of the number of unconstrained parameters by

$$N_i^{\rm uc} \equiv N_i - \mathcal{C}_i, \tag{4.1}$$

where N_i is the total number of free parameters of the model under consideration, i.e. the inflationary potential parameters, plus the reheating parameter. For models providing a reasonable good fit to the Planck data, one expects $N_i^{\rm uc} \geq 0$. However, if the best-fit log-likelihood of a given model is very poor, then the Bayesian complexity can be arbitrary large, as the second term in eq. (2.9) is large. This means that for such models $N_i^{\rm uc} < 0$. So we expect a negative measure of the number of unconstrained parameters to be correlated with a small value of the Bayes factor.

[4] The meaning of the different acronyms and the precise definition of the corresponding models can be found in appendix A.

JCAP03(2014)039

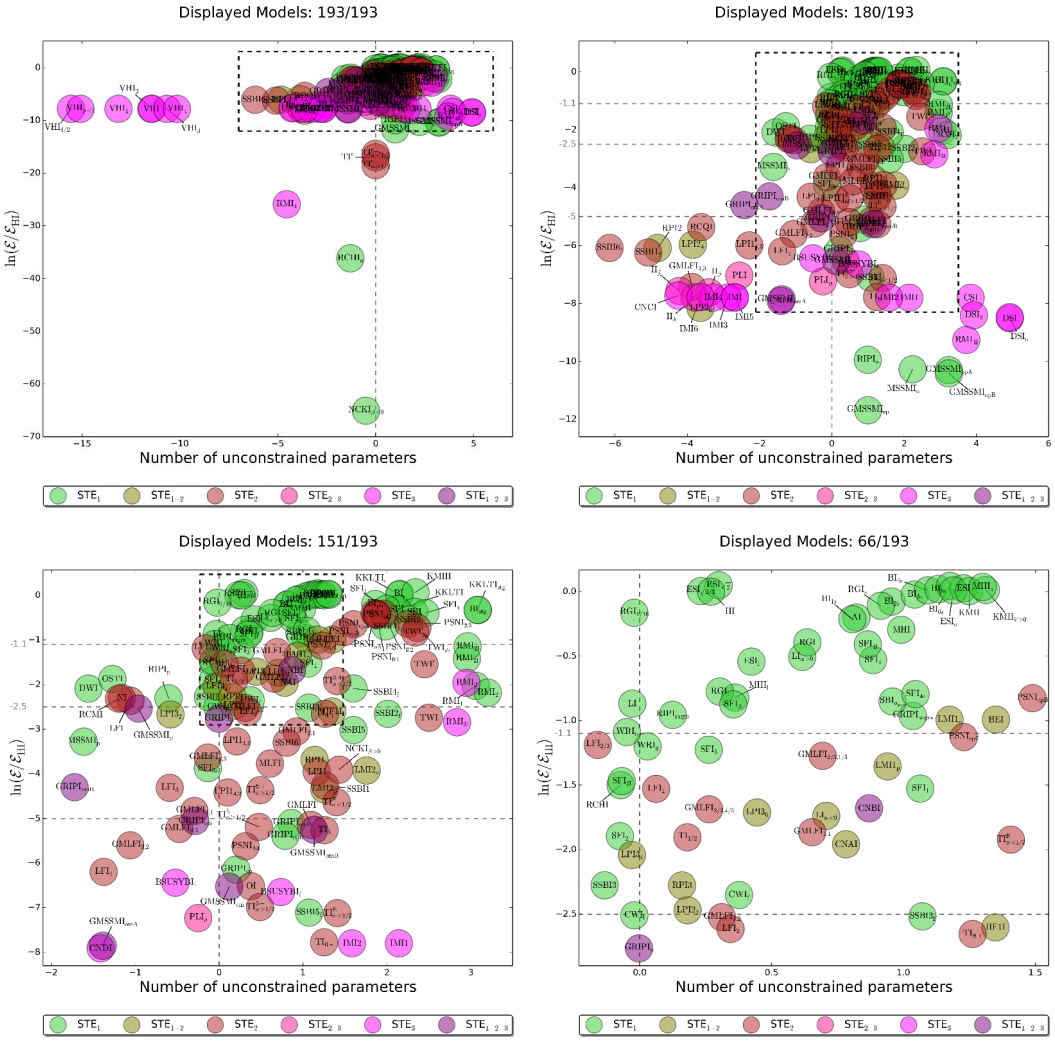

Figure 3. Logarithm of the Bayes factor versus the number of unconstrained parameters $N^{\rm uc}$ for all the inflationary models investigated. The $N^{\rm uc}$ dimension allows us to disambiguate models with the same evidence, by preferring those with the smallest number of unconstrained (i.e., unnecessary) parameters. Optimal models are clustered around Higgs Inflation and have $N^{\rm uc} \simeq 0$ together with $B_{\rm HI} \gtrsim 0$. The four plots (from upper left to bottom right) increasingly zoom into the "best region". Each model is represented by a filled circle for illustration purposes only, and the radius of a circle has no meaning.

In figure 3, we have plotted the location of all models in the two-dimensional plane $(N^{\rm uc}, \ln B_{\rm HI})$. Models appearing along the same horizontal lines have thus the same Bayes factor but different number of unconstrained parameters $N^{\rm uc}$. Models with the smallest, non-negative number of unconstrained parameters are to be preferred in that they can be deemed to be simpler, even if they have the same evidence as other models with a larger value of $N^{\rm uc}$.

We can observe in figure 3 that models with $N^{\rm uc} < 0$ do have poor values of the evidence as well ($\ln B^i_{\rm HI} \ll 0$), as expected from the above argument. Focusing on the models having the best evidences together with a minimal number of unconstrained parameters,

JCAP03(2014)039

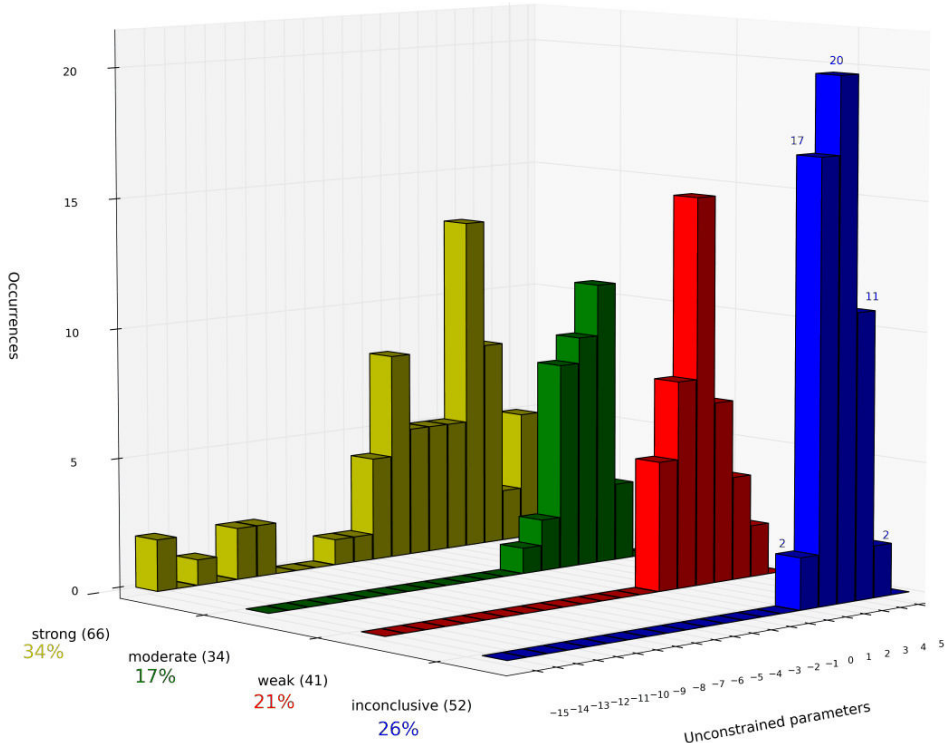

Figure 4. Histogram of the *Encyclopædia Inflationaris* models within the four Jeffreys' categories (inconclusive: blue, weakly disfavoured: red, moderately disfavoured: green and strongly disfavoured: yellow) and for different number of unconstrained parameters. The number of preferred models is 17, corresponding to 9 different types of potential.

i.e. $0 < N_i^{\rm uc} < 1$ narrows down the slow-roll landscape to a few preferred models: AI, $\mathrm{BI}_{1\mathrm{s}}$, $\mathrm{BI}_{2\mathrm{s}}$, ESI_{1}, $\mathrm{ESI}_{\sqrt{2/3}}$, $\mathrm{ESI}_{\sqrt{2}}$, HI, $\mathrm{LI}_{\alpha>0}$, MHI, MHI_{1}, RGI, $\mathrm{RGI}_{\mathrm{s}}$, RGI_{1}, $\mathrm{SBI}_{\alpha_{\rm min}}$, $\mathrm{SFI}_{3\mathrm{l}}$, SFI_{4} and $\mathrm{SFI}_{4\mathrm{l}}$. We have now 17 preferred models, that is to say roughly 9% of the initial numbers of models. They correspond to only 9 types of potential or scenarios. It is also interesting to notice that KMIII is not in this set of preferred models since it has $N^{\rm uc}_{\rm KMIII} \simeq 2.3$. While it cannot be concluded that the models with the best Bayes factors and $0 < N_i^{\rm uc} < 1$ are the "true" models, they are the simplest and most effective inflationary hypotheses that are compatible with the Planck 2013 CMB data. Obviously, allowing for more unconstrained parameters increases this list as displayed in figure 3.

Another interesting remark is that the 9 potentials mentioned above all belong to region 1 in the Schwarz-Terrero-Escalante classification (i.e. there are all "green"). This is of course consistent with the findings of ref. [5] which has shown that this region is the region favoured by the Planck data. This means that the corresponding models all belong to "plateau inflation" for which the potential does not necessarily grows to infinity when the *vev* of the field increases [54]. This type of potentials clearly appears to be the winners given the Planck data.

5 Conclusions

Let us now recap our main findings. Although this paper deals with slow-roll single-field inflation only, we do not expect multifield inflationary models to perform better than the

JCAP03(2014)039

optimal subset of single-field models that have been delineated in this work. This is because adding a field necessarily introduces extra-parameters encoding the shape of the potential in this new direction. Therefore, even if a multifield scenario would fit as well the Planck 2013 data as the best slow-roll single-field models, such a model would be penalised by its larger number of unconstrained parameters (in terms of complexity). This conclusion could be modified if a multifields model was able to fit the large scales glitches in the Planck data, thus achieving a better evidence. However, those glitches are of relatively weak statistical significance and cannot, currently, greatly improve the overall fit. Furthermore, the fit improvement would have to be sufficient to offset the extra Occam's factor penalty implied by additional free parameters. Such a situation may however change by considering additional and independent data sets which could not be fitted by the class of slow-roll models discussed in this paper such as, for instance, a small, but non-vanishing, level of non-Gaussianities. The same remarks also apply for single-field scenarios with non-minimal kinetic terms (or with features in the potential). These models are not necessarily ruled out. However, either they predict observable non-Gaussianities and the fact that Planck sees a Gaussian sky implies that those models will be penalised for this wasted parameter space. Or, they genuinely do not predict non-Gaussianities but introduce additional parameters that increase the model complexity (see for instance ref. [55–57]). Let us stress that, if we are not considering the small gain that might be associated with fitting Planck's glitches, the favoured models we have singled out in this paper already saturate the maximal possible value for the likelihood. As a result, even in the situation in which we would have missed an extremely good fitting and simple model, its Bayesian evidence would still be in the "inconclusive region".

Therefore, from a Bayesian point of view, it appears perfectly legitimate to focus on single-field slow-roll inflation (with a minimal kinetic term). These models have been studied and compared to the recent Planck data in ref. [5] which, therefore, represents a complete cartography of the inflationary landscape compatible with the most recent data. In the present article, we have computed the Bayes factors and the Bayesian complexity for all these *Encyclopædia Inflationaris* models. Our results are summarised in an histogram in figure figure 4, which gives the number of models in each Jeffreys' category (defined with respect to the best model) and for each number of unconstrained parameters with $n < N^{\mathrm{uc}} < n+1$, where n is an integer. This plot illustrates the power of the Planck data and allows us to summarise our main results: from a large number of models, one is able to single out a relatively small subset corresponding to the "best models". We rule out $\simeq 34\%$ of the models at a strong level of evidence and $\simeq 26\%$ of the models (9% if one includes the complexity) are preferred. All the favoured scenarios belong to the category 1 of the the Schwarz-Terrero-Escalante classification and have a shape consistent with "plateau inflation".

It is also worth pointing out that a few Bayesian evidences have been calculated in ref. [3]. The comparison is, however, difficult to carry out since the priors on reheating assumed in that paper greatly differ from those considered here.[5] Indeed, in ref. [3], a prior on ΔN_* is chosen while the reheating energy density is arbitrarily fixed. There is no physical motivations for picking up particular values of the reheating energy density. Moreover, choosing a prior on ΔN_* is surprising since this does not guarantee the validity of the physical prior,

[5]Let us also stress that the description made by refs. [3] of the work of ref. [29] on reheating is incorrect. It is claimed that the study of ref. [29] is restricted to equations of state of the form $\overline{w}_{\mathrm{reh}} = (p-2)/(p+2)$, which emerges in the case of a potential with the shape $\propto \phi^p$. This situation was indeed considered in ref. [29] but only as a particular example. The completely generic case $-1/3 < \overline{w}_{\mathrm{reh}} < 1$ was in fact the main concern of ref. [29].

JCAP03(2014)039

namely $\rho_{\rm nuc} < \rho_{\rm reh} < \rho_{\rm end}$. Another side effect is that this obviously modifies the calculation of the Bayesian evidences and, for this reason, comparing the two approaches does not lead to interesting insights.

To conclude this paper, let us present some speculations regarding what we have learnt about the physics of inflation. Firstly, let us stress that we have finally carried out one of the long standing task of primordial cosmology, namely put constraints on the shape of the inflationary potential. In some sense, this represents quite an impressive achievement since we are able to say something about physics at energy scales unreachable in accelerators. Indeed, with the Large Hardron Collider (LHC), it would obviously be impossible to establish the existence, at the Grand Unified Scale (GUT) scale, of a scalar field with a potential having a plateau shape. This perfectly illustrates the fact that cosmology can teach us something about high energy physics. On the other hand, this conclusion should be toned down: certainly, we have learnt a lot about the early Universe but, clearly, this does not give us the Lagrangian of particle physics at the GUT scales (i.e. the field content, their interactions etc ...). As a consequence, our knowledge of physics at such a high energy scale remains very limited. Hopefully, future analysis will help us to learn more about these questions. In this respect, constraining the reheating temperature of all the *Encyclopædia Inflationaris* models seems promising since this can tell us something about the interaction of the inflaton field with the rest of the world.

Finally, one cannot help making the connection between the results obtained here and the recent works about "conformal inflation" [49, 50, 58–66]. It is well-known that it is difficult to control the flatness of the inflaton potential that can easily be destroyed by quantum corrections. However, if one starts with any shape of $V(\phi)$, not necessarily very flat, and assumes a non-minimal coupling (for instance, of the form $\xi\phi^2 R$), then, in the Einstein frame, the potential automatically flattens out and, precisely takes the form of plateau inflation for some range of the field. A striking example is provided in figure 4 of ref. [61]: far from the origin, the potential automatically acquires the typical shape found in the present article to be favoured by the Planck data (see in particular right bottom of figure 4). Let us stress at this point that, although non-minimally coupled to gravity, this class of models belong to the `ASPIC` category since, after a conformal transformation to the Einstein frame, these models are in fact equivalent to single-field slow-roll inflation. In this representation, the non-triviality of the non-minimal coupling has been "transferred" to the complicated, non-minimal, interaction of ϕ with the other degrees of freedom present in the early Universe. In fact, Higgs inflation is the prototypical example of this class of scenarios and the ingredients necessary to describe the reheating phase in this case have been described in ref. [5]. Therefore, we are in a situation where two strong theoretical arguments (the flatness of the potential and the presence of a non-minimal coupling to gravity — recalling that, according to the standard lore, a term that is not forbidden by a symmetry must be present in the theory) point precisely to the models that appear favoured by recent data. Whether this is just a coincidence or whether we are starting to understand something deeper about Nature will hopefully be answered in the near future when even more accurate data become available.

Acknowledgments

This work is partially supported by the ESA Belgian Federal PRODEX Grant No. 4000103071 and the Wallonia-Brussels Federation grant ARC No. 11/15-040.

JCAP03(2014)039

A Choice of priors for inflationary models

In this appendix we detail the priors used in this article, and report the corresponding Bayesian evidences, complexities, number of parameters and likelihoods at the best fit point of all *Encyclopædia Inflationaris* scenarios. The priors are directly transcribed from considerations presented in ref. [5], which is assumed to be known to the reader.

As discussed in section 2.2, there are cases where it is difficult to numerically estimate the evidences. In particular, this happens when one tries to extend the prior ranges in order to study the impact of the prior choices on our physical conclusions. However, most of the time, this prior sensitivity can be trivially accounted for by means of simple analytical calculations that we now briefly review. There are few instances in the following where they are concretely used.

A common situation is when the support of the likelihood is included in the prior range $[\theta_{\rm min}, \theta_{\rm max}]$, i.e. $\mathcal{L}(D|\theta, \mathcal{M}) \simeq 0$ for $\theta \notin [\theta_{\rm min}, \theta_{\rm max}]$. The evidence of a model $\mathcal{M}$ is given by

$$\mathcal{E}(D|\mathcal{M}) = \int_{\theta_{\rm min}}^{\theta_{\rm max}} \mathrm{d}\theta \mathcal{L}(D|\theta, \mathcal{M}) \pi(\theta|\mathcal{M}), \tag{A.1}$$

where, for simplicity, we have assumed that there is only one parameter, θ (the argument can be generalised to any dimensions). For any proper (i.e., normalised) prior distribution $\pi(\theta|\mathcal{M})$, one has

$$\pi(\theta|\mathcal{M}) = \frac{\Pi(\theta)}{\displaystyle\int_{\theta_{\rm min}}^{\theta_{\rm max}} \mathrm{d}\theta\, \Pi(\theta)}, \quad \text{with} \quad \int_{\theta_{\rm min}}^{\theta_{\rm max}} \mathrm{d}\theta\, \pi(\theta|\mathcal{M}) = 1. \tag{A.2}$$

Let us assume that we change the prior range for the parameter θ and consider a new upper bound $\bar{\theta}_{\rm max}$. The new prior is now given by

$$\pi(\theta|\mathcal{M}) = \frac{\Pi(\theta)}{\displaystyle\int_{\theta_{\rm min}}^{\bar{\theta}_{\rm max}} \mathrm{d}\theta\, \Pi(\theta)}, \tag{A.3}$$

where, in accordance with the above discussion, the likelihood is vanishing in $[\theta_{\rm max}, \bar{\theta}_{\rm max}]$. As a consequence, the value of the evidence for the larger prior range is given by

$$\bar{\mathcal{E}}(D|\mathcal{M}) = \int_{\theta_{\rm min}}^{\bar{\theta}_{\rm max}} \mathrm{d}\theta \mathcal{L}(D|\theta, \mathcal{M}) \pi(\theta|\mathcal{M}) = \mathcal{E}(D|\mathcal{M}) \frac{\displaystyle\int_{\theta_{\rm min}}^{\theta_{\rm max}} \mathrm{d}\theta\, \Pi(\theta)}{\displaystyle\int_{\theta_{\rm min}}^{\bar{\theta}_{\rm max}} \mathrm{d}\theta\, \Pi(\theta)}, \tag{A.4}$$

and is obtained from the previous evidence value by simply rescaling it by the ratio of the prior volumes.

If instead the likelihood is flat along the θ direction, i.e. the data do not constrain the parameter under consideration, $\mathcal{L}(D|\theta, \mathcal{M}) = \mathcal{L}_0$, then the evidence is unchanged by modifying the prior bounds

$$\bar{\mathcal{E}}(D|\mathcal{M}) = \int_{\theta_{\rm min}}^{\bar{\theta}_{\rm max}} \mathrm{d}\theta \mathcal{L}(D|\theta, \mathcal{M}) \pi(\theta|\mathcal{M}) = \mathcal{L}_0 \int_{\theta_{\rm min}}^{\bar{\theta}_{\rm max}} \mathrm{d}\theta\, \pi(\theta|\mathcal{M}) = \mathcal{L}_0 = \mathcal{E}(D|\mathcal{M}), \tag{A.5}$$

and one should evaluate the Bayesian complexity to distinguish between the models.

JCAP03(2014)039

Let us notice that the complexity may also be modified when the prior range is extended to regions where the likelihood is known to be negligible. However, contrary to the evidence, there is no simple analytical treatment of how the complexity should be extrapolated in this case. One can nevertheless make further simplifying assumptions to roughly estimate how the complexity is sensitive to the choice of priors.

Assuming that the prior and likelihood distributions are Gaussian, the complexity is given by [23]

$$\mathcal{C} = \sum_{i=1}^{N} \frac{1}{1 + \left(\frac{\sigma^i_{\mathcal{L}}}{\sigma^i_{\Pi}}\right)^2} \simeq \frac{N}{1 + \left(\frac{\sigma_{\mathcal{L}}}{\sigma_{\Pi}}\right)^2}\,, \tag{A.6}$$

where N is the number of parameters, σ^i_{Π} and $\sigma^i_{\mathcal{L}}$ are the prior width and the standard deviations of the likelihood covariance matrix along its eigendirections i, respectively. The last approximation in the above equation assumes that one can define the averaged values σ_{Π} and $\sigma_{\mathcal{L}}$ over all the eigendirections. If the prior is widened along n directions (chosen among the N parameters), its averaged volume σ^n_{Π} gets multiplied by the same ratio $\bar{\mathcal{E}}/\mathcal{E}$ as computed above, i.e.

$$\sigma_{\bar{\Pi}} = \sigma_{\Pi} \left(\frac{\mathcal{E}}{\bar{\mathcal{E}}}\right)^{\frac{1}{n}}\,. \tag{A.7}$$

Plugging back this relation in eq. (A.6), one gets

$$\bar{\mathcal{C}} = \frac{N}{1 + \left(\frac{\bar{\mathcal{E}}}{\mathcal{E}}\right)^{2/n} \left(\frac{N}{\mathcal{C}} - 1\right)}\,, \tag{A.8}$$

where $\bar{\mathcal{E}}/\mathcal{E}$ is given by a volume ratio of the type eq. (A.4).

In the next subsections, we discuss, for each *Encyclopædia Inflationaris* scenarios, our choice of priors. We also give the definition of all the acronyms used in the paper, in particular in figure 2.

A.1 Higgs inflation (HI)

The Higgs inflation model the potential of which is given by [5]

$$V(\phi) = M^4 \left(1 - e^{-\sqrt{2/3}\phi/M_{\rm Pl}}\right)^2\,, \tag{A.9}$$

which contains only one parameter: the mass scale M. However, as discussed in section 3.3, this one has been traded for P_* in our analysis and there are no other free parameter in this potential. In total, including the reheating parameter, one ends up with a two-parameters model. For this reason, and besides the fact that it was actually the first model of inflation ever proposed, we have chosen to take HI as the "reference model".

Name	Priors	$\ln\left(\mathcal{E}/\mathcal{E}_{\rm HI}\right)$	$\mathcal{C}$	N	$\ln\left(\mathcal{L}_{\rm max}/\mathcal{E}_{\rm HI}\right)$
HI	–	0.00	1.73	2	2.22

JCAP03(2014)039

A.2 Radiatively corrected Higgs inflation (RCHI)

This model is a one-parameter model. The shape of the potential reads [5]

$$V(\phi) = M^4 \left(1 - 2e^{-2/\sqrt{6}\phi/M_{\rm Pl}} + \frac{A_{\rm I}}{16\pi^2}\frac{\phi}{\sqrt{6}M_{\rm Pl}}\right). \tag{A.10}$$

The parameter $A_{\rm I}$ controls the amplitude of the radiative corrections to the, tree level, HI potential. The one-loop expansion is valid under the condition $A_{\rm I} \ll 64\pi^2$, hence the physical prior $A_{\rm I} \in [-100, 100]$. However, numerically, when $A_{\rm I} < -65$, the likelihood is so small that it cannot be calculated in a reliable way. As a consequence, we choose the numerical prior to be $A_{\rm I} \in [-65, 100]$. Anyhow, as already mentioned, the range $A_{\rm I} \in [-100, -65]$ does not contribute to the likelihood. On the other hand, as discussed in ref. [5], particle physics implies $-48 < A_{\rm I} < -20$ and this defines a new model, the "original" one, that we denote RCHI$_{\rm o}$ in the following. We thus have two possible priors for this scenario as indicated by the following table:

Name	Priors	$\ln(\mathcal{E}/\mathcal{E}_{\rm HI})$	$\mathcal{C}$	N	$\ln(\mathcal{L}_{\rm max}/\mathcal{E}_{\rm HI})$
RCHI	$A_{\rm I} \in [-65, 100]$	-1.50	3.07	3	2.26
RCHI$_{\rm o}$	$A_{\rm I} \in [-48, -20]$	-36.16	4.29	3	-28.87

A.3 Large field inflation (LFI)

Large field inflation is characterised by the following potential [5]

$$V(\phi) = M^4 \left(\frac{\phi}{M_{\rm Pl}}\right)^p. \tag{A.11}$$

This potential depends on a mass scale M fixed by the CMB normalisation and a free index p of $\mathcal{O}(1)$ that can also take specific integer or rational values. Hence, one may assume a general prior on p such that one can calculate the evidence of this class of model. Here one takes $p \in [0.2, 5]$ because, for $p > 5$, one already knows that the models are ruled out and $p > 0.2$ instead of $p = 0$ for numerical reasons (in addition, the potential cannot be completely flat since one needs to stop inflation). Another possibility is simply to fix p to some interesting values: $p = 2/3$ corresponds to monodromy inflation [67] while $p = 1, \cdots, 4$ represents interesting phenomenological scenarios.

Name	Priors	$\ln(\mathcal{E}/\mathcal{E}_{\rm HI})$	$\mathcal{C}$	N	$\ln(\mathcal{L}_{\rm max}/\mathcal{E}_{\rm HI})$
LFI	$p \in [0.2, 5]$	-2.36	4.06	3	1.93
LFI$_{2/3}$	$p = 2/3$	-1.19	2.16	2	1.24
LFI$_1$	$p = 1$	-1.53	1.94	2	0.79
LFI$_2$	$p = 2$	-2.62	1.66	2	-0.08
LFI$_3$	$p = 3$	-4.31	2.59	2	-1.02
LFI$_4$	$p = 4$	-6.20	3.38	2	-2.91

A.4 Mixed large field inflation (MLFI)

This model possesses the following potential [5]

$$V(\phi) = M^4 \left(\frac{\phi}{M_{\rm Pl}}\right)^2 \left(1 + \alpha\frac{\phi^2}{M_{\rm Pl}^2}\right). \tag{A.12}$$

JCAP03(2014)039

Beside the usual mass scale M fixed by the CMB normalisation, MLFI contains only one parameter, α. Since the order of magnitude of this parameter is a priori unknown, a Jeffreys prior on α is assumed. In practice, when $\alpha < 10^{-5}$, the likelihood is numerically very close to that of LFI_2 and when $\alpha > 10$, the likelihood is numerically very close to that of LFI_4. As a consequence, we take the prior given in the following table:

Name	Priors	$\ln(\mathcal{E}/\mathcal{E}_{\mathrm{HI}})$	$\mathcal{C}$	N	$\ln(\mathcal{L}_{\max}/\mathcal{E}_{\mathrm{HI}})$
MLFI	$\log(\alpha) \in [-5, 1]$	-3.77	2.39	3	-0.09

A.5 Radiatively corrected massive inflation (RCMI)

The potential of this model is given by [5]

$$V(\phi) = M^4 \left(\frac{\phi}{M_{\mathrm{Pl}}}\right)^2 \left[1 - 2\alpha \frac{\phi^2}{M_{\mathrm{Pl}}^2} \ln\left(\frac{\phi}{M_{\mathrm{Pl}}}\right)\right]. \tag{A.13}$$

It depends on one parameter, α, which represents the amplitude of the radiative corrections to the potential of the LFI_2 scenario. Since the one-loop correction can vary over many orders of magnitude, it is meaningful to choose a Jeffreys prior on α. Then, clearly one must require $\alpha \ll 1$ in order for the perturbative expansion to be under control. On the other hand, the shape of the potential has been derived under the assumption that fermion loops dominate over self-interaction loops. This implies a lower bound on α, namely $\alpha > 10^{-15}$ [5]. However, when $\alpha < 10^{-7}$, the likelihood is numerically very close to that of LFI_2 and, therefore, it is not necessary to consider smaller values of α. There also exists an upper bound on α coming from the requirement of having a sufficient number of e-folds during inflation, $\alpha < 6 \times 10^{-4}$. Moreover, when $\alpha > 10^{-3}$, the likelihood is so small that the evidence cannot be properly computed. As a consequence, an upper bound on α of $\simeq 10^{-3}$ seems to be an appropriate choice. Our choice is summarised in the following table:

Name	Priors	$\ln(\mathcal{E}/\mathcal{E}_{\mathrm{HI}})$	$\mathcal{C}$	N	$\ln(\mathcal{L}_{\max}/\mathcal{E}_{\mathrm{HI}})$
RCMI	$\log(\alpha) \in [-7, -3]$	-2.32	4.19	3	1.77

A.6 Radiatively corrected quartic inflation (RCQI)

This model is a quartic large field model LFI_4 plus radiative corrections [5]. The potential reads

$$V(\phi) = M^4 \left(\frac{\phi}{M_{\mathrm{Pl}}}\right)^4 \left[1 - \alpha \ln\left(\frac{\phi}{M_{\mathrm{Pl}}}\right)\right]. \tag{A.14}$$

The amplitude of these corrections is controlled by the parameter α. As discussed in the previous subsection, the order of magnitude of α is not known and, therefore, a Jeffreys prior must be chosen. Moreover, the perturbative expansion making sense only if the radiative correction is small, one must have $\alpha \ll 1$. The physical prior is therefore $\log(\alpha) \in [-\infty, 0]$. However, in practice, when $\alpha < 10^{-3}$, the likelihood is numerically very close to that of LFI_4 and when $\alpha > 10^{-0.1}$, the likelihood is so small that it cannot be computed in a reliable way. Hence, the prior that we choose is the one indicated in the following table.

Name	Priors	$\ln(\mathcal{E}/\mathcal{E}_{\mathrm{HI}})$	$\mathcal{C}$	N	$\ln(\mathcal{L}_{\max}/\mathcal{E}_{\mathrm{HI}})$
RCQI	$\log(\alpha) \in [-3, -0.1]$	-5.36	6.62	3	1.27

JCAP03(2014)039

A.7 Natural inflation (NI)

This is a one parameter model and the potential is given by [5]

$$V(\phi) = M^4 \left[1 + \cos\left(\frac{\phi}{f}\right)\right]. \tag{A.15}$$

The order of magnitude of the free parameter f is not known and, therefore, a Jeffreys prior is chosen. Moreover, the model is compatible with the CMB only if the mass scale f is super-Planckian. It is not clear whether this condition makes sense at the fundamental level but, from the effective field point of view, several mechanisms have been invented such that this condition can be realised. In this situation f can scale from a few $M_{\rm Pl}$ to $\sim 100 M_{\rm Pl}$, hence the prior $\log(f/M_{\rm Pl}) \in [0, 2.5]$, see the following table.

Name	Priors	$\ln(\mathcal{E}/\mathcal{E}_{\rm HI})$	$\mathcal{C}$	N	$\ln(\mathcal{L}_{\rm max}/\mathcal{E}_{\rm HI})$
NI	$\log(f/M_{\rm Pl}) \in [0, 2.5]$	-2.30	4.16	3	2.05

A.8 Exponential SUSY inflation (ESI)

The potential of this model can be written as [5]

$$V(\phi) = M^4 \left(1 - e^{-q\phi/M_{\rm Pl}}\right), \tag{A.16}$$

where q is a free parameter. A priori, different priors on q are possible and this gives rise to different versions of this scenario. If we view ESI as a phenomenological model, then one can assume that the parameter q is a free $\mathcal{O}(1)$ quantity. In that case, a natural prior is $q \in [0.1, 6]$. But one can also assume that the order of magnitude of q is not known (in the following, we denote the corresponding version of the scenario by $\mathrm{ESI_l}$). In this situation, we must choose a Jeffreys prior, typically $\log(q) \in [-3, 3]$. However, when $q > 1$, the model is numerically difficult to track since it produces a too weak level of gravity waves. Moreover, in this regime, the likelihood reaches a stationary value. Therefore, as explained before, one can restrict ourselves to the numerical prior $\log(q) \in [-3, 1]$.

Another possible prior is based on the original derivation of the ESI scenario (we denote this version by $\mathrm{ESI_o}$ in what follows). Indeed, in that case, the model is based on supergravity and one has $q = \sqrt{2/\beta}$, where β is the coefficient which appears in front of the Kähler potential of the model. Hence, it seems reasonable to assume that this quantity is a coefficient of order one. This justifies our choice for the "original" prior, namely $\beta \in [1, 4]$. Of course, specific values of β are also very relevant. In particular, $\beta = 1$ or $\beta = 3$ represents the cases where the inflaton field is either a dilaton or a moduli ($\beta = 3$ corresponds to the "no scale" structure). In the following, we denote these versions of the ESI scenario by $\mathrm{ESI}_{\sqrt{2}}$ and $\mathrm{ESI}_{\sqrt{2/3}}$, respectively.

Name	Priors	$\ln(\mathcal{E}/\mathcal{E}_{\rm HI})$	$\mathcal{C}$	N	$\ln(\mathcal{L}_{\rm max}/\mathcal{E}_{\rm HI})$
ESI	$q \in [0.1, 6]$	0.03	1.77	3	2.29
$\mathrm{ESI_l}$	$\log(q) \in [-3, 1]$	-0.54	2.58	3	2.29
$\mathrm{ESI_o}$	$\beta = 2/q^2 \in [1, 4]$	0.01	1.81	3	2.25
$\mathrm{ESI}_{\sqrt{2}}$	$q = \sqrt{2}$	0.05	1.70	2	2.25
$\mathrm{ESI}_{\sqrt{2/3}}$	$q = \sqrt{2/3}$	0.00	1.77	2	2.22

JCAP03(2014)039

A.9 Power law inflation (PLI)

The potential of this class of models can be expressed as [5]

$$V(\phi) = M^4 e^{-\alpha\phi/M_{\rm Pl}}, \tag{A.17}$$

where α is a positive coefficient. A priori, it is a small quantity the order of magnitude of which is not known. As a consequence, a Jeffreys prior seems to be the most natural choice and we take $\log(\alpha) \in [-4, 0]$. On a more phenomenological viewpoint, inflation occurs when $\alpha < \sqrt{2}$ only and, therefore, it makes also sense to choose a flat prior on α, namely $\alpha \in [0, \sqrt{2}]$ (in the following, we denote this version of power law inflation by PLI$_p$). However, when $\alpha > 1.1$, the likelihood is so small that it cannot be properly calculated. Hence, we will restrict ourselves to the prior $\alpha \in [0, 1.1]$.

Name	Priors	$\ln(\mathcal{E}/\mathcal{E}_{\rm HI})$	$\mathcal{C}$	N	$\ln(\mathcal{L}_{\rm max}/\mathcal{E}_{\rm HI})$
PLI	$\log(\alpha) \in [-4, 0]$	-7.04	5.56	3	-2.54
PLI$_p$	$\alpha \in [0, 1.1]$	-7.23	3.25	3	-2.54

A.10 Kähler moduli inflation (KMII)

The potential of KMII inflation is given by [5]

$$V(\phi) = M^4 \left(1 - \alpha \frac{\phi}{M_{\rm Pl}} e^{-\phi/M_{\rm Pl}}\right), \tag{A.18}$$

where α is a free positive coefficient. As discussed in detail in ref. [5], in order for inflation to end by slow-roll violation, one must have $\alpha \gtrsim 2.4095$. On the other hand, the order of magnitude of this parameter is unspecified and this suggests a Jeffreys prior on α. Combining these two pieces of information, we are led to the prior $\log(\alpha) \in [\log(2.4095) \simeq 0.382, 4]$.

On the other hand, one can also choose α such that the potential is positive everywhere, as opposed to the previous situation where, for some values of the field, the potential can be negative and where one makes use of a finite portion of it only (the corresponding version of the scenario is denoted by KMII$_{V>0}$ in the following). In that case, one has the extra condition $\alpha < e \simeq 2.7183$. Since e is close to 2.4095, a Jeffreys prior no longer makes sense and a linear prior now seems a sensible choice. Hence our second choice $\alpha \in [2.4095, e \simeq 2.7183]$. Everything is summarised in the following table:

Name	Priors	$\ln(\mathcal{E}/\mathcal{E}_{\rm HI})$	$\mathcal{C}$	N	$\ln(\mathcal{L}_{\rm max}/\mathcal{E}_{\rm HI})$
KMII	$\log(\alpha) \in [0.382, 4]$	0.00	1.75	3	2.22
KMII$_{V>0}$	$\alpha \in [2.4095, 2.7183]$	0.01	1.69	3	2.22

A.11 Horizon flow inflation at first order (HF1I)

The potential of HF1I inflation reads [5]

$$V(\phi) = M^4 \left(1 + A_1 \frac{\phi}{M_{\rm Pl}}\right)^2 \left[1 - \frac{2}{3}\left(\frac{A_1}{1 + A_1\phi/M_{\rm Pl}}\right)^2\right]. \tag{A.19}$$

This model is obtained by an integration of the horizon flow equations truncated at a given order (here at second order). As such, this scenario is in fact purely phenomenological. Moreover, it turns out that the observational predictions are not very sensitive to the value of the free parameter A_1. Therefore, since its order of magnitude is not fixed, it makes sense to choose a Jeffrey prior on A_1 and we take $\log(A_1) \in [-3, 3]$ as indicated below:

JCAP03(2014)039

Name	Priors	$\ln(\mathcal{E}/\mathcal{E}_{\rm HI})$	$\mathcal{C}$	N	$\ln(\mathcal{L}_{\rm max}/\mathcal{E}_{\rm HI})$
HF1I	$\log(A_1) \in [-3,3]$	-2.60	1.65	3	-0.08

A.12 Coleman Weinberg inflation (CWI)

Coleman Weinberg inflation is based on the following potential [5]

$$V(\phi) = M^4 \left[1 + \alpha \left(\frac{\phi}{Q}\right)^4 \ln\left(\frac{\phi}{Q}\right)\right], \tag{A.20}$$

with $\alpha = 4e$ in order to have a vanishing minimum. The shape of $V(\phi)$ is therefore characterised by only one parameter, Q. In the original version of the scenario, Q is fixed by the GUT scale, $Q \sim 10^{14} - 10^{15}$GeV. Therefore, in this case, it is natural to choose a flat prior on Q (we denote this version of the scenario by $\mathrm{CWI_f}$). On the other hand, if one considers a more general situation, then there is a priori no criterion to fix the value (or the order of magnitude) of Q and, therefore, this justifies the choice of a Jeffreys prior, namely $\log(Q/M_{\rm Pl}) \in [-5,-3]$ (we denote this version of the scenario by $\mathrm{CWI_l}$).

Name	Priors	$\ln(\mathcal{E}/\mathcal{E}_{\rm HI})$	$\mathcal{C}$	N	$\ln(\mathcal{L}_{\rm max}/\mathcal{E}_{\rm HI})$
$\mathrm{CWI_f}$	$Q/M_{\rm Pl} \in [5\times10^{-5}, 5\times10^{-4}]$	-2.35	2.62	3	1.49
$\mathrm{CWI_l}$	$\log(Q/M_{\rm Pl}) \in [-5,-3]$	-2.51	3.02	3	1.60

A.13 Loop inflation (LI)

The potential of LI inflation can be written as [5]

$$V(\phi) = M^4 \left[1 + \alpha \ln\left(\frac{\phi}{M_{\rm Pl}}\right)\right], \tag{A.21}$$

where the parameter α controls the strength of the one loop correction to the tree level $V(\phi)$ (here the constant term) and must therefore be such that $\alpha \ll 1$. When $\alpha < 0$, in order to have a sufficient number of e-folds, one must require $\alpha > \alpha_{\rm min} \simeq -0.3$ [5]. In principle, the model makes sense only if inflation proceeds at sub-Planckian *vev*'s which is, strictly speaking, not possible in this regime. If we allow *vev*'s larger than the Planck mass, typically up to $\phi/M_{\rm Pl} \simeq 1000$, then this sets an additional condition, namely $\alpha < -0.1$. When $\alpha > 0$, there is no extra condition on α except, as already signaled, that α must be small in order for the perturbative expansion to make sense.

From the previous considerations, we assume a flat prior $\alpha \in [-0.3,-0.1]$ in the case where $\alpha < 0$ (we denote this version of the scenario by $\mathrm{LI}_{\alpha<0}$). We have seen that, when $\alpha > 0$, there exists no restrictions on this parameter. In particular, its order of magnitude is not specified and, therefore, it makes sense to choose a Jeffreys prior, namely $\log(\alpha) \in [\log(0.003), \log(0.3)]$ (in the following, this version of the scenario is denoted by $\mathrm{LI}_{\alpha>0}$). Finally, when the sign is left unspecified, we simply consider a flat prior $\alpha \in [\alpha_{\rm min}, -0.1] \cup [0, 0.3]$. These priors are summarised in the following table.

Name	Priors	$\ln(\mathcal{E}/\mathcal{E}_{\rm HI})$	$\mathcal{C}$	N	$\ln(\mathcal{L}_{\rm max}/\mathcal{E}_{\rm HI})$
LI	$\alpha \in [\alpha_{\rm min}, -0.1] \cup [0, 0.3]$	-0.87	3.03	3	2.27
$\mathrm{LI}_{\alpha>0}$	$\log(\alpha) \in [\log(0.003), \log(0.3)]$	-0.51	2.38	3	2.27
$\mathrm{LI}_{\alpha<0}$	$\alpha \in [\alpha_{\rm min}, -0.1]$	-1.74	2.29	3	0.79

JCAP03(2014)039

A.14 $R + R^{2p}$ inflation (RpI)

The potential of $R + R^{2p}$ inflation can be expressed as

$$V(\phi) = M^4 e^{-2\sqrt{2/3}\phi/M_{\rm Pl}} \left| e^{\sqrt{2/3}\phi/M_{\rm Pl}} - 1 \right|^{2p/(2p-1)}, \tag{A.22}$$

which depends on the parameter p. The case $p = 1$ is peculiar and corresponds to Higgs Inflation (HI). It has been shown in ref. [5] that, if p takes integer values different from $p = 1$, then the model is ruled out since it leads to values of r and $n_{\rm S}$ that are not compatible with the Planck data. As a consequence, p must be sufficiently close to 1, and therefore must be a real number. When $p > 1$, the potential possesses a maximum located at

$$\frac{\phi_{\rm max}}{M_{\rm Pl}} = \sqrt{\frac{3}{2}} \ln\left(\frac{2p-1}{p-1}\right). \tag{A.23}$$

and two regimes of inflation exist (denoted by RPI1 and RPI2 in what follows) depending on whether inflation takes place in $\phi \in [0, \phi_{\rm max}]$ or in $\phi \in [\phi_{\rm max}, \infty]$. In the first case, inflation stops by slow-roll violation and the model is therefore a one parameter model. In the second case, however, inflation must stop by instability at $\phi_{\rm end}$ and, hence, the corresponding model is in fact a two parameters model, p and $\phi_{\rm end}$. Since p must be close to one, we choose the flat prior $p \in [1, 1.5]$. In the case of RPI2, the order of magnitude of $\phi_{\rm end}$ being unspecified, we take the following Jeffreys prior on $\phi_{\rm end}$: $\log(\phi_{\rm end}/\phi_{\rm max}) \in [0.5, 2]$.

If $p < 1$, then there is a single regime where inflation can proceed. It is denoted by RPI3 in what follows. In that case, inflation stops by violation of the slow-roll conditions and, therefore, the model is a one parameter model. As a consequence, we choose to consider the following flat prior on p: $p \in [0.8, 1]$.

Name	Priors	$\ln(\mathcal{E}/\mathcal{E}_{\rm HI})$	$\mathcal{C}$	N	$\ln(\mathcal{L}_{\rm max}/\mathcal{E}_{\rm HI})$
RPI1	$p \in [1, 1.5]$	-3.69	1.86	3	2.26
RPI2	$p \in [1, 1.5]$ $\log(\phi_{\rm end}/\phi_{\rm max}) \in [0.8, 1]$	-6.08	8.82	4	1.80
RPI3	$p \in [0.8, 1]$	-2.28	2.84	3	2.22

A.15 Double well inflation (DWI)

Double Well inflation is a one parameter model characterised by the following potential

$$V(\phi) = M^4 \left[\left(\frac{\phi}{\phi_0} \right)^2 - 1 \right]^2. \tag{A.24}$$

As shown in ref. [5], slow-roll inflation takes place only if $\phi_0/M_{\rm Pl} > 2\sqrt{2}$. On the other hand, COBE normalising the model allows us to express the mass scale M in terms of the free parameter ϕ_0. Then, the requirement $M/M_{\rm Pl} < 1$ leads to to the constraint $\phi_0/M_{\rm Pl} \lesssim 10^5$. As a consequence, a Jeffreys logarithmic prior on ϕ_0 is chosen, namely $\log(\phi_0/M_{\rm Pl}) \in [\log(2\sqrt{2}) \simeq 0.45, 5]$.

Name	Priors	$\ln(\mathcal{E}/\mathcal{E}_{\rm HI})$	$\mathcal{C}$	N	$\ln(\mathcal{L}_{\rm max}/\mathcal{E}_{\rm HI})$
DWI	$\log(\phi_0/M_{\rm Pl}) \in [\log(2\sqrt{2}), 5]$	-2.09	4.56	3	2.14

JCAP03(2014)039

A.16 Mutated hilltop inflation (MHI)

The potential of Mutated Hilltop inflation is given by

$$V(\phi) = M^4 \left[1 - \mathrm{sech}\left(\frac{\phi}{\mu}\right)\right], \tag{A.25}$$

and depends on one free parameter, μ. This model is phenomenological although it is supposed to emerge from supergravity considerations. In this last case, only sub-Planckian values for μ probably make sense. This is the reason why it seems interesting to consider different priors. Given that the order of magnitude of μ/M_{Pl} is not specified, we take three Jeffreys priors corresponding to situations where μ is sub-Planckian (denoted by $\mathrm{MHI_l}$), super-Planckian (denoted by $\mathrm{MHI_s}$) or not specified. Those choices are summarised in the following table:

Name	Priors	$\ln(\mathcal{E}/\mathcal{E}_{\mathrm{HI}})$	$\mathcal{C}$	N	$\ln(\mathcal{L}_{\max}/\mathcal{E}_{\mathrm{HI}})$
MHI	$\log(\mu/M_{\mathrm{Pl}}) \in [-2, 2]$	-0.30	2.01	3	2.29
$\mathrm{MHI_l}$	$\log(\mu/M_{\mathrm{Pl}}) \in [-2, 0]$	-0.82	2.64	3	2.23
$\mathrm{MHI_s}$	$\log(\mu/M_{\mathrm{Pl}}) \in [0, 2]$	0.04	1.70	3	2.29

A.17 Radion gauge inflation (RGI)

The potential of Radion Gauge inflation can be expressed as

$$V(\phi) = M^4 \frac{(\phi/M_{\mathrm{Pl}})^2}{\alpha + (\phi/M_{\mathrm{Pl}})^2}, \tag{A.26}$$

where α is a dimensionless positive parameter. A priori, smaller than unity values are preferred but, at the same time, $\alpha > 1$ is not forbidden. This is why it is interesting to study how the Bayesian evidence of the model depends on the range of variation of α. Let us also notice that the order of magnitude of this parameter is not specified. As a consequence, we choose three Jeffreys priors, one such that $\log(\alpha) \in [-4, 4]$, one corresponding to a situation where $\alpha < 1$, namely $\log(\alpha) \in [-4, 0]$ (and we denote this version of the model by $\mathrm{RGI_s}$) and one corresponding to $\alpha > 1$, namely $\log(\alpha) \in [0, 4]$ (this version being referred to as $\mathrm{RGI_l}$). Finally, in ref. [68], the potential of Radion Gauge inflation was also obtained in the context of S-dual superstring models. In that case, the value of α is fixed and given by $\alpha = 1/16$ which leads to a fourth choice of prior. Everything is summarised in the following table:

Name	Priors	$\ln(\mathcal{E}/\mathcal{E}_{\mathrm{HI}})$	$\mathcal{C}$	N	$\ln(\mathcal{L}_{\max}/\mathcal{E}_{\mathrm{HI}})$
RGI	$\log(\alpha) \in [-4, 4]$	-0.39	2.36	3	2.29
$\mathrm{RGI_s}$	$\log(\alpha) \in [-4, 0]$	-0.11	2.09	3	2.29
$\mathrm{RGI_l}$	$\log(\alpha) \in [0, 4]$	-0.77	2.70	3	2.20
$\mathrm{RGI_{1/16}}$	$\alpha = 1/16$	-0.16	2.02	2	2.20

A.18 MSSM inflation (MSSMI)

In this scenario, inflation occurs along a flat direction of the MSSM potential. This flat direction is usually lifted by higher order non-renormalisable operators and SUSY soft terms. As a consequence, one can show that the potential takes the form [5]

$$V(\phi) = M^4 \left[\left(\frac{\phi}{\phi_0}\right)^2 - \frac{2}{3}\left(\frac{\phi}{\phi_0}\right)^6 + \frac{1}{5}\left(\frac{\phi}{\phi_0}\right)^{10}\right], \tag{A.27}$$

JCAP03(2014)039

where ϕ_0 is a free parameter which can be expressed as

$$\phi_0^8 = \frac{M_{\rm Pl}^6 m_\phi^2}{10\lambda_6^2}. \tag{A.28}$$

The quantity λ_6 is a coupling constant that is taken to be of order one while m_ϕ is a soft breaking mass and, thus, is chosen to be around $\simeq$ 1TeV. As a consequence, one has $\phi_0 \simeq 10^{14}$GeV. In this original form of the scenario (denoted in what follows by MSSMI$_{\rm o}$), it is therefore natural to take a flat prior on ϕ_0 such that $\phi_0/M_{\rm Pl} \in [2\times10^{-5}, 2\times10^{-4}]$.

This model can also be viewed as a phenomenological inflection point potential (denoted by MSSMI$_{\rm p}$) where the value of ϕ_0 is not fixed by high energy physics considerations. In that case, a Jeffreys prior on ϕ_0 is appropriate and, here, we take $\log(\phi_0/M_{\rm Pl}) \in [-3, 3]$.

Name	Priors	$\ln(\mathcal{E}/\mathcal{E}_{\rm HI})$	$\mathcal{C}$	N	$\ln(\mathcal{L}_{\rm max}/\mathcal{E}_{\rm HI})$
MSSMI$_{\rm o}$	$\phi_0/M_{\rm Pl} \in [2\times10^{-5}, 2\times10^{-4}]$	-10.27	0.76	3	-7.40
MSSMI$_{\rm p}$	$\log(\phi_0/M_{\rm Pl}) \in [-3, 3]$	-3.28	4.61	3	1.72

A.19 Renormalisable inflection point inflation (RIPI)

This model is derived in the same context as MSSM inflation except that an additional term in the superpotential involving right handed neutrinos is considered. The amplitude of this new term is controlled by the dimensionless coupling constant $h \simeq 10^{-12}$. This gives rise to a new flat direction parametrised by the inflaton field ϕ. This flat direction is lifted by the same mechanism discussed previously in the context of MSSM inflation and leads to the following potential [5]

$$V(\phi) = M^4\left[\left(\frac{\phi}{\phi_0}\right)^2 - \frac{4}{3}\left(\frac{\phi}{\phi_0}\right)^3 + \frac{1}{2}\left(\frac{\phi}{\phi_0}\right)^4\right], \tag{A.29}$$

where

$$\phi_0 = \sqrt{3}\frac{m_\phi}{h}, \tag{A.30}$$

m_ϕ, as a soft breaking mass, being between 100GeV and 10TeV. As a consequence, one has $\phi_0 \sim 10^{14}$GeV. For this version of the model (denoted as the "original version", RIPI$_{\rm o}$), a flat prior on ϕ_0 represents the preferred choice, $\phi_0/M_{\rm Pl} \in [2\times10^{-5}, 2\times10^{-4}]$. As for MSSM inflation, however, one can also see this scenario as a phenomenological scenario where ϕ_0 is not specified (denoted by RIPI$_{\rm p}$ in what follows). In this case, a Jeffreys prior on ϕ_0 is natural and we take $\log(\phi_0/M_{\rm Pl}) \in [-3, -3]$. Finally, the above potential can also arise in a supergravity framework with shift symmetry in the Kähler potential (denoted by RIPI$_{\rm sugra}$) which allows for super-Planckian *vev* of the inflaton field ϕ. For this reason, we also consider the prior $\phi_0/M_{\rm Pl} \in [10, 50]$.

Name	Priors	$\ln(\mathcal{E}/\mathcal{E}_{\rm HI})$	$\mathcal{C}$	N	$\ln(\mathcal{L}_{\rm max}/\mathcal{E}_{\rm HI})$
RIPI$_{\rm o}$	$\phi_0/M_{\rm Pl} \in [2\times10^{-5}, 2\times10^{-4}]$	-9.94	2.01	3	-6.76
RIPI$_{\rm p}$	$\log(\phi_0/M_{\rm Pl}) \in [-3, 3]$	-2.31	3.60	3	2.19
RIPI$_{\rm sugra}$	$\phi_0/M_{\rm Pl} \sim [10, 50]$	-0.96	2.87	3	2.19

JCAP03(2014)039

A.20 Arctan inflation (AI)

The potential of AI can be expressed as

$$V(\phi) = M^4 \left[1 - \frac{2}{\pi} \arctan\left(\frac{\phi}{\mu}\right)\right], \tag{A.31}$$

where μ is a free parameter. As shown in ref. [5], inflation stops by slow-roll violation only if $\mu/M_{\rm Pl} < 0.512378$. This model is purely phenomenological and, as a consequence, the scale μ is not fixed by any high energy physics considerations. As a consequence, its order of magnitude is a priori unspecified. Therefore, we choose a Jeffreys logarithmic prior on μ, namely $\log(\mu/M_{\rm Pl}) \in [-3, \log(0.51\cdots) \simeq -0.29]$.

Name	Priors	$\ln(\mathcal{E}/\mathcal{E}_{\rm HI})$	$\mathcal{C}$	N	$\ln(\mathcal{L}_{\rm max}/\mathcal{E}_{\rm HI})$
AI	$\log(\mu/M_{\rm Pl}) \in [-3, -0.29]$	-0.20	2.18	3	2.29

A.21 Constant ns A inflation (CNAI)

The potential of CNAI is given by the following expression

$$V(\phi) = M^4 \left[3 - \left(3 + \alpha^2\right) \tanh^2\left(\frac{\alpha}{\sqrt{2}} \frac{\phi}{M_{\rm Pl}}\right)\right], \tag{A.32}$$

where α is a dimensionless free parameter. It was demonstrated in ref. [5] that slow-roll inflation takes place provided $\alpha < \alpha_{\rm max} \simeq 0.66$. This model is phenomenological and is not based on high energy physics. It is in fact designed to produce an exact power law spectrum of density perturbations. As a consequence, the order of magnitude of α is not specified and one chooses to work with a Jeffreys prior $\log(\alpha) \in [-4, \log(\alpha_{\rm max}) \simeq -0.18]$.

Name	Priors	$\ln(\mathcal{E}/\mathcal{E}_{\rm HI})$	$\mathcal{C}$	N	$\ln(\mathcal{L}_{\rm max}/\mathcal{E}_{\rm HI})$
CNAI	$\log(\alpha) \in [-4, -0.18]$	-1.96	2.22	3	0.79

A.22 Constant ns B inflation (CNBI)

This model is very similar to CNAI inflation. It is also a phenomenological scenario designed to produce a constant spectral index and also depends on one dimensionless parameter α. The corresponding potential can be expressed as

$$V(\phi) = M^4 \left[\left(3 - \alpha^2\right) \tan^2\left(\frac{\alpha}{\sqrt{2}} \frac{\phi}{M_{\rm Pl}}\right) - 3\right]. \tag{A.33}$$

It was shown in ref. [5] that slow-roll inflation takes place if $\alpha < \alpha_{\rm max} \simeq 0.2975$. If one CMB normalises the model, then one can express the mass scale M in terms of α. It follows that the requirement $M/M_{\rm Pl} < 1$ implies $\alpha \lesssim 10^{-9}$. As a consequence, we should take a Jeffreys prior on α, namely $\log(\alpha) \in [-9, \log(\alpha_{\rm max}) \simeq -0.527]$. In practice, however, when $\alpha > 10^{-1.4}$, the likelihood is so small that it cannot be properly calculated. Moreover, when $\alpha < 10^{-5}$, the value of the likelihood reaches a numerical stationary value and, therefore, it is not necessary to numerically calculate it beyond that point. As a consequence, we consider the following prior: $\log(\alpha) \in [-5, -1.4]$.

Name	Priors	$\ln(\mathcal{E}/\mathcal{E}_{\rm HI})$	$\mathcal{C}$	N	$\ln(\mathcal{L}_{\rm max}/\mathcal{E}_{\rm HI})$
CNBI	$\log(\alpha) \in [-5, -1.4]$	-1.68	2.13	3	0.79

JCAP03(2014)039

A.23 Open string Tachyonic inflation (OSTI)

In this model, the inflaton field is a tachyon field on a D3-brane. In principle, its kinetic term is non-minimal but when higher order terms are neglected, it becomes a standard slow-roll model with a potential given by the following expression

$$V(\phi) = -M^4 \left(\frac{\phi}{\phi_0}\right)^2 \ln\left[\left(\frac{\phi}{\phi_0}\right)^2\right]. \tag{A.34}$$

In the original version of the model, ϕ_0 is set to the string scale $\phi_0 \sim M_{\rm s}$. However, ϕ_0 can also be viewed as a free sub-Planckian scale. In that case, a Jeffreys prior is appropriate, for instance $\log(\phi_0/M_{\rm Pl}) \in [0,4]$. However, when $\phi_0/M_{\rm Pl} < 10$, the likelihood is so small that it cannot be numerically calculated in a reliable way. As a consequence, in what follows, we consider the prior $\log(\phi_0/M_{\rm Pl}) \in [1,4]$ only.

Name	Priors	$\ln(\mathcal{E}/\mathcal{E}_{\rm HI})$	$\mathcal{C}$	N	$\ln(\mathcal{L}_{\rm max}/\mathcal{E}_{\rm HI})$
OSTI	$\log(\phi_0/M_{\rm Pl}) \in [1,4]$	-1.87	4.27	3	2.14

A.24 Witten-O'Raifeartaigh inflation (WRI)

The potential of WRI inflation can be expressed as

$$V(\phi) = M^4 \ln\left(\frac{\phi}{\phi_0}\right)^2. \tag{A.35}$$

When the high energy justifications of the scenario are considered, the condition $\phi_0 = M_{\rm Pl}$ holds. In what follows, we call this version of the model the "original WRI" and we denote it as $\mathrm{WRI_o}$. If this condition is relaxed (the corresponding version of the model is then denoted by $\mathrm{WRI_g}$) and if the model is now viewed as a more phenomenological one, then the order of magnitude and value of ϕ_0 are unspecified and a Jeffreys prior is appropriate. We choose $\log(\phi_0/M_{\rm Pl}) \in [-3,3]$. These considerations are summarised in the following table:

Name	Priors	$\ln(\mathcal{E}/\mathcal{E}_{\rm HI})$	$\mathcal{C}$	N	$\ln(\mathcal{L}_{\rm max}/\mathcal{E}_{\rm HI})$
$\mathrm{WRI_o}$	$\phi_0 = M_{\rm Pl}$	-1.09	2.05	2	1.29
$\mathrm{WRI_g}$	$\log(\phi_0/M_{\rm Pl}) \in [-3,3]$	-1.20	2.97	3	1.89

A.25 Small field inflation (SFI)

Small field inflation is characterised by the following potential

$$V(\phi) = M^4 \left[1 - \left(\frac{\phi}{\mu}\right)^p\right], \tag{A.36}$$

which depends on two parameters, the dimensionless index p and the mass scale μ. In most of high energy physics implementations, only the case $\mu < M_{\rm Pl}$ is sensible. It is, however, always possible to take a more phenomenological point of view and also consider the case $\mu > M_{\rm Pl}$. In what follows, for this reason, we will discuss a "small" version of the scenario for which $\log(\mu/M_{\rm Pl}) \in [-1,0]$ and a "large" version for which $\log(\mu/M_{\rm Pl}) \in [0,2]$. Two remarks are in order at this point. Firstly, a Jeffreys prior is chosen on μ because, a priori, its order of magnitude is unspecified. Secondly, in the small version of the model, we only consider $\log(\mu/M_{\rm Pl}) \in [-1,0]$ (and not, for instance, $\log(\mu/M_{\rm Pl}) \in [-2,0]$) because, when $\mu/M_{\rm Pl} < 0.1$, the likelihood is so small that it cannot be properly numerically calculated.

JCAP03(2014)039

The index p is an $\mathcal{O}(1)$ parameter that can also take specific integer values. We will treat the case where there is a flat prior on p, namely $p \in [2, 10]$, but also the case where p has specific values, $p = 1$, $p = 2$, $p = 3$ and $p = 4$. Let us also notice that for $p = 1$ and $p = 2$, the small version of the SFI inflation does not exist because slow-roll is violated in that case (for instance, for $p = 2$, one has $\epsilon_2 > 4$).

Our priors are summarised in the following table:

Name	Priors	$\ln(\mathcal{E}/\mathcal{E}_{\rm HI})$	$\mathcal{C}$	N	$\ln(\mathcal{L}_{\rm max}/\mathcal{E}_{\rm HI})$
SFI	$p \in [2, 10]$ $\log(\mu/M_{\rm Pl}) \in [-1, 2]$	-0.31	1.88	4	2.29
$\rm SFI_s$	$p \in [2, 10]$ $\log(\mu/M_{\rm Pl}) \in [-1, 0]$	-0.40	1.54	4	2.27
$\rm SFI_l$	$p \in [2, 10]$ $\log(\mu/M_{\rm Pl}) \in [0, 2]$	-0.30	2.01	4	2.29
$\rm SFI_1$	$p = 1$ $\log(\mu/M_{\rm Pl}) \in [-1, 2]$	-1.53	1.94	3	0.79
$\rm SFI_2$	$p = 2$ $\log(\mu/M_{\rm Pl}) \in [-1, 2]$	-1.90	3.07	3	2.19
$\rm SFI_{2l}$	$p = 2$ $\log(\mu/M_{\rm Pl}) \in [0, 2]$	-1.47	3.07	3	2.19
$\rm SFI_3$	$p = 3$ $\log(\mu/M_{\rm Pl}) \in [-1, 2]$	-1.23	2.74	3	2.26
$\rm SFI_{3s}$	$p = 3$ $\log(\mu/M_{\rm Pl}) \in [-1, 0]$	-3.88	3.13	3	0.67
$\rm SFI_{3l}$	$p = 3$ $\log(\mu/M_{\rm Pl}) \in [0, 2]$	-0.87	2.65	3	2.26
$\rm SFI_4$	$p = 4$ $\log(\mu/M_{\rm Pl}) \in [-1, 2]$	-0.53	2.12	3	2.29
$\rm SFI_{4s}$	$p = 4$ $\log(\mu/M_{\rm Pl}) \in [-1, 0]$	-0.79	1.95	3	2.26
$\rm SFI_{4l}$	$p = 4$ $\log(\mu/M_{\rm Pl}) \in [0, 2]$	-0.41	2.14	3	2.29

A.26 Intermediate inflation (II)

Intermediate Inflation is a phenomenological model that can be defined by demanding an equation of state during inflation of the form

$$\rho + p = \gamma \rho^{\lambda}, \tag{A.37}$$

where $\gamma > 0$ and $\lambda > 1$ are dimensionless parameters, ρ and p being the energy density and pressure stored in the inflaton field, respectively. This assumption is in fact equivalent to having a scale factor given by $a(t) \propto \exp\left(At^f\right)$ where

$$f = \frac{2(1-\lambda)}{1-2\lambda}. \tag{A.38}$$

Given that $\lambda > 1$, it follows that $0 < f < 1$. Finally, it is also equivalent to postulate the following potential

$$V(\phi) = M^4 \left[\left(\frac{\phi}{M_{\rm Pl}}\right)^{-\beta} - \frac{\beta^2}{6}\left(\frac{\phi}{M_{\rm Pl}}\right)^{-\beta-2}\right], \tag{A.39}$$

JCAP03(2014)039

with

$$\beta = 4\left(\frac{1}{f} - 1\right). \tag{A.40}$$

In this scenario, inflation cannot stop by violation of the slow-roll conditions and, hence, one needs to postulate an extra mechanism such as tachyonic instability. This implies that the scenario depends on another parameter, $\phi_{\rm end}$, the *vev* at which inflation ends. Intermediate inflation is therefore a two parameters models, $\phi_{\rm end}$ and λ (or f or β).

Given the above considerations, one can choose to take a flat prior on $\beta \in [0, 10]$ (in the following, we denote the corresponding version of the scenario by II_β). It makes also sense to work with a flat prior on $f \in [0, 1]$ (this version of the model is denoted II_f). In fact, in order to avoid an infinite value of β, we will consider the following prior $f \in [0.1, 1]$. Finally, we also investigate a Jeffreys prior on λ (this version is denoted by II_λ), namely $\log(\lambda) \in [0.1, 4]$, the lower bound $\log(\lambda) > 0.1$ being chosen to have finite values of β.

The prior on $\phi_{\rm end}$ also needs to be discussed. It was shown in ref. [5] that the parameter $x_{\rm end} = \phi_{\rm end}/M_{\rm Pl}$ must be larger than some value $x_{\rm end}^{\rm min}$ in order to have a sufficient number of e-folds during inflation. The parameter $x_{\rm end}$ is only known numerically and has been calculated in ref. [5]. Moreover, the order of magnitude of $x_{\rm end}$ is not known and, therefore, this suggests a Jeffreys prior. As a consequence, we take $\log(x_{\rm end}) \in [\log(x_{\rm end}^{\rm min}), 4]$. Everything is summarised in the following table.

Name	Priors	$\ln(\mathcal{E}/\mathcal{E}_{\rm HI})$	$\mathcal{C}$	N	$\ln(\mathcal{L}_{\rm max}/\mathcal{E}_{\rm HI})$
II_β	$\beta \in [0, 10]$ $\log(x_{\rm end}) \in [\log(x_{\rm end}^{\rm min}), 4]$	-7.61	7.39	4	-3.66
II_f	$f = 1/(1+\beta/4) \in [0.1, 1]$ $\log(x_{\rm end}) \in [\log(x_{\rm end}^{\rm min}), 4]$	-7.56	8.22	4	-3.02
II_λ	$\log(\lambda) = \log(1+2/\beta) \in [0.1, 4]$ $\log(x_{\rm end}) \in [\log(x_{\rm end}^{\rm min}), 4]$	-7.79	7.79	4	-3.89

A.27 Kähler moduli inflation II (KMIII)

Kähler Moduli Inflation III is a stringy inspired scenario the potential of which can be written as

$$V(\phi) = M^4\left[1 - \alpha\left(\frac{\phi}{M_{\rm Pl}}\right)^{4/3} e^{-\beta(\phi/M_{\rm Pl})^{4/3}}\right]. \tag{A.41}$$

In this model, the inflaton field is a modulus field. The potential depends on two parameters, α and β. As reviewed in ref. [5], the order of magnitude of the parameter β is in fact controlled by the compactification volume $\mathcal{V}$. More precisely, one can show that $\alpha = \mathcal{O}\left(\mathcal{V}_{\rm s}^{5/3}\right)$ and $\beta = \mathcal{O}\left(\mathcal{V}_{\rm s}^{2/3}\right)$ where $\mathcal{V}_{\rm s}$ is a dimensionless volume defined by $\mathcal{V}_{\rm s} = \mathcal{V}/\ell_{\rm s}^6$, $\ell_{\rm s}$ being the string length. Since typical values are usually chosen such that $\mathcal{V}_{\rm s} \sim 10^6$ and since the order of magnitude of $\mathcal{V}_{\rm s}$ is not precisely specified, we take a logarithmic prior on $\mathcal{V}_{\rm s}$, namely $\log(\mathcal{V}) \in [5, 7]$.

On the other hand, the ratio $\alpha/(\beta\mathcal{V})$ is a $\mathcal{O}(1)$ quantity, thanks to the scaling mentioned above. As a consequence, we choose a flat prior $\alpha/(\beta\mathcal{V}) \in [0.2, 5]$. In practice, once the number $\mathcal{V}_{\rm s}$ is fixed, one calculate β by means of $\beta = \mathcal{V}_{\rm s}^{2/3}$. Then, the ratio $\alpha/(\beta\mathcal{V})$ is chosen and one deduces the value of α.

JCAP03(2014)039

Name	Priors	$\ln(\mathcal{E}/\mathcal{E}_{\rm HI})$	$\mathcal{C}$	N	$\ln(\mathcal{L}_{\rm max}/\mathcal{E}_{\rm HI})$
KMIII	$\log(\mathcal{V}) \in [5,7]$ $\alpha/(\beta\mathcal{V}) \in [0.2,5]$	0.07	1.66	3	2.22

A.28 Logamediate inflation (LMI)

This model is a phenomenological model designed such that the scale factor during inflation behaves as

$$a(t) = a_0 \exp\left[A\left(\ln\frac{t}{t_0}\right)^{\lambda}\right], \tag{A.42}$$

where $A > 0$ and $\lambda > 1$ are two dimensionless parameters and t_0 is a third parameter the dimension of which is time. From this expression of the scale factor, one can infer the shape of the potential. Straightforward calculations [5] lead to

$$V(\phi) = M^4\left(\frac{\phi}{M_{\rm Pl}}\right)^{4(1-\gamma)} \exp\left[-\beta\left(\frac{\phi}{M_{\rm Pl}}\right)^{\gamma}\right] \tag{A.43}$$

where the parameters γ and β can be expressed as

$$\gamma = \frac{2}{\lambda+1}, \qquad \beta = 2\left(\frac{\lambda+1}{2\sqrt{2A\lambda}}\right)^{2/(\lambda+1)}. \tag{A.44}$$

These relations, together with the conditions on A and λ, imply $0 < \gamma \leq 1$ and $\beta > 0$. The potential (A.43) has a maximum located at

$$x_{\rm max} \equiv \frac{\phi_{\rm max}}{M_{\rm Pl}} = \left[\frac{4(1-\gamma)}{\beta\gamma}\right]^{1/\gamma}. \tag{A.45}$$

This gives rise to two different versions of the model [5]: either inflation proceeds on the left side of its maximum and the field *vev* decreases during inflation (we call this version LMI1 in the following) or it proceeds on the right side of its maximum and the field *vev* increases during inflation (this version is denoted LMI2). In the case of LMI1, inflation stops by slow-roll violation. The case of LMI2 is more complicated but, in brief, one needs an extra mechanism to end inflation and this introduces a new parameter in the model, $x_{\rm end}$, see ref. [5] for more details. LMI2 is therefore a three parameter model.

Regarding the priors, we essentially have two choices: either we specify them on the parameters characterising the potential or we specify them on the parameters controlling the behaviour of the scale factor. In the following, we consider both cases.

Let us start with the case where we choose priors on the parameters of the potential. In the following, we denote the two corresponding versions of the scenario by $\mathrm{LMI1_p}$ and $\mathrm{LMI2_p}$. For $\mathrm{LMI1_p}$, it is natural to take a flat prior on γ, namely $\gamma \in [0,1]$. In fact, $\gamma = 0$ is numerically pathological and, therefore, in practice, we consider $\gamma \in [0.1,1]$. For the parameter β, one takes a flat prior $\beta \in [0.01, \beta_{\rm max}(\gamma)]$, where

$$\beta_{\rm max}(\gamma) = 2^{2-3\gamma/2}\,(0.1)^{\gamma/2}\,\frac{(1-\gamma)^{1-\gamma/2}}{\gamma^{1+\gamma/2}}. \tag{A.46}$$

As discussed in ref. [5], the condition $\beta < \beta_{\rm max}(\gamma)$ is mandatory in order for the slow-roll conditions to be valid.

JCAP03(2014)039

Let us now turn to LMI2$_{\rm p}$. For this case, we also consider a flat prior on γ, $\gamma \in [0.1, 0.99]$. For this model, there is no condition on β in order to satisfy the slow-roll and, therefore, one takes a flat prior on this parameter, namely $\beta \in [0.01, 10]$. Finally, the order of magnitude of $x_{\rm end}$ is not specified and this suggests a Jeffreys prior. Notice also that one must have $x_{\rm end} > x_{\rm end}^{\rm min}(\gamma, \beta, \Delta N_{\rm min})$ in order to have at least $\Delta N_{\rm min}$ e-folds during inflation (typically $\Delta N_{\rm min} \simeq 50$). Combining these two pieces of information leads us to the following prior $\log(x_{\rm end}) \in [\log(x_{\rm end}^{\rm min}), \log(100\, x_{\rm end}^{\rm min})]$.

Let us now treat the case where the priors are chosen from considerations based on the form of the scale factor (A.42). We denote these versions LMI1$_{\rm o}$ and LMI2$_{\rm o}$. This means that we first choose A and λ and then infer γ and β from eqs. (A.44). For the LMI1$_{\rm o}$ model, since λ is a $\mathcal{O}(1)$ parameter, one takes a flat prior on this parameter, namely $\lambda \in [1, 6]$. For the parameter A, one needs to take into account the fact that there is a maximum value of β, see the above discussion. In fact, it is possible to invert eqs. (A.44) and to express A in terms of β and γ. One finds

$$A = \left(\frac{2}{\beta}\right)^{2/\gamma} \left(\frac{2}{\gamma}\right)^{2} \frac{1}{8(2/\gamma - 1)}. \tag{A.47}$$

Given that $2/\gamma > 1$, the presence of a $\beta_{\rm max}$ implies a $A_{\rm min}$ which can be expressed as

$$A_{\rm min} = \left(\frac{2}{\beta_{\rm max}}\right)^{2/\gamma} \left(\frac{2}{\gamma}\right)^{2} \frac{1}{8(2/\gamma - 1)}. \tag{A.48}$$

In addition, since the order of magnitude of A is a priori not fixed, one chooses to work with a Jeffreys prior. We therefore take $\log(A) \in [A_{\rm min}(\lambda), 2]$.

Let us finally examine the LMI2$_{\rm o}$ version. We take the same prior on λ and $x_{\rm end}$ as before. Since there is no maximum value of β anymore, there is no minimal value of A. As a consequence, we work with the following prior on A: $\log(A) \in [-2, 2]$.

All the above considerations are summarised in the following table:

Name	Priors	$\ln(\mathcal{E}/\mathcal{E}_{\rm HI})$	$\mathcal{C}$	N	$\ln(\mathcal{L}_{\rm max}/\mathcal{E}_{\rm HI})$
LMI1$_{\rm p}$	$\gamma \in [0.1, 1]$ $\beta \in [0.01, \beta_{\rm max}(\gamma)]$	-1.36	3.06	4	2.29
LMI1$_{\rm o}$	$\lambda \in [1, 6]$ $\log(A) \in [A_{\rm min}(\lambda), 2]$	-0.99	2.83	4	2.24
LMI2$_{\rm p}$	$\gamma \in [0.1, 0.99]$ $\beta \in [0.01, 10]$ $\log(x_{\rm end}) \in [\log(x_{\rm end}^{\rm min}), \log(100\, x_{\rm end}^{\rm min})]$	-4.35	3.74	5	2.29
LMI2$_{\rm o}$	$\lambda \in [1.1, 6]$ $\log(A) \in [-2, 2]$ $\log(x_{\rm end}) \in [\log(x_{\rm end}^{\rm min}), \log(100\, x_{\rm end}^{\rm min})]$	-3.93	3.24	5	2.29

A.29 Twisted inflation (TWI)

The potential of Twisted Inflation (TWI) is given by the following expression

$$V(\phi) = M^4 \left[1 - A \left(\frac{\phi}{\phi_0}\right)^2 e^{-\phi/\phi_0}\right], \tag{A.49}$$

JCAP03(2014)039

where the two parameters M and ϕ_0 can be expressed as

$$M^4 = \frac{8\mathcal{N}}{A\pi^2(2\pi R)^4}, \quad \frac{\phi_0}{M_{\rm Pl}} = \frac{1}{2\pi R M_{\rm Pl}}, \tag{A.50}$$

the constant A being defined by $A = 32/[93\zeta(5)] \simeq 0.33$. This model is based on higher dimensional supersymmetric gauge theories, more precisely U($\mathcal{N}$) Yang-Mills theory, and R represents the radius of compactification. The above potential is valid provided $RM_{\rm Pl} \gg 1$, that is to say $\phi_0/M_{\rm Pl} \ll 1$. In fact, the model makes sense if $\phi \ll M_{\rm Pl}$ for any *vev* and not only ϕ_0, see ref. [5] for more detail. Inflation cannot stop by violation of the slow-roll conditions and, as a consequence, one needs to introduce another mechanism which is characterised by a new parameter, $\phi_{\rm end}$. TWI inflation is therefore a two parameter model.

Let us now discuss the priors. We have just seen that ϕ_0 must be sub-Planckian. Since its order of magnitude is a priori unknown, it seems natural to take a Jeffreys prior, namely $\log(\phi_0/M_{\rm Pl}) \in [-4,-1]$. Concerning the *vev* at which inflation ends, we know that $\phi_{\rm end}/\phi_0 > 2$ because the minimum of the potential is located at $\phi/\phi_0 = 2$. Otherwise, as already discussed, the only other constraint is $\phi_{\rm end} \ll M_{\rm Pl}$. However, in practice, for values of $\phi_{\rm end}$ approaching the Planck mass, the potential is so flat that this regime is already strongly disfavoured (because $n_{\rm S} \simeq 1$). Therefore, it is better to choose an upper bound for $\log(\phi_{\rm end}/\phi_0)$ supplemented with the hard prior $\phi_{\rm end} < M_{\rm Pl}$. Then, one can study if the evidence is changed if we modify the upper bound. Since the order of magnitude of this parameter is a priori not specified, we must also take a Jeffreys prior on ϕ_0. To summarise, we consider the two following priors $\log(\phi_{\rm end}/\phi_0) \in [\log(2), \log(20)]$ and $\log(\phi_{\rm end}/\phi_0) \in [\log(2), \log(40)]$ and check that, indeed, the final result is not sensitive to the upper bound. In the following, we denote these priors by TWI_{ϕ_0} and $\mathrm{TWI}^{\rm r}_{\phi_0}$.

At the fundamental level, Twisted Inflation is in fact characterised by $\mathcal{N}$ and not by ϕ_0. If we CMB normalise the model, one can express the latter in terms of the former, namely $\phi_0/M_{\rm Pl} \simeq 10^{-5}/\sqrt{\mathcal{N}}$. In this version of the model, denoted by TWI and $\mathrm{TWI}^{\rm r}$ in what follows, the prior choices are now fixed on $\mathcal{N}$ (and the value of ϕ_0 is calculated using the above equation). Since $\mathcal{N}$ is a priori a number of order one, it makes sense to take a flat prior and we choose $\mathcal{N} \in [1, 100]$. Concerning $\phi_{\rm end}$, we just take the same priors as before.

Name	Priors	$\ln(\mathcal{E}/\mathcal{E}_{\rm HI})$	$\mathcal{C}$	N	$\ln(\mathcal{L}_{\rm max}/\mathcal{E}_{\rm HI})$
TWI_{ϕ_0}	$\log(\phi_0/M_{\rm Pl}) \in [-4,-1]$ $\log(\phi_{\rm end}/\phi_0) \in [\log(2), \log(20)]$ $\phi_{\rm end} < M_{\rm Pl}$	-0.73	1.64	4	2.27
$\mathrm{TWI}^{\rm r}_{\phi_0}$	$\log(\phi_0/M_{\rm Pl}) \in [-4,-1]$ $\log(\phi_{\rm end}/\phi_0) \in [\log(2), \log(40)]$ $\phi_{\rm end} < M_{\rm Pl}$	-0.83	1.66	4	2.27
TWI	$\mathcal{N} = 10^{-10}(\phi_0/M_{\rm Pl})^{-2} \in [1, 100]$ $\log(\phi_{\rm end}/\phi_0) \in [\log(2), \log(20)]$ $\phi_{\rm end} < M_{\rm Pl}$	-2.74	1.50	4	2.27
TWI	$\mathcal{N} = 10^{-10}(\phi_0/M_{\rm Pl})^{-2} \in [1, 100]$ $\log(\phi_{\rm end}/\phi_0) \in [\log(2), \log(40)]$ $\phi_{\rm end} < M_{\rm Pl}$	-1.55	1.55	4	2.27

JCAP03(2014)039

A.30 Generalised MSSM inflation (GMSSMI)

This model is a generalisation of MSSMI studied in section A.18. The potential can be expressed as [5]

$$V(\phi) = M^4 \left[\left(\frac{\phi}{\phi_0} \right)^2 - \frac{2}{3}\alpha \left(\frac{\phi}{\phi_0} \right)^6 + \frac{\alpha}{5} \left(\frac{\phi}{\phi_0} \right)^{10} \right]. \tag{A.51}$$

This is a two-parameters model, ϕ_0 and α, and the potential of MSSMI is recovered for $\alpha = 1$. As already discussed in section A.18 and in ref. [5], the typical value for the *vev* ϕ_0 is $\phi_0 \simeq 10^{14}$GeV. The model can also be viewed as a phenomenological one, that is to say as a representative of the class of the so-called inflection point inflationary scenario.

Let us now discuss the priors. Viewed as a phenomenological model (denoted by $\mathrm{GMSSMI_p}$ in what follows), the model is such that the scale of ϕ_0 is unspecified and, therefore, a Jeffreys prior is appropriate. We choose to work with $\log(\phi_0/M_{\mathrm{Pl}}) \in [-5, 5]$. On the other hand, the parameter α is of order one and, as a consequence, we take a flat prior: $\alpha \in [0.9, 1.1]$. Finally, a hard prior has been implemented to reject all non slow-roll cases (defined to have $|\epsilon_2| > 0.2$).

If we now want to calculate the evidence of the model motivated by particle physics, we must include in the analysis the fact that the *vev* ϕ_0 is around 10^{14}GeV. For this reason, we choose a flat prior such that $\phi_0/M_{\mathrm{Pl}} \in [2 \times 10^{-5}, 2 \times 10^{-4}]$. One also knows that, if α is not precisely tuned around $\alpha = 1$, then the model can not support slow-roll inflation and is, therefore, ruled out. Moreover, requiring at least $\Delta N \simeq 60$ e-fold during inflation leads to the constraint

$$|\alpha - 1| < \frac{\phi_0^4}{M_{\mathrm{Pl}}^4} \frac{\pi^2}{900 \Delta N^2}, \tag{A.52}$$

see ref. [5]. This formula tells us that, if $|\alpha - 1| \gtrsim 10^{-20}$, then the model is ruled out. This illustrates the extreme fine-tuning needed for this model to be compatible with the Planck data. When $\alpha > 1$, we implement this fine-tuning through two different choices of priors satisfying the above condition, namely $\log(1 - \alpha) \in [-28, -23]$ and $\log(1 - \alpha) \in [-28, -20]$, corresponding to the $\mathrm{GMSSMI_{omA}}$ and $\mathrm{GMSSMI_{omB}}$ versions of the model, $\mathrm{GMSSMI_{omB}}$ being on the validity threshold. If $\alpha > 1$, we define two other models denoted $\mathrm{GMSSMI_{opA}}$ and $\mathrm{GMSSMI_{opB}}$ such that $\log(\alpha - 1) \in [-28, -23]$ and $\log(\alpha - 1) \in [-28, -21.75]$. Our choices for the priors are summarised in the following table:

JCAP03(2014)039

Name	Priors	$\ln(\mathcal{E}/\mathcal{E}_{\rm HI})$	$\mathcal{C}$	N	$\ln(\mathcal{L}_{\rm max}/\mathcal{E}_{\rm HI})$
$\mathrm{GMSSMI_{p}}$	$\log(\phi_0/M_{\rm Pl}) \in [-5,5]$ $\alpha \in [0.9,1.1]$	-2.54	4.96	4	1.77
$\mathrm{GMSSMI_{opA}}$	$\phi_0/M_{\rm Pl} \in [2\times10^{-5}, 2\times10^{-4}]$ $\log(\alpha-1) \in [-28,-23]$ $\ln R \in [-46,0]$, $\Delta N > 60$	-10.30	0.76	4	-7.40
$\mathrm{GMSSMI_{opB}}$	$\phi_0/M_{\rm Pl} \in [2\times10^{-5}, 2\times10^{-4}]$ $\log(\alpha-1) \in [-28,-21.75]$ $\ln R \in [-46,0]$, $\Delta N > 60$	-10.41	0.76	4	-7.40
$\mathrm{GMSSMI_{omA}}$	$\phi_0/M_{\rm Pl} \in [2\times10^{-5}, 2\times10^{-4}]$ $\log(1-\alpha) \in [-28,-23]$ $\ln R \in [-46,0]$, $\Delta N > 60$	-7.85	5.39	4	2.23
$\mathrm{GMSSMI_{omB}}$	$\phi_0/M_{\rm Pl} \in [2\times10^{-5}, 2\times10^{-4}]$ $\log(1-\alpha) \in [-28,-20]$ $\ln R \in [-46,0]$, $\Delta N > 60$	-5.25	2.87	4	2.27

One may also wonder how the evidence would be changed if one penetrates the regime where eq. (A.52) is not satisfied (and where the slow-roll approximation is not satisfied). In that case, since all non slow-roll models are incompatible with the Planck data, the evidence should only be rescaled by the ratio of the prior volumes. Therefore, in the following, we study the more general situation where $\log|\alpha-1| \in [-28,-\ell]$, where ℓ is the variable with respect to which we want to study the behaviour of the Bayesian evidence. In the prior plane $[\phi_0/M_{\rm Pl}, \log|1-\alpha|]$, eq. (A.52) defines a line above which the likelihood vanishes (since, in that case and as already mentioned, the model becomes incompatible with the data). This curve approximately goes from $(2\times10^{-5}, -24 \equiv \ell_{\rm c}^{\rm min})$ to $(2\times10^{-4}, -20 \equiv \ell_{\rm c}^{\rm max})$ and, therefore, defines three different regions according to whether $-\ell < \ell_{\rm c}^{\rm min}$, $-\ell \in [\ell_{\rm c}^{\rm min}, \ell_{\rm c}^{\rm max}]$ or $-\ell > \ell_{\rm c}^{\rm max}$.

Let us first assume that $\alpha > 1$ and $\log(\alpha-1) \in [-28,-\ell]$. If $-\ell \lesssim -24$, then $\alpha-1$ is so small that one expects the model to be equivalent to MSSMI. If $\ell \in [\ell_{\rm c}^{\rm min}, \ell_{\rm c}^{\rm max}]$ (denoted the "transition region" in what follows), then only numerical calculations can track the behaviour of the evidence. Notice that $\mathrm{GMSSMI_{opA}}$ and $\mathrm{GMSSMI_{opB}}$ belongs to this region. Finally, for $-\ell > \ell_{\rm c}^{\rm max}$, one expects the evidence to scale with the ratio of the prior volumes. These expectations are confirmed in figure 5 (solid green line). However, for numerical reasons, we are in fact unable to follow the evidence beyond the point $-\ell \simeq -21.75$ ($\mathrm{GMSSMI_{opB}}$ model) which is still in the transition region. One can nevertheless assume that the evidence does not change much between that point and the edge of the transition region (hence the small horizontal dashed red segment inside the transition region in figure 5). In that case, in the regime $-\ell > \ell_{\rm c}^{\rm max}$, one can write

$$\ln\left[\frac{\mathcal{E}_{\log(\alpha-1)\in[-28,-\ell]}}{\mathcal{E}_{\rm HI}}\right] \simeq \ln\left(\frac{\mathcal{E}_{\rm GMSSMI_{opB}}}{\mathcal{E}_{\rm HI}}\right) + \ln(28-\ell_{\rm c}^{\rm max}) - \ln(28-\ell)\,. \tag{A.53}$$

This rough approximation can be considered as reasonable because it gives an upper bound on the value of the evidence (since the evidence can only decrease in the transition region) which is, anyhow, in a regime where the model is strongly disfavoured. Moreover, one should also keep in mind that we are close to a regime where the numerical calculations cannot really be trusted (light red shaded region).

The case $\alpha < 1$ is very similar and in figure 5, we have represented different numerical values of the Bayes factor versus $-\ell$ (blue solid line). The interpretation is very similar and

JCAP03(2014)039

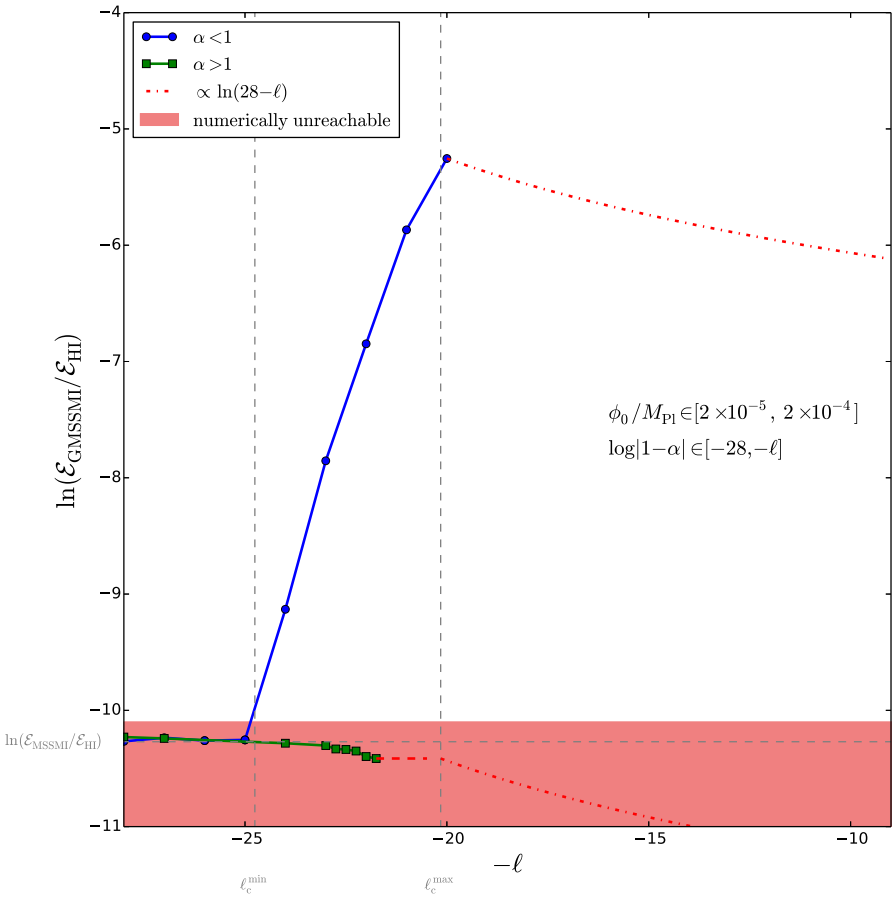

Figure 5. Evolution of the GMSSMI Bayes factor versus the upper bound $-\ell$ of the prior range on α for $\alpha > 1$ and $\alpha < 1$. The green squares and blue circles represent numerical values of the evidence. The dotted red curves represent the analytical laws giving the behaviour of the Bayes factor versus $-\ell$ for $-\ell \gtrsim \ell_{\rm c}^{\rm max}$ according to eqs. (A.53) and (A.54). These equations predict how the Bayes factor behaves with $-\ell$ and, therefore, can be used to extrapolate in regimes where α becomes of order one.

one notices that, this time, one can track the evidence until the end of the transition regime, i.e. until the GMSSMI$_{\rm omB}$ model. Then, one can extrapolate it using again the ratio of the prior volumes and this leads to the following expression

$$\ln\left(\frac{\mathcal{E}_{\log(1-\alpha)\in[-28,-\ell]}}{\mathcal{E}_{\rm HI}}\right) = \ln\left(\frac{\mathcal{E}_{\rm GMSSMI_{omB}}}{\mathcal{E}_{\rm HI}}\right) + \ln\left(28-\ell_{\rm c}^{\rm max}\right) - \ln\left(28-\ell\right). \tag{A.54}$$

This expression is plotted as the (upper) dotted red line in figure 5 and allows us to extrapolate, in a reliable way, the Bayes factor for values $-\ell \gtrsim -20$. Let us also notice that, in this case, the calculation is performed in a regime where numerical calculations are trustful.

In figure 5, one also notices that, for $\alpha > 1$, the evidence decreases in the transition region while, for $\alpha < 1$, it grows. This is because the spectral index of GMSSMI decreases with the value of α starting from the MSSMI value $n_{\rm S} \simeq 0.9$ when $|\alpha - 1| \simeq 0$. As a consequence, when $\alpha < 1$, if $-\ell$ is increased then $n_{\rm S}$ grows and, therefore, crosses the Planck best fit region. For this reason, the blue curve in figure 5 increases in the transition region.

JCAP03(2014)039

In the case $\alpha > 1$, one observes the opposite behaviour since, in that situation, the model moves away from the Planck best fit region.

The previous considerations allow us to extrapolate the evidence analytically to the theoretical prior in which α varies up to unity. Those two extrapolated models have been named $\mathrm{GMSSMI}_{\mathrm{ep}}$ and $\mathrm{GMSSMI}_{\mathrm{em}}$ in the next table and their evidence have been estimated using the two equations derived above, namely eqs. (A.53) and (A.54).

Name	Priors	$\ln(\mathcal{E}/\mathcal{E}_{\mathrm{HI}})$	$\mathcal{C}$	N	$\ln(\mathcal{L}_{\max}/\mathcal{E}_{\mathrm{HI}})$
$\mathrm{GMSSMI}_{\mathrm{ep}}$	$\phi_0/M_{\mathrm{Pl}} \in [2\times10^{-5}, 2\times10^{-4}]$ $\log(\alpha-1) \in [-28,-0]$ $\ln R \in [-46, 0]$	-11.69	3.00	4	-7.40
$\mathrm{GMSSMI}_{\mathrm{em}}$	$\phi_0/M_{\mathrm{Pl}} \in [2\times10^{-5}, 2\times10^{-4}]$ $\log(1-\alpha) \in [-28,-0]$ $\ln R \in [-46, 0]$	-6.53	3.88	4	2.27

In the above table, the complexities have been rescaled following the rough estimate given by eq. (A.8).

A.31 Generalised renormalisable point inflation (GRIPI)

In the very same way as GMSSMI is a generalisation of MSSMI, see section A.30, the GRIPI potential is a generalisation of the RIPI one, see section A.19. This potential can be written as

$$V(\phi) = M^4\left[\left(\frac{\phi}{\phi_0}\right)^2 - \frac{4\alpha}{3}\left(\frac{\phi}{\phi_0}\right)^3 + \frac{\alpha}{2}\left(\frac{\phi}{\phi_0}\right)^4\right], \tag{A.55}$$

and depends on two parameters, ϕ_0 and α. The case $\alpha = 1$ corresponds to the RIPI potential. As discussed in ref. [5], the typical value of the *vev* ϕ_0 is given by $\phi_0 \simeq 10^{14}\mathrm{GeV}$ and/or $\phi_0 \simeq 10^{17}\mathrm{GeV}$. In fact, in the case $\phi_0 \simeq 10^{14}\mathrm{GeV}$, the amount of fine-tuning is similar to the GMSSMI case. For this reason, it is not so interesting to replicate the discussion of the previous section and, here, one focuses on the case $\phi_0 \simeq 10^{17}\mathrm{GeV}$ where one can expect the fine tuning problem to be sligthly less severe.

Let us now discuss the priors. The GRIPI potential can always be viewed as a phenomenological model (simply denoted $\mathrm{GRIPI}_{\mathrm{p}}$ in what follows). In that case, the order of magnitude of the parameter ϕ_0 is not specified and, therefore, one chooses a Jeffreys prior, namely $\log(\phi_0/M_{\mathrm{Pl}}) \in [-5, 5]$. Regarding the parameter α, since it is of order one, we simply take $\alpha \in [0.9, 1.1]$. As for GMSSMI, we have also added a hard prior boundary, enforcing $|\epsilon_2| < 0.2$, as otherwise some regions of the parameter space would predict non-slow-roll inflation.

Returning to the original version of the model and considering the fact that, in this case, the *vev* ϕ_0 is specified, we choose the prior $\phi_0/M_{\mathrm{Pl}} \in [2\times10^{-2}, 2\times10^{-1}]$. As for GMSSMI, if α is not tuned around $\alpha = 1$, the model becomes inconsistent. Requiring at least $\Delta N \simeq 60$ e-fold during inflation leads to the condition

$$|\alpha - 1| < \frac{\phi_0^4}{M_{\mathrm{Pl}}^4}\frac{\pi^2}{576\Delta N^2}, \tag{A.56}$$

see ref. [5] and, therefore, if $|\alpha - 1| \gtrsim 10^{-8}$, then the model is a priori ruled out. As a consequence, when $\alpha > 1$, we consider two cases satisfying the above constraint namely

JCAP03(2014)039

$\log(1-\alpha) \in [-15, -10]$ and $\log(1-\alpha) \in [-28, -8]$, thus defining the $\mathrm{GRIPI}_{\mathrm{omA}}$ and $\mathrm{GRIPI}_{\mathrm{omB}}$ models. If $\alpha > 1$, we define two other models denoted $\mathrm{GRIPI}_{\mathrm{opA}}$ and $\mathrm{GRIPI}_{\mathrm{opB}}$ such that $\log(\alpha - 1) \in [-28, -10]$ and $\log(\alpha - 1) \in [-28, -8]$.

Finally, the GRIPI potential can also arise in a supergravity framework (we denote this version of the scenario $\mathrm{GRIPI}_{\mathrm{sugra}}$). In that case, there is usually a shift symmetry which allows us to consider super-Planckian *vev* of the field. For this reason, we also investigate the prior $\phi_0/M_{\mathrm{Pl}} \in [10, 50]$. The prior on α is still taken to be with $\alpha \in [0.9, 1.1]$ in agreement with the previous discussion. All the considerations presented in this section are summarised in the table below.

Name	Priors	$\ln(\mathcal{E}/\mathcal{E}_{\mathrm{HI}})$	$\mathcal{C}$	N	$\ln(\mathcal{L}_{\max}/\mathcal{E}_{\mathrm{HI}})$
$\mathrm{GRIPI}_{\mathrm{p}}$	$\log(\phi_0/M_{\mathrm{Pl}}) \in [-5, 5]$ $\alpha \in [0.9, 1.1]$	-2.77	4.00	4	2.29
$\mathrm{GRIPI}_{\mathrm{opA}}$	$\phi_0/M_{\mathrm{Pl}} \in [2\times10^{-2}, 2\times10^{-1}]$ $\log(\alpha-1) \in [-15, -10]$ $\ln R \in [-46, 0]$, $\Delta N > 60$	-5.10	3.14	4	-0.31
$\mathrm{GRIPI}_{\mathrm{opB}}$	$\phi_0/M_{\mathrm{Pl}} \in [2\times10^{-2}, 2\times10^{-1}]$ $\log(\alpha-1) \in [-15, -8]$ $\ln R \in [-46, 0]$, $\Delta N > 60$	-5.39	3.21	4	-0.31
$\mathrm{GRIPI}_{\mathrm{omA}}$	$\phi_0/M_{\mathrm{Pl}} \in [2\times10^{-2}, 2\times10^{-1}]$ $\log(1-\alpha) \in [-15, -10]$ $\ln R \in [-46, 0]$, $\Delta N > 60$	-4.60	6.42	4	1.87
$\mathrm{GRIPI}_{\mathrm{omB}}$	$\phi_0/M_{\mathrm{Pl}} \in [2\times10^{-2}, 2\times10^{-1}]$ $\log(1-\alpha) \in [-15, -8]$ $\ln R \in [-46, 0]$, $\Delta N > 60$	-4.30	5.72	4	1.99
$\mathrm{GRIPI}_{\mathrm{sugra}}$	$\phi_0/M_{\mathrm{Pl}} \in [10, 50]$ $\alpha \in [0.9, 1.1]$	-0.96	2.96	4	2.23

As was done in the case of GMSSM inflation in the previous section, one can also study how the choice of the prior on α affects the determination of the Bayesian evidence. For this reason, we consider the following priors: $\log(\alpha - 1) \in [-15, -\ell]$ for $\alpha > 1$ and $\log(1 - \alpha) \in [-15, -\ell]$ for $\alpha < 1$. The dependence of the evidence with respect to ℓ can be derived as in the previous section. In the prior plane $[\phi_0/M_{\mathrm{Pl}}, \log|1-\alpha|]$, eq. (A.56) defines a line above which the likelihood is tiny and can be considered to be vanishing. This line divides the prior space into two parts and goes from $(2\times10^{-2}, -12 \equiv \ell_{\mathrm{c}}^{\mathrm{min}})$ to $(2\times10^{-1}, -8 \equiv \ell_{\mathrm{c}}^{\mathrm{max}})$ and, therefore, defines three different regions according to whether $-\ell < \ell_{\mathrm{c}}^{\mathrm{min}}$, $-\ell \in [\ell_{\mathrm{c}}^{\mathrm{min}}, \ell_{\mathrm{c}}^{\mathrm{max}}]$ or $-\ell > \ell_{\mathrm{c}}^{\mathrm{max}}$.

Let us first assume that $\alpha > 1$. If $-\ell \lesssim -15$, then $\alpha - 1$ is tiny and one expects GRIPI to be equivalent to RIPI (with the same value of ϕ_0). If $\ell \in [\ell_{\mathrm{c}}^{\mathrm{min}}, \ell_{\mathrm{c}}^{\mathrm{max}}]$, then only numerical calculations can track the behaviour of the evidence. Notice that $\mathrm{GRIPI}_{\mathrm{opA}}$ and $\mathrm{GRIPI}_{\mathrm{opB}}$ belongs to this region. Finally, for $-\ell > \ell_{\mathrm{c}}^{\mathrm{max}}$, one expects the evidence to scale with the ratio of the prior volumes. In that case, one can write

$$\ln\left(\frac{\mathcal{E}_{\log(\alpha-1)\in[-15,-\ell]}}{\mathcal{E}_{\mathrm{HI}}}\right) = \ln\left(\frac{\mathcal{E}_{\mathrm{GRIPI}_{\mathrm{opB}}}}{\mathcal{E}_{\mathrm{HI}}}\right) + \ln(15 - \ell_{\mathrm{c}}^{\mathrm{max}}) - \ln(15 - \ell). \tag{A.57}$$

Here, we have taken $\mathrm{GRIPI}_{\mathrm{opB}}$ as the calibration model, a natural choice considering that this model lies at the frontier of the transition region. The corresponding results are represented

JCAP03(2014)039

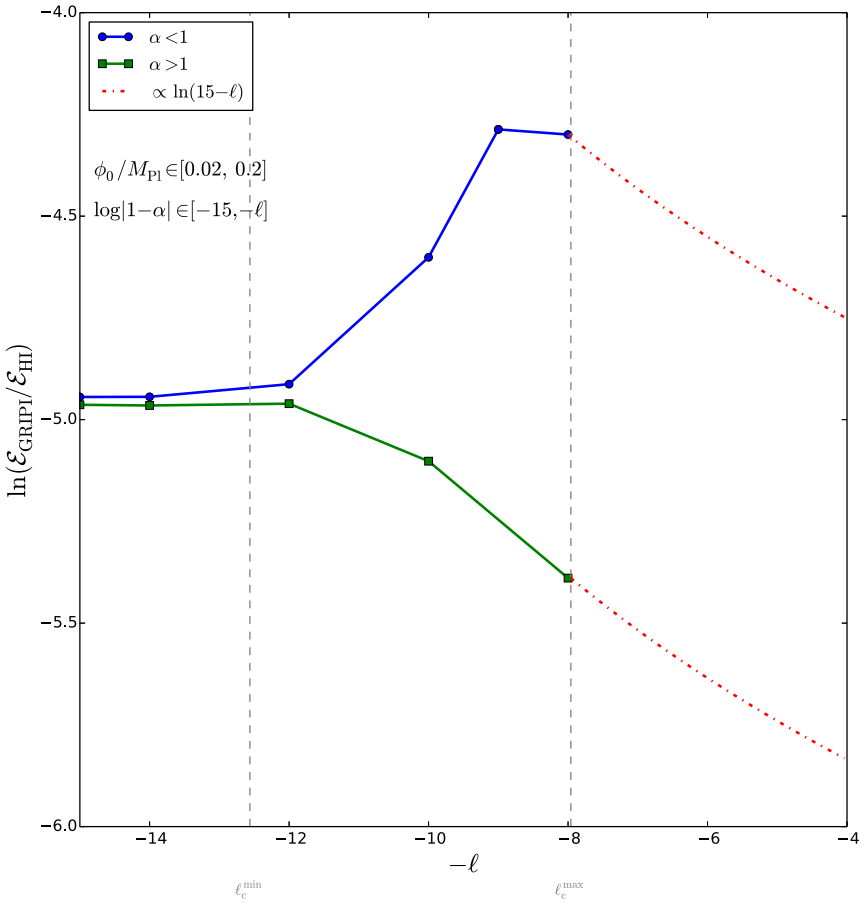

Figure 6. Evolution of the GRIPI Bayes factor versus the upper bound $-\ell$ of the prior range on α for $\alpha > 1$ and $\alpha < 1$. The green squares and blue circles represent numerical values of the evidence. The dotted red curves represent the analytical laws giving the behaviour of the Bayes factor versus $-\ell$ for $-\ell \gtrsim \ell_{\rm c}^{\rm max}$ according to eqs. (A.57) and (A.58). These equations predict how the Bayes factor behaves with $-\ell$ and, therefore, can be used to extrapolate in regimes where α becomes of order one. The behaviour of the evidences is very similar to what was found in the GMSSMI case, see figure 5. However, a difference with GMSSMI is that, in the case $\alpha > 1$, one is now able to track the Bayes factors through the entire transition region.

in figure 6 (solid green line for the numerical results and dashed red line for the extrapolated evidences).

For $\alpha < 1$, taking $\mathrm{GRIPI}_{\rm omB}$ as a calibration model, exactly the same discussion applies and one is led to (again, see figure 6)

$$\ln\left(\frac{\mathcal{E}_{\log(1-\alpha)\in[-15,-\ell]}}{\mathcal{E}_{\rm HI}}\right) = \ln\left(\frac{\mathcal{E}_{\mathrm{GRIPI}_{\rm omB}}}{\mathcal{E}_{\rm HI}}\right) + \ln(15-\ell_{\rm c}^{\rm max}) - \ln(15-\ell). \tag{A.58}$$

We can now use these formulae to rescale the evidence if α varies up to unity. Naming the two corresponding models $\mathrm{GRIPI}_{\rm ep}$ and $\mathrm{GRIPI}_{\rm em}$, their evidences have been reported below.

JCAP03(2014)039

Name	Priors	$\ln(\mathcal{E}/\mathcal{E}_{\rm HI})$	$\mathcal{C}$	N	$\ln(\mathcal{L}_{\rm max}/\mathcal{E}_{\rm HI})$
$\mathrm{GRIPI}_{\rm ep}$	$\phi_0/M_{\rm Pl} \in [2\times10^{-2}, 2\times10^{-1}]$ $\log(\alpha-1) \in [-15, 0]$	-6.15	3.79	4	-0.31
$\mathrm{GRIPI}_{\rm em}$	$\phi_0/M_{\rm Pl} \in [2\times10^{-2}, 2\times10^{-1}]$ $\log(1-\alpha) \in [-15, 0]$	-5.06	4.28	4	1.99

In this table, complexities have also been rescaled following the rough estimate given by eq. (A.8).

A.32 Brane SUSY breaking inflation (BSUSYBI)

The potential is a sum of two exponential and reads

$$V(\phi) = M^4\left(e^{\sqrt{6}\frac{\phi}{M_{\rm Pl}}} + e^{\sqrt{6}\gamma\frac{\phi}{M_{\rm Pl}}}\right). \tag{A.59}$$

In addition to the parameter γ, the field value $x_{\rm end} = \phi_{\rm end}/M_{\rm Pl}$ at which inflation ends has to be specified. Within the superstring scenario from which this model is inspired, $0 < \gamma < 1/\sqrt{3}$ [69]. However, the upper limit would already implies to $\epsilon_1(x) > 3\gamma^2 \simeq 1$ and slow-roll is violated everywhere. We have therefore limited the prior on γ to slightly lower values $\gamma < 0.3$ considering either a flat prior or a Jeffreys prior. Concerning, $x_{\rm end}$, one notices that inflation proceeds at decreasing field values and is confined in a region $x < x_{\epsilon_1=1}$, $x_{\epsilon_1=1}$ being the solution of $\epsilon_1(x) = 1$. As a result, there is a maximal bound $x_{\rm end}^{\rm max}$ which has been defined such that inflation last more than 120 e-folds. The quantity is only known numerically and is obtained by integrating the field trajectory from $x_{\rm ini} = x_{\epsilon_1=1}$ during 120 e-folds. On the contrary, there is no lower limit on the allowed values of $x_{\rm end}$ and the limit $x_{\rm end} \to -\infty$, would correspond to $n_{\rm S} = 1$ and $r = 0$. Therefore, for $x_{\rm end}$ negative enough, the likelihood, and therefore the evidence, becomes independent on the lower bound on $x_{\rm end}$. We have therefore considered the following priors:

Name	Priors	$\ln(\mathcal{E}/\mathcal{E}_{\rm HI})$	$\mathcal{C}$	N	$\ln(\mathcal{L}_{\rm max}/\mathcal{E}_{\rm HI})$
$\mathrm{BSUSYBI}_{\rm f}$	$\gamma \in [0, 0.3]$ $x_{\rm end} \in [-200, x_{\rm end}^{\rm max}]$	3.26	3.26	4	-2.54
$\mathrm{BSUSYBI}_{\rm l}$	$\log(\gamma) \in [-3, -1]$ $x_{\rm end} \in [-200, x_{\rm end}^{\rm max}]$	4.52	3.26	4	-2.54

A.33 Tip inflation (TI)

This string inspired potential has two parameters, a dimensionless coupling α and a typical *vev* μ:

$$V(\phi) = M^4\left[1 + \cos\left(\frac{\phi}{\mu}\right) + \alpha\sin^2\left(\frac{\phi}{\mu}\right)\right]. \tag{A.60}$$

As made explicit in ref. [5], these parameters encode combinations of geometrical quantities related to the relative position of branes within a conifold geometry. This potential supports inflation at its top provided $\alpha \simeq 1/2$, which amounts to some level of fine-tuning. When this condition is satisfied, μ actually gives the volume of the extra-dimensions

$$\frac{\mu}{M_{\rm Pl}} \simeq 2\times10^8\sigma_0^{9/4}, \tag{A.61}$$

where σ_0 is the stabilised value of the volume modulus in the absence of uplifting terms [70]. A typical value for σ_0 is $\sigma_0 \simeq 10^2$ which translates into $\mu/M_{\rm Pl} \simeq 10^{-4}$, up to a few orders

JCAP03(2014)039

of magnitude. Following these considerations, we have examined various priors designed to measure how important is the fine-tuning over α. In particular, the three sub-classes $\alpha \gtrsim 1/2$, $\alpha = 1/2$ and $\alpha \lesssim 1/2$ yield different observable predictions and have been treated as separated models. They are summarised below.

Name	Priors	$\ln(\mathcal{E}/\mathcal{E}_{\rm HI})$	$\mathcal{C}$	N	$\ln(\mathcal{L}_{\rm max}/\mathcal{E}_{\rm HI})$
$\mathrm{TI}^{\rm ft+}_{\alpha>1/2}$	$\alpha \in]0.5, 0.5+10^{-7}]$ $\log(\mu/M_{\rm Pl}) \in [-5,-3]$	-4.37	3.51	4	1.95
$\mathrm{TI}^{\rm ft}_{\alpha>1/2}$	$\alpha \in]0.5, 0.5+2\times10^{-7}]$ $\log(\mu/M_{\rm Pl}) \in [-5,-3]$	-5.19	3.53	4	1.95
$\mathrm{TI}^{\rm ft-}_{\alpha>1/2}$	$\alpha \in]0.5, 0.5+10^{-6}]$ $\log(\mu/M_{\rm Pl}) \in [-5,-3]$	-6.99	3.51	4	1.95
$\mathrm{TI}_{1/2}$	$\alpha = 1/2$ $\log(\mu/M_{\rm Pl}) \in [-5,-3]$	-1.90	2.82	3	1.95
$\mathrm{TI}^{\rm ft+}_{\alpha<1/2}$	$\alpha \in [0.5-10^{-7}, 0.5[$ $\log(\mu/M_{\rm Pl}) \in [-5,-3]$	-1.92	2.59	4	2.21
$\mathrm{TI}^{\rm ft}_{\alpha<1/2}$	$\alpha \in [0.5-10^{-6}, 0.5[$ $\log(\mu/M_{\rm Pl}) \in [-5,-3]$	-4.64	2.60	4	2.21
$\mathrm{TI}^{\rm ft-}_{\alpha<1/2}$	$\alpha \in [0.5-10^{-5}, 0.5[$ $\log(\mu/M_{\rm Pl}) \in [-5,-3]$	-7.12	2.59	4	2.21

For completeness, we have also considered models in which $\alpha \simeq 1/2$ without any prior prejudice on the sign of $\alpha - 1/2$. One gets the following evidences:

Name	Priors	$\ln(\mathcal{E}/\mathcal{E}_{\rm HI})$	$\mathcal{C}$	N	$\ln(\mathcal{L}_{\rm max}/\mathcal{E}_{\rm HI})$
$\mathrm{TI}_{\rm ft+}$	$\alpha \in [0.5-10^{-7}, 0.5+10^{-7}]$ $\log(\mu/M_{\rm Pl}) \in [-5,-3]$	-2.65	2.74	4	2.21
$\mathrm{TI}_{\rm ft}$	$\alpha \in [0.5-10^{-6}, 0.5+10^{-6}]$ $\log(\mu/M_{\rm Pl}) \in [-5,-3]$	-5.26	2.74	4	2.21
$\mathrm{TI}_{\rm ft-}$	$\alpha \in [0.5-10^{-5}, 0.5+10^{-5}]$ $\log(\mu/M_{\rm Pl}) \in [-5,-3]$	-7.78	2.75	4	2.21

One can also wonder what happens if one detunes the prior on α since, after all, this fine-tuning is not theoretically motivated. Let us first consider the case where $\alpha > 1/2$. We want to calculate the evidence if the prior on α is chosen such that $\alpha \in]0.5, 0.5+a]$. We assume that, for $a > 10^{-6}$, the likelihood vanishes (which is, according to the results presented in the tables, a realistic hypothesis). Applying the considerations presented earlier [see eq. (A.4)] and taking as a calibration model $\mathrm{TI}^{\rm ft-}_{\alpha>1/2}$, one obtains that for $a > 10^{-6}$

$$\mathcal{E}_{\alpha\in]0.5,0.5+a]} = \mathcal{E}_{\alpha\in]0.5,0.5+10^{-6}]}\frac{10^{-6}}{a}\,, \tag{A.62}$$

or

$$\ln\left(\frac{\mathcal{E}_{\alpha\in]0.5,0.5+a]}}{\mathcal{E}_{\rm HI}}\right) = \ln\left(\frac{\mathcal{E}_{\mathrm{TI}^{\rm ft-}_{\alpha>1/2}}}{\mathcal{E}_{\rm HI}}\right) - 6\ln(10) - \ln(a) \simeq -6.99 - 6\ln(10) - \ln(a). \tag{A.63}$$

If we now assume $\alpha < 1/2$, the same considerations lead to a similar formula, namely

$$\ln\left(\frac{\mathcal{E}_{\alpha\in]0.5-a,0.5]}}{\mathcal{E}_{\rm HI}}\right) = \ln\left(\frac{\mathcal{E}_{\mathrm{TI}^{\rm ft-}_{\alpha<1/2}}}{\mathcal{E}_{\rm HI}}\right) - 5\ln(10) - \ln(a) \simeq -7.12 - 5\ln(10) - \ln(a), \tag{A.64}$$

JCAP03(2014)039

for $a > 10^{-5}$. Finally, the case where the sign of $\alpha - 1/2$ is not specified yields

$$\ln\left(\frac{\mathcal{E}_{\alpha\in]0.5-a,0.5+a]}}{\mathcal{E}_{\rm HI}}\right) = \ln\left(\frac{\mathcal{E}_{\rm TI_{ft-}}}{\mathcal{E}_{\rm HI}}\right) - 5\ln(10) - \ln(a) \simeq -7.78 - 5\ln(10) - \ln(a), \quad \text{(A.65)}$$

for $a > 10^{-5}$. As expected, we see on these last three formulae that, if one increases the range of the prior in a region where the likelihood vanishes, then the corresponding models get penalised for the wasted parameter space. Therefore, the above calculations concretely illustrate the Occam's razor effect.

Applying these formulae allows us to extrapolate the evidence for a natural prior choice having $a = 10^{-1}$, i.e. assuming only $|\alpha - 0.5| < 0.1$.

Name	Priors	$\ln(\mathcal{E}/\mathcal{E}_{\rm HI})$	$\mathcal{C}$	N	$\ln(\mathcal{L}_{\rm max}/\mathcal{E}_{\rm HI})$
$\mathrm{TI}^{\rm e}_{\alpha<1/2}$	$\alpha \in [0.4, 0.5]$ $\log(\mu/M_{\rm Pl}) \in [-5, -3]$	-16.33	4.00	4	2.21
$\mathrm{TI}^{\rm e}_{\alpha>1/2}$	$\alpha \in [0.5, 0.6]$ $\log(\mu/M_{\rm Pl}) \in [-5, -3]$	-18.50	4.00	4	1.95
$\mathrm{TI}^{\rm e}$	$\alpha \in [0.4, 0.6]$ $\log(\mu/M_{\rm Pl}) \in [-5, -3]$	-16.99	4.00	4	2.21

In this table, complexities have also been rescaled following the rough estimate given by eq. (A.8). Here the volume ratio is so big that the rescaled complexities end up being very close to the number of parameters, which is certainly overestimated due to our crude assumptions in deriving eq. (A.8).

A.34 Beta exponential inflation (BEI)

This model is an extension of PLI to the generalised exponential function $\exp_{1\text{-}\beta}$ defined by $\exp_{1\text{-}\beta}(x) = (1+\beta x)^{1/\beta}$ for $1 + \beta x > 0$ and $\exp_{1\text{-}\beta}(x) = 0$ otherwise. The potential therefore reads

$$V(\phi) = M^4 \exp_{1\text{-}\beta}\left(\lambda\frac{\phi}{M_{\rm Pl}}\right), \quad \text{(A.66)}$$

where $\lambda > 0$ is a dimensionless parameter. As detailed in ref. [5], inflation ends naturally only for $\beta > 0$, which will be our prior. The model being phenomenological, there is no natural value for λ and we have chosen a Jeffreys prior. Moreover, one can show that the slow-roll observable predictions does not depend on λ, and thus the prior boundaries do not affect the evidence. In the limit $\beta \to 0$, the model becomes strongly disfavoured such that, changing the lower limit of the β-prior accordingly decreases the evidence of the model. This is summarised in the following table:

Name	Priors	$\ln(\mathcal{E}/\mathcal{E}_{\rm HI})$	$\mathcal{C}$	N	$\ln(\mathcal{L}_{\rm max}/\mathcal{E}_{\rm HI})$
BEI	$\log(\lambda) \in [-3, 3]$ $\log(\beta) \in [-1.5, 3]$	-0.99	2.65	4	2.29

A.35 Pseudo natural inflation (PSNI)

The potential of PSNI reads

$$V(\phi) = M^4\left[1 + \alpha\ln\left(\cos\frac{\phi}{f}\right)\right], \quad \text{(A.67)}$$

JCAP03(2014)039

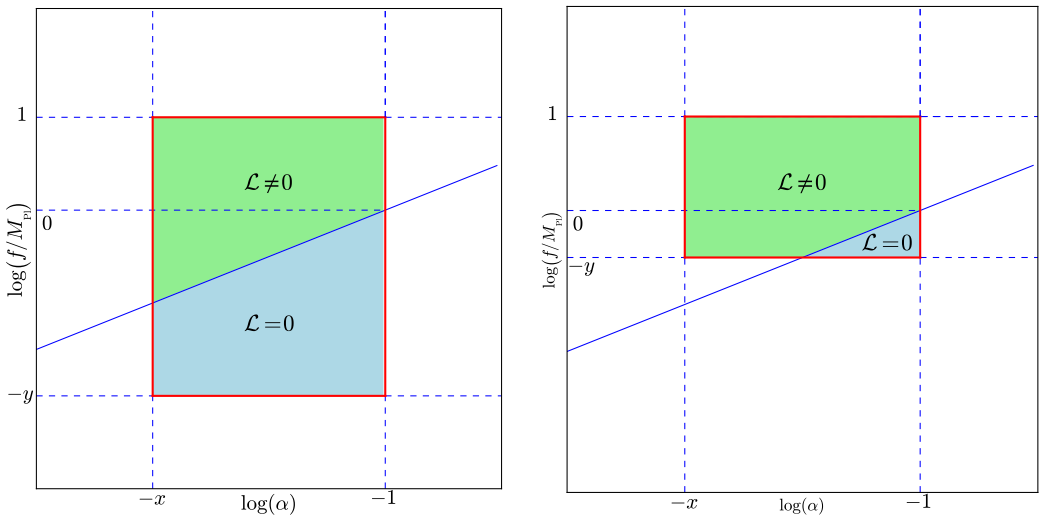

Figure 7. Priors for PSNI inflation in the plane $[\log\alpha, \log(f/M_{\rm Pl})]$. The red rectangle represents the theoretical motivated prior. The blue line represents the condition of validity of the slow-roll approximation, namely $\alpha f^2/M_{\rm Pl}^2 < 0.1$. Above this line (green region), slow-roll is satisfied and below (blue region) slow-roll is strongly violated. As a consequence, the likelihood vanishes in the blue region and is different from zero in the green one. Numerically, one can only determine the Bayesian evidence with a prior corresponding to the green region. The evidence corresponding to the red rectangle can be derived from analytical considerations (see text). The left panel corresponds to the situation where $y > (x-1)/2$ while the right panel is for $y < (x-1)/2$.

where α is a dimensionless coupling and f is an energy scale. In order for the model to be consistent, one should have $f < m_{\rm Pl} = \sqrt{8\pi}M_{\rm Pl}$ and $\alpha \ll 1$ [71]. As discussed in ref. [5], the above potential has $\epsilon_2 > \epsilon_2^{\rm min} = 2\alpha M_{\rm Pl}^2/f^2$ and slow-roll inflation can occur only if $\alpha M_{\rm Pl}^2/f^2$ is constrained to be small.

A first phenomenological choice of priors therefore consists in adopting prior boundaries for uniform priors in the quantities $\log(\alpha M_{\rm Pl}^2/f^2)$ and $\log(f/M_{\rm Pl})$. Taking $\log(f/M_{\rm Pl}) \in [-2,1]$ and $\log(\alpha M_{\rm Pl}^2/f^2) < -1$, different lower bounds on $\alpha M_{\rm Pl}^2/f^2$ have been studied, corresponding to different levels of fine-tuning of this parameter.

Name	Priors	$\ln(\mathcal{E}/\mathcal{E}_{\rm HI})$	$\mathcal{C}$	N	$\ln(\mathcal{L}_{\rm max}/\mathcal{E}_{\rm HI})$
$\rm PSNI_{ft1}$	$\log(\alpha M_{\rm Pl}^2/f^2) \in [-5,-1]$ $\log(f/M_{\rm Pl}) \in [-2,1]$	-0.42	2.13	4	2.29
$\rm PSNI_{ft2}$	$\log(\alpha M_{\rm Pl}^2/f^2) \in [-3,-1]$ $\log(f/M_{\rm Pl}) \in [-2,1]$	-0.41	2.04	4	2.29
$\rm PSNI_{ft3}$	$\log(\alpha M_{\rm Pl}^2/f^2) \in [-2,-1]$ $\log(f/M_{\rm Pl}) \in [-2,1]$	-0.64	1.74	4	2.29
$\rm PSNI_{ft4}$	$\log(\alpha M_{\rm Pl}^2/f^2) \in [-1.5,-1]$ $\log(f/M_{\rm Pl}) \in [-2,1]$	-5.62	3.68	4	0.02

One can see that the evidence increases as the lower bound on $\log(\alpha M_{\rm Pl}^2/f^2)$ decreases because the likelihood is better in the region where $\log(\alpha M_{\rm Pl}^2/f^2)$ is small.

Another sensible choice of priors, based on the previous considerations, is to take uniform priors on the theoretical motivated parameter $\log(\alpha) \in [-x,-1]$ and $\log(f/M_{\rm Pl}) \in [-y,1]$, where x and y are positive numbers left unspecified for the moment. In the plane

JCAP03(2014)039

$[\log(f/M_{\rm Pl}), \log\alpha]$ the two-dimensional prior range is represented in figure 7 by the red rectangle. As discussed previously, $\alpha M_{\rm Pl}^2/f^2$ must be a small quantity for slow-roll to be satisfied. In the numerical calculations, we have assumed that it is smaller than 0.1, i.e., we use the same hard prior boundary as before, $\epsilon_2 < 0.2$. Such a hard prior cuts the theoretical prior domain of figure 7 along the curve

$$\log\left(\frac{f}{M_{\rm Pl}}\right) > \frac{1}{2}\log\alpha + \frac{1}{2}, \tag{A.68}$$

which is represented by a blue line in figure 7. As for GMSSMI and GRIPI, we can estimate analytically how the evidence would be rescaled by removing this hard prior, but first we need to estimate how much prior volume is affected.

When $y \geq (x-1)/2$ (left panel of figure 7), the hard prior boundary line intersects the right vertical edge of the red rectangle at the point $(-1, 0)$ and the left vertical edge at $(-x, 1/2 - x/2)$. In the case where $y \leq (x-1)/2$ (right panel of figure 7), this line still intersects the right vertical edge of the red rectangle at the point $(-1, 0)$ but now meets the bottom horizontal edge at $(-1-2y, -y)$. The condition (A.68) corresponds to the green region in figure 7, where slow-roll is valid and the likelihood non-vanishing. The complementary domain has been represented in blue on the same figure. In this domain, slow-roll is violated and the predictions cannot be in agreement with the observations. As a consequence, the likelihood function $\mathcal{L}$ is very small and for the purpose of our analytical extrapolation it will be assumed to vanish. In the following table, we have numerically computed the evidences in the green domain, i.e. in the region where our computations can be trusted, for various prior choices.

Name	Priors	$\ln(\mathcal{E}/\mathcal{E}_{\rm HI})$	$\mathcal{C}$	N	$\ln(\mathcal{L}_{\rm max}/\mathcal{E}_{\rm HI})$
$\mathrm{PSNI_{oA}}$	$\log(\alpha) \in [-7,-1]$ $\log(f/M_{\rm Pl}) \in [-2,1]$ $\alpha M_{\rm Pl}^2/f^2 < 10^{-1}$	-0.40	2.15	4	2.29
$\mathrm{PSNI_{oB}}$	$\log(\alpha) \in [-5,-1]$ $\log(f/M_{\rm Pl}) \in [-2,1]$ $\alpha M_{\rm Pl}^2/f^2 < 10^{-1}$	-0.42	2.12	4	2.29
$\mathrm{PSNI_{oC}}$	$\log(\alpha) \in [-3,-1]$ $\log(f/M_{\rm Pl}) \in [-2,1]$ $\alpha M_{\rm Pl}^2/f^2 < 10^{-1}$	-0.43	2.12	4	2.29

We can now use these evidences calculated with the green domain prior and rescale them appropriately to obtain the evidences over the full domain, including the slow-roll violating regions, that is to say in the red rectangle. From eq. (A.4), generalised to a two-dimensional prior, one gets

$$\mathcal{E}_{\rm red} = \frac{\int_{\rm green} \mathrm{d}\log(\alpha)\,\mathrm{d}\log(f/M_{\rm Pl})}{\int_{\rm red} \mathrm{d}\log(\alpha)\,\mathrm{d}\log(f/M_{\rm Pl})}\mathcal{E}_{\rm green}, \tag{A.69}$$

i.e. the evidence is rescaled according to the ratio of the prior volumes between the green and red domains. Explicitly, one gets

$$\int_{\rm red} \mathrm{d}\log(\alpha)\,\mathrm{d}\log(f/M_{\rm Pl}) = (x-1)(y+1), \tag{A.70}$$

JCAP03(2014)039

and

$$\int_{\text{green}} \mathrm{d}\log(\alpha)\,\mathrm{d}\log(f/M_{\mathrm{Pl}}) = \begin{cases} \dfrac{(x-1)(x+3)}{4} & \text{if} \quad y \geq \dfrac{x-1}{2}\,, \\ (y+1)(x-1) - y^2 & \text{if} \quad y \leq \dfrac{x-1}{2}\,, \end{cases} \tag{A.71}$$

such that

$$\ln\left(\frac{\mathcal{E}_{\mathrm{red}}}{\mathcal{E}_{\mathrm{HI}}}\right) = \ln\left(\frac{\mathcal{E}_{\mathrm{green}}}{\mathcal{E}_{\mathrm{HI}}}\right) + \begin{cases} \ln\left[\dfrac{x+3}{4(y+1)}\right] & \text{if} \quad y \geq \dfrac{x-1}{2}\,, \\ \ln\left[1 - \dfrac{y^2}{(y+1)(x-1)}\right] & \text{if} \quad y \leq \dfrac{x-1}{2}\,. \end{cases} \tag{A.72}$$

Therefore, the rescaled evidence (for the red domain) can be obtained from the one in the green region by using the correction factor given by the above formula. The results are summarised below.

Name	Priors	$\ln(\mathcal{E}/\mathcal{E}_{\mathrm{HI}})$	$\mathcal{C}$	N	$\ln(\mathcal{L}_{\max}/\mathcal{E}_{\mathrm{HI}})$
$\mathrm{PSNI}_{\mathrm{epA}}$	$\log(\alpha) \in [-7,-1]$ $\log(f/M_{\mathrm{Pl}}) \in [-2,1]$	-0.65	2.39	4	2.29
$\mathrm{PSNI}_{\mathrm{epB}}$	$\log(\alpha) \in [-5,-1]$ $\log(f/M_{\mathrm{Pl}}) \in [-2,1]$	-0.83	2.51	4	2.29
$\mathrm{PSNI}_{\mathrm{epC}}$	$\log(\alpha) \in [-3,-1]$ $\log(f/M_{\mathrm{Pl}}) \in [-2,1]$	-1.13	2.77	4	2.29

In this table, complexities have also been rescaled following the rough estimate given by eq. (A.8).

A.36 Non canonical Kähker inflation (NCKI)

The model has two dimensionless parameters α and β and its potential reads

$$V(\phi) = M^4\left[1 + \alpha\ln\left(\frac{\phi}{M_{\mathrm{Pl}}}\right) + \beta\left(\frac{\phi}{M_{\mathrm{Pl}}}\right)^2\right]. \tag{A.73}$$

The logarithmic term encodes loop corrections to the monomial part of the potential [72] and, therefore, natural values of α are such $0 < \alpha \ll 1$ whereas $\beta = \mathcal{O}(1)$. As discussed in ref. [5], for $\beta > 0$, the first Hubble flow function has a maximum $\epsilon_1^{\max} \simeq \beta/2$ ($\alpha \ll 1$) at $x_{\epsilon_1^{\max}} \simeq 1/\sqrt{\beta}$, with $x \equiv \phi/M_{\mathrm{Pl}}$. Therefore, we require β to small enough to have $\epsilon_1^{\max} \ll 1$ to ensure slow-roll inflation. If this condition is not satisfied, inflation could still process in the large field limit, but would be equivalent to the LFI models. A similar requirement exists for $\beta < 0$ by noticing that the second Hubble flow function verifies $\epsilon_2^{\min} > -8\beta$ ($\alpha \ll 1$), which should be less than unity. The lower limit of $|\beta|$ is arbitrary but cannot not be too small in order to maintain the hierarchy between the loop corrections and the monomial term. On purely phenomenological grounds, taking the limit $\beta \to 0$ gives back the LI potential. We have accordingly chosen the following priors:

Name	Priors	$\ln(\mathcal{E}/\mathcal{E}_{\mathrm{HI}})$	$\mathcal{C}$	N	$\ln(\mathcal{L}_{\max}/\mathcal{E}_{\mathrm{HI}})$
$\mathrm{NCKI}_{\beta>0}$	$\log(\alpha) \in [-4,-1]$ $\beta \in [0.02, 0.2]$	-3.91	2.57	4	-0.11
$\mathrm{NCKI}_{\beta<0}$	$\log(\alpha) \in [-4,-1]$ $\beta \in [-0.1,-0.02]$	-65.07	4.50	4	-56.01

JCAP03(2014)039

A.37 Constant spectrum inflation (CSI)

This potential is designed to produce a scale invariant power spectrum $n_{\rm S} \simeq 1$ and reads

$$V(\phi) = \frac{M^4}{\left(1 - \alpha \dfrac{\phi}{M_{\rm Pl}}\right)}\,, \tag{A.74}$$

where α is supposed to be small. This potential requires the field value $x_{\rm end} = \phi_{\rm end}/M_{\rm Pl}$ at which inflation stops to be specified. In the branch $x = \phi/M_{\rm Pl} < 1/\alpha$, inflation proceeds at decreasing field value while it cannot start at too large initial field value $x_{\rm ini}$. Indeed, one has $\epsilon_1(x) < 1$ only for $x < x_{\epsilon_1=1}$ such that $x_{\rm ini}$ is bounded from above $x_{\rm ini} < x_{\epsilon_1=1}$. This implies that there is a maximal bound for $x_{\rm end}$, that is numerically determined by requesting inflation to last, at least, 120 e-folds from $x_{\rm ini} = x_{\epsilon_1=1}$ to $x_{\rm end} = x_{\rm end}^{\rm max}$. A priori, there is no lower limit for $x_{\rm end}$. However, for $x_{\rm end}^{\rm min} \to -\infty$, all the slow-roll functions vanish, $n_{\rm S} \to 1$, $r \to 0$. Therefore, the likelihood values become independent on $x_{\rm end}^{\rm min}$, as is the evidence. For convenience, we have chosen $x_{\rm end}^{\rm min}(\alpha)$ such that $\epsilon_1(x_{\rm end}^{\rm min}) > 10^{-16}$, the machine precision limit. Everything is summarised in the following table.

Name	Priors	$\ln(\mathcal{E}/\mathcal{E}_{\rm HI})$	$\mathcal{C}$	N	$\ln(\mathcal{L}_{\rm max}/\mathcal{E}_{\rm HI})$
CSI	$\log(\alpha) \in [-5,-1]$ $x_{\rm end} \in [x_{\rm end}^{\rm min}, x_{\rm end}^{\rm max}]$	-7.80	0.16	4	-7.72

A.38 Orientifold inflation (OI)

The potential of these models has two parameters, a coupling α and a *vev* ϕ_0, and reads

$$V(\phi) = M^4 \left(\frac{\phi}{\phi_0}\right)^4 \left[\ln^2\left(\frac{\phi}{\phi_0}\right) - \alpha\right]. \tag{A.75}$$

As the model is motivated by super Yang-Mills orientifold theories, the *vev* ϕ_0 should be related to the Grand Unified energy scale and the coupling α should be small since $\alpha = \mathcal{O}(1/N_{\rm c})$, $N_{\rm c} \gg 1$ being the number of colours [73]. Therefore, we have chosen the following priors.

Name	Priors	$\ln(\mathcal{E}/\mathcal{E}_{\rm HI})$	$\mathcal{C}$	N	$\ln(\mathcal{L}_{\rm max}/\mathcal{E}_{\rm HI})$
OI	$\log(\alpha) \in [-3,-1]$ $\log(\phi_0/M_{\rm Pl}) \in [-3,-1]$	-6.52	3.62	4	-3.21

A.39 Constant $n_{\rm S}$ C inflation (CNCI)

This is the class "C" of potentials, according to the classification of ref. [5], which produces a constant spectral index. The potential is parametrised by one parameter α and reads

$$V(\phi) = M^4 \left[\left(3 + \alpha^2\right) \coth^2\left(\frac{\alpha}{\sqrt{2}} \frac{\phi}{M_{\rm Pl}}\right) - 3\right]. \tag{A.76}$$

In addition to α, the model requires the field value $x_{\rm end} \equiv \phi_{\rm end}/M_{\rm Pl}$ at which inflation ends to be specified. These scenarios are phenomenological and motivated for α small. Moreover, inflation proceeds at increasing field values and there is a region at small $x = \phi/M_{\rm Pl}$ in which $\epsilon_1(x) > 1$. As the result, $x_{\rm ini} > x_{\epsilon_1=1}$, with $x_{\epsilon_1=1}$ the solution of $\epsilon_1 = 1$. Requesting inflation to support at least 120 e-folds from $x_{\epsilon_1=1}$ implies the existence of minimal value for $x_{\rm end} > x_{\rm end}^{\rm min}(\alpha)$. These considerations lead us to the following priors:

JCAP03(2014)039

Name	Priors	$\ln(\mathcal{E}/\mathcal{E}_{\rm HI})$	$\mathcal{C}$	N	$\ln(\mathcal{L}_{\rm max}/\mathcal{E}_{\rm HI})$
CNCI	$\log(\alpha) \in [-5,-1]$ $x_{\rm end}/x_{\rm end}^{\rm min} \in [1,10]$	-7.72	8.25	4	-3.53

A.40 Supergravity brane inflation (SBI)

The potential depends on two dimensionless parameters α and β and reads

$$V(\phi) = M^4 \left\{ 1 + \left[-\alpha + \beta \ln\left(\frac{\phi}{M_{\rm Pl}}\right)\right] \left(\frac{\phi}{M_{\rm Pl}}\right)^4 \right\}. \tag{A.77}$$

As discussed in ref. [5], the logarithmic term comes from loop corrections that should not dominate the field dynamics. As such, the potential supports inflation in the small field region in which it is convex. For inflation to end, one requires $\alpha \geq \alpha_{\rm min}(\beta)$ where $\alpha_{\rm min} = (\beta/4)[1-\ln(\beta/4)]$, and β should be a small parameter. For $\alpha > \alpha_{\rm min}$, inflation is well defined but, at larger field values, the potential exhibits a negative minimum showing that it cannot be extended to those regions. On the other hand, for $\alpha = \alpha_{\rm min}$, the potential has a vanishing minimum and is well defined everywhere. We have therefore considered these two cases.

Name	Priors	$\ln(\mathcal{E}/\mathcal{E}_{\rm HI})$	$\mathcal{C}$	N	$\ln(\mathcal{L}_{\rm max}/\mathcal{E}_{\rm HI})$
SBI	$\log(\alpha) \in [-5,-2]$ $\log(\beta) \in [-4,-1]$	-0.37	1.67	4	2.29
$\text{SBI}_{\alpha_{\rm min}}$	$\alpha = \alpha_{\rm min}$ $\log(\beta) \in [-4,-1]$	-0.85	2.04	3	2.23

A.41 Spontaneous symmetry breaking inflation (SSBI)

The SSBI models are described by potentials of the form

$$V(\phi) = M^4 \left[1 + \alpha \left(\frac{\phi}{M_{\rm Pl}}\right)^2 + \beta \left(\frac{\phi}{M_{\rm Pl}}\right)^4 \right], \tag{A.78}$$

where α and β are the two dimensionless parameters. As discussed in ref. [5], this potential supports six different inflationary regimes according the relative signs of α and β. They are SSBI1 for $\alpha > 0$, $\beta > 0$; SSBI2 for $\alpha < 0$, $\beta < 0$; SSBI3 and SSBI4 for $\alpha > 0$, $\beta < 0$; SSBI5 and SSBI6 for $\alpha < 0$, $\beta > 0$. A priori the parameters α and β may take very small values, or not, depending on the underlying theoretical motivations (see ref. [5]). As a result, we have both considered a Jeffreys and flat prior for those two parameters. There are however some additional restrictions. For SSBI1, inflation ends only for $\alpha > \alpha_{\rm min}(\beta)$ which fixes an absolute lower limit for the α-prior. Moreover, even when this condition is satisfied, SSBI1 is strongly disfavoured when α becomes small and we have only considered $\alpha > \max(10^{-3}, \alpha_{\rm min})$. For SSBI3 and SSBI4, inflation proceeds from the top of the potential, either at increasing field values or at decreasing field values. The shape of the SSBI potential is such that this may occur in a non slow-rolling way with ϵ_2 large. These situations violates the slow-roll approximation, and are strongly disfavoured. Therefore, we have added a hard prior rejecting all model parameter values yielding $\epsilon_2(x_{\rm top}) > 0.2$, $x_{\rm top}$ being the field value at the top of the potential. Finally, for SSBI5 and SSBI6, there is another value $\alpha_{\rm max}(\beta)$ above which inflation never ends. As a result, for those scenarios, the prior on α verifies $\alpha < \alpha_{\rm max}(\beta)$. The following table summarises all the SSBI models considered with the Jeffreys prior choices:

JCAP03(2014)039

Name	Priors	$\ln(\mathcal{E}/\mathcal{E}_{\rm HI})$	$\mathcal{C}$	N	$\ln(\mathcal{L}_{\rm max}/\mathcal{E}_{\rm HI})$
SSBI1	$\max[-3,\log(\alpha_{\rm min})]<\log(\alpha)<1$ $\log(\beta)\in[-5,1]$	-4.27	2.73	4	-0.08
SSBI2	$\log(-\alpha)\in[-5,1]$ $\log(-\beta)\in[-5,1]$	-0.54	1.74	4	2.29
SSBI3	$\log(\alpha)\in[\log(\alpha_{\rm min}),1]$ $\log(-\beta)\in[-5,1]$ $\epsilon_2(x_{\rm top})<0.2$	-2.28	4.13	4	1.83
SSBI4	$\log(\alpha)\in[\log(\alpha_{\rm min}),1]$ $\log(-\beta)\in[-5,1]$ $\epsilon_2(x_{\rm top})<0.2$	-0.70	2.02	4	2.29
SSBI5	$\log(-\alpha)\in[\log(-\alpha_{\rm max}),1]$ $\log(\beta)\in[-5,1]$	-3.02	2.40	4	2.19
SSBI6	$\log(-\alpha)\in[\log(-\alpha_{\rm max}),1]$ $\log(\beta)\in[-5,1]$	-3.30	3.19	4	0.72

We have also considered the same models but when the natural values of α and β are considered as being $\mathcal{O}(1)$, i.e. with flat priors rather than Jeffreys priors. They are listed in the table below.

Name	Priors	$\ln(\mathcal{E}/\mathcal{E}_{\rm HI})$	$\mathcal{C}$	N	$\ln(\mathcal{L}_{\rm max}/\mathcal{E}_{\rm HI})$
SSBI1$_{\rm f}$	$\alpha\in[\max(10^{-3},\alpha_{\rm min}),10]$ $\beta\in[10^{-5},10]$	-6.24	9.08	4	-0.08
SSBI2$_{\rm f}$	$\alpha\in[-10,-10^{-5}]$ $\log(-\beta)\in[-5,1]$	-2.65	1.99	4	2.29
SSBI3$_{\rm f}$	$\alpha\in[\alpha_{\rm min},10]$ $\beta\in[-10,-10^{-5}]$ $\epsilon_2(x_{\rm top})<0.2$	-2.52	2.93	4	1.83
SSBI4$_{\rm f}$	$\alpha\in[\alpha_{\rm min},10]$ $\beta\in[-10,-10^{-5}]$ $\epsilon_2(x_{\rm top})<0.2$	-2.09	2.40	4	2.29
SSBI5$_{\rm f}$	$\alpha\in[-10,\alpha_{\rm max}]$ $\beta\in[10^{-5},10]$	-7.11	2.93	4	2.19
SSBI6$_{\rm f}$	$\alpha\in[-10,\alpha_{\rm max}]$ $\beta\in[10^{-5},10]$	-6.08	10.15	4	0.71

A.42 Inverse monomial inflation (IMI)

The potential is a extension of the large field inflation potential to negative power indices and read

$$V(\phi)=M^4\left(\frac{\phi}{M_{\rm Pl}}\right)^{-p}, \tag{A.79}$$

with $p>0$. Inflation proceeds at increasing field values and ends at the field value $x_{\rm end}=\phi_{\rm end}/M_{\rm Pl}$, which is an additional model parameter. There is however a region, at small field values, which does not support inflation as $\epsilon_1(x)>1$. Denoting $x_{\epsilon_1=1}$ the solution of $\epsilon_1=1$, this implies that $x_{\rm ini}>x_{\epsilon_1=1}$ and there is a minimal acceptable value for $x_{\rm end}$ such that inflation lasts more than 120 e-folds. As for the other models, this value $x_{\rm end}^{\rm min}$ is numerically determined by solving the field trajectory starting at $x_{\rm ini}=x_{\epsilon_1=1}$ for the specified amount

JCAP03(2014)039

of e-folds. In the absence of definite constraints on $x_{\rm end}$, we have chosen a flat prior for $x_{\rm end}/x_{\rm end}^{\rm min} \in [1, 100]$ as well as various fixed values of $p = \mathcal{O}(1)$. They are summarised below.

Name	Priors	$\ln(\mathcal{E}/\mathcal{E}_{\rm HI})$	$\mathcal{C}$	N	$\ln(\mathcal{L}_{\rm max}/\mathcal{E}_{\rm HI})$
IMI	$p \in [1, 6]$ $x_{\rm end}/x_{\rm end}^{\rm min} \in [1, 100]$	-7.79	6.69	4	-4.44
IMI1	$p = 1$ $x_{\rm end}/x_{\rm end}^{\rm min} \in [1, 100]$	-7.80	0.85	3	-7.37
IMI2	$p = 2$ $x_{\rm end}/x_{\rm end}^{\rm min} \in [1, 100]$	-7.80	1.41	3	-7.09
IMI3	$p = 3$ $x_{\rm end}/x_{\rm end}^{\rm min} \in [1, 100]$	-7.80	5.88	3	-4.85
IMI4	$p = 4$ $x_{\rm end}/x_{\rm end}^{\rm min} \in [1, 100]$	-7.79	6.28	3	-4.65
IMI5	$p = 5$ $x_{\rm end}/x_{\rm end}^{\rm min} \in [1, 100]$	-7.79	5.68	3	-4.93
IMI6	$p = 6$ $x_{\rm end}/x_{\rm end}^{\rm min} \in [1, 100]$	-7.78	6.63	3	-4.44

A.43 Brane inflation (BI)

The potential of brane inflation reads

$$V_{\rm BI_{ph}}(\phi) = M^4 \left[1 - \left(\frac{\phi}{\mu}\right)^{-p}\right], \tag{A.80}$$

and depends explicitly on two parameters μ and p. This is an approximated expression derived from KKLMMT-like inflationary scenarios, in which $p = 4$ and $\mu \ll M_{\rm Pl}$ [74, 75]. In the following, we define $x \equiv \phi/\mu$ and inflation proceeds at decreasing x. It is induced by the motion of a brane inside the throat of some compactified extra-dimensions, ϕ referring to the position of this brane. Brane inflation can either ends naturally, i.e. when the acceleration of the universe stops, or before if a tachyonic preheating is triggered by brane annihilation. The model has therefore an additional parameter, $x_{\rm stg}$, which is the field value at which brane annihilation occurs. Denoting by $x_{\epsilon_1=1}$ the solution of $\epsilon_1(x) = 1$, inflation actually ends at the field value $x_{\rm end} = \max(x_{\rm stg}, x_{\epsilon_1=1})$. The parameter $x_{\rm stg}$ is related to various hidden string parameters such as the flux conserved quantum numbers and the volume of the throat. As shown in ref. [76], the internal consistency of the model implies that $x_{\rm stg} > 1$, its order of magnitude remaining unknown. Moreover, there is a maximal field value, $\phi_{\rm UV}$, which corresponds to the brane position at the edge of the throat. As the model only describes brane interactions within the throat, one should impose $\phi < \phi_{\rm UV}$. As discussed in ref. [76], the internal consistency of the model imposes that $\phi_{\rm UV} < 2M_{\rm Pl}$.

Following these considerations, we have first considered strict priors associated with the string scenario ($\rm BI_{stg}$), namely $p = 4$, $\log(\mu/M_{\rm Pl}) \in [-6, \log(2)]$, $\log(x_{\rm stg}) \in [0, 3]$ and $\log(\phi_{\rm UV}/M_{\rm Pl}) \in [-2, \log(2)]$. For the sake of generality, we have also considered the non-approximated potential associated with the KKLMMT model, namely

$$V_{\rm KKLTI}(\phi) = \frac{M^4}{1 + \left(\frac{\phi}{\mu}\right)^{-p}}, \tag{A.81}$$

JCAP03(2014)039

under the label $\mathrm{KKLTI_{stg}}$, and with the same priors as $\mathrm{BI_{stg}}$. As one can check in the following table, there is no difference between the two models under those priors.

Name	Priors	$\ln(\mathcal{E}/\mathcal{E}_{\rm HI})$	$\mathcal{C}$	N	$\ln(\mathcal{L}_{\rm max}/\mathcal{E}_{\rm HI})$
$\mathrm{BI_{stg}}$	$p=4$ $\log(\mu/M_{\rm Pl})\in[-6,\log(2)]$ $\log(x_{\rm stg})\in[0,3]$ $\log(\phi_{\rm UV}/M_{\rm Pl})\in[-2,\log(2)]$	-0.33	1.91	5	2.29
$\mathrm{KKLTI_{stg}}$	$p=4$ $\log(\mu/M_{\rm Pl})\in[-6,\log(2)]$ $\log(x_{\rm stg})\in[0,3]$ $\log(\phi_{\rm UV}/M_{\rm Pl})\in[-2,\log(2)]$	-0.32	1.92	5	2.29

Then, we have allowed for other phenomenological scenarios that would be based on the same potentials by relaxing p and allowing μ to become super-Planckian. Out of the string framework, there is no motivation to keep $x_{\rm stg}$ and $\phi_{\rm UV}$ as extra model parameters and we have instead assumed that inflation ends at $x_{\rm end}=x_{\epsilon_1=1}$. However, for $\mu>M_{\rm Pl}$, inflation within the potential (A.80) or (A.81) may yield different observable predictions. As a result, we have separated the models in which $\mu<M_{\rm Pl}$ from those in which μ can take any values. The phenomenological models considered, and their priors, are enumerated in the following table.

Name	Priors	$\ln(\mathcal{E}/\mathcal{E}_{\rm HI})$	$\mathcal{C}$	N	$\ln(\mathcal{L}_{\rm max}/\mathcal{E}_{\rm HI})$
KKLTI	$p\in[2,10]$ $\log(\mu/M_{\rm Pl})\in[-3,3]$	-0.34	1.90	4	2.29
$\mathrm{KKLTI_s}$	$p\in[2,10]$ $\log(\mu/M_{\rm Pl})\in[-3,0]$	0.02	1.85	4	2.29
$\mathrm{BI_{ph}}$	$p\in[2,10]$ $\log(\mu/M_{\rm Pl})\in[-3,3]$	-0.19	2.14	4	2.29
$\mathrm{BI_s}$	$p\in[2,10]$ $\log(\mu/M_{\rm Pl})\in[-3,0]$	0.03	1.84	4	2.29
$\mathrm{BI_{1s}}$	$p=1$ $\log(\mu/M_{\rm Pl})\in[-3,0]$	-0.21	2.19	3	2.29
$\mathrm{BI_{2s}}$	$p=2$ $\log(\mu/M_{\rm Pl})\in[-3,0]$	-0.08	2.05	3	2.29
$\mathrm{BI_{3s}}$	$p=3$ $\log(\mu/M_{\rm Pl})\in[-3,0]$	-0.02	1.96	3	2.29
$\mathrm{BI_{4s}}$	$p=4$ $\log(\mu/M_{\rm Pl})\in[-3,0]$	0.01	1.91	3	2.29
$\mathrm{BI_{5s}}$	$p=5$ $\log(\mu/M_{\rm Pl})\in[-3,0]$	0.02	1.87	3	2.29
$\mathrm{BI_{6s}}$	$p=6$ $\log(\mu/M_{\rm Pl})\in[-3,0]$	0.04	1.82	3	2.29

A.44 Running-mass inflation (RMI)

The running-mass inflationary models, denoted RMI, have a potential of the form

$$V(\phi)=M^4\left[1-\frac{c}{2}\left(-\frac{1}{2}+\ln\frac{\phi}{\phi_0}\right)\frac{\phi^2}{M_{\rm Pl}^2}\right], \tag{A.82}$$

JCAP03(2014)039

which supports four different inflationary regimes, namely RMI1 ($\phi < \phi_0$, $c > 0$), RMI2 ($\phi > \phi_0$, $c > 0$), RMI3 ($\phi < \phi_0$, $c < 0$) and RMI4 ($\phi > \phi_0$, $c < 0$), see ref. [5]. In addition to the constant c and the *vev* ϕ_0, the field value $\phi_{\rm end}$ at which inflation ends has to be specified making RMI a three-parameters model. The model describing loop corrections over a polynomial expansion, the constant c cannot be too small and the *vev* ϕ_0 must be sub-Planckian. The order of magnitude of ϕ_0 being unspecified, we have chosen a Jeffreys prior in $\log(\phi_0/M_{\rm Pl}) \in [-2, 0]$. For RMI1, RMI2 and RMI3, the likelihood has a flat direction along the parameter ϕ_0 such that the evidence is independent of the lower bound on ϕ_0. For RMI4, the likelihood is vanishing when ϕ_0 becomes small, and the evidence is accordingly decreased if the prior lower bound on $\log(\phi_0/M_{\rm Pl})$ is pushed to smaller values.

As discussed in ref. [5], within supersymmetry, natural values of $c \simeq 10^{-2}$ to 10^{-1} for soft masses values matching the energy scale of inflation. This suggest to take a flat prior for c encompassing those values. For other type of couplings, c may take smaller values and we therefore consider another motivated prior in which the order of magnitude of c is unknown, e.g. $\log(c) \in [-3, -1]$.

Finally, the field value $\phi_{\rm end}$ is constrained to be in the inflationary region of interest. The shape of the potential therefore gives the natural prior bounds for $x_{\rm end} \equiv \phi_{\rm end}/\phi_0$, i.e. $x_{\rm end} \in [1/e, 1]$ for RMI1 and RMI3, $x_{\rm end} \in [1, e]$ for RMI2. For RMI4, one still has $x_{\rm end} > 1$ but choosing the prior upper limit requires some precaution. Indeed, the potential is an increasing function of ϕ, which approaches large field inflation asymptotically, and inflation proceeds at decreasing field values, bounded from below by $x_{\rm end}$. Since the large field regime is not acceptable for RMI4, one has to require the *initial* field value $x_{\rm ini} < x_{\epsilon_1^{\rm max}}$. Here $x_{\epsilon_1^{\rm max}}$ is the field value at which the first Hubble flow function is maximal, which is the frontier between the vacuum dominated regime and the large field one. As for the other models, adding the "hard prior" that inflation lasts longer than 120 e-folds ensures the existence of a maximal value $x_{\rm end}^{\rm max}$, which is obtained by integrating the field trajectory from $x_{\rm ini} = x_{\epsilon_1^{\rm max}}$. This is a complicated functions of the other parameters which is only known numerically. The parameter space of RMI4 is therefore sampled with a flat prior for $x_{\rm end} \in [1, x_{\rm end}^{\rm max}]$.

Finally, for RMI1 and RMI2, we have added another "hard prior" to avoid an infinite number of e-folds to occur at the top of the potential by requiring $\epsilon_1(x_{\rm ini})$ to be larger than the numerical machine precision. This has no observable consequences as the parameter space volume cut remains extremely small and those cases would correspond otherwise to $n_{\rm S} = 1$ and are disfavoured. All these considerations are summarised in the following table.

JCAP03(2014)039

Name	Priors	$\ln(\mathcal{E}/\mathcal{E}_{\rm HI})$	$\mathcal{C}$	N	$\ln(\mathcal{L}_{\rm max}/\mathcal{E}_{\rm HI})$
RMI_1	$c \in [0.01, 0.2]$ $\log(\phi_0/M_{\rm Pl}) \in [-2, 0]$ $x_{\rm end} \in [1/e, 1]$	-2.03	1.94	5	2.29
RMI_{1l}	$\log(c) \in [-3, -1]$ $\log(\phi_0/M_{\rm Pl}) \in [-2, 0]$ $x_{\rm end} \in [1/e, 1]$	-1.41	2.04	5	2.29
RMI_2	$c \in [0.01, 0.2]$ $\log(\phi_0/M_{\rm Pl}) \in [-2, 0]$ $x_{\rm end} \in [1, e]$	-2.18	1.80	5	2.29
RMI_{2l}	$\log(c) \in [-3, -1]$ $\log(\phi_0/M_{\rm Pl}) \in [-2, 0]$ $x_{\rm end} \in [1, e]$	-1.14	2.04	5	2.29
RMI_3	$c \in [-0.2, -0.01]$ $\log(\phi_0/M_{\rm Pl}) \in [-2, 0]$ $x_{\rm end} \in [1/e, 1]$	-1.96	2.05	5	2.29
RMI_{3l}	$\log(-c) \in [-3, -1]$ $\log(\phi_0/M_{\rm Pl}) \in [-2, 0]$ $x_{\rm end} \in [1/e, 1]$	-2.84	2.16	5	2.29
RMI_4	$c \in [-0.2, -0.01]$ $\log(\phi_0/M_{\rm Pl}) \in [-2, 0]$ $x_{\rm end} \in [1, x_{\rm end}^{\rm max}]$	-25.90	9.54	5	-13.85
RMI_{4l}	$\log(-c) \in [-3, -1]$ $\log(\phi_0/M_{\rm Pl}) \in [-2, 0]$ $x_{\rm end} \in [1, x_{\rm end}^{\rm max}]$	-9.26	1.28	5	-7.13

A.45 Valley hybrid inflation (VHI)

The potential is parametrised by two parameters p and μ and reads

$$V(\phi) = M^4 \left[1 + \left(\frac{\phi}{\mu}\right)^p\right], \tag{A.83}$$

$p > 0$ being the power index and μ is a typical *vev*. Because this expression only describes inflation along the valley of the genuine two-field hybrid inflationary scenario, the *vev* μ is forced to be super-Planckian. As discussed in refs. [77–81], this condition is required to get enough e-folds of inflation occurring in the valley. Another implicit prior is to assume that the parameters associated with the other field are such that the regime of waterfall inflation does not take place. As discussed in ref. [5], the dynamics of VHI is significantly different if $p > 1$ or $p < 1$ and the two classes are considered. In addition to μ and p, hybrid inflation ends by tachyonic instability and the field value $x_{\rm end} \equiv \phi_{\rm end}/\mu$ at which this occurs is an extra model parameter. As for RMI, our prior is to restrain VHI to the vacuum dominated regime only, i.e. $x_{\rm ini} < x_{\epsilon_1^{\rm max}}$ where $x_{\epsilon_1^{\rm max}}$ is the frontier between the vacuum dominated regime and the large field one. From this limit, requiring inflation to support at least 120 e-folds gives a numerical upper bound $x_{\rm end} < x_{\rm end}^{\rm max}$. The quantity $x_{\rm end}^{\rm max}$ is determined numerically using the `ASPIC` code by integrating the field trajectory starting at $x_{\epsilon_1^{\rm max}}$. For the cases $p \leq 1$, the VHI potential does not support inflation around $x = 0$ as ϵ_1 diverges in this limit. For those, we therefore consider a prior $x_{\rm end} > x_{\rm end}^{\rm min}$ where $x_{\rm end}^{\rm min} = x^-_{\epsilon_1=1}$ is the solution of $\epsilon_1 = 1$ in the vacuum dominated region. For $p > 1$, the tachyonic instability can take place at arbitrarily

JCAP03(2014)039

small field values and $x_{\rm end}^{\rm min} = 0$ (up to machine precision limitations). Notice that the upper bounds of the p and μ priors have been fixed to arbitrary values. All the models considered for the VHI scenarios are listed below and are all ruled out, independently of their priors.

Name	Priors	$\ln(\mathcal{E}/\mathcal{E}_{\rm HI})$	$\mathcal{C}$	N	$\ln(\mathcal{L}_{\rm max}/\mathcal{E}_{\rm HI})$
VHI	$p \in]1,6]$ $\log(\mu/M_{\rm Pl}) \in [0,3]$ $x_{\rm end} \in [x_{\rm end}^{\rm min}, x_{\rm end}^{\rm max}]$	-7.81	16.46	5	0.43
VHI$_{p<1}$	$p \in [0,0.9]$ $\log(\mu/M_{\rm Pl}) \in [0,3]$ $x_{\rm end} \in [x_{\rm end}^{\rm min}, x_{\rm end}^{\rm max}]$	-7.80	20.09	5	2.27
VHI$_{1/2}$	$p = 1/2$ $\log(\mu/M_{\rm Pl}) \in [0,3]$ $x_{\rm end} \in [x_{\rm end}^{\rm min}, x_{\rm end}^{\rm max}]$	-7.80	19.57	4	1.99
VHI$_1$	$p = 1$ $\log(\mu/M_{\rm Pl}) \in [0,3]$ $x_{\rm end} \in [x_{\rm end}^{\rm min}, x_{\rm end}^{\rm max}]$	-7.80	17.14	4	0.79
VHI$_2$	$p = 2$ $\log(\mu/M_{\rm Pl}) \in [0,3]$ $x_{\rm end} \in [x_{\rm end}^{\rm min}, x_{\rm end}^{\rm max}]$	-7.80	15.42	4	-0.09
VHI$_3$	$p = 3$ $\log(\mu/M_{\rm Pl}) \in [0,3]$ $x_{\rm end} \in [x_{\rm end}^{\rm min}, x_{\rm end}^{\rm max}]$	-7.81	14.66	4	-0.47
VHI$_4$	$p = 4$ $\log(\mu/M_{\rm Pl}) \in [0,3]$ $x_{\rm end} \in [x_{\rm end}^{\rm min}, x_{\rm end}^{\rm max}]$	-7.82	14.15	4	-0.72

A.46 Dynamical supersymmetric inflation (DSI)

The potential is an extension of the VHI one to negative power index and reads

$$V(\phi) = M^4 \left[1 + \left(\frac{\phi}{\mu}\right)^{-p}\right], \tag{A.84}$$

while this class of model naturally appears in supersymmetric theories (see ref. [5]). As such, the *vev* μ should be always sub-Planckian. For the priors, we have either considered the typical values of refs. [82, 83], i.e. a flat prior for μ around 10^{-7} (model DSI$_{\rm o}$), which is also relaxed to allow for any other phenomenological models of the same kind (DSI). Inflation takes place at increasing field value and the end of inflation $x_{\rm end} = \phi_{\rm end}/\mu$ is an additional parameter. Moreover, as discussed in ref. [5], inflation can only take place in the region $x > x_{\epsilon_1=1}$, where $x_{\epsilon_1=1}$ is the solution of $\epsilon_1 = 1$. This provides a lower bound for $x_{\rm ini}$, and therefore, complemented with our hard prior that inflation lasts more than 120 e-folds, this gives $x_{\rm end} > x_{\rm end}^{\rm min}$. As for VHI, the quantity $x_{\rm end}^{\rm min}$ has to be numerically evaluated by integrating the field trajectory over 120 e-folds starting at $x_{\rm ini} = x_{\epsilon_1=1}$. Moreover, within the supersymmetric framework in which this potential is derived, there are additional terms lifting $V(\phi)$ at large field values which can be ignored provided ϕ is not too large. This gives a natural upper bound for the prior on $x_{\rm end}$. More specifically, these terms are of the form

JCAP03(2014)039

$\Delta V = \phi^{q+4}/M_{\rm Pl}^q$ such that the corrected potential exhibits a global minimum at a field value $x_{V^{\rm min}}$. Requiring $x_{\rm end} \ll x_{V^{\rm min}}$ gives the absolute upper bound

$$x_{\rm end} \ll x_{\rm end}^{\rm max} \equiv \left[43200\pi^2 \frac{p^3}{q+4} P_* \left(\frac{M_{\rm Pl}}{\mu}\right)^{q+6}\right]^{1/(3p+q+6)} . \tag{A.85}$$

As a motivated case, we have chosen $q = 8$ and a Jeffreys' prior on $x_{\rm end}$ in $[x_{\rm end}^{\rm min}, x_{\rm end}^{\rm max}]$. The case $p = 2$ has been considered as an independent model as it corresponds to the so-called inverse mutated scenarios. In summary, the following models and priors have been considered:

Name	Priors	$\ln(\mathcal{E}/\mathcal{E}_{\rm HI})$	$\mathcal{C}$	N	$\ln(\mathcal{L}_{\rm max}/\mathcal{E}_{\rm HI})$
DSI	$p \in]1, 6]$ $\log(\mu/M_{\rm Pl}) \in [-5, 0]$ $\log\left(\frac{x_{\rm end} - x_{\rm end}^{\rm min}}{x_{\rm end}^{\rm max} - x_{\rm end}^{\rm min}}\right) \in [-5, -0.7]$	-8.51	0.07	5	-7.71
$\rm DSI_o$	$p \in]1, 6]$ $\mu/M_{\rm Pl} \in \left[10^{-9}, 10^{-6}\right]$ $\log\left(\frac{x_{\rm end} - x_{\rm end}^{\rm min}}{x_{\rm end}^{\rm max} - x_{\rm end}^{\rm min}}\right) \in [-5, -0.7]$	-8.47	0.07	5	-7.71
$\rm DSI_2$	$p = 2$ $\mu/M_{\rm Pl} \in \left[10^{-9}, 10^{-6}\right]$ $\log\left(\frac{x_{\rm end} - x_{\rm end}^{\rm min}}{x_{\rm end}^{\rm max} - x_{\rm end}^{\rm min}}\right) \in [-5, -0.7]$	-8.40	0.07	4	-7.71

A.47 Generalised mixed large field inflation (GMLFI)

The potential mixes two large field monomials and reads

$$V(\phi) = M^4 \left(\frac{\phi}{M_{\rm Pl}}\right)^p \left[1 + \alpha \left(\frac{\phi}{M_{\rm Pl}}\right)^q\right], \tag{A.86}$$

where p and q are power indices and α a constant. The model has three parameters and their priors have been chosen on phenomenological grounds. In particular, because GMLFI allows to discuss the effects stemming from combining together two LFI models, it motivates to fix p and q to all the possible theoretically motivated combination of pure LFI models. One can also view GMLFI as a new class of models and let p, q and α freely varying. A priori, the parameter α can be very small such that it should be sampled along a Jeffreys prior. We have considered the following cases:

JCAP03(2014)039

Name	Priors	$\ln(\mathcal{E}/\mathcal{E}_{\rm HI})$	$\mathcal{C}$	N	$\ln(\mathcal{L}_{\rm max}/\mathcal{E}_{\rm HI})$
GMLFI	$p \in [1,6]$ $\log(\alpha) \in [-5,1]$ $q \in [1,6]$	-5.15	3.90	5	0.79
$\text{GMLFI}_{2/3,1/3}$	$p = 2/3$ $\log(\alpha) \in [-5,1]$ $q = 1/3$	-1.27	2.31	3	1.24
$\text{GMLFI}_{2/3,4/3}$	$p = 2/3$ $\log(\alpha) \in [-5,1]$ $q = 4/3$	-1.69	2.74	3	1.24
$\text{GMLFI}_{1,1}$	$p = 1$ $\log(\alpha) \in [-5,1]$ $q = 1$	-1.86	2.35	3	0.79
$\text{GMLFI}_{1,2}$	$p = 1$ $\log(\alpha) \in [-5,1]$ $q = 2$	-2.52	2.69	3	0.79
$\text{GMLFI}_{1,3}$	$p = 1$ $\log(\alpha) \in [-5,1]$ $q = 3$	-3.64	3.13	3	0.63
$\text{GMLFI}_{2,1}$	$p = 2$ $\log(\alpha) \in [-5,1]$ $q = 1$	-3.05	2.08	3	-0.08
MLFI	$p = 2$ $\log(\alpha) \in [-5,1]$ $q = 2$	-3.77	2.39	3	-0.09
$\text{GMLFI}_{2,3}$	$p = 2$ $\log(\alpha) \in [-5,1]$ $q = 3$	-5.23	3.47	3	-0.39
$\text{GMLFI}_{3,1}$	$p = 3$ $\log(\alpha) \in [-5,1]$ $q = 1$	-4.83	3.29	3	-1.02
$\text{GMLFI}_{3,2}$	$p = 3$ $\log(\alpha) \in [-5,1]$ $q = 2$	-5.60	4.06	3	-1.04
$\text{GMLFI}_{3,3}$	$p = 3$ $\log(\alpha) \in [-5,1]$ $q = 3$	-7.43	6.87	3	-1.90

Notice that the case $p = 2$, $q = 2$ is also referred to as MLFI in ref. [5].

A.48 Logarithmic potential inflation (LPI)

These scenarios are parametrised by a potential of the form

$$V(\phi) = M^4 \left(\frac{\phi}{\phi_0}\right)^p \left(\ln \frac{\phi}{\phi_0}\right)^q . \tag{A.87}$$

Some specific combinations of p and q match various Yang-Mills composite models $\text{LPI1}_{4,1}$ ($p = 4$, $q = 1$), $\text{LPI1}_{4,2}$ ($p = 1$, $q = 2$) and $\text{LPI1}_{4,3}$ ($p = 4$, $q = 3$) [73, 84]. Others

JCAP03(2014)039

combinations are phenomenological [85]. Because the potential admits a local maximum at $x = x_{V^{\max}}$, with $x = \phi/\phi_0$, inflation can take place in three domains: LPI1 for $x > 1$, LPI2 for $x_{V^{\max}} < x < 1$ and LPI3 for $x < x_{V^{\max}}$. Let us notice that for both LPI2 and LPI3, the potential is well-defined only if q is an even integer. For LPI1, both p and q can take arbitrary real values. The *vev* ϕ_0 is not constrained for LPI1, and we have chosen a Jeffreys prior encompassing both sub-Planckian and super-Planckian values. On the contrary, in the LPI1 and LPI2 domains, ϕ_0 must be deeply super-Planckian to allow for slow-rolling inflation. The models and priors considered are listed below.

Name	Priors	$\ln(\mathcal{E}/\mathcal{E}_{\rm HI})$	$\mathcal{C}$	N	$\ln(\mathcal{L}_{\max}/\mathcal{E}_{\rm HI})$
LPI1	$p \in [1,6]$ $\log(\phi_0/M_{\rm Pl}) \in [-3,3]$ $q \in [1,6]$	-3.95	3.84	5	0.77
$\mathrm{LPI1}_{4,1}$	$p = 4$ $\log(\phi_0/M_{\rm Pl}) \in [-3,3]$ $q = 1$	-3.27	2.79	3	0.69
$\mathrm{LPI1}_{4,2}$	$p = 4$ $\log(\phi_0/M_{\rm Pl}) \in [-3,3]$ $q = 2$	-4.42	2.90	3	-0.14
$\mathrm{LPI1}_{4,3}$	$p = 4$ $\log(\phi_0/M_{\rm Pl}) \in [-3,3]$ $q = 3$	-5.99	5.28	3	-1.14
$\mathrm{LPI2}_2$	$p \in [1,6]$ $\log(\phi_0/M_{\rm Pl}) \in [2,5]$ $q = 2$	-2.47	3.82	4	1.14
$\mathrm{LPI2}_4$	$p \in [1,6]$ $\log(\phi_0/M_{\rm Pl}) \in [2,5]$ $q = 4$	-5.97	7.85	4	-0.18
$\mathrm{LPI2}_6$	$p \in [1,6]$ $\log(\phi_0/M_{\rm Pl}) \in [2,5]$ $q = 6$	-8.15	7.64	4	-3.24
$\mathrm{LPI3}_2$	$p \in [1,6]$ $\log(\phi_0/M_{\rm Pl}) \in [2,5]$ $q = 2$	-2.67	4.58	4	1.98
$\mathrm{LPI3}_4$	$p \in [1,6]$ $\log(\phi_0/M_{\rm Pl}) \in [2,5]$ $q = 4$	-2.04	4.03	4	2.26
$\mathrm{LPI3}_6$	$p \in [1,6]$ $\log(\phi_0/M_{\rm Pl}) \in [2,5]$ $q = 6$	-1.71	3.56	4	2.28

A.49 Constant $n_{\rm S}$ D inflation (CNDI)

The potential has two parameters α, β and reads

$$V(\phi) = \frac{M^4}{\left[1 + \beta\cos\left(\alpha\dfrac{\phi}{M_{\rm Pl}}\right)\right]^2}\,. \tag{A.88}$$

JCAP03(2014)039

As discussed in ref. [5], the only regime of cosmological interest has $x = \phi/M_{\rm Pl}$ small and $\beta > 1$. In that situation, the field value at which inflation ends should be specified, namely $x_{\rm end} = \phi_{\rm end}/M_{\rm Pl}$. Moreover, if x becomes too large, inflation cannot even start because there exists a "forbidden" range of field values in which $\epsilon_1(x) > 1$. As a result, there is a maximal value for $x_{\rm ini} = x^{-}_{\epsilon_1=1}$, $x^{-}_{\epsilon_1=1}$ being the smallest root of the equation $\epsilon_1 = 1$. As for the other models, by imposing to get at least 120 e-folds of inflation, the maximal values of $x_{\rm ini}$ translates into a maximal value $x^{\rm max}_{\rm end}$ thereby constituting the upper bound of the $x_{\rm end}$'s prior. Concerning the parameter α, the genuine CNDI model is designed to produce a constant spectral index and, as discussed in ref. [5], this occurs for not too small, neither not too large values of α. The priors chosen are summarised in the following table.

Name	Priors	$\ln(\mathcal{E}/\mathcal{E}_{\rm HI})$	$\mathcal{C}$	N	$\ln(\mathcal{L}_{\rm max}/\mathcal{E}_{\rm HI})$
CNDI	$\beta \in [1.1, 6]$ $\log(\alpha) \in [-2, -1]$ $x_{\rm end} \in [0, x^{\rm max}_{\rm end}]$	-7.91	6.41	5	-4.55

References

[1] Planck collaboration, P.A.R. Ade et al., *Planck 2013 results. XVI. Cosmological parameters*, arXiv:1303.5076 [INSPIRE].

[2] R. Trotta, *Forecasting the Bayes factor of a future observation*, *Mon. Not. Roy. Astron. Soc.* **378** (2007) 819 [astro-ph/0703063] [INSPIRE].

[3] Planck collaboration, P.A.R. Ade et al., *Planck 2013 results. XXII. Constraints on inflation*, arXiv:1303.5082 [INSPIRE].

[4] Planck collaboration, P.A.R. Ade et al., *Planck 2013 Results. XXIV. Constraints on primordial non-Gaussianity*, arXiv:1303.5084 [INSPIRE].

[5] J. Martin, C. Ringeval and V. Vennin, *Encyclopaedia Inflationaris*, arXiv:1303.3787 [INSPIRE].

[6] C. Ringeval, *Fast Bayesian inference for slow-roll inflation*, arXiv:1312.2347 [INSPIRE].

[7] R.T. Cox, *Probability, Frequency and Reasonable Expectation*, *American Journal of Physics* **14** (1946) 1.

[8] H. Jeffreys, *Theory of probability*, Oxford University Press, Oxford Classics series, 1961, reprinted 1998.

[9] B. de Finetti, *Theory of probability*, John Wiley & Sons, Chichester, U.K., 1974, reprinted 1995.

[10] J.M. Bernardo and A.F. . Smith, *Bayesian Theory*, John Wiley and Sons, Chicester, U.K., 1994.

[11] G.E.P. Box and G.C. Tiao, *Bayesian Inference in Statistical Analysis*, John Wiley and Sons, Chicester, U.K., 1992.

[12] E.T. Jaynes, *Probability Theory. The logic of science*, Cambridge University Press, Cambridge, U.K., 2003.

[13] J. Berger, *Could fisher, jeffreys and neyman have agreed on testing?*, *Statistical Science* **18** (2003) 1.

[14] R. Trotta, *Applications of Bayesian model selection to cosmological parameters*, *Mon. Not. Roy. Astron. Soc.* **378** (2007) 72 [astro-ph/0504022] [INSPIRE].

[15] R. Trotta, *Bayes in the sky: Bayesian inference and model selection in cosmology*, *Contemp. Phys.* **49** (2008) 71 [arXiv:0803.4089] [INSPIRE].

JCAP03(2014)039

[16] C. Gordon and R. Trotta, *Bayesian Calibrated Significance Levels Applied to the Spectral Tilt and Hemispherical Asymmetry*, *Mon. Not. Roy. Astron. Soc.* **382** (2007) 1859 [arXiv:0706.3014] [INSPIRE].

[17] M.C. March, G.D. Starkman, R. Trotta and P.M. Vaudrevange, *Should we doubt the cosmological constant?*, *Mon. Not. Roy. Astron. Soc.* **410** (2011) 2488 [arXiv:1005.3655] [INSPIRE].

[18] J.O. Berger and T. Sellke, *Testing a Point Null Hypothesis: The Irreconcilability of P Values and Evidence*, *J. Am. Stat. Ass.* **82** (1987) 112.

[19] J. o. Berger and M. Bayarri, *The interplay of Bayesian and Frequentist analysis*, *Stat. Sci.* **19** (2004) 58.

[20] V. E. Johnson, *Revised standards for statistical evidence*, in *P. Natl. Acad. Sci. U.S.A.*, 2013.

[21] R.D. Cousins, *The Jeffreys-Lindley Paradox and Discovery Criteria in High Energy Physics*, arXiv:1310.3791.

[22] S. Kullback and R. Leibler, *On Information and Sufficiency*, *Ann. Math. Stat.* **22** (1951) 79.

[23] M. Kunz, R. Trotta and D. Parkinson, *Measuring the effective complexity of cosmological models*, *Phys. Rev.* **D 74** (2006) 023503 [astro-ph/0602378] [INSPIRE].

[24] D. Spiegelhalter et al., *Bayesian Measures of Model Complexity and Fit*, *J. Roy. Stat. Soc. B* **64** (2002) 583.

[25] F. Feroz, K. Cranmer, M. Hobson, R. Ruiz de Austri and R. Trotta, *Challenges of Profile Likelihood Evaluation in Multi-Dimensional SUSY Scans*, *JHEP* **06** (2011) 042 [arXiv:1101.3296] [INSPIRE].

[26] F. Feroz and M.P. Hobson, *Multimodal nested sampling: an efficient and robust alternative to MCMC methods for astronomical data analysis*, *Mon. Not. Roy. Astron. Soc.* **384** (2008) 449 [arXiv:0704.3704] [INSPIRE].

[27] F. Feroz, M.P. Hobson and M. Bridges, *MultiNest: an efficient and robust Bayesian inference tool for cosmology and particle physics*, *Mon. Not. Roy. Astron. Soc.* **398** (2009) 1601 [arXiv:0809.3437] [INSPIRE].

[28] J. Martin and C. Ringeval, *Inflation after WMAP3: Confronting the Slow-Roll and Exact Power Spectra to CMB Data*, *JCAP* **08** (2006) 009 [astro-ph/0605367] [INSPIRE].

[29] J. Martin and C. Ringeval, *First CMB Constraints on the Inflationary Reheating Temperature*, *Phys. Rev.* **D 82** (2010) 023511 [arXiv:1004.5525] [INSPIRE].

[30] J. Martin, C. Ringeval and R. Trotta, *Hunting Down the Best Model of Inflation with Bayesian Evidence*, *Phys. Rev.* **D 83** (2011) 063524 [arXiv:1009.4157] [INSPIRE].

[31] R. Easther and H.V. Peiris, *Bayesian Analysis of Inflation II: Model Selection and Constraints on Reheating*, *Phys. Rev.* **D 85** (2012) 103533 [arXiv:1112.0326] [INSPIRE].

[32] J. Norena, C. Wagner, L. Verde, H.V. Peiris and R. Easther, *Bayesian Analysis of Inflation III: Slow Roll Reconstruction Using Model Selection*, *Phys. Rev.* **D 86** (2012) 023505 [arXiv:1202.0304] [INSPIRE].

[33] C. Ringeval, *The exact numerical treatment of inflationary models*, *Lect. Notes Phys.* **738** (2008) 243 [astro-ph/0703486] [INSPIRE].

[34] J. Martin and J. Yokoyama, *Generation of Large-Scale Magnetic Fields in Single-Field Inflation*, *JCAP* **01** (2008) 025 [arXiv:0711.4307] [INSPIRE].

[35] V. Demozzi and C. Ringeval, *Reheating constraints in inflationary magnetogenesis*, *JCAP* **05** (2012) 009 [arXiv:1202.3022] [INSPIRE].

JCAP03(2014)039

[36] S. Kuroyanagi, C. Ringeval and T. Takahashi, *Early Universe Tomography with CMB and Gravitational Waves*, *Phys. Rev.* **D 87** (2013) 083502 [arXiv:1301.1778] [INSPIRE].

[37] C. Ringeval, T. Suyama and J. Yokoyama, *Magneto-reheating constraints from curvature perturbations*, *JCAP* **09** (2013) 020 [arXiv:1302.6013] [INSPIRE].

[38] PLANCK collaboration, P.A.R. Ade et al., *Planck 2013 results. XV. CMB power spectra and likelihood*, arXiv:1303.5075 [INSPIRE].

[39] D.J. Schwarz, C.A. Terrero-Escalante and A.A. Garcia, *Higher order corrections to primordial spectra from cosmological inflation*, *Phys. Lett.* **B 517** (2001) 243 [astro-ph/0106020] [INSPIRE].

[40] D.J. Schwarz and C.A. Terrero-Escalante, *Primordial fluctuations and cosmological inflation after WMAP 1.0*, *JCAP* **08** (2004) 003 [hep-ph/0403129] [INSPIRE].

[41] J. Martin, C. Ringeval and V. Vennin, *K-inflationary Power Spectra at Second Order*, *JCAP* **06** (2013) 021 [arXiv:1303.2120] [INSPIRE].

[42] PLANCK collaboration, P.A.R. Ade et al., *Planck 2013 results. I. Overview of products and scientific results*, arXiv:1303.5062 [INSPIRE].

[43] A. Lewis and S. Bridle, *Cosmological parameters from CMB and other data: A Monte Carlo approach*, *Phys. Rev.* **D 66** (2002) 103511 [astro-ph/0205436] [INSPIRE].

[44] A. Lewis, A. Challinor and A. Lasenby, *Efficient computation of CMB anisotropies in closed FRW models*, *Astrophys. J.* **538** (2000) 473 [astro-ph/9911177] [INSPIRE].

[45] D. Shepard, *A two-dimensional interpolation function for irregularly-spaced data*, in *Proceedings of the 1968 23rd ACM national conference*, ACM '68, New York, NY, U.S.A., pg. 517, ACM, 1968.

[46] W.I. Thacker, J. Zhang, L.T. Watson, J.B. Birch, M.A. Iyer, and M.W. Berry, *Algorithm 905: Sheppack: Modified shepard algorithm for interpolation of scattered multivariate data*, *ACM Trans. Math. Softw.* **37** (2010) 1.

[47] A. Mazumdar and B. Zaldivar, *Quantifying the reheating temperature of the universe*, arXiv:1310.5143 [INSPIRE].

[48] A.A. Starobinsky, *A New Type of Isotropic Cosmological Models Without Singularity*, *Phys. Lett.* **B 91** (1980) 99 [INSPIRE].

[49] J. Ellis, D.V. Nanopoulos and K.A. Olive, *Starobinsky-like Inflationary Models as Avatars of No-Scale Supergravity*, *JCAP* **10** (2013) 009 [arXiv:1307.3537] [INSPIRE].

[50] J. Ellis, D.V. Nanopoulos and K.A. Olive, *No-Scale Supergravity Realization of the Starobinsky Model of Inflation*, *Phys. Rev. Lett.* **111** (2013) 111301 [arXiv:1305.1247] [INSPIRE].

[51] J.P. Conlon and F. Quevedo, *Kähler moduli inflation*, *JHEP* **01** (2006) 146 [hep-th/0509012] [INSPIRE].

[52] S. Krippendorf and F. Quevedo, *Metastable SUSY Breaking, de Sitter Moduli Stabilisation and Kähler Moduli Inflation*, *JHEP* **11** (2009) 039 [arXiv:0901.0683] [INSPIRE].

[53] C.P. Burgess, M. Cicoli and F. Quevedo, *String Inflation After Planck 2013*, *JCAP* **11** (2013) 003 [arXiv:1306.3512] [INSPIRE].

[54] A. Ijjas, P.J. Steinhardt and A. Loeb, *Inflationary paradigm in trouble after PlancK2013*, *Phys. Lett.* **B 723** (2013) 261 [arXiv:1304.2785] [INSPIRE].

[55] C. Germani and A. Kehagias, *New Model of Inflation with Non-minimal Derivative Coupling of Standard Model Higgs Boson to Gravity*, *Phys. Rev. Lett.* **105** (2010) 011302 [arXiv:1003.2635] [INSPIRE].

JCAP03(2014)039

[56] C. Germani and A. Kehagias, *UV-Protected Inflation*, *Phys. Rev. Lett.* **106** (2011) 161302 [arXiv:1012.0853] [INSPIRE].

[57] C. Germani and Y. Watanabe, *UV-protected (Natural) Inflation: Primordial Fluctuations and non-Gaussian Features*, *JCAP* **07** (2011) 031 [*Addendum ibid.* **1107** (2011) A01] [arXiv:1106.0502] [INSPIRE].

[58] T. Futamase and K.-i. Maeda, *Chaotic Inflationary Scenario in Models Having Nonminimal Coupling With Curvature*, *Phys. Rev.* **D 39** (1989) 399 [INSPIRE].

[59] M.B. Einhorn and D.R.T. Jones, *Inflation with Non-minimal Gravitational Couplings in Supergravity*, *JHEP* **03** (2010) 026 [arXiv:0912.2718] [INSPIRE].

[60] W. Buchmüller, V. Domcke and K. Schmitz, *Superconformal D-Term Inflation*, *JCAP* **04** (2013) 019 [arXiv:1210.4105] [INSPIRE].

[61] R. Kallosh and A. Linde, *Universality Class in Conformal Inflation*, *JCAP* **07** (2013) 002 [arXiv:1306.5220] [INSPIRE].

[62] R. Kallosh and A. Linde, *Superconformal generalization of the chaotic inflation model* $\frac{\lambda}{4}\phi^4 - \frac{\xi}{2}\phi^2 R$, *JCAP* **06** (2013) 027 [arXiv:1306.3211] [INSPIRE].

[63] R. Kallosh and A. Linde, *Superconformal generalizations of the Starobinsky model*, *JCAP* **06** (2013) 028 [arXiv:1306.3214] [INSPIRE].

[64] S. Ferrara, R. Kallosh, A. Linde and M. Porrati, *Minimal Supergravity Models of Inflation*, arXiv:1307.7696 [INSPIRE].

[65] R. Kallosh and A. Linde, *Multi-field Conformal Cosmological Attractors*, *JCAP* **12** (2013) 006 [arXiv:1309.2015] [INSPIRE].

[66] R. Kallosh, A. Linde and D. Roest, *A universal attractor for inflation at strong coupling*, arXiv:1310.3950 [INSPIRE].

[67] E. Silverstein and A. Westphal, *Monodromy in the CMB: Gravity Waves and String Inflation*, *Phys. Rev.* **D 78** (2008) 106003 [arXiv:0803.3085] [INSPIRE].

[68] A. de la Macorra and S. Lola, *Inflation in S dual superstring models*, *Phys. Lett.* **B 373** (1996) 299 [hep-ph/9511470] [INSPIRE].

[69] E. Dudas, N. Kitazawa, S.P. Patil and A. Sagnotti, *CMB Imprints of a Pre-Inflationary Climbing Phase*, *JCAP* **05** (2012) 012 [arXiv:1202.6630] [INSPIRE].

[70] E. Pajer, *Inflation at the Tip*, *JCAP* **04** (2008) 031 [arXiv:0802.2916] [INSPIRE].

[71] N. Arkani-Hamed, H.-C. Cheng, P. Creminelli and L. Randall, *Pseudonatural inflation*, *JCAP* **07** (2003) 003 [hep-th/0302034] [INSPIRE].

[72] L. Boubekeur and D. Lyth, *Hilltop inflation*, *JCAP* **07** (2005) 010 [hep-ph/0502047] [INSPIRE].

[73] P. Channuie, J.J. Jorgensen and F. Sannino, *Composite Inflation from Super Yang-Mills, Orientifold and One-Flavor QCD*, *Phys. Rev.* **D 86** (2012) 125035 [arXiv:1209.6362] [INSPIRE].

[74] S. Kachru, R. Kallosh, A.D. Linde and S.P. Trivedi, *de Sitter vacua in string theory*, *Phys. Rev.* **D 68** (2003) 046005 [hep-th/0301240] [INSPIRE].

[75] S. Kachru, R. Kallosh, A.D. Linde, J.M. Maldacena, L.P. McAllister et al., *Towards inflation in string theory*, *JCAP* **10** (2003) 013 [hep-th/0308055] [INSPIRE].

[76] L. Lorenz, J. Martin and C. Ringeval, *Brane inflation and the WMAP data: A Bayesian analysis*, *JCAP* **04** (2008) 001 [arXiv:0709.3758] [INSPIRE].

[77] S. Clesse and J. Rocher, *Avoiding the blue spectrum and the fine-tuning of initial conditions in hybrid inflation*, *Phys. Rev.* **D 79** (2009) 103507 [arXiv:0809.4355] [INSPIRE].

JCAP03(2014)039

[78] S. Clesse, C. Ringeval and J. Rocher, *Fractal initial conditions and natural parameter values in hybrid inflation*, *Phys. Rev.* **D 80** (2009) 123534 [arXiv:0909.0402] [INSPIRE].

[79] S. Clesse, *Hybrid inflation along waterfall trajectories*, *Phys. Rev.* **D 83** (2011) 063518 [arXiv:1006.4522] [INSPIRE].

[80] S. Clesse and B. Garbrecht, *Slow Roll during the Waterfall Regime: The Small Coupling Window for SUSY Hybrid Inflation*, *Phys. Rev.* **D 86** (2012) 023525 [arXiv:1204.3540] [INSPIRE].

[81] S. Clesse, B. Garbrecht and Y. Zhu, *Non-Gaussianities and Curvature Perturbations from Hybrid Inflation*, arXiv:1304.7042 [INSPIRE].

[82] W.H. Kinney and A. Riotto, *Dynamical supersymmetric inflation*, *Astropart. Phys.* **10** (1999) 387 [hep-ph/9704388] [INSPIRE].

[83] W.H. Kinney and A. Riotto, *A Signature of inflation from dynamical supersymmetry breaking*, *Phys. Lett.* **B 435** (1998) 272 [hep-ph/9802443] [INSPIRE].

[84] F. Bezrukov, P. Channuie, J.J. Joergensen and F. Sannino, *Composite Inflation Setup and Glueball Inflation*, *Phys. Rev.* **D 86** (2012) 063513 [arXiv:1112.4054] [INSPIRE].

[85] J.D. Barrow and P. Parsons, *Inflationary models with logarithmic potentials*, *Phys. Rev.* **D 52** (1995) 5576 [astro-ph/9506049] [INSPIRE].

JCAP03(2014)039

Compatibility of Planck and BICEP2 in the Light of Inflation

Jérôme Martin,[1,*] Christophe Ringeval,[2,†] Roberto Trotta,[3,‡] and Vincent Vennin[1,§]

[1] *Institut d'Astrophysique de Paris, UMR 7095-CNRS, Université Pierre et Marie Curie, 98 bis boulevard Arago, 75014 Paris, France*

[2] *Centre for Cosmology, Particle Physics and Phenomenology, Institute of Mathematics and Physics, Louvain University, 2 Chemin du Cyclotron, 1348 Louvain-la-Neuve (Belgium)*

[3] *Imperial College London, Astrophysics & Imperial Centre for Inference and Cosmology, Blackett Laboratory, Prince Consort Road, London SW7 2AZ (United Kingdom)*

(Dated: May 29, 2014)

We investigate the implications for inflation of the detection of B-modes polarization in the Cosmic Microwave Background (CMB) by BICEP2. We show that the hypothesis of primordial origin of the measurement is only favored by the first four bandpowers, while the others would prefer unreasonably large values of the tensor-to-scalar ratio. Using only those four bandpowers, we carry out a complete analysis in the cosmological and inflationary slow-roll parameter space using the BICEP2 polarization measurements *alone* and extract the Bayesian evidences and complexities for all the *Encyclopædia Inflationaris* models. This allows us to determine the most probable and simplest BICEP2 inflationary scenarios. Although this list contains the simplest monomial potentials, it also includes many other scenarios, suggesting that focusing model building efforts on large field models only is unjustified at this stage. We demonstrate that the sets of inflationary models preferred by Planck alone and BICEP2 alone are almost disjoint, indicating a clear tension between the two data sets. We address this tension with a Bayesian measure of compatibility between BICEP2 and Planck. We find that for models favored by Planck the two data sets tend to be incompatible, whereas there is a moderate evidence of compatibility for the BICEP2 preferred models. As a result, it would be premature to draw any conclusion on the best Planck models, such as Starobinsky and/or Kähler moduli inflation. For the subset of scenarios not exhibiting data sets incompatibility, we update the evidences and complexities using both data sets together.

PACS numbers: 98.80.Cq

I. INTRODUCTION

The recent discovery of B-mode polarization in the Cosmic Microwave Background (CMB) by BICEP2 [1], if confirmed to be of primordial origin [2], would constitute a breakthrough for our understanding of early universe cosmology. In addition to lensing, B-mode can be generated by either vector perturbations or tensor perturbations [3]. Vectors do not propagate in a Friedmann-Lemaître universe (see however Ref. [4]) and can be a potential explanation of the BICEP2 data only if they are incessantly generated by active sources such as cosmic strings [5] or magnetic fields [6]. These, however, are severely constrained by other measurements [7, 8].

Tensor modes are a natural and expected outcome of cosmic inflation although the uncertainty on their amplitude is huge (several orders of magnitude). In this context, the BICEP2 result might represent the first detection of primordial gravity waves produced in the early Universe [9, 10] and, therefore, could give us precious information about the physical conditions that prevailed at that time. Of course, the BICEP2 result needs to be confirmed by other measurements before one can be sure that primordial B-mode have really been detected. In this paper, our working hypothesis will be that this is indeed the case. On general grounds, it is anyway always interesting to explore the implications for inflation of a non negligible level of primordial gravity waves.

The claimed amplitude of the signal corresponds to a tensor to scalar ratio of $r = 0.2^{+0.07}_{-0.05}$ or $r = 0.16^{+0.06}_{-0.05}$ depending on how polarized dust foregrounds are modeled and/or subtracted. Recent works [11] have however cast doubts on the modeling of the foreground dust, which could potentially lead to the amplitude of the tensor modes signal to be much lower, to the point of becoming undetectable. In the following, we shall take the BICEP2 result at face value, pending further investigation, most notably thanks to the recently released Planck dust maps [12]. The BICEP2 measurement, if, as already mentioned, interpreted as of primordial origin, has several important physical consequences that we now discuss.

Firstly, the energy scale of inflation [13–21] is fixed and roughly given by

$$\rho^{1/4} \simeq 2.2 \left(\frac{r}{0.2}\right)^{1/4} 10^{16}\,\mathrm{GeV}, \tag{1}$$

i.e. around the Grand Unified Theory (GUT) energy scale. A more accurate determination of this energy

*Electronic address: jmartin@iap.fr
†Electronic address: christophe.ringeval@uclouvain.be
‡Electronic address: r.trotta@imperial.ac.uk
§Electronic address: vennin@iap.fr

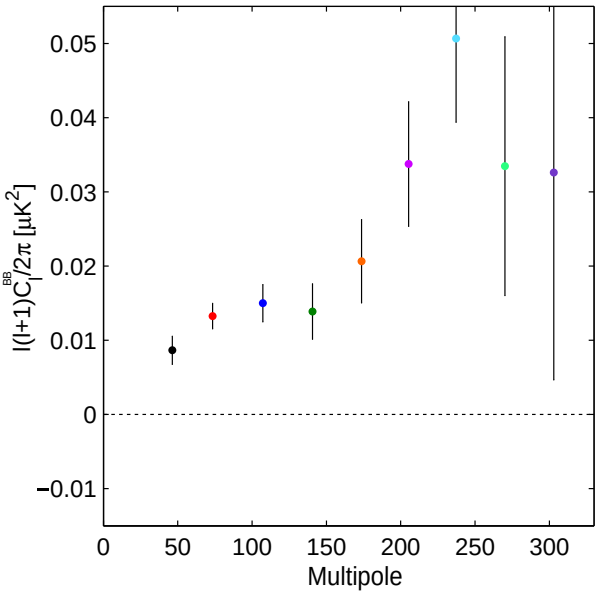

FIG. 1: B-mode angular power spectrum in the nine bandpowers measured by the BICEP2 experiment. Figure extracted from Ref. [1].

scale and the Hubble rate during inflation are given in Sec. III D. Inflation is therefore a high energy phenomenon by Particle Physics standard.

Secondly, this result would favor that single field slow-roll scenarios achieve the best compromise between quality of the fit and theoretical simplicity [22]. Indeed, in more complicated models, the tensor to scalar ratio is generically (but not necessarily) smaller than in the standard case[1]. For instance, for K-inflation [25], one has $r = -8n_{\rm T}c_{\rm S}$ where $c_{\rm S} < 1$ is the sound speed of the fluctuations [26]. For two-field inflation, one can write $r = -8n_{\rm T}\sin^2\Theta \leq -8n_{\rm T}$, where $\sin\Theta$ is a term taking into account the possible evolution of scalar modes on super Hubble scales [27]. For multiple field inflation, the above equality becomes an inequality, namely $r \leq -8n_{\rm T}\sin^2\Theta$, thus strengthening the argument presented before (up to the special case of massive Nflation which inherits some of the properties of a single $m^2\phi^2$ model [28–31]). Of course, this certainly does not mean that these more complicated models are ruled out by BICEP2 (as a matter of fact, they are not!), but together with the absence of detection of isocurvature modes and primordial non-Gaussianities, this reinforces the fact that there are not needed in order to give a satisfactory description of the data. Clearly, this argument should be toned down given that multiple field models are often well motivated from a high energy point of view and, moreover, can predict a non negligible r even if the field excursion is smaller than the Planck mass [32] (see below). Also notice that, for the simplest and preferred class of inflationary models mentioned above, the non-Gaussianities are characterized by $f_{\rm NL}^{\rm loc} = 5(1-n_{\rm S})/12 \simeq 1.6\times10^{-2}$ [33] since Planck [34, 35] has measured $n_{\rm S} = 0.9603 \pm 0.0073$. Therefore, unless one is able to reach the 10^{-2} level, it seems impossible to measure $V(\phi)$ using the precise shape of the three-point correlation function. The 10^{-2} level appears to be extremely challenging given our present day capabilities and, as a consequence, this reinforces the importance of a measurement of r since this opens a realistic opportunity to identify the correct inflationary scenario.

Thirdly, in the framework of single field slow-roll scenarios, BICEP2 result implies a lower bound on the first Hubble flow function, which is also given by $\epsilon_1 \simeq M_{\rm Pl}^2(V_\phi/V)^2/2$. Therefore, the first derivative of the inflaton potential can be constrained. Furthermore, since the deviation from scale invariance $n_{\rm S} - 1$ depends on a combination of the first and second derivatives of the potential (at leading order in slow roll), this automatically also provides a measurement of the second derivative of the potential. It is also interesting to notice that a constraint on ϵ_1 does not modify our estimate of the importance of the stochastic effects for CMB scales [36–38]. Indeed, if $\Delta_{\rm q}$ is the typical quantum excursion of the inflaton field during one e-fold and $\Delta_{\rm cl}$ its classical excursion, then $\Delta_{\rm q}/\Delta_{\rm cl} \simeq H/(M_{\rm Pl}\sqrt{\epsilon_1}) \simeq \sqrt{\mathcal{P}_\zeta} \simeq 10^{-5}$. The point is that $\Delta_{\rm q}/\Delta_{\rm cl}$ does not depend on ϵ_1 alone but on the combination $H/\sqrt{\epsilon_1}$ which was already measured before BICEP2 since it turns out to be exactly the amplitude of the scalar modes. However, a measurement of r also gives indications about the shape of the potential (see below) and, then, $\Delta_{\rm q}/\Delta_{\rm cl} > 1$ may become possible but necessarily outside the observable window. If $r \simeq 0.2$ favors potentials for which this systematically happens, one should still pay attention to how measurements made on the CMB scales should be extrapolated to the part of the inflaton's potential supporting a stochastic regime [39]. Therefore, observationally speaking, the question of knowing if non-perturbative quantum effects can play an important role in the early Universe is still open [40–42].

Fourthly, the model building problem is also impacted by the BICEP2 result. Indeed, by definition of the first Hubble flow function, one has $\Delta\phi/M_{\rm Pl} = \mathcal{O}(1)\,(r/0.2)^{1/2}$ [43, 44] which indicates that the excursion of the field during inflation is necessarily super-Planckian. The single field models discussed before are usually viewed as effective models only, valid up to a cut-off Λ [45]. This scale should be less than $M_{\rm Pl}$ since $M_{\rm Pl}$ is the cut-off of General Relativity and larger than H since the model should be able to describe what happens during inflation. In the framework of effective field theories, when physical effects beyond the cut-off are taken into account, the total Lagrangian of a given inflationary model can be expressed as $\mathcal{L} = \dot\phi^2/2 + V(\phi) + \sum_i c_i\mathcal{O}_i/\Lambda^{n_i-4}$,

[1] With the notable exception of G-inflation [23, 24] where $r = 16c_{\rm S}\sigma$, with σ a complicated function of the inflaton field and its derivative, possibly larger than one even in the slow-roll limit.

where $V(\phi)$ contains renormalizable terms only and $\mathcal{O}_i$ represents a higher order operator of dimension $n_i > 4$ (possibly a non minimal kinetic term) the amplitude of which is controlled by the coefficient c_i. When an inflationary model is designed, it usually makes use of $\mathcal{L} = \dot{\phi}^2/2 + V(\phi)$ only and the higher order operators are neglected. The validity of this approximation is questionable because of the following two problems. Firstly, as mentioned above, a large value of r implies a large value of $\Delta\phi$ compared to the Planck mass and the operators $\mathcal{O}_i$ may no longer be negligible. Solutions to these issues are either to fine-tune the couplings between the light and heavy fields or to assume the existence of a symmetry (typically the shift symmetry) to forbid the dangerous higher order operators. But, then, this raises the question of the origin of this symmetry in the full theory, that is to say the question of the UV completion of the model. For a nice and more complete discussion on all these issues, see for instance Ref. [45]. Secondly, the parameters of $V(\phi)$ usually get corrected by heavy field loops. For instance, a mass term typically acquires the following form: $m^2 \to m^2 + gM^2\ln(\Lambda/\mu)$, where μ is a renormalizable scale, $M > \Lambda$ the mass of a heavy field and g the coupling between ϕ and the heavy field[2]. This means that the mass of the inflaton becomes larger than the Hubble rate and that the potential is no longer flat enough to support inflation. Notice however that this issue is, a priori, always present even in a model where r is small.

Fifthly, the BICEP2 result exacerbates the problems of inflationary magnetogenesis [47–49]. Recent observations indicate the presence of magnetic fields of strength ranging from 10^{-17} to 10^{-15} Gauss on megaparsec scales and such a large coherence length suggests a cosmological origin [50–53]. In order to produce a magnetic field during inflation, one needs to break conformal invariance. For instance, this can be achieved by considering a term $f^2(\phi)F_{\mu\nu}F^{\mu\nu}$. A simple parametrization for the function $f(\eta)$ is given by $f \propto a^\alpha$ [49] since the choices $\alpha \simeq 2$ or $\alpha \simeq -3$ both lead to a flat spectrum. For $\alpha = 2$ f is a growing function of time, and since the gauge field A_μ is also coupled to charged fermions with a coupling constant $g_{\rm eff}(\eta) \propto g/f(\eta)$, this implies that the system is in a non perturbative regime during inflation [54] (for a possible solution, see Ref. [55]). On the other hand, the solution $\alpha = -3$ suffers from a backreaction problem. In order to avoid a too important production of the electric field, the only way out is then to lower the energy scale of inflation, i.e. $H/M_{\rm Pl} \lesssim 10^{-20}$ [49, 56, 57]. The BICEP2 result would invalidate this solution and, therefore, one is left in a situation where inflationary magnetogenesis appears to be more problematic than before.

Sixthly, the detection of a quite large value of r raises the question of whether one can directly see the primordial gravitational waves. With $r \simeq 0.2$ and $n_{\rm T} \simeq -r/8 \simeq -0.025$, see Eq. (28), one expects to have today $\Omega_{\rm gw} \simeq 10^{-15}$ and experiments such as VIRGO [58] and eLISA [59] cannot detect such a tiny signal. However, Japan's DECIGO [60, 61], Ultimate-DECIGO or NASA's Big Bang Observer (BBO) [62] have a priori the sensitivity required to directly probe the inflationary primordial gravity waves. Notice that these experiments operate in the frequency range $f \in [10^{-2}\,{\rm Hz}, 10\,{\rm Hz}]$ and this could render the measurements of the reheating parameters, such as the reheating temperature and/or the equation of state parameter, feasible [63, 64].

Seventhly, it has been claimed [65, 66] that the BICEP2 results would represent the first experimental evidence for quantum gravity since, in the framework of inflation, the transverse and traceless component of the perturbed metric is a quantum operator. This has indeed been known for forty years [9, 10] and more than twenty years in the context of inflation [67–69]. However, this was already the case for scalar modes [21, 67–69]. Indeed, their equation of motion derives from the perturbed quantum Einstein equations, $\delta\hat{G}_{\mu\nu} = 8\pi G\delta\hat{T}_{\mu\nu}$. To put it differently, the Mukhanov-Sasaki quantum operator $\hat{v}$, that characterizes the amplitude of scalar modes, is expressed in terms of the perturbed inflaton field $\delta\hat{\phi}$ and the Bardeen potential $\hat{\Phi}$, concretely $\hat{v} \equiv \delta\hat{\phi} + (\phi'/\mathcal{H})\hat{\psi} = \delta\hat{\phi}^{(\rm gi)} + (\phi'/\mathcal{H})\hat{\Phi}$ (where $\delta\hat{\phi}^{(\rm gi)}$ is the gauge invariant perturbed field and $\hat{\psi}$ is the scalar component of the perturbed metric proportional to δ_{ij}). We see that the perturbed metric is also a quantum operator in the scalar sector and is directly related to the CMB anisotropies. Notice that a semi-classical formulation of the problem, namely $\delta G_{\mu\nu} = 8\pi G\langle\delta\hat{T}_{\mu\nu}\rangle$, does not help since $\delta\hat{T}_{\mu\nu}$, being by definition linear in $\delta\hat{\phi}$, satisfies $\langle\delta\hat{T}_{\mu\nu}\rangle = 0$. One might argue that the scalar sector suffers from a gauge problem but this question has been discussed and solved with the help of the gauge-invariant formalism [70]. There exists a gauge (the spatially flat or uniform curvature gauge [71]) for which $\psi = 0$ and, therefore, $v = \delta\phi$. However, this cannot be used as an argument that only field fluctuations must be quantized. Indeed, there is another gauge (comoving orthogonal gauge [71]) where $\delta\phi = 0$ and, hence, $v = (\phi'/\mathcal{H})\psi$. As a consequence, the same logic leading to the above argument could also be used to reach an opposite conclusion, namely that only metric fluctuations (and not field perturbations) must be quantized. In fact, as it is

[2] Notice that regularizing the loop integral with a cut-off would have produced a correction proportional to Λ^2, namely $m^2 \to m^2 + g\Lambda^2$. However, this approach is not consistent as can be nicely illustrated on the example of the regularization of the cosmological constant. Indeed, if one regularizes $\rho_{\rm vac}$ with a cut-off, one obtains that $\rho_{\rm vac} \to \rho_{\rm vac} + \Lambda^4$. However, this method breaks Lorentz invariance and, as a consequence, one obtains the wrong equation of state, $w = p_{\rm vac}/\rho_{\rm vac} = 1/3$ instead of $w = -1$. If, on the contrary, the loop integral is regularized with a method that respects Lorentz invariance (for instance dimensional regularization), then one obtains $\rho_{\rm vac} \to \rho_{\rm vac} + M^4\ln(\Lambda/\mu)$ and $w = -1$, see Ref. [46]. In other words, if there is no new physics beyond the standard model, there is no hierarchy problem.

clear from the definition of the Mukhanov-Sasaki variable, field and metric perturbations cannot be disentangled [72] and the scalar modes are therefore already a genuine signature of the quantum-mechanical nature of the gravitational field. On the other hand, it is true that there still exist open issues related to the quantum to classical transition of these quantum fluctuations [73–81].

Eighthly, it is worth recalling that BICEP2 data do not only concern the B-mode polarization but also the E-modes ($C_\ell^{\rm TT,obs}$ and $C_\ell^{\rm TE,obs}$ are not yet publicly available). The fact that the polarization spectrum $C_\ell^{\rm EE,obs}$ has been also measured is fortunate since it allows us to constrain scalar perturbations, and cosmology, with the BICEP2 data alone [82]. This is discussed further in the following. Although not public, the BICEP2 team reports a $C_\ell^{\rm TB,obs}$ consistent with zero and this is relevant for models containing a gravitational Chern-Simons term [83–85]. This term is necessarily present since it is generated by quantum corrections and is generic in string theory. This implies that the two polarization states of a gravitational wave behave differently. As a consequence, the tensor-to-scalar ratio is modified and can even be enhanced [84] (to be fair, a calculation of r in a regime where the enhancement is large remains very challenging).

Another question which arises after BICEP2 is the implications of these new data with regards to the shape of the inflaton potential $V(\phi)$ and whether these implications are compatible with the conclusions reached previously, and notably from Planck data [22, 86–88]. Let us recall that, given Planck data, the best models in terms of evidences and complexities are such that their potential is of the plateau type, the prototypical example being the Starobinsky model [13]. In more quantitative terms, if one uses the Jeffreys' scale [89, 90] and count the number of models in the "inconclusive", "weak evidence", "moderate evidence" and "strong evidence" zones with respect to the best, one finds 26% in the first category (corresponding to 17 different shapes of the potential), 21% in the second, 17% in the third and, finally, 34% in the fourth and last one. These numbers can be further improved by another statistical indicator. If we restrict ourselves to models having a number of unconstrained parameters between zero and one, then only 9% of the scenarios are preferred, corresponding this time to 9 different potentials. And these 9 potentials are all of the plateau type. On the other hand, the Jeffreys scale has to be taken as indicative, and it is usually considered that only the models belonging to the strong evidence category (here, 34%) can really be considered as robustly "ruled out". Therefore, we see that the Planck data have been able to narrow down our theoretical uncertainties efficiently and to point to a particular type of potentials. As a consequence, an important question is whether the BICEP2 measurements are in agreement with these conclusions and, more generally, whether BICEP2 is compatible with Planck in the framework of single field slow-roll inflation.

The present article aims at discussing the issues presented above. As many inflationary models genuinely produce a small amount of tensor modes, one would expect the BICEP2 data to severely cut a large volume of the model space, thereby improving our knowledge of inflation compared to what has already been established with Planck data. However, one has first to address and quantify the compatibility between BICEP2 and Planck data. For this, it is required to first investigate both data sets independently. This may seem problematic for BICEP2 as B-modes alone do not give constraints on the scalar perturbations. But, as we show below, using both the E- and B modes polarization measurements in only four bandpowers already gives non-trivial constraints on both the standard cosmological parameters and the primordial ones (see also Ref. [82]). This allows us to derive the evidences and complexities of all the *Encyclopædia Inflationaris* models using BICEP2 data alone and thoroughly discuss the compatibility of Planck and BICEP2 using the so-called $\mathcal{R}$-factors [91–97]. These are the Bayes factors giving the ratio between the probability of compatibility to the probability of incompatibility assuming a given model. By evaluating $\mathcal{R}$ for slow-roll inflation and for each *Encyclopædia Inflationaris* scenarios, one can determine the subset of models for which Planck and BICEP2 data can be meaningfully combined to obtain evidences and complexities from the joint data sets.

This article is organized as follows. In the next section, we briefly describe the method used to compute the Bayesian evidence of any slow-roll inflationary model. In particular, our method is based on the determination of an effective likelihood for inflation which requires a slow-roll analysis of the Planck and BICEP2 data. The results of the analysis for Planck can be found in Ref. [22] and we present in Sec. III new results for BICEP2 alone, and BICEP2 combined with Planck. In particular, we discuss the compatibility of the data sets under the hypothesis of slow-roll. In Sec. IV, we present the evidences and complexities for all the *Encyclopædia Inflationaris* models stemming from the BICEP2 data alone and discuss what are the inflaton potential shapes favored and how they differ from the Planck results. We then move on to the compatibility of Planck and BICEP2 model by model and present joint evidences and complexities for the scenarios under which both data sets are not incompatible. Finally, in Sec. V, we summarize our findings and present our conclusions.

II. METHODOLOGY

A. Bayesian Evidence and Complexity

In this section, we briefly present the statistical methodology adopted here to compute the Bayesian evidence and complexity for each of the *Encyclopædia Inflationaris* models that, in the following, we denote by

$\mathcal{M}_i$.

The Bayesian evidence, given data D, is defined by [90]

$$P(D|\mathcal{M}_i) \equiv \mathcal{E}\left(D|\mathcal{M}_i\right) = \int \mathrm{d}\theta_{ij}\mathcal{L}\left(\theta_{ij}\right)\pi\left(\theta_{ij}|\mathcal{M}_i\right), \quad (2)$$

where θ_{ij} represents the parameters characterizing the model $\mathcal{M}_i$, $\mathcal{L}$ is the likelihood function (to be discussed below) and $\pi\left(\theta_{ij}|\mathcal{M}_i\right)$ is the prior distribution for the parameter θ_{ij}. As usual in Bayesian analysis, the choice of the priors plays a crucial role and a complete study of the $\pi\left(\theta_{ij}|\mathcal{M}_i\right)$ for all the *Encyclopædia Inflationaris* models can be found in Ref. [22]. Here, we adopt the same choices. The Bayesian complexity can be expressed as [98]

$$\mathcal{C}_i = \left\langle -2\log\mathcal{L}\left(\theta_{ij}\right)\right\rangle + 2\log\mathcal{L}\left(\theta_{ij}^{\mathrm{ML}}\right), \quad (3)$$

where $\langle\cdot\rangle$ means averaging over the posteriors and $\theta_{ij}^{\mathrm{ML}}$ represents the maximum likelihood estimate of the model's parameters.

The Bayesian evidences are often normalized to a reference model $\mathcal{M}_{\mathrm{REF}}$ and one defines $B^i_{\mathrm{REF}} \equiv \mathcal{E}(D|\mathcal{M}_i)/\mathcal{E}(D|\mathcal{M}_{\mathrm{REF}})$. They give us information about the posterior probability of the model $\mathcal{M}_i$ (for non-committal model priors),

$$P\left(\mathcal{M}_i|D\right) = \frac{B^i_{\mathrm{REF}}}{\sum_j B^j_{\mathrm{REF}}}. \quad (4)$$

On the other hand, the Bayesian complexities tell us something about the number of unconstrained parameters

$$N_i^{\mathrm{uc}} \equiv N_i - \mathcal{C}_i, \quad (5)$$

where N_i is the total number of parameters of the model under scrutiny. The above considerations show that, given a data set D, the performance of a model can be described by the numbers $(N^{\mathrm{uc}}, B_{\mathrm{REF}})$.

B. Compatibility of data sets

Although the previous discussion is readily applicable for either the Planck (D_{p}) or BICEP2 data (D_{b}) separately, computing a joint evidence from BICEP2 and Planck, namely using $D = \{D_{\mathrm{p}}, D_{\mathrm{b}}\}$, requires some precaution. Indeed, it is crucial to determine whether a small value of $P(D|\mathcal{M}_i)$ is the consequence of $\mathcal{M}_i$ being a poor explanation of the data, or whether this results from the tension between Planck and BICEP2.

As detailed below, there is a some tension between the two data sets, when interpreted in terms of tensor modes amplitude. Combining the two data sets blindly could potentially lead to a joint likelihood function that peaks in a region of parameter space that is not favored by either experiment–an obviously undesirable situation.

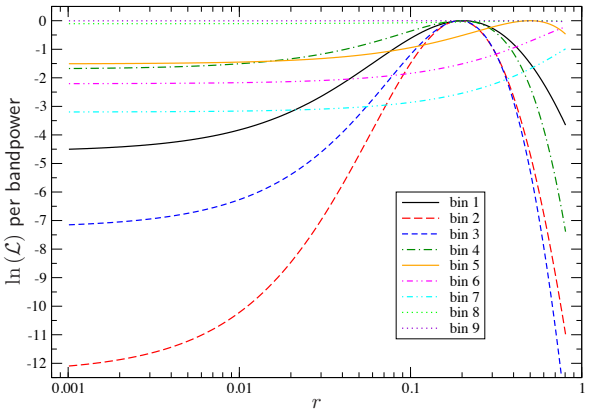

FIG. 2: BICEP2 likelihood function over the tensor-to-scalar ratio r, assuming power law primordial spectra and with the ΛCDM parameters fixed to their mean value obtained from the Planck data alone. B-modes from lensing are included and we have presented the contribution of each of the nine BICEP2 bandpowers. Only the first four bandpowers favor the hypothesis of primordial tensor modes of inflationary origin whereas the others exhibit a likelihood maximal at problematic large values of r.

In order to study the compatibility of BICEP2 and Planck, we resort to a Bayesian measure defined as follows [91–97, 99]:

$$\mathcal{R}_i \equiv \frac{P(D_{\mathrm{p}}, D_{\mathrm{b}}|\mathcal{M}_i, \mathcal{H}_{\mathrm{c}})}{P(D_{\mathrm{p}}|\mathcal{M}_i, \mathcal{H}_{\mathrm{ic}})P(D_{\mathrm{b}}|\mathcal{M}_i, \mathcal{H}_{\mathrm{ic}})}. \quad (6)$$

This quantity represents the posterior between the hypothesis that the two data sets are compatible, ($\mathcal{H}_{\mathrm{c}}$, when $\mathcal{R}_i > 1$) versus the hypothesis that they are not ($\mathcal{H}_{\mathrm{ic}}$ and thus described by different sets of parameters, when $\mathcal{R}_i < 1$), assuming the inflationary model $\mathcal{M}_i$ and noncommittal priors between the two hypotheses, $P(\mathcal{H}_{\mathrm{c}}) = P(\mathcal{H}_{\mathrm{ic}}) = 1/2$. Various proto-typical situations illustrating the behavior or $\mathcal{R}$ are presented in the appendix (see Sec. A 1), where one can gain some insight on why $\mathcal{R}$ measures compatibility. The $\mathcal{R}$ factor can also be re-expressed in terms of the conditional predictive probability for BICEP2 data, by noting that

$$P(D_{\mathrm{p}}, D_{\mathrm{b}}|\mathcal{M}_i) = P(D_{\mathrm{b}}|D_{\mathrm{p}}, \mathcal{M}_i)P(D_{\mathrm{p}}|\mathcal{M}_i). \quad (7)$$

Using Eq. (7), we obtain the simpler expression

$$\mathcal{R}_i = \frac{P(D_{\mathrm{b}}|D_{\mathrm{p}}, \mathcal{M}_i)}{P(D_{\mathrm{b}}|\mathcal{M}_i)}, \quad (8)$$

which shows that $\mathcal{R}_i$ is large if the probability of obtaining data D_{b}, given the Planck data D_{p}, is large.

C. Likelihood Functions

The likelihoods considered in the following have been provided by the Planck collaboration [100] and the BI-

CEP2 team [1, 101, 102]. Concerning the Planck likelihood, we have used the "CamSpec" likelihood for the temperature power spectrum in the multipole range $50 < \ell < 2500$ complemented with the "Commander" likelihood for $2 < \ell < 49$. Moreover, following the data analysis method of Refs. [34, 103], we have also used the WMAP polarization data for $\ell \leq 32$ [104–106]. These data sets are the same as the ones used in Ref. [22]. Concerning the BICEP2 likelihood, we have written a FORTRAN code from scratch based on the approximation of Ref. [101] and as implemented by the BICEP2 team (see Ref. [107]). Our results are identical to the ones obtained with the latest version of `COSMOMC` [108] in which the BICEP2 likelihood has also been implemented. The BICEP2 measurements are publicly available[3].

As discussed in Ref. [1], when assuming primordial power law power spectra, the BICEP2 likelihood for the tensor to scalar ratio r peaks at a value around 0.2, which is significantly larger than those favored by the Planck data. In Fig. 2, we have represented the BICEP2 likelihood profile along r, in each bandpower, when the ΛCDM cosmological parameters are fixed to their mean values obtained from the Planck data alone [34]. Let us notice that the likelihood has been estimated using `CAMB` [109] to provide the expected $C_\ell^{\rm BB,th}$ for each value of r while including the lensing effects which convert E-modes into B-modes. This figure shows that over the nine bandpowers provided by the BICEP2 team, the second bin carries most of the statistical weight and, moreover, only four bins are reasonable with the hypothesis that the measured $C_\ell^{\rm BB,obs}$ are sourced by tensor modes of inflationary origin. Indeed, already for the bandpower five, the likelihood peaks at a value $r > 0.5$. The bandpowers six to nine would even favor a tensor-to-scalar ratio larger than one. Those bandpowers do not significantly weigh in the total likelihood as their associated errors are relatively large (see Fig. 1). However, as they seem to suffer from a systematic excess, the origin of which not being inflation neither lensing, we have decided to perform our data analysis using only the first four bandpowers of the BICEP2 data hoping that they are not too much affected by such systematics. In fact, we have also checked that including all the bins in the analysis does not modify in a substantial way our conclusions.

D. Fast Evidence Computation

Given our likelihood function, we briefly summarize in this section how the Bayesian evidence of a given *Encyclopædia Inflationaris* model can be fast computed.

Any inflationary model is characterized by the parameters $\theta_{\rm inf}$ describing the shape of the potential [for instance, for large field inflation where $V(\phi) = M^4(\phi/M_{\rm Pl})^p$, one has $\theta_{\rm inf} = (M, p)$] and by the priors choice on those parameters [22]. We also need parameters describing the reheating phase, $\theta_{\rm reh}$, such as the reheating temperature and the equation of state. In fact, one can show that only one parameter is sufficient, the so-called rescaled reheating parameter R [110–114]. In the present paper, following Ref. [22], a Jeffreys' prior is assumed such that $\theta_{\rm reh} = \ln R \in [-46, 15]$. Finally, the parameters describing the post-inflationary phase are the standard cosmological parameters associated with a ΛCDM model, plus the astrophysical parameters entering the likelihood function. Those are referred to as $\theta_{\rm s}$ in the following. As a consequence, the evidence in Eq. (2), for a model $\mathcal{M}_i$, becomes

$$\mathcal{E}\left(D|\mathcal{M}_i\right) = \int {\rm d}\theta_{\rm s}{\rm d}\theta_{\rm reh}{\rm d}\theta_{\rm inf}\mathcal{L}\left(\theta_{\rm s},\theta_{\rm reh},\theta_{\rm inf}\right) \times \pi(\theta_{\rm s})\pi(\theta_{\rm reh})\pi(\theta_{\rm inf}), \tag{9}$$

where π represent the priors. The key remark here is to notice that, as opposed to the cosmological and astrophysics parameters, $\theta_{\rm reh}$ and $\theta_{\rm inf}$ affect the likelihood by modifying *only* the scalar $\mathcal{P}_\zeta(k)$ and tensor $\mathcal{P}_h(k)$ primordial power spectra. As a consequence, one possibility would be to numerically evaluate, for each inflationary model, $\mathcal{P}_\zeta$ and $\mathcal{P}_h$ [35, 114, 115]. This is, however, very time consuming.

Here, we rather choose to use the method developed in Ref. [116]. The main idea of this article is to bypass any mode integration by modeling through a small number of parameters the shape of the primordial spectra. Since we are only focused on slow-roll inflation, we consider the second order slow-roll expansion of the scalar and tensor primordial spectra around a pivot scale k_* [117–128], namely

$$\begin{aligned}\mathcal{P}_\zeta = \frac{H^2}{8\pi^2 M_{\rm Pl}^2\epsilon_1}\Bigg\{&1-2(1+C)\epsilon_1-C\epsilon_2\\&+\left(\frac{\pi^2}{2}-3+2C+2C^2\right)\epsilon_1^2+\left(\frac{\pi^2}{24}-\frac{C^2}{2}\right)\epsilon_2\epsilon_3\\&+\left(\frac{7\pi^2}{12}-6-C+C^2\right)\epsilon_1\epsilon_2+\left(\frac{\pi^2}{8}-1+\frac{C^2}{2}\right)\epsilon_2^2\\&+\Bigg[-2\epsilon_1-\epsilon_2+(2+4C)\epsilon_1^2+(-1+2C)\epsilon_1\epsilon_2\\&+C\epsilon_2^2-C\epsilon_2\epsilon_3\Bigg]\ln\left(\frac{k}{k_*}\right)+\left(2\epsilon_1^2+\epsilon_1\epsilon_2+\frac{1}{2}\epsilon_2^2\right.\\&\left.-\frac{1}{2}\epsilon_2\epsilon_3\right)\ln^2\left(\frac{k}{k_*}\right)\Bigg\}\end{aligned} \tag{10}$$

[3] See http://bicepkeck.org.

and

$$\mathcal{P}_h = \frac{2H^2}{\pi^2 M_{\rm Pl}^2} \times \left\{1 - 2(1+C)\epsilon_1 + \left(\frac{\pi^2}{2} - 3 + 2C + 2C^2\right)\epsilon_1^2 + \left(\frac{\pi^2}{12} - 2 - 2C - C^2\right)\epsilon_1\epsilon_2 + \left[-2\epsilon_1 + (2+4C)\epsilon_1^2 - 2(1+C)\epsilon_1\epsilon_2\right]\ln\left(\frac{k}{k_*}\right) + \left(2\epsilon_1^2 - \epsilon_1\epsilon_2\right)\ln^2\left(\frac{k}{k_*}\right)\right\}, \tag{11}$$

where $C = \gamma + \ln 2 - 2 \simeq -0.72$, γ being the Euler constant. The quantities ϵ_n are the Hubble-flow parameters evaluated at pivot Hubble exit, i.e. at the conformal time η_* solution of $k_*\eta_* = -1$. The Hubble parameter H entering the normalization is also evaluated at η_*. Let us notice that, by definition, $P_* \equiv \mathcal{P}_\zeta(k_*)$ is a well-measured quantity which fixes the amplitude of the CMB anisotropies. Let us also remark that, a priori, P_* is not directly proportional to $C_\ell^{\rm TT,obs}$ since, when the tensor-to-scalar ratio does not vanish, part of the signal also comes from $\mathcal{P}_h(k_*)$. However, for our choice of pivot scale, $k_* = 0.05\,{\rm Mpc}^{-1}$, the gravity waves contribution is already very small.

The inflationary model dependence now only appears through the explicit functionals $\epsilon_n(\theta_{\rm reh}, \theta_{\rm inf})$. These are explicitly derived for all models of the *Encyclopædia Inflationaris* in Ref. [86] and can be computed using the public library `ASPIC`[4]. In other words, the power spectra obtained in this way differ for different models because the functionals $\epsilon_n(\theta_{\rm reh}, \theta_{\rm inf})$ depend on the inflationary model considered. Then, the Bayesian evidence can be obtained from Eq. (9) by marginalizing over all parameters, i.e.

$$\mathcal{E}\left(D|\mathcal{M}_i\right) = \int \mathcal{L}_{\rm eff}\left[P_*(\theta_{\rm reh}, \theta_{\rm inf}), \epsilon_n(\theta_{\rm reh}, \theta_{\rm inf})\right] \times \pi(\theta_{\rm reh})\pi(\theta_{\rm inf})\,{\rm d}\theta_{\rm reh}{\rm d}\theta_{\rm inf}, \tag{12}$$

where we have defined the effective likelihood by

$$\mathcal{L}_{\rm eff}\left(P_*, \epsilon_n\right) \equiv \int \mathcal{L}\left(\theta_{\rm s}, P_*, \epsilon_n\right)\pi(\theta_{\rm s})\,{\rm d}\theta_{\rm s}. \tag{13}$$

The effective likelihood for inflation $\mathcal{L}_{\rm eff}$ is the full likelihood $\mathcal{L}$ marginalized over all the cosmological and astrophysics parameters. Its estimation therefore requires a complete data analysis that we present in the following. However, this has to be done once and for all as the evidences of all the inflationary models can be computed afterwards from Eq. (12). In practice, the functional shape of $\mathcal{L}_{\rm eff}(P_*, \epsilon_n)$ is fitted using a neural network interpolator allowing its very fast evaluation.

[4] http://theory.physics.unige.ch/~ringeval/aspic.html

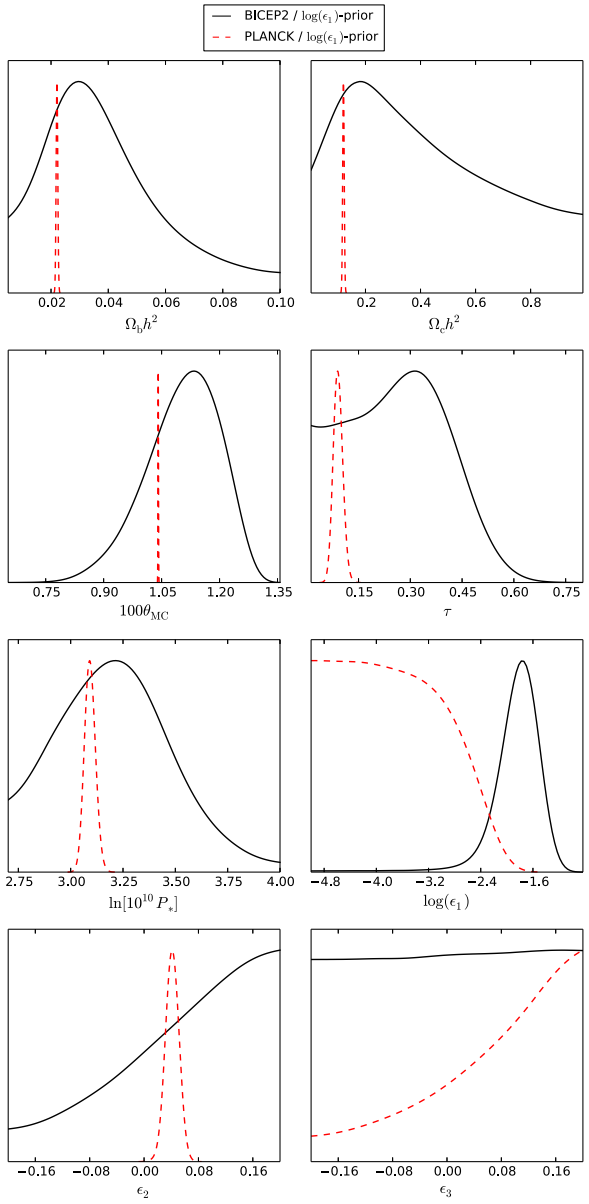

FIG. 3: One-dimensional marginalized posterior probability distributions for the cosmological and primordial slow-roll parameters obtained with BICEP2 data alone (solid black lines) compared to the corresponding Planck's posteriors (dashed red lines).

III. DATA ANALYSIS

In order to determine $\mathcal{L}_{\rm eff}$, we have performed a Markov-Chain-Monte-Carlo (MCMC) exploration of the slow-roll parameter space using the BICEP2 and Planck likelihood described above.

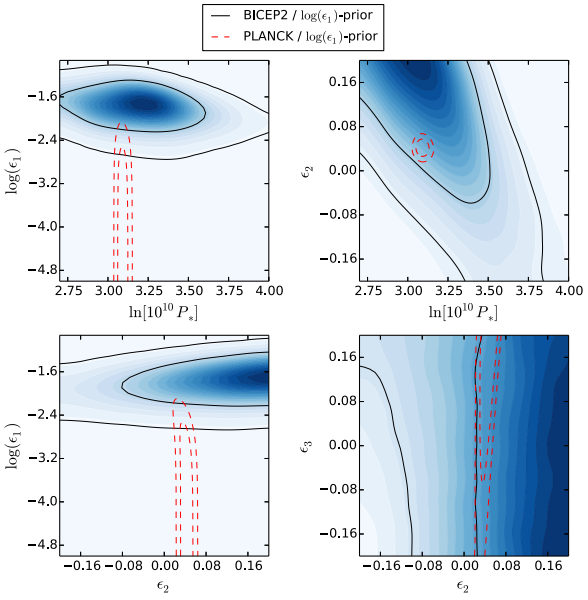

FIG. 4: Two-dimensional marginalized posterior probability distributions for the primordial slow-roll parameters obtained from BICEP2 data alone (solid black lines) compared to the corresponding Planck's posteriors (dashed red lines). The blue shading density traces the mean likelihood values for BICEP2 (Jeffreys' prior on ϵ_1).

A. Constraints from BICEP2

In this first section, we derive constraints on the cosmological parameters using the BICEP2 data alone. The post-inflationary universe, assumed to be a flat ΛCDM model, is described by the parameters $\theta_{\rm s}$:

$$\theta_{\rm s} = \left(\Omega_{\rm b}h^2, \Omega_{\rm c}h^2, \tau, 100\theta_{\rm MC}\right). \qquad (14)$$

The cosmological parameters are the baryons energy density (normalized to the critical energy density) $\Omega_{\rm b}$, the cold dark matter energy density $\Omega_{\rm c}$, the reduced Hubble parameter today h, the optical depth τ to last scattering and an angle, $\theta_{\rm MC}$, related to the angular size of the sound horizon on the last scattering surface [108]. The MCMC analysis was done by means of the public code `COSMOMC` [108] and a modified version of the `CAMB` code [109] taking into account that the initial power spectra are not simple power laws but are given by the expressions (10) and (11). The priors on the standard parameters are chosen in accordance with Ref. [100]. For the primordial parameters, we take a Jeffreys' prior for $\ln\left(10^{10}P_*\right) \in [2.7, 4.0]$ and for ϵ_1, namely $\log(\epsilon_1) \in [-5, -0.7]$. For the other slow-roll parameters, we choose flat priors on ϵ_2 and ϵ_3 in $[-0.2, 0.2]$. As already mentioned, the pivot scale is chosen at $k_* = 0.05\,{\rm Mpc}^{-1}$. These priors are the most uninformative within slow-roll inflation. Indeed, the order of magnitude of ϵ_1 (which is always positive) is a priori unknown as many models produce a level of tensor modes that can be extremely small. This prior was the one assumed in Ref. [22]

In Fig. 3, we have represented the one-dimensional marginalized posterior probability distributions for the standard and slow-roll parameters obtained with BICEP2 data alone (solid black lines) compared with the distributions inferred from Planck (dashed red lines). It does not come as a surprise to see that, as long as the $\theta_{\rm s}$'s are concerned, BICEP2 is much less constraining than Planck. Concerning the primordial parameters, we see that BICEP2 measures ϵ_1 (or r) since it is sensitive to both the amplitude of the tensor power spectrum through $C_\ell^{\rm BB,obs}$ and the amplitude of the scalar power spectrum through $C_\ell^{\rm EE,obs}$. The quantity P_*, that is to say $\mathcal{P}(k_*)$, is indeed constrained as can be seen on the figure. On the other hand, the second and third slow-roll parameters ϵ_2 and ϵ_3 are not constrained at all.

Fig. 4 shows the two-dimensional posterior probability distributions in the primordial parameter space from BICEP2 alone (solid black contours) and from Planck alone (red dashed contours). The upper and lower left panels are especially interesting since they illustrates the existing tension between the BICEP2 and Planck data in the sense that the one-sigma contours do not overlap (while the two-sigma contours do). Unsurprisingly, the first slow-roll parameter is well determined by BICEP2 while the second is well constrained by Planck.

B. Constraints from BICEP2 and Planck

We now turn to the joint analysis where the BICEP2 and Planck data are simultaneously considered. The post-inflationary universe is, as before, a flat ΛCDM model, and is now described by a larger set of parameters $\theta_{\rm s}$:

$$\theta_{\rm s} = \left(\Omega_{\rm b}h^2, \Omega_{\rm c}h^2, \tau, 100\theta_{\rm MC}, A_{100}^{\rm PS}, A_{143}^{\rm PS}, A_{217}^{\rm PS}, r_{143\times217}^{\rm PS}, A_{143}^{\rm CIB}, A_{217}^{\rm CIB}, r_{143\times217}^{\rm CIB}, \gamma^{\rm CIB}, A_{\rm tSZ}, A_{\rm kSZ}, \xi^{\rm tSZ\times CIB}, c_{100}, c_{217}, \beta_1^1\right). \qquad (15)$$

The cosmological parameters are the ones already considered in the previous section, $\Omega_{\rm b}$, $\Omega_{\rm c}$, h, τ and $\theta_{\rm MC}$, and their priors are the same. The remaining parameters are related to astrophysics, foregrounds and the instrumental systematics associated with the Planck satellite. A complete description of their meaning, and priors, can be found in Ref. [100].

In order to test the robustness against prior choices, we have also performed the same slow-roll analysis but starting from a flat prior on $\epsilon_1 \in [0.00001, 0.2]$. Such a prior implicitly favors models producing a larger tensor to scalar ratio.

In Fig. 5, we have represented the marginalized posteriors for all the cosmological, astrophysics and nuisance parameters obtained from either the Planck likelihood alone, or the Planck and BICEP2 likelihood combined.

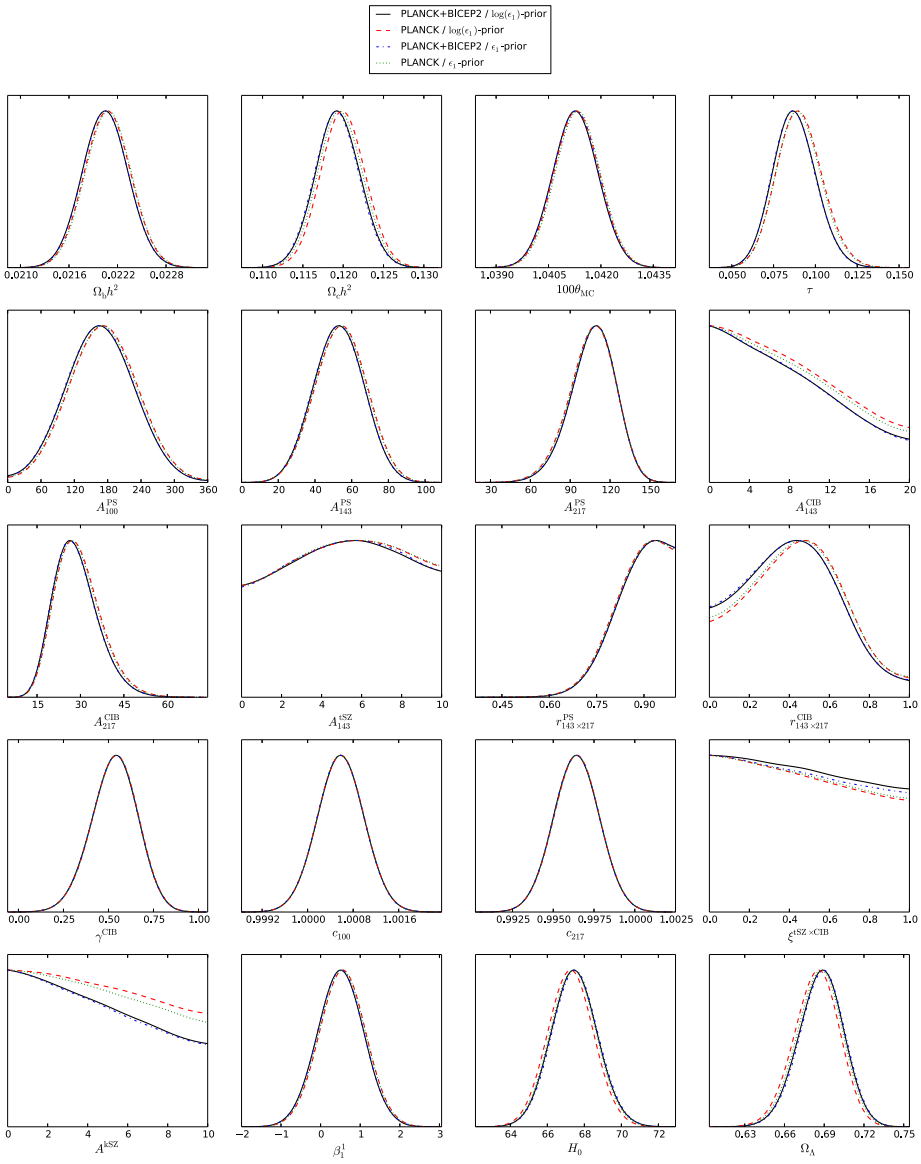

FIG. 5: One-dimensional marginalized posterior probability distributions on cosmological and astrophysics parameters associated with primordial power spectra having a second order slow-roll functional shape. These posteriors are robust against the four cases represented: Planck data alone, Planck and BICEP2 data combined, Jeffreys' prior on ϵ_1 or flat prior on ϵ_1.

This figure also shows these posteriors in the case of our two prior choices on ϵ_1. All of the θ_s posteriors are robust with respect to the prior choices and the combination of data used.

In Figs. 6 and 7, the one- and two-dimensional posteriors in the slow-roll parameter space have been represented for the same four combination of prior choices and data sets. The tension between Planck and BICEP2 is particularly visible on the posterior for $\log(\epsilon_1)$ (Jeffreys' prior on ϵ_1). As visible on the lower panels of Fig. 6, choosing a flat prior for ϵ_1 slightly reduces the tension but, as explained above, would implicitly favor models having a large tensor to scalar ratio. As expected, Planck and BICEP2 data together completely determine the first two Hubble flow functions and one obtains the two-sigma confidence intervals

$$0.0054 < \epsilon_1 < 0.013, \qquad 0.00013 < \epsilon_2 < 0.041, \quad (16)$$

for a Jeffreys' prior on ϵ_1 and

$$0.0056 < \epsilon_1 < 0.014, \qquad -0.0011 < \epsilon_2 < 0.039, \quad (17)$$

for a flat prior on ϵ_1. Because the spectral index is well constrained by Planck alone (see the discussion in Sec. III E), Figs. 6 and 7 show that combining Planck and

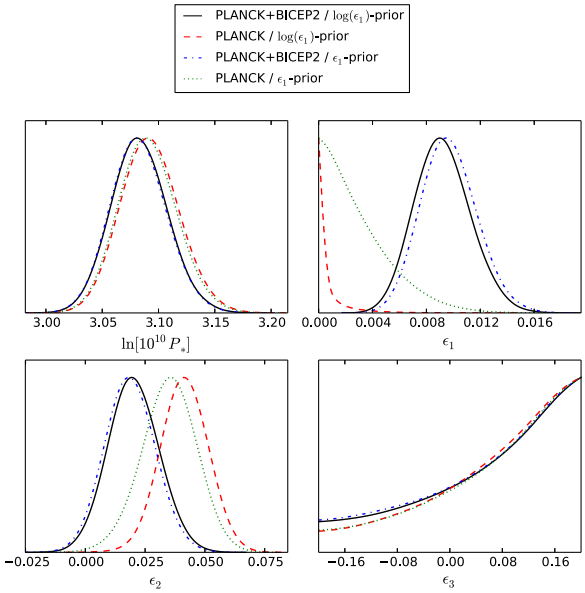

FIG. 6: One-dimensional marginalized posterior probability distributions for the primordial slow-roll parameters obtained with Planck and Planck plus BICEP2 data; with a Jeffreys' prior on ϵ_1 or a flat prior on ϵ_1. Notice the one-sigma shift of the ϵ_2 posterior towards smaller values when the BICEP2 data are included.

BICEP2 also induces a one-sigma shift of the posterior for the second Hubble flow function towards vanishing values. On the contrary, the third Hubble flow function ϵ_3 remains unconstrained and unaffected by the inclusion of BICEP2.

In order to assess how much of these results come from the tension between the Planck and BICEP2 data sets, we now estimate the Bayes factor $\mathcal{R}_{\rm SR}$ defined as the ratio between the probability of compatibility and the probability of incompatibility.

C. Compatibility for the Slow-Roll Model

As discussed in Sec. II B, the compatibility between BICEP2 and Planck can be evaluated from the Bayesian measure

$$\mathcal{R}_{\rm SR} = \frac{\mathcal{E}(D_{\rm p}, D_{\rm b}|{\rm SR})}{\mathcal{E}(D_{\rm p}|{\rm SR})\mathcal{E}(D_{\rm b}|{\rm SR})}\,, \tag{18}$$

where SR refers to the model under scrutiny, namely slow-roll. Here, we have not focused yet on a particular inflationary potential as we have sampled the whole slow-roll parameter space (in addition to the cosmological parameters). Nonetheless, this can still be interpreted as having chosen phenomenological inflationary priors, that we refer to as the slow-roll model, SR. These priors have been mentioned earlier and are $\ln(10^{10}P_*) \in [2.4, 4.0]$, $\log(\epsilon_1) \in [-5, -0.7]$, $\epsilon_2 \in [-0.2, 0.2]$ and $\epsilon_3 \in [-0.2, 0.2]$,

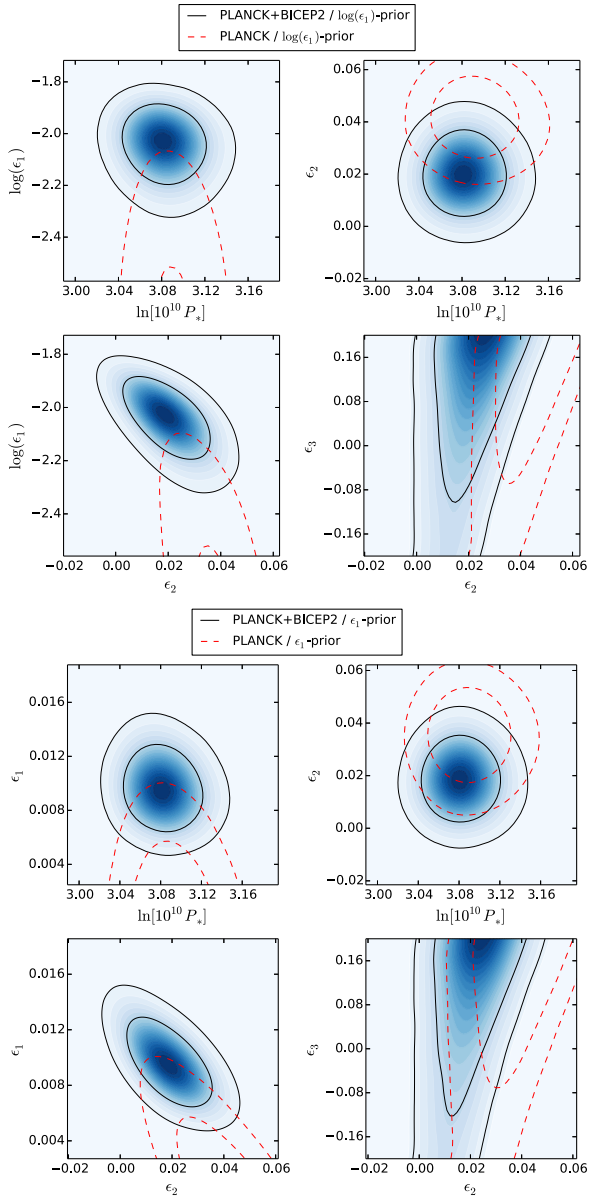

FIG. 7: One and two-sigma contour of the marginalized posterior probability distributions for the primordial slow-roll parameters obtained with Planck and Planck+BICEP2 data. The blue shading density traces the mean likelihood values for Planck+BICEP2 (Jeffreys' prior on ϵ_1). The tension between Planck and Planck+BICEP2 data induces a 1.5-sigma shift of the $\log(\epsilon_1)$ posterior towards higher values while shifting by one sigma the posterior of ϵ_2 towards zero.

plus the standard priors for the cosmological and astrophysical parameters (see Sec. III A). Evaluating Eq. (18) requires the computation of the three integrals given by Eq. (2) for $D_{\rm p}$ (Planck), $D_{\rm b}$ (BICEP2) and $\{D_{\rm p}, D_{\rm b}\}$ (combined) which are eight-dimensional for BICEP2 and twenty two-dimensional for the others. This is technically

non-trivial as evaluating the likelihood at each point of the parameter space requires a complete integration of the cosmological perturbations with `CAMB`. In order to minimize the number of likelihood evaluations and maximize convergence speed, we have used the nested sampling algorithm as implemented in `MultiNest` to estimate each evidence [95, 129, 130]. A target accuracy of 1% has been used together with a number of live points ranging from 1000 to 20000, depending on the dimensionality of space. Moreover, for each evidence, we have performed a few runs having half the number of live points in order to estimate any systematic uncertainties. The resulting numerical estimate is

$$\ln(\mathcal{R}_{\rm SR}) = -0.01 \pm 0.4, \tag{19}$$

where the quoted error is a systematic evaluated over the various runs. In appendix A 2, we discuss a semi-analytic method to calculate $\mathcal{R}_{\rm SR}$ that requires only one integration over the BICEP2 likelihood. The result quoted in Eq. (A11) matches the above numerical value.

Such a value for $\mathcal{R}_{\rm SR}$ is very close to unity and signals equal probability of Planck and BICEP2 data to be compatible or incompatible. Let us emphasize that, on the Jeffreys' scale, strong compatibility would have required $\ln(\mathcal{R}_{\rm SR}) > 5$ while strong incompatibility would have been $\ln(\mathcal{R}_{\rm SR}) < -5$. With values of $|\ln(\mathcal{R}_{\rm SR})| < 1$, we are in the inconclusive region, namely no conclusion can be drawn on the compatibility of the two data sets. As we illustrate in appendix A 1, the fact that we find $|\ln(\mathcal{R}_{\rm SR})| < 1$ is a non-trivial result. The tension between the Planck and BICEP2 posteriors on ϵ_1 (or r) visible in Fig. 3 ends up being compensated by the agreement between the informative posteriors for P_* and $\theta_{\rm MC}$ (see Fig. 3). Let us stress that discussing the compatibility of two data sets by estimating how much the likelihoods overlap in one direction only, without specifying any prior and without marginalizing over the other parameters, is misleading [131]. As can be seen in Fig. 6, even after marginalization, the amount of overlapping between the r-posteriors is by nature prior-dependent. For this reason, in the following, we will discuss the compatibility between Planck and BICEP2 by using the well defined Bayesian measure $\mathcal{R}$. In particular, even though all the *Encyclopædia Inflationaris* models belong to the slow-roll class, their prior space are completely different and their respective $\mathcal{R}$ value will accordingly be modified (see Fig. 15).

Since there is no evidence for incompatibility for the slow-roll model, we now derive various results applicable to the slow-roll class in general and obtained by combining Planck and BICEP2.

D. Energy Scale of Inflation

The correct Bayesian way to determine the energy scale of inflation is to compute the posterior distribution of the Hubble scale at the pivot crossing time, namely for the quantity H appearing in Eqs. (10) and (11). This can be done by importance sampling from the posteriors already obtained on P_*, ϵ_1, ϵ_2 and ϵ_3 [108]. From Eq. (10), one has at second order in slow roll

$$\frac{H^2}{M_{\rm Pl}^2} = 8\pi^2\epsilon_1 P_* \left[1 + 2(1+C)\epsilon_1 + C\epsilon_2\right], \tag{20}$$

and we have plotted its posterior in Fig. 8. Assuming a Jeffreys' prior on ϵ_1, Planck and BICEP2 data combined give the two-sigma confidence interval

$$1.1 < \ln\left(10^5 \frac{H}{M_{\rm Pl}}\right) < 1.6, \tag{21}$$

with a mean value at $\ln(10^5 H/M_{\rm Pl}) = 1.36$, namely $H \simeq 9.5 \times 10^{13}\,\mathrm{GeV}$. Starting from a flat prior on ϵ_1, one obtains instead

$$3.1 < 10^5 \frac{H}{M_{\rm Pl}} < 4.9, \tag{22}$$

and a mean value at $10^5 H/M_{\rm Pl} = 4.02$, giving $H \simeq 9.8 \times 10^{13}\,\mathrm{GeV}$. Those values can be converted into gravitating energy scales through the Friedmann-Lemaître equation, i.e.

$$\rho_*^{1/4} = 3^{1/4}\sqrt{H M_{\rm Pl}}. \tag{23}$$

One finds the corresponding values $\rho_*^{1/4} \simeq 2.00 \times 10^{16}\,\mathrm{GeV}$ (Jeffreys' prior on ϵ_1) and $\rho_*^{1/4} \simeq 2.03 \times 10^{16}\,\mathrm{GeV}$ (flat prior on ϵ_1).

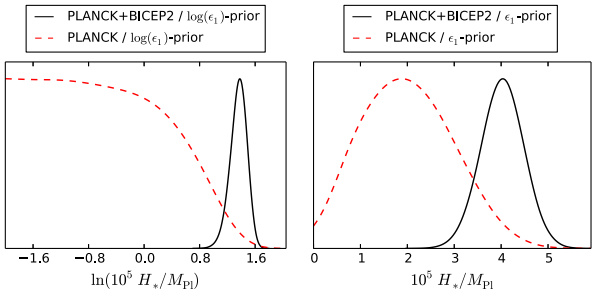

FIG. 8: Marginalized posterior distribution for the inflationary Hubble parameter at the time of pivot crossing. BICEP2 measures the energy scale of inflation.

E. Power Law Derived Parameters

Similarly, as it is explicit from Eqs. (10) and (11), the spectral indices $n_{\rm S}$ and $n_{\rm T}$, the tensor to scalar ratio r and the runnings $\alpha_{\rm S}$ and $\alpha_{\rm T}$ are completely given in terms of the Hubble flow functions. At second order in slow roll, the spectral indices read [127, 128]

$$\begin{aligned} n_{\rm S} &= 1 - (2\epsilon_1 + \epsilon_2) - 2\epsilon_1^2 - (3+2C)\epsilon_1\epsilon_2 - C\epsilon_2\epsilon_3, \\ n_{\rm T} &= -2\epsilon_1 - 2\epsilon_1^2 - 2(1+C)\epsilon_1\epsilon_2, \end{aligned} \tag{24}$$

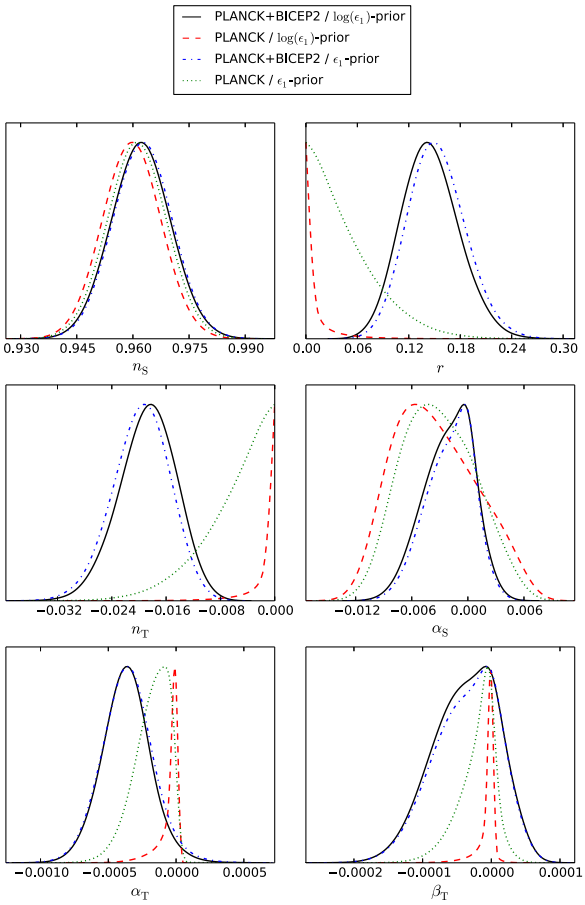

FIG. 9: Marginalized posterior distribution for the derived power law parameters $n_{\rm S}$, r, $n_{\rm T}$, $\alpha_{\rm S}$, $\alpha_{\rm T}$ and $\beta_{\rm T}$ obtained by importance sampling from the second order slow-roll parameters. Within slow-roll inflation, the running $\alpha_{\rm S}$ is more tightly constrained when the BICEP2 data are included.

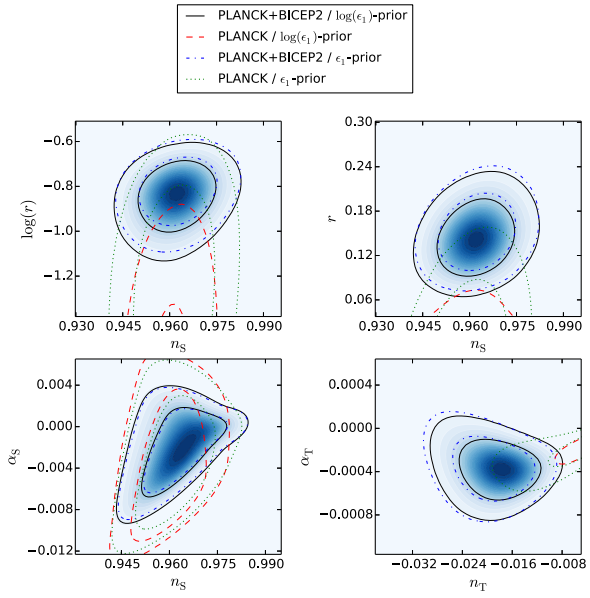

FIG. 10: Two-dimensional posterior distribution for some of the derived power law parameters. The blue shading density traces the mean likelihood values for Planck+BICEP2 (Jeffreys' prior on ϵ_1).

while the tensor to scalar ratio can be expressed as

$$r = 16\epsilon_1(1 + C\epsilon_2). \tag{25}$$

The scalar and tensor running are given by

$$\alpha_{\rm S} = -2\epsilon_1\epsilon_2 - \epsilon_2\epsilon_3, \qquad \alpha_{\rm T} = -2\epsilon_1\epsilon_2, \tag{26}$$

respectively. Finally, let us mention that the running of the running for the tensor mode is also completely specified by the first three Hubble flow functions and read

$$\beta_{\rm T} = -2\epsilon_1\epsilon_2\left(\epsilon_2 + \epsilon_3\right). \tag{27}$$

At leading order in slow roll, those equations can be recast into the so-called consistency relations

$$\begin{aligned} r &\simeq -8n_{\rm T}, \\ \alpha_{\rm T} &\simeq \frac{r}{8}\left[\frac{r}{8} + (n_{\rm S} - 1)\right], \\ \beta_{\rm T} &\simeq \alpha_{\rm T}(1 - n_{\rm S}) + \frac{r}{8}(\alpha_{\rm S} - 2\alpha_{\rm T}). \end{aligned} \tag{28}$$

Using again importance sampling, the posterior distribution for $n_{\rm S}$, $n_{\rm T}$, r, $\alpha_{\rm S}$, $\alpha_{\rm T}$ and $\beta_{\rm T}$ have been represented in Figs. 9 and 10. In particular, let us stress that, within slow roll inflation, a running spectral index for the scalar modes cannot help to alleviate the tension between Planck and BICEP2 data. On the contrary, we see that the posterior of $\alpha_{\rm S}$ is more restricted around vanishing values by adding the BICEP2 data. As it is explicit in Eq. (26), $\alpha_{\rm S}$ is a small quantity which is proportional to ϵ_2, the posterior of which is being shifted towards zero when the BICEP2 data are considered (see Sec. III B). From this equation one has

$$|\alpha_{\rm S}|_{\rm max} \simeq |\epsilon_2|_{\rm max}\left(2|\epsilon_1|_{\rm max} + |\epsilon_3|_{\rm max}\right) \simeq |\epsilon_2|_{\rm max}|\epsilon_3|_{\rm max}, \tag{29}$$

the third Hubble flow function ϵ_3 being the largest term since it is unconstrained [$\max\left(|\epsilon_3|\right) = 0.2$]. Therefore, shifting ϵ_2 towards small values implies the same for $\alpha_{\rm S}$. This effect could have been expected as Planck alone strongly constrains the spectral index, which is given by Eq. (24). Increasing ϵ_1 at fixed $n_{\rm S}$ imposes to decrease ϵ_2 by twice the amount. Therefore, Eq. (29) implies that the maximal values of $|\alpha_{\rm S}|$ will be accordingly reduced.

From the posteriors represented in Fig. 9, Planck and BICEP2 data combined yield the following 95% confidence intervals

$$\begin{aligned} 0.947 < n_{\rm S} < 0.978, \quad &-0.0074 < \alpha_{\rm S} < 0.0025, \\ -1.07 < \log(r) < -0.67, \quad &-0.027 < n_{\rm T} < -0.011, \end{aligned} \tag{30}$$

and

$$\begin{aligned} -7.1\times10^{-4} < \alpha_{\rm T} < -3.1\times10^{-6},\\ -1.3\times10^{-4} < \beta_{\rm T} < 5.0\times10^{-5}, \end{aligned} \tag{31}$$

when a Jeffreys' prior is assumed on ϵ_1. These bounds are relatively robust against the prior choices. Indeed, assuming instead a flat prior on ϵ_1 gives

$$\begin{aligned} 0.947 < n_{\rm S} < 0.978, \quad -0.0071 < \alpha_{\rm S} < 0.0027,\\ 0.088 < r < 0.22, \quad -0.028 < n_{\rm T} < -0.011, \end{aligned} \tag{32}$$

and

$$\begin{aligned} -7.1\times10^{-4} < \alpha_{\rm T} < 2.7\times10^{-5},\\ -1.3\times10^{-4} < \beta_{\rm T} < 5.0\times10^{-5}. \end{aligned} \tag{33}$$

To conclude this section, let us stress that although there is a tension between the Planck and BICEP2 data on the tensor-to-scalar ratio, it does not affect the posterior values of the cosmological and astrophysics parameters, those being already strongly constrained by the Planck data alone. Concerning the shape of the primordial power spectra, $n_{\rm S}$ remains also unaffected while the tensor-to-scalar ratio tension induces a drastic modification of the ϵ_1 posterior distribution and a one- to two-sigma shift of the ϵ_2 distribution compared to the Planck data alone. Moreover, as we have just discussed, the running of the scalar power spectrum cannot be used within slow-roll inflation to alleviate the above-mentioned tension, precisely because it cannot take large enough values. Solely in slow-roll violating models of inflation, such an explanation may be relevant [132–136].

Concerning the implications for inflation, BICEP2 results provide, for the first time, a measure of the energy scale of inflation which ends up being at GUT scale, see Eqs. (22) and (23), a major result indeed if confirmed. The mean value of $r = 0.15$ is slightly lower than what was inferred by the BICEP2 team but this is expected as we are here considering slow-roll inflation and have added the Planck data which disfavor larger tensor to scalar ratio values. As for the evidences, one should therefore expect all models predicting a very small tensor to scalar ratio to be now strongly penalized evidence-wise. That is why, if the BICEP2 measurements stands the test of time, this situation would be a pivotal moment for Cosmic Inflation models.

In the following, we use the multi-dimensional posterior on P_* and ϵ_i, derived under the Jeffreys' prior on ϵ_1, coming from the BICEP2 data as our effective likelihood $\mathcal{L}_{\rm eff}$.

IV. RESULTS AND DISCUSSION

In this section, we apply the method described previously in order to derive the Bayesian evidences and complexities for the $N^{\rm mod} = 193$ models of the *Encyclopædia Inflationaris*. The complete list of models as well as a careful discussion and justification of the priors on the free parameters $\theta_{\rm inf}$ can be found in Ref. [22]. In the present article, we use the same terminology and the same choices for the priors.

A. BICEP2 Evidences

In Fig. 11, we show the (logarithm) of the Bayes factors, $B^i_{\rm SR}$, normalized to the slow-roll model, and computed with the BICEP2 data only. The value of $\ln B^i_{\rm SR}$ is represented by an horizontal bar on the left if $\ln B^i_{\rm SR} < 0$ (the model $\mathcal{M}_i$ is disfavored with respect to the slow-roll model) and by an horizontal bar on the right if $\ln B^i_{\rm SR} > 0$ (the model $\mathcal{M}_i$ is favored with respect to the slow-roll model), the length of the bar being directly proportional to $\ln B^i_{\rm SR}$. There is also a color code which indicates the Schwarz Terrero-Escalante classification [137]. Let us briefly recall that, according to this classification, category one ("green" models) corresponds to models for which the kinetic energy and the kinetic to potential energy ratio increases during inflation. Typically, this region contains models having a plateau shape potential. As shown in Ref. [22], this class of models is favored by the Planck data (see below). Category two ("red" models) contains models for which the kinetic energy decreases but the kinetic to potential energy ratio increases during inflation. Large field models belongs to this region. Finally, category three ("purple" models) refers to models having a decreasing kinetic and kinetic to potential energy ratio. Valley hybrid inflation is an example of a model belonging to this category; for a more detailed explanation of this classification and its meaning, see Ref. [22]. We have also computed the maximum value of the evidences obtained when all the parameters have a Dirac function prior peaked at the best fit. This is indicated by the small black arrows. They can be interpreted as upper bounds on the evidences regardless of the priors. Finally the vertical dotted black lines refer to the Jeffreys' scale with respect to the best model and represent the four different categories, "inconclusive" (models between the first and the second vertical line, starting from the right), "weakly disfavored" (between the second and the third vertical line), "moderately disfavored" (between the third and the fourth vertical line) and "strongly disfavored" (left to the fourth vertical line), see Table 1 in Ref. [22].

As can be seen in Fig. 11, the best model according to BICEP2 is $\rm LFI_3$, for which $V(\phi) \propto \phi^3$. We see that there are in fact 52 models in the inconclusive zone (this one being defined with respect to the best model), namely $\rm LFI_3$, $\rm GMLFI_{2,1}$, HF1I, $\rm GMLFI_{3,1}$, $\rm LFI_2$, $\rm LPI2_2$, MLFI, $\rm GMSSMI_p$, SSBI1, $\rm LPI2_4$, $\rm SSBI6_f$, DWI, $\rm LFI_4$, SSBI6, $\rm LPI1_{4,2}$, $\rm SSBI1_f$, $\rm GMLFI_{1,2}$, RCMI, $\rm LPI1_{4,1}$, SSBI3, OI, $\rm NCKI_{\beta>0}$, $\rm LPI1_{4,3}$, $\rm LPI3_2$, $\rm GMLFI_{1,3}$, LPI1, $\rm GMLFI_{3,2}$, LFI, $\rm LPI3_4$, OSTI, RCQI, $\rm GMLFI_{2,3}$, $\rm GMLFI_{1,1}$, $\rm LPI3_6$, NI, $\rm LI_{\alpha<0}$, CNAI, CNBI, $\rm GMLFI_{2/3,4/3}$, $\rm GRIPI_{sugra}$, $\rm RIPI_{sugra}$, $\rm GMLFI_{3,3}$, $\rm LMI1_p$, $\rm LFI_1$, $\rm SFI_1$, $\rm LPI2_6$, $\rm MHI_l$,

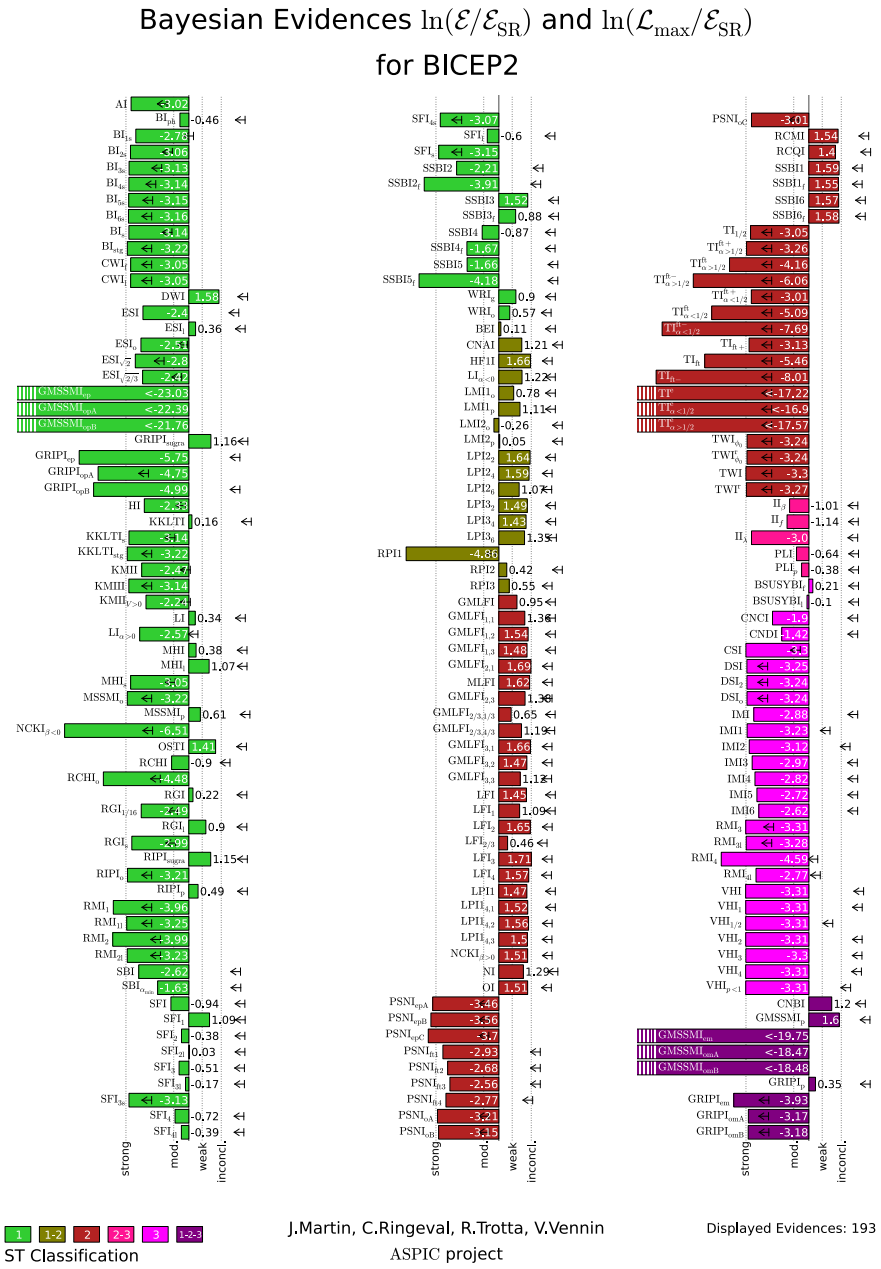

FIG. 11: Bayes factors and absolute upper bounds to the Bayes factors obtained from the BICEP2 data alone. The reference model is the slow-roll model (SR), here viewed as a scenario in itself having three parameters $\ln(10^{10}P_*)$, $\log(\epsilon_1)$ and ϵ_2 and whose priors are reported in the text. The vertical dotted lines refer to the Jeffreys' scale with respect to the best model, here LFI3.

GMLFI, $\mathrm{WRI_g}$, $\mathrm{RGI_l}$, $\mathrm{SSBI3_f}$ and $\mathrm{LMI1_o}$, where we have ordered the list in decreasing values of the evidences.

Let us now discuss these potentials and the physical context in which they arise. CNAI, CNBI, HF1I, $\mathrm{LMI1_o}$ and $\mathrm{MHI_l}$ are phenomenological and, therefore, difficult to embed in high energy physics. LFI is just the general family of monomial potentials $V(\phi) \propto \phi^p$ and, in the inconclusive zone, one finds $\mathrm{LFI_3}$, $\mathrm{LFI_2}$, $\mathrm{LFI_4}$ and $\mathrm{LFI_1}$. The $\mathrm{GMLFI}_{p,q}$ potentials (this includes MLFI for which $p = q = 2$) are of the form $V(\phi) \propto (\phi/M_{\rm Pl})^p\,[1+\alpha(\phi/M_{\rm Pl})^q]$, where α is a parameter controlling the amplitude of the second term. Physically, they could represent LFI modified by some quantum corrections [138, 139]. The following poten-

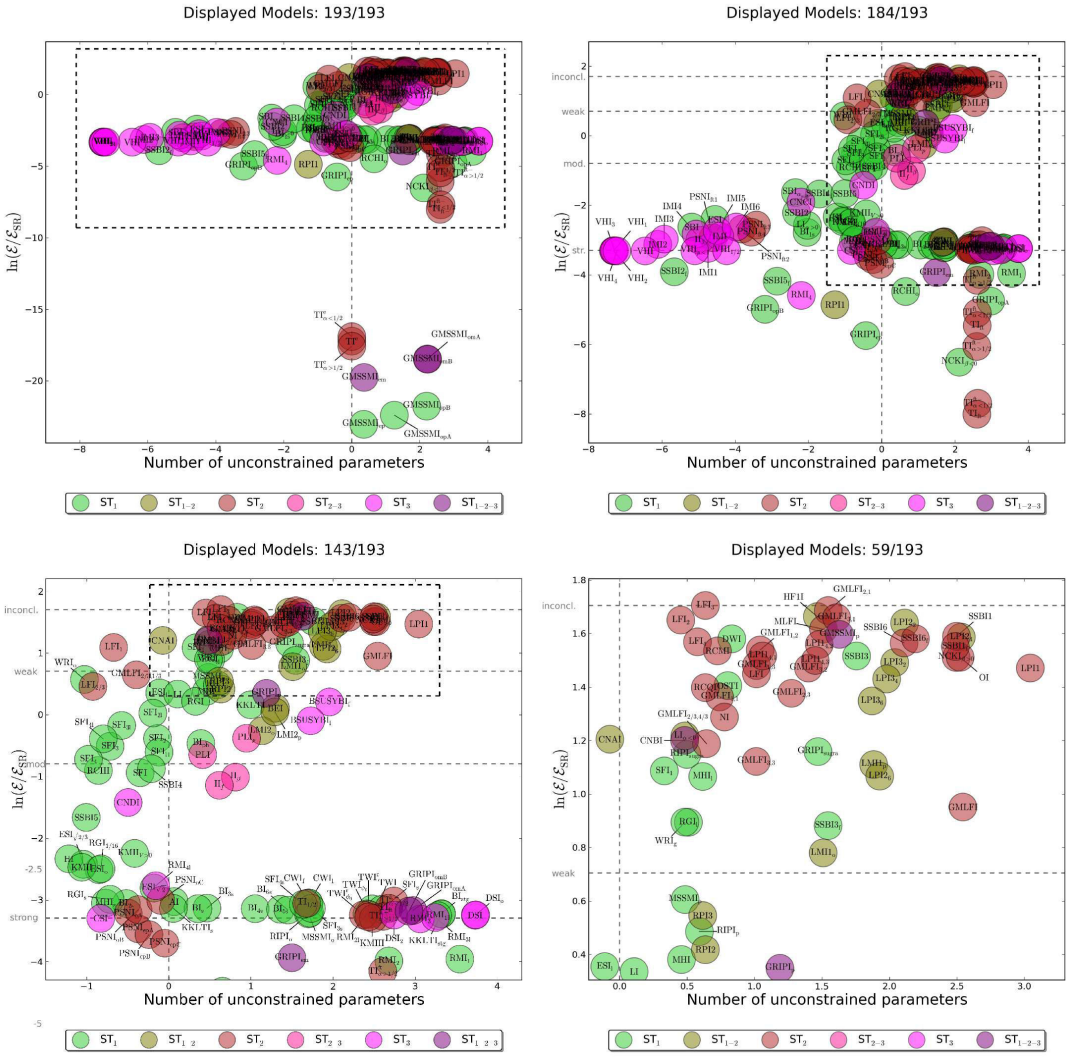

FIG. 12: Model performance assessed with both Bayesian evidence and number of unconstrained parameters for the BICEP2 data. The four panels represent different zooms in the models' space. They are to be read from the left to the right and from the top to the bottom—in this order, the black dashed rectangles frame the region comprised in the next panel.

tials can also be viewed as large field corrected models: RCMI, $V(\phi) \propto (\phi/M_{\rm Pl})^2\left[1-2\alpha(\phi/M_{\rm Pl})^2\ln(\phi/M_{\rm Pl})\right]$ and RCQI, $V(\phi)\propto(\phi/M_{\rm Pl})^4[1-\alpha\ln(\phi/M_{\rm Pl})]$. DWI has a $V(\phi)\propto\left[(\phi/\phi_0)-1\right]^2$ which is the sum of three monomials but was mainly used in the context of topological inflation. In the inconclusive zone, one also finds the SSBI potentials which are given by $V(\phi)\propto 1+\alpha(\phi/M_{\rm Pl})^2+\beta(\phi/M_{\rm Pl})^4$ and can be viewed as models where the vacuum energy part of the potential is corrected by higher order monomial terms. This is also the case for NCKI$_{\beta>0}$, $V(\phi)\propto 1+\alpha\ln(\phi/M_{\rm Pl})+\beta(\phi/M_{\rm Pl})^2$ where the corrections are also of radiative origin and loop inflation LI$_{\alpha<0}$, $V(\phi)=\propto[1+\alpha\ln(\phi/M_{\rm Pl})]$ with $\alpha<0$. Another class of models that are among the BICEP2 winners is LPI's, $V(\phi)\propto(\phi/\phi_0)^p[\ln(\phi/\phi_0)]^q$. These scenarios are based on super Yang-Mills theories and are also known as glue ball inflation. Notice, however, that the value of ϕ_0 must be super-Planckian. The model OI, $V(\phi)\propto(\phi/\phi_0)^4[\ln^2(\phi/\phi_0)-\alpha]$, possesses a similar potential as well as OSTI, $V(\phi)\propto(\phi/\phi_0)^2\ln\left[(\phi/\phi_0)^2\right]$. This last scenario is physically well motivated in the context of string theory. Unfortunately, it is used outside its natural domain of validity since Ref. [140] showed that it has severe problems in matching the amplitude of the CMB anisotropies. In the inconclusive zone, one also finds inflection point models such as GMSSMI$_{\rm p}$, RIPI$_{\rm sugra}$ and GRIPI$_{\rm sugra}$. Some of them are also used in a non physical region. For instance, this is the case for GMSSMI$_{\rm p}$, $V(\phi)\propto(\phi/\phi_0)^2-2\alpha/3(\phi/\phi_0)^6+\alpha/5(\phi/\phi_0)^5$. The model is based on the MSSM (Minimal Supersymmetric Standard Model) where the inflaton field evolves along a flat

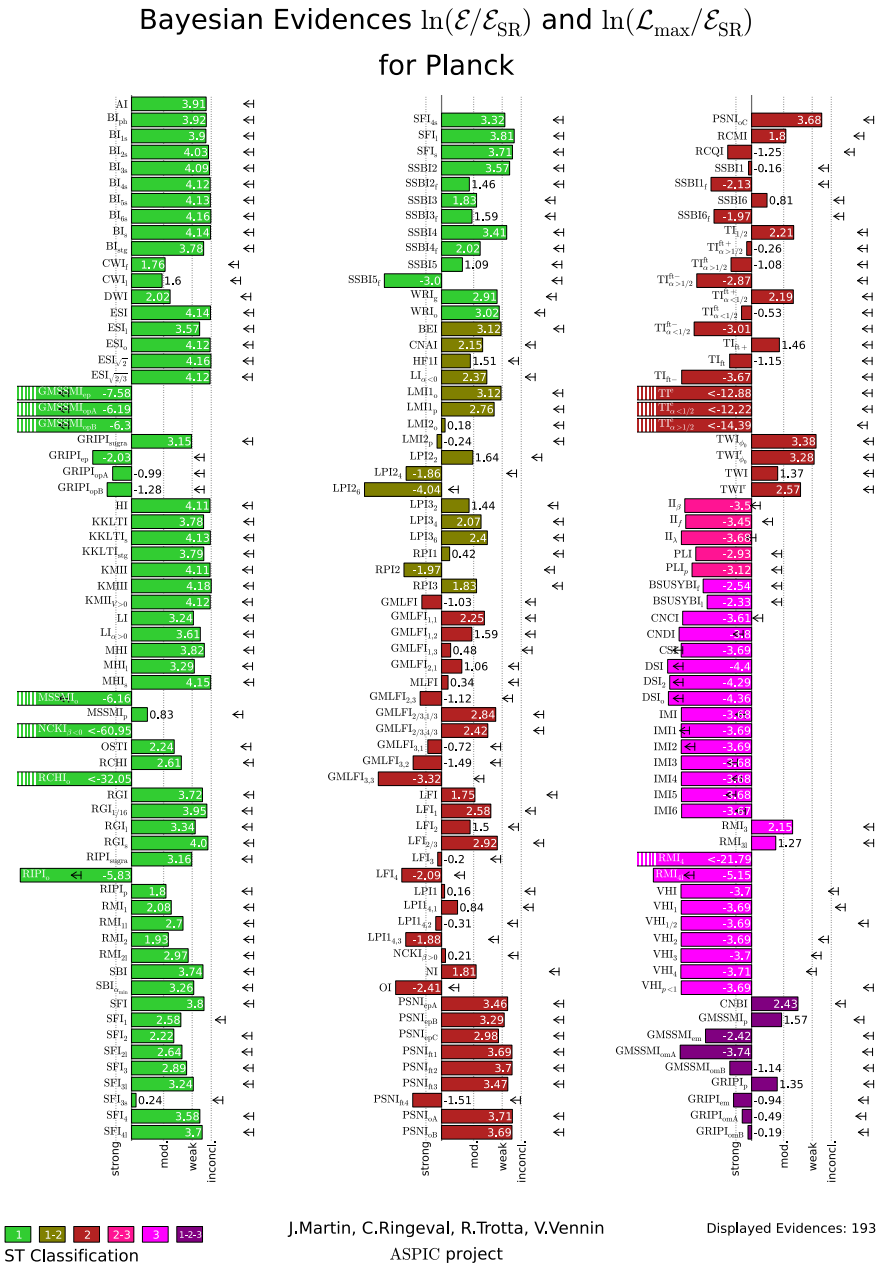

FIG. 13: Bayes factors and absolute upper bounds to the Bayes factors obtained from the Planck data as in Ref. [22]. The reference model is the same slow-roll model as in Fig. 11, and the vertical dotted lines refer to the Jeffreys' scale with respect to the best model, here KMIII.

direction and is, therefore, well justified from a high energy point of view. However, in order to be a satisfactory inflationary model, ϕ_0 must have a *vev* that is outside the natural MSSM values. $\mathrm{RGI_1}$ refers to radion gauge inflation and has a potential given by $V(\phi) \propto (\phi/M_{\rm Pl})^2/[\alpha + (\phi/M_{\rm Pl})^2]$. $\mathrm{SFI_1}$ is nothing but small field inflation, $V(\phi) \propto 1 - (\phi/\mu)^p$, with $p = 1$. Finally, natural inflation (NI), for which $V(\phi) \propto 1 + \cos(\phi/f)$ is also a good model but must be used in a domain where the scale f is super-Planckian.

We have also computed the Bayesian complexities, see Eq. (3), for all the *Encyclopædia Inflationaris* models, so that the performance of a model can be described by two numbers, its evidence and its complexity or, equivalently see Eq. (5), its evidence and its number of unconstrained parameters. We have represented the corre-

sponding result in the space $[N^{\rm uc}, \ln(\mathcal{E}/\mathcal{E}_{\rm best})]$ in Fig. 12. If one restricts oneself to models in the "inconclusive zone" with a minimal number of unconstrained parameters, i.e. $0 < N_i^{\rm uc} < 1$, then one finds only 17 models, namely: LFI_3, LFI_2, DWI, LFI_4, RCMI, OSTI, RCQI, $\mathrm{GMLFI}_{1,1}$, NI, $\mathrm{LI}_{\alpha<0}$, CNBI, $\mathrm{GMLFI}_{2/3,4/3}$, $\mathrm{RIPI}_{\rm sugra}$, SFI1, $\mathrm{MHI}_{\rm l}$, $\mathrm{WRI}_{\rm g}$ and $\mathrm{RGI}_{\rm l}$. It is interesting to notice that the $V(\phi) = m^2\phi^2/2$ model (i.e. LFI_2) is among the models favored by BICEP2 but is not the only one. At this stage, it would therefore be unjustified to focus model building efforts on this scenario only.

In order to compare the above results with what has been obtained by Planck, we have reproduced in Fig. 13 the values of the evidences, normalized to the slow-roll model, obtained with the Planck data in Ref. [22]. This figure is identical to Fig. 2 of Ref. [22] except that the reference model is now different (being HI in [22]). The best Planck model is KMIII and the 52 models that end up being in the inconclusive zone (with respect to the best) are: KMIII, $\mathrm{ESI}_{\sqrt{2}}$, $\mathrm{BI}_{6\rm s}$, $\mathrm{MHI}_{\rm s}$, $\mathrm{BI}_{\rm s}$, ESI, $\mathrm{BI}_{5\rm s}$, $\mathrm{KKLTI}_{\rm s}$, $\mathrm{KMII}_{V>0}$, $\mathrm{BI}_{4\rm s}$, $\mathrm{ESI}_{\rm o}$, $\mathrm{ESI}_{\sqrt{2/3}}$, KMII, HI, $\mathrm{BI}_{3\rm s}$, $\mathrm{BI}_{2\rm s}$, $\mathrm{RGI}_{\rm s}$, $\mathrm{RGI}_{1/16}$, $\mathrm{BI}_{\rm ph}$, AI, $\mathrm{BI}_{1\rm s}$, MHI, $\mathrm{SFI}_{\rm l}$, SFI, $\mathrm{KKLTI}_{\rm stg}$, $\mathrm{BI}_{\rm stg}$, KKLTI, SBI, RGI, $\mathrm{SFI}_{\rm s}$, $\mathrm{PSNI}_{\rm oA}$, $\mathrm{SFI}_{4\rm l}$, $\mathrm{PSNI}_{\rm ft2}$, $\mathrm{PSNI}_{\rm oB}$, $\mathrm{PSNI}_{\rm ft1}$, $\mathrm{PSNI}_{\rm oC}$, $\mathrm{LI}_{\alpha>0}$, SFI_4, $\mathrm{ESI}_{\rm l}$, SSBI2, $\mathrm{PSNI}_{\rm ft3}$, $\mathrm{PSNI}_{\rm epA}$, SSBI4, TWI_{ϕ_0}, $\mathrm{RGI}_{\rm l}$, $\mathrm{SFI}_{4\rm s}$, $\mathrm{MHI}_{\rm l}$, $\mathrm{PSNI}_{\rm epB}$, $\mathrm{TWI}^{\rm r}_{\phi_0}$, $\mathrm{SBI}_{\alpha_{\rm min}}$, LI, $\mathrm{SFI}_{3\rm l}$.

Two remarks are in order here. Firstly, the number of models favored is exactly the same for BICEP2 and Planck, namely 52. This probably illustrates the fact that r is an observable which is able to discriminate among the inflationary models much more efficiently that $n_{\rm S}$. Indeed, as above-mentioned, we have used only 4 bandpowers for the BICEP2 data, and this already singles out the same number of scenarios in the inconclusive zone. Secondly, there are only two models belonging to the two lists: $\mathrm{MHI}_{\rm l}$ and $\mathrm{RGI}_{\rm l}$. In particular, the fact that the Starobinsky (or Higgs) inflationary model was among the winners according to Planck is not recovered by BICEP2. On the contrary, this one becomes (almost) strongly disfavored compared to LFI_3.

In Ref. [22], the complexity was also calculated, see Fig. 3 of that article. We found that, among the models in the Planck inconclusive zone, those with a minimal number of unconstrained parameters, i.e. $0 < N_i^{\rm uc} < 1$, are: $\mathrm{ESI}_{\sqrt{2}}$, $\mathrm{ESI}_{\sqrt{2/3}}$, HI, $\mathrm{BI}_{2\rm s}$, $\mathrm{RGI}_{\rm s}$, AI, $\mathrm{BI}_{1\rm s}$, MHI, RGI, $\mathrm{SFI}_{4\rm l}$, $\mathrm{LI}_{\alpha>0}$, SFI_4, $\mathrm{ESI}_{\rm l}$, $\mathrm{RGI}_{\rm l}$, $\mathrm{MHI}_{\rm l}$, $\mathrm{SBI}_{\alpha_{\rm min}}$ and $\mathrm{SFI}_{3\rm l}$. Again, two models remain in the two lists, the same as above, namely $\mathrm{MHI}_{\rm l}$ and $\mathrm{RGI}_{\rm l}$.

Finally, we can summarize the data constraining power in an histogram for the four Jeffreys' categories as represented in Fig. 14. We have also represented the same histogram obtained from the Planck data. Noticing again that the BICEP2 data used here consist only of four bandpowers for E and B-modes, this plot illustrates the power of measuring r for inflationary physics. However, as discussed earlier, the models lying into these four categories weakly overlap between Planck and BICEP2 thereby showing some tension between the data sets. Since compatibility between data sets is a model dependent statement, we now move on to the determination of the $\mathcal{R}$ factors for all the *Encyclopædia Inflationaris* models.

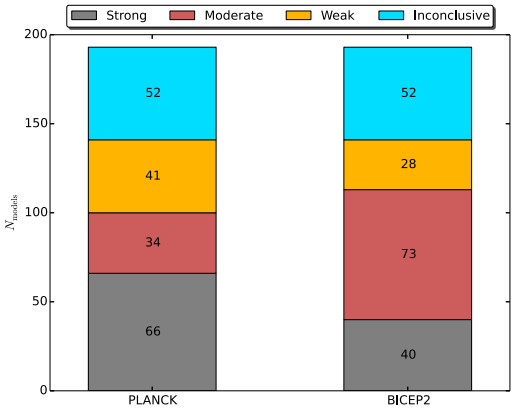

FIG. 14: Number of models within each Jeffreys' category (with respect to the best model) for Planck data alone and BICEP2 data alone.

B. Compatibility of Planck and BICEP2

In Fig. 15 we have represented the values of $\ln(\mathcal{R})$ for all the *Encyclopædia Inflationaris* models. These have been obtained using the fast likelihood method described in Sec. II. In this plot, one notices that the data sets are compatible with certainty [i.e. at the "strong" level, $\ln(\mathcal{R}) > 5$] for 36 models only. They are: $\mathrm{GMSSMI}_{\rm opA}$, $\mathrm{GMSSMI}_{\rm opB}$, $\mathrm{GMSSMI}_{\rm ep}$, $\mathrm{TI}^{\rm e}$, $\mathrm{TI}^{\rm e}_{\alpha<1/2}$, $\mathrm{TI}^{\rm e}_{\alpha>1/2}$, II_β, II_f, II_λ, PLI, PLI_p, $\mathrm{BSUSYBI}_{\rm f}$, $\mathrm{BSUSYBI}_{\rm l}$, CSI, DSI, DSI_2, $\mathrm{DSI}_{\rm o}$, IMI, IMI1, IMI2, IMI3, IMI4, IMI5, IMI6, RMI_4, $\mathrm{RMI}_{4\rm l}$, VHI, VHI_1, $\mathrm{VHI}_{1/2}$, VHI_2, VHI_3, VHI_4, $\mathrm{VHI}_{p<1}$, $\mathrm{GMSSMI}_{\rm em}$, $\mathrm{GMSSMI}_{\rm omA}$, and $\mathrm{GMSSMI}_{\rm omB}$. As one can check in Figs. 11 and 13, these models are disfavored by both PLANCK and BICEP2 separately; the ones exhibiting maximum compatibility are even ruled out. This is not surprising as $\mathcal{R}$ is a combined measure of both the reduction of prior volume brought about by the likelihood as well as their overlap (see appendix A 1). The statistical interpretation of these results is that both data sets agree in disfavoring those models.

On the other hand, one may be more interested in answering the question whether the data sets are compatible assuming the best Planck's scenarios. In Fig. 16, we have represented the same $\mathcal{R}$-factors of Fig. 15 plotted against the Bayes factor derived from the Planck data alone (the ones of Fig. 13). The shaded rectangles (yellow) trace the overlapping regions of maximal evidence and maximal compatibility over two units in the Jeffreys' scale: inconclusive plus weak zones along the evidence

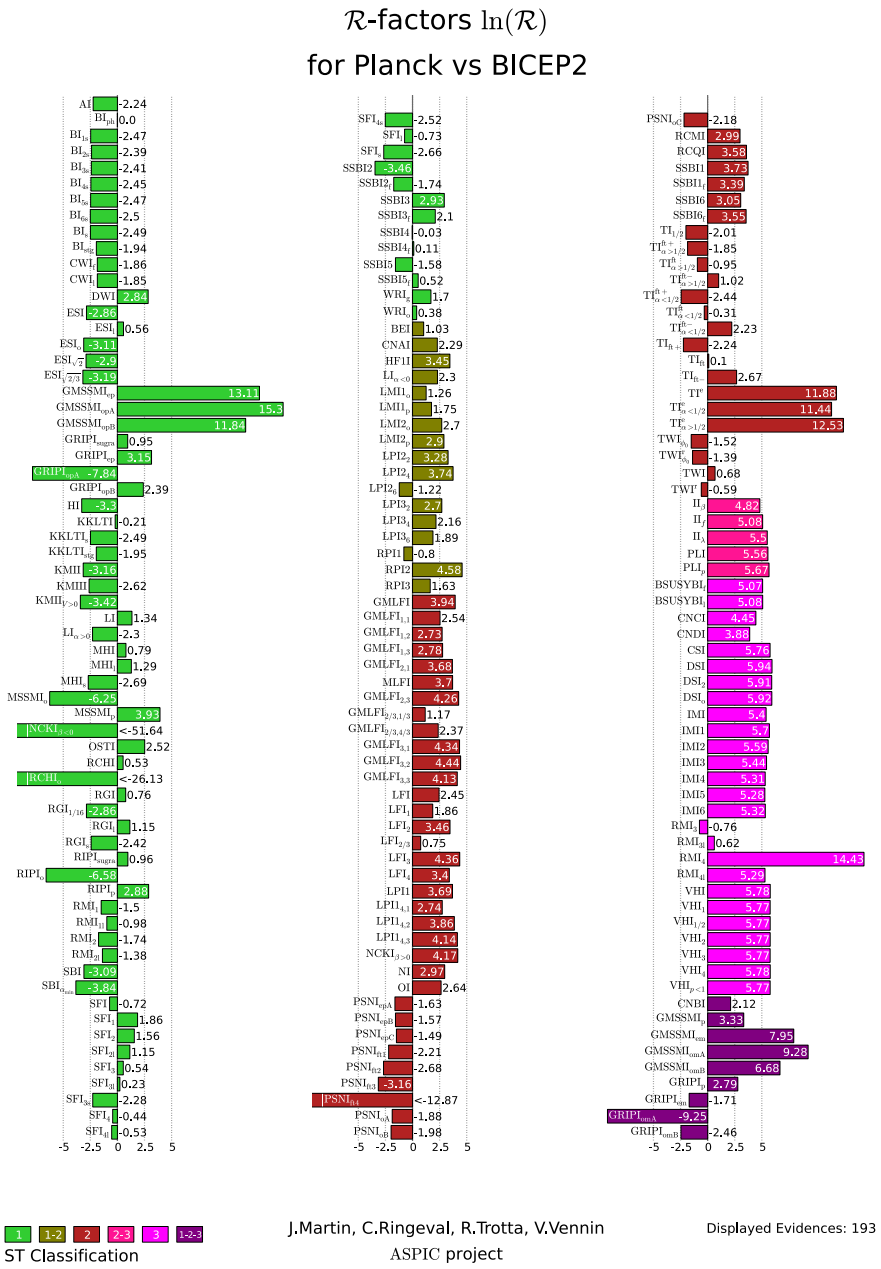

FIG. 15: Compatibility between the Planck and BICEP2 data for each model as measured by the $\mathcal{R}$-factors. Positive values correspond to compatibility, negative values to incompatibility.

direction and strong plus moderate zones along the compatibility direction. There is no model in these regions showing that, insofar the best inflationary models from Planck data alone are concerned, the two data sets are in tension. In fact, only a weak compatibility is reached for models which are already weakly disfavored by the Planck data alone. Many of these models belong to the ones listed earlier that were favored by BICEP2 alone (as NI, SSBI3, $\mathrm{RIPI_p}$ ...).

For Planck best models, the BICEP2 data cannot be brought into compatibility with Planck, and hence the two data sets cannot be combined to obtain meaningful updated inferences on these scenarios. In particular, this is the conclusion for Starobinsky inflation (HI) and, therefore, it is premature to conclude about its viability before compatibility is addressed. As we have just showed, both data sets can only be meaningfully combined if one focuses on scenarios which are, at least,

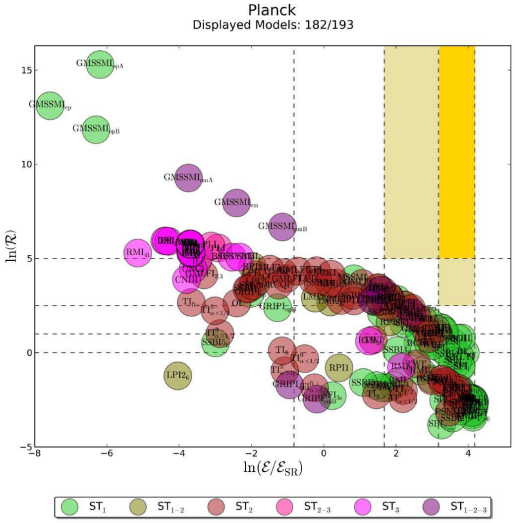

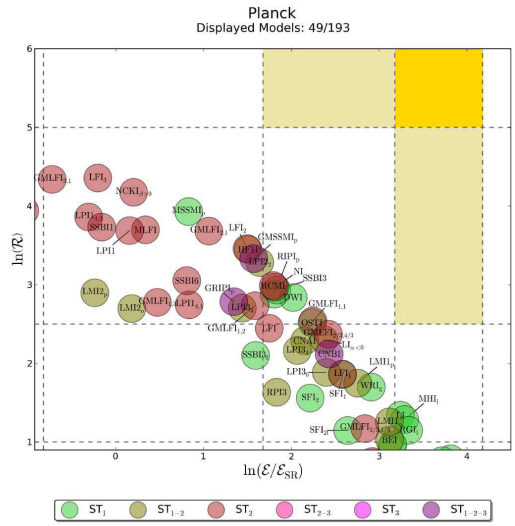

FIG. 16: Planck+BICEP2 compatibility measure, $\mathcal{R}$, versus Planck's evidences normalized to slow roll. The yellow rectangle in the top right encompasses the "strongly compatible" models that lie in the Planck-alone "inconclusive" zone (with respect to Planck's best model); the light yellow rectangles encompass the "strongly compatible" models that lie in the "weakly disfavored" zone (top left) and the "moderately compatible" models that lie in the "inconclusive" zone (bottom right). One can see that these rectangles are empty. The bottom panel is a zoom into the neighborhood of these regions. Among the models favored by Planck data alone, there are only a few for which Planck and BICEP2 data are, at most, weakly compatible [$1 < \ln(\mathcal{R}) < 2.5$].

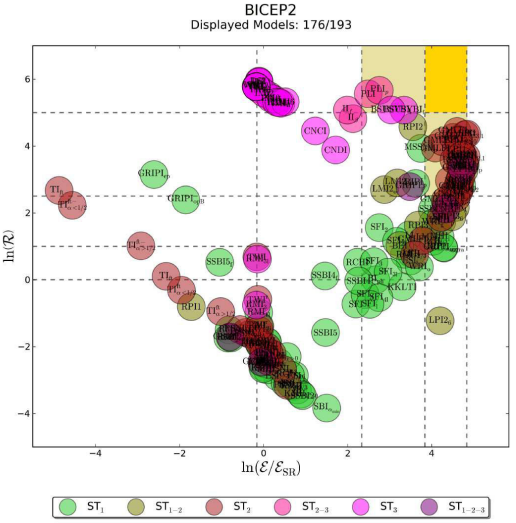

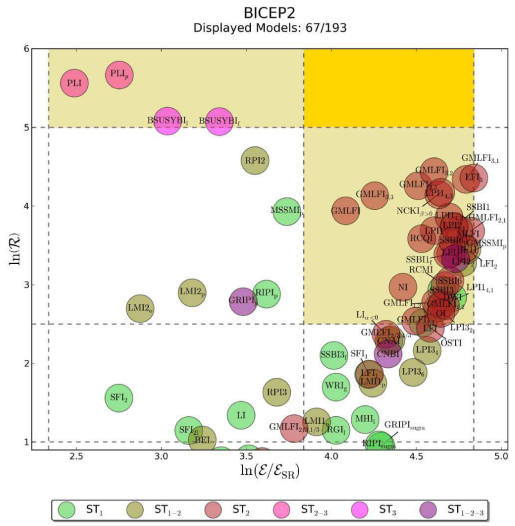

FIG. 17: Planck+BICEP2 compatibility measure, $\mathcal{R}$, versus BICEP2 evidences normalized to slow roll. The yellow rectangle in the top right encompasses the "strongly compatible" models that lie in the BICEP2-alone "inconclusive" zone (with respect to BICEP2's best model); the light yellow rectangles encompass the "strongly compatible" models that lie in the "weakly disfavored" zone (top left) and the "moderately compatible" models that lie in the "inconclusive" zone (bottom right). The bottom panel is a zoom into the neighborhood of these regions. The models favored by BICEP2 data alone are found in the region where Planck and BICEP2 are moderately compatible.

weakly disfavored by Planck.

It is also informative to assess the compatibility of the two data sets from the perspective of the BICEP2 best models. In Fig. 17 we have plotted the analogous of Fig. 16 for BICEP2, namely the $\mathcal{R}$-factors against the Bayes factors obtained from BICEP2 data alone (see Fig. 11). The BICEP2 best scenarios now spread into the region of moderate compatibility although there is again no model in the strong compatibility region. Nonetheless, for the BICEP2 best scenarios, Planck and BICEP2 data can be combined to get more information for these scenarios.

In the light of the above considerations, in Fig. 18 we

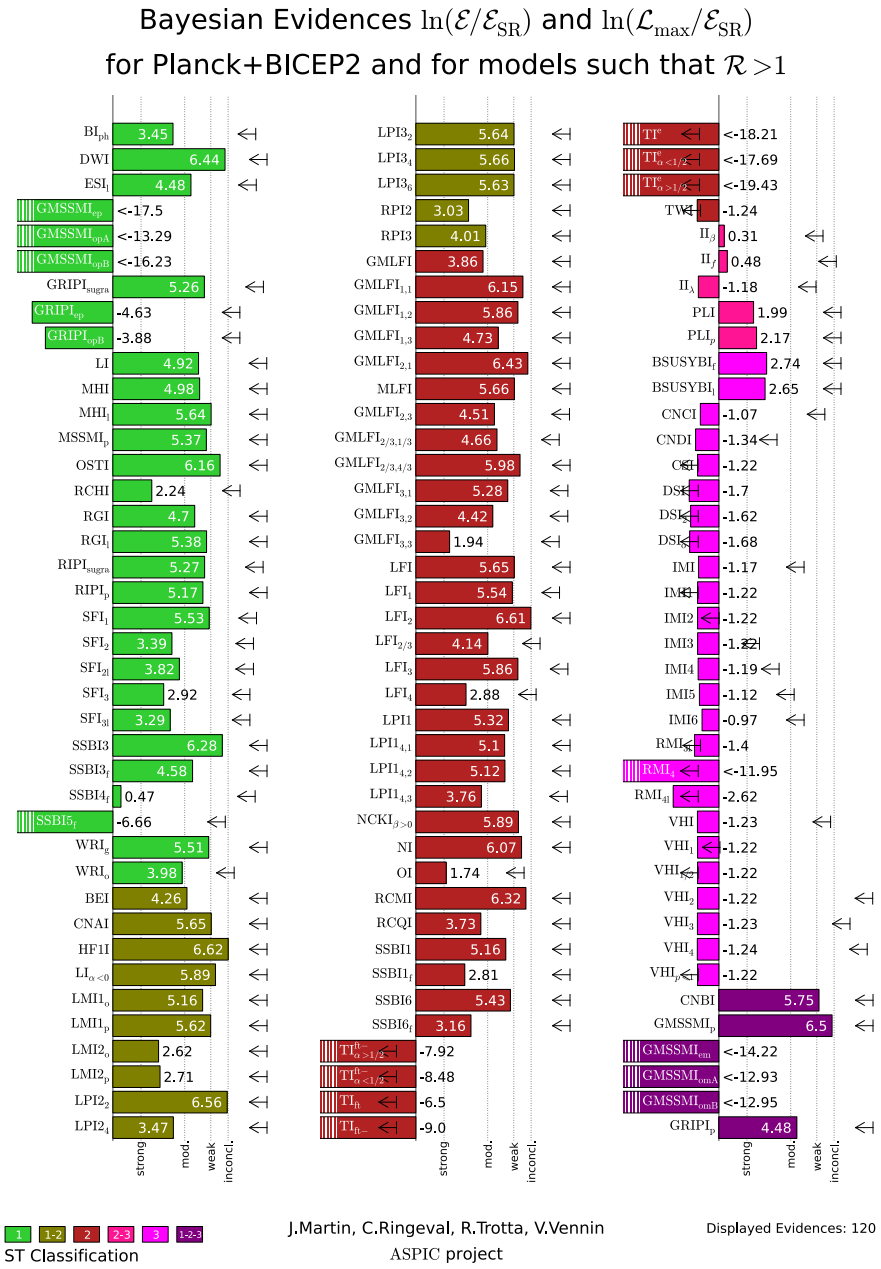

FIG. 18: Evidences (Bayes factor) and absolute upper bounds to the Bayes factors, from Planck and BICEP2 data combined, for the models such that $\mathcal{R} > 1$ only. The reference model is the same slow-roll model as in Figs. 11 and 13, and the vertical dotted lines refer to the Jeffreys' scale with respect to the best model, here HF1I.

have represented the Bayes factors obtained by combining Planck and BICEP2 together, but only for models having $\mathcal{R} > 1$ since combining models with $\mathcal{R} < 1$ is meaningless. Our chosen threshold of $\mathcal{R}$ is conservative (i.e., we are not requiring $\mathcal{R} \gg 1$), and it includes scenarios under which, in the present situation, one cannot conclude about compatibility according to the Jeffreys' scale (i.e. models having $0 < \ln\mathcal{R} \ll 5$). The two best models are now HF1I and LFI_2. Then, in the inconclusive zone (with respect to the new best model) one has $\mathrm{LPI2}_2$, $\mathrm{GMSSMI}_\mathrm{p}$, DWI, $\mathrm{GMLFI}_{2,1}$, RCMI, SSBI3, OSTI, $\mathrm{GMLFI}_{1,1}$, NI, $\mathrm{GMLFI}_{2/3,4/3}$, $\mathrm{LI}_{\alpha<0}$, $\mathrm{NCKI}_{\beta>0}$, $\mathrm{GMLFI}_{1,2}$, LFI_3, CNBI, $\mathrm{LPI3}_4$, MLFI, CNAI, LFI, MHI_l, $\mathrm{LPI3}_2$, $\mathrm{LPI3}_6$, $\mathrm{LMI1}_\mathrm{p}$, LFI_1 and SFI_1. It is interesting to notice that, among the previous models, none of them is in the strongly compatible zone. This is yet

another consequence of the tension between Planck and BICEP2 under an inflationary prior assumption. We also notice that all the models in the Planck+BICEP2 inconclusive zone are in the BICEP2 inconclusive zone while only one (i.e. $\mathrm{MHI_l}$) is in the Planck inconclusive zone. On the other hand, the $\mathrm{LFI_4}$ scenario which was in the list of inconclusive models for BICEP2 becomes moderately disfavored when adding Planck.

V. CONCLUSIONS

Let us now summarize our main conclusions. If the BICEP2 data stand the test of time and are confirmed as a signature of tensor modes of inflationary origin, they do represent a major advance in our understanding of inflation and primordial cosmology. Indeed, for the first time, we would now have a measurement of the energy scale of inflation: the GUT scale. Other important consequences were also discussed in the introduction.

The main issue addressed in the present article was the compatibility of the Planck data with the BICEP2 data assuming an inflationary prior. Several indicators have been used to quantify the tension between these two measurements. Firstly, assuming slow-roll, we have shown that our posterior odds measure of compatibility gives $\mathcal{R}_{\mathrm{SR}} \simeq 1$. This means that we are not in a position to establish that Planck and BICEP2 are compatible at a statistically significant level assuming a slow-roll model. But, clearly, we cannot either prove that the two data sets are incompatible (again, assuming slow-roll): we are precisely in a regime where one cannot conclude. Secondly, we have also computed the $\mathcal{R}$ factor for all the *Encyclopædia Inflationaris* scenarios and shown that the undecided situation just described is changed. We have found that the zone of strongly compatible models contain no "good" Planck or BICEP2 models (i.e. "good" models are defined to be models in the inconclusive zone with respect to the best models of each data set alone). Moreover, all the models for which we can be sure that Planck and BICEP2 are compatible ($\ln\mathcal{R} > 5$) are either strongly or moderately disfavored by Planck (except three models that are only weakly disfavored, i.e. $\mathrm{BSUSYBI_l}$, $\mathrm{GMSSMI_{omB}}$ and $\mathrm{GMSSMI_{em}}$). Thirdly, for models such that $\mathcal{R} > 1$, we have derived the updated value of the Bayesian evidence. We have found that, for all the best Planck+BICEP2 models (those which are in the inconclusive zone with respect to the best Planck+BICEP2 model $\mathrm{LFI_3}$), we have $1 < \ln\mathcal{R} < 5$, i.e. for none of them Planck and BICEP2 appear compatible at a strong evidence level. Fourthly, as was established in Ref. [22], the Planck data favor category 1 models, namely models with a potential having a plateau shape (the best model was KMIII but the inconclusive zone contained other scenarios, for instance the Starobinsky model). However, these models are disfavored by the BICEP2 data for which the best model is $\mathrm{LFI_3}$ (a category 2 model) and have $\mathcal{R}$-factors less than unity. Therefore, we face a situation where Planck and BICEP2 are not strongly compatible. Moreover, as discussed above, several hints all indicate that the two measurements could in fact be incompatible although, in the present situation, it is too early to make a final judgment.

Another important message of this work is that, assuming BICEP2 alone or Planck+BICEP2 when possible (i.e. for $\ln\mathcal{R} > 1$) does not single out a particular model, for instance $m^2\phi^2$. From a theoretical point of view, $m^2\phi^2$ may seem a priori quite attractive. However, given either BICEP2 or Planck+BICEP2, it is not the only winner and other types of models are still performing as well as this simple potential. As a consequence, in the present situation, it seems meaningless to focus the model building efforts only on large field models.

In view of our result, the most important next step is to confirm that the B-mode polarization detection by BICEP2 is truly of primordial origin. Hopefully, this will help to resolve the tension between the two data sets and thus their incompatibility for the Planck best scenarios.

Once done, if a the detection of a non-vanishing r is confirmed, one will have to measure the tensor spectral index n_{T}. The sign of n_{T} already carries very important information and has the potential to confirm or exclude different challengers to inflation. Indeed, inflation generically predicts a red spectrum, namely $n_{\mathrm{T}} < 0$, see Eq. (24). If one finds a blue spectrum $n_{\mathrm{T}} > 0$, this would certainly be difficult (and/or contrived) to explain in this framework and alternatives such as, for instance, string gas cosmology [141], which predicts a blue spectrum, would be a natural solution.

For a red spectrum, the next-to-next pressing question will be to verify the simplest consistency relation of Eq. (28), namely [142, 143]

$$\frac{r}{n_{\mathrm{T}}} \simeq -8, \tag{34}$$

which is independent of the shape of the potential (but not of the inflationary classes of models).

Only after these three steps have been completed, one would be in a position to claim that inflation has been really seen in the sky. It should be clear from the above considerations that this is not yet the case.

Acknowledgments

This work is partially supported by the ESA Belgian Federal PRODEX Grant No. 4000103071 and the Wallonia-Brussels Federation grant ARC No. 11/15-040.

Appendix A: Bayesian compatibility Between Data Sets

In this section we illustrate how the $\mathcal{R}$ factor measures the degree of compatibility/incompatibility between two data sets given a model $\mathcal{M}$.

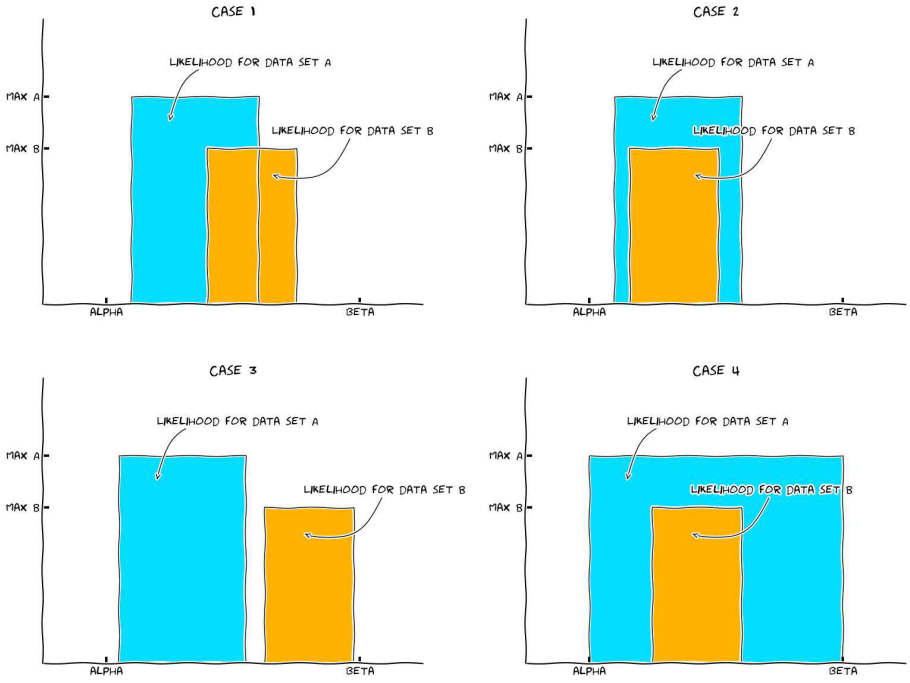

FIG. 19: Four proto-typical situations when combining two data sets $D_{\rm A}$ and $D_{\rm B}$. Their respective likelihoods may overlap, or not, within the prior volume, or not. As seen in Fig. 3, Planck and BICEP2 under the slow-roll model prior (SR) could be idealized as "case 2" for the cosmological parameters which ends up being constrained by BICEP2 alone ($\mathcal{R} > 1$), as "case 4" for those not constrained at all ($\mathcal{R} = 1$) and as "case 1" over the ϵ_1 direction ($\mathcal{R} < 1$).

1. Toy example

We consider a toy model $\mathcal{M}$ described by single parameter θ, the prior of which is uniform in the interval $[\alpha, \beta]$ and has a density $V_\pi^{-1} \equiv (\beta - \alpha)^{-1}$. Let us evaluate $\mathcal{R}$ associated with two data sets $D_{\rm A}$ and $D_{\rm B}$ in various idealized cases as sketched in Fig. 19. Their respective likelihoods are assumed to be Heaviside functions having a maximum value $\mathcal{L}_i^{\rm max}$ over a support $\delta\theta_i$ ($i = A, B$). For "case 1" represented in Fig. 19, one gets

$$\mathcal{R} = \frac{\displaystyle\int \mathcal{L}_{\rm A}(\theta)\mathcal{L}_{\rm B}(\theta)\pi(\theta){\rm d}\theta}{\displaystyle\int \mathcal{L}_{\rm A}(\theta)\pi(\theta){\rm d}\theta \int \mathcal{L}_{\rm B}(\theta)\pi(\theta){\rm d}\theta} = \frac{V_\pi \delta\theta_{\rm AB}}{\delta\theta_{\rm A}\delta\theta_{\rm B}} \qquad \text{(A1)}$$
$$= \frac{\delta\theta_{\rm AB}}{\min(\delta\theta_{\rm A}, \delta\theta_{\rm B})} \times \frac{1}{\max(\delta\theta_{\rm A}, \delta\theta_{\rm B})/V_\pi}\,.$$

The quantity $\delta\theta_{\rm AB}$ stands for the overlapping range of θ values between the two likelihoods. We point out that the maximum likelihood values cancel out and have no influence on $\mathcal{R}$. In the second line of Eq. (A1), we have highlighted a first factor which is always less than unity since $\delta\theta_{\rm AB} \leq \min(\delta\theta_{\rm A}, \delta\theta_{\rm B})$. The second term is the inverse of factor by which the prior volume has been reduce by the less constraining data set. Provided the less constraining data set (i.e., the one with the largest support of the likelihood) remains informative, namely $\max(\delta\theta_{\rm A}, \delta\theta_{\rm B}) < V_\pi$, this second term in Eq. (A1) is always greater than unity. As expected for a Bayesian quantity, $\mathcal{R}$ measures how much the likelihoods of the two data sets overlap balanced by how much information has been with respect to the initial prior volume. For instance, "case 2" in Fig. 19 yields $\delta\theta_{\rm AB} = \min(\delta\theta_{\rm A}, \delta\theta_{\rm B}) = \delta\theta_{\rm B}$ and $\mathcal{R} = V_\pi/\delta\theta_{\rm A} > 1$, so long as $D_{\rm A}$ is informative ($\delta\theta_{\rm A} < V_\pi$). Notice that one would get exactly the same result for $\delta\theta_{\rm AB} = \delta\theta_{\rm A} = \delta\theta_{\rm B}$. "Case 4" represents a situation in which the worse data set, here $D_{\rm A}$, becomes uninformative as the likelihood support encompasses the whole prior volume ($\delta\theta_{\rm A} = V_\pi$) and $\mathcal{R} = 1$. In other words, even though the likelihoods perfectly overlap, $\mathcal{R} = 1$ indicates that one cannot conclude on the compatibility of the two data sets precisely because one of them is uninformative. Finally, "case 3" is the worse case scenario $\delta\theta_{\rm AB} = 0$ and $\mathcal{R} = 0$ signaling a complete incompatibility between $D_{\rm A}$ and $D_{\rm B}$ under the model $\mathcal{M}$.

In view of the marginalized distributions represented in Fig. 3, the posterior of ϵ_1 exhibits a situation typical of "case 1". For all the other parameters, the BICEP2 posteriors are always encompassing those associated with Planck, some being informative and others uninformative. Therefore, some directions in the parameter space are typical of "case 4" (as for instance ϵ_2 and ϵ_3) while others are typical of "case 2" (as for instance $\theta_{\rm MC}$ and

P_*). As a result, one may expect the $\mathcal{R}_{\rm SR}$ factor between Planck and BICEP2 for the model $\mathcal{M} = {\rm SR}$ to be pushed towards unity by all the uninformative posteriors from BICEP2, less than unity by the ϵ_1-posterior and more than unity by the compatible posteriors; a situation more complex than what is advocated in Ref. [131]. In the following, we provide a semi-analytic calculation confirming the numerical calculation of Sec. III C and showing that those effects roughly compensate to give $\mathcal{R}_{\rm SR}$ close to unity.

2. Semi-analytic approach

In the following, we split the cosmological, astrophysical and instrumental parameters associated with the Planck likelihood into two sets $\theta_{\rm s} = (\theta_{\rm lcdm}, \theta_{\rm n})$ with

$$\begin{aligned}\theta_{\rm lcdm} &\equiv \left(\Omega_{\rm b}h^2, \Omega_{\rm c}h^2, \tau, 100\theta_{\rm MC}\right),\\ \theta_{\rm n} &\equiv \left(A^{\rm PS}_{100}, A^{\rm PS}_{143}, A^{\rm PS}_{217}, r^{\rm PS}_{143\times217}, A^{\rm CIB}_{143}, A^{\rm CIB}_{217}, r^{\rm CIB}_{143\times217},\right.\\ &\quad \left.\gamma^{\rm CIB}, A_{\rm tSZ}, A_{\rm kSZ}, \xi^{\rm tSZ\times CIB}, c_{100}, c_{217}, \beta^1_1\right),\end{aligned} \tag{A2}$$

noticing that the BICEP2 likelihood only involves the $\theta_{\rm lcdm}$ set. In order to simplify notation we denote by ε the set of primordial parameters $\ln(10^{10}P_*)$, $\log(\epsilon_1)$, ϵ_2 and ϵ_3 and by $D_{\rm p}$ and $D_{\rm b}$ the Planck and BICEP2 data sets. From the definition of $\mathcal{R}_{\rm SR}$ one has

$$\begin{aligned}\mathcal{R}_{\rm SR} &= \frac{\mathcal{E}(D_{\rm p}, D_{\rm b}|{\rm SR})}{\mathcal{E}(D_{\rm p}|{\rm SR})\mathcal{E}(D_{\rm b}|{\rm SR})}\\ &= \mathcal{R}_{\rm REF}\,\frac{\dfrac{\mathcal{E}(D_{\rm p}, D_{\rm b}|{\rm SR})}{\mathcal{E}(D_{\rm p}, D_{\rm b}|\mathcal{M}_{\rm REF})}}{\dfrac{\mathcal{E}(D_{\rm p}|{\rm SR})}{\mathcal{E}(D_{\rm p}|\mathcal{M}_{\rm REF})}\dfrac{\mathcal{E}(D_{\rm b}|{\rm SR})}{\mathcal{E}(D_{\rm b}|\mathcal{M}_{\rm REF})}}.\end{aligned} \tag{A3}$$

Here we have introduced a reference model $\mathcal{M}_{\rm REF}$ such that the last term in the above equation is a ratio of Bayes factors that can be computed quickly from the effective likelihood method discussed in Sec. II. The difficulty has been moved into estimating $\mathcal{R}_{\rm REF}$, i.e. the compatibility factor between Planck and BICEP2 under some reference model. However, the arbitrariness in choosing $\mathcal{M}_{\rm REF}$ allows us to define it with a very convenient prior, namely

$$\pi(\varepsilon) = \delta(\varepsilon - \varepsilon_{\rm f}), \tag{A4}$$

where $\varepsilon_{\rm f}$ are some fixed values of the primordial parameters. The evidence of $\mathcal{M}_{\rm REF}$ using Planck data alone is given by

$$\mathcal{E}(D_{\rm p}|\mathcal{M}_{\rm REF}) = \int \bar{\mathcal{L}}_{\rm p}(\varepsilon_{\rm f}, \theta_{\rm lcdm})\pi(\theta_{\rm lcdm})\,{\rm d}\theta_{\rm lcdm}, \tag{A5}$$

where we have defined

$$\bar{\mathcal{L}}_{\rm p}(\varepsilon_{\rm f}, \theta_{\rm lcdm}) \equiv \int \mathcal{L}_{\rm p}(\varepsilon_{\rm f}, \theta_{\rm lcdm}, \theta_{\rm n})\pi(\theta_{\rm n})\,{\rm d}\theta_{\rm n}. \tag{A6}$$

Similarly, for Planck and BICEP2 data combined, one has

$$\begin{aligned}\mathcal{E}(D_{\rm p}, D_{\rm b}|\mathcal{M}_{\rm REF}) = \int &\bar{\mathcal{L}}_{\rm p}(\varepsilon_{\rm f}, \theta_{\rm lcdm})\mathcal{L}_{\rm b}(\varepsilon_{\rm f}, \theta_{\rm lcdm})\\ &\times \pi(\theta_{\rm lcdm})\,{\rm d}\theta_{\rm lcdm}\,,\end{aligned} \tag{A7}$$

and for the BICEP2 data alone the evidence reads

$$\mathcal{E}(D_{\rm b}|\mathcal{M}_{\rm REF}) = \int \mathcal{L}_{\rm b}(\varepsilon_{\rm f}, \theta_{\rm lcdm})\pi(\theta_{\rm lcdm})\,{\rm d}\theta_{\rm lcdm}. \tag{A8}$$

These expressions are exact and we now make some approximations. From the posteriors of Fig. 3, one sees that, over all the cosmological parameters $\theta_{\rm lcdm}$, the marginalized Planck likelihood $\bar{\mathcal{L}}_{\rm p}(\varepsilon_{\rm f}, \theta_{\rm lcdm})$ is strongly peaked inside the support of $\mathcal{L}_{\rm b}(\varepsilon_{\rm f}, \theta_{\rm lcdm})$. Therefore, Eq. (A7) can be approximated by

$$\begin{aligned}\mathcal{E}(D_{\rm p}, D_{\rm b}|\mathcal{M}_{\rm REF}) \simeq\ &\mathcal{L}_{\rm b}(\varepsilon_{\rm f}, \theta^{\rm max}_{\rm lcdm})\\ &\times \int \bar{\mathcal{L}}_{\rm p}(\varepsilon_{\rm f}, \theta_{\rm lcdm})\pi(\theta_{\rm lcdm})\,{\rm d}\theta_{\rm lcdm},\end{aligned} \tag{A9}$$

where $\theta^{\rm max}_{\rm lcdm}$ are the cosmological parameters at which $\bar{\mathcal{L}}_{\rm p}$ is maximal given $\varepsilon_{\rm f}$. From this expression, together with Eqs. (A5) and (A8), one gets

$$\mathcal{R}_{\rm REF} \simeq \frac{\mathcal{L}_{\rm b}(\varepsilon_{\rm f}, \theta^{\rm max}_{\rm lcdm})}{\displaystyle\int \mathcal{L}_{\rm b}(\varepsilon_{\rm f}, \theta_{\rm lcdm})\pi(\theta_{\rm lcdm})\,{\rm d}\theta_{\rm lcdm}}, \tag{A10}$$

which, apart from the location $\theta^{\rm max}_{\rm lcdm}$, depends on the BICEP2 likelihood only. The evidence appearing in the denominator is a four-dimensional integral over $\theta_{\rm lcdm}$ (or five-dimensional if one marginalizes over ϵ_3), as opposed to a nineteen-dimensional integral for the bare Planck likelihood. In practice, we have chosen $\varepsilon_{\rm f}$ as the primordial parameters associated with the best fit model of Planck and BICEP2 combined and have evaluated Eq. (A10) using the `MultiNest` algorithm [129, 130]. This method yields

$$\ln(\mathcal{R}_{\rm SR}) \simeq -0.01 \pm 0.3, \tag{A11}$$

where the quoted error is a systematic estimated by performing various nested integrations having a number of live points between 500 to 1000. This value is compatible with the full numerical integration presented in Sec. III C.

[1] P. Ade et al. (BICEP2 Collaboration) (2014), 1403.3985.
[2] H. Liu, P. Mertsch, and S. Sarkar (2014), 1404.1899.
[3] S. Saga, M. Shiraishi, and K. Ichiki (2014), 1405.4810.

[4] C. Ringeval, T. Boehm, and R. Durrer, Phys.Rev.D (2003), hep-th/0307100.
[5] J. Lizarraga, J. Urrestilla, D. Daverio, M. Hindmarsh, M. Kunz, et al. (2014), 1403.4924.
[6] C. Bonvin, R. Durrer, and R. Maartens (2014), 1403.6768.
[7] C. Ringeval, Adv.Astron. **2010**, 380507 (2010), 1005.4842.
[8] P. Ade et al. (Planck Collaboration) (2013), 1303.5085.
[9] L. P. Grishchuk, Sov. Phys. JETP **40**, 409 (1975).
[10] L. P. Grishchuk, Nuovo Cim. Lett. **12**, 60 (1975).
[11] M. J. Mortonson and U. Seljak (2014), 1405.5857.
[12] P. Ade et al. (Planck Collaboration) (2014), 1405.0871.
[13] A. A. Starobinsky, Phys.Lett. **B91**, 99 (1980).
[14] A. H. Guth, Phys. Rev. **D23**, 347 (1981).
[15] A. D. Linde, Phys. Lett. **B108**, 389 (1982).
[16] A. A. Starobinsky, Phys. Lett. **B117**, 175 (1982).
[17] A. H. Guth and S. Y. Pi, Phys. Rev. Lett. **49**, 1110 (1982).
[18] A. Albrecht and P. J. Steinhardt, Phys. Rev. Lett. **48**, 1220 (1982).
[19] J. M. Bardeen, P. J. Steinhardt, and M. S. Turner, Phys. Rev. **D28**, 679 (1983).
[20] A. D. Linde, JETP Lett. **38**, 176 (1983).
[21] V. F. Mukhanov and G. V. Chibisov, JETP Lett. **33**, 532 (1981).
[22] J. Martin, C. Ringeval, R. Trotta, and V. Vennin, JCAP **1403**, 039 (2014), 1312.3529.
[23] T. Kobayashi, M. Yamaguchi, and J. Yokoyama, Phys.Rev.Lett. **105**, 231302 (2010), 1008.0603.
[24] T. Kobayashi, M. Yamaguchi, and J. Yokoyama, Phys.Rev. **D83**, 103524 (2011), 1103.1740.
[25] C. Armendariz-Picon, T. Damour, and V. F. Mukhanov, Phys.Lett. **B458**, 209 (1999), hep-th/9904075.
[26] J. Garriga and V. F. Mukhanov, Phys.Lett. **B458**, 219 (1999), hep-th/9904176.
[27] D. Wands, Lect.Notes Phys. **738**, 275 (2008), astro-ph/0702187.
[28] A. R. Liddle, A. Mazumdar, and F. E. Schunck, Phys.Rev. **D58**, 061301 (1998), astro-ph/9804177.
[29] S. A. Kim and A. R. Liddle, Phys.Rev. **D74**, 023513 (2006), astro-ph/0605604.
[30] Y.-S. Piao, Phys.Rev. **D74**, 047302 (2006), gr-qc/0606034.
[31] R. Easther, J. Frazer, H. V. Peiris, and L. C. Price, Phys.Rev.Lett. **112**, 161302 (2014), 1312.4035.
[32] S. Dimopoulos, S. Kachru, J. McGreevy, and J. G. Wacker, JCAP **0808**, 003 (2008), hep-th/0507205.
[33] J. M. Maldacena, JHEP **0305**, 013 (2003), astro-ph/0210603.
[34] P. Ade et al. (Planck Collaboration) (2013), 1303.5076.
[35] P. Ade et al. (Planck Collaboration) (2013), 1303.5082.
[36] A. A. Starobinsky, Lect.Notes Phys. **246**, 107 (1986).
[37] A. A. Starobinsky and J. Yokoyama, Phys.Rev. **D50**, 6357 (1994), astro-ph/9407016.
[38] J. Martin and M. Musso, Phys.Rev. **D73**, 043516 (2006), hep-th/0511214.
[39] W. H. Kinney and K. Freese (2014), 1404.4614.
[40] A. D. Linde, Mod.Phys.Lett. **A1**, 81 (1986).
[41] A. D. Linde, Phys.Lett. **B175**, 395 (1986).
[42] A. Goncharov, A. D. Linde, and V. F. Mukhanov, Int.J.Mod.Phys. **A2**, 561 (1987).
[43] D. H. Lyth, Phys.Rev.Lett. **78**, 1861 (1997), hep-ph/9606387.
[44] S. Antusch and D. Nolde (2014), 1404.1821.
[45] D. Baumann and L. McAllister (2014), 1404.2601.
[46] J. Martin, Comptes Rendus Physique **13**, 566 (2012), 1205.3365.
[47] M. S. Turner and L. M. Widrow, Phys.Rev. **D37**, 2743 (1988).
[48] B. Ratra, Astrophys.J. **391**, L1 (1992).
[49] J. Martin and J. Yokoyama, JCAP **0801**, 025 (2008), 0711.4307.
[50] W. Essey, S. Ando, and A. Kusenko, Astropart.Phys. **35**, 135 (2011), 1012.5313.
[51] K. Dolag, M. Kachelriess, S. Ostapchenko, and R. Tomas, Astrophys.J. **727**, L4 (2011), 1009.1782.
[52] A. Neronov and I. Vovk, Science **328**, 73 (2010), 1006.3504.
[53] F. Tavecchio, G. Ghisellini, L. Foschini, G. Bonnoli, G. Ghirlanda, et al., Mon.Not.Roy.Astron.Soc. **406**, L70 (2010), 1004.1329.
[54] V. Demozzi, V. Mukhanov, and H. Rubinstein, JCAP **0908**, 025 (2009), 0907.1030.
[55] R. J. Ferreira, R. K. Jain, and M. S. Sloth, JCAP **1310**, 004 (2013), 1305.7151.
[56] V. Demozzi and C. Ringeval, JCAP **1205**, 009 (2012), 1202.3022.
[57] C. Ringeval, T. Suyama, and J. Yokoyama, JCAP **1309**, 020 (2013), 1302.6013.
[58] T. Accadia, F. Acernese, P. Astone, G. Ballardin, F. Barone, et al., Nuovo Cim. **C034N06**, 189 (2011).
[59] P. Amaro-Seoane, S. Aoudia, S. Babak, P. Binetruy, E. Berti, et al., GW Notes **6**, 4 (2013), 1201.3621.
[60] S. Kawamura, M. Ando, N. Seto, S. Sato, T. Nakamura, et al., Class.Quant.Grav. **28**, 094011 (2011).
[61] M. Ando, S. Kawamura, N. Seto, S. Sato, T. Nakamura, et al., Class.Quant.Grav. **27**, 084010 (2010).
[62] J. Crowder and N. J. Cornish, Phys.Rev. **D72**, 083005 (2005), gr-qc/0506015.
[63] K. Nakayama, S. Saito, Y. Suwa, and J. Yokoyama, JCAP **0806**, 020 (2008), 0804.1827.
[64] S. Kuroyanagi, C. Ringeval, and T. Takahashi, Phys.Rev. **D87**, 083502 (2013), 1301.1778.
[65] L. M. Krauss and F. Wilczek, Phys.Rev. **D89**, 047501 (2014), 1309.5343.
[66] A. Ashoorioon, P. B. Dev, and A. Mazumdar (2012), 1211.4678.
[67] V. F. Mukhanov, H. Feldman, and R. H. Brandenberger, Phys.Rept. **215**, 203 (1992).
[68] J. Martin, Lect.Notes Phys. **669**, 199 (2005), hep-th/0406011.
[69] J. Martin, Lect.Notes Phys. **738**, 193 (2008), 0704.3540.
[70] J. M. Bardeen, Phys. Rev. **D22**, 1882 (1980).
[71] K. A. Malik and D. Wands, Phys.Rept. **475**, 1 (2009), 0809.4944.
[72] A. Riotto, pp. 317–413 (2002), hep-ph/0210162.
[73] L. P. Grishchuk and Y. V. Sidorov, Phys. Rev. **D42**, 3413 (1990).
[74] J. Lesgourgues, D. Polarski, and A. A. Starobinsky, Nucl. Phys. **B497**, 479 (1997), gr-qc/9611019.
[75] C. P. Burgess, R. Holman, and D. Hoover, Phys.Rev. **D77**, 063534 (2008), astro-ph/0601646.
[76] C. Kiefer and D. Polarski, Adv.Sci.Lett. **2**, 164 (2009), 0810.0087.
[77] D. Sudarsky, Int.J.Mod.Phys. **D20**, 509 (2011), 0906.0315.
[78] N. Pinto-Neto, G. Santos, and W. Struyve, Phys.Rev.

D85, 083506 (2012), 1110.1339.
[79] J. Martin, V. Vennin, and P. Peter, Phys.Rev. **D86**, 103524 (2012), 1207.2086.
[80] S. Das, K. Lochan, S. Sahu, and T. Singh, Phys.Rev. **D88**, 085020 (2013), 1304.5094.
[81] S. Das, S. Sahu, S. Banerjee, and T. Singh (2014), 1404.5740.
[82] S. Galli, K. Benabed, F. Bouchet, J.-F. Cardoso, F. Elsner, et al. (2014), 1403.5271.
[83] A. Lue, L.-M. Wang, and M. Kamionkowski, Phys.Rev.Lett. **83**, 1506 (1999), astro-ph/9812088.
[84] S. Alexander and J. Martin, Phys.Rev. **D71**, 063526 (2005), hep-th/0410230.
[85] C. R. Contaldi, J. Magueijo, and L. Smolin, Phys.Rev.Lett. **101**, 141101 (2008), 0806.3082.
[86] J. Martin, C. Ringeval, and V. Vennin (2013), 1303.3787.
[87] J. Martin (2013), 1312.3720.
[88] S. Dorn, E. Ramirez, K. E. Kunze, S. Hofmann, and T. A. Enlin (2014), 1403.5067.
[89] R. Trotta, Mon.Not.Roy.Astron.Soc. **378**, 72 (2007), astro-ph/0504022.
[90] R. Trotta, Contemp.Phys. **49**, 71 (2008), 0803.4089.
[91] M. Hobson, S. Bridle, and O. Lahav, Mon.Not.Roy.Astron.Soc. **335**, 377 (2002), astro-ph/0203259.
[92] P. Marshall, N. Rajguru, and A. Slosar, Phys.Rev. **D73**, 067302 (2006), astro-ph/0412535.
[93] F. Feroz, B. C. Allanach, M. Hobson, S. S. AbdusSalam, R. Trotta, et al., JHEP **0810**, 064 (2008), 0807.4512.
[94] M. E. Cabrera, J. A. Casas, R. Ruiz de Austri, and R. Trotta, Phys.Rev. **D84**, 015006 (2011), 1011.5935.
[95] F. Feroz, K. Cranmer, M. Hobson, R. Ruiz de Austri, and R. Trotta, JHEP **1106**, 042 (2011), 1101.3296.
[96] C. Arina, Phys.Rev. **D86**, 123527 (2012), 1210.4011.
[97] C. Arina (2013), 1310.5718.
[98] M. Kunz, R. Trotta, and D. Parkinson, Phys.Rev. **D74**, 023503 (2006), astro-ph/0602378.
[99] C. Arina, G. Bertone, and H. Silverwood, Phys.Rev. **D88**, 013002 (2013), 1304.5119.
[100] P. Ade et al. (Planck Collaboration) (2013), 1303.5075.
[101] S. Hamimeche and A. Lewis, Phys.Rev. **D77**, 103013 (2008), 0801.0554.
[102] H. Chiang, P. Ade, D. Barkats, J. Battle, E. Bierman, et al., Astrophys.J. **711**, 1123 (2010), 0906.1181.
[103] P. Ade et al. (Planck Collaboration) (2013), 1303.5062.
[104] J. Dunkley et al. (WMAP), Astrophys. J. Suppl. **180**, 306 (2009), 0803.0586.
[105] G. Hinshaw et al. (WMAP), Astrophys.J.Suppl. **208**, 19 (2013), 1212.5226.
[106] C. Bennett et al. (WMAP), Astrophys.J.Suppl. **208**, 20 (2013), 1212.5225.
[107] D. Barkats et al. (BICEP1 Collaboration) (2013), 1310.1422.
[108] A. Lewis and S. Bridle, Phys.Rev. **D66**, 103511 (2002), astro-ph/0205436.
[109] A. Lewis, A. Challinor, and A. Lasenby, Astrophys.J. **538**, 473 (2000), astro-ph/9911177.
[110] M. S. Turner, Phys. Rev. **D28**, 1243 (1983).
[111] J. Martin and C. Ringeval, JCAP **0608**, 009 (2006), astro-ph/0605367.
[112] C. Ringeval, Lect. Notes Phys. **738**, 243 (2008), astro-ph/0703486.
[113] J. Martin and C. Ringeval, Phys.Rev. **D82**, 023511 (2010), 1004.5525.
[114] R. Easther and H. V. Peiris, Phys.Rev. **D85**, 103533 (2012), 1112.0326.
[115] J. Martin, C. Ringeval, and R. Trotta, Phys.Rev. **D83**, 063524 (2011), 1009.4157.
[116] C. Ringeval, Mon. Not. Roy. Astron. Soc. **439**, 3253 (2014), 1312.2347.
[117] E. D. Stewart and D. H. Lyth, Phys.Lett. **B302**, 171 (1993), gr-qc/9302019.
[118] J.-O. Gong and E. D. Stewart, Phys.Lett. **B510**, 1 (2001), astro-ph/0101225.
[119] J. Martin and D. J. Schwarz, Phys.Rev. **D67**, 083512 (2003), astro-ph/0210090.
[120] S. Habib, K. Heitmann, G. Jungman, and C. Molina-Paris, Phys.Rev.Lett. **89**, 281301 (2002), astro-ph/0208443.
[121] D. J. Schwarz, C. A. Terrero-Escalante, and A. A. Garcia, Phys.Lett. **B517**, 243 (2001), astro-ph/0106020.
[122] S. M. Leach, A. R. Liddle, J. Martin, and D. J. Schwarz, Phys.Rev. **D66**, 023515 (2002), astro-ph/0202094.
[123] R. Casadio, F. Finelli, M. Luzzi, and G. Venturi, Phys. Rev. **D71**, 043517 (2005), gr-qc/0410092.
[124] R. Casadio, F. Finelli, M. Luzzi, and G. Venturi, Phys. Lett. **B625**, 1 (2005), gr-qc/0506043.
[125] R. Casadio, F. Finelli, M. Luzzi, and G. Venturi, Phys. Rev. **D72**, 103516 (2005), gr-qc/0510103.
[126] L. Lorenz, J. Martin, and C. Ringeval, Phys.Rev. **D78**, 083513 (2008), 0807.3037.
[127] J. Martin, C. Ringeval, and V. Vennin, JCAP **1306**, 021 (2013), 1303.2120.
[128] J. Beltran Jimenez, M. Musso, and C. Ringeval, Phys.Rev. **D88**, 043524 (2013), 1303.2788.
[129] F. Feroz and M. Hobson, Mon.Not.Roy.Astron.Soc. **384**, 449 (2008), 0704.3704.
[130] F. Feroz, M. Hobson, and M. Bridges, Mon.Not.Roy.Astron.Soc. **398**, 1601 (2009), 0809.3437.
[131] B. Audren, D. G. Figueroa, and T. Tram (2014), 1405.1390.
[132] R. K. Jain, P. Chingangbam, L. Sriramkumar, and T. Souradeep, Phys.Rev. **D82**, 023509 (2010), 0904.2518.
[133] C. R. Contaldi, M. Peloso, and L. Sorbo (2014), 1403.4596.
[134] D. K. Hazra, A. Shafieloo, G. F. Smoot, and A. A. Starobinsky (2014), 1404.0360.
[135] D. K. Hazra, A. Shafieloo, G. F. Smoot, and A. A. Starobinsky (2014), 1403.7786.
[136] K. N. Abazajian, G. Aslanyan, R. Easther, and L. C. Price (2014), 1403.5922.
[137] D. J. Schwarz and C. A. Terrero-Escalante, JCAP **0408**, 003 (2004), hep-ph/0403129.
[138] X. Calmet and V. Sanz (2014), 1403.5100.
[139] J. Ellis, M. A. G. Garcia, D. V. Nanopoulos, and K. A. Olive (2014), 1403.7518.
[140] L. Kofman and A. D. Linde, JHEP **0207**, 004 (2002), hep-th/0205121.
[141] R. H. Brandenberger, A. Nayeri, and S. P. Patil (2014), 1403.4927.
[142] J. Caligiuri and A. Kosowsky (2014), 1403.5324.
[143] S. Dodelson (2014), 1403.6310.

Journal of Cosmology and Astroparticle Physics
An IOP and SISSA journal

K-inflationary power spectra at second order

Jérôme Martin,[a] **Christophe Ringeval**[b] **and Vincent Vennin**[a]

[a]Institut d'Astrophysique de Paris, UMR 7095-CNRS, Université Pierre et Marie Curie, 98bis boulevard Arago, 75014 Paris, France

[b]Centre for Cosmology, Particle Physics and Phenomenology, Institute of Mathematics and Physics, Louvain University, 2 Chemin du Cyclotron, 1348 Louvain-la-Neuve, Belgium

E-mail: jmartin@iap.fr, christophe.ringeval@uclouvain.be, vennin@iap.fr

Received March 18, 2013
Revised April 23, 2013
Accepted May 30, 2013
Published June 17, 2013

Abstract. Within the class of inflationary models, k-inflation represents the most general single field framework that can be associated with an effective quadratic action for the curvature perturbations and a varying speed of sound. The incoming flow of high-precision cosmological data, such as those from the Planck satellite and small scale Cosmic Microwave Background (CMB) experiments, calls for greater accuracy in the inflationary predictions. In this work, we calculate for the first time the next-to-next-to-leading order scalar and tensor primordial power spectra in k-inflation needed in order to obtain robust constraints on the inflationary theory. The method used is the uniform approximation together with a second order expansion in the Hubble and sound flow functions. Our result is checked in various limits in which it reduces to already known situations.

Keywords: inflation, cosmological perturbation theory, physics of the early universe

ArXiv ePrint: 1303.2120

JCAP06(2013)021

doi:10.1088/1475-7516/2013/06/021

Contents

1 Introduction

Inflation [1, 2] (for reviews, see refs. [3–7]), which is currently the leading paradigm to describe the physical conditions that prevailed in the very early Universe, is now entering a new phase. With the advent of new high-accuracy cosmological data [8–21], among which are the Planck data [22], one can hope to obtain very tight constraints on the inflationary theory and even to pin-point the correct model of inflation. In order to achieve this ambitious goal, one must be able to compare the inflationary predictions to the data. The problem is that the inflationary landscape is very large [23] and that there is a whole zoo of different models making different predictions. Moreover, for many of these models, predictions can only be worked out by numerical methods. It is therefore not obvious how to extract model-independent constraints on the inflationary scenario.

How then should we proceed? Clearly, one can approach the problem step by step and start with the simplest models. In other words, it seems reasonable to consider more complicated models only if the data force us to do so and tell us that the simplest models are not enough. Then comes the question of identifying these models. One can convincingly argue that slow-roll Single Field with a Minimal Kinetic term (SFMK) scenarios are the simplest inflationary models since they are just characterized by one function, the potential $V(\phi)$. In order to establish their observational consequences, a possible approach is to scan models one by one and calculate the predictions exactly [24–29], most of the time numerically [30, 31].[1] This leads to an exact mapping of the inflationary landscape within this class of scenarios but, given that the number of SFMK models remains large, it would represent a huge effort. Another approach consists in developing a scheme of approximation allowing us to derive analytical, or semi-analytical, predictions. Although this is not always possible, such a method is available for the SFMK models and one can explicitly write a functional form for the primordial power spectrum of the cosmological perturbations [32], and even their higher order correlation functions [33–38].

In fact, one can enlarge the class of what we consider as the simplest models of inflation and assume that these ones are k-inflationary scenarios. K-inflation [39, 40] encompasses standard inflation and is more general since not only the potential but also the kinetic term

[1] See for instance http://theory.physics.unige.ch/~ringeval/fieldinf.html.

JCAP06(2013)021

is now a free function. At the perturbation level, the action for the comoving curvature perturbation has a varying speed of sound and this describes all possible quadratic terms within the effective field theory formalism [41, 42]. But, more interestingly, and despite the fact that this class of scenarios is more complicated to analyze, a properly generalized slow-roll approximation can still be used.

1.1 State-of-the-art

At this stage, it is interesting to recall the present status of the techniques that enable us to calculate the two-point correlation function for the primordial cosmological perturbations.

The spectrum of density perturbations during inflation was computed for the first time in refs. [43, 44] and for the gravity waves in ref. [45]. Then, in ref. [46], it was realized that it can be evaluated exactly in the case of power-law inflation. The first calculation at first order in the so-called "horizon flow parameters" and using the slow-roll approximation was performed in ref. [32]. This calculation was done for the SFMK models. This is a fundamental result since it allows to connect the deviations from scale invariance to the microphysics of inflation. This result was re-derived using the Green function methods in ref. [47], using the Wentzel-Kramers-Brillouin (WKB) method in ref. [48] and using the uniform approximation in refs. [49, 50]. In fact, the Green function method of ref. [47] made possible the first determination of the scalar power spectrum at second order in the "horizon flow parameters". Indeed, at second order, the mode equation describing the evolution of the cosmological perturbations can no longer be solved exactly, hence the need for a new method of approximation. Higher order corrections were also obtained in ref. [51]. The first derivation of the tensor power spectrum at second order using the Green function method was presented in ref. [52]. In refs. [53, 54], it was also shown how to improve the WKB method by adding more adiabatic terms. This improved WKB method has allowed a re-derivation of the scalar and tensor power spectra at second order and confirmed the results of the Green function approach.

After the advent of k-inflation, various attempts have been made to derive the corresponding power spectra. The problem is complicated due to the fact that density perturbations now propagate with a time-dependent speed (the speed of sound). In ref. [55], the Green function method has been used but with some extra-assumptions on the behavior of the sound speed. The question was also considered in refs. [56, 57] but the results obtained in those articles were not totally correct since the sound speed was (implicitly) assumed to be constant which is not the case in most of the k-inflationary scenarios (this result was also used afterward in ref. [58]). These works also missed the influence of the sound speed in the tensor power spectrum due to the shift between the scalar and tensor pivot scales [59, 60]. The first fully consistent result for the k-inflationary scalar power spectrum was presented in ref. [61]. The latter has been re-derived using the uniform approximation in ref. [59] together with the first fully consistent calculation of the tensor power spectrum at the same pivot scale. These spectra were compared to Cosmic Microwave Background Anisotropy (CMB) data first in ref. [62]. However, all of these calculations have been derived at first order only and no complete result at second order exists in the literature.

The main purpose of this article is to close this gap and to derive the slow-roll power spectra for the density and tensor perturbations in k-inflation, at second order in the Hubble and sound flow functions.[2] This calculation is interesting for two reasons. Firstly, the second order result is available for SFMK models and, for completeness, it should also be done for the

[2]Conforming to the modern usage, we will prefer the denomination of "Hubble flow functions" and "sound

JCAP06(2013)021

k-inflationary models. Secondly, according to the "blue book" [63], Planck will measure the spectral index with accuracy $\Delta n_{\rm S} \simeq 0.005$. Even if one expects the Hubble flow parameters to be less than 10^{-2}, second order corrections will be of order 10^{-4}, that is to say relevant for high-accuracy measurements of $n_{\rm S}$ and/or estimation of the corresponding error bars. Moreover, having at hand the second order terms allows to marginalize over, a procedure that should always be carried on to get robust Bayesian constraints on the first order terms.

Before moving to the calculation, let us briefly recall some well-known results about k-inflation at the background and perturbation levels.

1.2 K-inflation in brief

K-inflation corresponds to a class of models where gravity is described by General Relativity and where the action for the inflaton field is an arbitrary function, $P(\phi, X)$, the quantity X being defined by $X \equiv -(1/2)g^{\mu\nu}\partial_\mu\phi\partial_\nu\phi$. This action can be written as

$$S = \frac{M_{\rm Pl}^2}{2}\int {\rm d}^4x\sqrt{-g}\left[R + \frac{2}{M_{\rm Pl}^2}P\left(X,\phi\right)\right], \tag{1.1}$$

where $M_{\rm Pl}$ is the reduced Planck mass. In fact, in order to satisfy the requirements that the Hamiltonian is bounded from below and that the equations of motion remain hyperbolic, the function $P(X,\phi)$ must satisfy the following two conditions [64]

$$\frac{\partial P}{\partial X} > 0, \quad 2X\frac{\partial^2 P}{\partial X^2} + \frac{\partial P}{\partial X} > 0. \tag{1.2}$$

The general action (1.1) includes standard inflation for which $P = X - V(\phi)$, where $V(\phi)$ is the inflaton potential. This class of model is in fact characterized by an arbitrary function of ϕ only. K-inflation also includes the Dirac-Born-Infeld (DBI) class of inflationary models [65]. For those, one has $P = -T(\phi)\sqrt{1 - 2X/T(\phi)} + T(\phi) - V(\phi)$. This kind of action typically appears in brane inflation and $T(\phi)$ is interpreted as a warping function representing the bulk geometry in which various branes can move. It is of course possible to find even more complicated examples but, in the following, we will not need to specify explicitly the function $P(X,\phi)$.

As in standard inflation, the dynamics of the background space-time can be described by the Hubble flow functions ϵ_n defined by

$$\epsilon_{n+1} = \frac{{\rm d}\ln\epsilon_n}{{\rm d}N}, \qquad \epsilon_0 \equiv \frac{H_{\rm ini}}{H}, \tag{1.3}$$

where $N \equiv \ln(a/a_{\rm ini})$ is the number of e-folds. Inflation occurs if $\epsilon_1 < 1$ and the slow-roll approximation assumes that all these parameters are small during inflation $\epsilon_n \ll 1$. Let us notice that it is difficult to have an inflationary model without such a condition because otherwise one would obtain a deviation from scale invariance which would be too strong to be compatible with the cosmological data (see however ref. [42]).

At the perturbed level, we have density perturbations and gravity waves. As usual, rotational perturbations are unimportant since they quickly decay. Obviously, the tensorial sector of the theory is standard since the gravitational part of (1.1) is the ordinary Einstein-Hilbert

flow functions" to refer to the original, but confusing, appellation "horizon flow parameters". See section 1.2 for the definition of the Hubble and sound flow functions.

JCAP06(2013)021

action. As a consequence, the equation of motion for the amplitude $\mu_{\boldsymbol{k}}$ of gravity waves (re-scaled by a factor $1/a$ for convenience, where a is the Friedman-Lemaitre-Robertson-Walker scale factor) takes the usual form, namely

$$\mu_{\boldsymbol{k}}'' + \left[k^2 - U_{\mathrm{T}}(\eta)\right]\mu_{\boldsymbol{k}} = 0, \tag{1.4}$$

where η is the conformal time and a prime denotes a derivative with respect to η. The effective potential for the tensorial modes can be written as $U_{\mathrm{T}} = a^2H^2\,(2-\epsilon_1)$, i.e. only depends on the first Hubble flow function ($H = a'/a^2$ is the Hubble parameter).

For the density perturbations, the situation is slightly more complicated. One can show that the comoving curvature perturbation in Fourier space, $\zeta_{\boldsymbol{k}}$, can be written in terms of a modified Mukhanov-Sasaki variable $v_{\boldsymbol{k}}$ by means of the following expression, $v_{\boldsymbol{k}} = (a\sqrt{\epsilon_1})\zeta_{\boldsymbol{k}}/c_{\mathrm{s}}$ (in Planck units) where the quantity c_{s} is defined by the following equation

$$c_{\mathrm{s}}^2 \equiv \frac{P_{,X}}{P_{,X} + 2XP_{,XX}}\,, \tag{1.5}$$

a subscript "$,X$" denoting differentiation with respect to X. This quantity can be interpreted as the "sound speed" of density fluctuations. Notice that, because of the two consistency relations (1.2), we have $c_{\mathrm{s}}^2 > 0$. The fact that c_{s} is the sound speed can be most easily seen if one writes down the equation of motion of the Mukhanov-Sasaki variable. It reads

$$v_{\boldsymbol{k}}'' + \left[c_{\mathrm{s}}^2(\eta)k^2 - U_{\mathrm{S}}(\eta)\right]v_{\boldsymbol{k}} = 0. \tag{1.6}$$

This is similar to the equation of motion of a parametric oscillator. The quantity U_{S} is the effective potential for the density perturbations and is a function of time only. As expected, c_{s}^2 appears in front of the k^2 term, which is nothing but a gradient term in Fourier space and this confirms its interpretation as a time dependent sound speed. Since $c_{\mathrm{s}}(\eta)$ is not known a priori, one can introduce a second hierarchy of flow functions in order to describe its behavior. Therefore, we define the sound flow functions δ_n's by

$$\delta_{n+1} \equiv \frac{\mathrm{d}\ln\delta_n}{\mathrm{d}N}\,, \qquad \delta_0 \equiv \frac{c_{\mathrm{sini}}}{c_{\mathrm{s}}}\,. \tag{1.7}$$

Consistent models of inflation are obtained if $\delta_n \ll 1$, that is to say if the sound speed does not change too abruptly [59, 61]. A remark about terminology is in order at this point. In terms of the Hubble and sound flow functions, the effective potential for the density perturbations can be expressed as

$$U_{\mathrm{S}} = a^2H^2\left[2 - \epsilon_1 + \frac{3}{2}\epsilon_2 + \frac{1}{4}\epsilon_2^2 - \frac{1}{2}\epsilon_1\epsilon_2 + \frac{1}{2}\epsilon_2\epsilon_3 + (3 - \epsilon_1 + \epsilon_2)\,\delta_1 + \delta_1^2 + \delta_1\delta_2\right]. \tag{1.8}$$

The quantity U_{S} depends on the ϵ_n's up to ϵ_3 only and on the δ_n's up to δ_2 only. Despite this last property, it is important to remember that the above expression of U_{S} is *exact* and that no approximation has been made at this stage.

The cosmological observables we are interested in are the two point correlation functions of the fluctuations, i.e. in Fourier space, the power spectra of both gravity waves and density perturbations:

$$\mathcal{P}_h = \frac{2k^3}{\pi^2}\left|\frac{\mu_{\boldsymbol{k}}}{a}\right|^2, \quad \mathcal{P}_\zeta = \frac{k^3}{2\pi^2}\left|\zeta_{\boldsymbol{k}}\right|^2 = \frac{k^3}{4\pi^2}\frac{c_{\mathrm{s}}^2|v_{\boldsymbol{k}}|^2}{M_{\mathrm{Pl}}^2a^2\epsilon_1}. \tag{1.9}$$

JCAP06(2013)021

They have to be evaluated at the end of inflation and on large scales. After the inflationary era, and for single field models, these power spectra remain constant and can be directly used to compute various observable quantities such as the CMB anisotropies or the matter power spectrum. Our goal is now to integrate the equations of motion of $\mu_{\boldsymbol{k}}$ and $v_{\boldsymbol{k}}$ in order to explicitly evaluate the above power spectra.

This article is organized as follows. In the next section, after having very quickly reviewed how the uniform approximation can be used in the cosmological context, we apply it to the calculation of the scalar and tensor primordial power spectra. Our results are discussed section 3, in which we compare them, in the appropriate limits, with the existing literature and we present our conclusions.

2 K-inflationary power spectra

2.1 The uniform approximation

In this section, we use the uniform approximation to calculate the power spectrum of the density fluctuations in k-inflation, at second order in the Hubble and sound flow functions. We have seen in the previous section that the density perturbations in k-inflation propagate with a time-dependent velocity $c_{\rm s}(\eta)$. As the mode equation can no longer be solved exactly in terms of Bessel functions (even at first order for the sound flow functions), this prompts for the use of new techniques. Here, we choose to work with the well-suited uniform approximation [50]. The idea is to rewrite the effective potential according to $U_{\rm S} = (\nu^2 - 1/4)/\eta^2$, an equation which has to be understood as the definition of the function $\nu(\eta)$. Then, we introduce two new functions

$$g(\eta) \equiv \frac{\nu^2}{\eta^2} - c_{\rm s}^2 k^2, \qquad f(\eta) \equiv \frac{|\eta - \eta_*|}{\eta - \eta_*} \left| \frac{3}{2} \int_{\eta_*}^{\eta} {\rm d}\tau \sqrt{g(\tau)} \right|^{2/3}, \tag{2.1}$$

where the turning point time $\eta_*(k)$ is defined by the condition $g(\eta_*) = 0$, that is to say $\eta_* \equiv -\nu(\eta_*)/[kc_{\rm s}(\eta_*)]$. According to the uniform approximation, the Mukhanov-Sasaki variable can then be expressed as

$$v_{\boldsymbol{k}}(\eta) = A_{\boldsymbol{k}} \left(\frac{f}{g}\right)^{1/4} {\rm Ai}\,(f) + B_{\boldsymbol{k}} \left(\frac{f}{g}\right)^{1/4} {\rm Bi}\,(f)\,, \tag{2.2}$$

where the two constants $A_{\boldsymbol{k}}$ and $B_{\boldsymbol{k}}$ are fixed by the choice of the initial conditions and where Ai and Bi denotes the Airy function of the first and second kind respectively. Since one needs to compute $v_{\boldsymbol{k}}$ on large scales, only the asymptotic behavior of the Airy functions is needed and one arrives at a simpler formula, namely

$$\lim_{c_{\rm s}k\eta \to 0} v_{\boldsymbol{k}}(\eta) = \frac{B_{\boldsymbol{k}}}{g^{1/4}\pi^{1/2}} \exp\left(\frac{2}{3} f^{3/2}\right). \tag{2.3}$$

Here, the function $g(\eta)$ should be taken in its asymptotic limit, i.e. $g^{1/2} \simeq -\nu(\eta)/\eta$. Inserting the last equation for $v_{\boldsymbol{k}}(\eta)$ into the formula (1.9), one obtains the following expression for $\mathcal{P}_\zeta$

$$\mathcal{P}_\zeta = -\frac{k^3 \left|B_{\boldsymbol{k}}\right|^2}{4\pi^3 M_{\rm Pl}^2} \frac{\eta c_{\rm s}^2}{a^2 \nu \epsilon_1} e^{2\Psi}, \tag{2.4}$$

where we have defined $\Psi \equiv 2f^{3/2}/3$. One verifies that $\mathcal{P}_\zeta$ is positive definite since the conformal time is negative during inflation. Therefore, the only thing which remains to be done is to express the combination $c_{\rm s}^2/(a^2\nu\epsilon_1)$ and the quantity Ψ at second order in the Hubble and sound flow functions.

JCAP06(2013)021

2.2 Hubble and sound flow expansion

The first step of the calculation consists in determining the functions $a(\eta)$, $c_{\rm s}(\eta)$, $\nu(\eta)$ and $\epsilon_1(\eta)$ at second order in the Hubble and sound flow functions. Here, we first briefly explain the method in the case of the scale factor. By definition, the conformal time is given by $\eta = -\int \mathrm{d}t/a(t)$, where t is the cosmic time. By successive integrations by parts, one can re-write η as

$$\eta = \frac{1}{\mathcal{H}}\left\{1+\epsilon_1+\epsilon_1^2+\epsilon_1\epsilon_2 - aH\int \frac{1}{a}\frac{\mathrm{d}}{\mathrm{d}a}\left[\frac{1}{H}\left(\epsilon_1^2+\epsilon_1\epsilon_2\right)\right]\mathrm{d}a\right\}, \tag{2.5}$$

where $\mathcal{H} \equiv a'/a$ is the conformal Hubble parameter. It is important to stress that this equation is exact. In the last term, the integrand is third order in the ϵ_i. Indeed, differentiating the term $1/H$ produces a ϵ_1 which, multiplied with $(\epsilon_1^2+\epsilon_1\epsilon_2)$, is third order. We also have to differentiate expressions quadratic in the Hubble flow functions but, since $\mathrm{d}\epsilon_n/\mathrm{d}N = \epsilon_n\epsilon_{n+1}$, this also gives third order quantities. Therefore, the last term is $\mathcal{O}\left(\epsilon^3\right)$ and can be dropped for a second order calculation. In other words

$$\mathcal{H} = -\frac{1}{\eta}\left(1+\epsilon_1+\epsilon_1^2+\epsilon_1\epsilon_2\right)+\mathcal{O}\left(\epsilon^3\right). \tag{2.6}$$

In fact, this equation is not exactly what we want yet because, although the second order terms ϵ_1^2 and $\epsilon_1\epsilon_2$ can be considered as constant in time,[3] this is not the case for the term ϵ_1 which is first order. In order to render explicit the time-dependence, let us notice that the equations defining the Hubble-flow functions can also be written as $\mathrm{d}\epsilon_n/\mathrm{d}\eta = \mathcal{H}\epsilon_n\epsilon_{n+1}$. Given that $\epsilon_n\epsilon_{n+1}$ is already a second-order term, we can just replace $\mathcal{H}$ with $-1/\eta$ in this expression and one gets $\epsilon_n = \epsilon_{n*} - \epsilon_{n*}\epsilon_{n+1*}\ln\left(\eta/\eta_*\right)+\mathcal{O}\left(\epsilon^3\right)$, where we have chosen the integration constant such that this approximation is accurate around the time η_* of the turning point. Inserting this expression into eq. (2.6) gives

$$\mathcal{H} = -\frac{1}{\eta}\left(1+\epsilon_{1*}+\epsilon_{1*}^2+\epsilon_{1*}\epsilon_{2*}\right)+\epsilon_{1*}\epsilon_{2*}\frac{1}{\eta}\ln\left(\frac{\eta}{\eta_*}\right)+\mathcal{O}\left(\epsilon^3\right), \tag{2.7}$$

and, this time, the η-dependence of $\mathcal{H}$ is explicit. This equation can be further integrated leading to an expression for the e-folds number N, namely

$$N-N_* = \ln\left(\frac{a}{a_*}\right) \simeq -\left(1+\epsilon_{1*}+\epsilon_{1*}^2+\epsilon_{1*}\epsilon_{2*}\right)\ln\left(\frac{\eta}{\eta_*}\right)+\frac{1}{2}\epsilon_{1*}\epsilon_{2*}\ln^2\left(\frac{\eta}{\eta_*}\right). \tag{2.8}$$

Finally, by exponentiation the above formula and by expressing the constant $a_*\eta_*$ in terms of $1/H_*$, one obtains the following equation for the scale factor itself

$$\begin{aligned} a(\eta) \simeq -\frac{1}{H_*\eta}\Bigg[1+\epsilon_{1*}+\epsilon_{1*}^2+\epsilon_{1*}\epsilon_{2*}-\left(\epsilon_{1*}+2\epsilon_{1*}^2+\epsilon_{1*}\epsilon_{2*}\right)\ln\left(\frac{\eta}{\eta_*}\right) \\ +\frac{1}{2}\left(\epsilon_{1*}^2+\epsilon_{1*}\epsilon_{2*}\right)\ln^2\left(\frac{\eta}{\eta_*}\right)\Bigg]. \end{aligned} \tag{2.9}$$

We have reached our first goal, namely find an expression of $a(\eta)$ at second order in the Hubble flow parameters.

[3] Their derivative is indeed third order, i.e. zero at the order at which we work.

JCAP06(2013)021

Let us now discuss how the expression of $\epsilon_1(\eta)$ can be obtained. Let us notice that since ϵ_1 is appearing in eq. (2.4), we need to go to third order since a term $1/\epsilon_{1*}$ will remain in front of the final expression of $\mathcal{P}_\zeta$. This can however be obtained using the above formulas. Taylor expanding ϵ_1 around N_* one has

$$\epsilon_1 = \epsilon_{1*} + \left.\frac{\mathrm{d}\epsilon_1}{\mathrm{d}N}\right|_* (N - N_*) + \frac{1}{2}\left.\frac{\mathrm{d}^2\epsilon_1}{\mathrm{d}N^2}\right|_* (N - N_*)^2 + \cdots \tag{2.10}$$

Using the fact that $\mathrm{d}\epsilon_1/\mathrm{d}N = \epsilon_1\epsilon_2$, $\mathrm{d}^2\epsilon_1/\mathrm{d}N^2 = \epsilon_1\epsilon_2^2 + \epsilon_1\epsilon_2\epsilon_3$ and the expression of the number of e-folds at first order [see eq. (2.8) above], one arrives at

$$\epsilon_1 = \epsilon_{1*}\left[1 - \epsilon_{2*}\left(1 + \epsilon_{1*}\right)\ln\left(\frac{\eta}{\eta_*}\right) + \frac{1}{2}\left(\epsilon_{2*}^2 + \epsilon_{2*}\epsilon_{3*}\right)\ln^2\left(\frac{\eta}{\eta_*}\right)\right] + \mathcal{O}\left(\epsilon^4\right). \tag{2.11}$$

The very same method can be used to determine the second order expression of the sound speed. Taylor expanding c_s in e-fold gives

$$c_\mathrm{s}^2 = c_{\mathrm{s}*}^2 + \left.\frac{\mathrm{d}c_\mathrm{s}^2}{\mathrm{d}N}\right|_* (N - N_*) + \frac{1}{2}\left.\frac{\mathrm{d}^2c_\mathrm{s}^2}{\mathrm{d}N^2}\right|_* (N - N_*)^2 + \cdots, \tag{2.12}$$

and from the sound flow hierarchy one has $\mathrm{d}c_\mathrm{s}^2/\mathrm{d}N = -2c_\mathrm{s}^2\delta_1$, $\mathrm{d}^2c_\mathrm{s}^2/\mathrm{d}N^2 = -2c_\mathrm{s}^2\delta_1\delta_2 + 4c_\mathrm{s}^2\delta_1^2$. Together with the expression of $N - N_*$, it follows that

$$c_\mathrm{s}^2(\eta) = c_{\mathrm{s}*}^2 + 2c_{\mathrm{s}*}^2(\delta_{1*} + \delta_{1*}\epsilon_{1*})\ln\left(\frac{\eta}{\eta_*}\right) - c_{\mathrm{s}*}^2\left(\delta_{1*}\delta_{2*} - 2\delta_{1*}^2\right)\ln^2\left(\frac{\eta}{\eta_*}\right) + \mathcal{O}\left(\epsilon^3, \delta^3\right). \tag{2.13}$$

As expected the coefficients of the logarithms are expressed in terms of the parameters δ_1 and δ_2.

Finally, only the expression for $\nu(\eta)$ remains to be found. By definition, one has $\nu^2 = 1/4 + \eta^2 U_\mathrm{s}(\eta)$, i.e. Taylor expanding everything from the previous formulas, one gets

$$\nu(\eta) = \nu_* - \left(\epsilon_{1*}\epsilon_{2*} + \frac{1}{2}\epsilon_{2*}\epsilon_{3*} + \delta_{1*}\delta_{2*}\right)\ln\left(\frac{\eta}{\eta_*}\right) + \mathcal{O}\left(\epsilon^3, \delta^3\right), \tag{2.14}$$

with

$$\nu_* \equiv \frac{3}{2} + \epsilon_{1*} + \frac{1}{2}\epsilon_{2*} + \delta_{1*} + \epsilon_{1*}^2 + \frac{11}{6}\epsilon_{1*}\epsilon_{2*} + \frac{1}{6}\epsilon_{2*}\epsilon_{3*} + \epsilon_{1*}\delta_{1*} + \frac{1}{3}\delta_{1*}\delta_{2*}. \tag{2.15}$$

2.3 Comoving curvature power spectrum

We have now determined explicitly the four functions appearing in the expression of the power spectrum $\mathcal{P}_\zeta$, see eq. (2.4). It is straightforward, although lengthy, to calculate, at second order, the relevant combination $c_\mathrm{s}^2/(a^2\nu\epsilon_1)$ appearing in that expression. Moreover, we must also find Ψ. Upon using the expression of the function $g(\eta)$, one gets

$$\Psi = \int_{\eta_*}^{\eta} \mathrm{d}\tau \sqrt{\frac{\nu^2(\tau)}{\tau^2} - c_\mathrm{s}^2(\tau)k^2}\,. \tag{2.16}$$

JCAP06(2013)021

Inserting eqs. (2.13) and (2.14) into the previous formula and expanding everything to second order, the integrand in eq. (2.16) reads

$$\begin{aligned}\sqrt{\frac{\nu^2(\tau)}{\tau^2}-c_{\rm s}^2(\tau)k^2} = &-\frac{\nu_*}{\tau}\left(1-\frac{c_{\rm s*}^2k^2\tau^2}{\nu_*^2}\right)^{1/2}\\ &+\frac{3}{2\nu_*}\left(\epsilon_{1*}\epsilon_{2*}+\frac{1}{2}\epsilon_{2*}\epsilon_{3*}+\delta_{1*}\delta_{2*}\right)\frac{1}{\tau}\left(1-\frac{c_{\rm s*}^2k^2\tau^2}{\nu_*^2}\right)^{-1/2}\ln\left(\frac{\tau}{\eta_*}\right)\\ &+\frac{c_{\rm s*}^2}{\nu_*}\left(\delta_{1*}+\epsilon_{1*}\delta_{1*}\right)\frac{1}{\tau}\left(1-\frac{c_{\rm s*}^2k^2\tau^2}{\nu_*^2}\right)^{-1/2}k^2\tau^2\ln\left(\frac{\tau}{\eta_*}\right)\\ &-\frac{c_{\rm s*}^2}{2\nu_*}\left(\delta_{1*}\delta_{2*}-2\delta_{1*}^2\right)\frac{1}{\tau}\left(1-\frac{c_{\rm s*}^2k^2\tau^2}{\nu_*^2}\right)^{-1/2}k^2\tau^2\ln^2\left(\frac{\tau}{\eta_*}\right)\\ &+\frac{c_{\rm s*}^4}{2\nu_*^3}\left(\delta_{1*}+\epsilon_{1*}\delta_{1*}\right)^2\frac{1}{\tau}\left(1-\frac{c_{\rm s*}^2k^2\tau^2}{\nu_*^2}\right)^{-3/2}k^4\tau^4\ln^2\left(\frac{\tau}{\eta_*}\right). \end{aligned} \tag{2.17}$$

Therefore, we have five different integrals to calculate in order to evaluate the term Ψ. In the following, we write

$$\Psi=\sum_{i=1}^{i=5}I_i, \tag{2.18}$$

and calculate each of the I_i separately. Let us also notice that the way eq. (2.17) has been written is not yet fully consistent since all the terms have to be expanded to second-order. For instance, terms like $(\delta_{1*}+\epsilon_{1*}\delta_{1*})/\nu_*$ (in front of the second integral I_2) should clearly be expanded further on in order to keep only second order expressions. For the moment, however, we will be keeping them this way in order to maintain clarity. Only at the end of the calculation these terms will be expanded.

Let us now calculate the five integrals. Defining $w\equiv c_{\rm s*}k\eta/\nu_*$, which implies that $w_*\equiv c_{\rm s*}k\eta_*/\nu_*=-1$, the first integral, I_1, can be calculated exactly and reads

$$I_1=-\nu_*\left[\left(1-u^2\right)^{1/2}+\ln|u|-\ln\left|1+\left(1-u^2\right)^{1/2}\right|\right]\Bigg|_{u=w_*}^{u=w}. \tag{2.19}$$

On large scales, w approaches zero and one obtains

$$\lim_{w\to0}I_1=-\nu_*\left(1+\ln|w|-\ln 2\right). \tag{2.20}$$

The second integral is slightly more complicated but can also be carried out exactly. The result can be expressed as

$$\begin{aligned}I_2=&\frac{3}{16\nu_*}\left(\epsilon_{1*}\epsilon_{2*}+\frac{1}{2}\epsilon_{2*}\epsilon_{3*}+\delta_{1*}\delta_{2*}\right)\left[4\ln^2|u|-8\ln|u|\ln\left|\frac{1}{2}\left(1+\sqrt{1-u^2}\right)\right|\right.\\ &\left.+2\ln^2\left|\frac{1}{2}\left(1+\sqrt{1-u^2}\right)\right|-4\,{\rm Li}_2\left(\frac{1}{2}-\frac{\sqrt{1-u^2}}{2}\right)\right]\Bigg|_{u=w_*}^{u=w}, \end{aligned} \tag{2.21}$$

where $\rm Li_2$ denotes the Polygamma function of order two, or dilogarithm function [66]. On large scales the previous expression takes the form

$$\lim_{w\to0}I_2=\frac{3}{16\nu_*}\left(\epsilon_{1*}\epsilon_{2*}+\frac{1}{2}\epsilon_{2*}\epsilon_{3*}+\delta_{1*}\delta_{2*}\right)\left(4\ln^2|w|-4\ln^2 2+\frac{\pi^2}{3}\right), \tag{2.22}$$

JCAP06(2013)021

where we have used $\mathrm{Li}_2(0) = 0$ and $\mathrm{Li}_2(1/2) = \pi^2/12 - (\ln^2 2)/2$. We notice that I_1 and I_2 are logarithmically divergent in the limit $w \to 0$. We will see that this is not a problem and that those terms cancel out in the final expression of $\mathcal{P}_\zeta$. This is expected since we know that the power spectrum remains constant on larges scales, and as such an exact cancellation of those terms constitutes a consistency check of the method. On the contrary, the integrals I_3, I_4 and I_5 are convergent and can be directly computed. They read

$$I_3 = \nu_* \left(\delta_{1*} + \epsilon_{1*}\delta_{1*}\right)(1 - \ln 2)\,, \quad I_4 = -\frac{\nu_*}{2}\left(\delta_{1*}\delta_{2*} - 2\delta_{1*}^2\right)\left(\frac{\pi^2}{12} - 2 + 2\ln 2 - \ln^2 2\right),$$
$$I_5 = \frac{\nu_*}{2}\left(\delta_{1*} + \epsilon_{1*}\delta_{1*}\right)^2\left(2 - \frac{\pi^2}{6} - 2\ln 2 + 2\ln^2 2\right). \tag{2.23}$$

This completes our calculation of the quantity Ψ and we can now evaluate the expression (2.4). Collecting the expressions of a, ϵ_1, c_s and ν established previously, one gets $c_\mathrm{s}^2/(a^2\nu\epsilon_1)$ that has to be combined with $e^{2\Psi}$ using the above integrals. After some lengthy but straightforward manipulations, one obtains

$$\begin{aligned}\mathcal{P}_\zeta = \frac{H_*^2\left(18e^{-3}\right)}{8\pi^2 M_\mathrm{Pl}^2\epsilon_{1*}c_{\mathrm{s}*}}\Bigg[&1 + \left(-\frac{8}{3} + 2\ln 2\right)\epsilon_{1*} + \left(-\frac{1}{3} + \ln 2\right)\epsilon_{2*} + \left(\frac{7}{3} - \ln 2\right)\delta_{1*} \\ &+ \left(\frac{23}{18} - \frac{4}{3}\ln 2 + \frac{1}{2}\ln^2 2\right)\delta_{1*}^2 + \left(\frac{25}{9} - \frac{\pi^2}{24} - \frac{7}{3}\ln 2 + \frac{1}{2}\ln^2 2\right)\delta_{1*}\delta_{2*} \\ &+ \left(-\frac{25}{9} + \frac{13}{3}\ln 2 - 2\ln^2 2\right)\epsilon_{1*}\delta_{1*} + \left(\frac{13}{9} - \frac{10}{3}\ln 2 + 2\ln^2 2\right)\epsilon_{1*}^2 \\ &+ \left(-\frac{2}{9} + \frac{5}{3}\ln 2 - \ln^2 2\right)\epsilon_{2*}\delta_{1*} + \left(-\frac{25}{9} + \frac{\pi^2}{12} + \frac{1}{3}\ln 2 + \ln^2 2\right)\epsilon_{1*}\epsilon_{2*} \\ &+ \left(-\frac{1}{18} - \frac{1}{3}\ln 2 + \frac{1}{2}\ln^2 2\right)\epsilon_{2*}^2 + \left(-\frac{1}{9} + \frac{\pi^2}{24} + \frac{1}{3}\ln 2 - \frac{1}{2}\ln^2 2\right)\epsilon_{2*}\epsilon_{3*}\Bigg].\end{aligned} \tag{2.24}$$

Several remarks are in order at this stage. Firstly, in the above calculation, we have assumed that the initial state of the perturbations is the Bunch-Davies vacuum. This implies that $|B_{\boldsymbol{k}}|^2 = \pi/2$. Notice that, in the context of k-inflation, this is a non-trivial choice since, as discussed in ref. [59], the time dependence of the sound speed could be such that the adiabatic regime is not available anymore.[4] In this paper, we assume that this does not occur and that the function $c_\mathrm{s}(\eta)$ is initially smooth enough. Secondly, as announced above, all the time-dependent terms $\ln|w|$ have canceled out and the expression of $\mathcal{P}_\zeta$ is time-independent. Thirdly, eq. (2.24) should be compared with eq. (51) of ref. [59]. These two expressions coincide at first order, which is another indication that the above formula for $\mathcal{P}_\zeta$ is correct. Fourthly, in the overall amplitude, we notice the presence of the factor $18\,e^{-3}$. As explained in refs. [48] and [59], this is typical in a approximation scheme based on the WKB method or its extension (such as the uniform approximation). This leads to a $\simeq 10\%$ error in the estimation of the amplitude. In refs. [53, 54], it was shown that, by taking into account higher order terms in the adiabatic expansion, this shortcomings can easily be fixed. In that case, one obtains a new overall coefficient which dramatically reduces the error in the

[4] Let us notice however that one can still re-define a new time variable to absorb the c_s-dependence in the mode equation [42]. In terms of that new time variable, one could always set Bunch-Davies initial conditions for the scalar, but this would not be compatible with those of the tensor modes.

JCAP06(2013)021

amplitude. As a consequence, we do not really need to worry about the term $18\,e^{-3}$ and, for practical applications, one can simply renormalize it to one.

Finally, the above expression of $\mathcal{P}_\zeta$ depends on η_* which depends on k. Our goal is now to make this hidden scale dependence explicit and to re-express the power spectrum at a unique pivot scale defined by

$$k_\diamond \eta_\diamond \equiv -\frac{1}{c_{\mathrm{s}\diamond}}\,. \tag{2.25}$$

This is achieved by re-writing all the quantities appearing in the power spectrum at a single time, $\eta = \eta_\diamond$. Technically, this means that, say, ϵ_{1*} should be written as $\epsilon_{1*} = \epsilon_{1\diamond} - \epsilon_{1\diamond}\epsilon_{2\diamond}\ln(\eta_\diamond/\eta_*) + \mathcal{O}(\epsilon^3)$ and that the dependence in $\eta_\diamond/\eta_*$ should be replaced with a dependence in $k_\diamond/k$. This is performed by making use of the relation between the time $\eta_\diamond$ and η_*:

$$\frac{\eta_*}{\eta_\diamond} = \frac{k_\diamond}{k}\nu_*\frac{c_{\mathrm{s}\diamond}}{c_{\mathrm{s}*}}\,. \tag{2.26}$$

Working out the previous equation at second order, one obtains that

$$\begin{aligned}
\ln\left(\frac{\eta_*}{\eta_\diamond}\right) = {} & \left(\ln\frac{3}{2} + \ln\frac{k_\diamond}{k}\right)\left(1 - \delta_{1\diamond} - \epsilon_{1\diamond}\delta_{1\diamond} - \frac{2}{3}\epsilon_{1\diamond}\epsilon_{2\diamond} - \frac{1}{3}\epsilon_{2\diamond}\epsilon_{3\diamond} - \frac{2}{3}\delta_{1\diamond}\delta_{2\diamond} + \delta_{1\diamond}^2\right) \\
& + \frac{2}{3}\epsilon_{1\diamond} + \frac{1}{3}\epsilon_{2\diamond} + \frac{2}{3}\delta_{1\diamond} + \epsilon_{1\diamond}\epsilon_{2\diamond} - \frac{4}{9}\epsilon_{1\diamond}\delta_{1\diamond} + \frac{1}{9}\epsilon_{2\diamond}\epsilon_{3\diamond} + \frac{2}{9}\delta_{1\diamond}\delta_{2\diamond} + \frac{4}{9}\epsilon_{1\diamond}^2 - \frac{1}{18}\epsilon_{2\diamond}^2 \\
& - \frac{8}{9}\delta_{1\diamond}^2 - \frac{5}{9}\epsilon_{2\diamond}\delta_{1\diamond} + \frac{1}{2}\delta_{1\diamond}\delta_{2\diamond}\ln^2\frac{3}{2} + \delta_{1\diamond}\delta_{2\diamond}\ln\frac{3}{2}\ln\frac{k_\diamond}{k} + \frac{1}{2}\delta_{1\diamond}\delta_{2\diamond}\ln^2\frac{k_\diamond}{k}.
\end{aligned} \tag{2.27}$$

This finally leads to one of the two main new results of this paper, namely the expression of the scalar power spectrum in k-inflation at second order in the Hubble and sound flow functions

$$\begin{aligned}
\mathcal{P}_\zeta = {} & \frac{H_\diamond^2\left(18\,e^{-3}\right)}{8\pi^2 M_{\mathrm{Pl}}^2\epsilon_{1\diamond}c_{\mathrm{s}\diamond}}\Bigg\{1 - 2(1+D)\epsilon_{1\diamond} - D\epsilon_{2\diamond} + (2+D)\delta_{1\diamond} + \left(\frac{2}{9} + D + \frac{D^2}{2}\right)\delta_{1\diamond}^2 \\
& + \left(\frac{37}{18} + 2D + \frac{D^2}{2} - \frac{\pi^2}{24}\right)\delta_{1\diamond}\delta_{2\diamond} + \left(-\frac{8}{9} - 3D - 2D^2\right)\epsilon_{1\diamond}\delta_{1\diamond} + \left(\frac{17}{9} + 2D + 2D^2\right)\epsilon_{1\diamond}^2 \\
& + \left(\frac{5}{9} - D - D^2\right)\epsilon_{2\diamond}\delta_{1\diamond} + \left(-\frac{11}{9} - D + D^2 + \frac{\pi^2}{12}\right)\epsilon_{1\diamond}\epsilon_{2\diamond} + \left(\frac{2}{9} + \frac{D^2}{2}\right)\epsilon_{2\diamond}^2 \\
& + \left(\frac{\pi^2}{24} - \frac{1}{18} - \frac{D^2}{2}\right)\epsilon_{2\diamond}\epsilon_{3\diamond} + \big[-2\epsilon_{1\diamond} - \epsilon_{2\diamond} + \delta_{1\diamond} + (1+D)\delta_{1\diamond}^2 \\
& + (2+D)\delta_{1\diamond}\delta_{2\diamond} - (3+4D)\epsilon_{1\diamond}\delta_{1\diamond} + 2(1+2D)\epsilon_{1\diamond}^2 - (1+2D)\epsilon_{2\diamond}\delta_{1\diamond} - (1-2D)\epsilon_{1\diamond}\epsilon_{2\diamond} \\
& + D\epsilon_{2\diamond}^2 - D\epsilon_{2\diamond}\epsilon_{3\diamond}\big]\ln\frac{k}{k_\diamond} + \left(2\epsilon_{1\diamond}^2 + \epsilon_{1\diamond}\epsilon_{2\diamond} + \frac{1}{2}\epsilon_{2\diamond}^2 - \frac{1}{2}\epsilon_{2\diamond}\epsilon_{3\diamond} + \frac{1}{2}\delta_{1\diamond}^2 + \frac{1}{2}\delta_{1\diamond}\delta_{2\diamond}\right. \\
& \left. - 2\epsilon_{1\diamond}\delta_{1\diamond} - \epsilon_{2\diamond}\delta_{1\diamond}\right)\ln^2\frac{k}{k_\diamond}\Bigg\},
\end{aligned} \tag{2.28}$$

where we have introduced the quantity D defined by $D \equiv 1/3 - \ln 3$. One easily checks that, at first order, this expression exactly coincides with eq. (53) of ref. [59]. More details in the comparison of the above formula with the existing literature can be found in section 3.

JCAP06(2013)021

Using the method of ref. [68], one can also deduce the expression of the scalar spectral index which reads

$$
\begin{aligned}
n_{\rm S} - 1 = {} & -2\epsilon_{1\diamond} - \epsilon_{2\diamond} + \delta_{1\diamond} - 2\epsilon_{1\diamond}^2 - (2D+3)\,\epsilon_{1\diamond}\epsilon_{2\diamond} + 3\epsilon_{1\diamond}\delta_{1\diamond} + \epsilon_{2\diamond}\delta_{1\diamond} - D\epsilon_{2\diamond}\epsilon_{3\diamond} \\
& - \delta_{1\diamond}^2 + (D+2)\,\delta_{1\diamond}\delta_{2\diamond} - 2\epsilon_{1\diamond}^3 - \left(\frac{47}{9} + 6D\right)\epsilon_{1\diamond}^2\epsilon_{2\diamond} + 5\epsilon_{1\diamond}^2\delta_{1\diamond} \\
& + \left(-\frac{20}{9} - 3D - D^2 + \frac{\pi^2}{12}\right)\epsilon_{1\diamond}\epsilon_{2\diamond}^2 + \left(-\frac{11}{9} - 4D - D^2 + \frac{\pi^2}{12}\right)\epsilon_{1\diamond}\epsilon_{2\diamond}\epsilon_{3\diamond} \\
& + \left(\frac{73}{9} + 5D\right)\delta_{1\diamond}\epsilon_{1\diamond}\epsilon_{2\diamond} - 4\epsilon_{1\diamond}\delta_{1\diamond}^2 + \left(\frac{46}{9} + 4D\right)\epsilon_{1\diamond}\delta_{1\diamond}\delta_{2\diamond} + \frac{4}{9}\epsilon_{2\diamond}^2\epsilon_{3\diamond} \\
& + \left(-\frac{1}{18} - \frac{D^2}{2} + \frac{\pi^2}{24}\right)\epsilon_{2\diamond}\epsilon_{3\diamond}^2 + \left(\frac{5}{9} + 2D\right)\delta_{1\diamond}\epsilon_{2\diamond}\epsilon_{3\diamond} \\
& + \left(-\frac{1}{18} - \frac{D^2}{2} + \frac{\pi^2}{24}\right)\epsilon_{2\diamond}\epsilon_{3\diamond}\epsilon_{4\diamond} - \delta_{1\diamond}^2\epsilon_{2\diamond} + \left(\frac{5}{9} + D\right)\delta_{1\diamond}\delta_{2\diamond}\epsilon_{2\diamond} + \delta_{1\diamond}^3 \\
& - \left(\frac{50}{9} + 3D\right)\delta_{1\diamond}^2\delta_{2\diamond} + \left(\frac{37}{18} + 2D + \frac{D^2}{2} - \frac{\pi^2}{24}\right)\delta_{1\diamond}\delta_{2\diamond}^2 \\
& + \left(\frac{37}{18} + 2D + \frac{D^2}{2} - \frac{\pi^2}{24}\right)\delta_{1\diamond}\delta_{2\diamond}\delta_{3\diamond}
\end{aligned}
\tag{2.29}
$$

At first order in the flow parameters, one recovers the standard expression, i.e. $n_{\rm S} - 1 = -2\epsilon_{1\diamond} - \epsilon_{2\diamond} + \delta_{1\diamond}$. One can also check that the second order corrections are similar to those found in ref. [59]. Here, for the first time, we have given the formula of the spectral index at third order. This is of course possible only because we have determined the overall amplitude at second order. This also allows us to determine the higher order corrections to the running and to the running of the running. For instance, one can calculate $\alpha_{\rm S}$ at the fourth order and the running of the running at the fifth order. Here, in order to illustrate the efficiency of the method, we just present the expression of $\alpha_{\rm S}$. It reads

$$
\begin{aligned}
\alpha_{\rm S} = {} & -2\epsilon_{1\diamond}\epsilon_{2\diamond} - \epsilon_{2\diamond}\epsilon_{3\diamond} + \delta_{1\diamond}\delta_{2\diamond} - 6\epsilon_{1\diamond}^2\epsilon_{2\diamond} - (3+2D)\,\epsilon_{1\diamond}\epsilon_{2\diamond}^2 - (4+2D)\,\epsilon_{1\diamond}\epsilon_{2\diamond}\epsilon_{3\diamond} + 5\epsilon_{1\diamond}\epsilon_{2\diamond}\delta_{1\diamond} \\
& + 4\epsilon_{1\diamond}\delta_{1\diamond}\delta_{2\diamond} - D\epsilon_{2\diamond}\epsilon_{3\diamond}^2 - D\epsilon_{2\diamond}\epsilon_{3\diamond}\epsilon_{4\diamond} + 2\delta_{1\diamond}\epsilon_{2\diamond}\epsilon_{3\diamond} + \delta_{1\diamond}\delta_{2\diamond}\epsilon_{2\diamond} - 3\delta_{1\diamond}^2\delta_{2\diamond} + (2+D)\,\delta_{1\diamond}\delta_{2\diamond}^2 \\
& + (2+D)\,\delta_{1\diamond}\delta_{2\diamond}\delta_{3\diamond} - 12\epsilon_{1\diamond}^3\epsilon_{2\diamond} - \left(\frac{139}{9} + 14D\right)\epsilon_{1\diamond}^2\epsilon_{2\diamond}^2 - \left(\frac{83}{9} + 8D\right)\epsilon_{1\diamond}^2\epsilon_{2\diamond}\epsilon_{3\diamond} \\
& + 21\delta_{1\diamond}\epsilon_{1\diamond}^2\epsilon_{2\diamond} + 9\delta_{1\diamond}\delta_{2\diamond}\epsilon_{1\diamond}^2 + \left(-\frac{20}{9} - 3D - D^2 + \frac{\pi^2}{12}\right)\epsilon_{1\diamond}\epsilon_{2\diamond}^3 \\
& + \left(-\frac{20}{3} - 10D - 3D^2 + \frac{\pi^2}{4}\right)\epsilon_{1\diamond}\epsilon_{2\diamond}^2\epsilon_{2\diamond} + \left(\frac{100}{9} + 7D\right)\delta_{1\diamond}\epsilon_{1\diamond}\epsilon_{2\diamond}^2 \\
& + \left(-\frac{11}{9} - 5D - D^2 + \frac{\pi^2}{12}\right)\epsilon_{1\diamond}\epsilon_{2\diamond}\epsilon_{3\diamond}^2 + \left(-\frac{11}{9} - 5D - D^2 + \frac{\pi^2}{12}\right)\epsilon_{1\diamond}\epsilon_{2\diamond}\epsilon_{3\diamond}\epsilon_{4\diamond} \\
& + \left(\frac{127}{9} + 7D\right)\delta_{1\diamond}\epsilon_{1\diamond}\epsilon_{2\diamond}\epsilon_{3\diamond} - 9\delta_{1\diamond}^2\epsilon_{1\diamond}\epsilon_{2\diamond} + \left(\frac{137}{9} + 9D\right)\delta_{1\diamond}\delta_{2\diamond}\epsilon_{1\diamond}\epsilon_{2\diamond} - 15\delta_{1\diamond}^2\delta_{2\diamond}\epsilon_{1\diamond} \\
& + \left(\frac{64}{9} + 5D\right)\epsilon_{1\diamond}\delta_{1\diamond}\delta_{2\diamond}^2 + \left(\frac{64}{9} + 5D\right)\epsilon_{1\diamond}\delta_{1\diamond}\delta_{2\diamond}\delta_{3\diamond} + \frac{8}{9}\epsilon_{2\diamond}^2\epsilon_{3\diamond}^2 + \frac{4}{9}\epsilon_{2\diamond}^2\epsilon_{3\diamond}\epsilon_{4\diamond} \\
& + \left(-\frac{1}{18} - \frac{D^2}{2} + \frac{\pi^2}{24}\right)\epsilon_{2\diamond}\epsilon_{3\diamond}^3 + \left(-\frac{1}{6} - \frac{3D^2}{2} + \frac{\pi^2}{8}\right)\epsilon_{2\diamond}\epsilon_{3\diamond}^2\epsilon_{4\diamond} + \left(\frac{5}{9} + 3D\right)\delta_{1\diamond}\epsilon_{2\diamond}\epsilon_{3\diamond}^2
\end{aligned}
$$

JCAP06(2013)021

$$
\begin{aligned}
&+\left(-\frac{1}{18}-\frac{D^2}{2}+\frac{\pi^2}{24}\right)\epsilon_{2\diamond}\epsilon_{3\diamond}\epsilon_{4\diamond}^2+\left(-\frac{1}{18}-\frac{D^2}{2}+\frac{\pi^2}{24}\right)\epsilon_{2\diamond}\epsilon_{3\diamond}\epsilon_{4\diamond}\epsilon_{5\diamond}\\
&+\left(\frac{5}{9}+3D\right)\delta_{1\diamond}\epsilon_{2\diamond}\epsilon_{3\diamond}\epsilon_{4\diamond}-3\delta_{1\diamond}^2\epsilon_{2\diamond}\epsilon_{3\diamond}+\left(\frac{10}{9}+3D\right)\delta_{1\diamond}\delta_{2\diamond}\epsilon_{2\diamond}\epsilon_{3\diamond}-3\delta_{1\diamond}^2\delta_{2\diamond}\epsilon_{2\diamond}\\
&+\left(\frac{5}{9}+D\right)\delta_{1\diamond}\delta_{2\diamond}^2\epsilon_{2\diamond}+\left(\frac{5}{9}+D\right)\delta_{1\diamond}\delta_{2\diamond}\delta_{3\diamond}\epsilon_{2\diamond}+6\delta_{1\diamond}^3\delta_{2\diamond}-\left(\frac{118}{9}+7D\right)\delta_{1\diamond}^2\delta_{2\diamond}^2\\
&-\left(\frac{68}{9}+4D\right)\delta_{1\diamond}^2\delta_{2\diamond}\delta_{3\diamond}+\left(\frac{37}{18}+2D+\frac{D^2}{2}-\frac{\pi^2}{24}\right)\delta_{1\diamond}\delta_{2\diamond}^3\\
&+\left(\frac{37}{6}+6D+\frac{3D^2}{2}-\frac{\pi^2}{8}\right)\delta_{1\diamond}\delta_{2\diamond}^2\delta_{3\diamond}+\left(\frac{37}{18}+2D+\frac{D^2}{2}-\frac{\pi^2}{24}\right)\delta_{1\diamond}\delta_{2\diamond}\delta_{3\diamond}^2\\
&+\left(\frac{37}{18}+2D+\frac{D^2}{2}-\frac{\pi^2}{24}\right)\delta_{1\diamond}\delta_{2\diamond}\delta_{3\diamond}\delta_{4\diamond}
\end{aligned}
\tag{2.30}
$$

One can check that the second and third order corrections match the expression already found in ref. [59]. The fourth order corrections represent a new result.

2.4 Tensor power spectrum

In this section, we repeat the previous analysis but for tensor perturbations. Since the method is the same and, fortunately, the calculations are easier, the details will be skipped. The main difference between gravity waves and density perturbations is that their effective potential is not the same, see eqs. (1.4) and (1.6). This implies that the function $\nu(\eta)$ for tensors is different from the one of the scalars. One gets for the tensor

$$
\nu^2(\eta)=\frac{9}{4}+3\epsilon_{1*}+4\epsilon_{1*}^2+4\epsilon_{1*}\epsilon_{2*}-3\epsilon_{1*}\epsilon_{2*}\ln\left(\frac{\eta}{\eta_*}\right)+\mathcal{O}\bigl(\epsilon^3\bigr)\,. \tag{2.31}
$$

As a consequence, the functions $g(\eta)$, $f(\eta)$, and hence Ψ, are also different. Using the uniform approximation to evaluate $\mu_{\boldsymbol{k}}$ and inserting the corresponding formula into the expression of $\mathcal{P}_h$ given by eq. (1.9), one obtains

$$
\begin{aligned}
\mathcal{P}_h=\frac{2\left(18\,e^{-3}\right)H_*^2}{\pi^2M_{\mathrm{Pl}}^2}\biggl[1&+\left(-\frac{8}{3}+2\ln 2\right)\epsilon_{1*}+\left(\frac{\pi^2}{12}-\frac{26}{9}+\frac{8}{3}\ln 2-\ln^2 2\right)\epsilon_{1*}\epsilon_{2*}\\
&+\left(\frac{13}{9}-\frac{10}{3}\ln 2+2\ln^2 2\right)\epsilon_{1*}^2\biggr].
\end{aligned}
\tag{2.32}
$$

This equation is for the tensors what eq. (2.24) is for the scalars. As explained before, one has still to make explicit the scale dependence hidden in η_*. In the case of tensors, the pivot point is usually defined by $k_\star\eta_\star=-1$ since gravity waves propagate at the speed of light. This leads to the following expression for the power spectrum

$$
\begin{aligned}
\mathcal{P}_h=\frac{2\left(18\,e^{-3}\right)H_\star^2}{\pi^2M_{\mathrm{Pl}}^2}\biggl\{1&-2(1+D)\epsilon_{1\star}+\left(\frac{17}{9}+2D+2D^2\right)\epsilon_{1\star}^2+\left(-\frac{19}{9}+\frac{\pi^2}{12}\right.\\
&\left.-2D-D^2\right)\epsilon_{1\star}\epsilon_{2\star}+\left[-2\epsilon_{1\star}+2(1+2D)\epsilon_{1\star}^2-2(1+D)\epsilon_{1\star}\epsilon_{2\star}\right]\ln\frac{k_\star}{k}\\
&+\left(2\epsilon_{1\star}^2-\epsilon_{1\star}\epsilon_{2\star}\right)\ln^2\frac{k_\star}{k}\biggr\}.
\end{aligned}
\tag{2.33}
$$

JCAP06(2013)021

Let us notice that, in order to obtain this relationship, we have used the initial conditions for gravity waves $|B_{\boldsymbol{k}}| = 1/M_{\rm Pl}^2$. Otherwise, one notices the presence of the WKB factor $18\,e^3$ and one can check that, at first order, it coincides with the known expression for the tensor power spectrum. The above formula, being expressed at the time $\eta_\star$, is convenient for SFMK models only, but not for k-inflation. Indeed, all parameters here are functions evaluated at the time $\eta_\star$ which is different that the one at which the scalar power spectrum is calculated, namely $\eta_\diamond$. It has become a common mistake to try fitting data with both eq. (2.28) and eq. (2.33) while implicitly assuming that all Hubble and sound flow "parameters" are the same. As we have explicitly shown before, they do differ and such a fit would absolutely make no sense.

However, within slow-roll, one can re-express the tensor power spectrum at the same pivot point as for the scalar power spectrum. As before, each quantity in the tensor power spectrum should be re-expressed at the scalar pivot point, as for instance $\epsilon_{1\star} = \epsilon_{1\diamond} - \epsilon_{1\diamond}\epsilon_{2\diamond}\ln c_{\rm s\diamond} + \mathcal{O}\big(\epsilon^3, \delta^3\big)$. The quantity $c_{\rm s\diamond}$ appears because it is present in the ratio of the tensor to scalar pivot points. It follows that the final expression for the tensor power spectrum for k-inflation is

$$\begin{aligned}\mathcal{P}_h = \frac{2\left(18e^{-3}\right)H_\diamond^2}{\pi^2 M_{\rm Pl}^2}\Bigg\{1 - 2(1+D-\ln c_{\rm s\diamond})\epsilon_{1\diamond} + \Bigg[\frac{17}{9} + 2D + 2D^2 + 2\ln^2 c_{\rm s\diamond} \\ - 2(1+2D)\ln c_{\rm s\diamond}\Bigg]\epsilon_{1\diamond}^2 + \left[-\frac{19}{9} + \frac{\pi^2}{12} - 2D - D^2 + 2(1+D)\ln c_{\rm s\diamond} - \ln^2 c_{\rm s\diamond}\right]\epsilon_{1\diamond}\epsilon_{2\diamond} \\ + \left[-2\epsilon_{1\diamond} + (2 + 4D - 4\ln c_{\rm s\diamond})\epsilon_{1\diamond}^2 + (-2 - 2D + 2\ln c_{\rm s\diamond})\epsilon_{1\diamond}\epsilon_{2\diamond}\right]\ln\frac{k_\diamond}{k} \\ + \left(2\epsilon_{1\diamond}^2 - \epsilon_{1\diamond}\epsilon_{2\diamond}\right)\ln^2\frac{k_\diamond}{k}\Bigg\},\end{aligned} \tag{2.34}$$

where now "diamonded" terms are evaluated at the scalar pivot point. This new formula is the second main result of the present paper. It extends to second order the results of ref. [59]. As for the scalar modes, this expression also allows us to calculate the tensor spectral index at third order. One obtains

$$\begin{aligned}n_{\rm T} = -2\epsilon_{1\diamond} - 2\epsilon_{1\diamond}^2 + (-2 - 2D + 2\ln c_{\rm s\diamond})\,\epsilon_{1\diamond}\epsilon_{2\diamond} - 2\epsilon_{1\diamond}^3 + \left(-\frac{38}{9} - 6D + 6\ln c_{\rm s\diamond}\right)\epsilon_{1\diamond}^2\epsilon_{2\diamond} \\ + \left(-\frac{19}{9} - 2D - D^2 + \frac{\pi^2}{12} + 2\ln c_{\rm s\diamond} + 2D\ln c_{\rm s\diamond} - \ln^2 c_{\rm s\diamond}\right)\epsilon_{1\diamond}\epsilon_{2\diamond}^2 \\ + \left(-\frac{19}{9} - 2D - D^2 + \frac{\pi^2}{12} + 2\ln c_{\rm s\diamond} + 2D\ln c_{\rm s\diamond} - \ln^2 c_{\rm s\diamond}\right)\epsilon_{1\diamond}\epsilon_{2\diamond}\epsilon_{3\diamond}\end{aligned} \tag{2.35}$$

Of course, at first order, one recovers the standard formula, $n_{\rm T} = -2\epsilon_{1\diamond}$. We have already discussed before the relevance of higher order corrections for Bayesian parameter estimation. Notice that, in the case of primordial gravitational waves and as discussed in ref. [67], another motivation is the possibility of detecting them directly. Indeed, in that case, one needs to estimate their power spectrum today and, due to the very large lever arm between the cosmological scales and the smaller scales where a direct detection can be performed, it is necessay to calculate the power spectrum at the end of inflation very precisely. In this context, higher order corrections become mandatory. Similarly, the running of the tensors is

JCAP06(2013)021

obtained at fourth order and reads

$$\begin{aligned}\alpha_{\rm T} = &-2\epsilon_{1\diamond}\epsilon_{2\diamond} - 6\epsilon_{1\diamond}^2\epsilon_{2\diamond} + (-2-2D+2\ln c_{\rm s\diamond})\epsilon_{1\diamond}\epsilon_{2\diamond}^2 + (-2-2D+2\ln c_{\rm s\diamond})\epsilon_{1\diamond}\epsilon_{2\diamond}\epsilon_{3\diamond}\\ &- 12\epsilon_{1\diamond}^3\epsilon_{2\diamond} + \left(-\frac{112}{9} - 14D + 14\ln c_{\rm s\diamond}\right)\epsilon_{1\diamond}^2\epsilon_{2\diamond}^2 + \left(-\frac{56}{9} - 8D + 8\ln c_{\rm s\diamond}\right)\epsilon_{1\diamond}^2\epsilon_{2\diamond}\epsilon_{3\diamond}\\ &+ \left[-\frac{19}{9} - 2D - D^2 + \frac{\pi^2}{12} + 2(1+D)\ln c_{\rm s\diamond} - \ln^2 c_{\rm s\diamond}\right]\left(\epsilon_{1\diamond}\epsilon_{2\diamond}^3 + 3\epsilon_{1\diamond}\epsilon_{2\diamond}^2\epsilon_{3\diamond}\right.\\ &\left.+\epsilon_{1\diamond}\epsilon_{2\diamond}\epsilon_{3\diamond}^2 + \epsilon_{1\diamond}\epsilon_{2\diamond}\epsilon_{3\diamond}\epsilon_{4\diamond}\right).\end{aligned} \tag{2.36}$$

Finally, one can also deduce the tensor to scalar ratio at the third order. It reads

$$\begin{aligned}r = &\,16\epsilon_{1\diamond}c_{\rm s\diamond}\left[1 + 2\epsilon_{1\diamond}\ln c_{\rm s\diamond} + D\epsilon_{2\diamond} - (2+D)\,\delta_{1\diamond} + \left(\frac{34}{9} + 3D + \frac{D^2}{2}\right)\delta_{1\diamond}^2\right.\\ &+ \left(-\frac{37}{18} - 2D - \frac{D^2}{2} + \frac{\pi^2}{24}\right)\delta_{1\diamond}\delta_{2\diamond} - \left(\frac{5}{9} + 3D + D^2\right)\delta_{1\diamond}\epsilon_{2\diamond} + \left(-\frac{2}{9} + \frac{D^2}{2}\right)\epsilon_{2\diamond}^2\\ &+ \frac{1}{72}\left(4 + 36D^2 - 3\pi^2\right)\epsilon_{2\diamond}\epsilon_{3\diamond} + 2\epsilon_{1\diamond}^2\left(1+\ln c_{\rm s\diamond}\right)\ln c_{\rm s\diamond}\\ &+ \left(-\frac{28}{9} - 3D - 4\ln c_{\rm s\diamond} - 2D\ln c_{\rm s\diamond}\right)\delta_{1\diamond}\epsilon_{1\diamond}\\ &\left.+ \left(-\frac{8}{9} + D + 2\ln c_{\rm s\diamond} + 4D\ln c_{\rm s\diamond} - \ln^2 c_{\rm s\diamond}\right)\epsilon_{1\diamond}\epsilon_{2\diamond}\right].\end{aligned} \tag{2.37}$$

As usual the leading term is proportional to $\epsilon_{1\diamond}c_{\rm s\diamond}$ and the above formula shows that the corresponding corrections depend on the flow parameters but also on the sound speed.

3 Discussion and conclusions

The power spectra of eqs. (2.28) and (2.34) represent the main result of this article. There are the first calculation, at second order in the Hubble and sound flow functions, of the scalar and tensor power spectra in k-inflation within the uniform approximation. In this section, we discuss our results and check their consistency. In particular, in some limits, our calculation should reproduce known results already derived in the literature. As we show below, this is indeed the case.

We have seen before that the power spectrum is obtained as an expansion around the pivot scale and that the most general expression of $\mathcal{P}_\zeta$ can be written as

$$\mathcal{P}_\zeta(k) = \tilde{\mathcal{P}}_\zeta(k_\diamond)\sum_{n\geq 0}\frac{a_n}{n!}\ln^n\frac{k}{k_\diamond}, \tag{3.1}$$

where $\tilde{\mathcal{P}}_\zeta$ is the overall amplitude and the coefficients a_n are functions of the horizon flow parameters. The expression of a_n always starts at order n, i.e. a_0 starts with one, a_1 starts with a term of order $\mathcal{O}(\epsilon,\delta)$, a_2 with a term of order $\mathcal{O}\left(\epsilon^2,\delta^2,\epsilon\delta\right)$ and so on. As already mentioned before, k-inflationary power spectra were determined at first order in ref. [59]. This means that the expression found in that paper included only the first two terms, proportional to a_0 and a_1. There is however a trick derived in ref. [68] which allows us to determine some

JCAP06(2013)021

higher order terms. Indeed, the power spectrum should not depend on the choice of the pivot scale, which is arbitrary. As a consequence, one can establish the following recursion relation

$$a_{n+1} = \frac{\mathrm{d}\ln\tilde{\mathcal{P}}_\zeta}{\mathrm{d}\ln k_\diamond} a_n + \frac{\mathrm{d}a_n}{\mathrm{d}\ln k_\diamond}\,. \tag{3.2}$$

Given that a_0 was given at first order in ref. [59], it was then possible to calculate a_1 up to second order and a_2 to third order [see eqs. (64) and (65) in that reference]. Therefore, one can compare those formulas to the expression obtained in this article. One finds that they are the same, indicating the consistency of our results.

Another way to verify the validity of our expressions is to take the limit $c_\mathrm{s} = 1$ and to compare the resulting formulas to the results already obtained in the literature for SFMK models. As mentioned in the introduction, second order results were first obtained using the Green function method in ref. [47]. The corresponding expression for the scalar power spectrum reads

$$\begin{aligned}\mathcal{P}_\zeta = \frac{H^2}{8\pi^2 M_\mathrm{Pl}^2\epsilon_1}\Bigg\{&1 - 2(C+1)\epsilon_1 - C\epsilon_2 + \left(2C^2 + 2C + \frac{\pi^2}{2} - 5\right)\epsilon_1^2 \\ &+ \left(C^2 - C + \frac{7\pi^2}{12} - 7\right)\epsilon_1\epsilon_2 + \left(\frac{C^2}{2} + \frac{\pi^2}{8} - 1\right)\epsilon_2^2 + \left(-\frac{C^2}{2} + \frac{\pi^2}{24}\right)\epsilon_2\epsilon_3 \\ &+ \left[-2\epsilon_1 - \epsilon_2 + 2(2C+1)\epsilon_1^2 + (2C-1)\epsilon_1\epsilon_2 + C\epsilon_2^2 - C\epsilon_2\epsilon_3\right]\ln\frac{k}{k_\circledast} \\ &+ \left(2\epsilon_1^2 + \epsilon_2\epsilon_2 + \frac{1}{2}\epsilon_2^2 - \frac{1}{2}\epsilon_2\epsilon_3\right)\ln^2\frac{k}{k_\circledast}\Bigg\},\end{aligned} \tag{3.3}$$

where the constant C is defined by $C \equiv \gamma + \ln 2 - 2 \simeq -0.7296$, γ being the Euler constant, while the expression of the gravity wave power spectrum can be written as

$$\begin{aligned}\mathcal{P}_h = \frac{2H^2}{\pi^2 M_\mathrm{Pl}^2}\Bigg\{&1 - 2(C+1)\epsilon_1 + \left(2C^2 + 2C + \frac{\pi^2}{2} - 5\right)\epsilon_1^2 + \left(-C^2 - 2C + \frac{\pi^2}{12} - 2\right)\epsilon_1\epsilon_2 \\ &+ \left[-2\epsilon_1 + 2(2C+1)\epsilon_1^2 - 2(C+1)\epsilon_1\epsilon_2\right]\ln\frac{k}{k_\circledast} + \left(2\epsilon_1^2 - \epsilon_1\epsilon_2\right)\ln^2\frac{k}{k_\circledast}\Bigg\}.\end{aligned} \tag{3.4}$$

In the two previous formulas (3.3) and (3.4), the Hubble flow functions are evaluated at time $\eta_\circledast$ such that $a(\eta_\circledast)H(\eta_\circledast) = k_\circledast$ which slightly differs from the time $k_\diamond\eta_\diamond = -1$ (for $c_{\mathrm{s}\diamond} = 1$) used in the present paper. Therefore, if we want to compare eqs. (2.28) and (2.34) with $c_{\mathrm{s}\diamond} = 1$ to eqs. (3.3) and (3.4), one should first re-express the latter in terms of the Hubble flow parameters evaluated at time $k_\diamond\eta_\diamond = -1$. In the following, in order to simplify the discussion, we focus only on the scalar case but the tensor case could be treated in the same manner. From the definition of $\eta_\circledast$ one has $\eta_\circledast/\eta_\diamond = 1 + \epsilon_{1\diamond} + \epsilon_{1\diamond}^2 + \epsilon_{1\diamond}\epsilon_{2\diamond} + \mathcal{O}(\epsilon^3)$. As consequence, in eqs. (3.3) and (3.4), one should just replace ϵ_1, ϵ_2 with $\epsilon_{1\diamond}$, $\epsilon_{2\diamond}$ and H^2/ϵ_1

JCAP06(2013)021

with $H_\diamond^2/\epsilon_{1\diamond}(1+2\epsilon_{1\diamond}^2+\epsilon_{1\diamond}\epsilon_{2\diamond})$. This yields the following expression

$$\mathcal{P}_\zeta = \frac{H_\diamond^2}{8\pi^2 M_{\rm Pl}^2\epsilon_{1\diamond}}\Bigg\{1-2(C+1)\epsilon_{1\diamond}-C\epsilon_{2\diamond}+\left(2C^2+2C+\frac{\pi^2}{2}-3\right)\epsilon_{1\diamond}^2 + \left(C^2-C+\frac{7\pi^2}{12}-6\right)\epsilon_{1\diamond}\epsilon_{2\diamond}+\left(\frac{C^2}{2}+\frac{\pi^2}{8}-1\right)\epsilon_{2\diamond}^2+\left(-\frac{C^2}{2}+\frac{\pi^2}{24}\right)\epsilon_{2\diamond}\epsilon_{3\diamond} + \left[-2\epsilon_{1\diamond}-\epsilon_{2\diamond}+2(2C+1)\epsilon_{1\diamond}^2+(2C-1)\epsilon_{1\diamond}\epsilon_{2\diamond}+C\epsilon_{2\diamond}^2-C\epsilon_{2\diamond}\epsilon_{3\diamond}\right]\ln\frac{k}{k_\diamond} + \left(2\epsilon_{1\diamond}^2+\epsilon_{1\diamond}\epsilon_{2\diamond}+\frac{1}{2}\epsilon_{2\diamond}^2-\frac{1}{2}\epsilon_{2\diamond}\epsilon_{3\diamond}\right)\ln^2\frac{k}{k_\diamond}\Bigg\}, \tag{3.5}$$

that can be now compared to eq. (2.28). As already discussed, the overall amplitude differs by the WKB factor $18\,e^{-3}$. We also notice that the terms in D in eq. (2.28) exactly corresponds to the term in C in eq. (3.5). For instance, the coefficient of $\epsilon_{1\diamond}^2$ in eq. (2.28) contains a term $2D^2+2D$ while the coefficient of $\epsilon_{1\diamond}^2$ in eq. (3.5) contains a $2C^2+2C$. One easily checks that this is the rule for all first and second order terms. Provided one substitutes D with C, the first order term in the amplitude, the coefficient of $\ln k/k_\diamond$ and the coefficient of $\ln^2(k/k_\diamond)$ are identical. The only difference appears in the second order terms in the amplitude. For instance, the coefficients of $\epsilon_{1\diamond}^2$ in eq. (2.28) is $2D^2+2D+17/9$ while it is $2C^2+2C+\pi^2/2-3$ in eq. (3.5). But $17/9\simeq 1.88$ and $\pi^2/2-3\simeq 1.93$ and, therefore, the two terms are in fact numerically very close. The same is true for all the other terms in the amplitude. Therefore, we conclude that our result (2.28), specialized to SFMK models, is fully consistent with eq. (3.5) that comes from another approximation scheme. This confirms its validity.

Let us now compare our result to the one of refs. [53, 54] calculated with the help of the WKB approximation. The scalar power spectrum obtained in those articles reads

$$\mathcal{P}_\zeta = \frac{H^2}{8\pi^2 M_{\rm Pl}^2\epsilon_1}A_{\rm WKB}\Bigg\{1-2(D_{\rm WKB}+1)\epsilon_1-D_{\rm WKB}\epsilon_2+\left(2D_{\rm WKB}^2+2D_{\rm WKB}-\frac{1}{9}\right)\epsilon_1^2 + \left(D_{\rm WKB}^2-D_{\rm WKB}+\frac{\pi^2}{12}-\frac{20}{9}\right)\epsilon_1\epsilon_2+\left(\frac{D_{\rm WKB}^2}{2}+\frac{2}{9}\right)\epsilon_2^2+\left(-\frac{D_{\rm WKB}^2}{2}+\frac{\pi^2}{24}-\frac{1}{18}\right)\epsilon_2\epsilon_3 + \left[-2\epsilon_1-\epsilon_2+2(2D_{\rm WKB}+1)\epsilon_1^2+(2D_{\rm WKB}-1)\epsilon_1\epsilon_2+D_{\rm WKB}\epsilon_2^2-D_{\rm WKB}\epsilon_2\epsilon_3\right]\ln\frac{k}{k_\circledast} + \left(2\epsilon_1^2+\epsilon_1\epsilon_2+\frac{1}{2}\epsilon_2^2-\frac{1}{2}\epsilon_2\epsilon_3\right)\ln^2\frac{k}{k_\circledast}\Bigg\}, \tag{3.6}$$

while the tensor power spectrum is given by the following formula

$$\mathcal{P}_h = \frac{2H^2}{\pi^2 M_{\rm Pl}^2}A_{\rm WKB}\Bigg\{1-2(D_{\rm WKB}+1)\epsilon_1+\left(2D_{\rm WKB}^2+2D_{\rm WKB}-\frac{1}{9}\right)\epsilon_1^2+\left(-D_{\rm WKB}^2-2D_{\rm WKB} + \frac{\pi^2}{12}-\frac{19}{9}\right)\epsilon_1\epsilon_2+\left[-2\epsilon_1+2(2D_{\rm WKB}+1)\epsilon_1^2-2(D_{\rm WKB}+1)\epsilon_1\epsilon_2\right]\ln\frac{k}{k_\circledast} + \left(2\epsilon_1^2-\epsilon_1\epsilon_2\right)\ln^2\frac{k}{k_\circledast}\Bigg\}. \tag{3.7}$$

JCAP06(2013)021

In these equations, $A_{\rm WKB} = 18\,e^{-3}$ and $D_{\rm WKB} = 1/3 - \ln 3$, that is to say exactly what was found by means of the uniform approximation as $D_{\rm WKB} = D$. As already mentioned, refs. [53, 54] have shown that, by taking the next order in the adiabatic approximation into account, one obtains a new value for these two constants (in some sense, they are renormalized), namely $A_{\rm WKB}$ becomes $361/(18\,e^3) \simeq 0.99$ and $D_{\rm WKB} = 7/19 - \ln 3 \simeq -0.7302$. In particular, the new value of $D_{\rm WKB}$ is closer to the constant C than the non-renormalized one. Both eqs. (3.6) and (3.7) are evaluated at the pivot time $\eta_{\circledast}$ and have to be time-shifted to $\eta_\diamond$ to be compared with our results. Proceeding as previously, it is easy to show that this modifies the coefficients of ϵ_1^2 which now becomes $2D_{\rm WKB}^2 + 2D_{\rm WKB} + 17/9$, and the coefficient of $\epsilon_1\epsilon_2$ which becomes $2D_{\rm WKB}^2 - D_{\rm WKB} + \pi^2/12 - 11/9$. In other words eqs. (2.28) and eq. (3.6) expressed at $\eta_\diamond$ are exactly the same for $c_{\rm s\diamond} = 1$. This is maybe not so surprising considering the fact that the WKB and uniform approximations are closely related methods.

A few words are in order about ref. [55]. Historically, this is probably the first paper that attempted to evaluate the k-inflationary power spectrum at second order in some equivalent of the Hubble and sound flow functions used here. The method chosen is the Green function expansion discussed before. However, a specific form for the sound speed, which in the language of the present paper would be a first order approximation of $c_{\rm s}^2$, was also postulated. Together with a $k-$dependence kept implicit, this makes the comparison with the present work difficult. For this reason, we do not investigate further this issue.

To conclude, let us briefly recap our main result and discuss directions for future works. In this paper, using the uniform approximation, we have calculated the scalar and tensor power spectra in k-inflation, at second order in the Hubble and sound flow parameters, see eqs. (2.28) and (2.34). We have carefully checked that, in the various limits where our calculation reduces to known cases, consistent results are obtained. The next step is clearly to use these power spectra in order to constrain the values of the Hubble and sound flow parameters using CMB observations. This was done in ref. [62] but only for the first order power spectra (since only this result was available at that time). Given the on-going flux of high precision data, such as those from the Planck satellite, the results obtained in this article should be important to keep theoretical uncertainties at a minimal level. In this way, as discussed in the introduction, one may hope to obtain unprecedented information on the inflationary scenario.

References

[1] A.A. Starobinsky, *A New Type of Isotropic Cosmological Models Without Singularity*, *Phys. Lett.* **B 91** (1980) 99 [INSPIRE].

[2] A.H. Guth, *The Inflationary Universe: A Possible Solution to the Horizon and Flatness Problems*, *Phys. Rev.* **D 23** (1981) 347 [INSPIRE].

[3] P. Peter and J.-P. Uzan, *Primordial cosmology*. Oxford University Press, U.K. (2013).

[4] J. Martin, *Inflation and precision cosmology*, *Braz. J. Phys.* **34** (2004) 1307 [astro-ph/0312492] [INSPIRE].

[5] J. Martin, *Inflationary cosmological perturbations of quantum-mechanical origin*, *Lect. Notes Phys.* **669** (2005) 199 [hep-th/0406011] [INSPIRE].

[6] J. Martin, *Inflationary perturbations: The Cosmological Schwinger effect*, *Lect. Notes Phys.* **738** (2008) 193 [arXiv:0704.3540] [INSPIRE].

[7] L. Sriramkumar, *An introduction to inflation and cosmological perturbation theory*, arXiv:0904.4584 [INSPIRE].

JCAP06(2013)021

[8] Supernova Search Team collaboration, J.L. Tonry et al., *Cosmological results from high-z supernovae*, *Astrophys. J.* **594** (2003) 1 [astro-ph/0305008] [INSPIRE].

[9] Supernova Search Team collaboration, A.G. Riess et al., *Type Ia supernova discoveries at $z > 1$ from the Hubble Space Telescope: Evidence for past deceleration and constraints on dark energy evolution*, *Astrophys. J.* **607** (2004) 665 [astro-ph/0402512] [INSPIRE].

[10] A.G. Riess, L.-G. Strolger, S. Casertano, H.C. Ferguson, B. Mobasher et al., *New Hubble Space Telescope Discoveries of Type Ia Supernovae at z >=1: Narrowing Constraints on the Early Behavior of Dark Energy*, *Astrophys. J.* **659** (2007) 98 [astro-ph/0611572] [INSPIRE].

[11] SDSS collaboration, J.K. Adelman-McCarthy et al., *The Sixth Data Release of the Sloan Digital Sky Survey*, *Astrophys. J. Suppl.* **175** (2008) 297 [arXiv:0707.3413] [INSPIRE].

[12] SDSS collaboration, K.N. Abazajian et al., *The Seventh Data Release of the Sloan Digital Sky Survey*, *Astrophys. J. Suppl.* **182** (2009) 543 [arXiv:0812.0649] [INSPIRE].

[13] D. Larson, J. Dunkley, G. Hinshaw, E. Komatsu, M. Nolta et al., *Seven-Year Wilkinson Microwave Anisotropy Probe (WMAP) Observations: Power Spectra and WMAP-Derived Parameters*, *Astrophys. J. Suppl.* **192** (2011) 16 [arXiv:1001.4635] [INSPIRE].

[14] WMAP collaboration, E. Komatsu et al., *Seven-Year Wilkinson Microwave Anisotropy Probe (WMAP) Observations: Cosmological Interpretation*, *Astrophys. J. Suppl.* **192** (2011) 18 [arXiv:1001.4538] [INSPIRE].

[15] A.G. Riess, L. Macri, S. Casertano, H. Lampeitl, H.C. Ferguson et al., *A 3% Solution: Determination of the Hubble Constant with the Hubble Space Telescope and Wide Field Camera 3*, *Astrophys. J.* **730** (2011) 119 [*Erratum ibid.* **732** (2011) 129] [arXiv:1103.2976] [INSPIRE].

[16] WMAP collaboration, G. Hinshaw et al., *Nine-Year Wilkinson Microwave Anisotropy Probe (WMAP) Observations: Cosmological Parameter Results*, arXiv:1212.5226 [INSPIRE].

[17] C. Bennett, D. Larson, J. Weiland, N. Jarosik, G. Hinshaw et al., *Nine-Year Wilkinson Microwave Anisotropy Probe (WMAP) Observations: Final Maps and Results*, arXiv:1212.5225 [INSPIRE].

[18] Z. Hou, C. Reichardt, K. Story, B. Follin, R. Keisler et al., *Constraints on Cosmology from the Cosmic Microwave Background Power Spectrum of the 2500-square degree SPT-SZ Survey*, arXiv:1212.6267 [INSPIRE].

[19] K. Story, C. Reichardt, Z. Hou, R. Keisler, K. Aird et al., *A Measurement of the Cosmic Microwave Background Damping Tail from the 2500-square-degree SPT-SZ survey*, arXiv:1210.7231 [INSPIRE].

[20] J.L. Sievers, R.A. Hlozek, M.R. Nolta, V. Acquaviva, G.E. Addison et al., *The Atacama Cosmology Telescope: Cosmological parameters from three seasons of data*, arXiv:1301.0824 [INSPIRE].

[21] J. Dunkley, E. Calabrese, J. Sievers, G. Addison, N. Battaglia et al., *The Atacama Cosmology Telescope: likelihood for small-scale CMB data*, arXiv:1301.0776 [INSPIRE].

[22] Planck collaboration, J.-M. Lamarre et al., *Planck pre-launch status: The HFI instrument, from specification to actual performance*, *Astron. Astrophys.* **520** (2010) A9.

[23] J.D. Barrow and A.R. Liddle, *Can inflation be falsified?*, *Gen. Rel. Grav.* **29** (1997) 1503 [gr-qc/9705048] [INSPIRE].

[24] J. Martin and C. Ringeval, *Inflation after WMAP3: Confronting the Slow-Roll and Exact Power Spectra to CMB Data*, *JCAP* **08** (2006) 009 [astro-ph/0605367] [INSPIRE].

[25] R. Bean, X. Chen, H. Peiris and J. Xu, *Comparing Infrared Dirac-Born-Infeld Brane Inflation to Observations*, *Phys. Rev.* **D 77** (2008) 023527 [arXiv:0710.1812] [INSPIRE].

[26] L. Lorenz, J. Martin and C. Ringeval, *Brane inflation and the WMAP data: A Bayesian analysis*, *JCAP* **04** (2008) 001 [arXiv:0709.3758] [INSPIRE].

JCAP06(2013)021

[27] J. Martin and C. Ringeval, *First CMB Constraints on the Inflationary Reheating Temperature*, *Phys. Rev.* **D 82** (2010) 023511 [arXiv:1004.5525] [INSPIRE].

[28] J. Martin, C. Ringeval and R. Trotta, *Hunting Down the Best Model of Inflation with Bayesian Evidence*, *Phys. Rev.* **D 83** (2011) 063524 [arXiv:1009.4157] [INSPIRE].

[29] R. Easther and H.V. Peiris, *Bayesian Analysis of Inflation II: Model Selection and Constraints on Reheating*, *Phys. Rev.* **D 85** (2012) 103533 [arXiv:1112.0326] [INSPIRE].

[30] C. Ringeval, *The exact numerical treatment of inflationary models*, *Lect. Notes Phys.* **738** (2008) 243 [astro-ph/0703486] [INSPIRE].

[31] D.K. Hazra, L. Sriramkumar and J. Martin, *BINGO: A code for the efficient computation of the scalar bi-spectrum*, *JCAP* **05** (2013) 026 [arXiv:1201.0926] [INSPIRE].

[32] E.D. Stewart and D.H. Lyth, *A More accurate analytic calculation of the spectrum of cosmological perturbations produced during inflation*, *Phys. Lett.* **B 302** (1993) 171 [gr-qc/9302019] [INSPIRE].

[33] A. Gangui, F. Lucchin, S. Matarrese and S. Mollerach, *The Three point correlation function of the cosmic microwave background in inflationary models*, *Astrophys. J.* **430** (1994) 447 [astro-ph/9312033] [INSPIRE].

[34] A. Gangui, *NonGaussian effects in the cosmic microwave background from inflation*, *Phys. Rev.* **D 50** (1994) 3684 [astro-ph/9406014] [INSPIRE].

[35] A. Gangui and J. Martin, *Cosmic microwave background bispectrum and slow roll inflation*, *Mon. Not. Roy. Astron. Soc.* **313** (2000) 323 [astro-ph/9908009] [INSPIRE].

[36] L.-M. Wang and M. Kamionkowski, *The Cosmic microwave background bispectrum and inflation*, *Phys. Rev.* **D 61** (2000) 063504 [astro-ph/9907431] [INSPIRE].

[37] J.M. Maldacena, *Non-Gaussian features of primordial fluctuations in single field inflationary models*, *JHEP* **05** (2003) 013 [astro-ph/0210603] [INSPIRE].

[38] X. Chen, M.-x. Huang, S. Kachru and G. Shiu, *Observational signatures and non-Gaussianities of general single field inflation*, *JCAP* **01** (2007) 002 [hep-th/0605045] [INSPIRE].

[39] C. Armendariz-Picon, T. Damour and V.F. Mukhanov, *k-inflation*, *Phys. Lett.* **B 458** (1999) 209 [hep-th/9904075] [INSPIRE].

[40] J. Garriga and V.F. Mukhanov, *Perturbations in k-inflation*, *Phys. Lett.* **B 458** (1999) 219 [hep-th/9904176] [INSPIRE].

[41] C. Cheung, P. Creminelli, A.L. Fitzpatrick, J. Kaplan and L. Senatore, *The Effective Field Theory of Inflation*, *JHEP* **03** (2008) 014 [arXiv:0709.0293] [INSPIRE].

[42] D. Baumann, L. Senatore and M. Zaldarriaga, *Scale-Invariance and the Strong Coupling Problem*, *JCAP* **05** (2011) 004 [arXiv:1101.3320] [INSPIRE].

[43] V.F. Mukhanov, *Gravitational Instability of the Universe Filled with a Scalar Field*, *JETP Lett.* **41** (1985) 493 [INSPIRE].

[44] V.F. Mukhanov, *Quantum Theory of Gauge Invariant Cosmological Perturbations*, *Sov. Phys. JETP* **67** (1988) 1297 [INSPIRE].

[45] A.A. Starobinsky, *Relict Gravitation Radiation Spectrum and Initial State of the Universe. (In Russian)*, *JETP Lett.* **30** (1979) 682 [INSPIRE].

[46] F. Lucchin and S. Matarrese, *Power Law Inflation*, *Phys. Rev.* **D 32** (1985) 1316 [INSPIRE].

[47] J.-O. Gong and E.D. Stewart, *The Density perturbation power spectrum to second order corrections in the slow roll expansion*, *Phys. Lett.* **B 510** (2001) 1 [astro-ph/0101225] [INSPIRE].

[48] J. Martin and D.J. Schwarz, *WKB approximation for inflationary cosmological perturbations*, *Phys. Rev.* **D 67** (2003) 083512 [astro-ph/0210090] [INSPIRE].

JCAP06(2013)021

[49] S. Habib, K. Heitmann, G. Jungman and C. Molina-Paris, *The Inflationary perturbation spectrum*, *Phys. Rev. Lett.* **89** (2002) 281301 [astro-ph/0208443] [INSPIRE].

[50] S. Habib, A. Heinen, K. Heitmann, G. Jungman and C. Molina-Paris, *Characterizing inflationary perturbations: The Uniform approximation*, *Phys. Rev.* **D 70** (2004) 083507 [astro-ph/0406134] [INSPIRE].

[51] D.J. Schwarz, C.A. Terrero-Escalante and A.A. Garcia, *Higher order corrections to primordial spectra from cosmological inflation*, *Phys. Lett.* **B 517** (2001) 243 [astro-ph/0106020] [INSPIRE].

[52] S.M. Leach, A.R. Liddle, J. Martin and D.J. Schwarz, *Cosmological parameter estimation and the inflationary cosmology*, *Phys. Rev.* **D 66** (2002) 023515 [astro-ph/0202094] [INSPIRE].

[53] R. Casadio, F. Finelli, M. Luzzi and G. Venturi, *Improved WKB analysis of cosmological perturbations*, *Phys. Rev.* **D 71** (2005) 043517 [gr-qc/0410092] [INSPIRE].

[54] R. Casadio, F. Finelli, M. Luzzi and G. Venturi, *Higher order slow-roll predictions for inflation*, *Phys. Lett.* **B 625** (2005) 1 [gr-qc/0506043] [INSPIRE].

[55] H. Wei, R.-G. Cai and A. Wang, *Second-order corrections to the power spectrum in the slow-roll expansion with a time-dependent sound speed*, *Phys. Lett.* **B 603** (2004) 95 [hep-th/0409130] [INSPIRE].

[56] S.E. Shandera and S.-H.H. Tye, *Observing brane inflation*, *JCAP* **05** (2006) 007 [hep-th/0601099] [INSPIRE].

[57] R. Bean, S.E. Shandera, S.H. Henry Tye and J. Xu, *Comparing brane inflation to WMAP*, *JCAP* **05** (2007) 004 [hep-th/0702107] [INSPIRE].

[58] H.V. Peiris, D. Baumann, B. Friedman and A. Cooray, *Phenomenology of D-brane Inflation with General Speed of Sound*, *Phys. Rev.* **D 76** (2007) 103517 [arXiv:0706.1240] [INSPIRE].

[59] L. Lorenz, J. Martin and C. Ringeval, *K-inflationary Power Spectra in the Uniform Approximation*, *Phys. Rev.* **D 78** (2008) 083513 [arXiv:0807.3037] [INSPIRE].

[60] N. Agarwal and R. Bean, *Cosmological constraints on general, single field inflation*, *Phys. Rev.* **D 79** (2009) 023503 [arXiv:0809.2798] [INSPIRE].

[61] W.H. Kinney and K. Tzirakis, *Quantum modes in DBI inflation: exact solutions and constraints from vacuum selection*, *Phys. Rev.* **D 77** (2008) 103517 [arXiv:0712.2043] [INSPIRE].

[62] L. Lorenz, J. Martin and C. Ringeval, *Constraints on Kinetically Modified Inflation from WMAP5*, *Phys. Rev.* **D 78** (2008) 063543 [arXiv:0807.2414] [INSPIRE].

[63] PLANCK Collaboration, *The Scientific Program of Planck*, http://www.sciops.esa.int.

[64] J.-P. Bruneton, *On causality and superluminal behavior in classical field theories: Applications to k-essence theories and MOND-like theories of gravity*, *Phys. Rev.* **D 75** (2007) 085013 [gr-qc/0607055] [INSPIRE].

[65] M. Alishahiha, E. Silverstein and D. Tong, *DBI in the sky*, *Phys. Rev.* **D 70** (2004) 123505 [hep-th/0404084] [INSPIRE].

[66] M. Abramowitz and I. A. Stegun, *Handbook of mathematical functions with formulas, graphs, and mathematical tables*, ninth edition, National Bureau of Standards, Washington, U.S. (1970).

[67] S. Kuroyanagi and T. Takahashi, *Higher Order Corrections to the Primordial Gravitational Wave Spectrum and its Impact on Parameter Estimates for Inflation*, *JCAP* **10** (2011) 006 [arXiv:1106.3437] [INSPIRE].

[68] D.J. Schwarz and C.A. Terrero-Escalante, *Primordial fluctuations and cosmological inflation after WMAP 1.0*, *JCAP* **08** (2004) 003 [hep-ph/0403129] [INSPIRE].

JCAP06(2013)021

4. Quantum Aspects of Inflation and the Stochastic Formalism

One of the great achievements of inflation is that, combined with quantum mechanics, it provides a convincing mechanism for the origin of the cosmological fluctuations. Such a mechanism rests on General Relativity and Quantum Mechanics, two theories that are notoriously difficult to combine, and leads to predictions that can be tested experimentally. This is why inflation is an ideal playground to discuss deep questions at the fundamental level. This second chapter aims at studying issues related to the quantum nature of the theory, and in particular the stochastic formalism which enables to address some of them.

Publications

In the standard description of inflation, the homogeneous parts of the fields are usually assumed to behave classically while the small deviations from homogeneity and isotropy are treated quantum mechanically over this classical background. To go beyond this "semi-classical" approach, it seems interesting to incorporate quantum corrections to the inflationary dynamics. The stochastic inflation formalism aims at describing such an effect, by deriving the effective action for the fields coarse-grained over length scales larger than the Hubble radius, and integrating out the sub-Hubble degrees of freedom. At the technical level, such an approach boils down to solving Langevin equations for the coarse-grained fields, in which an additional, stochastic term, is added.

These stochastic equations give rise to non trivial inflationary dynamics, especially in the case where multiple fields are present. In order to understand how the quantum diffusion can affect the observable predictions in such models, in section 4.1, Ref. [210], we study the stochastic effects in hybrid inflation, a two-field model where inflation ends due to an instability triggered

by an auxiliary "waterfall" field. In the neighbourhood of the critical point, the potential is very flat and the quantum fluctuations dominate over the classical drifts of the fields. In practice, one has to deal with two coupled Langevin equations, and solving the corresponding system, even at the perturbative level, is a difficult task. This is why we numerically addressed this problem by simulating a large number of realizations of the stochastic processes, and studied the associated probability distributions in the hybrid potential, discussing in particular the impact of the stochastic effects on the realized number of e-folds.

We then studied how these results get modified when further backreaction effects are implemented. In the original version of stochastic inflation indeed, the correlations of the noise in the Langevin equations are controlled by the amplitude of the perturbations, calculated over the classical, *i.e.* without the stochastic corrections, background. At next-to-leading order however, these stochastic corrections modify the amplification of the perturbations, hence the properties of the stochastic corrections, so on and so forth. In section 4.2, Ref. [211], we designed a recursive formalism that addresses this issue and applied it to the case of hybrid inflation. We showed that the method converges in the valley (before the critical point) but points towards an expected instability in the waterfall (after the critical point). Notably, we found that the typical dispersion of the waterfall field at the critical point is diminished, thus jeopardizing the possibility of a short transition, and we showed that the blue-tilt problem present in the hybrid model is even worsened by recursive stochastic effects.

Finally, as an illustration of how inflationary physics enables to discuss deep questions related to the nature of the quantum theory itself, in section 4.3, Ref. [138], we addressed the issue of the quantum-to-classical transition and the quantum measurement problem in a cosmological context. We first reviewed how the quantum-to-classical transition of the cosmological perturbations is usually accounted for by the large squeezing of the quantum state of the perturbations and the phenomenon of decoherence. However, this does not explain how a specific outcome can be produced in the early Universe in the absence of any observer (referring to the Copenhagen interpretation of Quantum Mechanics). We then studied the continuous spontaneous localization (CLS) approach to quantum mechanics which attempts to solve the quantum measurement question by causing the wavefunction collapse by means of additional non-linear and stochastic terms to the Schrödinger equation. CSL is the only falsifiable solution to the quantum measurement problem proposed so far, since it makes predictions that, in some regimes, differ from standard quantum mechanics. We applied this theory to inflation, and we showed that reaching a satisfactory degree of collapse at the end of inflation requires to strongly break the almost scale invariance of the power spectrum of the scalar perturbations, at a level which is completely excluded by observations. These results illustrate the remarkable power of inflation in particular and cosmology in general to constrain new physics, in regimes complementary to what can be achieved in lab experiments. Let us mention that following our work, other authors [404] generalized our calculation to the case where the CSL strength parameter depends on physical scales through a phenomenological power law, so as to capture the CSL amplification mechanism. In particular, they showed that there exists a power index for which the problem we pointed out can be evaded.

PHYSICAL REVIEW D **85,** 043525 (2012)

Stochastic effects in hybrid inflation

Jérôme Martin* and Vincent Vennin†

Institut d'Astrophysique de Paris, UMR 7095-CNRS, Université Pierre et Marie Curie, 98bis boulevard Arago, 75014 Paris, France

(Received 2 November 2011; published 22 February 2012)

Hybrid inflation is a two-field model where inflation ends due to an instability. In the neighborhood of the instability point, the potential is very flat and the quantum fluctuations dominate over the classical motion of the inflaton and waterfall fields. In this article, we study this regime in the framework of stochastic inflation. We numerically solve the two coupled Langevin equations controlling the evolution of the fields and compute the probability distributions of the total number of e-folds and of the inflation exit point. Then, we discuss the physical consequences of our results, in particular, the question of how the quantum diffusion can affect the observable predictions of hybrid inflation.

DOI: 10.1103/PhysRevD.85.043525 PACS numbers: 98.80.Cq, 98.80.Qc

I. INTRODUCTION

Inflation is the leading scenario among the models attempting to describe the physical conditions that prevailed in the very early Universe. It consists in a phase of accelerated expansion which naturally solves the problems of the hot big bang theory [1–5] (for reviews, see Refs. [6–8]). In addition, it predicts an almost scale invariant power spectrum for the primordial cosmological fluctuations, the tiny deviations from scale invariance being related to the microphysics of inflation [9–14]. As is well known, this prediction turns out to be fully consistent with different types of astrophysical observations, among which is the measurement of the cosmic microwave background radiation (CMBR) anisotropies [15–19].

Inflation is usually driven by one or many scalar fields. In the context of general relativity, this represents the simplest mechanism to obtain the negative pressure necessary to produce an accelerated expansion. However, the physical nature of those scalar fields is presently unknown, and many different inflationary models have been suggested. The reason for such a situation originates from the fact that inflation is a high energy phenomenon. Indeed, the energy scale of inflation is somewhere between the TeV scale and the grand unified theory scale [15]. At those scales, particle physics remains elusive, and as a consequence there is presently a large variety of different inflationary scenarios.

However, given the extensions of the standard model of particle physics, notably those based on supersymmetry and supergravity, it is clear that some models appear to be more motivated and more generic than others. In particular, this is the case of hybrid inflation [20,21], which can be realized in various ways in the context of supersymmetry; see, for instance, the scenarios named F-term inflation and D-term inflation (among others) [22–25]. Hybrid inflation is a two-field model such that inflation occurs along a valley in the field space and ends by tachyonic instability along the so-called waterfall field direction. Hybrid inflation is known to lead to a blue spectrum for the fluctuations, a prediction which appears to be disfavored by the most recent observations [15]. However, it was shown recently [26–28] that, in some regions of the parameter space, a significant number of e-folds can occur in the waterfall regime. In this case, it was also demonstrated that the spectral index becomes red, which therefore implies that the model is in fact totally compatible with the data [26,27].

In the context of inflation, another interesting question is the role played by the quantum corrections [29–39]. Various works have shown that they can have a crucial impact on the inflationary dynamics. This is, for instance, the case for large field inflation if one starts inflation high enough in the potential. In this case, the quantum kicks undergone by the field can be so important that the field climbs its potential instead of rolling down it as should be the case according to the classical equations of motion. In such a situation, it is likely that one enters into a regime of eternal inflation [31,40,41].

Hybrid inflation is also a model where one expects the quantum corrections to be very important. It should be the case high in the inflationary valley but also around the critical point where the tachyonic instability is triggered [26,27,42]. The goal of this article is to investigate this last question in detail. In particular, we are interested in whether the quantum effects can significantly modify the classical dynamics and affect the observational predictions of the model.

In order to carry out our study, we use the stochastic inflation formalism [30,32–39,43,44]. It consists in modeling the quantum effects by a stochastic white noise. As a consequence, the equation describing the motion of the fields becomes a Langevin equation. As mentioned previously, hybrid inflation is a genuine two-field model, which implies that one has to deal with two coupled Langevin

*jmartin@iap.fr
†vennin@iap.fr

equations. Solving this system is a very complicated task, even if a perturbative expansion is used, as usually done in the context of single field inflation. This is the reason why, in this article, we use a numerical approach. This allows us to compute various interesting quantities such as the probability density function for the number of e-folds or for the location in field space of the end of inflation.

This article is organized as follows. In the next section, Sec. II, we review in some detail the classical behavior of the inflaton and waterfall fields. This allows us to clearly identify the region in the parameter space where a significant number of e-folds can occur during the waterfall regime. This also permits a comparison between the classical and stochastic dynamics. In Sec. III we numerically solve the two coupled Langevin equations that control the behavior of the two fields. We then use this result to compute various probability density functions, in particular, that of the number of e-folds and of the inflation exit point. Finally, in Sec. IV we summarize our main results and present our conclusions.

II. CLASSICAL REGIMES

There exist many ways to realize hybrid inflation. In this article, for simplicity, we focus on the first version studied in Ref. [20]; see also Ref. [45]. In this case, the potential in the field space (ϕ, ψ), where ϕ is the inflaton and ψ the waterfall field, is given by the following expression:

$$V(\phi, \psi) = \Lambda^4\left[\left(1 - \frac{\psi^2}{M^2}\right)^2 + \frac{\phi^2}{\mu^2} + 2\frac{\phi^2\psi^2}{\phi_c^2 M^2}\right]. \quad (1)$$

It contains four parameters (of dimension one), Λ, M, μ, and ϕ_c. The scale Λ is fixed by the Cosmic Background Explorer normalization (the other parameters being fixed). The true minimums of the potential are located at $\phi = 0$ and $\psi = \pm M$, while the instability point is given by $\phi = \phi_c$, $\psi = 0$. Along the inflationary valley, $\psi = 0$, the potential reduces to $\Lambda^4[1 + (\phi/\mu)^2]$ which shows that, in this regime, inflation cannot end by violation of the slow-roll conditions. The full hybrid inflation potential is shown in Fig. 1, where the inflationary valley is clearly visible.

In this section we study the classical behaviors of the inflaton and waterfall fields. The slow-roll equations controlling the evolution of the fields can be expressed as

$$3H^2\frac{\mathrm{d}\phi}{\mathrm{d}N} = -\frac{2\Lambda^4\phi}{\mu^2}\left(1 + \frac{2\psi^2\mu^2}{\phi_c^2 M^2}\right), \quad (2)$$

$$3H^2\frac{\mathrm{d}\psi}{\mathrm{d}N} = -\frac{4\Lambda^4}{M^2}\psi\left(\frac{\phi^2 - \phi_c^2}{\phi_c^2} + \frac{\psi^2}{M^2}\right), \quad (3)$$

where $H = \dot{a}/a$ is the Hubble parameter, $a(t)$ being the Friedman-Lemaitre-Robertson-Walker scale factor and a dot denoting a derivative with respect to cosmic time. The

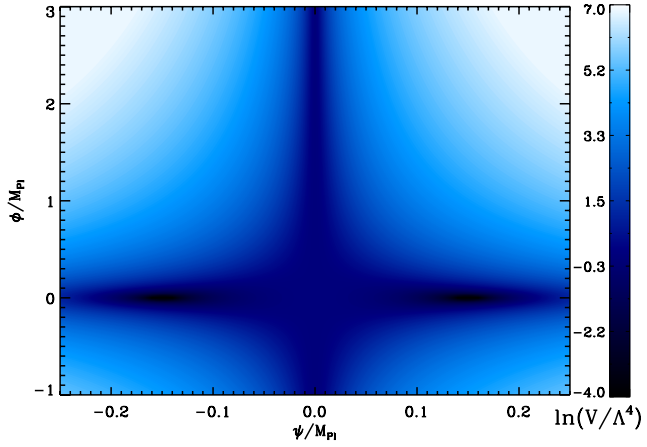

FIG. 1 (color online). Potential of hybrid inflation in the (ϕ, ψ) plane. The values of the parameters are $\mu = 3190.4 M_{\mathrm{Pl}}$, $M = \phi_c = 0.1503 M_{\mathrm{Pl}}$, with M_{Pl} being the reduced Planck mass.

quantity N is the number of e-folds, $N \equiv \ln(a/a_i)$, where a_i is the scale factor at the beginning of inflation.

In order to study the classical dynamics, it is interesting to calculate the slow-roll parameters. The hierarchy defined from the potential [46–49] is given by the following expressions:

$$\epsilon_\phi = \frac{2\phi^2 M_{\mathrm{Pl}}^2}{\mu^4}\left(1 + \frac{2\psi^2\mu^2}{\phi_c^2 M^2}\right), \quad (4)$$

$$\epsilon_\psi = \frac{8M_{\mathrm{Pl}}^2\psi^2}{M^4}\left(\frac{\phi^2 - \phi_c^2}{\phi_c^2} + \frac{\psi^2}{M^2}\right), \quad (5)$$

$$\eta_{\phi\phi} = \frac{2M_{\mathrm{Pl}}^2}{\mu^2}\left(1 + \frac{2\mu^2\psi^2}{\phi_c^2 M^2}\right), \quad (6)$$

$$\eta_{\phi\psi} = \frac{8M_{\mathrm{Pl}}^2\phi\psi}{\phi_c^2 M^2}, \quad (7)$$

$$\eta_{\psi\psi} = \frac{4M_{\mathrm{Pl}}^2}{M^2}\left(\frac{\phi^2 - \phi_c^2}{\phi_c^2} + 3\frac{\psi^2}{M^2}\right). \quad (8)$$

On the other hand, the hierarchy defined from the Hubble parameter, the so-called Hubble flow parameters [50,51], can be expressed as

$$\epsilon_{n+1} \equiv \frac{\mathrm{d}\ln|\epsilon_n|}{\mathrm{d}N}, \quad (9)$$

where $\epsilon_0 = H_i/H(N)$. The above expression implies that having inflation is strictly equivalent to $\epsilon_1 < 1$, where $\epsilon_1 = -\dot{H}/H^2$. Obviously, the two hierarchies are related by simple expressions. In particular, the first horizon flow parameter is

$$\epsilon_1 \simeq \epsilon_\phi + \epsilon_\psi, \tag{10}$$

where ϵ_ϕ and ϵ_ψ have been defined before.

Having specified the notation, we now turn to the choice of the free parameters controlling the shape of the inflationary potential.

A. Physical priors

It is usually assumed that hybrid inflation occurs in the vacuum dominated regime, for which $\phi \ll \mu$ and $\psi \ll M$. In this paper we also assume that this is the case. In any case, otherwise, hybrid inflation in the valley would be equivalent to a large field model, which is not the regime of interest here. For simplicity, in order to reduce the number of free parameters, and as also motivated by the supersymmetric version of the model, we take $\phi_c \simeq M$. Notice that this assumption does not imply a loss of generality, as we could easily relax it without drastically modifying the results obtained in this paper. Finally, in order for inflation to proceed for small values of the fields (compared to the Planck mass), one can consider that ϕ_c, $M \ll M_{\rm Pl}$, $M_{\rm Pl}$ being the reduced Planck mass.

In the valley and in the $\phi/\mu \ll 1$ limit, the slow-roll parameters ϵ_1 and ϵ_2 read

$$\epsilon_1(\phi, \psi = 0) \simeq 2\frac{M_{\rm Pl}^2}{\mu^2}\frac{\phi^2}{\mu^2}, \tag{11}$$

$$\epsilon_2(\phi, \psi = 0) \simeq 4\frac{M_{\rm Pl}^2}{\mu^2}. \tag{12}$$

Therefore, for the slow-roll approximation to be satisfied, these two parameters have to be much smaller than 1, which implies that $\mu \gg M_{\rm Pl}$.

In the next subsection we study the behavior of the two fields during the first phase of evolution, namely, when the inflaton field is moving along the valley.

B. The inflationary valley

The question of the initial conditions in hybrid inflation is a very interesting and nontrivial question. It has been studied in detail in Refs. [26,52–54]. Here, we simply argue that starting in the valley can be reasonably justified even if more complicated regimes can be found; see Ref. [53]. Indeed, if inflation starts beyond the critical line $\phi = \phi_c$, the system very quickly reaches the region where $\psi/M \ll 1$. In this regime, where the inflaton field is driving inflation, the slow-roll equation of motion for ϕ can be integrated, leading to

$$N = \frac{1}{4}\frac{\mu^2}{M_{\rm Pl}^2}\left[\frac{\phi_{\rm in}^2}{\mu^2} - \frac{\phi^2}{\mu^2} - 2\ln\left(\frac{\phi}{\phi_{\rm in}}\right)\right], \tag{13}$$

where $\phi_{\rm in}$ denotes the initial value of the inflaton field. This relation can be inverted, and one obtains [15]

$$\frac{\phi}{\mu} = \left[W_0\left(\frac{\phi_{\rm in}^2}{\mu^2}e^{\phi_{\rm in}^2/\mu^2 - 4M_{\rm Pl}^2 N/\mu^2}\right)\right]^{1/2}, \tag{14}$$

where W_0 denotes the 0-branch of the Lambert function. In the $\phi/\mu \ll 1$ limit, this formula simply reads

$$\phi = \phi_{\rm in}\exp\left(-2\frac{M_{\rm Pl}^2}{\mu^2}N\right). \tag{15}$$

This last expression is compared with an exact numerical integration of the full equations of motion in Fig. 2 (left panel), where it is shown that this is indeed an excellent approximation. Moreover, this allows us to calculate the number of e-folds "generated" in the valley, which reads

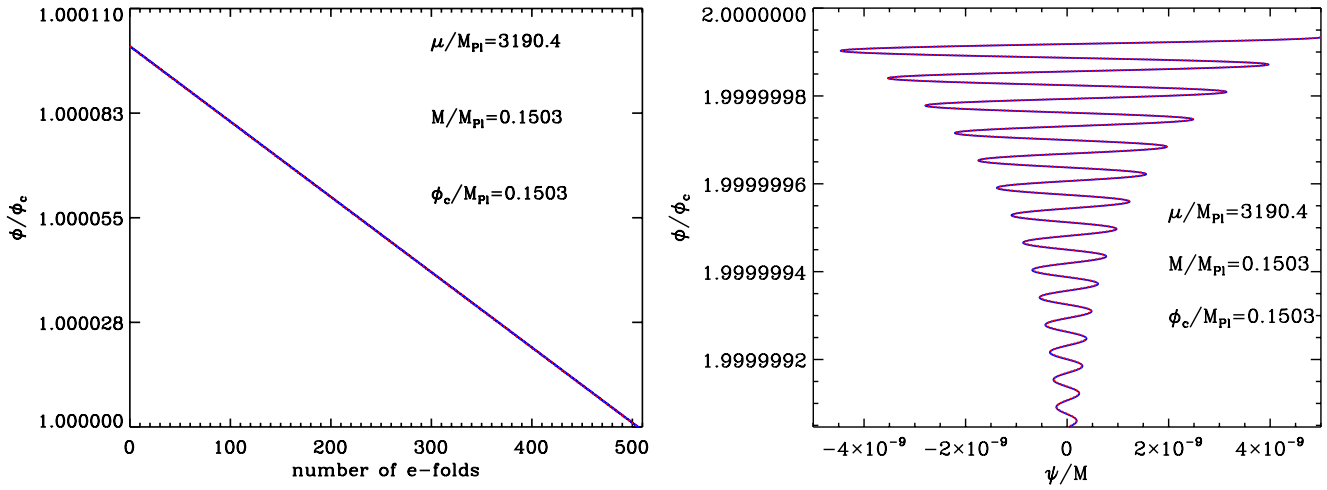

FIG. 2 (color online). Exact numerical solution for the inflaton (left panel, solid blue line) and waterfall (right panel, solid blue line) fields in the inflationary valley. The red dotted lines represent the analytical solution, and it is obvious that the approximation is very good. The damped oscillations of the waterfall field along the inflationary valley are clearly visible. The WKB analytical formula given by Eq. (17) is a very good approximation to the exact numerical solution.

$$N_{\rm c} = \frac{\mu^2}{2M_{\rm Pl}^2}\ln\left(\frac{\phi_{\rm in}}{\phi_{\rm c}}\right). \tag{16}$$

Clearly, this number is large because $\mu \gg M_{\rm Pl}$.

Let us now study the behavior of the waterfall field in the vicinity of the valley, when $\psi/M \ll 1$. Since ψ undergoes damped oscillations in this regime, it is clear that the slow-roll approximation cannot be used. On the other hand, since ψ oscillates much faster than ϕ moves, the WKB approximation can be used to describe this regime. The solution can be expressed as

$$\psi = \psi_{\rm in}\frac{{\rm e}^{-3N/2}}{\sqrt{2\omega(N)}}[C_1{\rm e}^{I(N)} + C_2{\rm e}^{-I(N)}], \tag{17}$$

where $\psi_{\rm in}$ is the initial value of the waterfall field, and where $I(N)$ is defined by the following expression (an unimportant sign has been ignored):

$$I(N) \equiv i\int \omega(n)dn, \tag{18}$$

$$= \frac{3}{2}\int_0^N \sqrt{1 - \frac{16}{3}\frac{M_{\rm Pl}^2}{M^2}\frac{\phi^2/\phi_{\rm c}^2 - 1}{1+\phi^2/\mu^2}}dn, \tag{19}$$

and where C_1 and C_2 are integration constants. The validity of the WKB approximation can be checked by estimating the following quantity, $({\rm d}\omega/{\rm d}N)/\omega \simeq \mathcal{O}(1)M_{\rm Pl}^2/\mu^2 \ll 1$. From the above expression one notices that oscillations in the ψ direction occur in the regime

$$\frac{16}{3}\frac{M_{\rm Pl}^2}{M^2}\frac{\phi^2/\phi_{\rm c}^2 - 1}{1+\phi^2/\mu^2} > 1, \tag{20}$$

that is to say, in the region

$$\frac{\phi}{\phi_{\rm c}} > 1 + \frac{3}{32}\frac{M^2}{M_{\rm Pl}^2}. \tag{21}$$

Since $M \ll M_{\rm Pl}$, we see that the field oscillates almost all the time before the critical point is met. In fact, it turns out that the integral $I(N)$ can be performed. One finds

$$I(N) \simeq -\sqrt{3}\frac{M_{\rm Pl}}{M}\frac{\mu^2}{M_{\rm Pl}^2}\left[\sqrt{\frac{\phi^2}{\phi_{\rm c}^2} - 1} - \arctan\left(\sqrt{\frac{\phi^2}{\phi_{\rm c}^2} - 1}\right)\right.$$
$$\left. - \sqrt{\frac{\phi_{\rm in}^2}{\phi_{\rm c}^2} - 1} + \arctan\left(\sqrt{\frac{\phi_{\rm in}^2}{\phi_{\rm c}^2} - 1}\right)\right]. \tag{22}$$

This solution is compared with the exact numerical solution in Fig. 2 (right panel). Clearly, the approximation is excellent.

When the condition (21) is not satisfied, $I(N) \simeq \pm 3N/2 + \cdots$ and the oscillations stop. Since the gradients become small, this time, one can use the slow-roll approximation in order to describe the motion of ψ. Notice that, since M is small (in Planck units), the above-mentioned regime occurs for a very small range of values for ϕ. However, a large number of e-folds $\propto \mu^2M^2/M_{\rm Pl}^4$ can be produced during this phase. The slow-roll equation of motion for ψ can be straightforwardly integrated and gives

$$\psi = \psi_{\rm in}\exp\left[4\frac{M_{\rm Pl}^2}{M^2}\int_0^N \frac{1 - \phi^2(n)/\phi_{\rm c}^2}{1+\phi^2(n)/\mu^2}dn\right], \tag{23}$$

where $\phi(n)$ is given by Eq. (14). Since $\phi > \phi_c$ in the valley, ψ decreases with N and obviously remains in the $\psi \ll M$ region. If one uses the fact that $\phi \ll \mu$, then the integral in the above formula can be performed exactly. Upon using Eq. (15), one obtains

$$\psi = \psi_{\rm in}\exp\left[4\frac{M_{\rm Pl}^2}{M^2}N - \frac{\phi_{\rm in}^2}{\phi_{\rm c}^2}\frac{\mu^2}{M^2} + \frac{\phi_{\rm in}^2}{\phi_{\rm c}^2}\frac{\mu^2}{M^2}\right.$$
$$\left.\times\exp\left(-4\frac{M_{\rm Pl}^2}{\mu^2}N\right)\right]$$
$$\simeq \psi_{\rm in}\exp\left[-4\frac{M_{\rm Pl}^2}{M^2}\left(\frac{\phi_{\rm in}}{\phi_{\rm c}} - 1\right)N\right], \tag{24}$$

where, in the last equation, we have used the fact that $\mu \gg M_{\rm Pl}$. In that case, one concludes that ψ is exponentially damped after the oscillations have stopped and before the critical point is reached. To our knowledge, this regime was not considered before. The above expression is compared with an exact numerical integration of the full equations of motion in Fig. 3. As one can notice, the agreement between the exact numerical solution and the analytical approximated expression is excellent. The previous formula also allows us to calculate the classical value of ψ when the system reaches the critical point. It is given by

$$\psi_c = \psi_{\rm in}\exp\left[-2\frac{\mu^2}{M^2}\left(\frac{\phi_{\rm in}}{\phi_{\rm c}} - 1\right)\ln\left(\frac{\phi_{\rm in}}{\phi_{\rm c}}\right)\right]. \tag{25}$$

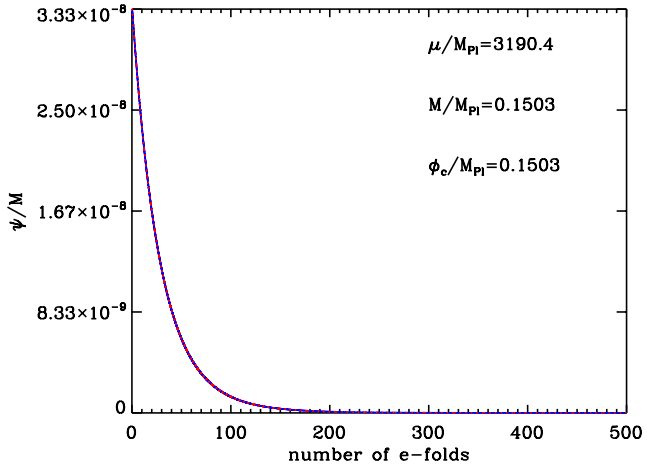

FIG. 3 (color online). Exact numerical solution for the waterfall field (solid blue line) in the inflationary valley after the oscillatory regime. The red dotted line represents the analytical solution, and it is obvious that the approximation is very good.

In practice, this value is always extremely small, thanks to the fact that $\mu \gg M_{\rm Pl}^2$ and, as was noticed in Refs. [27,42], the quantum fluctuations of ψ can be much larger than its classical value. We come back to this point in detail in the next section. However, before addressing this issue, in the next subsection, we describe the classical motion of the two fields during the waterfall stage.

C. The waterfall regime

The waterfall regime has recently been studied by various authors; see e.g. Refs. [27,55–58]. Here, we mainly follow the terminology used in Ref. [58]. We assume that slow roll is valid initially, at the critical point. We first study the so-called "phase 0" [58]. It consists in neglecting the last term in the inflaton slow-roll equation (2) and the first one in the right-hand side of the waterfall equation (3) (on the grounds that, initially, $\phi = \phi_{\rm c}$). Notice that, in this case, one could also solve the full inflaton equation, keeping the second time derivative, since in this approximation it becomes linear. On the other hand, the waterfall equation is nonlinear. In this sense, we do not start from a linear situation. It is easy to find the (slow-roll) solutions, and they read

$$\phi(N) = \phi_{\rm c} \exp\left[-2\frac{M_{\rm Pl}^2}{\mu^2}(N - N_{\rm c})\right], \tag{26}$$

$$\psi(N) = \psi_c\left[1 + \frac{8M_{\rm Pl}^2\psi_c^2}{M^4}(N - N_c)\right]^{-1/2}, \tag{27}$$

where $N_{\rm c}$ denotes the number of e-folds at the critical point, i.e. at the onset of the waterfall phase. In field space the trajectory reads

$$\phi = \phi_{\rm c} \exp\left[-\frac{M^4}{4\mu^2\psi_{\rm c}^2}\left(\frac{\psi_{\rm c}^2}{\psi^2} - 1\right)\right]. \tag{28}$$

Of course, instead of expressing ϕ in terms of ψ, one can also express ψ in terms of the inflaton field. In this case one obtains

$$\psi = \psi_{\rm c}\left[1 - \frac{4\mu^2\psi_{\rm c}^2}{M^4}\ln\left(\frac{\phi}{\phi_{\rm c}}\right)\right]^{-1/2}. \tag{29}$$

These expressions are fully consistent with Ref. [58].

The next question is when phase 0 stops. By definition, upon using Eqs. (2) and (3), it occurs when $\phi = \phi_1$ and $\psi = \psi_1$ such that

$$-\frac{\phi_1^2}{\phi_{\rm c}^2} + 1 = \frac{\psi_1^2}{M^2}. \tag{30}$$

Indeed, among the two conditions that we have required in order to derive the solutions (26) and (27), this one is the first to be violated since $\psi(N)$ decreases during phase 0. This condition can also be written as

$$2\ln\frac{\phi_1}{\phi_{\rm c}} = \ln\left(1 - \frac{\psi_1^2}{M^2}\right) \simeq -\frac{\psi_1^2}{M^2}. \tag{31}$$

Then, using the slow-roll trajectory one easily finds that

$$\ln\frac{\phi_1}{\phi_{\rm c}} \simeq \frac{M^4}{8\mu^2\psi_{\rm c}^2}\left(1 - \sqrt{1 + \frac{8\mu^2\psi_{\rm c}^4}{M^6}}\right) \tag{32}$$

and

$$\psi_1 \simeq M\sqrt{-2\ln\frac{\phi_1}{\phi_{\rm c}}}. \tag{33}$$

If we are in the regime where $8\mu^2\psi_{\rm c}^4/M^6 \ll 1$, then one has

$$\ln\frac{\phi_1}{\phi_{\rm c}} \simeq -\frac{\psi_{\rm c}^2}{2M^2} + \frac{\mu^2\psi_{\rm c}^6}{M^8} + \cdots, \tag{34}$$

$$\psi_1 \simeq \psi_{\rm c}\left(1 - \frac{\mu^2\psi_{\rm c}^4}{M^6} + \cdots\right). \tag{35}$$

From these expressions one can easily estimate the number of e-folds in phase 0. One obtains

$$N_1 - N_{\rm c} \simeq \frac{\mu^2\psi_{\rm c}^2}{4M_{\rm Pl}^2M^2} + \cdots \ll 1, \tag{36}$$

where N_1 denotes the number of e-folds at the end of phase 0. We see that the above quantity [as well as the parameter used in the expansion that leads to Eqs. (34) and (35)] is controlled by $\mu/M_{\rm Pl}$, which is large, and by $\psi_{\rm c}/M$, which is small. Therefore, the smallness of this parameter is *a priori* not obvious. The two situations, where it is small or large, have been studied in Ref. [58]. However, in practice, $\psi_{\rm c}/M$ is so small that the parameter mentioned previously is always small. In this case we conclude that phase 0 is unimportant since it lasts a negligible number of e-folds. As a consequence, the values of ϕ and ψ remain almost unchanged during that phase.

We now proceed with phase 1. By definition, the second term on the right-hand side of the waterfall equation (3) can be neglected. This means that this equation, as was already the case for the inflaton equation of motion (which remains unaffected during phase 1), becomes linear. For this reason, sometimes, this phase is also called the "linear phase." During this phase, the solution for the inflaton field is unchanged but, of course, one now has to solve the new approximated equation for the waterfall field. The solution can be easily calculated and reads

$$\ln\frac{\psi}{\psi_1} = \frac{\mu^2}{M^2}[e^{-4M_{\rm Pl}^2(N-N_{\rm c})/\mu^2} - e^{-4M_{\rm Pl}^2(N_1-N_{\rm c})/\mu^2}] + \frac{4M_{\rm Pl}^2}{M^2}(N - N_1). \tag{37}$$

Then, one can Taylor expand the exponential functions since we are in the regime where $\mu/M_{\rm Pl} \gg 1$. This gives

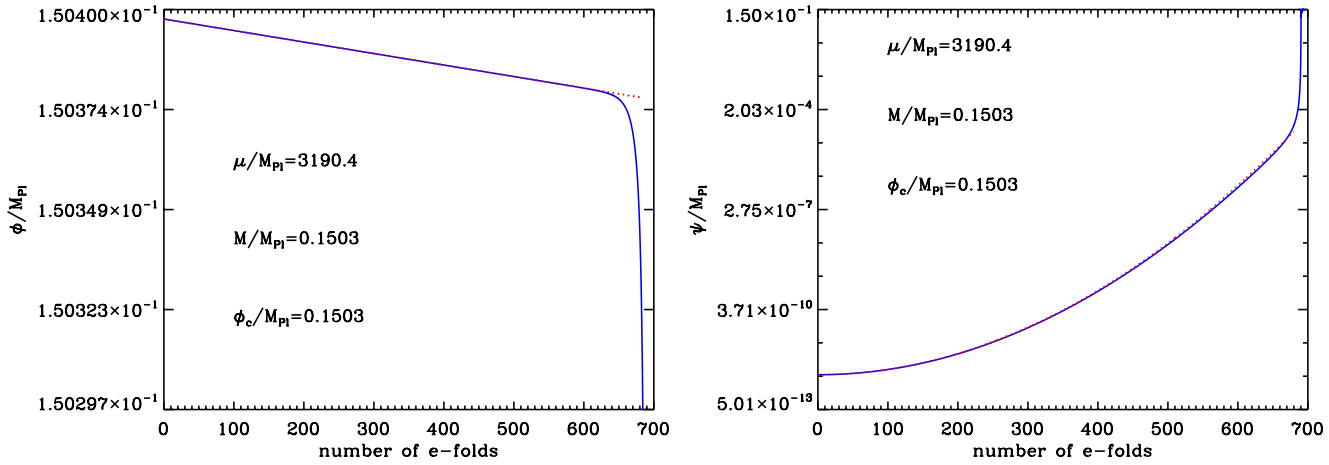

FIG. 4 (color online). Exact numerical solution for the inflaton (left panel, solid blue line) and waterfall (right panel, solid blue line) fields. The red dotted lines represents the slow-roll analytical solution during phase 1.

$$\psi = \psi_1 \exp\left\{\frac{8M_{\rm Pl}^4}{\mu^2 M^2}[(N-N_{\rm c})^2 - (N_1 - N_{\rm c})^2]\right\}. \quad (38)$$

This solution together with the solution for the inflaton is represented in Fig. 4. This plot confirms that the previous approximated solutions match the exact ones with a very good precision. Finally, in field space, the trajectory now reads

$$\psi = \psi_1 \exp\left[\frac{2\mu^2}{M^2}\left(\ln^2\frac{\phi}{\phi_{\rm c}} - \ln^2\frac{\phi_1}{\phi_{\rm c}}\right)\right], \quad (39)$$

or, equivalently,

$$\ln^2\frac{\phi}{\phi_{\rm c}} = \ln^2\frac{\phi_1}{\phi_{\rm c}} + \frac{M^2}{2\mu^2}\ln\frac{\psi}{\psi_1}. \quad (40)$$

Phase 1 stops when, on the right-hand side of the slow-roll inflaton equation of motion (2) for ϕ, the last term becomes 1. This occurs for $\psi \equiv \psi_2$, where

$$\psi_2^2 = \frac{\phi_{\rm c}^2 M^2}{2\mu^2}, \quad (41)$$

and $\phi = \phi_2$ with

$$\ln^2\frac{\phi_2}{\phi_{\rm c}} \simeq \ln^2\frac{\phi_1}{\phi_{\rm c}} + \frac{M^2}{2\mu^2}\ln\left(\frac{\phi_{\rm c} M}{\sqrt{2}\mu\psi_1}\right) \quad (42)$$

$$\simeq \frac{M^2}{2\mu^2}\ln\left(\frac{\phi_{\rm c} M}{\sqrt{2}\mu\psi_{\rm c}}\right), \quad (43)$$

the last approximated relation being obtained under the assumption that phase 0 can be neglected and, as a consequence, that $\phi_1 \simeq \phi_{\rm c}$ and $\psi_1 \simeq \psi_{\rm c}$. It is also important to realize that the terms $1 - \phi^2/\phi_{\rm c}^2$ and ψ^2/M^2 are equal at the onset of phase 1 and then both increase. It is therefore necessary to check that, at the end of phase 1, the term $1 - \phi^2/\phi_{\rm c}^2$ still dominates over ψ^2/M^2. In other words, one has to verify that ψ^2/M^2 has increased less rapidly than $1 - \phi^2/\phi_{\rm c}^2$. Using the solution for the waterfall, one has

$$N_2 - N_{\rm c} \simeq \frac{\mu M}{2\sqrt{2}M_{\rm Pl}^2}\ln^{1/2}\left(\frac{\psi_2}{\psi_{\rm c}}\right), \quad (44)$$

where N_2 denotes the number of e-folds at the end of phase 1 or, equivalently, at the onset of phase 2. Upon using this formula, this leads to

$$\frac{\phi_2^2}{\phi_{\rm c}^2} - 1 = -\sqrt{2}\frac{M}{\mu}\ln^{1/2}\left(\frac{\phi_{\rm c} M}{\sqrt{2}\mu\psi_{\rm c}}\right), \quad (45)$$

an expression that should be compared with

$$\frac{\psi_2^2}{M^2} = \frac{\phi_{\rm c}^2}{2\mu^2}. \quad (46)$$

We see that the condition $\phi_2^2/\phi_{\rm c}^2 - 1 \gg \psi_2^2/M^2$ is *a priori* not obvious. However, in the case under scrutiny in this article, one chooses $\phi_{\rm c}$ and M to be roughly of the same order of magnitude and $\mu \gg M_{\rm Pl}$. As a consequence, the condition is satisfied since $\phi_2^2/\phi_{\rm c}^2 - 1$ scales as the inverse of μ (neglecting the influence of the logarithm) while ψ_2^2/M^2 scales as the inverse of μ^2. However, it is also clear that one could easily design a situation where this is not true. Here, we restrict ourselves to situations where this does not happen.

Finally, let us express the number of e-folds produced during phase 1. It is given by

$$N_2 - N_{\rm c} \simeq \frac{\mu M}{2\sqrt{2}M_{\rm Pl}^2}\ln^{1/2}\left(\frac{\phi_{\rm c} M}{\sqrt{2}\mu\psi_{\rm c}}\right). \quad (47)$$

Upon using Eq. (25), one could also replace $\psi_{\rm c}$ by its expression in the above equation to obtain a formula depending on the initial conditions. We see that the number of e-folds during phase 1 is essentially controlled by the ratio $\mu M/M_{\rm Pl}^2$. This conclusion is in agreement with the results of Ref. [58]. As a consequence, for $\mu M/M_{\rm Pl}^2 > 1$,

$N_2 - N_c$ can be large. Hence, we conclude that the number of e-folds during the waterfall phase can indeed be much greater than the 60 required for inflation to be successful, as was noticed in Ref. [27]. The previous considerations allow us to identify where, in the parameter space, this regime occurs. We have studied this classical phase of evolution in some detail because this regime is of particular interest for the present article. Indeed, in the next section, we show that in this case the quantum effects play an important role.

Let us now briefly mention phase 2 (it was studied in more detail in Ref. [58]). This time one needs to keep the last term in the inflaton equation of motion (2). This means that the evolution for ϕ is modified and, as a consequence, the formula giving $\psi(N)$ is no longer valid since it made use of the evolution for ϕ established before. In this regime Eqs. (2) and (3) become fully coupled. However, it is still possible to find the slow-roll trajectory in the field space. One obtains [58]

$$\frac{\mathrm{d}\phi}{\mathrm{d}\psi} = \frac{\phi\psi}{\phi^2 - \phi_c^2} \tag{48}$$

which can be easily integrated, and the solution reads

$$\psi^2 = \psi_2^2 + \phi^2 - \phi_2^2 - 2\phi_c^2 \ln\frac{\phi}{\phi_2}\,. \tag{49}$$

This expression (green dotted line) is compared to the exact numerical solution (blue solid line) in Fig. 5. Clearly, the agreement is excellent. During phase 2, inflation stops and the system starts oscillating around one of the two true minimums of the potential. This is the onset of the reheating phase.

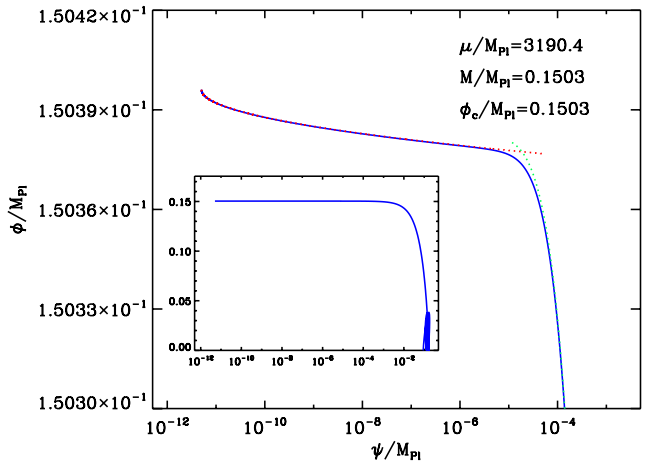

FIG. 5 (color online). Classical background evolution of the inflaton and waterfall fields starting from the critical point, $\phi = \phi_c$ and $\psi = 10^{-12} M_{\mathrm{Pl}}$. The solid blue curve represents the exact (i.e. numerical) trajectory, while the dotted red curve is the slow-roll approximation during phase 1 and the dotted green curve is the slow-roll approximation during phase 2. The inset shows the overall evolution of the two fields with, in particular, the oscillations around the true minimum of the potential at the end of inflation.

The above considerations complete this section. Having mastered the classical dynamics of the fields in the valley and during the waterfall regime, we are now in a position where we can turn to the main topic of this article, namely, studying the role played by the quantum effects. This is the goal of the next section.

III. STOCHASTIC EFFECTS

In this article, we use the stochastic inflation formalism to study the quantum effects. In this formalism, an effective Langevin equation can be derived for the "coarse-grained" field, i.e. the original field averaged over a physical volume, the size of which is typically larger than the Hubble radius H^{-1}. Applied to the case of hybrid inflation, one obtains two coupled Langevin equations for the inflaton and the waterfall fields, respectively. They read

$$3H^2\frac{\mathrm{d}\phi}{\mathrm{d}N} = -\frac{2\Lambda^4\phi}{\mu^2}\left(1 + \frac{2\psi^2\mu^2}{\phi_c^2 M^2}\right) + \frac{3H^3}{2\pi}\xi_\phi(N)\,, \tag{50}$$

$$3H^2\frac{\mathrm{d}\psi}{\mathrm{d}N} = -\frac{4\Lambda^4}{M^2}\psi\left(\frac{\phi^2 - \phi_c^2}{\phi_c^2} + \frac{\psi^2}{M^2}\right) + \frac{3H^3}{2\pi}\xi_\psi(N)\,, \tag{51}$$

where ξ_ϕ and ξ_ψ are two uncorrelated white Gaussian noises with 0-mean and 1-variance. Notice that the time variable used is the number of e-folds. It was argued in Refs. [59–61] that this choice is preferred.

A. Can the quantum effects be important?

Having at our disposal the two Langevin equations presented above, the first question is whether the stochastic noises can really play an important role and, if so, where in the field plane. This issue can be addressed in the following manner. During a typical time interval $\Delta t = H^{-1}$, both stochastic and classical evolutions of the fields ϕ and ψ can be read off directly from Eqs. (50) and (51). Roughly speaking, the typical classical change in the inflaton value is $\simeq M_{\mathrm{Pl}}^2(\partial V/\partial\phi)/V$, while the magnitude of the quantum kick is $H/(2\pi)$. Therefore, in order to assess the relative contribution of the stochastic effects over the classical ones, one can study the ratios Δ_ϕ and Δ_ψ of these two quantities for each field (in the context of a quartic large field model, this is how one can deduce that the quantum corrections dominate if the value of the field is larger than $\lambda^{-1/6} M_{\mathrm{Pl}}$, where λ is the self-coupling constant that appears in the potential). This amounts to taking $\Delta_\phi \equiv V^{3/2}/[2\pi\sqrt{3}M_{\mathrm{Pl}}^3(\partial V/\partial\phi)]$ and a similar definition for Δ_ψ. In the vacuum dominated regime, the two quantities Δ_ϕ and Δ_ψ read

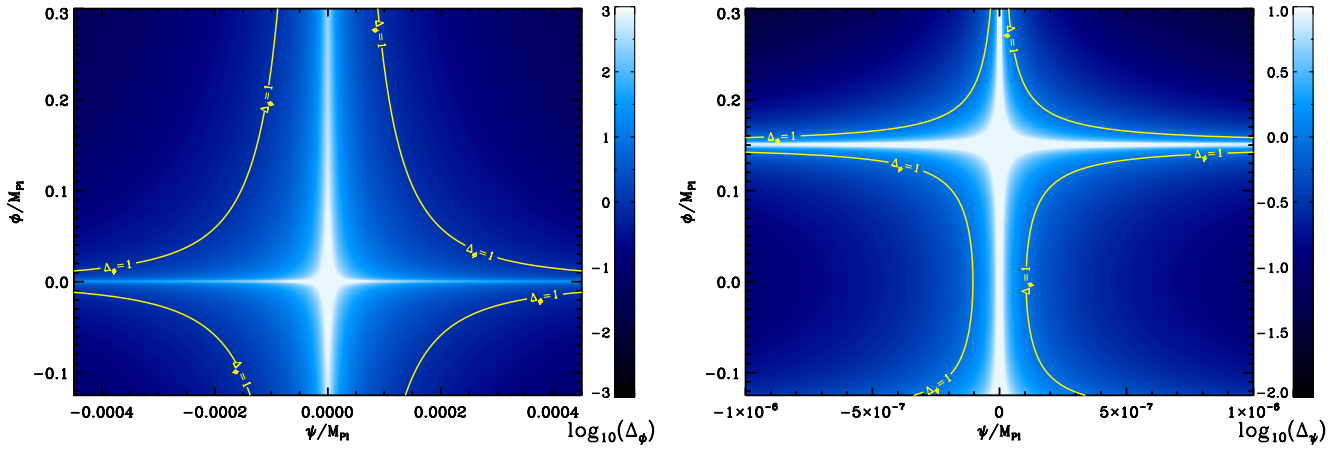

FIG. 6 (color online). Δ_ϕ and Δ_ψ plotted in the (ϕ, ψ) plane for the parameters $\mu = 3190.4 M_{\rm Pl}$, $M = \phi_c = 0.1503 M_{\rm Pl}$, $\Lambda = 0.014\,18 M_{\rm Pl}$. Δ_ϕ and/or Δ_ψ greater than 1 ($\sim$ in white on the plot) signal that the quantum effects are dominant. The stochastic effects in the ψ direction obviously dominate over the classical contributions in the valley and around the critical point, while the stochastic effects in the ϕ direction dominate in the valley and around the origin.

$$\Delta_\phi = \frac{1}{4\pi\sqrt{3}} \frac{\Lambda^2 \phi_{\rm c}}{M_{\rm Pl}^3} \frac{\phi_{\rm c}}{\phi} \left(\frac{\phi_{\rm c}^2}{\mu^2} + 2\frac{\psi^2}{M^2} \right)^{-1}, \tag{52}$$

$$\Delta_\psi = \frac{1}{8\pi\sqrt{3}} \frac{\Lambda^2 M}{M_{\rm Pl}^3} \frac{M}{\psi} \left(\frac{\psi^2}{M^2} - 1 + \frac{\phi^2}{\phi_{\rm c}^2} \right)^{-1}. \tag{53}$$

These quantities are plotted in Fig. 6 in the (ϕ, ψ) plane. Values such that $\Delta > 1$ indicate that the quantum effects dominate. Let us now discuss how Δ_ϕ and Δ_ψ behave in the field plane. Clearly, Δ_ϕ is infinite when $\phi = 0$ for any values of ψ. Therefore, the quantum effects are dominant along that direction. In the inflationary valley $\psi = 0$, which is perpendicular to the previously mentioned direction, one has

$$\Delta_\phi^{\rm valley} = \frac{1}{4\pi\sqrt{3}} \frac{\Lambda^2 \mu^2}{M_{\rm Pl}^3 \phi}. \tag{54}$$

This means that $\Delta_\phi > 1$ as long as

$$\frac{\phi}{M_{\rm Pl}} < \frac{\phi^{\rm valley}}{M_{\rm Pl}} \equiv \frac{1}{4\pi\sqrt{3}} \frac{\Lambda^2 \mu^2}{M_{\rm Pl}^4}. \tag{55}$$

For the parameters used in Fig. 6, one has $\phi^{\rm valley}/M_{\rm Pl} \simeq 94$, i.e. a value much larger than the upper limit of this plot. This means that the quantum effects dominate "very high" in the valley and, in particular, around the critical point. The previous considerations explain the cross-shaped white region centered at the origin observed in Fig. 6. In this regime, one expects a faithful description of the system to be obtained only if the stochastic noises for the two coupled fields are taken into account. In the following, we study this case, where treating one field (for instance, the inflaton) classically and the other (the waterfall field) stochastically is *a priori* not a good approximation.

Of course, these results also depend on the parameters, in particular, on Λ. It is interesting to determine the value of $\Lambda \equiv \Lambda_\phi$ such that $\phi^{\rm valley} = \phi_{\rm c}$. This value indicates the limit between the regime where it is mandatory to take into account the noise both in the inflaton and waterfall field directions and the regime where the waterfall field is still stochastic but where it is sufficient to treat the inflaton classically. It is given by

$$\Lambda_\phi^2 = 4\pi\sqrt{3} \frac{\phi_{\rm c} M_{\rm Pl}^3}{\mu^2}. \tag{56}$$

For our fiducial parameters, this leads to $\Lambda_\phi \simeq 5.7 \times 10^{-4} M_{\rm Pl}$. Obviously, for larger values of μ, Λ_ϕ is even smaller. In Fig. 7, we have represented Δ_ϕ for the

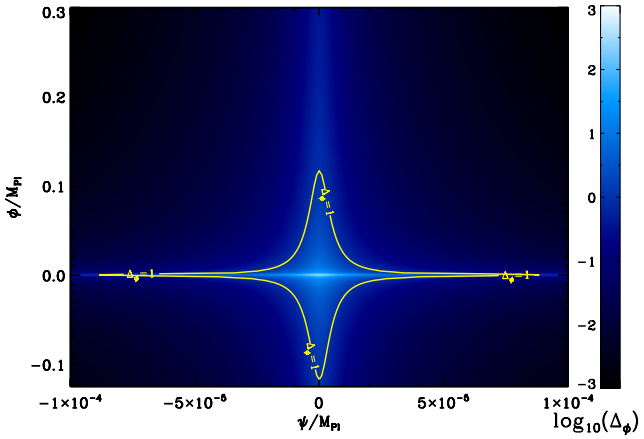

FIG. 7 (color online). Δ_ϕ plotted in the (ϕ, ψ) plane for the parameters $\mu = 3190.4 M_{\rm Pl}$, $M = \phi_c = 0.1503 M_{\rm Pl}$, $\Lambda = 0.0005 M_{\rm Pl} \lesssim \Lambda_\phi$. For this value of Λ, Δ_ϕ remains small along the valley and does not encompass the critical point. It becomes larger than 1 only in the vicinity of the origin.

same parameters, except that $\Lambda = 5 \times 10^{-4} M_{\rm Pl} \lesssim \Lambda_\phi$. This plot confirms that the region $\Delta_\phi > 1$ covers a much smaller area which does not encompass the critical point. In that case ϕ should behave almost classically in the valley, and we will also investigate this regime in Sec. III D.

Let us now describe Δ_ψ. It is infinite for $\psi = 0$, that is to say, in the valley. When $\psi \neq 0$, the quantum effects are dominant when $\phi^2/\phi_{\rm c}^2 \simeq 1 - \psi^2/M^2$, i.e. in the direction $\phi \simeq \phi_{\rm c}$ perpendicular to the valley (in the regime where $\psi/M \ll 1$). This explains the cross-shaped white region, this time centered at the critical point; see Fig. 6. This time, the previous considerations do not depend on Λ, which means that the noise in the waterfall field should always be taken into account in the valley and around the critical point. Since this corresponds to a very flat region of the potential where most of the e-folds are realized, one can already expect the inflationary dynamics to be significantly affected by the quantum effects.

B. Obstacles to a perturbative approach

Having justified that the quantum corrections play a crucial role, the next question is how to compute them, i.e. how to solve the two Langevin equations. It is clear that an exact analytical solution is not available. However, as proposed in Refs. [43,44], the Langevin equation can be solved perturbatively by considering the coarse-grained field as a perturbation on top of the classical solution. The corresponding formalism in the case of single field inflation was presented in Ref. [43]. However, in the present case, we are in a two-field situation, which means that both the inflaton and the waterfall fields must be expanded according to

$$\phi(N) = \phi_{\rm cl}(N) + \delta\phi_1(N) + \delta\phi_2(N) + \ldots, \tag{57}$$

$$\psi(N) = \psi_{\rm cl}(N) + \delta\psi_1(N) + \delta\psi_2(N) + \ldots, \tag{58}$$

where $\phi_{\rm cl}$ and $\psi_{\rm cl}$ are the classical values. We see that the corrections to the classical solutions are obtained by adding successive terms of higher and higher powers in the noise. In Ref. [43], general formulas valid at second order are provided, leading to a Gaussian probability density function for the field. The validity of this approach relies on the smallness of the stochastic effects compared to the classical ones and, obviously, the expansion is valid only in a limited regime; see Ref. [44]. Here, we have just seen that the quantum effects are dominant around the critical point and, therefore, there are already reasons to guess that a perturbative approach is not very appropriate.

Moreover, one can see that the perturbative approach is technically impossible to carry out in a multiple field situation since even the linearized coupled stochastic differential equations cannot be analytically solved. Indeed, in the hybrid inflation case, at first order in the noise, they can be written as

$$\frac{{\rm d}\delta\phi_1}{{\rm d}N} + 2\delta\psi_1\left(\frac{H_{\phi\psi}}{H} - \frac{H_\psi H_\phi}{H^2}\right) + 2\delta\phi_1\left(\frac{H_{\phi\phi}}{H} - \frac{H_\phi^2}{H^2}\right) = \frac{H}{2\pi}\xi_\phi(N), \tag{59}$$

$$\frac{{\rm d}\delta\psi_1}{{\rm d}N} + 2\delta\phi_1\left(\frac{H_{\phi\psi}}{H} - \frac{H_\psi H_\phi}{H^2}\right) + 2\delta\psi_1\left(\frac{H_{\psi\psi}}{H} - \frac{H_\psi^2}{H^2}\right) = \frac{H}{2\pi}\xi_\psi(N), \tag{60}$$

where H_ϕ is the derivative of $H = \sqrt{V}/(M_{\rm Pl}\sqrt{3})$ with respect to ϕ and the other notations used in this equation straightforwardly follow. The matrix of this differential system does not commute with itself at different times N and, as a consequence, one cannot solve the coupled perturbative problem in a simple way.

C. Testing the numerical approach

For all these reasons, the only method left seems to be a full numerical integration of the stochastic inflationary equations. This is the method used in the present article. Since the differential equations to be solved turn out to be stiff most of the time, we use a fourth order Rosenbrock method, monitoring a local truncation error to adjust step sizes, that we have adapted to take into account the presence of an extra random stochastic term. When possible, we have also used the Euler-Muruyama method in another independent code in order to check our numerical results.

In this section, we describe the tests that we have performed in order to check that our numerical codes work properly. A first verification of the consistency of our numerical treatment can be obtained in the following manner. If one considers that the dynamics of ϕ remains classical in the valley, then following Refs. [27,42] one can perturbatively estimate the typical dispersion of the waterfall field distribution (i.e. in the ψ direction) at the critical point. One obtains

$$\langle\psi_{\rm c}^2\rangle_{\rm pert} \simeq \frac{H^2\mu M}{32\pi^{3/2}M_{\rm Pl}^2}. \tag{61}$$

Therefore, numerically, in the regime $\Lambda < \Lambda_\phi$ (to ensure that the inflaton field behaves classically), one should recover the same result. As a consequence, it is interesting to plot the quantity $(\langle\psi_{\rm c}^2\rangle_{\rm num}/\langle\psi_{\rm c}^2\rangle_{\rm pert})^{1/2}$, where $\langle\psi_{\rm c}^2\rangle_{\rm num}$ is the dispersion in the waterfall direction (at $\phi = \phi_{\rm c}$) obtained numerically. This quantity as a function of Λ/Λ_ϕ is represented in Fig. 8. As it is clear from this plot, when $\Lambda < \Lambda_\phi$, the ratio $(\langle\psi_{\rm c}^2\rangle_{\rm num}/\langle\psi_{\rm c}^2\rangle_{\rm pert})^{1/2}$ is precisely 1, thus showing that our code correctly reproduces the known analytical result. We also see that when $\Lambda > \Lambda_\phi$, the perturbative regime breaks down. From what we have just discussed, the interpretation of this result is clearly that the stochastic effects in the ϕ direction play a role and

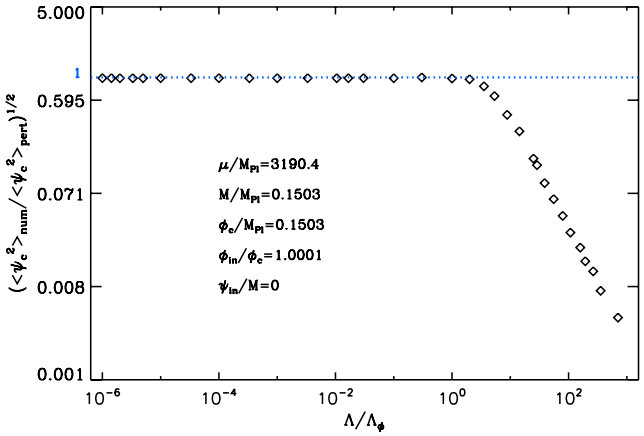

FIG. 8 (color online). Numerical predictions for $\langle\psi_c^2\rangle_{num}$ normalized to $\langle\psi_c^2\rangle_{pert}$ given by Eq. (61) for different values of Λ normalized to Λ_ϕ defined in Eq. (56).

kick the system below the critical point more rapidly. As a consequence, the distribution in ψ has much less e-folds to broaden than classically predicted, and hence $\langle\psi_c^2\rangle_{num} < \langle\psi_c^2\rangle_{pert}$. This behavior is similar to what has been found in Ref. [62], where it has been shown that, in case of a multiple field inflationary dynamics with one flat direction and several nonflat directions, the fluctuations of the nonflat directions can be sufficient to block the growth of the root-mean-square amplitude along the flat direction. The fact that $\langle\psi_c^2\rangle_{num}$ deviates from $\langle\psi_c^2\rangle_{pert}$ precisely at $\Lambda = \Lambda_\phi$ is another indication of the consistency of our numerical results.

Another type of consistency check can also be performed by investigating how given realizations behave for different values of the parameters. We present in Fig. 9 four different examples, for four different values of Λ, where four stochastic realizations (blue, cyan, purple, and pink lines) are compared with the classical trajectory (solid black line). The top left panel corresponds to

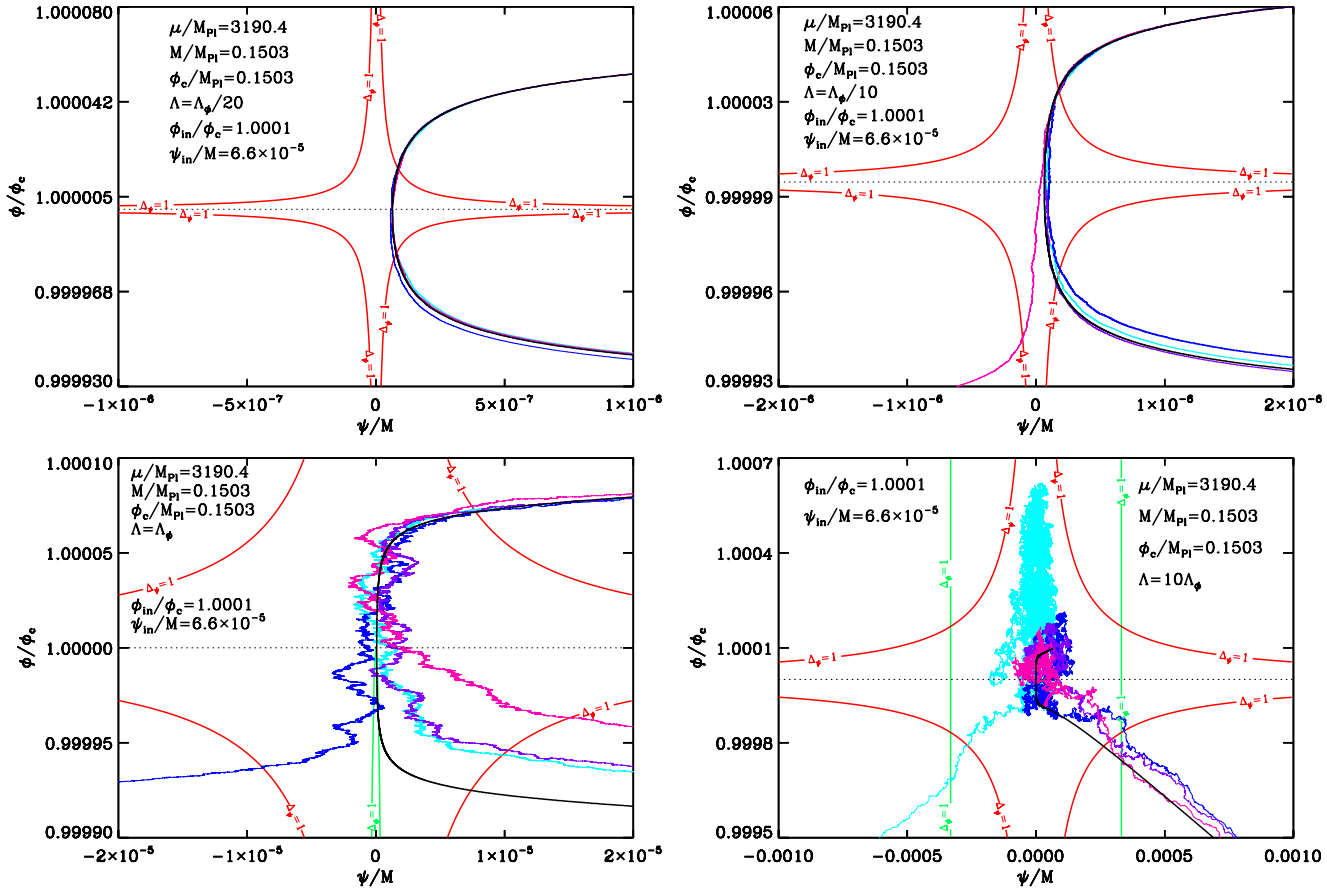

FIG. 9 (color online). Stochastic trajectories in field space for different values of Λ: $\Lambda = \Lambda_\phi/20$ (top left panel), $\Lambda = \Lambda_\phi/10$ (top right panel), $\Lambda = \Lambda_\phi$ (bottom left panel), and $\Lambda = 10\Lambda_\phi$ (bottom right panel). The solid black line represents the classical trajectory starting from the point $\phi_{in} = 1.0001\phi_c$ and $\psi_{in} = 6.6 \times 10^{-5}M$. The blue, cyan, pink, and purple lines represent four different stochastic trajectories. The parameters chosen are $\mu/M_{Pl} = 3190.4$ and $M/M_{Pl} = \phi_c/M_{Pl} \simeq 0.1503$. The contours $\Delta_\phi = 1$ (solid red line) and $\Delta_\psi = 1$ (solid green line) are also represented.

$\Lambda = \Lambda_\phi/20$. In this case, the noise is so small that the four stochastic realizations almost follow the classical trajectory. The top right panel corresponds to $\Lambda = \Lambda_\phi/10$, and the noise in the inflaton direction still plays no role in this case (i.e. the contour $\Delta_\phi = 1$ does not encompass the critical point). One sees that, when the trajectories enter the $\Delta_\psi > 1$ region, they start feeling the noise and that one of them (the pink realization) is even expelled towards the other global minimum. The bottom left panel corresponds to $\Lambda = \Lambda_\phi$, and the noise is stronger as revealed by the ''shaky'' behavior of the realizations. The contour $\Delta_\phi = 1$ appears but, clearly, the noise in the waterfall direction remains the main source of stochasticity. Finally, the bottom right panel corresponds to $\Lambda = 10\Lambda_\phi$ and, this time, we are in a regime where the noise in the two directions is *a priori* important as indicated by the contours $\Delta_\phi = 1$ and $\Delta_\psi = 1$. This is especially clear for the cyan realization which climbs the inflationary valley. Therefore, it seems fair to say that our numerical code gives results that are completely compatible with elementary expectations, which is an indication that it correctly calculates the behavior of the system.

Finally, by simulating a high number of realizations, we have been able to calculate the correlation functions of various quantities of interest as well as their probability distributions. As an example, Fig. 10 shows the probability density function in the (ϕ, ψ) plane, at different times N, starting from a peaked distribution in the valley. One can see that the distribution is first roughly Gaussian and goes down the valley before setting over the critical point with ''excrescences'' growing towards the two minimums of the potential, rendering the distribution highly non-Gaussian. Again, this plot confirms the previous discussion and shows that the numerical codes used in this article are able to reproduce expected results in regimes where it is possible to guess (or to approximately calculate) the behavior of the system.

In the following subsections, we present in more detail our numerical results.

D. Number of e-folds

A first relevant well-defined physical quantity to study is the total number of e-folds realized during inflation since it provides a straightforward way to investigate the deviations from the classical picture. Of course, in order to calculate this quantity, one has to choose some initial conditions. Here, we take $\phi_{\rm in}/\phi_{\rm c} = 1.0001$ and $\psi_{\rm in}/M = 10^{-9}$. The parameters describing the shape of the potential are $\mu/M_{\rm Pl} = 3190.4$, $M = \phi_{\rm c} = 0.1503 M_{\rm Pl}$, and $\Lambda/M_{\rm Pl} = 0.014\,18$. We see that this implies $\mu M/M_{\rm Pl}^2 > 1$ and, therefore, we already know from the previous section that the number of e-folds during the waterfall phase will be large. As a matter of fact, it can be easily estimated upon using Eq. (47). The above described choice is made in order to illustrate our point in the clearest way. It is important to stress that choosing other initial conditions would not drastically modify our conclusions. The classical prediction can be calculated in the slow-roll approximation using the formulas derived above, or using a numerical integration of the exact equations. It leads to a trajectory such that $\sim$505 e-folds are realized in the valley and $\sim$747 during the waterfall regime. The total number of e-folds is therefore $\sim$1252.

Then, we have computed the same quantity (for the same values of the initial conditions and of the parameters) in the stochastic case. Obviously, for each realization one gets a different number, and the corresponding distribution is displayed in Fig. 11. Let us now discuss this figure. Probably, the most striking property of Fig. 11 is that the distribution is peaked at a value which is completely different from the classical prediction. This clearly means that strong nonperturbative effects are at play. This also emphasizes the necessity of using a full numerical approach. Moreover, one sees that the stochastic contribution tends to diminish the total number of e-folds. This fact can be intuitively understood by noticing that most e-folds are realized in the region where the potential is very flat, around the critical point. Since this is precisely where the stochastic terms are dominant, the quantum kicks remove the system away from this region much faster than the classical roll; hence a lower number of e-folds is realized in this region.

The tendency to escape faster from a region where the potential is very flat can be understood analytically on the example of small field inflation. In this single field model, the potential is given by

$$V(\psi) = M^4\left[1 - \left(\frac{\psi}{\mu}\right)^p\right], \tag{62}$$

where μ is a mass scale. Inflation proceeds from small to large values of the field. At the beginning of inflation, the potential is very flat and a large number of e-folds can be realized. For $p = 2$, the slow-roll and the perturbative Langevin equations can be integrated and solved exactly; see Ref. [43]. Following Ref. [63], one can then calculate the mean value of the total number of e-folds,

$$\langle N\rangle = -\frac{1}{2M_{\rm Pl}^2}\int_{\psi_{\rm in}}^{\psi} {\rm d}\psi\, \frac{\langle H\rangle}{H'_{\rm cl}}\,. \tag{63}$$

In the present case and since $\phi \ll \mu$, one obtains

$$\langle N\rangle \simeq N_{\rm class} - \frac{1}{192\pi^2}\left(\frac{M}{M_{\rm Pl}}\right)^4\left(\frac{\mu}{M_{\rm Pl}}\right)^2\left[\ln\left(\frac{\psi_{\rm in}}{\psi}\right) + \frac{1}{2}\left(\frac{\psi^2}{\psi_{\rm in}^2} - 1\right)\right], \tag{64}$$

where $N_{\rm class}$ is the number of e-folds classically realized. From the above expression, it is clear that $\langle N\rangle$ is smaller than $N_{\rm class}$ since $\psi_{\rm in} < \psi_{\rm end}$ in this model. This result confirms the previous considerations: when the potential

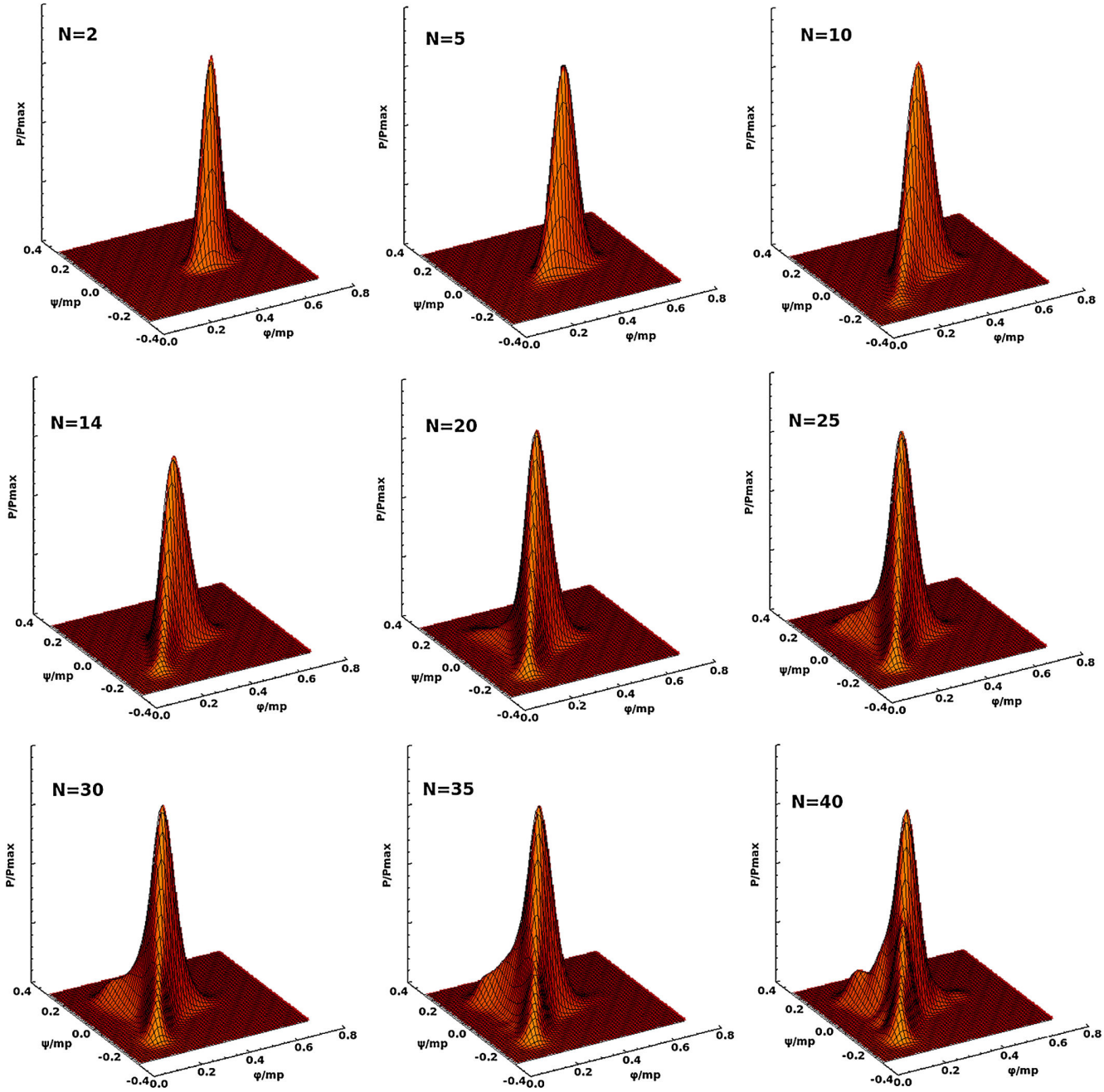

FIG. 10 (color online). Probability density functions in the (ϕ, ψ) plane, at different times N, starting from a Dirac distribution in the valley. The parameters chosen are $\Lambda = 1.063\,47 M_{\rm Pl}$, $\phi_{\rm c} = M = 1.503\,98 M_{\rm Pl}$, and $\mu = 7.745\,97 M_{\rm Pl}$.

is very flat, the quantum kicks undergone by the inflaton field push it out of the flat region and, as a consequence, the total number of e-folds becomes smaller.

Finally, it is also interesting to study how our results depend on the parameters of the model, especially on μ and Λ. As an example, Fig. 12 shows the normalized distribution of the total number of e-folds for different values of the parameter μ. From Eqs. (16) and (17), one can see that the classical number of e-folds realized during both the inflationary valley and the waterfall regime increases with μ, which is consistent with the behavior of the mean values of the stochastic distributions observed in Fig. 12. Moreover, the longer the field system stays in the flat region close to the critical point, the more its distribution gets stochastically broadened. This means that the dispersion of the distribution should evolve in a similar manner, which is exactly what is seen in Fig. 12. Moreover, if one keeps increasing μ, one observes that the mean value of the distribution saturates at a value of $\simeq 60$ e-folds.

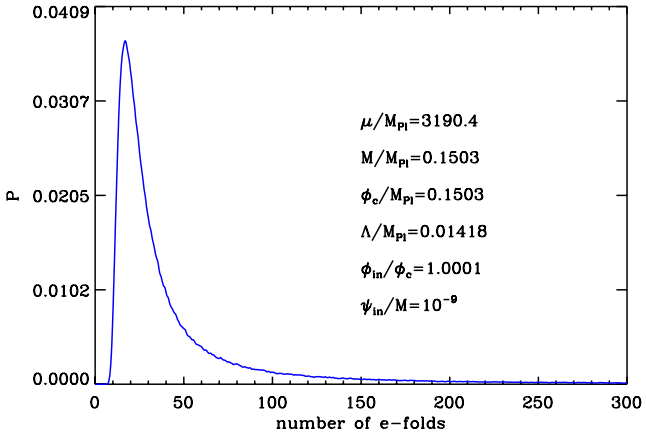

FIG. 11 (color online). Distribution of the total number of e-folds realized during inflation. Classically, 505 e-folds are realized in the valley and 747 e-folds are realized during the waterfall stage, accounting for a total of 1252 e-folds. Clearly the mean value $\langle N\rangle \sim 50$ is very different from the classical value which illustrates well how important the stochastic effects in the vicinity of the critical point are. Despite this fact, it is also interesting to notice that, in the tail of the distribution, one can find realizations with a total number of e-folds larger than the classical value.

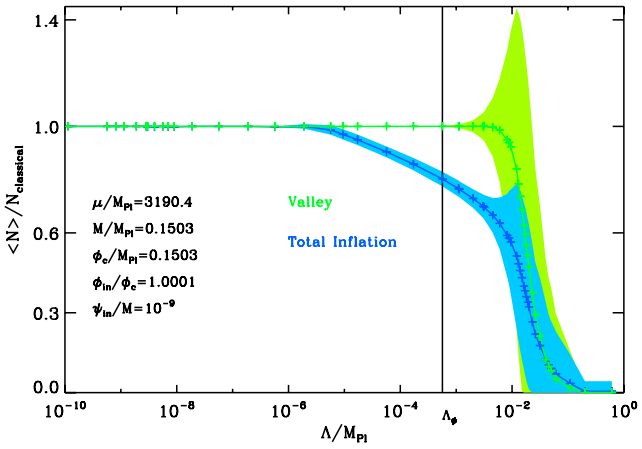

FIG. 13 (color online). Total number of e-folds (blue) and number of e-folds realized in the valley (green) as a function of $\Lambda/M_{\rm Pl}$ for the parameters indicated on the plot. The two numbers of e-folds are normalized to their classical counterparts. The solid lines represent the mean values of the distributions, while the colored surfaces represent the plus or minus 1 standard deviation areas. The vertical solid black line indicates the value of Λ_ϕ.

As mentioned above, we have also studied how our results depend on Λ. In the vacuum dominated regime, Λ is directly related to the energy scale of inflation. This quantity is constrained by the big bang nucleosynthesis and by the observations of the CMBR, namely,

$$10^{-17} M_{\rm Pl} \lesssim \Lambda \lesssim 5 \times 10^{-2} M_{\rm Pl}\,. \tag{65}$$

The previous figures correspond to a regime where $\Lambda > \Lambda_\phi$ (recall that, for the values of the parameters chosen here, we have $\Lambda_\phi \simeq 5.7 \times 10^{-4} M_{\rm Pl}$) since we wanted to study a regime where the noise in the two-field directions is important. However, one can also wonder if the previous conclusions, especially the fact that $\langle N\rangle < N_{\rm class}$, still hold in the regime $\Lambda < \Lambda_\phi$. In Fig. 13, we have computed the total number of e-folds as a function of Λ. The first thing we notice in this plot is that, for $\Lambda \gtrsim \Lambda_\phi$ (indicated by the vertical black line), the total number of e-folds and the number of e-folds in the valley are smaller than their classical counterparts. This is of course compatible with the previous considerations. In the regime $10^{-6} M_{\rm Pl} \lesssim \Lambda \lesssim \Lambda_\phi$, the number of e-folds in the valley is equal to its classical counterpart as expected, since the inflaton behaves classically but the total number of e-folds, hence the number of e-folds in the waterfall regime, is still smaller than $N_{\rm class}$. So even in the absence of noise along the inflaton direction, the conclusion obtained before remains valid. Finally, for $\Lambda \lesssim 10^{-6} M_{\rm Pl}$, the noise is so small that the stochastic and classical number of e-folds are equal.

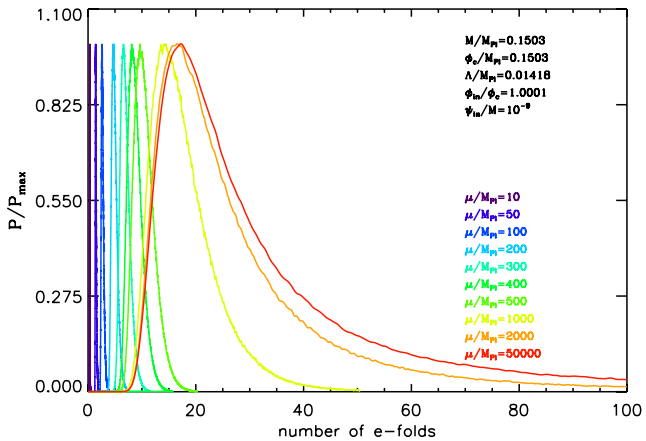

FIG. 12 (color online). Distribution of the total number of e-folds realized during inflation, normalized by its maximum value, for different values of μ. The dependence on μ of $\langle N\rangle$ is consistent with the qualitative predictions of Sec. II. One also notices that the dispersion of the distribution increases with the number of e-folds realized in the flat region. This is due to the fact that the quantum effects broaden the distribution.

In Fig. 11, we have seen that, for $\Lambda = 0.014\,18 M_{\rm Pl}$, one has $\langle N\rangle \simeq 50$. Since the scales of astrophysical interest today left the Hubble radius during inflation about 50–60 e-folds before the end of inflation, this would mean that we could have a direct observational window on the stochastic regime. In fact, this is not so because $\Delta = 1$ means that $H^2/\epsilon_1 \simeq 1$. But H^2/ϵ_1 is precisely the overall normalization of the density perturbations power spectrum which is observed to be $\simeq 10^{-5}$. So, in fact, this shows that the value $\Lambda = 0.014\,18 M_{\rm Pl}$ is simply excluded by the CMBR measurements. For this reason, it is interesting to plot the

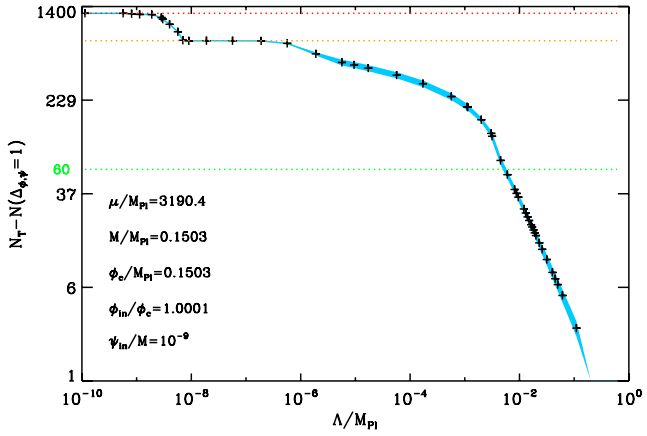

FIG. 14 (color online). Number of e-folds realized between the exit of the stochastic regime (i.e. the moment where Δ_ϕ and Δ_ψ are both smaller than 1) and the end of inflation. The cruxes stand for the mean values of the distributions, and the colored surfaces stand for the plus or minus 1 standard deviation areas. The horizontal dotted red line represents the total number of e-folds calculated in the absence of noise. The horizontal dotted orange line is the number of e-folds realized in the waterfall region in the absence of noise. Finally, the horizontal green dotted line represents the minimal number of e-folds required for inflation to be successful, i.e. 60.

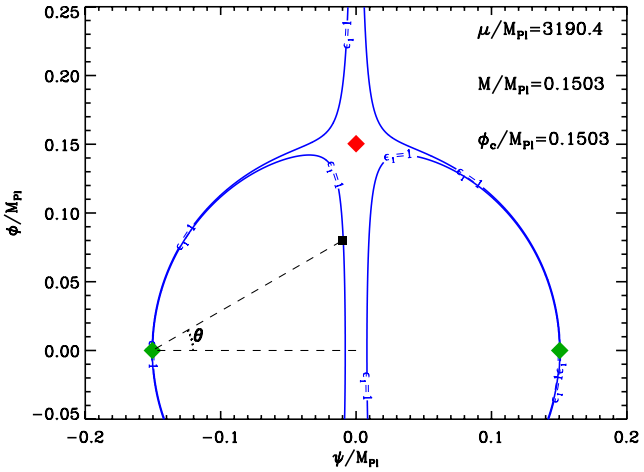

FIG. 15 (color online). Level lines $\epsilon_1 = 1$ in the (ϕ, ψ) plane. The parameters chosen are the same as in the other plots. The red rhombus sits at the critical point, while the two green ones are located at the two minima. The definition of the angle θ is shown for a trajectory leaving the inflationary region (i.e. crossing the $\epsilon_1 = 1$ line) at the black square.

number of e-folds performed between the moment the system becomes classical (i.e. when Δ_ϕ and Δ_ψ are both smaller than 1) and the end of inflation. If this number is smaller than ∼50–60, this means that the corresponding value of Λ is excluded due to the above argument. The plot is represented in Fig. 14. We see that for $\Lambda \gtrsim 10^{-2} M_{\rm Pl}$, the number mentioned above is indeed smaller than 60. All these values are therefore excluded. This means that for values of Λ such that $\Lambda_\phi \lesssim \Lambda \lesssim 10^{-2} M_{\rm Pl}$, we are in a regime where the perturbations are not too large to be directly in contradiction with the CMBR (of course this does not guarantee that the correct normalization can be obtained) and where it is mandatory to take into account the stochastic effects in the two-field directions. If $10^{-6} M_{\rm Pl} \lesssim \Lambda \lesssim \Lambda_\phi$, the stochastic effects dominate only in the ψ direction, both in the valley and the waterfall phase. For $10^{-8} M_{\rm Pl} \lesssim \Lambda \lesssim 10^{-6} M_{\rm Pl}$, the waterfall regime becomes completely classical and, finally, for $\Lambda \lesssim 10^{-8} M_{\rm Pl}$, the noise becomes so small that the full evolution in the valley and in the waterfall region can be described classically.

Let us end this subsection with some remarks. We have seen that the stochastic number of e-folds is smaller than its classical counterpart as soon as $\Lambda \gtrsim 10^{-6} M_{\rm Pl}$. If $\Lambda \gtrsim \Lambda_\phi \simeq 5.7 \times 10^{-4} M_{\rm Pl}$, we are in a two-field regime. Moreover, if $\Lambda \gtrsim 10^{-2} M_{\rm Pl}$, the stochastic effects are so strong that the model is in contradiction with the amplitude of the CMBR fluctuations. We expect these conclusions to be very roughly independent of the choice of the other parameters, provided, of course, that one remains in the regime described in Sec. II A. In fact, to go further, one should explore the full parameter space, and one should carefully apply Cosmic Background Explorer normalization to the model. When the waterfall regime plays an important role, this is not a trivial task.

E. Inflation exit point

Another relevant physical quantity is the inflation exit point, i.e. the location in the field space where inflation stops. The details of the subsequent (p)reheating phase strongly depend on these initial conditions, which are therefore important physical quantities [64,65]. Inflation stops when the system crosses the $\epsilon_1 = 1$ level line in the field space. As a consequence, the exit point is necessarily located on this level line. It can be characterized by the angle θ between the line joining the closest minimum to the origin and the line joining this same minimum to the exit point. This parametrization and the $\epsilon_1 = 1$ contours are represented in Fig. 15. Since the stochastic effects taking place in the valley quickly render the distribution symmetrical in ψ, the two minima are in fact put on an equal footing. Using the same method as before, one can calculate the classical prediction for this angle θ and compare it with the corresponding stochastic distribution. The result is shown in Fig. 16.

Here again, several comments are in order. First, unlike the distribution of the number of e-folds, the classical prediction lies within the stochastic distribution. It is even more remarkable that the distribution is very narrow. *A priori*, this is a surprising fact since the stochastic realizations in the vicinity of the critical point are extremely noisy, as can be seen in Fig. 9. Even if the

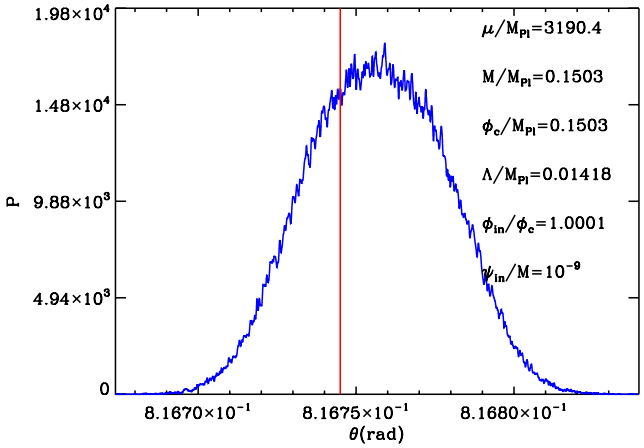

FIG. 16 (color online). Numerical distribution of the exit angle θ. The parameters are the same as in the other figures. The red line corresponds to the classical prediction. We notice that the distribution is extremely peaked, $\Delta\theta/\theta \sim 10^{-3}$.

stochastic trajectories are very different from one realization to another and spread over a large area in the field space, they eventually gather at the end of the waterfall phase to exit inflation at nearly the same point. We interpret this property in the following manner. Around the critical point, as was already mentioned before, the noise is quite strong and it quickly kicks the fields out of this region. As a consequence, the fields eventually land in a region where the noise is subdominant. Therefore, from that point, the fields will follow a classical trajectory. If there is a classical attractor, all the trajectories will converge towards this particular path, and inflation will always stop at the same point. This analysis is confirmed by Fig. 17, where we have plotted in the field plane the flow lines of the classical equations of motion, Eqs. (2) and (3). As can be seen in the

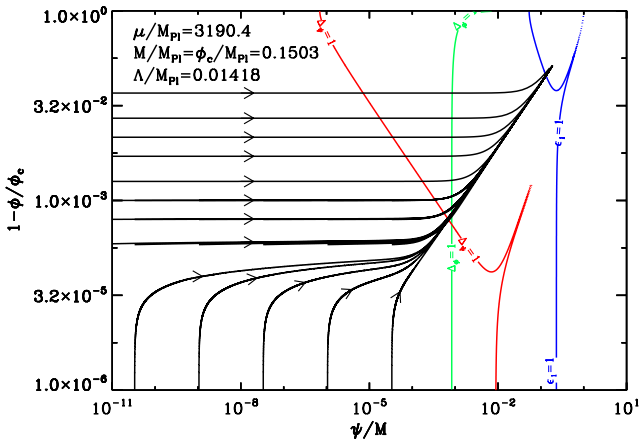

FIG. 17 (color online). Flow map of the classical slow-roll dynamics equations. Regardless of their initial conditions, all the trajectories end up at the same exit point.

figure, after crossing the $\Delta_\psi = 1$ and $\Delta_\phi = 1$ level lines, which implies that the fields enter a region where the stochastic terms are subdominant, all the classical trajectories merge into a single one before crossing the $\epsilon_1 = 1$ level line and thus exiting the inflationary region. Then, one can check that this point corresponds to the angle θ singled out in Fig. 16. This classical attractiveness can also be formally established by studying the Lyapounov exponent, in the direction orthogonal to the flow tangents. We conclude that, despite the strong quantum effects undergone by the fields during the inflationary phase, the exit point is always the same (approximately, of course) in hybrid inflation. Moreover, this point turns out to be the classical one which provides a straightforward way to calculate its location.

IV. CONCLUSION

Let us now summarize our main findings. We have found that the quantum effects play an important role in hybrid inflation, especially in the vicinity of the critical point (this seems to be a general feature of multiple field models of inflation, as soon as flat directions are present in the potential). As a consequence, the classical picture presented in Sec. II has to be substantially modified. This can be done in the framework of stochastic inflation, where the inflationary dynamics is driven by two coupled Langevin equations. Given that the stochastic effects can be strong in the two directions in field space, we have used a numerical approach to solve these equations. Then, we have derived the distributions of two relevant quantities, namely, the total number of e-folds realized during inflation and the exit point. We have shown that, when the stochastic noise plays a role, the distribution of the number of e-folds is peaked at a value which is different from the classical prediction. This is due to the fact that, in the neighborhood of the critical point, the potential is very flat and the quantum kicks quickly move the system away from this region. On the other hand, the distribution of the exit point of inflation leads to conclusions which are apparently at odds with this picture since it is extremely peaked over the classical prediction. But, in fact, this property is due to the attractiveness of the classical flow and is not at all in contradiction with the previous considerations.

An important question that remains to be addressed in more detail is the impact of our results on the observable predictions of hybrid inflation. For instance, it would be of utmost importance to study how the quantum effects can modify the power spectra of cosmological fluctuations. It was recently emphasized in Ref. [26] that hybrid inflation can lead to a red spectrum, and it would be interesting to investigate the influence of the quantum effects on this prediction, both for the adiabatic and entropy modes [66]. Also, the explicit computation of the probability density functions in the field space provides us with a

means to calculate the non-Gaussianities of this model. We intend to come back to those issues in the future. Maybe the most important conclusion of our work is that the richness of multiple inflation—namely, the presence of entropy modes *a priori* produced during the waterfall regime, the highly nontrivial phase of preheating, and the strong quantum effects—implies that it is not simple to derive the corresponding observable predictions and that, most of the time, these ones cannot be obtained in a simple single field effective model. This is an important conclusion that one should keep in mind when analyzing the future high accuracy CMB data and their implications for inflation.

ACKNOWLEDGMENTS

We would like to thank S. Clesse and C. Ringeval for useful discussions.

[1] A. A. Starobinsky, Phys. Lett. **91B**, 99 (1980).
[2] A. H. Guth, Phys. Rev. D **23**, 347 (1981).
[3] A. D. Linde, Phys. Lett. **108B**, 389 (1982).
[4] A. Albrecht and P. J. Steinhardt, Phys. Rev. Lett. **48**, 1220 (1982).
[5] A. D. Linde, Phys. Lett. **129B**, 177 (1983).
[6] J. Martin, Braz. J. Phys. **34**, 1307 (2004).
[7] J. Martin, Lect. Notes Phys. **669**, 199 (2005).
[8] J. Martin, Lect. Notes Phys. **738**, 193 (2008).
[9] V. F. Mukhanov and G. Chibisov, JETP Lett. **33**, 532 (1981).
[10] V. F. Mukhanov and G. Chibisov, Sov. Phys. JETP **56**, 258 (1982).
[11] S. Hawking, Phys. Lett. **115B**, 295 (1982), revised version.
[12] A. A. Starobinsky, Phys. Lett. **117B**, 175 (1982).
[13] A. H. Guth and S. Y. Pi, Phys. Rev. Lett. **49**, 1110 (1982).
[14] J. M. Bardeen, P. J. Steinhardt, and M. S. Turner, Phys. Rev. D **28**, 679 (1983).
[15] J. Martin and C. Ringeval, J. Cosmol. Astropart. Phys. 08 (2006) 009.
[16] L. Lorenz, J. Martin, and C. Ringeval, J. Cosmol. Astropart. Phys. 04 (2008) 001.
[17] L. Lorenz, J. Martin, and C. Ringeval, Phys. Rev. D **78**, 063543 (2008).
[18] J. Martin and C. Ringeval, Phys. Rev. D **82**, 023511 (2010).
[19] J. Martin, C. Ringeval, and R. Trotta, Phys. Rev. D **83**, 063524 (2011).
[20] A. D. Linde, Phys. Rev. D **49**, 748 (1994).
[21] E. J. Copeland, A. R. Liddle, D. H. Lyth, E. D. Stewart, and D. Wands, Phys. Rev. D **49**, 6410 (1994).
[22] E. Halyo, Phys. Lett. B **387**, 43 (1996).
[23] P. Binetruy and G. Dvali, Phys. Lett. B **388**, 241 (1996).
[24] G. Dvali, Q. Shafi, and R. K. Schaefer, Phys. Rev. Lett. **73**, 1886 (1994).
[25] R. Kallosh and A. D. Linde, J. Cosmol. Astropart. Phys. 10 (2003) 008.
[26] S. Clesse and J. Rocher, Phys. Rev. D **79**, 103507 (2009).
[27] S. Clesse, Phys. Rev. D **83**, 063518 (2011).
[28] A. A. Abolhasani, H. Firouzjahi, and M. H. Namjoo, Classical Quantum Gravity **28**, 075009 (2011).
[29] A. Vilenkin, Nucl. Phys. **B226**, 527 (1983).
[30] A. A. Starobinsky (unpublished).
[31] A. Goncharov, A. D. Linde, and V. F. Mukhanov, Int. J. Mod. Phys. A **2**, 561 (1987).
[32] Y. Nambu and M. Sasaki, Phys. Lett. B **205**, 441 (1988).
[33] Y. Nambu and M. Sasaki, Phys. Lett. B **219**, 240 (1989).
[34] H. E. Kandrup, Phys. Rev. D **39**, 2245 (1989).
[35] K.-i. Nakao, Y. Nambu, and M. Sasaki, Prog. Theor. Phys. **80**, 1041 (1988).
[36] Y. Nambu, Prog. Theor. Phys. **81**, 1037 (1989).
[37] S. Mollerach, S. Matarrese, A. Ortolan, and F. Lucchin, Phys. Rev. D **44**, 1670 (1991).
[38] A. D. Linde, D. A. Linde, and A. Mezhlumian, Phys. Rev. D **49**, 1783 (1994).
[39] A. A. Starobinsky and J. Yokoyama, Phys. Rev. D **50**, 6357 (1994).
[40] A. D. Linde, Phys. Lett. B **175**, 395 (1986).
[41] A. D. Linde, Mod. Phys. Lett. A **1**, 81 (1986).
[42] J. Garcia-Bellido, A. D. Linde, and D. Wands, Phys. Rev. D **54**, 6040 (1996).
[43] J. Martin and M. Musso, Phys. Rev. D **73**, 043516 (2006).
[44] J. Martin and M. Musso, Phys. Rev. D **73**, 043517 (2006).
[45] A. M. Green and A. Mazumdar, Phys. Rev. D **65**, 105022 (2002).
[46] E. D. Stewart and D. H. Lyth, Phys. Lett. B **302**, 171 (1993).
[47] A. R. Liddle, P. Parsons, and J. D. Barrow, Phys. Rev. D **50**, 7222 (1994).
[48] S. Groot Nibbelink and B. van Tent, Classical Quantum Gravity **19**, 613 (2002).
[49] R. Easther and J. T. Giblin, Phys. Rev. D **72**, 103505 (2005).
[50] D. J. Schwarz, C. A. Terrero-Escalante, and A. A. Garcia, Phys. Lett. B **517**, 243 (2001).
[51] S. M. Leach, A. R. Liddle, J. Martin, and D. J. Schwarz, Phys. Rev. D **66**, 023515 (2002).
[52] S. Clesse, AIP Conf. Proc. **1241**, 543 (2010).
[53] S. Clesse, arXiv:1006.4435.
[54] S. Clesse, C. Ringeval, and J. Rocher, Phys. Rev. D **80**, 123534 (2009).
[55] A. A. Abolhasani, H. Firouzjahi, and M. Sasaki, arXiv:1106.6315.
[56] D. H. Lyth, arXiv:1005.2461.

[57] A. A. Abolhasani and H. Firouzjahi, Phys. Rev. D **83**, 063513 (2011).
[58] H. Kodama, K. Kohri, and K. Nakayama, Prog. Theor. Phys. **126**, 331 (2011).
[59] F. Finelli, G. Marozzi, A. A. Starobinsky, G. P. Vacca, and G. Venturi, Phys. Rev. D **79**, 044007 (2009).
[60] F. Finelli, G. Marozzi, A. A. Starobinsky, G. P. Vacca, and G. Venturi, Phys. Rev. D **82**, 064020 (2010).
[61] F. Finelli, G. Marozzi, A. Starobinsky, G. Vacca, and G. Venturi, arXiv:1102.0216.
[62] K. Enqvist, D. G. Figueroa, and G. Rigopoulos, arXiv:1109.3024.
[63] S. Gratton and N. Turok, Phys. Rev. D **72**, 043507 (2005).
[64] J. Garcia-Bellido and A. D. Linde, Phys. Rev. D **57**, 6075 (1998).
[65] F. Finelli and R. H. Brandenberger, Phys. Rev. D **62**, 083502 (2000).
[66] L. P. Levasseur, G. Laporte, and R. Brandenberger, Phys. Rev. D **82**, 123524 (2010).

PHYSICAL REVIEW D **88,** 083538 (2013)

Recursive stochastic effects in valley hybrid inflation

Laurence Perreault Levasseur[*]
DAMTP, Center for Mathematical Sciences, University of Cambridge, Cambridge CB3 0WA, United Kingdom

Vincent Vennin[†]
Institut d'Astrophysique de Paris, UMR 7095-CNRS, Université Pierre et Marie Curie, 98bis boulevard Arago, 75014 Paris, France

Robert Brandenberger[‡]
Department of Physics, McGill University, Montréal, Quebec H3A 2T8, Canada
(Received 26 August 2013; published 31 October 2013)

Hybrid inflation is a two-field model where inflation ends because of a tachyonic instability, the duration of which is determined by stochastic effects and has important observational implications. Making use of the recursive approach to the stochastic formalism presented in [L. P. Levasseur, preceding article, Phys. Rev. D **88**, 083537 (2013)], these effects are consistently computed. Through an analysis of backreaction, this method is shown to converge in the valley but points toward an (expected) instability in the waterfall. It is further shown that the quasistationarity of the auxiliary field distribution breaks down in the case of a short-lived waterfall. We find that the typical dispersion of the waterfall field at the critical point is then diminished, thus increasing the duration of the waterfall phase and jeopardizing the possibility of a short transition. Finally, we find that stochastic effects worsen the blue tilt of the curvature perturbations by an $\mathcal{O}(1)$ factor when compared with the usual slow-roll contribution.

DOI: 10.1103/PhysRevD.88.083538 PACS numbers: 98.80.Cq, 98.70.Vc

I. INTRODUCTION

Inflation is currently the leading paradigm attempting to shed light on the physics of the very early Universe. It describes a phase of accelerated expansion, which solves many problems of the hot big bang scenario [1–8]. Inflation further provides a causal mechanism for generating fluctuations on cosmological scales, and it predicts that their spectrum should be almost scale invariant, with small deviations from scale invariance which can be traced back to the precise microphysics of inflation [9–14]. This prediction is consistent with the current astrophysical observation, such as the CMB, including the measurement of the cosmic microwave background anisotropies. For this specific observable, the latest results [15–17] give a slightly red-tilted spectral index $n_S \simeq 0.96$, ruling out exact scale invariance $n_S = 1$ at over 5σ and allowing us to constrain the inflationary models still allowed by the data [18].

With the ever-increasing precision of the experiments probing this window into the early Universe, it is now very important to develop robust and self-consistent methods for calculating inflationary predictions. For example, in the context of multifield inflation, it is complicated to disentangle the gravitational and matter degrees of freedom when describing fluctuations produced in the scalar fields using traditional methods. Typically, approximations are used to make the problem tractable, but these approximations ignore backreaction, that is, the effects of these fluctuations on the background spacetime and field trajectory. Restoring or even assessing the importance of these neglected effects then becomes extremely nontrivial, and it has been shown that such effects can have a crucial impact on the inflationary dynamics [19–22] (see also Ref. [23] for a review of early work).

One way to resum these effects, at least partially, is to make use of the stochastic inflation formalism [24–34]. The basic strategy is to derive an effective theory for the long-wavelength part of the fields, which are "coarse grained" at a scale larger than the Hubble radius. In this framework, the small-scale quantum fluctuations play the role of a "bath" and are collected in classical noise terms which affect the dynamics of the coarse-grained fields. The super-Hubble physics can thus be described by a stochastic classical theory.

The corresponding equations can be derived by making use of the Schwinger-Keldysh closed time path formalism [35–38], where the strategy is to split the degrees of freedom of the full quantum fields in momentum space through a window function, and perform the path integral over the small-scale fluctuations. In Ref. [39], this Lagrangian formulation of the theory is used to develop a recursive method for solving the stochastic equations when the background spacetime is taken to be dynamic. It is this recursive method which we now apply to models of multifield inflation, and specifically to hybrid inflation.

At the energy scale of inflation (typically around 10^{15}–10^{16} GeV), particle physics remains elusive, leaving room for a large variety of different inflationary scenarios.

[*]l.perreault-levasseur@damtp.cam.ac.uk
[†]vennin@iap.fr
[‡]rhb@hep.physics.mcgill.ca

However, the supersymmetry- and supergravity-based extensions of the standard model of particle physics yield a well-motivated model, hybrid inflation [40,41], which can be realized in various ways in the context of F-term or D-term inflation [42–45]. Hybrid Inflation is a two-field model in which inflation is driven by a light inflaton field in a valley, where the potential is dominated by a vacuum constant, and where the inflaton vacuum expectation value (vev) tunes the mass of an auxiliary field that becomes imaginary at some critical point, triggering the end of inflation by a "waterfall" phase. This auxiliary field is thus called the "waterfall field." This model is known to lead, in the valley, to a blue spectrum $n_S > 1$ for the cosmological fluctuations, a prediction which is strongly disfavored by current observations.

However, it was shown [46,47] that, in some regions of parameter space, a significant number of e-folds can occur in the waterfall regime. In this case, it was also demonstrated that the spectral index becomes red, eliminating this tension. Since the duration of the waterfall phase is determined by the stochastic dispersion of the waterfall field at the critical point, it is therefore crucial to compute this quantity accurately, and to properly include the stochastic effects in the description of the model.

Moreover, in Ref. [48], it was shown that stochastic effects can significantly alter the inflationary background dynamics in the context of hybrid inflation, especially close to the critical point where the two-field potential is very flat and where one enters a regime of stochastically driven saddle-point inflation. Backreaction is therefore expected to be important in this case. The associated mode coupling effects were investigated in Ref. [49].

In the current paper, these issues are addressed by applying the new recursive method developed in Ref. [39] to the specific example of two-field hybrid inflation potentials, to illustrate how this formalism can be implemented and how it yields new results when compared with standard techniques for computing observables of inflation beyond the leading order. The outline of the strategy is to first calculate the background evolution in the presence of a free noise, then calculate the corrected quantum noise on this shifted background, to finally come back to the background, coarse-grained dynamics shifted in light of the fluctuations, and so on until the process converges. We demonstrate the convergence of this method in the valley region, where the usual QFT methods of perturbation theory are known to be under control. In doing so, we calculate modified predictions emerging from a consistently implemented nonperturbative method for cosmological observables such as the tilt of the CMB power spectrum. Most interestingly, we identify regimes of hybrid inflation where stochastic effects dominate over regular perturbative corrections.

One of the main interests of this program of research is, however, the waterfall phase, where backreaction and mode coupling effects are expected to be important. We discuss important implications of the findings of the current work for this phase, but plan to pursue a more thorough study of the waterfall phase in the future.

The paper is organized as follows. In Sec. II, the background classical dynamics of valley hybrid inflation is computed, and the recursive approach to stochastic inflation of Ref. [39] is presented. A first-step massless de Sitter solution, valid up to leading order in $\hbar$ and to zeroth order in slow roll, is presented.

In Sec. III, we calculate the value of the noises up to next-to-leading order in $\hbar$ and to leading order in slow roll. To do so, we make use of the fact that solving for the propagators of the bath fields at this order is equivalent to solving the linearized quantum mode functions in a shifted background. We compute the amplitude of these linear perturbations in both fields, and identify different regimes for the waterfall field fluctuation evolution.

In Sec. IV, the corresponding modified amplitudes of the noise terms are implemented in the stochastic equations. Their effect on the mean deviation in the waterfall direction is carefully computed. Short-lived waterfalls are shown to be unlikely, since the quasistationary time behavior of the auxiliary field distribution breaks down in this regime, reducing its quantum dispersion at the critical point, hence lengthening this stage. Furthermore, an analysis of backreaction shows that the recursive process converges in the valley but blows up in the waterfall, suggesting perturbative instability there.

In Sec. V, we study how the classical inflation perturbations beyond zeroth order in the slow-roll expansion are influenced by stochastic effects, in particular, when it comes to the curvature perturbations' spectral tilt. We obtain that the stochastic effects worsen the blue-tilt problem, by a factor $\mathcal{O}(1)$ compared to the usual slow-roll contribution. Finally in Sec. VI, we summarize our main findings and suggest possible further investigations.

II. VALLEY HYBRID INFLATION

The potential of hybrid inflation in the field space (Φ, Ψ), where Φ is the inflaton and Ψ the waterfall field, is given by

$$V(\Phi, \Psi) = \frac{1}{2}m^2\Phi^2 + \frac{\lambda}{4}(\Psi^2 - v^2)^2 + \frac{g^2}{2}\Phi^2\Psi^2. \quad (1)$$

The true minima of the potential are located at $\Phi = 0$ and $\Psi = \pm v$, while the instability point is given by

$$\Phi_c^2 = \frac{v^2\lambda}{g^2}, \qquad \Psi_c = 0. \quad (2)$$

It is usually assumed that hybrid inflation occurs in the vacuum-dominated regime, for which $\Phi_c < \Phi \ll \lambda^{1/2}v^2/m$ and $\Psi \ll v$. In this approximation, the first slow-roll parameter in the valley ($\Phi > \Phi_c$, $\Psi = 0$) is given by $\varepsilon_1 \simeq 8m^4\phi^2M_{\rm Pl}^2/(\lambda^2v^8)$; hence for the slow-roll approximation

to be satisfied in the valley, one must assume that $\lambda v^4 \gg m^2 \Phi_c M_{\rm Pl}$, where $M_{\rm Pl}$ is the reduced Planck mass. In the same manner, the smallness of the second slow-roll parameter $\varepsilon_2 \simeq -8 M_{\rm Pl}^2 m^2/(\lambda v^4) \ll 1$ implies the more stringent condition $\lambda v^4 \gg m^2 M_{\rm Pl}^2$ (one then has $\varepsilon_1 \ll \varepsilon_2$). In this case, the total energy density is dominated by the constant term of the potential $\rho \simeq V \simeq \lambda v^4/4$. Motivated by the supersymmetric version of the model, we also take $\Phi_c \simeq v$ or, using the definition of Φ_c in terms of the potential parameters, $\lambda^{1/2} \simeq g$. Finally, in order for the model to be consistently derived, inflation must proceed at small values of the fields (compared to the Planck mass), and one can consider that Φ_c, $v \ll M_{\rm Pl}$. The constraints on the potential parameters coming from these considerations and the ones below are collected in Appendix A, together with a summary of the notations used throughout the paper.

Taken literally, this model produces a blue tilt for the spectrum of cosmological perturbations [50] when inflation is realized in the valley,

$$n_s \simeq 1 - \varepsilon_2 \simeq 1 + 8\frac{M_{\rm Pl}^2 m^2}{\lambda v^4}. \tag{3}$$

Recently, to alleviate this problem, it has been suggested to realize the last 60 e-folds of inflation in the waterfall phase [51]. In order to do so, one must choose the parameters of the potential in order for a sufficiently large number of e-folds to be realized in the waterfall phase, making the model behave in a fashion effectively similar to a (multifield) hilltop model. The duration of this stage being determined by the mean stochastic shift of the waterfall field at the critical point, an accurate calculation of the preceding stochastic effects in the valley is crucial to determine whether such a scenario is viable or not.

Note that one could also choose to glue a different potential for the inflaton in the valley phase, chosen specifically in order to produce the desired tilt, and then use the symmetry breaking shape of the hybrid potential for the sole purpose of ending inflation (see, e.g., Refs. [52–54]). However, as we will see, when choosing the potential, one has to be careful that stochastic effects do not reintroduce the blue tilt. In any case, $m^2\phi^2$ is the simplest choice for the inflaton potential, and in the absence of special symmetries (e.g., conformal symmetry), such a term will be present and will dominate at small field values. Thus, as a toy model for multifield inflation, the terms included in our potential are the lowest-order terms one would expect to find.

A. Classical dynamics

In this subsection, we study the classical behavior of the inflaton and waterfall fields at the background level, which represents the first step of the recursive method presented below. The slow-roll equations controlling the evolution of the classical background fields $\varphi^{(0)}$ and $\chi^{(0)}$ can be expressed as

$$3H^2 \frac{{\rm d}\varphi^{(0)}}{{\rm d}N} \simeq -m^2\varphi^{(0)}\left(1 + \frac{g^2\chi^{(0)2}}{m^2}\right), \tag{4}$$

$$3H^2 \frac{{\rm d}\chi^{(0)}}{{\rm d}N} \simeq -\lambda v^2 \chi^{(0)}\left(\frac{\varphi^{(0)2} - \Phi_c^2}{\Phi_c^2} + \frac{\chi^{(0)2}}{v^2}\right), \tag{5}$$

with

$$H^2 = \frac{1}{3M_{\rm Pl}^2}\rho \simeq \frac{\lambda v^4}{12 M_{\rm Pl}^2}. \tag{6}$$

The superscript $^{(0)}$ denotes a background, homogeneous quantity, and $H = \dot{a}/a$ is the Hubble parameter with the dot standing for a derivative with respect to cosmic time t. The quantity N is the number of e-folds, $N \equiv \ln(a/a_{\rm i})$, where[1] $a_{\rm i}$ is the scale factor at an initial reference point.

If inflation starts beyond the critical line $\Phi = \Phi_c$, the system very quickly reaches the region where $\chi^{(0)} \ll v$ and inflation is driven by the inflaton $\varphi^{(0)}$ which slowly rolls down towards the critical point, while the waterfall field $\chi^{(0)}$ first undergoes damped oscillations at the bottom of the valley, before experiencing a short, simple damping regime. Defining

$$\omega(N) = \frac{3}{2}\sqrt{1 - \frac{16}{3}\frac{M_{\rm Pl}^2}{v^2}\frac{\frac{\varphi^{(0)2}(N)}{\Phi_c^2} - 1}{1 + \frac{2m^2}{\lambda v^4}\varphi^{(0)2}(N)}}, \tag{7}$$

the homogeneous time evolution of these two fields is given by

$$\varphi^{(0)} = \varphi_{\rm in}\exp\left(-4\frac{M_{\rm Pl}^2 m^2}{\lambda v^4}N\right),$$
$$\chi^{(0)} = \begin{cases} \chi_{\rm in}\frac{{\rm e}^{-3N/2}}{\sqrt{2\omega(N)}}\left[C_1 {\rm e}^{I(N)} + C_2 {\rm e}^{-I(N)}\right] & \text{if } \frac{\varphi^{(0)}}{\Phi_c} > 1 + \frac{3}{32}\frac{v^2}{M_{\rm Pl}^2}, \\ \chi_{\rm in}\exp\left[-4\frac{M_{\rm Pl}^2}{M^2}\left(\frac{\varphi_{\rm in}}{\Phi_c} - 1\right)N\right] & \text{if } \frac{\varphi^{(0)}}{\Phi_c} < 1 + \frac{3}{32}\frac{v^2}{M_{\rm Pl}^2}, \end{cases} \tag{8}$$

where $\varphi_{\rm in}$ and $\chi_{\rm in}$ are the initial inflaton and waterfall values, C_1 and C_2 are integration constants, and where $I(N)$ is given by

$$I(N) \simeq -\frac{\sqrt{3}}{M_{\rm Pl}}\frac{\lambda v^3}{2m^2}\left[\sqrt{\frac{\varphi^{(0)2}}{\Phi_c^2} - 1} - \arctan\left(\sqrt{\frac{\varphi^{(0)}}{\Phi_c^2} - 1}\right) - \sqrt{\frac{\varphi_{\rm in}^2}{\Phi_c^2} - 1} + \arctan\left(\sqrt{\frac{\varphi_{\rm in}^2}{\Phi_c^2} - 1}\right)\right]. \tag{9}$$

From the previous equations, the total number of e-folds spent in the valley is

$$N_c = \frac{\lambda v^4}{4m^2 M_{\rm Pl}^2}\ln\left(\frac{\varphi_{\rm in}}{\Phi_c}\right). \tag{10}$$

[1]The cosmological scale factor is denoted by $a(t)$.

It is typically a large number because of our assumption $\lambda v^4/(2m^2) \gg M_{\rm Pl}^2$. Finally, the value of χ at the end of this stage reads

$$\chi_{\rm c}^{(0)} = \chi_{\rm in} \exp\left[-2\frac{\lambda v^2}{m^2}\left(\frac{\varphi_{\rm in}}{\Phi_{\rm c}} - 1\right)\ln\left(\frac{\varphi_{\rm in}}{\Phi_{\rm c}}\right)\right]. \quad (11)$$

With the assumptions made above on the potential parameters, this value is typically so small that it is completely washed out by the quantum noise that we calculate in the rest of the paper. The number of e-folds spent during the waterfall phase is given by [48,55]

$$N_{\rm end} - N_{\rm c} \simeq \frac{\lambda^{1/2} v^3}{4mM_{\rm Pl}^2} \ln^{1/2}\left(\frac{m}{g\chi_{\rm c}}\right). \quad (12)$$

From this, if one is interested in the regime where the required $\sim$60 e-folds of inflation take place during the waterfall phase, one needs to work with $\lambda^{1/2} v^3 \gg mM_{\rm Pl}^2$. Note that a more detailed description of the waterfall phase is reviewed in Appendix B.

Finally, inflation stops when $\varepsilon_1 = 1$, and the system starts oscillating around one of the two true minima of the potential, triggering a phase of (p)reheating [56–59].

B. Stochastic formalism and recursive strategy

The previous subsection details the dynamics of two classical fields $\varphi^{(0)}$ and $\chi^{(0)}$, each obeying a homogeneous Klein-Gordon equation. The system we are interested in studying, however, is a system consisting of two inhomogeneous four-dimensional quantum fields, Φ and Ψ. Solving the full Heisenberg field equations that they obey in curved spacetime is, in general, impossible with current techniques, and so different approximation schemes are typically applied to make the calculations tractable.

One such strategy is to derive an effective theory for the classicalized, long-wavelength part of the fields, which can be shown [60,61] to behave as a classical stochastic system. The super-Hubble Fourier modes of the full quantum fields, corresponding to scales with $k < \epsilon aH$ ($\epsilon < 1$ being a small dimensionless parameter setting the averaging scale and collecting only the super-Hubble sufficiently squeezed and decohered modes), are collected into coarse-grained fields φ and χ. These coarse-grained fields evolve in the presence of a quantum bath made of the remaining, sub-Hubble modes with $k > \epsilon aH$, which are collected using a window function $W_H(k, t)$ in the Fourier expansion of the corresponding full quantum fields. The fields of the quantum bath and the coarse-grained fields are thus given by

$$\phi_> = \int \frac{{\rm d}^3k}{(2\pi)^3} W_H(k,t)[\phi_{\mathbf{k}} \hat{a}_{\mathbf{k}} e^{-i\mathbf{x}\cdot\mathbf{k}} + \phi_{\mathbf{k}}^* \hat{a}_{\mathbf{k}}^\dagger e^{i\mathbf{x}\cdot\mathbf{k}}], \quad (13)$$

$$\varphi \equiv \Phi - \phi_>,$$

$$\psi_> = \int \frac{{\rm d}^3k}{(2\pi)^3} W_H(k,t)[\psi_{\mathbf{k}} \hat{b}_{\mathbf{k}} e^{-i\mathbf{x}\cdot\mathbf{k}} + \psi_{\mathbf{k}}^* \hat{b}_{\mathbf{k}}^\dagger e^{i\mathbf{x}\cdot\mathbf{k}}],$$

$$\chi \equiv \Psi - \psi_>, \quad (14)$$

where the quantum bath fields have been written in terms of their linearized mode functions $\phi_{\mathbf{k}}$ and $\psi_{\mathbf{k}}$, and the creation and annihilation operators $\hat{a}_{\mathbf{k}}^\dagger$, $\hat{a}_{\mathbf{k}}$, $\hat{b}_{\mathbf{k}}^\dagger$, $\hat{b}_{\mathbf{k}}$.

Because Fourier modes constantly cross the Hubble radius during inflation, leaving the quantum bath to join the coarse-grained fields, the quantum bath sources the coarse-grained part of the fields. This effect adds to the equations of motion a stochastic noise term, yielding, to leading order[2] in $\hbar$,

$$3H^2 \frac{{\rm d}\varphi}{{\rm d}N} = -m^2\varphi\left(1 + \frac{g^2\chi^2}{m^2}\right) + 3H\xi_\phi(N), \quad (15)$$

$$3H^2 \frac{{\rm d}\chi}{{\rm d}N} = -\lambda v^2 \chi\left(\frac{\varphi^2 - \Phi_{\rm c}^2}{\Phi_{\rm c}^2} + \frac{\chi^2}{v^2}\right) + 3H\xi_\psi(N), \quad (16)$$

where ξ_ϕ and ξ_ψ are two uncorrelated white Gaussian noises with zero mean and variance given by

$$\langle \xi_\phi(N)\xi_\phi(N')\rangle = \frac{\epsilon^3 H^5}{2\pi^2} a^3 |\phi_k|^2_{k=\epsilon aH}(1 - 2\varepsilon_1)\delta(N - N'), \quad (17)$$

$$\langle \xi_\psi(N)\xi_\psi(N')\rangle = \frac{\epsilon^3 H^5}{2\pi^2} a^3 |\psi_k|^2_{k=\epsilon aH}(1 - 2\varepsilon_1)\delta(N - N'). \quad (18)$$

Here, ψ_k and ϕ_k are evaluated at the time when they join the coarse-grained scales.

In principle, other noise terms arise in Eqs. (15) and (16), which are either suppressed by factors of $\varepsilon_1 \ll 1$, or come from higher-order contributions of the loop expansion in the quantum piece of the fields, and are therefore suppressed by higher powers of $\hbar$. The latter contribution mainly implements mode coupling effects, which are not taken into account in the current paper.

Notice that the time variable used in these equations is the number of e-folds N, since it was shown in Refs. [62,63] that this time gauge must be used to describe the stochastic dynamics of the gauge-invariant Mukhanov variables for the fields. Other choices of the time variable would, in principle, correspond to different stochastic processes. However, note that, under the vacuum-domination approximation (which we are assuming here), the mapping between number of e-folds, cosmic time and conformal

[2]We work in units where $\hbar = 1$ throughout the paper, and we will not write explicitly the factors of $\hbar$, to avoid making the notation heavier. However, the power counting from the expansion in $\hbar$ should be straightforward to restore from the text.

time is nonstochastic, and one can equivalently work in different time gauges.

Equations (15) and (16) are Langevin equations that describe Markovian processes, which means that instead of having to solve a single equation of motion (single "realization"), one now has to calculate a whole probability distribution $\rho(\varphi, \chi, N)$ over many realizations, through a Fokker-Planck equation. Expectation values of functionals of the stochastic fields, in particular, their correlation functions, can be calculated by averaging over realizations using ρ as an integral kernel [34].

One can see that the noise amplitudes appearing in Eqs. (17) and (18) at a given time N are computed from the amplitudes of the linearized Fourier modes of the bath fields crossing the ϵ-scaled Hubble radius at time N. This simple form holds only if one chooses the window function entering the definition of the quantum fields to be a Heaviside step function, with a transition at $k = \epsilon aH$ (for a discussion of the influence of the choice of the window function, see e.g., Refs. [64,65]). Regardless of the choice of window function, one needs to solve the linearized Fourier mode function equations for each field and evaluate the solutions ϕ_k and ψ_k at Hubble crossing in order to obtain the noise amplitudes.

We therefore obtain a system of two coupled sets of equations: on one hand, the set of Langevin equations for the two stochastic processes φ and χ, and, on the other, the set of linearized mode function equations for ϕ_k and ψ_k. This is where the recursive strategy of Ref. [39] comes into play. Let us see how it proceeds. One should keep in mind that the Langevin equations (15) and (16) arise from a Lagrangian theory, in which the small-wavelength fluctuations are integrated out to yield an effective theory for the coarse-grained field. Such fluctuations are evolved by equations of motion that involve coarse-grained—or "background"—quantities, the dynamics of which is itself shifted by these small-wavelength fluctuations. This forms a closed system of equations that is, in general, very difficult to solve. Indeed, at each time N, one needs to compute the amplitude of the modes that are crossing the Hubble radius, which depends on the previous history of the background, which is itself determined by the amplitude of all the modes that previously crossed the Hubble radius.

Considered as a whole in this manner, the process stops being Markovian since the amplitudes of the noise at a given time N depend on all the realizations of the noises at previous times $N' < N$, and one needs to assign a so-called "prescription" $\alpha \in [0, 1]$ to the Langevin equations (which determines at which point $N + \alpha \mathrm{d}N$ the noises must be calculated when the fields are incremented between N and $N + \mathrm{d}N$, when defining the Langevin dynamics as a limit of a discrete stochastic process). The resulting integro-differential equation becomes, in practice, impossible to solve.

However, as argued in Ref. [39], a perturbative solution can be obtained by recursively solving a sequence of Markovian processes. To this end, one first evolves the linearized Fourier mode functions for each field to zeroth order in the slow-roll parameters and to leading order in $\hbar$. This means evolving the mode equations truncated as if they were massless equations over exact de Sitter space. This enables one to calculate the (zeroth-order) noise amplitudes at each time N, and to obtain the corresponding driving term at each time in Eqs. (15) and (16), giving us the leading $\hbar$ quantum effects to the coarse-grained equations. Solving the latter, now keeping only terms to zeroth order in slow roll and leading order in $\hbar$, then provides one with the shifted (or renormalized) associated background fields.

One can then solve again the equations of motion for the linearized mode functions of the quantum fields, this time in the presence of a "mean" background calculated from averaging over many realizations of the coarse-grained system described by the Langevin equations at this order (or using the probability density function obtained by solving the Fokker-Planck equation). This enables one to calculate new noise amplitudes which include corrections of leading order in slow roll and next-to-leading order in $\hbar$ (note, however, that at this point one cannot yet make predictions about the classical spectrum of perturbations).

From these noise amplitudes valid to higher order, one can go back to the Langevin system for the coarse-grained fields, Eqs. (15) and (16), and find new, corrected solutions. These will now be valid up to next-to-leading order in $\hbar$ and to leading order in slow-roll parameters. From these corrected solutions to the classical system, one can study classical perturbations of the coarse-grained fields and make predictions beyond zeroth order in slow roll, for example, for the spectral index.

One can keep solving recursively the linearized mode functions (describing the quantum bath and required to calculate the noise amplitudes) and the Langevin equations (describing the coarse-grained classical fields) until one reaches the required level of accuracy. If such a process converges towards a limit point, it should be close to the actual solution of the implicit closed equations. If, on the contrary, it does not possess any fixed point, this should be interpreted as a sign that the backreaction effects may be out of control and that the whole model is under pressure. In any case, performing such a program is of interest, and we now carry it out for the model being considered in this paper.

C. Coarse-grained system up to zeroth order: Massless de Sitter solution

As a first step, let us assume that the linearized mode functions for the bath fields, ϕ_k and ψ_k with $k > \epsilon aH$, are free and massless and evolving in a de Sitter background. Since the potential is vacuum dominated in the valley

phase, the de Sitter approximation seems to be well justified. The inflaton perturbations $\phi_{\boldsymbol{k}}$ also need to be very light with $m \ll H$ in order for slow-roll inflation to proceed, as already mentioned. However, the waterfall perturbations $\psi_{\boldsymbol{k}}$ can *a priori* be very massive (it is precisely the mass of the waterfall field that quickly brings the system to the bottom of the valley), and thus the approximation of masslessness may be totally unjustified for this field. This is the object of the calculation and discussion of Sec. IV. For now, we will assume that since inflation proceeds as Φ approaches the critical point, and Ψ becomes lighter and lighter, the approximation correspondingly becomes better and better, so that close enough to the critical point, the following calculation is a reliable first step.

The standard massless de Sitter solution gives

$$|\phi_{\mathbf{k}}|^2_{k=\epsilon aH} = |\psi_{\mathbf{k}}|^2_{k=\epsilon aH} = \frac{H^2}{2(\epsilon aH)^3}, \tag{19}$$

so that, to leading order, we obtain the correlators

$$\langle \xi_\phi(N)\xi_\phi(N')\rangle = \frac{H^4}{4\pi^2}\,\delta(N-N'), \tag{20}$$

$$\langle \xi_\psi(N)\xi_\psi(N')\rangle = \frac{H^4}{4\pi^2}\,\delta(N-N'), \tag{21}$$

and hence the well-known $H/2\pi$ noise amplitude commonly used in stochastic inflation. Let us now try to assess the typical dispersion acquired by the field distributions when subjected to the influence of these stochastic effects.

The importance of the stochastic effects in the Φ direction can be estimated through the ratio, which we call Δ_Φ, of the mean magnitude of the quantum kick $H/(2\pi)$ during a typical time interval of one e-fold, to the typical classical change in the inflaton value $\simeq M^2(\partial V/\partial\varphi)/V$ during the same time interval. In the valley close to the critical point, one obtains

$$\Delta_\Phi = \frac{1}{16\sqrt{3}\pi}\lambda g\frac{\upsilon^5}{m^2M_{\rm Pl}^3}. \tag{22}$$

If $\Delta_\Phi \ll 1$, the inflaton dynamics in the valley phase is dominated by its classical drift so that the classical solution (8) can be used in Eq. (16). We will restrict our attention to this case. In particular, we will not consider the eternal version of hybrid inflation which is obtained if the mass is chosen to be so small that $\Delta_\phi \gg 1$. Letting

$$x \equiv \mathrm{e}^{-8\frac{M_{\rm Pl}^2m^2}{\lambda\upsilon^4}(N-N_{\rm c})}, \tag{23}$$

the χ equation of motion (16) can be rewritten as

$$\frac{\mathrm{d}\chi}{\mathrm{d}x} = \frac{\lambda\upsilon^2}{2m^2}\frac{x-1}{x}\chi - \sqrt{\frac{3}{2x}}\frac{\xi_\psi(x)}{m}, \tag{24}$$

where $\xi_\psi(x)$ shares the same statistical properties (18) as $\xi_\psi(N)$, replacing N by x in the delta function argument. The solution to this equation is given by

$$\chi(x) = C\exp\left[\frac{\lambda\upsilon^2}{2m^2}(x-\ln x)\right] - \sqrt{\frac{3}{2}}\exp\left[\frac{\lambda\upsilon^2}{2m^2}(x-\ln x)\right] \times \int_\infty^x \exp\left[-\frac{\lambda\upsilon^2}{2m^2}(x'-\ln x')\right]\frac{\xi_\psi(x')}{m}\frac{\mathrm{d}x'}{\sqrt{x'}}, \tag{25}$$

where C is a constant of integration. It is set to $C=0$, provided one assumes an initial delta distribution for χ at $\varphi \gg \Phi_{\rm c}$ (i.e., $x\to\infty$). In this case, using Eq. (21), the two-point correlation function can be calculated as

$$\langle\chi^2\rangle = \frac{1}{384\pi^2}\frac{\lambda^2\upsilon^8}{m^2M_{\rm Pl}^4}\left(\frac{m^2\mathrm{e}^x}{\lambda\upsilon^2x}\right)^{\frac{\lambda\upsilon^2}{m^2}}\Gamma\left(\frac{\lambda\upsilon^2}{m^2},\frac{\lambda\upsilon^2}{m^2}x\right), \tag{26}$$

where Γ is the upper incomplete gamma function. Therefore, the dispersion of the distribution for χ is found to be

$$\sigma_\chi \equiv \sqrt{\langle\chi^2\rangle - \langle\chi\rangle^2} = \frac{\lambda\upsilon^4}{8\sqrt{6}\pi mM_{\rm Pl}^2}\left(\frac{m^2\mathrm{e}^x}{\lambda\upsilon^2x}\right)^{\frac{\lambda\upsilon^2}{2m^2}}\Gamma^{\frac{1}{2}}\left(\frac{\lambda\upsilon^2}{m^2},\frac{\lambda\upsilon^2}{m^2}x\right). \tag{27}$$

This analytical formula is compared with a numerical integration of the Langevin equations in Fig. 1, where the matching appears to be very good in the valley (i.e., for $N<N_{\rm c}$). At the critical point where $x=1$, in the limit $\lambda\upsilon^2/m^2 \gg 1$, one can make use of the asymptotic behavior $(e/y)^y\Gamma(y,y) \simeq \sqrt{\pi/(2y)}$ when $y\to\infty$, and the previous expression reduces to

$$\sigma_{\chi_{\rm c}} \simeq \left(\frac{\lambda}{2\pi}\right)^{3/4}\left(\frac{\upsilon}{3m}\right)^{1/2}\frac{\upsilon^3}{8M_{\rm Pl}^2}. \tag{28}$$

In the supersymmetric version of the model, where $\Phi_{\rm c}=\upsilon$, one then has $\sigma_{\chi_{\rm c}}/\upsilon \propto \sqrt{m/M_{\rm Pl}\Delta_\Phi}$, where $\propto$ signals the presence of a numerical $\mathcal{O}(1)$ factor. Since we are working under the $\Delta_\Phi \ll 1$ assumption, for light inflaton fields compared to the Planck mass, this means that $\sigma_{\chi_{\rm c}} \ll \upsilon$. Therefore, one can safely use the approximation $\chi \ll \upsilon$ in Eq. (15), even when the stochastic diffusion in the χ direction is taken into account. So one can now integrate Eq. (15). If the initial condition for φ is chosen to be a delta distribution, this leads to

$$\varphi = \exp\left[-4\frac{m^2M_{\rm Pl}^2}{\lambda\upsilon^4}(N-N_{\rm in})\right]\left[\varphi_{\rm in} + 2\sqrt{\frac{3}{\lambda}}\frac{M_{\rm Pl}}{\upsilon^2} \times \int_{N_{\rm in}}^N \exp\left(4\frac{m^2M_{\rm Pl}^2}{\lambda\upsilon^4}n\right)\xi_\phi(n)\mathrm{d}n\right], \tag{29}$$

from which one gets a distribution for φ centered around its classical counterpart $\langle\varphi\rangle = \varphi^{(0)}$, with a constant dispersion given by

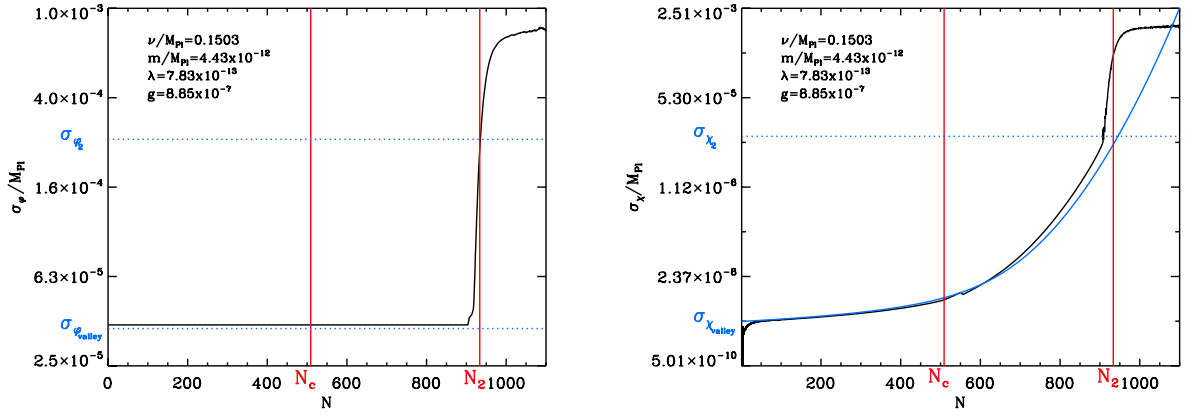

FIG. 1 (color online). Dispersion of the inflaton field (left panel) and of the waterfall field (right panel) during inflation. The values of N_c and N_2 are given by Eqs. (10) and (B8), respectively. The constant dispersion in the valley $\sigma_{\varphi_{\text{valley}}}$ (blue dotted line) and the time-dependent dispersion $\sigma_{\chi_{\text{valley}}}$ (blue solid line) correspond to the values given by Eqs. (30) and (27), respectively, while the dispersions in the φ direction σ_{φ_2} and in the χ direction σ_{χ_2} (blue dotted lines) at the end of subphase 2 of the waterfall phase correspond to the value given by Eqs. (32) and (31), respectively. The black lines correspond to numerical results coming from solving $\sim 10^7$ realizations of the Langevin equations.

$$\sigma_\varphi = \frac{\lambda v^4}{8\sqrt{6}\pi m M_{\text{Pl}}^2}, \tag{30}$$

where Eq. (21) has been used to obtain the above. In Fig. 1, the dispersion given by this formula is compared with the dispersion obtained numerically, from solving $\sim 10^7$ realizations of the Langevin equations. The figure confirms that σ_φ is indeed constant during the valley phase (i.e., for $N < N_c$) and shows good agreement between numerical and analytical methods.

Let us now say a few words about the waterfall phase. The classical dynamics of this phase is reviewed in Appendix B, where the notations of Ref. [55] are adopted, dividing this stage into three subphases, labeled 0, 1, and 2. At the classical level, subphase 2 ends up with the values of the fields given by Eqs. (B6) and (B7), which implies that $\chi_2/v \ll 1$ and that $\varphi_2 \simeq \Phi_c$. Therefore, the approximation scheme used for the calculation of the diffusion in the χ direction in the valley is still roughly valid, as can be confirmed by comparing with the numerical results displayed in Fig. 1.

On the other hand, a straightforward way to estimate the dispersion of the distribution for χ at the end of subphase 2 is to use the following qualitative argument. The stochastic diffusion in the valley phase randomizes which minimum of the potential is eventually taken on by the coarse-grained field, in such a way that half of the Langevin realizations end up in each minimum. If the classical estimation of χ_2 given by Eq. (B6) is roughly correct, the typical dispersion should be twice this value, namely,

$$\sigma_{\chi_2} \simeq \frac{2m}{g}. \tag{31}$$

This expression, obtained from a heuristic argument, is shown to agree with the numerical calculation in Fig. 1.

Equation (B7) and the fact that χ_c is a stochastic quantity both lead to the conclusion that the value φ_2 of the inflaton at the end of phase 1 of the waterfall is also a stochastic quantity. Going back to Eq. (B7), we see that σ_{χ_c} and σ_{φ_2} can be related to each other. Using the Gaussianity of the distribution for χ_c, one obtains

$$\sigma_{\varphi_2} = \Phi_c\left\{\exp\left[-\frac{2m}{\lambda^{1/4}v}\left|\ln\left(\frac{m}{g\sigma_{\psi_c}}\right)\right|^{\frac{1}{2}}\right] - \exp\left[-\frac{2m}{\lambda^{1/4}v}\left|\ln\left(\frac{m\sqrt{2\pi}}{g\sigma_{\psi_c}}\right)\right|^{\frac{1}{2}}\right]\right\}^{\frac{1}{2}}. \tag{32}$$

Again, this value is compared with a numerical calculation in Fig. 1 which confirms the validity of this approach.

This calculation provides a leading-order result for the field dispersions σ_φ and σ_χ. To go beyond this approximation, we now proceed to step 3 of our recursive method.

III. LINEARIZED MODE FUNCTION CALCULATION

We now go back to the mode function equations for the bath fields and solve them again, this time in the presence of the "shifted" background calculated in the previous subsection (this now represents keeping corrections up to next-to-leading order in $\hbar$) and keeping corrections up to leading order in slow roll.

As shown in Ref. [39], at this order in $\hbar$, the mode functions we need to solve for correspond to the linear perturbation equations for the scalar fields in a shifted background. We can therefore apply here the usual methods from the theory of linearized cosmological perturbations. This also means that one need not worry about mode

coupling effects at this order, at least for what concerns the calculation of the bath propagators and noise amplitudes.[3]

From the split of the full fields into the bath and system in (14) and (15), one can think about this as performing the following expansion in the bath fields:

$$\begin{aligned}\phi_>(x,N) &= \delta\phi_>^{(1)}(x,N) + \delta\phi_>^{(2)}(x,N) + \cdots,\\ \psi_>(x,N) &= \delta\psi_>^{(1)}(x,N) + \delta\psi_>^{(2)}(x,N) + \cdots,\end{aligned} \tag{33}$$

where the zero mode of the bath fields is zero, by definition. The background quantities are given by the homogeneous coarse-grained fields $\varphi^{(0)}$ and $\chi^{(0)}$, and we aim at solving for the first-order fluctuations, $\delta\phi_>^{(1)}$ and $\delta\psi_>^{(1)}$. The different notations referring to the different quantities derived from the quantum fields Φ and Ψ are summed up in Appendix A. Following the recursive scheme presented above, in the equations of motion driving these quantities, all the occurrences of the coarse-grained quantities $\varphi^{(0)}$ and $\chi^{(0)}$, which are stochastic quantities, shall be replaced by their stochastic means, namely,

$$F[\varphi^{(0)},\chi^{(0)}] \to \langle F[\varphi^{(0)},\chi^{(0)}]\rangle, \tag{34}$$

where F is any functional of the two fields. Moreover, in order for this expansion to be consistent, we also need to include metric perturbations. In the following, we will only be interested in the scalar mode and will therefore neglect the tensor modes. We choose to work in the uniform curvature gauge at linear order in metric perturbations.

A. First-order metric perturbations

For the Friedmann-Lemaître-Robertson-Walker (FLRW) metric at linear order, scalar, vector and tensor metric perturbations decouple (see Refs. [66–69] and references therein for a review of the theory of cosmological perturbations). We therefore only need to consider scalar perturbations at this order. For a flat FLRW spacetime, they are parametrized by

$$\begin{aligned}\mathrm{d}s^2 = &-(1+2\alpha)\mathrm{d}t^2 - aB_{,i}\mathrm{d}t\mathrm{d}x^i\\ &+ a^2[\delta_{ij}(1-2\beta) + E_{,ij}]\mathrm{d}x^i\mathrm{d}x^j.\end{aligned} \tag{35}$$

Using the conventions of Ref. [70], in the following we work in the spatially flat, or uniform curvature, gauge, which is defined by making the scale factor of the metric homogeneous, choosing $\beta = E = 0$:

$$\mathrm{d}s^2 = -(1+2\alpha)\mathrm{d}t^2 - aB_{,i}\mathrm{d}t\mathrm{d}x^i + a^2\mathrm{d}x^2. \tag{36}$$

This choice uniquely fixes the gauge. The Einstein equations then reduce to

$$3H^2\alpha + \frac{k^2}{2a^2}(aHB) = -\frac{\delta\rho}{2M_{\rm Pl}^2}, \tag{37}$$

$$H\alpha = -4\pi G\delta q, \tag{38}$$

$$H\dot\alpha + (3H^2 + 2\dot H)\alpha = \frac{1}{2M_{\rm Pl}^2}\left(\delta p - \frac{2}{3}k^2\delta\Sigma\right), \tag{39}$$

$$(\partial_t + 3H)\frac{B}{2a} - \frac{\alpha}{a^2} = \frac{\delta\Sigma}{2M_{\rm Pl}^2}, \tag{40}$$

where Σ stands for the anisotropic stress, which we set to zero from now on since it cannot be seeded by scalar field matter to linear order in perturbation theory. The total density and momentum perturbations are given by

$$\begin{aligned}\delta\rho = &\dot\varphi^{(0)}(\delta\dot\phi_>^{(1)} - \dot\varphi^{(0)}\alpha) + \dot\chi^{(0)}(\delta\dot\psi_>^{(1)} - \dot\chi^{(0)}\alpha)\\ &+ V_{,\Phi}(\varphi,\chi)\delta\phi_>^{(1)} + V_{,\Psi}(\varphi,\chi)\delta\psi_>^{(1)},\end{aligned} \tag{41}$$

$$\delta q = \dot\varphi^{(0)}\delta\phi_>^{(1)} + \dot\chi^{(0)}\delta\psi_>^{(1)}, \tag{42}$$

where $V_{,\Phi}$ and $V_{,\Psi}$ stand for the derivatives of the potential with respect to the fields Φ and Ψ, evaluated at their coarse-grained values. In order to obtain equations for $\phi_>$ and $\psi_>$ only, one just needs to consider the first two Einstein equations in Eqs. (37)–(40), that is, the G_0^0 and G_i^0 equations, which can be expressed as

$$\begin{aligned}-\frac{H}{a}k^2B &= 8\pi G[\dot\varphi^{(0)}\delta\dot\phi_>^{(1)} + V_{,\Phi}\delta\phi_>^{(1)} + \dot\chi^{(0)}\delta\dot\psi_>^{(1)}\\ &\quad + V_{,\Phi}\delta\psi_>^{(1)} + 2V\alpha]\\ &= \frac{8\pi G}{H}\left\{\dot\varphi^{(0)2}\frac{\mathrm{d}}{\mathrm{d}t}\left[\frac{H\delta\phi_>^{(1)}}{\dot\varphi^{(0)}}\right] + \dot\chi^{(0)2}\frac{\mathrm{d}}{\mathrm{d}t}\left[\frac{H\delta\psi_>^{(1)}}{\dot\chi^{(0)}}\right]\right\},\end{aligned} \tag{43}$$

$$\alpha_{,i} = \frac{4\pi G}{H}[\dot\varphi^{(0)}\delta\phi_{>,i}^{(1)} + \dot\chi^{(0)}\delta\psi_{>,i}^{(1)}], \tag{44}$$

where $G = 1/(8\pi M_{\rm Pl}^2)$ is the gravitational constant. Also, since we are assuming the absence of anisotropic stress, we have the extra constraint $\dot B + 2HB = 2\alpha/a$ (which is

[3]However, technically, at this order in $\hbar$, we should include the loop corrections to the Langevin equations calculated in Ref. [39], which would appear in the fourth and last stages of the recursive method applied in the present paper. Despite this, since these effects represent mode coupling between bath and system fields, we expect them to be negligible in the valley phase of inflation because they are both loop and slow-roll parameters suppressed. We therefore neglect them at this order and plan on coming back to this calculation in a future work focused on the waterfall phase of inflation, where those effects are known to be important (see e.g., Ref. [49]).

equivalent to the usual $\Phi = \Psi$ equality in the longitudinal gauge).

B. Inflaton fluctuations $\delta\phi^{(1)}$

Following the recursive strategy presented above, let us now write down [71] the equation of motion for the first-order inflaton fluctuations $\delta\phi^{(1)}_{>}$, replacing the functions of the background fields $\varphi^{(0)}$ and $\chi^{(0)}$ by the stochastic mean values of the same functions of the coarse-grained quantities φ and χ:

$$\delta\ddot{\phi}^{(1)}_{\boldsymbol{k}} + 3H\delta\dot{\phi}^{(1)}_{\boldsymbol{k}} + \left(\frac{k^2}{a^2} + m^2 + g^2\langle\chi^2\rangle\right)\delta\phi^{(1)}_{\boldsymbol{k}} + 2g^2\langle\varphi\chi\rangle\delta\psi^{(1)}_{\boldsymbol{k}} = 2\alpha\langle\ddot{\varphi}\rangle + \langle\dot{\varphi}\rangle\left(\dot{\alpha} + 6H\alpha + \frac{k^2}{2a}B\right). \tag{45}$$

The notation ">" has been dropped for simplicity. As derived above, the distribution for φ is centered around its classical counterpart $\langle\varphi\rangle = \varphi^{(0)}$, and therefore, one can replace $\langle\dot{\varphi}\rangle = \dot{\varphi}^0$ and $\langle\ddot{\varphi}\rangle = \ddot{\varphi}^0$. Then, for $\Delta_\Phi \ll 1$, which is an assumption we are currently working under, the noise effects in the φ direction do not affect the inflaton dynamics much, i.e., $\sigma_\varphi/\varphi \ll 1$. Assuming independence of the two coarse-grained field probability density functions, one can then approximate $\langle\varphi\chi\rangle \simeq \langle\varphi\rangle\langle\chi\rangle = \varphi^{(0)}\langle\chi\rangle = 0$, with the last approximation justified by the fact that the χ distribution is quickly centered around 0 in the valley phase.[4] Finally replacing $\langle\chi^2\rangle$ by σ^2_χ, one obtains

$$\delta\ddot{\phi}^{(1)}_{\boldsymbol{k}} + 3H\delta\dot{\phi}^{(1)}_{\boldsymbol{k}} + \left(\frac{k^2}{a^2} + m^2 + g^2\sigma^2_\chi\right)\delta\phi^{(1)}_{\boldsymbol{k}} = 2\alpha\ddot{\varphi}^{(0)} + \dot{\varphi}^{(0)}\left(\dot{\alpha} + 6H\alpha + \frac{k^2}{2a}B\right). \tag{46}$$

One can see that, in general, the inflaton and the waterfall fields also couple through the metric perturbations on the right-hand side. Indeed, since there really are only 2 degrees of freedom in the problem, it is possible to replace the metric fluctuations in favor of the fields using the constraint equations (43) and (44). In this process, we set terms with odd powers of $\chi^{(0)}$ to zero, while terms with a quadratic power of $\chi^{(0)}$ we set to $\langle\chi^2\rangle = \sigma^2_\chi$. We obtain

$$\delta\ddot{\phi}^{(1)}_{\boldsymbol{k}} + 3H\delta\dot{\phi}^{(1)}_{\boldsymbol{k}} + \left[\frac{k^2}{a^2} + m^2 + g^2\sigma^2_\chi - \frac{8\pi G}{a^3}\frac{\mathrm{d}}{\mathrm{d}t}\left(\frac{a^3\dot{\varphi}^{(0)^2}}{H}\right)\right]\delta\phi^{(1)}_{\boldsymbol{k}} = 0. \tag{47}$$

Here, the last term is clearly identifiable as coming from gravitational interactions since it is proportional to the gravitational constant. One also sees that, written in this way, the waterfall field seems to decouple from the inflaton field. Indeed, this same equation would have been obtained for a single scalar field (with a stochastically shifted mass) coupled to the metric perturbations.

This equation can also be rewritten in a way that makes explicit what order in slow roll the gravitational corrections are, and in a way that makes the corrections coming from σ_χ appear clearly:

$$\delta\ddot{\phi}^{(1)}_{\boldsymbol{k}} + 3H\delta\dot{\phi}^{(1)}_{\boldsymbol{k}} + \left[\frac{k^2}{a^2} + m^2 + g^2\sigma^2_\chi + 2\frac{\dot{H}}{H} \times \left(\frac{\ddot{\varphi}^{(0)}}{\dot{\varphi}^{(0)}} - \frac{\dot{H}}{H} + 3H\right)\left(1 + \frac{1}{\dot{\varphi}^{(0)^2}/\dot{\sigma}^2_\chi + 1}\right)\right]\delta\phi^{(1)}_{\boldsymbol{k}} = 0. \tag{48}$$

From Eq. (27), one can calculate the time variation of σ_χ at the critical point

$$\mathrm{d}\,\sigma_\chi/\mathrm{d}N|_{\mathrm{c}} = (2\pi)^{5/4}\lambda^{1/4}\sqrt{m\upsilon/3}. \tag{49}$$

From this one obtains a value

$$\dot{\varphi}^{(0)^2}/\dot{\sigma}^2_\chi \simeq 192\sqrt{2}\pi^{5/2}m^3M^4_{\mathrm{Pl}}/(g^2\lambda^{3/2}\upsilon^7) \tag{50}$$

which is typically very big (e.g., for the parameter values used in Fig. 1, one obtains $\simeq 0.5 \times 10^6$). One can therefore approximate the second term in parentheses of Eq. (48) to be $\simeq 1$.

In Eq. (48) also, the H factors should be understood as $\langle H(\varphi,\chi)\rangle_{\xi_\varphi,\xi_\chi}$ and similarly for any function of H ($\dot{H}/H$, etc.) and, more generally, any function of coarse-grained quantities. However, in the valley H is assumed to be vacuum dominated, and its time dependence mostly comes from $\varphi \simeq \varphi^{(0)}$. The Hubble parameter can therefore be treated in the standard way without impacting the result much. This is why a lighter notation is adopted for this parameter.

Since $(\dot{\varphi}^{(0)})^2$ dominates the contribution to $\dot{H}$, one finds that the corrections due to χ are negligible and recovers that the metric perturbations cause a shift in the mass of a single field coupled to the metric. The effective mass for the inflaton can therefore be rewritten in terms of the first slow-roll parameter:

$$m^2 + g^2\sigma^2_\chi + 2\frac{\dot{H}}{H}\left(\frac{\ddot{\varphi}^{(0)}}{\dot{\varphi}^{(0)}} - \frac{\dot{H}}{H} + 3H\right) \approx m^2 + g^2\sigma^2_\chi - 6H^2\left(\varepsilon_1 - \frac{1}{3}\varepsilon_1^2 + \frac{\dot{\varepsilon}_1}{3H}\right). \tag{51}$$

Upon the standard field redefinition to obtain the canonically normalized field,

$$\delta\phi^{(1)}_{\boldsymbol{k}} = a^{-1}\upsilon_{\boldsymbol{k}}, \tag{52}$$

and the change of the time coordinate to conformal time $\mathrm{d}\tau = a^{-1}\mathrm{d}t$, one obtains an equation analogous to the

[4] This approximation is no longer valid in the waterfall phase.

usual mode function for a single scalar field in de Sitter space:

$$v_k'' + \left\{k^2 - \frac{a''}{a} + a^2\left[m^2 + g^2\sigma_\chi^2 - 6H^2\left(\varepsilon_1 - \frac{1}{3}\varepsilon_1^2 + \frac{\dot{\varepsilon}_1}{3H}\right)\right]\right\}v_k = 0, \quad (53)$$

where the prime denotes a derivative with respect to the conformal time τ. Or, to first order in slow roll (which we assume is sufficient in the valley), $aH = -\tau^{-1}(1-\varepsilon_1)$, and

$$v_k'' + \left[k^2 - \frac{2 - m^2/H^2 - g^2\sigma_\chi^2/H^2 + 9\varepsilon_1}{\tau^2}\right]v_k = 0. \quad (54)$$

We can then quantize the modes by promoting v_k to an operator

$$\hat{v}_k(\tau) = v_k(\tau)\hat{a}_k + v_k^\star(\tau)\hat{a}_{-k}^\dagger \quad (55)$$

and imposing the usual commutation relations

$$[a_k, a_{-k'}^\dagger] = (2\pi)^3\delta^{(3)}(k + k'). \quad (56)$$

Noticing that, from Eq. (27), one has

$$\mathrm{d}/\mathrm{d}N(\sigma_\chi^2/H^2)|_c = 1/(4\pi^2) \quad (57)$$

at the critical point, the time variation of σ_χ^2 in the above equation is suppressed by a g^2 factor and can be neglected in the adiabatic limit, allowing us to express the solution to the mode function in terms of Hankel functions:

$$v_k = -ie^{i(\nu+\frac{1}{2})\frac{\pi}{2}}\frac{\sqrt{\pi}}{2}(-\tau)^{1/2}H_\nu^{(1)}(-k\tau), \quad (58)$$

where

$$\nu^2 = 9/4 - (m^2 + g^2\sigma_\chi^2)/H^2 + 9\varepsilon_1 \approx \frac{9}{4} + \frac{3}{2}\varepsilon_2 + \frac{g^2\sigma_\chi^2}{H^2} + 9\varepsilon_1. \quad (59)$$

In the second line, we have reintroduced the second slow-roll parameter to make explicit which corrections in slow roll we are keeping. This term is the term which propagates to yield the well-known classical blue tilt for the canonical hybrid inflation model. The last term is the correction from metric fluctuations which induces a red tilt. The second-to-last term, however, is a new term which is induced by stochastic effects and which tends to increase the blue tilt.

The mode functions have been normalized so that deep inside the Hubble radius, when the k^2 term dominates the mass in Eq. (54), one recovers the Bunch-Davies vacuum:

$$v_k \to \frac{e^{-ik\tau}}{\sqrt{2k}}, \qquad \tau \to -\infty. \quad (60)$$

Here, a few comments are in order. First, note that what we have calculated so far are only the linearized mode functions of the bath quantum fields, not the perturbations that will arise in the coarse-grained system once we perturb the Langevin equations; these are the ones giving rise to the classical curvature perturbations. As such, to be technically correct we are not yet allowed to predict the modified spectral index (even though we can suspect that the result we obtain here should propagate to the final answer). We first have to use this corrected amplitude of linearized mode functions to calculate a shifted noise through Eq. (17), and then we use the latter to source a new solution to the Langevin equation (15). Linear perturbations around this classical system will allow us to predict n_s to leading order in slow roll.

Second, note that the effect of σ_χ^2 on $\delta\phi_k^{(1)}$ is to make each mode more massive. Therefore, having the sub-Hubble modes evolve in a background that has been shifted by the integration to first order of all modes that have already frozen out has the effect of making the tilt of the inflaton modes bluer when they freeze out. It should be highlighted that this conclusion does not depend on the specific value of σ_χ, and it will remain true when its calculation is refined in Sec. IV. Moreover, for typical values of the potential (and, in particular, in the supersymmetric version of the model $\Phi_c \sim v$), one has

$$g^2\sigma_\chi^2/H^2 \sim \varepsilon_1^{-1/4}\frac{\lambda v^3}{\Phi_c^{3/2}M_{\mathrm{Pl}}^{3/2}} \gg 9\varepsilon_1. \quad (61)$$

Therefore, the blue tilt induced by the stochastic background will always overcome the tendency of metric perturbations to make the spectrum of quantum fluctuations red.

This result is not *a priori* obvious since the two effects are antagonistic (the coupling to metric perturbations rendering the spectral tilt redder and the stochastic shift of the background rendering it bluer). It is necessary to rigorously work out the two contributions in order to conclude that the latter wins over the former, yielding a shifted and a blue-tilted spectrum of the quantum noise sourcing the Langevin equations once the mode functions are plugged back into Eqs. (17) and (18).

We once again insist that whether the blue shift and time dependence in the noise amplitude also yield a worsened blue-tilt problem, by translating into a bluer spectrum of classical curvature perturbations of the coarse-grained field φ (which are the observable ones), is a different question which requires further calculation. To provide a satisfactory answer, we shall wait until we feed this new quantum noise amplitude back into the Langevin equations (15) and (16) and calculate the spectrum.

As a second remark, note that if the collective effect of the inflaton mass and σ_χ is a small enough correction, i.e., if $(m^2 + g\sigma_\chi^2)/H^2 - 9\varepsilon_1 \leq 9/4$, then as the modes v_k cross their Hubble radius, their oscillations stop and freeze out as one would expect. However, the modes of the original field $\delta\phi_k^{(1)}$ also contain a decay factor

$a^{-1}(-k\tau)^{-\nu+1/2} \sim \tau(-k\tau)^{-\nu+1/2}$ as $-k\tau \to 0$, which indicates that they eventually roll back down to zero. (Recall that the observable quantity here is the curvature perturbation, $\mathcal{R} = \frac{H}{\dot\phi}\delta\phi$). This means that the modes become overdamped after horizon exit. The full solution in this limit is given by

$$v_k \to \begin{cases} -e^{i(\nu+\frac{1}{2})\frac{\pi}{2}}\frac{2^{\nu-1}}{\sqrt{\pi}}\Gamma(\nu)\frac{(-\tau)^{-\nu+1/2}}{k^\nu} & 0 < \nu \leq 3/2 \\ e^{i\frac{\pi}{2}}(-\tau)^{1/2}\ln(-k\tau) & \nu = 0. \end{cases} \quad (62)$$

The k^ν factor shows the deviation from scale invariance, and we therefore recover that the mass of the inflaton causes the spectrum to be blue tilted in the valley (scale invariance has $k^{3/2}$, which is the massless case). The power of τ shows the time dependence, and in the massless case one recovers τ^{-1}, which is canceled by multiplying by a^{-1} to recover $\delta\phi_k^{(1)}$.

C. Waterfall fluctuations $\delta\psi^{(1)}$

1. Mode function evolution equation

Let us now proceed with $\delta\psi^{(1)}$, similarly expanding the equations of motion to first order, once again in the flat-slicing gauge. One obtains

$$\delta\ddot\psi_k^{(1)} + 3H\delta\dot\psi_k^{(1)} + \left(\frac{k^2}{a^2} + 3\lambda\chi^2 - \lambda v^2 + g^2\varphi^2\right)\delta\psi_k^{(1)} + 2g^2\varphi\chi\delta\phi_k^{(1)} = \dot\alpha\,\dot\chi - 2\alpha V_{,\Psi}(\varphi,\chi) - \dot\varphi\frac{k^2}{2a}B. \quad (63)$$

As in the previous subsection, on the left-hand side, one replaces χ^2 by σ_χ^2, φ^2 by $\langle\varphi^2\rangle \simeq \varphi^{(0)2}$, and $\varphi\chi$ by $\langle\varphi\chi\rangle = 0$. On the right-hand side, using the linearized Einstein equations to replace the metric fluctuations by field perturbations, and setting to zero all terms with stochastic mean values with odd powers of χ (remembering that the distribution of χ is even), one obtains

$$\delta\ddot\psi_k^{(1)} + 3H\delta\dot\psi_k^{(1)} + \left[\frac{k^2}{a^2} + 3\lambda\sigma_\chi^2 - \lambda v^2 + g^2\varphi^{(0)^2} - \frac{8\pi G}{a^3}\frac{\mathrm{d}}{\mathrm{d}t}\left(\frac{a^3\langle\dot\chi^2\rangle}{H}\right)\right]\delta\psi_k^{(1)} = 0, \quad (64)$$

where, again, H is approximated by its classical value $H(\varphi^{(0)}, \chi = 0)$. Note that, as opposed to what would have been obtained using perturbation theory around a classical background for Ψ, the stochastically shifted background causes the $\delta\psi_k^{(1)}$ perturbations not to decouple completely. Indeed, in the case of a classical background, unless the trajectory is turning in field space, the perturbations reduce to those of a scalar field in an unperturbed FLRW spacetime [71]. This is not the case here: The field space trajectory is straight, but the stochastic dispersion of the waterfall allows for nonvanishing corrections due to gravity.

We again rewrite the term coming from gravitational interactions in terms of the slow-roll parameters:

$$2\frac{\dot H}{H}\left(\frac{\ddot\chi}{\dot\chi} - \frac{\dot H}{H} + 3H\right)\left(1 + \frac{1}{\dot\sigma_\chi^2/\dot\varphi^{(0)^2} + 1}\right) \simeq 4\frac{\dot H}{H}\left(-\frac{\dot H}{H} + 3H\right) = 12H^2\left(\varepsilon_1 - \frac{1}{3}\varepsilon_1^2\right). \quad (65)$$

As above, one proceeds to the field redefinition

$$\delta\psi_k^{(1)} = a^{-1}u_k \quad (66)$$

and changes coordinates to conformal time, $\mathrm{d}t = a\mathrm{d}\tau$, to find the mode function expressed in terms of the canonical variable u_k:

$$u_k'' + \left\{k^2 - \frac{a''}{a} + a^2\left[3\lambda\sigma_\chi^2 - \lambda v^2 + g^2\varphi^{(0)^2} + 12H^2\left(\varepsilon - \frac{1}{3}\varepsilon^2\right)\right]\right\}u_k = 0. \quad (67)$$

Using the explicit expression for a during inflation to first order in slow roll, $aH = -\tau^{-1}(1-\varepsilon_1)$, and under the assumption of vacuum domination, this gives rise to

$$u_k'' + \left[k^2 - \frac{1}{\tau^2}\times\left(2 - 3\frac{\lambda\sigma_\chi^2}{H^2} + \frac{12M_{\mathrm{Pl}}^2}{v^2} - \frac{g^2\varphi^{(0)^2}}{H^2} + 15\varepsilon_1\right)\right]u_k = 0. \quad (68)$$

In contrast to what happens for the fluctuations of the rescaled inflaton field, the correction terms in the mode equation for the fluctuations of the waterfall field are large. This is a reflection of the tachyonic instability in the direction of the waterfall field. More specifically, the mass term of this equation contains terms of different orders of magnitude. Indeed, in the vacuum-dominated regime, under the slow-roll approximation, and since $\sigma_\chi^2 < \sigma_{\chi_c}^2$ in the valley, one has

$$15\varepsilon_1, \qquad 3\frac{\lambda\sigma_\chi^2}{H^2} \ll 2 \ll \frac{12M_{\mathrm{Pl}}^2}{v^2}, \qquad \frac{g^2\phi^{(0)^2}}{H^2}. \quad (69)$$

Moreover, for typical parameter values, one also has

$$15\varepsilon_1 \ll 3\frac{\lambda\sigma_\chi^2}{H^2}, \quad (70)$$

although it would, in principle, be possible to find a range of fine-tuned parameters for which this inequality does not hold.

Finally, one can use Eq. (10) to rewrite $\varphi_{\rm in}^{(0)}$ in terms of $\Phi_{\rm c}$ and the total number of e-folds of inflation $N_{\rm c}$ produced in the valley when φ crosses the critical point, and one obtains

$$\frac{g^2\varphi^{(0)2}}{H^2} = \frac{12M_{\rm Pl}^2}{v^2}\frac{\varphi^{(0)2}}{\Phi_{\rm c}^2} \tag{71}$$

$$\simeq \frac{12M_{\rm Pl}^2}{v^2}\left[e^{N_c - N(\tau)}\right]^{8M_{\rm Pl}^2 m^2/(v^4\lambda)}, \tag{72}$$

where at first order in ε_1 one has

$$N(\tau) = \ln\left[-(1+\varepsilon_1)/(H\tau)\right] \approx -\ln(-H\tau) + \varepsilon_1, \tag{73}$$

if one initializes N to 0 when $\tau = -(1+\varepsilon_1)/H$.

2. Qualitative mode evolution analysis

Let us now try to gain some qualitative insight about the time evolution of the $\boldsymbol{k}$ modes. First of all, one can see that there is some explicit τ dependence in the time-dependent mass of the $u_{\boldsymbol{k}}$'s (through the $\phi^{(0)2}$) in addition to the usual $1/\tau^2$ dependence. One needs to make sure that this term goes to zero at early times, i.e., when the limit $k\tau \to -\infty$ is formally taken, so that the Bunch-Davies vacuum initial condition can be recovered in that limit. That is, one needs to make sure that at arbitrary early times (as $k\tau \to -\infty$), any given mode is at small enough scales so that it feels a Minkowski flat spacetime and lies in the Bunch-Davies state.

Bearing this in mind, since $8M_{\rm Pl}^2 m^2/(v^4\lambda) \ll 1$, from our assumption of vacuum domination of the Hubble constant in the valley, one is safe since

$$\frac{(-H\tau)^{\frac{8M_{\rm Pl}^2 m^2}{v^4\lambda}}}{\tau^2} \to 0 \quad \text{as } (-k\tau) \to \infty. \tag{74}$$

One can therefore quantize the mode functions as usual using the Bunch-Davies vacuum solution as a limiting initial condition at early times.

Also, the $\varphi^{(0)}$ dependence of the mass was written in the form (71) in order to get a better insight on the qualitative behavior of the modes after they exit the Hubble radius. Inserting this expression into the mode function equations of motion, one obtains

$$u_{\boldsymbol{k}}'' + [k^2 - m_u^2(\tau)]u_{\boldsymbol{k}} = 0, \tag{75}$$

where the effective mass m_u is defined as

$$m_u^2(\tau) \equiv \frac{2 - m_\psi^2/H^2}{\tau^2} \tag{76}$$

$$= \frac{1}{\tau^2}\left[2 + 15\varepsilon_1 - 3\frac{\lambda\sigma_\chi^2}{H^2} - \frac{12M_{\rm Pl}^2}{v^2}\left(\frac{\varphi^{(0)2}}{\varphi_{\rm c}^2} - 1\right)\right]. \tag{77}$$

The time evolution of the squared mass m_u^2 is sketched in Fig. 2. Very small scales for which $k^2 \gg m_u^2(\tau)$ are still oscillating in their Bunch-Davies state. However, when a mode crosses the value $k_{H_{\rm eff}}^2 = m_u^2(\tau)$, its qualitative behavior changes. We call this point the crossing of the "effective" Hubble radius (since in standard massless-single-field inflation this corresponds to the point where every mode crosses the Hubble radius and then freezes out). The evolution of modes with wavelength larger than this effective Hubble crossing scale, i.e., satisfying $k^2 < k_{H_{\rm eff}}^2 = m_u^2(\tau)$, will be driven according to the behavior of $m_u^2(\tau)$.

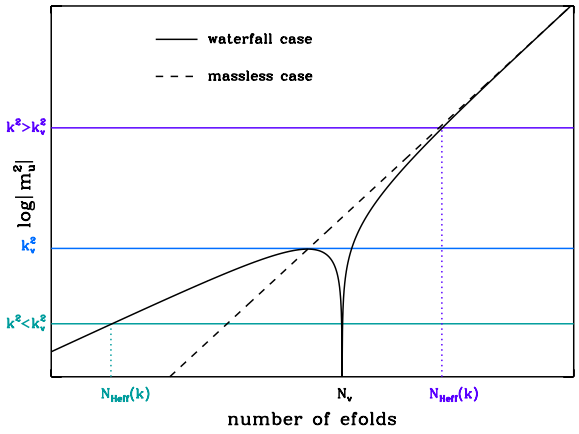

FIG. 2 (color online). Sketch of the time evolution of the squared mass m_u^2 appearing in Eq. (75), as a function of the number of e-folds. As a comparison, the dashed line represents the massless situation where $m_\psi = 0$ and $m_u^2 = 2/\tau^2$. For $N < N_{\rm v}$ (respectively, $N > N_{\rm v}$), one has $m_u^2 < 0$ (respectively, $m_u^2 > 0$). The first time a mode $\boldsymbol{k}$ crosses the squared mass scale is given by $N_{H_{\rm eff}}(k)$. Its behavior then depends on whether $N_{H_{\rm eff}}(k) < N_{\rm v}$ or $N_{H_{\rm eff}}(k) > N_{\rm v}$ (see discussion in the text). The separation between these two regimes is given by $k_{\rm v}$.

Let us see in more detail how the evolution proceeds. The time of the "effective" Hubble radius crossing $N_{H_{\rm eff}}(k)$ is defined by $k^2 = m_u^2[N_{H_{\rm eff}}(k)]$. This happens during the valley phase if $N_{H_{\rm eff}} < N_{\rm c}$, i.e., for modes such that $k < k_{\rm c}$, where

$$k_{\rm c}^2 = m_u^2(\tau_{\rm c}) \simeq 2H^2 {\rm e}^{2N_{\rm c}}. \tag{78}$$

The comoving wave number k_c thus corresponds to the wavelength that freezes out when $\varphi = \Phi_{\rm c}$. Now, for $k < k_{\rm c}$, two different behaviors for m_u^2 right after the effective Hubble radius crossing can occur, which we now investigate. Recall that typically one has $\frac{12M_{\rm Pl}^2}{v^2} \gg 2 \gg 3\frac{\lambda\sigma_\chi^2}{H^2}$. Therefore, the modes with $m_u^2 < 0$, when they cross their effective Hubble radius, are such that

$$N_{\rm c} - N_{H_{\rm eff}}(k) > \frac{v^4\lambda}{8M_{\rm Pl}^2 m^2}\ln\left(1 + \frac{v^2}{6M_{\rm Pl}^2}\right) = \frac{v^2H^2}{4M_{\rm Pl}^2 m^2} + \mathcal{O}\left(\frac{v^4}{M_{\rm Pl}^4}\right).$$

This means that it happens at long wavelengths, for $k < k_{\rm v}$, where

$$k_{\rm v}^2 = m_u^2(\tau_{\rm v}) \simeq \frac{H^2\upsilon^2}{6M_{\rm Pl}^2}\, {\rm e}^{2N_{\rm c}-\frac{\upsilon^2H^2}{2M_{\rm Pl}^2m^2}}. \tag{79}$$

From this formula it is very easy to check that $k_{\rm v} < k_{\rm c}$, since $\upsilon/M_{\rm Pl} \ll 1$ for this model to proceed at small fields. If $k < k_{\rm v}$, the modes do not freeze out as they escape their effective Hubble radius, but rather continue their oscillations until the time $N_{\rm v}$ given by

$$N_{\rm c} - N_{\rm v} = \frac{\upsilon^2H^2}{4M_{\rm Pl}^2m^2} \tag{80}$$

when the distance between φ^2 and its critical value becomes such that $\varphi^2 - \Phi_{\rm c}^2 \lesssim (\upsilon^2/6M_{\rm Pl}^2)\Phi_{\rm c}^2$, at which point they freeze out. Mapping back to $\delta\psi_{\boldsymbol{k}}^{(1)} = a^{-1}u_{\boldsymbol{k}}$, this oscillation period for the $u_{\boldsymbol{k}}$ modes corresponds to a fast underdamping of the perturbations $\delta\psi_{\boldsymbol{k}}^{(1)}$. This means that those modes do not undergo squeezing and therefore do not experience classicalization.

From Fig. 2, one can see that between $N_{H_{\rm eff}}$ and $N_{\rm v}$, these modes actually experience a very brief stage during which k^2 dominates over m_u^2 again. Since this period is very short in time, we will neglect its effect for now (and this approximation will be shown to be consistent *a posteriori*). Finally, in the $N \ll N_{\rm v}$ limit, one has $m_u^2 \simeq -12/\tau^2M_{\rm Pl}^2/\upsilon^2\varphi^{(0)2}/\Phi_{\rm c}^2$, which leads to

$$\begin{aligned} N_{H_{\rm eff}} &\simeq \frac{\log\left(\frac{\upsilon^2}{M_{\rm Pl}^2}\frac{k^2}{12H^2}\right)}{2\left(1-4\frac{m^2M_{\rm Pl}^2}{\lambda\upsilon^4}\right)} - \frac{4}{\frac{\lambda\upsilon^4}{2m^2M_{\rm Pl}^2}-2}N_{\rm c} \\ &\simeq \frac{1}{2}\log\left(\frac{\upsilon^2}{M_{\rm Pl}^2}\frac{k^2}{12H^2}\right) - 8\frac{m^2M_{\rm Pl}^2}{\lambda\upsilon^4}N_{\rm c}, \end{aligned} \tag{81}$$

the second expression being simplified using the slow-roll condition $\varepsilon_1(\Phi_{\rm c}, \Psi = 0) \ll 1$.

On the other hand, if $k_{\rm v} < k < k_{\rm c}$, the modes freeze out and cease to oscillate right after effective Hubble crossing. They consequently undergo squeezing, which allows for classicalization. This phase typically extends over much more than 60 e-folds before the inflaton reaches its critical value, which makes it the most important one to study. Close to the inflaton critical value, $m_u^2(\tau)$ is dominated by the $2/\tau^2$ term, and therefore modes freezing out and growing in this range of conformal time behave very similarly to the perturbations of a light scalar field in de Sitter space, with a slight positive mass given by $3\lambda\sigma_\chi^2/H^2 - 15\varepsilon + 12M_{\rm Pl}^2/\upsilon^2(\varphi^{(0)2}/\Phi_{\rm c}^2 - 1)$, which gives the spectrum a blue tilt. In this limit where $N_{\rm v} \ll N < N_{\rm c}$, one has

$$N_{H_{\rm eff}}(k) \simeq \left[\log\left(\frac{k}{\sqrt{2}H}\right) + 2\frac{m^2}{\upsilon^2}\frac{k^2M_{\rm Pl}^2}{H^4}N_{\rm c}\right]\Big/\left(1-2\frac{m^2}{\upsilon^2}\frac{k^2M_{\rm Pl}^2}{H^4}\right). \tag{82}$$

3. Quantitative mode evolution analysis

Now that we have qualitatively analyzed the behavior of the mode functions as they cross their "effective" Hubble radius, let us now manipulate the equation for the mode function into a more practical form for calculations. Considering the form (72) of writing the last term appearing in $m_u^2(\tau)$, one has

$$m_u^2(\tau) = \frac{2 + 15\varepsilon - 3\frac{\lambda\sigma_\chi^2}{H^2} - \frac{12M_{\rm Pl}^2}{\upsilon^2}\{{\rm e}^{[N_c - N(\tau)]\frac{2m^2}{3H^2}} - 1\}}{\tau^2}. \tag{83}$$

Now, since we are interested in the late-time behavior of the mode functions, that is, after they exit their effective Hubble radius, we use an asymptotic approximate solution for the scaling of their amplitude. To do this, let us define a differential equation for an "effective" scale factor $\mathfrak{a}$:

$$\frac{\mathfrak{a}''}{\mathfrak{a}} = m_u^2(\tau). \tag{84}$$

We call this quantity the effective scale factor because it allows us to rewrite the equation for the mode functions in the standard form for a massless field in de Sitter space:

$$u_{\boldsymbol{k}}'' + \left(k^2 - \frac{\mathfrak{a}''}{\mathfrak{a}}\right)u_{\boldsymbol{k}} = 0. \tag{85}$$

Moreover, for a single massless scalar field in de Sitter space, on super-Hubble scales, the mode functions (which we call $z_{\boldsymbol{k}}$) scale as the scale factor a if one waits long enough for the decaying mode to become negligible. This means that for small $k^2 < \min(2/\tau_1^2, 2/\tau_2^2)$, one has $a(\tau_1)/a(\tau_2) \approx z_{\boldsymbol{k}}(\tau_1)/z_{\boldsymbol{k}}(\tau_2)$ (neglecting an overall irrelevant constant phase), provided that τ_1 and τ_2 are chosen to be long enough after the Hubble crossing of the $\boldsymbol{k}$ mode (which usually means only a few e-folds).

Here, we are facing a similar situation. Qualitatively, once the modes $u_{\boldsymbol{k}}$ cross their effective Hubble radius (technically, a few e-folds after the crossing), they scale as the effective scale factor $\mathfrak{a}(\tau)$ (if the modes are underdamped after their effective Hubble crossing, i.e., for the modes such that $k < k_{\rm c}$, one simply needs to somehow be more careful about the matching of the sub- and super-$H_{\rm eff}$ scalings, but the same argument essentially still holds). Since $\mathfrak{a}$ is basically given by the background equation of motion with a nonvanishing σ_χ, one finds that the $u_{\boldsymbol{k}}$'s evolve asymptotically as the linearized background after $H_{\rm eff}$ crossing.

This argument provides one with the asymptotic behavior for the evolution of the norm of the super-$H_{\rm eff}$ $\delta\psi_{\boldsymbol{k}}^{(1)}$ modes:

$$\begin{aligned} \delta\psi_{\boldsymbol{k}}^{(1)}(\tau) &= a^{-1}(\tau)|u_{\boldsymbol{k}}(\tau)| \\ &\simeq a^{-1}(\tau)\frac{\mathfrak{a}(\tau)}{\mathfrak{a}(\tau_{H_{\rm eff}})}|u_{\boldsymbol{k}}(\tau_{H_{\rm eff}})| \\ &\simeq a^{-1}(\tau)\frac{\mathfrak{a}(\tau)}{\mathfrak{a}(\tau_{H_{\rm eff}})}|u_{\boldsymbol{k}}(\tau_i)|. \end{aligned} \tag{86}$$

Here, $\tau_{H_{\rm eff}}$ is defined as the conformal time at which the $\boldsymbol{k}$ mode crosses its effective Hubble radius. As before, an overall irrelevant phase factor is neglected. Also, in the last step we use the fact that, before effective Hubble crossing, one has $m_u \ll k^2$ and the modes just oscillate with constant amplitude. Then, $|u_{\boldsymbol{k}}(\tau_i)|$ can be evaluated in the Bunch-Davies initial vacuum. A more precise calculation would consist in finding the exact sub-Hubble solution, given in terms of Hankel functions of the first kind (once the Bunch-Davies initial conditions are imposed), and evaluating it at the effective Hubble crossing. However, not much accuracy would be gained by doing so.

That being said, one is only left with the problem of solving the differential equation for the effective scale factor $\mathfrak{a}$ and inverting the relation $k^2 = m_u^2[\tau_{H_{\rm eff}}(k)]$ to obtain $\tau_{H_{\rm eff}}(k)$.

The first problem is an easy one since it just corresponds to solving the linearized background equation of motion. Expressed in terms of the number of e-folds, it is given by

$$\frac{\mathrm{d}^2\mathfrak{a}}{\mathrm{d}N^2} + \frac{\mathrm{d}\mathfrak{a}}{\mathrm{d}N} - \mathfrak{a}\Bigg(2 + 15\varepsilon_1 - 3\frac{\lambda\sigma_\chi^2}{H^2} - \frac{12M_{\rm Pl}^2}{v^2}\{e^{[N_c - N(\tau)]\frac{2m^2}{3H^2}} - 1\}\Bigg) = 0. \tag{87}$$

As before, $\mathrm{d}/\mathrm{d}N(\sigma_\chi^2/H^2) = 1/(4\pi^2)$ and the time variation of the σ_χ term in the above equation is suppressed by a λ factor. It can therefore be neglected, allowing the solution to be approximated in terms of Bessel functions of the first and second kinds:

$$\mathfrak{a} = e^{-\frac{N(\tau)}{2}}[C_1 \mathrm{J}_\nu(x) + C_2 \mathrm{Y}_\nu(x)],$$

$$\text{where } \nu = \frac{3H^2}{m^2}\sqrt{\frac{9}{4} + 15\varepsilon_1 - 3\frac{\lambda\sigma_\chi^2}{H^2} + \frac{12M_{\rm Pl}^2}{v^2}}$$

$$\text{and } \quad x = \frac{3H^2}{m^2}\frac{2\sqrt{3}M_{\rm Pl}}{v}e^{(N_c - N)\frac{m^2}{3H^2}}, \tag{88}$$

where C_1 and C_2 are integrating constants. To fix them, one first notices that an overall constant in $\mathfrak{a}$ bears no physical meaning, since only the ratio $\mathfrak{a}(\tau)/\mathfrak{a}(\tau_i)$ enters in the quantities to be computed. Therefore, one only needs to fix the ratio in which the two independent solutions enter in the mode function. To do so, one notes that in the formal limit $k\tau \to -\infty$, the positive mode function starts out in the Bunch-Davies vacuum, and its evolution deep inside its effective Hubble radius is given by a Hankel function of the first kind. It is therefore natural that its approximate behavior after the crossing of its effective Hubble radius also be mapped to another Hankel function of the first kind. One can therefore choose the constants C_1 and C_2 so that the solution is written in the form of an $H_\nu(x)$ function.

To give another, maybe more convincing, argument to fix C_1 and C_2, we note that if $k < k_{\rm v}$, that is, if the mode is still underdamped and continues its oscillations outside its Hubble radius for a (more or less long) time before freezing out at $N = N_{\rm v}$, the requirement of having oscillations damped by a factor of $e^{-N/2}$ in Eq. (88) basically fixes the constants to $C_1 = 1$ and $C_2 = i$, up to an overall irrelevant constant phase. This is precisely the choice that allows us to recover the Hankel function of the first kind discussed above.

If, on the contrary, $k_{\rm v} < k < k_{\rm c}$, i.e., if the $\boldsymbol{k}$ mode of interest crosses its effective Hubble radius late enough so that it is overdamped and freezes out immediately after the crossing, then, provided the mapping is done a few e-folds after the crossing, the decaying mode J_ν of the fundamental solution (88) completely decays and the positive mode function is exclusively mapped to the growing mode Y_ν to great accuracy. This corresponds to only using the Bessel function of the second kind Y_ν as a solution, which is also approximately what using a Hankel function of the first kind would mean in the relevant range of values for ν and x.

However it might be cumbersome to work in terms of Bessel or Hankel functions, mainly because for the regime of parameters ν and x one is interested in, none of the asymptotic forms of these functions is a good approximation when the mode function freezes out and is mapped to the growing mode. Indeed, the small-argument form holds if $x \ll \sqrt{\nu}$, which is not the case here since one works under vacuum domination, and the large-argument expansion is valid provided that $x \gg \nu^2$, which is not the case either, again because of vacuum domination.

It is therefore useful to note that, since $\frac{2m^2}{3H^2} \ll 1$, one can Taylor expand to first order the exponential in Eq. (87), in order to obtain a simpler differential equation which can be solved in terms of Airy functions:

$$\frac{\mathrm{d}^2\mathfrak{a}}{\mathrm{d}N^2} + \frac{\mathrm{d}\mathfrak{a}}{\mathrm{d}N} - \mathfrak{a}\Bigg\{2 + 15\varepsilon - 3\frac{\lambda\sigma_\chi^2}{H^2} - \frac{8M_{\rm Pl}^2 m^2}{v^2H^2}[N_{\rm c} - N(\tau)]\Bigg\} = 0, \tag{89}$$

which is solved by

$$\mathfrak{a} = e^{-\frac{N}{2}}[\mathrm{Ai}(x)C_1 + \mathrm{Bi}(x)C_2], \tag{90}$$

with

$$x = \left(\frac{v^6\lambda}{96m^2M_{\rm Pl}^4}\right)^{\frac{2}{3}}\left[\frac{96m^2M_{\rm Pl}^4}{v^6\lambda}(N - N_c) - 3\frac{\lambda\sigma_\chi^2}{H^2} + 15\varepsilon_1 + \frac{9}{4}\right], \tag{91}$$

where C_1 and C_2 are integration constants which are not necessarily the same as before. For the $\boldsymbol{k}$ modes such that $k < k_{\rm v}$, which are underdamped when they cross their effective Hubble radius, one has $x \ll 0$, and the asymptotic forms of the Airy functions for large and negative arguments in terms of sine and cosine can be used. Since oscillations are expected, one can choose $C_1 = i$

and $C_2 = 1$. Then, deep inside the valley when these modes cross their effective Hubble radius, one obtains

$$\mathfrak{a} \underset{x\to-\infty}{=} \frac{e^{-N/2}}{\sqrt{\pi}}|x|^{-1/4}e^{i\frac{2}{3}|x|^{3/2}+\frac{i}{4}\pi}. \tag{92}$$

The modes that freeze out in that limit evolve according to

$$\delta\psi_{\boldsymbol{k}}^{(1)} \approx e^{\frac{1}{2}(N_{H_{\rm eff}}-3N)}\left|\frac{x(N)}{x(N_{H_{\rm eff}})}\right|^{-\frac{1}{4}}\frac{e^{i\frac{2}{3}|x(N)|^{\frac{3}{2}}}}{e^{i\frac{2}{3}|x(N_{H_{\rm eff}})|^{\frac{3}{2}}}}|u_{\boldsymbol{k}}(N_{H_{\rm eff}})| \tag{93}$$

$$\approx e^{\frac{1}{2}[N_{H_{\rm eff}}-3N]-i\frac{2}{3}[|x(N_{H_{\rm eff}})|^{\frac{3}{2}}-|x(N)|^{\frac{3}{2}}]}\left|\frac{x(N_{H_{\rm eff}})}{x(N)}\right|^{\frac{1}{4}}\frac{1}{\sqrt{2k}}$$
$$\text{for } x(N), x(N_{H_{\rm eff}}) \ll 0 \quad (\text{and} \quad k^2 < m_u^2). \tag{94}$$

In the first line of this equation one can see the previously mentioned oscillations, which were expected to be found since in that limit one has $m_u^2(N) < 0$. One also finds the decay factor $e^{-3N/2}$. Recall that in order to express $N_{H_{\rm eff}}$ in terms of k in that regime, one needs to solve $|k^2_{H_{\rm eff}}| = |m_u^2(N_{H_{\rm eff}})|$.

If $k > k_{\rm v}$, $m_u^2(N_{H_{\rm eff}})$ becomes positive, the oscillations cease and the modes freeze out. To see this, one can equivalently examine x, which becomes positive as $x \to$ constant $\times\,[9/4 + 15\varepsilon - 3\lambda\sigma_\chi^2/(H^2)]^-$, and the above approximation for the Airy functions breaks down. However, to find how the behavior of the modes $k < k_{\rm v}$ changes when $N > N_{\rm v}$, and to derive the behavior of the modes with $k_{\rm v} < k < k_{\rm c}$ which cross their effective Hubble radius in that limit, one can assume a long waterfall takes place (which we recall is necessary in order to evade the blue-tilt problem) and suppose $v^6\lambda \gg m^2M_{\rm Pl}^4$ [see Eq. (12)], to use the large-argument expansion of the Airy functions and proceed as above. In this limit, one obtains a growing mode and a decaying mode, and keeping only the former in the asymptotic solution, one gets

$$\mathfrak{a} \underset{x\to+\infty}{=} \frac{e^{-\frac{N}{2}}}{\sqrt{\pi}}|x|^{-1/4}e^{\frac{2}{3}x^{3/2}}. \tag{95}$$

Using this asymptotic expression, one obtains, for the underdamped modes $k < k_{\rm v}$, once frozen out (for $N > N_{\rm v}$),

$$\delta\psi_{\boldsymbol{k}}^{(1)} \simeq e^{\frac{1}{2}(N_{H_{\rm eff}}-3N)}\left|\frac{x(N_{H_{\rm eff}})}{x(N)}\right|^{\frac{1}{4}}\frac{e^{\frac{2}{3}x(N)^{\frac{3}{2}}}}{e^{\frac{2}{3}x(N_{\rm v})^{\frac{3}{2}}}}\frac{1}{\sqrt{2k}}$$
$$\text{for } x(N) \gg 0, x(N_{H_{\rm eff}}) \ll 0 \quad (\text{and} \quad k^2 < m_u^2), \tag{96}$$

and where a constant irrelevant phase factor is neglected. For modes $k > k_{\rm v}$ freezing out in that regime [for which $x(N_{H_{\rm eff}}) > 0$], one has

$$\delta\psi_{\boldsymbol{k}}^{(1)} \simeq e^{\frac{1}{2}(N_{H_{\rm eff}}-3N)}\left|\frac{x(N)}{x(N_{H_{\rm eff}})}\right|^{-\frac{1}{4}}\frac{e^{\frac{2}{3}x(N)^{\frac{3}{2}}}}{e^{\frac{2}{3}x(N_{H_{\rm eff}})^{\frac{3}{2}}}}|u_{\boldsymbol{k}}(N_{H_{\rm eff}})| \tag{97}$$

$$\simeq e^{\frac{1}{2}[N_{H_{\rm eff}}-3N]+\frac{2}{3}[x(N)^{\frac{3}{2}}-x(N_{H_{\rm eff}})^{\frac{2}{3}}]}\left|\frac{x(N_{H_{\rm eff}})}{x(N)}\right|^{\frac{1}{4}}\frac{1}{\sqrt{2k}}$$
$$\text{for } x(N), x(N_{H_{\rm eff}}) \gg 0 \quad (\text{and} \quad k^2 < m_u^2). \tag{98}$$

The formulas derived above for the amplitude of the first-order perturbations in the ψ direction are collected in Appendix C [see Eqs. (C2)–(C6)], for practical convenience.

Before proceeding, since several approximations have been performed, it seems useful to first check their validity by comparing them with the full numerical integrations of Eq. (68). We also check the validity of the commonly used so-called adiabatic approximation. This scheme is defined as follows: Since the inflaton field is slowly rolling down the bottom of the valley, the effective mass for the waterfall field m_ψ, defined as $m_u^2 \equiv (2 - m_\psi^2/H^2)/\tau^2$ in Eq. (76) (m_u is sketched in Fig. 2), is varying slowly, and therefore its time dependence can be neglected. Hence, when solving Eq. (68), the usual constant-mass mode function solution

$$u_{\boldsymbol{k}} \simeq -ie^{i(\nu+\frac{1}{2})\frac{\pi}{2}}\frac{\sqrt{\pi}}{2}(-\tau)^{1/2}H_\nu^{(1)}(-k\tau) \tag{99}$$

can be used, with ν now given by the time varying quantity $\nu \equiv \sqrt{9/4 - m_\psi^2/H^2}$, which is complex when $N < N_{\rm v}$. This approximate solution is referred to as the adiabatic one since it is derived under the approximation of a slowly varying mass. We check its validity in Fig. 3, where results from an exact integration of Eq. (68) are compared to the analytical approximations (C2)–(C6) and to the adiabatic solution Eq. (99).

Let us comment on what has been obtained. The case $k > k_{\rm v}$ is similar to the standard well-known massless case, where $|u_{\boldsymbol{k}}|$ is constant on sub-Hubble scales and $|\delta\psi_{\boldsymbol{k}}^{(1)}|$ is constant on super-Hubble scales. The matching between the analytical expressions (C2)–(C6) and the numerical solution is excellent. The adiabatic approximation also holds during the whole evolution of such modes.

If $k < k_{\rm v}$, there is an intermediate regime when $N_{H_{\rm eff}}(k) < N < N_{\rm v}$ where the field fluctuations are overdamped and oscillations continue to take place. As noticed in Fig. 2, during that phase, at some point, such modes experience a short period during which k^2 dominates over m_u^2 again. Since this period is very short in time, it was not taken into account when deriving the analytical expressions Eqs. (C2)–(C6), and checking this assumption was postponed until later. One can now check that it indeed leads to rather reliable expressions. However, this short phase of rapid evolution of m_u^2 obviously breaks the adiabatic approximation, and one can indeed see that the

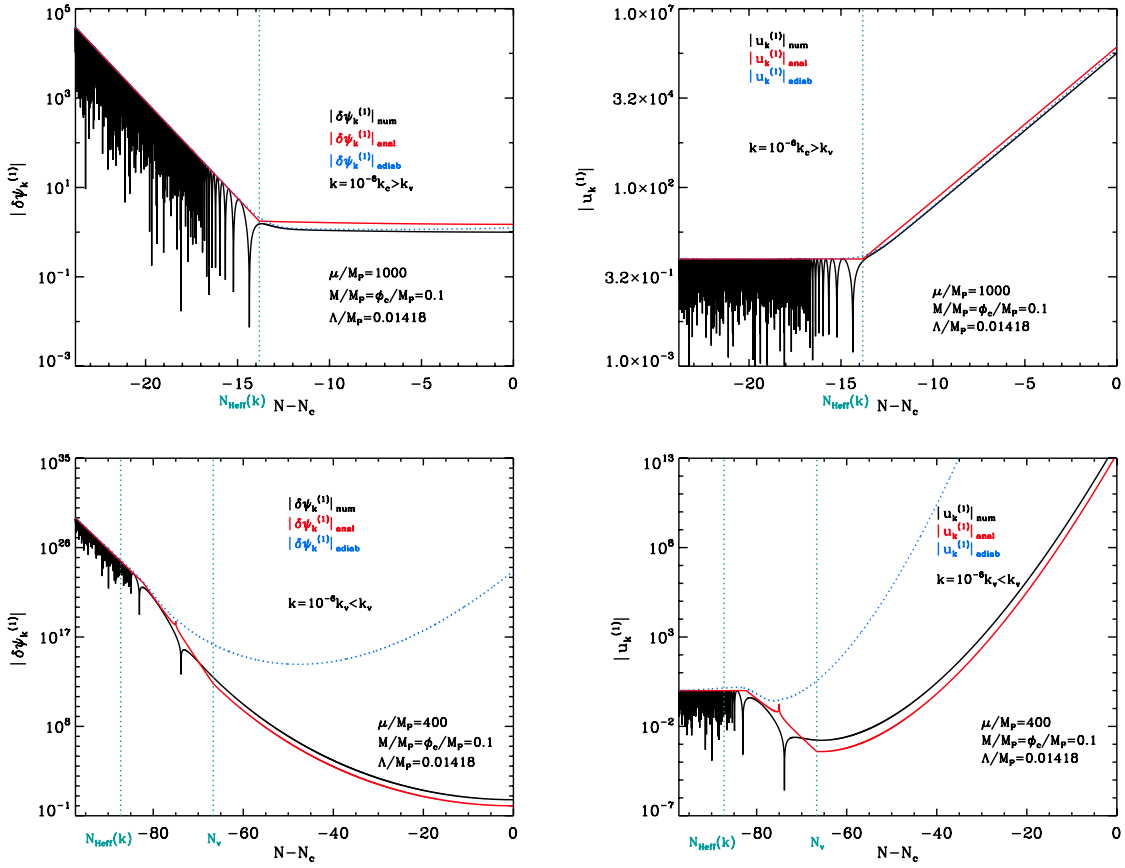

FIG. 3 (color online). Time evolution of the first-order perturbation amplitudes of the waterfall field $|\delta\psi_k^{(1)}|$ (left panels) and its scaled counterpart u_k (right panels) in the cases $k > k_v$ (top panels) and $k < k_v$ (bottom panels). The black solid lines are numerical results from an exact integration of Eq. (68). The red solid lines represent the analytical approximated results Eqs. (C2)–(C6). The blue dotted lines represent the adiabatic solution Eq. (99). When $k > k_v$ the modes evolve in the standard well-known way, $|u_k|$ being constant on sub-Hubble scales and $|\delta\psi_k^{(1)}|$ being constant on super-Hubble scales. When $k < k_v$, however, there is an intermediate phase $N_{H_{\rm eff}}(k) < N < N_v$ during which the adiabatic evolution of the effective mass of the waterfall breaks down and the fluctuations are overdamped.

adiabatic formula stops being valid at this point. The subsequent evolution is therefore also different from the one we expect under the adiabatic approximation. When $N > N_v$, the field fluctuations continue to experience overdamping.

The validity of the analytical expressions derived above is thus confirmed, as is the schematic description previously sketched, and the adiabatic method is shown not to be valid for the modes such that $k < k_v$, when N approaches N_v and afterward.

IV. CALCULATION OF σ_χ AND THE BACKREACTION PROBLEM

So far, we have calculated to leading order in the slow-roll parameters the amplitude of the linearized quantum fluctuations in both fields in the presence of a shifted background. These are the mode functions valid up to next-to-leading order in $\hbar$ and up to leading order in slow roll as defined in Eqs. (13) and (14), which enter in the bath field propagators evaluated at the time when a given mode of the quantum fields joins the coarse-grained fields. We can therefore use these results to directly calculate a shifted classical noise for Eqs. (15) and (16), which will now be valid to next-to-leading order in $\hbar$ and to leading order in slow roll.

This higher accuracy calculation does bear some importance. Indeed, the typical deviation in the waterfall direction acquired during the valley phase sets typical initial conditions for the subsequent waterfall phase, hence determining how many e-folds this tachyonic period should last. One should therefore calculate $\sigma_{\chi c}$ as accurately as possible.

A first estimate was given in Sec. II C using the standard massless de Sitter solutions for the modes $\delta\phi^{(1)}$ and $\delta\chi^{(1)}$ to calculate the amplitude of the noises; see Eq. (27). This was a first step towards a more accurate calculation, carried out mainly to obtain qualitative results. We now wish to include the higher-accuracy noises derived from the mode amplitude results of the previous subsection, and study

how this impacts on the stochastic dispersions of the coarse-grained fields, which we discuss here, and on the statistics of the inflaton perturbations, which we discuss in the next section.

For the coarse-grained inflaton field φ, we expect the solution of Eq. (15), including higher noise accuracy, to closely follow the noiseless, classical solution. This is because we already assumed the values of the potential parameters to be such that the dynamics of the inflaton in the valley phase is dominated by its classical drift at leading order in $\hbar$. We can convince ourselves that this assumption is preserved up to next-to-leading order in $\hbar$ and to leading order in the first two slow-roll parameters by looking at the corrected inflaton noise autocorrelation, which shows a suppressed correction compared to its leading $\hbar$ and $\mathcal{O}(\epsilon_1^0, \varepsilon_2^0)$ value:

$$\langle \xi_\phi(N)\xi_\phi(N')\rangle = \frac{H^4}{4\pi^2}\delta(N-N')\times\left[1+\frac{2}{3}\left(\frac{m^2+g\sigma_\chi^2}{H^2}-9\varepsilon_1\right)\times(\ln 2\epsilon+\gamma-2)\right]. \quad (100)$$

Here, $\gamma \simeq 0.577$ is the Euler-Mascheroni constant, and recall that $\varepsilon_2 \approx -\frac{2}{3}\frac{m^2}{H^2}$. The correction to the de Sitter massless formula (20) is indeed small for a light inflaton field, and one does not expect important effects on the background trajectory coming from a better calculation of σ_ϕ. Important effects concerning the inflaton, however, are to be expected when it comes to the statistics of the fluctuations of the coarse-grained field, and they will be calculated in the next section.

As a final remark concerning the background inflaton coarse-grained field, it is interesting to remember that in spite of the fact that the condition $\epsilon \ll 1$ was required in order to only collect the squeezed super-Hubble modes in the coarse-grained part of the field, the splitting parameter ϵ cannot be arbitrarily small if one wants the deviations from the free massless case to remain small. More precisely, from the previous equation, one can see that the condition $\exp(-H^2/m^2) \ll \epsilon \ll 1$ should be imposed. This is exactly the condition that was obtained by Starobinsky and Yokoyama in their first paper [34] on the subject [see Eq. (80) there], requiring ϵ-independent results for the two-point equilibrium correlation function of test scalar fields in de Sitter space. Here, we make the origins of such a condition rather clear.

On the other hand, the waterfall field is significantly massive far enough in the valley. Therefore, important effects on its dispersion coming from a higher-order calculation of the noise sourcing its coarse-grained evolution are expected to arise in this region. We shall investigate this question in detail in what follows. Whether these effects can lie in the observational window or not is also a question which shall be answered.

Concretely, the higher-order white Gaussian noise $\xi_\psi(N)$ sourcing the Langevin equation (16) for the coarse-grained waterfall field is given by

$$\langle \xi_\psi(N)\xi_\psi(N')\rangle \propto |\delta\psi_{\boldsymbol{k}}^{(1)}|^2_{k=\epsilon aH}\delta(N-N'), \quad (101)$$

with $|\delta\psi_{\boldsymbol{k}}^{(1)}|$ now evaluated using Eqs. (C2)–(C6).

Before proceeding to this evaluation, a verification is in order. In the computational program described above, one should remember that $|\delta\psi_{\boldsymbol{k}}^{(1)}|$ takes different forms depending on whether $N \lessgtr N_{\rm v}$, $N_{H_{\rm eff}}$ and one needs to know which piece of the function should be used. Furthermore, ϵ is usually taken to be such that $\epsilon \ll 1$ in order to keep only the super-Hubble highly squeezed modes in the coarse-grained field (squeezing being the condition for classical behavior; see Refs. [60,61,72]).

However, here, the effective Hubble radius $H_{\rm eff}^{-1}$ intervenes rather than the Hubble radius itself, and therefore one first needs to be sure that no modification to the standard picture arises from this fact. In Ref. [73], the original analysis of Guth and Pi [72] is generalized to heavy fields, and it is found that there is no emergence of classical correlations for $\nu^2 < 0$ (recall that $\nu_\psi^2 = 9/4 - m_\psi^2/H^2$). Such classical correlations, usually obtained through turning quantum oscillators upside-down or by rapid squeezing of upside-right oscillators, are a key point of the stochastic inflation formalism, as they enable us to model the dynamics of the large-wavelength fluctuations as the evolution of a stochastic classical distribution.

For our purpose, this means that when $N < N_{\rm v}$, the stochastic equations driving the evolution of the coarse-grained field are questionable, and that a full field theoretic approach should be used instead. Therefore, in the following, one should be careful when interpreting the results derived for $N < N_{\rm v}$.

Recalling that

$$N_{\rm c} - N_{\rm v} = \lambda v^6/(48m^2M_{\rm Pl}^4) \propto (N_{\rm end}-N_{\rm c})^2 \quad (102)$$

[see Eq. (12)], this means that such a "problematic" period happens long before the critical point is reached if the waterfall lasts for a long number of e-folds. In this case, this possible issue does not affect the fluctuations in the observational window. However, in the case of a short-lived waterfall, the potentially problematic phase lasts almost until the inflaton crosses the critical point, just before the end of inflation. Note, however, that in this case the noise amplitude would be accordingly suppressed by the heavy mass of the waterfall field, rendering this problem mostly academic for all practical and observational purposes. This suggests that, in accordance with the intuition that heavy fields should be irrelevant to the dynamics of the light fields, rather than using the stochastic formalism, one should integrate out the waterfall entirely for the whole problematic period. Here, our study focuses mainly on long-lived waterfall scenarios, and hence we avoid these issues.

A. Quasistationary approximation

Let us now turn to the concrete calculation of σ_χ. One first notices that Eq. (25) is completely general and is correct no matter what the amplitude of the ξ_ψ noise is. However, Eq. (26) makes use of the specific de Sitter massless statistics (21), and the lower incomplete gamma function solution arises when the amplitude of the noise $\langle \xi_\psi^2 \rangle$ is time independent. This is not true in general. However, the relaxation time of the statistical distribution (25) is extremely small since $\lambda v^4/(mM_{\rm Pl}^2) \gg 1$, which means, in practical terms, that the mass of Ψ decreases so slowly that at each given time, the χ distribution swiftly acquires its "stationary" local dispersion. This kind of adiabatic scheme should not be confused with the adiabatic approximation mentioned in Sec. III C in the calculation of $\delta\psi^{(1)}$. The former describes quasistationary stochastic distributions, while the latter relies on fluctuation modes crossing the relevant scales faster than their typical mass variation times. This is why, to avoid confusion, we may refer to the former as the "quasistationary" frame in what follows. Under this quasistationary approximation, one has $\sigma_\chi^2/\sigma_\chi^2|_{\rm massless} \simeq \langle \xi_\psi^2 \rangle / \langle \xi_\psi^2 \rangle_{\rm massless} = |\delta\psi^{(1)}|^2/|\delta\psi^{(1)}|^2_{\rm massless}$, so that

$$\sigma_\chi^2 \simeq \frac{|\delta\psi^{(1)}|^2}{H^4/(4\pi^2)} \sigma_\chi^2|_{\rm massless}, \tag{103}$$

where $\sigma_\chi^2|_{\rm massless}$ is given by Eq. (27).

It is of particular interest to notice that Eq. (103) is actually an implicit relation involving σ_χ, since $|\delta\psi^{(1)}|$ involves σ_χ itself [see Eqs. (C2)–(C6)]. In some sense, the whole recursive strategy presented in Sec. II B is now summarized in a single implicit equation for σ_χ. The situation is summarized in Fig. 4, where the left-hand side and the right-hand side of Eq. (103) are displayed, as a function of σ_χ^2. The solution of Eq. (103) lies at the intersection of these two curves, the location of which can be calculated using a recursive scheme which exactly translates the one presented in Sec. II B. The red circle labeled "1" in Fig. 4 represents the solution of Eq. (103) when setting $\sigma_\chi = 0$ in the right-hand side. This is the solution calculated in Sec. II C (where one has also neglected the mass of Ψ). This corresponds to evolving the perturbations $\delta\psi^{(1)}$ on a "classical" unshifted background. Then, one can source the equation of motion for these perturbations with a background shifted by the value of σ_χ just calculated. This new solution is represented by the red point labeled "2" in Fig. 4. This iterative procedure can be continued until obtaining the exact solution labeled by the red circle "3."

One can remark that the "classical" guess (labeled "1") lies in the attraction basin of the exact solution (labeled "3"). This is an indication that the perturbative expansion is under control, since at each step, one gets closer to the exact solution and decreases the absolute value of its

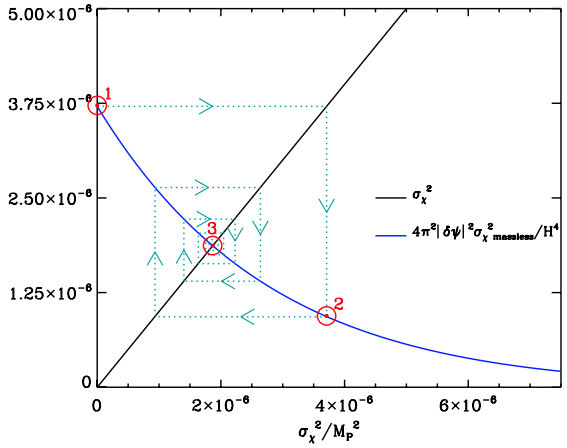

FIG. 4 (color online). Right hand side of Eq. (103), namely $4\pi^2|\delta\psi^{(1)}|^2\sigma^2_{\chi\rm massless}/H^4$ (blue solid line), normalized to $M_{\rm Pl}^2$, as a function of σ_χ^2, for $v = 0.1503M_{\rm Pl}$, $m = 7\times10^{-5}M_{\rm Pl}$, $g = \sqrt{\lambda} = 0.885$, computed one e-fold before crossing the critical point. These values may not be physical (especially for g and λ) but they have been chosen for display convenience. The black solid line is the left hand side of Eq. (103), namely σ_χ^2, normalized to $M_{\rm Pl}^2$, so that the solution of Eq. (103) lies at the intersection of these two lines. The green dotted lines and the arrows indicate how an iterative (perturbative) process leads to this solution, hence showing that the "classical" guess lies in the attraction basin of the solution. The meaning of the red circles and the associated labels 1, 2 and 3 is detailed in the text body.

displacement. This is a direct consequence of the fact that the right-hand side of Eq. (103) is a decreasing function of σ_χ, which is always true since as σ_χ increases, the mass "seen" by the perturbations $\delta\psi^{(1)}$ increases; hence, the amplitude of the noise decreases, and so does the resulting σ_ψ. However, this may not be the case during the waterfall, where this mass becomes more negative as σ_χ increases, rendering the amplitude of the noise more important. This signals a tachyonic breakdown of the perturbative expansion which indicates that the model may face serious issues when carefully studied in the waterfall (especially if this phase is long). We will come back to this point later, explaining how the start of the waterfall can be delayed.

Let us now see how these different estimations of σ_χ evolve in time. In Fig. 5, we display the free massless result (27), the result of a calculation taking into account the mass of Ψ but no backreaction (corresponding to the point labeled "1" in Fig. 4), and the exact solution of Eq. (103) (corresponding to the point labeled "3" in Fig. 4), as a function of time. When $N \ll N_{\rm c}$ (remember that $N < N_{\rm v}$ is not obvious to interpret), the inclusion of the mass of Ψ significantly decreases the value obtained for σ_χ, since a positive mass better confines the distribution for χ. In this regime σ_χ remains small and the inclusion of backreaction does not alter the result much. As the system gets closer to the critical point, σ_ψ increases and a discrepancy due to

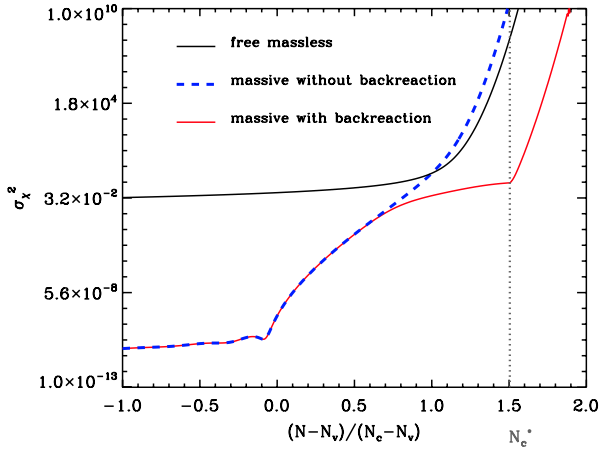

FIG. 5 (color online). Stochastic dispersion in the χ direction σ_χ^2, rescaled by its value (28) at the critical point in the free massless case, as a function of time labeled by $(N - N_v)/(N_c - N_c)$ (which is 1 at the critical point and 0 at the point $N = N_v$). The black solid line represents the free massless result (27). The blue dashed line takes the mass of Ψ into account but does not include backreaction. Technically, it corresponds to the right-hand side of Eq. (103), setting $\sigma_\chi = 0$, i.e., the value at the point labeled "1" in Fig. 4. The red solid line represents the exact solution of Eq. (103), i.e., the value at the point labeled "3" in Fig. 4. The parameter values used are $v = 0.1503 M_{\rm Pl}$, $m = 2.24 \times 10^{-4} M_{\rm Pl}$, $g = \sqrt{\lambda} = 4.2$. These values may not be physical (especially for g and λ) but they have been chosen for convenience of display. The grey dotted line represents the value of $N_c^\star$ defined in Eq. (105) (see text).

backreaction starts to become visible, which decreases the actual value of σ_χ (in agreement with what is noticed in Fig. 4 where the point labeled "3" lies below the point labeled "1"). At the critical point itself, one can see that there is no difference due to taking the mass of Ψ into account, since in the quasistationary approximation, the result only depends on the instantaneous value of the mass, which vanishes precisely at the critical point. We will come back to this point in the next subsection.

After the critical point, the calculations performed in the present work may be extrapolated for a few e-folds, and one can see that the inclusion of the mass effects increases the value of σ_χ, which makes sense since the fluctuation modes become tachyonic during the waterfall; hence, the amplitude of the noise increases. However, when looking at the exact solution of Eq. (103), one can see that the actual value of σ_ψ remains smaller. This can be understood as a time delay in the waterfall start. Indeed, when the field system crosses the critical point, two minima in the Ψ direction appear at

$$\Psi_\pm^2 = v^2\left(1 - \frac{\Phi^2}{\Phi_c^2}\right). \tag{104}$$

In between these two minima, the curvature of the potential in the Ψ direction is negative, whereas it is positive elsewhere. This is why when no backreaction is taken into account, the fluctuations $\delta\psi^{(1)}$ become tachyonic as soon as the critical point is crossed. On the other hand, if backreaction is "switched on" and if the fluctuations evolve about a σ_χ-shifted background, the fluctuations keep on "seeing" a potential with positive curvature in the Ψ direction as long as $\sigma_\psi > |\Psi_\pm|$. This means that the waterfall begins at a delayed time $N_c^\star$ instead of N_c, where $N_c^\star$ is defined by

$$\sigma_\chi(N_c^\star) = |\Psi_\pm(N_c^\star)| = v\sqrt{1 - \frac{\Phi^2(N_c^\star)}{\Phi_c^2}}. \tag{105}$$

This "effective" critical time is displayed as the grey dotted line in Fig. 5. One can check that it coincides with the moment when the exact solution of Eq. (103) starts to strongly increase, i.e., with the beginning of the "effective" waterfall phase. One could ask whether such an effect could save the model from the tachyonic breakdown of the perturbative expansion mentioned above. Indeed, if the waterfall start is sufficiently delayed so that it somehow "never" occurs, the effective potential curvature felt by the field system is always positive and no pathological growth of the fluctuations occurs.

This can be rephrased as follows. Once the critical point is crossed, the χ distribution splits into two pieces, each moving towards each minimum of the potential at $\Phi = 0$, $\Psi = \pm v$. This is confirmed e.g., by the numerical simulations of Ref. [48] (see Fig. 10 there). Now, if one extends the quasistationary treatment presented above in the valley and assumes that the inflationary trajectory constantly tracks the local minimum in the χ direction, this implies that each piece of the distribution is centered over one of the two instantaneous minimums $\Psi_\pm(\Phi)$, so that most of the distribution settles over a positive potential curvature region. Obviously, this can occur only if the waterfall is sufficiently slowly driven by φ so that a quasistationary distribution settles in the χ direction. This means that stochastic effects, combined with a long waterfall, may protect the hybrid model from the tachyonic issues mentioned above.

B. Beyond the quasistationary approximation

As already mentioned and as can be seen e.g., in Eq. (12), the number of e-folds realized in the waterfall phase depends on the typical dispersion in the χ direction at the critical point, σ_{χ_c}. In the previous subsection, we made use of a quasistationary approximation where σ_χ only depends on the instantaneous value of the Ψ mass. At the critical point itself, this mass vanishes; hence, no correction coming from the mass and its dynamical variation can be accounted for in this framework, and the obtained result coincides with the massless one (28). To check that this approximation scheme is reliable, and to identify the typical corrections appearing when it is not, the

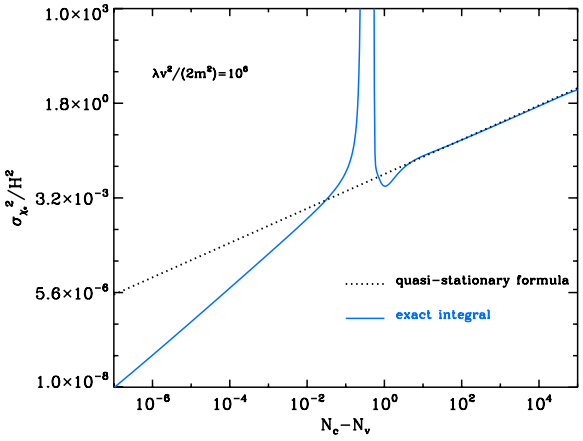

FIG. 6 (color online). Stochastic dispersion in the χ direction σ_χ^2 at the critical point when $\varphi = \Phi_c$, normalized by the Hubble scale H^2, as a function of the number of e-folds spent between N_v and the critical point. The black dotted line corresponds to the massless formula (28), which is the expected result in the quasistationary approximation, where the dispersion in the χ direction only depends on the instantaneous mass of χ, which vanishes at the critical point. The blue solid line corresponds to the exact integral (106). The parameters are chosen as follows. If one defines $\alpha = \lambda v^2/(2m^2)$, the calculation can be shown to depend only on the two parameters α and $v/M_{\rm Pl}$. More precisely, the quantities appearing in Eqs. (28) and (106) are α, $\alpha v^2/M_{\rm Pl}^2$ [which roughly corresponds to the typical number of e-folds one can spend in the valley; see Eq. (10)] and $\alpha v^4/M_{\rm Pl}^4$ [which corresponds to both the squared number of e-folds spent in the waterfall phase—see Eq. (12)—and to the number of e-folds spent between N_v and the critical point—see Eq. (80)]. In the figure, α is fixed to $\alpha = 10^6$ and v is varied below the Planck mass and labeled by $N_c - N_v$. One can check that the qualitative behavior is independent of the chosen value for α.

value of σ_{χ_c} is calculated in this section beyond the quasistationary approximation. Combining Eqs. (18) and (25), one obtains the general formula

$$\sigma_{\chi_c}^2 = \frac{9}{8\pi^2}\frac{H^4}{m^2}e^{\frac{\lambda v^2}{2m^2}} \times \int_1^\infty e^{-\frac{\lambda v^2}{2m^2}(x-\ln x)}(\epsilon a H)^3 \frac{|\delta\psi_{\boldsymbol{k}}^{(1)}|^2_{k=\epsilon a H}}{H^2}\frac{\mathrm{d}x}{x}, \tag{106}$$

where one recalls that the argument of the integral is to be evaluated at $x \equiv \exp[-8M_{\rm Pl}^2 m^2(N - N_c)/(\lambda v^4)]$. Making use of Eqs. (C2)–(C6), this integral can be computed numerically. The result is displayed in Fig. 6, as a function of the number of e-folds spent between N_v and the critical point. It is compared with the quasistationary formula, which coincides with the massless equation (28). The parameters are chosen according to what is explained in the caption of the figure. Three regimes of interest appear, which can easily be understood and described, keeping in mind the evolution of the effective mass m_u of the waterfall perturbations displayed in Fig. 2.

When $N_c - N_v \gg 1$, a large number of e-folds are spent between N_v and the critical point, which means that the effective mass of the waterfall perturbations varies slowly. In this case the quasistationary approximation is valid; the modes contributing the most to $\sigma_{\chi_c}^2$ are the ones that crossed their effective Hubble radius right before the critical point, which is far after N_v. In Fig. 2, one can correspondingly check that the effective mass m_u is well approximated by that of a massless field in this regime, and accordingly in Fig. 6, the quasistationary formula and the exact integral match perfectly. One concludes that the quasistationary approximation holds for parameters such that $N_c - N_v \gg 1$, which is equivalent to requiring a long-lasting waterfall.

When $N_c - N_v \ll 1$, a very small number of e-folds are spent between N_v and the critical point. Remembering that m_u vanishes at N_v, this means that the effective mass of the waterfall perturbations varies very quickly, and one expects the quasistationary approximation to break. More precisely, in this case $\sigma_{\chi_c}^2$ is still dominated by the modes that crossed their effective Hubble radius during, say, the last e-fold before crossing the critical point, but because $N_v \sim N_c$, they did this long before N_v. In this regime the potential curvature in the Ψ direction is not negligible anymore, and one can indeed check in Fig. 2 that the effective mass of the waterfall perturbations becomes much larger than the one for a massless field. The larger the potential curvature, the stronger it "holds" the field at its bottom; hence, we have a decreased dispersion σ_χ. This is exactly what is noticed in Fig. 6, where for $N_c - N_v \ll 1$, the dispersion is much smaller than what is predicted by the quasistationary formula.

Finally, these two cases are connected by the regime $N_c - N_v \sim 1$, where a more singular behavior occurs. In this case, $\sigma_{\chi_c}^2$ is again dominated by the modes that crossed their effective Hubble radius during the last few e-folds before crossing the critical point, that is, exactly around N_v since $N_c - N_v \sim 1$. Remembering that the effective mass of the waterfall perturbations vanishes at N_v, one can check in Fig. 2 that there is a small time interval around N_v during which m_u is suppressed, and it is much smaller than its massless counterpart. During this short period, χ diffuses almost freely, hence the peak noted in Fig. 6. This regime is, however, rather fine-tuned, since there is *a priori* no reason why $N_c - N_v \sim 1$.

In conclusion, the quasistationary approximation which enables us to develop the calculations and the results of the previous subsection holds in the regime of parameters for which a long waterfall occurs (or equivalently $N_c - N_v \gg 1$), and when this is not the case, the actual dispersion in the χ direction is decreased. However, since the number of e-folds spent in the waterfall precisely depends on this typical dispersion at the critical point, one can see that even in this regime, this number of e-folds may not be that small.

V. INFLATON PERTURBATIONS BEYOND ZEROTH ORDER IN SLOW ROLL

Let us now recapitulate our progress so far. The formalism of stochastic inflation has allowed us to split the full quantum system formed by the two scalar fields in quasi-de Sitter space into a quantum bath and a coarse-grained, classical system, and to integrate out the bath to obtain an effective theory for the coarse-grained system. In this effective theory formalism, the quantum effects are modeled through a classical stochastic noise term in the equation of motion for each field, which can be calculated from the propagator of the quantum fields.

Assuming propagators valid up to zeroth order in slow roll, we have obtained a first approximation for the coarse-grained field dynamics, valid to leading order in $\hbar$ and zeroth order in slow roll, in Sec. II. However, many cosmological observables are known to depend primarily on higher-order quantities, for example, the spectral index of curvature perturbations, n_s. To increase the order of precision of our answer, we had to calculate the noise sourcing the Langevin equations to higher order. This is what we did in Sec. III, where we calculated the linearized mode functions for the quantum fields in the presence of a stochastically shifted background, which allowed us to obtain shifted noise amplitudes valid to leading order in slow roll and up to next-to-leading order in $\hbar$. Note that this did not allow us, however, to calculate the corrected classical observables, such as the spectral index, because in the stochastic formalism these are quantities which must be calculated from perturbations of the classical stochastic system, rather than the quantum bath.

We then calculated the classical effects of a shifted noise on the one-point statistics of the coarse-grained waterfall field in Sec. IV, insisting, in particular, on its dispersion as the critical point is approached. Now that we have developed a good understanding of the coarse-grained waterfall field behavior beyond $\mathcal{O}(\varepsilon_1^0, \varepsilon_2^0)$ and leading order in $\hbar$, we can turn to the question of how stochastic effects will affect the details of the statistics of the coarse-grained inflaton field to leading order in slow roll (and to next-to-leading order in $\hbar$). In particular, we are interested in calculating how stochastic effects modify the tilt of the curvature perturbation power spectrum.

First, we need to incorporate the shifted noise from Sec. III in the Langevin equation. This is the noise amplitude we already wrote in Eq. (100) and which we rewrite here for clarity:

$$\langle \xi_\phi(N)\xi_\phi(N')\rangle = \frac{H^4}{4\pi^2}\delta(N-N')\times\left[1+\frac{2}{3}\left(\frac{m^2+g\sigma_\chi^2}{H^2}\right)\times(\ln 2\epsilon+\gamma-2)\right]. \tag{107}$$

Note that, in the following, we will only keep the leading contribution from the second slow-roll parameter ε_2, since we want to capture the leading effect in magnitude and $\varepsilon_2^2 \gg \varepsilon_1$ for the values of the parameters we are considering. Since we are neglecting all powers of ε_2 higher than 1, we have neglected the factor of ε_1 in the derivation presented below.

Next, to address the question of the classical coarse-grained inflaton spectrum, one would technically need to solve the Fokker-Planck equations corresponding to Eqs. (15) and (16) with the noises calculated from the results of Sec. III through Eqs. (17) and (18). However, this turns out to be a rather difficult task analytically, and the result is not readily usable to get concrete observable predictions.

Fortunately, we can perform a simpler calculation which circumvents the difficulties of solving the Fokker-Planck equations. In the previous section, we obtained a solution of Eq. (16) to derive the mean and dispersion of χ, which holds provided that $\langle\varphi\rangle$ remains close to the classical, noiseless solution (we have verified this is indeed the case for the regime of parameters we are considering in the current work, i.e., $\Delta_\phi \ll 1$). We could perform a similar analysis for φ, but this would not be of much help since we are really interested in separating the power in φ coming from the "mean" uniform background *classical* evolution, and the one coming from the fluctuations in φ which give rise to the power spectrum in the CMB.

The strategy we adopt is therefore to expand Eq. (15) as follows[5]:

$$\varphi = \varphi_0 + \delta\varphi^{(1)} + \cdots. \tag{108}$$

Our goal here is to find the average power in the linear inflaton classical fluctuations squared $\langle(\delta\varphi^{(1)})^2\rangle$, analogously to what is done in Ref. [62], and then take its time derivative to recover the k dependence of its power spectrum. Assuming that the noises should be treated perturbatively, we obtain the usual $\frac{\mathrm{d}\varphi_0}{N} = -\frac{-V_\phi}{3H^2}$ for the equation of motion of the classical mean φ_0 field, while for the linear perturbations $\delta\varphi^{(1)}$ we obtain

$$\frac{\mathrm{d}\delta\varphi^{(1)}}{\mathrm{d}N} + 2M_{\mathrm{Pl}}^2\left(\frac{H_{,\Phi}}{H}\right)_{,\Phi}\delta\varphi^{(1)} = \frac{\xi_\phi}{H}, \tag{109}$$

where, as before, ξ_ϕ is the contribution of the stochastic noise in φ. Here, the occurrences of χ in H are the full coarse-grained fields since we are not performing an expansion in the coarse-grained waterfall field, only in the coarse-grained inflaton field. Multiplying this equation by $\delta\varphi^{(1)}$ and taking the average, we obtain

$$\frac{\mathrm{d}\langle(\delta\varphi^{(1)})^2\rangle}{\mathrm{d}N} + 4M_{\mathrm{Pl}}^2\left(\frac{H_{,\Phi}}{H}\right)_{,\Phi}\langle(\delta\varphi^{(1)})^2\rangle = \frac{H^2}{4\pi^2}\left(1+\frac{2}{3}\frac{A}{H^2}\right), \tag{110}$$

[5]Note, however, that even though we are splitting the classical fields into mean classical field and classical perturbations, the mean background felt by the quantum fields is still $\langle\varphi = \varphi_0 + \delta\varphi^{(1)} + \cdots\rangle$, and similarly for higher powers.

where we have defined $A = \tilde{m}^2(\ln 2\epsilon + \gamma - 2)$, with $\tilde{m}^2 = (m^2 + g^2\sigma_\chi^2)$, and where we assumed that $\delta\varphi^{(1)}$ and χ are mutually independent and used $\langle\chi\rangle = 0$, as well as $\langle\chi^2\rangle = \sigma_\chi^2$, which have already been calculated at the required order. We have also used the relation[6] $\langle\xi_\phi\delta\varphi^{(1)}\rangle = H^3(1 + \frac{2}{3}\frac{A}{H^2})/(8\pi^2)$.

Integrating and using the zeroth-order equation to rewrite the solution in terms of an integral over φ, we get the solution

$$\langle(\delta\varphi^{(1)})^2\rangle = \left(\frac{H_{,\Phi}}{H}\right)^2 \frac{1}{8M_{\rm Pl}^2}\int_{\varphi_0}^{\varphi_{0,\rm in}}\left(\frac{H^5}{H_{,\Phi}^3}\right)\left(1 + \frac{2}{3}\frac{A}{H^2}\right)\mathrm{d}\varphi. \tag{111}$$

Using the solutions for φ_0 and H_0, this integral can easily be performed, keeping expressions for H to leading order in m^2. We obtain (by analogy to e.g., Ref. [63])

$$\langle(\delta\varphi^{(1)})^2\rangle \approx \frac{3H^4\varphi_0^2}{8\pi^2\tilde{m}^2}\left[1 - \frac{\varphi_0^2}{(\varphi_0)_{\rm in}^2}\right]\left(1 + \frac{2}{3}\frac{A}{H^2}\right). \tag{112}$$

This result is sensible since at the beginning of inflation, when $\varphi_0^2 = (\varphi_0)_{\rm in}^2$, there is no power in the inflaton fluctuations. As inflation proceeds and the classical background inflaton rolls downs its potential, there is more and more power (qualitatively because modes are joining the coarse-grained field and, in doing so, adding power to the classical fluctuations), and at sufficiently late times, the system approaches a ''quasi-equilibrium'' average power in the fluctuations.[7] If we were to carry through and calculate the tilt induced by this piece of the time dependence of $\langle(\delta\varphi^{(1)})^2\rangle$, we would obtain a contribution to the final tilt which is subdominant.[8] We therefore neglect the time dependence coming from $\varphi_0^2/(\varphi_0)_{\rm in}^2$ in the rest of this calculation.

Comparing with the usual QFT methods, we know that the general formula for massive modes far outside the Hubble radius is given by [70]

$$\phi_k = \frac{1}{a^{3/2}}\left(\frac{\pi\lambda}{4H}\right)^{1/2}\left[\frac{H(t_k)}{H(t)}\right]^2 H_{3/2}^{(1)}\left[\frac{k(1+\varepsilon)}{\epsilon aH}\right], \tag{113}$$

$$\text{with}\quad H(t_k) = H_{\rm in}\sqrt{1 + 2\frac{\dot{H}_{\rm in}}{H_{\rm in}^2}\ln\left[\frac{(1+\varepsilon_{\rm in})k}{H_{\rm in}\nu_{\rm in}}\right]}. \tag{114}$$

Therefore, when one is interested in the average power in the fluctuations, one needs to calculate the following integral:

$$\langle\phi_k^2\rangle^{\rm IR} = \frac{1}{4\pi^2}\left(\frac{H_{\rm in}}{H}\right)^2\frac{H_{\rm in}^2}{(1+\varepsilon)^2}\int_l^{\epsilon aH} D^2(k), \tag{115}$$

where we have defined the function $D(k)$ to have only k/aH and ν dependence and no other time dependence (all the modes' time dependence has been brought to the front of the integral).

Therefore, we find that

$$\int_l^{\epsilon aH}\frac{\mathrm{d}k}{k}k^3|\delta\varphi_k^{(1)}|^2 \tag{116}$$

$$\sim 4\pi^2(1+\epsilon)^2\frac{H^6}{H_{\rm in}^4}\frac{\varphi_0^2}{\tilde{m}^2}\frac{3}{8\pi^2}\left[1 - \frac{\varphi_0^2}{(\varphi_0)_{\rm in}^2}\right]\left(1 + \frac{2}{3}\frac{A}{H^2}\right)$$
$$\approx \frac{3H^4}{2\tilde{m}^2}\left(1 + \frac{2}{3}\frac{A}{H^2}\right)\left[1 - \frac{\varphi_0^2}{(\varphi_0)_{\rm in}^2}\right] \tag{117}$$

where in the last line we have used the fact that at this order in m, H is a constant. From the leading coefficient, we recognize the standard result for the blue-tilted spectrum of a massive field. We therefore obtain

$$\frac{\mathrm{d}k}{k}k^3|\delta\varphi_k^{(1)}|^2 \propto \frac{\mathrm{d}k}{k}\left(\frac{k}{aH}\right)^{\frac{2\tilde{m}^2}{3H^2}\frac{1}{(1+\frac{2}{3}\frac{A}{H^2})}} \tag{118}$$

$$\Rightarrow k^3|\delta\varphi_k^{(1)}|^2 \approx \left(\frac{k}{aH}\right)^{\frac{2\tilde{m}^2}{3H^2} - \frac{4\tilde{m}^2}{9H^2}\left(\frac{\tilde{m}^2}{H^2}\right)(\ln 2\epsilon + \gamma - 2)}. \tag{119}$$

Here, the second term in the exponent is the one coming from the modified amplitude of the noise sourcing the $\delta\varphi^{(1)}$ equation of motion, while the fact that we took the full χ field to source the mass of φ_0 is the reason why $\tilde{m}^2$ appears instead of the usual m^2. Even though, at this order, the conceptually different methods of, on one side, perturbing the classical coarse-grained inflaton to obtain its classical spectrum and, on the other side, reading it off from the spectrum of quantum mode functions directly give the same result, there is no guarantee that this will indeed be the case when one computes higher-order corrections in slow roll. One should therefore be careful when it comes to taking short cuts to obtain observables in stochastic inflation, as this expansion strategy separates the bath and the coarse-grained system into distinct theories sourcing each other.

Note that the shifted noise has a contribution which is higher order in $\tilde{m}^2/H^2$, in such a way that it actually gives rise to a correction which is higher order in $\hbar$. Thus, we cannot retain it while neglecting contributions of similar order coming from different sources. Hence, we find as our final result that the spectral index to leading order in slow roll is

[6]This relation can be obtained by plugging a formal solution of Eq. (110), $\delta\varphi^{(1)} = \int \mathrm{d}N[f/H - 2M_{\rm Pl}^2(H_{,\Phi}/H)_{,\Phi}\delta\varphi^{(1)}]$, into $\langle\xi_\phi\delta\varphi^{(1)}\rangle$, and using Eq. (107) as well as the identity $\int_a^{x_0}\delta(x - x_0)f(x)dx = f(x_0)/2$.

[7]This picture holds given our assumption that H is truly constant. In a more realistic scenario, this is only approximately true but can still provide intuition on what is actually happening.

[8]More specifically, its contribution to the tilt is blue, but initially less by half than the contribution to the tilt we calculate in what follows, and it has a decaying prefactor which becomes negligible as this quasi-equilibrium is approached.

$$n_S = 1 + \frac{2(m^2 + g^2\sigma_\chi^2)}{3H^2} = 1 + \frac{2g^2\sigma_\chi^2}{3H^2} - \varepsilon_2. \quad (120)$$

This result (which is the main result of this section) can be understood as being the standard one, provided that we perform the replacement $m^2 \to \tilde{m}^2$ for the mass of the inflaton, which comes from using the shifted χ rather than the zeroth-order background value $\chi^{(0)} = 0$. The interesting point here is that this modification of the standard spectral index formula shows an example of resummed quantum corrections competing with the usual slow-roll corrections. Indeed, since $g^2\sigma_\chi^2$ can be comparable to m^2, mainly close to the critical point, there is a region of parameter space where stochastic corrections can dominate over slow-roll effects.

Finally, and more importantly, since $\tilde{m}^2 > m^2$, the stochastic dispersion of χ makes the inflaton more massive. Therefore, as suspected by looking at the spectrum of the quantum fluctuations causing the noise, the spectrum becomes bluer due to stochastic effects. Moreover, we obtain that the tilt is modified by an $\mathcal{O}(1)$ factor compared to an estimate based solely on slow-roll parameters. This is one of the main results of the paper.

Note that this effect is, however, not expected to occur in all models of inflation, since it is due to the particular way various mass scales are set in hybrid inflation. In particular, the reason why metric perturbations cannot overcome the tendency of the mass of the inflaton m to make the tilt blue is because the first slow-roll parameter is set by the vacuum energy dominating H, which is independent of the adiabatic direction in the potential. In other words, the ratio m^2/H^2 is proportional to the second slow-roll parameter, rather than the first, as is the case in single-field inflation. As the system approaches the critical point, the waterfall field becomes lighter, and its dispersion approaches that of a light field, i.e., becomes comparable to that of the inflaton, allowing the two corrections to the tilt to be comparable in size if the transition is sufficiently slow.

VI. CONCLUSION

In this paper we have investigated the effects of a recursive stochastic approach to the valley phase of hybrid inflation, making use of the method presented in Ref. [39], where the noise amplitude is calculated from the scalar perturbations evolving about a background continuously shifted by the modes sourcing the coarse-grained fields.

This paper therefore presented an illustration of how to consistently implement this recursive method of stochastic inflation in multifield cases, and applied it to derive interesting novel results. In particular, we provided a concrete example where leading corrections to observables can be dominated by stochastic effects rather than slow-roll parameters. In the valley of the hybrid potential, it was found that this consistent calculation yields a blue-tilt problem which is worse by an $\mathcal{O}(1)$ factor compared with the usual slow-roll contribution. This indicates that if one wishes to modify the valley potential to generate a red tilt, it is crucial to take into account the stochastic contribution to the spectral index.

We also demonstrated how to obtain the correct dispersions at a given order for both the inflaton and the waterfall fields. The latter sets the length of the waterfall, which in turn can potentially determine the viability of the model, and must therefore be computed accurately. Short-lived waterfalls were shown to be unlikely, since the quasistationary time behavior of the auxiliary field distribution breaks down in this regime, reducing its quantum dispersion at the critical point, hence lengthening this final stage. In addition, short-lived waterfalls imply that the long wavelengths of the auxiliary field do not experience quantum squeezing, in which case the usual interpretation of the stochastic formalism is problematic. Furthermore, an analysis of backreaction showed that the recursive process converges in the valley but fails during the waterfall, suggesting the presence of an expected perturbative instability.

Even though, to find a regime where the spectral tilt n_S is compatible with current constraints, a long waterfall phase containing the observational window may seem like an attractive solution, the tachyonic growth of the waterfall field and the exponential growth of entropy scalar perturbations make a traditional perturbative approach unstable and out of control in this final stage. If at all, a solution may be found if the stochastic effects combined with a long and a slow waterfall phase allow for the fields' distribution to continuously settle over the two local Ψ minimums in a quasistationary way. This is why it becomes crucial to be able to consistently compute the physical predictions of such a genuine two-field phase, properly including the stochastic contribution on the background. This shall be the purpose of future work.

ACKNOWLEDGMENTS

The authors would like to thank Giovanni Marozzi for useful discussions. The work of L. P. L. is supported in part by a NSERC PGS-D and by Girton College. The research of R. B. is supported in part by a NSERC Discovery Grant and by funds from the Canada Research Chair program.

APPENDIX A: NOTATIONS AND ASSUMPTIONS ON THE PARAMETERS

In this appendix we summarize the notations used in this paper, as well as the assumptions made on the potential parameters. The potential of hybrid inflation is given by

$$V(\Phi, \Psi) = \frac{1}{2}m^2\Phi^2 + \frac{\lambda}{4}(\Psi^2 - v^2)^2 + \frac{g^2}{2}\Phi^2\Psi^2,$$

where Φ and Ψ are the inflaton and waterfall fields, g and λ are supposedly small coupling constants, m is the mass

of the inflaton, and v is the vev of the waterfall at the global minima of the potential $\Phi = 0$, $\Psi = \pm v$. The critical point is located at $\Phi = \Phi_c \equiv v\sqrt{\lambda}/g$, $\Psi = 0$, and the "valley" corresponds to $\Phi > \Phi_c$, $\Psi \simeq 0$. If the model is derived in the framework of supersymmetry, one has

$$\Phi_c = v \Rightarrow \lambda = g^2. \tag{A1}$$

For inflation to proceed at "small field" values, the parameters Φ_c and v must be small compared to the Planck mass,

$$\Phi_c, \qquad v \ll M_{\rm Pl}. \tag{A2}$$

The vacuum-dominated regime corresponds to vevs of the fields for which the potential is dominated by its constant term $V \simeq \lambda v^4/4$, that is, $\Psi \ll v$, and $\Phi_c < \Phi \ll \lambda v^2/m$. The former is well verified in the valley, even if one starts from sizable values of $\Psi_{\rm in}/v$ (in which case the bottom of the valley is reached very quickly), and even in the presence of stochastic effects, as shown e.g., after Eq. (28), while the latter implies that

$$gv \gg m. \tag{A3}$$

It is also assumed that a slow-roll regime of inflation takes place in the valley. The smallness of the first slow-roll parameter $\varepsilon_1 \ll 1$ implies that

$$\lambda v^4 \gg m^2 \Phi_c M_{\rm Pl}, \tag{A4}$$

while the smallness of the second slow-roll parameter $\varepsilon_2 \ll 1$ implies the more stringent condition

$$\lambda v^4 \gg m^2 M_{\rm Pl}^2. \tag{A5}$$

Finally, to avoid the blue-tilt problem one may wish to realize the last ~ 60 e-folds of inflation in the waterfall stage. From Eq. (12) this is the case only if

$$\sqrt{\lambda} v^3 \gg m M_{\rm Pl}^2. \tag{A6}$$

We now explain the notation employed to refer to different quantities associated with each quantum field. In Eq. (1), the potential was written in terms of the full quantum operator fields Φ and Ψ. Their classical homogeneous background counterparts are denoted by $\varphi^{(0)}$ and $\chi^{(0)}$. Φ and Ψ are Fourier expanded in terms of the classical mode functions $\phi_{\mathbf{k}}$ and $\psi_{\mathbf{k}}$ (and the creation and annihilation operators $\hat{a}_{\mathbf{k}}^\dagger$, $\hat{a}_{\mathbf{k}}$, $\hat{b}_{\mathbf{k}}^\dagger$, $\hat{b}_{\mathbf{k}}$).

One collects the small-wavelength modes of the full quantum fields to define the quantum bath $\phi_>$ and $\psi_>$, with their linearized counterparts denoted by $\delta\phi_>^{(1)}$ and $\delta\psi_>^{(1)}$. The large-wavelength modes collectively form the classical stochastic coarse-grained system fields φ and χ, formally defined by $\varphi = \Phi - \phi_>$ and $\chi = \Psi - \psi_>$. Classical linearized fluctuations around the coarse-grained fields are denoted $\delta\varphi^{(1)}$ and $\delta\chi^{(1)}$.

APPENDIX B: CLASSICAL DYNAMICS OF THE WATERFALL PHASE

Following the terminology used in Ref. [55], this phase can be divided into three consecutive subphases.

"Phase 0" consists in neglecting the last term in the inflaton slow-roll equation (4) and the first one on the right-hand side of the waterfall equation (5) (on the grounds that initially $\varphi = \Phi_c$). The slow-roll solutions read

$$\varphi^{(0)}(N) = \Phi_c \exp\left[-4\frac{M_{\rm Pl}^2 m^2}{\lambda v^4}(N - N_c)\right], \tag{B1}$$

$$\chi^{(0)}(N) = \chi_c\left[1 + \frac{8M_{\rm Pl}^2\chi_c^2}{v^4}(N - N_c)\right]^{-1/2}, \tag{B2}$$

where N_c denotes the number of e-folds at the critical point, i.e., at the onset of the waterfall phase. This phase ends when $\varphi = \varphi_1$ and $\chi = \chi_1$, with

$$\ln\frac{\varphi_1}{\Phi_c} \simeq \frac{m^2}{4\lambda\chi_c^2}\left(1 - \sqrt{1 + \frac{4\lambda\chi_c^4}{m^2 v^2}}\right), \qquad \chi_1 \simeq v\sqrt{-2\ln\frac{\varphi_1}{\Phi_c}}. \tag{B3}$$

If we are in the regime where $4\lambda\chi_c^4/(m^2v^2) \ll 1$, then the number of e-folds realized in this phase is given by

$$N_1 - N_c \simeq \frac{\lambda v^2 \chi_c^2}{8M_{\rm Pl}^2 m^2} \ll 1, \tag{B4}$$

where N_1 denotes the number of e-folds at the end of phase 0. In practice, χ_c/v is so small that $N_1 - N_c$ is always very small. In this case, we conclude that the phase 0 is unimportant since it lasts a negligible number of e-folds and since the values of φ and χ remain almost unchanged during that phase.

We now proceed with phase 1, where the second term on the right-hand side of the waterfall equation (5) can be neglected. During this phase, the solution for the inflaton field is unchanged, but the waterfall field evolution now reads

$$\chi^{(0)} = \chi_1 \exp\left\{\frac{16m^2M_{\rm Pl}^4}{\lambda v^6}[(N - N_c)^2 - (N_1 - N_c)^2]\right\}. \tag{B5}$$

Phase 1 stops when the first term on the right-hand side of the waterfall field equation becomes important, i.e., when $\chi \equiv \chi_2$ and $\varphi \equiv \varphi_2$, where

$$\chi_2^2 = \frac{\Phi_c^2 m^2}{\lambda v^2} = \frac{m^2}{g^2}, \tag{B6}$$

$$\ln^2\frac{\varphi_2}{\Phi_c} \simeq \frac{m^2}{\lambda v^2}\ln\left(\frac{m}{g\chi_c}\right). \tag{B7}$$

Finally, the number of e-folds produced during phase 1 is given by

$$N_2 - N_c \simeq \frac{\lambda^{1/2}v^3}{4mM_{\rm Pl}^2}\ln^{1/2}\left(\frac{m}{g\chi_c}\right). \tag{B8}$$

Therefore, if one were interested in the regime where the required 60 e-folds of inflation take place during the waterfall phase, one needs to work in the $\frac{\lambda v^6}{m^2 M_{\rm Pl}^4} \gg 1$ regime.

Finally, let us now briefly mention phase 2, where one needs to keep the last term in the inflaton equation of motion (4); hence, Eqs. (4) and (5) become fully coupled. The slow-roll trajectory in field space obeys

$$\chi^2 = \chi_2^2 + \varphi^2 - \varphi_2^2 - 2\Phi_c^2 \ln\frac{\varphi}{\varphi_2}. \tag{B9}$$

During phase 2, inflation quickly stops and the system starts oscillating around one of the two true minimums of the potential.

APPENDIX C: FORMULAS FOR $\delta\psi_k^{(1)}$

In this appendix we summarize, for practical convenience, the derived formula for the amplitude of the first-order perturbations in the Ψ direction $\delta\psi_k^{(1)}$. Defining

$$x(N) = \left[\frac{v^2H^2}{8m^2M_{\rm Pl}^2}\right]^{\frac{2}{3}}\left[\frac{8m^2M_{\rm Pl}^2}{v^2H^2}(N-N_c) - 3\frac{\lambda\sigma_\chi^2}{H^2} + 15\varepsilon_1 + \frac{9}{4}\right], \tag{C1}$$

one has

$$\begin{aligned}
&\text{If } k < k_{\rm v} = \frac{Hv}{\sqrt{6}M_{\rm Pl}}\, e^{N_c - \frac{v^2H^2}{4M_{\rm Pl}^2m^2}},\\
&\text{if } N < N_{H_{\rm eff}} \simeq \frac{1}{2}\log\left(\frac{v^2}{M_{\rm Pl}^2}\frac{k^2}{12H^2}\right) - 8\frac{M_{\rm Pl}^2m^2}{\lambda v^4}N_c,\\
&|\delta\psi_k^{(1)}| \approx \frac{e^{-N}}{\sqrt{2k}},
\end{aligned} \tag{C2}$$

$$\begin{aligned}
&\text{if } N_{H_{\rm eff}} < N < N_{\rm v} = N_c - \frac{v^2H^2}{4M_{\rm Pl}^2m^2},\\
&|\delta\psi_k^{(1)}| \approx e^{\frac{1}{2}[N_{H_{\rm eff}} - 3N]}\left|\frac{x(N_{H_{\rm eff}})}{x(N)}\right|^{\frac{1}{4}}\frac{1}{\sqrt{2k}},
\end{aligned} \tag{C3}$$

$$\begin{aligned}
&\text{if } N_{\rm v} < N < N_c,\\
&|\delta\psi_k^{(1)}| \approx e^{\frac{1}{2}(N_{H_{\rm eff}} - 3N)}\left|\frac{x(N_{H_{\rm eff}})}{x(N)}\right|^{\frac{1}{4}}\frac{e^{\frac{2}{3}x(N)^{\frac{3}{2}} - \frac{2}{3}x(N_{\rm v})^{\frac{3}{2}}}}{\sqrt{2k}},
\end{aligned} \tag{C4}$$

$$\begin{aligned}
&\text{If } k_{\rm v} < k < k_c = \sqrt{2}He^{N_c},\\
&\text{if } N < N_{H_{\rm eff}} \simeq \left[\log\left(\frac{k}{\sqrt{2}H}\right) + \frac{24m^2M_{\rm Pl}^4}{\lambda v^6}\frac{k^2}{H^2}N_c\right]\Big/\left(1 - \frac{24m^2M_{\rm Pl}^4}{\lambda v^6}\frac{k^2}{H^2}\right),\\
&|\delta\psi_k^{(1)}| \approx \frac{e^{-N}}{\sqrt{2k}},
\end{aligned} \tag{C5}$$

$$\begin{aligned}
&\text{if } N_{H_{\rm eff}} < N < N_c,\\
&|\delta\psi_k^{(1)}| \approx e^{\frac{1}{2}[N_{H_{\rm eff}} - 3N]}\left|\frac{x(N_{H_{\rm eff}})}{x(N)}\right|^{\frac{1}{4}}e^{\frac{2}{3}[x(N)^{\frac{3}{2}} - x(N_{H_{\rm eff}})^{\frac{3}{2}}]}\frac{1}{\sqrt{2k}}.
\end{aligned} \tag{C6}$$

[1] R. Brout, F. Englert, and E. Gunzig, Ann. Phys. (N.Y.) **115**, 78 (1978).
[2] K. Sato, Mon. Not. R. Astron. Soc. **195**, 467 (1981).
[3] D. Kazanas, Astrophys. J. **241**, L59 (1980).
[4] A. A. Starobinsky, Phys. Lett. **91B**, 99 (1980).
[5] A. H. Guth, Phys. Rev. D **23**, 347 (1981).
[6] A. D. Linde, Phys. Lett. **108B**, 389 (1982).
[7] A. Albrecht and P. J. Steinhardt, Phys. Rev. Lett. **48**, 1220 (1982).
[8] A. D. Linde, Phys. Lett. **129B**, 177 (1983).
[9] V. F. Mukhanov and G. Chibisov, JETP Lett. **33**, 532 (1981).
[10] V. F. Mukhanov and G. Chibisov, Sov. Phys. JETP **56**, 258 (1982).
[11] S. Hawking, Phys. Lett. **115B**, 295 (1982), revised version.
[12] A. A. Starobinsky, Phys. Lett. **117B**, 175 (1982).
[13] A. H. Guth and S. Y. Pi, Phys. Rev. Lett. **49**, 1110 (1982).
[14] J. M. Bardeen, P. J. Steinhardt, and M. S. Turner, Phys. Rev. D **28**, 679 (1983).
[15] Z. Hou, C. Reichardt, K. Story, B. Follin, R. Keisler *et al.*, arXiv:1212.6267.
[16] J. L. Sievers, R. A. Hlozek, M. R. Nolta, V. Acquaviva, and G. E. Addison, arXiv:1301.0824.
[17] P. Ade *et al.* (Planck Collaboration), arXiv:1303.5082.
[18] J. Martin, C. Ringeval, and V. Vennin, arXiv:1303.3787.
[19] N. Tsamis and R. Woodard, Phys. Lett. B **301**, 351 (1993).
[20] N. Tsamis and R. Woodard, Ann. Phys. (N.Y.) **238**, 1 (1995).
[21] V. F. Mukhanov, L. R. W. Abramo, and R. H. Brandenberger, Phys. Rev. Lett. **78**, 1624 (1997).

[22] L. R. W. Abramo, R. H. Brandenberger, and V. F. Mukhanov, Phys. Rev. D **56**, 3248 (1997).
[23] R. H. Brandenberger, arXiv:hep-th/0210165.
[24] A. Vilenkin, Nucl. Phys. **B226**, 527 (1983).
[25] A. A. Starobinsky, Lect. Notes Phys. **246**, 107 (1986).
[26] A. Goncharov, A. D. Linde, and V. F. Mukhanov, Int. J. Mod. Phys. A **02**, 561 (1987).
[27] Y. Nambu and M. Sasaki, Phys. Lett. B **205**, 441 (1988).
[28] Y. Nambu and M. Sasaki, Phys. Lett. B **219**, 240 (1989).
[29] H. E. Kandrup, Phys. Rev. D **39**, 2245 (1989).
[30] K.-i. Nakao, Y. Nambu, and M. Sasaki, Prog. Theor. Phys. **80**, 1041 (1988).
[31] Y. Nambu, Prog. Theor. Phys. **81**, 1037 (1989).
[32] S. Mollerach, S. Matarrese, A. Ortolan, and F. Lucchin, Phys. Rev. D **44**, 1670 (1991).
[33] A. D. Linde, D. A. Linde, and A. Mezhlumian, Phys. Rev. D **49**, 1783 (1994).
[34] A. A. Starobinsky and J. Yokoyama, Phys. Rev. D **50**, 6357 (1994).
[35] L. V. Keldysh, Zh. Eksp. Teor. Fiz. **47**, 1515 (1964) [Sov. Phys. JETP **20**, 1018 (1965)].
[36] J. S. Schwinger, J. Math. Phys. (N.Y.) **2**, 407 (1961).
[37] R. Jordan, Phys. Rev. D **33**, 444 (1986).
[38] E. Calzetta and B. Hu, Phys. Rev. D **35**, 495 (1987).
[39] L. P. Levasseur, preceding article, Phys. Rev. D **88**, 083537 (2013).
[40] A. D. Linde, Phys. Rev. D **49**, 748 (1994).
[41] E. J. Copeland, A. R. Liddle, D. H. Lyth, E. D. Stewart, and D. Wands, Phys. Rev. D **49**, 6410 (1994).
[42] E. Halyo, Phys. Lett. B **387**, 43 (1996).
[43] P. Binetruy and G. Dvali, Phys. Lett. B **388**, 241 (1996).
[44] G. Dvali, Q. Shafi, and R. K. Schaefer, Phys. Rev. Lett. **73**, 1886 (1994).
[45] R. Kallosh and A. D. Linde, J. Cosmol. Astropart. Phys. 10 (2003) 008.
[46] S. Clesse and J. Rocher, Phys. Rev. D **79**, 103507 (2009).
[47] A. A. Abolhasani, H. Firouzjahi, and M. H. Namjoo, Classical Quantum Gravity **28**, 075009 (2011).
[48] J. Martin and V. Vennin, Phys. Rev. D **85**, 043525 (2012).
[49] L. Levasseur Perreault, G. Laporte, and R. Brandenberger, Phys. Rev. D **82**, 123524 (2010).
[50] D. H. Lyth and A. Riotto, Phys. Rep. **314**, 1 (1999).
[51] S. Clesse, Phys. Rev. D **83**, 063518 (2011).
[52] D. H. Lyth, arXiv:hep-ph/9609431.
[53] D. H. Lyth and E. D. Stewart, Phys. Rev. D **54**, 7186 (1996).
[54] S. King and J. Sanderson, Phys. Lett. B **412**, 19 (1997).
[55] H. Kodama, K. Kohri, and K. Nakayama, Prog. Theor. Phys. **126**, 331 (2011).
[56] J. Garcia-Bellido and A. D. Linde, Phys. Rev. D **57**, 6075 (1998).
[57] J. Garcia-Bellido, arXiv:hep-ph/9804205.
[58] E. J. Copeland, S. Pascoli, and A. Rajantie, Phys. Rev. D **65**, 103517 (2002).
[59] F. Finelli and R. H. Brandenberger, Phys. Rev. D **62**, 083502 (2000).
[60] C. Kiefer, D. Polarski, and A. A. Starobinsky, Int. J. Mod. Phys. D **07**, 455 (1998).
[61] D. Polarski and A. A. Starobinsky, Classical Quantum Gravity **13**, 377 (1996).
[62] F. Finelli, G. Marozzi, A. A. Starobinsky, G. P. Vacca, and G. Venturi, Phys. Rev. D **79**, 044007 (2009).
[63] F. Finelli, G. Marozzi, A. A. Starobinsky, G. P. Vacca, and G. Venturi, Phys. Rev. D **82**, 064020 (2010).
[64] S. Winitzki and A. Vilenkin, Phys. Rev. D **61**, 084008 (2000).
[65] H. Casini, R. Montemayor, and P. Sisterna, Phys. Rev. D **59**, 063512 (1999).
[66] V. F. Mukhanov, H. Feldman, and R. H. Brandenberger, Phys. Rep. **215**, 203 (1992).
[67] R. H. Brandenberger, Lect. Notes Phys. **646**, 127 (2004).
[68] K. A. Malik and D. Wands, Phys. Rep. **475**, 1 (2009).
[69] D. Baumann, arXiv:0907.5424.
[70] F. Finelli, G. Marozzi, G. Vacca, and G. Venturi, Phys. Rev. D **69**, 123508 (2004).
[71] C. Gordon, D. Wands, B. A. Bassett, and R. Maartens, Phys. Rev. D **63**, 023506 (2000).
[72] A. H. Guth and S.-Y. Pi, Phys. Rev. D **32**, 1899 (1985).
[73] M. Mijic, Int. J. Mod. Phys. D **06**, 505 (1997).

PHYSICAL REVIEW D **86,** 103524 (2012)

Cosmological inflation and the quantum measurement problem

Jérôme Martin,* Vincent Vennin,† and Patrick Peter‡

Institut d'Astrophysique de Paris, UMR 7095-CNRS, Université Pierre et Marie Curie, 98 bis boulevard Arago, 75014 Paris, France

(Received 17 July 2012; published 26 November 2012)

According to cosmological inflation, the inhomogeneities in our Universe are of quantum-mechanical origin. This scenario is phenomenologically very appealing as it solves the puzzles of the standard hot big bang model and naturally explains why the spectrum of cosmological perturbations is almost scale invariant. It is also an ideal playground to discuss deep questions among which is the quantum measurement problem in a cosmological context. Although the large squeezing of the quantum state of the perturbations and the phenomenon of decoherence explain many aspects of the quantum-to-classical transition, it remains to understand how a specific outcome can be produced in the early Universe, in the absence of any observer. The continuous spontaneous localization (CSL) approach to quantum mechanics attempts to solve the quantum measurement question in a general context. In this framework, the wave function collapse is caused by adding new nonlinear and stochastic terms to the Schrödinger equation. In this paper, we apply this theory to inflation, which amounts to solving the CSL parametric oscillator case. We choose the wave function collapse to occur on an eigenstate of the Mukhanov-Sasaki variable and discuss the corresponding modified Schrödinger equation. Then, we compute the power spectrum of the perturbations and show that it acquires a universal shape with two branches, one which remains scale invariant and one with $n_S = 4$, a spectral index in obvious contradiction with the cosmic microwave background anisotropy observations. The requirement that the non-scale-invariant part be outside the observational window puts stringent constraints on the parameter controlling the deviations from ordinary quantum mechanics. Due to the absence of a CSL amplification mechanism in field theory, this also has the consequence that the collapse mechanism of the inflationary fluctuations is not efficient. Then, we determine the collapse time. On small scales the collapse is almost instantaneous, and we recover exactly the behavior of the CSL harmonic oscillator (a case for which we present new results), whereas, on large scales, we find that the collapse is delayed and can take several e-folds to happen. We conclude that recovering the observational successes of inflation and, at the same time, reaching a satisfactory resolution of the inflationary ''macro-objectification'' issue seems problematic in the framework considered here. This work also provides a complete solution to the CSL parametric oscillator system, a topic we suggest could play a very important role to further constrain the CSL parameters. Our results illustrate the remarkable power of inflation and cosmology to constrain new physics.

DOI: 10.1103/PhysRevD.86.103524 PACS numbers: 98.80.Cq, 98.80.Qc, 03.65.Ta, 03.65.Yz

I. INTRODUCTION

Inflation is currently the leading paradigm for explaining the physical conditions that prevailed in the very early Universe [1–5]. It solves the puzzles of the standard hot big bang phase and it explains the origin of the inhomogeneities in our Universe [6–11] (for reviews, see Refs. [12–18]). According to the inflationary scenario, these inhomogeneities result from the amplification of the unavoidable vacuum quantum fluctuations of the gravitational and inflaton fields during a phase of accelerated expansion. In particular, inflation predicts an almost scale invariant power spectrum for the cosmological fluctuations [19], a prediction which fits very well the high accuracy astrophysical data now at our disposal [20–26].

Often less emphasized is the fact that inflation is also particularly remarkable from the theoretical point of view. Indeed, the inflationary mechanism for the production of cosmological perturbations makes use of general relativity and quantum mechanics, two theories that are notoriously difficult to combine. Moreover, this mechanism leads to theoretical predictions that are possible to study observationally with great accuracy. In fact, inflation is probably the only case in physics where an effect based on general relativity and quantum mechanics leads to predictions that, given our present day technological capabilities, can be tested experimentally.

The situation described above can be used to investigate deep questions. Among these deep questions is how the quantum measurement problem looks in a cosmological context. According to inflation, the cosmic microwave background (CMB) radiation anisotropy [27] is an observable and is therefore described by a quantum operator. As a consequence, when one looks at a CMB map, one observes

*jmartin@iap.fr
†vennin@iap.fr
‡peter@iap.fr

the result of a measurement of that observable. According to the postulates of quantum mechanics in the Copenhagen interpretation, this means that the wave function of the inflationary perturbations has collapsed to an eigenvector of this operator and that the CMB map corresponds to one of its eigenvalues. The problem with this approach is that the collapse is supposed to occur only when an observer performs a measurement on the system. Clearly, there was no observer before or when the CMB was emitted. This seems to contradict the phenomenological fact that large-scale structure formation started early in the history of the Universe since these structures are seeded by the same early physics which led to CMB fluctuations. As a matter of fact, CMB fluctuations can also be understood as the earliest hint that primordial inhomogeneities had already started to grow at that time. Furthermore, in some sense, the observers are actually the end product of the structure formation process. Of course, this measurement problem is already present in conventional laboratory situations but it seems to be exacerbated (to use the words of Ref. [28]) in a cosmological context.

Important steps towards a better understanding of these issues have already been accomplished. In particular, it was shown that the inflationary accelerated expansion transforms a coherent vacuum state into a strongly squeezed state [29], the corresponding squeezing being much more important than whatever can be realized in the laboratory [30]. In this limit, the predictions of the quantum formalism are indistinguishable from that of a theory where the fluctuations are just assumed to be realizations of a classical stochastic process [31–33]. The classical limit is a subtle concept in quantum mechanics but, in this sense (and in this sense only), the system can be characterized as being classical [34]. Moreover, the large-scale cosmological perturbations are not isolated and, as a consequence, the phenomenon of decoherence [35–37] is relevant for them. This has the consequence that their density matrix becomes diagonal before recombination, a criterion which is also considered as necessary in order to understand the quantum-to-classical transition [31,32,38–43]. However, it is known that decoherence *per se* does not solve the measurement problem [44,45]. Indeed, it remains to understand how a single outcome can be produced. This point is particularly important given that we only have one CMB map, that is to say only one measurement of the corresponding observable. In other words, even if the cosmological fluctuations can be viewed as a classical stochastic problem, this does not explain how a given realization of this process becomes an actual perception. This ''macro-objectivation'' problem is already present in a conventional situation but, as already mentioned before, it becomes particularly embarrassing in the context of inflation where the collapse of the wave function cannot be due to the presence of a conscious observer. Facing this situation, the common attitude is to postulate that decoherence should be combined with a new interpretational scheme, different from the Copenhagen interpretation [46,47]. Typically, in cosmology, the many world approach is often implicitly assumed [34,46–50]. Another frequently mentioned possibility, which seems to be particularly well suited to the cosmological context, is to consider that the wave function only represents the information that we have on the system [51]. In this case, the issue of the wave function collapse becomes irrelevant since it just corresponds to a situation where the observer updates their knowledge (in the Bayesian sense) about the physical properties of the system. Other attempts, such as the nonlocal hidden variable theories, have also been tried [52–57]. In all of these cases, the cosmological situation does not differ much from a conventional laboratory situation and, moreover, does not lead to new, falsifiable, predictions.[1] Then, it becomes a question of taste which approach best fits one's own prejudices.

However, there exists an exception to the conclusion of the previous discussion, namely the case of the collapse models [61–66] (for reviews, see Refs. [67,68]). In this approach, the Schrödinger equation is modified by adding nonlinear and stochastic terms which render dynamical the collapse of the wave function. The model has nice features: first, the approach seems to follow a conservative strategy since, in physics, it is standard to first consider a linear theory and then, in order to have a more accurate description, to consider nonlinear corrections; in some sense, the collapse theories follow this line of argument. Second, there is now a single law of evolution for the state vector and, third, the Born laws can be derived instead of postulated. There are also disadvantages such as the property that energy is not conserved or the fact that the relativistic formulation of the theory appears to be technically and conceptually difficult to develop (however, see Ref. [69]). But, clearly, the main advantage in comparison to the possibilities discussed above is that this approach is falsifiable since it leads to predictions different from that of conventional quantum mechanics. This fact has been widely used in order to constrain collapse theories in the laboratory [68,70–73] but, clearly, it is also important to see whether this could be done in a cosmological context [74–76]. It is therefore interesting to investigate what the collapse theories have to say about the inflationary mechanism. Notice that, regardless of one's opinion about collapse theories, the subject is worth studying: a supporter would argue that the cosmological measurement problem can possibly find a natural solution within this theory and an opponent would hope that the constraints obtained in a cosmological context can rule out the theory. In fact, this last question turns out to be very important. Indeed, as

[1]In the case of the Bohm-de Broglie approach, there could be a transitory regime, before ''quantum equilibrium'' is reached, where the predictions differ from conventional quantum mechanics [58]. Cosmology is also precisely considered as a situation where this regime could be relevant [59,60].

already mentioned, the constraints that exist on collapse theories are usually obtained from physical phenomena that can be observed in the laboratory. Therefore, by studying collapse theories in the context of cosmology and inflation, one can hope to derive very relevant new constraints since one now deals with characteristic scales (energy, length, etc.) which typically differ by many orders of magnitude from those used in a down-to-earth context. This illustrates again the conceptual relevance of inflation when it comes to very fundamental questions and its power to constrain alternatives to gravity but also to quantum mechanics. In some sense, inflation represents an ideal playground to test new theories. Notice in passing that the very same strategy was used in the case of the so-called trans-Planckian problem of inflation [77–79] where it was shown that the inflationary observables could possibly contain an imprint (although probably small) of string theory.

We are using a (modified) Schrödinger-type of equation to describe the behavior of cosmological perturbations. This is justified because each Fourier mode of those effectively evolves in an independent way and cosmological expansion permits one to define a privileged time. This allows for a sensible treatment of cosmological perturbations even though a fully relativistic continuous spontaneous localization (CSL) model, which could be naively expected to be required, is still lacking. At this moment, surprisingly, it is easier to treat inflationary perturbations than ordinary particle physics.

It should also be emphasized that the idea of applying collapse theories to inflationary perturbations of quantum-mechanical origin was first considered in Refs. [80–82]. In these articles, a phenomenological model for the collapse process was assumed and the corresponding physical properties were derived. In particular, the power spectrum of the perturbations was calculated and was shown to deviate from the standard predictions. Therefore, Refs. [80–82] have demonstrated that, in principle, it is possible to observationally test collapse theories in a cosmological context. Our approach differs from that of Refs. [80–82] in the fact that we use the CSL model to implement the collapse dynamics. This has the advantage that our calculations can be directly confronted and compared to other results obtained in other branches of physics.

This paper is organized as follows. In the next section, Sec. II, we present a brief review of the theory of inflationary cosmological perturbations of quantum-mechanical origin. We especially focus on the calculation of the power spectrum since this quantity is the tool that allows us to relate the inflationary theory with the CMB observations. Then, in Sec. III, we discuss the cosmological measurement problem and we explain how high accuracy CMB measurements can constrain inflation. In Sec. IV, we consider collapse theories, in particular, its CSL version, which is, as already mentioned, the case we use in this article. These sections aim at rendering the present work self-contained for readers with different expertise. Then, we show how the harmonic oscillator can be treated in this context. This case is particularly relevant for cosmological fluctuations since it corresponds to the small-scale limit (in comparison to the Hubble radius) of the theory of cosmological perturbations. In Sec. V, we apply the CSL theory to inflation and to the calculation of the power spectrum. We use this result to constrain the parameter that controls the deviations from ordinary quantum mechanics. In Sec. VI, we study in more details the collapse phenomenon and explicitly compute the collapse time on small and large scales. In Sec. VII, we summarize our results and present our conclusions. We end the paper with an Appendix where it is shown that changing the "temporal gauge" in which the modified Schrödinger equation is written does not affect the shape of the power spectrum. This calculation reinforces the generic character of the results obtained in this work.

II. INFLATIONARY COSMOLOGICAL PERTURBATIONS

A. Basic formalism

By definition, inflation is a phase of accelerated expansion that took place in the very early Universe, prior to the standard hot big bang phase [1–5] (for reviews, see Refs. [13–15]). As is well known, postulating such a phase of evolution allows us to solve the standard problems of the hot big bang model. Given that at very high energies, field theory is the relevant framework to describe matter, a natural way to realize inflation is to consider that a real scalar field (the "inflaton" field) dominated the energy density budget of matter in the early Universe. Moreover, this assumption is compatible with the observed homogeneity, isotropy and flatness of the early Universe. Technically, the above-mentioned situation can be described by the metric tensor $\mathrm{d}s^2 = -\mathrm{d}t^2 + a^2(t)\delta_{ij}\mathrm{d}x^i\mathrm{d}x^j$, where $a(t)$ is the Friedman-Lemaître-Robertson-Walker (FLRW) scale factor and t the cosmic time.[2] The Einstein equations imply that $\ddot{a}/a = -(\rho + 3p)/(6M_{\mathrm{Pl}}^2)$, ρ and p being the energy density and pressure of the matter sourcing the gravitational field and M_{Pl} the Planck mass (a dot denotes a derivative with respect to the cosmic time t). For a scalar field, this reduces to $\ddot{a}/a = V(\varphi) \times (1 - \dot{\varphi}^2/V)/(3M_{\mathrm{Pl}}^2)$, where $V(\varphi)$ is the scalar field potential. This means that inflation (i.e., $\ddot{a} > 0$) can be obtained provided the inflaton slowly rolls down its potential so that its potential energy dominates over its kinetic energy. This also shows that the inflaton potential must be sufficiently flat, a requirement which is not always easy to obtain in

[2]Unless explicit mention of the contrary, we shall in what follows assume natural units in which $\hbar = c = 1$ so that the Newton constant G_{N} is related with the Planck mass M_{Pl} through $8\pi G_{\mathrm{N}} = M_{\mathrm{Pl}}^{-2}$.

realistic situations and makes the inflationary model building problem a difficult issue [83]. The physical nature of the inflaton field has not been identified (there are many candidates) and, as a consequence, the shape of $V(\varphi)$ is not known. Of course, different $V(\varphi)$ lead to different inflationary expansions but, since these different potentials must all be sufficiently flat, the corresponding scale factors are all approximately given by the de Sitter solution. This solution is described by the scale factor $a(t) \simeq \mathrm{e}^{Ht}$, where $H \equiv \dot{a}/a$ is the Hubble parameter, a slowly-varying quantity directly related to the energy scale of inflation. Observationally, this last quantity is not known but is constrained [22] to be between the grand unified theory (GUT) scale, that is to say $\sim 10^{15}$ GeV, and ~ 1 TeV. The previous considerations show that inflation can also be viewed as a phase of quasiexponential expansion.

A concrete illustration of the above discussion consists in considering power-law inflation [84]. Although it is based on a specific model with potential $V(\varphi) = M^4 \mathrm{e}^{-\alpha\varphi/M_{\mathrm{Pl}}}$ (with α constant), it captures, in a simple way, all the essential properties of inflation and, moreover, is the only scenario which permits an exact integration of the equations of motion (at the background level but also at the perturbative level, see below). The corresponding scale factor is given by

$$a(\eta) = \ell_0(-\eta)^{1+\beta}, \tag{1}$$

where ℓ_0 is a length the value of which is fixed once the energy scale of inflation is known and η in the conformal time defined by $\mathrm{d}t = a\mathrm{d}\eta$, see Eq. (2). The quantity β is a free parameter such that $\beta \leq -2$ and is related to α through $\alpha^2/2 = (\beta + 2)/(\beta + 1)$. The case $\beta = -2$ represents the de Sitter solution since it implies $\alpha = 0$, i.e., a flat potential (and, of course, in cosmic time, the solution $a \propto 1/\eta$ is given by an exponential). Therefore, different β represents different inflationary solutions and β must always be close to -2 in order for the potential to be sufficiently flat. As announced, power-law inflation illustrates well the discussion of the previous paragraph.

The above arguments can be considered as strong hints in favor of inflation. However, soon after its advent, it was realized that inflation, combined with quantum mechanics, leads to an even more impressive result, namely it naturally explains the origin of the CMB anisotropies and of the large-scale structures. According to the inflationary paradigm, these deviations from homogeneity and isotropy originate from the unavoidable zero-point quantum fluctuations of the coupled inflaton and gravitational fields. Statistically, the fluctuations are characterized by their two-point correlation function or power spectrum. The observations [20–26] indicate that the corresponding power spectrum is close to the Harrison-Zel'dovich, scale invariant, power spectrum with equal power on all scales. That this power spectrum represents a good fit to the astrophysical data was in fact realized before the advent of inflation but no convincing fundamental theory was known to explain this result.

The main success of inflation is that it precisely predicts an almost scale invariant power spectrum, the small deviations from scale invariance being connected with the microphysics of inflation [6–11]. The fact that different types of inflationary scenarios lead to a power spectrum which is, at leading order, always close to scale invariance is connected with the fact that the inflationary scale factor is always close to the de Sitter solution (see above) or, equivalently, with the fact that the inflaton potential is always almost flat. The deviations from scale invariance are related to the deviations from a flat potential and, therefore, depend on the detailed shape of the potential. As a consequence, measuring them allows us to say something about $V(\varphi)$ and there is currently an important effort in this direction using the high accuracy CMB data that have been released in the past years.

Let us now see how the results reviewed before can be derived. Clearly, in order to model the cosmological fluctuations, one needs to go beyond homogeneity and isotropy. The most general metric describing small fluctuations of the scalar type on top of a FLRW Universe can be written as [12]

$$\begin{aligned} \mathrm{d}s^2 = a^2(\eta)\{&-(1-2\phi)\mathrm{d}\eta^2 + 2(\partial_i B)\mathrm{d}x^i\mathrm{d}\eta \\ &+ [(1-2\psi)\delta_{ij} + 2\partial_i\partial_j E]\mathrm{d}x^i\mathrm{d}x^j\}. \end{aligned} \tag{2}$$

A similar approach could be used to take into account tensor perturbations (i.e., gravity waves). Here, we do not include them since they are subdominant in the CMB, representing less than $\sim 20\%$ at 2σ confidence level [22] and, in addition, doing it would not bring any new aspects to the question we want to investigate in this article. In Eq. (2), the four functions ϕ, B, ψ and E are of course functions of time and space since we consider an inhomogeneous and anisotropic situation. As is well known, the above approach is redundant because of gauge freedom [12,85,86]. A careful study of this question shows that the gravitational sector can in fact be described by a single, gauge-invariant, quantity, the Bardeen potential Φ_{B} defined by [85]

$$\Phi_{\mathrm{B}}(\eta, \boldsymbol{x}) = \phi + \frac{1}{a}[a(B - E')]', \tag{3}$$

where a prime denotes a derivative with respect to the conformal time η. In the same manner, the matter sector can be modeled by the gauge invariant fluctuation of the scalar field

$$\delta\varphi^{(\mathrm{gi})}(\eta, \boldsymbol{x}) = \delta\varphi + \varphi'(B - E'). \tag{4}$$

The two quantities Φ_{B} and $\delta\varphi^{(\mathrm{gi})}$ are related by a perturbed Einstein constraint. This implies that the scalar sector can in fact be described by a single quantity. For this reason, we now introduce the so-called Mukhanov-Sasaki variable [6,87] which is a combination of the Bardeen potential and of the gauge invariant field

$$v(\eta, \boldsymbol{x}) = a\left[\delta\varphi^{(\mathrm{gi})} + \varphi'\frac{\Phi_{\mathrm{B}}}{\mathcal{H}}\right], \tag{5}$$

where $\mathcal{H} \equiv a'/a$. All the other relevant quantities can be expressed in terms of $v(\eta, \boldsymbol{x})$ which, therefore, fully characterizes the scalar sector.

The next step consists in deriving an equation of motion for $v(\eta, \boldsymbol{x})$. This can be done directly from the perturbed Einstein equations but, here, we first establish the action for the quantity $v(\eta, \boldsymbol{x})$. Expanding the action of the system (i.e., Einstein-Hilbert action plus the action of a scalar field) up to second order in the perturbations, one obtains [12]

$$^{(2)}\delta S = \frac{1}{2}\int \mathrm{d}^4x\left[(v')^2 - \delta^{ij}\partial_i v\partial_j v + \frac{(a\sqrt{\epsilon_1})''}{a\sqrt{\epsilon_1}}v^2\right], \tag{6}$$

where $\epsilon_1 = 1 - \mathcal{H}'/\mathcal{H}^2$ is the first slow-roll parameter [88,89]. As the formula $\ddot{a}/a = H^2(1-\epsilon_1)$ shows, the condition $\epsilon_1 < 1$ is in fact sufficient to have inflation. Moreover, we have slow-roll inflation [19,88–91] if $\epsilon_1 \ll 1$. In this case, it is easy to show that $\epsilon_1 \simeq (M_{\mathrm{Pl}}^2/2V^2)(\mathrm{d}V/\mathrm{d}\varphi)^2$, i.e., ϵ_1 is in fact a measure of how much the inflaton potential deviates from a flat potential. Equivalently, according to the previous considerations, this is also a measure of how much the inflationary expansion deviates from a pure de Sitter solution. In the case of power-law inflation, one has $\epsilon_1 = (2+\beta)/(1+\beta)$ and, of course, $\epsilon_1 = 0$ when $\beta = -2$ (de Sitter solution). The scale factor can also be rewritten as $a(\eta) \simeq \ell_0(-\eta)^{-1-\epsilon_1}$ and this formula is in fact valid for any slow-roll model of inflation, i.e., for arbitrary shaped potentials, not necessarily of the exponential type. In this sense, power-law inflation with $\beta \lesssim -2$ is a simple representative of all the slow-roll scenarios. Therefore, the fact that, in this paper, we focus on this particular model for technical reasons (again, because this model allows an easy integration of the equations of motion at the background and perturbative level) does not restrict in any way the generality of our considerations.

Our next move consists in Fourier transforming the quantity $v(\eta, \boldsymbol{x})$. This is of course justified by the fact that we work with a linear theory and, hence, all the modes evolve independently. We have

$$v(\eta, \boldsymbol{x}) = \frac{1}{(2\pi)^{3/2}}\int_{\mathbb{R}^3}\mathrm{d}^3\boldsymbol{k}\, v_{\boldsymbol{k}}(\eta)\mathrm{e}^{i\boldsymbol{k}\cdot\boldsymbol{x}}, \tag{7}$$

with $v_{-\boldsymbol{k}} = v_{\boldsymbol{k}}^*$ because $v(\eta, \boldsymbol{x})$ is real. Then inserting this expansion into Eq. (6), one arrives at [12]

$$^{(2)}\delta S = \int \mathrm{d}\eta \int \mathrm{d}^3\boldsymbol{k}\left\{v_{\boldsymbol{k}}' v_{\boldsymbol{k}}^{*\prime} + v_{\boldsymbol{k}} v_{\boldsymbol{k}}^*\left[\frac{(a\sqrt{\epsilon_1})''}{a\sqrt{\epsilon_1}} - k^2\right]\right\}, \tag{8}$$

where the integral over $\boldsymbol{k}$ is taken over half the Fourier space only. Next, we define $p_{\boldsymbol{k}}$, the variable canonically conjugate to $v_{\boldsymbol{k}}$

$$p_{\boldsymbol{k}} = \frac{\delta\mathcal{L}}{\delta v_{\boldsymbol{k}}^{*\prime}} = v_{\boldsymbol{k}}', \tag{9}$$

where $\mathcal{L}$ is the Lagrangian density in Fourier space that can be derived from Eq. (8). This allows us to calculate the Hamiltonian which reads

$$H = \int \mathrm{d}^3\boldsymbol{k}\left\{p_{\boldsymbol{k}}p_{\boldsymbol{k}}^* + v_{\boldsymbol{k}}v_{\boldsymbol{k}}^*\left[k^2 - \frac{(a\sqrt{\epsilon_1})''}{a\sqrt{\epsilon_1}}\right]\right\}. \tag{10}$$

This Hamiltonian represents a collection of parametric oscillators (i.e., one oscillator per mode), the time-dependent frequency of which can be expressed as

$$\omega^2(\eta, \boldsymbol{k}) = k^2 - \frac{(a\sqrt{\epsilon_1})''}{a\sqrt{\epsilon_1}}. \tag{11}$$

We see that the frequency depends on the scale factors and its derivatives (up to the fourth). This means that different inflationary backgrounds (i.e., different inflaton potentials) lead to different $\omega(\eta, \boldsymbol{k})$ and, therefore, to different behaviors for $v_{\boldsymbol{k}}(\eta)$. From Eq. (10) or Eq. (8), it is easy to derive the equation of motion for the Mukhanov-Sasaki variable. One obtains

$$v_{\boldsymbol{k}}'' + \omega^2(\eta, \boldsymbol{k})v_{\boldsymbol{k}} = 0, \tag{12}$$

which confirms that each mode behaves as a parametric oscillator. Once a model of inflation has been chosen, the potential $V(\varphi)$ is known and, hence, the corresponding scale factor can be calculated. This, in turn, allows us to determine $\omega^2(\eta, \boldsymbol{k})$ and, then, one can solve the equation of motion (12). However, in order to find the solution for the Fourier component of the Mukhanov-Sasaki variable, one also needs to specify the initial conditions. Classically, there does not seem to exist a natural criterion to choose them. However, when quantization has been performed, the requirement that it be initially in the vacuum state of the theory leads to well-defined initial conditions. We now turn to these questions.

B. Quantization in the Schrödinger picture

In this section, we review how the cosmological perturbations are quantized. Very often in the literature, this is done in the Heisenberg picture. Here, we carry out the quantization in the Schrödinger picture [15] because this is more convenient for the problem we want to investigate in this article. In order to quantize the system, it is also more convenient to work with real variables. Therefore, we introduce the following definitions:

$$v_{\boldsymbol{k}} \equiv \frac{1}{\sqrt{2}}(v_{\boldsymbol{k}}^{\mathrm{R}} + iv_{\boldsymbol{k}}^{\mathrm{I}}), \qquad p_{\boldsymbol{k}} \equiv \frac{1}{\sqrt{2}}(p_{\boldsymbol{k}}^{\mathrm{R}} + ip_{\boldsymbol{k}}^{\mathrm{I}}). \tag{13}$$

In the Schrödinger approach, the quantum state of the system is described by a wave functional, $\Psi[v(\eta, \boldsymbol{x})]$. Since we work in Fourier space (and since the theory is still free in the sense that it does not contain terms with power higher than 2 in the Lagrangian), the wave functional can also be factorized into mode components as

$$\Psi[v(\eta,\boldsymbol{x})] = \prod_{\boldsymbol{k}} \Psi_{\boldsymbol{k}}(v_{\boldsymbol{k}}^{\mathrm{R}}, v_{\boldsymbol{k}}^{\mathrm{I}}) = \prod_{\boldsymbol{k}} \Psi_{\boldsymbol{k}}^{\mathrm{R}}(v_{\boldsymbol{k}}^{\mathrm{R}}) \Psi_{\boldsymbol{k}}^{\mathrm{I}}(v_{\boldsymbol{k}}^{\mathrm{I}}). \quad (14)$$

Quantization is achieved by promoting $v_{\boldsymbol{k}}$ and $p_{\boldsymbol{k}}$ to quantum operators, $\hat{v}_{\boldsymbol{k}}$ and $\hat{p}_{\boldsymbol{k}}$, and by requiring the canonical commutation relations

$$[\hat{v}_{\boldsymbol{k}}^{\mathrm{R}}, \hat{p}_{\boldsymbol{q}}^{\mathrm{R}}] = i\delta(\boldsymbol{k}-\boldsymbol{q}), \qquad [\hat{v}_{\boldsymbol{k}}^{\mathrm{I}}, \hat{p}_{\boldsymbol{q}}^{\mathrm{I}}] = i\delta(\boldsymbol{k}-\boldsymbol{q}). \quad (15)$$

These relations admit the following representation:

$$\hat{v}_{\boldsymbol{k}}^{\mathrm{R,I}}\Psi = v_{\boldsymbol{k}}^{\mathrm{R,I}}\Psi, \qquad \hat{p}_{\boldsymbol{k}}^{\mathrm{R,I}}\Psi = -i\frac{\partial\Psi}{\partial v_{\boldsymbol{k}}^{\mathrm{R,I}}}. \quad (16)$$

The wave functional $\Psi[v(\eta,\boldsymbol{x})]$ obeys the Schrödinger equation which, in this context, is a functional differential equation. However, since each mode evolves independently, this functional differential equation can be reduced to an infinite number of differential equations for each $\Psi_{\boldsymbol{k}}$. Concretely, we have

$$i\frac{\Psi_{\boldsymbol{k}}^{\mathrm{R,I}}}{\partial\eta} = \hat{\mathcal{H}}_{\boldsymbol{k}}^{\mathrm{R,I}}\Psi_{\boldsymbol{k}}^{\mathrm{R,I}}, \quad (17)$$

where the Hamiltonian densities $\hat{\mathcal{H}}_{\boldsymbol{k}}^{\mathrm{R,I}}$ are related to the Hamiltonian by $\hat{H} = \int \mathrm{d}^3\boldsymbol{k}(\hat{\mathcal{H}}_{\boldsymbol{k}}^{\mathrm{R}} + \hat{\mathcal{H}}_{\boldsymbol{k}}^{\mathrm{I}})$. They can be expressed as

$$\hat{\mathcal{H}}_{\boldsymbol{k}}^{\mathrm{R,I}} = -\frac{1}{2}\frac{\partial^2}{\partial(v_{\boldsymbol{k}}^{\mathrm{R,I}})^2} + \frac{1}{2}\omega^2(\eta,\boldsymbol{k})(\hat{v}_{\boldsymbol{k}}^{\mathrm{R,I}})^2, \quad (18)$$

where we have made use of the representations (16).

We are now in a position where we can solve the Schrödinger equation. Let us consider the following Gaussian state

$$\Psi_{\boldsymbol{k}}^{\mathrm{R,I}}(\eta, v_{\boldsymbol{k}}^{\mathrm{R,I}}) = N_{\boldsymbol{k}}(\eta)\mathrm{e}^{-\Omega_{\boldsymbol{k}}(\eta)(v_{\boldsymbol{k}}^{\mathrm{R,I}})^2}. \quad (19)$$

The functions $N_{\boldsymbol{k}}(\eta)$ and $\Omega_{\boldsymbol{k}}(\eta)$ are time dependent and do not carry the subscripts "R" and/or "I" because they are the same for the wave functions of the real and imaginary parts of the Mukhanov-Sasaki variable (see below). Then, inserting $\Psi_{\boldsymbol{k}}$ given by Eq. (19) into the Schrödinger equation (17) implies that $N_{\boldsymbol{k}}$ and $\Omega_{\boldsymbol{k}}$ obey the differential equations

$$i\frac{N_{\boldsymbol{k}}'}{N_{\boldsymbol{k}}} = \Omega_{\boldsymbol{k}}, \qquad \Omega_{\boldsymbol{k}}' = -2i\Omega_{\boldsymbol{k}}^2 + \frac{i}{2}\omega^2(\eta,\boldsymbol{k}). \quad (20)$$

The solutions can be easily found and read

$$|N_{\boldsymbol{k}}| = \left(\frac{2\Re\mathrm{e}\Omega_{\boldsymbol{k}}}{\pi}\right)^{1/4}, \qquad \Omega_{\boldsymbol{k}} = -\frac{i}{2}\frac{f_{\boldsymbol{k}}'}{f_{\boldsymbol{k}}}, \quad (21)$$

where $f_{\boldsymbol{k}}$ is a function obeying the equation $f_{\boldsymbol{k}}'' + \omega^2 f_{\boldsymbol{k}} = 0$, that is to say exactly Eq. (12). The first equation (21) guarantees that the wave function is properly normalized, i.e.,

$$\int \Psi_{\boldsymbol{k}}^{\mathrm{R,I}}\Psi_{\boldsymbol{k}}^{\mathrm{R,I}*}\mathrm{d}v_{\boldsymbol{k}}^{\mathrm{R,I}} = 1. \quad (22)$$

Let us now discuss the initial conditions. The fundamental assumption of inflation is that the perturbations are initially in their ground state. At the beginning of inflation, all the modes of astrophysical interest today have a physical wavelength smaller than the Hubble radius, i.e., $k/(aH) \to \infty$. In this regime, one has $\omega^2(\eta,\boldsymbol{k}) \to k^2$ and each mode now behaves as an harmonic oscillator (as opposed to a parametric oscillator in the generic case) with frequency $\omega = k$. As a consequence, the differential equation for $f_{\boldsymbol{k}}(\eta)$ can easily be solved and the solution reads $f_{\boldsymbol{k}} = A_{\boldsymbol{k}}\mathrm{e}^{ik\eta} + B_{\boldsymbol{k}}\mathrm{e}^{-ik\eta}$, $A_{\boldsymbol{k}}$ and $B_{\boldsymbol{k}}$ being integration constants. Upon using the second equation (21), one has

$$\Omega_{\boldsymbol{k}} \to \frac{k}{2}\frac{A_{\boldsymbol{k}}\mathrm{e}^{ik\eta} - B_{\boldsymbol{k}}\mathrm{e}^{-ik\eta}}{A_{\boldsymbol{k}}\mathrm{e}^{ik\eta} + B_{\boldsymbol{k}}\mathrm{e}^{-ik\eta}}. \quad (23)$$

The wave function (19) represents the ground state wave function of an harmonic oscillator if $\Omega_{\boldsymbol{k}} = k/2$. Therefore, one must choose the initial conditions such that $B_{\boldsymbol{k}} = 0$. Moreover, it is easy to check that the Wronskian $W \equiv f_{\boldsymbol{k}}'f_{\boldsymbol{k}}^* - f_{\boldsymbol{k}}'^*f_{\boldsymbol{k}}$ is a conserved quantity, $\mathrm{d}W/\mathrm{d}\eta = 0$, thanks to the equation of motion of $f_{\boldsymbol{k}}$. Straightforward calculation leads to $W = 2ik|A_{\boldsymbol{k}}|^2$. In the Heisenberg picture the canonical commutation relations require that $W = i$. Even if in the Schrödinger picture presently used, the specific value of W is irrelevant since it cancels out on all calculable physical quantities, this value is conventionally adopted, which amounts to setting $A_{\boldsymbol{k}} = 1/\sqrt{2k}$. As announced, requiring the initial state to be the ground state has completely fixed the initial conditions. We see that Eq. (12) (or, equivalently, the equation for $f_{\boldsymbol{k}}$) should thus be solved with the boundary condition

$$\lim_{k/(aH)\to+\infty} f_{\boldsymbol{k}} = \frac{1}{\sqrt{2k}}\mathrm{e}^{ik\eta}. \quad (24)$$

This choice of initial conditions is referred to as the Bunch-Davies vacuum.

C. The power spectrum

Let us now turn to the calculation of the power spectrum and first introduce the two-point correlation function, defined by

$$\langle\Psi|\hat{v}(\eta,\boldsymbol{x})\hat{v}(\eta,\boldsymbol{x}+\boldsymbol{r})|\Psi\rangle = \int\prod_{\boldsymbol{k}}\mathrm{d}v_{\boldsymbol{k}}^{\mathrm{R}}\mathrm{d}v_{\boldsymbol{k}}^{\mathrm{I}}\Psi_{\boldsymbol{k}}^*(v_{\boldsymbol{k}}^{\mathrm{R}}, v_{\boldsymbol{k}}^{\mathrm{I}})v(\eta,\boldsymbol{x})v(\eta,\boldsymbol{x}+\boldsymbol{r})\Psi_{\boldsymbol{k}}(v_{\boldsymbol{k}}^{\mathrm{R}}, v_{\boldsymbol{k}}^{\mathrm{I}}). \quad (25)$$

The next step consists in using the Fourier transform of the Mukhanov-Sasaki variable, see Eq. (7) and the explicit form of the wave function of Eq. (19). One arrives at

$$\langle\Psi|\hat{v}(\eta,\boldsymbol{x})\hat{v}(\eta,\boldsymbol{x}+\boldsymbol{r})|\Psi\rangle = \frac{1}{(2\pi)^3}\int \mathrm{d}\boldsymbol{p}\mathrm{d}\boldsymbol{q}\,\mathrm{e}^{i\boldsymbol{p}\cdot\boldsymbol{x}}\,\mathrm{e}^{i\boldsymbol{q}\cdot(\boldsymbol{x}+\boldsymbol{r})}\prod_{\boldsymbol{k}}\left(\frac{2\Re\mathrm{e}\Omega_{\boldsymbol{k}}}{\pi}\right) \times \int\prod_{\boldsymbol{k}}\mathrm{d}v_{\boldsymbol{k}}^{\mathrm{R}}\mathrm{d}v_{\boldsymbol{k}}^{\mathrm{I}}\,\mathrm{e}^{-2\sum_{\boldsymbol{k}}\Re\mathrm{e}\Omega_{\boldsymbol{k}}[(v_{\boldsymbol{k}}^{\mathrm{R}})^2+(v_{\boldsymbol{k}}^{\mathrm{I}})^2]}\,v_{\boldsymbol{p}}v_{\boldsymbol{q}}. \quad (26)$$

If $\boldsymbol{p}\neq\pm\boldsymbol{q}$, the result of the integration is zero since the integrand (up to the Gaussian weight) becomes linear in $v_{\boldsymbol{p}}^{\mathrm{R,I}}$ or $v_{\boldsymbol{q}}^{\mathrm{R,I}}$. If $\boldsymbol{p}=\boldsymbol{q}$, then the only nonlinear term in the integrand is given by $[(v_{\boldsymbol{p}}^{\mathrm{R}})^2-(v_{\boldsymbol{p}}^{\mathrm{I}})^2]/2$. Each term contributes the same amount, so the difference vanishes. The only possibility left is therefore $\boldsymbol{p}=-\boldsymbol{q}$, such that $v_{\boldsymbol{p}}v_{\boldsymbol{q}}=[(v_{\boldsymbol{p}}^{\mathrm{R}})^2+(v_{\boldsymbol{p}}^{\mathrm{I}})^2]/2$, the factor $1/2$ coming from the definition of $v_{\boldsymbol{k}}^{\mathrm{R,I}}$, see Eqs. (13). This leads to

$$\langle\Psi|\hat{v}(\eta,\boldsymbol{x})\hat{v}(\eta,\boldsymbol{x}+\boldsymbol{r})|\Psi\rangle = \frac{2}{(2\pi)^3}\frac{1}{2}\int \mathrm{d}\boldsymbol{p}\,\mathrm{e}^{-i\boldsymbol{p}\cdot\boldsymbol{r}}\prod_{\boldsymbol{k}}^{N}\left(\frac{2\Re\mathrm{e}\Omega_{\boldsymbol{k}}}{\pi}\right) \times \int\prod_{\boldsymbol{k}}^{N}\mathrm{d}v_{\boldsymbol{k}}^{\mathrm{R}}\mathrm{d}v_{\boldsymbol{k}}^{\mathrm{I}}\,\mathrm{e}^{-2\sum_{\boldsymbol{k}}\Re\mathrm{e}\Omega_{\boldsymbol{k}}[(v_{\boldsymbol{k}}^{\mathrm{R}})^2+(v_{\boldsymbol{k}}^{\mathrm{I}})^2]}(v_{\boldsymbol{p}}^{\mathrm{R}})^2, \quad (27)$$

the factor of 2 originating from the fact that we have two contributions, one given by the term $(v_{\boldsymbol{p}}^{\mathrm{R}})^2$ and the other by $(v_{\boldsymbol{p}}^{\mathrm{I}})^2$. The Gaussian integrals can easily be carried out. They are all of the form "$\int \mathrm{d}x\mathrm{e}^{-\alpha x^2}$," except of course the one over $v_{\boldsymbol{p}}^{\mathrm{R}}$ which is of the form "$\int \mathrm{d}x x^2\mathrm{e}^{-\alpha x^2}$." As a consequence, one obtains

$$\langle\Psi|\hat{v}(\eta,\boldsymbol{x})\hat{v}(\eta,\boldsymbol{x}+\boldsymbol{r})|\Psi\rangle = \frac{1}{(2\pi)^3}\int \mathrm{d}\boldsymbol{p}\,\mathrm{e}^{-i\boldsymbol{p}\cdot\boldsymbol{r}}\prod_{\boldsymbol{k}}^{N}\left(\frac{2\Re\mathrm{e}\Omega_{\boldsymbol{k}}}{\pi}\right)\frac{1}{2}\left[\frac{\sqrt{\pi}}{\left(\sqrt{2\Re\mathrm{e}\Omega_{\boldsymbol{p}}}\right)^3}\right] \times\prod_{\boldsymbol{k}}^{N}\left(\frac{\sqrt{\pi}}{\sqrt{2\Re\mathrm{e}\Omega_{\boldsymbol{k}}}}\right)\prod_{\boldsymbol{k}}^{N-1}\left(\frac{\sqrt{\pi}}{\sqrt{2\Re\mathrm{e}\Omega_{\boldsymbol{k}}}}\right). \quad (28)$$

The infinite product "$\prod_{\boldsymbol{k}}^{N-1}$" means a product over all the wave vectors but $\boldsymbol{p}$. One can always write this product as "$\sqrt{2\Re\mathrm{e}\Omega_{\boldsymbol{p}}/\pi}\prod_{\boldsymbol{k}}^{N}$," then the two last infinite products in the above expression exactly cancel the first one. Therefore, we are left with

$$\langle\Psi|\hat{v}(\eta,\boldsymbol{x})\hat{v}(\eta,\boldsymbol{x}+\boldsymbol{r})|\Psi\rangle = \frac{1}{(2\pi)^3}\int \mathrm{d}\boldsymbol{p}\,\mathrm{e}^{-i\boldsymbol{p}\cdot\boldsymbol{r}}\frac{1}{4\Re\mathrm{e}\Omega_{\boldsymbol{p}}}. \quad (29)$$

We now need to express $\Re\mathrm{e}\Omega_{\boldsymbol{p}}$ in terms of the function $f_{\boldsymbol{p}}$. From the second Eq. (21), one easily shows that

$$\Re\mathrm{e}\Omega_{\boldsymbol{p}} = -\frac{i}{4}\frac{W}{|f_{\boldsymbol{p}}|^2}, \quad (30)$$

and we obtain our final expression for the two-point correlation function

$$\langle\Psi|\hat{v}(\eta,\boldsymbol{x})\hat{v}(\eta,\boldsymbol{x}+\boldsymbol{r})|\Psi\rangle = \frac{1}{(2\pi)^3}\int \mathrm{d}\boldsymbol{p}\,\mathrm{e}^{-i\boldsymbol{p}\cdot\boldsymbol{r}}\frac{i}{W}|f_{\boldsymbol{p}}|^2 = \frac{1}{2\pi^2}\int_0^{+\infty}\frac{\mathrm{d}p}{p}\frac{\sin pr}{pr}p^3|f_{\boldsymbol{p}}|^2, \quad (31)$$

where, in the last expression, we have used our choice $W=i$. The power spectrum is just defined as the square of the Fourier amplitude per logarithmic interval at a given scale, i.e.,

$$\mathcal{P}_{v}(k) = \frac{k^3}{2\pi^2}|f_{\boldsymbol{k}}|^2. \quad (32)$$

The same manipulations allow us to express the two-point correlation of two Fourier amplitudes. It can be written as

$$\langle\Psi|\hat{v}_{\boldsymbol{k}}\hat{v}_{\boldsymbol{p}}^{*}|\Psi\rangle = \int\prod_{\boldsymbol{q}}\mathrm{d}v_{\boldsymbol{q}}^{\mathrm{R}}\mathrm{d}v_{\boldsymbol{q}}^{\mathrm{I}}\Psi_{\boldsymbol{q}}^{*}\hat{v}_{\boldsymbol{k}}\hat{v}_{\boldsymbol{p}}^{*}\Psi_{\boldsymbol{q}}. \quad (33)$$

This integral is nonvanishing only if $\boldsymbol{k}=\boldsymbol{p}$ (otherwise one has to integrate an odd function) and receives two contributions, one from $(v_{\boldsymbol{k}}^{\mathrm{R}})^2$ and the other from $(v_{\boldsymbol{k}}^{\mathrm{I}})^2$. Repeating calculations already performed before, one finally arrives at

$$\langle\Psi|\hat{v}_{\boldsymbol{k}}\hat{v}_{\boldsymbol{p}}^{*}|\Psi\rangle = \frac{2\pi^2}{k^3}\mathcal{P}_{v}(k)\delta(\boldsymbol{k}-\boldsymbol{p}). \quad (34)$$

We now need to explain how the cosmological perturbations of quantum-mechanical origin studied above are related to observables in cosmology. This is the goal of the next section.

D. From quantum fluctuations to CMB anisotropies

The presence of quantum fluctuations in the inflaton and gravitational fields has many observational implications. Here, we focus on one of them, namely the existence of CMB temperature anisotropies. The importance of this observable is that we now have at our disposal very high accuracy measurements of those anisotropies [20,21]. Moreover, even more accurate data will be released soon [92]. The relation between the temperature fluctuations along a given direction $\boldsymbol{e}$ and the cosmological perturbations is expressed by the so-called Sachs-Wolfe effect [93,94]. A simplified version of this result, valid on large angular scales only, can be written as [94]

$$\frac{\delta T}{T}(\boldsymbol{e}) = \frac{1}{5}\zeta[\eta_{\ell\mathrm{ss}}, -\boldsymbol{e}(\eta_{\ell\mathrm{ss}}-\eta_0)+\boldsymbol{x}_0], \quad (35)$$

where T represents the averaged background temperature, i.e., $T\simeq 2.7$ K, $\eta_{\ell\mathrm{ss}}$ is the conformal time at emission (that is to say at the surface of last scattering) and η_0 is the present conformal time. The vector $\boldsymbol{x}_0$ landmarks the place of reception, in the present case Earth (or a satellite orbiting the Earth). The quantity ζ denotes the curvature perturbation. It is related to the Bardeen potential defined in Eq. (3) through the following expression [12,86,95]:

$$\zeta = \frac{2}{3}\frac{\mathcal{H}^{-1}\Phi_{\mathrm{B}}' + \Phi_{\mathrm{B}}}{1+w} + \Phi_{\mathrm{B}}, \tag{36}$$

where $w \equiv p/\rho$ is the equation of state parameter, that is to say the energy density to pressure ratio of the dominant fluid. For instance, for the matter dominated era ($w = 0$), during which recombination takes place (at a redshift of $z_{\ell\mathrm{ss}} \simeq 1100$), on large scales, one simply has $\zeta \simeq 5\Phi_{\mathrm{B}}/3$ since the Bardeen potential is constant. The importance of ζ lies in the fact that it is a conserved quantity on large scales [86,95]. Therefore, its spectrum, calculated at the end of inflation, can directly be propagated to the recombination time as it is not sensitive to the details of the cosmological evolution, in particular to those of the complicated reheating era [96–100]. The curvature perturbation can also be expressed in terms of the Mukhanov-Sasaki variable as

$$\zeta = \frac{1}{a\sqrt{2\epsilon_1}}\frac{v}{M_{\mathrm{Pl}}}. \tag{37}$$

Finally, in the framework of the theory of inflationary cosmological perturbations of quantum-mechanical origin, we have seen that v is in fact an operator. This implies that ζ and $\delta T/T$ are also quantum operators and, for this reason, from now on, we will denote them with a hat.

Since the operator $\widehat{\delta T}/T$ lives on the celestial sphere, it can be expanded over the spherical harmonic basis according to

$$\frac{\widehat{\delta T}}{T}(\boldsymbol{e}) = \sum_{\ell=2}^{\infty}\sum_{m=-\ell}^{m=\ell}\hat{a}_{\ell m}Y_{\ell m}(\theta,\phi), \tag{38}$$

where θ and ϕ are the angles defining the direction along which the vector $\boldsymbol{e}$ is pointing. Then, the angular two-point correlation function can be expressed in terms of the multipole moments C_ℓ as

$$\langle\Psi|\hat{a}_{\ell m}\hat{a}^{*}_{\ell' m'}|\Psi\rangle = C_\ell\delta_{\ell\ell'}\delta_{mm'}, \tag{39}$$

and, as a consequence, the two-point correlation function of the temperature fluctuations operator can be written as

$$\left\langle\Psi\left|\frac{\widehat{\delta T}}{T}(\boldsymbol{e}_1)\frac{\widehat{\delta T}}{T}(\boldsymbol{e}_2)\right|\Psi\right\rangle = \frac{1}{4\pi}\sum_{\ell=2}^{\infty}(2\ell+1)C_\ell P_\ell(\boldsymbol{e}_1\cdot\boldsymbol{e}_2), \tag{40}$$

the quantity P_ℓ denoting Legendre polynomials.

In order to pursue our demonstration that the CMB anisotropies are entirely determined by the quantum fluctuations, let us now express the multipole moments in terms of the cosmological perturbation power spectrum. Upon using Eqs. (35) and (38), one obtains

$$\hat{a}_{\ell m} = \frac{1}{(2\pi)^{3/2}}\int \mathrm{d}\Omega_{\boldsymbol{e}}\mathrm{d}\boldsymbol{k}\frac{\hat{\zeta}_{\boldsymbol{k}}(\eta_{\ell\mathrm{ss}})}{5}\mathrm{e}^{-i\boldsymbol{k}\cdot[\boldsymbol{e}(\eta_{\ell\mathrm{ss}}-\eta_0)-\boldsymbol{x}_0]}Y^{*}_{\ell m}(\boldsymbol{e}) \tag{41}$$

and, from this expression, it is easy to show that

$$C_\ell = \frac{1}{2a^2M_{\mathrm{Pl}}^2\epsilon_1}\frac{4\pi}{25}\int\frac{\mathrm{d}k}{k}j_\ell^2[k(\eta_0-\eta_{\ell\mathrm{ss}})]\mathcal{P}_v(k), \tag{42}$$

where j_ℓ is a spherical Bessel function and where we used Eq. (34) to show that

$$\langle\Psi|\hat{\zeta}_{\boldsymbol{k}}\hat{\zeta}^{*}_{\boldsymbol{p}}|\Psi\rangle = \frac{1}{2a^2M_{\mathrm{Pl}}^2\epsilon_1}\frac{2\pi^2}{k^3}\mathcal{P}_v(k)\delta(\boldsymbol{k}-\boldsymbol{p}). \tag{43}$$

We see that C_ℓ is given by an integral over wave numbers of the Mukhanov-Sasaki power spectrum times a quantity that can be viewed as a "transfer matrix $j_{l\boldsymbol{k}} \equiv j_\ell^2[k(\eta_0-\eta_{\ell\mathrm{ss}})]$" which allows us to "translate" a three dimensional spatial frequency $\boldsymbol{k}$ into a two-dimensional spatial frequency ℓ on the celestial sphere. We emphasize again that the above result is valid on large scales only; otherwise the integral in Eq. (42) contains another transfer function $T_\zeta(k)$ which takes into account the subsequent evolution of the modes when they reenter the Hubble radius after inflation. Since ζ is a conserved quantity, we have $T_\zeta(k\to 0) = 1$.

Finally, let us also notice that Eq. (41) implies that $\langle\Psi|\hat{a}_{\ell m}|\Psi\rangle = 0$ since $\langle\Psi|\hat{\zeta}_{\boldsymbol{k}}|\Psi\rangle = 0$. Of course, this also means that $\langle\Psi|\widehat{\delta T}/T|\Psi\rangle = 0$.

E. Inflationary predictions

We have just seen that, in order to calculate the CMB multipole moments, we need to evaluate the curvature perturbation power spectrum. In this section, we calculate this quantity for power-law inflation.

The first step consists in solving the equation of motion (12). Upon using Eq. (11), one obtains the time dependence of the frequency of the parametric oscillator, which reads

$$\omega^2(\eta,\boldsymbol{k}) = k^2 - \frac{\beta(\beta+1)}{\eta^2}. \tag{44}$$

From this expression, one sees that there are two regimes depending on whether the first term is dominant or subdominant. The Hubble radius is given by $\ell_{\mathrm{H}} \equiv 1/H = a\eta/(1+\beta)$ and the Fourier mode wavelength can be expressed in terms of the comoving wave number as $\lambda = 2\pi a/k$. The first term dominates if $|k\eta| \gg 1$ or, equivalently, $\lambda \ll \ell_{\mathrm{H}}$. In this case $\omega \simeq k$ and we expect the mode function to oscillate as it would in Minkowski spacetime since, at those scales, spacetime curvature is negligible for the mode evolution. On the contrary, if $|k\eta| \ll 1$, or $\lambda \gg \ell_{\mathrm{H}}$, one has $\omega \sim 1/\eta$, so curvature dominates and one obtains one growing mode and one decaying mode. These arguments are confirmed when one studies the exact solution for the mode function $f_{\boldsymbol{k}}$. It can be expressed in terms of Bessel functions $J_\nu(z)$ as [101,102]

$$f_{\boldsymbol{k}} = (-k\eta)^{1/2}[C_{\boldsymbol{k}}J_{\beta+1/2}(-k\eta) + D_{\boldsymbol{k}}J_{-(\beta+1/2)}(-k\eta)], \tag{45}$$

where $C_{\boldsymbol{k}}$ and $D_{\boldsymbol{k}}$ are two integration constants. In order to match the initial vacuum behavior (24), one must choose

$$C_k = -D_k e^{i\pi(\beta+1/2)}, \qquad D_k = \frac{i}{2}\sqrt{\frac{\pi}{k}}\frac{e^{-i\pi/4-i\pi(\beta+1/2)/2}}{\sin[\pi(\beta+1/2)]}. \tag{46}$$

In particular, one notices that both coefficients C_k and D_k scale as $1/\sqrt{k}$.

Since we want to evaluate the power spectrum on large scales, it is sufficient to take the limit $k\eta \to 0$ in Eq. (45). Then, one is led to

$$\mathcal{P}_\zeta|_{\rm stand} = \frac{1}{2a^2 M_{\rm Pl}^2 \epsilon_1}\mathcal{P}_v(k) = \frac{1}{\pi\epsilon_1 m_{\rm Pl}^2 \ell_0^2} f(\beta) k^{2\beta+4} \equiv A_{\rm S} k^{n_{\rm S}-1}, \tag{47}$$

where $M_{\rm Pl} = m_{\rm Pl}/\sqrt{8\pi}$ and the function $f(\beta)$ is defined by [90]

$$f(\beta) \equiv \frac{1}{\pi}\left[\frac{\Gamma(-\beta-1/2)}{2^{1+\beta}}\right]^2, \tag{48}$$

where $\Gamma(z)$ is the Euler integral of the first kind [101,102]. This function is such that, for the de Sitter case $\beta = -2$, one has $f(\beta = -2) = 1$. The scalar spectral index $n_{\rm S} = 2\beta + 5$ and, for solutions close to the de Sitter solutions, one has $n_{\rm S} \simeq 1$, i.e., we have an almost scale invariant power spectrum. As discussed before, the deviations from scale invariance are related to the deviation from the de Sitter case $\beta = -2$. This conclusion is in fact valid for any slow-roll models. The amplitude $A_{\rm S}$ determines the level of the temperature fluctuations observed in the sky, namely $\delta T/T \sim 10^{-5}$.

Finally, let us evaluate the multipole moments explicitly. Upon using Eq. (42) and the expression of the power spectrum established above, one arrives at

$$C_\ell = \frac{\pi^{3/2}\Gamma[(3-n_{\rm S})/2]\Gamma[\ell+(n_{\rm S}-1)/2]}{\Gamma[(4-n_{\rm S})/2]\Gamma[\ell+2-(n_{\rm S}-1)/2]}(r_{\ell_{\rm ss}})^{1-n_{\rm S}}\frac{A_{\rm S}}{25}, \tag{49}$$

where we have defined $r_{\ell_{\rm ss}} \equiv \eta_0 - \eta_{\ell_{\rm ss}}$. Since this equation has been derived for large scales, roughly speaking one can estimate it to be valid in the regime $\ell \ll 20$. For $n_{\rm S} \simeq 1$, the above expression implies that $C_\ell \propto 1/[\ell(\ell+1)]$.

Of course, in the real world, the argument goes the other way around. From measurements of the CMB anisotropies, we observe that, on large scales, $C_\ell \propto 1/[\ell(\ell+1)]$ and, therefore, we deduce that the corresponding power spectrum is close to scale invariance, i.e., $n_{\rm S} \simeq 1$. Obviously, this also means that a spectrum that is not very close to scale invariance is now ruled out (more precisely, the WMAP data indicate that $1 - n_{\rm S} = 0.018^{+0.019}_{-0.02}$ [20–22]). As already emphasized, the great success of inflation is that it precisely leads to such a power spectrum.

It should also be clear that the above discussion, although perfectly correct at the level of principles, is oversimplified at the technical level. The multipole moments are in fact computed at any scale (i.e., for any value of ℓ) by means of numerical calculations (since, in the most general case, they are solutions of more involved differential equations) [103]. Moreover, their shape is not only determined by the spectral index but is also affected by the other cosmological parameters. The constraints on the different inflationary models are then obtained by a Markov chain exploration of the parameter space [104]. But these technical considerations do not affect the considerations presented in this paper. Once again, as far as physical principles are concerned, the discussion presented in this section is accurate.

III. THE COSMOLOGICAL MEASUREMENT PROBLEM

A. Squeezed state

In this section, we study in more detail the properties of the quantum state in which the cosmological perturbations are placed [29,31,34,105]. As already mentioned around Eq. (19), it is described by the wave function

$$\Psi_k(\eta, v_k^{\rm R}, v_k^{\rm I}) = \left(\frac{2\Re{\rm e}\Omega_k}{\pi}\right)^{1/2} e^{-\Omega_k[(v_k^{\rm R})^2+(v_k^{\rm I})^2]} \tag{50}$$

$$= \left(\frac{2\Re{\rm e}\Omega_k}{\pi}\right)^{1/2} e^{-2\Omega_k(\eta)v_k v_k^*}. \tag{51}$$

We see that this quantum state is completely known once the time dependence of $\Omega_k(\eta)$ has been determined. The differential equation controlling the evolution of $\Omega_k(\eta)$ is given by the second part of Eq. (20). This equation is a Ricatti equation (i.e., a first order, nonlinear, differential equation). As is well known, it can always be reduced to a second order but linear differential equation. As already mentioned, this is achieved through the change of variable $\Omega_k = -if_k'/(2f_k)$. The function $f_k(\eta)$ obeys $f_k'' + \omega^2 f_k = 0$ and has been solved in Eq. (45). In the small-scale limit, one has $\Omega_k \to k/2$ and the wave function (50) is the ground state of an harmonic oscillator. In the large-scale limit, a lengthy but straightforward calculation leads to

$$\frac{\Omega_k(\eta)}{k} = -\frac{i}{2k\eta}(1+\beta) - \frac{i}{4(\beta+3/2)}(-k\eta) - \frac{i}{\pi}2^{2\beta}\sin(2\pi\beta)\Gamma^2\left(\beta+\frac{3}{2}\right)(-k\eta)^{-2\beta-2} + \frac{\pi 2^{2\beta+1}}{\Gamma^2(-\beta-1/2)}(-k\eta)^{-2\beta-2} + \cdots. \tag{52}$$

From this expression, one deduces that

$$\Re{\rm e}\Omega_k(\eta) = \frac{k\pi 2^{2\beta+1}}{\Gamma^2(-\beta-1/2)}(-k\eta)^{-2\beta-2} + \cdots \to 0, \tag{53}$$

and

$$\Im{\rm m}\Omega_k(\eta) = -\frac{1}{2\eta}(1+\beta) + \cdots = -\frac{a'}{2a} \to \infty, \tag{54}$$

where the limits are taken in the super-Hubble regime in which $k\eta \to 0$.

We have mentioned above that the Ricatti equation (20) can always be reduced to a linear second order differential equation. Of course, it can also be expressed as two linear, first order, differential equations. Therefore, one can introduce the functions $u_k(\eta)$ and $v_k(\eta)$ such that $f_k \equiv (u_k + v_k^*)/\sqrt{2k}$, the normalization $1/\sqrt{2k}$ being introduced for convenience. Then it is easy to show that these two functions obey

$$u_k' = iku_k + \frac{(a\sqrt{\epsilon_1})'}{a\sqrt{\epsilon_1}} v_k^*, \tag{55}$$

$$v_k' = ikv_k + \frac{(a\sqrt{\epsilon_1})'}{a\sqrt{\epsilon_1}} u_k^*. \tag{56}$$

The Wronskian $W = f_k' f_k^* - f_k'^* f_k$ can be straightforwardly evaluated as $W = i(|u_k|^2 - |v_k|^2)$. This means that, if we want to work with the choice $W = i$, one must have $|u_k|^2 - |v_k|^2 = 1$. This suggests to introduce the following parametrization:

$$u_k(\eta) = \mathrm{e}^{i\theta_k} \cosh r_k, \tag{57}$$

$$v_k(\eta) = \mathrm{e}^{-i\theta_k + 2i\phi_k} \sinh r_k. \tag{58}$$

The three functions $r_k(\eta)$, $\theta_k(\eta)$ and $\phi_k(\eta)$ are called the squeezing parameter, rotation angle and squeezing angle, respectively. It is clear that the knowledge of these three functions is equivalent to that of the function $\Omega_k(\eta)$ and, therefore, of the wave function. Upon using Eqs. (57) and (58), it is easy to show that

$$r_k' = \frac{(a\sqrt{\epsilon_1})'}{a\sqrt{\epsilon_1}} \cos(2\phi_k), \tag{59}$$

$$\phi_k' = k - \frac{(a\sqrt{\epsilon_1})'}{a\sqrt{\epsilon_1}} \coth(2r_k) \sin(2\phi_k), \tag{60}$$

$$\theta_k' = k - \frac{(a\sqrt{\epsilon_1})'}{a\sqrt{\epsilon_1}} \tanh r_k \sin(2\phi_k). \tag{61}$$

The explicit relation between Ω_k and the three squeezing parameters is given by

$$\Omega_k = \frac{k}{2} \frac{\cosh r_k - \mathrm{e}^{-2i\phi_k} \sinh r_k}{\cosh r_k + \mathrm{e}^{-2i\phi_k} \sinh r_k} - i\frac{a'}{2a}, \tag{62}$$

from which one deduces that

$$\Re\mathrm{e}\Omega_k = \frac{k}{2} \frac{1}{\cosh(2r_k) + \cos(2\phi_k)\sinh(2r_k)}, \tag{63}$$

$$\Im\mathrm{m}\Omega_k = \frac{k}{2} \frac{\sin(2\phi_k)\sinh(2r_k)}{\cosh(2r_k) + \cos(2\phi_k)\sinh(2r_k)} - \frac{a'}{2a}. \tag{64}$$

Equations (59)–(61), are highly nonlinear differential equations and cannot be solved in general. We notice that Eqs. (59) and (60) are in fact decoupled from Eq. (61). Therefore, they can be solved in a first step and then the solutions can be inserted in Eq. (61) to find the behavior of θ_k. In the case of power-law inflation, one can find explicit solutions for the de Sitter case, $\beta = -2$. Although this is not a solution for an arbitrary value of β, it is sufficient to understand the main features of the phenomenon of squeezing. One obtains

$$r_k(\eta) = -\mathrm{argsinh}\left(\frac{1}{2k\eta}\right), \tag{65}$$

$$\phi_k(\eta) = \frac{\pi}{4} + \frac{1}{2}\arctan\left(\frac{1}{2k\eta}\right). \tag{66}$$

Therefore, we see that, initially in the sub-Hubble limit, $r_k = 0$ (and $\phi_k = \pi/4$) while the super-Hubble limit corresponds to the limit of strong squeezing $r_k \to +\infty$ (and $\phi_k \to 0$).

Based on the previous considerations, it is clear that the super-Hubble limit is always associated with strong squeezing, even if we do not deal with the exact de Sitter solution. Indeed, now for an arbitrary β, Eq. (60) can be written as $\phi_k' \simeq -(\beta+1)\sin(2\phi_k)/\eta$ which can be integrated and leads to $\phi_k \simeq \arctan[C|\eta|^{-2(\beta+1)}]$. For $\beta \lesssim -2$, this confirms the fact that $\phi_k \to 0$. In the same limit, one has $r_k' \simeq 1/\eta$ from which one obtains $r_k \propto (1+\beta)\ln a$. This confirms that the super-Hubble limit is the strong squeezing limit and, given the fact that modes of astrophysical interest today leave the Hubble scale 50–60 e-folds before the end of inflation, one can deduce that $r_k \simeq 120$ for those modes [29,30]. Compared to what can be achieved in the laboratory in quantum optics, this is a very large value [106].

In order to understand better the features of the quantum state (50), it is also interesting to calculate the mean values and dispersion of various quantities. First of all, it is clear that

$$\langle\Psi|\hat{v}_k^{\mathrm{R,I}}|\Psi\rangle = \langle\Psi|\hat{p}_k^{\mathrm{R,I}}|\Psi\rangle = 0. \tag{67}$$

Second, we also have

$$\langle\Psi|(\hat{v}_k^{\mathrm{R,I}})^2|\Psi\rangle = \frac{1}{4\Re\mathrm{e}\Omega_k}, \tag{68}$$

$$\langle\Psi|(\hat{p}_k^{\mathrm{R,I}})^2|\Psi\rangle = \Re\mathrm{e}\Omega_k + \frac{(\Im\mathrm{m}\Omega_k)^2}{\Re\mathrm{e}\Omega_k}. \tag{69}$$

Finally, the cross products can be expressed as

$$\langle\Psi|\hat{v}_k^{\mathrm{R}}\hat{p}_k^{\mathrm{R}}|\Psi\rangle = \frac{i\Omega_k}{2\Re\mathrm{e}\Omega_k}, \tag{70}$$

$$\langle\Psi|\hat{p}_k^{\mathrm{R}}\hat{v}_k^{\mathrm{R}}|\Psi\rangle = -i + \frac{i\Omega_k}{2\Re\mathrm{e}\Omega_k}, \tag{71}$$

and, of course, similar expressions for the operators $\hat{v}_k^{\mathrm{I}}$ and $\hat{p}_k^{\mathrm{I}}$. It is also interesting to notice that $\langle\Psi|\hat{v}_k^{\mathrm{R}}\hat{p}_k^{\mathrm{I}}|\Psi\rangle = \langle\Psi|\hat{v}_k^{\mathrm{I}}\hat{p}_k^{\mathrm{R}}|\Psi\rangle = 0$.

At this point, it is worth digressing about the definition of the conjugate momentum. The action (6) is of course defined up to a total derivative. In Ref. [15], it was shown that adding the term $\mathrm{d}[(a'/a)(v_k^{\mathrm{R}})^2 + (a'/a)(v_k^{\mathrm{I}})^2]/(2\mathrm{d}\eta)$ can also be viewed as a canonical transformation. This generates an additional term $(a'/a)(p_{\mathrm{k}}^{\mathrm{R,I}} v_{\mathrm{k}}^{\mathrm{R,I}*} + p_{\mathrm{k}}^{\mathrm{R,I}*} v_k^{\mathrm{R,I}})$ in the Hamiltonian. A complete study was presented in Ref. [15] and, here, we only quote the main results. It was shown that, at the quantum level, this canonical transformation leaves the amplitude $\hat{v}_k^{\mathrm{R,I}}$ invariant but induces the following transformations for the momentum: $\hat{p}_k^{\mathrm{R,I}} \to \hat{\pi}_k^{\mathrm{R,I}}$ with

$$\hat{\pi}_k^{\mathrm{R,I}} = \hat{p}_k^{\mathrm{R,I}} - \frac{a'}{a}\hat{v}_k^{\mathrm{R,I}}. \tag{72}$$

On the other hand, the wave function is also modified, $\Psi_k \to \bar{\Psi}_k$, and the function Ω_k changes according to $\Omega_k \to \bar{\Omega}_k$, where

$$\bar{\Omega}_k = \Omega_k + i\frac{a'}{2a}. \tag{73}$$

In particular, we see that the canonical transformation is such that the term $ia'/(2a)$ in the expression (62) of the function $\Omega_k(\eta)$ is exactly canceled. The factor N_k of the wave function is not modified and is still given by the first of Eq. (21) (but of course should be used either with Ω_k or $\bar{\Omega}_k$ according to which set of variables is used). This also means that when the averages (67)–(71) are computed in the state $|\bar{\Psi}\rangle$, one obtains exactly the same expression, Ω_k being just replaced with $\bar{\Omega}_k$ (of course, $|\Psi\rangle$ and $|\bar{\Psi}\rangle$, being related by a canonical transformation, represent the same physical state).

We now come back to our calculation of the dispersion of amplitude operator and its conjugate momentum. Upon using Eqs. (68) and (63), one obtains

$$\langle\bar{\Psi}|(\hat{v}_k^{\mathrm{R,I}})^2|\bar{\Psi}\rangle = \frac{1}{2k}[\cosh(2r_k) + \cos(2\phi_k)\sinh(2r_k)]. \tag{74}$$

In the same manner, the dispersion of the operator $\hat{\pi}_k^{\mathrm{R,I}}$ is given by

$$\langle\bar{\Psi}|(\hat{\pi}_k^{\mathrm{R,I}})^2|\bar{\Psi}\rangle = \frac{k}{2}\frac{1 + \sin^2(2\phi_k)\sinh^2(2r_k)}{\cosh(2r_k) + \cos(2\phi_k)\sinh(2r_k)}. \tag{75}$$

Let us now consider two new operators $\hat{\mathcal{A}}_k^{\mathrm{R,I}}$ and $\hat{\mathcal{B}}_k^{\mathrm{R,I}}$, defined from $\hat{\pi}_k^{\mathrm{R,I}}/\sqrt{k}$ and $\sqrt{k}\hat{v}_k^{\mathrm{R,I}}$ through a rotation by the squeezing angle ϕ_k,

$$\hat{\mathcal{A}}_k^{\mathrm{R,I}} = \frac{\hat{\pi}_k^{\mathrm{R,I}}}{\sqrt{k}}\cos\phi_k + \sqrt{k}\hat{v}_k^{\mathrm{R,I}}\sin\phi_k, \tag{76}$$

$$\hat{\mathcal{B}}_k^{\mathrm{R,I}} = \frac{\hat{\pi}_k^{\mathrm{R,I}}}{\sqrt{k}}\sin\phi_k - \sqrt{k}\hat{v}_k^{\mathrm{R,I}}\cos\phi_k. \tag{77}$$

It is easy to check that $[\hat{\mathcal{A}}_k, \hat{\mathcal{B}}_k] = i$. Then, a lengthy but straightforward calculation leads to

$$\langle\bar{\Psi}|\hat{\mathcal{A}}_k^{\mathrm{R,I}}|\bar{\Psi}\rangle = \frac{\mathrm{e}^{-2r_k}}{2}, \tag{78}$$

$$\langle\bar{\Psi}|\hat{\mathcal{B}}_k^{\mathrm{R,I}}|\bar{\Psi}\rangle = \frac{\mathrm{e}^{2r_k}}{2}. \tag{79}$$

Therefore, we see that there exists a direction in the plane (π_k, v_k) where the dispersion is extremely small. This is why the corresponding state is called a squeezed state. In order to satisfy the Heisenberg inequality, the dispersion along the direction perpendicular to the previous one becomes very large. As already mentioned, the phenomenon of squeezing is widely studied in many different branches of physics, in particular in quantum optics. Squeezing occurs each time the quantization of a parametric oscillator is carried out. It is remarkable that the quantization of small fluctuations on top of an expanding universe also leads to that concept (squeezing here, i.e., $r_k \neq 0$, does not require an accelerated expansion, only a dynamical background is necessary).

B. The classical limit

We have seen in the last section that the super-Hubble limit corresponds to a limit where the squeezing parameter r_k is large. In the literature, this regime is very often described as a regime where the cosmological perturbations have classicalized [31,32,39,39,107]. Since this concept is subtle in quantum mechanics (and particularly when quantum mechanics is applied to cosmology), we need to come back to this issue and to describe accurately what is meant by a "classical limit" in this context. In particular, it may seem strange at first sight that a quantum system placed in a strongly squeezed state can be described as a classical state since, in the context of, say, quantum optics, a similar situation would precisely be described as a nonclassical situation [108,109].

A convenient tool to study this question is the Wigner function, defined by

$$W(v_k^{\mathrm{R}}, v_k^{\mathrm{I}}, p_k^{\mathrm{R}}, p_k^{\mathrm{I}}) = \frac{1}{(2\pi)^2}\int \mathrm{d}x\mathrm{d}y\Psi^*\left(v_k^{\mathrm{R}} - \frac{x}{2}, v_k^{\mathrm{I}} - \frac{y}{2}\right) \times \mathrm{e}^{-ip_k^{\mathrm{R}}x - ip_k^{\mathrm{I}}y}\Psi\left(v_k^{\mathrm{R}} + \frac{x}{2}, v_k^{\mathrm{I}} + \frac{y}{2}\right). \tag{80}$$

Indeed, it is well known that the Wigner function can be understood as a classical probability distribution function whenever it is positive definite. Then, upon using the quantum state (50), the following explicit form is obtained

$$W(v_k^{\mathrm{R}}, v_k^{\mathrm{I}}, p_k^{\mathrm{R}}, p_k^{\mathrm{I}}) = \Psi\Psi^*\frac{1}{2\pi\Re\mathrm{e}\Omega_k}\exp\left[-\frac{1}{2\Re\mathrm{e}\Omega_k}(p_k^{\mathrm{R}} + 2\Im\mathrm{m}\Omega_k v_k^{\mathrm{R}})^2\right] \times \exp\left[-\frac{1}{2\Re\mathrm{e}\Omega_k}(p_k^{\mathrm{I}} + 2\Im\mathrm{m}\Omega_k v_k^{\mathrm{I}})^2\right]. \tag{81}$$

The following remark is in order at this stage. One could have calculated the Wigner function with the state $\bar{\Psi}_k$.

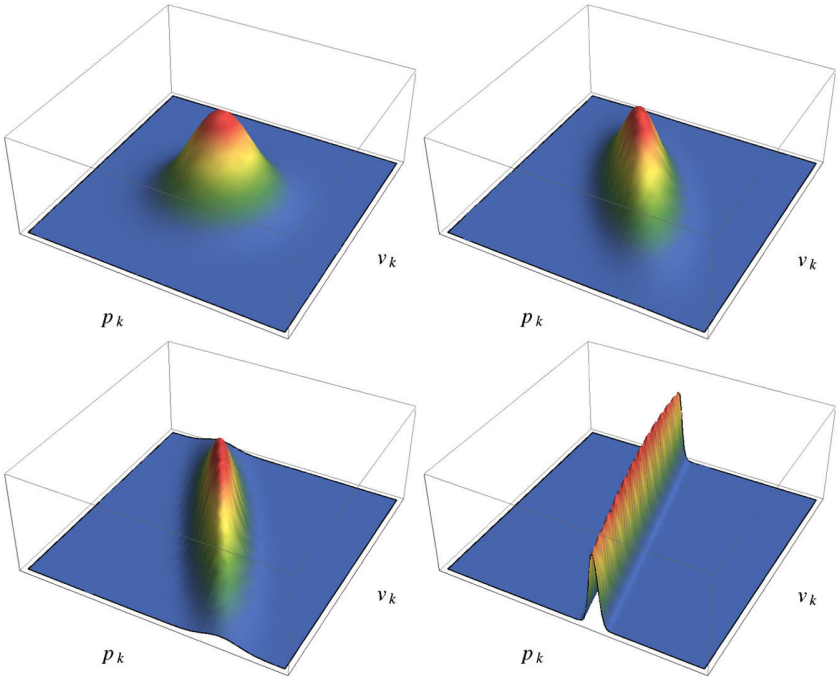

FIG. 1 (color online). Wigner function of a squeezed quantum state at different times during inflation. Only the two-dimensional function corresponding to the set of variables $(v_k^{\mathrm{R}}, p_k^{\mathrm{R}})$ has been represented, see Eq. (81). The time evolution of $\Re\mathrm{e}\Omega_k$ and $\Im\mathrm{m}\Omega_k$ has been expressed in terms of the two squeezing parameters r_k and ϕ_k. These ones are given by the solutions (65) and (66). The left upper panel corresponds to $r_{\mathrm{k}} = 0.0005$ and the corresponding state is almost a coherent one. The right upper panel corresponds to $r_k = 0.48$, the left bottom one to $r_k = 0.88$ and, finally, the right bottom one to $r_k = 2.31$. The effect of the squeezing and the cigar shape of Eq. (82) are clearly visible.

Obviously, one would have obtained exactly the same expression except that all the Ω_k terms would have been replaced with $\bar{\Omega}_k$ and $p_k^{\mathrm{R,I}}$ with $\pi_k^{\mathrm{R,I}}$. In particular, this means that the term in parenthesis in the argument of the exponentials would have read $\pi_k^{\mathrm{R,I}} + 2\Im\mathrm{m}\bar{\Omega}_k v_k^{\mathrm{R,I}}$. But, thanks to Eqs. (72) and (73), this is precisely $p_k^{\mathrm{R,I}} + 2\Im\mathrm{m}\Omega_k v_k^{\mathrm{R,I}}$ since the two terms proportional to a'/a exactly cancel out. This is of course related to the fact that the Wigner function is invariant under a canonical transformation.

The Wigner function (81) is represented in Fig. 1 at different times or, equivalently, at different values of r_k ($r_k = 0.0005$, 0.48, 0.88 and 2.31). The effect of the strong squeezing is clearly visible. Initially, in the sub-Hubble regime, r_k is small and the Wigner function is peaked over a small region in phase space. As inflation proceeds, the modes become super Hubble and r_k increases. As a consequence, the Wigner function spreads and acquires a cigar shape typical of squeezed states. In fact, in the strong squeezing limit, one has $\Re\mathrm{e}\bar{\Omega}_k \to 0$ and $\Im\mathrm{m}\bar{\Omega}_k \to k\sin\phi_k/(2\cos\phi_k) \to 0$, see Eqs. (63) and (64). Let us notice in passing that this last equation is consistent with Eq. (54). On the other hand, if one considers $\Im\mathrm{m}\bar{\Omega}_k$, then the leading term $a'/(2a)$ is absent and one has to go to the next order in Eq. (64). This one is given by $k/[4(\beta+3/2)](-k\eta)$ and represents the leading term of $\Im\mathrm{m}\bar{\Omega}_k$. It goes to zero in agreement with the fact that $\phi_k \to 0$ in the strong squeezing limit. In this regime, the Wigner function can be written as

$$W(v_k^{\mathrm{R}}, v_k^{\mathrm{I}}, p_k^{\mathrm{R}}, p_k^{\mathrm{I}}) \to \Psi\Psi^* \delta\left(p_k^{\mathrm{R}} + k\frac{\sin\phi_k}{\cos\phi_k} v_k^{\mathrm{R}}\right) \times \delta\left(p_k^{\mathrm{I}} + k\frac{\sin\phi_k}{\cos\phi_k} v_k^{\mathrm{I}}\right). \tag{82}$$

This last equation represents the mathematical formulation of the cigar shape mentioned above.

It is important to notice that the behavior described above is very different from the behavior of the Wigner function of a coherent state. The coherent states are usually considered as the "most classical" states and their Wigner function is given by

$$W(v_k^{\mathrm{R}}, p_k^{\mathrm{R}}) = \frac{1}{\pi}\, \mathrm{e}^{-k[v_k^{\mathrm{R}} - v_k^{\mathrm{R,cl}}(\eta)]^2}\, \mathrm{e}^{-[p_k^{\mathrm{R}} - p_k^{\mathrm{R,cl}}(\eta)]^2/k}, \tag{83}$$

where $v_k^{\mathrm{R,cl}}$ and $p_k^{\mathrm{R,cl}}$ represent the classical solutions. The typical shape is plotted in Fig. 2. One sees that the Wigner functions remain peaked over a small region in phase space and that this packet follows the classical trajectory (an ellipse in this context). Comparing Figs. 1 and 2, we understand why a coherent state is usually considered as classical while a squeezed state is considered as highly nonclassical. In the case of the coherent state, if one is given, say, the value of v_k^{R}, then one obtains a value for the

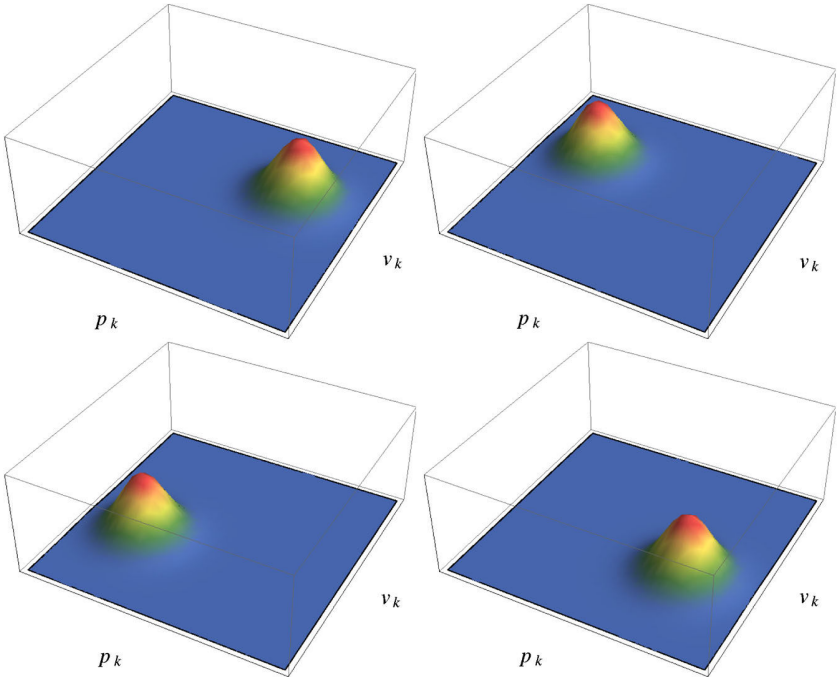

FIG. 2 (color online). Wigner function of a coherent state (83), represented at different times during inflation. Contrary to the Wigner function of a squeezed state of Fig. 1, the shape remains unchanged during the cosmological evolution. The Wigner function just follows the classical trajectory, an ellipse here since we deal with an harmonic oscillator. This justifies the fact that a coherent state can be viewed as the "most classical quantum state."

momentum, p_k^{R}, which is very close to the one we would have inferred in the classical case. This is of course due to the fact that the Wigner function follows the classical trajectory and has minimal spread around it in all phase space directions. On the contrary, in the case of the squeezed state, if one is given p_k^{R} then the value of v_k^{R} is very uncertain since the Wigner function is spread over a large region in phase space. Therefore, we conclude that the cosmological perturbations do not behave classically in the usual sense.

Given the previous discussion, it may seem relatively easy to observe genuine quantum effects in the CMB. Unfortunately this is not so, essentially because, in the strong squeezed limit, all quantum predictions can be in fact obtained from averages performed by mean of a classical stochastic process.

Let us first study how this question is usually treated. For this purpose, let us consider again the expectation of the operator $(\hat{\pi}_k^{\mathrm{R}})^2$ [of course, one could also treat the case of $(\hat{\pi}_k^{\mathrm{R}})^n$]. The quantum average is given by Eq. (69), namely

$$\langle\bar{\Psi}|(\hat{\pi}_k^{\mathrm{R}})^2|\bar{\Psi}\rangle = \Re\mathrm{e}\bar{\Omega}_k + \frac{(\Im\mathrm{m}\bar{\Omega}_k)^2}{\Re\mathrm{e}\bar{\Omega}_k}. \tag{84}$$

On the other hand, if one computes the quantity

$$\int \mathrm{d}v_k^{\mathrm{R}}\mathrm{d}\pi_k^{\mathrm{R}} W_{r_k\to\infty}(v_k^{\mathrm{R}}, \pi_k^{\mathrm{R}})(\pi_k^{\mathrm{R}})^2, \tag{85}$$

where $W_{r_k\to\infty}(v_k^{\mathrm{R}}, \pi_k^{\mathrm{R}})$ refers to the Wigner function in the strong squeezing limit (82), then one obtains $(\Im\mathrm{m}\bar{\Omega}_k)^2/\Re\mathrm{e}\bar{\Omega}_k$, which coincides with Eq. (84) in the limit $r_k \to \infty$. This result is often taken as a proof that a strongly squeezed state can be described as a classical stochastic process. However, this argument is not very convincing since it is a theorem [31] that the exact Wigner function [we stress again that, in Eq. (85), we have not used the general Wigner function but its limit when r_k is large] satisfies the following property:

$$\langle\hat{A}(\hat{v}_k^{\mathrm{R}}, \hat{\pi}_k^{\mathrm{R}})\rangle = \int \mathrm{d}v_k^{\mathrm{R}}\mathrm{d}\pi_k^{\mathrm{R}} W(v_k^{\mathrm{R}}, \pi_k^{\mathrm{R}})A(v_k^{\mathrm{R}}, \pi_k^{\mathrm{R}}), \tag{86}$$

where $\hat{A}$ is an arbitrary operator. Therefore, it does not come as a surprise that an expression like Eq. (85) reproduces the corresponding quantum average in the limit $r_k \to \infty$.

In fact, as was discussed in Refs. [34,39,110], what makes the situation so peculiar is something different. The point is that, in the limit $r_k \to \infty$, all the quantum predictions can be reproduced if one assumes that the system always followed classical laws but had random initial conditions with a given probably density function. This can be easily understood on the example of a free particle [34,39,110]. Let us assume that, initially (at $t = 0$), the probability to find the particle at x is given by

$$|\Psi(x, 0)|^2 = \sqrt{\frac{2}{\pi b^2}}\,\mathrm{e}^{-2x^2/b^2}, \tag{87}$$

where b is a parameter that characterizes the width of the distribution. At time t, this probability is given by

$$|\Psi(x,t)|^2 = \sqrt{\frac{2}{\pi b^2}}\frac{1}{\sqrt{1+4t^2/(m^2b^4)}} \times \exp\biggl[-\frac{2b^2(x-k_0t/m)^2}{b^4+4t^2/m^2}\biggr], \tag{88}$$

where m is the mass of the particle and k_0 the center of the Gaussian wave packet in Fourier space.

Now let us consider a situation where we repeat many times an experiment consisting in sending a classical particle from the origin with a velocity v (equivalently, instead of repeating the experiments many times, one could also consider an ensemble of classical particles) and detecting it at a position $x \neq 0$. By definition, the particle follows the laws of classical physics which means that its motion can be described by the equation: $x = vt$ (they all start from $x = 0$ at $t = 0$). Then, let us assume that the velocities are classical random variables with a probability distribution function given by

$$P(v) = \frac{1}{\sqrt{\pi}\Delta v}\,\mathrm{e}^{-v^2/(\Delta v)^2}. \tag{89}$$

This means that according to the particle considered, the velocity is in fact not always the same. But because different particles have different velocities, they will not reach the position x at the same time. It is important to stress that, here, only the initial conditions are random and that the trajectory is purely classical. From the above distribution, we can easily infer that the probability of finding a particle at x, at time t, is

$$P(x,t) = \frac{1}{\sqrt{\pi}t\Delta v}\,\mathrm{e}^{-(x-vt)^2/(t\Delta v)^2}. \tag{90}$$

This distribution is in fact exactly $|\Psi(x,t)|^2$ in the limit $t\to\infty$ provided we identify $v = k_0/m$ and $\Delta v = \sqrt{2}/(mb)$. Let us notice that this last relation is exactly what is obtained at the quantum level since x and v are conjugate variables. As a matter of fact, Eqs. (87) and (89) are Fourier transforms of each other. We conclude that, provided we detect the particles far from the origin, the quantum predictions for the particles can be completely mimicked by means of a classical stochastic process.

As discussed in Ref. [110], the situation is exactly similar for the inflationary perturbations. The limit $r_k \to \infty$ is in fact equivalent to the limit of large times in the example above. One can even calculate the Wigner function of the free particle described by the wave function (88) and show that it takes the same form as the one of Eq. (81). Therefore, the inflationary perturbations are said to be classical in the sense explained before: they can be described by a classical stochastic process. In practice, for instance, one can consider the $\hat{a}_{\ell m}$ in Eqs. (38) and (39) as classical random variables with probability density functions given by

$$P(a^{\mathrm{R}}_{\ell 0}) = \frac{1}{\sqrt{2\pi}C_\ell}\,\mathrm{e}^{-(a^{\mathrm{R}}_{\ell 0})^2/(2C_\ell)}, \tag{91}$$

$$P(a^{\mathrm{R}}_{\ell m}) = \frac{1}{\sqrt{\pi}C_\ell}\,\mathrm{e}^{-(a^{\mathrm{R}}_{\ell m})^2/C_\ell}, \qquad m \neq 0, \tag{92}$$

$$P(a^{\mathrm{I}}_{\ell m}) = \frac{1}{\sqrt{\pi}C_\ell}\,\mathrm{e}^{-(a^{\mathrm{I}}_{\ell m})^2/C_\ell}, \qquad m \neq 0. \tag{93}$$

Of course one can check that $\langle a^{\mathrm{R,I}}_{\ell m} a^{\mathrm{R,I}}_{\ell' m'}\rangle = C_\ell \delta_{\ell\ell'}\delta_{mm'}$ where, now, the bracket means a classical average calculated by means of the above distributions.

Finally, we conclude this section by a few words on the density matrix $\hat{\rho}^{\mathrm{R}}_k$. In fact, the density matrix is nothing but the Fourier transform of the Wigner function. Let us denote by $|v^{\mathrm{R}}_k\rangle$ the eigenstates of the operator $\hat{v}^{\mathrm{R}}_k$. Then, we have

$$\langle v^{\mathrm{R}\prime}_k|\hat{\rho}^{\mathrm{R}}_k|v^{\mathrm{R}}_k\rangle = \int_{-\infty}^{\infty}\mathrm{d}y\,\mathrm{e}^{iy(v^{\mathrm{R}\prime}_k - v^{\mathrm{R}}_k)}W\biggl(\frac{v^{\mathrm{R}\prime}_k + v^{\mathrm{R}}_k}{2}, y\biggr). \tag{94}$$

Upon using Eq. (81) in the above equation, one arrives at

$$\langle v^{\mathrm{R}\prime}_k|\hat{\rho}^{\mathrm{R}}_k|v^{\mathrm{R}}_k\rangle = \biggl(\frac{2\Re\mathrm{e}\Omega_k}{\pi}\biggr)^{1/2}\mathrm{e}^{-\Re\mathrm{e}\Omega_k[(v^{\mathrm{R}\prime}_k)^2+(v^{\mathrm{R}}_k)^2]} \times \mathrm{e}^{-i\Im\mathrm{m}\Omega_k[(v^{\mathrm{R}\prime}_k)^2-(v^{\mathrm{R}}_k)^2]}. \tag{95}$$

We notice that the off-diagonal terms, $v^{\mathrm{R}\prime}_k \neq v^{\mathrm{R}}_k$, oscillate very rapidly in the strong squeezing limit. This means that decoherence (defined as the disappearance of those off-diagonal terms) does not occur without taking into account an environment for the perturbations. Various discussions on what this environment may be can be found in Refs. [41–43].

C. Ergodicity

Let us now discuss how, in practice, we can check the predictions of the theory previously reviewed. Initially, the system is placed in an eigenstate of the Hamiltonian (the vacuum state) of Eq. (19), which can also be expressed as a superposition in the basis of the states $|v^{\mathrm{R}}_k\rangle$, namely

$$|\Psi\rangle = \int \mathrm{d}v^{\mathrm{R}}_k N_k(\eta)\,\mathrm{e}^{-\Omega_k(\eta)(v^{\mathrm{R}}_k)^2}|v^{\mathrm{R}}_k\rangle. \tag{96}$$

The corresponding mean value of the Hamiltonian operator can be expressed as

$$\langle\Psi|\mathcal{H}^{\mathrm{R}}_k|\Psi\rangle = \frac{1}{2}\Re\mathrm{e}\Omega_k + \frac{1}{2}\frac{(\Im\mathrm{m}\Omega_k)^2}{2\Re\mathrm{e}\Omega_k} + \frac{\omega^2}{2}\frac{1}{4\Re\mathrm{e}\Omega_k}. \tag{97}$$

Of course, initially $\Omega_k = k/2$ and the energy is nothing but $\omega/2$ as expected for the vacuum state.

In the real world, we measure the temperature anisotropies. As we have seen (and as is appropriate for an observable in the quantum-mechanical framework), this quantity is represented by an operator. According to Eq. (38), measuring the temperature anisotropies is equivalent to measuring the observables $\hat{a}_{\ell m}$ which, in turn, according to

Eq. (41), is equivalent to measuring the observables $\hat{\zeta}_{\boldsymbol{k}}$ or $\hat{v}_{\boldsymbol{k}}$ (that is to say $\hat{v}^{\mathrm{R}}_{\boldsymbol{k}}$ and $\hat{v}^{\mathrm{I}}_{\boldsymbol{k}}$).

According to the postulates of quantum mechanics, measuring the observable $\hat{v}^{\mathrm{R}}_{\boldsymbol{k}}$ gives an eigenvalue $v^{\mathrm{R}}_{\boldsymbol{k}}$ (no hat, it is a number) with probability $|\langle v^{\mathrm{R}}_{\boldsymbol{k}}|\Psi\rangle|^2$ and, immediately after this measurement, the system is placed in the eigenstate $|v^{\mathrm{R}}_{\boldsymbol{k}}\rangle$. More concretely, after the measurement, we "see" a specific CMB map and we say that the measurement has produced a specific "realization." The result is given in terms of coefficients $a_{\ell m}$ (again, no hat) expressed in terms of the numbers $v^{\mathrm{R}}_{\boldsymbol{k}}$ through Eq. (41) (except, of course, that this equation should now be used with no hat on both sides). Equivalently, we see a specific temperature pattern $\delta T(\boldsymbol{e})/T$ (no hat) corresponding to the set of numbers $a_{\ell m}$, see also Eq. (38). In conclusion, the CMB map observed, say, by the WMAP satellite corresponds to one measurement (or one realization) of the operator $\widehat{\delta T}(\boldsymbol{e})/T$.

Then comes the question of how one can operationally verify these theoretical predictions. In quantum mechanics, in an ordinary laboratory situation, one would check that the theory is correct by repeating the experiment many times. In this way, one would generate many realizations of $\hat{v}^{\mathrm{R}}_{\boldsymbol{k}}$ (or, equivalently, of $\hat{a}_{\ell m}$ or $\widehat{\delta T}/T$) i.e., one would obtain N_{real} numbers $v^{\mathrm{R}i}_{\boldsymbol{k}}$, $i = 1, \cdots, N_{\mathrm{real}}$ [or $a^i_{\ell m}$ or $(\delta T/T)^i$] where N_{real} is the number of realizations (that is to say the number of times the experiments have been performed). With these N_{real} CMB maps, one could then check that the $v^{\mathrm{R}i}_{\boldsymbol{k}}$ are indeed distributed with a Gaussian probability density function in agreement with Eq. (50) or, with the N_{real} sets of numbers $a^i_{\ell m}$, one could infer whether they follow Eqs. (91)–(93), determine the corresponding variance and check that it is given by the C_ℓ predicted by the theory. Let us notice that the above discussion is independent from the fact that the perturbations can be described classically or not. If we are in the classical limit (in the restricted sense defined in the previous section), then we showed that measuring the observable $\hat{a}_{\ell m}$ can be viewed as measuring a classical system with random initial conditions but this does not change the fact that we need many realizations to check that the probability density function predicted by the theory is the correct one.

Clearly, in cosmology, the program described above cannot be carried out because one cannot repeat the experiment many times since we are given only one CMB map [33]. How, then, can we check the predictions of the theory of cosmological perturbations? To discuss this question, let us be more accurate about the operator $\widehat{\delta T}/T(\boldsymbol{e})$. In the large-squeezing limit, we have seen that it can be viewed as a classical stochastic process and, therefore, it is convenient to write it as

$$\frac{\delta T}{T}(\xi, \boldsymbol{e}), \tag{98}$$

where the symbol ξ labels the realizations. A given realization of a stochastic process is a function of $\boldsymbol{e}$. By contrast, a given realization of a random variable is not a function but a number. This is for instance the case of $a_{\ell m}(\xi)$. The idea is then to replace ensemble averages by spatial averages (i.e., averages over different directions $\boldsymbol{e}$) [33]. If the process is ergodic, these two types of averages are equal [33]. In that case, one can check the predictions of the theory even if one has only one realization at our disposal. Unfortunately, one can also show that a stochastic process living on a sphere (here, of course, the celestial sphere) cannot be ergodic [33]. Therefore, we are left with the task of constructing unbiased estimators with minimal variances. For instance, let us assume that we have calculated the number C_ℓ in some inflationary scenario and that we would like to compare its value to an actual measurement. How would we proceed? We would consider the random variable $\mathcal{C}_\ell(\xi)$ defined by the following expression [33]:

$$\mathcal{C}_\ell(\xi) = \frac{1}{4\pi}\int_{S^2} \mathrm{d}\Omega_1 \mathrm{d}\Omega_2 P_\ell(\cos\delta_{12}) \frac{\delta T}{T}(\xi, \boldsymbol{e}_1)\frac{\delta T}{T}(\xi, \boldsymbol{e}_2), \tag{99}$$

where δ_{12} is the angle between the direction $\boldsymbol{e}_1$ and $\boldsymbol{e}_2$. As announced, the estimator $\mathcal{C}_\ell(\xi)$ is expressed as a spatial average of the stochastic process $\delta T/T$. It is easy to show that it is unbiased, $\langle\langle \mathcal{C}_\ell \rangle\rangle = C_\ell$ and has the minimum variance [33] (called the "cosmic variance") given by $\sqrt{2/(2\ell+1)}C_\ell$. The double brackets $\langle\langle\rangle\rangle$ mean an ensemble average, which amounts to a quantum average in the high squeezing limit as mentioned before. One should be careful that this ensemble average has nothing to do with the one introduced below (denoted $\mathbb{E}$) for the CSL modifications of the Schrödinger equation, since these two stochasticities have completely different natures, the former being effective and the later intrinsic.

In practice, we would proceed as follows. From our CMB map $\delta T(\xi, \boldsymbol{e})/T$, we compute the integral in Eq. (99) and this gives a number representing one realization of the estimator $\mathcal{C}_\ell$, the only one we can have access to. It is unlikely that this number will be C_ℓ because it is unlikely that one realization of a random variable will be exactly equal to the mean value of that variable. However, if the variance is small (i.e., if the estimator is good), the corresponding probability density function will be sharply peaked around the mean value and any realization will therefore be close to the mean (and, in our case, it is not possible to decrease the value of the variance since we work with the best estimator). Therefore, we can study where the number we have obtained by following the above described procedure falls, compared to the interval $C_\ell \pm \sqrt{2/(2\ell+1)}C_\ell$, where C_ℓ is the theoretically predicted multipole moment. Then, for instance, one can start a calculation of the χ^2 to assess to which confidence we have verified the theory. In fact, the cosmic variance can simply be seen as another source of error, besides those coming from the instruments.

Given the previous discussion, there is one issue that one can raise and which is the subject of the present paper. The

question is how a specific outcome (a realization) is produced. Above, we have just assumed that this happens without discussing this point. According to the postulates of quantum mechanics in the Copenhagen interpretation, this macro-objectification takes place when a measurement is performed. Since the CMB anisotropies were produced at a redshift of $z_{\ell\mathrm{ss}} \simeq 1100$, this means that it should have happened prior to that epoch (possibly during inflation itself). But, clearly, there was no observer at those early times. We face here the conventional measurement problem of quantum mechanics which is, in the context of cosmology, exacerbated.

IV. THE PEARLE-GHIRARDI-RIMINI-WEBER THEORY

A. A dynamical collapse model

Although one can manage to obtain, based on primordial vacuum quantum fluctuations, a set of correlation functions that are formally indistinguishable from a classical stochastic distribution, one still has to face the problem of reaching a specific realization before cosmological perturbations can start to grow in a classical way. This amounts to the question of the measurement problem in quantum mechanics, namely that there are two distinct evolution processes: the unitary and linear Schrödinger time evolution on the one hand, and the stochastic and nonlinear wave packet reduction on the other.

In what follows, we briefly present the collapse theories and explain how the Schrödinger equation can be modified in order to allow a dynamical description of the wave packet reduction. In fact, to be more precise, we shall restrict attention to the case of CSL [62,63,65,67].

The CSL model relies on the idea that an extra stochastic behavior should be added to the Schrödinger linear evolution, encoded through a Wiener process W_t, whose differential acts as a random square root of that of time, namely

$$\mathbb{E}(\mathrm{d}W_t) = 0, \quad \text{and} \quad \mathbb{E}(\mathrm{d}W_t \mathrm{d}W_{t'}) = \delta(t - t')\mathrm{d}t^2, \tag{100}$$

where $\mathbb{E}$ stands for an ensemble average. One then expands the state vector variation $\mathrm{d}|\chi\rangle$ up to first order in time through

$$\mathrm{d}|\chi\rangle = (\hat{A}\mathrm{d}t + \hat{B}\mathrm{d}W_t)|\chi\rangle, \tag{101}$$

where $\hat{A}$ and $\hat{B}$ are operators acting on the Hilbert space of available states. One then demands that, on average, the wave function will be normalized, i.e.,

$$\mathbb{E}(\langle\chi|\chi\rangle) = 1 \Rightarrow \mathbb{E}[\mathrm{d}(\langle\chi|\chi\rangle)] = 0, \tag{102}$$

which, upon using Itô calculus[3] for the differentials and Eq. (100), yields

$$\hat{A}^\dagger + \hat{A} = -\hat{B}^\dagger\hat{B}, \tag{103}$$

since the state $|\chi\rangle$ is arbitrary. The general solution of Eq. (103) is $\hat{A} = -i\hat{H} - \frac{1}{2}\hat{B}^\dagger\hat{B}$, where $\hat{H}$ is Hermitian and to be identified with the Hamiltonian leading to the usual Schrödinger dynamics.

In order to assign a probabilistic meaning to the norm of the wave function, it should be normalized. However, according to Eq. (101), although this is true on average, it varies stochastically according to

$$\mathrm{d}\||\chi\||^2 = \langle\chi|(\hat{B} + \hat{B}^\dagger)|\chi\rangle\mathrm{d}W_t = 2\langle\chi|\hat{B}|\chi\rangle\mathrm{d}W_t, \tag{104}$$

where from now on we assume that $\hat{B}$ is Hermitian.

Equation (104) implies that the state $|\chi\rangle$ is not normalized, and one can define a normalized one whose probability distribution will thus be interpretable in terms of measurements. We then set

$$|\psi\rangle \equiv \frac{|\chi\rangle}{\||\chi\||}, \tag{105}$$

whose dynamics can be computed using the previously derived rules. One finds

$$\mathrm{d}|\psi\rangle = \left\{\left[-i\hat{H} - \frac{1}{2}(\hat{B} - \langle\hat{B}\rangle)^2\right]\mathrm{d}t + (\hat{B} - \langle\hat{B}\rangle)\mathrm{d}W_t\right\}|\psi\rangle, \tag{106}$$

where the quantum expectation value is taken on the normalized state vector and thus defined as

$$\langle\hat{B}\rangle \equiv \langle\psi|\hat{B}|\psi\rangle. \tag{107}$$

The operator $\hat{B}$ can be decomposed as $\hat{B} = \sqrt{\gamma}\hat{Q}$. The coupling constant γ is the product of the localization rate with the width of the Gaussian wave function inducing the localizations [62], and sets the strength of the nonlinear effects and therefore the characteristic time scale over which these are measurable. The observable $\hat{Q}$, for instance the position operator, is the basis on which the states are to spontaneously collapse to (in the following, we also call the operator $\hat{Q}$, the "collapse operator").

As it turns out, and this is exemplified later in the case where the operator $\hat{Q}$ is identified with a cosmological perturbation Fourier mode (see Sec. V A), the natural evolution of Eq. (106) is to project an initial state $|\psi_0\rangle$ on an eigenstate $|\alpha\rangle$ of the operator $\hat{Q}$ setting

$$\hat{Q} = \sum_\alpha q_\alpha|\alpha\rangle\langle\alpha|, \tag{108}$$

(the sum being replaced by an integral in the case of a continuous spectrum for $\hat{Q}$) such that $\hat{Q}|\alpha\rangle = q_\alpha|\alpha\rangle$, one finds that $\lim_{t\to\infty}|\Psi(t)\rangle = |\alpha\rangle$ for a given value of α, and this with a probability $P(\alpha) = |\langle\Psi|\alpha\rangle|^2$. In other words, the Born rule is naturally implemented as a dynamical consequence instead of being imposed as an extra hypothesis.

[3]This means that for two functions f and g of the stochastic variable W, one has $\mathrm{d}(fg) = f\mathrm{d}g + (\mathrm{d}f)g + \mathbb{E}[(\mathrm{d}f)(\mathrm{d}g)]$ and $\mathrm{d}f(W) = f'(W)\mathrm{d}W + \frac{1}{2}f''(W)\mathbb{E}[(\mathrm{d}W)^2]$, where a prime stands for ordinary derivative with respect to the argument W. It is necessary to expand up to second order in the noise because Eq. (100) means $\mathbb{E}(\mathrm{d}W_t^2) = \mathrm{d}t$.

Finally, defining the density operator as

$$\hat{\rho} \equiv \mathbb{E}(|\Psi\rangle\langle\Psi|), \tag{109}$$

one obtains, using Eq. (106) the so-called Lindblad equation, namely

$$\frac{\mathrm{d}\hat{\rho}}{\mathrm{d}t} = -i[\hat{H}, \hat{\rho}] - \frac{\gamma}{2}[\hat{Q}, [\hat{Q}, \hat{\rho}]], \tag{110}$$

providing its time development.

Let us now come to another very important aspect of the CSL theory and describe the so-called "amplification mechanism" which enables one to understand why the dynamics of microscopic systems is not much altered by the extra stochastic and nonlinear terms in Eq. (106). This is phenomenologically very important since this means that the laboratory experiments performed on "small" quantum systems are still accurately predicted by the standard Schrödinger equation while the macroscopic objects are quickly and efficiently localized. Let us consider an ensemble of N identical particles, assuming that, for each of them, the collapse operator is the physical position in space. Therefore, we can identify the operator and Wiener processes according to

$$\hat{B} \rightarrow \sqrt{\gamma}\sum_{i=1}^{N}\hat{x}_i \quad \text{and} \quad \mathrm{d}W_t \rightarrow \mathrm{d}W_t^{(i)} \tag{111}$$

in Eq. (106), with $\hat{x}_i$ the position operator for the ith particle. Note that in this case, one has as many independent Wiener processes as there are particles; they satisfy

$$\mathbb{E}[\mathrm{d}W_t^{(i)}\mathrm{d}W_{t'}^{(j)}] = \delta^{ij}\delta(t-t')\mathrm{d}t^2. \tag{112}$$

This naturally generalizes Eq. (106) to a set of operators and particles on which to project the relevant states.

We now assume that one can decompose the total wave vector $|\Psi\rangle$ in the form

$$|\Psi(\{x_i\})\rangle = |\Psi_{\mathrm{CM}}(R)\rangle \otimes |\Psi_{\mathrm{rel}}(\{r_i\})\rangle, \tag{113}$$

where the total wave function depends on the set of all of the position operators $\{x_i\}$, while the "macroscopic" part of it, $|\Psi_{\mathrm{CM}}\rangle$, depends only on the position $R \equiv N^{-1}\sum_i x_i$ of the center of mass, and the rest is a function only of the relative coordinates r_i defined through $x_i = R + r_i$.

Using Itô calculus to evaluate the differential of the tensor product in Eq. (113), it is easily checked that $|\Psi(\{x_i\})\rangle$ satisfies Eq. (106) with $\hat{B}$ and dW_t given by Eq. (111) if the components of the product respectively satisfy

$$\mathrm{d}\,|\Psi_{\mathrm{CM}}(R)\rangle = \left\{\left[-i\hat{H}_{\mathrm{CM}} - \frac{\gamma_{\mathrm{CM}}}{2}(\hat{R} - \langle\hat{R}\rangle)^2\right]\mathrm{d}t + \sqrt{\gamma_{\mathrm{CM}}}(\hat{R} - \langle\hat{R}\rangle)dW_t\right\}|\Psi_{\mathrm{CM}}(R)\rangle, \tag{114}$$

and

$$\mathrm{d}\,|\Psi_{\mathrm{rel}}(\{r_i\})\rangle = \left\{\left[-i\hat{H}_{\mathrm{rel}} - \frac{\gamma}{2}\sum_{i=1}^{N-1}(\hat{r}_i - \langle\hat{r}_i\rangle)^2\right]\mathrm{d}t + \sqrt{\gamma}\sum_{i=1}^{N-1}(\hat{r}_i - \langle\hat{r}_i\rangle)\mathrm{d}W_t^{(i)}\right\}|\Psi_{\mathrm{rel}}(\{r_i\})\rangle, \tag{115}$$

where we have assumed the total Hamiltonian could be split into $\hat{H} = \hat{H}_{\mathrm{CM}}(\hat{R}) + \hat{H}_{\mathrm{rel}}(\{\hat{r}_i\})$ and the new constant γ_{CM} appearing in Eq. (114) is given by $\gamma_{\mathrm{CM}} = N\gamma$. This illustrates the mechanism thanks to which localization is amplified for a macroscopic object containing a large number (in practice $N \sim 10^{23} \gg 1$ for usual classical systems) of particles, while the usual quantum spread is mostly conserved for the internal degrees of freedom. A recent inventory of all the constraints derived so far in various physical situations on the CSL parameter γ can be found in Ref. [111].

B. An illustrative example: The harmonic oscillator

In this section, we illustrate how the CSL theory works on the example of the harmonic oscillator, resetting the Planck constant $\hbar$ for easier comparison with previous works. This is an interesting case because it represents the prototypical example of a quantum system and, to our knowledge, this case has not been solved explicitly in the case of the CSL theory. Moreover, in cosmology, as explained before, we deal with a parametric oscillator, a case which shares some similarities with an harmonic oscillator, at least in some regimes. It is therefore important to understand first this simplest case in the CSL framework. In the following, we assume that the operator $\hat{B}$ introduced in the previous section is the position operator $\hat{x}$. As a consequence, the modified Schrödinger equation can be written as

$$\mathrm{d}\,\Psi = \left[-\frac{i}{\hbar}\hat{H}\mathrm{d}t + \sqrt{\gamma}(\hat{x} - \langle\hat{x}\rangle)\mathrm{d}W_t - \frac{\gamma}{2}(\hat{x} - \langle\hat{x}\rangle)^2\mathrm{d}t\right]\Psi, \tag{116}$$

where $\hat{H} = \hat{p}^2/(2m) + m\omega^2\hat{x}^2/2$ is the Hamiltonian. The parameter γ sets the strength of the collapse mechanism and, since we have chosen the position as the preferred basis, it has dimension $L^{-2} \times T^{-1}$. Following Ref. [73], the wave function can be taken as a Gaussian state and the most general form can be expressed as

$$\Psi(t, x) = |N(t)|\exp\{-\Re\mathrm{e}\Omega(t)[x - \bar{x}(t)]^2 + i\sigma(t) + i\chi(t)x - i\Im\mathrm{m}\Omega(t)x^2\}, \tag{117}$$

where, *a priori*, $|N|$, $\Re\mathrm{e}\Omega$, $\bar{x}$, σ, χ and $\Im\mathrm{m}\Omega$ are real stochastic variables. Introducing this wave function in Eq. (118), one obtains the following set of equations:

$$\frac{|N|'}{|N|} = \frac{1}{4}\frac{(\Re\mathrm{e}\Omega)'}{\Re\mathrm{e}\Omega} = \frac{\hbar}{m}\Im\mathrm{m}\Omega + \frac{\gamma}{4\Re\mathrm{e}\Omega}, \tag{118}$$

$$(\Re\mathrm{e}\Omega)' = \gamma + 4\frac{\hbar}{m}(\Re\mathrm{e}\Omega)(\Im\mathrm{m}\Omega), \tag{119}$$

$$(\Im\mathrm{m}\Omega)' = -\frac{\hbar}{m}[2(\Re\mathrm{e}\Omega)^2 - 2(\Im\mathrm{m}\Omega)^2] + \frac{m}{\hbar}\frac{\omega^2}{2}, \tag{120}$$

$$\bar{x}' = \frac{\hbar}{m}[\chi - 2(\Im\mathrm{m}\Omega)\bar{x}] + \frac{\sqrt{\gamma}}{2\Re\mathrm{e}\Omega}\frac{\mathrm{d}W_t}{\mathrm{d}t}, \tag{121}$$

$$\sigma' = \frac{\hbar}{m}\left[-\Re\mathrm{e}\Omega + 2(\Re\mathrm{e}\Omega)^2\bar{x}^2 - \frac{1}{2}\chi^2\right], \tag{122}$$

$$\chi' = -\frac{\hbar}{m}[4(\Re\mathrm{e}\Omega)^2\bar{x} - 2\chi\Im\mathrm{m}\Omega], \tag{123}$$

where a prime means a derivative with respect to time. We see that the first equation can be integrated to give $|N| = (2\Re\mathrm{e}\Omega/\pi)^{1/4}$, which ensures that the wave function is properly normalized. Then, the two following equations, Eqs. (119) and (120) "decouple" from the other equations and can be integrated separately. In particular, if we add them up, we arrive at

$$\Omega' = -2i\frac{\hbar}{m}\Omega^2 + \gamma + \frac{im}{2\hbar}\omega^2. \tag{124}$$

This equation should be compared to Eq. (21). As expected, they are identical provided we take $\hbar = m = 1$ and $\gamma = 0$. Of course, in the present case, the frequency ω is constant since we deal with a harmonic oscillator rather than a parametric oscillator as is the case for cosmological perturbations. Equation (124) is a Ricatti equation and we have already seen that the appropriate change of variable to transform it into a linear second order differential equation is $\Omega = -imf'/(2\hbar f)$, where the function $f(t)$ obeys the equation

$$f'' + \left(\omega^2 - 2i\frac{\hbar}{m}\gamma\right)f = 0. \tag{125}$$

This equation admits simple solutions that can be expressed in terms of exponentials, namely $f(t) \propto \exp(\pm\alpha t)$ where α is defined by

$$\alpha \equiv \sqrt{\frac{2i\gamma\hbar}{m} - \omega^2}. \tag{126}$$

As a consequence, the solution for $\Omega(t)$ can be written as

$$\Omega(t) = -\frac{im}{2\hbar}\alpha\tanh(\alpha t + \phi), \tag{127}$$

where ϕ is an integration constant that can be expressed in terms of the initial value of the function $\Omega(t)$

$$\phi = \mathrm{argtanh}\left[-\frac{2\hbar}{im}\frac{\Omega(t=0)}{\alpha}\right]. \tag{128}$$

This solution resembles the formula obtained in the case of the free particle, see Ref. [73].

At this stage, we need to discuss the initial conditions. Our assumption is that, at $t = 0$, the quantum state is simply given by the ground state of the harmonic oscillator in conventional quantum mechanics. Technically, this means that we require the wave function to be

$$\Psi(t=0,x) = \left(\frac{m\omega}{\pi\hbar}\right)^{1/4}\mathrm{e}^{-m\omega x^2/(2\hbar)}, \tag{129}$$

which implies that $\Re\mathrm{e}\Omega = m\omega/(2\hbar)$ and $\Im\mathrm{m}\Omega = 0$ or, equivalently, $\phi = \mathrm{argtanh}(i\omega/\alpha)$. Notice that this choice is fully compatible with the normalization established above, $|N| = (2\Re\mathrm{e}\Omega/\pi)^{1/4}$. Of course, our choice also amounts to imposing $\bar{x}(t=0) = \sigma(t=0) = \chi(t=0) = 0$.

Since the evolution of the stochastic wave function is controlled by the function $\Omega(t)$, it is interesting to study how it evolves with time. Writing the number α as $\alpha \equiv \alpha^{\mathrm{R}} + i\alpha^{\mathrm{I}}$, where it is easy to show that

$$\alpha^{\mathrm{R}} = \frac{\omega}{\sqrt{2}}\left(\sqrt{1 + 4\frac{\hbar^2\gamma^2}{m^2\omega^4}} - 1\right)^{1/2}, \tag{130}$$

$$\alpha^{\mathrm{I}} = \frac{\sqrt{2}}{\omega}\frac{\hbar\gamma}{m}\left(\sqrt{1 + 4\frac{\hbar^2\gamma^2}{m^2\omega^4}} - 1\right)^{-1/2}, \tag{131}$$

and $\phi \equiv \phi^{\mathrm{R}} + i\phi^{\mathrm{I}}$, straightforward algebraic manipulations lead to the following expressions for $\Re\mathrm{e}\Omega$ and $\Im\mathrm{m}\Omega$:

$$\Re\mathrm{e}\Omega(t) = \frac{m}{2\hbar}\frac{\alpha^{\mathrm{I}}\sinh[2(\alpha^{\mathrm{R}}t + \phi^{\mathrm{R}})] + \alpha^{\mathrm{R}}\sin[2(\alpha^{\mathrm{I}}t + \phi^{\mathrm{I}})]}{\cos[2(\alpha^{\mathrm{I}}t + \phi^{\mathrm{I}})] + \cosh[2(\alpha^{\mathrm{R}}t + \phi^{\mathrm{R}})]}, \tag{132}$$

$$\Im\mathrm{m}\Omega(t) = \frac{m}{2\hbar}\frac{\alpha^{\mathrm{I}}\sin[2(\alpha^{\mathrm{I}}t + \phi^{\mathrm{I}})] - \alpha^{\mathrm{R}}\sinh[2(\alpha^{\mathrm{R}}t + \phi^{\mathrm{R}})]}{\cos[2(\alpha^{\mathrm{I}}t + \phi^{\mathrm{I}})] + \cosh[2(\alpha^{\mathrm{R}}t + \phi^{\mathrm{R}})]}. \tag{133}$$

In particular, the function $\Re\mathrm{e}\Omega(t)$, with the initial condition specified above, is always positive. Notice also that there is a sign ambiguity in the definitions of the quantities α^{R} and α^{I} in Eqs. (130) and (131), but one can show that this does not affect the physical predictions of the model. It is also interesting to calculate the limit for large times of the two functions in Eqs. (132) and (133). One obtains

$$\lim_{t\to\infty}\Re\mathrm{e}\Omega = \frac{m\alpha^{\mathrm{I}}}{2\hbar} \simeq \frac{m\omega}{2\hbar}\left(1 + \frac{1}{2}\frac{\hbar^2\gamma^2}{m^2\omega^4} + \cdots\right), \tag{134}$$

$$\lim_{t\to+\infty}\Im\mathrm{m}\Omega = -\frac{m\alpha^{\mathrm{R}}}{2\hbar} \simeq -\frac{\gamma}{2\omega}\left(1 - \frac{1}{2}\frac{\hbar^2\gamma^2}{m^2\omega^4} + \cdots\right), \tag{135}$$

where the dots indicate an expansion in the small dimensionless parameter $\hbar\gamma/(m\omega^2)$. We see that, if $\gamma = 0$, we obtain the ground state given by Eq. (129). Deviations from that solution are controlled by the parameter $\hbar\gamma/(m\omega^2)$.

We are now in a position where one can investigate the physical properties of the quantum state (117). In particular, it is easy to show that $\langle\hat{x}\rangle = \bar{x}$ and $\langle\hat{p}\rangle = \chi - 2(\Im\mathrm{m}\Omega)\bar{x}$. Initially, $\bar{x} = 0$ and the position operator has a

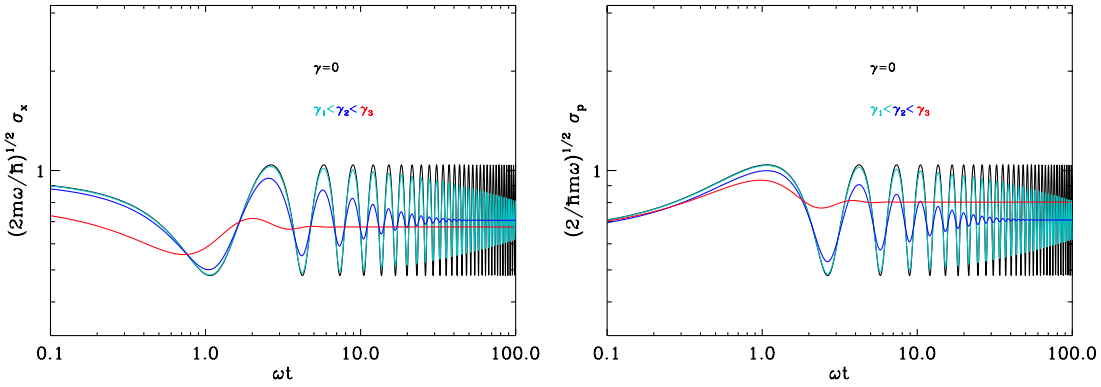

FIG. 3 (color online). Spread in position and momentum for different values of γ in the case of the harmonic oscillator; see Eq. (138). The conventional Schrödinger evolution corresponds to $\gamma = 0$ and is represented by the black curve which oscillates with constant amplitude. On the contrary, when the collapse mechanism is turned on, the oscillations are damped (blue and red curves), the spreads tend toward a constant value and localization occurs.

vanishing mean value as expected for the ground state of the harmonic oscillator but, at later times, due to the stochastic evolution of the wave function, it acquires a nonzero value. It is also possible to calculate the spread in position and momentum. One obtains

$$\sigma_x \equiv \sqrt{\langle \hat{x}^2 \rangle - \langle \hat{x} \rangle^2} = \frac{1}{2} \frac{1}{\sqrt{\Re\mathrm{e}\Omega}}, \tag{136}$$

$$\sigma_p \equiv \sqrt{\langle \hat{p}^2 \rangle - \langle \hat{p} \rangle^2} = \hbar \sqrt{\frac{(\Re\mathrm{e}\Omega)^2 + (\Im\mathrm{m}\Omega)^2}{\Re\mathrm{e}\Omega}}. \tag{137}$$

We see that these quantities only depend on $\Re\mathrm{e}\Omega$ and $\Im\mathrm{m}\Omega$. As a consequence, inserting Eqs. (132) and (133) in the above expressions of σ_x and σ_p, one arrives at

$$\sigma_x = \sqrt{\frac{\hbar}{2m}} \sqrt{\frac{\cosh[2(\alpha^{\mathrm{I}} t + \phi^{\mathrm{I}})] + \cosh[2(\alpha^{\mathrm{R}} t + \phi^{\mathrm{R}})]}{\alpha^{\mathrm{I}} \sinh[2(\alpha^{\mathrm{R}} t + \phi^{\mathrm{R}})] + \alpha^{\mathrm{R}} \sin[2(\alpha^{\mathrm{I}} t + \phi^{\mathrm{I}})]}},$$

$$\sigma_p = \sqrt{\frac{m\hbar}{2}} \sqrt{(\alpha^{\mathrm{R}})^2 + (\alpha^{\mathrm{I}})^2} \times \sqrt{\frac{\cosh[2(\alpha^{\mathrm{R}} t + \phi^{\mathrm{R}})] - \cos[2(\alpha^{\mathrm{I}} t + \phi^{\mathrm{I}})]}{\alpha^{\mathrm{I}} \sinh[2(\alpha^{\mathrm{R}} t + \phi^{\mathrm{R}})] + \alpha^{\mathrm{R}} \sin[2(\alpha^{\mathrm{I}} t + \phi^{\mathrm{I}})]}}. \tag{138}$$

The time evolution of these quantities is displayed in Fig. 3. The black curves correspond to the conventional Schrödinger evolution, i.e., the case $\gamma = 0$. They show the usual oscillatory behavior. On the contrary, when $\gamma \neq 0$, we see that the oscillations are damped (see the smaller amplitude decaying red and blue curves). Then, the spreads converge towards a constant value, which only depends on γ, ω and m. This value is easy to evaluate and one finds

$$\lim_{t\to\infty} \sigma_x = \frac{1}{2^{3/4}} \sqrt{\frac{\omega}{\gamma}} \left(\sqrt{1 + 4\frac{\hbar^2\gamma^2}{m^2\omega^4}} - 1 \right)^{1/4}, \tag{139}$$

$$\lim_{t\to\infty} \sigma_p = m\omega \left(1 + 4\frac{\hbar^2\gamma^2}{m^2\omega^4} \right)^{1/4} \times \lim_{t\to\infty} \sigma_x. \tag{140}$$

From these formulas one can see that the spread in position at infinity decreases with γ, from $\sqrt{\hbar/(2m\omega)}$ for $\gamma = 0$ to 0 for $\gamma \to \infty$. We see that the modified Schrödinger equation, as expected, implies a localization in position. We also notice that the microscopic behavior of the system is altered by the nonlinear and stochastic terms added to the theory. By contrast, in order to satisfy the Heisenberg uncertainty relation, the spread in momentum increases with γ, from $\sqrt{m\omega\hbar/2}$ for $\gamma = 0$ to infinity for $\gamma \to \infty$. For $\gamma = 0$ and at large times, one finds that the Heisenberg relation is saturated, $\sigma_x\sigma_p = \hbar/2$, as appropriate for a coherent state. In the limit $\gamma \to \infty$, one finds a larger value $\sigma_x\sigma_p = \hbar/\sqrt{2}$. Let us also remark that an exact eigenstate of the operator $\hat{x}$ is given by a Dirac function $\delta(x - \bar{x})$ centered at some value $\bar{x}$. On the other hand, we see that adding nonlinear and stochastic terms results in a spreading of the Dirac function into a Gaussian wave function with a finite width decreasing for increasing γ. Therefore, the modified Schrödinger equation does not exactly lead to an eigenstate of the position operator. In fact, the asymptotic value of σ_x obtained above defines the "precision" of the collapse and characterizes how close to an eigenstate of the collapse operator the final state is. In that sense, since σ_x decreases with γ, the bigger γ, the more "precise" the collapse.

To conclude this section, it is also interesting to calculate the time derivative of the quantum mean value of the Hamiltonian operator. One obtains

$$\frac{\mathrm{d}\langle \hat{H} \rangle}{\mathrm{d}t} = \frac{\hbar^2}{2m}\gamma - \frac{\hbar}{m}\sqrt{\gamma}\frac{\Im\mathrm{m}\Omega}{\Re\mathrm{e}\Omega}\langle \hat{p} \rangle \frac{\mathrm{d}W_t}{\mathrm{d}t} + \frac{1}{2}m\omega^2\langle \hat{x} \rangle \frac{\sqrt{\gamma}}{\Re\mathrm{e}\Omega}\frac{\mathrm{d}W_t}{\mathrm{d}t}. \tag{141}$$

This equation implies that

$$\frac{\mathrm{d}\mathbb{E}[\langle\hat{H}\rangle]}{\mathrm{d}t} = \frac{\hbar^2}{2m}\gamma. \tag{142}$$

As is well know, this formula expresses the nonconservation of energy in the CSL theory. From a phenomenological point of view, this increase of energy is usually so small (given the values of γ usually considered) that it cannot be detected. Put differently, the nonconservation of energy in the CSL theory cannot be used to rule out this theory [68].

V. THE INFLATIONARY CSL THEORY

The dynamical collapse model of the previous sections should apply to any quantum system, and hence in particular to cosmological perturbations as they arise from vacuum fluctuations. Spontaneously collapsing these happens to be a tremendously complicated task for many reasons discussed below, so in what follows, we suggest a much simplified modeling method which we then apply to the inflationary situation.

A. The modified Schrödinger equation for the Mukhanov-Sasaki variable

The first obvious problem one encounters when dealing with quantum cosmological perturbations is that the underlying theory ought to be relativistic. The straightforward relativistic generalization of the CSL model for quantum field theory, starting with the action (6) in the Tomonaga picture for instance, leads to unremovable divergences [65] (see however Ref. [69]), even more so when nonlinearities inherent to general relativity are taken into account.

The second option which happens to lead to a model in which calculations are actually possible consists in noting, as mentioned earlier in Sec. II D, that the spectrum of primordial perturbations depends on the wave number $\boldsymbol{k}$. In other words, once the Fourier spectrum is known, all of the observable quantities related with the CMB can be computed and compared with actual data. This means that mere knowledge of the modes $\hat{v}_{\boldsymbol{k}}$ ought to be enough in order for a complete description of the possible observations to be realized.

We shall therefore accordingly assume in what follows that the modified Schrödinger equation of motion for the wave function will be done at the level of the Fourier mode $\Psi_{\boldsymbol{k}}$, with spontaneous localization on the $\hat{v}_{\boldsymbol{k}}$ eigenmanifolds. This is consistent with previous approaches aimed at studying decoherence of cosmological perturbations where the pointer basis is often assumed to be precisely the Mukhanov-Sasaki operators, see Ref. [38]. Separating as before into real and imaginary parts, we shall thus assume the following basic equation:

$$\begin{aligned}\mathrm{d}\Psi^{\mathrm{R}}_{\boldsymbol{k}} = \Big[&-i\hat{\mathcal{H}}^{\mathrm{R}}_{\boldsymbol{k}}\mathrm{d}\eta + \sqrt{\gamma}(\hat{v}^{\mathrm{R}}_{\boldsymbol{k}} - \langle\hat{v}^{\mathrm{R}}_{\boldsymbol{k}}\rangle)\mathrm{d}W_\eta \\ &- \frac{\gamma}{2}(\hat{v}^{\mathrm{R}}_{\boldsymbol{k}} - \langle\hat{v}^{\mathrm{R}}_{\boldsymbol{k}}\rangle)^2\mathrm{d}\eta\Big]\Psi^{\mathrm{R}}_{\boldsymbol{k}},\end{aligned} \tag{143}$$

and a similar equation for $\Psi^{\mathrm{I}}_{\boldsymbol{k}}$. Here, the quantity γ is a positive constant with mass dimension 2 if the scale factor is chosen to be dimensionless but is dimensionless if the scale factor is chosen to have mass dimension -1, which is the convention adopted here. As in Sec. IV, the parameter γ sets the strength of the collapse mechanism.

Let us now review all the limitations of postulating an ansatz equation such as Eq. (143). First, one should note that the constant γ in Eq. (143) cannot be the same as the one associated with the choice of the position operator as the collapse operator appearing in Eq. (116), despite our choice of the same notation. It is clear that each time one considers different collapse operators, this leads to different CSL parameters with different mass dimension. The same phenomenon is observed in Ref. [70] where the collapse operator is chosen to be a spin operator. In this case, it is clear that the corresponding CSL parameter cannot be the same as the one corresponding to the case where the collapse operator is the position (as it is for the case of the free particle [73]). This is unfortunate when it comes to a comparison of the constraints obtained in the laboratory with the constraints obtained in cosmology. In fact, what could be done is to consider the strict CSL theory where the collapse operator is usually taken to be the averaged density operator. In the language of cosmological perturbations, this amounts to assuming that there is spontaneous localization on the $\widehat{\delta\rho}(\eta, \boldsymbol{x})$ eigenmanifold, where $\delta\rho(\eta, \boldsymbol{x})$ is the perturbed energy density. This would have the advantage to introduce a universal γ with always the same dimension. Unfortunately, $\delta\rho(\eta, \boldsymbol{x})$ is a complicated functional of $v_{\boldsymbol{k}}$ and this would probably render the whole approach untractable. Let us also notice that γ could be taken as a function of the wave number $\boldsymbol{k}$, i.e., different CSL parameters for different modes. In this article, for simplicity, we do not follow this route.

Another issue is that we moved from real to reciprocal space while keeping the structure of the equation unchanged. In doing so, we also avoid from the outset any mode mixing that would be naturally arising from a real space modified Schrödinger equation: its stochastic version being nonlinear, one would expect a coupling of the Fourier modes, which is here automatically set to zero. Note this approximation is justified by data observations of the CMB.

Another important limitation of our treatment is the fact that the collapse concerns the modes independently. As a result, the amplification mechanism, so crucial to explain why the quantum behavior becomes increasingly less important for increasingly large systems (the effective collapse time being inversely proportional to the number of particles involved and, hence, to the size of the system), is simply not operating here. Therefore, even though one might consider cosmological size effects, the collapse will occur just as it would for an independent quantum particle. As we will see, that implies a severe constraint on the constant γ when comparison of the

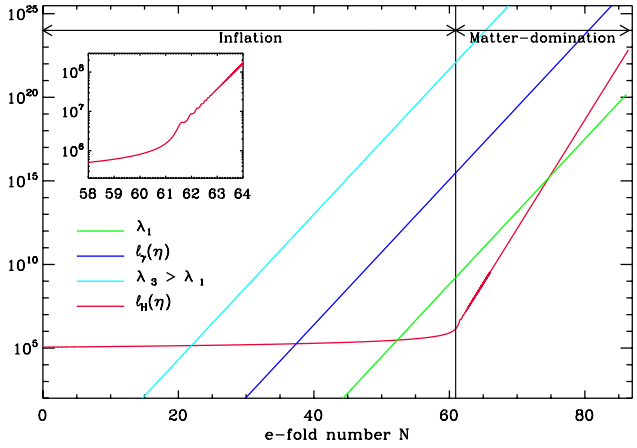

FIG. 4 (color online). Evolution of various physical length scales with time during the cosmic history in the CSL model described by Eq. (143) with a zoom on the transition from inflation to reheating inserted (see the concluding section). The solid line represents the Hubble radius ℓ_{H} and the dashed-dotted green and red lines, the physical wavelengths of two Fourier modes of cosmological relevance today. The solid blue line represents the built-in CSL scale ℓ_γ, see the discussion above Eq. (157). It is a preferred comoving scale and can also be viewed as a time-dependent preferred physical scale. Therefore, when a mode is below (above) ℓ_γ it remains so during the whole history of the Universe as is clear from the plot. This means that, contrary to the Hubble scale, there is no "ℓ_γ crossing" during the cosmic evolution. As a consequence, one expects the power spectrum to acquire a broken power-law shape, with two different branches, an expectation confirmed by the calculations in Sec. V D.

modified spectrum is made to actual observations on Hubble-size scales.

Finally, Eq. (143) is written in terms of the conformal Fourier mode of the original action. Because its normalization implies the equation be nonlinear, this means the constant γ can be translated, as we will show later, into a privileged *conformal* scale, and hence a time-dependent privileged length ℓ_γ, as shown in Fig. 4 and the discussion above Eq. (157). This is somehow similar to the fact, except at the perturbative and conformal levels, that considering nonflat spatial sections permits to define a curvature length and thus forbids to renormalize the scale factor arbitrarily. However, as shown in the Appendix, this last limitation does not affect the general conclusions drawn here.

B. Gaussian state

Our goal is now to solve Eq. (143). As was done for the standard case (50), one considers that the wave function assumes a Gaussian shape. Concretely, we take the most general form, namely

$$\Psi_k^{\mathrm{R,I}}(\eta, v_k^{\mathrm{R,I}}) = |N_k(\eta)| \exp\{-\Re\mathrm{e}\Omega_k(\eta)[v_k^{\mathrm{R,I}} - \bar{v}_k^{\mathrm{R,I}}(\eta)]^2 + i\sigma_k^{\mathrm{R,I}}(\eta) + i\chi_k^{\mathrm{R,I}}(\eta) v_k^{\mathrm{R,I}} - i\Im\mathrm{m}\Omega_k(\eta)(v_k^{\mathrm{R,I}})^2\}, \tag{144}$$

where $\bar{v}_k^{\mathrm{R,I}}$, $\sigma_k^{\mathrm{R,I}}$ and $\chi_k^{\mathrm{R,I}}$ are real numbers. The fact that one can assume $|N_k|$ and Ω_k to be independent of "R" or "I" will be justified in the following. Compared to Eq. (50), we see that Eq. (144) is more general and, therefore, contains more parameters. The case of Eq. (50) corresponds to $\bar{v}_k^{\mathrm{R,I}} = 0$, $\chi_k^{\mathrm{R,I}} = 0$ and $\arg N_k = \sigma_k$. Of course, the above Gaussian is similar to the wave function considered in the case of the harmonic oscillator of Eq. (117). The only difference is that the stochastic functions characterizing the wave function now depend on the wave number $\boldsymbol{k}$ and the role of the position is played by the Fourier amplitude of the Mukhanov-Sasaki variable.

The next step is to insert Eq. (144) into Eq. (143) in order to derive the differential equations obeyed by the functions parametrizing the Gaussian state. Straightforward manipulations making use of the Itô calculus lead to the following expressions:

$$\frac{|N_k|'}{|N_k|} = \frac{1}{4}\frac{(\Re\mathrm{e}\Omega_k)'}{\Re\mathrm{e}\Omega_k} = \Im\mathrm{m}\Omega_k + \frac{\gamma}{4\Re\mathrm{e}\Omega_k}, \tag{145}$$

$$(\Re\mathrm{e}\Omega_k)' = \gamma + 4(\Re\mathrm{e}\Omega_k)(\Im\mathrm{m}\Omega_k), \tag{146}$$

$$(\Im\mathrm{m}\Omega_k)' = -2(\Re\mathrm{e}\Omega_k)^2 + 2(\Im\mathrm{m}\Omega_k)^2 + \frac{1}{2}\omega^2(\eta, \boldsymbol{k}), \tag{147}$$

$$(\bar{v}_k^{\mathrm{R,I}})' = \chi_k^{\mathrm{R,I}} + \frac{\sqrt{\gamma}}{2\Re\mathrm{e}\Omega_k}\frac{\mathrm{d}W_\eta}{\mathrm{d}\eta} - 2(\Im\mathrm{m}\Omega_k)\bar{v}_k^{\mathrm{R,I}}, \tag{148}$$

$$(\sigma_k^{\mathrm{R,I}})' = -\Re\mathrm{e}\Omega_k + 2(\Re\mathrm{e}\Omega_k)^2(\bar{v}_k^{\mathrm{R,I}})^2 - \frac{1}{2}(\chi_k^{\mathrm{R,I}})^2, \tag{149}$$

$$(\chi_k^{\mathrm{R,I}})' = -4(\Re\mathrm{e}\Omega_k)^2\bar{v}_k^{\mathrm{R,I}} + 2\chi_k^{\mathrm{R,I}}(\Im\mathrm{m}\Omega_k). \tag{150}$$

Several remarks are in order at this point. First, we see that the evolution equations for $|N_k|$, $\Re\mathrm{e}\Omega_k$ and $\Im\mathrm{m}\Omega_k$ are deterministic and independent of that of $\bar{v}_k^{\mathrm{R,I}}$, $\sigma_k^{\mathrm{R,I}}$ or $\chi_k^{\mathrm{R,I}}$. This justifies the fact that one can assume these quantities to be independent on R, I provided similar initial conditions are chosen for R, I. This also means that these three quantities are not random (but their evolution is still explicitly modified by the stochastic dynamics when $\gamma \neq 0$). Second, Eq. (145) explicitly implies the conservation of the wave function norm: if one initially has a normalized state, i.e.,

$$|N_k| = \left(\frac{2\Re\mathrm{e}\Omega_k}{\pi}\right)^{1/4}, \tag{151}$$

it will remain so at any time. In fact, this equation is similar to Eq. (21) which is therefore not modified by the introduction of the nonlinear stochastic terms. Moreover, in the present case where the wave function is given by a single Gaussian, $\sigma_k^{\mathrm{R,I}}$ is just an irrelevant global phase and can be ignored (this will no longer be the case when the quantum state is the sum of two Gaussians, see below). Third, it is easy to check that Eqs. (145)–(150), are the exact counter parts of Eqs. (118)–(123). The only difference is that ω is

now a time-dependent quantity as expected since we deal with a parametric oscillator. We conclude that, instead of six coupled stochastic differential equations, we have in fact to solve two sets of two coupled differential equations, the first one being deterministic and the second one being stochastic. In particular Eqs. (146) and (147) can be combined and lead to the following Ricatti equation for the quantity $\Re\mathrm{e}\Omega_k + i\Im\mathrm{m}\Omega_k = \Omega_k$:

$$\Omega_k' = -2i\Omega_k^2 + \gamma + \frac{i}{2}\omega^2(\eta, \boldsymbol{k}). \tag{152}$$

This equation is similar to Eq. (124) obtained for the harmonic oscillator. Of course, if $\gamma = 0$, then one exactly recovers the Ricatti equation (20). As discussed before, a Ricatti equation can always be reduced to a linear but second order differential equation: this is achieved through the transformation $\Omega_k = -if_k'/(2f_k)$, where f_k is a solution of the following linear differential equation:

$$f_k'' + [\omega^2(\eta, \boldsymbol{k}) - 2i\gamma]f_k = 0. \tag{153}$$

This equation is very similar to the equation for the mode function considered before. The only difference is the appearance of the term $-2i\gamma$ in the effective frequency. Obviously, if $\gamma = 0$, then one recovers the conventional case. Moreover, the fact that this is the counterpart of Eq. (125) is obvious.

C. Evolution of the stochastic wave function during inflation

We now study the time evolution of the quantum state (144) in more detail. We start with the evolution of $\Re\mathrm{e}\Omega_k$ and $\Im\mathrm{m}\Omega_k$ since we have shown in the last section that it decouples from the other equations of motion. To derive the corresponding solutions, it is sufficient to solve Eq. (153). If the background is driven by a phase of power-law inflation, $\omega(\eta, \boldsymbol{k})$ is given by $\omega(\eta, \boldsymbol{k}) = k^2 - \beta(\beta + 1)/\eta^2$ and the differential equation (153) reads

$$f_k'' + \left[k^2 - \frac{\beta(\beta + 1)}{\eta^2} - 2i\gamma\right]f_k = 0. \tag{154}$$

We see that the only effect of the CSL term $-2i\gamma$ is to modify the comoving wave number $k^2 \to k^2 - 2i\gamma$. The solution of Eq. (154) can be written in terms of Bessel functions

$$f_k(\eta) = (-z_k k\eta)^{1/2}[C_k J_{\beta+\frac{1}{2}}(-z_k k\eta) + D_k J_{-(\beta+1/2)}(-z_k k\eta)], \tag{155}$$

where C_k and D_k are integration constants and where the complex number z_k is defined by

$$z_k \equiv \sqrt{1 - i\frac{2\gamma}{k^2}} = \left(1 + 4\frac{\gamma^2}{k^4}\right)^{1/4} \mathrm{e}^{-\frac{i}{2}\arctan(2\gamma/k^2)}. \tag{156}$$

Equation (155) should be compared to its non-CSL counterpart, Eq. (45). The only difference is the appearance of the z_k factor. This is consistent with the remark made above since this factor always multiplies the expression $k\eta$ and can, therefore, be viewed as a "renormalization" of the wave number k. In the non-CSL case where $\gamma = 0$, one obviously has $z_k = 1$ and Eq. (155) reduces to Eq. (45). It is interesting to remark that z_k for the parametric oscillator plays a role similar to that of α for the harmonic oscillator, see the definition (126). In fact, strictly following this last definition, one can introduce a mode-dependent α_k parameter, namely $\alpha_k \equiv \sqrt{2i\gamma - k^2}$ (using $\omega = k$ for massless perturbations) and, then, z_k appears to be just a rescaled α_k parameter: $\alpha_k = ikz_k$. Finally, notice also that the sign ambiguity in the definition of z_k due to the presence of a square root has absolutely no impact on the results presented below.

Let us now discuss the solution $f_k(\eta)$ and what this implies for the behavior of the wave function. In the presence of the CSL term, the problem is characterized by three scales: the wavelength of the Fourier mode given by $\lambda_k(\eta) = a(\eta)/k$, the Hubble radius $\ell_{\mathrm{H}}(\eta) = a^2/a'$ and a new scale associated with the parameter γ defined by $\ell_\gamma \equiv a(\eta)/\sqrt{\gamma}$ or, in terms of mass scale, $M_\gamma \equiv \sqrt{\gamma}/a(\eta)$. Notice that ℓ_γ is a new, time-dependent, physical scale that is built in the inflationary CSL theory, see Fig. 4. In terms of these three physical scales, the quantity $z_k k\eta$ which appears in Eq. (155) can be written as

$$z_k k\eta = (1 + \beta)\frac{\ell_{\mathrm{H}}}{\lambda_k}\sqrt{1 - 2i\frac{M_\gamma^2}{k_{\mathrm{phys}}^2}}, \tag{157}$$

where $k_{\mathrm{phys}} = k/a$ is the physical wave number. At the beginning of inflation, the modes of cosmological interest today laid far inside the Hubble radius, which means $\lambda_k \ll \ell_{\mathrm{H}}$, i.e., $k\eta \to -\infty$. Notice that these considerations are independent of the value of M_γ. Indeed, if $k_{\mathrm{phys}} \gg M_\gamma$, then $z_k \simeq 1$ and the previous limit is not changed. On the contrary, if $k_{\mathrm{phys}} \ll M_\gamma$, then the condition $|z_k| \gg 1$ is even better satisfied. It is also interesting to remark that, in this last case, $z_k k\eta$ does not go to $-\infty$ along the real axis but along a direction that is inclined in the complex plane. However, this does not change the asymptotic behavior of the Bessel functions in this regime. Upon using Eq. (155), one obtains

$$\lim_{\lambda_k/\ell_{\mathrm{H}}\to 0} f_k(\eta) = \sqrt{\frac{2}{\pi}}\left[C_k \sin\left(-z_k k\eta - \frac{\pi}{2}\beta\right) + D_k \cos\left(-z_k k\eta + \frac{\pi}{2}\beta\right)\right]. \tag{158}$$

This expression can also be re-expressed in term of "plane wave" functions (writing $\alpha_k \equiv \alpha_k^{\mathrm{R}} + i\alpha_k^{\mathrm{I}}$)

$$\lim_{\lambda_k/\ell_{\mathrm{H}}\to 0} f_k(\eta) = \frac{A_k}{\sqrt{2\pi}}\mathrm{e}^{\alpha_k^{\mathrm{R}}|\eta| - i\alpha_k^{\mathrm{I}}\eta - i\pi/4} + \frac{B_k}{\sqrt{2\pi}}\mathrm{e}^{-\alpha_k^{\mathrm{R}}|\eta| + i\alpha_k^{\mathrm{I}}\eta + i\pi/4}, \tag{159}$$

where the coefficients A_k and B_k can be expressed as linear combinations of C_k and D_k, namely

$$A_k = C_k\, \mathrm{e}^{-i\pi(\beta+1/2)/2} + D_k\, \mathrm{e}^{i\pi(\beta+1/2)/2} \tag{160}$$

$$B_k = C_k\, \mathrm{e}^{i\pi(\beta+1/2)/2} + D_k\, \mathrm{e}^{-i\pi(\beta+1/2)/2}. \tag{161}$$

The solution (159) is nothing but the Wentzel-Kramers-Brillouin (WKB) mode function $\exp(\pm i \int \omega \mathrm{d}\tau)/\sqrt{2\omega}$. The reason for this result is that, in the sub-Hubble regime, the WKB approximation is still valid even in presence of the CSL term. As is well known, this approximation is satisfied when the quantity $|Q/\omega^2| \ll 1$, where Q is given by

$$Q \equiv \frac{3}{4}\frac{1}{\omega^2}\left(\frac{\mathrm{d}\omega}{\mathrm{d}\eta}\right)^2 - \frac{1}{2\omega}\frac{\mathrm{d}^2\omega}{\mathrm{d}\eta^2}. \tag{162}$$

Since, in the limit under consideration, ω^2 tends toward a constant, namely $\omega^2 = k^2 - 2i\gamma$, and since Q is given in terms of derivatives of ω, it is obvious that the criterion is satisfied. As already mentioned, the only effect of the CSL theory is to add the constant term $-2i\gamma$ to ω^2. Although this modifies the solution for the mode function, clearly, this cannot change the fact that WKB is valid at the beginning of inflation.

Let us now comment on Eq. (159). When $|\eta|$ goes to infinity, the second branch of the above solution is going to die away since $\alpha_k^{\mathrm{R}} > 0$. As a consequence, only the first branch remains and, since Ω_k is given in terms of a ratio, i.e., $-if_k'/(2f_k)$, the remaining constant A_k disappears from the final expression. Therefore, Ω_k becomes independent of the initial conditions and is given by $\Omega_k \simeq i\alpha_k/2$, which implies that $\Re\mathrm{e}\Omega_k \simeq -\alpha_k^{\mathrm{I}}/2 \simeq -k/2$. Returning to Eq. (144), this means that the wave function is not bounded at infinity and is not normalizable. The deep reason is that, in the CSL context, z_k (or α_k) is complex and this implies that the WKB solution acquires either a growing or a decaying exponential component which automatically kills one of the two branches. And, of course, z_k (or α_k) is complex because of the CSL term $-2i\gamma$.

Based on the previous discussion, it is clear that the only meaningful choice of initial conditions is to require that $A_k = 0$. From Eqs. (160) and (161), we see that this implies

$$C_k = -D_k\, \mathrm{e}^{i\pi(\beta+1/2)}. \tag{163}$$

This choice exactly coincides with the Bunch-Davies initial conditions (46). From now on, we assume Eq. (163) but we will come back soon to this discussion. Then, one can rederive the behavior of Ω_k in the sub-Hubble regime. One obtains

$$\lim_{\lambda_k/\ell_{\mathrm{H}}\to 0} \Omega_k(\eta) = -\frac{i}{2}\alpha_k, \tag{164}$$

which is fully consistent with Eqs. (134) and (135). In particular, one can check that, now, $\Re\mathrm{e}\Omega_k \to k/2$ and the wave function becomes normalizable (of course, it tends to the ground state wave function). Therefore, we have proven that, as expected, the cosmological perturbations behave, in the sub-Hubble regime, exactly as the CSL harmonic oscillator.

Having studied the behavior of the stochastic wave function in the sub-Hubble regime, we now turn to the super-Hubble case. In the framework of CSL, and contrary to the sub-Hubble regime studied before, it is clear that this regime has no counter part in the case of the harmonic oscillator. It corresponds to the limit $\ell_{\mathrm{H}} \ll \lambda_k$ and, from Eq. (157), we see that this means $|z_k k\eta| \to 0$. Let us notice that one could also consider the case where $k_{\mathrm{phys}} \ll M_\gamma$ such that $M_\gamma/k_{\mathrm{phys}} \gg 1$ compensates the ratio $\ell_{\mathrm{H}}/\lambda_k$ in Eq. (157) resulting in a large $|z_k k\eta|$, even in the super-Hubble regime. Below, we briefly comment on this case. Here, we assume that M_γ is such that this does not happen. Then, upon using the asymptotic behavior of the Bessel functions for small values of their argument, one arrives at

$$\begin{aligned}\frac{\Omega_k}{k} = &-\frac{i(1+\beta)}{2k\eta} - \frac{i(-k\eta)}{4(\beta+3/2)} - \frac{(-k\eta)}{2(\beta+3/2)}\frac{\gamma}{k^2} \\ &+ i\frac{D_k}{C_k}\left(1-2i\frac{\gamma}{k^2}\right)^{-\beta-1/2} 2^{2\beta+1}\left(\beta+\frac{1}{2}\right) \\ &\times \frac{\Gamma(\beta+1/2)}{\Gamma(-\beta-1/2)}(-k\eta)^{-2\beta-2} + \cdots.\end{aligned} \tag{165}$$

This equation should be compared to the corresponding non-CSL formula (52). If $\gamma = 0$ and if one takes the Bunch-Davies initial conditions, $D_k = -C_k \mathrm{e}^{-i\pi(\beta+1/2)}$, then the above equation exactly reduces to Eq. (52). Here, although we argued before that one should use the Bunch-Davies initial conditions (163), we temporarily keep the coefficients C_k and D_k arbitrary because, later on, we shall want to comment on their influence on the shape of the CSL power spectrum. Let us also notice that the last term of the above expression is in fact proportional to $z_k^{-(2\beta+1)}$. If we write z_k in polar form, $z_k \equiv |z_k|\mathrm{e}^{i\theta_k}$ (of course, θ_k should not be confused with the squeezing angle) where the modulus and the phase can be read off directly from Eq. (156), and parametrize the initial conditions as $C_k = |C_k|\mathrm{e}^{i\theta_c}$ and $D_k = |D_k|\mathrm{e}^{i\theta_d - i\pi\beta + i\pi/2}$ (so that the Bunch-Davies limit is simply $\theta_d - \theta_c = 0$), then it is easy to determine the real and imaginary parts of the function Ω_k. One finds

$$\begin{aligned}\Re\mathrm{e}\Omega_k(\eta) = &-\frac{k}{2(\beta+3/2)}\frac{\gamma}{k^2}(-k\eta) + \frac{|D_k|}{|C_k|}|z_k|^{-(2\beta+1)} \\ &\times \cos[\pi\beta + (2\beta+1)\theta_k - \theta_d + \theta_c] \\ &\times \frac{k\pi 2^{2\beta+1}}{\Gamma^2(-\beta-1/2)\cos(\pi\beta)} \\ &\times (-k\eta)^{-2\beta-2} + \cdots,\end{aligned} \tag{166}$$

$$\Im\mathrm{m}\Omega_k(\eta) = -\frac{k}{2k\eta}(1+\beta) - \frac{k}{4(\beta+3/2)}(-k\eta) - \frac{k}{\pi}\frac{|D_k|}{|C_k|}|z_k|^{-(2\beta+1)} \times 2^{2\beta}\frac{1}{2}\sin[\pi\beta + (2\beta+1)\theta_k - \theta_d + \theta_c] \times \cos(\pi\beta)\Gamma^2\left(\beta+\frac{3}{2}\right)(-k\eta)^{-2\beta-2} + \cdots. \quad (167)$$

These equations are the CSL counterparts of Eqs. (53) and (54). Of course, for $\gamma = 0$ and the Bunch-Davies initial conditions, they exactly reduce to those equations. We see that the main effect of the CSL theory is to strongly modify $\Re\mathrm{e}\Omega_k$ since its leading term in the above expansion is a term which cancels if $\gamma = 0$. We also see that we still have $\Re\mathrm{e}\Omega_k \to 0$ in the super-Hubble limit. In the absence of the CSL term, we would obtain the same limit but not with the same power. Compared to $\Re\mathrm{e}\Omega_k$, $\Im\mathrm{m}\Omega_k$ is much less modified since the first correction show up only in the third term of the expansion. As a consequence, we still have $\Im\mathrm{m}\Omega_k \to \infty$ in the super-Hubble regime.

We now use the above results to discuss the collapse of the wave function in more detail. Since we have assumed in Eq. (143) that the "collapse operator" is $\hat{v}_k$, we expect the nonlinear and stochastic terms in the modified Schrödinger equation to drive the initial Gaussian state to an eigenvector of $\hat{v}_k$, that is to say to the Dirac function $\delta(v_k - \bar{v}_k)$. However, in practice, as we learned from the harmonic oscillator example in Sec. IV B, this is not what happens. In practice, we find that the wave function tends towards a Gaussian state with a constant spread in position and that the larger the value of γ, the smaller the amplitude of this spread, i.e., $\lim_{t\to\infty}\sigma_x \to [\hbar/(4m\gamma)]^{1/4}$ when $\gamma \to \infty$. Therefore, strictly speaking, the exact localization is obtained only in the $\gamma \to \infty$ limit. Of course, if the spread is very small, then for all practical purposes, the collapse has been achieved. In fact, this is the essence of the amplification mechanism discussed in Sec. IV A. The effective value γ_{CM} of γ for a macroscopic object (or for its center of mass) is the fundamental γ times the number of particles in that object which results in a huge effective γ and, therefore, a very efficient localization. As a consequence, a collapse can occur for macroscopic objects while it does not happen for microscopic particles even if their behavior is slightly disturbed.

Let us now see how the previous discussion applies to inflation. The first difference is that the standard deviation, $1/(2\sqrt{\Re\mathrm{e}\Omega_k})$, does not go to a constant as for the harmonic oscillator but to infinity since Eq. (166) implies that $\Omega_k \propto \eta \to 0$. We remark that the divergence is less violent than when $\gamma \neq 0$ since, in that case, $\Omega_k \propto \eta^2 \to 0$, according to Eq. (53). This is of course due to the influence of the nonlinear and stochastic terms. However, this influence is not sufficient to prevent the divergence of the variance and, therefore, to ensure an efficient localization. As a matter of fact, we see that, in the limit $\eta \to 0$, the main divergence in the Hamiltonian comes from the term $\propto \omega^2 v_k^2$ while the CSL term goes like γv_k^2. Hence, it is because the term $\omega^2 \propto \eta^{-2}$ diverges at the end of inflation that the Hamiltonian strongly dominates the dynamics of the system, preventing the CSL terms $\propto \gamma v_k^2$ to carry out its job and to localize v_k (however, see the Appendix). This is certainly a problem for the inflationary CSL theory. This issue can also be related to the fact that it is unclear how an amplification mechanism could be implemented in quantum field theory. As a consequence, the collapse mechanism is controlled by the parameter γ and no effective γ can be derived which would ensure a better localization.

Finally, let us mention that one could wonder whether the localization can be achieved during the radiation dominated era that takes place after inflation. In this case, the scale factor behaves as $a(\eta) \propto \eta$ and, therefore, $\epsilon_1 = 2$ and $(a\sqrt{\epsilon_1})''/(a\sqrt{\epsilon_1}) = 0$. As consequence, the mode equation for f_k is exactly that of a harmonic oscillator. This means that the variance now goes to a constant, see Sec. IV B, which seems to cure the problem discussed above. However, one can show that the corresponding value remains large for modes of astrophysical interest today. Therefore, this remains an unsatisfactory solution.

D. The CSL power spectrum

We now turn to one of the main goal of the present paper, namely the determination of the power spectrum predicted by the CSL theory. It was shown in Eqs. (29) and (37) that the power spectrum of the conserved quantity ζ_k can be expressed as

$$\mathcal{P}_\zeta(k) = \frac{k^3}{16\pi^2 M_{\mathrm{Pl}}^2}\frac{1}{a^2\epsilon_1\Re\mathrm{e}\Omega_k}. \quad (168)$$

Since we have determined the quantity $\Re\mathrm{e}\Omega_k$ in Eq. (166), the calculation of $\mathcal{P}_\zeta$ becomes straightforward. One obtains

$$\mathcal{P}_\zeta(k) = g_\gamma(k,\beta)\left[1 - \frac{\gamma}{k^2}g_\gamma(k,\beta)f(\beta) \times \frac{(-k\eta)^{2\beta+3}}{\beta+3/2}\right]^{-1}\mathcal{P}_\zeta(k)|_{\mathrm{stand}}, \quad (169)$$

where $\mathcal{P}_\zeta|_{\mathrm{stand}}$ is the standard power spectrum given by Eq. (47) and the function $f(\beta)$ has been defined in Eq. (48). The function $g_\gamma(k,\beta)$

$$g_\gamma(k,\beta) \equiv \frac{|C_k|}{|D_k|}|z_k|^{2\beta+1}\frac{\cos(\pi\beta)}{\cos[\pi\beta + (2\beta+1)\theta_k - \theta_d + \theta_c]} \quad (170)$$

is seen to depend on the choice of the initial conditions. It has the property that, for $\gamma = 0$ and the Bunch-Davies initial conditions, $g_{\gamma=0}(k,\beta) = 1$. In this case, and as expected, one

can check that the modified power spectrum (169) reduces to the standard inflationary power spectrum. We also notice that the power spectrum (169) is still a time-dependent quantity, contrary to the conventional case where the time dependence cancels out. For this reason, it is convenient to evaluate it at the end of inflation. In that case, the quantity $-k\eta$ can be rewritten as

$$-k\eta = -\frac{k}{k_0}(1+\beta)\,\mathrm{e}^{\Delta N_*/(1+\beta)}, \tag{171}$$

where k_0 is the comoving wave number of the Fourier mode, the wavelength of which equals the Hubble radius today, i.e., $k_0 = a_0 H_0$. The quantity ΔN_* denotes the number of e-folds spent by a mode of cosmological relevance today outside the Hubble radius during inflation; typically, one has $\Delta N_* \simeq 50$–60. As a consequence, the power spectrum (169) can be reexpressed as

$$\mathcal{P}_\zeta(k) = g_\gamma(k,\beta)\Bigg[1 - \frac{\gamma}{k_0^2} g_\gamma(k,\beta) f(\beta) \frac{|1+\beta|^{2\beta+3}}{(\beta+3/2)} \times \mathrm{e}^{(2\beta+3)\Delta N_*/(1+\beta)} \left(\frac{k}{k_0}\right)^{2\beta+1}\Bigg]^{-1} \mathcal{P}_\zeta(k)|_{\mathrm{stand}}. \tag{172}$$

Let us notice that, in Eq. (170), the quantities $|z_{\boldsymbol{k}}|$ of Eq. (156) and $\theta_{\boldsymbol{k}}$ must now be written as

$$|z_{\boldsymbol{k}}| = \left[1 + 4\frac{\gamma^2}{k_0^4}\left(\frac{k_0}{k}\right)^4\right]^{1/4}, \tag{173}$$

$$\theta_{\boldsymbol{k}} = -\frac{1}{2}\arctan\left[2\frac{\gamma}{k_0^2}\left(\frac{k_0}{k}\right)^2\right], \tag{174}$$

such that the amplitude of the CSL correction is controlled by the dimensionless ratio γ/k_0^2. The formula (172) is one of the main results of this article and the corresponding power spectra for different values of the ratio γ/k_0^2 are represented in Fig. 5.

Let us now discuss in more detail the CSL power spectrum (172). First, we notice that, in the short-wavelength regime $k/k_0 \to \infty$, the power spectrum reduces to $\mathcal{P}_\zeta(k) \simeq g_\gamma(k,\beta)\mathcal{P}_\zeta|_{\mathrm{stand}}$. Moreover, in this limit, we see that $|z_{\boldsymbol{k}}| \to 1$ and $\theta_{\boldsymbol{k}} \to 0$. As a consequence, an almost scale invariant (namely, $n_S = 2\beta + 4$ with $\beta \lesssim -2$) power spectrum is recovered if one assumes the Bunch-Davies initial conditions, $|C_{\boldsymbol{k}}| = |D_{\boldsymbol{k}}|$ and $\theta_d - \theta_c = 0$ since, in that case, $g_\gamma(k,\beta) = 1$. This almost scale invariant branch of the power spectrum is clearly seen in Fig. 5. Second, there is clearly another regime which corresponds to the case where the second term in the square brackets in Eq. (172) starts playing a role. If we neglect factors of order one, this happens at $k = k_\gamma$, where k_γ solves

$$\frac{\gamma}{k_0^2} g_\gamma(k_\gamma,\beta)\,\mathrm{e}^{(2\beta+3)\Delta N_*/(1+\beta)}\left(\frac{k_\gamma}{k_0}\right)^{2\beta+1} \simeq 1. \tag{175}$$

The value of g_γ is mainly controlled by the value of $|z_{\boldsymbol{k}}|$ which is always close to unity provided that $k \ll k_z$ with

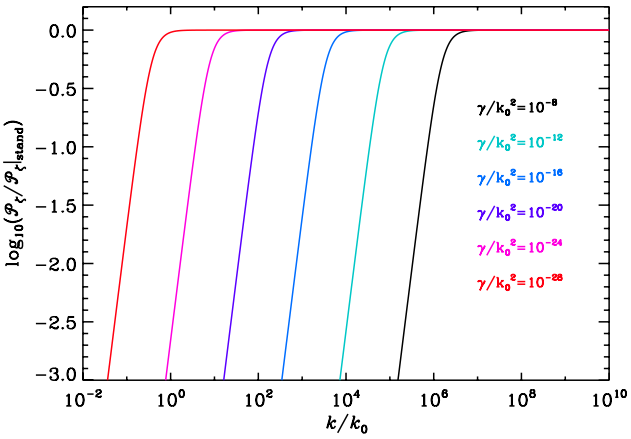

FIG. 5 (color online). Ratio of the power spectrum given by Eq. (172) to the standard power spectrum given by Eq. (47) for different values of the parameter γ/k_0^2 (and for $\beta = -2.01$, a value leading to a standard power spectrum close to scale invariance). The number of e-folds between Hubble radius crossing and the end of inflation (for the modes of cosmological interest today) has been taken to $\Delta N_* = 60$ and the initial conditions have been chosen to be the adiabatic vacuum.

$$\frac{k_z}{k_0} \equiv \sqrt{2}\left(\frac{\gamma}{k_0^2}\right)^{1/2}. \tag{176}$$

Then, let us assume that $g_\gamma \simeq 1$ when the condition (175) is met. In this case, the scale k_γ can be expressed as

$$\frac{k_\gamma}{k_0} \sim \left(\frac{\gamma}{k_0^2}\right)^{-1/(1+2\beta)} \exp\left[-\frac{2\beta+3}{(\beta+1)(2\beta+1)}\Delta N_*\right]. \tag{177}$$

Choosing the fiducial value $\beta \simeq -2$ leads to $k_\gamma/k_0 \sim (\gamma/k_0^2)^{1/3}\exp(\Delta N_*/3)$. One can check that, indeed, $k_\gamma \gg k_z$ and, therefore, assuming $g_\gamma \simeq 1$ was, in retrospect, valid. As a consequence, in the range $k \ll k_\gamma$, the spectrum approximately behaves as $\propto k^{2\beta+4}/k^{2\beta+1} = k^3$, that is to say with a spectral index of $n_S \simeq 4$. This second branch is also clearly visible in Fig. 5. In addition, the dependence in g_γ is canceled out which means that this prediction is actually independent of the choice of the initial conditions, a remarkable property indeed (this also means that, even if $k \ll k_z$, the spectral index remains the same). Moreover, we see that this spectral index is also independent of β which is also remarkable. In this sense, the CSL branch of the power spectrum can be said to be "universal" (unfortunately not scale invariant).

We are now in a position where we can discuss the cosmological constraints on the parameter γ. From the high accuracy measurements of the CMB anisotropies [20–22], we know that the power spectrum is almost scale invariant, $n_S \simeq 1$, and that a spectral index $n_S = 4$ is completely excluded. This means that the CSL branch must correspond to scales much larger than the present Hubble radius, in other words $k_\gamma/k_0 \ll 1$. This condition means that, for $\beta \simeq -2$, one has

$$\frac{\gamma}{k_0^2} \ll \mathrm{e}^{-\Delta N_*} \simeq 10^{-28}. \tag{178}$$

To our knowledge, this is the first time that a constraint on the parameter γ is obtained from cosmological considerations (see, however, Ref. [76]). We see that the constraint is expressed as a limit not on γ itself but on the combination γ/k_0^2 where we remind the reader that k_0 is the comoving wave number of the Hubble radius today. Looking at Eqs. (143) and (153), this was expected since the CSL modification amounts to a redefinition of the comoving wave number $k^2 \to k^2 - 2i\gamma$. This means that, in order to characterize the amplitude of the modification, one has to compare the comoving wave number to γ, hence the ratio γ/k_0^2. The appearance of the comoving wave number in the observational constraint reflects the fact that the theory contains a built-in "time-dependent physical preferred scale" $\ell_\gamma(\eta)$. In terms of physical scales, the constraint (178) can be rewritten as

$$\left.\frac{\ell_{\mathrm{H}}}{\ell_\gamma}\right|_{\mathrm{today}} \ll 10^{-13}. \tag{179}$$

Clearly, the constraint is very strong and means that the scale ℓ_γ is very large in comparison to the Hubble radius today. This is another illustration of the fact that squeezed states are fragile and easily perturbed. For the CSL theory itself, this probably means that, in order to be compatible with cosmological inflation, an important fine-tuning is required. Of course, this conclusion should be toned down given the uncertainty that exists on a CSL formulation of quantum field theory as discussed in Sec. V A. One might argue for instance that the above result could be due to the fact that our modified Schrödinger equation is not necessarily the appropriate one in the context of quantum field theory. It would also be interesting to compare the cosmological constraint with the other constraints on γ derived in the literature. But, as explained before, because we assumed $\hat{v}_{\boldsymbol{k}}$ to be the preferred basis for the collapse, our parameter γ is actually different from the parameter γ considered elsewhere, in particular it has a different dimension. This complicates tremendously any comparison with other systems.

Finally, before closing this section, let us discuss the following question. In this article, we have defined the power spectrum in the CSL theory by means of the formula $\mathbb{E}(\langle\hat{v}_{\boldsymbol{k}}^2\rangle) - \mathbb{E}(\langle\hat{v}_{\boldsymbol{k}}\rangle^2)$. However, there is an issue regarding this definition. Indeed, it is clear that it does not go to zero when the parameter γ vanishes. Actually, it tends towards the standard result when the Schrödinger equation is recovered. However, it was argued in Ref. [112] that the power spectrum should go to zero in the limit where $\gamma \to 0$ and, therefore, cannot be given by the definition used above. The reason advocated by Ref. [112] is that, without a collapse, the theory remains homogeneous and isotropic and, as a consequence, there is simply no perturbations at all. This has led Ref. [112] to define the CSL power spectrum by $\mathbb{E}(\langle\hat{v}_{\boldsymbol{k}}\rangle^2) - \mathbb{E}^2(\langle\hat{v}_{\boldsymbol{k}}\rangle)$, a quantity which indeed vanishes when $\gamma \to 0$ and differs from the previous one. In this last paragraph, we explore the difference between these two alternative definitions. At any time, the wave function can always be expanded as

$$\Psi(\eta, v_{\boldsymbol{k}}) = \int \Psi(\eta, \bar{v}_{\boldsymbol{k}})\delta(v_{\boldsymbol{k}} - \bar{v}_{\boldsymbol{k}})\mathrm{d}\bar{v}_{\boldsymbol{k}}, \tag{180}$$

where the superscripts "R, I" have been ignored for convenience. If a dynamical collapse of the wave function takes place then Ψ is projected (collapsed) on an eigenstate of the operator $\hat{v}_{\boldsymbol{k}}$, namely

$$\Psi \to \Psi_{\mathrm{col}} \equiv \delta(v_{\boldsymbol{k}} - \bar{v}_{\boldsymbol{k}}), \tag{181}$$

where $\bar{v}_{\boldsymbol{k}}$ depends on the specific realization under consideration, then one obviously has

$$\begin{aligned}\langle\Psi_{\mathrm{col}}|\hat{v}_{\boldsymbol{k}}^2|\Psi_{\mathrm{col}}\rangle &= \langle\Psi_{\mathrm{col}}|\hat{v}_{\boldsymbol{k}}|\psi_{\mathrm{col}}\rangle^2, \\ &= \bar{v}_{\boldsymbol{k}}^2.\end{aligned} \tag{182}$$

Therefore, for each realization, one has $\langle\hat{v}_{\boldsymbol{k}}^2\rangle = \langle\hat{v}_{\boldsymbol{k}}\rangle^2$, once the wave function has collapsed. Since this is true for all realizations, it remains the case after taking the stochastic average. Therefore, after the collapse, one can write

$$\mathbb{E}\left(\langle\hat{v}_{\boldsymbol{k}}^2\rangle\right) = \mathbb{E}(\langle\hat{v}_{\boldsymbol{k}}\rangle^2), \tag{183}$$

and this remains true for any Hermitian operator. Note that this argument strongly depends on the fact that the wave function has actually collapsed to an eigenstate of the operator $\hat{v}_{\boldsymbol{k}}$. For instance, in the case of a harmonic oscillator studied in Sec. IV B, it was shown that the asymptotic state is not exactly a Dirac wave function, but a Gaussian state the spread of which does not vanish for finite values of γ. In that situation, the two above expressions are not identical.

On the other hand, the second terms in both definitions of the power spectrum differ

$$\mathbb{E}\left(\langle\hat{v}_{\boldsymbol{k}}\rangle^2\right) \neq \mathbb{E}^2(\langle\hat{v}_{\boldsymbol{k}}\rangle), \tag{184}$$

so the two spectra do not coincide even after the collapse. The difference ultimately boils down to the fact that it is built out of a standard deviation which is not a Hermitian operator. This is a generic question for the predictions of any theory mixing different kinds of averages (in the case at hand, quantum and stochastic) whenever nonlinear combinations of Hermitian operators are involved.

VI. THE COLLAPSE OF COSMOLOGICAL PERTURBATIONS

In this section, we investigate the collapse mechanism and its dynamics in more detail. In particular, we calculate the collapse time and compare it with the cosmological characteristic times. For this purpose, we now consider the following double Gaussian quantum state [73]:

$$\Psi_k(\eta, v_k) = |N_k^{(1)}(\eta)| \exp\{-\Re\mathrm{e}\Omega_k^{(1)}(\eta)[v_k - \bar{v}_k^{(1)}(\eta)]^2 + i\sigma_k^{(1)}(\eta) + i\chi_k^{(1)}(\eta)v_k - i\Im\mathrm{m}\Omega_k^{(1)}(\eta)(v_k)^2\} + |N_k^{(2)}(\eta)| \exp\{-\Re\mathrm{e}\Omega_k^{(2)}(\eta)[v_k - \bar{v}_k^{(2)}(\eta)]^2 + i\sigma_k^{(2)}(\eta) + i\chi_k^{(2)}(\eta)v_k - i\Im\mathrm{m}\Omega_k^{(2)}(\eta)(v_k)^2\}, \tag{185}$$

where, as before, $|N_k^{(1,2)}|$, $\Re\mathrm{e}\Omega_k^{(1,2)}$, $\bar{v}_k^{(1,2)}$, $\sigma_k^{(1,2)}$, $\chi_k^{(1,2)}$ and $\Im\mathrm{m}\Omega_k^{(1,2)}$ are real, possibly stochastic, numbers. The superscripts "R, I" have not been written for convenience but it should be remembered that they are of course present. Inserting the above state into the modified Schrödinger equation leads to the following set of formulas:

$$\frac{|N_k^{(1,2)}|'}{|N_k^{(1,2)}|} = \Im\mathrm{m}\Omega_k^{(1,2)} + \frac{\gamma}{4\Re\mathrm{e}\Omega_k^{(1,2)}} - \sqrt{\gamma}[\langle\hat{v}_k\rangle - \bar{v}_k^{(1,2)}] \times \frac{\mathrm{d}W_\eta}{\mathrm{d}\eta} - \frac{\gamma}{2}[\langle\hat{v}_k\rangle - \bar{v}_k^{(1,2)}]^2, \tag{186}$$

$$[\Re\mathrm{e}\Omega_k^{(1,2)}]' = \gamma + 4[\Re\mathrm{e}\Omega_k^{(1,2)}][\Im\mathrm{m}\Omega_k^{(1,2)}], \tag{187}$$

$$[\Im\mathrm{m}\Omega_k^{(1,2)}]' = -2[\Re\mathrm{e}\Omega_k^{(1,2)}]^2 + 2[\Im\mathrm{m}\Omega_k^{(1,2)}]^2 + \frac{1}{2}\omega^2(\eta, \boldsymbol{k}), \tag{188}$$

$$[\bar{v}_k^{(1,2)}]' = \chi_k^{(1,2)} + \frac{\sqrt{\gamma}}{2\Re\mathrm{e}\Omega_k^{(1,2)}}\frac{\mathrm{d}W_\eta}{\mathrm{d}\eta} - 2[\Im\mathrm{m}\Omega_k^{(1,2)}]\bar{v}_k^{(1,2)} + \frac{\gamma}{\Re\mathrm{e}\Omega_k^{(1,2)}}[\langle\hat{v}_k\rangle - \bar{v}_k^{(1,2)}], \tag{189}$$

$$[\sigma_k^{(1,2)}]' = -\Re\mathrm{e}\Omega_k^{(1,2)} + 2[\Re\mathrm{e}\Omega_k^{(1,2)}]^2[\bar{v}_k^{(1,2)}]^2 - \frac{1}{2}[\chi_k^{(1,2)}]^2, \tag{190}$$

$$[\chi_k^{(1,2)}]' = -4[\Re\mathrm{e}\Omega_k^{(1,2)}]^2\bar{v}_k^{(1,2)} + 2\chi_k^{(1,2)}[\Im\mathrm{m}\Omega_k^{(1,2)}]. \tag{191}$$

These equations should be compared to Eqs. (145)–(150). They are obviously very similar except the two last terms of Eq. (186) and the last term of Eq. (189) which are new. In the case of a single Gaussian, one has $\langle\hat{v}_k\rangle = \bar{v}_k$ and these terms disappear. In the present case, the expression of $\langle\hat{v}_k\rangle$ is a very complicated function of all the parameters describing the wave function. Let us also notice that, since the evolution of $\sigma_k^{(1,2)}$ and $\chi_k^{(1,2)}$ depends on $\bar{v}_k^{(1,2)}$, these quantities also feel the coupling between the two Gaussian components. However, one can see that the equations of motion for $\Re\mathrm{e}\Omega_k^{(1,2)}$ and $\Im\mathrm{m}\Omega_k^{(1,2)}$ decouple from the other equations of motion and form an independent and closed subsystem. This means that the evolution of these two functions is identical to that of their counterpart in the simple Gaussian case and, moreover, that, if the initial conditions are chosen to be the same, $\Omega_k^{(1)} = \Omega_k^{(2)}$ at any subsequent time. From now on, for this reason, the superscripts "(1)" and/or "(2)" on these quantities will be dropped.

It should be clear that the above system of differential equations is rather complicated to study. However, as we shall see, the most relevant properties of the evolution of the double Gaussian quantum state can be analyzed in a rigorous way. In particular, it is interesting to introduce the function $\Gamma_k(\eta) \equiv \ln[|N_k^{(2)}|/|N_k^{(1)}|]$, see Ref. [73]. This quantity characterizes the relative importance of one Gaussian component to the other and, therefore, provides a criterion to decide whether the collapse has taken place. The superposition of the two Gaussian quantum states reduces to one of them when $|\Gamma_k|$ goes to infinity. In practice, the collapse will be said to have occurred when $|\Gamma_k| > b$ with, say, $b \sim 10$ [73]. Then, by subtracting the two equations (186), one arrives at the following evolution equation for Γ_k

$$\frac{\mathrm{d}\Gamma_k}{\mathrm{d}\eta} = \sqrt{\gamma}[\bar{v}_k^{(2)} - \bar{v}_k^{(1)}]\frac{\mathrm{d}W}{\mathrm{d}\eta} - \gamma[\bar{v}_k^{(2)} - \bar{v}_k^{(1)}][\bar{v}_k^{(1)} + \bar{v}_k^{(2)} - 2\langle\hat{v}_k\rangle]. \tag{192}$$

This equation remains complicated because of the presence of the term $\langle\hat{v}_k\rangle$. However, the calculation can be simplified if one assumes that the two Gaussian components of the wave function do not overlap, i.e., have separate supports. Technically, this means that $\Re\mathrm{e}\Omega_k[\bar{v}_k^{(2)} - \bar{v}_k^{(1)}]^2 \gg 1$, leading to the following simple formula:

$$\langle\hat{v}_k\rangle \simeq \frac{|N_k^{(1)}|^2\bar{v}_k^{(1)} + |N_k^{(2)}|^2\bar{v}_k^{(2)}}{|N_k^{(1)}|^2 + |N_k^{(2)}|^2}. \tag{193}$$

Inserting this formula into Eq. (192) and defining X_k by $X_k \equiv \bar{v}_k^{(2)} - \bar{v}_k^{(1)}$, one obtains the following expression:

$$\frac{\mathrm{d}\Gamma_k}{\mathrm{d}\eta} = \sqrt{\gamma}X_k\frac{\mathrm{d}W_\eta}{\mathrm{d}\eta} + \gamma X_k^2\tanh(\Gamma_k). \tag{194}$$

This stochastic differential equation can be further simplified. Indeed, using the new timelike variable [73]

$$s_k \equiv \gamma\int_{\eta_{\mathrm{ini}}}^{\eta} X_k^2(u)\mathrm{d}u, \tag{195}$$

Eq. (194) can be rewritten as

$$\frac{\mathrm{d}\Gamma_k}{\mathrm{d}s_k} = \frac{\mathrm{d}W_s}{\mathrm{d}s_k} + \tanh(\Gamma_k), \tag{196}$$

where

$$W_s = \sqrt{\gamma}\int_0^{s_k} X_k\mathrm{d}W_\eta \tag{197}$$

is another Wiener process with respect to the time variable s_k.

A. Collapse time: Definition

Let us now study the stochastic differential equation driving the evolution of Γ_k in more detail. In particular, we would like to know how much time it takes for the wave function to collapse or, in technical terms, we would like to determine the value of s_k such that $|\Gamma_k| > b$. The quantity Γ_k being stochastic, two complications arise. First, once it has reached a value larger than b, there is no guarantee that it will stay in this region. The random behavior of Γ_k could temporally bring it back to the region $|\Gamma_k| \leq b$. However, since the average trend is clearly to have a collapse, this would happen for a limited amount of time only before Γ_k returns in the regime where $|\Gamma_k| \geq b$. For this reason, we will consider that the wave function has collapsed when Γ_k has crossed the value $\pm b$ for the first time. Technically, this means that we are led to define the "collapse time," S_k, as $S_k \equiv \inf(s_k)$ such that $|\Gamma_k(s_k)| > b$, see also Ref. [73]. A second issue is that, clearly, the value of S_k will differ from one realization to the other or, in other words, that S_k is still a random variable. Therefore, we will rather define the collapse time as the ensemble average value of S_k but we will also be interested in calculating its higher order momenta.

We now seek an explicit expression for the quantity S_k. It can be obtained in the following manner. Let us consider a function $c(\Gamma_k)$ that we do not characterize in more detail for the moment (but see below). It can always be Taylor expanded in $\mathrm{d}\Gamma_k$. At second order, the result reads

$$c(\Gamma_k + \mathrm{d}\Gamma_k) = c(\Gamma_k) + c'(\Gamma_k)\mathrm{d}\Gamma_k + \frac{1}{2}c''(\Gamma_k)\mathrm{d}\Gamma_k^2 + \mathcal{O}(\mathrm{d}\Gamma_k^3), \tag{198}$$

where $\mathrm{d}\Gamma_k$ is given by Eq. (196). At first order in $\mathrm{d}s_k$, this leads to

$$\mathrm{d}c[\Gamma_k(s_k)] = c'[\Gamma_k(s_k)]\mathrm{d}W_s + c'[\Gamma_k(s_k)]\tanh[\Gamma_k(s_k)]\mathrm{d}s_k + \frac{1}{2}c''[\Gamma_k(s_k)]\mathrm{d}s_k. \tag{199}$$

Then, integrating the above expression between $s_k = 0$ where $\Gamma_k(s_k = 0) = b_0$ and $s_k = S_k$ where $\Gamma_k(s_k = S_k) = \pm b$, one gets the following (Itô) formula:

$$c(\pm b) - c(b_0) = \int_0^{S_k} c'[\Gamma_k(s_k)]\mathrm{d}W_s + \int_0^{S_k}\left\{c'[\Gamma_k(s_k)] \times \tanh[\Gamma_k(s_k)] + \frac{1}{2}c''[\Gamma_k(s_k)]\right\}\mathrm{d}s_k. \tag{200}$$

At this stage, we now specify the function c. We require it to be the solution of the differential ordinary equation

$$\frac{1}{2}c''(x) + \tanh(x)c'(x) = -1, \tag{201}$$

with boundary conditions $c(-b) = c(+b) = 0$. It is easy to show that $c(x) = b\tanh(b) - x\tanh(x)$. This means that the first term on the left-hand side of Eq. (200) vanishes and that the integrand of the second term on the right-hand side is just -1. Therefore, Eq. (200) can be rewritten as

$$S_k = c(b_0) + \int_0^{S_k} c'[\Gamma_k(s_k)]\mathrm{d}W_s, \tag{202}$$

and this gives an (implicit) expression for the quantity S_k. Finally, by averaging over all realizations, one obtains [73]

$$\mathbb{E}(S_k) = c(b_0) = b\tanh(b) - b_0\tanh(b_0). \tag{203}$$

The fact that the stochastic average of the integral in Eq. (202) vanishes comes from the fact that $c'[\Gamma_k(s_k)]$ depends only on stochastic events occurring at $s_k' < s_k$. As a consequence, it can be expressed as an integration over $\mathrm{d}s_k'$ and $\mathrm{d}W_{s'}$ where $s_k' < s_k$. Since $\mathbb{E}(\mathrm{d}W_{s'}\mathrm{d}W_s) = \delta(s_k' - s_k)\mathrm{d}s_k'^2$, at first order in $\mathrm{d}s_k$, the stochastic average of the integral term in Eq. (202) vanishes. Actually, things are slightly more complicated since the upper bound of this integral, S_k, is a stochastic quantity itself. Therefore, the averaging process should also be carried out on this upper bound, and a generalized demonstration which includes this case can be found in Ref. [113] (theorem 1 on p. 28).

In order to characterize better the properties of this collapse time, it is also important to determine its variance. Interestingly enough, the same technique described above can be used in order to calculate iteratively higher orders of S_k. Upon using Eq. (202) one has

$$\mathbb{E}(S_k^2) = c^2(b_0) + \int_0^{S_k} c'^2[\Gamma_k(s_k)]\mathrm{d}s_k. \tag{204}$$

We see that we now need to evaluate the integral in the above expression. For this purpose, we consider a new function $e(\Gamma_k)$. As was done before, it can be Taylor expanded and this leads exactly to Eq. (200) (with, of course, c replaced by e). Compared with the proof that allowed us to obtain $\mathbb{E}(S_k)$, at this point, the strategy changes. We now require the function $e(x)$ to be the solution of the following ordinary differential equation [compare with Eq. (201)]:

$$\frac{1}{2}e''(x) + \tanh(x)e'(x) = -e'^2(x), \tag{205}$$

with boundary conditions $e(-b) = e(b) = 0$. As before, one can use this differential equation into the Itô formula to simplify the second integral in Eq. (204) [more precisely, the integrand is replaced by $-e'^2(x)$]. Taking the stochastic average of the resulting equation, one gets

$$e(b_0) = \int_0^{S_k} e'^2[\Gamma_k(s_k)]\mathrm{d}s_k. \tag{206}$$

As a consequence, we deduce that

$$\mathbb{E}(S_k^2) = c^2(b_0) + e(b_0). \tag{207}$$

The only thing which remains to be done is to solve Eq. (205). In fact, it turns out to be more convenient to

solve the slightly simpler differential equation satisfied by $e_1(x) \equiv c^2(x) + e(x)$, namely $e_1''(x)/2 + \tanh(x)e_1'(x) = -2c(x)$, with boundary conditions $e_1(-b) = e_1(b) = 0$. It is straightforward to show that $e_1(x) = x^2 - b^2 + [1 + 2b\tanh(b)][b\tanh(b) - x\tanh(x)]$. Then, the second moment of S can be simply expressed as $\mathbb{E}(S_k^2) = e_1(b_0)$ which, therefore, gives an explicit expression for the variance of the collapse time. Since b is supposed to be a large number $b \gg 1$ and if we assume that the two Gaussians have comparable initial weights which implies that $b_0 \sim 0$, then one obtains, at leading order in b,

$$\mathbb{E}(S_k) \simeq b, \tag{208}$$

$$\sqrt{\mathbb{E}(S_k^2) - \mathbb{E}^2(S_k)} \simeq \sqrt{b}. \tag{209}$$

These two equations tell us that the relative standard deviation scales as $1/\sqrt{b}$ and, therefore, that the distribution of S_k becomes more peaked as b increases. For this reason, in the following, we will simply estimate the collapse time by means of the sloppy requirement that $s_k = b$. Finally, let us mention that one could also apply the technique used in this section in order to determine the higher order correlation functions of the process S_k.

B. Collapse time in the sub-Hubble regime

In the last section, we have explained how to determine the collapse time in terms of the variable s_k. In order to translate this result in terms of a more physical time (conformal time or, better, number of e-folds), we need to use Eq. (195) which, in turn, requires the knowledge of the function X_k. This one cannot be determined in full generality but it is easy to characterize it in the sub- and super-Hubble regimes. In this section, we investigate the sub-Hubble regime.

Let us define $K_k \equiv \chi_k^{(2)} - \chi_k^{(1)}$. This quantity measures the shift in momentum between the two Gaussian components of the wave function (185) (we recall that X_k measures the shift in position). Then, taking the difference between the versions "(1)" and "(2)" of Eq. (189) on the one hand, and versions "(1)" and "(2)" of Eq. (191) on the other hand, we arrive at a closed system which can be written in a matrix form, namely

$$\frac{\mathrm{d}}{\mathrm{d}\eta}\begin{pmatrix} X_k \\ K_k \end{pmatrix} = \begin{pmatrix} -2\Im\mathrm{m}\Omega_k - \frac{\gamma}{\Re\mathrm{e}\Omega_k} & 1 \\ -4(\Re\mathrm{e}\Omega_k)^2 & 2\Im\mathrm{m}\Omega_k \end{pmatrix}\begin{pmatrix} X_k \\ K_k \end{pmatrix}. \tag{210}$$

At this stage, there is no approximation and the above equation is general. In the sub-Hubble regime, one can use Eq. (164) to simplify the expressions of $\Re\mathrm{e}\Omega_k$ and $\Im\mathrm{m}\Omega_k$. Moreover, we are mainly interested in computing the collapse time for the modes that correspond to the (almost) scale invariant part of the power spectrum since it is clearly less interesting to compute this quantity in a regime that is already excluded by the data. As was discussed before, this amounts to considering that $\gamma/k^2 \ll 1$. Under those conditions, one has $\Re\mathrm{e}\Omega_k \to k/2$ and $\Im\mathrm{m}\Omega_k \to -\gamma/(2k)$ and Eq. (210) can be reexpressed as

$$\frac{\mathrm{d}}{\mathrm{d}\eta}\begin{pmatrix} X_k \\ K_k \end{pmatrix} = \begin{pmatrix} -\gamma/k & 1 \\ -k^2 & -\gamma/k \end{pmatrix}\begin{pmatrix} X_k \\ K_k \end{pmatrix}. \tag{211}$$

This system of differential equations can be integrated and the solution reads

$$K_k(\eta) = \mathrm{e}^{-\gamma(\eta-\eta_{\mathrm{ini}})/k}\{K_{k,\mathrm{ini}}\cos[k(\eta-\eta_{\mathrm{ini}})] - kX_{k,\mathrm{ini}}\sin[k(\eta-\eta_{\mathrm{ini}})]\}, \tag{212}$$

$$X_k(\eta) = \mathrm{e}^{-\gamma(\eta-\eta_{\mathrm{ini}})/k}\left\{X_{k,\mathrm{ini}}\cos[k(\eta-\eta_{\mathrm{ini}})] + \frac{K_{k,\mathrm{ini}}}{k}\sin[k(\eta-\eta_{\mathrm{ini}})]\right\}, \tag{213}$$

where $K_{k,\mathrm{ini}}$ and $X_{k,\mathrm{ini}}$ are two integration constants conveniently chosen to be the values of K_k and X_k at initial time $\eta = \eta_{\mathrm{ini}}$. For simplicity, we now consider a situation such that $K_{k,\mathrm{ini}} = 0$. Upon using Eq. (195), one finds that

$$s_k = -\frac{k}{4}X_{k,\mathrm{ini}}^2[\mathrm{e}^{-2\gamma(\eta-\eta_{\mathrm{ini}})/k} - 1] - \frac{\gamma^2}{k^3}X_{k,\mathrm{ini}}^2\frac{1}{1+4\gamma^2/k^4}\mathrm{e}^{-2\gamma(\eta-\eta_{\mathrm{ini}})/k}\{\cos[2k(\eta-\eta_{\mathrm{ini}})] - \sin[2k(\eta-\eta_{\mathrm{ini}})] - 1\}. \tag{214}$$

If we expand the above result in γ/k^2 for the reason discussed before then, at leading order, one obtains an approximated expression for the mapping between the variables η and s_k

$$s_k \simeq \frac{kX_{k,\mathrm{ini}}^2}{4}[1 - \mathrm{e}^{-2\gamma(\eta-\eta_{\mathrm{ini}})/k}]. \tag{215}$$

This expression means that s_k runs from 0 to $kX_{k,\mathrm{ini}}^2/4$ when η runs from η_{ini} to infinity. Therefore, the time s_k evolves in a finite range. However, in order to be consistent, one must have $\eta < \eta_* = -1/k$ since the equations that have been used in order to derive s_k are valid only in the sub-Hubble regime. As a consequence, we have in fact $s_k \in [0, s_*]$ where $s_* \equiv kX_{k,\mathrm{ini}}^2/4\{1 - \exp[(2\gamma/k^2)(1 + k\eta_{\mathrm{ini}})]\}$. Since we have $|k\eta_{\mathrm{ini}}| \gg 1$, one can thus write $s_* \simeq kX_{k,\mathrm{ini}}^2/4[1 - \exp(2\gamma\eta_{\mathrm{ini}}/k)]$. If $s < s_*$, then Eq. (215) can be inverted in order to evaluate the (total) number of e-folds in terms of the time variable s_k. One finds

$$N_k = (1+\beta)\ln\left[1 - \frac{k^2}{2\gamma}\frac{1}{k\eta_{\mathrm{ini}}}\ln\left(1 - \frac{4s_k}{kX_{k,\mathrm{ini}}^2}\right)\right], \tag{216}$$

and one checks that if $s_k = 0$ then $N_k = 0$, if $s_k = s_*$ then $N \to \infty$, and that the condition $s < s_*$ is sufficient to guarantee that the above expression is well defined.

Let us now discuss the above results in more detail. First, we notice in Eqs. (212) and (213) that the functions $K_k(\eta)$

and $X_k(\eta)$ tend to zero when $\eta - \eta_{\rm ini} \gg 1$. When this happens, the two Gaussians have the same mean in position and momentum; in other words the two Gaussians have merged. This "merging phenomenon" seems to be a generic feature and can also be observed for the free particle [73] and/or the harmonic oscillator in Minkowski spacetime. Therefore, it does not come as a surprise that it also shows up in the sub-Hubble regime where the Fourier mode under consideration does not feel spacetime curvature. This also means that it is not a peculiar property of inflation.

The free particle situation can be studied [73] by returning to Eqs. (118)–(123). It is sufficient to consider that $\omega = 0$ in those equations to obtain this case. This means that the mode equation (125) now reads $f_k'' - \alpha^2 f_k = 0$, where the quantity α, defined in Eq. (126) for the harmonic oscillator, now reads $\alpha = \sqrt{2i\gamma\hbar/m} = \sqrt{\gamma\hbar/m}(1+i)$ and is obtained from Eq. (126) by taking $\omega = 0$. As a consequence, the solution for $\Omega(t)$ has exactly the same form as in Eq. (127) but now with the new α given above. This implies that $\Re\mathrm{e}\Omega \to \sqrt{\gamma m/\hbar}/2$ and $\Im\mathrm{m}\Omega \to \sqrt{\gamma m/\hbar}/2$ when $t \to \infty$. These formulas should be compared to Eqs. (134) and (135). Then, considering the equations of motion for a double Gaussian state, and defining $X \equiv \bar{x}_2 - \bar{x}_1$ and $K \equiv \chi_2 - \chi_1$, upon using Eq. (210), one obtains the following set of equations:

$$\frac{\mathrm{d}}{\mathrm{d}t}\begin{pmatrix} X \\ K \end{pmatrix} = \begin{pmatrix} -\sqrt{\gamma\hbar/m} & \hbar/m \\ -\gamma & -\sqrt{\gamma\hbar/m} \end{pmatrix}\begin{pmatrix} X \\ K \end{pmatrix}. \tag{217}$$

This equation should be compared to Eq. (211). In particular, one notices that, here, the free particle case is not simply obtained from this equation by considering $k = \omega = 0$. If we assume that $K(0) = 0$, then the solution for $X(t)$ is given by $X(t) = X(0)\exp(-t\sqrt{\hbar\gamma/m})\cos(t\sqrt{\hbar\gamma/m})$. We see that this solution resembles solutions (213) and (212) obtained before. Therefore, the merging is indeed already present for a free particle in flat spacetime and is not a specific feature of inflation. The exponential factor is mainly responsible for the merging and this means that the "merging time" of the free particle is given by

$$T_{\rm merge}^{\rm fp} = \sqrt{\frac{m}{\hbar\gamma}}. \tag{218}$$

This expression is consistent with the merging time derived in Ref. [73].

In order to discuss our inflationary result, one should consider the merging time of the harmonic oscillator instead of that of the free particle since this is the appropriate limit in the sub-Hubble regime. Following the same logic as before, it is easy to show that, for the harmonic oscillator, Eq. (217) is replaced by

$$\frac{\mathrm{d}}{\mathrm{d}t}\begin{pmatrix} X \\ K \end{pmatrix} = \begin{pmatrix} -\gamma\hbar/(m\omega) & \hbar/m \\ -m\omega^2/\hbar & -\gamma\hbar/(m\omega) \end{pmatrix}\begin{pmatrix} X \\ K \end{pmatrix}. \tag{219}$$

We see that it is indeed similar to Eq. (211) if we take $\omega = k$ (and $m = \hbar = 1$). The solution for $X(t)$ can be expressed as $X(t) = X(0)\exp[-\hbar\gamma/(m\omega)t]\cos(\omega t)$, assuming as before $K(0) = 0$. This solution is perfectly consistent with (212) and (213). Compared to the free particle case, one notices that the coefficient in the exponential is now different from the frequency of the trigonometric function. But the most important result that one can deduce from the above considerations is that the merging phenomenon is also present for the harmonic oscillator and that the corresponding merging time is given by

$$T_{\rm merge}^{\rm ho} = \frac{m\omega}{\hbar\gamma} = \omega(T_{\rm merge}^{\rm fp})^2. \tag{220}$$

Let us remark that the last expression could have been guessed on dimensional grounds.

In the case of inflation, the conformal merging time is given by [see Eqs. (212) and (213)]

$$k(\eta_{\rm merge} - \eta_{\rm ini}) = \frac{k^2}{\gamma}. \tag{221}$$

However, there is a new twist in the discussion. It is not obvious that the above equation admits a solution because, in some sense, we have a limited amount of time from $\eta_{\rm ini}$ to η_*, the time of Hubble horizon crossing (defined by $|k\eta_*| = 1$). For times such that $|k\eta| < 1$, we are no longer in the sub-Hubble regime and the above equation can no longer be used. But, given a value of k^2/γ, and an initial time $\eta_{\rm ini}$, it is not obvious that there exists a time $\eta_{\rm merge}$ such that Eq. (221) is satisfied. In fact, there exists a solution only if $|k\eta_{\rm ini}| > 1 + k^2/\gamma$. This condition means that, for a given k^2/γ, one can always give more time to the system to satisfy Eq. (221) by starting its evolution earlier (which is equivalent to increasing $|\eta_{\rm ini}|$). It is easy to show that the previous inequality is in fact a condition on the total number of e-folds during inflation ($\beta \lesssim -2$), namely

$$N_{\rm T} \gtrsim \Delta N_* + \ln\left(1 + \frac{k^2}{\gamma}\right), \tag{222}$$

where $\Delta N_* \simeq 50$ for the modes of cosmological interest today. If this condition is met, then the merging occurs after $N_k^{\rm merge}$ with

$$N_k^{\rm merge} = -\ln\left(1 + \frac{k^2}{\gamma k\eta_{\rm ini}}\right). \tag{223}$$

Moreover, the term $k^2/(\gamma k\eta_{\rm ini})$ is of the order $\sim k^2 \mathrm{e}^{-N_{\rm T}+50}/\gamma$ and it seems reasonable to assume that it is small. Indeed, typically, the total number of e-folds during inflation is very large and, even if $k^2/\gamma \gg 1$, the factor $\mathrm{e}^{-N_{\rm T}}$ will entirely compensate its influence (to be more concrete, we know that $k^2/\gamma \gtrsim 10^{28}$ but $N_{\rm T}$ can easily be larger than, say, 1000 and can even be as large as 10^8). Then, the merging time during inflation can be approximated by

$$N_{\boldsymbol{k}}^{\mathrm{merge}} \simeq -\frac{k^2}{\gamma k \eta_{\mathrm{ini}}} \ll 1. \tag{224}$$

We see that this expression scales as $\propto k/\gamma$, in full agreement with the previous considerations on the harmonic oscillator, see Eq. (220).

Let us now study the collapse time. First of all, the collapse can occur in the sub-Hubble regime only if $b < s_*$. If we use the expression of s_* and assume, as before, that $k^2/(\gamma k \eta_{\mathrm{ini}}) \ll 1$, then $s_* \simeq k X_{\boldsymbol{k},\mathrm{ini}}^2/4$ and the condition for having the collapse in the sub-Hubble regime can be simply rewritten as

$$b \ll \frac{k X_{\boldsymbol{k},\mathrm{ini}}^2}{4}. \tag{225}$$

If this condition is satisfied, then the "e-fold collapse number" of the mode under consideration is obtained by putting $s_{\boldsymbol{k}} = b$ in the above expression (216). Upon using the same assumptions as before, we obtain that

$$N_{\boldsymbol{k}}^{\mathrm{col}} \simeq -\frac{2b}{\gamma X_{\boldsymbol{k},\mathrm{ini}}^2 \eta_{\mathrm{ini}}} \ll 1. \tag{226}$$

At this point, several remarks are in order. First, we notice that $N_{\boldsymbol{k}}^{\mathrm{col}}/N_{\boldsymbol{k}}^{\mathrm{merge}} = 4b/(k X_{\boldsymbol{k},\mathrm{ini}}^2) \ll 1$. This means that the collapse occurs on a much smaller time scale than the merging. This property was also noticed in the case of a free particle in Ref. [73]. This means that the merging cannot be viewed as a substitute for the collapse. Second, we notice that $N_{\boldsymbol{k}}^{\mathrm{col}}$ is actually independent of k. We interpret this fact as meaning that, on sub-Hubble scales, the mode under consideration must behave as in flat spacetime. Indeed, for a free particle or the harmonic oscillator in Minkowski spacetime, the condition for the collapse to occur can be written as $s = \gamma \int X^2(\tau) \mathrm{d}\tau \simeq \gamma X(0)^2 T_{\mathrm{col}}^{\mathrm{fp,ho}} = b$, where we have used $X(t) \simeq X(0)$ since we have shown that the merging takes place on a much longer time scale. This implies that

$$T_{\mathrm{col}}^{\mathrm{fp,ho}} \simeq \frac{b}{\gamma X(0)^2}, \tag{227}$$

and one verifies that it is similar to Eq. (226). Therefore, if the collapse occurs on sub-Hubble scales, its properties are, as expected, similar to what happens in flat spacetime. Finally, if one starts from an initial state made of several well-separated Gaussian wave functions, the previous calculation suggests that it will almost instantaneously turn into a single Gaussian state. As a matter of fact, it is a general property [64,114] of the CSL dynamics that it asymptotically leads to Gaussian states. *A posteriori*, this remark reinforces the assumption of using a Gaussian state for the calculation of the spectrum in Sec. V D.

When condition (225) is not satisfied, there will be no collapse on sub-Hubble scales. However, we can still hope it will happen on super-Hubble scales. In fact, the claim that the collapse has occurred depends on the value chosen for b. Before, we used $b \simeq 10$ and for this value, given that our working assumption is $k X_{\boldsymbol{k},\mathrm{ini}}^2 \gg 1$, condition (225) is probably always satisfied. Therefore, it is only if we are more demanding about the criterion that defines the collapse that this condition can be violated. It is clear that a more stringent criterion takes more time to be satisfied and, in this case, the time "at our disposal" in the sub-Hubble regime may not be sufficient. In this situation, we have to consider the super-Hubble regime. In the next section, we turn to this case and show that the collapse is less efficient on large scales than it is on small scales.

C. Collapse time in the super-Hubble regime

In this section, we repeat the previous discussion but now in the super-Hubble regime. Therefore, we restart from equations (210) but now use the super-Hubble limit (166) and (167) for $\Re\mathrm{e}\Omega_{\boldsymbol{k}}$ and $\Im\mathrm{m}\Omega_{\boldsymbol{k}}$. For the modes of cosmological interest today in the (almost) scale invariant branch of the CSL power spectrum, one has $\gamma/k^2 \lll 1$ and the solution for $X_{\boldsymbol{k}}(\eta)$ can be simply written as

$$X_{\boldsymbol{k}}(\eta) \simeq X_{\boldsymbol{k}*}(-k\eta)^{\beta+1}, \tag{228}$$

where $X_{\boldsymbol{k}*}$ is the value of $X_{\boldsymbol{k}}(\eta)$ when the mode under consideration $\boldsymbol{k}$ crosses the Hubble radius. One can see that $X_{\boldsymbol{k}}(\eta)$ increases with time contrary to what happens in the sub-Hubble regime. From this expression, it is easy to derive the relation between $s_{\boldsymbol{k}}$ and the conformal time. One obtains

$$s_{\boldsymbol{k}} = -\frac{\gamma}{k^2}\frac{k X_{\boldsymbol{k}*}^2}{2\beta+3}[(-k\eta)^{2\beta+3} - 1]. \tag{229}$$

The last formula is valid only on super-Hubble time, that is to say for $\eta > \eta_* = -1/k$. At $\eta = \eta_*$, $s_{\boldsymbol{k}} = 0$ and then $s_{\boldsymbol{k}} \to \infty$ as $\eta \to 0$. From this expression, it is also possible to relate the time variable $s_{\boldsymbol{k}}$ and the number of e-folds. One arrives at

$$N_{\boldsymbol{k}} = N_* + \frac{1+\beta}{2\beta+3}\ln\left(1 - \frac{k^2}{\gamma}\frac{2\beta+3}{k X_{\boldsymbol{k}*}^2} s_{\boldsymbol{k}}\right). \tag{230}$$

This expression is always well defined because $2\beta + 3 < 0$. One verifies that $s_{\boldsymbol{k}} = 0$ corresponds to $N_{\boldsymbol{k}} = N_*$.

Let us now derive the time of collapse. As usual, it is obtained by $s_{\boldsymbol{k}} = b$. As a consequence, it is simply given by

$$N_{\boldsymbol{k}}^{\mathrm{col}} = N_* + \frac{1+\beta}{2\beta+3}\ln\left(1 - \frac{k^2}{\gamma}\frac{2\beta+3}{k X_{\boldsymbol{k}*}^2} b\right). \tag{231}$$

As a first check of this equation, we notice that, when $\gamma \to \infty$, $N_{\boldsymbol{k}}^{\mathrm{col}} \simeq N_*$. Of course, this result is expected since a large value of γ means that the collapse mechanism is very efficient and, therefore, that the wave function almost instantaneously collapses. On the other hand, formula (231) can be further simplified. Indeed, if the collapse has not taken place on sub-Hubble scales, it is also the case for the merging since $N_{\boldsymbol{k}}^{\mathrm{col}}/N_{\boldsymbol{k}}^{\mathrm{merge}} \ll 1$. As a consequence, $X_{\boldsymbol{k}}(\eta)$ has not evolved much and one can replace $X_{\boldsymbol{k}*}$ by $X_{\boldsymbol{k},\mathrm{ini}}$. Moreover, for the same reason, one must have $b \gtrsim k X_{\boldsymbol{k},\mathrm{ini}}^2/4$, see also Eq. (225). In addition, we know that

$k^2/\gamma \gg 1$. Therefore, the first term in the argument of the logarithm in Eq. (231) can be neglected. For $\beta \simeq -2$, this equation can be rewritten as

$$N_{\boldsymbol{k}}^{\mathrm{col}} - N_* \simeq \ln\left(\frac{k^2}{\gamma}\right) + \ln\left(\frac{b}{kX_{\boldsymbol{k},\mathrm{ini}}^2}\right). \tag{232}$$

Of course the result will depend on what we require for b and what we assume for $X_{\boldsymbol{k},\mathrm{ini}}$. However, it seems reasonable to assume that the second logarithm will not lead to a dominant contribution. If this is the case, then our result simply says that the wave function collapses just $\ln(k^2/\gamma)$ e-folds after the Hubble radius crossing. Given the constraint obtained from the measurement of the power spectrum in Eq. (178), one already knows that $N_{\boldsymbol{k}}^{\mathrm{col}} - N_* \gtrsim 28$. Smaller values of γ/k^2 would of course lead to a larger number of e-folds. We conclude this section by noticing that the constraint (178) is compatible with a collapse occurring during inflation. Only for values of γ such that $\gamma/k^2 \ll 10^{-50}$ (and $b \gtrsim kX_{\boldsymbol{k},\mathrm{ini}}^2/4$) would the collapse happen after inflation.

D. The Born rule derived

Finally, we conclude with a section where we calculate the probabilities of collapsing to each of the two branches of the wave function. We show that these probabilities are given by the Born rule, which is of course expected since the CSL theory is precisely designed to reproduce this result, as already discussed in Sec. IV (see also Ref. [73]).

Let us denote by p_1 the probability that the system collapses on the first Gaussian branch of the wave function. This is also the probability that, from given initial conditions, the stochastic quantity $\Gamma_{\boldsymbol{k}}$ reaches first the region $\Gamma_{\boldsymbol{k}} < -b$ (i.e., before the region $\Gamma_{\boldsymbol{k}} > b$) and that, therefore, one has $\Gamma_{\boldsymbol{k}}(S_{\boldsymbol{k}}) = -b$. Clearly, the probability p_2 that the wave function collapses on the second branch is the probability that $\Gamma_{\boldsymbol{k}}(S_{\boldsymbol{k}}) = b$. Now, let us introduce a function $\psi(x)$ which is defined by

$$\psi(x) \equiv \frac{g(x) - g(b)}{g(-b) - g(b)}, \tag{233}$$

where $g(x)$ will be specified soon. By construction, one has $\psi(-b) = 1$ and $\psi(b) = 0$. Since, by definition, $\Gamma_{\boldsymbol{k}}(S_{\boldsymbol{k}})$ can only take two values (namely $\pm b$), one has

$$\mathbb{E}\{\psi[\Gamma_{\boldsymbol{k}}(S_{\boldsymbol{k}})]\} = p_1\psi(-b) + p_2\psi(b) = p_1, \tag{234}$$

and this gives us a method to calculate p_1. To do so, we follow what was explained in Sec. VI A, see in particular Eq. (200), and we write the corresponding Itô formula

$$\begin{aligned}\psi[\Gamma_{\boldsymbol{k}}(S_{\boldsymbol{k}})] - \psi(b_0) &= \int_0^{S_{\boldsymbol{k}}} \psi'[\Gamma_{\boldsymbol{k}}(s_{\boldsymbol{k}})]\mathrm{d}W_s + \int_0^{S_{\boldsymbol{k}}}\Big\{\psi'[\Gamma_{\boldsymbol{k}}(s_{\boldsymbol{k}})]\tanh[\Gamma_{\boldsymbol{k}}(s_{\boldsymbol{k}})] \\ &\quad + \frac{1}{2}\psi''[\Gamma_{\boldsymbol{k}}(s_{\boldsymbol{k}})]\Big\}\mathrm{d}s_{\boldsymbol{k}}.\end{aligned} \tag{235}$$

Then, let us choose the function $g(x)$ such that it obeys the equation

$$\frac{1}{2}g''(x) + \tanh(x)g'(x) = 0, \tag{236}$$

or, equivalently, $g(x) = \tanh(x)$. Since Eq. (233) implies that $\psi(x)$ and $g(x)$ are linearly related, $\psi(x)$ also obeys the above differential equation. As a consequence, the second integral in Eq. (235) vanishes. Taking the stochastic average, one obtains

$$\mathbb{E}\{\psi[\Gamma_{\boldsymbol{k}}(S_{\boldsymbol{k}})]\} = p_1 = \psi(b_0), \tag{237}$$

which is explicitly known since $g(x)$ has been determined.

The probability p_2 can be deduced along the same lines, by introducing a new function ψ such that, this time, $\psi(-b) = 0$ and $\psi(b) = 1$. Another method, much simpler, is just to use the condition $p_1 + p_2 = 1$. The final result reads

$$p_1 = \frac{\tanh(b_0) - \tanh(b)}{\tanh(-b) - \tanh(b)}, \tag{238}$$

$$p_2 = \frac{\tanh(b_0) - \tanh(-b)}{\tanh(b) - \tanh(-b)}. \tag{239}$$

From the definition of $\Gamma_{\boldsymbol{k}}$, these two formula can be rewritten as [73]

$$p_1 = \frac{|N_1(\eta_{\mathrm{ini}})|^2}{|N_1(\eta_{\mathrm{ini}})|^2 + |N_2(\eta_{\mathrm{ini}})|^2}, \tag{240}$$

$$p_2 = \frac{|N_2(\eta_{\mathrm{ini}})|^2}{|N_1(\eta_{\mathrm{ini}})|^2 + |N_2(\eta_{\mathrm{ini}})|^2}, \tag{241}$$

which are exactly the Born rules of conventional quantum mechanics.

VII. CONCLUSION

Let us now summarize our main findings. In this paper, we have applied the CSL theory to inflation. Since the CSL scenario addresses the measurement problem in quantum mechanics, it is *a priori* relevant to explain how the wave packet reduction took place in the early Universe, in the absence of any observer. Assuming that the wave function has to collapse on an eigenstate of the Mukhanov-Sasaki operator, we have computed the scalar power spectrum of cosmological perturbations and studied the dynamics of the wave function collapse. We have found that, in order to preserve the scale invariance of the power spectrum, it is necessary to fine-tune the parameter γ which controls the amplitude of the CSL corrections. Typically, depending on which temporal gauge is chosen (see the Appendix), we have found that the dimensionless parameter that can be constructed out of γ must be smaller than $\exp(-\text{a few}\Delta N_*)$, where $\Delta N_* \simeq 50$–60 is the number of e-folds spent by the relevant modes outside the Hubble radius during inflation. We have also found that the time

available during the inflationary phase is sufficient in order for the perturbations' wave function to collapse. However, due to the smallness of γ, the spread of the final wave function is too important, rendering the collapse process not sufficiently efficient. Therefore, under the assumptions made in this paper, it seems fair to claim that the collapse theories cannot solve the inflationary macro-objectification question.

The conclusions drawn above may not be as drastic as they appear at first sight, because they are subject to some assumptions, and in particular the choice of the collapse operator as the Fourier space Mukhanov-Sasaki $v_{\boldsymbol{k}}$ variable: all cosmological predictions made to date are based on this variable, rendering this choice very sensible, but it is by no means unique (see, e.g., the discussion in Sec. V A). Moreover, $v_{\boldsymbol{k}}$ can be understood as a quantum field living in a curved spacetime, so it should be treated by a quantum field theory version of the CSL mechanism. The present state of the art of this subject technically forbids such a direct treatment, hence our simplifying hypothesis. Could it be that a full relativistic version of CSL, reproducing the many successes of quantum field theory and of the ensuing particle physics, is needed before we can even embark in examining cosmological perturbations? We doubt so, because cosmology, contrary to ordinary quantum field theory, is endowed with a preferred timelike direction that renders the "time-dependent Minkowski approximation" accurate enough for all practical purposes. It is left for future investigations to verify that the potential problems raised and stringent constraints obtained in this work could be naturally solved in a more general, yet unknown, framework.

There are other questions that could be the subject of further works. In particular, there is the issue that energy is not conserved in the CSL theory. In the case of the harmonic oscillator, this is expressed through Eq. (142). In the case of cosmological perturbations, it is easy to show that this leads to

$$\frac{\mathrm{d}}{\mathrm{d}\eta}\langle\hat{\mathcal{H}}_{\boldsymbol{k}}\rangle = \frac{\gamma}{2} + \omega\omega'\langle v_{\boldsymbol{k}}^2\rangle. \tag{242}$$

The CSL contribution can easily be integrated and gives $\langle\hat{\mathcal{H}}_{\boldsymbol{k}}\rangle|_{\mathrm{CSL}} \simeq \gamma\eta_{\mathrm{ini}}/2$ at the end of inflation. Expressed in terms of the Hamiltonian rather than the Hamiltonian density, one arrives at

$$\langle\hat{H}\rangle|_{\mathrm{CSL}} \simeq -4\pi^2\frac{\gamma}{2}\eta_{\mathrm{ini}}\int k^2\mathrm{d}k, \tag{243}$$

which is infinite. It does not come as a surprise as it is known that the CSL Tomanaga-Schwinger equation precisely leads to this type of divergence [67,68]. It could be regularized by introducing an ultraviolet cutoff although we notice on the above equation the weird property that the infinite integral is over comoving wave numbers rather than over physical ones. This energy nonconservation should cause a continuous increase of energy density during inflation. It is interesting to notice that it cannot occur at first order in the perturbations since $\mathbb{E}(\langle\widehat{\delta\rho}_{\boldsymbol{k}}\rangle) = 0$. This means that it will be important at second order only. Then, it would be important to quantify this effect and, in particular, to compare it to the background energy density $\simeq H^2M_{\mathrm{Pl}}^2$ in order to check whether this leads to a back-reaction problem.

Another point is that we have shown that the power spectrum, contrary to what happens in the standard case, remains a time-dependent quantity, i.e., still evolves with time on large scales during inflation. It is therefore not obvious that $\mathcal{P}_\zeta$ evaluated at the end of inflation is exactly the power spectrum that should be used at recombination. In fact, what happens just after the end of inflation is of great interest for the cosmological consequences of CSL. Indeed, just after inflation, the stages of preheating and reheating begin [96–98]; this is also shown in Fig. 4. During this phase of evolution, the inflaton field oscillates at the bottom of its potential, $\varphi(t) \propto \sin(mt + \Delta)/(mt)$ where Δ is a phase and m the mass of the inflaton (in the case of power-law inflation, the potential has no minimum and, therefore, can only be used to describe the slow-roll regime; here, we assume that the potential can be approximated by $m^2\varphi^2$ in the vicinity of the minimum). In this case, the equation of motion (12) for the Mukhanov-Sasaki variable takes the form of a Mathieu equation [99]. As is well known, this equation possesses unstable solutions when the parameters falls in the resonant bands. In the case of inflation, one can show that the large-scale perturbations are in the first instability band which makes $v_{\boldsymbol{k}}$ growing and $\zeta_{\boldsymbol{k}}$ staying constant [99,100]. In the CSL case, the corresponding Mathieu equation would read

$$\frac{\mathrm{d}^2v_{\boldsymbol{k}}}{\mathrm{d}z^2} + [\mathcal{A}_{\boldsymbol{k}} - 2q\cos(2z + 2\Delta)]v_{\boldsymbol{k}} = 0, \tag{244}$$

where $z \equiv mt + \pi/4$, a_{e}, t_{e} denoting the scale factor and the cosmic time at the end of inflation and with

$$\mathcal{A}_{\boldsymbol{k}} = 1 + \frac{k^2 - 2i\gamma}{m^2a^2}, \tag{245}$$

$$q = \frac{2}{mt_{\mathrm{e}}}\left(\frac{a_{\mathrm{e}}}{a}\right)^{3/2}. \tag{246}$$

Since $q \ll 1$, in the regular case when $\gamma = 0$, the condition to be in the first resonant bands, $1 - q < \mathcal{A}_{\boldsymbol{k}} < 1 + q$, is equivalent to $0 < k/a < \sqrt{3Hm}$. In the CSL case, the coefficient $\mathcal{A}_{\boldsymbol{k}}$ becomes complex. Therefore, in order to determine the corresponding Floquet index, it now becomes necessary to study the instability chart of the Mathieu equation in the complex domain. Although this is beyond the scope of this paper, this is certainly a subject worth investigating. In particular, it would be interesting to see whether the instability is enhanced in this case as one can, maybe naively, suspect. If so, maybe the preheating

stage can put even more stringent constraints on the parameter γ.

We have seen that the study of the CSL cosmological perturbations is in fact equivalent to the study of the CSL parametric oscillator (i.e., a harmonic oscillator with a time-dependent frequency). The previous discussion suggests that it would be interesting to investigate the case of a parametric oscillator in the presence of a resonance in the CSL framework. In quantum field theory, this is a common situation and typical examples are the dynamical Schwinger effect [115] (the analogy between cosmological perturbations and the Schwinger effect was discussed in Ref. [15]) or the dynamical Casimir effect [116] which was recently observed for the first time [117] in the laboratory. In fact, if we want to avoid the objection that the quantum field CSL theory is not yet ready, it would be even more interesting to find a nonrelativistic system governed by a Mathieu equation and to investigate its behavior within the CSL theory. We believe that all of the equations presented in the present article can be straightforwardly applied to this case. Here, we suggest that a Paul trap [118] could be such an example. As for the inflationary preheating, we expect the coefficients of the Mathieu equation to become complex because of the $-2i\gamma$ term. This will probably make the system extremely unstable and, as a consequence, it will probably be possible to put very tight constraints on the value of γ. We hope that this case will be treated in details soon.

ACKNOWLEDGMENTS

We would like to thank D. Sudarsky for interesting and enjoyable discussions.

APPENDIX: "GAUGE INVARIANCE" OF THE CSL POWER SPECTRUM

In section VA, we discussed the choice of the collapse operator, i.e., the operator that appears in the nonlinear and stochastic part of the modified Schrödinger equation. In principle, this operator should be determined by a more fundamental theory. However, the CSL model is just a phenomenological approach and the collapse operator is just put by hand in order to match what we observe when an experiment or an observation is performed (the position of a spot in a detector, the energy density of a field, etc.). In the case of the cosmological primordial perturbations, we have argued that the Mukhanov-Sasaki variable $\hat{v}_{\boldsymbol{k}}$ is the most sensible choice. But this variable often appears factorized by a background quantity, typically a power of the scale factor $a(\eta)$. Therefore, instead of $\hat{v}_{\boldsymbol{k}}$, one could very well choose the collapse operator to be $h(a)\hat{v}_{\boldsymbol{k}}$, where h is *a priori* an arbitrary function of the scale factor a. After all, $\hat{v}_{\boldsymbol{k}}$ and $h(a)\hat{v}_{\boldsymbol{k}}$ share the same eigenspectrum and drive the system towards the same target states with the same probabilities. But the point is that, *a priori* and as is discussed in detail below, this does not lead to the same solution for the mode function $f_{\boldsymbol{k}}(\eta)$ and, therefore, *a priori*, for the power spectrum.

In fact, this issue is related to an even more fundamental problem. Indeed, one could claim that the conformal time η used in this paper to write the modified Schrödinger equation is not the physical one and that one should use instead, say, the cosmic time t (of course, the discussion also applies to any other time variables related to η through a transformation that depends only on the background). In fact, a choice of time is equivalent to a choice of h since it has the same effect on the modified Schrödinger equation. And, of course, as already mentioned, one could worry that different choices lead to different predictions. Therefore, the phenomenological approach used in this article suffers from what can be called a temporal gauge problem. This problem probably originates from the fact that the CSL equation is not covariant under diffeomorphisms (contrary to the standard theory of cosmological perturbations).

In this appendix, we investigate this question, showing the remarkable property that the conclusions obtained in this paper for $h(a) = 1$ are in fact valid for any other functions h. It is true that the detailed shape of the power spectrum depends on the gauge but its global properties are independent of the choice of h. This means that, *a priori* for any h allowing meaningful initial conditions, the power spectrum of cosmological perturbations has a broken power-law shape, with $n_{\mathrm{S}} = 1$ at small wavelengths and $n_{\mathrm{S}} = 4$ at large wavelengths. As a consequence, the requirement of moving the non-scale-invariant part of the spectrum beyond the Hubble radius today always leads to extreme constraints on the parameter γ.

Let us now consider the modified Schrödinger equation of motion for $\Psi_{\boldsymbol{k}}$ in the CSL picture, with spontaneous localization on the $h(a)\hat{v}_{\boldsymbol{k}}$ eigenmanifolds. It reads

$$\mathrm{d}\Psi_{\boldsymbol{k}}^{\mathrm{R}} = \Big[-i\hat{\mathcal{H}}_{\boldsymbol{k}}^{\mathrm{R}}\mathrm{d}\eta + \sqrt{\gamma}h(a)(\hat{v}_{\boldsymbol{k}}^{\mathrm{R}} - \langle\hat{v}_{\boldsymbol{k}}^{\mathrm{R}}\rangle)\mathrm{d}W_\eta - \frac{\gamma}{2}h^2(a)(\hat{v}_{\boldsymbol{k}}^{\mathrm{R}} - \langle\hat{v}_{\boldsymbol{k}}^{\mathrm{R}}\rangle)^2\mathrm{d}\eta\Big]\Psi_{\boldsymbol{k}}^{\mathrm{R}}, \tag{A1}$$

and a similar equation for $\Psi_{\boldsymbol{k}}^{\mathrm{I}}$. This equation should be compared with Eq. (143), the only difference being that the operator $\hat{v}_{\boldsymbol{k}}$ is now multiplied by $h(a)$. Parametrizing $\Psi_{\boldsymbol{k}}$ as in Eq. (144) using again $\Omega_{\boldsymbol{k}} = -if_{\boldsymbol{k}}'/(2f_{\boldsymbol{k}})$, one is led to the following equation for the mode function

$$f_{\boldsymbol{k}}'' + [\omega^2(\eta, \boldsymbol{k}) - 2i\gamma h^2(a)]f_{\boldsymbol{k}} = 0. \tag{A2}$$

This expression should be compared with Eq. (153): as expected, the only difference is that an extra $h^2(a)$ appears in front of the γ term. For simplicity, let us choose h to be a simple power law and let us assume the inflationary dynamics to be close to a de Sitter universe $a(\eta) \simeq -\ell_0/\eta$. Then, the mode function can be reexpressed as

$$f_{\boldsymbol{k}}'' + \left(k^2 - \frac{2}{\eta^2} - 2i\gamma a^p\right)f_{\boldsymbol{k}} = 0. \tag{A3}$$

If $p < 0$, the Bunch-Davies vacuum state cannot be chosen at the onset of inflation since the k^2 term does not dominate in the parenthesis. This means that one must work with $p \geq 0$. In this paper the case $p = 0$ [i.e., $h(a) = 1$] has been studied, hence one only needs to study the $p > 0$ cases. It is interesting first to notice that the cases $p > 0$ provide a natural amplification phenomenon depending on the physical length of the mode since the amplitude of the term proportional to γ now increases as the mode is stretched by the growth of the scale factor. This is consistent with the physical intuition which tells us that the collapse should occur for macro extended objects only. If $p > 2$, the term proportional to γ dominates the dynamics at the end of inflation, when $k\eta$ goes to 0, and one can expect the power spectrum scale invariance to be destroyed. Therefore, if p is an integer, we are left with the cases $p = 1$ and $p = 2$ that we now study.

If $p = 1$, the general solutions of Eq. (A3) can be expressed in terms of Whittaker functions $W_{\mu,\kappa}(z)$ [101,102] as

$$f_k(\eta) = C_k W_{\gamma\ell_0/k,3/2}(2ik\eta) + D_k W_{-\gamma\ell_0/k,3/2}(-2ik\eta), \tag{A4}$$

where C_k and D_k are integration constants that can be determined by choosing the Bunch-Davies vacuum state for the initial conditions. This leads to $C_k = 0$. Then, in the limit where $k\eta$ goes to 0, $\Re\mathrm{e}\Omega_k(\eta)$ can be Taylor expanded, and this provides a simple expression for this quantity. In particular, we find that $\Re\mathrm{e}\Omega_k/k = \gamma\ell_0/(2k) + \mathcal{O}(k\eta)$, showing that, in this case, the spread does not diverge in the large-scale limit and that, as a consequence, the localization of the wave function becomes much more accurate. Moreover, since the inverse of $\Re\mathrm{e}\Omega_k$ is basically $\mathcal{P}_\zeta$, this allows us to calculate the power spectrum, provided we push the expansion to higher orders. One obtains

$$\mathcal{P}_\zeta(k) = g\left(\frac{\ell_0\gamma}{k}\right)\left[1 + \frac{\ell_0\gamma}{k_0}g\left(\frac{\ell_0\gamma}{k}\right)\mathrm{e}^{2\Delta N_*}\left(\frac{k_0}{k}\right)^3 - 2\frac{\ell_0\gamma}{k}g\left(\frac{\ell_0\gamma}{k}\right)\left(1 - \frac{\ell_0^2\gamma^2}{k^2}\right)\ln\left(2\frac{k}{k_0}\,\mathrm{e}^{-\Delta N_*}\right)\right]^{-1} \times \mathcal{P}_\zeta(k)|_{\mathrm{stand}}, \tag{A5}$$

where $\mathcal{P}_\zeta|_{\mathrm{stand}}$ is the standard power spectrum (47), and where $g(x)$ is defined by

$$\frac{1}{g(x)} \equiv 1 + 3x - 3x^2 - x^3 - 2x(1-x^2)[\psi(2+x) - 2\psi(1)], \tag{A6}$$

$\psi(x)$ being the digamma Euler function [101,102]. Let us notice that, in Eq. (A5), we have sometimes introduced the quantity $\ell_0\gamma/k$. Of course, the most convenient way of dealing with this quantity is to express it as $(\ell_0\gamma/k_0)k_0/k$ such that the dimensionless small parameter $\ell_0\gamma/k_0$ explicitly appears. The spectrum given by Eq. (A5) should be compared with the one obtained in Eq. (172) with the choice

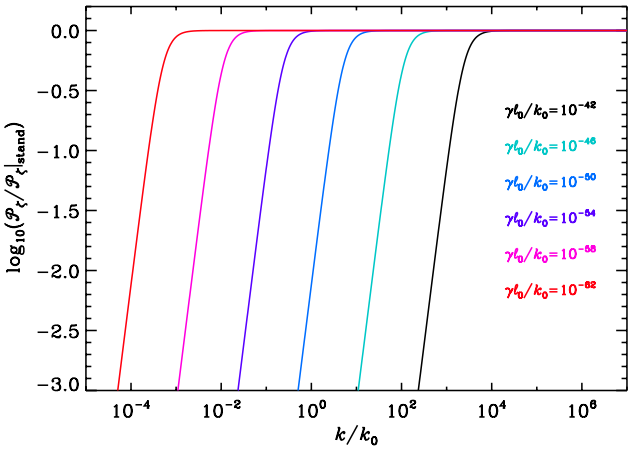

FIG. 6 (color online). Ratio of the power spectrum given by Eq. (A5) ($p = 1$) to the standard power spectrum given by Eq. (47) for different values of the parameter $\gamma\ell_0/k_0$.

$h = 1$. They share the same broken power-law structure, with a scale-invariant part $n_S \simeq 1$ at small scales and a branch with $n_S = 4$ on large scales. This spectrum is displayed in Fig. 6 for different values of the parameter $\ell_0\gamma/k_0$.

The break in the power spectrum appears at $k^3/k_0^3 \simeq \ell_0\gamma/k_0\mathrm{e}^{2\Delta N_*}$. Therefore, in order for the non-scale-invariant part of the power spectrum to be outside the Hubble radius, one must have

$$\frac{\gamma\ell_0}{k_0} \ll \mathrm{e}^{-2\Delta N_*} \simeq 10^{-53}. \tag{A7}$$

This equation should be compared to Eq. (178). We see that, in the present case, we also obtain a constraint that can be considered as "extreme". In other words, it seems that a very important fine-tuning is necessary to maintain the consistency of the CSL predictions with the CMB observations. We also notice that, instead of γ/k_0^2, it is now the combination $\gamma\ell_0/k_0$ that is constrained. Of course, this is just the consequence of the fact that, as already discussed, changing the collapse operator can change the dimension of the parameter γ. In some sense, we face again the discussion of the temporal gauge issue.

Let us now turn to the case $p = 2$ in Eq. (A3). The general solutions of this equation can be expressed in terms of Bessel functions with a complex order [101,102], namely

$$f_k(\eta) = C_k\sqrt{-k\eta}J_{\frac{3}{2}\sqrt{1+\frac{8}{9}i\gamma\ell_0^2}}(-k\eta) + D_k\sqrt{-k\eta}J_{-\frac{3}{2}\sqrt{1+\frac{8}{9}i\gamma\ell_0^2}}(-k\eta), \tag{A8}$$

where C_k and D_k are integration constants that can be determined by requiring, as usual, the initial state to be the Bunch-Davies vacuum. This leads to $C_k = -D_k\mathrm{e}^{3i\pi/2\sqrt{1+8/9i\gamma\ell_0^2}}$. In the limit where $k\eta$ goes to 0,

$\Re\mathrm{e}\Omega_k$ can be Taylor expanded and, at first order in the parameter $\gamma\ell_0^2$, the power spectrum reads

$$\mathcal{P}_\zeta(k) \simeq \left(1+\frac{2\pi}{3}\gamma\ell_0^2\right)\left[1+\frac{2\gamma\ell_0^2}{3}\,\mathrm{e}^{3\Delta N_*}\left(\frac{k_0}{k}\right)^3 + \frac{4}{3}\gamma\ell_0^2\frac{k_0}{k}\,\mathrm{e}^{\Delta N_*}\right]^{-1}\mathcal{P}_\zeta(k)|_{\mathrm{stand}}. \tag{A9}$$

The formula (A9) should be compared with Eqs. (172) and (A5). Again, the power spectrum has the same shape, with a scale invariant part on small scales and a noninvariant branch with $n_\mathrm{S}=4$ on large scales. This is clearly seen in Fig. 7, where the spectrum (A9) is represented for different values of the parameter $\gamma\ell_0^2$. The break in the power spectrum appears at $k^3/k_0^3 \simeq \gamma\ell_0^2/3\mathrm{e}^{3\Delta N_*}$. Therefore, in order for the non-scale-invariant part of the power spectrum to be outside the observational window, one must require that

$$\gamma\ell_0^2 \ll \mathrm{e}^{-3\Delta N_*} \simeq 10^{-79}. \tag{A10}$$

Again, we can consider the above constraint as a fine-tuning. It is also interesting to notice that, contrary to Eqs. (178) or (A7) and (A10) involves physical quantities only. This is because, when $p=2$, the CSL correction that should be compared to the comoving wave number squared is $\propto \gamma a^2$, see Eq. (A3). In other words, γ should now be compared to the physical wave number. If we take $\ell_0 \simeq 10^5\ell_{\mathrm{Pl}}$, which comes from the CMB normalization, then one arrives at $\gamma \ll 10^{-89}$.

Let us conclude this appendix by noticing that the above results are in fact generic and do not depend on the value of p. Technically, the power spectrum is obtained by taking the super-Hubble limit of the mode function $f_k(\eta)$, by inserting it in the expression of $\Re\mathrm{e}\Omega_k = \Re\mathrm{e}[-if_k'/(2f_k)]$ and by retaining only the leading order in $k\eta$. In the standard case, the leading terms of the mode function expansion turn out to cancel out in $\Re\mathrm{e}\Omega_k$, leaving an expression which precisely gives a scale-invariant power spectrum. This cancellation originates from the fact that the Wronskian is conserved. In the CSL case, the fact that $\gamma \neq 0$ implies that this symmetry no longer exists, and, as a consequence, the nice cancellations mentioned above no longer show up and scale invariance is immediately broken. In some sense, the fact that the γ term destroys the scale invariance of the power spectrum does not come from the fact that its presence modifies the time dependence of the effective frequency (the value of p or the choice of h), but is rather due to the fact that it makes the effective frequency a complex quantity. We conclude that modifying the definition of the collapse operator by multiplying it with a background function, despite changing the dimension of γ, always constrains this parameter to be extremely fine-tuned.

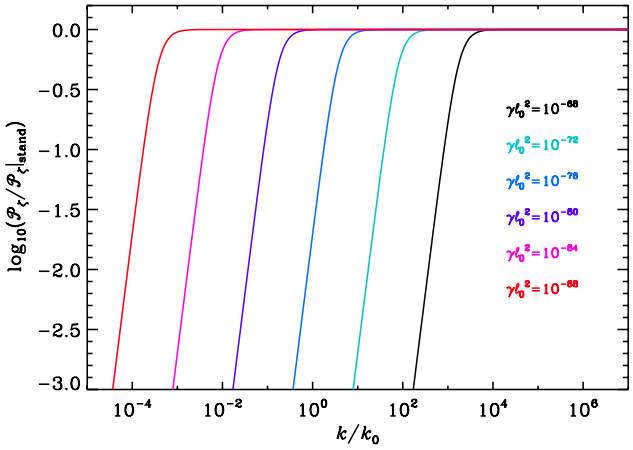

FIG. 7 (color online). Ratio of the power spectrum given by Eq. (A9) ($p=2$) to the standard power spectrum given by Eq. (47) for different values of the parameter $\gamma\ell_0^2$.

[1] A. A. Starobinsky, Phys. Lett. **91B**, 99 (1980).
[2] A. H. Guth, Phys. Rev. D **23**, 347 (1981).
[3] A. D. Linde, Phys. Lett. **108B**, 389 (1982).
[4] A. Albrecht and P. J. Steinhardt, Phys. Rev. Lett. **48**, 1220 (1982).
[5] A. D. Linde, Phys. Lett. **129B**, 177 (1983).
[6] V. F. Mukhanov and G. Chibisov, Pis'ma Zh. Eksp. Teor. Fiz. **33**, 549 (1981) [JETP Lett. **33**, 532 (1981)].
[7] V. F. Mukhanov and G. Chibisov, Zh. Eksp. Teor. Fiz. **22**, 549 (1981) [Sov. Phys. JETP **56**, 258 (1982)].
[8] A. A. Starobinsky, Phys. Lett. **117B**, 175 (1982).
[9] A. H. Guth and S. Y. Pi, Phys. Rev. Lett. **49**, 1110 (1982).
[10] S. Hawking, Phys. Lett. **115B**, 295 (1982), revised version.
[11] J. M. Bardeen, P. J. Steinhardt, and M. S. Turner, Phys. Rev. D **28**, 679 (1983).
[12] V. F. Mukhanov, H. Feldman, and R. H. Brandenberger, Phys. Rep. **215**, 203 (1992).
[13] J. Martin, Braz. J. Phys. **34**, 1307 (2004).
[14] J. Martin, Lect. Notes Phys. **669**, 199 (2005).
[15] J. Martin, Lect. Notes Phys. **738**, 193 (2008); S. Kundu, J. Cosmol. Astropart. Phys. 02 (2012) 005.
[16] A. D. Linde, Lect. Notes Phys. **738**, 1 (2008).
[17] L. Sriramkumar, arXiv:0904.4584.
[18] P. Peter and J.-P. Uzan, *Primordial Cosmology*, Oxford Graduate Texts (Oxford University Press, New York, 2009).
[19] E. D. Stewart and D. H. Lyth, Phys. Lett. B **302**, 171 (1993).
[20] D. Larson, J. Dunkley, G. Hinshaw, E. Komatsu, M. Nolta *et al.*, Astrophys. J. Suppl. Ser. **192**, 16 (2011).

[21] E. Komatsu *et al.* (WMAP Collaboration), Astrophys. J. Suppl. Ser. **192**, 18 (2011).
[22] J. Martin and C. Ringeval, J. Cosmol. Astropart. Phys. 08 (2006) 009.
[23] L. Lorenz, J. Martin, and C. Ringeval, J. Cosmol. Astropart. Phys. 04 (2008) 001.
[24] L. Lorenz, J. Martin, and C. Ringeval, Phys. Rev. D **78**, 063543 (2008).
[25] J. Martin and C. Ringeval, Phys. Rev. D **82**, 023511 (2010).
[26] J. Martin, C. Ringeval, and R. Trotta, Phys. Rev. D **83**, 063524 (2011).
[27] G. F. Smoot, C. Bennett, A. Kogut, E. Wright, J. Aymon *et al.*, Astrophys. J. **396**, L1 (1992).
[28] D. Sudarsky, Int. J. Mod. Phys. D **20**, 509 (2011).
[29] L. Grishchuk and Y. Sidorov, Phys. Rev. D **42**, 3413 (1990).
[30] L. Grishchuk, H. Haus, and K. Bergman, Phys. Rev. D **46**, 1440 (1992).
[31] D. Polarski and A. A. Starobinsky, Classical Quantum Gravity **13**, 377 (1996).
[32] J. Lesgourgues, D. Polarski, and A. A. Starobinsky, Nucl. Phys. **B497**, 479 (1997).
[33] L. Grishchuk and J. Martin, Phys. Rev. D **56**, 1924 (1997).
[34] C. Kiefer and D. Polarski, Adv. Sci. Lett. **2**, 164 (2009).
[35] W. Zurek, Phys. Rev. D **24**, 1516 (1981).
[36] W. Zurek, Phys. Rev. D **26**, 1862 (1982).
[37] E. Joos and H. Zeh, Z. Phys. B **59**, 223 (1985).
[38] C. Kiefer, I. Lohmar, D. Polarski, and A. A. Starobinsky, Classical Quantum Gravity **24**, 1699 (2007).
[39] C. Kiefer, D. Polarski, and A. A. Starobinsky, Int. J. Mod. Phys. D **7**, 455 (1998).
[40] I. Egusquiza, A. Feinstein, M. Perez Sebastian, and M. Valle Basagoiti, Classical Quantum Gravity **15**, 1927 (1998).
[41] P. R. Anderson, C. Molina-Paris, and E. Mottola, Phys. Rev. D **72**, 043515 (2005).
[42] C. P. Burgess, R. Holman, and D. Hoover, Phys. Rev. D **77**, 063534 (2008).
[43] P. Martineau, Classical Quantum Gravity **24**, 5817 (2007).
[44] S. L. Adler, Stud. Hist. Phil. Mod. Phys. **34**, 135 (2003).
[45] M. Schlosshauer, Rev. Mod. Phys. **76**, 1267 (2005).
[46] Y. Nomura, J. High Energy Phys. 11 (2011) 063.
[47] Y. Nomura, arXiv:1110.4630.
[48] V. Mukhanov, *Physical Foundations of Cosmology* (Cambridge University Press, Cambridge, England, 2005).
[49] R. Bousso and L. Susskind, Phys. Rev. D **85**, 045007 (2012).
[50] S. Weinberg, *Cosmology* (Oxford University Press, New York, 2008).
[51] C. A. Fuchs, arXiv:quant-ph/0205039; arXiv:quant-ph/0205039.
[52] P. Holland, Phys. Rep. **224**, 95 (1993).
[53] P. Peter, E. Pinho, and N. Pinto-Neto, J. Cosmol. Astropart. Phys. 07 (2005) 014.
[54] P. Peter, E. J. Pinho, and N. Pinto-Neto, Phys. Rev. D **73**, 104017 (2006).
[55] P. Peter, E. J. Pinho, and N. Pinto-Neto, Phys. Rev. D **75**, 023516 (2007).
[56] P. Peter and N. Pinto-Neto, Phys. Rev. D **78**, 063506 (2008).
[57] N. Pinto-Neto, G. Santos, and W. Struyve, Phys. Rev. D **85**, 083506 (2012).
[58] A. Valentini, J. Phys. A **40**, 3285 (2007); A. Valentini, Phys. Rev. D **82**, 063513 (2010).
[59] A. Valentini, arXiv:0804.4656.
[60] P. M. Pearle and A. Valentini, arXiv:quant-ph/0506115.
[61] P. M. Pearle, Phys. Rev. D **13**, 857 (1976).
[62] G. Ghirardi, A. Rimini, and T. Weber, Phys. Rev. D **34**, 470 (1986).
[63] P. M. Pearle, Phys. Rev. A **39**, 2277 (1989).
[64] L. Diósi, Phys. Lett. A **132**, 233 (1988).
[65] G. C. Ghirardi, P. M. Pearle, and A. Rimini, Phys. Rev. A **42**, 78 (1990).
[66] S. Weinberg, Phys. Rev. A **85**, 062116 (2012).
[67] A. Bassi and G. C. Ghirardi, Phys. Rep. **379**, 257 (2003).
[68] A. Bassi, K. Lochan, S. Satin, T. P. Singh, and H. Ulbricht, arXiv:1204.4325.
[69] D. J. Bedingham, Found. Phys. **41**, 686 (2011).
[70] A. Bassi and E. Ippoliti, Phys. Rev. A **69**, 012105 (2004).
[71] S. L. Adler, J. Phys. A **38**, 2729 (2005).
[72] S. L. Adler, A. Bassi, and E. Ippoliti, J. Phys. A **38**, 2715 (2005).
[73] A. Bassi, J. Phys. G **38**, 3173 (2005).
[74] P. Pearle, arXiv:0710.0567.
[75] P. Pearle, Found. Phys. **42**, 4 (2012).
[76] K. Lochan, S. Das, and A. Bassi, Phys. Rev. D **86**, 065016 (2012).
[77] R. H. Brandenberger and J. Martin, Mod. Phys. Lett. A **16**, 999 (2001).
[78] J. Martin and R. H. Brandenberger, Phys. Rev. D **63**, 123501 (2001).
[79] J. Martin and R. H. Brandenberger, arXiv:astro-ph/0012031.
[80] A. Perez, H. Sahlmann, and D. Sudarsky, Classical Quantum Gravity **23**, 2317 (2006).
[81] A. De Unanue and D. Sudarsky, Phys. Rev. D **78**, 043510 (2008).
[82] A. Diez-Tejedor, G. Leon, and D. Sudarsky, Gen. Relativ. Gravit. (in press).
[83] D. H. Lyth and A. Riotto, Phys. Rep. **314**, 1 (1999).
[84] F. Lucchin and S. Matarrese, Phys. Rev. D **32**, 1316 (1985).
[85] J. M. Bardeen, Phys. Rev. D **22**, 1882 (1980).
[86] J. Martin and D. J. Schwarz, Phys. Rev. D **57**, 3302 (1998).
[87] H. Kodama and M. Sasaki, Prog. Theor. Phys. Suppl. **78**, 1 (1984).
[88] D. J. Schwarz, C. A. Terrero-Escalante, and A. A. Garcia, Phys. Lett. B **517**, 243 (2001).
[89] S. M. Leach, A. R. Liddle, J. Martin, and D. J. Schwarz, Phys. Rev. D **66**, 023515 (2002).
[90] J. Martin and D. J. Schwarz, Phys. Rev. D **62**, 103520 (2000).
[91] J. Martin, A. Riazuelo, and D. J. Schwarz, Astrophys. J. **543**, L99 (2000).
[92] F. Bouchet, arXiv:0911.3101.
[93] R. Sachs and A. Wolfe, Astrophys. J. **147**, 73 (1967).
[94] M. Panek, Phys. Rev. D **34**, 416 (1986).
[95] D. Lyth, Phys. Rev. D **31**, 1792 (1985).
[96] J. H. Traschen and R. H. Brandenberger, Phys. Rev. D **42**, 2491 (1990).

[97] Y. Shtanov, J. H. Traschen, and R. H. Brandenberger, Phys. Rev. D **51**, 5438 (1995).
[98] L. Kofman, A. D. Linde, and A. A. Starobinsky, Phys. Rev. D **56**, 3258 (1997).
[99] F. Finelli and R. H. Brandenberger, Phys. Rev. Lett. **82**, 1362 (1999).
[100] K. Jedamzik, M. Lemoine, and J. Martin, J. Cosmol. Astropart. Phys. 09 (2010) 034.
[101] M. Abramowitz and I. A. Stegun, *Handbook of Mathematical Functions with Formulas, Graphs, and Mathematical Tables* (National Bureau of Standards, Washington, 1970), ninth ed.
[102] I. S. Gradshteyn and I. M. Ryzhik, *Table of Integrals, Series, and Products* (Academic Press, New York, 1965).
[103] C. Ringeval, Lect. Notes Phys. **738**, 243 (2008).
[104] A. Lewis and S. Bridle, Phys. Rev. D **66**, 103511 (2002).
[105] C. Kiefer, J. Lesgourgues, D. Polarski, and A. A. Starobinsky, Classical Quantum Gravity **15**, L67 (1998).
[106] H. Vahlbruch, M. Mehmet, S. Chelkowski, B. Hage, A. Franzen, N. Lastzka, S. Goßler, K. Danzmann, and R. Schnabel, Phys. Rev. Lett. **100**, 033602 (2008).
[107] C. Kiefer, Nucl. Phys. B, Proc. Suppl. **88**, 255 (2000).
[108] C. M. Caves and B. L. Schumaker, Phys. Rev. A **31**, 3068 (1985).
[109] B. L. Schumaker and C. M. Caves, Phys. Rev. A **31**, 3093 (1985).
[110] C. Kiefer and D. Polarski, Ann. Phys. (N.Y.) **7**, 137 (1998).
[111] W. Feldmann and R. Tumulka, J. Phys. A **45**, 065304 (2012).
[112] D. Sudarsky (private communication).
[113] I. Gihman and A. Skorohod, *Stochastic Differential Equations* (Springer Verlag, Berlin, 1972).
[114] J. Halliwell and A. Zoupas, Phys. Rev. D **52**, 7294 (1995).
[115] E. Brezin and C. Itzykson, Phys. Rev. D **2**, 1191 (1970).
[116] G. Moore, J. Math. Phys. (N.Y.) **11**, 2679 (1970).
[117] C. M. Wilson, G. Johansson, A. Pourkabirian, M. Simoen, J. R. Johansson, T. Duty, F. Nori, and P. Delsing, Nature (London) **479**, 376 (2011).
[118] D. Leibfried, R. Blatt, C. Monroe, and D. Wineland, Rev. Mod. Phys. **75**, 281 (2003).

Conclusion

The goal of this thesis was to derive observational constraints on cosmological inflation models, and to investigate some fundamental aspects related to the quantum nature of the inflationary setup. In this last section we summarize the main results we obtained, drawing a few concluding remarks and suggesting possible prospects.

The phenomenological successes of inflation have provided the motivation for numerous efforts to establish its connection with the standard model of particle physics. Our ability to see through the inflationary window turns the early Universe into a laboratory for ultra-high energy physics, at scales entirely inaccessible to conventional experimentation. A crowd of inflationary candidates have thus been proposed, among which it is *a priori* difficult to discriminate the most promising ones since inflation takes place at energy scales where particle physics remain elusive. As a consequence, despite the fact that it has become a cornerstone, the inflationary era is not as well constrained as the other parts of the standard model of Cosmology. However, there is now a flow of increasingly accurate astrophysical data which gives us a unique opportunity to learn more about inflation. We have now entered the era of massive multi-data analysis, and a change of scale is clearly required compared to previous analyses.

The first goal of this thesis was to develop methods that allow us to constrain the inflationary scenario at a level matching the accuracy of the data. We chose to adopt a systematic and somewhat "industrial" approach of this issue. We first focused on the single-field models of inflation, with canonical kinetic terms, and studied them in the slow-roll approximation. Indeed, these are the simplest inflationary models, and there is currently no observational evidence (as would be for example the detection of substantial primordial non-Gaussianities or entropic perturbations) that forces us to consider more complicated models. Obviously, this does not mean that more complicated models are ruled out, but simply that single-field slow-roll scenarios achieve the best compromise between quality of the fit and theoretical simplicity. This still left us with a very populated landscape.

Going through the literature, we identified ~ 75 different inflationary potentials that we studied one by one. Without any other approximation than slow roll, we calculated the predictions of these models. For many of them, we thus derived new results since in most cases, they were studied under additional approximations. The errors associated with these approximations cannot be ignored given the current accuracy of the data, and it is therefore necessary to do without them. We also developed a publicly available runtime library that computes the reheating consistent predictions for these models. This project is an evolutive one and it is intended to be completed as new models appear.

Then, the Planck 2013 Cosmic Microwave Background (CMB) data were released and we computed the Bayesian evidences and complexities of the ~ 200 inflationary scenarios that arise from the previously studied potentials. At the technical level, we actually interfaced the slow-roll library mentioned above with a machine-learning effective likelihood and a nested sampling algorithm. Doing so, we identified the most probable models that are compatible with the Planck

data, while ruling out with very strong evidence one third of the models considered. Among the preferred models, we identified that most potentials are of the plateau type, *i.e.* they are such that the kinetic energy and the kinetic-to-total energy density ratio increase during inflation. Prototypical examples of such models are the Starobinsky model or the Kähler moduli model.

Later on in the course of this thesis, the BICEP2 experiment reported the detection of B-mode signal in the polarization of the CMB, at the level of $r \sim 0.16$. Beyond the strong implications that such a detection would have for inflation in general if confirmed, it was clear that it could drastically refine our analysis arising from the Planck data only. In particular, the Planck likelihood is consistent with $r = 0$ (so far), and indicates that $r < 0.1$ at the two-sigma confidence level. A measurement of r obviously puts further constrains on the inflationary models. This is why we re-processed the same computational pipeline, but including the BICEP2 data in the analysis. The results we obtained showed that the sets of inflationary models preferred by Planck alone and BICEP2 alone are almost disjoint, indicating a clear tension between the two data sets.

We then decided to quantify this tension with a Bayesian measure of compatibility between BICEP2 and Planck. The compatibility of these two experiments is widely discussed in the literature, but the improvement of our approach is that we quantify compatibility *under the assumption* of inflation or *under the assumption* of a specific inflationary model. In this manner, we could draw stronger and more reliable conclusions. Under the generic assumption of slow-roll inflation, we established that the Bayesian test is inconclusive, *i.e.* there is neither indication towards compatibility nor incompatibility. However, when computing the compatibility level model by model, we found that for models favoured by Planck the two data sets tend to be incompatible, whereas there is a moderate evidence of compatibility for the BICEP2 preferred models. As a result, it is premature to draw any conclusion on the best Planck models at this point, such as Starobinsky inflation or Kähler moduli inflation. Furthermore, we established that the data are strongly compatible only for models that are disfavoured by both Planck and BICEP2 separately. Indeed, both data sets agree in disfavouring those models and in this sense only, they can be said to be "compatible". This is why one still needs to wait for some clarification about the data before being able to properly combine them and draw definitive conclusions as for the Planck best models. In particular, the polarization measurements by Planck that should be released by the end of the year, and a possible reconsideration of the dust contribution in the B-mode signal measured by BICEP2, may help to unveil the tension.

As a possible prospect of this work, the inclusion of k-inflation models in the analysis needs to be considered. Indeed, in this class of models, the action for the scalar perturbations at linear order is still quadratic, but the speed of sound c_{S} is now a function of time. As a consequence, there exists a frame of approximation similar to slow roll that applies to the time variation of c_{S}, and the same machinery can be extended to these cases without implying an unreasonable increase in its complexity level. Since the accuracy of the data requires to work at next-to-next-to leading order at least, we have calculated, for the first time, the power spectra of scalar and tensor perturbations at this order in k-inflation to pave the way for such an extension. However, such models can produce a large amount of primordial non-Gaussianities, and this observable needs also be included in the analysis to properly constrain k-inflation.

Obviously, on could go beyond and include multi-field models, non scalar-field models, *etc.* However, this represents much more complicated situations with strong dependence on the initial conditions, and where there is no such thing as a frame of approximation in which the background trajectory and the amplitude of the perturbations can be calculated perturbatively. As a consequence, one needs to numerically integrate all equations, and it seems difficult to

process our complete Bayesian pipeline in a realistic amount of time for such models, at least in the generic situation.

Another relevant study to carry out is the one about reheating. From the beginning, we have taken care of consistently describing reheating in the analysis, which boils down to including a single parameter combining the mean energy density and the average equation of state during reheating. From the results we obtained, it is clear that we are in a position where we can put explicit constraints on the reheating parameters, either model by model, or in a model averaged way. We are currently working on such a follow-up.

There is also an ongoing debate about what the next instrumental move should be. If the urge for a clear detection of r is obvious, the sensitivity of future experiments must be such that, in case of a non detection, the improvement in the constraint on the gravity wave level would still significantly improve our knowledge about the early Universe. This is why we are also currently examinating future experiments specifications in the light of this issue. For the few ones that have been planned, we are deriving the likelihood it would provide given a fiducial model, and we are processing our Bayesian pipeline for the ~ 200 inflationary models we have at hand, to determine how much the constraints on these models would improve. Repeating the analysis for a few different fiducial models, this allows us to derive clear forecasts about the actual performance of these experiments.

It is also worth mentioning that the reliability of our approach, compared with model independent parametrizations of inflation, was strengthened by our analysis of the horizon-flow framework. In this setup, inflation is parametrized by means of truncated flow equations. Typically, potential reconstruction has been investigated with the help of this technique, as well as the search for "generic" inflationary predictions. We showed that horizon flow only samples a phenomenological class of inflationary potentials, which are at the origins of such wrongly concluded generic predictions. Furthermore, we established that the horizon-flow setup rests on trajectories in phase space that differ from the slow roll one. Such trajectories are sometimes unstable, and given a potential, they render horizon flow blind to entire inflationary regimes, hence making this parametrization a biased one.

Together with this data-oriented approach of inflationary models, we also studied more fundamental aspects related to the quantum nature of the inflationary setup. In particular, we got interested in the stochastic inflation formalism which incorporates quantum corrections to the classical background by means of stochastic Langevin equations. Such a formalism is theoretically well founded and technically appealing since it is notably able to reproduce a number of results from Quantum Field Theories, even beyond the perturbative level. It gives rise to non trivial dynamics, in particular when multiple fields are present, since in these cases, due to quantum diffusion, the system can explore parts of the inflationary potential to which the classical trajectory is insensitive. This is why we studied the stochastic effects in hybrid inflation, a two-field model where inflation ends by tachyonic instability, triggered by an auxiliary "waterfall" field, close to a critical saddle point. There, the potential is very flat and the quantum fluctuations dominate over the classical drifts of the fields. The two Langevin equations become highly coupled, and their solving requires a numerical approach. It is however important to well understand what happens in this regime, since it determines the amount of e-folds that can be realized in the waterfall phase. If the scales of astrophysical interest today cross the Hubble radius before the critical point, that is if the number of e-folds realized in the waterfall is smaller than ~ 50, then the power spectrum of scalar perturbations was shown to be blue and the model is therefore ruled out. Only if the last 50 e-folds are realized in the waterfall phase can this problem be evaded, and it is then crucial to properly determine the amount of e-folds realized in

the waterfall. This is why we mainly focused on this quantity, and we computed its distribution for different sets of parameters.

To go beyond, one needs to investigate more the regime of parameters for which ~ 50 e-folds are realized during the waterfall, and scales of astrophysical interest today cross the Hubble radius in the neighbourhood of the critical point, that is where the stochastic effects do not represent a tiny correction to the classical trajectory anymore. In such a case, the calculation of the power spectrum is more involved. In the introductory part of this manuscript, we have derived an entirely analytical method for calculating the power spectrum in stochastic inflation in a non perturbative manner, that is without relying on an expansion in the noise term, for single-field models. If such an approach should be employed to calculate the power spectrum and the non Gaussianity levels in some single-field models where important stochastic effects are expected to play a role, it still remains to be generalized to multiple-fields setups in order to address the case of models such as hybrid inflation.

Another issue we studied is the fact that in standard stochastic inflation, the correlations of noise terms in the Langevin equations depend on the amplitude of perturbations that are calculated over a classical background. Now, if the background is stochastically shifted, the perturbations should be affected, hence the noise correlations, hence the way the background is shifted, so on and so forth. In order to try and take into account such an effect, we designed a recursive approach to stochastic inflation that we applied to the hybrid models. As expected, such a formalism converges in the valley but blows up in the waterfall. Interestingly enough, the corresponding effects tend to increase the duration of the waterfall phase by decreasing the waterfall field dispersion at the critical point, and worsen the blue tilt problem in the valley, hence reinforcing the plausibility of long lasting waterfall scenarios.

Finally, we addressed the issue of the quantum measurement problem in a cosmological context, so as to illustrate how inflationary physics can help to discuss deep questions related to the nature of the quantum theory itself. The quantum-to-classical transition of cosmological perturbations is a subject of great interest at the fundamental level, since perturbations originate from zero point quantum fluctuation but are usually treated as purely classical quantities after inflation ends. This transition is often accounted for by the large squeezing of the quantum state of the perturbations, for which one can show that it is phenomenologically equivalent to a stochastic set of classical processes. The phenomenon of quantum decoherence is also usually mentioned as being part of the explanation. However, at the fundamental level, this does not explain how a specific outcome can be produced in the early Universe, in the absence of any observer. A possible way out is the continuous spontaneous localization (CSL) approach to quantum mechanics in which the wavefunction collapse is caused by adding non linear and stochastic terms to the Schrödinger equation. We applied this theory to inflation, and calculated both the collapse level of the wavefunction at the end of inflation and the power spectrum of perturbations. We found that reaching a satisfactory level of collapse for the scales of astrophysical interest today implies to strongly break the scale invariance of the power spectrum, hence rendering the direct application of the theory in the early Universe problematic. In a later work, other authors have extended our calculation in the case where the CSL strength parameter depends on physical scales through a phenomenological power law, and they showed that there exists a power index for which the problem we point out is evaded. In any case, this illustrates the remarkable power of inflation in particular, and Cosmology in general, to constrain new physics.

In this thesis, we have thus shown that theoretical developments and observational achievements of the past years make possible to constrain the inflationary physics and to learn more about the physical conditions that prevailed in the early Universe. However, one might fear that the

built-in phenomenological robustness of inflation may keep us from learning too much about its microphysical origin since inflationary predictions depend on a few generic observables and the window of scales through which we may grasp a look at early Universe physics is restricted to a few e-folds.

Actually, we may indeed be at a turning point with the possible detection of primordial gravity waves. Indeed, if the detection of r is confirmed, it is clear that we should undertake all possible and reasonable efforts to provide an accurate measurement of its value. If it is of the same order of magnitude as the one announced by BICEP2, $r \sim 0.1 - 0.2$, it also means that the spectral index of gravity waves, $n_{\rm T}$, may also be measured [405] in the medium term. This would double the number of inflationary parameters for which we have a measurement, going from $\{\mathcal{P}_{\zeta,*}, n_{\rm S}\}$ to $\{\mathcal{P}_{\zeta,*}, n_{\rm S}, r, n_{\rm T}\}$. If this is the case, considering also the EE and TE signals measured by Planck and that will be released soon, it seems realistic to try and really constrain the shape of the inflationary potential and its energy scale. This is a very exciting perspective.

However, if a more accurate determination of the foregrounds contribution to the BICEP2 signal makes its detection disappear, measurement of new inflationary parameters in the short run seem quite unlikely. Indeed, some plateau models, such as Khäler moduli inflation or brane inflation, can predict tiny values of r, typically $r < 10^{-6}$. At the present day, it seems technologically unrealistic to try and detect such small amount of primordial gravity waves. Moreover, for single-field slow-roll models of inflation with canonical kinetic terms, the level of non-Gaussianities is very small, $f_{\rm NL} \sim \epsilon$, and still beyond what we can reach observationally [406]. The same applies for entropic perturbations which may well be far beyond what we will be able to detect in the years to come if the other fields contributing to ρ during inflation are very massive. The running of the scalar power spectrum is also very small in the slow-roll regime, $\alpha_{\rm S} \sim \epsilon^2$, and if no deviation from slow roll occurred in the observational window (as it seems to be the case so far), it is also quite unlikely to be detected in the years to come. Of course, there is still the possibility that slow roll be mildly violated at some point, or that a "massive but not so massive" auxiliary field contributes to the energy density during inflation, or that a "small but not so small" deviation from minimal coupling to gravity appear, so that the quantities mentioned above may still be measured soon, but this would represent a rather fine-tuned situation, considering what we already know. This is why in that second case, it is possible that the observational constraints on inflationary models stagnate for a decade or even more.

To continue to improve our knowledge of early universe physics, two routes may then be followed. One is to try and discriminate among models on a theoretical basis, dedicating more efforts in the model building programme, better understanding how inflationary models are sensitive to radiative corrections, how they can be connected to the standard model of particle physics and its extensions, *etc.* Another is to investigate more the connections between inflationary predictions and other astrophysical probes such as supernovae, galaxy surveys, 21 cm astrophysics, the reconstruction of the initial conditions large scale structures simulations, *etc.* For example, the "lever arm" in length scales between CMB and galaxy power spectra is huge and it increases the sensitivity to the small deviations from scale invariance.

Cosmology has now entered a "big data" era where measurements very different in nature have to be cleverly combined to derive constraints on physical processes equally different. In this manner, advances in the different fields of Cosmology and even Astrophysics are highly entangled, and the decryption of the early Universe physics is an ongoing adventure.

List of Figures

List of Tables

Bibliography

[1] E. W. Kolb and M. S. Turner, *The Early Universe*, vol. 69. Front.Phys., 1990.

[2] P. Peebles, *Principles of physical cosmology*. Princeton University Press, 1994.

[3] A. R. Liddle, *An introduction to modern cosmology*. Wiley, 1998.

[4] A. R. Liddle and D. Lyth, *Cosmological inflation and large scale structure*. Cambridge, UK: Univ. Pr., 2000.

[5] S. Dodelson, *Modern cosmology*. Amsterdam, Netherlands: Academic Pr., 2003.

[6] V. Mukhanov, *Physical foundations of cosmology*. Cambridge, UK: Univ. Pr., 2005.

[7] D. H. Lyth and A. R. Liddle, *The primordial density perturbation: Cosmology, inflation and the origin of structure*. Cambridge, UK: Cambridge Univ. Pr., 2009.

[8] P. Peter and J.-P. Uzan, *Primordial cosmology*. Oxford University Press, UK, 2009.

[9] A. Friedmann, "On the Possibility of a world with constant negative curvature of space," *Z.Phys.* **21** (1924) 326–332.

[10] G. Lemaitre, "A homogeneous Universe of constant mass and growing radius accounting for the radial velocity of extragalactic nebulae," *Annales Soc.Sci.Brux.Ser.I Sci.Math.Astron.Phys.* **A47** (1927) 49–59.

[11] H. Robertson, "Kinematics and World-Structure," *Astrophys.J.* **82** (1935) 284–301.

[12] A. G. Walker, "On the formal comparison of Milne's kinematical system with the systems of general relativity," *Mon.Not.Roy.Astron.Soc.* **95** (1935) 263–269.

[13] E. Hubble, "A relation between distance and radial velocity among extra-galactic nebulae," *Proc.Nat.Acad.Sci.* **15** (1929) 168–173.

[14] A. Sandage, "Current Problems in the Extragalactic Distance Scale," *Astrophys.J.* **127** (1958) 513–526.

[15] **Planck Collaboration** Collaboration, P. Ade *et al.*, "Planck 2013 results. XVI. Cosmological parameters," `arXiv:1303.5076 [astro-ph.CO]`.

[16] L. Verde, P. Protopapas, and R. Jimenez, "Planck and the local Universe: Quantifying the tension," *Phys.Dark Univ.* **2** (2013) 166–175, `arXiv:1306.6766 [astro-ph.CO]`.

[17] J.-Q. Xia, H. Li, and X. Zhang, "Dark Energy Constraints after Planck," *Phys.Rev.* **D88** (2013) 063501, `arXiv:1308.0188 [astro-ph.CO]`.

[18] A. Caramete and L. Popa, "Cosmological evidence for leptonic asymmetry after Planck," *JCAP* **1402** (2014) 012, arXiv:1311.3856 [astro-ph.CO].

[19] A. E. Romano and S. A. Vallejo, "Can the tension in the H_0 estimation be solved by a local overdensity?," arXiv:1403.2034 [astro-ph.CO].

[20] L. Verde, P. Protopapas, and R. Jimenez, "The expansion rate of the intermediate Universe in light of Planck," arXiv:1403.2181 [astro-ph.CO].

[21] B. Leistedt, H. V. Peiris, and L. Verde, "No new cosmological concordance with massive sterile neutrinos," arXiv:1404.5950 [astro-ph.CO].

[22] A. Einstein, "The Field Equations of Gravitation," *Sitzungsber.Preuss.Akad.Wiss.Berlin (Math.Phys.)* **1915** (1915) 844–847.

[23] A. Einstein, "On the General Theory of Relativity," *Sitzungsber.Preuss.Akad.Wiss.Berlin (Math.Phys.)* **1915** (1915) 778–786.

[24] D. Hilbert, "Die Grundlagen der Physik. 1.," *Gott.Nachr.* **27** (1915) 395–407.

[25] A. Friedman, "On the Curvature of space," *Z.Phys.* **10** (1922) 377–386.

[26] A. Raychaudhuri, "Relativistic cosmology. 1.," *Phys.Rev.* **98** (1955) 1123–1126.

[27] J. Khoury, B. A. Ovrut, P. J. Steinhardt, and N. Turok, "The Ekpyrotic universe: Colliding branes and the origin of the hot big bang," *Phys.Rev.* **D64** (2001) 123522, arXiv:hep-th/0103239 [hep-th].

[28] J. Khoury, B. A. Ovrut, P. J. Steinhardt, and N. Turok, "Density perturbations in the ekpyrotic scenario," *Phys.Rev.* **D66** (2002) 046005, arXiv:hep-th/0109050 [hep-th].

[29] P. J. Steinhardt and N. Turok, "Cosmic evolution in a cyclic universe," *Phys.Rev.* **D65** (2002) 126003, arXiv:hep-th/0111098 [hep-th].

[30] M. Gasperini and G. Veneziano, "The Pre - big bang scenario in string cosmology," *Phys.Rept.* **373** (2003) 1–212, arXiv:hep-th/0207130 [hep-th].

[31] J. Martin and P. Peter, "On the causality argument in bouncing cosmologies," *Phys.Rev.Lett.* **92** (2004) 061301, arXiv:astro-ph/0312488 [astro-ph].

[32] L. R. Abramo and P. Peter, "K-Bounce," *JCAP* **0709** (2007) 001, arXiv:0705.2893 [astro-ph].

[33] P. Peter and N. Pinto-Neto, "Cosmology without inflation," *Phys.Rev.* **D78** (2008) 063506, arXiv:0809.2022 [gr-qc].

[34] J. Martin and P. Peter, "Parametric amplification of metric fluctuations through a bouncing phase," *Phys.Rev.* **D68** (2003) 103517, arXiv:hep-th/0307077 [hep-th].

[35] E. A. Milne, "A Newtonian expanding Universe," *The Quarterly Journal of Mathematics* **5** (1934) 64–72.

[36] W. H. McCrea and E. A. Milne, "Newtonian Universes and the curvature of space," *The*

Quarterly Journal of Mathematics **5** (1934) 73–80.

[37] C. G. Wells, "On The Equivalence of the FRW Field Equations and those of Newtonian Cosmology," arXiv:1405.1656 [gr-qc].

[38] A. Narimani, N. Afshordi, and D. Scott, "How does pressure gravitate? Cosmological constant problem confronts observational cosmology," arXiv:1406.0479 [gr-qc].

[39] S. Rappaport, J. Schwab, S. Burles, and G. Steigman, "Big Bang Nucleosynthesis Constraints on the Self-Gravity of Pressure," *Phys.Rev.* **D77** (2008) 023515, arXiv:0710.5300 [astro-ph].

[40] J. Schwab, S. A. Hughes, and S. Rappaport, "The Self-Gravity of Pressure in Neutron Stars," arXiv:0806.0798 [astro-ph].

[41] F. Kamiab and N. Afshordi, "Neutron Stars and the Cosmological Constant Problem," *Phys.Rev.* **D84** (2011) 063011, arXiv:1104.5704 [astro-ph.CO].

[42] J. Martin, "Everything You Always Wanted To Know About The Cosmological Constant Problem (But Were Afraid To Ask)," *Comptes Rendus Physique* **13** (2012) 566–665, arXiv:1205.3365 [astro-ph.CO].

[43] D. Kirzhnits and A. D. Linde, "Macroscopic Consequences of the Weinberg Model," *Phys.Lett.* **B42** (1972) 471–474.

[44] S. Weinberg, "Gauge and Global Symmetries at High Temperature," *Phys.Rev.* **D9** (1974) 3357–3378.

[45] D. Kirzhnits, "Weinberg model in the hot universe," *JETP Lett.* **15** (1972) 529–531.

[46] L. Dolan and R. Jackiw, "Symmetry Behavior at Finite Temperature," *Phys.Rev.* **D9** (1974) 3320–3341.

[47] D. Kirzhnits and A. D. Linde, "A Relativistic phase transition," *Sov.Phys.JETP* **40** (1975) 628.

[48] D. Kirzhnits and A. D. Linde, "Symmetry Behavior in Gauge Theories," *Annals Phys.* **101** (1976) 195–238.

[49] M. Dine, R. G. Leigh, P. Y. Huet, A. D. Linde, and D. A. Linde, "Towards the theory of the electroweak phase transition," *Phys.Rev.* **D46** (1992) 550–571, arXiv:hep-ph/9203203 [hep-ph].

[50] A. Sakharov, "Violation of CP Invariance, c Asymmetry, and Baryon Asymmetry of the Universe," *Pisma Zh.Eksp.Teor.Fiz.* **5** (1967) 32–35.

[51] G. W. Anderson and L. J. Hall, "The Electroweak phase transition and baryogenesis," *Phys.Rev.* **D45** (1992) 2685–2698.

[52] G. R. Farrar and M. Shaposhnikov, "Baryon asymmetry of the universe in the standard electroweak theory," *Phys.Rev.* **D50** (1994) 774, arXiv:hep-ph/9305275 [hep-ph].

[53] A. G. Cohen, D. Kaplan, and A. Nelson, "Progress in electroweak baryogenesis,"

Ann.Rev.Nucl.Part.Sci. **43** (1993) 27–70, arXiv:hep-ph/9302210 [hep-ph].

[54] A. Riotto and M. Trodden, "Recent progress in baryogenesis," *Ann.Rev.Nucl.Part.Sci.* **49** (1999) 35–75, arXiv:hep-ph/9901362 [hep-ph].

[55] K. A. Olive, "The Thermodynamics of the Quark - Hadron Phase Transition in the Early Universe," *Nucl.Phys.* **B190** (1981) 483.

[56] E. Suhonen, "The Quark - Hadron Phase Transition in the Early Universe," *Phys.Lett.* **B119** (1982) 81.

[57] M. Crawford and D. N. Schramm, "Spontaneous Generation of Density Perturbations in the Early Universe," *Nature* **298** (1982) 538–540.

[58] J. Applegate and C. Hogan, "Relics of Cosmic Quark Condensation," *Phys.Rev.* **D31** (1985) 3037–3045.

[59] H. Satz, "The Transition From Hadron Matter to Quark - Gluon Plasma," *Ann.Rev.Nucl.Part.Sci.* **35** (1985) 245–270.

[60] G. Fuller, G. Mathews, and C. Alcock, "The Quark - Hadron Phase Transition in the Early Universe: Isothermal Baryon Number Fluctuations and Primordial Nucleosynthesis," *Phys.Rev.* **D37** (1988) 1380.

[61] B.-l. Cheng and A. V. Olinto, "Primordial magnetic fields generated in the quark - hadron transition," *Phys.Rev.* **D50** (1994) 2421–2424.

[62] C. Alcock, G. Fuller, and G. Mathews, "The Quark - hadron phase transition and primordial nucleosynthesis," *Astrophys.J.* **320** (1987) 439–447.

[63] **WMAP** Collaboration, G. Hinshaw *et al.*, "Nine-Year Wilkinson Microwave Anisotropy Probe (WMAP) Observations: Cosmological Parameter Results," *Astrophys.J.Suppl.* **208** (2013) 19, arXiv:1212.5226 [astro-ph.CO].

[64] R. Alpher, H. Bethe, and G. Gamow, "The origin of chemical elements," *Phys.Rev.* **73** (1948) 803–804.

[65] R. V. Wagoner, W. A. Fowler, and F. Hoyle, "On the Synthesis of elements at very high temperatures," *Astrophys.J.* **148** (1967) 3–49.

[66] S. Sarkar, "Big bang nucleosynthesis and physics beyond the standard model," *Rept.Prog.Phys.* **59** (1996) 1493–1610, arXiv:hep-ph/9602260 [hep-ph].

[67] D. N. Schramm and M. S. Turner, "Big bang nucleosynthesis enters the precision era," *Rev.Mod.Phys.* **70** (1998) 303–318, arXiv:astro-ph/9706069 [astro-ph].

[68] A. Coc, E. Vangioni-Flam, P. Descouvemont, A. Adahchour, and C. Angulo, "Updated Big Bang nucleosynthesis confronted to WMAP observations and to the abundance of light elements," *Astrophys.J.* **600** (2004) 544–552, arXiv:astro-ph/0309480 [astro-ph].

[69] G. Steigman, "Big bang nucleosynthesis: Probing the first 20 minutes," arXiv:astro-ph/0307244 [astro-ph].

[70] G. Steigman, "Primordial Nucleosynthesis in the Precision Cosmology Era," *Ann.Rev.Nucl.Part.Sci.* **57** (2007) 463–491, arXiv:0712.1100 [astro-ph].

[71] F. Iocco, G. Mangano, G. Miele, O. Pisanti, and P. D. Serpico, "Primordial Nucleosynthesis: from precision cosmology to fundamental physics," *Phys.Rept.* **472** (2009) 1–76, arXiv:0809.0631 [astro-ph].

[72] K. Jedamzik and M. Pospelov, "Big Bang Nucleosynthesis and Particle Dark Matter," *New J.Phys.* **11** (2009) 105028, arXiv:0906.2087 [hep-ph].

[73] M. Pospelov and J. Pradler, "Big Bang Nucleosynthesis as a Probe of New Physics," *Ann.Rev.Nucl.Part.Sci.* **60** (2010) 539–568, arXiv:1011.1054 [hep-ph].

[74] B. D. Fields, "The primordial lithium problem," *Ann.Rev.Nucl.Part.Sci.* **61** (2011) 47–68, arXiv:1203.3551 [astro-ph.CO].

[75] A. Coc, J.-P. Uzan, and E. Vangioni, "Standard Big-Bang Nucleosynthesis after Planck," arXiv:1307.6955 [astro-ph.CO].

[76] **Planck Collaboration** Collaboration, P. Ade *et al.*, "Planck 2013 results. I. Overview of products and scientific results," arXiv:1303.5062 [astro-ph.CO].

[77] A. A. Penzias and R. W. Wilson, "A Measurement of excess antenna temperature at 4080-Mc/s," *Astrophys.J.* **142** (1965) 419–421.

[78] J. E. Gunn and B. A. Peterson, "On the Density of Neutral Hydrogen in Intergalactic Space," *Astrophys.J.* **142** (1965) 1633.

[79] **SDSS Collaboration** Collaboration, R. H. Becker *et al.*, "Evidence for reionization at Z 6: Detection of a Gunn-Peterson trough in a Z = 6.28 quasar," *Astron.J.* **122** (2001) 2850, arXiv:astro-ph/0108097 [astro-ph].

[80] R. Barkana and A. Loeb, "In the beginning: The First sources of light and the reionization of the Universe," *Phys.Rept.* **349** (2001) 125–238, arXiv:astro-ph/0010468 [astro-ph].

[81] E. T. Vishniac, "Reionization and small-scale fluctuations in the microwave background," *Astrophys.J.* **322** (1987) 597–604.

[82] K. Heitmann, P. M. Ricker, M. S. Warren, and S. Habib, "Robustness of cosmological simulations. 1. Large scale structure," *Astrophys.J.Suppl.* **160** (2005) 28–58, arXiv:astro-ph/0411795 [astro-ph].

[83] K. Heitmann. Personal communication.

[84] **Supernova Search Team** Collaboration, A. G. Riess *et al.*, "Observational evidence from supernovae for an accelerating universe and a cosmological constant," *Astron.J.* **116** (1998) 1009–1038, arXiv:astro-ph/9805201 [astro-ph].

[85] **Supernova Cosmology Project** Collaboration, S. Perlmutter *et al.*, "Measurements of Omega and Lambda from 42 high redshift supernovae," *Astrophys.J.* **517** (1999) 565–586, arXiv:astro-ph/9812133 [astro-ph].

[86] G. Ellis and S. Stoeger, William R., "Horizons in Inflationary Universes," *Class.Quant.Grav.* **5** (1988) 207–220.

[87] J. Martin, "Inflation and precision cosmology," *Braz.J.Phys.* **34** (2004) 1307–1321, arXiv:astro-ph/0312492 [astro-ph].

[88] W. Rindler, "Visual horizons in world-models," *Mon.Not.Roy.Astron.Soc.* **116** (1956) 662–677.

[89] C. W. Misner, "The Isotropy of the Universe," *The Astrophysical Journal* **151** (1967) 431.

[90] A. H. Guth, "The Inflationary Universe: A Possible Solution to the Horizon and Flatness Problems," *Phys.Rev.* **D23** (1981) 347–356.

[91] A. A. Starobinsky, "A New Type of Isotropic Cosmological Models Without Singularity," *Phys.Lett.* **B91** (1980) 99–102.

[92] R. Dicke, "Gravitation and the Universe: The Jayne Lectures for 1969," *Philadelphia: American Philosophical Institute* (1970) 61–62.

[93] R. Dicke and P. Peebles, "General Relativity: An Einstein Centenary Survey," *Cambridge University Press, edited by S.W. Hawking and W. Israel* (1979) .

[94] H. Georgi and S. Glashow, "Unity of All Elementary Particle Forces," *Phys.Rev.Lett.* **32** (1974) 438–441.

[95] J. C. Pati and A. Salam, "Lepton Number as the Fourth Color," *Phys.Rev.* **D10** (1974) 275–289.

[96] A. Buras, J. R. Ellis, M. Gaillard, and D. V. Nanopoulos, "Aspects of the Grand Unification of Strong, Weak and Electromagnetic Interactions," *Nucl.Phys.* **B135** (1978) 66–92.

[97] G. 't Hooft, "Magnetic Monopoles in Unified Gauge Theories," *Nucl.Phys.* **B79** (1974) 276–284.

[98] A. M. Polyakov, "Particle Spectrum in the Quantum Field Theory," *JETP Lett.* **20** (1974) 194–195.

[99] A. H. Guth and S. Tye, "Phase Transitions and Magnetic Monopole Production in the Very Early Universe," *Phys.Rev.Lett.* **44** (1980) 631.

[100] M. B. Einhorn, D. Stein, and D. Toussaint, "Are Grand Unified Theories Compatible with Standard Cosmology?," *Phys.Rev.* **D21** (1980) 3295.

[101] Y. Zeldovich and M. Y. Khlopov, "On the Concentration of Relic Magnetic Monopoles in the Universe," *Phys.Lett.* **B79** (1978) 239–241.

[102] J. Preskill, "Cosmological Production of Superheavy Magnetic Monopoles," *Phys.Rev.Lett.* **43** (1979) 1365.

[103] L. W. Alvarez, "Analysis of a Reported Magnetic Monopole,".

[104] P. Price, E. Shirk, W. Osborne, and L. S. Pinsky, "Evidence for Detection of a Moving Magnetic Monopole," *Phys.Rev.Lett.* **35** (1975) 487–490.

[105] B. Cabrera, "First Results from a Superconductive Detector for Moving Magnetic Monopoles," *Phys.Rev.Lett.* **48** (1982) 1378–1380.

[106] P. Price, S.-l. Guo, S. Ahlen, and R. Fleischer, "Search for GUT Magnetic Monopoles at a Flux Level Below the Parker Limit," *Phys.Rev.Lett.* **52** (1984) 1265.

[107] **MACRO Collaboration** Collaboration, M. Ambrosio *et al.*, "Search for nucleon decays induced by GUT magnetic monopoles with the MACRO experiment," *Eur.Phys.J.* **C26** (2002) 163–172, arXiv:hep-ex/0207024 [hep-ex].

[108] **MOEDAL Collaboration** Collaboration, J. Pinfold, "MoEDAL becomes the LHC's magnificent seventh," *CERN Cour.* **50N4** (2010) 19–20.

[109] A. D. Linde and R. Brandenberger, *Inflation and quantum cosmology*. Boston, USA: Academic, 1990.

[110] A. D. Linde, *Particle physics and inflationary cosmology*, vol. 5. Contemp.Concepts Phys., 1990. arXiv:hep-th/0503203 [hep-th].

[111] A. H. Guth, *The inflationary universe: The quest for a new theory of cosmic origins*. Reading, USA: Addison-Wesley, 1997.

[112] S. Winitzki, *Eternal inflation*. Hackensack, USA: World Scientific, 2008.

[113] M. Lemoine, J. Martin, and P. Peter, *Inflationary cosmology*. Lemoine, Martin, 2008.

[114] A. H. Guth, "The Inflationary Universe: A Possible Solution to the Horizon and Flatness Problems," *Phys.Rev.* **D23** (1981) 347–356.

[115] D. Kazanas, "Dynamics of the Universe and Spontaneous Symmetry Breaking," *Astrophys.J.* **241** (1980) L59–L63.

[116] A. D. Linde, "A New Inflationary Universe Scenario: A Possible Solution of the Horizon, Flatness, Homogeneity, Isotropy and Primordial Monopole Problems," *Phys.Lett.* **B108** (1982) 389–393.

[117] K. Sato, "Cosmological Baryon Number Domain Structure and the First Order Phase Transition of a Vacuum," *Phys.Lett.* **B99** (1981) 66–70.

[118] A. Albrecht and P. J. Steinhardt, "Cosmology for Grand Unified Theories with Radiatively Induced Symmetry Breaking," *Phys.Rev.Lett.* **48** (1982) 1220–1223.

[119] A. D. Linde, "Chaotic Inflation," *Phys.Lett.* **B129** (1983) 177–181.

[120] J. Martin and C. Ringeval, "Inflation after WMAP3: Confronting the Slow-Roll and Exact Power Spectra to CMB Data," *JCAP* **0608** (2006) 009, arXiv:astro-ph/0605367 [astro-ph].

[121] A. A. Starobinsky, "Relict Gravitation Radiation Spectrum and Initial State of the Universe. (In Russian)," *JETP Lett.* **30** (1979) 682–685.

[122] V. F. Mukhanov and G. Chibisov, "Quantum Fluctuation and Nonsingular Universe. (In Russian)," *JETP Lett.* **33** (1981) 532–535.

[123] V. F. Mukhanov and G. Chibisov, "The Vacuum energy and large scale structure of the universe," *Sov.Phys.JETP* **56** (1982) 258–265.

[124] S. Hawking, "The Development of Irregularities in a Single Bubble Inflationary Universe," *Phys.Lett.* **B115** (1982) 295.

[125] A. A. Starobinsky, "Dynamics of Phase Transition in the New Inflationary Universe Scenario and Generation of Perturbations," *Phys.Lett.* **B117** (1982) 175–178.

[126] A. H. Guth and S. Pi, "Fluctuations in the New Inflationary Universe," *Phys.Rev.Lett.* **49** (1982) 1110–1113.

[127] J. M. Bardeen, P. J. Steinhardt, and M. S. Turner, "Spontaneous Creation of Almost Scale - Free Density Perturbations in an Inflationary Universe," *Phys.Rev.* **D28** (1983) 679.

[128] E. D. Stewart and D. H. Lyth, "A More accurate analytic calculation of the spectrum of cosmological perturbations produced during inflation," *Phys.Lett.* **B302** (1993) 171–175, arXiv:gr-qc/9302019 [gr-qc].

[129] V. F. Mukhanov, H. Feldman, and R. H. Brandenberger, "Theory of cosmological perturbations. Part 1. Classical perturbations. Part 2. Quantum theory of perturbations. Part 3. Extensions," *Phys.Rept.* **215** (1992) 203–333.

[130] A. R. Liddle, P. Parsons, and J. D. Barrow, "Formalizing the slow roll approximation in inflation," *Phys. Rev.* **D50** (1994) 7222–7232, arXiv:astro-ph/9408015.

[131] L. Grishchuk and Y. Sidorov, "Squeezed quantum states of relic gravitons and primordial density fluctuations," *Phys.Rev.* **D42** (1990) 3413–3421.

[132] D. Polarski and A. A. Starobinsky, "Semiclassicality and decoherence of cosmological perturbations," *Class.Quant.Grav.* **13** (1996) 377–392, arXiv:gr-qc/9504030 [gr-qc].

[133] C. Kiefer, D. Polarski, and A. A. Starobinsky, "Quantum to classical transition for fluctuations in the early universe," *Int.J.Mod.Phys.* **D7** (1998) 455–462, arXiv:gr-qc/9802003 [gr-qc].

[134] J. Martin, "Inflationary cosmological perturbations of quantum- mechanical origin," *Lect. Notes Phys.* **669** (2005) 199–244, arXiv:hep-th/0406011.

[135] J. Martin, "Inflationary perturbations: The Cosmological Schwinger effect," *Lect.Notes Phys.* **738** (2008) 193–241, arXiv:0704.3540 [hep-th].

[136] C. Kiefer and D. Polarski, "Why do cosmological perturbations look classical to us?," *Adv.Sci.Lett.* **2** (2009) 164–173, arXiv:0810.0087 [astro-ph].

[137] D. Sudarsky, "Shortcomings in the Understanding of Why Cosmological Perturbations Look Classical," *Int.J.Mod.Phys.* **D20** (2011) 509–552, arXiv:0906.0315 [gr-qc].

[138] J. Martin, V. Vennin, and P. Peter, "Cosmological Inflation and the Quantum

Measurement Problem," *Phys.Rev.* **D86** (2012) 103524, arXiv:1207.2086 [hep-th].

[139] J. Martin, "The Quantum State of Inflationary Perturbations," *J.Phys.Conf.Ser.* **405** (2012) 012004, arXiv:1209.3092 [hep-th].

[140] S. Alexander, R. H. Brandenberger, and D. Easson, "Brane gases in the early universe," *Phys.Rev.* **D62** (2000) 103509, arXiv:hep-th/0005212 [hep-th].

[141] J. Khoury, B. A. Ovrut, N. Seiberg, P. J. Steinhardt, and N. Turok, "From big crunch to big bang," *Phys.Rev.* **D65** (2002) 086007, arXiv:hep-th/0108187 [hep-th].

[142] J. Martin, P. Peter, N. Pinto Neto, and D. J. Schwarz, "Passing through the bounce in the ekpyrotic models," *Phys.Rev.* **D65** (2002) 123513, arXiv:hep-th/0112128 [hep-th].

[143] P. Steinhardt and N. Turok, "A cyclic model of the universe," *Science* **296** (2002) 1436–1439.

[144] F. Finelli and R. Brandenberger, "On the generation of a scale invariant spectrum of adiabatic fluctuations in cosmological models with a contracting phase," *Phys.Rev.* **D65** (2002) 103522, arXiv:hep-th/0112249 [hep-th].

[145] R. Brandenberger, D. A. Easson, and D. Kimberly, "Loitering phase in brane gas cosmology," *Nucl.Phys.* **B623** (2002) 421–436, arXiv:hep-th/0109165 [hep-th].

[146] R. Kallosh, L. Kofman, and A. D. Linde, "Pyrotechnic universe," *Phys.Rev.* **D64** (2001) 123523, arXiv:hep-th/0104073 [hep-th].

[147] P. Peter and N. Pinto-Neto, "Primordial perturbations in a non singular bouncing universe model," *Phys.Rev.* **D66** (2002) 063509, arXiv:hep-th/0203013 [hep-th].

[148] S. Tsujikawa, R. Brandenberger, and F. Finelli, "On the construction of nonsingular pre - big bang and ekpyrotic cosmologies and the resulting density perturbations," *Phys.Rev.* **D66** (2002) 083513, arXiv:hep-th/0207228 [hep-th].

[149] L. Kofman, A. D. Linde, and V. F. Mukhanov, "Inflationary theory and alternative cosmology," *JHEP* **0210** (2002) 057, arXiv:hep-th/0206088 [hep-th].

[150] J. Khoury, P. J. Steinhardt, and N. Turok, "Designing cyclic universe models," *Phys.Rev.Lett.* **92** (2004) 031302, arXiv:hep-th/0307132 [hep-th].

[151] J. Martin and P. Peter, "On the properties of the transition matrix in bouncing cosmologies," *Phys.Rev.* **D69** (2004) 107301, arXiv:hep-th/0403173 [hep-th].

[152] A. Nayeri, R. H. Brandenberger, and C. Vafa, "Producing a scale-invariant spectrum of perturbations in a Hagedorn phase of string cosmology," *Phys.Rev.Lett.* **97** (2006) 021302, arXiv:hep-th/0511140 [hep-th].

[153] P. Peter, E. J. Pinho, and N. Pinto-Neto, "A Non inflationary model with scale invariant cosmological perturbations," *Phys.Rev.* **D75** (2007) 023516, arXiv:hep-th/0610205 [hep-th].

[154] F. Finelli, P. Peter, and N. Pinto-Neto, "Spectra of primordial fluctuations in

two-perfect-fluid regular bounces," *Phys.Rev.* **D77** (2008) 103508, arXiv:0709.3074 [gr-qc].

[155] F. T. Falciano, M. Lilley, and P. Peter, "A Classical bounce: Constraints and consequences," *Phys.Rev.* **D77** (2008) 083513, arXiv:0802.1196 [gr-qc].

[156] A. Linde, V. Mukhanov, and A. Vikman, "On adiabatic perturbations in the ekpyrotic scenario," *JCAP* **1002** (2010) 006, arXiv:0912.0944 [hep-th].

[157] L. R. Abramo, I. Yasuda, and P. Peter, "Non singular bounce in modified gravity," *Phys.Rev.* **D81** (2010) 023511, arXiv:0910.3422 [hep-th].

[158] R. Brandenberger, "Matter Bounce in Horava-Lifshitz Cosmology," *Phys.Rev.* **D80** (2009) 043516, arXiv:0904.2835 [hep-th].

[159] R. H. Brandenberger, "String Gas Cosmology: Progress and Problems," *Class.Quant.Grav.* **28** (2011) 204005, arXiv:1105.3247 [hep-th].

[160] R. H. Brandenberger, "The Matter Bounce Alternative to Inflationary Cosmology," arXiv:1206.4196 [astro-ph.CO].

[161] Y.-F. Cai, D. A. Easson, and R. Brandenberger, "Towards a Nonsingular Bouncing Cosmology," *JCAP* **1208** (2012) 020, arXiv:1206.2382 [hep-th].

[162] Y.-F. Cai, R. Brandenberger, and P. Peter, "Anisotropy in a Nonsingular Bounce," arXiv:1301.4703 [gr-qc].

[163] **Planck Collaboration** Collaboration, P. Ade *et al.*, "Planck 2013 results. XV. CMB power spectra and likelihood," arXiv:1303.5075 [astro-ph.CO].

[164] **BICEP2 Collaboration** Collaboration, P. Ade *et al.*, "BICEP2 I: Detection Of B-mode Polarization at Degree Angular Scales," arXiv:1403.3985 [astro-ph.CO].

[165] C. Bennett, D. Larson, J. Weiland, N. Jarosik, G. Hinshaw, *et al.*, "Nine-Year Wilkinson Microwave Anisotropy Probe (WMAP) Observations: Final Maps and Results," arXiv:1212.5225 [astro-ph.CO].

[166] G. Hinshaw, D. Larson, E. Komatsu, D. Spergel, C. Bennett, *et al.*, "Nine-Year Wilkinson Microwave Anisotropy Probe (WMAP) Observations: Cosmological Parameter Results," arXiv:1212.5226 [astro-ph.CO].

[167] **Planck Collaboration** Collaboration, P. Ade *et al.*, "Planck 2013 results. XXII. Constraints on inflation," arXiv:1303.5082 [astro-ph.CO].

[168] **Planck Collaboration** Collaboration, P. Ade *et al.*, "Planck 2013 Results. XXIV. Constraints on primordial non-Gaussianity," arXiv:1303.5084 [astro-ph.CO].

[169] J. Dunkley, E. Calabrese, J. Sievers, G. Addison, N. Battaglia, *et al.*, "The Atacama Cosmology Telescope: likelihood for small-scale CMB data," arXiv:1301.0776 [astro-ph.CO].

[170] J. L. Sievers, R. A. Hlozek, M. R. Nolta, V. Acquaviva, G. E. Addison, *et al.*, "The Atacama Cosmology Telescope: Cosmological parameters from three seasons of data,"

arXiv:1301.0824 [astro-ph.CO].

[171] Z. Hou, C. Reichardt, K. Story, B. Follin, R. Keisler, *et al.*, "Constraints on Cosmology from the Cosmic Microwave Background Power Spectrum of the 2500-square degree SPT-SZ Survey," arXiv:1212.6267 [astro-ph.CO].

[172] K. Story, C. Reichardt, Z. Hou, R. Keisler, K. Aird, *et al.*, "A Measurement of the Cosmic Microwave Background Damping Tail from the 2500-square-degree SPT-SZ survey," arXiv:1210.7231 [astro-ph.CO].

[173] **CMBPol Study Team** Collaboration, D. Baumann *et al.*, "CMBPol Mission Concept Study: Probing Inflation with CMB Polarization," *AIP Conf.Proc.* **1141** (2009) 10–120, arXiv:0811.3919 [astro-ph].

[174] J. Bock, A. Cooray, S. Hanany, B. Keating, A. Lee, *et al.*, "The Experimental Probe of Inflationary Cosmology (EPIC): A Mission Concept Study for NASA's Einstein Inflation Probe," arXiv:0805.4207 [astro-ph].

[175] B. Crill, P. Ade, E. Battistelli, S. Benton, R. Bihary, *et al.*, "SPIDER: A Balloon-borne Large-scale CMB Polarimeter," arXiv:0807.1548 [astro-ph].

[176] A. Kogut, D. Fixsen, D. Chuss, J. Dotson, E. Dwek, *et al.*, "The Primordial Inflation Explorer (PIXIE): A Nulling Polarimeter for Cosmic Microwave Background Observations," *JCAP* **1107** (2011) 025, arXiv:1105.2044 [astro-ph.CO].

[177] T. Matsumura, Y. Akiba, J. Borrill, Y. Chinone, M. Dobbs, *et al.*, "Mission design of LiteBIRD," arXiv:1311.2847 [astro-ph.IM].

[178] **PRISM Collaboration** Collaboration, P. Andre *et al.*, "PRISM (Polarized Radiation Imaging and Spectroscopy Mission): A White Paper on the Ultimate Polarimetric Spectro-Imaging of the Microwave and Far-Infrared Sky," arXiv:1306.2259 [astro-ph.CO].

[179] **Supernova Search Team** Collaboration, J. L. Tonry *et al.*, "Cosmological results from high-z supernovae," *Astrophys.J.* **594** (2003) 1–24, arXiv:astro-ph/0305008 [astro-ph].

[180] **Supernova Search Team** Collaboration, A. G. Riess *et al.*, "Type Ia supernova discoveries at z¿1 from the Hubble Space Telescope: Evidence for past deceleration and constraints on dark energy evolution," *Astrophys.J.* **607** (2004) 665–687, arXiv:astro-ph/0402512 [astro-ph].

[181] A. G. Riess, L.-G. Strolger, S. Casertano, H. C. Ferguson, B. Mobasher, *et al.*, "New Hubble Space Telescope Discoveries of Type Ia Supernovae at z¿1: Narrowing Constraints on the Early Behavior of Dark Energy," *Astrophys.J.* **659** (2007) 98–121, arXiv:astro-ph/0611572 [astro-ph].

[182] A. G. Riess, L. Macri, S. Casertano, H. Lampeitl, H. C. Ferguson, *et al.*, "A 3Telescope and Wide Field Camera 3," *Astrophys.J.* **730** (2011) 119, arXiv:1103.2976 [astro-ph.CO].

[183] **SDSS Collaboration** Collaboration, J. K. Adelman-McCarthy *et al.*, "The Sixth Data

Release of the Sloan Digital Sky Survey," *Astrophys.J.Suppl.* **175** (2008) 297–313, arXiv:0707.3413 [astro-ph].

[184] **SDSS Collaboration** Collaboration, K. N. Abazajian *et al.*, "The Seventh Data Release of the Sloan Digital Sky Survey," *Astrophys.J.Suppl.* **182** (2009) 543–558, arXiv:0812.0649 [astro-ph].

[185] **Euclid collaboration** Collaboration, J. Amiaux *et al.*, "Euclid Mission: building of a Reference Survey," arXiv:1209.2228 [astro-ph.IM].

[186] M. S. Turner, M. J. White, and J. E. Lidsey, "Tensor perturbations in inflationary models as a probe of cosmology," *Phys.Rev.* **D48** (1993) 4613–4622, arXiv:astro-ph/9306029 [astro-ph].

[187] M. Maggiore, "Gravitational wave experiments and early universe cosmology," *Phys.Rept.* **331** (2000) 283–367, arXiv:gr-qc/9909001 [gr-qc].

[188] H. Kudoh, A. Taruya, T. Hiramatsu, and Y. Himemoto, "Detecting a gravitational-wave background with next-generation space interferometers," *Phys.Rev.* **D73** (2006) 064006, arXiv:gr-qc/0511145 [gr-qc].

[189] K. Nakayama, S. Saito, Y. Suwa, and J. Yokoyama, "Probing reheating temperature of the universe with gravitational wave background," *JCAP* **0806** (2008) 020, arXiv:0804.1827 [astro-ph].

[190] S. Kuroyanagi, C. Gordon, J. Silk, and N. Sugiyama, "Forecast Constraints on Inflation from Combined CMB and Gravitational Wave Direct Detection Experiments," *Phys.Rev.* **D81** (2010) 083524, arXiv:0912.3683 [astro-ph.CO].

[191] J. Crowder and N. J. Cornish, "Beyond LISA: Exploring future gravitational wave missions," *Phys.Rev.* **D72** (2005) 083005, arXiv:gr-qc/0506015 [gr-qc].

[192] M. Ando, S. Kawamura, N. Seto, S. Sato, T. Nakamura, *et al.*, "DECIGO and DECIGO pathfinder," *Class.Quant.Grav.* **27** (2010) 084010.

[193] S. Kawamura, M. Ando, N. Seto, S. Sato, T. Nakamura, *et al.*, "The Japanese space gravitational wave antenna: DECIGO," *Class.Quant.Grav.* **28** (2011) 094011.

[194] P. Amaro-Seoane, S. Aoudia, S. Babak, P. Binetruy, E. Berti, *et al.*, "eLISA: Astrophysics and cosmology in the millihertz regime," arXiv:1201.3621 [astro-ph.CO].

[195] S. Kuroyanagi, C. Ringeval, and T. Takahashi, "Early Universe Tomography with CMB and Gravitational Waves," *Phys. Rev. D* **87** (2013) 083502, arXiv:1301.1778 [astro-ph.CO].

[196] K. Jedamzik, M. Lemoine, and J. Martin, "Generation of gravitational waves during early structure formation between cosmic inflation and reheating," *JCAP* **1004** (2010) 021, arXiv:1002.3278 [astro-ph.CO].

[197] D. Gorbunov and A. Tokareva, "R^2-inflation with conformal SM Higgs field," *JCAP* **1312** (2013) 021, arXiv:1212.4466 [astro-ph.CO].

[198] M. Zaldarriaga, S. R. Furlanetto, and L. Hernquist, "21 Centimeter fluctuations from cosmic gas at high redshifts," *Astrophys.J.* **608** (2004) 622–635, arXiv:astro-ph/0311514 [astro-ph].

[199] A. Lewis and A. Challinor, "The 21cm angular-power spectrum from the dark ages," *Phys. Rev.* **D76** (2007) 083005, arXiv:astro-ph/0702600.

[200] M. Tegmark and M. Zaldarriaga, "The Fast Fourier Transform Telescope," *Phys. Rev.* **D79** (2009) 083530, arXiv:0805.4414 [astro-ph].

[201] V. Barger, Y. Gao, Y. Mao, and D. Marfatia, "Inflationary Potential from 21 cm Tomography and Planck," *Phys. Lett.* **B673** (2009) 173–178, arXiv:0810.3337 [astro-ph].

[202] Y. Mao, M. Tegmark, M. McQuinn, M. Zaldarriaga, and O. Zahn, "How accurately can 21 cm tomography constrain cosmology?," *Phys. Rev.* **D78** (2008) 023529, arXiv:0802.1710 [astro-ph].

[203] P. Adshead, R. Easther, J. Pritchard, and A. Loeb, "Inflation and the Scale Dependent Spectral Index: Prospects and Strategies," *JCAP* **1102** (2011) 021, arXiv:1007.3748 [astro-ph.CO].

[204] S. Clesse, L. Lopez-Honorez, C. Ringeval, H. Tashiro, and M. H. Tytgat, "Background reionization history from omniscopes," *Phys.Rev.* **D86** (2012) 123506, arXiv:1208.4277 [astro-ph.CO].

[205] J. Martin, C. Ringeval, and V. Vennin, "Encyclopædia Inflationaris," *Phys.Dark Univ.* (2014) , arXiv:1303.3787 [astro-ph.CO].

[206] J. Martin, C. Ringeval, R. Trotta, and V. Vennin, "The Best Inflationary Models After Planck," *JCAP* **1403** (2014) 039, arXiv:1312.3529 [astro-ph.CO].

[207] J. Martin, C. Ringeval, R. Trotta, and V. Vennin, "Compatibility of Planck and BICEP2 in the Light of Inflation," arXiv:1405.7272 [astro-ph.CO].

[208] V. Vennin, "Horizon-Flow off-track for Inflation," *Phys. Rev. D89,* **083526** (2014) 083526, arXiv:1401.2926 [astro-ph.CO].

[209] J. Martin, C. Ringeval, and V. Vennin, "K-inflationary Power Spectra at Second Order," *JCAP* **1306** (2013) 021, arXiv:1303.2120 [astro-ph.CO].

[210] J. Martin and V. Vennin, "Stochastic Effects in Hybrid Inflation," *Phys.Rev.* **D85** (2012) 043525, arXiv:1110.2070 [astro-ph.CO].

[211] L. Perreault Levasseur, V. Vennin, and R. Brandenberger, "Recursive Stochastic Effects in Valley Hybrid Inflation," *Phys. Rev. D88,* **083538** (2013) 083538, arXiv:1307.2575.

[212] D. H. Lyth and A. Riotto, "Particle physics models of inflation and the cosmological density perturbation," *Phys. Rept.* **314** (1999) 1–146, arXiv:hep-ph/9807278.

[213] M. S. Turner, "Coherent Scalar Field Oscillations in an Expanding Universe," *Phys. Rev.* **D28** (1983) 1243.

[214] L. Kofman, A. D. Linde, and A. A. Starobinsky, "Towards the theory of reheating after inflation," *Phys.Rev.* **D56** (1997) 3258–3295, arXiv:hep-ph/9704452 [hep-ph].

[215] B. A. Bassett, D. I. Kaiser, and R. Maartens, "General relativistic preheating after inflation," *Phys.Lett.* **B455** (1999) 84–89, arXiv:hep-ph/9808404 [hep-ph].

[216] F. Finelli and R. H. Brandenberger, "Parametric amplification of metric fluctuations during reheating in two field models," *Phys. Rev.* **D62** (2000) 083502, arXiv:hep-ph/0003172 [hep-ph].

[217] B. A. Bassett, S. Tsujikawa, and D. Wands, "Inflation dynamics and reheating," *Rev. Mod. Phys.* **78** (2006) 537–589, arXiv:astro-ph/0507632.

[218] A. Mazumdar and J. Rocher, "Particle physics models of inflation and curvaton scenarios," *Phys. Rept.* **497** (2011) 85–215, arXiv:1001.0993 [hep-ph].

[219] K. Jedamzik, M. Lemoine, and J. Martin, "Collapse of Small-Scale Density Perturbations during Preheating in Single Field Inflation," *JCAP* **1009** (2010) 034, arXiv:1002.3039 [astro-ph.CO].

[220] R. Easther, R. Flauger, and J. B. Gilmore, "Delayed Reheating and the Breakdown of Coherent Oscillations," *JCAP* **1104** (2011) 027, arXiv:1003.3011 [astro-ph.CO].

[221] A. Albrecht, P. J. Steinhardt, M. S. Turner, and F. Wilczek, "Reheating an Inflationary Universe," *Phys.Rev.Lett.* **48** (1982) 1437.

[222] L. Kofman, A. D. Linde, and A. A. Starobinsky, "Reheating after inflation," *Phys.Rev.Lett.* **73** (1994) 3195–3198, arXiv:hep-th/9405187 [hep-th].

[223] Y. Shtanov, J. H. Traschen, and R. H. Brandenberger, "Universe reheating after inflation," *Phys.Rev.* **D51** (1995) 5438–5455, arXiv:hep-ph/9407247 [hep-ph].

[224] V. Kuzmin and V. Rubakov, "Ultrahigh-energy cosmic rays: A Window to postinflationary reheating epoch of the universe?," *Phys.Atom.Nucl.* **61** (1998) 1028–1030, arXiv:astro-ph/9709187 [astro-ph].

[225] F. Finelli and R. H. Brandenberger, "Parametric amplification of gravitational fluctuations during reheating," *Phys.Rev.Lett.* **82** (1999) 1362–1365, arXiv:hep-ph/9809490 [hep-ph].

[226] D. J. Schwarz, C. A. Terrero-Escalante, and A. A. Garcia, "Higher order corrections to primordial spectra from cosmological inflation," *Phys.Lett.* **B517** (2001) 243–249, arXiv:astro-ph/0106020 [astro-ph].

[227] D. J. Schwarz and C. A. Terrero-Escalante, "Primordial fluctuations and cosmological inflation after WMAP 1.0," *JCAP* **0408** (2004) 003, arXiv:hep-ph/0403129 [hep-ph].

[228] G. N. Remmen and S. M. Carroll, "Attractor Solutions in Scalar-Field Cosmology," *Phys.Rev.* **D88** (2013) 083518, arXiv:1309.2611 [gr-qc].

[229] D. Larson, J. Dunkley, G. Hinshaw, E. Komatsu, M. Nolta, *et al.*, "Seven-Year Wilkinson Microwave Anisotropy Probe (WMAP) Observations: Power Spectra and WMAP-Derived Parameters," *Astrophys.J.Suppl.* **192** (2011) 16, arXiv:1001.4635

[astro-ph.CO].

[230] **WMAP Collaboration** Collaboration, E. Komatsu *et al.*, "Seven-Year Wilkinson Microwave Anisotropy Probe (WMAP) Observations: Cosmological Interpretation," *Astrophys.J.Suppl.* **192** (2011) 18, arXiv:1001.4538 [astro-ph.CO].

[231] L. Lorenz, J. Martin, and C. Ringeval, "Constraints on Kinetically Modified Inflation from WMAP5," *Phys.Rev.* **D78** (2008) 063543, arXiv:0807.2414 [astro-ph].

[232] J. Martin and C. Ringeval, "First CMB Constraints on the Inflationary Reheating Temperature," *Phys.Rev.* **D82** (2010) 023511, arXiv:1004.5525 [astro-ph.CO].

[233] R. Easther and W. H. Kinney, "Monte Carlo reconstruction of the inflationary potential," *Phys.Rev.* **D67** (2003) 043511, arXiv:astro-ph/0210345 [astro-ph].

[234] W. H. Kinney, E. W. Kolb, A. Melchiorri, and A. Riotto, "WMAPping inflationary physics," *Phys.Rev.* **D69** (2004) 103516, arXiv:hep-ph/0305130 [hep-ph].

[235] C.-Y. Chen, B. Feng, X.-L. Wang, and Z.-Y. Yang, "Reconstructing large running-index inflaton potentials," *Class.Quant.Grav.* **21** (2004) 3223–3236, arXiv:astro-ph/0404419 [astro-ph].

[236] B. A. Powell, K. Tzirakis, and W. H. Kinney, "Tensors, non-Gaussianities, and the future of potential reconstruction," *JCAP* **0904** (2009) 019, arXiv:0812.1797 [astro-ph].

[237] J. Martin, C. Ringeval, and R. Trotta, "Hunting Down the Best Model of Inflation with Bayesian Evidence," *Phys.Rev.* **D83** (2011) 063524, arXiv:1009.4157 [astro-ph.CO].

[238] J. Bardeen, "Gauge invariant cosmological perturbations," *Phys.Rev.* **D22** (1981) 1882.

[239] J. M. Bardeen, "Gauge Invariant Cosmological Perturbations," *Phys.Rev.* **D22** (1980) 1882–1905.

[240] J. Martin and D. J. Schwarz, "The Influence of cosmological transitions on the evolution of density perturbations," *Phys.Rev.* **D57** (1998) 3302–3316, arXiv:gr-qc/9704049 [gr-qc].

[241] H. Kodama and M. Sasaki, "Cosmological Perturbation Theory," *Prog.Theor.Phys.Suppl.* **78** (1984) 1–166.

[242] V. F. Mukhanov, "Quantum Theory of Gauge Invariant Cosmological Perturbations," *Sov.Phys.JETP* **67** (1988) 1297–1302.

[243] F. L. Claude Cohen-Tannoudji, Bernard Diu, *Quantum Mechanics*. Hermann, 1973.

[244] T. Bunch and P. Davies, "Quantum Field Theory in de Sitter Space: Renormalization by Point Splitting," *Proc.Roy.Soc.Lond.* **A360** (1978) 117–134.

[245] N. Birrell and P. Davies, "Quantum Fields in Curved Space," *Cambridge Monogr.Math.Phys.* (1982) .

[246] J. Martin and R. H. Brandenberger, "The TransPlanckian problem of inflationary cosmology," *Phys.Rev.* **D63** (2001) 123501, arXiv:hep-th/0005209 [hep-th].

[247] J. Martin and R. H. Brandenberger, "The Corley-Jacobson dispersion relation and transPlanckian inflation," *Phys.Rev.* **D65** (2002) 103514, arXiv:hep-th/0201189 [hep-th].

[248] J. Martin and R. Brandenberger, "On the dependence of the spectra of fluctuations in inflationary cosmology on transPlanckian physics," *Phys.Rev.* **D68** (2003) 063513, arXiv:hep-th/0305161 [hep-th].

[249] R. H. Brandenberger and J. Martin, "Back-reaction and the trans-Planckian problem of inflation revisited," *Phys.Rev.* **D71** (2005) 023504, arXiv:hep-th/0410223 [hep-th].

[250] N. Kaloper, M. Kleban, A. Lawrence, S. Shenker, and L. Susskind, "Initial conditions for inflation," *JHEP* **0211** (2002) 037, arXiv:hep-th/0209231 [hep-th].

[251] U. H. Danielsson, "A Note on inflation and transPlanckian physics," *Phys.Rev.* **D66** (2002) 023511, arXiv:hep-th/0203198 [hep-th].

[252] K. Goldstein and D. A. Lowe, "A Note on alpha vacua and interacting field theory in de Sitter space," *Nucl.Phys.* **B669** (2003) 325–340, arXiv:hep-th/0302050 [hep-th].

[253] H. Collins and R. Holman, "Taming the alpha vacuum," *Phys.Rev.* **D70** (2004) 084019, arXiv:hep-th/0312143 [hep-th].

[254] H. Collins, R. Holman, and M. R. Martin, "The Fate of the alpha vacuum," *Phys.Rev.* **D68** (2003) 124012, arXiv:hep-th/0306028 [hep-th].

[255] R. Brunetti, K. Fredenhagen, and S. Hollands, "A Remark on alpha vacua for quantum field theories on de Sitter space," *JHEP* **0505** (2005) 063, arXiv:hep-th/0503022 [hep-th].

[256] U. H. Danielsson, "Transplanckian energy production and slow roll inflation," *Phys.Rev.* **D71** (2005) 023516, arXiv:hep-th/0411172 [hep-th].

[257] B. Greene, K. Schalm, J. P. van der Schaar, and G. Shiu, "Extracting new physics from the CMB," *eConf* **C041213** (2004) 0001, arXiv:astro-ph/0503458 [astro-ph].

[258] K. Bhattacharya, S. Mohanty, and R. Rangarajan, "Temperature of the inflaton and duration of inflation from WMAP data," *Phys.Rev.Lett.* **96** (2006) 121302, arXiv:hep-ph/0508070 [hep-ph].

[259] R. Easther, W. H. Kinney, and H. Peiris, "Boundary effective field theory and trans-Planckian perturbations: Astrophysical implications," *JCAP* **0508** (2005) 001, arXiv:astro-ph/0505426 [astro-ph].

[260] M. Giovannini, "Hanbury Brown-Twiss interferometry and second-order correlations of inflaton quanta," *Phys.Rev.* **D83** (2011) 023515, arXiv:1011.1673 [astro-ph.CO].

[261] A. Ashoorioon and G. Shiu, "A Note on Calm Excited States of Inflation," *JCAP* **1103** (2011) 025, arXiv:1012.3392 [astro-ph.CO].

[262] I. Agullo and L. Parker, "Non-gaussianities and the Stimulated creation of quanta in the inflationary universe," *Phys.Rev.* **D83** (2011) 063526, arXiv:1010.5766 [astro-ph.CO].

[263] D. Carney, W. Fischler, S. Paban, and N. Sivanandam, "The Inflationary Wavefunction and its Initial Conditions," *JCAP* **1212** (2012) 012, arXiv:1109.6566 [hep-th].

[264] A. Dey and S. Paban, "Non-Gaussianities in the Cosmological Perturbation Spectrum due to Primordial Anisotropy," *JCAP* **1204** (2012) 039, arXiv:1106.5840 [hep-th].

[265] A. Dey, E. Kovetz, and S. Paban, "Non-Gaussianities in the Cosmological Perturbation Spectrum due to Primordial Anisotropy II," *JCAP* **1210** (2012) 055, arXiv:1205.2758 [astro-ph.CO].

[266] S. Kundu, "Inflation with General Initial Conditions for Scalar Perturbations," *JCAP* **1202** (2012) 005, arXiv:1110.4688 [astro-ph.CO].

[267] D. Lyth, "Large Scale Energy Density Perturbations and Inflation," *Phys.Rev.* **D31** (1985) 1792–1798.

[268] J. H. Traschen and R. H. Brandenberger, "Particle Production During Out-of-equilibrium Phase Transitions," *Phys.Rev.* **D42** (1990) 2491–2504.

[269] M. Abramowitz and I. Stegun, *Handbook of Mathematical Functions*. Dover, New York, fifth ed., 1964.

[270] V. F. Mukhanov, "Gravitational Instability of the Universe Filled with a Scalar Field," *JETP Lett.* **41** (1985) 493–496.

[271] F. Lucchin and S. Matarrese, "Power Law Inflation," *Phys.Rev.* **D32** (1985) 1316.

[272] J.-O. Gong and E. D. Stewart, "The Density perturbation power spectrum to second order corrections in the slow roll expansion," *Phys.Lett.* **B510** (2001) 1–9, arXiv:astro-ph/0101225 [astro-ph].

[273] J. Martin and D. J. Schwarz, "WKB approximation for inflationary cosmological perturbations," *Phys.Rev.* **D67** (2003) 083512, arXiv:astro-ph/0210090 [astro-ph].

[274] S. Habib, K. Heitmann, G. Jungman, and C. Molina-Paris, "The Inflationary perturbation spectrum," *Phys.Rev.Lett.* **89** (2002) 281301, arXiv:astro-ph/0208443 [astro-ph].

[275] S. Habib, A. Heinen, K. Heitmann, G. Jungman, and C. Molina-Paris, "Characterizing inflationary perturbations: The Uniform approximation," *Phys.Rev.* **D70** (2004) 083507, arXiv:astro-ph/0406134 [astro-ph].

[276] R. Casadio, F. Finelli, M. Luzzi, and G. Venturi, "Improved WKB analysis of cosmological perturbations," *Phys.Rev.* **D71** (2005) 043517, arXiv:gr-qc/0410092 [gr-qc].

[277] R. Casadio, F. Finelli, M. Luzzi, and G. Venturi, "Higher order slow-roll predictions for inflation," *Phys.Lett.* **B625** (2005) 1–6, arXiv:gr-qc/0506043 [gr-qc].

[278] S. M. Leach, A. R. Liddle, J. Martin, and D. J. Schwarz, "Cosmological parameter estimation and the inflationary cosmology," *Phys.Rev.* **D66** (2002) 023515, arXiv:astro-ph/0202094 [astro-ph].

[279] V. Mukhanov, "Quantum Cosmological Perturbations: Predictions and Observations," *Eur.Phys.J.* **C73** (2013) 2486, arXiv:1303.3925 [astro-ph.CO].

[280] R. H. Brandenberger, A. Nayeri, and S. P. Patil, "Closed String Thermodynamics and a Blue Tensor Spectrum," arXiv:1403.4927 [astro-ph.CO].

[281] D. H. Lyth, "What would we learn by detecting a gravitational wave signal in the cosmic microwave background anisotropy?," *Phys.Rev.Lett.* **78** (1997) 1861–1863, arXiv:hep-ph/9606387 [hep-ph].

[282] S. Antusch and D. Nolde, "BICEP2 implications for single-field slow-roll inflation revisited," *JCAP* **1405** (2014) 035, arXiv:1404.1821 [hep-ph].

[283] D. Baumann and L. McAllister, "Inflation and String Theory," arXiv:1404.2601 [hep-th].

[284] A. Vilenkin, "Quantum Fluctuations in the New Inflationary Universe," *Nucl.Phys.* **B226** (1983) 527.

[285] A. Vilenkin, "The Birth of Inflationary Universes," *Phys.Rev.* **D27** (1983) 2848.

[286] M. Sasaki, Y. Nambu, and K.-i. Nakao, "Classical Behavior of a Scalar Field in the Inflationary Universe," *Nucl.Phys.* **B308** (1988) 868.

[287] A. Goncharov, A. D. Linde, and V. F. Mukhanov, "The Global Structure of the Inflationary Universe," *Int.J.Mod.Phys.* **A2** (1987) 561–591.

[288] D. Salopek and J. Bond, "Nonlinear evolution of long wavelength metric fluctuations in inflationary models," *Phys.Rev.* **D42** (1990) 3936–3962.

[289] A. D. Linde, D. A. Linde, and A. Mezhlumian, "From the Big Bang theory to the theory of a stationary universe," *Phys.Rev.* **D49** (1994) 1783–1826, arXiv:gr-qc/9306035 [gr-qc].

[290] A. A. Starobinsky, "STOCHASTIC DE SITTER (INFLATIONARY) STAGE IN THE EARLY UNIVERSE," *Lect.Notes Phys.* **246** (1986) 107–126.

[291] Y. Nambu and M. Sasaki, "Stochastic Stage of an Inflationary Universe Model," *Phys.Lett.* **B205** (1988) 441.

[292] Y. Nambu and M. Sasaki, "Stochastic Approach to Chaotic Inflation and the Distribution of Universes," *Phys.Lett.* **B219** (1989) 240.

[293] H. E. Kandrup, "Stochastic inflation as a time dependent random walk," *Phys.Rev.* **D39** (1989) 2245.

[294] K.-i. Nakao, Y. Nambu, and M. Sasaki, "Stochastic Dynamics of New Inflation," *Prog.Theor.Phys.* **80** (1988) 1041.

[295] Y. Nambu, "Stochastic Dynamics of an Inflationary Model and Initial Distribution of Universes," *Prog.Theor.Phys.* **81** (1989) 1037.

[296] D. Salopek and J. Bond, "Stochastic inflation and nonlinear gravity," *Phys.Rev.* **D43**

(1991) 1005–1031.

[297] S. Mollerach, S. Matarrese, A. Ortolan, and F. Lucchin, "Stochastic inflation in a simple two field model," *Phys.Rev.* **D44** (1991) 1670–1679.

[298] A. A. Starobinsky and J. Yokoyama, "Equilibrium state of a selfinteracting scalar field in the De Sitter background," *Phys.Rev.* **D50** (1994) 6357–6368, arXiv:astro-ph/9407016 [astro-ph].

[299] F. Finelli, G. Marozzi, A. Starobinsky, G. Vacca, and G. Venturi, "Generation of fluctuations during inflation: Comparison of stochastic and field-theoretic approaches," *Phys.Rev.* **D79** (2009) 044007, arXiv:0808.1786 [hep-th].

[300] F. Finelli, G. Marozzi, A. Starobinsky, G. Vacca, and G. Venturi, "Stochastic growth of quantum fluctuations during slow-roll inflation," *Phys.Rev.* **D82** (2010) 064020, arXiv:1003.1327 [hep-th].

[301] B. Garbrecht, G. Rigopoulos, and Y. Zhu, "Infrared Correlations in de Sitter Space: Field Theoretic vs. Stochastic Approach," *Phys.Rev.* **D89** (2014) 063506, arXiv:1310.0367 [hep-th].

[302] N. Tsamis and R. Woodard, "Stochastic quantum gravitational inflation," *Nucl.Phys.* **B724** (2005) 295–328, arXiv:gr-qc/0505115 [gr-qc].

[303] T. Prokopec, N. Tsamis, and R. Woodard, "Stochastic Inflationary Scalar Electrodynamics," *Annals Phys.* **323** (2008) 1324–1360, arXiv:0707.0847 [gr-qc].

[304] T. Prokopec, N. C. Tsamis, and R. P. Woodard, "Two loop stress-energy tensor for inflationary scalar electrodynamics," *Phys.Rev.* **D78** (2008) 043523, arXiv:0802.3673 [gr-qc].

[305] M. Morikawa, "Dissipation and Fluctuation of Quantum Fields in Expanding Universes," *Phys.Rev.* **D42** (1990) 1027–1034.

[306] B. Hu and S. Sinha, "A Fluctuation - dissipation relation for semiclassical cosmology," *Phys.Rev.* **D51** (1995) 1587–1606, arXiv:gr-qc/9403054 [gr-qc].

[307] L. Grishchuk, H. Haus, and K. Bergman, "Generation of squeezed radiation from vacuum in the cosmos and the laboratory," *Phys.Rev.* **D46** (1992) 1440–1449.

[308] A. H. Guth and S.-Y. Pi, "The Quantum Mechanics of the Scalar Field in the New Inflationary Universe," *Phys.Rev.* **D32** (1985) 1899–1920.

[309] J. Lesgourgues, D. Polarski, and A. A. Starobinsky, "Quantum to classical transition of cosmological perturbations for nonvacuum initial states," *Nucl.Phys.* **B497** (1997) 479–510, arXiv:gr-qc/9611019 [gr-qc].

[310] M. Mijic, "Quantum squeezing and late time classical behavior of massive fields in expanding Robertson-Walker universe," *Int.J.Mod.Phys.* **D6** (1997) 505–514, arXiv:gr-qc/9706016 [gr-qc].

[311] W. Zurek, "Pointer Basis of Quantum Apparatus: Into What Mixture Does the Wave Packet Collapse?," *Phys.Rev.* **D24** (1981) 1516–1525.

[312] W. Zurek, "Environment induced superselection rules," *Phys.Rev.* **D26** (1982) 1862–1880.

[313] E. Joos and H. Zeh, "The Emergence of classical properties through interaction with the environment," *Z.Phys.* **B59** (1985) 223–243.

[314] E. Calzetta and B. Hu, "Quantum fluctuations, decoherence of the mean field, and structure formation in the early universe," *Phys.Rev.* **D52** (1995) 6770–6788, arXiv:gr-qc/9505046 [gr-qc].

[315] C. Kiefer, I. Lohmar, D. Polarski, and A. A. Starobinsky, "Pointer states for primordial fluctuations in inflationary cosmology," *Class.Quant.Grav.* **24** (2007) 1699–1718, arXiv:astro-ph/0610700 [astro-ph].

[316] I. Egusquiza, A. Feinstein, M. Perez Sebastian, and M. Valle Basagoiti, "On the entropy and the density matrix of cosmological perturbations," *Class.Quant.Grav.* **15** (1998) 1927–1936, arXiv:gr-qc/9709061 [gr-qc].

[317] P. R. Anderson, C. Molina-Paris, and E. Mottola, "Short distance and initial state effects in inflation: Stress tensor and decoherence," *Phys.Rev.* **D72** (2005) 043515, arXiv:hep-th/0504134 [hep-th].

[318] C. P. Burgess, R. Holman, and D. Hoover, "Decoherence of inflationary primordial fluctuations," *Phys.Rev.* **D77** (2008) 063534, arXiv:astro-ph/0601646 [astro-ph].

[319] P. Martineau, "On the decoherence of primordial fluctuations during inflation," *Class.Quant.Grav.* **24** (2007) 5817–5834, arXiv:astro-ph/0601134 [astro-ph].

[320] H. Casini, R. Montemayor, and P. Sisterna, "Stochastic approach to inflation. 2. Classicality, coarse graining and noises," *Phys.Rev.* **D59** (1999) 063512, arXiv:gr-qc/9811083 [gr-qc].

[321] S. Matarrese, M. A. Musso, and A. Riotto, "Influence of superhorizon scales on cosmological observables generated during inflation," *JCAP* **0405** (2004) 008, arXiv:hep-th/0311059 [hep-th].

[322] M. Liguori, S. Matarrese, M. Musso, and A. Riotto, "Stochastic inflation and the lower multipoles in the CMB anisotropies," *JCAP* **0408** (2004) 011, arXiv:astro-ph/0405544 [astro-ph].

[323] B. Hu, J. P. Paz, and Y. Zhang, "Quantum origin of noise and fluctuations in cosmology," arXiv:gr-qc/9512049 [gr-qc].

[324] S. Winitzki and A. Vilenkin, "Effective noise in stochastic description of inflation," *Phys.Rev.* **D61** (2000) 084008, arXiv:gr-qc/9911029 [gr-qc].

[325] H. M. Hodges, "Analytic Solution of a Chaotic Inflaton," *Phys.Rev.* **D39** (1989) 3568–3570.

[326] H. M. Hodges, "Is double inflation likely?," *Phys.Rev.Lett.* **64** (1990) 1080.

[327] A. Matacz, "Inflation and the fine tuning problem," *Phys.Rev.* **D56** (1997) 1836–1840, arXiv:gr-qc/9611063 [gr-qc].

[328] J. Martin and M. Musso, "Solving stochastic inflation for arbitrary potentials," *Phys.Rev.* **D73** (2006) 043516, arXiv:hep-th/0511214 [hep-th].

[329] J. Martin and M. Musso, "On the reliability of the Langevin perturbative solution in stochastic inflation," *Phys.Rev.* **D73** (2006) 043517, arXiv:hep-th/0511292 [hep-th].

[330] S. Gratton and N. Turok, "Langevin analysis of eternal inflation," *Phys.Rev.* **D72** (2005) 043507, arXiv:hep-th/0503063 [hep-th].

[331] K. E. Kunze, "Perturbations in stochastic inflation," *JCAP* **0607** (2006) 014, arXiv:astro-ph/0603575 [astro-ph].

[332] J. Garcia-Bellido and A. D. Linde, "Stationarity of inflation and predictions of quantum cosmology," *Phys.Rev.* **D51** (1995) 429–443, arXiv:hep-th/9408023 [hep-th].

[333] A. Vilenkin, "Making predictions in eternally inflating universe," *Phys.Rev.* **D52** (1995) 3365–3374, arXiv:gr-qc/9505031 [gr-qc].

[334] H. Risken, *The Fokker-Planck Equation*, vol. 18. Spinger Series in Synergetics, 1984.

[335] F. Finelli, G. Marozzi, A. Starobinsky, G. Vacca, and G. Venturi, "Stochastic growth of quantum fluctuations during inflation," *AIP Conf.Proc.* **1446** (2010) 320–332, arXiv:1102.0216 [hep-th].

[336] K. A. Malik, "Gauge-invariant perturbations at second order: Multiple scalar fields on large scales," *JCAP* **0511** (2005) 005, arXiv:astro-ph/0506532 [astro-ph].

[337] K. A. Malik and D. Wands, "Evolution of second-order cosmological perturbations," *Class.Quant.Grav.* **21** (2004) L65–L72, arXiv:astro-ph/0307055 [astro-ph].

[338] H. Noh and J.-c. Hwang, "Second-order perturbations of the friedmann world model," arXiv:astro-ph/0305123 [astro-ph].

[339] D. Wands, K. A. Malik, D. H. Lyth, and A. R. Liddle, "A New approach to the evolution of cosmological perturbations on large scales," *Phys.Rev.* **D62** (2000) 043527, arXiv:astro-ph/0003278 [astro-ph].

[340] F. Finelli, G. Marozzi, G. Vacca, and G. Venturi, "Energy momentum tensor of cosmological fluctuations during inflation," *Phys.Rev.* **D69** (2004) 123508, arXiv:gr-qc/0310086 [gr-qc].

[341] G. Marozzi, "Back-reaction of Cosmological Fluctuations during Power-Law Inflation," *Phys.Rev.* **D76** (2007) 043504, arXiv:gr-qc/0612148 [gr-qc].

[342] K. A. Malik, "A not so short note on the Klein-Gordon equation at second order," *JCAP* **0703** (2007) 004, arXiv:astro-ph/0610864 [astro-ph].

[343] K. A. Malik and D. Wands, "Cosmological perturbations," *Phys.Rept.* **475** (2009) 1–51, arXiv:0809.4944 [astro-ph].

[344] K. A. Malik and D. R. Matravers, "A Concise Introduction to Perturbation Theory in Cosmology," *Class.Quant.Grav.* **25** (2008) 193001, arXiv:0804.3276 [astro-ph].

[345] I. Huston and K. A. Malik, "Numerical calculation of second order perturbations," *JCAP* **0909** (2009) 019, arXiv:0907.2917 [astro-ph.CO].

[346] I. Huston and K. A. Malik, "Second Order Perturbations During Inflation Beyond Slow-roll," *JCAP* **1110** (2011) 029, arXiv:1103.0912 [astro-ph.CO].

[347] F. Kuhnel and D. J. Schwarz, "Stochastic Inflation and Dimensional Reduction," *Phys.Rev.* **D78** (2008) 103501, arXiv:0805.1998 [gr-qc].

[348] F. Kuhnel and D. J. Schwarz, "Stochastic Inflation and Replica Field Theory," *Phys.Rev.* **D79** (2009) 044009, arXiv:0810.5686 [gr-qc].

[349] F. Kuhnel and D. J. Schwarz, "Large-Scale Suppression from Stochastic Inflation," *Phys.Rev.Lett.* **105** (2010) 211302, arXiv:1003.3014 [hep-ph].

[350] T. Fujita, M. Kawasaki, Y. Tada, and T. Takesako, "A new algorithm for calculating the curvature perturbations in stochastic inflation," *JCAP* **1312** (2013) 036, arXiv:1308.4754 [astro-ph.CO].

[351] T. Fujita, M. Kawasaki, and Y. Tada, "Non-perturbative approach for curvature perturbations in stochastic-δN formalism," arXiv:1405.2187 [astro-ph.CO].

[352] A. A. Starobinsky, "Multicomponent de Sitter (Inflationary) Stages and the Generation of Perturbations," *JETP Lett.* **42** (1985) 152–155.

[353] M. Sasaki and E. D. Stewart, "A General analytic formula for the spectral index of the density perturbations produced during inflation," *Prog.Theor.Phys.* **95** (1996) 71–78, arXiv:astro-ph/9507001 [astro-ph].

[354] M. Sasaki and T. Tanaka, "Superhorizon scale dynamics of multiscalar inflation," *Prog.Theor.Phys.* **99** (1998) 763–782, arXiv:gr-qc/9801017 [gr-qc].

[355] D. H. Lyth, K. A. Malik, and M. Sasaki, "A General proof of the conservation of the curvature perturbation," *JCAP* **0505** (2005) 004, arXiv:astro-ph/0411220 [astro-ph].

[356] D. H. Lyth and Y. Rodriguez, "The Inflationary prediction for primordial non-Gaussianity," *Phys.Rev.Lett.* **95** (2005) 121302, arXiv:astro-ph/0504045 [astro-ph].

[357] P. Creminelli and M. Zaldarriaga, "Single field consistency relation for the 3-point function," *JCAP* **0410** (2004) 006, arXiv:astro-ph/0407059 [astro-ph].

[358] D. H. Lyth and D. Wands, "Conserved cosmological perturbations," *Phys.Rev.* **D68** (2003) 103515, arXiv:astro-ph/0306498 [astro-ph].

[359] J. Garcia-Bellido, "Flat direction MSSM (A-term) inflation," *AIP Conf.Proc.* **878** (2006) 277–283, arXiv:hep-ph/0610152 [hep-ph].

[360] R. Allahverdi, "MSSM flat direction inflation," *eConf* **C0605151** (2006) 0020, arXiv:hep-ph/0610180 [hep-ph].

[361] D. H. Lyth, "MSSM inflation," *JCAP* **0704** (2007) 006, arXiv:hep-ph/0605283

[hep-ph].

[362] R. Allahverdi and A. Mazumdar, "Spectral tilt in A-term inflation," arXiv:hep-ph/0610069 [hep-ph].

[363] R. Allahverdi, B. Dutta, and A. Mazumdar, "Probing the parameter space for an MSSM inflation and the neutralino dark matter," *Phys.Rev.* **D75** (2007) 075018, arXiv:hep-ph/0702112 [HEP-PH].

[364] K. Enqvist, L. Mether, and S. Nurmi, "Supergravity origin of the MSSM inflation," *JCAP* **0711** (2007) 014, arXiv:0706.2355 [hep-th].

[365] R. Allahverdi, B. Dutta, and A. Mazumdar, "Attraction towards an inflection point inflation," *Phys.Rev.* **D78** (2008) 063507, arXiv:0806.4557 [hep-ph].

[366] K. Kamada and J. Yokoyama, "On the realization of the MSSM inflation," *Prog.Theor.Phys.* **122** (2010) 969–986, arXiv:0906.3402 [hep-ph].

[367] R. Allahverdi, B. Dutta, and Y. Santoso, "MSSM inflation, dark matter, and the LHC," *Phys.Rev.* **D82** (2010) 035012, arXiv:1004.2741 [hep-ph].

[368] K. Enqvist, A. Mazumdar, and P. Stephens, "Inflection point inflation within supersymmetry," *JCAP* **1006** (2010) 020, arXiv:1004.3724 [hep-ph].

[369] K. Kohri and C.-M. Lin, "Hilltop Supernatural Inflation and Gravitino Problem," *JCAP* **1011** (2010) 010, arXiv:1008.3200 [hep-ph].

[370] S. Choudhury and A. Mazumdar, "An accurate bound on tensor-to-scalar ratio and the scale of inflation," *Nucl.Phys.* **B882** (2014) 386–396, arXiv:1306.4496 [hep-ph].

[371] R. K. Jain, P. Chingangbam, J.-O. Gong, L. Sriramkumar, and T. Souradeep, "Punctuated inflation and the low CMB multipoles," *JCAP* **0901** (2009) 009, arXiv:0809.3915 [astro-ph].

[372] R. K. Jain, P. Chingangbam, L. Sriramkumar, and T. Souradeep, "The tensor-to-scalar ratio in punctuated inflation," *Phys.Rev.* **D82** (2010) 023509, arXiv:0904.2518 [astro-ph.CO].

[373] D. A. Lowe and S. Roy, "Punctuated eternal inflation via AdS/CFT," *Phys.Rev.* **D82** (2010) 063508, arXiv:1004.1402 [hep-th].

[374] A. D. Linde, "Hybrid inflation," *Phys.Rev.* **D49** (1994) 748–754, arXiv:astro-ph/9307002 [astro-ph].

[375] L. Covi, "Models of inflation, supersymmetry breaking and observational constraints," arXiv:hep-ph/0012245 [hep-ph].

[376] A. D. Linde, "Axions in inflationary cosmology," *Phys. Lett.* **B259** (1991) 38–47.

[377] C. Panagiotakopoulos, "Hybrid inflation and supergravity," arXiv:hep-ph/0011261 [hep-ph].

[378] G. Lazarides, "Supersymmetric hybrid inflation," arXiv:hep-ph/0011130 [hep-ph].

[379] G. Dvali and S. H. Tye, "Brane inflation," *Phys.Lett.* **B450** (1999) 72–82, arXiv:hep-ph/9812483 [hep-ph].

[380] R. Maartens, D. Wands, B. A. Bassett, and I. Heard, "Chaotic inflation on the brane," *Phys.Rev.* **D62** (2000) 041301, arXiv:hep-ph/9912464 [hep-ph].

[381] S. H. Alexander, "Inflation from D - anti-D-brane annihilation," *Phys.Rev.* **D65** (2002) 023507, arXiv:hep-th/0105032 [hep-th].

[382] N. T. Jones, H. Stoica, and S. H. Tye, "Brane interaction as the origin of inflation," *JHEP* **0207** (2002) 051, arXiv:hep-th/0203163 [hep-th].

[383] I. Gihman and A. Skorohod, *Stochastic Differential Equations*. p.108, Springer Verlag, Berlin Heidelberg New York, 1972.

[384] K. Itô, "Stochastic integral," *Proceedings of the Imperial Academy* **20** (1944) no. 8, 519–524. http://dx.doi.org/10.3792/pia/1195572786.

[385] R. W. Butler, *Saddlepoint approximations and applications*. Cambridge University Press, 2007.

[386] L. Smolin, "Gravitational Radiative Corrections as the Origin of Spontaneous Symmetry Breaking!," *Phys.Lett.* **B93** (1980) 95.

[387] A. D. Linde, "Chaotic Inflation With Constrained Fields," *Phys.Lett.* **B202** (1988) 194.

[388] Y. Watanabe, "δN versus covariant perturbative approach to non-Gaussianity outside the horizon in multifield inflation," *Phys.Rev.* **D85** (2012) 103505, arXiv:1110.2462 [astro-ph.CO].

[389] T. Tanaka, T. Suyama, and S. Yokoyama, "Use of delta N formalism - Difficulties in generating large local-type non-Gaussianity during inflation -," *Class.Quant.Grav.* **27** (2010) 124003, arXiv:1003.5057 [astro-ph.CO].

[390] C. Burgess, M. Majumdar, D. Nolte, F. Quevedo, G. Rajesh, *et al.*, "The Inflationary brane anti-brane universe," *JHEP* **0107** (2001) 047, arXiv:hep-th/0105204 [hep-th].

[391] S. Kachru, R. Kallosh, A. D. Linde, J. M. Maldacena, L. P. McAllister, *et al.*, "Towards inflation in string theory," *JCAP* **0310** (2003) 013, arXiv:hep-th/0308055 [hep-th].

[392] E. Silverstein and D. Tong, "Scalar speed limits and cosmology: Acceleration from D-cceleration," *Phys.Rev.* **D70** (2004) 103505, arXiv:hep-th/0310221 [hep-th].

[393] M. Alishahiha, E. Silverstein, and D. Tong, "DBI in the sky," *Phys.Rev.* **D70** (2004) 123505, arXiv:hep-th/0404084 [hep-th].

[394] D. Baumann, A. Dymarsky, I. R. Klebanov, J. M. Maldacena, L. P. McAllister, *et al.*, "On D3-brane Potentials in Compactifications with Fluxes and Wrapped D-branes," *JHEP* **0611** (2006) 031, arXiv:hep-th/0607050 [hep-th].

[395] D. Baumann, A. Dymarsky, I. R. Klebanov, L. McAllister, and P. J. Steinhardt, "A Delicate universe," *Phys.Rev.Lett.* **99** (2007) 141601, arXiv:0705.3837 [hep-th].

[396] D. Baumann, A. Dymarsky, I. R. Klebanov, and L. McAllister, "Towards an Explicit Model of D-brane Inflation," *JCAP* **0801** (2008) 024, arXiv:0706.0360 [hep-th].

[397] A. Krause and E. Pajer, "Chasing brane inflation in string-theory," *JCAP* **0807** (2008) 023, arXiv:0705.4682 [hep-th].

[398] E. Pajer, "Inflation at the Tip," *JCAP* **0804** (2008) 031, arXiv:0802.2916 [hep-th].

[399] D. Baumann, A. Dymarsky, S. Kachru, I. R. Klebanov, and L. McAllister, "Holographic Systematics of D-brane Inflation," *JHEP* **0903** (2009) 093, arXiv:0808.2811 [hep-th].

[400] X. Chen, S. Sarangi, S.-H. Henry Tye, and J. Xu, "Is brane inflation eternal?," *JCAP* **0611** (2006) 015, arXiv:hep-th/0608082 [hep-th].

[401] F. Helmer and S. Winitzki, "Self-reproduction in k-inflation," *Phys.Rev.* **D74** (2006) 063528, arXiv:gr-qc/0608019 [gr-qc].

[402] A. J. Tolley and M. Wyman, "Stochastic Inflation Revisited: Non-Slow Roll Statistics and DBI Inflation," *JCAP* **0804** (2008) 028, arXiv:0801.1854 [hep-th].

[403] L. Lorenz, J. Martin, and J. Yokoyama, "Geometrically Consistent Approach to Stochastic DBI Inflation," *Phys.Rev.* **D82** (2010) 023515, arXiv:1004.3734 [hep-th].

[404] S. Das, K. Lochan, S. Sahu, and T. Singh, "Quantum to Classical Transition of Inflationary Perturbations - Continuous Spontaneous Localization as a Possible Mechanism -," *Phys.Rev.* **D88** (2013) 085020, arXiv:1304.5094 [astro-ph.CO].

[405] S. Dodelson, "How much can we learn about the physics of inflation?," *Phys.Rev.Lett.* **112** (2014) 191301, arXiv:1403.6310 [astro-ph.CO].

[406] G. W. Pettinari, C. Fidler, R. Crittenden, K. Koyama, A. Lewis, *et al.*, "Impact of polarisation on the intrinsic CMB bispectrum," arXiv:1406.2981 [astro-ph.CO].

[407] I. Ogburn, R.W., P. Ade, R. Aikin, M. Amiri, S. Benton, *et al.*, "BICEP2 and Keck Array operational overview and status of observations," arXiv:1208.0638 [astro-ph.IM].

[408] C. Kiefer, "Origin of classical structure from inflation," *Nucl.Phys.Proc.Suppl.* **88** (2000) 255–258, arXiv:astro-ph/0006252 [astro-ph].

[409] C. Kiefer and D. Polarski, "Emergence of classicality for primordial fluctuations: Concepts and analogies," *Annalen Phys.* **7** (1998) 137–158, arXiv:gr-qc/9805014 [gr-qc].

[410] S. L. Adler, "Why decoherence has not solved the measurement problem: A Response to P. W. Anderson," *Stud.Hist.Philos.Mod.Phys.* **34** (2003) 135–142, arXiv:quant-ph/0112095 [quant-ph].

[411] M. Schlosshauer, "Decoherence, the measurement problem, and interpretations of quantum mechanics," *Rev.Mod.Phys.* **76** (2004) 1267–1305, arXiv:quant-ph/0312059 [quant-ph].

[412] Y. Nomura, "Physical Theories, Eternal Inflation, and Quantum Universe," *JHEP* **1111**

(2011) 063, arXiv:1104.2324 [hep-th].

[413] Y. Nomura, "Quantum Mechanics, Spacetime Locality, and Gravity," *Found.Phys.* **43** (2013) 978–1007, arXiv:1110.4630 [hep-th].

[414] R. Bousso and L. Susskind, "The Multiverse Interpretation of Quantum Mechanics," *Phys.Rev.* **D85** (2012) 045007, arXiv:1105.3796 [hep-th].

[415] C. A. Fuchs, "Quantum Mechanics as Quantum Information (and only a little more)," arXiv:quant-ph/0205039.

[416] P. Holland, "The de Broglie-Bohm theory of motion and quantum field theory," *Phys.Rept.* **224** (1993) 95–150.

[417] P. Peter, E. Pinho, and N. Pinto-Neto, "Tensor perturbations in quantum cosmological backgrounds," *JCAP* **0507** (2005) 014, arXiv:hep-th/0509232 [hep-th].

[418] P. Peter, E. J. Pinho, and N. Pinto-Neto, "Gravitational wave background in perfect fluid quantum cosmologies," *Phys. Rev.* **D73** (2006) 104017, arXiv:gr-qc/0605060 [gr-qc].

[419] N. Pinto-Neto, G. Santos, and W. Struyve, "Quantum-to-classical transition of primordial cosmological perturbations in de Broglie–Bohm quantum theory," *Phys.Rev.* **D85** (2012) 083506, arXiv:1110.1339 [gr-qc].

[420] P. M. Pearle, "Reduction of the State Vector by a Nonlinear Schrodinger Equation," *Phys.Rev.* **D13** (1976) 857–868.

[421] G. Ghirardi, A. Rimini, and T. Weber, "A Unified Dynamics for Micro and MACRO Systems," *Phys.Rev.* **D34** (1986) 470.

[422] P. M. Pearle, "Combining Stochastic Dynamical State Vector Reduction With Spontaneous Localization," *Phys.Rev.* **A39** (1989) 2277–2289.

[423] L. Diosi, "LOCALIZED SOLUTION OF SIMPLE NONLINEAR QUANTUM LANGEVIN EQUATION,".

[424] G. C. Ghirardi, P. M. Pearle, and A. Rimini, "MARKOV PROCESSES IN HILBERT SPACE AND CONTINUOUS SPONTANEOUS LOCALIZATION OF SYSTEMS OF IDENTICAL PARTICLES," *Phys.Rev.* **A42** (1990) 78–79.

[425] A. Bassi and G. C. Ghirardi, "Dynamical reduction models," *Phys.Rept.* **379** (2003) 257, arXiv:quant-ph/0302164 [quant-ph].

[426] S. Weinberg, "Collapse of the State Vector," arXiv:1109.6462 [quant-ph].

[427] A. Bassi, K. Lochan, S. Satin, T. P. Singh, and H. Ulbricht, "Models of Wave-function Collapse, Underlying Theories, and Experimental Tests," arXiv:1204.4325 [quant-ph].

Compte Rendu Français

Ce court compte rendu contient une description en langue française des résultats importants obtenus lors de la thèse et présentés dans ce document.

5.1. L'inflation et le Modèle Standard de la Cosmologie

Nous commençons par rappeler les aspects essentiels du modèle standard de la cosmologie. Le modèle du Big Bang chaud décrit avec succès une série d'événements se déroulant dans un univers en expansion, dont la densité d'énergie et la température décroissent au cours du temps depuis une singularité initiale il y a 13.7 milliards d'année. Un certain nombre de questions sont néanmoins laissées en suspens, et nous expliquons comment une phase d'inflation, c'est à dire d'expansion accélérée, permet d'y répondre.

5.1.1. L'Univers Homogène

Les observations faites à grandes échelles de la distribution de matière dans l'Univers laissent apparaître que notre Univers est isotrope sur des distances supérieures à $\sim$ 100 Mpc. Ce constat, combiné au principe Copernicien qui suppose que nous n'occupons pas une place spécifique ou "centrale" dans l'Univers, nous amène à considérer un Univers homogène aux grandes échelles. Sous l'hypothèse de cette symétrie, la métrique de l'espace-temps $\mathrm{d}s^2 = g_{\mu\nu}\mathrm{d}x^\mu \mathrm{d}x^\nu$ est entièrement déterminée par une fonction du temps $a(t)$ appelée facteur d'échelle, et un paramètre discret $\mathcal{K} = -1, 0, 1$ qui caractérise la courbure spatiale de l'Univers (ouvert, plat ou fermé). Cette métrique est celle des espaces-temps de Friedmann-Lemaître-Robertson-Walker (FLRW), et elle peut s'écrire [9, 10, 11, 12]

$$\mathrm{d}s^2 = -\mathrm{d}t^2 + a^2(t)\left[\frac{\mathrm{d}r^2}{1-\mathcal{K}r^2} + r^2\left(\mathrm{d}\theta^2 + \sin^2\theta \mathrm{d}\phi^2\right)\right] . \tag{5.1}$$

Dans cette paramétrisation, t est le temps cosmique, r est la coordonnée radiale comobile, et θ et ϕ sont des coordonnées angulaires comobiles. A l'intérieur de ces espaces-temps, la distance physique L_{phys} séparant deux points, mesurée sur une hypersurface à t constant, est proportionnelle au facteur d'échelle a. En pratique, nous avons donc $L_{\mathrm{phys}} = a(t)L_{\mathrm{com}}$, où L_{com} est la distance comobile, constante pour deux objets au repos dans les coordonnées FLRW. Ainsi, le facteur d'échelle a définit le niveau global d'expansion (ou de contraction) des hypersurfaces de type espace. Une autre conséquence de la forme de la métrique (5.1) est l'existence d'une relation linéaire entre vitesse et distance, appelée loi de Hubble [13]. En effet, lorsque l'on dérive la relation $L_{\mathrm{phys}} = a(t)L_{\mathrm{com}}$ par rapport au temps, on obtient

$$v = \frac{\mathrm{d}L_{\mathrm{phys}}}{\mathrm{d}t} = \frac{\dot{a}}{a}L_{\mathrm{phys}} = HL_{\mathrm{phys}} , \tag{5.2}$$

où nous avons défini le paramètre de Hubble $H = \dot{a}/a$. La valeur actuelle de H, souvent dénotée H_0, a été mesurée [15] autour de 67 km/sec/Mpc.

Dans le cadre de la relativité générale, la dynamique des espaces-temps est décrite par l'action de Einstein-Hilbert [22, 23, 24],

$$\mathcal{S} = \mathcal{S}_{\rm grav} + \mathcal{S}_{\rm mat} = \frac{1}{2\kappa}\int \mathrm{d}^4x\sqrt{-g}\,(R - 2\Lambda) + \mathcal{S}_{\rm mat}\,. \tag{5.3}$$

Dans cette expression, $\kappa \equiv 8\pi G = 1/M_{\rm Pl}^2$ où G est la constante de Newton et $M_{\rm Pl}$ est la masse de Planck réduite $M_{\rm Pl} \simeq 2.4 \times 10^{18}$ GeV. La partie gravitationnelle de l'action $\mathcal{S}_{\rm grav}$ fait intervenir une constante cosmologique éventuelle Λ, le déterminant g de la métrique $g_{\mu\nu}$ et la courbure de Ricci R associée à la métrique. La partie de matière $\mathcal{S}_{\rm mat}$ contient tous les champs du modèle standard de la physique des particules et de ses extensions éventuelles. Sa forme exacte est donc en général relativement complexe. Néanmoins, dans la limite où le constituant dominant (en terme de densité d'énergie) est un fluide parfait homogène, son expression peut être largement simplifiée et la variation de l'action (5.3) par rapport aux composantes de la métrique $g_{\mu\nu}$ donne lieu à deux équations dynamiques,

$$H^2 = \frac{\kappa}{3}\rho - \frac{\mathcal{K}}{a^2} + \frac{\Lambda}{3}\,, \tag{5.4}$$

$$\frac{\ddot{a}}{a} = -\frac{\kappa}{6}(\rho + 3p) + \frac{\Lambda}{3}\,, \tag{5.5}$$

où ρ et p sont respectivement la densité d'énergie et la pression du fluide parfait. La première de ces équations s'appelle équation de Friedmann [25] et relie le taux d'expansion de l'Univers à sa densité d'énergie, sa courbure spatiale et la valeur de la constante cosmologique. La deuxième équation s'appelle équation de Raychaudhuri [26] et relie son accélération à une combinaison de la densité d'énergie et de la pression, ainsi qu'à la valeur de la constante cosmologique. Lorsque l'on combine ces deux relations, on obtient l'équation de continuité[1]

$$\dot{\rho} + 3H(\rho + p) = 0\,. \tag{5.6}$$

De façon heuristique, cette équation peut être comprise comme étant une traduction de la première loi de la thermodynamique, $\mathrm{d}U = -p\mathrm{d}V$, avec $U = \rho V$ and $V = a^3$.

5.1.2. Le Modèle du Big Bang Chaud et ses Problèmes

Nous venons d'établir que pour un Univers homogène et isotrope, la Relativité Générale décrit un espace-temps en expansion, le taux d'expansion et son accélération étant reliés au contenu en matière de l'Univers, à sa courbure et à une éventuelle constante cosmologique. Cela implique qu'en remontant le temps et en regardant dans le passé, l'Univers est de plus en plus contracté, les densités d'énergie sont de plus en plus importantes, jusqu'à une singularité initiale où $a = 0$. Pour un univers principalement constitué de matière froide et de rayonnement, ces considérations donnent lieu au modèle dit du Big Bang chaud, dans lequel les éléments constitutifs de la matière baryonique aujourd'hui s'assemblent peu à peu, au fur et à mesure que les énergies en jeux diminuent et permettent leur existence stable, et les grandes structures de l'Univers (galaxies, amas, filaments, ...) se forment et croissent par instabilité gravitationnelle.

[1] L'équation de continuité s'obtient également à partir de la relation de conservation $\nabla_\mu T^{\mu\nu} = 0$, ce qui une conséquence des identités de Bianchi.

Néanmoins, ce scénario pose un certain nombre de questions appelés "problèmes" du modèle du Big Bang chaud. Ce ne sont pas des problèmes d'impossibilité pure à proprement parler, mais ils montrent que le modèle du Big Bang chaud repose en fait sur des hypothèses très fortes concernant ses conditions initiales, qui doivent être finement réglées autour de configurations peu "naturelles" pour pouvoir expliquer les propriétés de l'Univers telles que nous les observons aujourd'hui.

Le premier de ces problèmes est celui dit de l'horizon [88, 89]. Une des propriétés fondamentales des espaces-temps décrits plus haut est le fait qu'ils sont dotés d'horizon causaux, c'est à dire de frontières séparant les événements observables des événements non observables, définis relativement à un observateur. Par causalité, aucun processus physique ne peut agir sur des distances plus grandes que l'horizon, et l'on s'attend donc à ce que l'Univers soit relativement inhomogène sur ces échelles. Cette hypothèse naturelle est en contradiction avec les observations, qui mettent en évidence un Univers redoutablement homogène sur des échelles qui, sous l'hypothèse du modèle standard du Big Bang chaud, devraient être bien plus étendues que l'horizon. Le modèle du Big Bang chaud suppose donc pour commencer que l'Univers ait été initialement parfaitement homogène, y compris au delà de son horizon causal.

Le deuxième problème est celui de la platitude [92, 93], qui se pose à partir des mesures actuelles de la courbure spatiale de l'Univers. Ces observations sont compatibles avec l'hypothèse d'un univers parfaitement plat, et contraignent en tout état de cause la courbure spatiale à des niveaux extrêmement faibles. Or, dans un Univers dominé par de la matière froide ou du rayonnement, la déviation à un Univers plat ne peut qu'augmenter avec le temps. Par conséquent, si l'Univers actuel est redoutablement plat, cela implique qu'il l'était encore bien davantage dans le passé. Malheureusement, il n'y a aucune raison qui explique a priori que la courbure ait été initialement si faible. Là aussi, le modèle du Big Bang chaud suppose le réglage ultra-fin d'un paramètre (la courbure) à une valeur initiale minuscule.

Finalement, le troisième problème, plus spéculatif, est celui des monopôles [101, 102, 99, 100], qui sont des défauts topologiques pouvant apparaître notamment lors de la transition de phase entre une théorie de grande unification et la symétrie de jauge du modèle standard $SU(3) \times SU(2) \times U(1)$. Ces transitions se produisent à une échelle d'énergie de l'ordre de $M_{\mathrm{GUT}} \simeq 10^{16}$ GeV, et donnent lieu à la production de monopôles magnétiques qui devraient perdurer jusqu'à l'heure actuelle. Lorsqu'on la calcule dans le cadre du modèle standard du Big Bang chaud, la densité de ces monopôles aujourd'hui devrait être colossale, en fait, ils devraient même dominer le contenu énergétique de l'Univers actuel. Ce n'est clairement pas le cas. Des recherches pour leur détection ont même été menées et des contraintes très importantes [103, 104, 105, 106, 107, 108] sur leur densité ont pu être dérivées (typiquement, moins de 1 monopôle par $\sim 10^{30}$ nucléon). Ce troisième problème est bien entendu plus délicat à cerner, car il met en jeu de la physique au delà du modèle standard.

5.1.3. L'Inflation Cosmologique

Dans la section précédente, nous avons vu que le modèle standard du Big Bang chaud, dans lequel l'Univers est principalement constitué de matière froide et de rayonnement, souffre d'hypothèses très fortes et peu naturelles concernant ses conditions initiales et sur lesquelles il repose. Un remède possible est de supposer qu'une phase initiale d'accélération de l'expansion (c'est à dire lors de laquelle $\ddot{a} > 0$), a eu lieu dans l'Univers primordial [90, 91]. C'est ce que l'on appelle l'inflation cosmologique [114, 116, 118, 119].

L'équation de Raychaudhuri (5.5) nous indique que pour avoir $\ddot{a} > 0$, en l'absence de constante cosmologique, la quantité $\rho + 3p$ doit être négative. Puisque la densité d'énergie ρ est toujours positive, la pression doit donc être, a fortiori, négative. Bien entendu, la question est de savoir quel système physique est susceptible de générer une telle pression négative. Ce qui rend l'idée inflationnaire relativement attractive est le fait que le système physique le plus simple compatible avec les symétries du problème, à savoir un champ scalaire homogène ϕ minimalement couplé à la gravité, permet de réaliser cette condition. La partie de matière $\mathcal{S}_{\rm mat}$ de l'action pour un tel champ est donnée par

$$S_\phi = -\int \mathrm{d}^4x\sqrt{-g}\left[\frac{1}{2}g^{\mu\nu}\partial_\mu\phi\partial_\nu\phi + V(\phi)\right], \tag{5.7}$$

où $V(\phi)$ est un terme potentiel que nous ne spécifions pas pour le moment. En effet, la nature physique du champ ϕ, dénommé inflaton, et ses relations avec les autres champs du modèle standard de la physique des particules n'a toujours pas été établi et bon nombre de candidats ont été proposés et sont étudiés à l'heure actuelle. Il est intéressant de noter que l'action écrite plus haut peut être vue comme celle d'un fluide parfait, dont la densité d'énergie et la pression sont respectivement données par

$$\rho = \frac{\dot{\phi}^2}{2} + V, \tag{5.8}$$

$$p = \frac{\dot{\phi}^2}{2} - V. \tag{5.9}$$

Une conséquence directe de ce résultat est le fait que la condition d'accélération de l'expansion, $\rho + 3p < 0$, est remplie dès lors que $V > \dot{\phi}^2$. Cela implique qu'une phase d'inflation peut être obtenue lorsque l'inflaton descend lentement le long de son potentiel, suffisamment lentement pour que son énergie potentielle dépasse le double de son énergie cinétique. Son potentiel doit donc être suffisamment plat, ce qui n'est pas toujours facile à réaliser en pratique.

5.2. Prédictions Inflationnaires et Observations en Données Massives

Nous entrons à présent dans la description résumée des principaux résultats obtenus lors de cette thèse. La cosmologie moderne est entrée dans une "ère de précision" avec l'arrivée de données astrophysiques massives, en particulier celles concernant le fonds diffus cosmologique (FDC). Notamment, au cours de cette thèse, le satellite Planck a publié des mesures sans précédent des fluctuations primordiales de température du FDC. D'un autre côté, comme nous venons de le mentionner, de nombreux candidats à l'inflation ont été proposés jusqu'à aujourd'hui et il reste a priori difficile de déterminer lesquels sont favorisés par les observations. Un des objectifs de cette thèse a donc été de développer les méthodes et les outils permettant une approche systématique de ce problème, et menant à un changement d'échelle à la fois dans la prise en compte des données et dans le nombre de modèles traités.

5.2.1. Roulement Lent et Flot de Hubble

Une des manières d'aborder la question est d'utiliser des approches indépendantes du modèle inflationnaire. Dans la Ref. [208] (section 3.1), nous nous sommes intéressés à l'une d'entre elles, le "flot de Hubble". Dans cette paramétrisation, la hiérarchie des paramètres de roulement lent

est tronquée à un certain ordre M, c'est à dire que l'ensemble des paramètres d'ordre supérieur à M sont pris comme identiquement nuls. L'évolution des paramètres restants est intégrée numériquement à partir de conditions initiales tirées au hasard dans des intervalles prédéfinis, et en utilisant l'inflaton ϕ lui-même comme variable temporelle. Le même processus est réitéré pour différentes conditions initiales, et ce un grand nombre de fois. De cette manière, on cherche à dériver des prédictions typiques pour l'inflation, ne reposant pas sur une forme explicite du potentiel mais ayant une portée "générique".

Nous avons montré qu'une telle approche comporte en réalité un certain nombre de biais. Premièrement, puisque les paramètres de roulement lent sont reliés à une fonction de Hubble $H(\phi)$ et à ses dérivées successives, tronquer leur hiérarchie à un ordre M revient à imposer une forme polynomiale pour $H(\phi)$, d'ordre $M+1$. Dans la mesure où V et H sont explicitement reliés via la relation $V = 3M_{\rm Pl}^2 H^2 - 2M_{\rm Pl}^4 H'^2$ (où un prime signifie une dérivation par rapport à l'inflaton ϕ), une famille spécifique de potentiels est en fait implicitement étudiée par l'approche du flot de Hubble. Ces potentiels sont des polynômes d'ordre $2M+2$ dans le champ scalaire ϕ, avec certaines relations imposées entre les coefficients. Nous avons étudié cette famille de potentiels et nous avons montré qu'elle est directement responsable des prédictions soit-disant "génériques" qui semblaient avoir été dérivées dans la littérature. Cette méthode n'est donc pas indépendante du modèle dans la mesure où elle ne permet d'étudier qu'une famille restreinte de potentiels, qui n'ont par ailleurs pas de justification physique et sont purement phénoménologiques.

Ensuite, nous avons établi qu'une fois le potentiel fixé, le flot de Hubble résout la dynamique inflationnaire le long d'une seule trajectoire dans l'espace des phases uniquement. En effet, puisqu'en toute généralité, $\dot{\phi} = -2M_{\rm Pl}^2 H'$, partir d'une fonction $H(\phi)$ revient à fixer à l'avance la trajectoire inflationnaire. Ceci pose deux types de problèmes. Tout d'abord, cette trajectoire est en général différente de la trajectoire de roulement lent, qui est pourtant un attracteur du système dynamique. Par conséquent, autant cela fait du sens d'étudier l'inflation le long de la trajectoire de roulement lent puisqu'elle est asymptotiquement approchée depuis un large bassin de conditions initiales, autant la trajectoire reliée au flot de Hubble ne jouit pas d'une telle justification physique.[2] Ensuite, à l'intérieur d'un potentiel, il arrive souvent que l'inflation puisse se produire le long de différentes branches, notamment lorsque le potentiel n'est pas une fonction monotone du champ scalaire ϕ (ce qui est courant pour les potentiels décrits par le flot de Hubble et mentionnés plus haut). La trajectoire "imposée" par la fonction $H(\phi)$ ne permet d'étudier l'inflation que sur l'une de ces branches, ce qui représente un biais supplémentaire dans l'étude de ces potentiels.

Pour l'ensemble de ces raisons, nous avons conclu que le flot de Hubble conduit à une analyse biaisée des dynamiques inflationnaires et de leurs prédictions physiques, et avons donc opté pour une étude systématique de l'ensemble des potentiels inflationnaires proposés dans la littérature, le long des trajectoires de roulement lent.

5.2.2. Modèles à un Champ et *Encyclopædia Inflationaris*

Dans la mesure où plusieurs centaines de scénarios inflationnaires ont été proposés dans la littérature, il semble naturel de commencer par étudier les plus simples, à savoir les modèles à un champ scalaire, avec terme cinétique standard, et dont la dynamique satisfait à l'approximation

[2] Dans certains cas, nous avons même montré que les trajectoire reliées au flot de Hubble sont instables dans l'espace des phases.

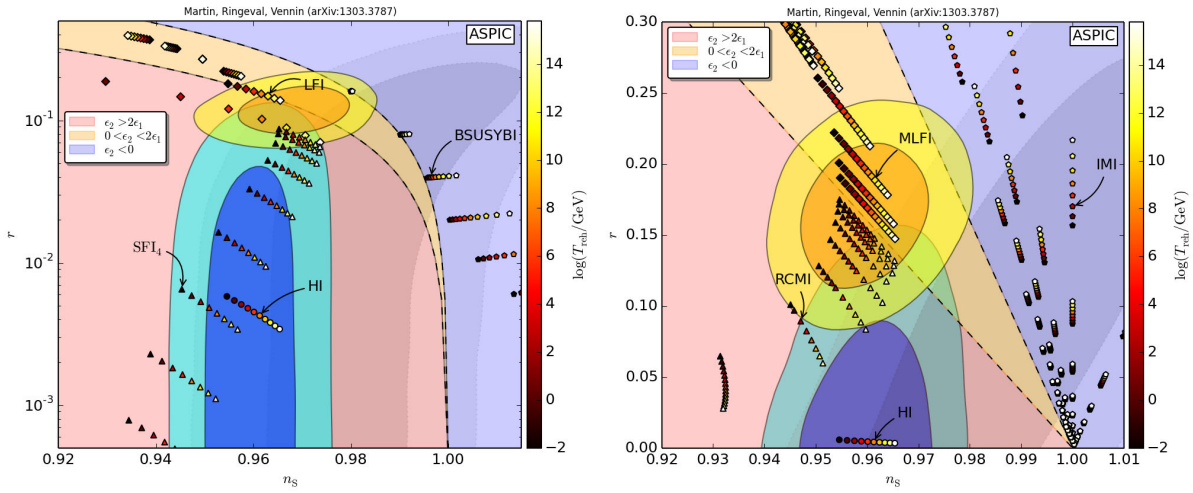

Figure 5.1.: Prédictions de quelques modèles implémentés dans la bibliothèque `ASPIC`, calculées dans l'approximation du roulement lent et en intégrant de façon cohérente la phase de réchauffement. Ces prédictions sont tracées dans le plan $(n_{\rm S}, r)$, et sont superposées aux contours à un et deux sigma de WMAP9 (en gris), PLANCK (en bleu) et PLANCK+BICEP2 (en jaune). Une loi a priori de Jeffreys a été utilisée pour le premier paramètre de roulement lent dans la figure de gauche, tandis qu'une loi a priori plate a été utilisée dans la figure de droite. Les valeurs annotées représentent le logarithme de l'échelle d'énergie, $\log(T_{\rm reh}/{\rm GeV})$, à laquelle une phase de réchauffement dominée par de la matière se termine. La zone rose délimite les modèles pour lesquels l'énergie cinétique et son rapport avec l'énergie totale augmentent, la zone jaune indique les modèles pour lesquels l'énergie cinétique diminue mais son rapport avec l'énergie totale augmente, et la zone violette recouvre les modèles pour lesquels l'énergie cinétique et son rapport avec l'énergie totale diminuent, au moment où les prédictions sont calculées.

du roulement lent. En effet, les extensions à ce cadre minimal (terme cinétique non-standard, présence de champs multiples, sortie transitoire du régime de roulement lent, *etc.*) prédisent souvent la présence de signaux (non-Gaussianités, perturbations entropiques, running, *etc.*) qui n'ont pour l'instant jamais été détectés. C'est pourquoi à ce stade, et tant que les données ne les excluent pas, il semble raisonnable de commencer en abordant les scénarios les moins complexes.

Nous avons recensé environ 75 potentiels appartenant à cette catégorie, pour lesquelles nous avons dérivé les prédictions dans l'approximation du roulement lent, que nous avons présentées dans la Ref. [205], *Encyclopædia Inflationaris* (section 3.2). Nous avons également conçu une bibliothèque numérique publique dénommée `ASPIC`[3] (pour "Accurate Slow-roll Predictions for Inflationary Cosmology") qui contient l'ensemble des programmes permettant le calcul numérique des prédictions inflationnaires de ces modèles et leur comparaison aux observations. Ce code libre d'accès est un projet évolutif, et est amené à être complété au fur et à mesure que de nouveaux modèles sont considérés.

Il est important de noter qu'aucune autre approximation que celle du roulement n'a été effectuée dans cette analyse, là où des approximations supplémentaires ont souvent été utilisées dans la littérature. En effet, nous avons montré que la précision actuelle des données est telle que le calcul

[3] http://theory.physics.unige.ch/~ringeval/aspic.html

des prédictions se doit d'être le plus précis possible, et que ces approximations supplémentaires conduisent souvent à des résultats erronés. La phase de réchauffement a également été prise en compte de façon cohérente, là où la plupart des travaux se contentent de tirer le paramètre ΔN_* (représentant le nombre d'e-folds entre le croisement de l'échelle de pivot des spectres de puissance avec le rayon de Hubble et la fin de l'inflation) dans un intervalle prédéfini. Cette procédure peut conduire à des situations non-physiques où l'énergie à la fin de l'ère de réchauffement est plus élevée que l'énergie à la fin de l'inflation, ou plus faible que l'énergie au moment de la nucléation.

Le détail des prédictions dérivées potentiel par potentiel est présenté dans la section 3.2 et nous ne donnons ici que quelques éléments conclusifs. Une manière de résumer les résultats obtenus est d'utiliser une classification des modèles d'inflation basée sur la variation temporelle des énergies qui leur sont associées et permettant de découper le plan $(n_{\rm S}, r)$ (où $n_{\rm S}$ est l'indice spectral des perturbations scalaires et r est l'amplitude du spectre des ondes gravitationnelles normalisé au spectre des perturbations scalaires) en trois zones, représentées sur la figure 5.1. La première zone, en rose, contient les modèles pour lesquels l'énergie cinétique $\dot{\phi}^2/2$ et le rapport de l'énergie cinétique avec l'énergie totale $\dot{\phi}^2/2/(V + \dot{\phi}^2/2)$ augmentent au moment où les prédictions sont calculées, c'est à dire lorsque l'échelle pivot des spectres de puissance croise le rayon de Hubble. La deuxième zone, en jaune pâle, recouvre les modèles pour lesquels l'énergie cinétique diminue mais son rapport avec l'énergie totale augmente, tandis que la troisième zone, en bleu, indique les modèles pour lesquels l'énergie cinétique et son rapport avec l'énergie totale diminuent. S'il est clair que les données du satellite WMAP ne sont pas discriminantes vis à vis de cette classification, dans la mesure où des modèles compatibles avec ses mesures existent dans chacune des trois zones, l'apport du satellite PLANCK apparaît clairement dans le fait que ses observations indiquent une nette préférence pour les modèles de la première catégorie. Ces modèles ont des potentiels concaves, soit en forme de "sommet de colline", soit en forme de "plateau". Parmi les 75 familles de potentiels que nous avons étudiées, ce sont donc ces potentiels qui semblent être "préférés" par les données (le fait que BICEP2 nous amène à reconsidérer ou non cette affirmation sera discutée plus bas).

Pour aller plus loin que ce simple constat "à l'œil", pour quantifier précisément cette préférence et pour dégager les tout meilleurs modèles, nous avons ensuite appliqué les méthodes de l'inférence Bayésienne au problème étudié.

5.2.3. Inférence Bayésienne et Meilleurs Modèles Inflationnaires selon Planck

Étant donné le nombre important de modèles à traiter (75 familles de potentiels, et près de 200 modèles), il nous faut disposer d'un moyen de quantifier rigoureusement une affirmation du type "le modèle A est meilleur que le modèle B". Le programme Bayésien de comparaison de modèles répond à ce besoin, et nécessite de calculer l'évidence Bayésienne, c'est à dire l'intégrale de la fonction de vraisemblance sur l'espace des lois a priori, pour chaque modèle. Le rapport entre ces évidences donne le facteur de Bayes, qui représente le degré avec lequel les données ont modifié notre niveau de confiance relative entre les différents modèles. De cette manière, nous pouvons identifier les "meilleurs" (au sens Bayésien du terme) modèles d'inflation.

Dans la Ref. [206] (section 3.3), nous avons donc calculé l'évidence Bayésienne de l'ensemble des modèles implémentés dans la bibliothèque `ASPIC`. Pour ce faire, nous avons mis au point un bloc de traitement numérique qui réalise l'interface entre une fonction de vraisemblance inflationnaire effective, la bibliothèque `ASPIC`, et un algorithme d'échantillonnage adaptatif. De

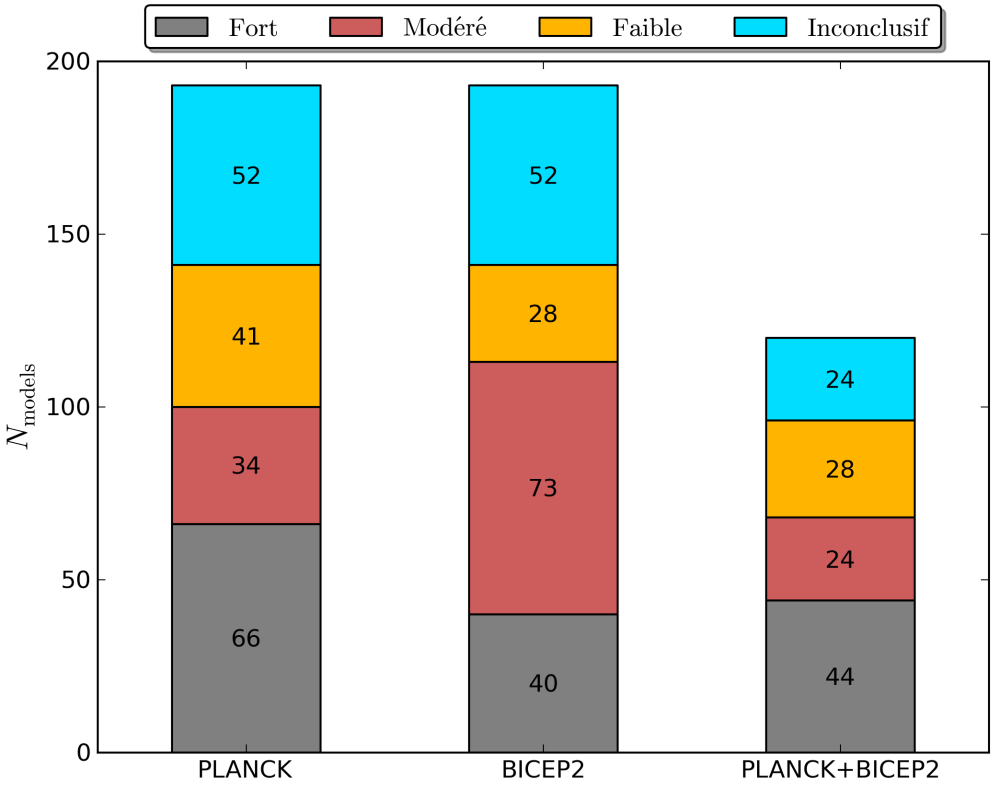

Figure 5.2.: Nombre de modèles inflationnaires dans chaque catégorie de Jeffreys (définies par rapport au meilleur modèle pour chaque expérience) pour les jeux de données PLANCK, BICEP2 et PLANCK+BICEP2. Pour les données de PLANCK et BICEP2 combinées, seuls les modèles n'indiquant pas d'incompatibilité entre PLANCK et BICEP2 sont comptabilisés.

cette manière, nous avons identifié les 26% des modèles qui sont favorisés[4] par les données de PLANCK, ce qui correspond à 15 familles de potentiels. Le détail des effectifs au sein de chaque catégorie de Jeffreys est présenté dans la figure 5.2. En incluant la complexité Bayésienne dans l'analyse, qui permet d'identifier le nombre de paramètres non contraints par les observations et d'estimer ainsi le niveaux de complexité superflue, seulement 9% des modèles arrivent en tête, qui correspondent tous à des potentiels ayant une forme de "plateau". Le détail des résultats est donné dans la section 3.3.

5.2.4. Inflation et Tension entre Planck et BICEP2

Si l'on regarde attentivement la figure 5.1, l'on est en droit de se demander si les mesures de l'expérience BICEP2 ne remettent pas en cause ces conclusions, dans la mesure où la zone

[4]Le terme "favorisé" doit être entendu ici comme appartenant à la zone inconclusive de la classification de Jeffreys, définie relativement au meilleur modèle. L'échelle de Jeffreys permet de qualifier conventionnellement le rapport entre les évidences $\mathcal{E}_A$ et $\mathcal{E}_B$ de deux modèles A et B selon quatre catégories. Lorsque $\ln(\mathcal{E}_A/\mathcal{E}_B) < 1$, la situation est dite "inconclusive", lorsque $1 < \ln(\mathcal{E}_A/\mathcal{E}_B) < 2.5$, la conclusion que le modèle A est meilleur que le modèle B est dite "faible", lorsque $2.5 < \ln(\mathcal{E}_A/\mathcal{E}_B) < 5$ elle est dite "modérée", et lorsque $\ln(\mathcal{E}_A/\mathcal{E}_B) > 5$ elle est dite "forte".

préférée par la combinaison PLANCK+BICEP2 recouvre à présent certains modèles de la deuxième zone, celle en jaune pâle. Ces modèles correspondent typiquement à des potentiels convexes, s'annulant à leur minimum. D'un autre côté, l'existence d'une possible tension entre PLANCK et BICEP2 a été discutée dans la littérature, ainsi que la question de la correcte prise en compte des avant plans de poussière par BICEP2. En attendant une clarification de cette situation, il s'agit donc d'être prudent lorsque l'on combine ces deux jeux de données.

Dans la Ref. [207] (section 3.4), nous avons donc discuté les conséquences de la détection du mode B de polarisation dans le FDC par l'expérience BICEP2, si cette détection est confirmée. En particulier, nous avons mené une étude complète dans l'espace des paramètres cosmologiques et des paramètres inflationnaires de roulement lent, en utilisant les données de polarisation de BICEP2 seules. Nous avons ensuite extrait les évidences Bayésiennes et les complexités des ~ 200 modèles que nous avions traités avec PLANCK. De cette manière, nous avons là aussi identifié les meilleurs modèles d'après BICEP2. Cela nous a permis de constater que la liste des modèles préférés par PLANCK et la liste des modèles préférés par BICEP2 sont presque disjointes, ce qui confirme l'existence d'une possible tension entre les deux jeux de données.

Pour aller plus loin, nous avons donc cherché à quantifier cette tension à l'aide d'une mesure Bayésienne de la compatibilité entre PLANCK et BICEP2, définie relativement à chaque modèle. Nous avons ainsi établi que pour les modèles préférés par PLANCK, les deux jeux de données montrent une tendance à l'incompatibilité, alors qu'il y a une indication modérée de compatibilité pour certains des modèles préférés par BICEP2. C'est pourquoi il est en particulier prématuré de tirer des conclusions trop hâtives et définitives concernant les modèles favorisés par PLANCK tels que le modèle de Starobinsky. Pour le sous-ensemble constitué des modèles n'indiquant pas d'incompatibilité, nous avons finalement mis à jour nos calculs d'évidence et de complexité en utilisant la combinaison des deux jeux de données PLANCK+BICEP2. La distribution des modèles au sein des différentes catégories de Jeffreys est présentée dans la figure 5.2 pour BICEP2 seul, et pour la combinaison des données de PLANCK et de BICEP2 où seuls les modèles n'indiquant pas d'incompatibilité entre les deux jeux de données sont dénombrés.

Ce travail ouvre de nombreuses perspectives. Tout d'abord, le projet `ASPIC` est évolutif, dans le sens qu'il a vocation a être complété par de nouveaux modèles au gré de leur apparition, qu'il peut être étendu à d'autres classes de modèles que celle considérée ici (modèles à un champ scalaire avec terme cinétique standard et dans l'approximation du roulement lent), et qu'il se doit enfin d'intégrer de nouveaux jeux de données au fur et à mesure que ceux-ci sont publiés. Ainsi, dès l'automne 2014, les mesures de polarisation réalisées par le satellite Planck devraient être disponibles, et d'autres expériences viendront bientôt les compléter [174, 407, 178, 177].

L'exploitation des résultats de notre analyse Bayésienne peut également se poursuivre concernant la phase de réchauffement. En effet, comme nous l'avons mentionné, les prédictions inflationnaires sont sensibles à la phase de réchauffement à travers deux quantités, le paramètre d'équation d'état moyen (c'est à dire moyenné sur le nombre d'e-folds) $\bar{w}_{\rm reh}$ pendant la phase de réchauffement, et la densité d'énergie $\rho_{\rm reh}$ au moment où $w = 1/3$ et où la phase de radiation commence. Ces deux paramètres décrivent l'expansion réalisée entre la fin de l'inflation et le début de la phase de radiation, et sont contraints par l'analyse Bayésienne que nous avons menée. Nous travaillons actuellement à caractériser précisément ces contraintes pour l'ensemble des modèles implémentés.

Enfin, un problème largement discuté par la communauté à l'heure actuelle est celle des caractéristiques techniques requises pour les prochaines expériences. La question générale est de savoir quel niveau de précision doit être atteint dans les mesures pour permettre une progres-

sion notable de notre niveau de connaissance de l'Univers primordial. En particulier, le niveau de sensibilité en r, l'amplitude du spectre de puissance des ondes gravitationnelles normalisé au spectre des perturbations scalaires, semble crucial. Notre approche permet de répondre très explicitement à cette question. En effet, en dérivant la vraisemblance effective que nous observerions pour un niveau de bruit fixé dans les détecteurs et pour un modèle fiduciel donné, nous pouvons calculer les évidences de chaque modèle de la bibliothèque `ASPIC` sous ces hypothèses et caractériser ainsi le gain d'information associé sur les modèles d'inflation. Nous menons actuellement cette étude prospective, qui va permettre de quantifier exactement l'apport des futures expériences.

Finalement, on est en droit de se demander si le niveau de précision théorique des approches calculatoires utilisées sera suffisant. En particulier, les résultats présentés ici sont dérivés à partir d'un calcul au premier ou au deuxième ordre dans l'approximation du roulement lent, et il faut établir à quel ordre il sera nécessaire de travailler avec les données des futures expériences. L'étude prospective que nous venons d'évoquer permettra aussi d'étudier cette question en détail.

5.2.5. Spectres de Puissance au Deuxième Ordre en Inflation-k

Comme nous venons de l'expliquer, un prolongement possible à ce travail est l'intégration de nouveaux modèles d'inflation, et de nouvelles catégories de modèles. Par exemple, l'inflation-k représente le cadre le plus général décrivant les modèles avec une action effective quadratique pour les perturbations de courbure et une vitesse du son $c_{\rm S}$ variable. Si ces modèles prédisent souvent la production de non-Gaussianités à un niveau exclu par les observations, il reste intéressant de pouvoir les contraindre précisément. C'est pourquoi dans la Ref. [209] (section 3.5), nous avons calculé pour la première fois les spectres de puissance scalaire et tensorielle au deuxième ordre pour l'inflation-k. Techniquement, nous avons utilisé l'approximation uniforme assortie d'un développement au deuxième ordre dans les paramètres de roulement lent et dans les paramètres de flot de la vitesse du son. A titre illustratif, le résultat obtenu pour le spectre de puissance des perturbations de courbure s'écrit

$$
\begin{aligned}
\mathcal{P}_\zeta = \frac{H_\diamond^2\left(18\,\mathrm{e}^{-3}\right)}{8\pi^2 M_{\rm Pl}^2 \epsilon_{1\diamond} c_{\rm s\diamond}}\Bigg\{ & 1 - 2(1+D)\epsilon_{1\diamond} - D\epsilon_{2\diamond} + (2+D)\delta_{1\diamond} + \left(\frac{2}{9} + D + \frac{D^2}{2}\right)\delta_{1\diamond}^2 \\
& + \left(\frac{37}{18} + 2D + \frac{D^2}{2} - \frac{\pi^2}{24}\right)\delta_{1\diamond}\delta_{2\diamond} + \left(-\frac{8}{9} - 3D - 2D^2\right)\epsilon_{1\diamond}\delta_{1\diamond} + \left(\frac{17}{9} + 2D + 2D^2\right)\epsilon_{1\diamond}^2 \\
& + \left(\frac{5}{9} - D - D^2\right)\epsilon_{2\diamond}\delta_{1\diamond} + \left(-\frac{11}{9} - D + D^2 + \frac{\pi^2}{12}\right)\epsilon_{1\diamond}\epsilon_{2\diamond} + \left(\frac{2}{9} + \frac{D^2}{2}\right)\epsilon_{2\diamond}^2 \\
& + \left(\frac{\pi^2}{24} - \frac{1}{18} - \frac{D^2}{2}\right)\epsilon_{2\diamond}\epsilon_{3\diamond} + \big[-2\epsilon_{1\diamond} - \epsilon_{2\diamond} + \delta_{1\diamond} + (1+D)\delta_{1\diamond}^2 \\
& + (2+D)\delta_{1\diamond}\delta_{2\diamond} - (3+4D)\epsilon_{1\diamond}\delta_{1\diamond} + 2(1+2D)\epsilon_{1\diamond}^2 - (1+2D)\epsilon_{2\diamond}\delta_{1\diamond} - (1-2D)\epsilon_{1\diamond}\epsilon_{2\diamond} \\
& + D\epsilon_{2\diamond}^2 - D\epsilon_{2\diamond}\epsilon_{3\diamond}\big]\ln\frac{k}{k_\diamond} + \left(2\epsilon_{1\diamond}^2 + \epsilon_{1\diamond}\epsilon_{2\diamond} + \frac{1}{2}\epsilon_{2\diamond}^2 - \frac{1}{2}\epsilon_{2\diamond}\epsilon_{3\diamond} + \frac{1}{2}\delta_{1\diamond}^2 + \frac{1}{2}\delta_{1\diamond}\delta_{2\diamond}\right. \\
& \left. - 2\epsilon_{1\diamond}\delta_{1\diamond} - \epsilon_{2\diamond}\delta_{1\diamond}\right)\ln^2\frac{k}{k_\diamond}\Bigg\},
\end{aligned}
\tag{5.10}
$$

où nous avons introduit la quantité D définie par $D \equiv 1/3 - \ln 3$. Les paramètres ϵ_i sont les paramètres de roulement lent et les paramètres δ_i sont les paramètres de flot de la vitesse du son. La présence du $\diamond$ en indice indique que les quantités sont calculées au moment où l'échelle

de pivot $k_\diamond$ croise le rayon de Hubble. Avec les mêmes notations, le spectre de puissance des ondes gravitationnelles est donné par

$$\begin{aligned}\mathcal{P}_h =& \frac{2\left(18\mathrm{e}^{-3}\right)H_\diamond^2}{\pi^2 M_{\mathrm{Pl}}^2}\Bigg\{1-2(1+D-\ln c_{\mathrm{s}\diamond})\epsilon_{1\diamond}+\left[\frac{17}{9}+2D+2D^2+2\ln^2 c_{\mathrm{s}\diamond}\right.\\ &\left.-2(1+2D)\ln c_{\mathrm{s}\diamond}\right]\epsilon_{1\diamond}^2+\left[-\frac{19}{9}+\frac{\pi^2}{12}-2D-D^2+2(1+D)\ln c_{\mathrm{s}\diamond}-\ln^2 c_{\mathrm{s}\diamond}\right]\epsilon_{1\diamond}\epsilon_{2\diamond}\\ &+\left[-2\epsilon_{1\diamond}+(2+4D-4\ln c_{\mathrm{s}\diamond})\epsilon_{1\diamond}^2+(-2-2D+2\ln c_{\mathrm{s}\diamond})\epsilon_{1\diamond}\epsilon_{2\diamond}\right]\ln\frac{k}{k_\diamond}\\ &+\left(2\epsilon_{1\diamond}^2-\epsilon_{1\diamond}\epsilon_{2\diamond}\right)\ln^2\frac{k}{k_\diamond}\Bigg\}. \end{aligned} \tag{5.11}$$

Ces deux résultats mettent en évidence qu'à l'ordre dominant dans l'approximation du roulement lent et lorsque $c_{\mathrm{S}}=1$, les spectres de puissances sont invariants d'échelle, c'est à dire qu'ils ne dépendent pas de k. La dépendance en k apparaît de façon logarithmique uniquement, et son amplitude dépend des paramètres de roulement lent et des paramètres de flot de la vitesse du son. Les termes correspondants sont en rouge dans les équations (5.10) et (5.11). Dans ce contexte, une expression au "deuxième" ordre en $\{\epsilon_i,\delta_i\}$ des spectres implique que l'on étende le résultat jusqu'à l'ordre $\ln^2(k/k_\diamond)$.

5.3. Aspects Quantiques de l'Inflation et Formalisme Stochastique

Sur le plan théorique, un des aspects intéressants de l'inflation est qu'elle permet d'expliquer l'existence de fluctuations cosmologiques et de caractériser leurs propriétés statistiques à partir de considérations quantiques. D'une certaine manière, un tel mécanisme repose à la fois sur la Relativité Générale et sur la Mécanique Quantique, deux théories que l'on sait difficile à combiner, et conduit à des prédictions que l'on peut tester expérimentalement. C'est pourquoi la physique inflationnaire représente un objet d'étude intéressant pour aborder un certain nombre de questions fondamentales.

Dans la description standard des champs en inflation, on considère la plupart du temps que la partie homogène des champs se comporte de façon classique, tandis que les petites déviations à l'homogénéité sont traitées comme des fluctuations quantiques, évoluant sur ce fonds classique. Dans le sens où seule une partie du système est ainsi quantifiée, l'approche standard peut donc être qualifiée de semi-classique.

Le formalisme de l'inflation stochastique [290, 291, 292, 293, 294, 295, 296, 297, 289, 298] permet d'aller au delà et d'incorporer les corrections quantiques à la trajectoire classique. L'idée est de dériver une théorie effective pour les modes scalaires de grandes longueurs d'onde uniquement, en intégrant les modes de petites longueurs d'onde dans l'action du champ scalaire. Les modes de grandes longueurs d'onde sont rassemblés dans un champ filtré φ, que l'on peut définir à partir du champ total ϕ de la manière suivante:

$$\varphi(\boldsymbol{x},N)=\int\frac{\mathrm{d}^3\boldsymbol{k}}{(2\pi)^{3/2}}W\left(\frac{k}{\sigma aH}\right)\left[\phi_{\boldsymbol{k}}(N)\,\hat{a}_{\boldsymbol{k}}\mathrm{e}^{i\boldsymbol{k}\cdot\boldsymbol{x}}+\phi_{\boldsymbol{k}}^*(N)\,\hat{a}_{\boldsymbol{k}}^\dagger\mathrm{e}^{-i\boldsymbol{k}\cdot\boldsymbol{x}}\right]. \tag{5.12}$$

Dans cette expression, W est une fonction de filtrage qui sélectionne les modes de grandes longueurs d'onde, c'est à dire que $W\simeq 0$ lorsque $k\gg\sigma aH$ et $W\simeq 1$ lorsque $k\ll\sigma aH$. Le paramètre $\sigma\ll 1$ est une constante fixant l'échelle à laquelle le lissage a lieu. En écrivant le

champ total comme $\phi = \varphi + \delta\phi$, l'idée est donc de dériver une théorie effective pour φ uniquement en intégrant $\delta\phi$. On peut alors montrer que les fluctuations quantiques présentes dans le secteur $\delta\phi$ affectent la dynamique de φ par l'introduction d'un terme de bruit stochastique dans son équation du mouvement. A l'ordre dominant dans l'approximation du roulement lent, celle-ci s'écrit

$$\frac{\mathrm{d}\varphi}{\mathrm{d}N} = -\frac{V'}{3H^2} + \frac{H}{2\pi}\xi\left(N\right) . \tag{5.13}$$

Dans cette équation, le premier terme $-V'/(3H^2)$ est le terme classique standard de l'équation de Klein-Gordon et ξ est un bruit blanc Gaussien (pour une fonction filtre de Heaviside), telle que $\langle\xi\left(N\right)\rangle = 0$ et $\langle\xi\left(N_1\right)\xi\left(N_2\right)\rangle = \delta\left(N_1 - N_2\right)$. L'équation du mouvement pour le champ scalaire devient donc une équation stochastique appelée équation de Langevin. Sa résolution permet de calculer efficacement des effets de pure théorie quantique des champs, comme cela est montré pour différents systèmes dans les Refs. [298, 302, 303, 304, 299, 300, 301]. Dans la section 2.4.3, nous avons notamment montré que l'équation de Langevin permet de calculer la statistique des fluctuations du champ, c'est à dire le spectre de puissance des perturbations scalaires. Plus précisément, nous avons établi que l'intégration exacte de l'équation (5.13) conduit au spectre de puissance des perturbations de courbure

$$\mathcal{P}_\zeta\left(\phi\right) = 2\int_\phi^{\hat{\phi}} \mathrm{d}\psi \frac{f'^2\left(\psi\right)}{f\left(\phi\right)} \exp\left[\frac{24\pi^2 M_{\mathrm{Pl}}^4}{V\left(\psi\right)} - \frac{24\pi^2 M_{\mathrm{Pl}}^4}{V\left(\phi\right)}\right] , \tag{5.14}$$

où $\mathcal{P}_\zeta\left(\phi\right)$ représente le spectre de puissance calculé au mode k pour lequel la valeur du champ scalaire lorsque k croise le rayon de Hubble vaut ϕ, et où la fonction $f(\phi)$ est définie par

$$f\left(\phi\right) = -24\pi^2 M_{\mathrm{Pl}}^2 \int_{\phi_{\mathrm{end}}}^{\phi} \mathrm{d}u \int_{\bar{\phi}}^{u} \frac{\mathrm{d}v}{V\left(v\right)} \exp\left\{24\pi^2 M_{\mathrm{Pl}}^4 \left[\frac{1}{V\left(v\right)} - \frac{1}{V\left(u\right)}\right]\right\} . \tag{5.15}$$

Dans ces deux expressions, $\hat{\phi}$ et $\bar{\phi}$ sont des constantes d'intégration qui valent dans la plupart des cas $\hat{\phi} = \bar{\phi} = \pm\infty$. A l'ordre dominant dans l'approximation classique, c'est à dire lorsque $V \ll M_{\mathrm{Pl}}^4$ et que les corrections attendues en gravité quantiques sont faibles, l'expression standard du spectre de puissance est retrouvée comme cas limite de l'équation (5.14).

5.3.1. Effets Stochastiques en Inflation Hybride

Une situation d'intérêt pour l'inflation stochastique est celle des modèles à champs multiples, pour lesquels plusieurs équations de Langevin couplées régissent les trajectoires inflationnaires et donnent lieu à une dynamique non triviale. Dans la Ref. [210] (section 4.1) nous nous sommes intéressés à l'un d'entre eux, le modèle d'inflation hybride.

Ce modèle est celui d'un potentiel à deux champs, un inflaton φ et un champ auxiliaire ψ dont la masse est proportionnelle à $\varphi^2 - \phi_{\mathrm{c}}^2$, où ϕ_{c} est une constante fixant la valeur de l'inflaton à partir de laquelle le champ auxiliaire devient tachyonique. L'inflation a d'abord lieu dans la "vallée" $\varphi > \phi_{\mathrm{c}}$ où elle est conduite par l'inflaton et où le champ auxiliaire, lourd, est tel que $\psi \simeq 0$. Puis, lorsque φ passe la valeur critique ϕ_{c}, la masse du champ auxiliaire devient négative ce qui déclenche son instabilité tachyonique et termine l'inflation. Au voisinage de ce point critique, les corrections stochastiques sont importantes et donnent lieu à des effets que nous avons étudiés numériquement. A titre illustratif, nous avons représenté dans la Fig. 5.3 la densité de probabilité de présence du système dans le plan (φ, ψ), en partant d'une distribution de Dirac initialisée suffisamment haut dans la vallée. Dans un premier temps, le système descend le long de la vallée et la distribution reste relativement piquée. Puis, arrivée au point critique,

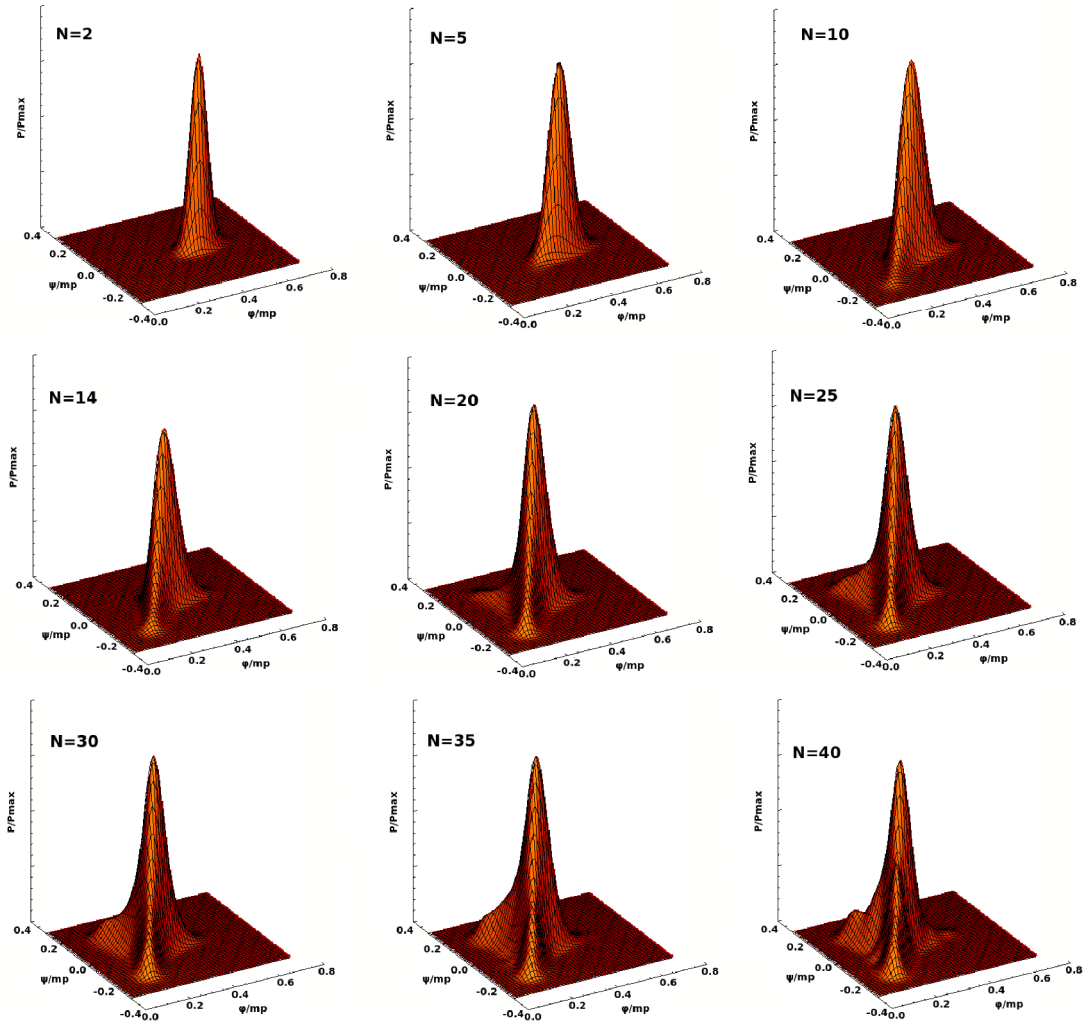

Figure 5.3.: Densité de probabilité de présence calculée à différents temps N pour le modèle d'inflation hybride, et représentée dans le plan (φ, ψ). La distribution initiale est celle d'une fonction de Dirac prise suffisamment haute dans la vallée. Le potentiel hybride est donné par $V = \Lambda^4 \left[\left(1 - \psi^2/M^2\right)^2 + \varphi^2/\mu^2 + 2\varphi^2\psi^2/(\phi_c^2 M^2)\right]$, et les paramètres utilisés sont $\Lambda = 1.06347 M_{\rm Pl}$, $\phi_c = M = 1.50398 M_{\rm Pl}$ et $\mu = 7.74597 M_{\rm Pl}$.

elle s'étend rapidement, notamment dans la direction des deux vallées secondaires menant le système aux minimas $(\varphi = 0, \psi = \pm M)$.

Une question importante relative à ce modèle est la durée de la période d'instabilité tachyonique lors de laquelle $\varphi < \phi_c$. En effet, si la fenêtre observationnelle du FDC se trouve à l'extérieur de cette phase, l'indice spectral des perturbations scalaires est bleu, ce qui est en désaccord avec les observations. Typiquement, le modèle est donc viable uniquement si la période d'instabilité tachyonique s'étend sur plus de 40 ou 50 e-folds. Cette durée étant essentiellement dépendante des effets stochastiques et de la dispersion moyenne des champs au point critique qui en découle, nous avons étudié cette quantité avec attention. En particulier, nous avons caractérisé, en fonction des paramètres du potentiel, la dispersion stochastique dans le champ ψ au point critique et la distribution du nombre d'e-folds réalisé dans la période d'instabilité tachyonique.

Une autre quantité à laquelle nous nous sommes intéressés est le point de sortie de l'inflation.

Lorsque l'inflation est réalisée par un seul champ φ, le point de sortie de l'inflation $\varphi_{\rm end}$ est unique (du moins dans l'approximation du roulement lent) et ne dépend pas des conditions initiales ou de la réalisation stochastique. Dans le modèle d'inflation hybride en revanche, la ligne de niveau $\epsilon_1 = 1$ définit une infinité de points de sortie possibles $(\varphi_{\rm end}, \psi_{\rm end})$, qui dépendent a priori de la réalisation stochastique. Or, nous avons montré qu'en pratique, les trajectoires stochastiques terminent toutes l'inflation très près du point de sortie classique (c'est à dire là où sort la solution des équations du mouvement sans le terme stochastique). En effet, lors des derniers e-folds avant la fin de l'inflation, les termes de bruit dans les équations de Langevin sont fortement sous-dominants. Puisque la trajectoire de roulement lent est un attracteur dynamique, le système se rapproche alors rapidement de cette trajectoire classique, peu importe l'endroit par lequel les effets stochastiques lui ont fait quitter la zone du potentiel dominée par le bruit. Cela explique que la distribution finale soit très piquée autour de la valeur classique.

5.3.2. Formalisme Stochastique Récursif

Dans l'approche standard de l'inflation stochastique, les corrélations des termes de bruit dans l'équation de Langevin sont calculées à partir de l'amplitude des perturbations en champs scalaires, lorsqu'elles croisent l'échelle de lissage σaH. Ces perturbations sont elles-mêmes obtenues à partir de leur équation d'évolution sur un fonds classique. Ce schéma est valable dans la limite où les effets stochastiques ne représentent qu'une petite perturbation à la trajectoire classique, mais en principe, si l'on évolue les perturbations sur un fonds corrigé par les effets stochastiques, leur amplitude devrait en être légèrement affectée. Ainsi, les corrélations du bruit devraient être corrigées par cet effet, et donc la dynamique du fonds, et donc l'amplitude du bruit, et ainsi de suite.

Pour étudier plus en détails cet effet, dans la Ref. [211] (section 4.2), nous avons mis au point un formalisme récursif intégrant la correction des corrélations du bruit par les effets stochastiques eux-mêmes. Nous avons ensuite appliqué ce formalisme au modèle d'inflation hybride, pour l'illustrer concrètement. Nous avons également pris soin d'incorporer les effets de la masse du champs auxiliaire ψ dans le calcul des corrélations du bruit agissant sur ψ, puisque dans la vallée cette masse n'est plus négligeable devant le paramètre de Hubble H et a tendance à diminuer l'amplitude des perturbations. De cette manière, la dispersion stochastique dans le champs auxiliaire est réduite au point critique, ce qui augmente la durée de la phase d'instabilité tachyonique.

Une bonne prise en compte des effets stochastiques dans la vallée montre également que le problème de l'indice spectral bleu est plus grave encore lorsque les corrections quantiques à la trajectoire sont implémentées. Cela renforce l'hypothèse d'une instabilité tachyonique longue. D'un autre côté, nous avons établi que le formalisme récursif présente de bonnes propriétés de convergence dans la vallée mais diverge dans la phase d'instabilité tachyonique. Cette période peut donc difficilement être décrite par une approche perturbative, ce qui rend son traitement délicat en général. Pourtant, outre le problème de l'indice spectral, le scénario d'une instabilité courte pose le problème de l'évolution de la distribution du champ auxiliaire qui n'est plus quasi-statique dans la vallée. Cela induit des valeurs de sa dispersion encore plus faibles au point critique que ce que le calcul usuel suggère, et qui sont incompatibles avec l'hypothèse d'une instabilité courte. Enfin, dans le cas d'une instabilité courte, les grandes longueurs d'onde du champs auxiliaire ne sont plus dans un état quantique comprimé. Cette caractéristique de la fonction d'onde des perturbations est pourtant un ingrédient important de la transition quantique-classique que nous décrivons dans la section suivante.

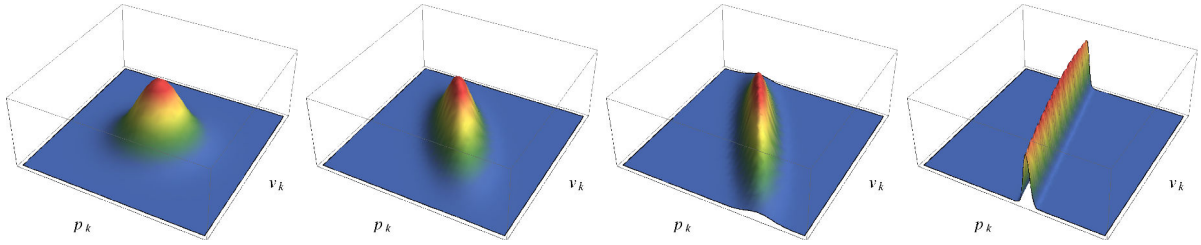

Figure 5.4.: Fonction de Wigner de l'état quantique comprimé d'un mode k de perturbation scalaire à différents instants durant l'inflation, correspondants successivement à $r_{\boldsymbol{k}} = 0.0005$, $r_{\boldsymbol{k}} = 0.48$, $r_{\boldsymbol{k}} = 0.88$ et $r_{\boldsymbol{k}} = 2.31$.

5.3.3. Le Problème de la Mesure Quantique en Cosmologie

Une des questions largement discutées dans le contexte de l'inflation est la transition quantique-classique des perturbations cosmologiques. En effet, si les fluctuations des champs inflationnaires sont traitées quantiquement, il est d'usage de considérer que les coefficients a_{lm} mesurés sur le FDC par exemple se comportent comme des réalisations stochastiques de ces variables quantiques. Ils sont alors interprétés comme des graines de perturbations classiques donnant lieu à la croissance de structures cosmologiques par instabilité gravitationnelle telles que les galaxies, les amas de galaxies, *etc.* Il s'agit donc de savoir comment cette projection sur des états classiques s'effectue en pratique.

Une première réponse souvent avancée est la compression des états quantiques [131, 307, 132, 309, 133, 408]. En effet, lorsqu'elles évoluent sur des échelles plus grandes que le rayon de Hubble durant l'inflation, les perturbations cosmologiques subissent une compression de leur état quantique. Cette compression peut être décrite via la fonction de Wigner W, qui est une distribution de quasi-probabilité définie dans l'espace des phases $(v_{\boldsymbol{k}}, p_{\boldsymbol{k}})$ pour chaque mode k, où v est la variable de Mukhanov et p est son moment canoniquement conjugué. Pour un état quantique $|\Psi_{\boldsymbol{k}}(v_{\boldsymbol{k}})\rangle$ Gaussien, cette fonction est de la forme

$$W\left(v_{\boldsymbol{k}}, p_{\boldsymbol{k}}\right) \propto \exp\left[-\frac{k}{\cosh\left(2r_{\boldsymbol{k}}\right)+\cos\left(2\phi_{\boldsymbol{k}}\right)\sinh\left(2r_{\boldsymbol{k}}\right)}v_{\boldsymbol{k}}^2\right]\times \exp\left\{-k\left[\cosh\left(2r_{\boldsymbol{k}}\right)+\cos\left(2\phi_{\boldsymbol{k}}\right)\sinh\left(2r_{\boldsymbol{k}}\right)\right]\left[\frac{p_{\boldsymbol{k}}}{k}+v_{\boldsymbol{k}}\frac{\sin\left(2\phi_{\boldsymbol{k}}\right)\sinh\left(2r_{\boldsymbol{k}}\right)}{\cosh\left(2r_{\boldsymbol{k}}\right)+\cos\left(2\phi_{\boldsymbol{k}}\right)\sinh\left(2r_{\boldsymbol{k}}\right)}\right]^2\right\}. \tag{5.16}$$

Dans cette expression, $r_{\boldsymbol{k}}$ et $\phi_{\boldsymbol{k}}$ sont deux fonctions du temps appelées respectivement paramètre de compression et angle de compression. Dans un espace-temps de de Sitter (c'est à dire dans lequel le paramètre de Hubble H est constant), elles sont données par

$$r_{\boldsymbol{k}} = \operatorname{argsinh}\left(\frac{aH}{2k}\right), \tag{5.17}$$

$$\phi_{\boldsymbol{k}} = \frac{\pi}{4}-\frac{1}{2}\arctan\left(\frac{aH}{2k}\right). \tag{5.18}$$

La fonction de Wigner décrite par ces relations est représentée sur la figure 5.4 à différents temps, ou de façon équivalente, à différentes valeurs de $r_{\boldsymbol{k}}$ ($r_{\boldsymbol{k}} = 0.0005$, $r_{\boldsymbol{k}} = 0.48$, $r_{\boldsymbol{k}} = 0.88$ et $r_{\boldsymbol{k}} = 2.31$). Initialement, dans le régime où le mode considéré correspond à une échelle de longueur plus petite que le rayon de Hubble, $k \gg aH$, on a $r_{\boldsymbol{k}} \simeq 0$ et $\phi_{\boldsymbol{k}} \simeq \pi/4$. Dans cette

limite, la fonction de Wigner (5.16) est de la forme $W \propto \exp\left(-kv_{\boldsymbol{k}}^2 - p_{\boldsymbol{k}}^2/k\right)$, ce qui correspond à un état cohérent pour lequel l'extension de la fonction de Wigner est la même dans toutes les directions et sature l'inégalité de Heisenberg. En revanche, à la fin de l'inflation lorsque le mode considéré est largement au delà du rayon de Hubble, $k \ll aH$, on a[5] $r_{\boldsymbol{k}} \gg 1$ et $\phi_{\boldsymbol{k}} \simeq 0$. La fonction de Wigner est alors de la forme $W \propto \delta[p_{\boldsymbol{k}} + k\tan(\phi_{\boldsymbol{k}})v_{\boldsymbol{k}}]$, ce qui correspond à un état comprimé dans la direction donnée par l'angle $\phi_{\boldsymbol{k}}$.

Les états comprimés sont bien connus en mécanique quantique (en particulier dans le domaine de l'optique quantique) car ils présentent des propriétés statistiques intéressantes. Notamment, leur évolution temporelle peut être décrite en terme d'une collection stochastique de processus classiques [136, 133, 409]. En d'autres termes, la fonction de Wigner peut être vue dans cette limite comme une véritable distribution de probabilité, répartissant un ensemble de processus dans l'espace des phases qui suivent tous les équations classiques du mouvement. La valeur moyenne de n'importe quelle observable définie dans l'espace des phases et calculée à l'aide de cette distribution coïncide alors avec les moyennes d'opérateurs quantiques. C'est pour cette raison qu'à partir de la fin de l'inflation, les perturbations cosmologiques aux grandes longueurs d'onde peuvent être traitées comme étant des fluctuations classiques, suivant une distribution initiale dont les propriétés statistiques coïncident avec les prédictions quantiques calculées pendant la phase inflationnaire. Dans ce sens, la compression des états quantiques joue un rôle clé pour l'ensemble du scénario cosmologique.

Un autre phénomène associé à la transition quantique-classique est celui de la décohérence. Les perturbations cosmologiques ne sont pas totalement isolées d'un environnement extérieur auquel elles sont nécessairement couplées [317, 318, 319]. Ce couplage a pour conséquence que leur matrice densité est dynamiquement diagonalisée avant la recombinaison [132, 309, 315, 133, 316], et le système peut alors être vu comme un mélange statistique d'état purs. Néanmoins, la décohérence des perturbations ne résout pas le problème de la mesure en mécanique quantique [410, 411], c'est à dire la production d'une réalisation unique. Ce problème apparaît de manière encore plus nette en cosmologie puisque nous disposons alors, par définition, d'une seule carte du FDC. L'interprétation standard de Copenhague de la mécanique quantique, qui stipule qu'une réalisation unique d'un processus quantique est produite par le biais d'une mesure réalisée par un expérimentateur extérieur qui projette la fonction d'onde du système sur un état propre de l'observable en question, pose problème dans le cas présent vue la difficulté à définir un observateur extérieur à l'Univers lui même. C'est pourquoi il est courant de postuler que le phénomène de décohérence est combiné avec une autre interprétation que celle de Copenhague, comme par exemple celle des mondes multiples [136, 412, 413, 414], de l'information quantique [415], ou en invoquant des variables cachées non locales [416, 417, 418, 153, 33, 419]. En fait, la seule alternative à la formulation standard de Copenhague qui propose une solution au problème de la mesure tout en étant falsifiable, est un modèle de réduction dynamique de la fonction d'onde [420, 421, 422, 423, 424, 425, 426, 427]. En effet, le problème de la mesure réside dans le fait que deux processus très différents par nature prennent place: l'évolution linéaire et unitaire de Schrödinger d'un côté et la réduction non linéaire et stochastique du paquet d'onde de l'autre.

Dans la Ref. [138] (section 4.3), nous nous sommes ainsi intéressés au modèle de CSL (pour "continuous spontaneous localization") de Pearle, Ghirardi, Rimini et Weber [421, 422, 424,

[5] Plus précisément, on a $a_{\rm end}H/k = \mathrm{e}^{\Delta N_*}$, où ΔN_* est le nombre d'e-folds réalisés entre le moment où le mode k croise le rayon de Hubble et la fin de l'inflation. Si k est à l'intérieur de la fenêtre observationnelle, on a typiquement $\Delta N_* \simeq 50$, et d'après l'équation (5.17), $r_{\boldsymbol{k}}$ à la fin de l'inflation est de l'ordre de $r_{\boldsymbol{k}} \simeq \Delta N_* \simeq 50$. Il est intéressant de noter que le niveau de compression associé à de tels paramètres est colossal, et typiquement bien plus grand que ce qui peut être réalisé en laboratoire [307].

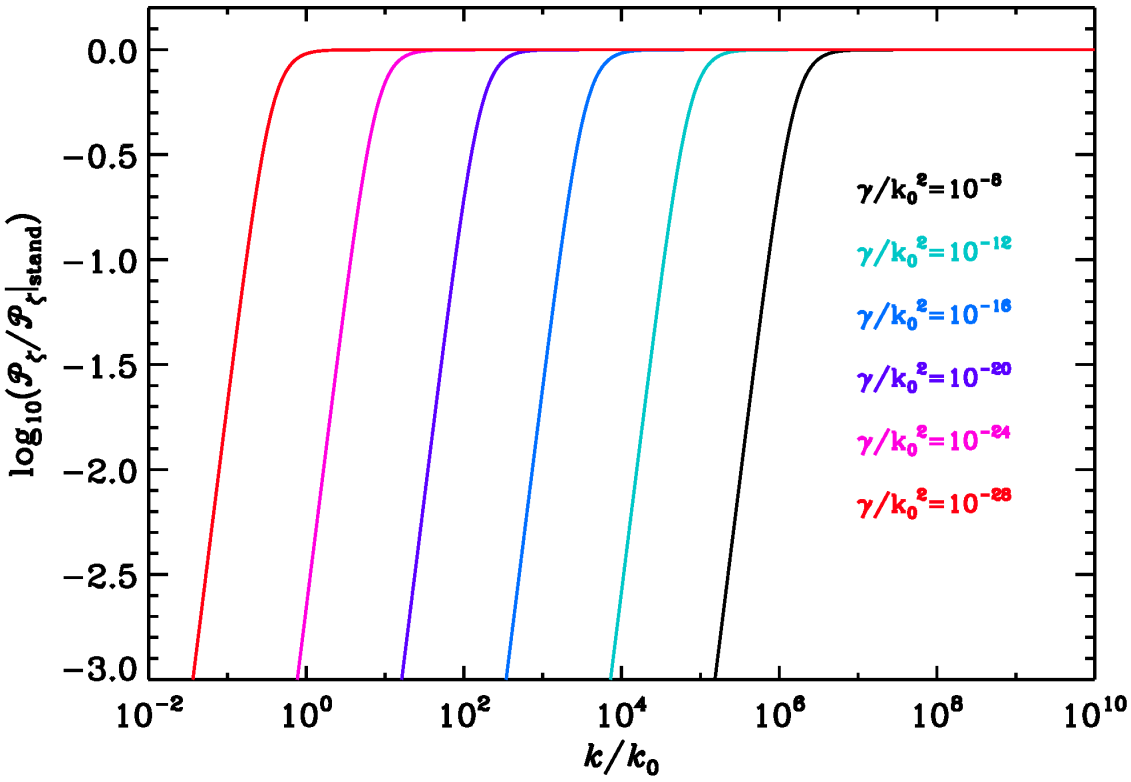

Figure 5.5.: Spectre de puissance des perturbations scalaires obtenu avec l'équation de Schrödinger modifiée (5.19), en prenant $\hat{C} = \hat{v_k}$ pour chaque mode k, et pour différentes valeurs de γ. La quantité représentée est le spectre normalisé à sa valeur standard (c'est à dire lorsque $\gamma = 0$). Le mode k_0 correspond à une échelle pivot autour de laquelle le spectre est calculé.

425], dans lequel l'équation de Schrödinger est modifiée par l'ajout de termes non linéaires et stochastiques:

$$\mathrm{d}\,|\psi\rangle = -i\hat{H}\mathrm{d}t\,|\psi\rangle + \sqrt{\gamma}\left(\hat{C} - \left\langle\hat{C}\right\rangle\right)\mathrm{d}W_t\,|\psi\rangle - \frac{\gamma}{2}\left(\hat{C} - \left\langle\hat{C}\right\rangle\right)^2\mathrm{d}t\,|\psi\rangle\ . \tag{5.19}$$

L'opérateur $\hat{H}$ est le hamiltonien du système et le premier terme correspond donc à l'équation de Schrödinger standard. L'opérateur $\hat{C}$ est l'opérateur de projection dont les états propres sont les directions le long desquelles on souhaite réaliser la réduction de la fonction d'onde. La non linéarité apparaît dans les termes $\langle\hat{C}\rangle = \langle\psi|\hat{C}|\psi\rangle$. La nature stochastique de cette équation de Schrödinger modifiée se traduit quant à elle par la présence d'un processus de Wiener W_t, et l'amplitude des termes non standards est définie par une constante de couplage γ. Cette théorie permet de projeter la fonction d'onde $|\psi\rangle$ sur un des états propres de $\hat{C}$ de façon dynamique, avec un temps caractéristique et à une précision près qui dépendent de γ, et selon des probabilités qui suivent la règle de Born.[6] De plus, ce modèle est doté d'un mécanisme d'amplification grâce auquel la constante de couplage γ effective d'un système constitué de N particules croît proportionnellement avec N. Cela permet d'expliquer que les objets macroscopiques soient bien

[6] De cette manière, les règles de Born n'ont pas besoin d'être postulées dans cette théorie, contrairement à ce qui est fait en mécanique quantique standard. Ici elles peuvent être démontrées à partir de l'équation d'évolution (5.19).

localisés, tout en laissant la dynamique des systèmes microscopiques, dont on sait qu'ils sont parfaitement décrits par la mécanique quantique standard, essentiellement inchangée.

Nous avons donc utilisé ce modèle pour décrire l'évolution des perturbations scalaires pendant l'inflation, afin d'établir quelles contraintes sur la théorie (c'est à dire principalement sur le paramètre γ) la nécessité de réduire la fonction d'onde pendant l'inflation pouvait imposer. Nous avons choisi comme opérateur de projection la variable de Mukhanov-Sasaki v puisqu'elle est invariante de jauge. Un premier résultat a été obtenu en calculant le spectre de puissance produit par cette théorie, et représenté sur la figure 5.5 pour différentes valeurs de γ. Deux branches apparaissent nettement: une branche qui reste quasi invariante d'échelle et où les termes non standards jouent un rôle négligeable, et une branche très fortement dépendante de l'échelle où $n_{\rm S} = 4$ et où les termes non standards dominent. Afin que cette branche se situe au delà des échelles observables et pour préserver l'invariance d'échelle observée, la constante de couplage γ doit être suffisamment petite,

$$\frac{\gamma}{k_0^2} \ll e^{-\Delta N_*} \simeq 10^{-28}\,. \tag{5.20}$$

Dans cette expression, k_0 est l'échelle pivot autour de laquelle le spectre de puissance est calculé. Néanmoins, γ ne peut pas être arbitrairement petit si l'on souhaite que la réduction du paquet d'onde se produise avant la fin de l'inflation. Pour des échelles situées à l'extérieur du rayon de Hubble, le nombre d'e-folds requis pour que la réduction ait lieu est de l'ordre de $\log(k^2/\gamma)$, qui d'après la contrainte précédente doit être plus grand que ~ 28. Les $\Delta N_* \sim 60$ e-folds dont nous disposons sont donc suffisants. En revanche, dans la branche invariante d'échelle, l'efficacité de la réduction du paquet d'onde, mesurée par sa dispersion $\sigma_{v_{\boldsymbol{k}}}$ dans son état final, est donnée par

$$k\sigma_{v_{\boldsymbol{k}}} \simeq \exp\left(2\Delta N_*\right) \gg 1\,. \tag{5.21}$$

En conclusion, l'invariance d'échelle contraint γ à prendre des valeurs si petites que la fonction d'onde est très mal localisée à la fin de l'inflation et que le modèle discuté ici ne peut pas expliquer correctement la production d'une réalisation bien définie au cours de l'inflation.

Notons néanmoins que les auteurs de la Ref. [404] ont généralisé notre calcul au cas où γ dépend de k par le biais d'une loi de puissance. Ils ont établi pour quel exposant dans cette loi l'indice spectral de la branche du spectre dominée par les termes non standards est invariante d'échelle. Dans ce cas, il n'y a plus de borne supérieure sur γ et quitte à prendre des grandes valeurs de γ, il est toujours possible de réaliser efficacement la réduction du paquet d'onde sans altérer l'invariance d'échelle du spectre.

5.4. Conclusion

Dans cette thèse, nous avons illustré la manière dont le paradigme inflationnaire permet de mieux cerner un certain nombre de questions fondamentales en physique, et d'appréhender leurs implications concrètes dans un cadre théorique pertinent. D'un autre côté, nous avons vu que de nombreuses mesures cosmologiques et astrophysiques permettent de contraindre explicitement les paramètres microphysiques décrivant cette phase d'expansion accélérée et de cette manière, d'en apprendre d'avantage sur les caractéristiques physiques de l'Univers primordial.

Pour conclure, il convient de discuter à présent les perspectives offertes par une telle démarche à moyen et long terme. Le paradigme inflationnaire est doté d'une solidité phénoménologique

qui peut rendre difficile l'identification de son origine microphysique, puisque ses prédictions dépendent d'un petit nombre d'observables génériques et que les échelles nous permettant de les sonder sont restreintes à quelques e-folds. Par conséquent, si la détection de r revendiquée par l'expérience BICEP2 se confirme, il est clair que tout doit être entrepris pour en mesurer précisément la valeur. Si l'ordre de grandeur annoncé $r \sim 0.1$ est correct, cela signifie également que l'indice spectral des ondes gravitationnelles, $n_{\rm T}$, peut aussi être mesuré [405] à moyen terme. De cette manière, le nombre de paramètres inflationnaires dont on aurait une mesure doublerait, passant de $\{\mathcal{P}_{\zeta,*}, n_{\rm S}\}$ à $\{\mathcal{P}_{\zeta,*}, n_{\rm S}, r, n_{\rm T}\}$. Si l'on ajoute à cela les corrélations EE et TE mesurées par Planck et qui devraient être publiées sous peu, il semble réaliste de vouloir réellement contraindre la forme du potentiel et son échelle d'énergie.

En revanche, si une détermination plus précise de la contribution des avant plans de poussière dans l'expérience BICEP2 fait disparaître le signal sur r, ce projet risque d'être fortement ralenti. En effet, pour bon nombre de modèles dont le potentiel a une forme de "plateau" (les modèles favorisés par Planck), tels que les modèles d'inflation branaire ou les modèles d'inflation avec module de Khähler, la valeur prédite pour r est minuscule, typiquement $r < 10^{-6}$. Pour l'instant, il semble totalement impossible d'atteindre de tels seuils de détection. De la même manière, pour les modèles d'inflation à un champ scalaire et avec terme cinétique standard (qui semblent pour le moment favorisés par les données), le niveau de non Gaussianités primordiales est très faible, $f_{\rm NL} \sim \epsilon$, et ne semble pas être détectable pour le moment [406]. Le même constat s'applique pour les perturbations entropiques qui pourraient provenir de la présence d'autres champs massifs, ou pour le running du spectre de puissance $\alpha_{\rm S} \sim \epsilon^2$. C'est pourquoi dans ce cas, il est fort possible que l'on assiste à un certain ralentissement de l'entreprise visant à contraindre l'inflation par les mesures du FDC.

Pour continuer à progresser dans notre compréhension de l'Univers primordial, deux chemins peuvent alors être empruntés. Le premier consiste à discriminer les modèles par des arguments théoriques, en continuant à examiner les possibilités offertes par les extensions du modèle standard de la physique des particules, en comprenant mieux le rôle des corrections radiatives, des couplages aux autres champs, des propriétés physiques de la phase de réchauffement qui en découlent, etc. Car indépendamment des observations, l'inflation soulève un certain nombre de problème fondamentaux qu'il reste à résoudre. Une autre possibilité est d'étudier plus en détails les connections existant entre les prédictions inflationnaires et d'autres sondes astrophysiques telles que les supernovae, la répartition des galaxies et des amas de galaxies, l'astrophysique à 21 cm, la reconstruction des conditions initiales par les simulations de grandes structures, etc. Le bras de levier entre les différentes échelles associées à ces objets est énorme et devrait nous permettre de mieux cerner l'Univers dans lequel ils évoluent.

La cosmologie est entrée dans une ère de données massives où des mesures d'observables fondamentalement différentes par nature doivent être intelligemment combinées dans le but de contraindre des processus physiques tout aussi différents. De cette manière, les avancées dans l'ensemble des champs de la cosmologie et même de l'astrophysique sont étroitement liées et dépendantes les unes des autres. Le décryptage de l'Univers primordial repose donc sur une compréhension de phénomènes physiques très variés, et sur la réalisation de mesures qui mettent au défi la technologie moderne. Seulement à ce prix pourrons nous avancer dans cette quête universelle qu'est la compréhension du monde dans lequel nous vivons.